USDA
United States Department of Agriculture

Proceedings

19th International Nondestructive Testing and Evaluation of Wood Symposium

Rio de Janeiro, Brazil
2015

Forest Service, Forest Products Laboratory
University of Campinas, College of Agricultural Engineering
Brazilian Society of Non-Destructive Testing and Inspection

General Technical Report
FPL–GTR–239

September
2015

Abstract

The 19th International Nondestructive Testing and Evaluation of Wood Symposium was hosted by the University of Campinas, College of Agricultural Engineering (FEAGRI/UNICAMP), and the Brazilian Association of Nondestructive Testing and Evaluation (ABENDI) in Rio de Janeiro, Brazil, on September 22–25, 2015. This Symposium was a forum for those involved in nondestructive testing and evaluation (NDT/NDE) of wood and brought together many NDT/NDE users, suppliers, international researchers, representatives from various government agencies, and other groups to share research results, products, and technology for evaluating a wide range of wood products, including standing trees, logs, lumber, and wood structures. Networking among participants encouraged international collaborative efforts and fostered the implementation of NDT/NDE technologies around the world. The technical content of the 19th Symposium is captured in these proceedings.

Keywords: International Nondestructive Testing and Evaluation of Wood Symposium, nondestructive testing, nondestructive evaluation, wood, wood products

Contents

September 2015

Ross, Robert J.; Gonçalves, Raquel; Wang, Xiping, eds. 2015. Proceedings: 19th International Nondestructive Testing and Evaluation of Wood Symposium. General Technical Report FPL-GTR-239. Madison, WI: U.S. Department of Agriculture, Forest Service, Forest Products Laboratory. 688 p.

A limited number of free copies of this publication are available to the public from the Forest Products Laboratory, One Gifford Pinchot Drive, Madison, WI 53726–2398. This publication is also available online at www.fpl.fs.fed.us. Laboratory publications are sent to hundreds of libraries in the United States and elsewhere.

The Forest Products Laboratory is maintained in cooperation with the University of Wisconsin.

Proceedings

19th International Nondestructive Testing and Evaluation of Wood Symposium

Rio de Janeiro, Brazil
2015

Edited by

Robert J. Ross, Supervisory Research General Engineer
Forest Products Laboratory, Madison, Wisconsin

Raquel Gonçalves, Professor
University of Campinas, Brazil

Xiping Wang, Research Forest Products Technologist
Forest Products Laboratory, Madison, Wisconsin

Preface

The International Nondestructive Testing and Evaluation of Wood Symposium Series started in Madison, Wisconsin, USA, in 1963. Since its inception, 18 symposia have been held in various countries around the world, including China, Germany, Hungary, Switzerland, and the United States.

The 19th International Nondestructive Testing and Evaluation of Wood Symposium was hosted by the University of Campinas, College of Agricultural Engineering (FEAGRI/UNICAMP), and the Brazilian Association of Nondestructive Testing and Evaluation (ABENDI). It was held in Rio de Janeiro, Brazil, on September 23–25, 2015. This symposium was a forum for those involved in nondestructive testing and evaluation (NDT/NDE) of wood and brought together many NDT/NDE users, suppliers, international researchers, representatives from various government agencies, and other groups to share research results, products, and technology for evaluating a wide range of wood products, including standing trees, logs, lumber, and wood structures. Networking among participants encouraged international collaborative efforts and fostered the implementation of NDT/NDE technologies around the world.

The 19th symposium was especially important because, in addition to its strong technical content, it was the first one held in South America. The opening session, "Importance of Nondestructive Evaluation in a Global Forest Products Community," included keynote speakers from around the globe who presented the state-of-the-art in nondestructive testing and evaluation of wood. Special recognition at the symposium's banquet was made to ABENDI and the University of Campinas for their outstanding efforts in support of this meeting. Engraved plaques were awarded to representatives from ABENDI and the University of Campinas. An engraved plaque was presented to Dr. Raquel Gonçalves for her leadership of this meeting.

Special events included a pre-symposium workshop on nondestructive evaluation of trees that was held at Tijuca National Park, Rio de Janeiro.

Two special publications, *Wood and Timber Condition Assessment Manual—Second Edition* and *Nondestructive Evaluation of Wood—Second Edition*, were published by the Forest Products Laboratory for this symposium. Each attendee received complimentary printed copies of these publications.

The technical content of the 19th symposium is captured in the following proceedings. Full-length, in-depth technical papers for the oral presentations and several of the poster presentation are published herein. The papers were not peer-reviewed and are reproduced here as they were submitted by the authors.

The organization of the following proceedings follows that of the sessions at the 19th symposium. Technical sessions covered the following topics:

- Material Characterization
- Evaluation of Solid Sawn Products
- Evaluation of Engineered Wood Products
- Standing Timber Assessment
- In-Place Assessment of Structures
- Urban Tree Assessment
- Logs and Round Wood Assessment
- Biomass and Pulpwood Assessment

We express our sincere appreciation and gratitude to members of the Organizing Committee, International Nondestructive Testing and Evaluation of Wood Symposium Series, for their efforts in making this symposium a success:

- Brian K. Brashaw, Program Manager, USDA Forest Products Laboratory, USA
- Francisco Arriaga Martitegui, Professor, Universidad Politécnica de Madrid, Spain
- Ferenc Divos, Professor, University of Western Hungary, Hungary
- Roy F. Pellerin, Professor Emeritus, Washington State University, USA
- Adam Senalik, Research Engineer, USDA Forest Products Laboratory, USA
- Xiping Wang, Research Forest Products Technologist, USDA Forest Products Laboratory, USA

We thank the International Union of Forestry Research Organizations (IUFRO) for their support. Thanks also go to the following organizations for providing financial support in the form of sponsorships or who exhibited equipment: Apoena Engineering Ltda; ATCP Physical Engineering; PD Instrumentos; Agricef Technological Solutions for Agriculture; Fakopp Enterprise; ABENDI; Coordination for the Improvement of Higher Education Personnel (CAPES); National Council for Scientific and Technological Development (CNPq); Background Support Teaching, Research and Extension (FAEPEX/UNICAMP); São Paulo Research Foundation (FAPESP); Washington State University (WSU); USDA Forest Service; Beijing Forestry University (BFU); Research Institute of Wood Industry (CRIWI), Chinese Academy of Forestry (CAF).

A very special thank you to Ms. Pamela Byrd (FPL) and Thais Nunes (ABENDI) for their outstanding efforts—especially for serving as our main point of contact for speakers. Thank you, Pam and Thais!

We thank the following staff at FPL for their outstanding efforts in preparing these proceedings: Jim Anderson, Xiping Wang, and Adam Senalik.

A note of thanks to the many individuals who prepared papers for inclusion in the symposium. Your dedication and efforts make this Symposium Series a success!

We hope that these proceedings provide inspiration to those who read its papers. And welcome to new participants in the global wood NDT/NDE family!

Robert J. Ross, Project Leader, USDA Forest Products Laboratory, USA

Raquel Gonçalves, Professor, University of Campinas, Brazil

Symposium Co-Chairs

Thank you to this year's sponsors and exhibitors.
Your support has helped make this symposium possible!

Session 1

Material Characterization—Ultrasound

Prediction of Young's Modulus in Three Orthotropic Directions for Some Important Turkish Wood Species Using Ultrasound

Ergün Güntekin
Suleyman Demirel University, Faculty of Forestry, Department of Forest Products Engineering, 32260 Isparta, Turkey, ergunguntekin@sdu.edu.tr

Tuğba Yılmaz Aydın
Suleyman Demirel University, Faculty of Forestry, Department of Forest Products Engineering, 32260 Isparta, Turkey, tugbayilmaz@sdu.edu.tr

Peter Niemz
ETH Zürich, Institute for Building Materials, Wood Physics Group, Zürich, Switzerland, niemz.p@ethz.ch

Abstract

The materials used in the study consisted of 720 small clear specimens of nominal dimensions 20 x 20 x 60 mm, of Turkish Red Pine (*Pinus brutia*) Lebanon cedar (*Cedrus libani*), Oriental beech (*Fagus oriantalis*), and English oak (*Quercus robur*) from Turkey. The specimens were grouped into 4 batches of 15 specimens each and were tested in the ETH laboratories in Zurich, Switzerland. The influence of EMC was studied over four batches of 15 specimens each, conditioned for 6-8 weeks before testing at a temperature of 20 ± 2ºC and at four different relative humidities (50%, 65%, 85%, and 95%). Time of flight value was measured with an ultrasonic commercial device Steinkamp BP-V. Measurements were made end to end directions (*L, R, T*) on each specimen, with a constant sensor coupling pressure. According to the time results of ultrasound devices, the wave velocities (length/time) and E_{dyn} were calculated. Samples were also tested in uniaxial compression in order to determine *E* values in three orthotropic directions using a Zwick Z 100 universal testing machine. A load cell with 100-kN maximum capacity was used for compression tests performed in all directions. The feed rate was defined in such a way that the failure of the specimen should be reached in 90 (±30) s. The strains were evaluated using the digital image correlation DIC technique. Wood MC was determined by the oven-drying method. The R^2 values between E and E_{dyn} ranged from 0.79 to 0.96 for the species tested. Moisture content seems to be an influencing factor on sound velocities.

Keywords: young modulus, prediction, ultrasound

Introduction

Compression properties, particularly Young’s modulus, in the three principal directions are important in design of wood members in structures. Young's modulus, also known as the elastic modulus, is a measure of the stiffness of an elastic material and is a quantity used to characterize materials. In general, there are many physical parameters that may affect Young’s modulus such as moisture content (MC), specific gravity, temperature, creep, knots, number of annual growth rings and grain angle. Investigations regarding the influence of MC on Young’s modulus have shown that if MC increases the Young’ moduli decrease. While the influence of MC on the mechanical behavior of wood in the L direction is relatively well known (Gerhards 1982), investigations on the behavior in the perpendicular directions (R and T) are limited. The interest on the moisture dependent orthotropic behavior is not new. So far, only few studies studied moisture dependent elastic properties of wood in

the R and T directions (McBurney and Drow 1962; Hering et al. 2012a; Hering et al. 2012b; Ozyhar et al. 2013). Furthermore, moisture-dependent wood strength in the R and T directions, remain widely unrevealed for most wood species. The usable data are limited to a few references (Kretshmann and Green 1996; Ozyhar et al. 2013). While selected moisture dependent elastic properties for some wood species can be found in (Kretshmann and Green 1996; Ross 2010). Young's modulus can be determined using both destructive and non-destructive methods.

Use of non-destructive testing (NDT) and non-destructive evaluation (NDE) in the field of wood and wood based materials is advancing every day. There are wide spread NDT techniques, equipment and evaluation procedures available today which resulted from early NDT researches (Brashaw et al. 2009; Dündar and Divos 2014). Ultrasonic wave velocity has more advantages over other techniques in practical terms (Estaban et al. 2009).

The ultrasonic technique has been utilized in many applications including tree quality evaluation in forests (Wang et al. 2004) and condition assessment of wood structures in service (Ross and Pellerin 1994). The ultrasonic modulus of elasticity determination in a solid depends on its elastic properties and its density (Oliveira and Sales 2006). The velocity of sound in wood is influenced by many factors such as moisture content, grain orientation, density, decay, temperature and geometry (Beall 2002; Oliveria et al. 2005).

Information on the Young's modulus of wood in the orthotropic directions is not available for majority of Turkish species. Most of the studies deal with bending MOE, bending, tensile and compression strength at constant MC. Although data needed for three dimensional modeling of mechanical behavior depending on the MC change, no information is available for this purpose. In this study, Young's modulus in compression for some important Turkish wood species is determined by non-destructive and destructive testing at different moisture conditions.

Materials and Methods

Materials

For the study, two softwood and two hardwood species are chosen. The sample trees for Sessile oak (*Quercus petraea*) and Oriental beech (*Fagus orientalis*), were selected from a beech-oak mixed stand in the Devrek Forest Region of the Western Black Sea region of Turkey. The sample tress for Calabrian pine (*Pinus brutia Ten.)* and Taurus cedar (*Cedrus libani*) were selected from pine-cedar mixed stand in the Bucak Forest Region of the Southwest region of Turkey.

The materials used in testing consisted of 720 small clear specimens of nominal dimensions 20 x 20 x 60 m. The specimens were grouped into 4 batches of 15 specimens each and were tested in the ETH laboratories in Zurich, Switzerland. The influence of EMC was studied over four batches of nearly 15 specimens each, conditioned for 6-8 weeks before testing at a temperature of 20 ± 2ºC and at four different relative humidity conditions (50%, 65%, 85%, and 95%).

Methods

Time of flight value was measured with an ultrasonic commercial device Steinkamp BP-V using conical sensors of 22 kHz frequency. Measures were made end to end directions (L, R, T) on each specimen, with a constant sensor coupling pressure. According to the time results of ultrasound devices, the sound velocities (SV, length/time) and Edyn were calculated using the fallowing equation:

$$E_{dyn} = \rho V^2 10^6 \quad (1)$$

Where E_{dyn} is the dynamic modulus of elasticity, in N/mm^2, ρ is the density, in kg/m^3, V is the velocity of the ultrasound wave, in m/s.

After completing ultrasonic measurements, uniaxial compression tests were carried out using a Zwick 100 universal testing machine at standard climatic conditions (65 % RH and 20 °C). To minimize the influence of the MC change, specimens were tested immediately after removal from the climatic chamber. Wood MC was determined by the oven-drying method. The feed rate was defined in such a way that the failure of the specimen should be reached in 90 (±30) s. The strains were evaluated using the digital image correlation (DIC) technique. A high contrast random dot texture was sprayed on the surface of the specimen with air-brush to ensure the contrast needed for the evaluation of the displacements. Pictures were taken with a frequency of 4 Hz of the cross-sectional surface area of the specimen during testing. By means of the mapping software (VIC 2D, Correlated Solution), the surface strains were calculated from the displacements that occurred during deformation. A more detailed description of the strain computation by the DIC technique is given in Keunecke et al. (2008). Density of the samples was calculated according to TS 2472. The stress-strain curves obtained were used in order to evaluate Young's moduli and strength properties of the specimens. The Young's modulus was calculated from the ratio of the stress σ to the strain ε measured in the linear elastic range:

$$E_i = \frac{\Delta\sigma_i}{\Delta\varepsilon_i} = \frac{\sigma_{i,2}-\sigma_{i,1}}{\varepsilon_{i,2}-\varepsilon_{i,1}} \quad i \in R, L, T \tag{2}$$

Since the strength behavior of wood in R and T directions is obscure, maximum compression strength was calculated using 0.2% yield values using following formula.

$$\sigma UCS = P_{max}/A \tag{3}$$

Where; σ_{UCS} represents yield strength, P_{max} is the yield load and A is the cross-sectional area of the specimen.

Analysis of variance (ANOVA) general linear model procedure was run for data with SAS statistical analysis software to interpret the interrelationships among the properties measured of the clear wood samples.

Results and Discussion

Average values for density, MC, sound velocities (SV), Edyn, Young's modulus and compression strength (CS) values of the specimens tested are presented in Tables 1-4. There was a good match among the density values in the different MC groups. In comparison to available literature references at similar MC, the measured density values were comparable. The ratios of SV and Young's modulus in the principal direction are presented in Table 5.

The SV values obtained in this study are similar to those reported by Bucur (2006) except Sessile oak which has much lower SV values than common oak and many hardwood species. Results indicate that there is negative weak correlation between density and SV for each species tested . There is a contradiction in the literature on whether SV is correlated with wood density or not. Some authors (Oliveria et al. 2002; Ilic 2003; Teles et al. 2011) identified that there is no relationship between density and velocity while others (Oliveira and Sales, 2006; Baradit and Niemz, 2012) reported positive relationship of density and velocity. Some authors (Ilic 2003; Krauss and Kudela 2011) claimed that velocity is related to the micro-fibrilar angle while Gerhards (1982) and Beall (2002) pointed out that grain angle has major impact on the SV.

Table 1. Sound velocity, Edyn, Young's modulus and CS values for Calabrian pine.

Direction	Density g/cm^3	MC (%)	Velocity (m/s) Mean	cov (%)	E_{dyn} (N/mm^2) Mean	cov (%)	Young's Modulus Mean	cov (%)	CS Mean	cov(%)
L	0.53	10.57	5302	3.66	14968	10.26	9131	19	38.42	6.67
R	0.53	10.76	2304	4.86	2860	12.08	1114	19	8.70	12.23
T	0.55	10.89	1680	4,02	1545	7.54	646	11	7.55	5.38
L	0.53	13.47	5045	3.26	13240	8.86	8650	14	33.14	578
R	0.53	12.76	2261	4.31	2713	10.57	917	16	8.25	10.69
T	0.54	13.42	1651	2.97	1480	5.58	624	14	6.71	7.23
L	0.52	19.85	5016	4.29	13222	9.32	7731	16	24.42	6.71
R	0.54	20.00	2120	6.36	2451	14.97	766	9	5.83	9.2
T	0.55	20.05	1570	1.84	1354	3.78	431	14	4.67	4.98
L	0.56	24.35	4821	3.45	13085	8.18	7380	13	21.16	5.15
R	0.57	24.64	2037	4.28	2360	8.07	676	15	5.21	5.49
T	0.56	24.37	1504	1.97	1265	3.60	402	23	3.85	8.26

Table 2. Sound velocity, Edyn, Young's modulus and CS values for Taurus cedar.

Direction	Density g/cm^3	MC (%)	Velocity (m/s) Mean	cov (%)	E_{dyn} (N/mm^2) Mean	cov (%)	Young's modulus Mean	cov(%)	CS Mean	cov (%)
L	0.54	10.74	4458	5.41	10706	12.80	7857	18	45.82	6.41
R	0.58	10.88	2243	2.26	2933	7.96	1298	16	9.84	1.51
T	0.58	10,50	1902	5,01	2107	8,04	716	14	6.90	19.03
L	0.57	12,89	4388	7,55	10929	11,59	7496	11	41.33	5.98
R	0.57	12,87	2142	3,29	2605	11,74	974	21	9.21	13.03
T	0.53	14,80	1756	2,11	1641	7,94	663	21	6.17	13.87
L	0.62	20,59	4229	9,27	11115	13,66	6831	10	35.80	7.18
R	0.57	20,27	20,39	2,23	2360	9,41	850	11	7.86	11.63
T	0.54	20,72	1678	2,76	1532	8,49	490	19	5.20	10.42
L	0.59	26,05	4406	6,64	11428	9,03	6683	18	31.02	8.09
R	0.59	26,05	2001	2,87	2387	9,30	809	9	7.15	8.68
T	0.56	23,50	1612	2,40	1445	8,09	437	23	4.46	12.85

Table 3. Sound velocity, Edyn, Young's modulus and CS values for Oriental beech.

Direction	Density g/cm3	MC (%)	Velocity (m/s) Mean	cov (%)	E_{dyn} (N/mm^2) Mean	cov (%)	Young's Modulus Mean	cov(%)	CS Mean	cov (%)
L	0.68	10,65	5168	4,09	18235	8,40	14092	24	54.13	23.67
R	0.66	10,23	2244	1,42	3302	4,10	2137	26	14.04	7.86
T	0.64	10,97	1572	1,87	1586	7,08	902	14	8.40	24.17
L	0.69	13,40	5100	5,27	17941	8,95	13360	10	49.07	19.12
R	0.67	11,82	2200	1,69	3222	3,11	1684	21	12.60	5.99
T	0.64	13,64	1560	2,22	1568	9,04	824	8	7.65	21.65
L	0.68	16,53	4792	4,72	15732	8,94	11586	18	38.88	15.73
R	0.68	16,53	2070	1,52	2926	3,19	1481	8	10.81	10.61
T	0.64	16,62	1500	2,04	1442	8,11	706	11	6.58	38.51
L	0.67	20,36	4901	2,56	16176	4,89	10135	12	33.91	14.60
R	0.68	20,40	2032	1,09	2794	3,18	1214	10	9.29	15.00
T	0.65	20,95	1495	2,47	1455	9,80	616	17	5.96	36.65

In general, the results indicate clear differences between the SV along the principal directions (SVL > SVR> SVT). The ratios found in this study are somewhat smaller than those reported by Bucur (2006), Keunecke et al. (2011) and Baradith and Niemz (1012).

Table 4. Sound velocity, Edyn, Young's modulus, and CS values for Sessile oak.

Direction	Density g/cm3	MC (%)	Velocity (m/s) Mean	cov (%)	E_{dyn}(N/mm^2) Mean	cov (%)	Young's Modulus Mean	cov (%)	CS Mean	cov (%)
L	0.65	12,27	4168	4,66	11239	13,06	8305	30	37.57	24.20
R	0.72	11,60	2001	2,61	2890	4,41	2001	21	14.32	8.33
T	0.67	11,95	1661	1,34	1864	4,80	1249	12	10.23	13.21
L	0.66	12,81	4160	4,67	11505	9,16	7691	21	34.86	15.11
R	0.73	13,78	1996	2,81	2895	4,24	1883	31	12.76	7.45
T	0.67	14,33	1638	1,09	1792	4,12	1033	15	9.08	17.61
L	0.68	20,81	4042	5,92	11088	14,07	6583	32	27.20	13.79
R	0.72	18,50	1882	2,46	2560	3,89	1312	25	10.23	12.63
T	0.68	20,93	1592	0,76	1729	2,51	892	32	7.55	25.93
L	0.70	23,38	3912	7,55	10752	16,34	5016	37	25.32	11.54
R	0.79	20,67	2615	3,51	2615	3,51	1132	31	9.60	13.65
T	0.68	22,16	1589	1,41	1723	4,10	715	18	7.14	28.50

Table 5. Ratios of sound velocity and Edyn for the main directions

Species	MC (%)	Ratio of sound velocities (T:R:L)	Ratio of Young's modulus (T:R:L)
Calabrian pine	10-11	1: 1.37 : 3.15	1: 1.72 : 14.13
	13-14	1: 1.36 : 3.05	1: 1.46 : 13.86
	16-17	1: 1.45 : 3.19	1: 1.77 : 17.93
	20-21	1: 1.35 : 3.20	1: 1.68 : 18.35
Cedar	11-12	1: 1.17 : 2.34	1: 1.72 : 10.97
	13-14	1: 1.21 : 2.49	1: 1.46 : 11.30
	18-20	1: 1.21 : 2.52	1: 1.73 : 13.94
	21-23	1: 1.24 : 2.73	1: 1.85 : 15.29
Oriental beech	10-11	1: 1.42 : 3.28	1: 2.36 : 15.62
	13-14	1: 1.41 : 3.26	1: 2.04 : 16.21
	16-17	1: 1.38 : 3.19	1: 2.09 : 16.41
	20-21	1: 1.35 : 3.27	1: 1.97 : 16.45
Oak	11-12	1: 1.20 : 2.50	1: 1.60 : 6.64
	13-14	1: 1.21 : 2.53	1: 1.82 : 7.44
	19-21	1: 1.18 : 2.53	1: 1.47 : 7.38
	21-23	1: 1.64 : 2.46	1: 1.58 : 7.01

The softwoods Calabrian pine and cedar significantly differ regarding their SV in the longitudinal direction at 20 °C and 65% RH. Their SV are identical in the perpendicular directions. Average SV ranged from 4821 to 5302 m/s parallel to grain direction and 1504 to 2304 m/s perpendicular direction for Calabrian pine. Average SV ranged from 4229 to 4458 m/s parallel to grain direction and 1612 to 2243 m/s perpendicular direction for cedar. Although cedar has higher average density than Calabrian pine, its SV was lower for all principal directions. The higher SV of Calabrian pine can be due to longer fiber length.

The hardwoods Oriental beech and Sessile oak also clearly differs concerning their SV in the longitudinal direction at all humidity conditions. Their SV are similar in the perpendicular directions. Average SV ranged from 4901 to 5168 m/s parallel to grain direction and 1495 to 2244 m/s perpendicular direction for Oriental beech. Average SV ranged from 3912 to 4168 m/s parallel to grain direction and 1589 to 2615 m/s perpendicular direction for sessile oak. Although Sessile oak has higher average density than Oriental beech, its SV was lower for all principal directions. Oriental beech has also longer fibers than sessile oak which has also large earlywood pores and rays. The SV of Sessile oak is much lower than those reported for common oak (Bucur 2006). According to Beall (2002) the SV in the radial direction range from 1000 to 2000 m/s and can be twice as the SV in the

tangential direction. The results obtained between species indicated that SV tends to decrease with increasing density. While oak had the highest average density, it had the lowest average SV. In general, there is a good negative correlation between MC and SV, and the correlations are higher in perpendicular directions (Table 5). According to Gerhards (1982) SV decreases by 1% when the MC increases by 1% within the hygroscopic range. The SV in all directions seem to decrease with increasing MC except Sessile oak samples tested at 20 °C and 95% which showed an increase in comparison to other levels of RH. The rate of change with changing humidity (%) ranged from 0.36 for Cedar in L direction to 1.38 for Cedar in T direction. SV in Calabrian pine showed the closest rate of decrease with increasing MC confirming Gerhards (1982) statement. In the L and T directions, Sessile oak wood showed very low rate of decrease in sound velocity with increasing MC. The effect of moisture content (MC) on velocity has been studied by number of researchers, who have shown that the velocity of acoustic waves decreases with moisture content up to the fiber saturation point (Booker et al. 1996; Bucur, 2006; Gao et al. 2011).

The wood species tested clearly differ regarding their calculated Young's moduli. Between softwoods, the values of Cedar are lower than those of Calabrian pine, although Cedar has slightly higher average density (0.56 g/cm3) than Calabrian pine (0.54 g/cm3). Between hardwoods, Sessile oak wood has higher density (0.69 g/cm3) than Oriental beech (0.66 g/cm3) but its average calculated Young's moduli values are lower.

The E_{dyn} calculated from sound propagation is much higher than the static Young's modulus because the measurements were not corrected with the Poisson's ratios. According to Bucur (2006) the ultrasonic values of Young's modulus, EL, are slightly higher than the corresponding static measured moduli, under compression. It is known that dynamically determined elastic properties are 10-20% (or even more, depending on the frequency of ultrasonic waves) increased compared with statically calculated values (Keunecke et al. 2011).

In general, Young's modulus in all anatomical directions tended to increase at lower MC as expected. The three Young's moduli values are affected by moisture, but to a different degree. Young's modulus in the direction perpendicular to the grain changes with MC at higher rates. It seems that anisotropy is higher for Oriental beech and Calabrian pine than Sessile oak and Cedar. It was reported by Baradit and Niemz (2012) that anisotropy is higher in softwood than hardwoods in Europe while it is contrary for some Chilean wood species. Bodig and Jayne (1993) stated that EL:ET ratio is nearly 24:1 in softwoods while Bucur (2006) reported the largest EL:ET ratio which is nearly 28:1 for Scotch pine. Similar trend in mechanical properties due to the MC changes was reported by Gerhards (1982), Ross (2010), Hering et al. (2012a) and Ozyhar et al. (2013). The ratio of Young's modulus in L, R and T directions was approximately 16:2:1 for Oriental beech which is identical to European beech (Hering et al. 2012a). Sessile oak had the lower difference between the parallel and perpendicular to the grain values which is similar to results reported by Bucur (2006) and contrary to those reported by Baradit and Niemz (2012) for the Chilean hardwoods. The ratios calculated in this study are clearly below those published by Bodig and Jayne (1993).

Depending on the type of species, the ratio of CS parallel to the grain to that perpendicular to the grain varied between 3.54 and 6.64 that are lower than those reported for poplar, fir, and pine (Aydın et al. 2007) and similar to those stated by Kretschmann and Green (1996). The corresponding value is 6.69 for cedar and 3.54 for Sessile oak due to its lower anisotropy. The ratios of between principal direction is almost constant for Sessile oak, higher for increasing MC for Calabrian pine and lower for increasing MC for Oriental beech and Taurus cedar. The effect of MC on CS is the highest for Calabrian pine while it is the lowest for Taurus cedar

CONCLUSIONS

Compression properties of species tested in all anatomical direction can be predicted using sound velocity. The coefficient of correlations between E_{dyn} and Young's modulus; E_{dyn} and CS are significantly high. The ratios of E_{dyn}, Young Modulus and CS in principal anatomic directions are

similar to those reported in the literature. The effect of MC on SV is more pronounced than density of the samples. The differences between the parallel and perpendicular to the grain values for the species tested seem to be influenced by the MC and anatomical structure. In general, the ratio between main directions is increasing with increasing MC. The Young's modulus in principal directions significantly different among the species tested. Sessile oak showed the minimum anisotropy while oriental beech showed the maximum. The effect of MC on strength is more noticeable than elasticity for the species tested. Compression properties of Calabrian pine seemed to be more sensitive than other species tested.

ACKNOWLEDGMENTS

The data presented here is a part of results obtained through projects sponsored by SDU BAP 3670-D2-2013, TUBITAK 2214/A and TUBITAK 2219 programs.

References

Aydın, S.; Yardımcı, M.Y. ; Ramyar, K. 2007. Mechanical properties of four timber species commonly used in Turkey, Turkish Journal of Eng. Env. Sci. (31), 19-27.

Baradit, E.; Niemz P. 2012. Elastic constants of some native Chilean wood species using ultrasound techniques, Wood Research 57(3), 497-504.

Beall, F.C. 2002. Overview of the use of ultrasonic technologies in research on wood properties, Wood Science and Technology 36(3):197-212. DOI 10.1007/s00226-002-0138-4

Bodig, J.; Jayne, B.A. 1993. Mechanics of wood and wood composites, Malabar, USA: Krieger Publishing Company.

Booker, R.E.; Froneberg, J.; Collins, F. 1996. Variation of sound velocity and dynamic Young's modulus with moisture content in the three principal directions, Proceedings, 10th Symposium Nondestructive Testing of Wood, Lausanne, Switzerland, pp. 279-295.

Brashaw, B.K.; Bucur, V.; Divos, F.; Gonçalves, R.; Lu, J.; Meder, R. 2009. Nondestructive testing and evaluation of wood: A worldwide research update, Forest Products Journal 59(3), 7-14.

Bucur, V. 2006. Acoustics of wood, Springer Verlag, Berlin.

Dündar, T.;Divos, F. 2014. European wood NDT&NDE research and practical applications, Eurasian Journal of Forest Science 1(1), 35-43.

Esteban, L.G.; Fernandez, F.G.; de Palacios, P. 2009. MOE prediction in Abies pinsapo Boiss. timber: Application of an artificial neural network using non-destructive testing, Comput Struct 87, 1360-1365.

Gao, S.; Wang, X.; Wan, L.; Allison, R.B. 2011. Modeling temperature and moisture state effects on acoustic velocity in wood. In: Proceedings, 17th Symposium Nondestructive Testing of Wood, Vol. 2. Sopron, Hungary, pp.411-418.

Gerhards, C.C. 1982a. Effect of moisture content and temperature on the mechanical properties of wood: An analysis of immediate effects, Wood and Fiber Science 14(1), 4-36.

Gerhards, C.C. 1982b. Longitudinal stress waves for lumber stress grading: factors affecting applications: state of the art, Forest Products Journal 32: 20-25.

Hering, S.; Keunecke, D.; Niemz, P. 2012a. Moisture-dependent orthotropic elasticity of beech wood, Wood Sci. Technology 45, 927-938.

Hering, S.; Saft, S.; Resch, E.; Niemz, P.; Kaliske, M. 2012b. Characterization of moisture-dependent plasticity of beech wood and its application to a multi-surface plasticity model, Holzforschung 66, 373-380.

Ilic, J. 2003. Dynamic MOE of 55 species using small wood beams, Holz als-Roh Werkstoff 61(3), 167-172.

Keunecke, D.; Hering, S.; Niemz, P. 2008. Three-dimensional elastic behavior of common yew and Norway spruce, Wood Science Technology 42, 633-647.

Keunecke, D.; Merz, T.; Sonderegger, W.; Schnider, T.; Niemz, P. 2011. Stiffness moduli of various softwood and hardwood species determined with ultrasound, Wood Material Science and Engineering 6, 91-94.

Krauss, A.; Kúdela, J. 2011. Ultrasonic wave propagation and Young´s modulus of elasticity along the grain of Scots pine wood (Pinus Sylvestris L.) varying with distance from the pith, Wood Research 56(4), 479-488.

Kretschmann, D.E.; Green, D.W. 1996. Modeling moisture content-mechanical property relationships for clear Southern Pine,'' Wood and Fiber Science 28(3), 320-337.

McBurney, R.S.; Drow, J.T. 1962. The elastic properties of wood: Young's moduli and Poisson's ratios of Douglas-fir and their relations to moisture content, USDA Forest Products Laboratory, Report No. 1528-D, Madison.

Oliveira, F.G.R.; Campos, J.A.O.; Sales, A. 2002. Ultrasonic measurements in Brazilian hardwood, Materials Research 5(1), 51-55.

Oliveria, F.G.R.; Candian, M.; Lucchette, F.F.; Salgon, J.L.; Sales, A. 2005. Moisture content effect on ultrasonic velocity in Goupia Glabra, Materials Research 8(1),11-14.

Oliveira, F.G.R.; Sales, A. 2006. Relationship between density and ultrasonic velocity in Brazilian tropical woods,'' Bioresource Technology 97, 2443-2446.

Ozyhar, T.; Hering, S.; Niemz, P. 2013. Moisture-dependent orthotropic tension compression asymmetry of wood, Holzforschung 67(4), 395-404.

Ross, R.J.(Ed.). 2010. Wood Handbook: Wood as an Engineering Material, General Technical Report FPL-GTR 190, USDA Forest Products Laboratory, Madison.

Ross, R.J.; Pellerin, R.F. 1994. Nondestructive testing for assessing wood members in structures: Areview, USDA Forest Products Laboratory, Madison, Technical Report 70, pp. 42.

Teles, F.T.; Del Menezzi, C.S.; de Souza, F.; de Souza, M.R. 2011. Nondestructive evaluation of a tropical hardwood: Interrelationship between methods and physical-acoustical variables, Ciência da Madeira 02(01), 01-14.

Wang, X.; Divos, F.; Pilon, C.; Brashaw, B.K.; Ross, R.J.; Pellerin, R.F. 2004. Assessment of decay in standing timber using stress wave timing nondestructive evaluation tools, USDA Forest Products Laboratory, Technical Report: 147. Madison, WI, pp. 14.

Monitoring of wood Degradation caused by Fungi using ultrasonic tomography with Brazilian technology

Alex J. Trinca
PhD, Visiting Professor, Laboratory of Nondestructive Testing - LabEND, College of Agricultural Engineering - FEAGRI - University of Campinas - UNICAMP, Brazil – E-mail: alexjuliotrinca@gmail.com

Stella S.S.A. Palma
Master student, Laboratory of Nondestructive Testing – LabEND, College of Agricultural Engineering - FEAGRI - University of Campinas - UNICAMP, Brazil – E-mail:ssapalma@gmail.com

Raquel Gonçalves
Professor, Coordinator of the Laboratory of Nondestructive Testing – LabEND, College of Agricultural Engineering - FEAGRI - University of Campinas - UNICAMP, Brazil – E-mail: Raquel@agr.unicamp.br

Abstract

In wood, the decay generated by the action of fungi is one of the most recurring defects causing degradation and making its detection extremely important. The objective of this study was to evaluate the viability to detect the evolution of degradation of wood causing by action of fungi using ultrasonic tomography (equipment and software) performed in Brazil. To achieve this goal we used five *Pinus sp*. discs inoculated with the fungi from the specie *Lentinula edodes* which acted on the material for 11 months. During the period we measured the weight change, performed ultrasound tests on the discs and generated the corresponding images. The technology was able to detect and track the degradation of wood and the detection was consistent with the weight loss of the discs.

Keywords: Ultrasonic tomography, action of fungi, degradation of wood.

Introduction

The construction of images from the internal structure of trees is possible using wave propagation parameters, producing ultrasonic tomography, which may be based on propagation delay time, amplitude or frequency response (Bucur 2005).

The fungi are considered the most effective microorganisms in the biodegradation of wood (Rowell, 2005). Its action is caused by the consumption of the cellulose and hemicellulose of the cell walls while the lignin is maintained, making the wood less resistant and propitious to rupture. They may also generate cavities inside the trunk, making the timber less resistant in bending (Piccinin, 2000). For inspection matters, this degradation is usually divided into incipient, intermediate and advanced. In the advanced stage, the cellular structure of the wood is destroyed by hydrolase and oxidase enzymes (Arantes and Miracles 2009).

Deflorio et al (2007) inoculated artificially 6 types of fungi in trunks from four wood species (Douglas fir, Beech , Oak and Sycamore) and analyzed the images produced by acoustic tomography (stress waves) of the logs after 2, 6, 16 and 27 months after inoculation. The trees were 40 to 70 years old and had

diameters ranging from 414-498 mm. To determine the final weight loss (after 28 months after inoculation), the authors used a healthy tree disc from each species as reference. Even considering the large diameter and the old age of the trees, the authors have obtained high weight losses (up to 54.6 %) for some types of fungi. Tomographic images only showed deterioration for the Sycamore specie (with lowest density) and the beginning of the deterioration was visible on the images starting at 2 months of inoculation.

The pine specie has low resistance to degradation by decay fungi (Ziglio, 2010) and high susceptibility to be attacked by xylophagous organisms. For this reason it is widely used in trials aiming the deterioration analysis.

Acoustic methods are used successfully in tree assessments, complementing the visual inspections. Its use is possible because the wave propagation is affected by the presence of materials with different acoustic impedance characteristics, such as, defects or irregularities of different patterns (grain deviation, resin bags, etc.) and anomalies caused by biological attacks by insects and fungi (Bucur et al. , 2006) . When the propagation is affected there is variation in wave velocity and amplitude of the signal emitted, which can be detected by equipment and studied for the development of a behavioral profile. Technological advances in techniques and equipment allow improvements in inspection reports (Oliveira, 2001).

The fungus *Lentinula edodes* (shitake), used in this research, belongs to the class of *Basidiomycetes*, classified as white rot. Its action occurs by the deterioration without any discrimination between polysaccharides and lignin. During the attack, the wood usually has whitish appearance. The attack of this fungus causes gradual erosion of the cell wall, but also the lignin (Rowell 2005). Although lignin resist the attack of most microorganisms, white rot fungi are capable of degrading lignin efficiently (Wong 2009). The main conditions for the development of fungi in wood pieces are wood moisture content above 20%, low-light environment, temperature ranging between 25 and 30 ° and oxygen availability (Gonzaga, 2006).

This research aimed to evaluate the performance of ultrasonic tomography using Brazilian technology (equipment and software), in monitoring the evolution of the wood degradation by fungi attack.

Methodology

To follow up the evolution of fungi degradation on wood we used 5 *Pinus elliottii* discs. The diameters of the discs had around 300 mm and 440 $kg.m^{-3}$ average density (12% moisture content). The disks were freshly cut (saturated condition) and free of contamination, fundamental condition for fungi development. For the inoculation we used 30 strains of *Lentinula edodes* fungus (shiitake).

Initially we cleaned the surface of the disk to receive the fungi, following we drilled a hole to insert the strains and finally we covered the strains with the waste from drilling (Figure 1). After this preparation the disks were placed in wet room with low light and humidity control and temperature

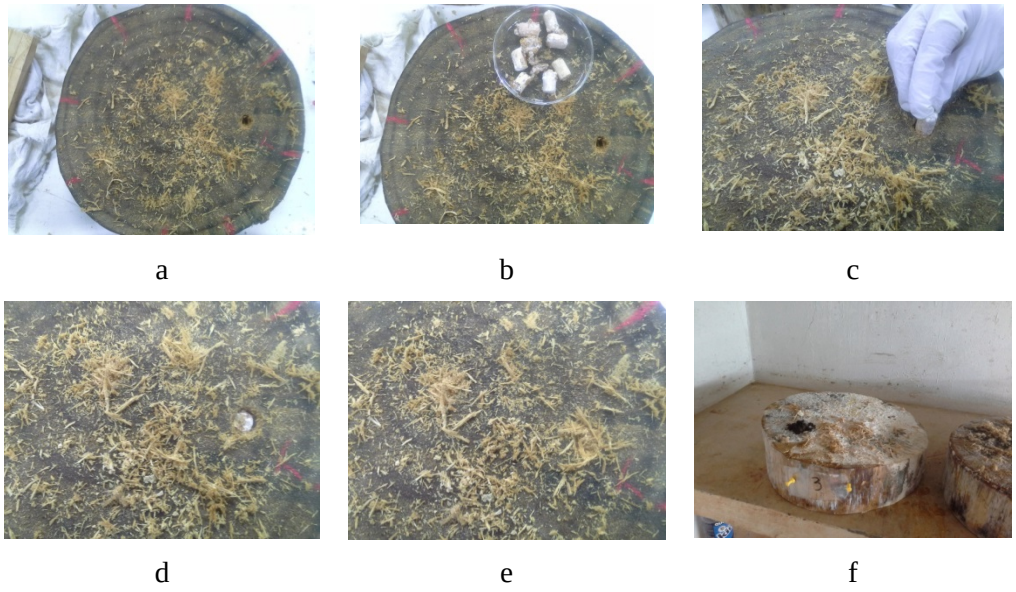

Figure 1. *Lentinula edodes* fungus inoculation process in *Pinus elliottii* discs.

The first ultrasonic measuring of each disk was performed before the inoculation. The second measurement of the discs was performed 3 months after inoculation and other four measurements every 2 months, a total of 11 months of measurements. Measurements were performed with ultrasound equipment developed in the research group in partnership with spin-off company (USLab , Agricef , Brazil) and 45 kHz dry points transducers. In addition to ultrasound measurements, we also monitored the loss of mass of the discs measuring its weight.

Ultrasound measurements on the discs (Figure 2) were performed using diffraction mesh (Figure 3), already used by several researchers (Divos , 2002 and Secco , 2011). For these measurements the transmitter transducer is positioned on one point of the mesh while the receiver transducer is placed in the other points, so that the wave propagation occurs under different routes (Figure 2).

Figure 2: Example of ultrasonic tomography in a disc.

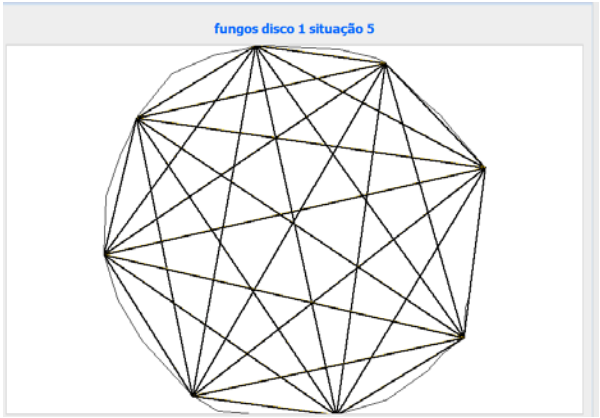

Figure 3. Wave propagation routes in diffraction mesh

The measurement results in diffraction mesh were used in a software also developed by the research group (*ImageWood 2.0*). With this software we generated the ultrasonic tomography images.

In each disc we used two velocities ranges (colors). The lower velocity obtained in each disc before the fungi inoculation was always set as the minimum velocity of the disk in the subsequent measurements (after inoculation). This reasoning has been done in order to take into account the disk areas that, since the initial situation, had lower velocities due to some internal uniqueness.

Results

Although we adopted the more visually similar disks, the initial condition of each one was not exactly the same. This differences on initial condition was reflected in the initial ranges of velocity obtained before inoculation, and also in the advancement of degradation over time.

The Images generated by *ImageWood 2.0* over time showed evolution of the zones with velocities lower than the minimum obtained in the initial condition (yellow areas) - Example in Figure 4. According to the methodology used to generate the images, zones with velocities below the minimum obtained in the initial condition represent the degraded areas of the disk.

In neither disk the images indicated degradation in the first 3 months after inoculation. Except for one of the disks in which the images indicated the presence of damaged areas only after 11 months of inoculation, the others showed significant deterioration after 7 months.

The results of images after 11 months of inoculation showed degraded areas filling almost all area of the disks. These images correspond to actual condition of the discs, because they all had soft the internal structure and no resistance. The results of images also corresponded, approximately, to the weight losses of the disks (Figure 5).

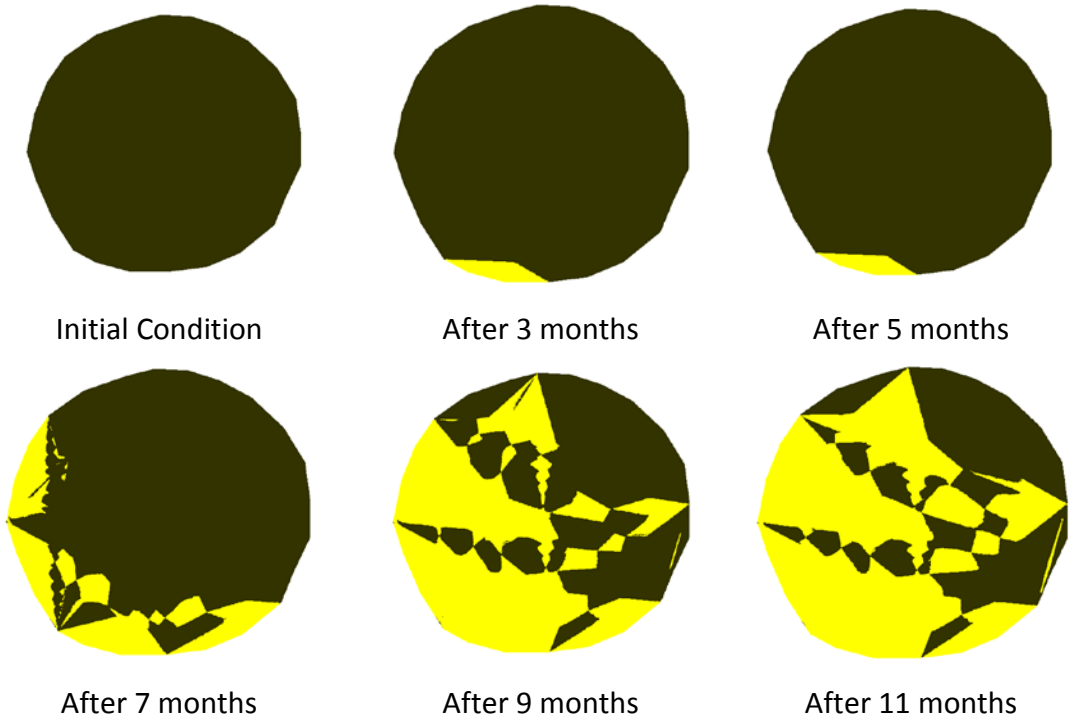

Figure 4. Example of images generated by Wood Image 2.0 software during the development of fungi on the disk 2. The yellow areas indicate limited speed ranges the minimum speed obtained at the initial condition.

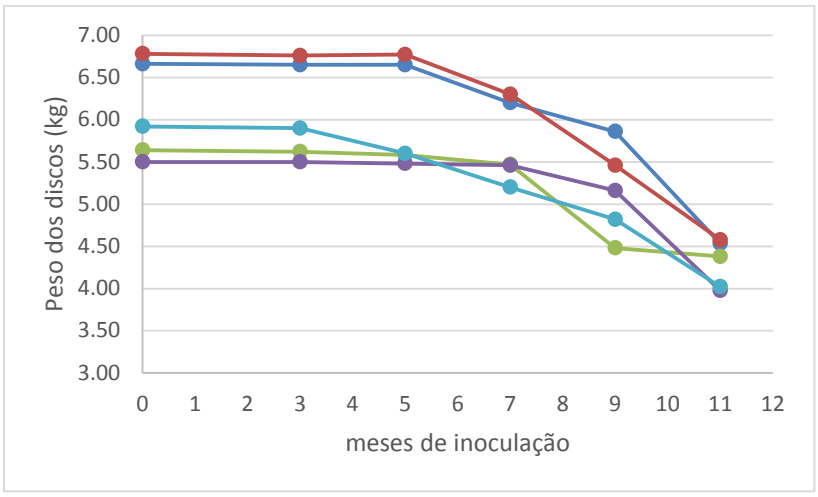

Figure 5. Behavior of the variation in weight of the disks during the analysis period of degradation

CONCLUSION

Tomographic images produced with the equipment and software developed in Brazil described adequately the evolution of fungi degradation of the discs and the results was compatible with the mass loss of the disks and the visual analysis.

ACKNOWLEDGEMENTS

The authors thank the São Paulo Research Foundation (FAPESP – Proc. n.2012/22599-9; Proc. 2011/08286-5 e Proc. 2015/05692-3) for the support. We also thank the Sguario Forest Company S/A for the material (logs of Pinus elliottii) and Fungi and Flora Company for the fungal strains.

REFERENCES

BUCUR, V. (2005). Ultrasonic techniques for nondestructive testing of standing trees. Ultrasonics, 43:237-239.

DEFLORIO, G; FINK, S; SCHWARZE, F.W.M.R.; Detection of incipient decay in tree stems with sonic tomography after wounding and fungal inoculation. Wood Sci Technol, 2007. 42:117-132.

DIVOS, F.; SZALAI, L. 2002. Tree evaluation by acoustic tomography. In: Proceedings of the 13th International symposium on nondestructive testing of wood; 2002 August 19. 21; Berkeley, CA. Madison, WI: Forest Products Society: 251.256. 2002.

GONZAGA, A.L; Madeira: uso e conservação. Brasília/DF: IPHAN/MONUMENTA 2006. 248p.

OLIVEIRA, F.G.R. Estudo de propriedades mecânicas de dicotiledôneas por meio de ensaios não destrutivos utilizando equipamento de ultra-som. São Carlos: USP, 2001. 55f. Tese (Mestrado em Ciência e Engenharia de Materiais). Universidade de São Paulo, 2001.

PICCININ, E.; Cultivo do cogumelo Shiitake (Lentinula edodes) em toras de eucalipto: Teoria e Prática, 48p, Série Produtor Rural, edição especial, Piracicaba (SP), 2000.

ROEWLL, R. M.; Handbook of Wood Chemistry and Wood Composites, 1st ed., CRC Press: Madison, 2005.

SECCO, C.B. Detecção de ocos em toras utilizando métodos de propagação de ondas. ultrassonicas.112p. Tese (Mestrado em Engenharia Agrícola), Na área de concentração de Construções Rurais, Faculdade de Engenharia Agrícola, Universidade Estadual de Campinas, Campinas (SP), 2011.

WANG, X.; CARTER, P.; ROSS, R.J.; BRASHAW. Acoustic assessment of wood quality of raw forest materials – a path to increased profitability. Forest Products Journal, Madison, v.57, n.5, p.6-14, 2007.

WONG, D.W. (2009). Structure and action mechanism of ligninolytic enzymes. Applied Microbiology and Biotechnology, v.157 (2), pp.174-209

ZIGLIO, A.C. Uso da capsaicina como preservante de madeiras ao ataque do fungo apodrecedor. Dissertação (Mestrado – Programa de Pós-Graduação Interunidades em Ciência e Engenharia de Materiais. Área de Concentração: Desenvolvimento, Caracterização e Aplicação de Materiais) – Escola de Engenharia de São Carlos, Instituto de Física de São Carlos, Instituto de Química de São Carlos da Universidade de São Paulo. edição revisada - São Carlos, 2010. 80p.

African mahogany wood defects detected by ultrasound waves

Tamara Suely Filgueira Amorim França
Department of Sustainable Bioproducts, Mississippi State University, Starkville, Mississippi, United States, tsf97@msstate.edu

Frederico Jose Nistal França
Department of Sustainable Bioproducts, Mississippi State University, Starkville, Mississippi, United States, fn90@msstate.edu

Robert John Ross
U.S. Forest Service, Forest Product Laboratory, Madison, Wisconsin, USA, rjross@fs.fed.us

Xiping Wang
U.S. Forest Service, Forest Product Laboratory, Madison, Wisconsin, USA, xwang@fs.fed.us

Marina Donaria Chaves Arantes
Departamento de Ciências Florestais e da Madeira, Universidade Federal do Espírito Santo, Jerônimo Monteira, Espírito Santo, Brasil, marina.arantes@ufes.br

Roy Daniel Seale
Department of Sustainable Bioproducts, Mississippi State University, Starkville, Mississippi, United States, rds9@msstate.edu

Abstract

This study aims to investigate the potential of ultrasound wave to detect defects in 19 years old of two species of African mahogany planted in Brazil. Were used five 76 x 5 x 5 cm samples from each species with different types of defects, and were conditioned to 12% moisture content. The samples were scanned with ultrasound wave in longitudinal direction and every 2,54 cm in radial and tangential directions along the samples. It was possible to identify end split and pin knots in *Khaya ivorensis* and reaction wood in *Khaya senegalensis* wood. Beetle galleries did not affect wave velocities in *Khaya senegalensis* wood. Grain angle had a large effect in ultrasound velocities in radial and tangential directions. *Khaya senegalensis* exhibit lower longitudinal velocities related to larger amount of interlocked grain in this species. The ultrasound waves can be useful in lumber classification process in wood industry.

Keywords: *Khaya ivorensis*. *Khaya senegalensis*. Nondestructive test

Introduction

African mahogany has been an important multipurpose species in its natural range in Africa. It is valued for a range of non-timber traditional use products. *Khaya* is a genus of seven species of trees in the family Meliaceae, native from this continent and called African mahogany, the only timber widely accepted as mahogany besides the South American mahogany from genus *Swietenia* (Arnold, 2004; Robertson and Reilly, 2012).

The use of ultrasonic wave propagation as a nondestructive testing method has proved to be a viable method to characterizing wood. Research on ultrasound method has evidence the efficacy of the method to determine the mechanical properties of wood. The method was tested and significant correlations were found between nondestructive and destructive results (Karlinasari, 2006).

Detection of defects in wood by nondestructive ultrasonic methods have been investigated by many researchers with a variety of ultrasonic parameters (McDonald, 1980; Patton-Mallory and Degroot, 1990; Ross et al., 1992) showing that ultrasound method can detect defects in wood, like knots, interlocked grain, bark pockets, insect holes, splits, decay, and reaction wood.

Based on studies that showed the effects of defects change ultrasonic signal propagation in wood, this study aims to scan African mahogany (*Khaya ivorensis* and *Khaya senegalensis*) wood samples searching for variations in wood (sapwood/heartwood, grain angle, knots, and end checks reaction wood) using ultrasound waves.

Material and Methods

The species studied were two 19-year-old African mahogany species (*Khaya ivorensis* and *Khaya senegalensis*) from Vale Nature Reserve located in Sooretama, ES, Brazil. Five trees from each species were cut and sawed into boards. After air dry (9 month), 5x5x76 cm static bending test specimens (ASTM D143, 2005) were cut and conditioned into 12% moisture content. Six samples of *Khaya ivorensis* and seven samples of *Khaya senegalensis* showed different characteristics and defects were selected for this study.

Nondestructive testing was conducted by ultrasonic wave velocity measurements. The wave propagation was measured by Sylvatest Duo® (f=22kHz) ultrasonic device. The equipment consists in two accelerometer transducers located in opposite sides of the material that was being evaluated. The wave flows through the wood from one transducer (transmitter) to other one (receiver) and the time in microseconds is recorded by the equipment.

Twenty-eight readings of propagation times were taken at intervals of 2.54 cm along the specimen in radial and tangential directions and two readings in longitudinal direction were collected while the velocities of wave propagation in all three directions were calculated.

Results and Discussion

Average velocities and coefficient of variation for longitudinal, radial, and tangential directions, specific gravity and wood characteristics of the two species of African mahogany specimens are shown in Table 1.

Table 1. Average of wave velocities, specific gravity, and wood characteristics of *Khaya ivorensis* and *Khaya senegalensis* samples

SPECIES	SAMPLE	VELOCITY (m/s)			S.G. ($Kg.m^{-3}$)	Characteristics
		Longitudinal	Radial	Tangential		
Khaya ivorensis	1	5135	1795 (12.82)	1804 (3.43)	566	45° + end check
	2	4903	2138 (5.73)	1459 (4.41)	510	No defects
	3	4967	2093 (3.06)	1783 (10.13)	557	Pin knots
	4	4935	2351 (1.96)	1731 (3.09)	486	Pin knots

	5	5170	2381 (2.29)	1539 (3.98)	541	Sapwood + heartwood
	6	4779	2355 (3.29)	1542 (2.75)	566	Sapwood
	Average	4981 (2.95)	2185 (4.86)	1643 (4.63)	538 (6.13)	
Khaya senegalensis	1	4294	2396 (3.93)	2009 (3.53)	567	Sapwood + heartwood
	2	4343	2221 (3.25)	1955 (5.18)	783	Heartwood
	3	4471	2039 (2.93)	1592 (2.60)	709	Sapwood
	4	4903	2270 (9.79)	1680 (8.69)	795	Reaction wood+ beetle galleries
	5	5170	1686 (8.29)	1558 (4.57)	758	45° + reaction wood beetle galleries
	6	4393	2576 (2.72)	1965 (2.59)	737	No defects
	7	4841	2468 (3.47)	1931 (3.51)	707	No defects
	Average	4631 (7.31)	2237 (4.91)	1813 (4.38)	723 (10.57)	

** Parentheses: coefficient of variance (%).

For *Khaya ivorensis* wood samples, the average longitudinal velocities ranged from 4780 to 5170 m/s. Radial velocities ranged from 1724 to 2630 m/s and in tangential direction from 1087 to 1923 m/s. In *Khaya senegalensis* wood specimens, the longitudinal velocities ranged from 4294 to 5171 m/s. In radial direction velocities ranged from 1515 to 2940 m/s. Tangential velocities ranged from 1390 to 2380 m/s. Higher specific gravity were found in *Khaya senegalensis* wood, ranging from 567 to 795 kgm^{-3}. In *Khaya ivorensis* it ranged from 486 to 566 kgm^{-3}.

K. ivorensis sample no. 1 with a 45° grain orientation showed high tangential and reduced radial velocities (Fig. 1-a). A tangential end check was easily detected by the ultrasound techniques (higher coefficient of variation in radial velocities). Sample no. 2 with no defects showed radial velocity 47% higher than tangential velocity (Fig. 1-b). Pin knots changed tangential velocities in sample no. 3 (Fig. 1-c), but were not detected in sample no. 4 (Fig. 1-d) because there were reduced amount of defects. Sample no. 5 (Fig. 1-e) made with sapwood and heartwood had greater longitudinal velocity if compared with sapwood sample no. 6 (Fig 1-f).

K. senegalensis sample no. 1 (Fig 2-a) made with sapwood had greater longitudinal velocity if compared with sapwood/heartwood sample no. 2 (Fig. 2-b) and heartwood sample no. 3 (Fig. 2-c). Reaction wood in sample no. 4 (Fig. 2-d) and no. 5 (Fig. 2-e) increased in longitudinal velocities. Beetle galleries in the same samples did not affect radial and tangential ultrasound velocities. Sample no. 6 (Fig. 2-f) showed low longitudinal velocity (interlocked grain). No defects in sample no. 7 (Fig. 2-g) showed radial velocity 28% higher than tangential velocities. Samples with 45° grain had low difference between radial and tangential velocities.

The velocities in sapwood, heartwood, reaction wood, grain angle, pin knots, and beetle galleries on ultrasound velocities for *Khaya ivorensis* wood are shown in Figure 2 and *Khaya senegalensis* wood are shown in Figure 3.

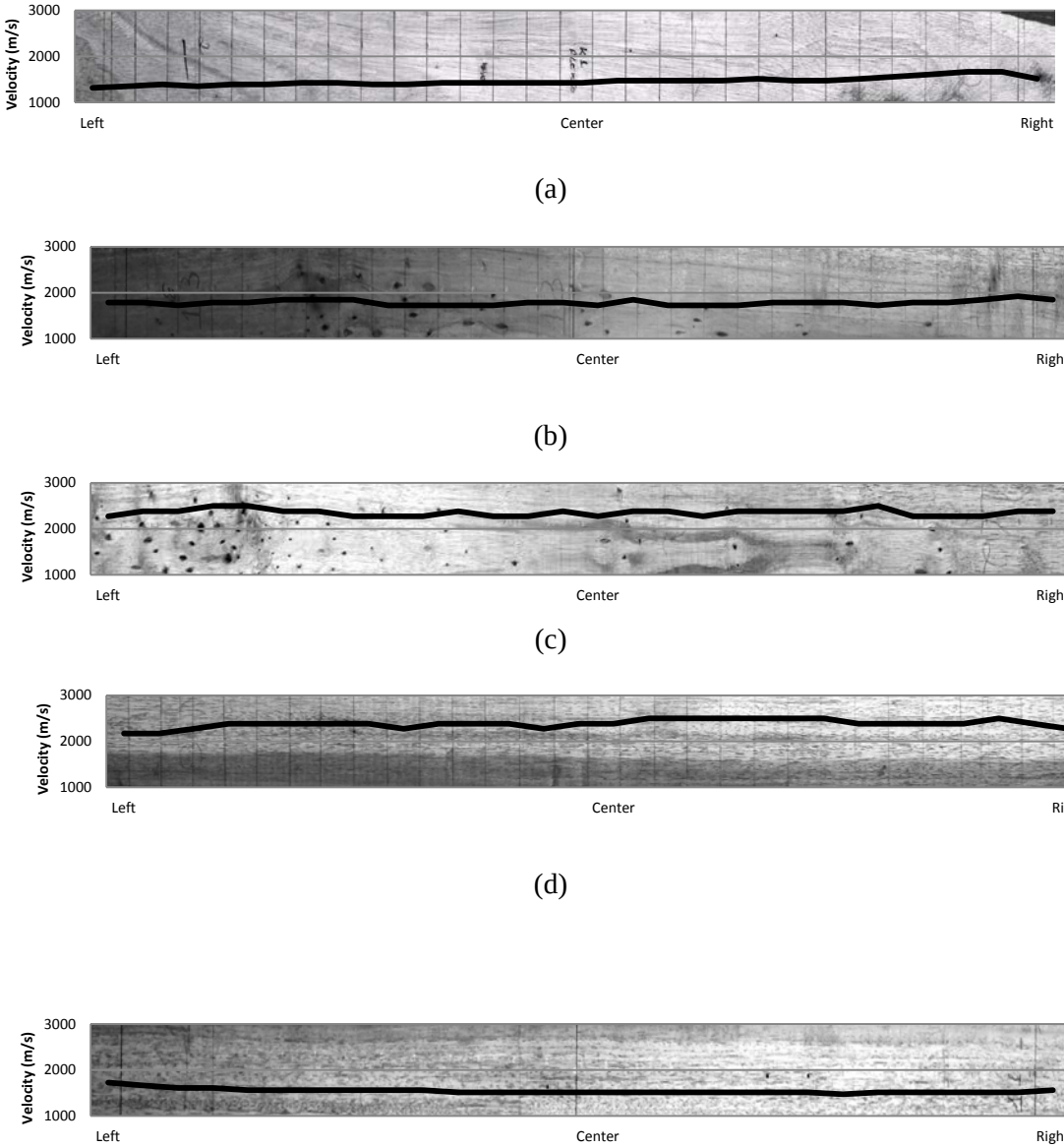

Figure 2. Ultrasonic measurements in *Khaya ivorensis* wood specimen: a) 45° grain + end check; b) no defects; c and, d) pin knots; e) sapwood/heartwood; f) sapwood

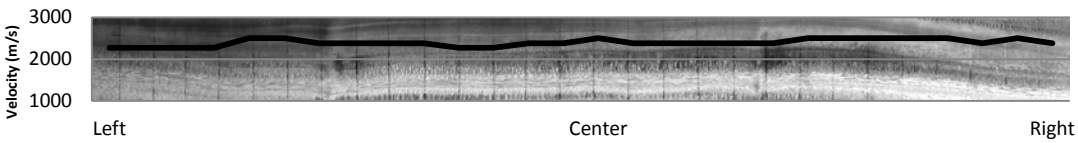

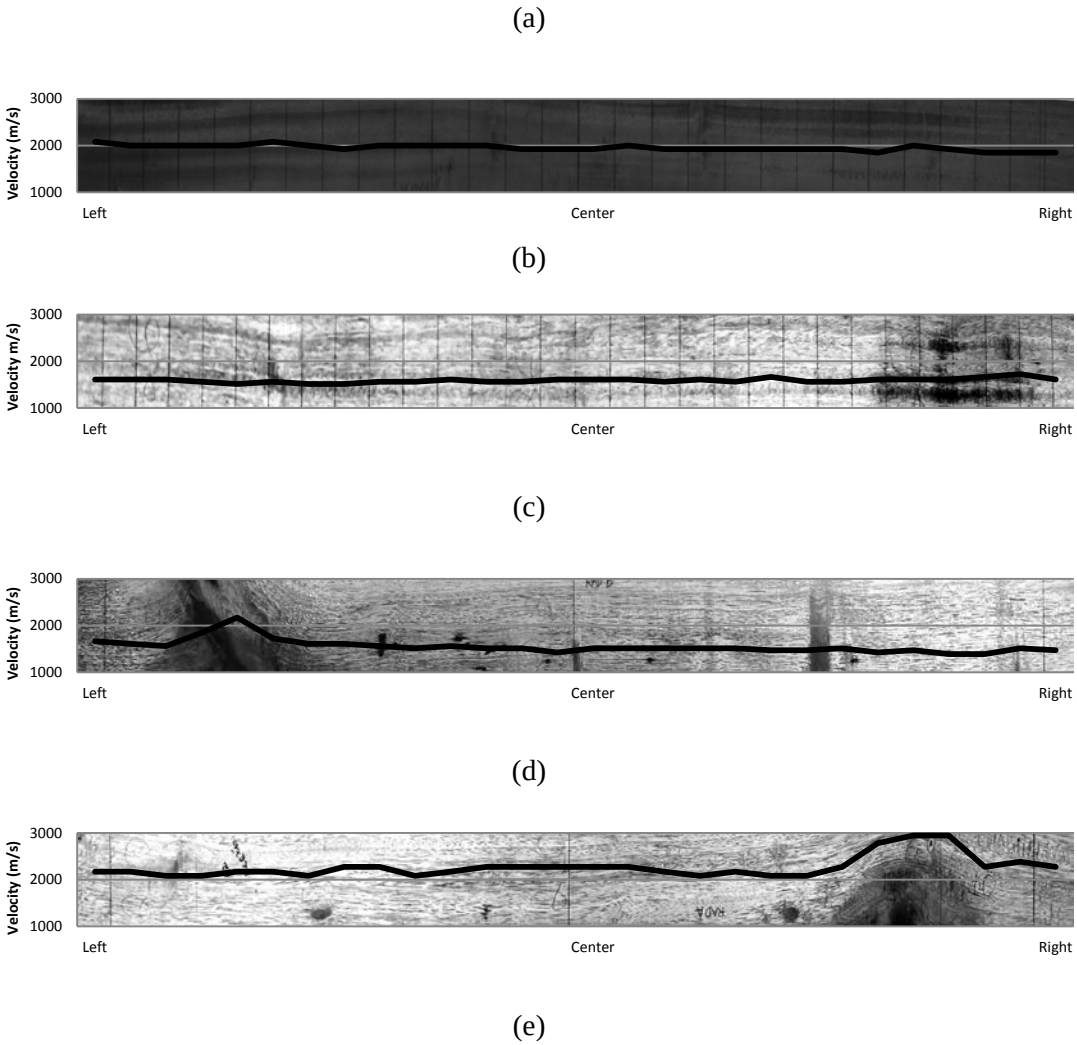

Figure 3. Ultrasonic measurements in *Khaya senegalensis* wood specimen: a) sapwood/heartwood; b) heartwood; c) sapwood; d) reaction wood and beetle galleries; e) 45° grain + reaction wood; f and g) no defects.

Longitudinal velocities in *K. senegalensis* wood were lower if compared to *K. ivorensis*. Interlocked grain present in *K. senegalensis* wood is the reason for reduced velocities. No correlations were found between specific gravity and longitudinal velocities for *Khaya ivorensis* (r^2=0.02) and a low correlation were found for *Khaya senegalensis* (r^2=0.20). Oliveira and Sales (2005) reported that the ultrasonic velocity tends to increase with increasing wood density. Vun et al. (2002) studying ultrasonic transmission systems for measuring OSB properties as panel density, flake alignment level, and layering structures reported high correlation between wave transmission velocity and density.

Higher longitudinal velocities were found in sapwood/heartwood in *Khaya ivorensis* and in sapwood for *Khaya senegalensis*. This may occur because adult wood has better wood properties in the sapwood/heartwood transition areas. Sapwood may be heavier than heartwood at the time of cutting the tree due to higher moisture content. However, the basic density may be less than that of heartwood because of the absence of materials that may have been infiltrated into heartwood (Panshin and De Zeeuw, 1980; Wellwood and Jurazs, 1968).

A large end split and pin knots in *Kaya ivorensis* were detected by the increasing the ultrasound time of flight. Fuller et al., (1995) concluded that defect, such as a knot, checks, and honeycomb, in a small increase in transit time tended to result in a localized increase in transit time. Sound transmission time perpendicular to the grain was significantly increased by the presence of honeycomb and surface checks in red oak lumber.

Reaction wood in *Khaya senegalensis* increased the ultrasound velocities in all three directions. The higher group velocity values in tension wood could be related to the longer fibers and to the existence of the G-layer. Bucur and Feeney (1991) reported higher sound velocity values in beech tension wood. In reaction wood and normal wood of two species, wave velocity variations were greater in the longitudinal direction than in the transverse direction.

Nondestructive tests such as those involving ultrasound have been developed to detect reaction wood (Bucur, 2003). Ultrasonic waves are affected by the anatomical structure of wood. Thus the main descriptors of ultrasonic waves (velocity, rate of energy flow, and attenuation) change during propagation. As the anatomical structure of reaction wood differs from that of normal wood, some differences may be observed in the wave descriptors (Saadat-Nia et al., 2011). The main problem associated with the quality and use of wood and timber containing reaction tissue is that their shrinkage characteristics differ from those of adjacent normal wood (Barnett and Jeronimidis, 2003).

Conclusion

Adult wood had greater velocities if compared to juvenile wood. It was possible to detect an end crack and pin knots in *Khaya ivorensis* wood and reaction wood in *Khaya senegalensis*. However, it was not possible to detect beetle galleries in *Khaya senegalensis* wood. Grain angle had a large effect in ultrasound velocities in radial and tangential directions for both species.

Acknowledgments

The authors would like to thank the USDA Forest Product Laboratory (USA), Fundação de Amparo à Pesquisa e Inovação do Espírito Santo (Brazil), VALE S.A. (Brazil), and Universidade Federal do Espírito Santo (Brazil).

References

American Society For Testing And Materials. 2006. *ASTM D – 143*: Standard methods of testing small clear specimens timber. Annual Book of ASTM Standards. v. 4.10, West Conshohocken.

Arnold, R. *Khaya senegalensis* - current use from its natural range and its potential in Sri Lanka and elsewhere in Asia. In: *Prospect for high-value hardwood timber plantations in the 'dry' tropics of northern Australia.* 2004; Queensland.

Barnett, J.R.; Jeronimidis, G. 2003. *Wood Quality and Its Biological Basis*, Blackwell Scientific Publisher, Oxford.

Bucur, V, Feeney, F. 1991. Attenuation of ultrasound in solid wood. *Ultrasonics*. 2:76–81.

Bucur, V. 2003. Nondestructive Characterization and Imaging of Wood, *Springer Series in Wood Science.*

Fuller, J.J.; Ross, R.J.; Dramm J.R. 1995. Non destructive evaluation of Honeycomb and surface check in Red Oak lumber. *Forest Products Journal,* 45(5):42-44.

Karlinasari, L. 2006.*Study on wood bending strength evaluation based on nondestructive testing ultrasonic method.* Department of Forest Products Faculty of Forestry, Bogor Agricultural University Indonesia.

McDonald, K.A. 1980. Lumber defect detection by ultrasonics. *Research Paper FPL*-311, USDA Forest Service, 20p.

Oliveira, F.G.R.; Sales, A. 2005. Efeito da densidade e do teor de umidade na velocidade ultrasônica da madeira. *Minerva,* 2(1):25-31.

Panshin, A.J.; De Zeeuw C. 1980. *Textbook of wood technology*. McGraw-Hill, New York; 722 pp.
Patton-Mallory, M.; Degroot, R.C. 1990. Detecting brown-rot decay in southern yellow pine by acousto-ultrasonics. Pages 29-44 In: *Proceedings of the 7th International Nondestructive Testing of Wood Symposium,* United State.

Robertson, B.; Reilly, D. 2012. *Growing African Mahogany in Northern Australia*. Northern Territory Government.

Ross, R. J.; Ward, J. C.; Tenwolde, A. 1992. Identifying bacterially infected oak by stress wave non-destructive evaluation. *Research Paper FPL*-512, USDA Forest Service.

Saadat-Nia, M. A.; Brancheriau, L.; Gallet P.; Enayati, A. A.; Pourtahmasi, K.; Honarvar, F. 2011. Ultrasonic wave parameter changes during propagation through poplar and spruce reaction wood, *Bioresource*, 6(2):1172-1185.

Vun, R. Y.; Wu, Q.; Bhardwaj, M. C.; Stead, G. 2003. Ultrasonic characterization of structural properties of oriented strandboard: a comparison of direct-contact and non-contact methods. *Wood and Fiber Science*, 35(3):381-386.

Wellwood, R. W.; Jurazs, P. E. 1968. Variation in sapwood thickness, specific gravity, and tracheid length in western Cedar. *Forest Product Journal,* 18(12):37-46.

Ultrasound Transmission Times in Biologically Deteriorated Wood

Adam Senalik, USDA Forest Service, Forest Products Laboratory, Madison, WI USA, christopherasenalik@fs.fed.us

Robert Ross, USDA Forest Service, Forest Products Laboratory, Madison, WI USA, rross@fs.fed.us

Rodney C. DeGroot, Research Plant Pathologist (Retired), USDA Forest Service, Forest Products Laboratory, Madison, WI USA

Abstract
The use of a variety of stress wave transmission techniques for the in-service condition assessment of deteriorated wood is well documented. This paper summarizes results from an extensive study designed to examine the relationship between ultrasound transmission times and the deterioration of exposed wood. Two hundred seventy (270) southern pine lumber specimens were evaluated nondestructively using a through transmission ultrasound technique after field exposure for periods of up to fifty seven (57) months. Ultrasound transmission times increased with exposure time. Several statistical models of the relationship between transmission time and length of exposure were developed and are presented.

Keywords
Ultrasound, stress wave transmission, deterioration model, weathering, exposure

Introduction

Wood is used extensively for both interior and exterior applications in the construction of a variety of structures (residential, agricultural, commercial, government, religious). The deterioration of an in-service wood member may result from a variety of causes during the life of a structure. It is important, therefore, to periodically assess the condition of wood used in structures to determine the extent of deterioration so that degraded members may be replaced or repaired to avoid structural failure. An assessment is especially critical for building officials in municipalities affected by catastrophic events.

Assessment of the condition of wood in a building can be conducted for a variety of reasons. Code compliance, historic preservation, or alternative uses of a structure are frequently cited reasons for conducting a condition assessment. A structural condition assessment consists of the following: 1) a systematic collection and analysis of data pertaining to the physical and mechanical properties of materials in use; 2) evaluation of the data collected; and 3) providing recommendations, based on evaluation of the collected data, regarding portions of an existing structure that affect its current or proposed use. Such an assessment relies upon an in-depth inspection of the wood members in the structure. A wide variety of techniques are used to assess the condition of wood in structures. Visual assessment, probing, resistance drilling, and stress

wave or ultra-sound-based techniques are all used either individually or in combination to evaluate the condition of in-service members (Ross and others 2006).

The use of a variety of stress wave transmission techniques for the in-service condition assessment of deteriorated wood is well documented, from the evaluation of historic artifacts (Dundar and Ross 2012) to timber bridges (Brashaw and others 2005a; Brashaw and others 2005b; Emerson and others 2002; Ross and others 1999), to historic structures and ships (Allison and others 2008; Clausen and others 2001; Ross and others 1998; Ross and Wang 2005; Wang and others 2008). Of particular note are the *Wood and Timber Condition Assessment Manual-Second Edition* (White and Ross 2014) and an extensive literature review on the use of ultrasound techniques for evaluating wood by Senalik and others (2014).

Pellerin and others (1985) were the first to report on a systematic examination of the effect of biological attack on the acoustic properties of clear wood. They used small, clear southern pine specimens in a laboratory study designed to examine the effect brown-rot decay fungi and termite attack have on acoustic velocity and static strength. Time-of-flight measurements, parallel to the fiber axis, were made using a pitch/catch system on specimens after various exposure times. They observed a considerable change in acoustic time-of-flight with exposure time. More importantly, they were able to conclude the following:

1. Changes in time-of-flight occurred well before measureable weight loss (density), and before strength loss, were observed.
2. Significant correlation was observed between residual strength and acoustic time-of-flight.
3. Because termite attack was preferential to the early wood sections of the specimens, time-of-flight measurements parallel to the fiber axis were not useful for monitoring changes in corresponding strength.

DeGroot and others (1994, 1995, 1998) reported on a follow-up study they performed to examine both energy storage and loss parameters for monitoring the deterioration of clear wood when exposed to natural populations of decay fungi and subterranean termites. They used a pulse echo test setup (Ross and others 1994) to measure speed of sound transmission and wave attenuation, parallel to the fiber axis, in small clear southern pine specimens in field exposure conditions and developed empirical models which used both parameters that were capable of predicting residual compressive strength with a high level of accuracy (Ross and others 1996, 1997). A similar relationship was reported by Ross and others (2001) for timbers removed from service.

The objective of this research was to examine the relationship between ultrasound transmission and wood deterioration. This paper presents a mathematical relationship between the changes in transmission times along the length of the wood board specimens and the months of weathering exposure time.

Materials and Methods

Clear, southern pine lumber specimens, nominal 5.1 cm (2 in.) by 10.2 cm (4 in.) by 243.8 cm (96 in.) in length, were used in this study. All specimens were obtained from southern pine sapwood lumber, Class C or better, obtained from a mill in Georgia. The species of trees from

which the wood was cut could not be identified but is assumed to be from a major southern pine species in the area. These species are longleaf pine (*Pinus palustris*), shortleaf pine, (*P. echinata*), loblolly pine (*P. taeda*), and slash pine (*P. elliottii*). Clear sapwood was used in this study to maximize the opportunity to establish relationships between ultrasound transmission and the deterioration of the wood. From a sample of 400 specimens, 270 were selected for inclusion in the study. After conditioning to approximately 10% moisture content, the modulus of elasticity (MOE) of each piece was nondestructively determined using stress wave techniques. The specimens were sorted into nine groups, 30 specimens per group, with each group having nearly identical MOE distributions (mean values and standard deviations).

One group of 30 specimens was randomly selected as the reference or control group. This group was retained in a controlled environment room until the conclusion of the field phase of the study. The remaining specimens were installed in a field plot on the Harrison Experimental Forest in April 1990. Note that the specimens were not in ground contact; they were placed horizontally on racks approximately 1 m above the ground. This forest is located in southern Mississippi, approximately 32 km from the Gulf of Mexico. Specimens were removed from the field after 2, 9, 14, 21, 26, 35, 45, and 57 months of exposure.

Upon removal from the field, each specimen was shipped to FPL and reconditioned in a controlled environment room. After conditioning, each specimen was tested nondestructively using the experimental setup shown in Figure 1. The setup consisted of two 84 kHz rolling transducers, coupled to an ultrasonic transmitting and receiving unit (Ross and DeGroot 1998). A stress wave was induced into the specimen through the width of the board by the transmitting transducer. The wave was then received by the opposing transducer. Stress wave transmission times were displayed by the unit and recorded on a personal computer. Transmission times were measured at increments along the length of the specimens at the locations illustrated in Figure 2. Note that measurements were made in 76 mm (3 in.) increments near the ends of the specimens and in 152 mm (6 in.) increments elsewhere along the length. Each specimen was tested several times; excellent agreement was observed between scans for individual specimens.

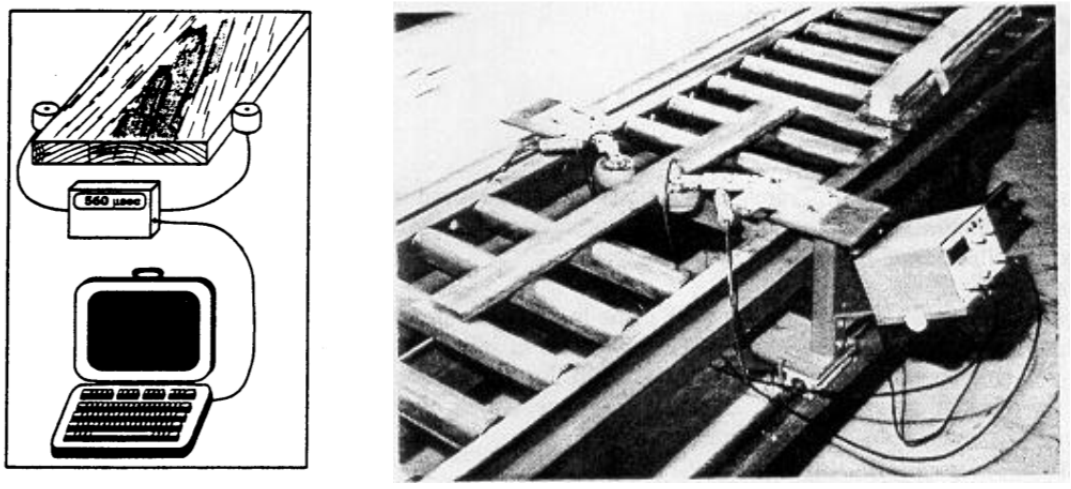

a. **b.**

Figure 1–Nondestructive experimental setup used to measure ultrasonic transmission times across the width of timber boards. **a.** experimental setup schematic, **b.** photograph of experimental setup

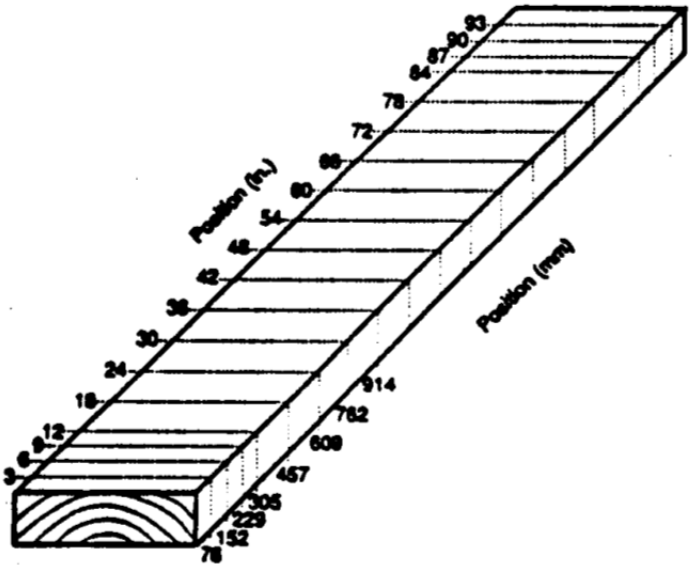

Figure 2–Transmission time measurement locations. Measurements were made in 76 mm (3 in.) increments near the ends of the specimens and in 152 mm (6 in.) increments elsewhere along the length.

Deterioration Model

Wood can be considered a cylindrically orthotropic, hygroscopic material. The three principle directions of wood are longitudinal, tangential, and radial. Wood draws water into itself from all directions; however, the rate at which it draws water longitudinally is much greater than the rate it draws water in either tangentially or radially. The presence of water is one of the four key ingredients for wood decay: wood, water, air, and acceptable temperatures. As a result of the higher rate of water absorption in the longitudinal direction, cut timber tends to decay more quickly at the ends that were cut normal to the longitudinal axis of the original tree.

It should be noted that the model presented was constructed using data collected from specimens including up to 45 months of exposure. The transit times recorded using specimens exposed for 57 months were several times higher than any other transit time and were excluded from the model.

At the time of the deterioration model construction, it was believed that the boards would have end regions of decay and then center portions that were largely sound. As a result, the transit times near the ends of the board should be high and transition to a lower value as the distance from the end increased. The form of equation chosen to model this behavior was a second order exponentially decaying function, shown in Equation (1).

$$T_s = (A_H - A_L)\exp\left[-\left(\frac{2l}{d_t}\right)^2\right] + A_L \qquad (1)$$

Where
T_s is the transit time in microseconds,
A_H is transit time near board end (NE),

A_L is the transit time along the center board (CB),
l is the distance to the nearest end of the board, and
d_t is the distance from the board end that the decay has intruded into the board.

Figure 3 shows predicted values versus the actual board transmission data. Near the end of the board, the transit time, T_s will have a high value of A_H. As the distance from the end of the board, l, increases, the transit time will decrease. At a distance, d_t, the transit time will be near to the low value, A_L. The transit time was recorded over several months at constant distances from the ends of the boards. The transit time at the same distance from both ends of the board were averaged to construct representative transit time transition curves for modelling. The high and low transit time values were extracted from the curves and each curve was fitted to a second order exponentially decaying function. Microsoft Excel Solver function was used to find a transition distance, d_t, that maximized the coefficient of determination, r^2, and minimized the root mean square error.

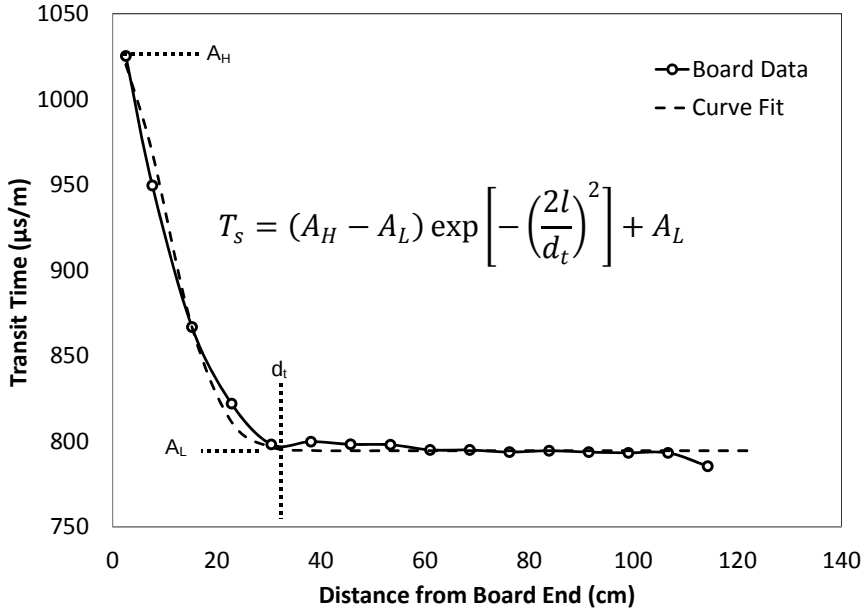

Figure 3–Average transit time as a function of distance from the end of the board for a specimen weathered for 21 months. Also shown is the curve fit of the data using a second order exponentially decaying function.

2

The general form of the mathematical relationships relating high and the low transit values to months of weathering are presented in Equations (2a) and (3a), respectively. The terms Δ_H and Δ_L are adjustments applied to the trends based upon precipitation within three months prior to testing, and are discussed later in this report. Simple linear regression (LR) was used to determine the values of the coefficients. The LR coefficients for the high values were constrained such that the constant term matched the constant term of the low value coefficients; the underlying assumption is that without weathering (0 months of exposure), the high and low transit values should be equal. The equations with the numerical coefficients are given for high ($r^2 = 0.9136$) and low ($r^2 = 0.8739$) are given in Equations (2b) and (3b), respectively. The r^2 values presented above include no adjustments for precipitation (Δ_H, $\Delta_L = 0$).

$$A_H = a_{H1}t + a_{H0} + \Delta_H \quad (2a)$$
$$A_H = 13.93t + 721.4 + \Delta_H \quad (2b)$$

$$A_L = a_{L1}t + a_{L0} + \Delta_L \quad (3a)$$
$$A_L = 4.497t + 721.4 + \Delta_L \quad (3b)$$

Where
t is the weathering time in months,
a_{H1} and a_{H0} are linear regression (LR) coefficients for the near board end (NE) 1st and 0th order terms,
Δ_H is the NE precipitation adjustment applied after the third month of weathering,
a_{L1} and a_{L0} are LR coefficients for the center board (CB) 1st and 0th order terms, and
Δ_L is the CB precipitation adjustment applied after the third month of weathering.

Simple linear regression (LR) was used to relate the natural logarithm of the transition distance ($r^2 = 0.8531$) to months of weathering. The general form of the equation is given in Equation (4a); the equation with numerical coefficients is given in Equation (4b). Precipitation occurring near the time of testing did not significantly influence the transition distance.

$$\ln d_t = a_{d1}t + a_{d0} \quad (4a)$$
$$\ln d_t = 0.036t + 2.494 \quad (4b)$$

Where a_{d1} and a_{d0} are LR coefficients for the transition distance 1st and 0th order terms.

The precipitation for the three months prior to specimen testing was found to influence the high and low transit values. Equations (5a) and (6a) are the general form of the relationships between the high and low adjustment values, respectively, and a weighted average precipitation for the three months prior to the removal of the specimen from the test environment. Equations (5b) and (6b) have the coefficient values shown. The method of determining the coefficient values is given below.

$$\Delta_H = a_{\Delta H1}p_w + a_{\Delta H0} \quad (5a)$$
$$\Delta_H = 10.25p_w - 171.7 \quad (5b)$$

$$\Delta_L = a_{\Delta L1}p_w + a_{\Delta L0} \quad (6a)$$
$$\Delta_L = 4.661p_w - 65.52 \quad (6b)$$

Where
p_w is the weighted average precipitation,
$a_{\Delta H1}$, $a_{\Delta H0}$ are 1st and 0th order term LR coefficients for the NE precipitation adjustment, and
$a_{\Delta L1}$, $a_{\Delta L0}$ are 1st and 0th order term LR coefficients for the CB precipitation adjustment.

Equation (7a) has the general form the weighted average precipitation for the three months prior to the removal of the specimens from the test environment. Microsoft Excel Solver was used to find three weighted averages that maximized the minimum of the coefficients of determination for Equations (5a) and (6a). Equation (7b) has the numerical values for the weighted coefficients. Table 1 shows the precipitation values, the weighted average precipitation, and the deviations of

the transit time for the high and low values. The precipitation adjustment trends are shown in Figure 4; the r^2 values for both trends are 0.9156.

$$p_w = \frac{a_{r-2}p_{r-2} + a_{r-1}p_{r-1} + a_r p_r}{a_{r-2} + a_{r-1} + a_r} \quad (7a)$$

$$p_w = \frac{0.315p_{-2} + 1.125p_{-1} + 0.721p_0}{0.315 + 1.125 + 0.721} \quad (7b)$$

Where p_r, p_{r-1}, and p_{r-2} are the precipitation levels for the month of removal, one month prior to removal, and two months prior to removal, respectively. a_r, a_{r-1}, and a_{r-2} are the weight factors for the precipitation levels for the month of removal, one month prior to removal, and two months prior to removal, respectively.

Table 1–Adjustment for precipitation at the time of specimen collection

Exposure	Precip. (cm) Relative to Removal			Precip. (cm)	Deviation from Model	
(Months)	-2 Months	-1 Month	0 Months	Weighted	NE Val.	CB Val.
4	10.0	10.4	5.7	8.8	–92.99	–26.05
9	4.8	13.0	31.7	18.1	12.40	10.15
14	17.8	39.3	9.7	26.3	107.49	57.67
21	6.2	7.0	26.5	13.4	–3.98	13.27
26	6.1	3.3	24.1	10.7	–61.10	–23.95
33	42.3	13.1	17.9	19.0	–6.31	23.83
45	15.3	6.0	11.8	9.3	14.13	–27.49

NE and CB denote near board end and center board, respectively.

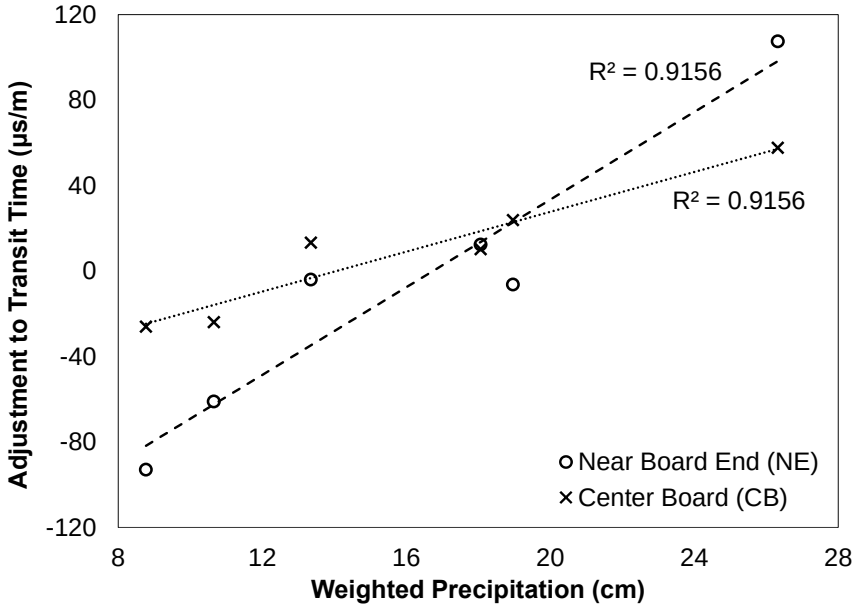

Figure 4–Precipitation adjustment to transit time.

Table 2 describes the variables and constants used in deterioration model.

Table 2–Symbols and coefficient descriptions

Symbol	Value	Description
T_s	Calculated	Transit time in microseconds
A_H	Calculated	Transit time near board end (NE)
A_L	Calculated	Transit time along the center board (CB)
l	Independent	Distance to the nearest end of the board
d_t	Calculated	Distance from board end where transit time transitions from NE to CB
t	Independent	Time of weathering in months
a_{H1}	13.93	Coef. 1st order term NE linear regression method (LRM)
a_{H0}	721.4	Coef. 0th order term NE LRM
Δ_H	Calculated	NE precip. adjustment applied after 3rd month of weathering
a_{L1}	4.497	Coef. 1st order term CB LRM
a_{L0}	721.4	Coef. 0th order term CB LRM
Δ_L	Calculated	CB precip. adjustment applied after 3rd month of weathering
a_{d1}	0.036	Coef. 1st order term transition distance LRM
a_{d0}	2.494	Coef. 0th order term transition distance LRM
p_w	Calculated	Weighted average precipitation
p_{r-2}	Independent	Precipitation two months prior to specimen removal
p_{r-1}	Independent	Precipitation one month prior to specimen removal
p_r	Independent	Precipitation the month of removal
a_{r-2}	0.315	Weight factor for precipitation two months prior to removal
a_{r-1}	1.125	Weight factor for precipitation one month prior to removal
a_r	0.721	Weight factor for precipitation the month of removal
$a_{\Delta H1}$	10.25	Coef. 1st order term NE precip. adjustment LRM
$a_{\Delta H0}$	–171.7	Coef. 0th order term NE precip. adjustment LRM
$a_{\Delta L1}$	4.661	Coef. 1st order term CB precip. adjustment LRM
$a_{\Delta L0}$	–65.52	Coef. 0th order term CB precip. adjustment LRM

Results and Discussion

The transit times predicted by the deterioration model are plotted alongside the transit times measured from the test specimens in Figures 5 through 12. The vertical dotted lines represent the transition distance from the end of the boards. At that point, it is predicted that the transit time will begin transitioning from the low value of the center of the board to the high value of the deteriorated ends of the board. The model developed here attempts to explain variation in transit times caused by wood decay, not variation in transit times inherent to the wood specimens. The model predicts a uniform transit time for the control specimen (0 months exposure); the underlying assumption is that the control boards have no variation in the transit times. In reality,

the wood does have variation in transit times that are inherent to the wood boards themselves. The r^2 value is the percentage of the variation explained by the model. For the control specimens, any variation from the starting control transit time would therefore be unexplained by the model and be indicative of variation inherent to the wood, not variation caused by decay. As a result, the r^2 value for the control group is near zero. The low r^2 value for the control group does not mean the model poorly fits the data. The average percentage error between the control data and the predicted values is 0.24% indicating that the model closely matches the control data. With increased exposure, decay causes the transit times to increase; a larger percentage of the transit time variation is explained by the model, and the r^2 values increase.

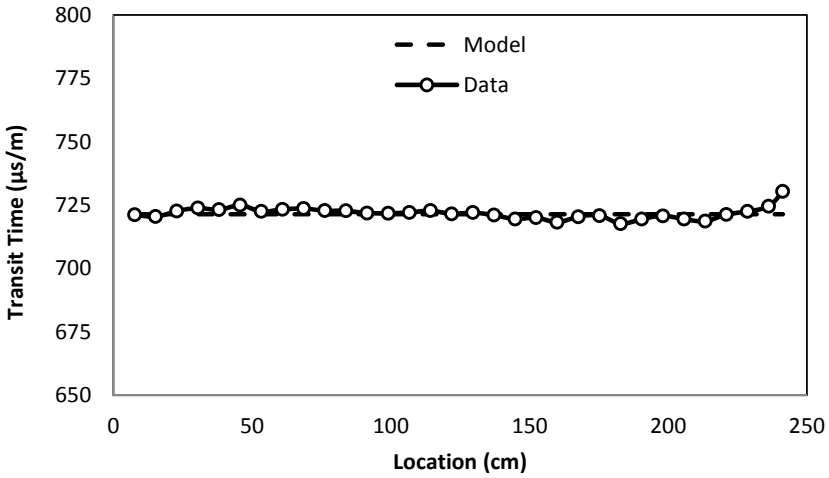

Figure 5–Transit time data and predicted transit time for 0 months (Control) of weathering. Average percentage error = 0.24%, r^2 = NA.

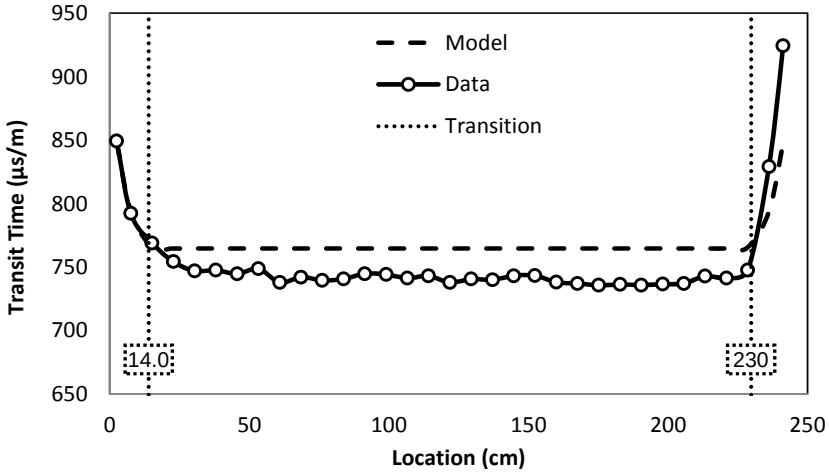

Figure 6–Transit time data and predicted transit time for 4 months of weathering. Average percentage error = 2.9%, r^2 = 0.8958.

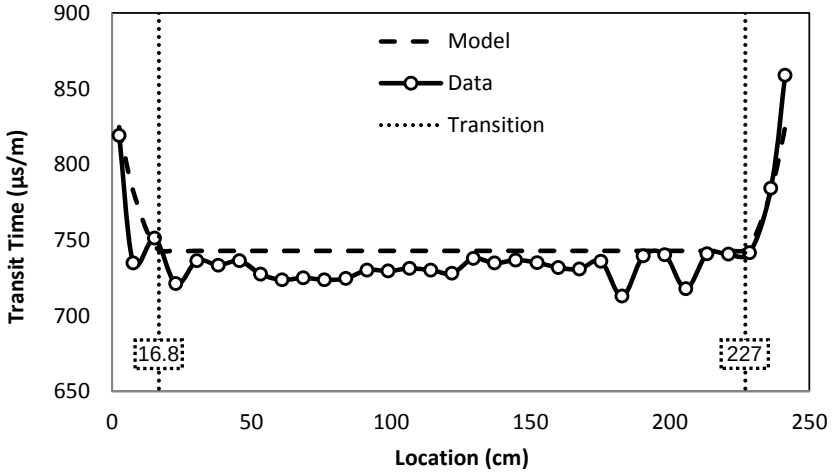

Figure 7–Transit time data and predicted transit time for 9 months of weathering. Average percentage error = 1.7%, r^2 = 0.8254.

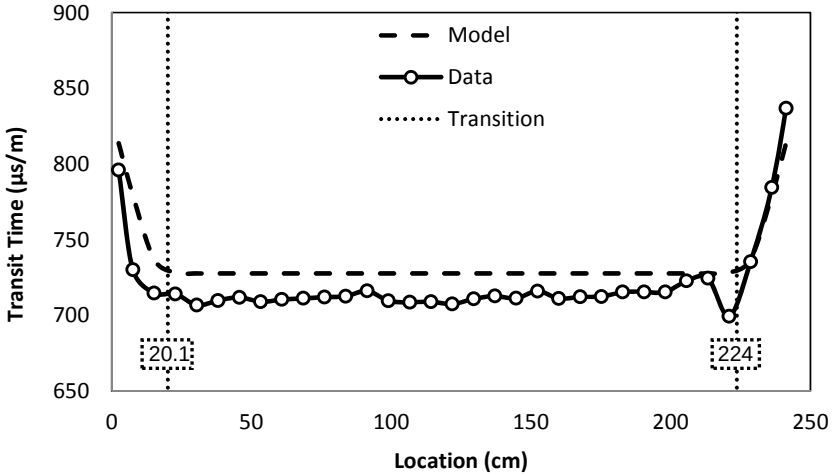

Figure 8–Transit time data and predicted transit time for 14 months of weathering. Average percentage error = 2.2%, r^2 = 0.8620.

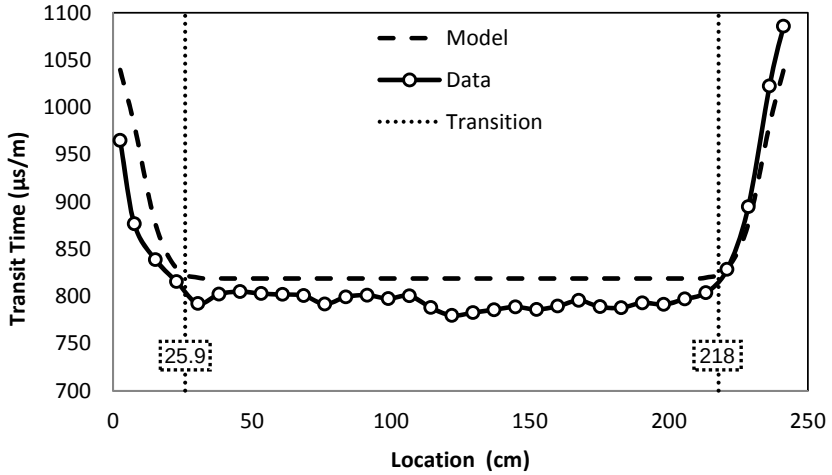

Figure 9–Transit time data and predicted transit time for 21 months of weathering. Average percentage error = 3.3%, r^2 = 0.8620.

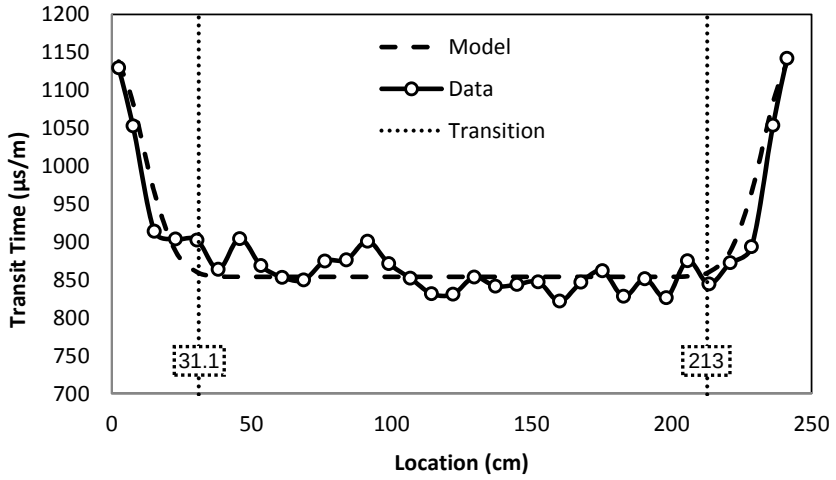

Figure 10–Transit time data and predicted transit time for 26 months of weathering. Average percentage error = 2.3%, r^2 = 0.9068.

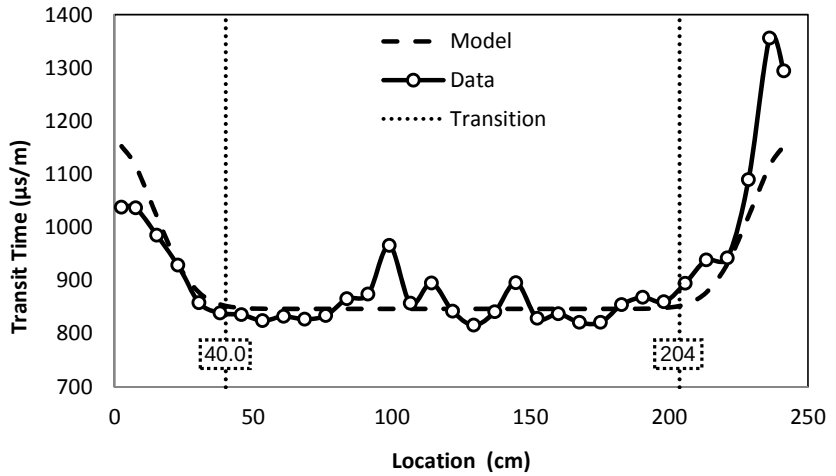

Figure 11–Transit time data and predicted transit time for 33 months of weathering. Average percentage error = 4.2%, r^2 = 0.7609.

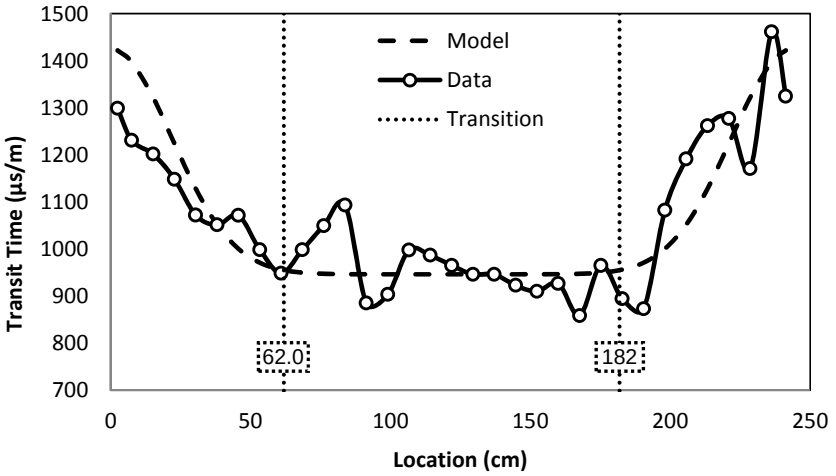

Figure 12–Transit time data and predicted transit time for 45 months of weathering. Average percentage error = 6.1%, r^2 = 0.7608.

Conclusions

The deterioration model presented in this report describes the change in ultrasonic wave transit times along the length of the wood specimens subjected to weathering of up to 45 months. The model was a second order exponentially decaying function. The transit times were found to be dependent upon of the months of weathering, the distance from the end of the boards, and the precipitation for the three months prior to testing. Precipitation for the three months prior to the removal of the specimens from the weathering environment was found to influence the transit times of the tested specimens despite the fact the specimens underwent conditioning prior to testing. Accounting for precipitation, the model was capable of estimating the transit times within the specimens to an average percentage error of 6.1% for 45 months of weathering. If precipitation was excluded from the analysis, the average percentage error exceeded 9% during the wettest months.

Literature Cited

Allison, R.B.; Wang, X.; Ross, R.J. 2008. Visual and nondestructive evaluation of red pines supporting a ropes course in the USFS Nesbit Lake Camp, Sidnaw, MI. Proceedings, 15th Nondestructive Testing of Wood Symposium, September 10–12, 2007; Duluth, MN. Forest Products Society: 43–48.

Brashaw, B.K.; Vatalaro, R.J.; Wacker, J.P.; Ross R.J. 2005 (a). Condition assessment of timber bridges. 1. Evaluation of a micro-drilling resistance tool. General Technical Report FPL–GTR–159, USDA Forest Products Laboratory, Madison, WI. 8 p.

Brashaw, B.K.; Vatalaro, R.J.; Wang, X.; Ross, R. J.; Wacker, J.P. 2005 (b). Condition assessment of timber bridges. 2. Evaluation of several stress wave tools. General Technical Report FPL–GTR–160, USDA Forest Products Laboratory, Madison, WI. 11 p.

Clausen, C.A.; Ross, R.J.; Forsman, J.W., Balachowski, J.D. 2001. Condition assessment of roof trusses of Quincy Mine Blacksmith Shop in Keweenaw National Historical Park. Res. Note. FPL–RN–0281. Madison, WI: U.S. Department of Agriculture, Forest Service, Forest Products Laboratory: 4 p.

De Groot, R.; Ross, R.; Nelson, W. 1994. Nondestructive assessment of biodegradation in southern pine sapwood exposed to attack by natural populations of decay fungi and subterranean termites. Proceedings, Twenty-Fifth Annual Meeting, The International Research Group on Wood Preservation, Bali, Indonesia, May 29–June 3, 1994. 13 p.

De Groot, R.C.; Ross, R.J.; Nelson, W.J. 1995. Natural progression of decay in unrestrained, southern pine sapwood lumber exposed above ground. Proceedings, Twenty Sixth Annual Meeting, IRG, Helsinger, Denmark. June 11–16, 1995.

De Groot, R.C.; Ross, R.J. Nelson, W.J. 1998. Nondestructive assessment of wood decay and termite attack in southern pine sapwood. Wood Protection 3(2): 25–34.

Dundar, T.; Ross, R.J. 2012. Condition assessment of 2500 year old wood coffin. Res. Note FPL–RN–0327. Madison, WI: U.S. Department of Agriculture, Forest Service, Forest Products Laboratory: 3 p.

Emerson, R.; Pollock, D.; McLean, D.; Fridley, K.; Pellerin, R.; Ross, R.J. 2002. Ultrasonic inspection of large timber bridge members. Forest Products Journal. 52(9): 88–95.

Pellerin, R.F.; DeGroot, R.C.; Esenther, G.R. 1985. Nondestructive stress wave measurements of decay and termite attack in experimental wood units. In: Proceedings, 5th Nondestructive Testing of Wood Symposium, 1985 September 9–11; Pullman, WA. Pullman, WA: Washington State University: 319–353.

Ross, R.J.; De Groot, R.C.; Nelson, W.J. 1994. Technique for nondestructive evaluation of biologically degraded wood. Experimental Techniques 18(5): 29–32.

Ross, R.J.; De Groot, R.C.; Nelson, W.J.; Lebow, P.K. 1996. In: C. Sjostrom, ed. Assessment of the strength of biologically degraded wood by stress wave NDE. Proceedings, Seventh International Symposium on Durability of Building Materials and Components, Volume 1. E&FN Spon, 2–6 Boundary Row, London SE1 8HN, UK. pp. 637–644.

Ross, R.J.; De Groot, R.C.; Nelson, W.J.; Lebow, P.K. 1997. Relationship between stress wave transmission characteristics and the compressive strength of biologically degraded wood. Forest Products Journal 47(5): 89–93.

Ross, R.J.; De Groot, R.C. 1998. Scanning technique for identifying biologically degraded areas in wood members. Experimental Techniques 22(3): 32–33.

Ross; R.J.; Soltis, L.A.; Otton, P. 1998. Assessing wood members in the USS Constitution using nondestructive evaluation methods. APT Bulletin 29(2): 21–25.

Ross, R.J.; Volny, N.; Pellerin, R.F.; Salsig, W.W.; Falk, R.H. 1999. Inspection of timber bridges with stress wave nondestructive evaluation tools. A guide for use and interpretation. FPL–GTR–114. U.S. Department of Agriculture, Forest Service, Forest Products Laboratory, Madison, WI.

Ross, R.J.; Pellerin, R.F.; Forsman, J.W.; Erickson, J.R.; Lavinder, J.A. 2001. Relationship between stress wave transmission time and compressive properties of timbers removed from service. Res. Note FPL–RN–0280. Madison, WI: U.S. Department of Agriculture, Forest Service, Forest Products Laboratory: 4 p.

Ross, R.J.; Wang, X. 2005. Quincy Mine Blacksmith Shop-condition assessment of timbers. Structure Magazine, September 2005, pp. 32–34.

Ross, R.J.; Brashaw, B.K.; Wang, X. 2006. Structural condition assessment of in-service wood. Forest Products Journal 56(6):4–8.

Senalik, C.A.; Schueneman, G.; Ross, R.J. 2014. Ultrasonic-based nondestructive evaluation methods for wood: a primer and historical review. General Technical Report FPL–GTR–235. Madison, WI: U.S. Department of Agriculture, Forest Service, Forest Products Laboratory. 31 p.

Wang X.; Wacker, J.P.; Ross, R.J.; Brashaw, B.K. 2008. Condition assessment of the main structural members of historic steam schooner Wapama. Res. Pap. FPL–RP–649. Madison, WI: U.S. Department of Agriculture, Forest Service, Forest Products Laboratory.

White, R.H.; Ross, R.J. 2014. Wood and Timber Condition Assessment Manual. Second Edition. General Technical Report. FPL–GTR–324. Madison, WI: U.S. Department of Agriculture, Forest Service, Forest Products Laboratory: 102 p.

Ultrasound Tests for Evaluating Sensitivity to Identify Cracks in a Piece of Pinus spp.

Isabelle Tavares Cardoso
Civil Engineering Undergraduate Student, Civil Engineering Department, UFSC - Federal University of Santa Catarina, Campus Universitário, Trindade, CEP 88040-970, Florianópolis, Santa Catarina, Brasil, isabelletcardoso@gmail.com

Giancarlo Zibetti Mantovani
Civil Engineer Master Student, Civil Engineering Department, UFSC - Federal University of Santa Catarina, Campus Universitário, Trindade, CEP 88040-970, Florianópolis, Santa Catarina, Brasil, gzmantovani@gmail.com

Ângela do Valle
Dr. Professor, Civil Engineering Department, UFSC - Federal University of Santa Catarina, Campus Universitário, Trindade, CEP 88040-970, Florianópolis, Santa Catarina, Brasil, angela.valle@ufsc.br

Abstract

Ultrasound technique presents several possible applications, and one of them is the investigation of internal imperfections presence such as cracks and galleries of wood-destroying insects. The research presents experimental results performed to evaluate ultrasound technique sensitivity in detecting internal non-homogeneities in a wood piece of *Pinus spp*. with dimensions of 7 cm x 15 cm x 300 cm. Some cracks were produced with a saw in a radial-tangential plane of wood and radial-longitudinal plane of the piece. Each one of these cracks presents 2 cm, 4 cm and 6 cm depth. Wave propagation time through crack direction was measured by using ultrasound equipment and transducers of 200 kHz with flat faces. Spacing between transducers is chosen with different values to identify how far is possible to detect internal voids from a crack, in that wood piece.

Keywords: structure, wood, mechanical characterization, diagnostic.

Introduction

Wood is an ancient building material that presents several advantages such as potential for renewing on nature and very low power consumption during processing. On the other hand, it is difficult to get the raw material free of defects since wood is a biological material. Also, it will be subjected to deterioration processes if it is not adopted proper care in design, construction, use and maintenance phases. Periodic planning of building inspections is essential to prevent problems or act before worse consequences arise. During the inspections, it is necessary to investigate the structural elements integrity. The performance of non-destructive evaluations is an interesting alternative for evaluating the conservation status of buildings. Non-destructive techniques are a way to identify physical and mechanical properties of a structural piece without altering its use capability under service (Ross and Pellerin 1994). Ultrasonic wave propagation is an important technique among non-destructive evaluation ones. It is essential to understand how the ultrasonic wave propagation phenomenon works, in materials, to use it correctly. Therefore, it is necessary to determinate relations among factors involved in the phenomena. In general, physical and mechanical properties of wood present a high degree of variability as a consequence of its biological formation. Also, wood may show structure defects such as knots and cracks that interfere directly with its mechanical properties. Density and

moisture content are quite notorious among the most important physical characteristics of wood (Bodig and Jayne 1993). The application of ultrasound technique involves the analysis of high-frequency sound waves characteristics during wave propagation through the material. According to Zombori (2001), the frequency range used for timber study is relatively small (20 kHz - 500 kHz) due to the high signal dissipation. It is a limiting factor to apply the technique in wooden structures. Ultrasound tests are non-destructive, and ultrasonic wave velocity is one parameter used for evaluating the elastic properties of wood. Ultrasound technique is also used for detecting internal non-homogeneity in wood pieces. In this case, inhomogeneities could be detected by changes in ultrasonic pulse velocity (Bucur 2006). Propagation of sound wave in the wood is considered an extremely complex phenomenon. The wave propagation velocity is significantly affected by various factors such as anatomical properties, density, moisture content, temperature, specimen geometric configuration, transducer frequency and presence of internal inhomogeneities.

One of the parameters used for analyzing tests results with ultrasound equipment is wave propagation velocity. Wave velocity can be expressed by Equation 1 (Halliday and Resnick 1991):

$$V = \lambda . f \tag{1}$$

where V is longitudinal wave velocity, l is wavelength, and f is ultrasound transducer frequency.

To verify solid consistency via ultrasound, the classic method measures several points in the piece with the aid of transducers positioned in a direct, semi-direct or indirect path, aligned over an orthogonal or an oblique imaginary line. In a zone with a low quality material, ultrasonic pulse velocity is lower than the values in the rest of the solid. If a linear propagation is considered, travel time to the wave transit through that area is higher than the rest of the element. Various researchers investigated the use of ultrasound technique for detecting no exterior apparent homogeneities (Carrasco and Teixeira 2012; Emerson et al. 2002). Carrasco and Teixeira (2012) performed an inspection of a glued laminated timber beam with 8.5 x 15 x 95.8 cm. According to the authors, the propagation time measurement circa 60-80 ms represents sound wood and higher values means the presence of some degradation. Visual examination of the beam interior confirmed the existence of cracks and insect galleries in regions where the pulse was slow. Emerson et al. (2002) evaluated the damage level of a timber beam from an ancient bridge. Measurements were made perpendicular to the wood grain. Results permitted to detect the section in which there is no homogeneity; however, they are unable to determine its location, size and shape within the section.

It was possible to observe that ultrasound technique can work in damage detection of timber structures; nevertheless, it requires even further study. During research it was possible to test distance influence between the measuring point and defect on the wave velocity of propagation to evaluate the ultrasound technique sensitivity for structures inspections.

Materials and methods

Wood and equipment

The species chosen for this research was Pinus (*Pinus elliottii*) extracted from planted forests, in Santa Catarina, with a specific gravity of 400 kg/m³. That species was selected since it is often commercially available in Brazil and shows an abundant presence of nodes. Also, it was considered its potential in prefabricated structures. Ultrasound tests were performed on a specimen of $7 \times 15 \times 300$ m^3 (Figure 1 and 2). These dimensions were chosen to approach them to dimensions of a wood piece under service conditions.

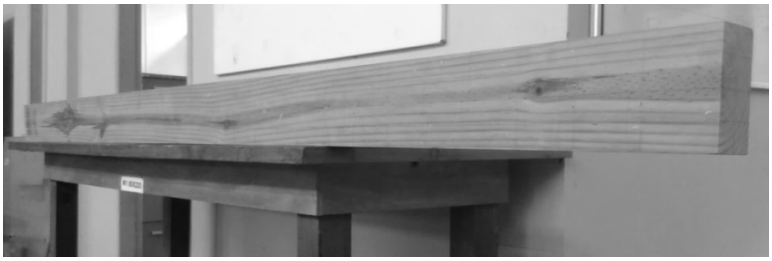

Figure 1 – Specimen of Pinus used in the research.

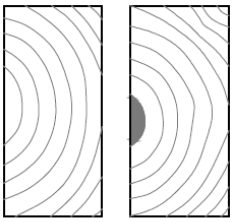

Figure 2 – Cross section of the Pinus specimen.

Just before each ultrasound test, the wood moisture content was evaluated by resistive hygrometer equipment model H-DI-3.10 from BES-BOLLMANN to avoid affecting the specimen integrity. The moisture content was measured at 29 points in specimen faces, and the average value was 15 %. The ultrasound equipment used in tests is PUNDIT 6 (Portable Ultrasonic Non-Destructive Digital Indicating Tester) whose accuracy is 0,1μs. Transducers have plane faces and emit longitudinal waves with 200 kHz frequency and a diameter of 2 cm. It was used a couplant gel from Carbogel for minimizing the air presence in contact surfaces during ultrasound tests. Before each series of tests, the equipment was calibrated according to the fabricator's specification.

Method of investigation

An artificial crack was made, in the longitudinal direction of the wood (Figure 3), to analyze the influence of cracks presence in ultrasound wave propagation velocity in the wood specimen. The ultrasound emission was applied in a transversal section of the specimen that coincides with the predominant radial-tangential plane of the wood. A mesh was created for indicating ultrasound transducers position along the wood specimen as seen in Figure 4. The specimen faces are identified as A, A', B, B', C and C'. In that mesh, the columns identify different transversal sections along a piece length, and they are numbered from face A (column 0) until face A' (column 30), with subdivisions named 0A, 0B, 0C, 1A and 1B. The mesh had a dimension of 2.5 cm between columns, from column 0 till column 1B, 5 cm, from column 1B and column 2, and 10 cm, from column 2 until column 30. The line mesh position, in faces B, B', C and C', is identified by the Roman algorisms I, II, III and by the letters a, b, c, d, e and f, with 1.875 cm of distance between each other.

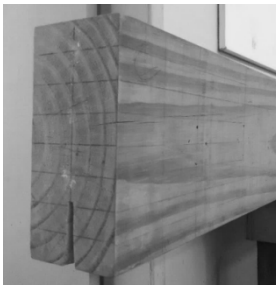

Figure 3 – Longitudinal crack artificially produced.

Nomenclature of columns and lines in the mesh was chosen to facilitate the understanding and interpretation of the tests performed and their results. The specimen and its mesh are illustrated in

Figure 4. Detail 1 (Figure 4), zoomed in Figure 5, shows the mesh of transducers positioning in the crack proximity.

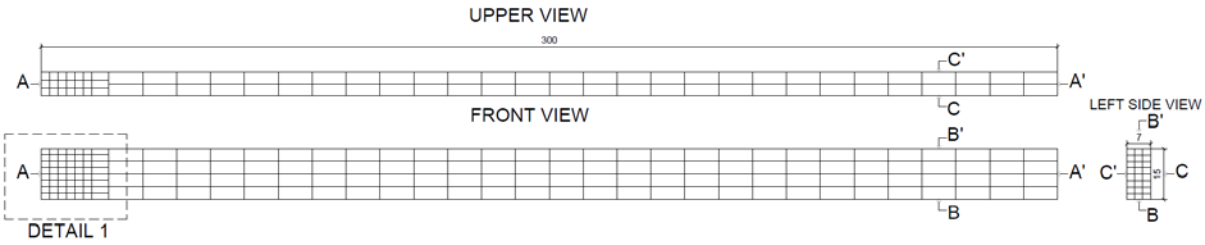

Figure 4 – Mesh for positioning ultrasound transducers in the wood specimen.

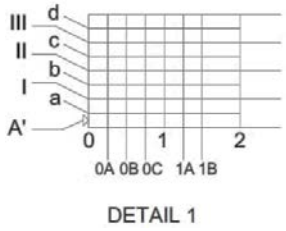

Figure 5 – Mesh for positioning ultrasound transducers in the surrounding area of the crack.

Experimental measurements of a nearby longitudinal crack are organized in three Stages. Stage 0 corresponds to a piece without cracks and the other Stages are classified according to the depth (d) of the crack, with a constant length of 15 cm (Table 1) as presented in Figure 6.

Table 1 – Crack depth (d) in different stages

Stage	Depth (cm)
0	-
1	2.0
2	4.0

During the tests, transducers were positioned on the specimen, in the opposite lateral faces (C and C'), between columns 0 and 2. In Figure 6, it is possible to notice that the mesh in Stage 0 is different from the mesh in Stages 1 and 2. That happens because it was noted the need for more measurements after executing a crack of 2 cm (Stage 1) to improve the analysis.

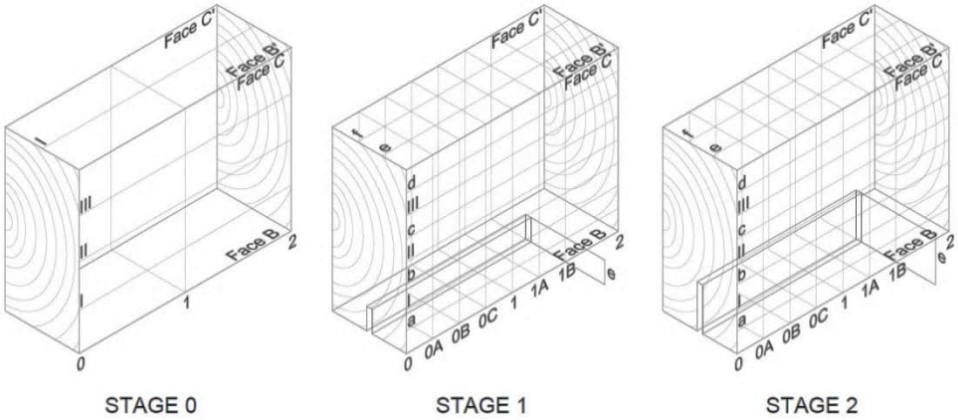

Figure 6 – Mesh for positioning transducers for testing a nearby longitudinal crack.

Results and analysis

Ultrasonic wave propagation velocities are calculated from pulse time measured on a transversal direction in the specimen, along different positions identified by the presented mesh. Velocities obtained are shown in Table 2 and organized by Stages of tests (0, 1 and 2), and by each mesh line in

the specimen. As stated before, the mesh used for transducers position in Stage 0 (without a crack) was less refined than other Stages after the crack execution.

Table 2 – Ultrasonic velocities in proximity of longitudinal crack in each Stage

Stage	Position	Ultrasound velocities aligned per column (m/s)						
		0A (a)	0B (b)	0C (c)	1 (d)	1A (e)	1B (f)	Avg. Vel per line (g)
Stage 0 - Without crack	a	-	-	-	-	-	-	-
	I	-	1808.8	-	1772.2	-	1818.2	1799.7
	b	-	-	-	-	-	-	-
	II	-	2095.8	-	2114.8	-	2095.8	2102.1
	c	-	-	-	-	-	-	-
	III	-	1781.2	-	1790.3	-	1776.6	1782.7
	d	-	-	-	-	-	-	-
Stage 1 – Crack 2 cm	a	1732.7	1730.5	1724.1	1713.6	1717.8	1732.7	1725.2
	I	1825.3	1822.9	1804.1	1792.6	1818.2	1806.5	1811.6
	b	1966.3	1997.1	1966.3	1936.4	1963.5	1969.1	1966.4
	II	2124.4	2118.0	2095.8	2095.8	2099.0	2114.8	2108.0
	c	1988.6	1969.1	1969.1	1910.0	1955.3	1917.8	1951.6
	III	1778.9	1776.6	1778.9	1776.6	1783.4	1774.4	1778.2
	d	1734.8	1726.3	1719.9	1728.4	1707.3	1709.4	1721.0
Stage 2 – Crack 4 cm	a	1587.3	1587.3	1585.5	1590.9	1616.6	1647.1	1602.5
	I	1781.2	1801.8	1790.3	1785.7	1801.8	1808.8	1794.9
	b	1963.5	1974.6	2002.9	1920.4	1985.8	1969.1	1969.4
	II	2105.3	2092.7	2074.1	2080.2	2067.9	2061.9	2080.3
	c	1941.7	1904.8	1894.5	1907.4	1869.2	1859.2	1896.1
	III	1765.4	1756.6	1763.2	1752.2	1763.2	1763.2	1760.6
	d	1726.3	1711.5	1709.4	1722.0	1705.2	1684.7	1709.9

The values of velocities calculated were submitted to statistics tests with a significance level of 95% to evaluate the existence or not of significant differences between values for several lines. The Shapiro-Wilk normality Test identified that data in Stages 0 and 1 presented non-normal distributions, and data in Stage 2 had a normal distribution. Then, the Wilcoxon Test, indicated for non-normal distributions, and the Paired T-Test, indicated for normal distributions, was performed to compare results with each other in various stages. It is possible to conclude there is a difference between measurements from Stages 1 (d = 2 cm) and 2 (d = 4 cm), according to results of statistical tests. That is, the presence of a 4 cm depth crack shows a statistically different velocity in comparison to 2 cm depth. On the other hand, it is not possible to prove that there is a statistical difference from comparisons between Stages 0 (d = 0 cm) and 1 (d = 2 cm), and Stages 0 (d = 0 cm) and 2 (d = 4 cm). One possible reason for non-identification of these differences could be the data amount since there are less measured points in Stage 0 than Stages 1 and 2. Then, it can result in less accurate analysis.

In Table 2, it is possible to observe that velocity values increase as the line position is away from the crack and cross section edge (Face B'). It is because the transducers are positioned closer to a discontinuity with higher interference and longer wave path. For measurements on lines that are far away from the crack edge and Face B', lines II and c, a shorter propagation time means a higher velocity. The percentage differences between Steps 0 and 1, in the velocity of each line, are analyzed, and values are shown in Table 3.

In Stage 1, the crack is 2 cm depth (d = 2 cm) and located between the height of line a (1.875 cm) and the line I (3.750 cm). Since line I is not crossed by the crack, it is noticed in Table 3 (line a, column g) an increase of 4.76 % in the average velocity of propagation from the velocity in line a to the one in line I. When comparing lines I and b (Table 3, line b, column g), it is possible to note a greater

variation than the last situation, with an average increase of 7.87 %. The crack does not cross any of the lines (lines I and b); however, there are different propagation velocities on each other. It means that the line distance from the crack edge affects the velocity. Line b, which is distant from the crack edge 3.625 cm, presents higher velocities than the line I, which is distant 1.750 cm from the crack. It evidences that there is less influence in line b that is at a greater distance from the crack.

Table 3 – Percentage difference between each line in Stage 1 (d = 2 cm).

Horizontal Position	0A (a)	0B (b)	0C (c)	1 (d)	1A (e)	1B (f)	Avg. Dif % (g)
Distance from column 0	25 mm	50 mm	75 mm	100 mm	125 mm	150 mm	-
Dif. % a x I (a)	5.07	5.07	4.43	4.41	5.52	4.08	4.76
Dif. % I x b (b)	7.17	8.72	8.25	7.43	7.40	8.26	7.87
Dif. % b x II (c)	7.44	5.71	6.18	7.61	6.45	6.89	6.71
Dif. % II x c (d)	-6.83	-7.56	-6.44	-9.73	-7.35	-10.27	-8.03
Dif. % c x III (e)	-11.79	-10.83	-10.69	-7.50	-9.64	-8.08	-9.76
Dif. % III x d (f)	-2.54	-2.92	-3.43	-2.79	-4.46	-3.80	-3.32

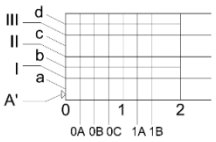

DETAIL 1

Furthermore, in Stage 1, the comparison between velocity values in line b (distant 3.625 cm of the crack) and line II (distant 5.500 cm of the crack) shows that there is an increase of 6.71 % (Table 3, line c, column g). The value will increase if it is far away from the crack. However, the amount of variation is lower than the last increase of 7.87 % (Table 3, line b, column g), for a position nearer to the crack. For heights above the line II position (Table 3, lines d, e and f, column g), it is worth mentioning that velocity decreases between adjacent lines. For lines II and c (Table 3, line d) the variation decrease is 8.03 %; for lines c and III (Table 3, line e) it is 9.76% and for lines III and d (Table 3, line f) there is a reduction of 3.32%. Decrease of variation rates of propagation velocity between adjacent lines, in higher positions from the crack edge (line c, distant 7.375 cm; line III, distant 9.250 cm and line d, distant 11.125 cm) could be justified by gradual approximation of the cross section upper border as well as possible variations of the wood internal structure. In the same way that propagation velocity increases in the lines that are furthest from the crack, there is a higher velocity in positions that are farther away from the upper section border. That behavior related to the upper face and crack edges proximity demonstrates the influence of solid discontinuities presence in the path and propagation velocity of the ultrasonic pulse.

For Stage 2, in which the crack depth is 4 cm, the percentage variations of ultrasound propagation velocity appear in Table 4. In that Stage, the crack edge (d = 4 cm) is between the height of line I (3.750 cm) and line b (5.625 cm). Values observed in Table 4 have the same behavior observed in Table 3 (Stage 1). The average propagation velocity variations show an increase when adjacent lines values are compared.

In Table 4 (lines d, e and f, column g), the variation rate between velocities on lines II e c, lines c e III and lines III e d presents decreasing reduction. The variation rate decreases for lines that are closer to the upper face (Face B'), that is, to lines to positions higher than the crack edge (line c, distant 5.375 cm; line III, distant 7.250 cm and line d, distant 9.125 cm) decrease as the lines move away from the crack. The variation rate decreased -7.7 %, from line c to line III, and -2.78 %, from line III to line d.

In Stage 2, that behavior confirms the same effect observed in Stage 1 about propagation velocity of ultrasonic pulse in the presence of discontinuities. The comparison of velocities variation values between lines a and I, in Stage 1 (Table 3, line a, column g, 4.76 %), and Stage 2 (Table 4, line a, column g, 10.73%) enables to observe a higher variation in the second case. That fact can be justified because both lines a and I are interrupted by the crack in Stage 2, and it does not occur the same in Stage 1.

Table 4 – Percentage difference between each line in Stage 2 (d = 4 cm).

Horizontal Position	0A (a)	0B (b)	0C (c)	1 (d)	1A (e)	1B (f)	Avg. Dif. % (g)
Distance from column 0	25 mm	50 mm	75 mm	100 mm	125 mm	150 mm	-
Dif. % a x I (a)	10.88	11.90	11.44	10.91	10.28	8.94	10.73
Dif. % I x b (b)	9.29	8.75	10.61	7.02	9.27	8.14	8.85
Dif. % b x II (c)	6.73	5.64	3.43	7.68	3.97	4.50	5.33
Dif. % II x c (d)	-8.42	-9.87	-9.48	-9.06	-10.64	-10.90	-9.73
Dif. % c x III (e)	-9,99	-8.44	-7.44	-8.86	-6.01	-5.44	-7.70
Dif. % III x d (f)	-2.27	-2.63	-3.15	-1.75	-3.40	-4.66	-2.98

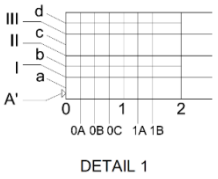

DETAIL 1

In Stage 2 (d = 4 cm), propagation velocities measured in the section lines c, III and d decreases when related to Stage 1 (d = 2 cm). Velocities in the height of line III were measured in all three Stages, and they presented maximum values in Stage 0 (d = 0 cm), and minimum in Stage 2 (d = 4 cm). Once measurements made in line III, for any stage, are with the same value of 3.75 cm far from the upper face of the wood piece, there must be another factor influencing the velocity change.

As tests were performed on the same day, it was possible to discard the influence of moisture content, temperature variation and internal imperfections on the wood. Crack depth is the different parameter among three stages. Thus, it is possible to conclude that ultrasound equipment had captured the presence of a longitudinal crack situated 9.250 cm in Stage 1, and 7.250 cm at Stage 2. One possible way of expressing these distances under a dimensionless manner is by converting values of propagation velocity, in line III, to some wavelengths (l) by using Equation 1. Substituting the frequency of 200 kHz, the wavelength in each Stage is l_m = 0.8906 cm, in Stage 0, l_m = 0.8889 cm, in Stage 1 and l_m = 0.8816 cm in Stage 2, all of them on line III. Expressing the distance between line III and the crack edge as a wavelength function (l), it is possible to say that an ultrasound equipment with transducers of 200 kHz has captured an artificial imperfection within the reach of 10.41 l_m, in Stage 1, and 8.22 l_m in Stage 2. It is possible to state from these results that the ultrasound technique is sensitive to detect a crack distant, at least, 9.250 cm (Stage 1, line III), and under particular conditions of the research. That distance may be represented as the number of wavelength 10.41 l_m.

It is possible to conclude, considering the result, that the ultrasound method was sensitive to capture a wooden inhomogeneity 10.41 l_m far from the measuring point. During each stage, further analysis of velocities values in line III is shown in Table 5. In the same position of measurement and variable distance from the crack edge is observed that the propagation velocity average value decreased -0.25 %, in Stage 1 (d = 2 cm), and -1.24 % (d = 4 cm) in comparison to velocities in the sound wood condition. The fail influence is more significantly in Stage 2, where the crack distance expressed in a wavelength form is 8.22 l_m.

Table 5 – Velocities in line III on each Stage

Stage	Distance between line III and crack	Velocity in line III per column (m/s)			Avg.Vel.in line III per Stage (m/s)	CV % Vel. related Stage 0
	(a)	0B (b)	1 (c)	1B (d)	(e)	(f)
Stage 0 (a)	0 cm	1781.2	1790.3	1776.6	1782.7	0
Stage 1 (b)	9.25cm	1776.6	1776.6	1774.4	1778.2	-0.25
Stage 2 (c)	7.25 cm	1756.6	1752.2	1763.2	1760.6	-1.24

Conclusions

The study analyzes a piece of *Pinus elliottii* with a rectangular cross-section of 7 cm x 15 cm and 300 cm length. An artificial crack was made with a circular saw along the wood, in a longitudinal direction, with a gradual depth of 2 cm and 4 cm, respectively. Ultrasound wave measurements were

conducted on a cross-section specimen by using plane face transducers and a frequency of 200 kHz. Ultrasound readings were performed in three stages: Stage 0 - without a crack; Stage 1 - with a crack of 2 cm depth and Stage 2 – with a crack of 4 cm depth. Tests were made with transducers on different positions to investigate the crack influence.

In line III, the ultrasound velocities presented variations in the three Stages. It was possible to observe that the propagation velocity average value decreased -0.25 % in Stage 1 (d = 2 cm), and -1.24 % (d = 4 cm) in comparison to the velocities without a crack. The fail influence is more significantly in Stage 2, where the distance of line III from a crack expressed in a wavelength form is 8.22 l_m.

It was confirmed that the propagation speed progressively increases as the distance measurement points from the crack edge are higher. The farthest position, where the influence of velocities values is perceived, is line III, distant 9.250 cm from a crack in Stage 1 (d = 2 cm), and 7.250 cm at Stage 2 (d = 4 cm). Converting distances to a wavelength, the values are 10.41 l_m in Stage 1, and 8.22 l_m in Stage 2. The ultrasound velocity values measured in the position of line III suffered a decrease of -0.25 % in Stage 1, and -1.24 % in Stage 2.

References

Bodig, J; Jayne, B. A. Mechanics of wood and wood composites. New York, U.S.: Krieger Publishing, 1993. 712 p.

Bucur, V. Acoustics of wood. Germany: Springer-Verlag, 2006. 403 p.

Carrasco, E. V. M.; Teixeira, R. A. Methodology for inspection of wood pathologies using ultrasonic pulses. Cerne, v. 18, n. 3, p. 479–486, mar. 2012.

Emerson, R. et al. Ultrasonic inspection of large bridge timbers. Forest Products Journal, v. 52, n. 9, p. 88–95, 2002.

Halliday, R.; Resnick, R. Fundamentos de física: gravitação, ondas e termodinâmica. 2 ed. Rio de Janeiro: LTC, 1991.

Ross, R. J.; Pellerin, R. F. Nondestructive testing for assessing wood members in structures: A review. Madison: U.S. Department of Agriculture, Forest Service, Forest Products Laboratory, 1994. 40 p.

Zombori, B. "In situ" Nondestructive Testing of Built in Wooden Members. Disponível em: http://www.ndt.net/article/v06n03/skatter /skatter.htm. [20 may 2015].

Determination of the Mechanical Properties of Castanea Sativa Mill. using Ultrasonic Wave Propagation and Comparison with Static Compression and Bending Methods

C. Vázquez
Department of Agroforestry Engineering, University of Santiago de Compostela, Campus Universitario. 27002 Lugo, Spain, +34686844575: c.vazquez@outlook.com
R. Gonçalves
Faculty of Agricultural Engineering (FEAGRI), University of Campinas (UNICAMP) Av. Candido Rondon, 501 – 13083310 Barão Geraldo, Campinas, São Paulo, Brasil: raquel@feagri.unicamp
M. Guaita
Department of Agroforestry Engineering, University of Santiago de Compostela, Campus Universitario. 27002 Lugo, Spain: m.guaita@usc.es

Abstract

The goal of this paper was to analyse the mechanical properties of Castanea sativa determined using an ultrasonic wave method. The results were compared with those obtained using the traditional static compression and bending methods with the same sample. The results were also compared with expected values for this species, and relationships among properties were determined to verify if there were differences between the results and the expected behaviour of the wood. The elastic constants determined using ultrasound did not reveal statistically significant differences compared with the static methods, and the results were generally within the expected range for this species. This result makes ultrasound a powerful method for determining the elastic constants of wood, in addition to its feasibility and low cost. Future studies regarding optimisation of the specimen are important to improve the results of the Poisson's ratios.

Keywords

Orthotropic material, elastic constants, stiffness, wood, moduli.

Introduction

Some species with very good features are not yet being used in the Iberian Peninsula because the mechanical properties of such species have never been determined. Castanea sativa wood is well known among professionals and has been traditionally used for construction (with no design), carpentry and furniture in Portugal, Italy and northern Spain. The growing importance of this species in Spain for structural uses has raised research interest regarding identification of proprieties (characterisation) and grading. Vega et al. (2012) presented results of grading this species by ultrasound.

As an orthotropic material, wood presents different properties according to the direction to the grain. Often, the longitudinal modulus (E_L) is the only known; however, many projects, due to modern

calculation methods, require all of the elastic constants. For this reason, means or relationships between constants are commonly used, such as the ones suggested by Arguelles Álvarez et al. (2000) or Bodig and Jayne (1984). Currently, rapid and efficient methods for the determination of the material properties are desired. Authors such as Bucur (1983, 2006), Bucur and Archer (1984), and Keunecke et al. (2007) highlighted the benefits of the ultrasonic technique for the determination of the properties of wood, among which are the capability to test small specimens and the possibility of testing the same specimen several times due to the non-destructive nature of these measurements.

Zimmer and Cost (1970) first determined the elastic constants of a material using longitudinal and transverse ultrasonic wave propagation and obtained the five independent elements of the stiffness matrix for a material with transverse isotropy. The value of the Young's modulus obtained by inverting the stiffness matrix (37714 $N \cdot mm^{-2}$) was very near its theoretical value (39644 $N \cdot mm^{-2}$).

Since the 1980s, there has been a search for methods that allow for the use of the Christoffel's equations (Bucur 2006) to determine all of the elastic constants of fibrous materials, including wood.

Preziosa et al. (1981) and Preziosa (1982) pioneered the use of the ultrasonic technique for the determination of the stiffness matrix of wood. François (1995) proposed the use of a polyhedral specimen with 26 faces to measure the elastic constants of wood. Polyhedral specimens with 26 faces allow for the determination of all of the elements in the stiffness matrix from a single specimen. More recently, studies have presented results and insightful discussions regarding the use of the ultrasound technology, with different approaches and specimens, to more completely characterise wood (Gonçalves et al. 2014, Ozyhar et al. 2013, Kohlhouser and Hellmich 2012, Longo et al. 2012, Gonçalves et al. 2011a, El Mouridi et al 2011, Dahmen et al. 2010).

Therefore, the goal of this paper was to determine and analyse the three Young's moduli (E_L, E_R, and E_T), the three shear moduli (G_{LR}, G_{LT}, and G_{RT}) and the six Poisson's ratios (ν_{LR}, ν_{LT}, ν_{RL}, ν_{RT}, ν_{TL}, and ν_{TR}) of Spanish Castanea sativa Mill. using ultrasonic testing, and to compare the results with the values obtained by bending (for the E_L Young's modulus) and compression testing (for all of the elastic constants) using the same timber sample. Additionally, the results were compared with expected values proposed by other authors

Materials and methods

Materials

We used 13 beams of Castanea sativa with a 70x150 mm nominal transversal section and a 3500 mm length from 3 regions of Spain (Cataluña, Asturias and Galicia). The different regions of Spain were used only to include a greater variability of the properties of the species and not for comparison.

Material was extracted from each beam to produce 13 polyhedral specimens for the ultrasound test. The material was selected to provide pieces with no pith or knots, as well as to be well defined in the three directions. In addition, each face of the polyhedron was sufficiently large to allow for full, direct contact with the transducer (13 mm). For this geometry, the nominal length of the wave propagation was always 70 mm for the measurements in all directions (Figure1).

For the compression tests, we produced 6 prismatic specimens to compose one group of tests – 3 in axis and 3 out of axis (Gonçalves et al., 2011). 3 beams were chosen to extract the 18 prismatic specimens with dimensions of 20x20x60 mm for the compression tests. All of the specimens were conditioned in a chamber at 20ºC and 65% humidity in compliance with UNE 56528.

To conduct ultrasonic testing on the polyhedral specimens, an ultrasonic wave pulser (Olympus /Panametrics NDT Inc. San Diego, CA) was used. The ultrasonic wave pulser has two sets of nominal 1 MHz longitudinal and transverse wave transducers. Starch glucose was applied as a couplant between the transducers and the specimen to perform the ultrasound measurements (Gonçalves et al. 2011b).

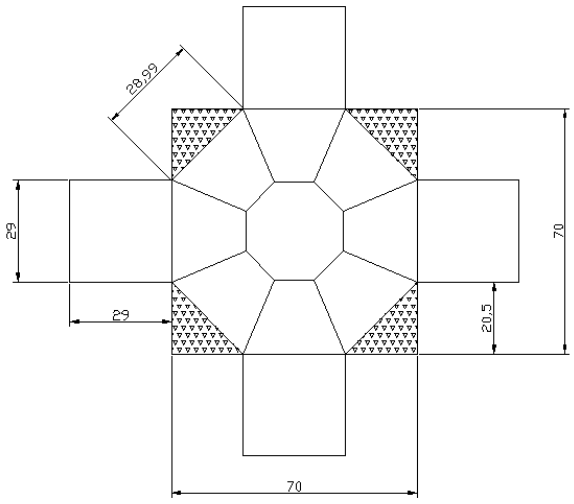

Figure 1-Plane view of a polyhedron with 26 faces, measured in mm

The specimens used in this research were larger than those used by Bucur (1984, 1983) and Ozyhar et al. (2013). Because of the signal attenuation in wood, the effective frequency (FEFF) is different than the nominal frequency of the transducer, and the largest specimen is expected to have largest frequency lost. To obtain FEFF we analysed the waveform recorded by the equipment (Fig. 2) and used the time difference (Δt) between two successive wave oscillations or picks (FEFF = 1/t). To minimise the effects of wave propagation in a finite medium, the distance between the transducers must be greater than the wavelength (λ) (Bucur 2006, Trinca and Gonçalves 2009, Kohlhauser and Hellmich 2012). Some researchers (Bucur 2006, Oliveira et al. 2006, Trinca and Gonçalves 2009) reported that values among 3 to 5 λ indicate good conditions for the ultrasound test. Considering the geometry and dimensions of the specimens used in this research and although the effective frequency was smaller than the nominal frequency, the theoretical aspects were observed, and the distance between the transducers was greater than 5 λ in all measurement directions (Table 1). Bucur and Böhnke (1994) and Trinca and Gonçalves (2009) indicated to the importance of the propagation phenomena occurring out of the near field (N). In the case of the polyhedral specimens used in this research, the propagation length was almost 8 times the near field (Table 1).

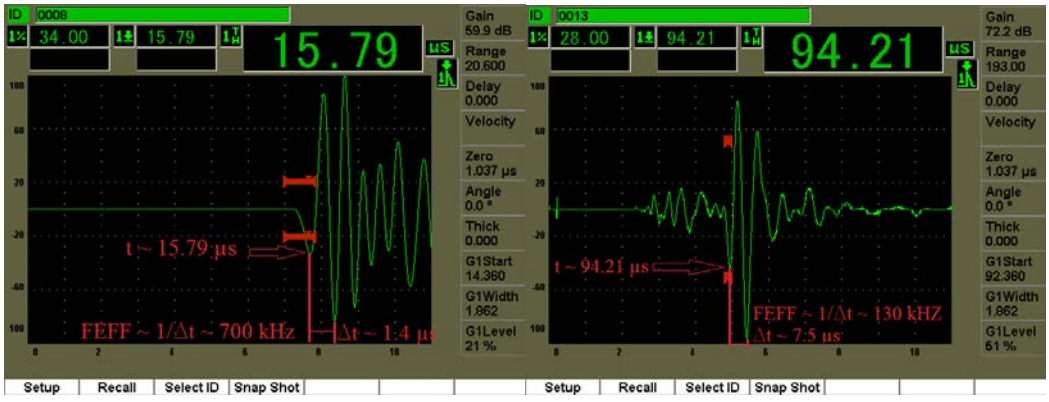

a b

Figure 2- Examples of Screen captures of Longitudinal (a) and transversal (b) waves.

The polyhedral specimens allowed us to measure the time wave propagation, and with this time and the length of the specimen, we calculate the velocities required to determine the stiffness matrix. The

time of the longitudinal wave is obtained from the arrival of the first signal (Figure 2a). For the transversal transducer, the equipment shows the two types of waves – longitudinal and transversal (Figure 2b). The longitudinal wave arrives firstly, represented by the first group of signals. After the reduction of signal amplitude, there are a new peak; which represents the arrival of the transversal waves (Figure 2b). So, the time of the transversal wave is obtained on this second peak (Figure 2b).

Table 1: *Average values of velocity (V in* $m.s^{-1}$*), effective frequency (FEFF in* kHz*), wave length (*λ *in* mm*), relation between propagation length (L) and wave length and near field (N in mm) in measurements obtained on different directions (LL, RR, TT, LR, LT, RT,* LR_{45}*,* LT_{45}*,* RT_{45}*) of the polyhedral specimen*

	LL	RR	TT	LR	LT	RT	LR_{45}	LT_{45}	RT_{45}
V	4835	2188	1594	1616	1306	763	1705	1358	853
EFFF	800	400	200	200	200	150	200	150	100
λ	6.04	5.47	7.97	8.08	6.53	5.09	8.53	9.05	8.53
L*/λ	11.6	12.8	8.8	8.7	10.7	13.8	8.2	7.7	8.2
N	7.0	7.7	5.3	5.2	6.5	8.3	5.0	4.7	5.0

*nominal propagation length = 70 mm in all directions of the polyhedral specimen

$N = \phi^2/4\lambda$ were ϕ = diameter of the transducer element (informed by the transducer manufacturer) = 13 mm

The velocities were: V_{LL}, V_{RR}, and V_{TT} for longitudinal waves measured in the axial direction; V_{RT}, V_{TR}, V_{LR}, V_{RL}, V_{TL}, and V_{LT} for transverse waves measured in the axial direction with polarisation along the perpendicular axes; and V_{QLR}, V_{QRT}, and V_{QLT} for quasi-transverse waves measured with 45^o angular displacement within the plane. The first subscript letter on the velocity names corresponds to the direction of wave propagation, and the second letter corresponds to the polarisation direction. For quasi-transversal waves, the polarisation was in the corresponding measuring plane. The tests were performed using direct measurements.

The stiffness matrix [C] was determined based on the velocities and by using the Christoffel tensor (Bucur 2006).

The compliance matrix [S] was determined as the inverse of the stiffness matrix $[C]^{-1}$.

Compression tests

Compression tests were conducted using a testing frame with a 200kN load cell, and data were collected using a Quantum X-HBM data acquisition system and Microtest data collection software. To measure the strain during testing, strain gauges (Micro-Measurements C2A-13-250LW-350 and C2A-13-250LT-350) were placed on the specimens according to their different arrangements in or out of the axes.

The specimens positioned in the longitudinal axis were tested under compression according to the UNE 56535 standard for the determination of compression stress parallel to the grain. For this arrangement, the constants E_L, ν_{LR} and ν_{LT} were obtained.

The specimens positioned in the radial and tangential directions were tested according to UNE 56542 standard for the determination of compression stress perpendicular to the grain. For this arrangement, the constants E_R, ν_{RL}, ν_{RT}, E_T, ν_{TR} and ν_{TL} were obtained.

Finally, the specimens positioned in the inclined longitudinal-tangential, tangential-radial and longitudinal-radial planes were tested according to UNE 56542. For this arrangement, the constants G_{LT}, G_{TR} and G_{LR} were obtained, respectively.

To determine the elastic constants, the data were analysed using Microsoft Excel, and lines with R^2 above 0.99 were fitted to the ε/σ graphs. Equations aporting by Gonçalves et al. (2011a) were used to determine elastic constants.

The Young's moduli in the axial direction (E_L, E_R and E_T) were determined from the slope of the stress/strain curve (σ/ε) between 20 - 60% of the maximum stress with R^2 above 0.99.

Bending tests

Static bending tests were performed on the 13 beams (70x150x3000 mm) from which the polyhedral and prismatic specimens were cut. The bending tests were performed according to the UNE-EN 408:2011 standard to obtain the longitudinal Young's modulus for each beam.

Results and Discussion

The stiffness term C_{LL} (dynamic modulus attending to Iñiguez, 2007) obtained from the ultrasound test and the E obtained from the bending test were highly correlated (R^2= 0.89) what agrees well with the values obtained by Iñiguez (2007) who reports correlation coefficients of 0.74 for other species. As expected and commented by Ozyhar et al (2013) and Gonçalves et al (2011a and 2014), the values of C_{LL} are larger than values obtained by static tests.

The average modulus of elasticity obtained from the bending tests of the 13 beams was 10675 MPa (CV of 18.6%). This result is 2.9% less than the average modulus (E_L) obtained by ultrasound (10985 MPa and CV = 23.2%) using the 13 polyhedron extracted from the same beams. The t-test (95% confidence level) applied to the 13 pairs of values shows, that there are no significant differences between the moduli of elasticity determined by the ultrasound or by bending tests (P-value = 0.177).

To compare all the elastic parameters we must use the results of the compression tests. The results of compression tests and ultrasound tests are numerically similar for E_L, E_R, E_T, G_{TL} and G_{LR} (Table 2). The means were not significantly different between both methods (ultrasound and compression) for any constant (Table 2). For the shear modulus (G_{RT}) and Poisson's ratios (ν_{RL}, ν_{LR}, and ν_{TL}), attention must be given to the statistical equivalence because of the large coefficients of variation (Table 2) that affect the statistical analysis (difference of means). In the case of G_{RT}, the large variability confirms discrepancies observed by other authors (Kohlhauser and Hellmich 2012) in static shear testing.

Gonçalves et al. (2011a and 2014) obtained statistical equivalence between the modulus of elasticity (E_L, E_R and E_T) and shear modulus (G_{TR}, G_{TL} and G_{RT}) using compression and ultrasound tests for tree species. The results for the moduli in the longitudinal direction (E_L) obtained using ultrasound (complete stiffness matrix) and compression tests varied from 1% to 4% depending on the species, which is very similar to that obtained by us (2.2%) for Castanea sativa (Table 2). Ozyhar et al (2013) also obtained all of the elastic constants for Fagus sylvatica using ultrasound on cubic specimens, and their results were in agreement with those obtained by other authors (literature data). Longo et al (2012) used resonant ultrasound spectroscopy (RUS) on cubic specimens of Fagus sylvatica and obtained the full stiffness matrix. The results for the diagonal elements of the stiffness matrix obtained by Longo et al (2012) are in agreement with the elements of the stiffness matrix obtained by RUS and values from literature data; however, the authors did not calculate or compare the elastic constants (longitudinal modulus, shear modulus and Poisson ratio). El Mouridi et al (2011) used contact ultrasound on spherical samples and obtained 28.6%, 12.5%, and 4.2% differences with predicted values (Guitard 1987) for C_{11}, C_{22} and C_{33}, respectively.

Using the intervals suggested by Bodig and Jayne (1982), any constant obtained by ultrasound and compression tests presented values far outside of the expected range (Table 3).

The differences between the results proposed by Arguelles et al. (2000) for hardwood from Spain and the results obtained for Castanea sativa using both methods (ultrasound and compression) do not allow us to define a best method because each presents small differences for the half elastic constants.

Table 2: Average Results for modulus of elasticity in longitudinal (E_L), radial (E_R) and tangential (E_T) directions; shear modulus in tangential-radial (G_{TR}), tangential-longitudinal (G_{TL}) and longitudinal-radial (G_{LR}) planes and Poisson ratios on tangential-radial (ν_{TR} and ν_{RT}), tangential-longitudinal (ν_{TL} and ν_{LT}) and longitudinal-radial (ν_{RL} and ν_{LR}) planes obtained from Ultrasound and compression tests

Test	E_L	E_R	E_T	G_{TR}	G_{TL}	G_{LR}	ν_{RL}	ν_{TL}	ν_{LR}	ν_{TR}	ν_{LT}	ν_{RT}
Ultrasound	9973	1441	790	299	760	1139	0.08	0.05	0.60	0.39	0.66	0.70
	(22.3)	(27.7)	(21.5)	(24.5)	(14.8)	(17.9)	(18.7)	(20.2)	(50.9)	(16.5)	(43.2)	(3.6)
Compression	9757	1336	707	485	822	1082	0.08	0.04	0.47	0.47	0.52	0.82
	(29.6)	(19.5)	(6.6)	(52.9)	(24.5)	(26.6)	(55.0)	(66.1)	(3.7)	(10.8)	(11.8)	(19.1)
Dif. (%)	2.2	7.9	11.7	62.2	8.2	5.3	0.00	25.0	27.7	20.5	26.9	17.1
Statistical Differences	-2084 +2516	-396 +605	-225 +389	-801 +430	-491 +368	-1065 +1180	-0.15 +0.14	-0.07 +0.09	-0.64 +0.91	-0.17 +0.015	-0.53 +0.83	-0.54 +0.30

Values in brackets are the Coefficient of Variation (%)

Table 3: Relationship between terms of the compliance matrix (10^{-5}) obtained in this research using ultrasound and compression tests and interval obtained by Bodig and Jayne (1982)

Test	$\frac{\nu_{RL}}{E_R}$	$\frac{\nu_{LR}}{E_L}$	$\frac{\nu_{TL}}{E_T}$	$\frac{\nu_{LT}}{E_L}$	$\frac{\nu_{TR}}{E_T}$	$\frac{\nu_{RT}}{E_R}$
Ultrasound	4.58	5.04	7.20	7.31	48.11	47.74
compression	6.06	4.82	5.66	5.33	66.5	61.4
Bodig and Jayne	1.52 to 5.13	1.34 to 4.27	1.79 to 6.14	1.59 to 6.48	20.68 to 128	21 to 104

Table 4: Values suggested by Arguelles et al. (2000) for elastic constants of hardwood from Spain and differences (%) between these values and the mean values of elastic constants obtained by ultrasound and by compression tests to *Castanea sativa*

	E_L	E_R	E_T	G_{RT}	G_{LT}	G_{LR}	ν_{RL}	ν_{TL}	ν_{LR}	ν_{TR}	ν_{LT}	ν_{RT}
Arguelles et al. (2000)	10674	$E_L/8$	$E_L/13.5$	366	971	1260	0.048	0.033	0.39	0.38	0.46	0.67
Ultras. Arguelles et al. (2000)	2.9	8.8	2.2	42.4	23.2	11.4	37.5	69.7	42.1	2.2	74.6	3.4
Comp. Arguelles et al. (2000)	9.4	0.0	11.8	32.5	18.1	16.4	66.7	21.2	20.5	23.7	13.0	22.4

Where: E_L, E_R,E_T, G_{RT}, G_{LT}, G_{LR} in $N \cdot mm^{-2}$

Our research and the work of other authors (Gonçalves et al. 2011a and 2014, Ozyhar 2013, Longo et al. 2012, El Mouridi et al 2011, Dahmen et al. 2010) shows that although the longitudinal and shear moduli (or their corresponding stiffness parameters on the stiffness diagonal) present good agreement with those obtained using static methods, the results of the Poisson's ratio (or their corresponding parameters of off-diagonal stiffness) are less precise. The results are affected by the deviation of the

energy flux because the thickness of the specimen increases the influence of the grain and ring orientations on the wave propagation. This behaviour is well explained by Kohlhauser and Hellmich (2012) who show that the ultrasound measurements on non-principal directions are very sensitive to errors, yielding errors in the non-diagonal components (off-diagonal stiffness) and affecting the calculation of the Poisson's ratio. A combined mechanical-ultrasonic method is proposed by Kohlhauser (2012) to obtain the Poisson's ratio of spruce, and the results agree well with results obtained from mechanical measurements in this species.

Conclusions

The new way to characterize the wood of Castanea sativa, proposed in this research, provides important scientifically contribution. The use of this specie in rehabilitation of traditional structures is growing in Spain, due to its natural durability and dimensional stability. Increase this use and open new markets is very important to the forest sector from North of Spain, where this specie is largely found. The ultrasound wave propagation method shows great potential to determine the mechanical properties of Castanea sativa, presenting values compatible with those obtained from a static compression method. The polyhedral specimen allows the elastic constants to be easily obtained because only one specimen is necessary, besides is fast, reliable and economic system. To following contributions, we are working to propose an optimization of the specimen. We are also applying the method to other species of wood and to engineered wood.

References

AENOR (1988). UNE 56542:1988; Características físico-mecánicas de la madera. Determinación de la resistencia a la compresión perpendicular a las fibras (Physical-Mechanical Properties of Wood. Determination of Compression Strength Perpendicular to the Grain.) AENOR, Madrid

AENOR (1977). UNE 56535:1977; Características físico-mecánicas de la madera. Determinación de la resistencia a la compresión. (Physical-Mechanical Properties of Wood. Determination of axial compression strength.) AENOR, Madrid

AENOR (1978). UNE 56528:1978; Características físico-mecánicas de la madera. Preparación de probetas para. (Physical-Mechanical Properties of Wood. Preparation of Specimens for Testing.) AENOR, Madrid

AENOR (2011). UNE EN 408:2011; Estructuras de madera. Madera aserrada y madera laminada encolada para uso estructural. Determinación de algunas propiedades físicas y mecánicas. (Timber Structures. Sawn and Glued Laminated Timber for Structural Use. Determination of some Physical-Mechanical Properties.) AENOR, Madrid

Argüelles Álvarez, R.; Arriaga Martitegui, F.: Martínez Calleja, J. (2000) Estructuras de madera. Diseño y cálculo (Wooden structures. Design and calculation). AITIM, Madrid, p 712

Bodig, J.; Jayne, B.A. (1981) Mechanics of wood and wood composites. Van Nostrand Reinhold, New York, p 419

Bucur, V. (1983) An ultrasonic method for measuring the elastic constants of wood increment cores bored from living trees. Ultrasonics 21: 116-126

Bucur, V.; Böhnke, I. (1994) Factors affecting ultrasonic measurements in solid wood. Ultrassonics 32(5): 385-390

Bucur, V. (2006) Acoustics of wood. 2nd Edn. Springer. New York p 394. 978-3540261230

Bucur, V.; Archer, R. (1984) Elastic-Constants for Wood by an Ultrasonic Method. Wood Sci Technol 18: 255-265

Dahmen ,S. et al. (2010) Elastic constants measurement of anisotropic Olivier wood plates using air-coupled transducers generated lumb wave and ultrasonic bulk wave. Ultrasonics 50: 502-507

El Mouridi et al. (2011) Searching for material symmetries in the burr wood of thuja by a direct contact ultrasonic method on spherical samples. Maderas. Ciencia y tecnología 13 (3): 285-296

François, M.L.M. (1995) Identification des symétries matérielles de matériaux anisotropes (Identification of the material symmetries of anisotropic materials) (Doctoral dissertation, Université Pierre et Marie Curie-Paris VI)

Gonçalves, R.; Trinca, A.J.; Cerri, D.G.P. (2011a) Comparison of Elastic Constants of Wood Determined by Ultrasonic Wave Propagation and Static Compression Testing. Wood Fiber Sci 43: 64-75

Gonçalves, R.: Trinca, A.J.; Ferreira, G.C.S. (2011b) Effect of coupling media on velocity and attenuation of ultrasonic waves in Brazilian wood. J Wood Sci 57(4): 282-287

Gonçalves, R.; Trinca, A. J.; Pellis, B.P. (2014). Elastic constans of wood determined by ultrasound using three geometries of specimens. Wood Sci Technol 48: 269-287.

Guitard, D. 1987. Mécanique du matériau bois et composites (Mechanic of wood and composites). Cépadues, France. 118-127.

Iñiguez Gonzalez, G. (2007) Clasificación mediante técnicas no destructivas y evaluación de las propiedades mecánicas de la madera aserrada de coníferas de gran escuadría para uso estructural (Classification by nondestructive techniques and evaluation of mechanical properties of sawn softwood large cross for structural use)(Doctoral disersation) . Universidad Politécnica de Madrid. Madrid

Keunecke, D.; Sonderegger, W.; Pereteanu, K.; Lüthi, T.; Niemz, P. (2007) Determination of Young's and shear moduli of common yew and Norway spruce by means of ultrasonic waves. Wood Sci Technol 41: 309-327

Kohlhauser, C.; Hellmich, C. (2012) Determination of Poisson's ratios in isotropic, transversely isotropic, and orthotropic materials by means of combined ultrasonic-mechanical testing of normal stiffnesses: application to metals and wood. Eur J Mech A-Solid 33: 82-98

Longo, R. et al. (2012) Wood elastic characterization from a single sample by resonant ultrasound spectroscopy. Ultrasonics 52: 971-974

Oliveira, F.G.R.; Sales, A.; Lucchette, F.F.; Candian, M. (2006) Efeito do comprimento do corpo de prova na velocidade ultrassonica em madeiras (Effect of specimen lengh on ultrasonic velociy of wood). Rev Árvore 30(1): 141-145

Ozyhar, T.; Hering, S.; Sanabria, S.J.; Niemz, P. (2013) Determining moisture-dependent elastic characteristics of beech wood by means of ultrasonic waves. Wood Sci Technol 47(2): 329-341.

Preziosa, C. (1982). Méthode de détermination des constantes élastiques du matériau bois par utilisation des ultrasons (Method for determining elastic constants of wood material by use of ultrasound) (Doctoral dissertation). Université d'Orléans, Orléans

Preziosa, C. ; Mudry, M. ; Launay, J. ; Gilletta, F. (1981) Détermination des constantes élastiques du bois par une méthode acoustique goniométrique (Determination of the elastic constants of wood by an acoustic method using immersion). CR Acad.Sc.Paris, Série II 293: 91-94

Trinca, A.J.; Gonçalves, R. (2009) Efeito das dimensões da seção transversal e da frequência do transdutor na velocidade de propagação de ondas de ultrassom na madeira (Effect of the transversal section dimensions and transducer frequency on ultrasound wave propagation velocity in wood). R. Árvore 33 (1): 177-184

Vega, A.; Dieste, A.; Guaita, M.; Majada, J.; Baño, V. (2012) Modelling of the mechanical properties of Castanea sativa Mill. structural timber by a combination of non-destructive variables and visual grading parameters. Eur J Wood Wood Prod, 70(6): 839-844

Zimmer, J.; Cost, J.R. (1970) Determination of the elastic constants of a unidirectional fiber composite using ultrasonic velocity measurements. J Acoust Soc Am 47: 795-803.

Ultrasonic testing with different orientations throughout cross section of *Eucalyptus grandis*

Lourenço Panosso Perlin
PhD Student of Civil Engineering Department, Federal University of Santa Catarina – UFSC, Florianópolis, Santa Catarina, Brazil, lourencopp@gmail.com

Roberto Caldas de Andrade Pinto
PhD Professor of Civil Engineering Department, Federal University of Santa Catarina – UFSC, Florianópolis, Santa Catarina, Brazil, rcapinto@gmail.com

Ângela do Valle
PhD Professor of Civil Engineering Department, Federal University of Santa Catarina – UFSC, Florianópolis, Santa Catarina, Brazil, angela.valle@ufsc.br

Abstract

Wood, as an orthotropic material, shows different mechanical behavior depending on the analyzed angle with its main axes. Since wood is also hygroscopic, its mechanical properties are also function of the humidity rate. This research investigates the mechanical properties of *Eucalyptus grandis* specimens using ultrasound. Ultrasonic readings through a cross section were performed at different angles with the tangential axis at several moisture content. The gathered results were compared to the Hankinson equation, allowing to model wood mechanical behavior.

Keywords: ultrasound, velocity, humidity, transversal.

Introduction

Currently, the use of wood as a structural material in civil engineering applications is not as frequent as it could be. There are several reasons for this low use, among which some stand out: insufficient technology dissemination of their structural behavior; lack of qualified professionals for project design; lack of skilled workers; susceptibility to fungal decay and insect attack; action of water and the presence of cracks and nodes (Calil Junior and Lahr, 2010; Pfeil and Pfeil, 2003).

As far as the physical properties are concerned, wood can be regarded as an anisotropic material. Hence, its elastic properties vary depending on the reference system considered. However, with the choice of a particular reference system, the axes of symmetry can be taken into account, allowing to analyze timber as an orthotropic material. As a result, in order to investigate the mechanical properties of wood, several experimental methods should be used. These methods can be classified in two major groups: destructive and nondestructive ones. The latter ones have the advantage of not causing any damage to the element under analysis, which allow an inspected structure to remain in service with a consequent reduction of time and cost. Among the various nondestructive test methods to be used in timber structures, the ultrasonic technique stands out.

The propagation of the ultrasonic pulse is affected by many factors including wood species, plane wave propagation, specific gravity, existence of empty regions or biological deterioration, humidity level, temperature and specimen geometry (Bucur, 2006).

An experimental research with four species carried out by Sakai et al. (1990), evidenced that the ultrasonic pulse propagation velocity is influenced by the relationship between the moisture content and the fiber saturation point (FSP). FSP is considered to be reached when wood cell cavities contain no liquid water, but the cell walls are saturated with moisture. Figure 1 displays the ultrasonic pulse velocity in the longitudinal direction for different species at various moisture content.

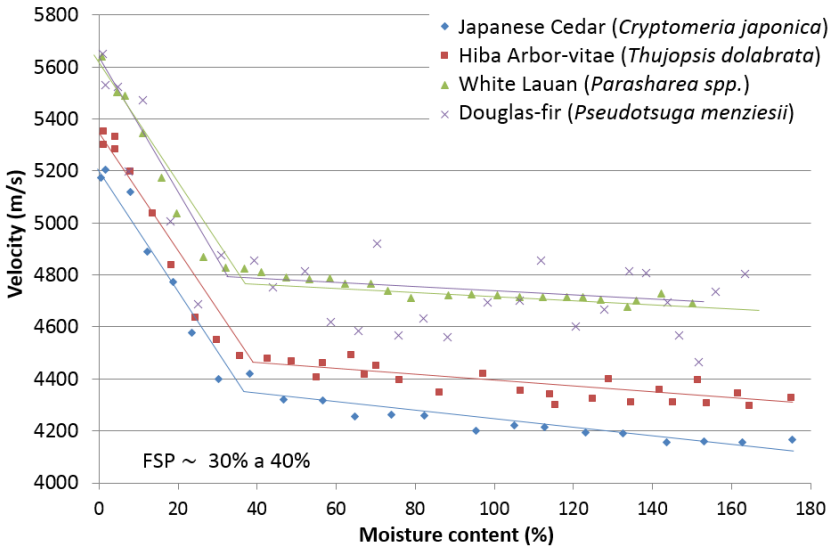

Figure 1 — Ultrasound pulse velocity variation in the longitudinal direction due to the moisture content
Source: modified from Sakai et al. (1990)

As can be noted in Figure 1, the behavior of ultrasonic pulse velocity is different depending on whether the moisture content is lower or higher than the FSP. Physical and mechanical properties change when the moisture content value is lower than FSP; in that case there is no inward or outward diffusion of free water inside the wood. On the other hand, when the moisture content is higher than the FSP, free water moves inside wood cells, reducing its influence on wood properties (Bucur, 2006). Figure 1 shows a much greater rate of change in the pulse velocity values when moisture is lower than the FSP.

The ultrasonic pulse velocity values range from 5000 to 6000 m/s when the pulse propagates parallel to the grain direction of solid wood, or in the longitudinal direction (V_L). When the propagation occurs perpendicular to the grain direction, such values are usually much smaller in the range of 1000 to 2500 m/s. In that case, the pulse velocity also changes if the propagation occurs in the radial or tangential to the growth rings. The radial velocity (V_R) is approximately 50% higher than the tangential velocity (V_T) (Beall, 2002).

Using the ultrasonic test, Amstrong et al. (1991) *apud* Bucur (2006) proposed the use of the Hankinson empirical equation to model the ultrasonic pulse velocity in the longitudinal-radial plane, as shown in Equation 1.

$$V_\theta = \frac{V_R * V_L}{V_R * sen^2(\theta) + V_L * cos^2(\theta)} \quad (1)$$

where V_R is the velocity at radial axis, V_L is the velocity at longitudinal axis and V_θ is the velocity at θ degree from longitudinal axis.

Inspired by the Armstrong research, this research aims to confirm the possibility of use the Hankinson equation to also model the behavior of ultrasonic pulse velocity in the radial-tangential plane, according to Equation 2.

$$V_\alpha = \frac{V_T * V_R}{V_T * sen^2(\alpha) + V_R * cos^2(\alpha)} \quad (2)$$

where V_α is the velocity at α degree from the tangential direction.

Therefore, an experimental investigation was designed. Several ultrasonic readings at different orientations relative to the transverse axes were performed on pieces of *Eucalyptus grandis*. Such measurements were carried out with the specimen at different moisture content values in order to investigate the influence of moisture content on the ultrasonic measurements.

Materials and methods

Specimens preparation and characterization

Eucalyptus grandis logs, with 25 cm of diameter, were extracted from the same tree and placed in the laboratory (Figure 2 (a)). After two months of natural air drying, transverse discs were cut (Figure 2b).

(a) (b)

Figure 2 — Logs used in the research (a) cut in the field (b) making the transverse discs

From these discs, four specimens were extracted with dimensions of $3.9 \times 3.9 \times 3.8\ cm$, $4.0 \times 4.2 \times 3.8\ cm$, $5.5 \times 4.9 \times 4.7\ cm$ *and* $4.0 \times 3.4 \times 5.9\ cm$. These specimens differ from their angles between one face and tangential axis of 0°, 15°, 30° and 45°. The same specimens provide angles of 60°, 75° and 90° if used the other faces of the specimens (Figure 3).

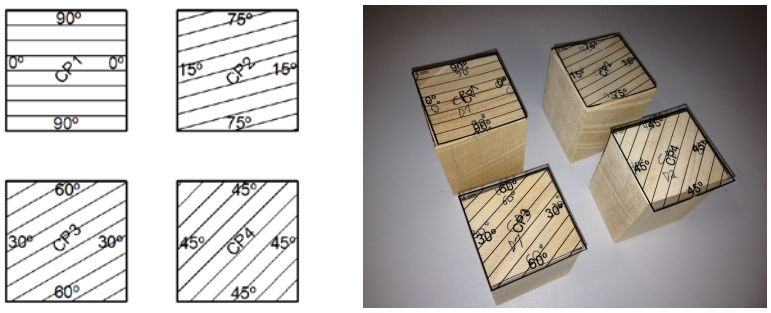

(a) (b)

Figure 3 — Grains orientation of specimens with angle identification (a) markers (b) specimens and markers

In order to define the actual species of wood tested, the micrograph technique, with Microm HM 400 was used to create the slides together with the photomicroscope Leica DM 2500 to generate the image. The microscopic technique used Safranin, which makes the lignin appears in red color, and Astra, which makes the cellulose appears in blue color.

Moisture content and ultrasound testing

The specimens were stored for five months in a box, without ventilation, in order to promote a slow drying. The mass of each specimen was monitored approximate every 10 days until no further mass loss was measured.

After reaching a constant moisture content, the specimens were oven-dried at 103 °C ± 2 °C, as established by NBR7190:1997. The dry mass of the specimens was obtained when no appreciable weight change occurred. The value of dry mass of each specimen was used to determinate its moisture content in each mass measurement step along the drying process.

The ultrasonic tests were performed at each mass measurement step, at all angles previously described in Figure 3. This process allows to correlate the ultrasonic pulse velocity and the moisture content of each specimens. A commercial ultrasonic equipment with a 200 kHz cylindrical transducer of 20 mm diameter was used.

The experimental values of ultrasonic velocities were then correlated to the values obtained with the modified Hankinson empirical equation (Equation 2). The values of V_T ($\alpha = 0°$) e V_R ($\alpha = 90°$), used to estimate velocities for different angles, were acquired from the ultrasound tests at angles of 0° and 90°, respectively.

Results and analysis

The used microscopic technique provided the production of photos of the slides as shown in Figure 4. The photos allowed the wood species to be classified as *Eucalyptus grandis*.

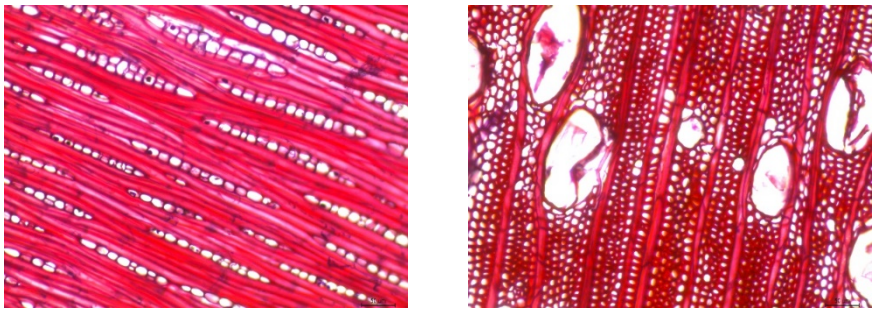

(a) (b)

Figure 4 — Micrographs of the tested wood sample magnified by 20 times (a) the tangential-longitudinal section (b) cross-section

During the initial air drying period, 64 measurements of the specimen's masses were recorded with approximate 0.4-month intervals (10 days), as shown in Figure 5.

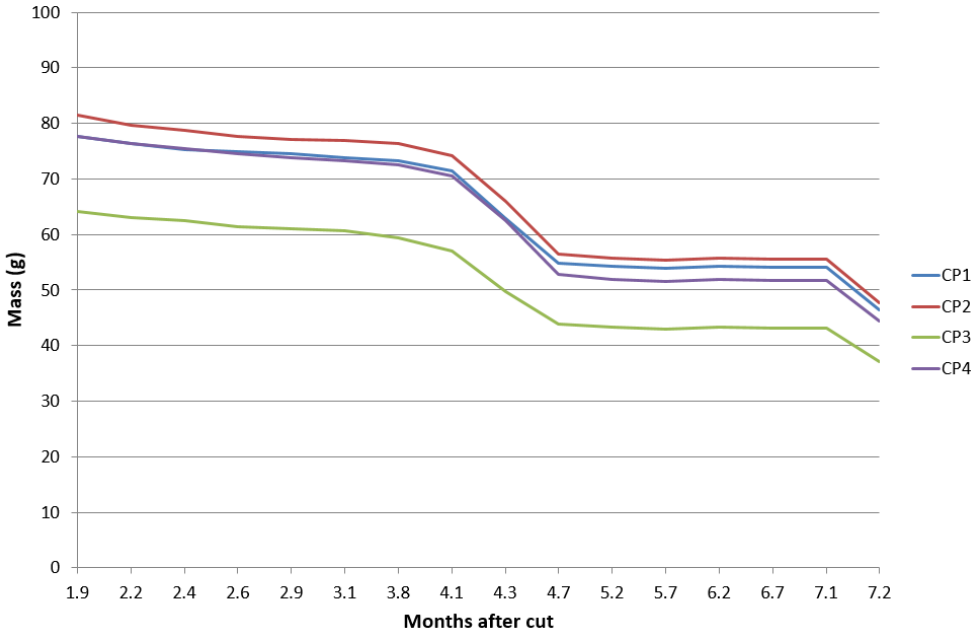

Figure 5 — Mass evolution of the specimens

From Figure 5, it can be noticed that the period of 4.1 to 4.7 months after cut, corresponded to the greatest mass loss variation of the whole drying period for all specimens. In fact, that period of time coincided with summer, and therefore increased heat intensified moisture loss rate. Between 4.7 and 7.1 months after cut there was no significant change in mass, indicating that the moisture of the wood specimens was in balance with the environment as a consequence oven-drying followed. An age of 7.2 months after cut dry mass was achieved which allowed the calculation of all moisture content of each specimens at each mass measurement step along the natural drying process (Figure 6).

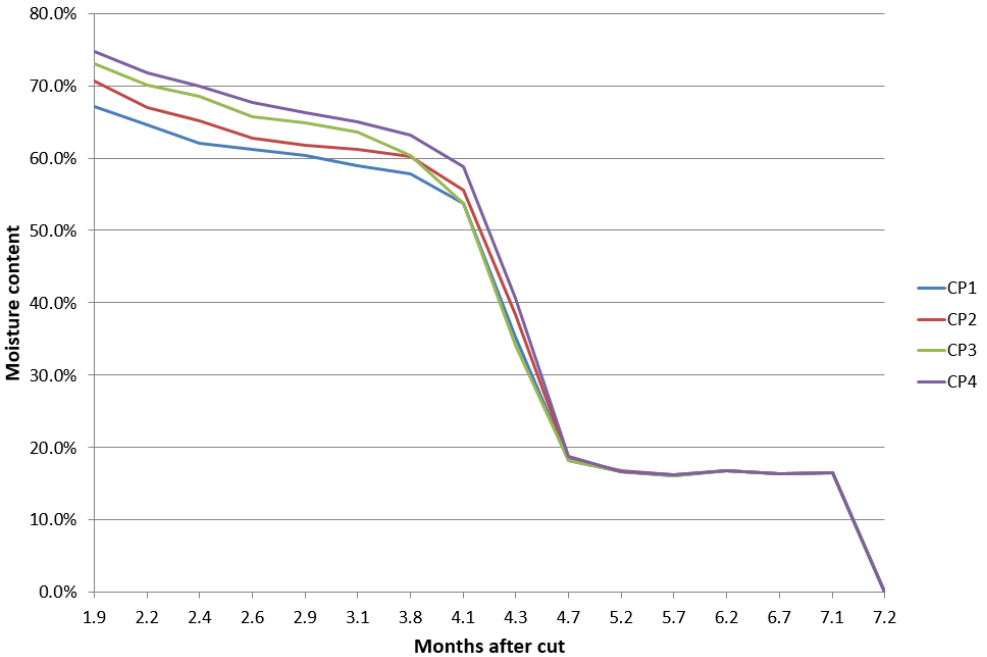

Figure 6 — Moisture content over natural drying process

The results of the ultrasound measurements at all the angles previously mentioned were correlated with each moisture content as shown in Figure 7. A total, of 256 ultrasonic readings were performed on this research.

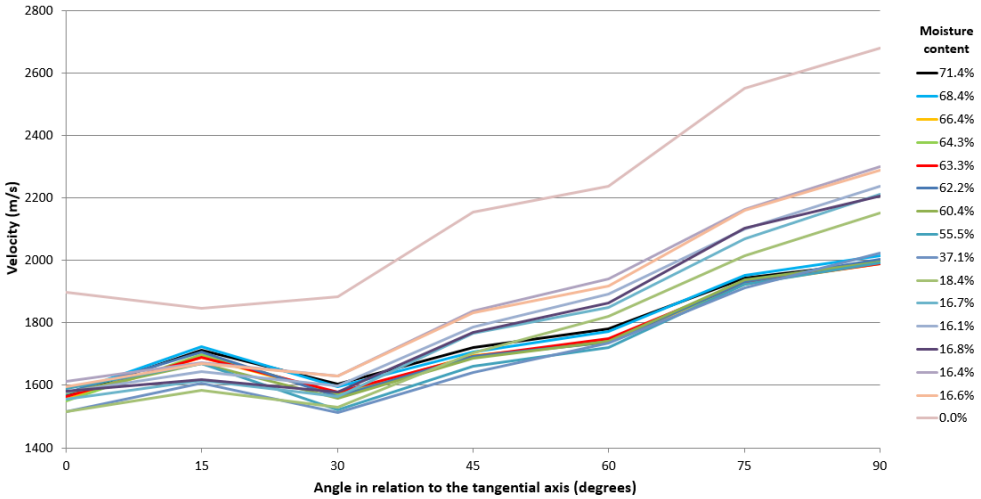

Figure 7 — Evolution of ultrasonic readings in specimens to different angles relative to the tangential axis

From Figure 7, it can be noticed that, as the wood specimens moisture content decreased, the ultrasonic pulse velocity increased. This behavior was particularly seen at 0% moisture content, where the ultrasonic pulse velocities were significantly greater than at other moisture content values.

Figure 8 presents the comparison between the Modified-Hankinson Equation (Equation 2) and the experimental values at moisture content of 0%, 16.1% and 71.4%.

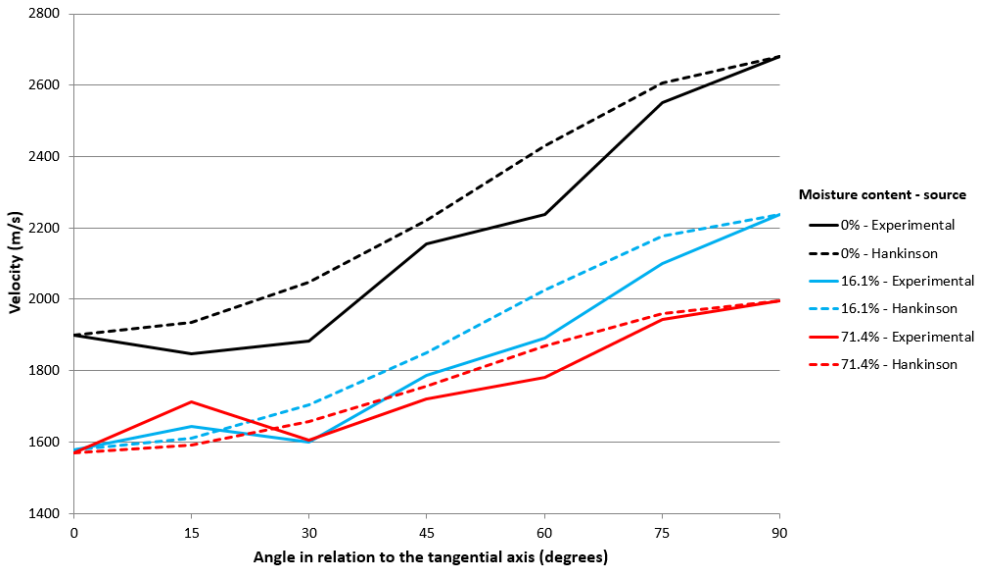

Figure 8 — Comparison between the experimental and the Modified-Hankinson curves for three different moisture contents

The comparison between the experimental and Modified-Hankinson curves shows similar behavior, even though the experimental values were lower than the Hankinson values for most of the curves.

The difference between the experimental and Modified-Hankinson values were of the order of 1% to 9%. This low magnitude would allow one to use the Modified-Hankinson equation to model the behavior of the ultrasonic pulse velocity at different angles between the longitudinal plane and the tangential direction of the timber. This conclusion applies only for the species sample of *Eucalyptus grandis* and size of the specimens investigated here. In order to be able to apply to other species and specimens dimensions, it is necessary to perform further investigations since differences in orthotropic material properties could affect this relationship.

The rate of V_T/V_R can also be correlated as a function of moisture content, as displayed in Figure 9. It is possible to identify two groups of V_T/V_R values depending on the moisture content. One is located in the neighborhood of 16% and another 65%. This behavior can be related to the fiber saturation point (FSP), which value is usually between 30% and 40%. Unfortunately, the FSP content of the tested specimens probably occurred between the period of 4.1 to 4.7 months after cut, corresponding to 55.5% and 18.4% of moisture content, which showed fast drying caused by summer heat.

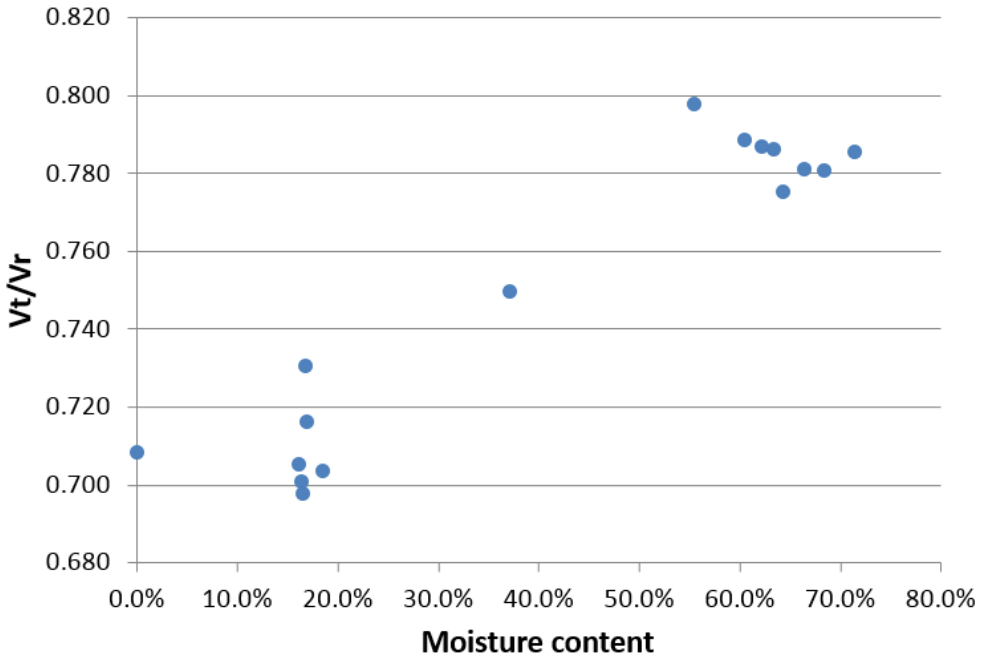

Figure 9 — Relationship between V_T/V_R and moisture content

The data in Figure 9 show a value for V_T/V_R approximately equal to 0.7 for a moisture content below fiber saturation point (FSP) and approximately equal to 0.78 for moisture content above FPS.

A similar conclusion was obtained in the thesis of Costa (2005), where, among other studies, ultrasonic readings were made in the tangential and radial axis. These readings were made in samples of *Eucaliptus citriodora*, with moisture content below and above the FSP. His results showed the existence of two defined levels of V_T/V_R, as function of moisture content. When moisture content was below FSP, the value of V_T/V_R was equal to 0.81, and above FSP equal to 0.90.

Conclusions

This paper investigated and demonstrated that there is similar behavior between the Hankinson empirical equation and experimental values for ultrasonic pulse velocity in cross section of *Eucalyptus grandis* regardless its moisture content. Such a conclusion allows one to apply the Hankinson equation when modeling the orthotropic behavior of the ultrasonic pulse velocity for this species.

It was also observed that there is variation in the relation V_T/V_R depending on the moisture content of the wood, with higher values at higher moisture content values. These results are also useful when modeling the ultrasonic pulse velocity at different planes of cross-section. For these conclusions to be extended to other species, it is necessary that the procedure applied here is tested to other types of wood.

Acknowledgments

The authors wish to thanks Professor João de Deus Medeiros, from Botany Department of Federal University of Santa Catarina, for their help in identifying the species of used wood.

References

ASSOCIAÇÃO BRASILEIRA DE NORMAS TÉCNICAS. **NBR 7190**: Projeto de estruturas de madeira. Rio de Janeiro, 1997. 107 p.

Amstrong, J.P.; Patterson, D.W.; Sneckenberger, J.E. 1991. Comparison of three equations for predicting stress wave velocity as a function of grain angle. Wood and Fiber Science. 14: 32–43.

Beall, F.C. 2002. Overview of the use of ultrasonic technologies in research on wood properties, Wood Science and Technology. 36(3), 197-212.

Bucur, V. 2006. Acoustics of Wood. New York: Springer. 393 p.

Calil Junior, C.; Lahr, F.A.R. 2010. Madeiras na construção civil. In: Isaia, G.C. ed. Materiais de construção civil e princípios de ciência e engenharia de materiais. São Paulo: IBRACON. 1712 p.

Costa, O.A.L. 2005. Velocidade de propagação de ondas de ultra-som na madeira para diferentes condições de umidade. Campinas, OR: Estadual de Campinas University. 95 p. Ph.D. thesis.

Pfeil, W.; Pfeil, M. 2003. Estruturas de Madeira. Rio de Janeiro: LTC. 224 p.

Sakai, H.; Minamisawa, A.; Takagi, K. 1990. Effect of moisture content on ultrasonic velocity and attenuation in woods. Ultrasonics. 28: 0–3.

Changes on color and wave velocity by ultrasound of Eucalyptus decayed woods.

Patrícia Soares Bilhalva Dos Santos
Chemical and Environmental Engineering Department, University of the Basque Country, San Sebastian, Spain, patricia.bilhalva@hotmail.com

Silvia Helena Fuentes Da Silva
Chemical and Environmental Engineering Department, University of the Basque Country, San Sebastian, Spain,silviahfuente@hotmail.com

Pedro Henrique Gonzalez de Cademartori
Forest Engineering Department, Federal University of Paraná and Embrapa Forestry, Curitiba, Brazil, pedrocademartori@gmail.com

Roberto Lessa Pereira
Center Engineering, Federal University of Pelotas, Pelotas, Brazil,roberto-lessa93@hotmail.com

Fernanda Regina Andrade
Forestry Engineering, Federal University of Santa Maria, Santa Maria, Brazil,fernandaalpf@gmail.com

Francieli De Vargas
Forestry Engineering, Federal University of Santa Maria, Brazil,devargasfrancieli@gmail.com

Darci Alberto Gatto
Center Engineering, Federal University of Pelotas, Pelotas, Brazil, darcigatto@yahoo.com

Jalel Labidi
Chemical and Environmental Engineering Department, University of the Basque Country, San Sebastian, Spain, jalel.labidi@ehu.es

Abstract

In this study, four non-destructive techniques methods were used to assess the natural durability of eucalypt wood exposed to field test. Wood from two *Eucalyptus* hybrid clones was exposed in a field test in southern of Brazil for 360 days. Wood samples were collected every 45 days. Changes in density, weight loss, wave propagation, dynamic modulus of elasticity and color were investigated. The main results showed *Eucalyptus urophylla x Eucalyptus grandis* wood is more susceptible to deterioration by xylophages agents than *Eucalyptus globulus x Eucalyptus grandis* wood. The highest weight loss values of wood were found after 360 days of exposure. Dynamic modulus of elasticity tends to decrease as a function of exposure time. Color variation increased with increasing time of exposure in field test.

Keywords: natural durability, dynamic modulus of elasticity, CIE L*a*b*, velocity of propagation.

Introduction

Wood is a natural, versatile and renewable material widely used in different industrial and commercial sectors. Use of wood in building is essential (Ashori et al. 2012) and represents a significant market share in many countries, especially in Northern Hemisphere.
Wood and wood-based products can be used indoor and outdoor. However, outdoor applications result in high susceptibility to the action of climatic agents (weathering) and, consequently, photodegradation (Feist and Hon 1984). Among the damages caused by weathering, surface cracks can significantly changes wood properties and its durability in service. Furthermore, wood exposure in indoor or outdoor increase the susceptibility to xylophages' agents, which deteriorate wood chemical components (hemicelluloses, cellulose and lignin) and could affect its integrity.
Natural durability of wood depends to the geographical location of exposure, since climatic conditions and soil micro flora influences durability in ground. (Brischke et al. 2013). Thus, field tests are an interesting alternative to expose wood in natural and more realistic conditions (Meyer et al. 2014).
Eucalypt is one of the most important commercial wood in Brazil. However, natural durability of eucalypt wood is commonly lower than tropical woods. Thus, genetic improvement of *Eucalyptus* species are necessary to increase both quality and homogeneity of wood.
This study aimed to characterize some physical properties and color changes of eucalypt wood after field test exposure. Wood from two eucalypt hybrid clones (*Eucalyptus globulus x Eucalyptus grandis* and *Eucalyptus uruphilla x Eucalyptus grandis*) are exposed to decay for 360 days in southern of Brazil. Changes in density, wave propagation, dynamic modulus of elasticity and color were investigated by non-destructive techniques.

EXPERIMENTAL METHODS

Selection and preparation of material

Two hybrid clones - *Eucalyptus globulus x Eucalyptus grandis* (GG) and *Eucalyptus urophylla x Eucalyptus grandis* (UG) with 11 years old were selected from a homogenous plantation located in the city of Tapes (30º40'24"S, 51º23'45" W), Rio Grande do Sul, Brazil.
Central plank was cut from each tree as described in ASTM D5536-94. Thickness of each central plank was reduced from 8 to 6 cm. Wood samples were prepared and were kept in a climatic chamber (20°C and 65% of relative humidity) to reach the equilibrium moisture content.

Installation of field test

Field test was installed in the city of Morro Redondo, Rio Grande do Sul (S 31º58'18"; W 52º63'55", sea level of 245 m. According to Köppen classification, climate in the experimental site is Cfa (Humid Subtropical Mild) with no dry season and hot summer. Average temperature during the warmest months are over 22°C and average temperature of the coldest month is under 18°C. The average annual temperature is 18.6°C. Soil temperature at 5 cm is 20.3 °C and the average annual rainfall is 1445 mm (Embrapa - CPTAC, 2015).
Local of installation was a forest plantation of *Eucalyptus* spp. with six years planted with spacing of 2 x 3 m. Wood samples were put in a vertical position with half length (12.5 cm) below the soil. Spacing between samples were 10 cm and blocks 100 cm. Seven wood samples of each species were collected every 45 days for 360 days. All the samples were cleaned with a brush and kept in a climatic chamber at 20°C of temperature and 65% of relative humidity. Weight loss (%) was determined by Eq. 1.

$$WL(\%) = \frac{(w_i - w_0)}{w_i} * 100 \quad (1)$$

In which: WL= weight loss (%), Wi = initial weight and W0= final weight

Ultrasonic evaluation

Wave propagation time was measured by ultrasound equipment (μs). Three readings in longitudinal direction were performed using dry point type transducers with 54 Hz frequency. Wood samples were tested before and after the field test exposure.
Dynamic modulus of elasticity was determined using the velocity of ultrasound wave (V) and the wood density (D) as described in Eq. 2. The loss of ultrasonic wave was determined by Eq. 3.

$$E_d = V^2 * D \quad (2)$$

$$VL(\%) = (V_i - V_0)V_i * 100 \quad (3)$$

In which: VL = Loss of ultrasonic wave velocity (%) Vi = initial velocity (m.s-1) and V0 = final velocity (m.s-1).

Color measurement

Color changes were measured in radial and tangential section of five samples by *CIEL*a*b** method. Parameters L* (lightness), a* (green-red chromatic coordinate) and b* (blue-yellow chromatic coordinate) were determined using a colorimeter (Konica Minolta- CR-400) with opening sensor of 8 mm. Colorimetric parameters were measured in three different regions, above ground (region 1), ground zone (region 2) and below soil (3).

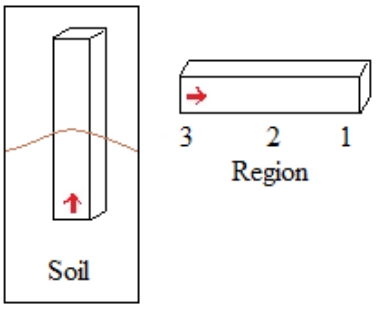

Figure 1—Scheme of color measurement in different positions in wood sample.

Results and Discussion

Physical properties

Density of UG wood (492.4 kg/m³) was higher than value found in GG wood (537 kg/m³). Both wood densities presented similar values observed in previous studies (Santos, 2009; Queiroz et al. 2004; Milagres 2009). However, after field test wood density decreased, especially after 360 days exposure time (Figure 3)
Weight loss increased with increasing time of exposure (Figure 3). Main changes in weight loss of both woods occurred from 135 days of exposure. UG wood was more susceptible to decay than GG wood.

This high susceptibility to decay could be attributed to soil conditions, humid climate and abundant presence of xylophages' organisms in the environment. In contrast of other countries, Brazil has a propitious climate for development of these organisms, which results in high rating of decay.

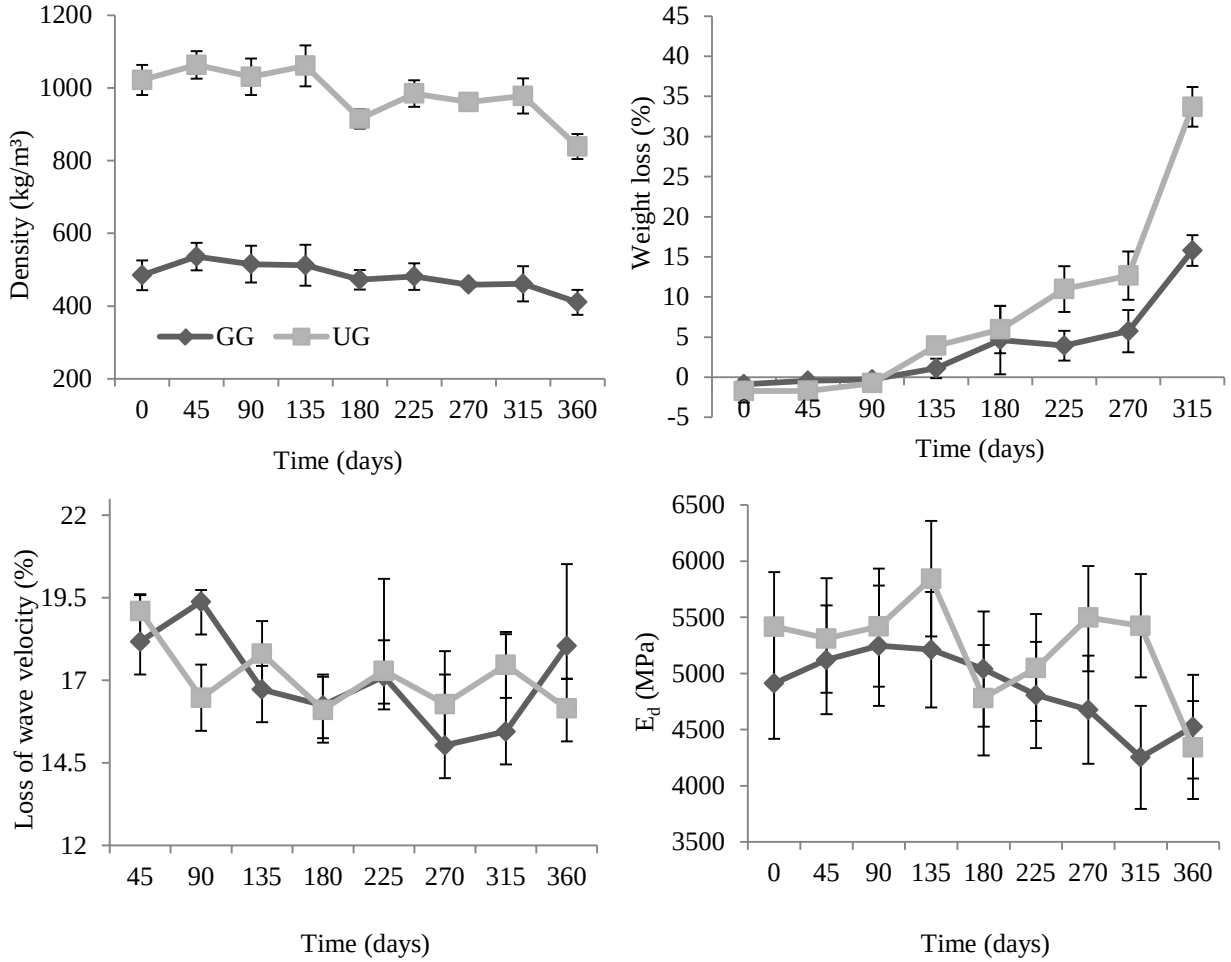

Figure 2— Density, weight loss, loss of wave velocity and E_d of eucalypt woods as a function of exposure time in field test.

Loss of wave velocity was similar in both woods (around 16%). After exposure in the field test, elasticity of wood tends to decrease in comparison to unexposed wood (Figure 4). Liñan et al. (2004) affirmed elasticity loss of 10-30% implies in a maintenance or replacement of wood pieces, which could be suggested to UG and GG decayed wood if in service. Dynamic modulus of elasticity (E_d) showed a tendency to decrease as a function of exposure time. The lowest values of E_d were found after 360 days of exposure. This decrease of E_d corroborates with the results found by Mattos et al. (2013).

Color changes

Exposure in field testing for 360 days significantly influenced wood color. Darkening of wood is verified as a function of time of exposure. Ground zone was the most affected region on the sample due to intense activity of xylophages' agents in comparison to region 1 and 3.

Table 2—Effect of color parameters for two wood species as a function of exposure time.

Time (days)	UG									GG								
	Region									Region								
	1			2			3			1			2			3		
	L*	a*	b*	L*	a*	b*	L*	a*	b*	L*	a*	b*	L*	a*	b*	L*	a*	b*
0	65.20	5.15	15.55	66.19	5.04	15.54	65.21	5.12	15.58	65.54	4.76	15.12	66.19	5.05	15.07	66.06	4.76	15.14
45	60.37	4.95	17.33	53.58	5.19	16.12	55.87	5.26	16.07	60.74	5.15	17.47	56.49	5.13	16.68	59.05	5.14	17.22
90	61.31	4.43	17.09	53.46	5.02	15.97	52.80	5.44	15.91	59.68	4.80	16.71	57.03	4.93	16.28	58.77	4.64	16.17
135	57.63	4.58	16.44	52.13	4.97	15.48	50.26	4.91	14.75	55.60	4.09	15.36	54.14	4.41	15.04	56.70	4.46	15.83
180	57.53	4.12	15.55	52.17	4.68	15.12	55.32	5.37	16.59	61.42	3.80	15.72	55.02	4.23	14.94	57.31	4.87	15.82
225	51.94	4.70	14.70	49.49	4.79	14.01	54.78	4.42	14.84	58.08	3.72	15.01	47.00	4.96	14.23	54.11	5.49	17.25
270	52.35	4.37	14.41	47.52	4.57	12.35	47.33	4.41	12.92	50.10	5.76	16.34	48.32	5.32	15.29	54.95	3.87	13.68
315	58.93	3.69	14.37	43.78	4.73	11.98	44.01	4.90	14.21	47.63	5.47	13.93	46.41	5.17	13.65	58.68	3.70	13.90
360	55.33	4.44	14.86	49.47	5.34	15.02	37.16	7.71	13.46	55.88	3.95	14.69	46.75	5.02	13.99	46.88	5.27	13.84

Color variation (ΔE) increased with increasing exposure time. UG wood presented ΔE values from 7.10 to 13.7 in region 1. On the other hand, variation of ΔE in region 1 in GG wood was higher than in UG (7.95 - 20.65). Region 1 (above ground) presents high color variation due to the exposure to xylophages' agents and weathering. Likewise, region 2 (ground zone) showed high color variation because is the position with intense decay by microorganisms.

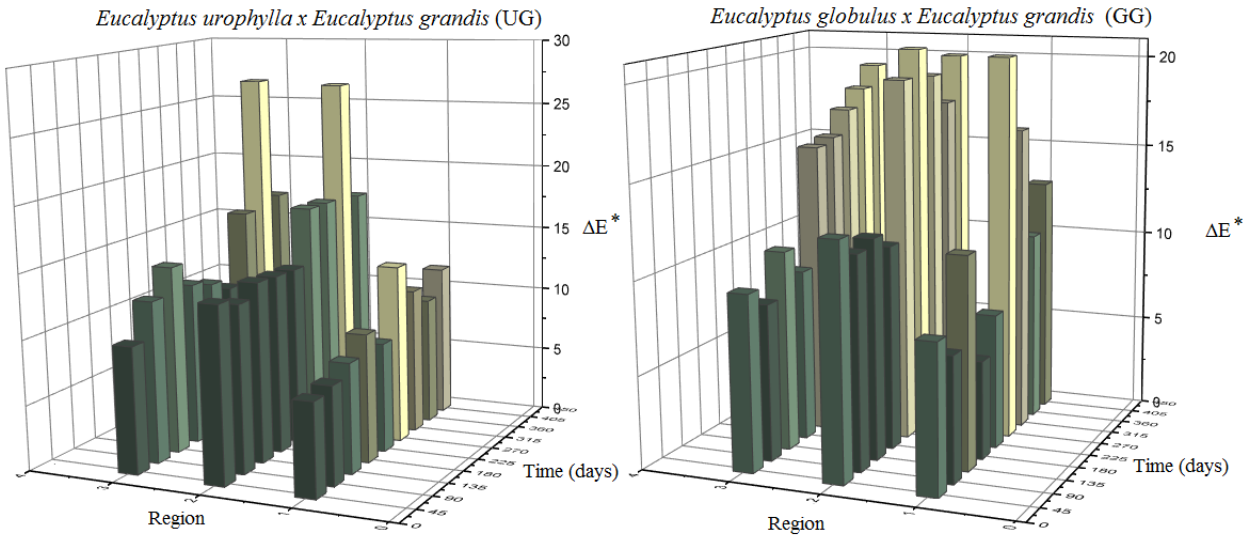

Figure 6—Color variation (ΔE) of eucalypt wood as a function of exposure time.

Conclusions

Eucalyptus urophylla x Eucalyptus grandis wood was more susceptible to biodeterioration by xylophageous agents than *Eucalyptus globulus x Eucalyptus grandis* wood. This biodeterioration was well-characterized by weight loss, decrease of wood density and color changes on wood surface.

Acknowledgments

The authors would like to thank to National Council for Scientific and Technological Development CNPq-Brazil, PhD scholarship DGE (207252/2014-9 and 246018/2012-7),Coordination for the Improvement of Higher Level Personnel (CAPES 014/2012), the University of the Basque Country, and the Federal University of Pelotas for financial and technical support; and the CMPC-Celulose Riograndense for supplying wood.

References

Ashori, A.; Tabarsa, T.; Amosi, F. 2012. Evaluation of using waste timber railway sleepers in wood–cement composite materials. Construction and Building Materials. 27(1): 126–129.

ASTM International, American Society for Te sting and Materials, ASTM D5536-94-Standard method of Sampling Forest Trees for Determination of Clear Wood Properties, Annual Book of ASTM Standards, Philadelphia, PA, USA; 2008.

Brischke, C., Meyer, L., Olberding, S. 2013. Durability of wood exposed in ground e Comparative field trials with different soil substrates.International Biodeterioration & Biodegradation. 86: 108-114.

Empresa Brasileira de Pesquisa Agropecuária - EMBRAPA. 2015. Dados meteorológicos. Laboratório de Agrometereologia. http://www.cpact.embrapa.br/agromet/. 08jun. 2015.

Feist, William C.; Hon, Dn-S., 1984. Chemistry of weathering and protection. Advances in chemistry series. 207: 401–451.

Liñán, C. R.; Hita, P. R.; Cózar, J. C. G.; Gálvez, F. P. 2004. Diagnóstico mediante técnicas de ultrasonidos del forjado de madera del refectorio del convento de santa clara en Carmona (Sevilla). Informes de la Construcción. 55.(490): 17-28.

Mattos, B. D., Gatto, D. A., de Cademartori, P. H. G. [and others]. 2013. Durabilidade a campo da madeira de três espécies de Eucalyptus tratadas por imersão simples. Brazilian Journal of Agricultural Sciences, 8(4): 648-655.

Meyer, L., Brischke, C., Melcher, E., Brandt, K., Lenz, M.T., Soetbeer, A. 2014. Durability of English oak (*Quercus robur* L.) - Comparison of decay progress and resistance under various laboratory and field conditions.International Biodeterioration & Biodegradation. 86: 79-85.

Milagres, F. R. Avaliação da madeira de híbidos de *Eucalyptus globulus* com *Eucalyptus grandis* e *Eucalyptus urophyllla*, para produção de celulose, utilizando espectroscopia NIR. 2009. 142f. (Magister Scientiae)-Universidade Federal de Viçosa, Minas Gerais.

Queiroz, S. C. S.; Gomide, J. L.; Colodette, J. L. [and others]. 2004. Influência da densidade

básica da madeira na qualidade da polpa Kraft de clones híbridos de *Eucalyptus grandis* W. Hill ex Maiden x *Eucalyptus urophylla* S. T. Blake. Revista Árvore, 28(6): 901-909.

Santos, S. R., Influência da qualidade da madeira de híbridos de *Eucaplytus grandis* x *Eucalyptus urophylla* e do processo Kraft de polpação na qualidade de polpa branqueada. 2005. 178f. (Mestrado em Recursos Florestais)-Universidade de São Paulo, São Paulo.

Session 2

Material Characterization—Infrared and Laser

An Application of 3D Fiber Angles Identified through Laser Scanning Based on Tracheid Effect

Min Hu
Dept of Building Technology, Linnaeus University, Växjö, Sweden, min.hu@lnu.se

Anders Olsson
Dept of Building Technology, Linnaeus University, Växjö, Sweden, anders.olsson@lnu.se

Marie Johansson
Dept of Building Technology, Linnaeus University, Växjö, Sweden, marie.johansson@lnu.se

Jan Oscarsson
Dept of Building Technology, Linnaeus University, Växjö, Sweden, jan.oscarsson@lnu.se

Abstract

It is well known that the tracheid effect can be used for determination of in-plane fiber orientation on timber surfaces. Recent research indicates that out-of-plane angle, i.e. diving angle can also be determined on the basis of scanning data. This paper presents a finite element (FE) model based on knowledge of 3D fiber orientation obtained through high resolution laser scanning of a side board of Norway spruce of dimensions 24 × 95 × 2000 mm. For assessment, strain fields in the vicinity of knots due to a simulated moment load case are compared to strain fields obtained from 3D displacement measurement using digital image correlation (DIC) technique applied during a laboratory bending test. The results from simulation and measurement show good agreement regarding the strain fields. This indicates that the 3D fiber orientation model gives basis for an FE model that can be used for accurate assessment of local strains.

Keywords: diving angle, FE-model, grain angle, machine strength grading, Norway spruce, wood

Introduction

Today high resolution scanning of timber is often performed at sawmills in order to detect defects that are not allowed in applications for which the timber is intended to be used. Information regarding fiber orientation can be collected on a very local scale and such information may be used for prediction of stiffness and strength of timber, but it has not until very recently been utilized for timber strength grading. Olsson et al. (2013) presented a new method for strength grading of timber based on a combination of laser scanning, dynamic excitation and weighing of boards. The scanning of face and edge surfaces was performed using a scanner of make WoodEye® equipped with four sets of multi-sensor cameras and dot lasers. The system is based on the so called *tracheid effect*, where one of the principal axes of the light intensity distribution around a laser dot indicates the fiber orientation in the plane of the surface (e.g. Matthews and Beech 1976, Nyström 2003). An initial type testing procedure (ITT), see EN 14081-2, were performed and in March 2015 the method and procedure were approved by the technical group (TG1) established under the technical committee (TC 124) within the European Committee for Standardization, and the method is now available on the market. The suggested IP of the new method can predict the bending strength with high accuracy. On a sample consisting of more than 900 boards of Norway spruce of various dimensions the coefficient of correlation between IP and bending strength was $R^2 = 0.70$ (cf. $R^2 = 0.53$ obtained for dynamic longitudinal MOE vs. bending strength).

One of the simplifying assumptions made in the new method was that the angle between a wood fiber and the scanned surface, i.e. the so called diving angle, was ignored. It has been shown that the tracheid effect may be utilized for determination of the diving angle by considering the ratio between the two principal axes of the elliptically shaped light spots on the wood surface (Simonaho *et al.* 2004). It has not yet been investigated, however, if this can be utilized for accurate and robust high-speed identification of the diving angles on timber surfaces of e.g. spruce consisting of a mixture of early wood and late wood, knots, compression wood and so on. Nor has it been shown that fiber orientation on surfaces identified using the tracheid effect give basis for accurate 3D fiber orientation for the entire volume of a wooden board.

The aims of the present study are 1) to investigate the potential of establishing full-field 3D fiber orientation within the entire board volume using the surface fiber orientation indentified from the laser scanning; 2) to assess the significance and usefullness of such determined full-field 3D fiber information by applying it in a Finite Element (FE) model of a wooden board subjected to bending and comparison of calculated results in terms of strains with those obtained from laboratory tests with the aid of digital image correlation (DIC) system.

Material

In the study a board of Norway spruce with dimensions 24×95×2000 mm is used. The board was flat sawn taken far from the pith with annual rings almost parallel to the wide face of the board. One of the wide faces of the board was planned while the rest of the surfaces were fine sawn. The studied board has an edge knot at about the mid-length of it. Before tests, the boards had been stored in a climate room at a temperature of 20 °C and 65 % relative humidity for about eight months. After that, the average moisture content was 12.9 %.

3D modelling of fiber orientations

Scanning and calculation scheme

The board was fed through a scanner of make WoodEye® in a speed of about 75 meters per minute, by which all four longitudinal surfaces of the board were exposed to laser rays and photographed. The raw data from the scanning consists of images of elliptic laser dots. The resolution achieved regarding the laser dot information was approximately 1.3 mm in the longitudinal board direction and 4 mm in the transversal direction for each of the examined surfaces. The reason the laser dots are elliptic rather than circular in shape is that the light spread more along the tracheid cells, i.e. along the fibers, than across. The elliptical shape of the laser dots can be used to determine the full field 3D orientation on the wide faces of the board using the following five steps:

1. Finding the in-plane fiber angle. Truncation at a fixed threshold value of the light intensity was applied to determine the directions and lengths of the main axes of the elliptical spots. The direction of the longer axis is interpreted as the local direction of the fibers in the plane of the investigated surface.

2. Finding the diving angle. The ratio between the shorter and the longer axis of an elliptical light spot is used to determine the angle between the surface and the local fiber, i.e. the diving angle. The ratio was calibrated by the diving angle seen on the edge faces of the board. The ratio can however only give the absolute value of the diving angle; to find the direction of the fiber it is necessary also to determine the location of the pith of the log and the piths of knots.

3. Identifying knots and their piths. Areas where the diving angle is larger than 50° is set to be knots. When knot areas are found on both the wide faces with a distance between the centroids of the knots being smaller than 24mm (the board thickness) they are assumed to be parts of the same knot. The pith of the knot is defined as the line through the centroid of each of the knot area.

4. Identifying pith in the log. The lines through all the knots in a board are used to find the pith of the log. An estimated intersection point of all the lines representing the knot directions, as seen from the end of the log/board is set as the pith position in the log.

5. Determining the direction of the fiber angle. The fiber is then assumed to be orientated such that with respect two ends of a fiber, the end closer to the pith of the knot has a longer distance to the pith of the log.

A thorough description for the method to establish the size and orientation of the diving angle can be found in Olsson and Oscarsson (2014).

Obtained 3D fiber angles

An example of resulted 3D fiber orientation is shown in Figure 1. The fiber orientation that can be seen in the *xy*-plane, Figure 1b and Figure 1e, follow the longer main axis of the elliptic laser dots on the surface from the scanning and it is known that the result is reliable in this plane in clear wood areas (Olsson et al. 2013). The ratio, *R*, that determines the diving angle, only affects the result in the *xy*-plane in the sense that the length of the lines representing the local fiber orientation are shorter in positions where the diving angle is substantial, which is in the area of the knot. In the *xz*-plane (c) and in the *yz*-plane (d) the picture depends more directly on the values of *R*. The results show that the calculated orientation of fibers around the knot agrees quite well with what is known about the fiber orientation around/with some distance to knots in general (Shigo 1990 for example). The rule applied to decide the sign of the diving angle also works well.

Comparison of strain fields from measurement and simulation

Measurement of strains

A test is arranged as four-point bending, loaded edgewise, to apply a constant bending moment to a 570 mm long part of the board located between two point loads. The edge knot in the middle of the board, the same one as displayed in Figure 1, is placed at the tension side. Both sides of the board were photographed during loading with a DIC system (ARAMIS) to register the complete displacement field around the knot on both the wide faces. The bending test was run up to ultimate failure of the board and the time-force-displacement history was recorded all along. The ARAMIS systems work with triggers to ensure that the registration of images on both sides of the board is done simultaneously- the systems take the images and sample load signals approximately at every 15 seconds time increment and every 100 N load increment.

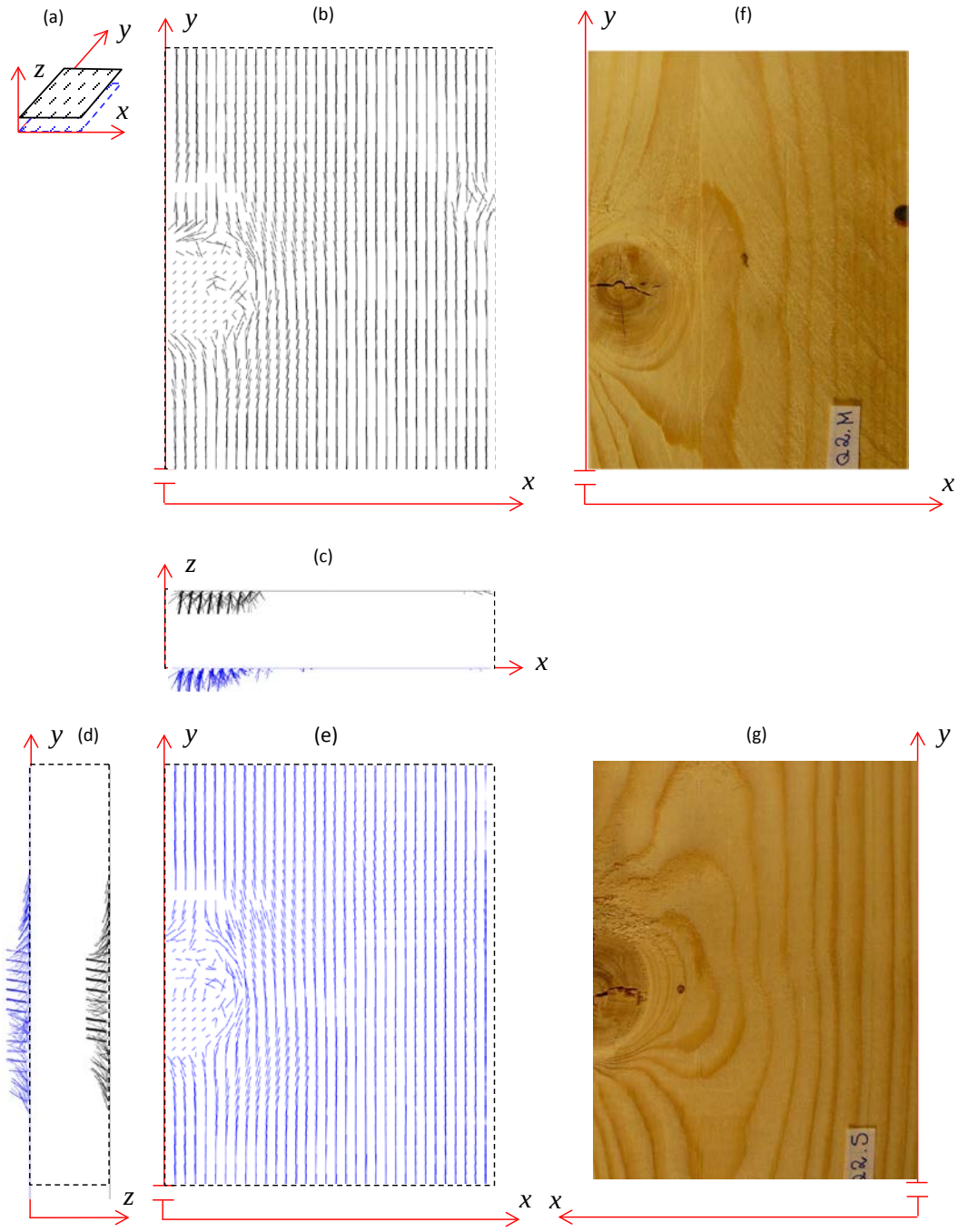

Figure 1- Identified 3D fiber orientation on the two wide faces of a part of the board including a knot; (a) schematic perspective image, (b) fiber orientation of the top surface in the *xy*-plane, (c) fiber orientation of both surfaces in the *xz*-plane, (d) fiber orientation of both surfaces in the *yz*-plane,(e) fiber orientation of the bottom surface in the *xy*-plane and (f) - (g) photographs of the two wide faces of the board.

FE Model based on 3D fiber orientation

The FE modeling is performed using the commercial software ABAQUS in which a 3D model of the board, using linear solid elements, were created. The material is defined as linearly elastic and transversely isotropic, with detailed material properties with respect to the local directions as presented in

the row with "Nominal value" in Table 1. A distinction is made between stiffness in the fiber direction and the across fiber directions but not between the tangential and the radial direction.

From the images of the board, see Figure 1, it was possible to see that there was a crack through the center of the knot already before loading. The crack goes almost perpendicularly throughout the board in the thickness, i.e. *z*-direction. The crack will influence the strain behavior of the board and was therefore included in the FE-model as an area with lower stiffness. The solid FE model was therefore prepared such that the elements marked with red in Figure 2 may be assigned either the nominal value for the material parameters, just as the material in all other elements of the model, or the "Reduced stiffness" defined in Table 1 in order to mimic the locally reduced stiffness caused by the crack.

In the practical handling the identified 3D fiber orientation on the two wide faces of the board as described in the previous section are sufficient inputs to represent the 3D fiber orientation model all over the board volume. The fiber angles between the two surfaces are calculated through linear interpolation between the values on the two surfaces. The data supplied consists of five parts, *x*-, *y*-, *z*-coordinates and two angles φ_{xy} and φ_{diving}. The input files organize the position and fiber angle information in such a way that one pair of specific values of φ_{xy} and φ_{diving} are allocated for each position (*x*, *y*, *z*) on the board surfaces.

Table 1- Material parameters adopted in the FE model, where 1, 2 and 3 correspond to the tangential, longitudinal and radial directions of the fibers, respectively.

Parameter	E_1 [MPa]	E_2 [MPa]	E_3 [MPa]	υ_{12} [-]	υ_{13} [-]	υ_{23} [-]	G_{12} [MPa]	G_{13} [MPa]	G_{23} [MPa]
Norminal value	533	14300	533	0.015	0.45	0.45	1000	50	1000
Reduced stiffness	5.3	143	5.3	0.015	0.45	0.45	10	0.5	10

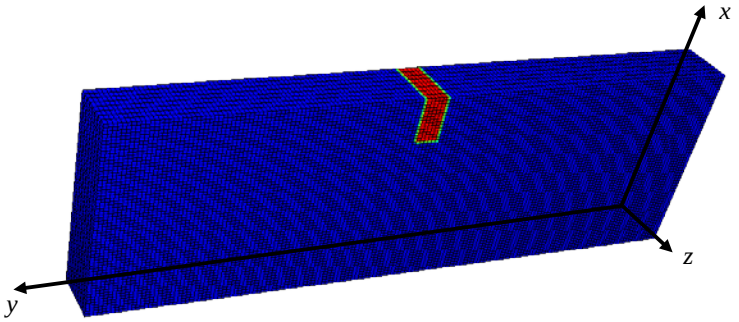

Figure 2-The FE-model of the board with a possibility of introducing an initial crack. The material property of the red part is defined either by nominal value or redueced stiffness in Table 1.

Strains calculated based on 3D fiber orientation

Figure 3 shows normal strains in the longitudinal board direction according to (a-b) a FE model and simulation employing only the nominal material stiffness properties (cf. Table 1); (c-d) the DIC results; (e-f) the FE model with reduced material stiffness, i.e. with consideration to the initial crack in the knot. The left images of Figure 3, i.e. (a), (c) and (e), display strains for the pith side surface and the right images, i.e. (b), (d) and (f), displays the strains for the bark side surface. The FE models employed had an in-plane element size of 1.5×1.5 mm but the strains displayed in Figure 3 (a, b, e and f) are average values over surrounding areas of 6×6 mm^2.

Comparing the different strain plots of Figure 3 there is an obvious resemblance between the results from the FE models based on the fiber orientation model and the result from the DIC measurement, regarding

both the strain pattern and the strain levels. The FE model that ignores the initial crack in the knot (a-b) gives large positive strains over an area slightly larger than the knot itself. Of course, this is due to the low stiffness in positions where fibers are directed perpendicularly to the longitudinal direction of the board. Thus, locally this model gives a different strain pattern compared to the other strain plots. In this respect the FE model that takes the crack into account (e-f) shows better agreement with the DIC results (c-d). Note, however, that the crack only causes a local effect. Apart from an area only slightly larger than the knot there is hardly any difference between (a-b) and (e-f). Both FE models and the DIC images show concentrated positive strains just below the knot, both to the left and to the right of it. Also, the concentrated negative strain on the compression edge of the board, slightly to the right of the knot on the pith side surface (caused by a hole visible in Figure 1a) can be distinguished in (a), (c) and (e). However, the FE model also shows a few local strain concentrations, far away from the knot; those are not shown by the DIC results. These can be explained by laser dots in the scanning that detect fiber deviation in single measurement position. A chip or some sawdust on one of the board surface may be the cause and, since a single laser dot represents a width of 4 mm in the vertical direction, this may explain the small strain concentrations.

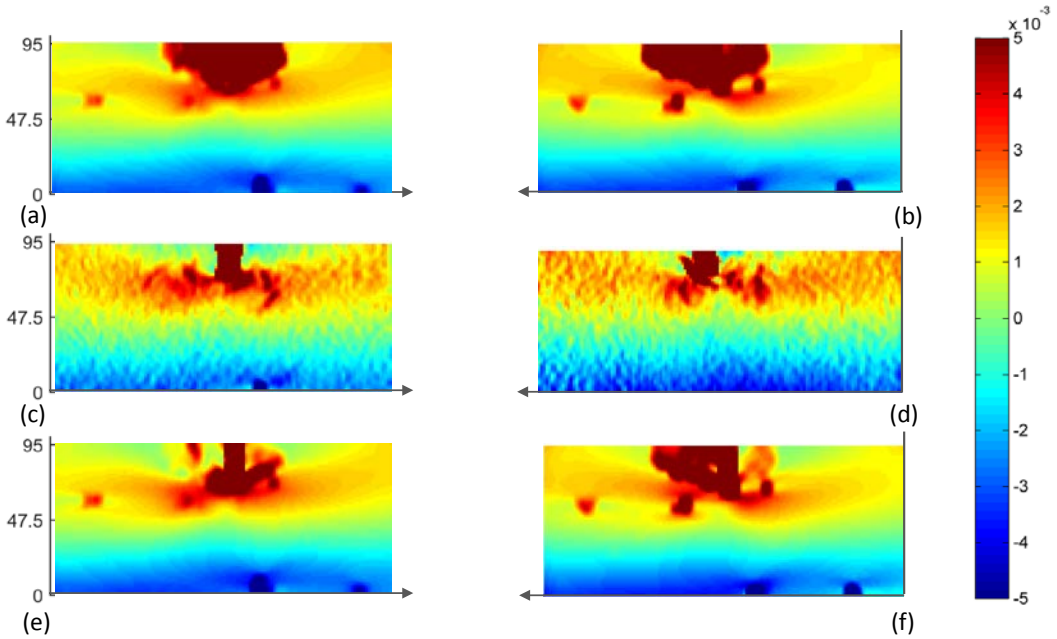

Figure 3- Longitudinal/horizontal normal strains valid for the board corresponding to a nominal stress level at the outmost fiber of the board about 33MPa obtained from (a-b) a FE model considering only the nominal material stiffness properties, (c-d) the DIC results and (e-f) the FE model with reduced material stiffness, i.e. with consideration to the initial crack in the knot. Left images (a), (c) and (e) display strains for the pith side surface. Right images (b), (d) and (f) display the strains for the bark side surface.

Figure 4 shows, for the same load case as for Figure 3, normal strains in the transversal board direction, i.e. vertical direction, according to (a-b) the DIC results; (c-d) the FE model with reduced stiffness, i.e. with consideration to the initial crack in the knot. Figure 5 shows the corresponding shear strains. As for the normal strains in longitudinal direction there is, both for transversal normal strains and for shear strains, an obvious resemblance between the results from the FE model and the result from the DIC measurements. Regarding transversal normal strains, see Figure 4, large positive strains appear just beneath the knot on all the plots. Bending tests of sideboards with a knot on the tension side also show that the failure mode in most cases consists of the development of a horizontal crack beneath the knot that propagate along the fiber direction, i.e. almost horizontally, on both sides of it.

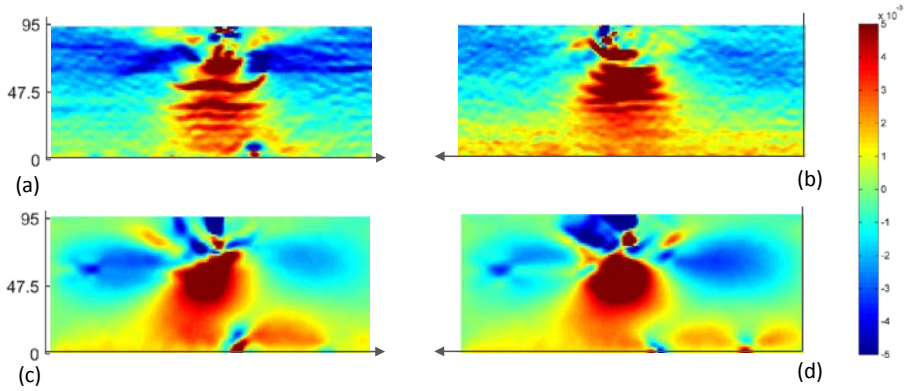

Figure 4-Transversal/vertical normal strains valid for the board corresponding to a nominal stress level at the outmost fiber of the board about 33MPa obtained from (a-b) the DIC results and (c-d) the FE model with reduced material stiffness, i.e. with consideration to the initial crack in the knot. Left images, (a) and (c), display strains for the pith side surface. Right images, (b) and (d), displays the strains for the bark side surface.

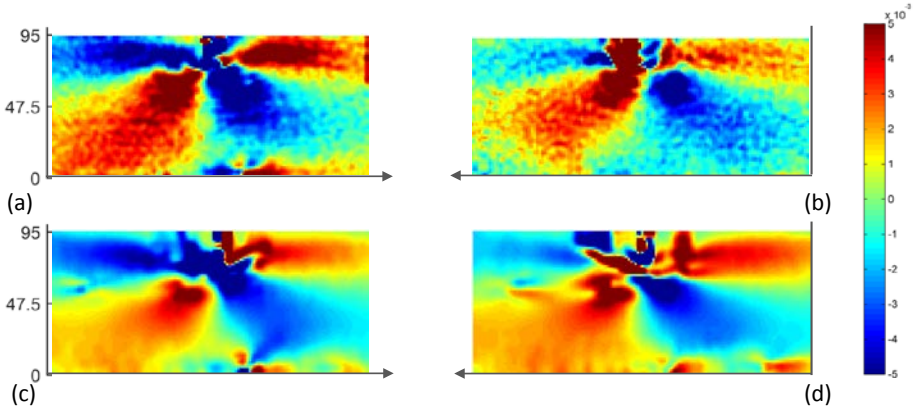

Figure 5-Shear strains valid for the board corresponding to a nominal stress level at the outmost fiber of the board about 33MPa derived from (a-b) the DIC results and (c-d) the FE model with reduced material stiffness, i.e. with consideration to the initial crack in the knot. Left images, (a) and (c), display strains for the pith side surface. Right images, (b) and (d) display the strains for the bark side surface.

Discussion and Conclusions

A modelling scheme for the 3D fiber orientation of the entire volume of a side board of Norway spruce, based on data from dot laser scanning and utilization of the tracheid effect, was presented. The diving angle was determined based on the ratio between the shorter and longer axis from the tracheid effect.The direction of the diving angle was set to follow the direction of the pith of the knot in question defined as areas where the diving angles were larger than 50°. The fiber orientation derived in areas around knots seems to be in fair agreement with the actual fiber orientation seen on such surfaces.

The 3D fiber orientation models established were conveniently integrated with the FE model using the software ABAQUS. The model was used to simulate four point bending test on the board with transversing knots located at the tension edge. The same board as evaluated and modelled with respect to their individual fiber orientation in 3D were also tested in four point bending in laboratory and strains on the wide faces were estimated using DIC technique which enabled comparison to strains calculated on the

basis of the FE model including fiber orientation information. Comparisons of strain fields, i.e. normal strains in longitudinal and transversal board direction and shear strains, from the measurement and simulations showed close agreement regarding both strain patterns and strain levels. The large positive normal strains in direction perpendicular to grain that occur beneath a knot located on the upper/tension edge of the board, and normally cause fracture in the board subjected to bending, were well captured by the FE model. Also, small defects in the wood, e.g. a very small hole on one of the wide faces rather close to the edge in compression, caused local strain concentrations that were clearly detectable both on the strain plots from the laboratory measurement and from the simulations.

In conclusion the modelling approach presented using the 3D fiber orientation information shows promissing results. It can be used for accurate calculations of strain fields and it could be used also for assessment of stresses, provided that sufficient knowledge of the stiffness parameters of wood material in direction along and across fibers is available.

Further work would be (1) to make the modelling scheme more general, i.e. to make it able to handle wooden boards also from the centre part of logs and not only side boards, (2) to address the fiber orientation in the transit zone between knots and clear wood and (3) to evaluate the usefulness of the fiber orientation model on more challenging applications such as prediction of strength and failure modes of timber.

References

EN 14081-2:2010E. Timber structures- Strength graded structural timber with rectangular cross section- Part 2: Machine grading; additional requirements for initial type of testing. European Committee for Standardization.

Matthews, P.C., and Beech, B.H., 1976. Method and apparatus for detecting timber defects. U.S. Patent 3, 976,384.

Nyström, J., 2003. Automatic measurement of fiber orientation in softwoods by using the tracheid effect. Computer and Electronic in Agriculture 41:91-99.

Olsson, A., Oscarsson, J. (2014). Three dimensional fiber orientation models for wood based on laser scanning utilizing the tracheid effect. Proceedings of the 2014 World Conference on Timber Engineering (WCTE), Quebec City, Canada, August 10-14, 2014.

Olsson, A., Oscarsson, J., Serrano, E., Källsner, B., Johansson, M. and Enquist, B., 2013. Prediction of timber bending strength and in-member cross-sectional stiffness variation on basis of local wood fiber orientation. European Journal of Wood and Wood Products 71(3):319-333.

Shigo,A.L., 1990. Tree branch attachment to trunks and branch pruning. HotrScience 2(1):54-59.

Simonaho, S.-P., Palviainen, J., Tolonen, Y. and Silvennoinen, R., 2004. Determination of wood grain direction from laser light scattering pattern. Optics and Lasers in Engineering 41(1):95-103.

Three dimensional knot models based on surface laser scanning

Andreas Briggert
Dept. of Building Technology, Linnaeus University, Växjö, Sweden, andreas.briggert@lnu.se

Anders Olsson
Dept. of Building Technology, Linnaeus University, Växjö, Sweden, anders.olsson@lnu.se

Jan Oscarsson
Dept. of Building Technology, Linnaeus University, Växjö, Sweden, jan.oscarsson@lnu.se

Abstract

Most machine strength grading methods of today result in limited grading accuracy and poor yield in higher strength classes. A new and more accurate grading method utilizing laser scanning technique to determine the in-plane fibre directions on board surfaces was recently approved for the European market. In this, however, no consideration is taken to the out-of-plane direction of the fibres. A first step towards scanning-based 3D models of the fibre orientation is the establishment of 3D knot models. In this investigation laser scanning was used to identify knot surfaces on longitudinal board surfaces. By means of developed algorithms knot surfaces that belonged to the same physical knot visible on different sides of the board were identified. All knots with surface areas larger than 100 mm^2 were correctly identified and modeled in 3D. This is a promising starting point for further development of the new grading method based on laser scanning.

Keywords: structural timber, knots, laser scanning, tracheid effect, local fibre direction, diving angle

Introduction

Background

Destructive testing of structural timber typically results in the conclusion that failures are strongly related to the occurrence of knots. For example, Johansson (2003) evaluated results from about 1800 boards tested in bending or tension and found that more than 90 % of the failures were connected to the existence of this kind of defects. On the contrary, other investigations highlight the fact that the statistical relationship between strength and *indicating properties* (IPs) reflecting size and position of knots is rather weak. The *coefficient of determination* (R^2) between such IPs and bending strength typically vary between 0.16–0.27 (Hoffmeyer 1995), which is poor in comparison with common grading methods in which *modulus of elasticity* (MoE) measures based on axial dynamic excitation or flatwise bending are applied as IPs. Such methods, which typically result in R^2 values of about 0.5 (Johansson 2003), utilize the fact that the best single predictor of strength is stiffness expressed in terms of different MoEs.

There is in a sense a contradiction between, on one hand, failure of timber being dependent on the occurrence of knots and, on the other hand, the statistical relationship between knot measures and strength being poor. However, this can be understood from the fact that failure in bending or tension is typically not initiated in an actual knot, but in adjacent clear wood areas where the fibre orientation deviates strongly from the longitudinal direction of the tested piece (e.g. Boughton 1994). Furthermore, Foley (2003) concluded that the strength reducing effect related to knots was most likely caused by a combination of *inter alia* fibre deviations and reduced area of clear wood in the cross-

section. Thus, development and application of new IPs that include the strength- and stiffness-reducing effect of both knots and fibre deviations could be expected to be very useful in the development of new strength grading methods.

It is well known that dot laser scanning and utilization of the so called tracheid effect, see below, can be applied for the purpose of determining local fibre directions with high resolution on board surfaces (Åstrand 1996). Commercial equipment for laser scanning carried out at sawmill production speed has been available on the market for several years but it is not until very recently that such information has been used for strength grading purposes. A new grading method based on dot laser scanning using an optical scanner of make WoodEye (Innovativ Vision 2015), in combination with axial dynamic excitation and weighing using a grading machine of make Precigrader (Dynalyse 2015), was approved on the 3rd of March 2015 by the technical group TG1 set up under the technical committee TC 124 within the European Committee for Standardization. The method, which is presented in Olsson et al. (2013), is based on the fact that local fibre directions deviating from the longitudinal direction of a board result in a reduction of local stiffness in longitudinal board direction. By means of integration over cross-sections, a bending MoE profile is calculated across a board and the lowest local bending MoE found across this profile is used as IP. It has been shown that the new method will provide grading with high accuracy (Olsson et al. 2013; Oscarsson et al. 2014) in spite of the fact that the method, as approved, is based on several assumptions. For example, it is assumed that measured fibre directions are 1) located in the longitudinal-tangential plane, 2) valid to a certain depth, and 3) coinciding with the scanned board surface. The latter means that the so called diving angle, i.e. the out-of-plane angle, is set to zero, which it is not in reality. A further assumption is that the occurrence of knots is not considered, i.e. scanned fibres within knots are assumed to be clear wood fibres, but with directions that strongly deviate from the longitudinal board direction. Consequently, the intricate three-dimensional (3D) fibre pattern that occurs in the transition zone between knot and clear wood (Shigo 1997; Foley 2003) is neglected, although failures are frequently initiated in, or close to, such areas.

If the present two-dimensional (2D) fibre orientation model implemented in the grading method described in Olsson et al. (2013) was replaced by an accurate 3D fibre orientation model in which also the occurrence of knots was included, it is very likely that a further improvement of the relationship between IP and strength would be achieved. Such a fibre orientation model would also enable even more advanced calculations for assessment of strength, considering the development of cracks and fracture. The purpose of this paper is to initiate the development towards accurate knot and fibre orientation models in 3D.

Tracheid effect and determination of fibre direction

The in-plane fibre orientation on surfaces of softwood timber can be determined using the so called *tracheid effect*, which means that the tracheids (fibres) in softwood conduct concentrated light such as laser light better along the fibres than across. When a beam of such light illuminates a board, some of the light will penetrate the surface and scatter within the wood. A part of the scattered light will be reflected back to the surface and due to the tracheid effect the reflected light will take the shape of an ellipse with the major axis following the direction of the fibres at the surface. The left image in Figure 1a shows a softwood surface in which a knot is included; the right image displays the light scattering on the same surface when illuminated by dot lasers. By determining the major axis of each light spot the in-plane fibre orientation at the surface can be determined. Inside the knot, where the fibre direction is close to perpendicular to the surface, the fiber direction is determined more or less at random. This is a consequence of the fact that the shape of the ellipse becomes close to circular when fibres with a large diving angle are illuminated by a dot laser and, hence, making it difficult to determine the major axis of the ellipse that corresponds to in-plane direction of the fibre.

Methods based on the tracheid effect have also been developed for the purpose of determining the diving angle on board surfaces. Simonaho et al. (2004) suggested that the diving angle could be interpreted by a shape factor ratio determined as the ratio between the minor- and major axis of a

reflected light spot. Olsson and Oscarsson (2014) used this in an attempt to model the 3D fibre orientation on the wide faces on sideboards of Norway spruce. The value of the diving angle (β) was calculated as

$$\beta = cos^{-1}\left(\left(\frac{l_1 + l_2}{2} - R\right)\frac{2}{l_2 - l_1}\right) , \qquad l_1 < R < l_2 \tag{1}$$

where l_1 and l_2 are the ratios between the lengths of the minor- and major axis below and above which diving angles are assumed to be 0° and 90°, respectively, and R is the shape factor ratio of the studied ellipse. A consequence of this equation is that the more circular the ellipse, the higher the value of the diving angle. The mapping suggested by Olsson and Oscarsson (2014) for Norway spruce is shown in Figure 1b, in which the boundary values l_1 and l_2 are set to 0.54 and 0.82, respectively.

The theories presented above regarding determination of in-plane and out-of-plane angles must be adopted with caution when modelling fibre orientation in timber and there are two reasons for this. Firstly, in the 3D fibre orientation modelling carried out by in Olsson and Oscarsson (2014) the complicated 3D fibre pattern that occurs around knots, in the transition zone between knot and clear wood, was not captured accurately since no distinction between fibres that integrate with the knot and fibres that grow around the knot was made in the model. Thus, the result is not consistent with theories concerning growth such as Shigo's knot formation theory (Shigo 1997). Secondly, the mapping between the shape factor ratio and the diving angle, see Figure 1b, may be sensitive to the roughness and the colour of the wood surface. Still, however, the method is useful and reliable for certain purposes.

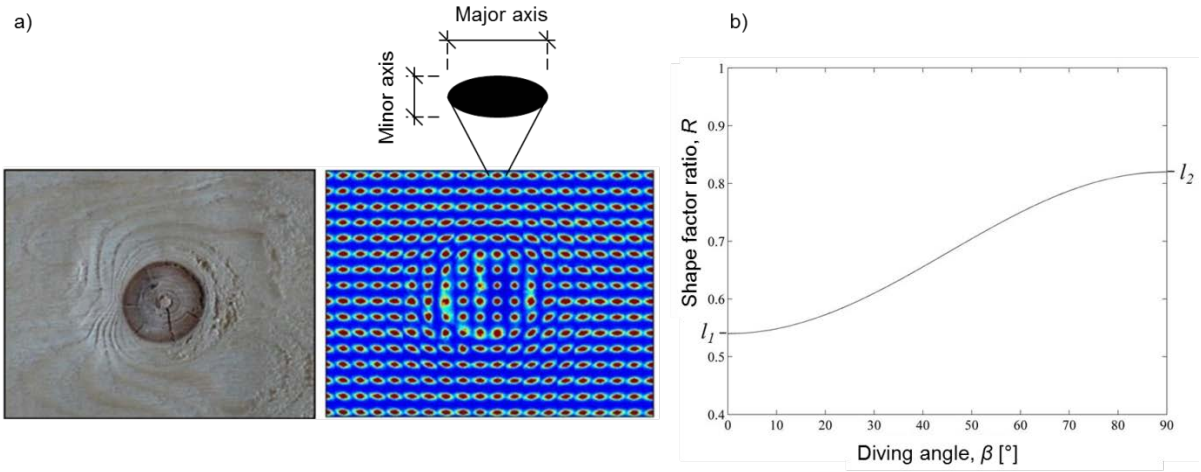

Figure 1— a) Left: surface of softwood timber including a knot. Right: spread of light (tracheid effect) due to dot laser illumination. Figure originates from Petersson (2010). b) Mapping between shape factor ratio and value of the diving angle. Figure originates from Olsson and Oscarsson (2014).

Purpose, aims and limitations

The purpose of the present paper is to define a scheme for how models of the 3D orientation of knots in boards can be established on the basis of data from high speed laser scanning and utilization of the tracheid effect. Since the orientation of a knot is decisive for the orientation of fibres flowing around or integrating with it, the development of 3D knot models is regarded as an important step towards modelling the entire 3D fibre structure within a board. The aims of the present research are

- to determine positions and areas of knot surfaces visible on different sides of a board,
- to identify knot surfaces belonging to the same physical knot and create a complete 3D model of all knots within the board (knots smaller than 10 mm^2 are ignored).

Material and equipment

The test sample used in this study comprises in total 10 boards of Norway spruce with dimensions 45×145×4800 mm delivered from Södra Wood's sawmill in Torsås, Kalmar County, Sweden. All surfaces were planed prior to scanning but the planing was not satisfactory everywhere on all surfaces since limited areas on some of the boards were left raw even after the planing. In two of the boards the pith was located within the cross-section. The boards contained both live and dead knots. The dot laser scanning was performed by a high resolution laser scanner of the make WoodEye. The WoodEye also contains an end scanning camera that may be used to determine an approximate location of pith for the first board end leaving the system.

Methods and measurements

Detection of knots on timber surfaces using the tracheid effect

Dot laser scanning using the tracheid effect means that the fibre orientation is determined with a certain resolution across flatwise and edgewise board surfaces. The resolution was in this study set to 1 mm in the longitudinal direction and 4 mm in the transverse direction. To create smooth transitions between local dot laser observations a moving average of 5×5 mm^2 was applied to both the in-plane angle and the shape factor ratio determining the value of the diving angle. The latter value was calculated according to Equation (1). The values used for l_1 and l_2 in this equation were set to 0.54 and 0.82 which are the same values as suggested by Olsson and Oscarsson (2014). It should be mentioned that the diving angle could be defined as either positive or negative. For example, if 3D fibre directions determined on wide surfaces of a board are projected to the *yz*-plane, see Figure 2f, then a positive diving angle is assigned to those projected fibre directions that present a positive slope in the *yz*-plane. Consequently, a negative slope results in a negative sign of the mentioned angle. For fibre directions determined on edge surfaces the sign of the angle can be determined in a similar way, but in this case on the basis of projections to the *xy*-plane. A different method for determining the sign of the diving angle is presented in Olsson and Oscarsson (2014). However, for the purposes of this investigation the sign is not important since only the magnitude of deviation between the fibre direction and the longitudinal direction of the board is actually considered.

In order to identify all knots of various types along board surfaces by means of high resolution laser scanning, both the in-plane angle and the diving angle should be considered. To do this a 3D vector, based upon both these angles, was created for each dot laser observation, which means that an assumed local 3D fibre orientation was established for each such observation. Further, by assuming that the pith of the log was parallel with the longitudinal direction of the board, a new local angle between the assumed 3D fibre orientation and the pith of the log was calculated as

$$\varphi = cos^{-1}\left(\frac{u \cdot v}{|u| \cdot |v|}\right) \quad (2)$$

where u and v are the local 3D fibre orientation vector and the pith vector, respectively. All such new local angles (φ) determined over a board's surfaces were then used to identify where the 3D fibre orientation deviated substantially from the pith direction. Such deviations exceeding a set threshold value was interpreted as indications that the dot laser observation belonged to a knot surfaces. On the basis of repeated trials, it was found that an optimum relationship between indicated and actual knot surfaces was achieved for a value of φ equal to 56°. This value was subsequently used as threshold value for determination of both the position of knot surfaces and their corresponding areas on the board's longitudinal surfaces. The practical procedure for subsequent identification of knot surfaces can be summarized as follows; (a) for every dot laser observation the position in the coordinate system was defined by the scanning, (b) by using a binary numbering system, all observations for which the threshold value (56°) was exceeded, the binary value was set to 1, c) all observations which had a binary value equal to 1 and was located next to each other on a board surface was regarded as

one coherent knot surface, and (d) even if two such knot surfaces were not located exactly next to each other, but had a distance between the centroids of them that was smaller than

$$r_{crit} = \sqrt{A_1/\pi} + \sqrt{A_2/\pi} \tag{3}$$

where A_1 and A_2 are the areas of the two knot surfaces, the two knot surfaces were considered as a single knot of size $A_1 + A_2$. Figure 2a shows photographs of four longitudinal surfaces of a part of one of the investigated boards. Figure 2b shows colour plots, for the same surfaces, of the calculated angle φ between the assumed fibre orientation in 3D and the direction of the pith. The colour bar describes the angle between the direction of the pith and the assumed fibre orientation; colours from yellow/orange to red implies a large angle, which indicates a knot surface, whereas blue colour means that the angle is small, i.e. indicating clear wood areas. The viewing principle of these figures is that the images can be folded around their longitudinal direction, i.e. the *y*-direction and thus, creating a 3D view of the board. The results displayed in Figure 2b show good resemblance with the actual surfaces of the board shown in Figure 2a.

Three-dimensional modeling of knots

In the following it is described how it can be concluded whether knot surfaces that are visible on different board surfaces are actually parts of the same physical knot. It is common knowledge that branches grow outwards from the pith of the log and usually slightly upwards and it is assumed that the centroid of a knot area correspond to the location of the pith of the branch at a distance r_i from the pith of the log, see Figure 2c. As mentioned in section *Material and equipment*, the WoodEye scanner may be used to determine the location of the pith of the log at the first board end leaving the system. However, due to poor calibration of the end scanning camera in the WoodEye scanner used in this investigation, the described determination of the pith location had to be carried out manually. Having knowledge of an approximate location of the pith of the log (illustrated by the filled circle in Figure 2c), the positions of the centroids of the knot areas identified could be transformed to a polar coordinate system. Then, by comparing the position of two knot surfaces that are visible on different sides of the board, with respect to their tangential and longitudinal coordinates, respectively, it becomes obvious if the two knot surfaces belong to the same physical knot, see Figure 2c. The difference between two tangential coordinates can be denoted $\Delta\theta$, see Figure 2c. Of course, depending on 1) limited accuracy regarding the assumed location of the pith of the log, 2) limited accuracy in the interpretation of knot surfaces 3) limited knowledge regarding the actual growth direction of the branch and 4) misinterpretation of the location of the pith within the knot, *e.g.* because the knot surfaces may be cut off at an edge of the board, some difference in the polar and longitudinal coordinates, i.e. some tolerance that can be expressed as $\Delta\theta_{\text{limit}}$ and Δl_{limit}, respectively, have to be allowed for when comparing tangential coordinates and longitudinal position. Thus it is assumed that two knot surfaces, *i* and *j*, visible on different surfaces, are parts of the same physical knot if

$$\left|\theta_i - \theta_j\right| < \Delta\theta_{limit} \tag{4}$$

and

$$\left|y_i - y_j\right| < \Delta l_{limit} \tag{5}$$

in which

$$\Delta l_{limit} = a \cdot \left|r_i - r_j\right| \tag{6}$$

where $\Delta\theta_{\text{limit}}$ was set to 18.5° and a was set to 0.8. The constant a is dimensionless and can be changed if another species of timber is examined in a similar way. Both these values where set by repeated trial. With knowledge of which knot surfaces that were parts of the same physical knot, it was then possible to model knots in 3D as convex hulls, i.e. with the smallest convex volume that

connected the different knot surfaces as shown in Figure 2d–e. Figure 2f shows a complete 3D knot model for a part of one of the investigated board. The four knots with the highest *y*-coordinates correspond to the knots visible in Figure 2a.

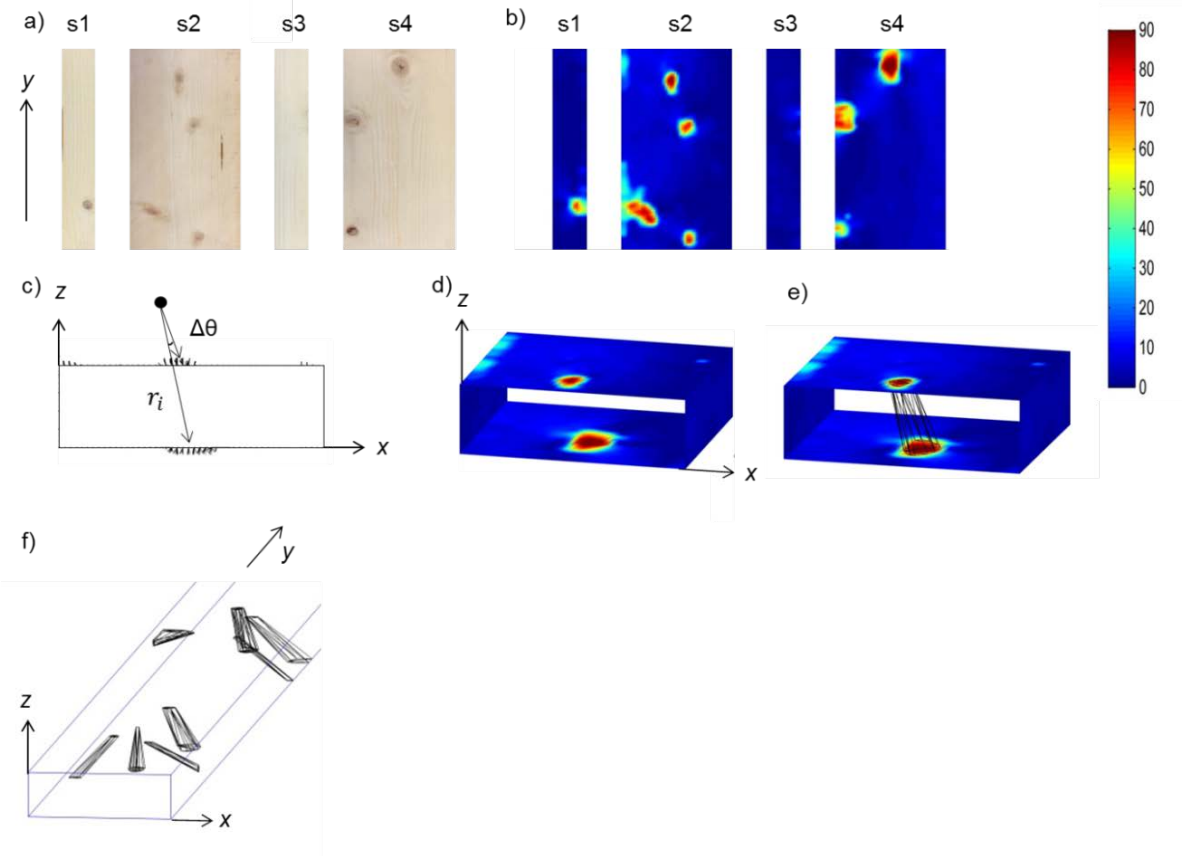

Figure 2—a) Photographs of a part of one of the investigate boards. b) The angle φ between the assumed 3D fibre orientation and the longitudinal direction of the board, for the same surfaces as in (a). The colourbar indicates the size of φ. c) Projection onto the *xz*-plane of the assumed 3D fibre orientation for the uppermost knot shown in (b). The knot is marked on two surfaces and indicated with respect to position with polar coordinates. d) A three dimensional view of the uppermost knot surfaces visible in (b). e) The knot volume inside the board modelled as convex hull. f) A complete 3D knot model for a part of a board. The four knots with the highest *y*-coordinate correspond to the knots visible in (a).

Results and discussion

Validation of identified knot surfaces areas

The ability of the algorithm to determine areas of knot surfaces were verified by manually measuring the knot area on photographs of the board surfaces in the software AutoCAD Architecture. The knot areas measured on photographs and the knot areas assessed by means of the algorithm, for all the knots that are visible on the part of a board that is shown in Figure 2a–b, respectively, are presented in Table 1. In this part of the board there are in total seven round knots, i.e. knots that are cut off in a plane that is fairly close to an *lt*-plane, and one oval knot, i.e. a knot that is cut off in a plane between the *lt*-plane and *lr*-plane. In some photograph, the size of the knot areas is difficult to assess manually since the border between the knot and the surrounding clear wood is fuzzy. Such knots are indicated with an approximately-equal-to sign in Table 1 and the knot area is rounded off to the nearest fiftieth mm^2. The radius given are, for the round knots, simply the square root of the knot area divided by π, and the lengths given for the major- and minor radius of the oval knot were determined manually by approximating the oval knot area with an ellipse of the same size. As shown in Table 1, the radius of the round knots, estimated by means of the algorithm and manually from photographs, respectively, is

quite similar. Considering the knots with well-defined boundaries the largest error of the radius is only 2 mm. The mean error of the radius is smaller than 1 mm and it can be concluded that the algorithm that is based on a criterion for the angle between the assessed fibre direction and the direction of the board is able to determine the areas of the knot surfaces accurately.

Table 1—Knot areas measured on photographs and knot areas assessed by means of the proposed algorithm. The knots considered are those of the part of the board that is shown in Figure 2a–b. Numbering starts with the knot having the lowest *y*-coordinate on each side.

Knot no. (side)	Knot type	y-coordinate *(mm)*	Knot area algorithm *(mm^2)*	Knot area photograph *(mm^2)*	Radius round knots		Major and minor radius of elliptically shaped knots			
					Algorithm *(mm)*	Photograph *(mm)*	Algorithm *(mm)*		Photograph *(mm)*	
							Major	Minor	Major	Minor
1 (s1)	Round	1040	99	77	6	5	-	-	-	-
2 (s2)	Round	998	118	114	6	6	-	-	-	-
3 (s2)	Elliptic	1032	616	≈ 350	-	-	19	10	16	7
4 (s2)	Round	1144	181	179	8	8	-	-	-	-
5 (s2)	Round	1204	218	190	8	8	-	-	-	-
6 (s4)	Round	1013	54	93	4	5	-	-	-	-
7 (s4)	Round	1155	616	≈ 400	14	11	-	-	-	-
8 (s4)	Round	1225	670	515	15	13	-	-	-	-

Validation of the 3D knot model

In section *Three-dimensional modelling of knots* it was explained how it can be concluded if knot surfaces that are visible on different surfaces of a board are parts of o the same physical knot, and how 3D models of knots can be established on the basis of such knowledge. A complete 3D model of knots for a part of a board was shown in Figure 2f. An account of the knots identified by means of the proposed algorithm and by manual inspection, respectively, is given in Table 2 for two different boards. The comparison show that all knots with surface areas larger than 100 mm^2 were identified by the algorithm and also that all knots having at least one surface larger than that 100 mm^2 were correctly associated with other surfaces of the same knot. For knot surfaces with areas between 10–100 mm^2 approximately 60 % of them were correctly associated and modeled in 3D by the algorithm. In two cases spots on the board surfaces that were poorly planed were erroneously identified as knot surfaces. This also led to a connection between one such spurious knot surface and a real knot surface which meant that one knot was modelled as a volume in an incorrect manner. The reason why a rough clear wood surface could be identified as a knot is that the laser dots illuminating such a surfaces may display more round shapes than what they would have done on a corresponding planed clear wood surface. The result is, of course, that large diving angles of fibres are incorrectly identified on such surface.

Table 2—An account of knot surfaces and knots in 3D identified by means of the proposed algorithm and by manual inspection, respectively, for board number 7 and board number 9.

Board no.	7		9*	
Knot surface area (mm^2)	*10-100*	>100	*10-100*	>100
No. of knot surfaces (determined visually)	40	44	36	50
No. of knot surfaces identified by the algorithm	29	44	19	50
No. of knots in the board (determined visually)	18	14	15	20
No. of knots correctly identified by the algorithm	11	14	8	20
No. of knots incorrectly identified by the algorithm	0	0	1	0

***** One 20 cm long section of board number 9 is excluded due to a large and uncommon defect.

Conclusions and further research

The method used in this paper to identify knots through laser scanning and 3D modelling has proven to work well. For the two boards closely examined all knots with surface areas larger than 100 mm^2 were correctly identified and modelled in 3D. Further, for knots with surfaces between 10–100 mm^2 approximately 60 % were correctly identified and modelled. However, it has also been found that when utilizing the tracheid effect for the purposes of identifying knots it is important that the surfaces are thoroughly planed. Otherwise there is a risk that a poorly planed surface will be identified as a knot surfaces. A limitation of the described method for 3D modelling of knots is that it only works when the pith of the log is placed outside the cross-section.

Reference list

Boughton, G. (1994) *Superior sorting of timber using localized stiffness on edge.* In: Proceedings of the Pacific Timber Engineering Conference, Gold Coast, Australia, July 11–15.

Dynalyse AB (2015) Precigrader. http://dynalyse.se/precigrader/ (2 June 2015).

Foley, C. (2003) *Modeling the effect of knots in structural timber.* Doctoral thesis, Division of Structural Engineering, Report TVBK-1027, Lund Institute of Technology, Lund, Sweden

Hoffmeyer, P. (ed.) (1995) *Styrkesortering ger mervärde, Del 2 – Tillgaengelig teknik (Strength grading adds value, Part 2 – Available technique).* Laboratoriet for Bygningsmaterialer, Danmarks Tekniske Universitet, Teknisk Rapport 335-1995, ISSN 0908-3871 (in Danish, Norwegian and Swedish).

Innovativ Vision (2015) WoodEye. http://woodeye.se/ (18 June 2015).

Johansson, C.-J. (2003) *Grading of timber with respect to mechanical properties.* In: Thelandersson, S. and Larsen, H. J. (eds.) *Timber engineering*, John Wiley & Sons, Chichester, England, pp. 23–43.

Olsson, A., Oscarsson, J., Serrano, E., Källsner, B., Johansson, M., Enquist, B. (2013) *Prediction of timber bending strength and in-member cross-sectional stiffness variation on the basis of local wood fibre orientation.* European Journal of Wood and Wood Products, 71(3):319–333.

Olsson, A., Oscarsson, J. (2014) *Three dimensional fibre orientation models for wood based on laser scanning utilizing the tracheid effect.* In: World Conference on Timber Engineering, Quebec City, Canada, August 10–14.

Oscarsson, J., Olsson, A., Enquist, B. (2014) *Localized modulus of elasticity in timber and its significance for the accuracy of machine strength grading*. Wood and Fiber Science, 46(4):489−501.

Petersson, H. (2010) *Use of optical and laser scanning techniques as tools for obtaining improved FE-input data for strength and shape stability analysis of wood and timber.* In: 5th European Conference on Computational Mechanics, Paris, France, May 16–21.

Shigo, A. L. (1997) *A new tree biology; facts photos and philosophies on trees and their problems and proper care.* Eighth printing. Shigo and Trees, Associates. Durham, NE, U.S.

Simonaho, S.-P., Palvianien, J., Tolonen, Y., Silvennoinen, R. (2004) *Determination of wood grain direction from laser light scattering pattern.* Optics and Lasers in Engineering, 41:95–103.

Åstrand, E. (1996) *Automatic inspection of sawn wood.* Dissertation No. 424, Department of Electrical Engineering, Linköping University, Sweden.

Surface Defect Detection in Solid Wood using Infrared Techniques: A Preliminary Study.

Roberto Aedo Garcia
Physics Department, Universidad del Bío-Bío. Av. Collao 1202. Concepción-Chile,
raedogar@ubiobio.cl

Erik Baradit Allendes
Physics Department, Universidad del Bío-Bío. Av. Collao 1202. Concepción-Chile
ebaradit@ubiobio.cl

Miguel Yañez Alvarado
Statistic Department, Universidad del Bío-Bío. Av. Collao 1202. Concepción-Chile,
myanez@ubiobio.cl

Abstract

Among the major irregularities and defects in solid wood, knots and woods specks, which affect its quality and limit the production of laminated wood for exportation. Nowadays wood industry needs a diversity and variety of technology to detect these irregularities, being important extract relevant information in order to determine a good classification of quality. The electromagnetic radiation reflected and absorbed fields in the Near Infrared (NIR), its frequently used to identify different features and properties in the wood. This work, through multivariate statistical techniques, studies the average spectral behavior from different zones of the wood samples in a rank from 900 to 1700 (nm). This was made by using an optoelectronic sensor for two different defects: knots and wood specks. The infrared images obtained from the sensor were studied by spectral signature and infrastructure graphs.

Keywords: Defects, NIR, statistical.

Introduction

Currently, in the ranges of the electromagnetic spectrum, visible, ultraviolet, and infrared, different cameras are widely used in various industrials processes for both quality control and automation of production lines. The principle used is to consider the information that comes from the reflected ligth, as a function of the source, and the reflectivity and absorption properties of material. The light reflected from a surface, its luminance, has a spectrum given by:

$$L(\lambda) = E(\lambda)R(\lambda) \ \ [\mathrm{W/m^{-2}}] \qquad (1)$$

where E(λ) is the incident light from the source, and R (λ) is the reflectivity of the surface, both are functions of wavelength. In the range of near infrared (NIR) between 750-2500 [nm] various studies related to the forest industry are found (Kelly et al 2004), specifically for characteration of the wood properties. There are many studies in the literature related to the prediction of physical properties such as density, microfibrillar angle, tracheid length (Schimleck et al. 2001, 2002, 2003, 2004, Via 2004, Jones et al. 2005), mechanical properties, modulus of rupture (MOR), modulus of elasticity (MOE), chemical (glucose, lignin and extractives content) and different studies for a number of softwoods and hardwoods (Bailleres et al. 2002, 2003 Kludt, Yazaki Schimleck and 2003, Kelley et al. 2004ab). In general, these techniques used for classification of wood defects are based on changes in the mechanical properties, mainly the changes in wood density and fiber orientation (Echols 1973; Cowen

and Clement 1983; Kanowski 1985. Others have demonstrated the ability of NIRS to measure flexural strength and modulus of elasticity for the radiata pine for moving samples at 900 [mm/min] (Thumm 2001 and Gindl Meder et al. 2004).

The quality of the data recorded by the camera depends on the response of the photodetectors, which capture the reflected light. In the construction process of the image the following mathematical model of focal plane array is used (FPA). In this process the photodetector array is found, delivering a first-order relationship between the irradiance input and output for the (i, j) is - th detector in the FPA arrangement. Then k-th time sample is expressed as:

$$Y_{(i,j)}[k]=A_{(i,j)}\bullet X_{(i,j)}+ B_{(i,j)}+ N_{(i,j)}[k] \quad (2)$$

where Y (i, j) - radiation measured in the (i, j) detector, A(i, j) - gain of (i, j) detector, X(i, j) - actual radiation incident on the (i, j) detector, B (i, j) - of the offset (i,j) detector and N (i, j) [k] - temporal noise for (i, j) detector in frame k. The gain and offset are based on the parameters obtained with the two-point calibration (TPC) which takes a diffuse body at two different temperatures T1 and T2. By combining these measurements the individual response of each photodetector is calibrated. The values of gain and offset are given by:

$$A_{i,j} = \frac{Y_{i,j}^{T_2} - Y_{i,j}^{T_1}}{X_{i,j}^{T_2} + X_{i,j}^{T_2}} \quad (3)$$

$$B_{i,j} = Y_{i,j}^{T_1} - A_{i,j} \cdot X_{i,j}^{T_1} \quad (4)$$

The spectral response for these samples using the average and standard deviation of the calibration matrix is achieved. This matrix is correlated with vector Ln (Number of pixels in different positions of the sample) and characterizes the reflectance values for each one of the areas according to the wavelengths involved.

Multivariate statistics can work with large volumes of data, such as information contained in the infrared images. Given the complexity in obtaining spectral signatures, the method Biplot Principal Component (Gabriel, 1971; Clark 2007) is applied to characterize the various irregularities study (wood specks and knots). To perform the Principal Component Biplot, considered the covariance matrix between the reflectance of the areas under study. Indeed S is the covariance matrix, then the breakdown in values and eigenvectors of S, is given by:

$$S = V\ D\ V^t \quad (3)$$

$$V^t V = I \quad (4)$$

where V - matrix of eigenvectors, D - diagonal matrix of eigenvalues. Finally, the Biplot Principal Component reflectance zones are obtained by plotting on a two-dimensional space H the following coordinates:

$$H_{(2)} = \frac{1}{\sqrt{n-1}} V_{(2)}\ D_{(2)} \quad (5)$$

where H_2 – zones coordinate averages in the two dimensional space Biplot, V_2 - matrix of eigenvectors in the two dimensional space and n - number of k-frames from 1 to 253.

Materials and Methods

Solid wood samples of Pinus Radiata D. Don with dimensions 10x30x1.5 [cm] and irregularities like knots and wood specks are studied. The next optical parameters for measurement were used: sampling

height of 13 [cm], instantaneous field of view (IFOV) of 0.055 [rad], field of view (FOV) 17.6 [rad], sampling rate 0.375 [cm/s]. For measurements an excitation source based on a calibrated quartz lamp and tungsten halogen QTH ORIEL Model 100 watt was used. This lamp covered from ultraviolet to near-infrared range. The spectral reflectance was performed by a multispectral camera in the near infrared range between 700-1700 [nm] Fig 1.

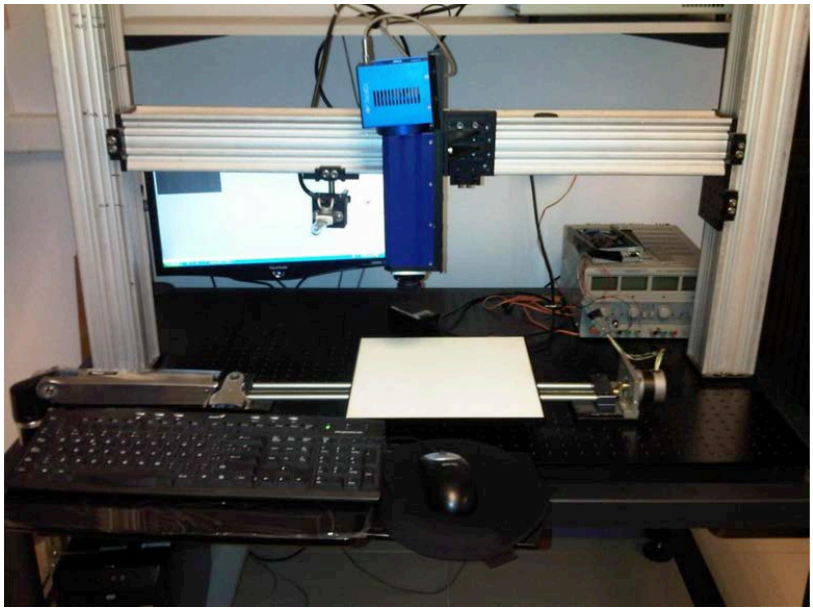

Figure 1— Image Acquisition System

The camera spectral range of work defined by the difference between the maximum and minimum wavelengths was Δλ=800[nm]. For the image analysis 236 pixels were used in the spectral axis reaching a resolution of 3 [nm] and stored in image files with extension Raw Fig2.

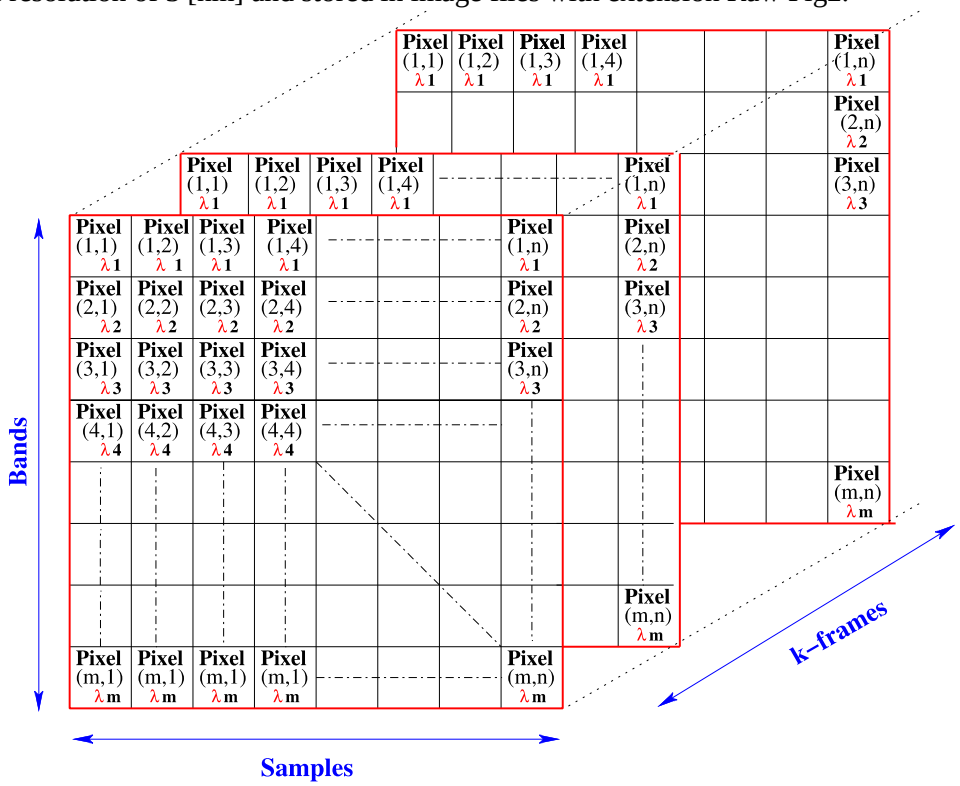

Figure 2— Structure of hyperspectral images

Results

Some of the results are shown as graphs of spectral reflectance v/s wavelength in the figures 3-6. In Figure 3 the average reflectance and standard deviation is shown for an area with knots given by the vector **Ln4** in comparison with three zones free of knots **Ln1, Ln2 and Ln3**.

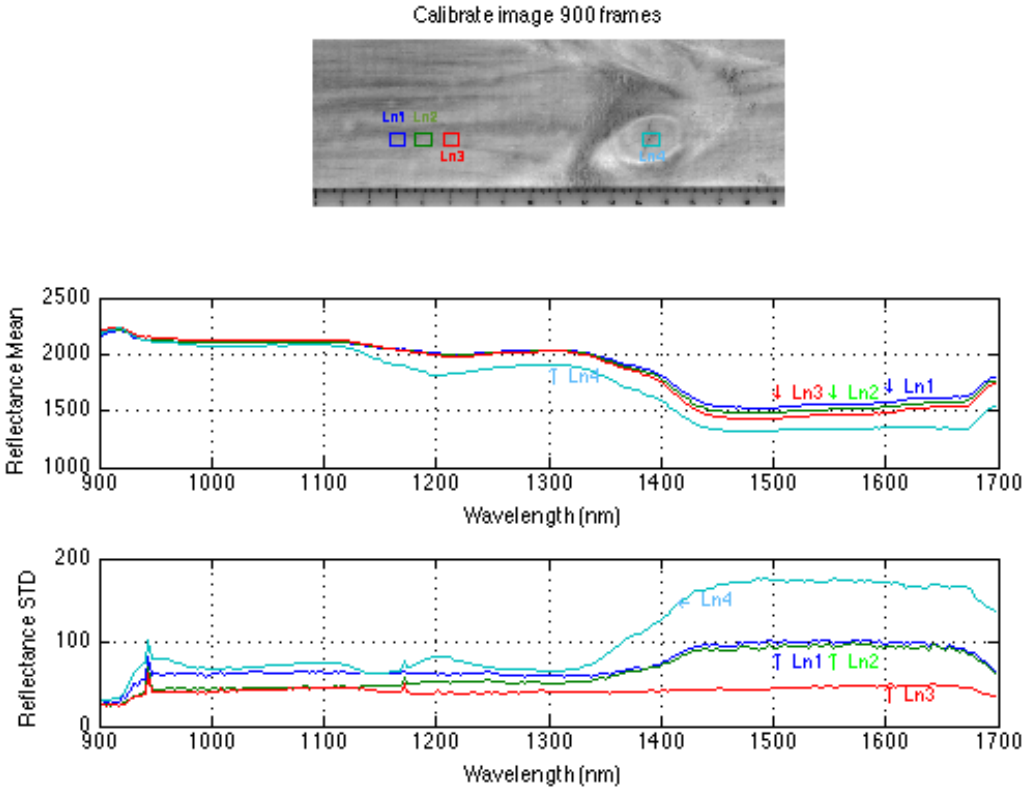

Figure 3— Reflectance in areas with knots (Ln4) and without knots (Ln1, Ln2 and Ln3) and standard deviation.

For wavelengths between 1400-1700 [nm] the reflectance intensity decrease in all this spectral region with lower values for the intensity in the zones with knots. Moreover, the standard deviations of the Ln vectors show increased values for areas with knots in the wavelength range from 1350 to 1700 [nm].

In the Fig. 4 the multivariant analysis applied shows the two first Biplot principal component of reflectance and represent the 98.9% of total variance. A clear discrimination between areas without knots (Ln, Ln2 and Ln3) respect to the area with knot (LN4) is observed. The three areas free of knots present a reflectance strongly correlated with each other, interpreted as areas of similar texture. Instead, LN4 reflectance area is not correlated with the above three areas, and has a higher dispersion, reflecting very different texture area.

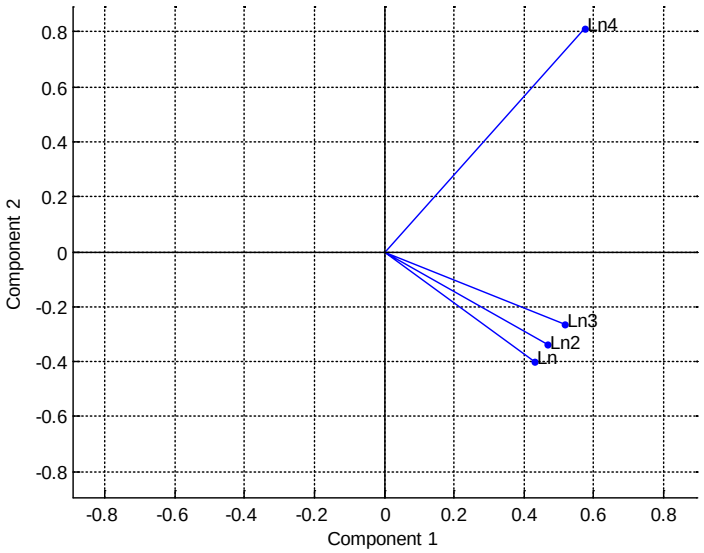

Figure 4— Biplot principal Component of reflectance for areas with and without knots (covariance structure).

The reflectance and standard deviation for woods specks zones are shown in Figure 5. Here **Ln** and **Ln2** areas are free of woods specks while ***Ln3*** y ***Ln4*** areas contain woods specks. The results of the correlation with the average shows that areas with woods specks have lower intensity values in reflectance in comparison with woods specks free zone. Furthermore, for the standard deviation occurs otherwise.

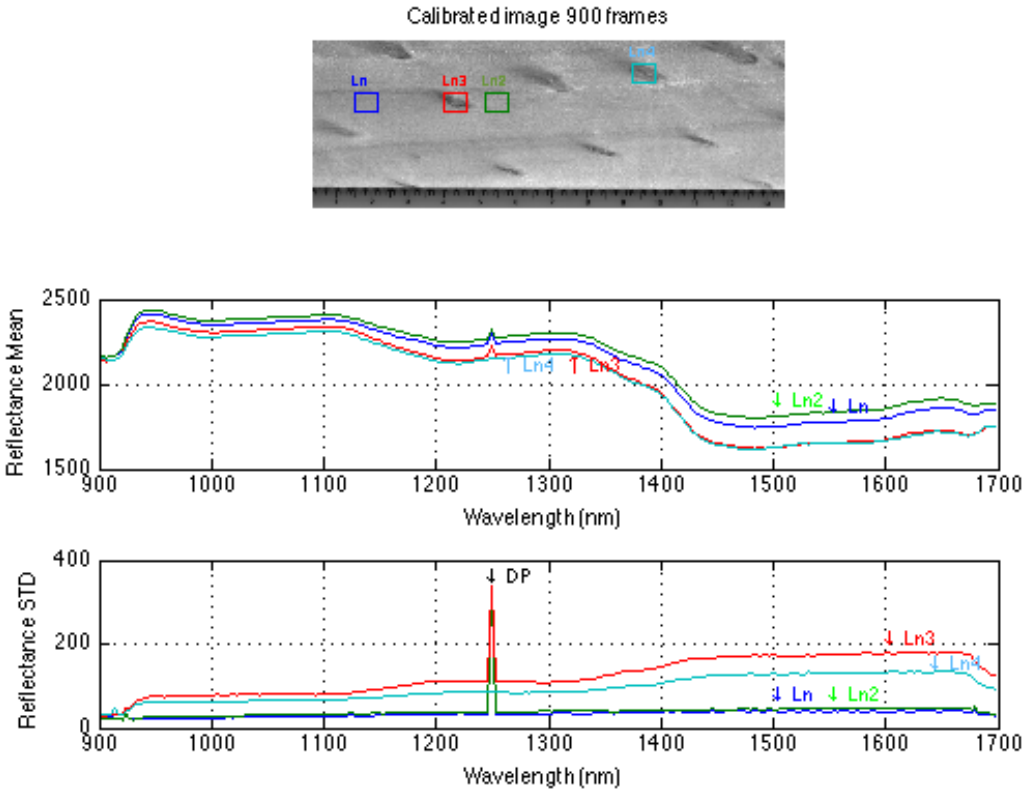

Figure 5— Reflectance average and standard deviation without specks (Ln and Ln2) and with specks (IN3 and IN4).

Finally, the first two dimensions of Biplot principal components of reflactancias (Fig. 6) for the areas with and without woods specks, account for 97.8% of the total variance. The differentiation between areas with Specks (Ln3 and Ln4) and areas without Specks (Ln and Ln2) is notorious.

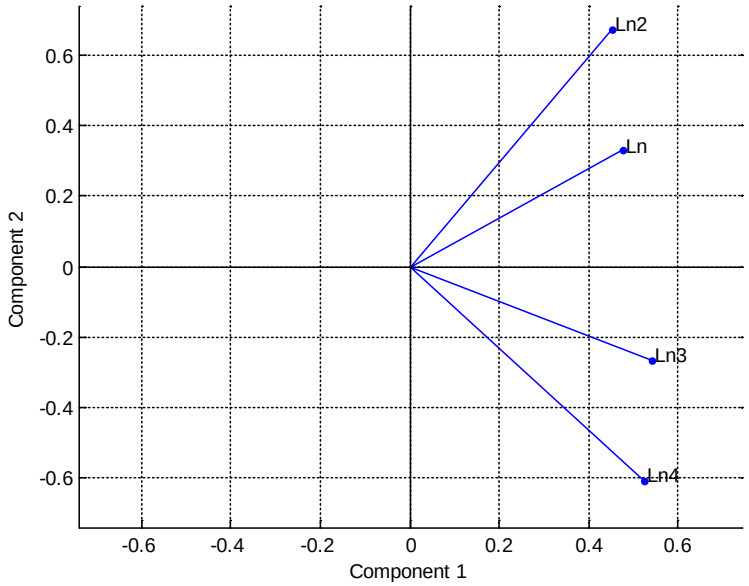

Figure 6— Principal Component Biplot reflectance for areas without specks

Conclusions

The analysis of this works show that the use of infrared technology in conjunction with a multivariate statistical analysis allows detection defects in solid wood due to their characteristic patterns. Certainly, a future research more accurate in this direction should be made in order to confirm or reject the potential of these techniques.

Acknowledgments

This work was supported by research project GI 152007 /VC of Dirección de investigación, Universidad del Bío-Bío, Concepción, Chile.

References

Bailleres H, F Davrieux, F Ham-Pichavant. 2002. Near infrared analysis as a tool for rapid screening of some major wood characteristics in a eucalyptus breeding program. *Annals For. Sc.* 59: 479-490.

Cardenas, Olesia; Galindo, P y Vicente-Villardon, J. L. (2007). Los métodos Biplot: Evolución y aplicaciones. *Análisis de Coyuntura* [online]. vol.13, n.1, pp. 279-303. ISSN 1315-3617.

Cown, D.J., and B.C. Clement 1983. A wood densitometer using direct scanning with X-rays. Wood Sci. Technol. 17:91–99.

Echols, R.M. 1973. Uniformity of wood density assessed from X-rays of increment cores. Wood Sci. Technol. 7:34–44.

Gabriel, K. R. (1971). “The biplot graphic display of matrices with application to principal component analysis”. Biometrika 58(3), 453-467.

Gindl, W., Gupta, H. S., Schoberl, T., Lichtenegger, H. C., and Fratzl, P. (2004). "Mechanical properties of spruce wood cell walls by nanoindentation," Appl. Phys. A- Mater. 79(8), 2069-2073

Jones PD, LR Schimleck, GF Peter, RF Daniels, A Clark III. 2005. Nondestructive estimation of *Pinus taeda* L. wood properties for samples from a wide range of sites in Georgia. *Can. J. For. Res.* 35: 85-92.

Kanowski, P. 1985. Densitometric analysis of a large number of wood samples. J. Inst. Wood Sci. 10:145–151.

Kelley SS, TG Rials, LH Groom, C So. 2004b. Use of near infrared spectroscopy to predict the mechanical properties of six softwoods. *Holzforschung* 58(3): 252-260

Kludt KD. 2003. Use of near infrared spectroscopy technology for predicting bending properties of clear wood specimens. MSc Thesis. Washington State University. USA. 86 p.

Schimleck LR, AJ Michell, CA Raymond, A Muneri. 1999. Estimation of basic density of *Eucalyptus globulus* using near-infrared spectroscopy. *Can. J. For. Res.* 29: 194-201.

Schimleck LR, R Evans, J Ilic. 2001. Estimation of *Eucalyptus delegatensis* wood properties by near infrared spectroscopy. *Can. J. For. Res.* 31(10): 1671-1675.

Schimleck LR, R Evans, J Ilic, AC Matheson. 2002. Estimation of wood stiffness of increment cores by near-infrared spec- troscopy. *Can. J. For. Res.* 32(1): 129-135.

Schimleck LR, Y Yazaki. 2003. Analysis of *Pinus radiata* D. Don bark by near infrared spectroscopy. *Holzforschung* 57: 520-526.

Schimleck LR, C Mora, RF Daniels. 2003. Estimation of the physical wood properties of green *Pinus taeda* radial samples by near infrared spectroscopy. *Can. J. For. Res.* 33: 2297-2305.

Schimleck LR, PD Jones, GF Peter, RF Daniels, A Clark III. 2004. Nondestructive estimation of tracheid length from sections of radial wood strips by near infrared spectroscopy. *Holzforschung* 58: 375-381.

Thumm, A., and Meder, R. (2001). "Stiffness prediction of radiata pine clearwood test pieces using near infrared spectroscopy," Journal of Near Infrared Spectroscopy 9(2), 117-122

Via BK, T Shupe, L Groom, M Stine, C So. 2003. Multivariate modeling of density, strength and stiffness from near infrared spectra for mature, juvenile and pith wood of longleaf pine (*Pinus palustris*). *J. Near Infrared Spectr.* 11: 365-378.

Near infrared laser reflection based wood moisture content determination

Ferenc Divos
Simonyi Karoly Faculty of Engineering, Wood Sciences and Applied Arts, University of West Hungary, Sopron, ferenc.divos@skk.nyme.hu

Laszlo Bejo
Simonyi Karoly Faculty of Engineering, Wood Sciences and Applied Arts, University of West Hungary, Sopron, laszlo.bejo@skk.nyme.hu

Miriam Bradley
Faculty of Forestry, Technical University Madrid, Spain, mbradleyvaldenebro@gmail.com

Abstract

The present project describes a method of measuring moisture content in wood chips based on infrared absorption spectroscopy of water. The theoretical basis of this technique is that in the near-infrared range, liquid water has absorption bands around 1950 nm (5128 cm^{-1}), 1450 nm (6896 cm^{-1}), 1200 nm (8333 cm^{-1}) and 970 nm, (10300 cm^{-1}), Günzler (2003). The electrical signals generated by the reflection on wood chips of three infrared lasers with very narrow wave lengths, provide a value that depends on the quantity of water contained in the measured material. This value will increase when concentration of water in chips decreases, Dalal (1986)

At the present time, there are instruments applying this kind of technique to determine moisture in wood chips, makers are: JWII (Australia), M.C.TEC (The Netherlands), and NDC Technologies (USA) These instruments are composed of NIR lamps and filters in such a way that reflection light at different wave lengths, can be measured. The objective of this project is to offer an alternative to determine moisture content in wood products by a non contact method and providing higher accuracy by removing filters.

Material and Methods

The infrared device is composed of three near-infrared laser diodes with the following wavelengths, 1450 nm, 1310 nm and 980 nm. These wavelengths are close to the main absorption bands of liquid water. The three laser diodes are emitting infrared light which is absorbed by the material providing a value of the reflected light that is proportional to the concentration of liquid water.

The reflected light is collected by a receiver diode placed on the centre of a parabolic mirror whose main objective is to increase the signal of the received reflected light.

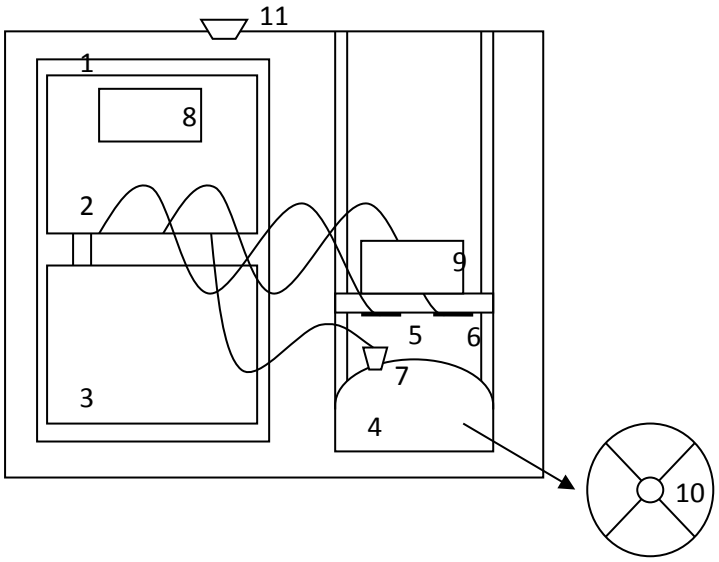

1. Electronic circuit
2. Power Stage
3. Processor
4. Parabolic mirror
5. Diode A
6. Diode B
7. Diode C
8. Power Stage´s cooling plate
9. Diodes´ cooling plate
10. Reflected light detector (Front view of the parabolic mirror)
11. Serial connection to the PC

Figure 1. The internal structure of the infrared device

The electronic device can be connected to the PC using a Serial to USB converter cable; the electrical signals of the emitted and reflected light are displayed on the computer through a simple software called Putty. (Figure 2)

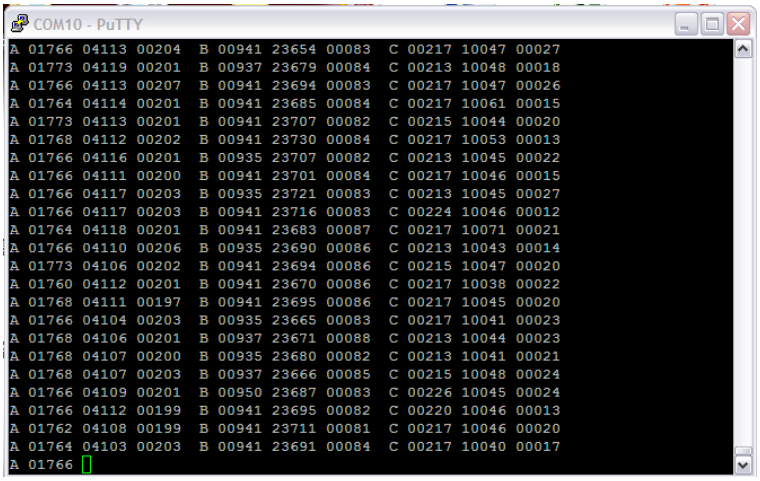

Figure 2. PUTTY software display window

Putty software shows three different data for each diode which are represented by channels A (1450 nm), B (1310 nm) and C (980 nm). Thus, the first column presents the current of the laser diode in mA (mili Amper) ; the second one, the emitted light and the third one, the reflected light intensity. The parameter that is sensitive for moisture content is the one on the third column.

Wood chips of two distinct seizes were measured. The chips were received from Company FALCO, producer of particle boards, they were originally green material, which means, that their moisture content was above 30%. The first step was to obtain samples with different moisture content, for that, it was necessary to dry or moist the chips until they had reached the

equilibrium humidity. To make sure the equilibrium humidity was reached, we made three moisture content measurements picking distinct samples of the same sum of chips. In this procedure it was utilized a special particle-moisture meter (*KERN MLS 50-3).*

The next step was to measure the reflected light parameter of the amount of chips in evaluation with its specific moisture content, that would be, the average of the three measurements previously made. The infrared device used to measure the reflected light, had to be placed opposite to the holder that contains the chips, so that they are directly exposed to the emitted infrared light. For the collecting of data it was important to utilize the same holder and to apply the same distance between the upper layer of the chips and the infrared device. This is because distance has a significant effect on the readings of the reflected light, in such a way that when the distance increases; the electric signal of the reflected light loses intensity. By means of Putty software, these data were recorded into the PC and exported to Excel were the calibration was made.

The presence of water in wood chips increases the absorption of infrared light and consequently the reflected light parameter decreases. The resultant lineal regression is based on this idea and it was obtained representing MC in percentage as a function of the ratios *a/b*, *a/c* and *b/c*. Where *a*, is the average of the readings of the reflected light parameter of diode A (1450 nm), *b* is the average of the same readings of diode B (1310 nm) and *c* is the average corresponding to diode C (980 nm).

Results and conclusions

The results of the collected data are presented in the table below where *a/b*, *a/c* and *b/c* show the averages of the reflected light parameter with its corresponding MC percentage in the left.

Table 1. Summary of results, moisture contentMC and reflected infrared light intensity ratios

MC (%)	a/b	a/c	b/c
2,87	1,311	4,196	3,202
8,58	1,301	4,003	3,076
11,55	1,253	4,039	3,222
18,25	1,211	3,893	3,214
30,01	1,121	3,345	2,985
31,17	1,218	3,534	2,901
107,81	0,784	1,990	3,693

Three lineal regressions were obtained by plotting the points on Table 1. They represent the relationship between moisture content of chips in percentage and each of the ratios mentioned above.

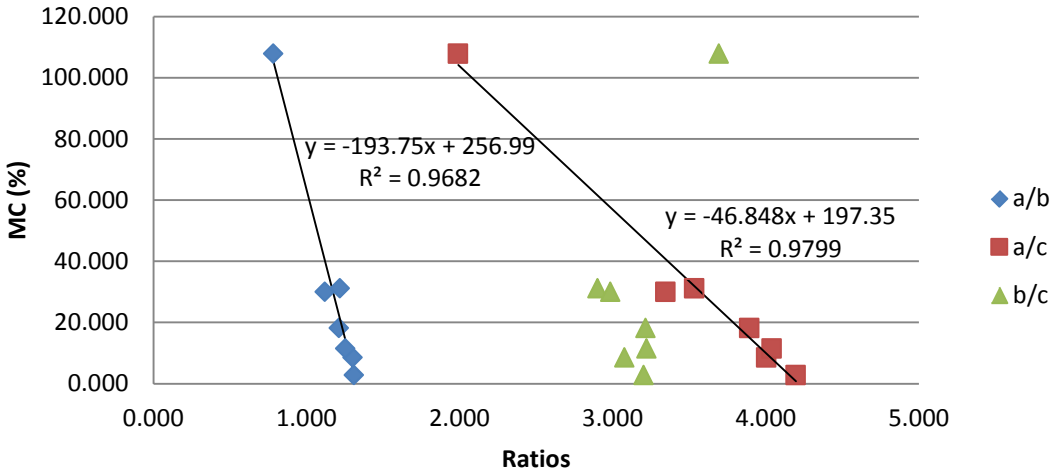

Figure 3. Relation between MC (%) and reflected infrared light intensity ratios. 0,5-2 cm chips.

Figure 3 above shows that the ratio between b and c does not follow a lineal proportion therefore it is not a reliable value to estimate the MC as a function of the readings given by the infrared device. However, the regression got from ratios a/b and a/c have a R^2 value close to 1 and show a clear relation between MC and the reflected light intensity.

As mentioned before, two distinct sizes of chips were evaluated. This appeared to have influence on the measurements and the final results were not the same in each case. The graph below (Figure 4) was generated with the measurements of 2-3 cm chips, the one above was generated by 0,5-2 cm chips. It is clear how the resultant equations of MC vary, depending on the kind of chip size.

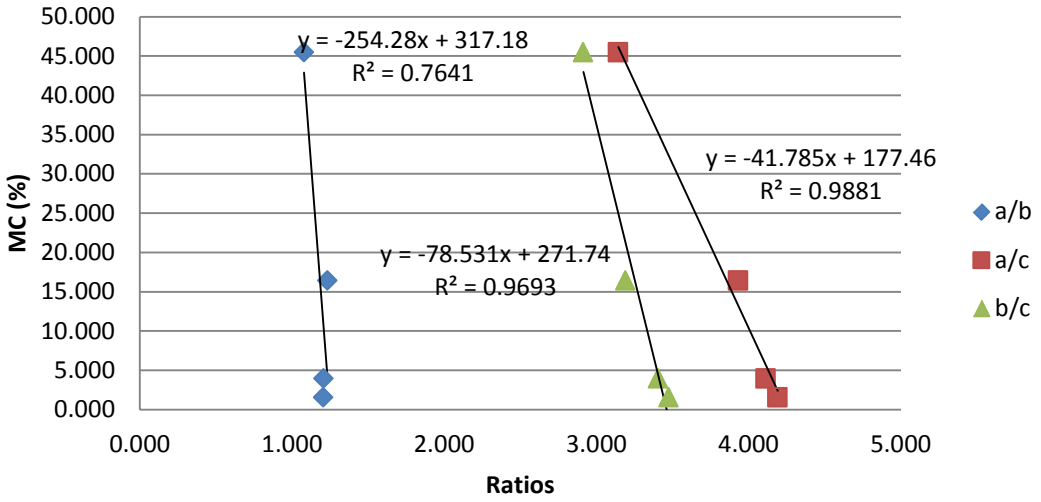

Figure 4. Relation between MC (%) and reflected infrared light intensity ratios. 2-3 cm chips.

The main objective of the data collecting was to create an equation that presents the MC as a function of the calculated ratios, to this end statistical software was used, namely *STATISTICA*. To take into consideration all the variables that had been measured we worked with the multiple regression model. The result of the analysis is shown on figure 5.

Regression Summary for Dependent Variable: Var1 (Spreadsheet1)
R= ,99988895 R²= ,99977792 Adjusted R²= ,99944480
F(3,2)=3001,2 p<,00033 Std.Error of estimate: ,92643

N=6	b*	Std.Err. of b*	b	Std.Err. of b	t(2)	p-value
Intercept			238,1324	29,16250	8,16571	0,014668
Var2	-0,352427	0,130411	-69,9245	25,87463	-2,70244	0,113987
Var3	-0,668119	0,106172	-31,8977	5,06893	-6,29278	0,024335
Var4	-0,021774	0,035024	-3,2531	5,23264	-0,62170	0,597563

Statistic	Summary Statistics Value
Multiple R	0,999888953
Multiple R²	0,999777919
Adjusted R²	0,999444797
F(3,2)	3001,24007
p	0,000333103118
Std.Err. of Estimate	0,926431625

Figure 5 . Results of the multiple regression analysis with STATISTICA, VAR2=a/b, VAR3=a/c and VAR4=b/c

Resulting function: $MC\ (\%) = -69.924\frac{a}{b} - 31.898\frac{a}{c} - 3.253\frac{b}{c} + 238.132$

The standard error of moisture content determination is less than 1%! The last step was to compose a software which displays the final MC in percentage from the readings of the reflected light that get to the PC. It was programmed by means of the resulting function above.

The conclusions of the measurements and the data calibration were the following:

- Distance between the surface of the volume of chips and the device affects the signal received of the reflected light by the detector and it is a critical factor. Therefore, when measuring, it is important to keep the same distance.
- The density of the material is also an influencing factor. This was demonstrated by measuring different chip sizes; as a result, we got distinct relationships between MC and channel ratios.
- The infrared device is a good estimator of MC in chips because it is sensitive for changes in concentration of water in the material.

References

Dalal R. C. n Henry R. J. : Simultaneous Determination of Moisture, Organic Carbon, and Total Nitrogen by Near Infrared Reflectance Spectrophotometry, Journal of Soil Science Society of America, Vol. 50 No. 1, p. 120-123 (1986)

Günzler H., Gremlich H.-U.: IR-Spektroskopie, Wiley-VCH Verlag, Weinheim, (2003)

Chemistry of wood in 3D: new infrared imaging

Barbara L. Illman
U.S. Forest Service, Forest Products Lab, Madison, Wisconsin, USA, billman@fs.fed.us

Julia Sedlmair
U.S. Forest Service Forest Products Laboratory, Madison, Wisconsin, USA, Currently at Bruker AXS, Madison, WI, USA, jul.sedl@gmail.com

Miriam Unger
University of Wisconsin-Milwaukee and University of Wisconsin-Madison, Synchrotron Radiation Center, Madison, Wisconsin, USA, MiriamUnger@gmx.de

Casey Crooks
U.S. Forest Service, Forest Products Lab, Madison, Wisconsin, USA, ccrooks@fs.fed.us

Marli Oliveira
Federal University of Espirito Santo, Alegre, Espirito Santo, Brazil, marlourd.o@gmail.com

Carol Hirschmugl
University of Wisconsin-Milwaukee, Milwaukee, Wisconsin; and University of Wisconsin-Madison, Synchrotron Radiation Center, Madison, Wisconsin, USA, chirschmugl@gmail.com

Abstract

Chemical detection, mapping, and imaging in three dimensions will help refine our understanding of wood properties and durability. We describe here a pioneering infrared method to create visual 3D images of the chemicals in wood, providing for the first time spatial and architectural information at the cellular level without liquid extraction or prior fixation. Analysis used high-resolution Fourier transform infrared (FTIR) microspectroscopy that obtains infrared light from a synchrotron beamline facility at the University of Wisconsin Synchrotron Radiation Center that is equipped with a unique design for illuminating samples. An advanced detector allows multiple mid-infrared spectra to be collected simultaneously. Chemical images were generated in 3D for cell wall layers of *Populus deltoides* Bartr. A complete mid-infrared spectrum was obtained for each data point in the 3D image.

Keywords**:** wood, tomography, Populus, infrared, FTIR, synchrotron, 3D imaging

Introduction

A nondestructive three-dimensional (3D) infrared imaging technique has been developed that allows generation of color images depicting spatial distribution of the chemical constituents of wood. The tomographic images provide structural and chemical information that can be missed by a monolayer approach that may result from manual slicing and staining. We published the first infrared tomographic images of wood in *Nature Methods* (Martin et al. 2013).

This infrared tomography technique was developed at the specialized synchrotron beamline IRENI (InfraRed Environmental Imaging) at the Synchrotron Radiation Center (SRC), University of Wisconsin,

Madison, WI, USA. The technique couples the IRENI rapid 2D spectral image acquisition capability (Hirschmugl and Gough 2012) to a system that enables acquisition of transmission images as a sample is precisely rotated. A tomographic data set corresponds to projection images as a function of sample angle and includes the *complete mid-infrared spectrum for each data point*. A full 3D image of the sample can be reconstructed for one or more infrared wavelengths. The combined Fourier transform infrared (FTIR) spectroscopy and tomography create color images where colors can be assigned by specific spectral identification or spectral changes. Each data point on the 3D grid (voxel) provides a wealth of information for advanced spectral analysis. A 3D image of the object can be visualized by a number of methods, including volume rendering or digitally slicing through the sample along any arbitrary plane.

Tomographic chemical images will provide information about wood artifacts, adhesives, weathering, coatings, and fungal decay. Knowledge about chemical identification and distribution will aid the design of protocols to breakdown cell walls for conversion of lignocellulose to bioplastics, liquid biofuels, nanocellulose, and chemical feedstock for industry (Illman et al. 2013).

We describe here the nondestructive 3D infrared imaging approach, revealing distribution of the chemicals throughout an intact solid wood sample. The objective was to determine the architectural distribution of lignin, hemicellulose, and cellulose in a sample of Populus wood.

Methods

Commercial kiln-dried poplar wood (*Populus deltoides* Bartr.) was hand sectioned (50–100 μm thick) longitudinally with a scalpel or cross-sectioned with a Reichert sliding microtome (5–10 μm thick), stored at room temperature and transferred to the microscope stage for infrared data collection.

The novel IRENI synchrotron beamline configuration collects a section of synchrotron radiation (320 × 27 mrad) generated by a bending magnet, collimates 12 light beams that are arranged side by side to illuminate the sample (Nasse et al. 2011a; Nasse et al. 2011b). Infrared microspectroscopy was performed at the IRENI beamline facility using a Bruker Optics Hyperion 3000 and a Santa Barbara (Santa Barbara Infrared, Inc., Santa Barbara, CA) focal plane array detector (FPA) coupled to a Fourier Transform Infrared (FTIR) vertex 70 spectrometer. The FTIR spectra from every pixel in the 128 × 128 pixel detector array was collected and processed by OPUS 6.5 software (Bruker Optiks, Billerica, MA). The infrared microscope stage with sample rotation mount is described in Figure 1.

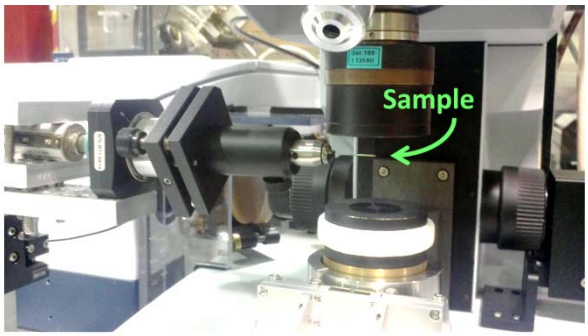

Figure 1—Infrared microscope where the sample is held by a pin on a tip-tilt alignment stage at the focus position of the 15× condenser (NA = 0.5). Sample and stage are rotated by a computer-controlled Agilis rotation mount. The angle of rotation is measured by a potentiometer. Sample and stage above are mounted on an x-z-y stage to position and focus the point of interest on the axis of rotation and at center of the field of view of the FPA detector.

Computed tomography, sample rotation, and tomographic and spectral reconstructions are described by Martin et al. (2013). Briefly, spectral images were acquired in transmission mode with a 15× (numerical aperture (NA) = 0.5) condenser and a 36× (NA = 0.5) objective resulting in an effective projected sample pixel size of 1.1 × 1.1 µm. A series of Java scripts were written for reconstruction of one (or all) mid-IR wavelengths. Reconstruction of the transmission image of an infrared wavelength is similar to x-ray tomography (Illman 2013), using Open Source imaging software such as Fiji.

Wood cellulose, lignin, and hemicellulose were identified by characteristic absorption bands (Pandey 1999, Marchessault 1962, Fengel 1992, Gorzsás 2011).

Results and Discussion

The full mid-IR spectrum was collected for each data point in poplar wood, giving more accurate data than traditional techniques where a single spectrum is collected and averaged. A representative spectrum for lignin, hemicellulose, and cellulose were selected from the full spectrum for analysis. Color images were generated to reveal the distribution of lignin, hemicellulose, and cellulose in 3D.

Computer assisted tomography (CAT) scans based on x-ray energy sources do not provide the range of chemical detection that are obtained with infrared. This new ability to rapidly obtain high quality FTIR spectral images provides complementary information to the density differences of chemicals in x-ray tomography (Illman and Dowd 1999).

Representative FTIR images of Populus wood are given in Figure 2, where three virtual slices of wood are taken at different locations along the sample (d-f).

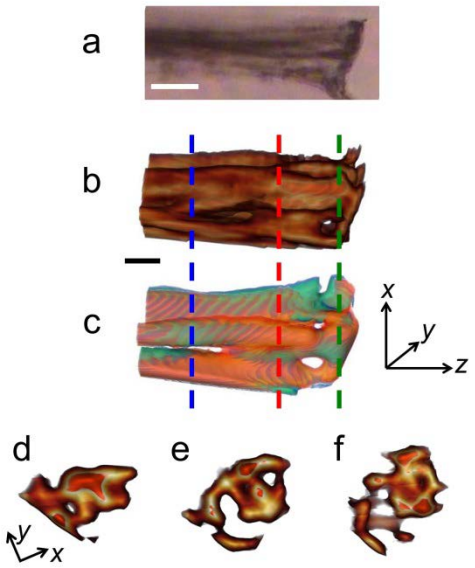

Figure 2—Populus wood: 2D representations of 3D reconstructions. (a) Visible microscope image of a longitudinal sliver of wood (80-µm diameter) (b through f). Tomographic images, where red and blue-green colors are spectrally associated with lignin (1523-1627 cm^{-1}) and hemicellulose (1689-1781 cm^{-1}), respectively. d and f show digital cuts through the middle of the wood cells. e and f show two views of reconstructions of hydrocarbon stretching absorption modes between 2804-3023 cm^{-1}, similar to views a and b (b–c in Martin et al. 2013).

Conclusions

Tomographic mid-infrared chemical images were obtained with the IRENI synchrotron beamline facility. Sample preparation required no fixative, staining, or special storage. This FTIR spectro-microtomography provided spectrally rich 3D visualizations of lignin, cellulose, and hemicellulose in wood samples. The large data sets contain the full mid-infrared spectrum for each data point, allowing future comprehensive analysis of all chemicals in the sample. This technique addresses the challenging problem of determining the 3D molecular architecture of wood cell walls, and promises to be a tool for analysis of wood decay, chemical modification of wood. and many other applications.

Acknowledgments

This work was funded by the USDA Forest Service, Forest Products Lab; the University of Wisconsin-Milwaukee, and the U.S. National Science Foundation awards CHE-1112433 and DMR-0619759. The research was conducted at the USDA Forest Service, Forest Products Lab, Madison, WI, and at the Synchrotron Radiation Center, University of Wisconsin-Madison, which was supported by the National Science Foundation under award DMR- 0537588, and by the University of Wisconsin-Milwaukee and University of Wisconsin-Madison.

References

Fengel, D. 1992. Möglichkeiten und Grenzen der FTIR-Spektroskopie bei der Charakterisierung von Cellulose. Das Papier 46(1): 7–11.

Gorzsás, A. 2011 Cell-specific chemotyping and multivariate imaging by combined FT-IR microspectroscopy and orthogonal projections to latent structures (OPLS) analysis reveals the chemical landscape of secondary xylem. Plant Journal. 66(5): 903–914.

Hischmugl, C.J.; Gough, K.M. 2012. Fourier transform infrared spectrochemical imaging: review of design and applications with a focal plane array and multiple beam synchrotron radiation source. Applied Spectroscopy. 66(5): 475–490.

Illman B.L., Dowd, B.A. 1999. High resolution microtomography for density and spatial information about wood structures. In: Bonse, U., ed. Developments in x-ray tomography II. SPIE 3772: 198–204.

Illman, B.L. 2003. Synchrotron applications in wood preservation and deterioration. In: Wood deterioration and preservation: advances in our changing world. B. Goodell, D.D. Nicholas, T.P. Schultz, eds. ACS Symposium Series 845. American Chemical Society, Washington, D.C.: 337–345.

Illman, B.L., et al. 2013. Nondestructive chemical imaging of wood at the micro-scale: advanced technology to complement macro-scale evaluations. In: USDA Forest Service, Forest Products Laboratory, General Technical Report, Proceedings,18th International Nondestructive Testing and Evaluation of Wood Symposium, Madison, Wisconsin, USA 2013, FPL-GTR-226. pp. 331–335.

Marchessault, R. 1962. Application of infra-red spectroscopy to cellulose and wood polysaccharides. Pure Applied Chemistry. 5(1–2): 107–130.

Martin, M, et al. 2013. 3D spectral imaging with synchrotron Fourier transform infrared spectro-microtomography. Nature Methods. 10: 861–864.

Nasse, M.J. et al. 2011a. High-resolution Fourier-transform infrared chemical imaging with multiple synchrotron beams. Nature Methods. 8(5): 413–416.

Nasse, M.J. et al. 2011b. Multi-beam synchrotron infrared chemical imaging with high spatial resolution: beamline realization and first reports on image restoration. Nuclear Instruments & Methods in Physics Research, Section A: Accelerators, Spectrometers, Detectors, and Associated Equipment. 649: 172–176.

Pandey, K.K. 1999. A study of chemical structure of soft and hardwood and wood polymers by FTIR spectroscopy. Journal of Applied Polymer Science. 71(12): 1969–1975.

Application of near infrared spectroscopy in the screening of disease tolerant *Pinus taeda* (Loblolly pine) families for chemistry, strength and bioenergy

Gifty Acquah
Forest Products Development Center (FPDC), School of Forestry and Wildlife Sciences (SFWS), Auburn University, Auburn, AL, USA, gea0002@auburn.edu

Brian Via
FPDC, SFWS, Auburn University, Auburn, AL, USA, bkv0003@auburn.edu

Lori Eckhardt
Forest Health Dynamics Laboratory, SFWS, Auburn University, Auburn, AL, USA, eckhalg@auburn.edu

Oladiran Fasina
Dept. of Biosystems Engineering, Auburn University, Auburn, AL, USA, fasinoo@aubrun.edu

Nedret Billor
Department of Mathematics and Statistics, Auburn University, Auburn, AL, USA, billone@auburn.edu

Abstract

This study used near infrared spectroscopy coupled with partial least squares regression to rapidly and non-destructively predict the density, modulus of elasticity, modulus of rupture, extractives content and higher heating value of *Pinus taeda* genetic families that have been selectively bred to be disease tolerant.
Calibration models were developed with 1st-derivative treated NIR spectra collected from six positions of southern pines solid wood specimen. Smaller errors of NIR models, as compared to the relatively larger standard deviations associated with the conventional methods gave RPD values greater than 2.5. The R^2_{adj} values of cross-validated models ranged from 0.81 for MOR to 0.89 for MOE. One-way anova used to determine statistical differences (at 95% confidence level) between means of conventionally-measured and NIR-predicted property for each of the loblolly pine families showed that, all models were able to accurately estimate the various properties of at least eleven out of the fifteen families.

Keywords: Near infrared spectroscopy, *Pinus taeda*, tree improvement, wood strength, density, chemical composition, bioenergy

Introduction

Pinus taeda (loblolly pine) is the most economically important tree species in the USA. It provides 110,000 jobs and contributes approximately $30 billion to the economy of the southern US alone, where some 30 million acres of this species have been planted. Reduced growth, decline and eventual mortality have however been associated with loblolly pine trees over the past five decades (Eckhardt and others 2010). In a bid to control this disease complex, stakeholders are selecting and deploying genetically

superior families that have been selectively bred to be disease tolerant. It is vital that we do not compromise other important properties while breeding for disease tolerance; the only way to determine this is to measure them. However, with the large number of trees involved in tree breeding programs, it is not feasible to determine these properties with the conventional methods that require considerable sample preparation and analysis that are time consuming, expensive and mostly destructive. There is therefore the need for alternative analytical tools that have high throughput and are cost effective.

In this study, near infrared spectroscopy (NIRS) coupled with multivariate data analysis was used to characterize and then rapidly predict the basic density, modulus of elasticity (MOE), modulus of rupture (MOR), extractives content and higher heating value (HHV) of loblolly pine families that have been selectively bred to be disease tolerant. These properties are important because any changes in them will impact the yield and/or quality of final products – whether it be paper, lumber, engineered wood product or bioenergy. Furthermore, it is essential that strength is not compromised else mortality due to reasons other than forest disease such as wind failure could occur.

Materials

Fifteen loblolly pine families (one tree per family) were used in this study. Trees were harvested in the winter of 2014 from two forest sites; seven families from Yulee FL and eight from Waycross GA. The average diameter at breast height (DBH) of the trees was 16.8 cm. Trees were crosscut into 1.5 m bolts along the bole, then 50 cm ‘disks’ were taken from the mid portions for further processing into the final test specimen. Nominal 2 x 4-in southern pine boards were also acquired from West Fraser Inc., a sawmill located in Opelika, AL.

Methods

Conventional Testing

Three-point bending test, as specified in ASTM D143 was used to determine the strength properties of samples. Test specimens (2.5 x 2.5 x 41 cm) were conditioned to an average moisture content (MC) of 9 % in a control chamber (temp: 22 ^{o}C; relative humidity: 55 percent) before testing. Basic density was determined as the ratio of the oven-dry mass of a test specimen to its volume. Samples were loaded into a Zwick-Roell load frame equipped with 10KN load cell and a computer controlled screw-drive crosshead. Force was applied to the tangential surface at a loading speed of 1.3 mm/min. The MOE (i.e. Stiffness) was computed as the slope of the linear portion of the load-deflection curve; and the MOR (i.e. Ultimate strength) was calculated as the breaking load divided by the cross-sectional area. After failure, test samples were ground to pass a 40-mesh screen size and used for extractives content and higher heating value determination. Extractives content of test samples was determined following NREL/TP-510-42619 and TAPPI T- 204. Industrial grade acetone (150 ml) was used to extract 5 g of test sample for 6 hours in a Soxhlet Apparatus. For the energy content, approximately 0.5 g of material was pelletized and completely combusted in the presence of oxygen, as specified in ASTM D5865. An IKA C-200 bomb calorimeter was utilized.

Near Infrared Spectroscopy (NIRS)

NIRS measures the amount of near infrared light a sample absorbs, transmits or reflects based on its chemical composition. Spectra (10000 – 4000 cm^{-1}) was collected from six positions (encompassing the cross-sectional, radial and tangential surfaces) on a 2.5 x 2.5 x 41 cm test specimen using the fiber optic probe of a PerkinElmer Spectrum Model 400 NIR spectrometer. Each position was scanned thirty-two times at a resolution of 4 cm^{-1}. Spectra from all positions were then averaged into one spectrum for

analysis. NIR spectra were acquired before the same specimen were used in the destructive three-point bending tests.

Multivariate Data Analysis – Model Calibration and Validation

Raw NIR spectra were preprocessed with 1st-derivatives (5-point filter) before analysis. The PerkinElmer Spectrum Quant+ software was used to develop Partial Least Squares regression (PLS) models. First derivative treated spectra (i.e. independent X variables) were regressed against parameters determined with conventional testing methods (i.e. dependent Y variables). Thirty-five southern pines samples were used for calibration and a leave-one-out cross-validation (LOO-CV). LOO-CV uses all samples except the first to build/calibrate a model which is used to predict the property of the interest for the first sample. The process is iterated so that all samples are used as single-element test sets.

To assess the performance of calibration models, several statistics were employed. The standard error of calibration (SEC) was used to evaluate how precisely the regression line fitted the data, whereas standard error of cross validation (SECV) measured a model's predictive ability during validation.

$$\mathrm{SEC} = \sqrt{\frac{\sum_{i=1}^{n}(\hat{y}_i - y_i)^2}{n-lv-1}} \qquad (1) \qquad\qquad \mathrm{SECV_{lv}} = \sqrt{\frac{\sum_{i=1}^{n}(\hat{x}_{ilv} - x_i)^2}{n}} \qquad (2)$$

Where $\hat{y}_i$ is the value estimated for sample i by the calibration model; y_i is the known value for sample i; n is the number of samples used in model development; and lv is the number of latent variables used to develop the model: xi is the known value for sample i; and $\hat{x}_{ilv}$ is the value for sample i predicted by the model (without sample i) developed with lv factors.
Latent variables are successive linear combinations of the x and y variables chosen such that variations in both the dependent and independent variables are optimally explained (Acquah *et. al* 2015).

The residual predictive deviation (RPD) was used to evaluate the SECV with respect to the standard deviation of the reference data; and the coefficient of determination (R^2) was used to measure the total variance between measured and predicted that could be modeled linearly.

Selected models were then applied in the prediction of some physical, mechanical, chemical and thermal properties of genetically superior loblolly pine families. One-way anova (with MS-Excel) was used to determine the differences between means of conventionally-measured and NIR-predicted property of interest for each of the fifteen loblolly pine families. Tukey pairwise comparison test was used to identify significant differences between treatment (i.e. method) means at 95% confidence level.

Results and Discussion

Conventional Lab Results

Descriptive statistics of density, MOE, MOR, percent extractives and HHV of southern pines (used in model calibration) and loblolly pine determined by the conventional methods are presented in Table 1. The density for the calibration set ranged from a low of 0.38 cm^{-3} to a high of 0.63 cm^{-3}; whereas for the prediction set, the range was 0.42 to 0.73 cm^{-3}. The average MOE and MOR were respectively 9935 MPa and 82 MPa for the southern pines and 9684 MPa and 93 MPa for the selectively bred loblolly pine families. The range of the stiffness and extractives content were not as wide as has been reported in the literature -- 2200 to 26000 MPa; 2.6 to 26.9 % respectively (Kelley *et. al* 2004). Wide and overlapping ranges are known to generally improve the performance of models in the prediction of future unknowns.

Table 1 - Conventional lab results used for model development and independent prediction

	Calibration/ Cross-validation set (n=35)				Prediction set (n=15)			
	Min	Max	Average	SD	Min	Max	Average	SD
Basic Density (g/cm^3)	0.38	0.63	0.49	0.06	0.42	0.73	0.54	0.07
MOE (MPa)	5780	14300	9935	2094	5830	15100	9684	2361
MOR (MPa)	41	113	82	15	26	132	93	28
Extractives (%)	0.4	9.4	4.0	2.2	0.4	3.7	2.3	0.9
HHV (MJ/kg)	16.7	19.3	17.9	0.5	17.5	19.2	18.2	0.5

NIR Spectra

Raw and 1st-derivative treated NIR spectra characteristic of the calibration/cross-validation set, and prediction set are shown in Figure 1; spectra of both sets followed a general pattern. Several important peaks that have been assigned to specific chemical components of wood have been highlighted. For example, peaks occurring at 4063 cm^{-1} is known to result from carbohydrates; 5220 cm^{-1} from water, 5245 cm^{-1} from hemicelluloses; 6945 cm^{-1} from lignin; 7092 cm^{-1} from phenolic hydroxyl groups either in lignin or extractives; and 8425 cm^{-1} from CH_3 – groups in cellulose or lignin (Schwanninger *et. al* 2011). These chemical constituents form the basis on which NIRS is applicable in the prediction of other non-chemical properties such as density, strength and HHV. It has for instance been shown that, cellulose has a strong relationship with density, which in turn has an influence on the stiffness and ultimate strength of wood (Via *et. al* 2003); and the amount of extractives in biomass affect its calorific value (So and Eberhardt 2010). NIR spectra typically have broad overlapping bands that can limit analysis. Raw spectra was thus pre-treated with 1st-derivatives to narrow bands, as well as to correct baseline shift and reduce the non-linearity and multicollinearity between factors (Via *et al*. 2013).

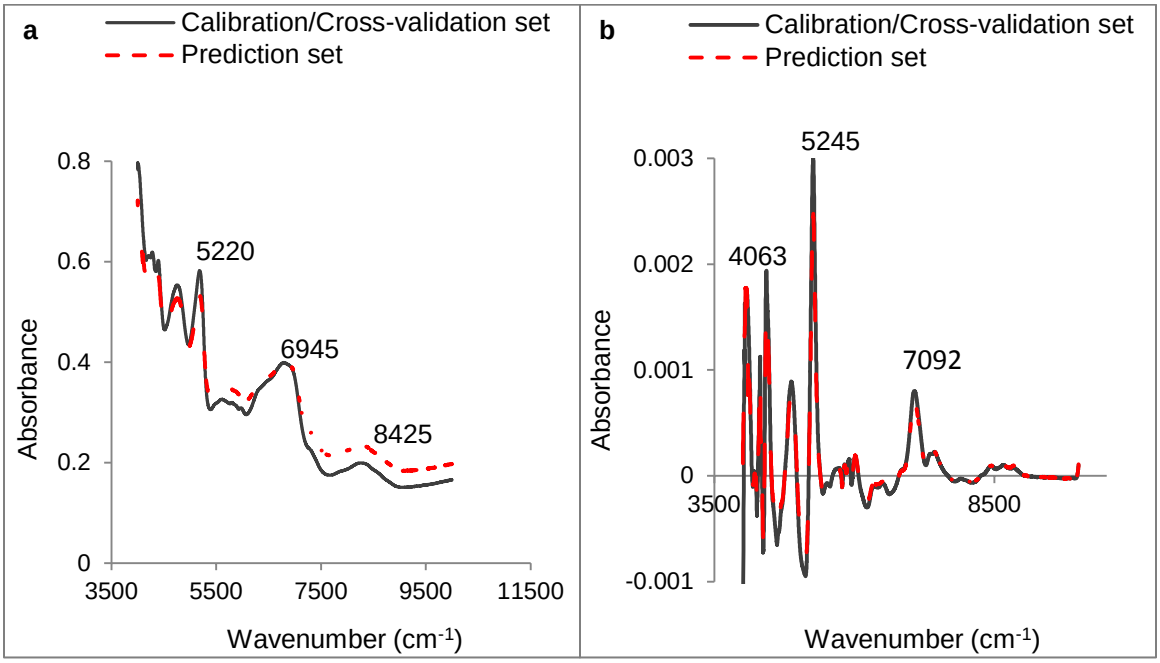

Figure 1 – Raw (a) and 1st-derivative treated (b) NIR spectra characteristic of the calibration/cross-validation and prediction sets.

Performance of calibration models for property prediction

The best performing models were developed with 1st-derivative treated spectra using three or four LVs. Fit statistics showing how models performed are presented in Table 2. The small differences between SEC and SECV is an indication that the validation sets were well predicted by calibration models. Calibration and cross-validation errors were 723 MPa and 697 MPa for the stiffness; and 0.9 % and 0.8 % for extractives content.

Table 2 - Fit statistics of calibration models using 1st-derivative-treated NIR spectra

Property	LVs	SEC	SECV	SD	RPD	R^2	R^2_{adj}
Basic Density (g/cm^3)	4	0.02	0.02	0.06	2.9	0.88	0.88
MOE (MPa)	4	723	697	2093	3.0	0.89	0.89
MOR (MPa)	3	7	6	15	2.4	0.82	0.81
Extractives (%)	3	0.9	0.8	2.2	2.6	0.85	0.84
HHV (MJ/kg)	3	0.2	0.2	0.5	2.7	0.86	0.85

R^2 values for the five propetries studied ranged from a low of 0.81 for MOR, to a high of 0.89 for MOR. R^2 is a measure of the total variance between measured and predicted that can be modeled linearly; it usually keeps increasing as more LVs are added in the development of a model. The adjusted R^2 (R^2_{adj}) of calibration models were thus calculated to ensure that insignificant LVs were not included in model development. R^2_{adj} values were very similar to, or even in some cases same as the R^2 values. Another statistic that was also employed in model diagnostics was the RPD. A higher RPD is an indication of a robust model; a model with an RPD greater than 2.5 can be used for preliminary screening in tree breeding programs (Hein *et. al* 2009). Except for MOR, the RPD of all calibration models passed the 2.5 threshold.

Fit statistics of validated models developed in this study compared well with other results as reported in literature. So and Eberhardt (2010) used NIRS coupled with PLS to predict the HHV of seventy year old *Pinus palustris* (Longleaf pine). Their model for extractives (acetone-soluble) had an SEC of 1.75 %, standard error of prediction (i.e. SEP which is synonymous to SECV in this study) of 2.51 % and R^2 of 0.88, using 2 LVs. For HHV, the fit statistics were as follows: SEC = 0.32, SEP = 0.41, R^2 = 0.37 and LVs = 2. Schimleck *et. al* (2005) also developed models to predict the specific gravity, MOE, and MOR of solid clear wood samples of loblolly pine obtained from 81 plantation sites across southern United States. For MOE, the authors reported that the model developed from NIR spectra collected from the radial surface had SEC, SECV, R^2 and RPD of 1450 MPa, 1570 MPa, 0.82 % and 2.19 respectively; whereas model developed with NIR spectra acquired from a cross-sectional surface (cut with a band saw and designated 'rough') had 1240 MPa, 1250 MPa, 0.87 % and 2.74 respectively. MOR models had 9.61 MPa (SEC), 10.16 MPa (SECV), 0.84% (R^2) and 2.4 (RPD) for the radial surface; and 9.55 MPa (SEC), 9.65 MPa (SECV), 0.84% (R2) and 2.69 (RPD) for the rough cross-sectional surface. The models the authors developed for specific density also had good diagnostics -- radial surface: SEC = 0.03, SECV = 0.03, R^2 = 0.90, RPD = 2.88; rough cross-sectional surface: SEC = 0.03, SECV = 0.04, R^2 = 0.88, RPD = 2.77.

Partial least squares regression models validated in this study were used to predict the aforementioned properties of the fifteen disease-tolerant loblolly pine families. One-way anova was used to determine differences between means of NIR-predicted and conventionally-measured property of interest, Figure 2.

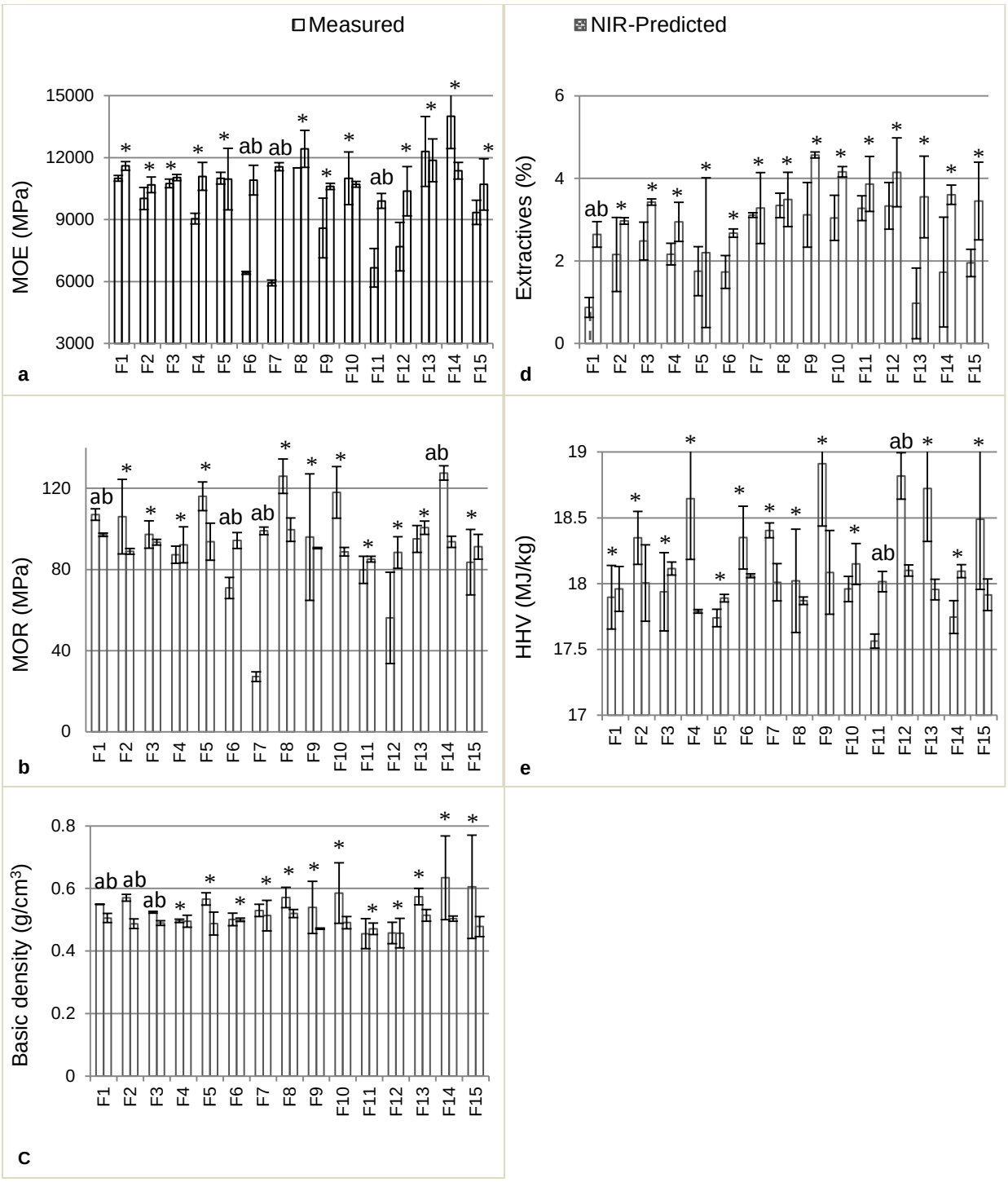

Figure 2 – Bar charts of conventionally-measured versus NIR-predicted properties of the 15 loblolly pine families. A: MOE, B: MOR, C: Basic density, D: Extractives and E: HHV. Note: NIR-predicted and conventionally-measured property are statistically the same for families with an asterisk (*) (Tukey Test, $P > 0.05$).

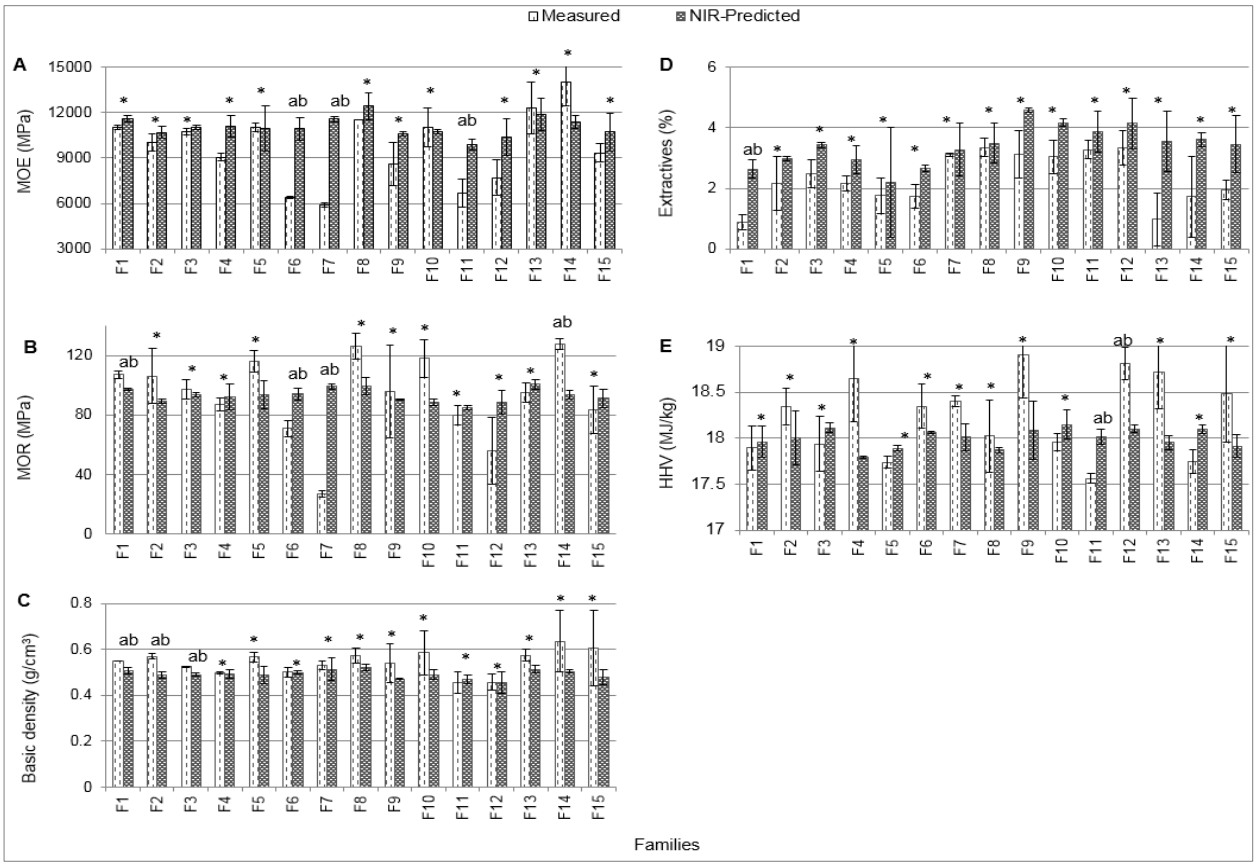

Figure 2 – Bar charts of conventionally-measured versus NIR-predicted properties of the 15 loblolly pine families. a: MOE, b: MOR, c: Basic density, d: Extractives and e: HHV. Note: NIR-predicted and conventionally-measured property are statistically the same for families with an asterisk (*) (Tukey Test, P > 0.05).

With respect to prediction, the best performing model was for extractives, and the worst was for MOR. Developed models were able to accurately estimate the extractives content of all but one of the families, whereas for the MOR, four out of the fifteen families were wrongly predicted. The model for HHV was able to rightly predict thirteen out of the fifteen families; and the models for MOE and density correctly predicted all but three of the families.

Conclusions

In this preliminary study, PLS regression models were developed with 1st-derivative treated NIR spectra of southern pines and reference data acquired through standard methods. These models were used to rapidly predict the basic density, Modulus of Elasticity (Stiffness), Modulus of Rupture (Ultimate strength), extractives content and higher heating value of fifteen *Pinus taeda* families that have been selectively bred to be disease tolerant.

Mean density and MOR for the calibration/cross-validation set were 0.49 g/cm^3 MPa and 82 MPa respectively; and 0.54 g/cm^3 and 93 MPa for the independent prediction set. The range of the stiffness and extractives content were not as wide as has been reported in the literature (i.e. 5780 to 15100 MPa, and 0.4 to 9.4 % respectively). The average HHV of all samples used in this study was 18.0 MJ/kg (SD= 0.5 MJ/kg). The R^2_{adj} values of cross-validated models ranged from a low of 0.81 for MOR, to a high of 0.89 for MOE. With the RPD values being over or very close to the 2.5 threshold, all models were expected to meet the criteria as a preliminary screening tool in tree breeding programs. When the various models were

applied in the rapid and non-destructive prediction of properties, all models were able to accurately estimate the various properties of at least eleven out of the fifteen loblolly pine families.

Further studies is ongoing to improve the predictive capability of these calibration models. At the completion of this project, models should be able to rapidly predict not only the studied properties of these 15 families, but also other genetically superior loblolly pine families that are currently being deployed by stakeholders. The long term goal of this study is to make the right feedstocks available for the conventional forest industry, as well as to support the emerging bioeconomy.

Acknowledgments

The authors are grateful for the financial and/ and or material support of NSF IGERT: Integrated Biorefining for Sustainable Production of Fuels and Chemicals (Award #: 1069004), Auburn University; the Forest Health Cooperative, Auburn University, Regions Bank; the USDA Southeastern Partnership for Integrated Biomass Supply Systems (Grant #:2011-68005-30410); and West Fraser Inc.

Literature cited

Acquah, G.E.; Via, B.K.; Fasina, O.O. [and others]. 2015. Nondestructive prediction of the properties of forest biomass for bio energy, fuel and chemical applications using near infrared spectroscopy (NIRS). Journal of Near Infrared Spectroscopy. 23: 93-102.

Eckhardt, L.; Sword Sayer M.A.; Imm, D. 2010. State of Pine Decline in the southeastern United States. Southern Journal of Applied Forestry. 34: 138-141.

Hein, P.R.G.; Campos, A.C.M.; Trugilho, P.F. [and others]. 2009. Near infrared spectroscopy for estimating wood basic density in *Eucalyptus uroplylla* and *Eucalyptus grandis*. Cerne, Lavras. 15: 133-141.

Kelley, S.S.; Rials, T.G.; Snell, R. [and others]. 2004. Use of near infrared spectroscopy to measure the chemical and mechanical properties of solid wood. Journal of Wood Science and Technology. 38: 257-276.

Schimleck, L.R.; Jones, P.D.; Clark III, A. [and others]. Near infrared spectroscopy for the nondestructive estimation of clear wood properties of *Pinus taeda* L. from the southern United States. Forest Products Journal. 55 (12): 21-28.

Schwanninger, M.; Rogrigues, J.; Fackler, J. 2011. A review of band assignments in near infrared spectra of wood and wood components. Journal of Near Infrared Spectroscopy. 19: 287-308.

So, C-L.; Eberhardt, T.L. 2010. Chemical and calorific characterization of longleaf pine using near infrared spectroscopy. Journal of Near Infrared Spectroscopy. 18: 417-423.

Via, B.K.; Shupe, T.; Groom, L. [and others]. 2003. Multivariate modeling of density, strength and stiffness from near infrared spectra for mature, juvenile and pith wood of longleaf pine (*Pinus palustris*). Journal of Near Infrared Spectroscopy. 11: 365-378.

Via, B.K.; Adhikari, S.; Taylor, S. 2013. Modeling for proximate analysis and heating value of torrefied biomass with vibration spectroscopy. Bioresources Technology. 133: 1-8.

Session 3

Material Characterization—Mechanical, Optical, and Electrical

Surface roughness determination of MDF using speckle interferometry.

Erik Baradit
Physics Department ,University of Bio-Bio, Av. Collao 1202. Concepción. Chile ebaradit@ubiobio.cl

Cristobal Gatica
Physics Department ,University of Bio-Bio, Av. Collao 1202. Concepción. Chile. cgatica@ubiobio.cl

Victor Mora
Physics Department, University of Bio-Bio, Av. Collao 1202. Concepción. Chile. ved@ubiobio.cl

Miguel Yañez
Statistical Department ,University of Bio-Bio, Av. Collao 1202. Concepción. Chile. myanez@ubiobio.cl

Abstract

In this work the speckle interferometry is applied for measurements of surface roughness for MDF or trupán (*Chile)*. The recorded images are saved in a lineal array and then, processed to obtain the correlation level between each and other using a correlation algorithm. Different surfaces are measured using laser speckle interferometry and compared with mechanical measurements. The values for roughness were between 21.84 μm and 26.63 μm and a good correlation between both experimental measurements was obtained.

Keywords. Speckle interferometry, surface roughness, MDF.

Introduction

In the Chilean forest industry there is a very important production of wood composites, flake boards, particle boards and others. These wood products are widely used in Chile and also exported to other countries. The majority of these wood boards are used in walls, furniture and other applications. Sometimes without treatment, but usually different surface coatings are applied. In the latter case, the adhesion of these coatings and wood panels presents some problems due to the formation of gaps between surfaces. In the last case, the adhesion of this covers present problems due to flaws between the surface and the cover increasing the percentage of product rejection. This problem can be solved if the roughness values are known with high accuracy.

Traditional measurements of surface roughness of materials are based on the use of a mechanical profilometer, however non-contact techniques are also used for rugosity measurements. Thus, the speckle interferometry is widely used for roughness determination of different materials [1-4]. In this work this technique is used for determination of the surface roughness of a wood board [5].

Theory

We suppose a rough surface with a Gaussian amplitude distribution ε(x) and variance σ. When a plane wave of a coherent light incides on the surface under an angle θ_1 the distribution of reflected light under a reflection angle θ_2 is given by [6]

$$A(\theta_2) = \frac{A_0}{2L}\int e^{iV_x\, x\, +\, V_z \varepsilon(x)} dx \tag{1}$$

where: $V_x = \frac{2\pi}{\lambda}(\sin\theta_1 - \sin\theta_2)$ and $V_z = -\frac{2\pi}{\lambda}(\cos\theta_1 - \cos\theta_2)$

where A_0 –Amplitude of incident wave, λ-wavelength, 2L-iluminated pupil dimension.

Under an angle rotation $\delta\theta$ of the sample, a correlation between the amplitude distribution $A(\theta_2)\ and\ A(\theta_2 + \delta\theta)$ is given by[7]:

$$\gamma(\delta\theta_2) = \frac{\langle A(\theta_2)A^*(\theta_2 + \delta\theta)\rangle}{A(\theta_2)A^*(\theta_2)} = \mathrm{sinc}(\Delta V_x L)\, e^{(-\frac{\sigma^2}{2}\Delta {V_z}^2)} \tag{2}$$

where $A^*(\theta_2 + \delta\theta)$, is the conjugated wave amplitude in the new direction of reflection

$$\Delta V_x = \frac{2\pi}{\lambda}(\delta\theta_1 \cos\theta_1 - \delta\theta_2 \cos\theta_2) \tag{3}$$

when $\Delta V_x = 0$, we have $\mathrm{sinc}(\Delta V_x L) = 1$ and $\delta\theta_2 = \delta\theta_1 \frac{\cos\theta_1}{\cos\theta_2}$. Then

$$\Delta V_z = \frac{2\pi}{\lambda}(\delta\theta_1 \sin\theta_1 + \delta\theta_2 \sin\theta_2) = \frac{2\pi}{\lambda}\delta\theta_1 \frac{\sin(\theta_1 + \theta_2)}{\cos\theta_2} \tag{4}$$

This way, the next expression for the correlation γ is obtained

$$\gamma(\delta\theta_2) = e^{-\frac{\sigma^2}{2}\Delta V_z^2} \tag{5}$$

This expression shows that the amplitude correlation is related to the roughness. When the speckle is observed in the specular direction we have $\theta_1 = \theta_2 = \theta$ and $\delta\theta_1 = \delta\theta_2 = \delta\theta$ (Figure 1).

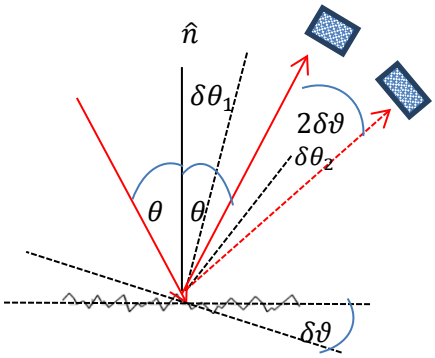

Figure 1— Optical geometry.

The intensities are recorded for both angle positions and the correlation between them is given by

$$\gamma_I(\delta\theta) = \frac{\langle I(\theta)\, I(\theta+\delta\theta)\rangle - \langle I(\theta)\rangle\langle I(\theta+\delta\theta)\rangle}{\sqrt{(\langle I^2(\theta)\rangle - \langle I(\theta)\rangle^2)(\langle I^2(\theta+\delta\theta)\rangle - \langle I(\theta+\delta\theta)\rangle^2)}} = intensity\ correlations \tag{6}$$

where $I(\theta) = \langle A(\theta)\, A^*(\theta)\rangle$ e $I(\theta+\delta\theta) = \langle A(\theta+\delta\theta)\, A^*(\theta+\delta\theta)\rangle$, and

$$\gamma_I(\delta\theta) = \gamma_A^2(\delta\theta) \tag{7}$$

Finally, the next equation for roughness measurements is obtained

$$\gamma_I(\delta\theta) = e^{-\sigma^2\left(\frac{4\pi}{\lambda}\sin\theta\,\delta\theta\right)^2} \tag{8}$$

Experimental setup

The experimental setup was realized using two concentric goniometers with a sensibility of 1/60 degrees. On the goniometers both, the sample and the CCD camera were mounted (fig 2). Using an optical system of lenses a coherent beam of light incides on the rough surface. The system of optical lenses consists of a spherical one L_1 and, and a cylindrical lens L_2 . The first lens L_1 determines the Fourier plane on the detector, and the second lens L_2 is focused on the sample

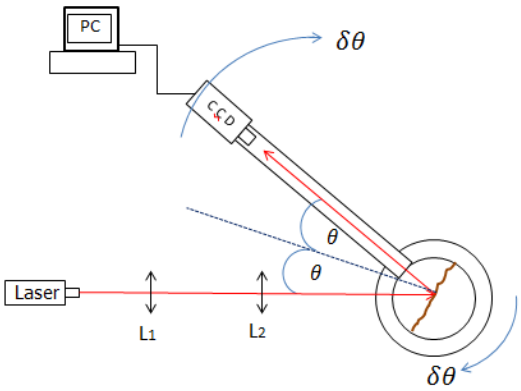

Figure 2—Experimental setup.

The sample is mounted on the goniometer allowing a rotational movement around the axe centered on the middle rough plane. A CCD camera also mounted on the goniometer is used for register of the distribution of the speckle pattern intensities in the specular direction of reflection. Different speckle intensities are registered by the CCD camera under various reflection angles and the images are recorded using a PC. Using an algorithm to find the intensity correlations of speckle patterns, and adjusting the experimental data by mean of a numerical regression the roughness values are obtained.

Results and conclusions

The speckle pattern results of roughness measurements in boards using speckle interferometry are shown in figures 3 and 4, and Table 1 for two different samples. In both patterns a laser beam of $\lambda = 0.520[\mu m]$ was used.

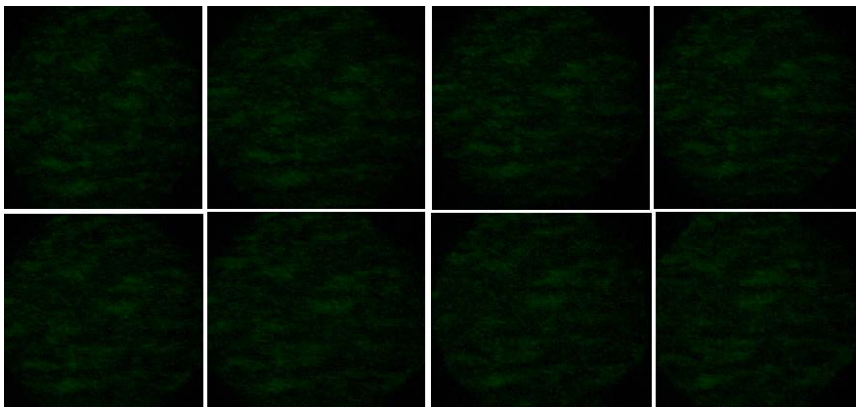

Figure 3: Speckle images obtained for sample 1 using a laser beam of λ=520 nm.

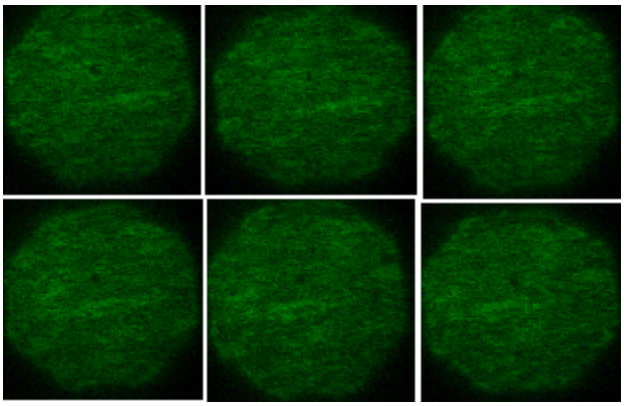

Figure 4: Speckle images obtained for sample 2 using a laser beam of λ= 520 nm.

In the Table 1 the values of roughness using the speckle interferometry (σ) and the mechanical testing (R_r) are shown. The values obtained by mean of the mechanical roughness meter were 26.12 µm for sample 1 and 21.84 µm for sample 2, while using the speckle interferometry were 26.63 µm and 23.7 µm respectively.

$\sigma\ [\mu m]$	$R_r\ [\mu m]$
26.63	26.12
23.7	21.84

Table 1: Results obtained for roughness values using both methods.

In the figure 5 the Gaussian theorical curves are shown using σ experimental data. The difference between the theorical curves and experimental data is due to the surface roughness of the real boards does not have an exactly Gaussian form.

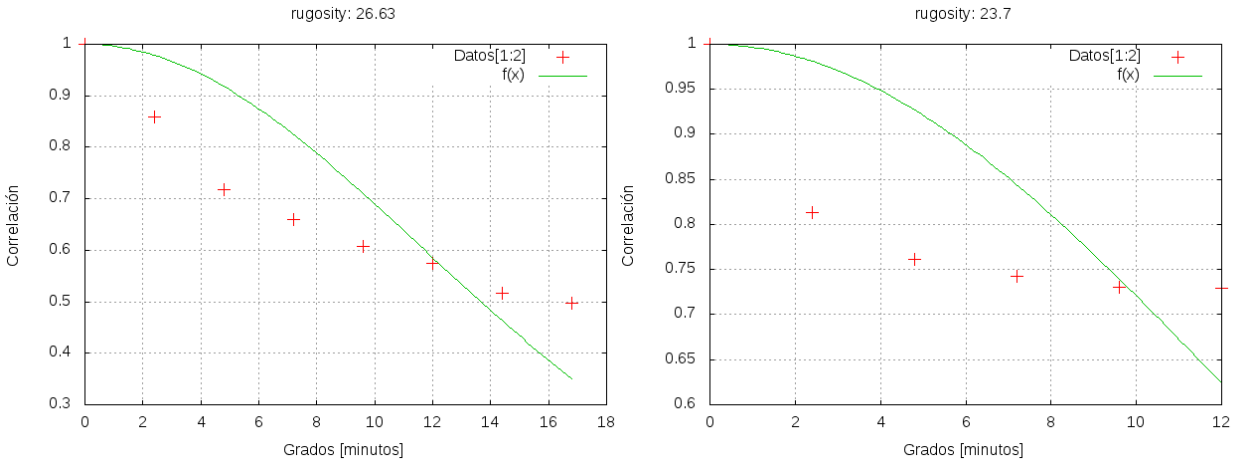

Figure 5: Gaussian theorical functions f(x) = $\gamma_I(\delta\theta)$ **(----) and** experimental data (+++).

This way, the application of the speckle correlation techniques allowed a preliminary calculation of surface roughness of this type of boards. To improve this research, future studies should be performed.

Aknowledgments

This work was supported by research Project GI 152007 /VC of Dirección de Investigación, Universidad del Bio-Bio, Concepcion, Chile.

References

[1] M. R. Landau. et al;245- ANALES ALFA, vol 5, Rosario (1993). “Método visual para la determinación de rugosidad de superficies”.

[2] M. R. Landau. et al; 247-ANALES ALFA, vol 5, Rosario (1993). “Relación entre rugosidad y rocas”.

[3] F. Perez Quinitán et al;40- ANALES ALFA, vol 7, Bariloche (1995). “Determinación de la Rugosidad de una Transparencia Mediante Técnica de Correlación Digital de Speckles”.

[4] M. F. Ruiz Gale et al; Laboratorio de Optica y laser – IAMEND – ENDE - CNA, Buenos Aires, Argentina. “Modelo Teórico de la variación de la rugosidad de una superficie erosionada”.

[5] Roman Castañeda; Universidad Nacional de Colombia, Medellín. (1994). “Interferometría de speckle”.

[6] P. Beckmann and Spizzichino; Pergamon Press, N.Y. (1963). “The scattering of electromagnetic waves from rough surface”.

[7] D. Leger; Tesis de Doctorado Universiadad de Paris-Sud, Francia (1976). “Deux methods de mesure de rugosités par correlation de speckles”.

Modulus of elasticity and rebound coefficient correlated for tropical species

Nádia Schiavon da Veiga
PhD Student, Laboratory of Nondestructive Testing - LabEND, College of Agricultural Engineering – FEAGRI – University of Campinas – UNICAMP, Campinas, Brazil – e-mail: nadiasveiga@gmail.com

Julio Soriano
Assistant Professor, Laboratory of Nondestructive Testing – LabEND, College of Agricultural Engineering – FEAGRI – University of Campinas – UNICAMP, Campinas, Brazil – e-mail: julio.soriano@feagri.unicamp.br. Tel +55-19-35211040; fax +55-19-35211005

Paulo Gustavo Krejci Nunes
Agricultural Engineer, Laboratory of Nondestructive Testing – LabEND, College of Agricultural Engineering – FEAGRI – University of Campinas – UNICAMP, Campinas, Brazil.

Abstract

Modulus of elasticity of wood is a stiffness property that needs to be known for developing engineering designs. Methods to determine this property that requires the extraction of specimens shows difficulties in some applications. In this study, we evaluated the correlations between rebound coefficient obtained by sclerometry and the modulus of elasticity parallel to the grain. We used two species of tropical wood: *Cedrela ssp* and *Apuleia leiocarpa*, and for each species were extracted 12 prisms of different beams. These prisms, with moisture content stabilized, were subjected to the sclerometric test. One specimen of each prism was obtained to test the compression parallel to the grain, from which we obtained the modulus of elasticity. The results allowed us to conclude that the correlation between elasticity modulus and rebound coefficient is significant (r = 0.82), showing that the sclerometric method can be used to estimate this property of wood.

Keywords: sclerometry, compression parallel to the grain, stabilized timber

Introduction

To develop timber designs, several properties are required, for example, the modulus of elasticity that is associated to the behavior of the material stiffness. This property is also of fundamental importance to the classification of wood (Kretschmann and Hernandez, 2006), as well as to evaluate the performance of structures *in situ*.

According to ABNT NBR 7190 (1997) the modulus of elasticity can be obtained by the test of compression parallel to fibers of specimens, with cross section equal to 5 cm x 5 cm and 15 cm in length or, by three point flexural testing, requiring specimens with section measuring 5 cm x 5 cm and with span equal to 105 cm. Therefore, in both testing methods, the confection of specimens is required. According to the ABNT NBR 7190 (1997), the relationship between the flexural elasticity modulus and the compression parallel to the fibers is equal to 0.85 for softwood and 0.90 for hardwood, respectively.

Researches have been made to generate correlations between modulus of elasticity of wood and the results of nondestructive methods. Del Menezzi et al. (2010), working with six Amazonian species, established correlations between the results of the dynamic elastic modulus obtained by the stress waves and flexure test. In that study, considering all species, they obtained correlation coefficients greater than 0.91. However, when considering the species separately, the correlation coefficients were less than 0.75.

Baar et al. (2015), using five species of tropical timber in stabilized moisture condition (8% moisture content), evaluated the correlation between the dynamic modulus of elasticity (obtained by ultrasound, by longitudinal resonance and resonance in flexion) with the static modulus of elasticity (obtained by three-point flexural method). In the case of ultrasound elastic modulus and the static modulus of elasticity, the established correlation resulted R = 0.83. For the results obtained by the resonance method correlated to the static modulus of elasticity, correlation coefficients obtained were between 0.86 and 0.87. Sales et al. (2011) evaluated beams of the species *Goupia Glaba*, and concluded that the dynamic elastic modulus obtained by ultrasound and the static modulus of elasticity obtained by flexural by 4 points have strong correlations with R = 0.94. With the same order, the authors obtained the correlation between the modulus of elasticity for transverse vibration and static modulus of elasticity.

The combination of several techniques has been used to predict properties of wood by artificial networks. With this methodology, Esteban et al. (2009) by associating properties such as density, moisture content and dimensions of the cross section with the ultrasonic wave velocity, were able to predict the elastic modulus of timber with R^2 = 75%. Cavalli and Togni (2013) evaluated the use of old structures, showing that the pylodin method associated with the stress wave method is capable of estimating the modulus of flexural elasticity, by four points, with a correlation coefficient higher than 0.87.

The sclerometry is a nondestructive testing method used to evaluate the homogeneity of the concrete and, its results may also be correlated to estimate of compression strength, according to ASTM C805 (2013). The method has been researched at the Non-Destructive Testing Laboratory (LabEND) at the College of Agricultural Engineering of University of Campinas and, some results showed that the method has great potential to estimate some of the wood properties, such as compressive strength (Soriano *et al.*, 2011) and the density (Soriano et al., 2013).

The objective of this study was to evaluate the correlation between the values of sclerometric index and the elastic modulus obtained by compression parallel to fibers of two species of hardwoods.

Material and Methods

To reach the objectives of this study two species of tropical wood with different densities were used, *Cedrela ssp* and *Apuleia leiocarpa*. For each species we selected twelve beams cross-section measuring 80 mm by 200 mm. Of each beam, we cut a prism free from defects with length of 300 mm.
At these prisms, in the wood stabilized condition, the esclerometric impacts were applied, with a total of 10 impacts in the direction parallel to the fibers, 10 in the tangential direction and 18 in the radial direction.

In Figure 1 are shown the anatomical directions and points marked for application of impacts, with the same number of points were marked to the corresponding opposing faces. The distance between the points of impact is equal to 25.4 mm.

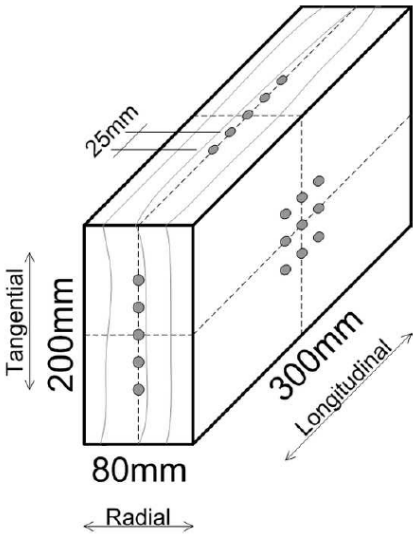

Figure 1. Prism and marked points for application of sclerometry

As proposed by Soriano et al. (2011) during application of impacts, each prism that was fixed to the universal press by a load estimated at 15% of the normal to the fiber strength, considering the timber in the saturated condition. For *Apuleia leiocarpa* species was applied a load of 20 kN, whereas for *Cedrela odorata* was applied a load equal to 4kN. For the application of this load, in both cases it was considered an area of approximately 114 cm². The application of impacts in the tangential direction is shown in Figure 2.

Figure 2. Application of sclerometric impacts.

In order to obtain the static modulus of elasticity, according to Brazilian standards ABNT NBR 7190 (1997), after the performance of esclerometrics tests, of each prism was extracted a specimen of 50 mm x 50 mm x 150 mm (Figure 3), which was submitted to the parallel compression to fibers test.

To obtain the moisture content, of each prism it was also extracted a specimen (20 mm x 30 mm x 50 mm). The specimens were kept for drying in an oven at a temperature of 103 ± 2 ° C, i.e., to stabilize the mass, given by the difference between two consecutive measurements less than 0.5%.

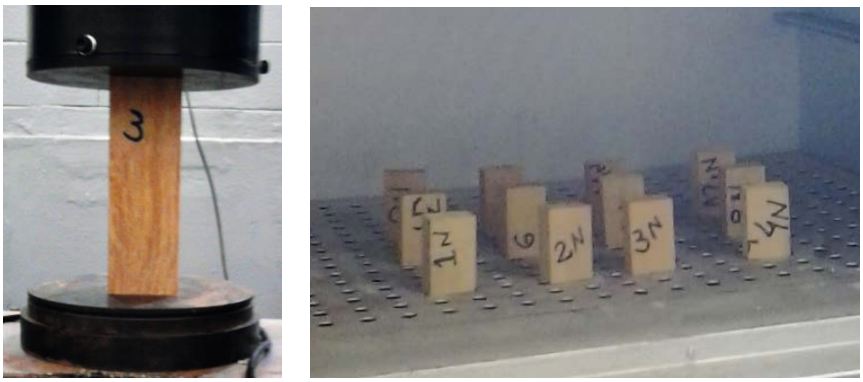

Figure 3. Specimens. **a)** Parallel compression strength to the fibers, **b)** Moisture content.

Results and discussions

The results presented refer to the specimens in equilibrium with the environment, whose moisture content was verified equal to 17% for Garapa and 24.5% for Cedar.

To obtain the esclerometric indexes, the normality of the data was analyzed and the average of impact was used for each anatomical direction of the wood. For the statistical analysis we used the Minitab software (16.1.0), were considered normal data with p-value less than 5%, thereby ensuring 95% confidence in the data normality.

The analysis of results of the static modulus of elasticity generated two groups, indicating that the species used had different mechanical properties as shown in Table 1. The groupings of sclerometric indexes for each species were performed, thus enabling differentiating the three anatomical directions (Table 2).

Table 1. Groupings generated for the static modulus of elasticity.

	Specie	Mean (MPa)	StDev (%)	Grouping (*)
E_L	Apuleia leiocarpa	17384	1597	A
	Cedrela odorata	11949	1639	B

*Similar letters indicate homogeneous groups. StDev = Standard Deviation.

Table 2. Groupings generated for esclerométricos indices relating to anatomical directions.

Specie	Direction	SI Mean	StDev (%)	Grouping (*)
Apuleia Leiocarpa	Tangential	36.1	1.62	A
	Radial	32.6	2.23	B
	Longitudinal	28.5	2.02	C
Cedrela odorata	Tangential	27.6	3.36	A
	Radial	23.9	2.93	B
	Longitudinal	17.0	2.99	C

*Similar letters indicate homogeneous groups. StDev = Standard Deviation..

Given the normality of the data, correlations were established between the values of sclerometrics indexes (obtained for each of the anatomical directions: longitudinal, radial and tangential) and the values of modulus of elasticity parallel to the fibers (Figures 4 to 6).

In the abscissa (Fig. 4 to 6) each value represents the average of impact obtained on a prism. The value of the sclerometric impact is dimensionless to represent the relationship between restored and applied energy. For each anatomical direction with the linear adjustments taking into account the data of both species, the correlations between the properties studied were established.

The use of distinct species favors stronger correlations than those generated with the data of the same species. The example of this can be seen by the results presented Del Menezzi et al. (2010), reaching correlations with R>0.8 (considering different species) and R<0.75 (for the same species).

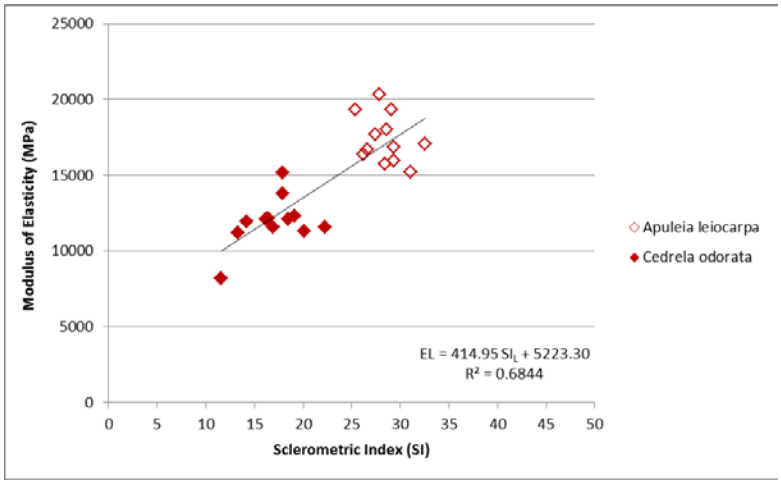

Figure 4. Modulus of elasticity parallel to the fibers versus SI in the longitudinal direction.

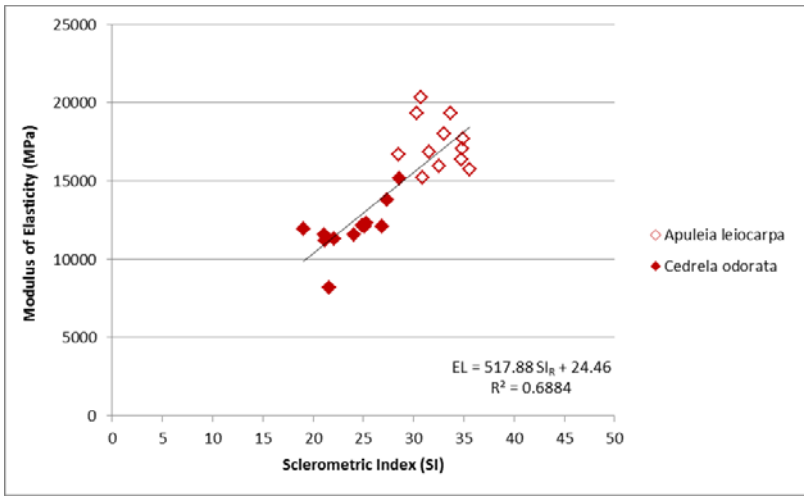

Figure 5. Modulus of elasticity parallel to the fibers versus SI in the radial direction.

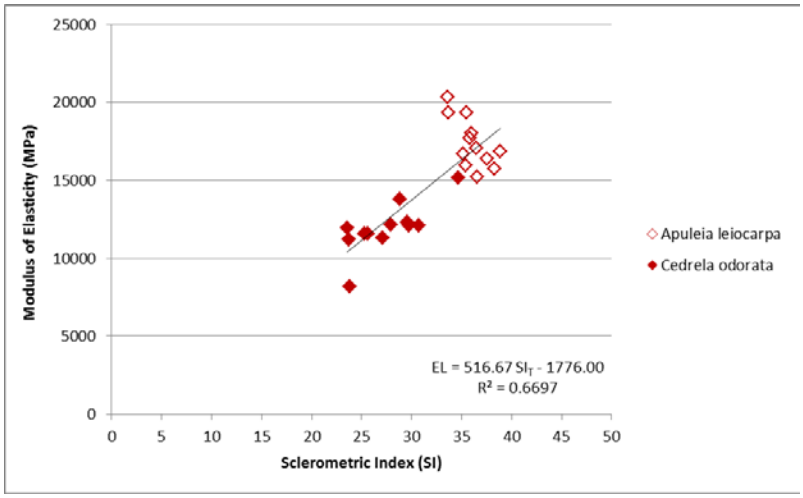

Figure 6. Modulus of elasticity parallel to the fibers versus SI in the tangential direction.

The correlations established that the behavior differs for each anatomical directions, given that the values of the different sclerometry resulted for each of the three anatomical directions. Therefore, three different equations are generated. The radial direction (Fig. 5) showed stronger correlation with R = 0.83. While the weaker correlation was observed for tangential direction with the R = 0.82. These results can be considered satisfactory as compared to correlations between NDT results and the static modulus of elasticity, established by Sales et al. (2011), Cavalli et al. (2013) e Baar (2015).

With the results obtained in this study was shown the possibility of using sclerometry to predict the wood elastic modulus. However, it is necessary to continue this research to increase the confidence of the proposed method. Therefore, other species should also be evaluated and included in the generation of these correlations. The effects of moisture content in these results should also be studied.

Conclusions

With analysis of the results obtained for tropical wood species we concluded that:

- The rebound hammer method has a great potential to be used in estimating the modulus of elasticity of wood. The corresponding correlation coefficient for each anatomical direction was greater than 0.8, with the highest value obtained for the radial direction.
- The equations established to correlation of modulus of elasticity parallel to the fibers and the sclerometric index resulted differently for each anatomical direction.
- Other wood species should be included in this analysis in order to increase the reliability of the proposed method.

Acknowledgments

The authors would like to thank the support of the Brazilian Federal Agency of Coordination for the Improvement of Higher Education Personnel (CAPES) for the Scholarship grants, the Fund to Support to Teaching, Research and Extension (FAEPEX) from the University of Campinas for the financial support and São Paulo Research Foundation (FAPESP).

References

ABNT. 1997. Design of timber structures. NBR 7190. Brazilian Association of Technical Standards. Rio de Janeiro. (in Portuguese).

ASTM. 2013. Standard test method for rebound number of hardened concrete. C805 / C805M-13a, ASTM International, West Conshohocken, PA.

Baar, J.; Tippner, J.; Rademacher, P. 2015. Prediction of mechanical properties-modulus of rupture and modulus of elasticity-of five tropical species by nondestructive methods. *Maderas. Ciencia y tecnología*, (AHEAD), 0-0.

Cavalli, A.; Togni, M. 2013. How to improve the on-site MOE assessment of old timber beams combining NDT and visual strength grading. Nondestructive Testing and Evaluation, 28 (3): 252-262.

Del Menezzi, C. H. S.; Silveira, R. R.; Souza, M. R. 2010. Predicting flexural properties of six Amazonian hardwoods using stress wave nondestructive. Acta Amazonica, 40 (2): 325-332. (in Portuguese)

Esteban, L. G.; Fernandez, F. G.; Palacios, P. 2009. MOE prediction in Abies pinsapo Boiss. timber: Application of an artificial neural network using non-destructive testing. Computers and Structures, 87: 1360‑1365.

Kretschmann, D.; Hernandez, R. 2006. Grading timber and glued structural members. Primary wood processing: principles and practice. Dordrecht, Springer, 339-390.

Sales, A.; Candian, M.; Cardin, V. S. 2011. Evaluation of the mechanical properties of Brazilian lumber (Goupia glabra)by nondestructive techniques Construction and Building Materials, 25: 1450‑1454.

Soriano, J.; Gonçalves, R.; Bertoldo, C. [and other]. 2011b. Application of esclerometer test method in specimens of eucalyptus saligna. Revista Brasileira de Engenharia Agrícola e Ambiental 15(3): 322-328. (in Portuguese)

Soriano, J.; Gonçalves, R.; Trinca. [and other]. 2013. Esclerometer test methods for estimating density of wood. In: 18th International Nondestructive Testing and Evaluation of Wood Symposium, Madison, WI.

Development of an automated portable tester for evaluating dynamic hardness of wood

Adriano Ballarin
Department of Rural Engineering, College of Agronomical Sciences, Botucatu, Sao Paulo, Brazil, awballarin@fca.unesp.br

Albert Assis
Graduate Student, College of Agronomical Sciences, Botucatu, Sao Paulo, Brazil, albert_assis@fca.unesp.br

Rogério Alexandre
Graduate Student, College of Agronomical Sciences, Botucatu, Sao Paulo, Brazil, rpalexandre@fca.unesp.br

Abstract

In Europe the most widely used method for determining wood hardness is the Brinell test, whereas in the Americas the Janka test is predominant. More recently, international studies have reported the use of dynamic hardness for wood, claiming as main advantage the feasibility of tests under field conditions. This paper presents results obtained in the development of the third generation of a portable hardness tester for wood, which uses displacement transducer and embedded electronic processor in order to automate the dynamic hardness measurement. Functional tests of the equipment, carried out using seven species of Eucalyptus, revealed strong correlation to Janka hardness and the possibility of its prediction by dynamic hardness. Beyond that, the classical problems of “sinking-in” and recovery of the indented area where solved by the equipment using under-load measurements of indentation’s depth. Furthermore, this paper introduces a new methodology for dynamic hardness calculation.

Keywords: dynamic hardness, wood, portable hardness tester, Janka hardness, Brinell hardness

Introduction

The quality of wood can be assessed by several different properties, depending on their importance to the end-use of the material (Heräjärvi 2004). For parquet flooring, the hardness is considered to be one of the most important surface property (Meyer et al. 2011), affecting the resistance against abrasion, scratching and wearing (Grekin and Verkasalo 2013). The hardness is also accounted among the major indices of wood quality, due to its good relation with other mechanical properties (Ibama 1993, Hirata 2001, Colenci 2002).

Basically, the hardness expresses the material resistance to the indentation (or penetration) of a body. In a typical test, a hard tool of known geometry is pressed into the body, and the hardness is given by the ratio between the applied force and the size of the indentation (Doyle and Walker 1985). In Europe the most widely used method for determining wood hardness is the Brinell test, whereas in the Americas the Janka test is predominant (Heräjärvi 2004, Grekin and Verkasalo 2013).

Despite of the proven effectiveness of Janka tests, the method has been criticized because of the deformation promoted when the indenter is embedded beyond a certain limit of the material (Doyle 1980). In accordance with International Standard ISO 3350-1975E, the Polish standard PN 90/D-04109 admits Janka Hardness test with half of the original indentation, considering that with the full indentation there is the possibility of wood rupture under and around the indenter (Helinska-Raczkowska and Molinski 2003). For the same reason, the Janka test has not been accepted in Europe (Niemz and Stübi 2000).

The Brinell test is also associated with some inconveniences, especially the difficulty to measure accurately the diameter of the indentation promoted in the material (Niemz and Stubi 2000, Heräjärvi 2004, Colenci 2006, Hansson and Antti 2006). Beyond the sinking-in phenomena around the edge of the indenter tool, the elastic portion recovery of the indentation affects significantly the accuracy of those measurements (Doyle and Walker 1985, Holmberg 2000, Grekin and Verkasalo 2013).

Regardless of advantages or inconveniences of each methodology, traditional hardness tests don't support mobility. The Janka test is predominantly applied in laboratory conditions (Dubovský and Rohanová, 2007) due to the high forces demanded by the method and difficulty to control the indenter depth under field conditions (Colenci 2006, Ballarin et al. 2012). On the other hand, the Brinell test, which involves lower magnitude forces, is dependent on precision both to control the loading rate and measure the indentation diameter.

More recently, international studies have reported the use of dynamic hardness for wood, claiming as main advantage the feasibility of tests under field conditions (Augutis et al. 2005, Colenci 2006, Dubovský and Rohanová, 2007, Meyer et al. 2011, Ballarin et al. 2012).

This paper presents results obtained in the development of a portable hardness tester which uses displacement transducer and embedded electronic processor in order to automate the dynamic hardness evaluation in wood. Two previous generations of this equipment were developed reporting great functionality and good correlation with Janka hardness (Colenci 2006, Ballarin et al. 2010, Ballarin et al. 2012). Despite of their remarkable progress, these previous generations were not automated and thence, led the development of the present generation. Beyond the basic aspects of the third generation, which were already introduced in Ballarin et al. (2013) and Ballarin et al. (2014), this paper brings forward new findings, specifically the methodology for dynamic hardness calculation.

Materials and Methods

The portable hardness tester – DPM3 (Figure 1 - patent pending), is an electro-mechanical equipment whose operating principle is similar to Brinell hardness test, i.e., a cap with spherical format and known diameter is indented into wood using a known force. In this case, the force mobilized to promote indentation is obtained by the free fall of a mass and the hardness value is determined by the ratio between the average impulse force promoted by the indentation and its depth according to equation:

$$HD = \frac{F}{\pi D h} = \frac{m\frac{\Delta v}{\Delta t}}{\pi D h} \quad (1)$$

where *HD* is the dynamic hardness (MPa), *F* is the average impulse force promoted by the indentation (N), *D* is the diameter of the metal sphere (mm), h is the indentation depth (mm), *m* is the mass of the

dropping component, including the indenter (kg*)*, Δv is the velocity variation during the indentation (m.s^{-1}*)* and Δt is the duration time of the indentation (*s*).

Figure 1 - Portable Hardness Tester - DPM3: a) electronic display, b) equipment in the operation position and c) general view

Both the previous generations of the equipment and the early introduction of the third generation used the energy mobilized by the dropping mass instead of the force presented in Equation 1 (Colenci 2006, Ballarin et al. 2010, Ballarin et al. 2012, Ballarin et al. 2013, Ballarin et al. 2014). In the same way, another researcher introducing similar equipment suggested the momentum instead of that force (Meyer et al. 2011). These approaches take into account just the dynamics before the impact between the indenter and the wood; therefore the impulse force of the indentation (reaction force) is ignored. The reaction force is very significant to be disregarded because the harder the material, the lower the duration time to promote that indentation, consequently the impulse force of the indentation varies for each different hardness levels. In order to provide a reasonable meaning to the dynamic hardness, the current

progress of the third generation regards the impulse force of the indentation in the dynamic hardness calculation, as presented in the Equation 1.

An embedded electronic processor was employed in order to record the indentation readings, calculate the velocity variation and duration time of the indentation, and hence compute the dynamic hardness according to Equation 1. The indentation readings were gauged with a displacement transducer linked directly to the processor and the results were displayed in a LCD colored screen.

The dynamic hardness HD (Equation 1) measured by the DPM3was associated with Janka hardness obtained by a universal servo controlled testing machine EMIC, model DL 30000 according to requirements of the Brazilian standard NBR 7190 (ABNT, 1997). Both hardness were determined classically, i.e., direction perpendicular to the grain of wood.

An additional association was performed between the dynamic hardness HD and Janka read with half indentation depth (2.82 mm) in order to verify the correlation of tests with similar indentation depths. Another reason to perform this association was the limitations reported about the Janka hardness, which are related to the over-indentation and consequently possibility of material's failure (Doyle 1980, Helinska-Raczkowska and Molinski 2003, Niemz e Stübi 2000).

The experimental tests were conducted on sixteen specimens (50 mm x 50 mm x 150 mm) obtained from seven species of eucalyptus (Table 1), totalizing 112 specimens.

Table 1 - Main characteristics of the groups of Eucalyptus wood

Group	Specie	Age of the Plantation (years)	Average density(*) ($kg.m^{-3}$)
1	*E.maculata*	35	810
2	*E.microcorys*	35	770
3	*E. tereticornis*	40	950
4	*E. citriodora*	44	980
5	*E. saligna*	50	690
6	*E. dunnii*	20-23	750
7	*E. viminalis*	20	720

(*) – Apparent density based on mass and volume at 12%MC – values reported by suppliers

Results and discussion

As already reported in the early introduction of the equipment (Ballarin et al. 2013, Ballarin et al. 2014), the DPM3 promoted quick and effortless operation, revealing consistent indentation readings. The dynamic hardness HD (Equation 1) was calculated by the electronic processor and showed immediately after the test, as well as additional data as velocity variation and duration time of the indentation.

The procedure for dynamic hardness evaluation using the DPM3 took nearly five seconds, since the placement of the equipment on the specimen until the accomplishment of the test. On the other hand, the Janka test performed by the laboratory machine spent two minutes, excluding the placement of the specimen into the machine.

The indentation was determined under load, avoiding the influence of elastic recovery of the indentation area. Furthermore, by measuring the indentation depth instead of the indented area, the influence of "sinking in" phenomenon was also avoided.

The association of the dynamic hardness HD and Janka expressed moderate to strong correlation (R^2 = 0,873 – Figure 2) furthermore, the similarity of the coefficient of variation for both hardness (Table 2) revealed a fine sensibility of the DPM3 to the Janka hardness variations. This sensibility could be related to the new methodology adopted for dynamic hardness calculation, since the previous methodology (Ballarin et al. 2013, Ballarin et al. 2014) presented half of this coefficient variations for the same specimens set.

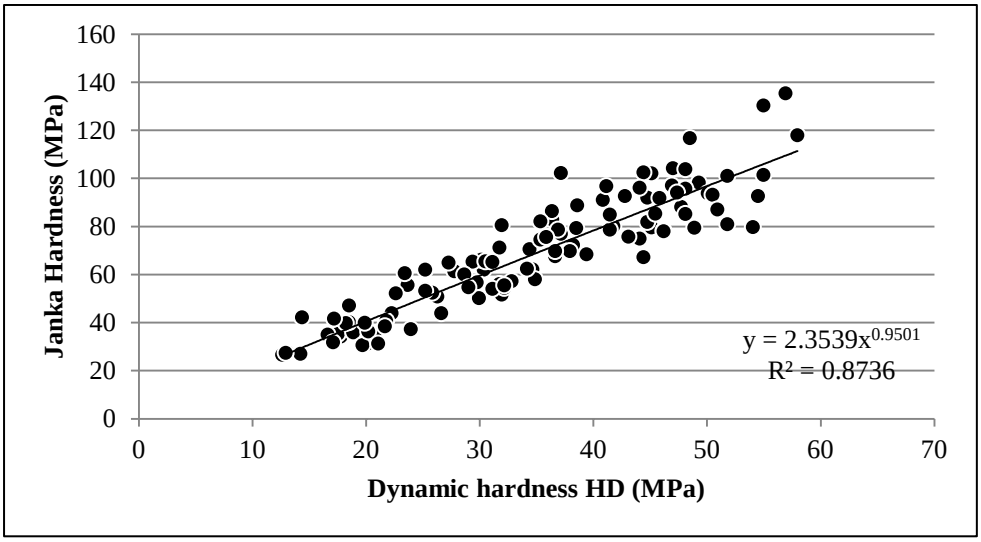

Figure 2 – Hardness Janka versus dynamic hardness HD evaluated by the portable hardness tester - DPM3

Table 2 - Main characteristics of the groups of Eucalyptus wood

Descrip.	Janka Hardness	Dynamic hardness HD
Stat.	(Mpa)	(Mpa)
Mean	69,75	34,84
sd	24,86	12,16
Min	26,70	12,63
Max	135,40	57,96
CV	35,64	34,89
N	112	112

Another positive aspect in considering the reaction force to compute the dynamic hardness is the interrelationship of this hardness and the Janka test. Previously, disregarding the reaction force, the exponent of the power model fitted were expressive ($x^{1,915}$ - in Ballarin et al. 2013 and Ballarin et al 2014) providing necessarily a curvilinear fitting, but using the current methodology, the exponent ($x^{0,95}$) denoted tendency to linear regression.

The Figure 3 compares the regression models for the association between the dynamic hardness HD* and HD with the Janka hardness. The HD* hardness was fitted by $y = 0{,}052\ x^{1,915}$, stated in previous reports

cited above, in turn, the HD was fitted regarding the reaction force, according to the model presented in the Figure 2 ($y = 2{,}353\ x^{0{,}950}$).

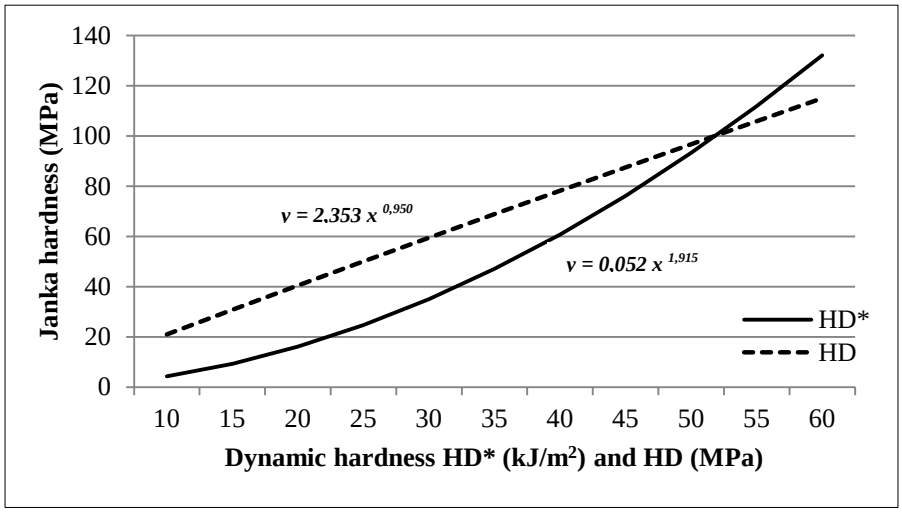

Figure 3 – Fitting model comparison in the association between dynamic hardness HD* and HD versus Janka hardness.

The HD hardness regression tending to linear, expressed in Figure 3, implies a suitable adequacy of this hardness to the Janka hardness, so those higher hardness values of the first one are related to the higher values of the second one likewise the lower values are for both hardness. A nonlinear regression model usually include an extra meaning, in such a way the higher values are not only a magnified version of the lower ones.

The association of the dynamic hardness HD and Janka obtained with half indentation (2.82 mm) expressed a strong correlation ($R^2 = 0{,}912$ – Figure 4) and low dispersion of results in comparison with those seen in Figure 2. These results could be, in a first moment, explained by the similarity of the indentation depths of the associated data but, the already mentioned limitations associated to Janka test (Doyle 1980, Helinska-Raczkowska and Molinski 2003, Niemz and Stübi 2000) suggest the possibility of divergence in the traditional Janka test (performed with full indentation). Therefore, the better correlation of the dynamic hardness with Janka in half indentation (instead of full) could be also explained by the ruptures promoted in the specimens when using the full indentation of Janka test, fact observed in this experimental set.

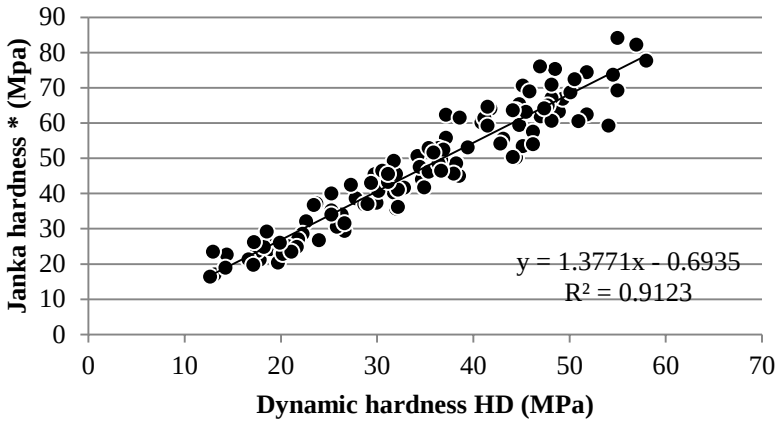

Figure 4 – Hardness Janka (indentation of 2,82 mm) versus dynamic hardness HD - DPM3

The alternative use of shallower indentation depths instead of traditional Janka test were reported in Lewis (1968), where the hardness modulus (obtained from the slope force-penetration) was achieved with 2.5 mm of indentation's depth. In the same way, the American standard ASTM D1037-78 advocates the hardness modulus with 2.5 mm in depth, especially for thin materials, where the traditional Janka test could not be performed.

Conclusions

The following main conclusions can be pointed:

- The Portable Hardness Tester – DPM3 promoted quick, easy and reliable readings of the indentation, as well as evaluation of hardness HD;
- Classical problems of Brinell hardness related to "sinking in" phenomenon and recovery of indented area were solved by the equipment using under loading measurement of the indentation;
- The hardness HD measured from the equipment revealed moderate to strong association to conventional Janka Hardness ($R^2 = 0.87$) and stronger association ($R^2 = 0.91$) to Janka hardness test performed with half the conventional indentation (2.82mm);
- The suggested equation for dynamic hardness calculation, using the reaction force of the indentation, provided a reasonable meaning for the dynamic hardness and suitable adequacy of it to Janka hardness.

Acknowledgments

The authors express their gratitude to FAPESP – Fundação de Amparo à Pesquisa do Estado de São Paulo (08/08414-0) and to the Graduate Program in Agronomy- Energy in Agriculture – FCA/UNESP, for their financial support.

References

American Society for Testing Materials. 1987. ASTM D1037-78: Hardness Modulus Test - Number of Penetrations, 234, 1987.

Associação Brasileira de Normas Técnicas. 1997. Projeto de estruturas de madeira. NBR 7190. Rio de Janeiro.

Augutis, S. V. et al. 2005. The hardness testing by means of indentation for low density materials. Matavimai = Measurements/Kauno Technologijos Universitetas. p. 1292-1323.

Ballarin, A. W. et al. 2010. Portable hardness tester for timber classification. In: WCTE 2010 – Word Conference on Timber Engineering, 8p.

Ballarin, A.W. et al. 2012. Estimating hardness of eucalyptus wood with a portable hardness tester. In: WCTE 2012 – World Conference on Timber Engineering, 4p.

Ballarin, A. W. et al. 2013. Development of a portable hardness tester for wood using displacement transducer. In: 18th International Nondestructive Testing and Evaluation of Wood Symposium, Madison / WI – EUA, FS - Forest Products Laboratory - Forest Service, v. 1. p. 511-517

Ballarin, A. W. et al. 2014. Development of a portable hardness tester for wood using displacement transducer. In: WCTE - World Conference on Timber Engineering, 2014, Quebec – Canadá, University of Laval, 2014. v. 1. p. 1-5.

Colenci, R.A. 2002. Qualificação mecânica de madeiras para uso como dormente ferroviário. Botucatu, SP: Sao Paulo State University, 90p. M.S. thesis.

Colenci, R. A. 2006. Desenvolvimento de equipamento para avaliação em campo da dureza de madeiras para dormente ferroviário. Botucatu, SP: Sao Paulo State University, 83p. PhD thesis.

Doyle, J. 1980. The hardness of wood. Ph.D.- Thesis, University of Canterbury, Christchurch, N.Z.

Doyle, J.; Walker, J.C.F. 1985. Indentation hardness of wood. Wood and Fiber Science. 17(3): 369-376

Dubovský, J.; Rohanová, A. 2007. Static and dynamic hardness of chosen wood species. In: Proceedings of the 2nd International Scientific Conference Woodworking Technique, Zalesina, Croatia, 11-15 September, 2007. Faculty of Forestry, University of Zagreb, p. 27-32.

Grekin, M.; Verkasalo, E. 2013. Variations in and Models for Brinell Hardness of Scots Pine Wood from Finland and Sweden. Baltic Forestry, v. 19, p. 128-136.

Hansson, L.; Antti, A. L. 2006. The effect of drying method and temperature level on the hardness of wood. Journal of Materials Processing Technology, v. 171, n. 3, p. 467-470.

Helinska-Raczkowska, L.; Molinski, W. 2003. The effect of the Janka ball indentation depth on the hardness number determined for selected species. Folia Forestalia Polonica. 34: 27-36

Heräjärvi, H. 2004. Variation of basic density and Brinell hardness within mature Finnish Betula pendula and B. pubescens stems. Wood and fiber science, v. 36, n. 2, p. 216-227.

Hirata, S. et al. 2001. Hardness distribution on wood surface. Journal of Wood Science, v. 47, n. 1, p. 1-7.

Holmberg, H. 2000. Influence of grain angle on Brinell hardness of Scots pine (Pinus sylvestris L.). Holz als Roh-und Werkstoff. 28: 91-95

Instituto Brasileiro do Meio Ambiente e dos Recursos Renováveis. 1993. Amostragem e propriedades físico-mecânicas de madeiras amazônicas. Brasília: IBAMA, Coleção Meio Ambiente – Serie estudo floresta, nº 1.

Lewis W. C. 1968. Hardness modulus as an alternative measure of hardness to the standard Janka ball for wood and wood-base materials. Forest Products Lab Madison WIS.

Niemz, P.; Stübi, T. 2000. Investigations of hardness measurements on wood based materials using a new universal measurement system. In:_____ Proceedings of the symposium on wood machining, properties of wood and wood composites related to wood machining. Vienna, p. 51-61.

Meyer, L. et al. Dynamic and static hardness of wood: method development and comparative studies. International Wood Products Journal, v. 2, n. 1, p. 5-11, 2011.

Analysis of Wood Transversal Tension Mechanical Behavior by Digital Image Correlation

Far-Ching Lin
School of Forestry and Resources Conservation, National Taiwan University, Taipei, Taiwan,
farching@ntu.edu.tw

Chung-Cheng Chiu
School of Forestry and Resources Conservation, National Taiwan University, Taipei, Taiwan,
r01625037@ntu.edu.tw

Feng-Cheng Chang
School of Forestry and Resources Conservation, National Taiwan University, Taipei, Taiwan,
fcchang@ntu.edu.tw

Abstract

The purpose of study was to predict wood strength through analysis of strain distribution. Transversal tension test with specimens of China fir (*Cunninghamia lanceolata*) was conducted and global strain was measured by DIC (Digital image correlation). Then, the data was drawn strain-area cumulative curve and benchmark strain location curve that could quantize strain concentration.

Results show the maximum strain at pith is 0.36, far greater than 0.002 of that at latewood both were discontinue of material lead to strain concentration.

It was hard to categorize the characteristic of each specimen from different cutting location by area ratio of strain integral-time curve calculated from strain-area cumulative curve. Only specimens with pith curve type could be found. There is significant positive linear relationship between area ratio of strain integral and strength expect the specimens with defects beneath the wood surface which severely deteriorated the strain concentration.

Both ultimate strain gradient calculated from benchmark strain location curve and the distance of maximum strain area to crack showed positive correlation to strength exponential with R-square values 0.78 and 0.68, respectively. The slope of maximum strain gradient-time curve could predict strength before failure which has negative correlation to strength exponential with R-square values of 0.82. Thus, strain concentration owing to wood structure transition determined the fracture type and failure time.

Keywords: Digital image correlation, strain concentration, transversal tension

Introduction

The knowledge regarding wood mechanical properties is fundamental in determining structural applications of wood. However, predicting stress distribution in wood is difficult. Stress concentration could occur because of many reasons, such as knot, notch, pith, internal void structure, earlywood -latewood boundary, juvenile-mature boundary (Oscarsson *et al*.,2012). Digital image correlation (DIC) techniques can be employed to observe and measure the deformation or displacement of materials, and consequently obtain the overall strain distribution, there by facilitating determining strain concentration areas and the degree of strain concentration.

DIC offers a highly accurate means for measuring strains in wood. Specifically, the advantages of

DIC are that it enables a noncontact measurement; moreover, such measurement process is not affected by the deformation or failure of a specimen. These advantages render DIC suitable for detecting wood deformation during strength testing. Tensile strains of wood were typically determined by measuring deformations of specimens; conversely, DIC detects the intensity change of pixels on a specimen image to estimate strain. For example, summing up the pixel change of all grid points along the longitudinal direction of a specimen provides the overall longitudinal change of the specimen.

The occurrence of wood defects is associated with the orthotropic, cellular structure of wood. Samarasinghe and Kulasiri (2000) used a DIC technique to observe wood tensile strain distribution. They revealed that despite the direction of loading, the variation of displacement in longitudinal direction was greater than that in transversal directions. This phenomenon can be explained that buckling of wood cell walls and internal shear forces caused an uneven stress distribution in wood. In addition, connecting parts in wood internal structure may contain various contents and voids, therefore resulting in a change of failure occurring at such locations.

Buksnowitz et al.(2010) employed DIC to compare the strain distribution of wood knots and artificial holes and concluded that the local fiber orientation at defects could affect load transfer and strain distribution in wood. Dill-Langer (2002) proposed a model to monitor micro fracture in wood.

According to Dill-Langer, cracks in radial direction propagated in the interface zone between adjacent tracheids, whereas tangential tension caused rupture in radial direction. Furthermore, some studies (Jernkvist and Thuvander, 2001; Farugia and Perré, 2000) have applied DIC to measure the radial deformation behaviors of spruce and indicated that the lowest and highest strains occurred at the latewood and the adjacent earlywood, respectively. Therefore, the correlation between strain variation and material failure was confirmed.

The variation of displacement is more readily to be determined in transversal directions than in longitudinal direction (Samarasinghe and Kulasiri, 2000).Therefore, this study explored transversal tensile behaviors of wood by using a DIC technique and investigated strain distributions generated because of structural variability and defect existence. In addition, this study determined the change of strain concentration with time and provided a reference for the prediction of wood tensile strength and other basic mechanical properties.

Materials and Methods

The specimens were fabricated using the heartwood of 25-year-old China fir (*Cunninghamia lanceolate*), which was obtained from National Taiwan University Experimental Forest in Xitou, Taiwan. Forty tensile specimens were machined by centering the log pith and cutting specimens at the locations marked as *L0–L3* (Figure 1-a). All the specimens were sampled from one tree log.
The procedure of Wood-Determination of Tensile Properties, CNS 456, was adopted to fabricate tensile specimens (Figure1-b). The specimens had the length of 150 mm, width and thickness of same 20 mm, radius of curvature of 145 mm, and curve length of 75 mm. The specific gravity (SG) and moisture content (MC) were determined according to Wood-Determination of Density for Physical and Mechanical Tests, CNS 451, and Wood-Determination of MC for Physical and Mechanical Tests, CNS 452, respectively. Concurrently, the specimens were prepared by using particular white and black inks to produce a random dot pattern (speckle pattern) to their cross-sectional surfaces. Therefore strains on such surface scan be measured using DIC (Figure1-c).

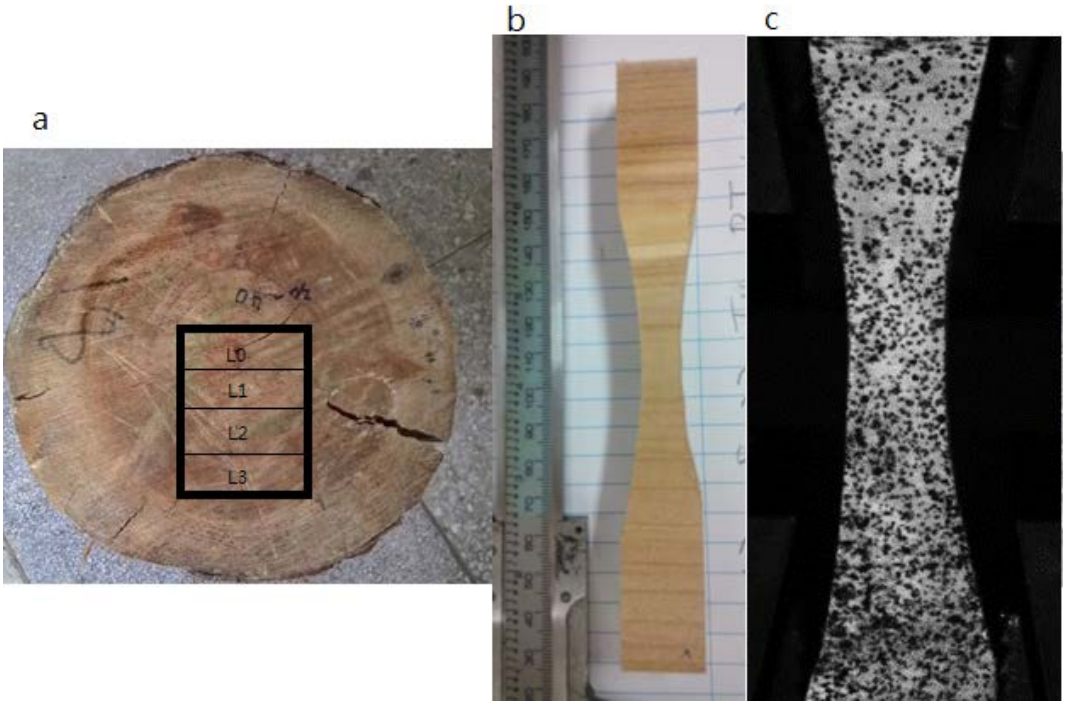

Figure1--Tensile test specimen: (a) Scheme of specimens cut location on disk; (b) clear surface; (c) random speckle pattern cover.

Tension tests were conducted using a universal testing machine (Shimadzu UH-10A). Loading speed was set to 2mm/min. A charge-coupled device (CCD; GRAS-20S4M, Lens M5018-MP2; f= 50mm and F= 1.8, pixel size 4.4 μm, and resolution is 2 megapixel, 1624 ×1224)) was used to capture images. To conduct the DIC analysis, a single light source was used, and images were capture at a frequency of 2Hz. Images were captured using a DIC software, Vic-2D. By comparing the images of a specimen before and after its deformation, the full-field strain distribution of the specimen can be determined.

Because of the mechanism of DIC, the internal strain of specimens cannot be calculated. However, breakages of specimens did not always take place on the surface. Therefore, this study involved two methods to explore how strains distributed on the surface change with time and space and how such strains affect specimen strength.

To determine the variation of strain distribution at various time points, the images were arranged according to the strain value and employed to plot the strain-area cumulative curve (SACC) at each time point (Figure 2).Point *B* has the maximum strain value of the curve. By differentiating the curve, the inflection point *A* was identified, which was also the median point of the overall strain range. Strains whose value was higher than that of point *A* were integrated along the curve to calculate the area of the high-strain zone. As shown in Figure 2, the points *A* and *B* define an *A*-*B* rectangular zone. Through dividing the calculated the area of the high-strain zone by the *A*-*B* total area, an area ratio of strain integral (ARSI) was obtained. The function of calculating such ratio was also shown in Figure 2. The ARSI can be used to describe the path of the strain curve, thereby presenting the changes of strain.

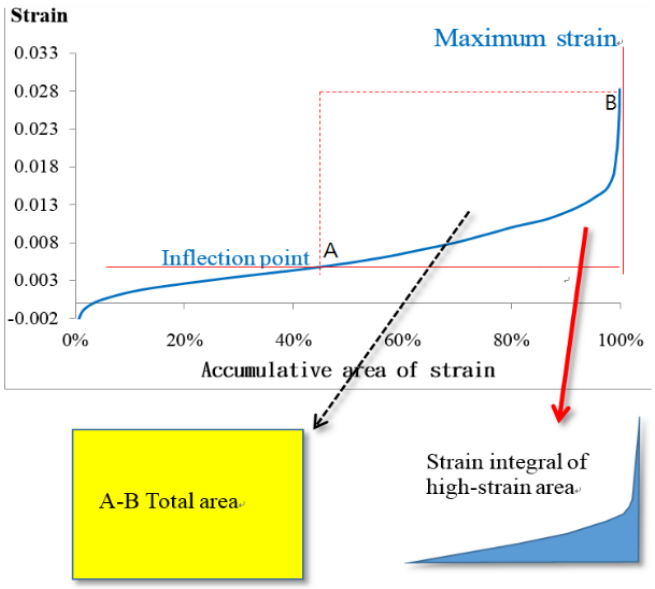

$$\frac{Strain\ integral}{A-B\ Total\ area} = Area\ ratio\ of\ Strain\ Integral$$

Figure2--Calculation for area ratio of strain integral

Subsequently, by using DIC, the maximum strain location on the specimen surface was identified. Moreover, strains along a line normal to the tensile direction of the specimen were averaged at the middle point of the line. By plotting all the average strains along the tensile direction, a benchmark strain location curve (BSLC) was formed (Figure 3). Such curve was then applied to determine the gradients at the measured maximum strain location and the actual failure location. The maximum strain and failure location on the BSLC was marked with dash lines.

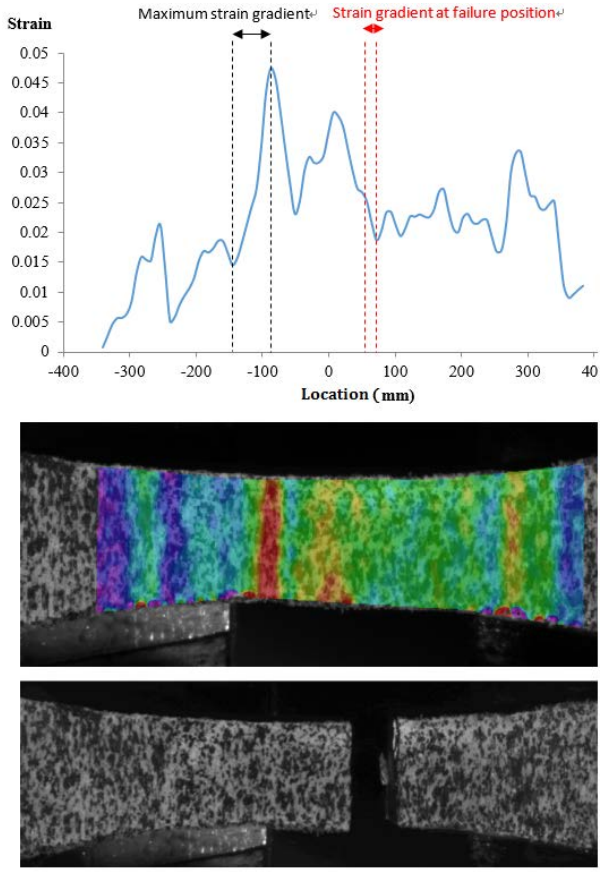

Figure3--Schematic graph of strain gradient determination

Specifically, the strain gradient of a peak strain on the BSLC was estimated by calculating the strain difference between the peak and adjacent valley values and dividing the difference by the distance between the peak and valley. The strain gradient generated quantified the degree of strain change of the specimen. The maximum strain gradient and strain gradient at failure location were demonstrated in Figure 3.

Results and Discussion

The physical and mechanical properties of the specimens were summarized in Table 1. The tensile strength of the specimens ranged from 0.5 to 6.3MPa; the mean value was 3.649MPa and the coefficient of variation (COV) was 38.73%. The strength was found clustered at a range of 3.5–4.5MPa while the first and third quartiles being 2.7 MPa and 4.5 MPa, respectively. Moreover, obvious defects or strain concentration was observed in the specimens whose strength is lower than 2.7 MPa. The mean of Young's modulus and COV of all the specimens were 270MPa and 36.3%, respectively. Furthermore, specimens obtained by cutting the log at the *L0* and *L1* locations (Figure 1-a) exhibited a relatively large tensile strength variation.

Table 1-- Physical and mechanical properties of the specimens

Young's modulus （MPa）	Tensile strength （MPa）	SG	MC （%）
264(34.2%)	3.64(41.1%)	0.464(12.2%)	23.63(10.1%)

Numbers in parentheses are coefficient of variation

The strain distribution and occurrence of strain concentration on the specimen surface were affected by defects, grain orientation, and earlywood-latewood boundary on the surface. In the full-field strain distribution images captured by DIC, different colors were used to demonstrate distinct strain levels; namely, the color varies from red to purple indicates the strain ranges from the highest to lowest (Figure 4). The red and yellow colors indicate the high-strain zone, which accounts for one-fourth of the overall strain range. Most the specimens in this zone possessed structural flaws on their surfaces, such as pith, earlywood-latewood boundary, thereby resulting in strain concentration.

According to the specimen cut location, the variation of strain distribution on the specimen surface caused by defects was readily to identify. For example, regarding the specimens obtained from *L0* location of the log (Figure 1-a), their critical defect was the pith. The strain values of these specimens were higher than 0.3, and the maximum was 0.36; which indicated a strain concentration and strength reduction among these specimens.

However, when the pith did not present on the specimen surface, the strain value of the specimen was relatively low, and no strain concentration was detected. Moreover, the earlywood-latewood boundary was commonly observed in the specimens sampled from the *L1* and *L3*locations of the log. When a load transferred from the earlywood to latewood, strain absurdly decreased, conversely, a sudden strain increase occurred when the load transfer process reversed. In addition, the strain of the latewood ranged 0.002–0.005 in the specimens, whereas that of the earlywood had a broader range of 0.02–0.065.

In this study, DIC was employed to acquire images of the specimens at various time points throughout the loading process until the specimen failure; therefore, the strain distribution at each time point was determined. By arranging these images in a strain increasing order, SACCs were plotted (Figure 5). As Figure 5 shows, the SACC was affected by time. A long loading time generated a large high-strain integral area, therefore resulting in a large ARSI, vice versa. Consequently, a large ARSI indicated the occurrence of strain concentration. Therefore, time critically affected the strain distribution of the specimen.

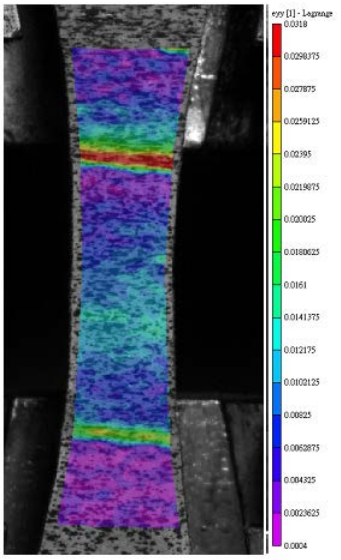

Figure4--Strain distribution in a DIC image

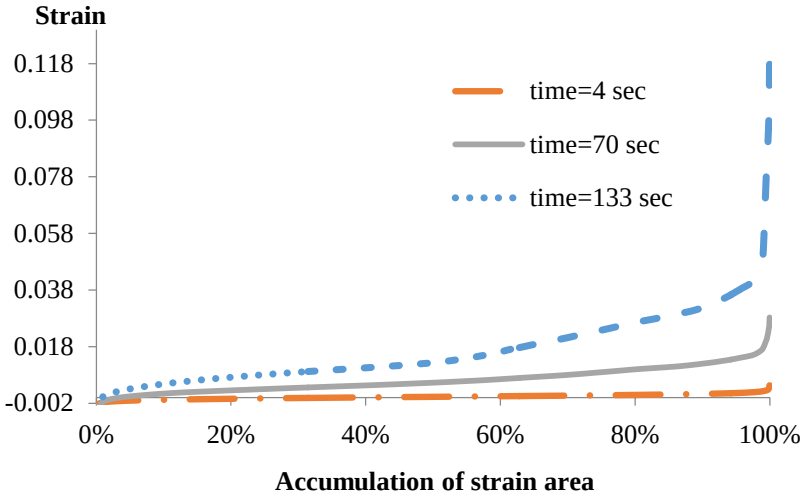

Figure5--Strain accumulation over time

The structural characteristics on the specimen surface (e.g., pith, earlywood-latewood boundary) caused maximum strain gradient values. By applying a regression analysis, the maximum and failure strain-gradient-to-strength relationship curves were obtained (Figure 6-a, b). Both the maximum and failure strain gradients were highly correlated the strength with the R-square of 0.78 and 0.68, respectively. Moreover, both strain gradients specimens exhibited a negative exponential relationship with the strength (Figure 6-a,b). Furthermore, the specimens with low strength values were observed to fail at the maximum strain gradient location, which closed to the maximum strain location. This observation indicated that strain variation caused by defects.

By comparing the strain distribution with the derived BSLC, relatively detailed strain differences can be observed. Depending on where the specimen acquired from the log, the maximum strain and possible strain concentration could occur at three locations, namely the pith, central area of the earlywood, and earlywood-latewood boundary. Such distinct locations indicated that the load transfer in wood was affected by wood structural characteristics. For example, the maximum strain occurred at the pith in only the specimens acquired from the *L0* location and at the central area of earlywood for most the specimens from the *L0* and *L1* locations. Among the specimens from *L2* location, high strains (including the maximum strain) existed at both the central area of the earlywood and earlywood-latewood boundary. In addition, most the specimens from *L3*location exhibited high strains at the earlywood-latewood boundary.

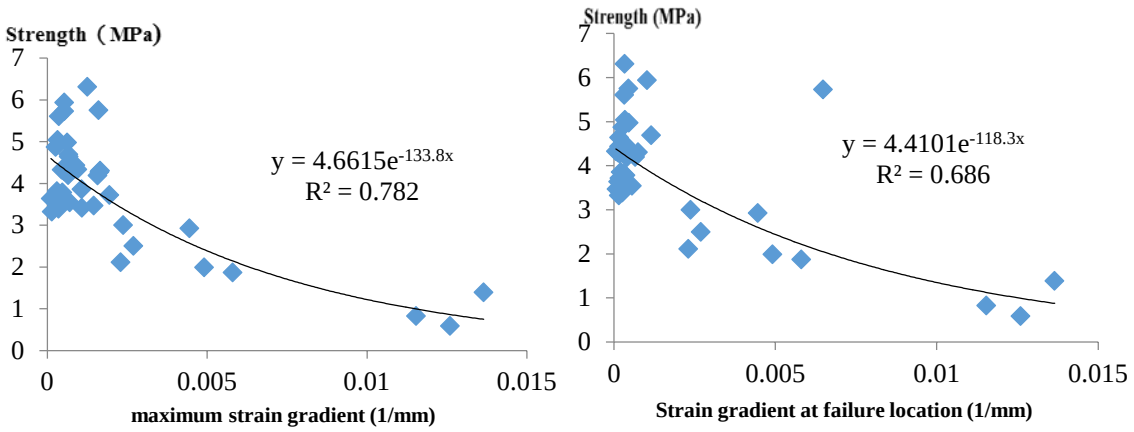

Figure 6--Relationship between strength and (a) maximum strain gradient; (b) failure strain gradient

By differentiating the specimen strain gradient in the maximal strain zone with respect to time, a slope at each strain point was obtained. Through a regression analysis, a slope-strength relationship at the time point right before failure was determined, and the R-square was 0.82, indicating that the change of strain gradient was highly correlated with the strength (Figure7). Additionally, the results showed that the change rate of strain gradient increased during loading and the strain concentration occurred would affect the ultimate strength.

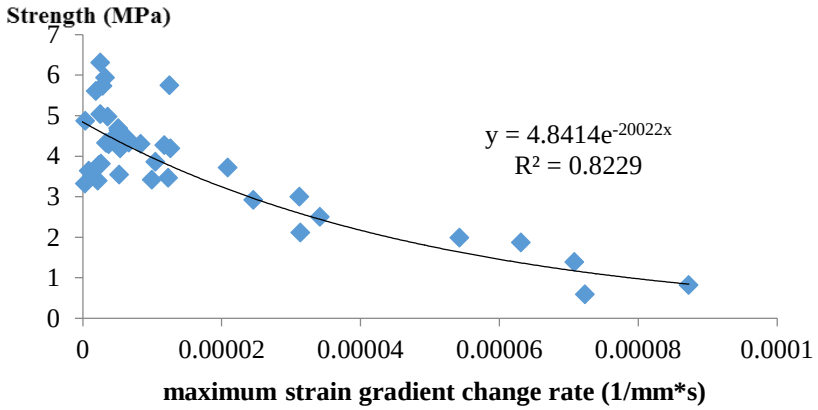

Figure 7--Relationship between strength-maximum strain gradient change rate

Conclusion

This study aimed to investigate the relationship between the wood transversal strain distribution and tensile strength. For this purpose, this study adopted a DIC technique to measure the full-field strain distribution data, and such data were presented in the SACCs and a BSLC.
The ARSIs were calculated from the SACCs; small ARSIs indicated a high degree of strain concentration. The regression between ARSIs and wood tensile strength generated an R-square value of 0.66. Moreover, the BSLC was an explicit presentation of strain distribution and was applied to determine strain changes in wood.

The maximum strain and the strain gradient at the failure location on the verge of failure were calculated. The maximum and failure strain-gradient-to-strength curves derived showed a negative exponential relationship between the strain gradient and strength, and the R-square value was0.78 and 0.68, respectively.

The relationship of the slope of time-dependent maximum strain gradient and strength also showed a negative exponential correlation with as R-square value of0.82.Such high correlation implied that the change rate of the maximum strain gradient may predict wood transversal tensile strength; namely an increased strain gradient change rate indicated a decrease of wood strength.

References

Buksnowitz, C.; Hackspiel, C.; Hofstetter, K.; Mueller, U.; Gindl, W.; Teischinger, A. 2010. Knots in trees: strain distribution in a naturally optimised structure. Wood Science and Technology. 44: 389-398.

Dill-Langer, G.; Lütze, S.; Aicher, S.2002. Microfracture in wood monitored by confocal laser scanning microscopy. Wood Science and Technology. 36(6): 487-499.

Farruggia, F.; Perré, P.2000. Microscopic tensile tests in the transverse plane of earlywood and latewood parts of spruce. Wood Science and Technology. 34(2): 65-82.

Griffith, A.A.1920. The Phenomena of Rupture and Flow in Solids. Philosophical Transactions. 221: 163-198.

Jernkvist, L.O.; Thuvander, F.2001. Experimental determination of stiffness variation across growth rings in Picea abies. Holzforschung. 55(3): 309-317.

Oscarsson, J.; Olsson, A.; Enquist, B.2012. Strain fields around knots in Norway spruce specimens exposed to tensile forces. Wood Science and Technology. 46: 593-610.

Samarasinghe, S.; Kulasiri, G.D.2000. Displacement fields of wood in tension based on image processing: Part 1. Silva Fennica. 34(3): 251-259.

Schreier, H.; Orteu, J.J.; Sutton, M.A.2009. Image Correlation for Shape, Motion and Deformation Measurements : Basic Concepts,Theory and Applications. Springer, NewYork.
Thomason, P.F.1990. Ductile Fracture of Metals. Pergamon Press. Oxford.

Contact angle technique to infer wettability of plasma treated solid wood

Pedro Henrique G. de Cademartori
Wood and Forestry Science Center, Federal University of Paraná, Curitiba, Brazil, pedrocademartori@gmail.com

Bruno D. Mattos
Integrate program in Engineering & Materials Science, Federal University of Paraná, Curitiba, Brazil, brunodufaumattos@gmail.com

André L. Missio
Forestry Engineering, Forest Products Laboratory, Federal University of Santa Maria, Santa Maria, Brazil, andreluizmissio@gmail.com

Graciela I. B. de Muniz
Wood and Forestry Science Center, Federal University of Paraná, Curitiba, Brazil, gbmunize@ufpr.br

Washington L. E. Magalhães
Embrapa Forestry, Estrada da Ribeira, Km 111 – P.O Box: 319, ZIP code: 83411-000, Colombo, Brazil, washington.magalhaes@embrapa.br

Abstract

This study aimed to investigate the effect of plasma treatment on wettability of furfurylated pine wood using contact angle technique. Free-defect Loblolly pine samples were immersed at atmospheric pressure in two different furfuryl alcohol solutions to obtain two levels of weight percent gain, 15 and 40%. Surface of untreated and furfurylated wood samples were modified by plasma treatment in a RF cold-plasma reactor. The argon plasma treatment were performed in low-pressure at 80 W for 120 s. Wettability parameters were measured by non-destructive sessile drop type contact angle at 1, 4, 8, 12 and 20 days after the plasma treatment. Apparent contact angle, work of adhesion and surface free energy were determined. The wettability of untreated and furfurylated wood was enhanced significantly. Apparent contact angle decreased and the pine wood surface became highly wetted. The plasma treatment converts the hydrophobic furfurylated wood surface into a hydrophilic surface. Furfurylated wood partially recovered their natural hydrophobicity after aging. Nevertheless, even after the aging effects, the high degree of wettability may be important for future applications in industrial processes.

Keywords: glow discharge, furfurylation, contact angle, wood surface, wood technology.

Introduction

In the last decades, many alternatives have been developed to improve wood properties, especially related to mechanical strength, dimensional stability and decay resistance. Nevertheless, some of these alternatives could inactivate wood surface, which is undesirable for coating and adhesion aspects. *In situ* polymerization (Mattos et al. 2015; Venas and Rinnan 2008), heat treatment (Cademartori et al.

2013; Missio et al. 2015) and wax impregnation (Scholz et al. 2010) are examples of treatments that improve wood properties – especially hydrophobicity - but could inactive wood surface. This phenomenon of surface inactivation reduces the materials' surface free energy, resulting in liquid poor wettability (Nussbaum 1999). According to Christiansen (1991), some mechanisms of attractive reduction on wood surface influencing wood inactivation, such as migration of wood extractives to surface, micropores closure, surface oxidation and reorientation of molecular surface.

Taking the surface inactivation into consideration, changes on wood surface are interesting to increase wettability and adhesion without modify their bulk structure. Plasma technique is a high-tech alternative to improve the performance of materials' surface. Among the applications in forest sector, plasma has been widely used to increase surface adhesion of wood-based panels (Cademartori et al. 2015), solid wood (Acda et al. 2012, Asandulesa et al. 2012) and natural fibers (Xiao et al. 2015).

One of the most simple and efficient tools to evaluate plasma changes on materials' surface is the non-destructive contact angle. This technique has been commonly applied in recent studies of plasma treated wood-based products (Magalhães and Souza 2002; Aydin and Demirkir 2010; Liu et al. 2010; Poaty et al. 2013; Cademartori et al. 2015). Contact angle of polar and nonpolar solvents could infers changes on surface free energy, which is in relation to coating characteristics of wood and wood-based products (Pétrissans et al. 2003). Nevertheless, determination of contact angle should considers both chemical nature and roughness of surface (Adamsom 1990). Among the methods for non-destructive contact angle measurement, sessile drop is commonly applied to evaluate surface of wood and wood-based products. Sessile drop directly measures a droplet of a liquid resting on a flat surface of a solid (Adamsom 1990).

In this study, pine wood was treated with furfuryl alcohol to create a hydrophobicity surface with poor wettability. The effect of argon plasma treatment on wettability of furfurylated wood was evaluated. Plasma-treated furfurylated wood samples were stored at room environment for 20 days and the effect of aging was evaluated by contact angle technique.

Material and Methods

Raw material

Free-defect Loblolly pine (*Pinus taeda*) wood was cut into small pieces of 50 x 50 x 25 mm (length, width and thickness, respectively). All the samples' surface were sanded and kept in a climatic chamber (20°C and 65% of relative humidity) to reach the equilibrium moisture content.

Furfurylation

Loblolly pine samples were kept immersed at atmospheric pressure in two different furfuryl alcohol solutions. Wood samples were impregnated with furfuryl alcohol (Aldrich, 98% purity) for 4 and 72 hours to obtain two levels of weight percent gain, 15 and 40%. Citric acid at 4% w/v was used as the catalyst of the polymerization. After the impregnation, wood samples were kept wrapped in aluminum foil and were oven-dried at 90±2ºC for 24 hours. These steps are based on the methodology described by Magalhães and Silva (2004).

Plasma treatment

Plasma treatment was performed in a cold plasma stainless steel cylindrical reactor previously described in Cademartori et al. (2015). This reactor was developed in Embrapa Forestry and works at low-pressure in a RF (radio frequency, 13.5 MHz) system (Figure 1A).

Before the plasma treatment, argon was introduced inside the reactor to remove contaminants. Subsequently, glow discharge (Figure 1B) was performed at ~0.3 torr pressure with a gas flow of 20 sccm. Power applied was 80 W and time of discharge was 120 seconds. After plasma treatment, all the wood samples were kept in a desiccator to avoid contact with air humidity.

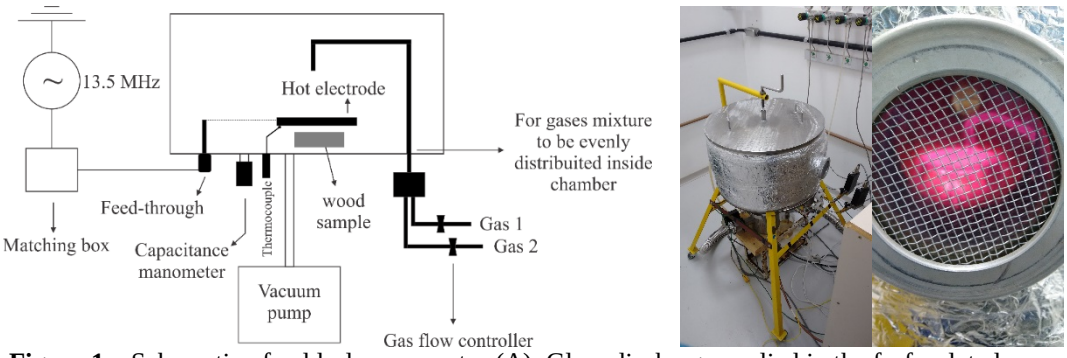

Figure 1—Schematic of cold-plasma reactor (A); Glow discharge applied in the furfurylated wood.

Wettability

The sessile drop type contact angle technique was used to measure changes on wettability of plasma treated pine wood. Apparent contact angle, work of adhesion and surface free energy parameters were determined in a goniometer Krüss DSA25 as a function of the time of droplet deposition. The first measurement was twenty-four hours after the plasma treatments by depositing three droplets of deionized water (surface tension of 72.80 mN m^{-1}) with 5 µl volume on the surface of each sample. The apparent contact angle was measured after 5 s and 15 s of droplet deposition on samples' surface.
Aging effects on untreated and plasma-treated furfurylated wood surface were evaluated after storage in a room at 20±5ºC and 65±5% of relative humidity for 20 days. Wettability parameters were measured after 1, 4, 8, 12, 20 and 20 days of storage.

Results and Discussion

Before the plasma treatment, apparent contact angle (CA) at 5s of droplet deposition of untreated wood was similar to CA of furfurylated wood. Nevertheless, CA of furfurylated wood showed a stabilization after 15s on wood surface, while CA of untreated wood decreased around 14%. This confirms the efficiency of treatment with furfuryl alcohol to improve hydrophobicity of wood surface.

Table 1— Apparent contact angle of untreated and furfurylated wood before the plasma treatment.

Treatment	Contact Angle (°)	
	After 5 s	After 15 s
Untreated	95.18 ± 17.13	82.48 ± 16.36
15% load level (15% FA)	107.54 ± 9.66	105.28 ± 8.16
40% load level (40% FA)	101.28 ± 6.67	99.33 ± 5.55

Plasma treatment affected significantly wood surface of untreated and furfurylated wood. Plasma treatment converts hydrophobic furfurylated wood into a hydrophilic material, especially 15% FA samples (CA reduction of ~93%). Wood samples with 40% FA were less susceptible to the plasma treatment, wherein CA reduction was ~68% in the first day after the surface activation (Figure 2A). Work of adhesion (WoA) and surface free energy (SFE) presented an inverse behavior of CA (Figure 2B and 2C). Activation of surface reduces apparent contact angle, which results in higher wood surface reactivity. Thus, efficiency of finishing steps – coating and bonding – should be better. Previous studies

infer this CA decrease to introduction or formation of oxygen-containing functional groups on materials' surface (De Geyter et al. 2007; Liu et al. 2013; Cademartori et al. 2015).

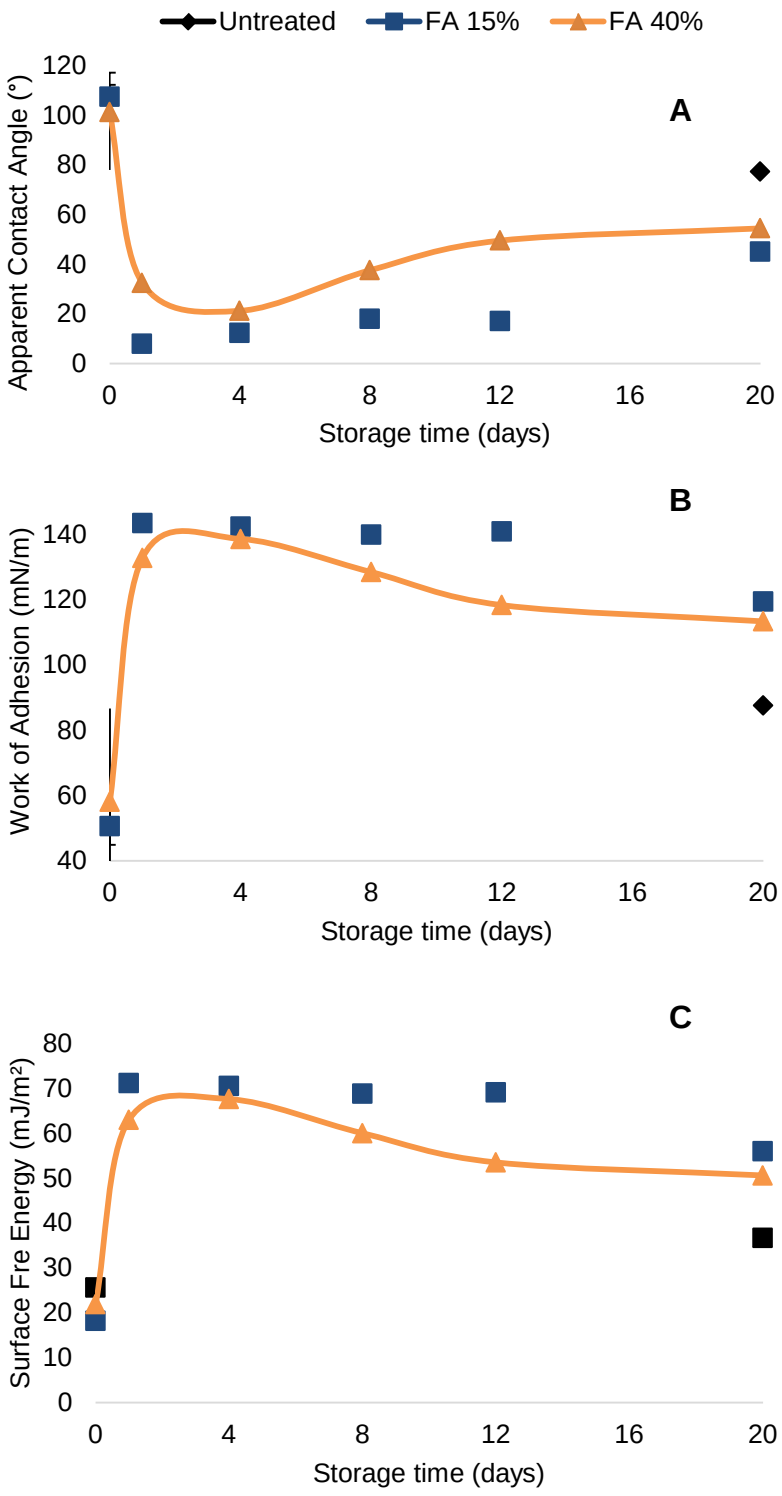

Figure 2—The effect of aging on apparent contact angle (CA), work of adhesion (WoA) and surface free energy (SFE) of untreated and furfurylated wood before (time=0) and after plasma treatment.

Figure 2A illustrates the aging effect on untreated and furfurylated wood surface after the plasma treatment. CA of both woods increased with increasing storage time. This loss of plasma effect during aging was described by previous studies with polypropylene (Yun et al. 2004), synthetic fibers (Liu et al. 2013) and solid wood (Novák et al. 2015). Plasma treatment is not permanent, since species generated by plasma are high instable (Sanchis et al. 2008). The same authors concluded partial hydrophobic recovery occurs due to the rearrangement of polar species on materials' surface.
The effect of aging is more intense in untreated samples, mainly after 8 storage days. After 20 storage days, furfurylated wood samples recovery part of their surface hydrophobicity. Nevertheless, CA average values are significant lower than CA measured before the plasma treatment. From industrial process point of view, this behavior is interesting, in the course of which the plasma treated wood samples remain with high surface reactivity for application of finishing products. This is also proved by the WoA behavior of plasma treated furfurylated wood after 20 storage days (Figure 2B).

Conclusions

Wettability of untreated and furfurylated pine wood increased significantly after plasma treatment. Apparent contact angle, work of adhesion and surface free energy clearly showed loss of plasma effects during aging, wherein untreated and furfurylated wood recovery part of its hydrophobicity after 20 storage days. Surface of furfurylated wood was less susceptible to the plasma treatment due to its natural water repellence in comparison to untreated wood.

Acknowledgments

This work was partially supported by the National Counsel of Technological and Scientific Development (CNPq), Coordination for the Improvement of Higher Education Personnel (CAPES), Araucaria Foundation and Embrapa Forestry.

References

Acda, M.N.; Devera, E.E.; Cabangon, R.J.; Ramos, H.J. 2012. Effects of plasma modification on adhesion properties of wood. International Journal of Adhesion and Adhesives. 32(0): 70-75.

Asandulesa, M.; Topala, I.; Dumitrascu, N. 2010. Effect of helium DBD plasma treatment on the surface of wood samples. Holzforschung. 64(2): 223-227.

Aydin, I.; Demirkir, C. 2010. Activation of Spruce Wood Surfaces by Plasma Treatment After Long Terms of Natural Surface Inactivation. Plasma Chemistry and Plasma Processing. 30(5): 697-706.

Bai, Y.; Gao, Z. 2011. The ambient aging of wood fiber and its effect on mechanical properties of MDF panels. Wood Sci Technol. 45(3): 501-510.

Cademartori, P.H.G.; dos Santos, P.S.B.; Serrano, L.; Labidi, J.; Gatto, D.A. 2013. Effect of thermal treatment on physicochemical properties of Gympie messmate wood. Industrial Crops and Products. 45(0): 360-366.

Cademartori, P.H.G.; Muniz, G.I.B.; Magalhães, W.L.E. 2015. Changes of wettability of medium density fiberboard (MDF) treated with He-DBD plasma Holzforschung. 69(2): 187-192.

Christiansen, A.W. 1991. How overdrying wood reduces its bonding to phenol-formaldehyde adhesives : a critical review of the literature. Part II, Chemical reactions. Wood and Fiber Science. 23(1): 69-84.

De Geyter, N.; Morent, R.; Leys, C.; Gengembre, L.; Payen, E. 2007. Treatment of polymer films with a dielectric barrier discharge in air, helium and argon at medium pressure. Surface and Coatings Technology. 201(16–17): 7066-7075.

Liu, Y.; Tao, Y.; Lv, X.; Zhang, Y.; Di, M. 2010. Study on the surface properties of wood/polyethylene composites treated under plasma. Applied Surface Science. 257(3): 1112-1118.

Liu, Z.; Chen, P.; Han, D.; Lu, F.; Yu, Q.; Ding, Z. 2013. Atmospheric air plasma treated PBO fibers: Wettability, adhesion and aging behaviors. Vacuum. 92(0): 13-19.

Magalhães, W.L.E.; da Silva, R.R. 2004. Treatment of Caribbean pine by in situ polymerization of styrene and furfuryl alcohol. Journal of Applied Polymer Science. 91(3): 1763-1769.

Magalhães, W.L.E.; Souza, M.F.d. 2002. Solid softwood coated with plasma-polymer for water repellence. Surface and Coatings Technology. 155(1): 11-15.

Mattos, B.D.; Missio, A.L.; Cademartori, P.H.G.; Lourençon, T.V.; Gatto, D.A.; Magalhães, W.L.E. 2015. Pinewood Composite Prepared by In Situ Graft Polymerization of Epoxy Monomer. Polymer Composites. Online First

Novák, I.; Popelka, A.; Špitalský, Z.; Mičušík, M.; Omastová, M.; Valentin, M., et al. 2015. Investigation of beech wood modified by radio-frequency discharge plasma. Vacuum. 119(0): 88-94.

Poaty, B.; Riedl, B.; Blanchet, P.; Blanchard, V.; Stafford, L. 2013. Improved water repellency of black spruce wood surfaces after treatment in carbon tetrafluoride plasmas. Wood Sci Technol. 47(2): 411-422.

Sanchis, M.R.; Calvo, O.; Fenollar, O.; Garcia, D.; Balart, R. 2008. Characterization of the surface changes and the aging effects of low-pressure nitrogen plasma treatment in a polyurethane film. Polymer Testing. 27(1): 75-83.

Scholz, G.; Militz, H.; Gascón-Garrido, P.; Ibiza-Palacios, M.S.; Oliver-Villanueva, J.V.; Peters, B.C., et al. 2010. Improved termite resistance of wood by wax impregnation. International Biodeterioration & Biodegradation. 64(8): 688-693.

Yun, Y.I.; Kim, K.S.; Uhm, S.-J.; Khatua, B.B.; Cho, K.; Kim, J.K., et al. 2004. Aging behavior of oxygen plasma-treated polypropylene with different crystallinities. Journal of Adhesion Science and Technology. 18(11): 1279-1291.

Drilling resistance measurement and the effect of shaft friction – using feed force information for improving decay identification on hard tropical wood

Leif Nutto
Malinovski Florestal – Rua Itupava 1541, Alto da XV, Curitiba PR, Brazil, leif@malinovski.com.br

Tobias Biechele
IML System GmbH, Parkstraße 33, 69168 Wiesloch, Germany, tobias.biechele@iml.de

Abstract

Drilling resistance measurement is widely applied since several years for detecting internal decay and cavities in trees and construction timber. When drilling hard wood with high density, such as tropical hardwoods, the drilling curve tends to rise with drilling depth. This is due to the shavings from the drilling which remain in the drilling hole causing friction on the needle shaft.
This rising drilling curve makes it difficult to identify a dropdown in drilling resistance due to decay especially when it is an early stage of decay. Operators often struggle with the interpretation of the drilling curve results. Having this in mind, in this study tropical hardwood trees with different stages of decay were drilled with the drill resistance device IML-RESI PD® which simultaneously records drilling resistance and feed force with two independent motors. The feed force which is needed to enter the needle into the wood is measured and recorded in a feed curve. Results of this study clearly indicate the high potential of this feed curve which is only marginally affected by shaft friction and therefore improves the identification of decayed areas within the resistance drilling profiles.

Keywords: IML-RESI PD®, drilling resistance, shaft friction, feed curve, decay

Introduction

In urban areas trees have to be controlled to assure public safety and to avoid damage to humans and properties. Next to visual tree inspections in selected cases technical inspections with specialized equipment are necessary to clearly determine the internal wood condition of a tree and to derive conclusions about its breaking stability.
Drilling resistance is a semi destructive testing technique widely applied for identifying internal decay or cavities in trees and timber constructions (Brashaw et al. 2015; Brashaw et al. 2005; Fruewald et. al 2011; Johnstone et al. 2010; Kubus 2009; Wang et al. 2008). A drilling needle with 3mm needle tip diameter (1,5mm needle shaft diameter) is being drilled into the wood measuring drilling resistance (drilling torque) (Wang et al. 2005). Resistances are electronically or mechanically recorded depending on drilling device and changes in wood resistance illustrated on a graph as changes in amplitude. Sound wood has higher resistance than decayed wood.
When the needle drill cuts its way through the wood, wood chips remain in the drilling channel causing friction on the rotating needle shaft (Rinn 2012). Also internal stresses in the stem may cause that the wood closes the drilling hole and this way squeezes the needle. This so called shaft friction increases drilling resistance causing a rising drilling curve with deeper drilling depth. The rising drilling resistance curve (drilling trend) make the identification of decayed wood difficult. Especially when it is an early stage of decay shaft friction can overlay and cover resistance dropdowns (Rinn 2012; Tannert et al. 2013).

Shaft friction on the drilling curve is only clearly determined when the drilling needle exits the wood on the other side of the tree or timber and the difference between beginning and end height of the drilling curve amplitude is recorded. In urban tree inspection needle penetration through the tree diameter is a case that nearly never occurs, hence software correction of shaft friction is only possible on construction timber of minor diameter (Rinn 2012). Furthermore shaft friction may not have a linear trend.
The electronically recording drilling resistance device IML RESI PD® from IML records additionally to drilling torque the feed force that is needed for needle penetration into the wood.
Experiences on wood with high density show that this second feed force measurement of the feed motor recorded on a feed curve is only marginally affected by shaft friction.
In this study the feed curve information was examined and tested on standing hard tropical trees commonly found in urban areas of Brazil. With the results authors hope to give further information about the improvement of decay detection with feed force measurement. This will improve drilling resistance profile interpretation for the operators.

Material and Method

Drilling resistance

Drilling resistance is measured with a rotating wood cutting needle penetrating the wood. The rotating needle cuts the wood which results in resistance amplitudes in the resistance curve. Intact or sound wood has higher resistance than decayed wood. The wood chips being cut at the front tip remain in the drilling channel causing friction on the drilling needle shaft (Figure 1). Hence drilling resistance is a combination of drilling torque resistance and shaft friction (Weber and Mattheck 2001). Feed force measurement with the IML RESI PD® is displayed in a separate feed curve.

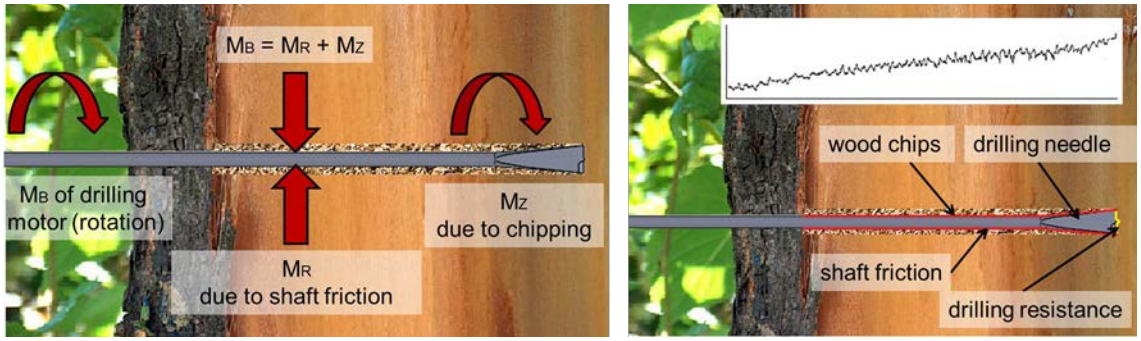

Figure 1 -- Rotating needle cuts wood at needle tip. Remaining wood chips cause friction on needle shaft leading to an increase in drilling resistance amplitude with deeper drilling depth. Drilling resistance (M_B) is a combination of drilling torque (M_Z) and shaft friction (M_R)

Feed and drilling speed adjustment depending on wood hardness

The IML RESI PD® has different feed (cm/min) and needle speed (rounds per minute) stages. Feed speed can be adjusted from 15 cm/min to 200 cm/min depending on wood hardness, needle rotation speed between 1500 r/min and 5000 r/min. Operators should have basic knowledge about the tree species wood hardness to correctly select feed speed. In soft wood high feed speed is necessary to produce sufficient amplitude to identify curve dropdowns. In hardwood feed speed has to be reduced and needle speed increased to enable the needle penetration into the wood. If the operator selected the feed speed too fast for the wood hardness, the drilling needle will automatically retract and the operator advised to reduce feed speed.
In the present study feed and needle speeds were adjusted according to wood hardness of the trees.

Needle sharpness and its effect on shaft friction

Blunt needles are visually identified by a less sharp blade and rounded needle tip edges. A reduction in needle tip diameter results in a higher shaft friction due to a narrower ratio between drill bit and needle shaft diameter. For this study only sharp drilling needles were used.

Hardwood tree species selected for this study

The effect of shaft friction and inclining drilling curve increases with average wood densities above 600 kg/m³ (Tannert et al. 2013). Five tree species commonly found in urban areas of Brazil were selected to match the criteria of hardness (density > 600 kg/m³) and presence of defects (Table 1).

Table 1 – Hardwood species selected and feed and needle speed selection

Common name	Scientific name	Average wood density [kg/m³]	feed speed [cm/min]	needle speed [r/min]
Pau Ferro	*Caesalpinia ferrea*	982	25	5000
Rosewood	*Tipuana tipu*	670 - 750	100	2500
Arueira	*Lithraea molleoides*	725	100	2500
Imbuia	*Ocotea porosa*	660	100	2500
Pitangueira	*Eugenia uniflora*	765	100	2500
Parana Pine	*Araucaria angustifolia*	418 - 537	175	2000

Source: Paula and Alves (1997)

Results

In the following drilling resistance profiles of the IML RESI PD® are shown, where the feed curve and drilling curve of a variety of hardwoods show differences.

Drilling resistance profile of Pau Ferro (*Caesalpinia ferrea*)

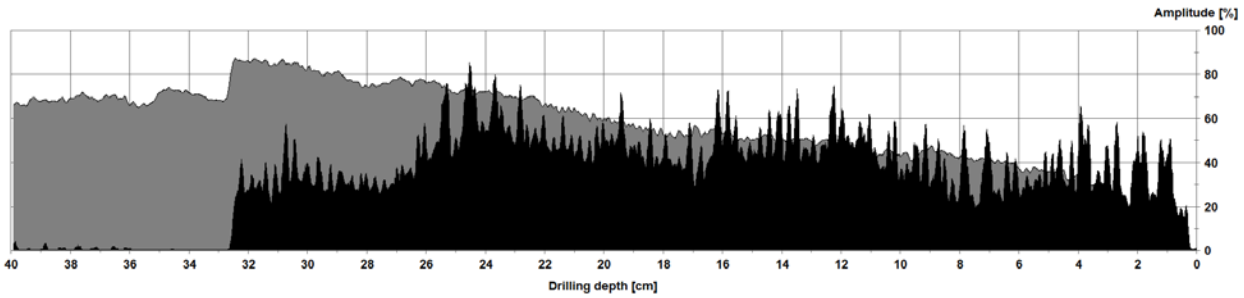

Figure 2 -- Drilling resistance profile of Pau Ferro. Drilling curve = grey; feed curve = black

Drilling resistance curve rises steeply being strongly affected by shaft friction (Figure 2). The amount of shaft friction is visible when the drilling needle exits the tree at 33 cm of drilling depth. Drilling curve amplitude remains at 70% amplitude while the feed curve drops down to 0% not being affected by shaft friction.

Drilling resistance profile of Pau Ferro (*Caesalpinia ferrea*)

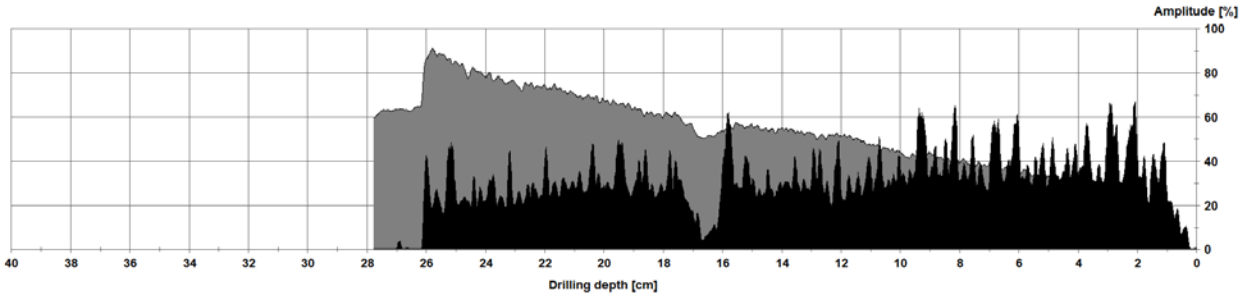

Figure 3 -- Drilling resistance profile of a smaller diameter Pau Ferro tree. Drilling curve = grey; feed curve = black

Drilling resistance curve rises steeply being strongly affected by shaft friction (Figure 3). The amount of shaft friction is visible when the drilling needle exits the tree at 26 cm of drilling depth. At 17 cm drilling depth a dropdown of the feed curve and to minor extend also of the drilling curve is detected. In Pau Ferro this phenomena is often observed when the needle passes directly through the pith, where wood density is extremely low. In other cases the dropdown may indicate a crack or bark inclusion.

Drilling resistance profiles of a Rosewood (*Tipuana tipu*)

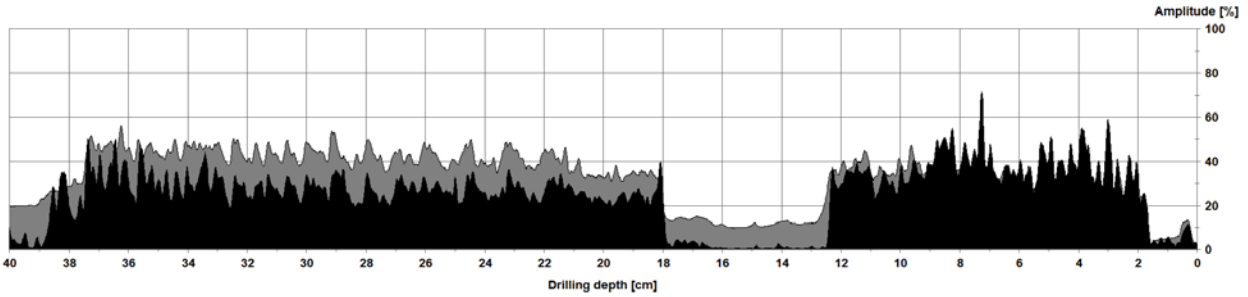

Figure 4 -- Drilling resistance profile of a Tipuana tree.
Drilling curve = grey; feed curve = black

Drilling resistance curve is less affected by shaft friction due to lower wood density of the tree (Figure 4). At 12 to 18 cm drilling depth both curves, drilling and feed curve drop down, indicating a mayor defect. The abrupt dropdown indicates a good compartmentalization of the wood at this measurement position.

Drilling resistance profiles of a fresh Rosewood crosscut (*Tipuana tipu*)

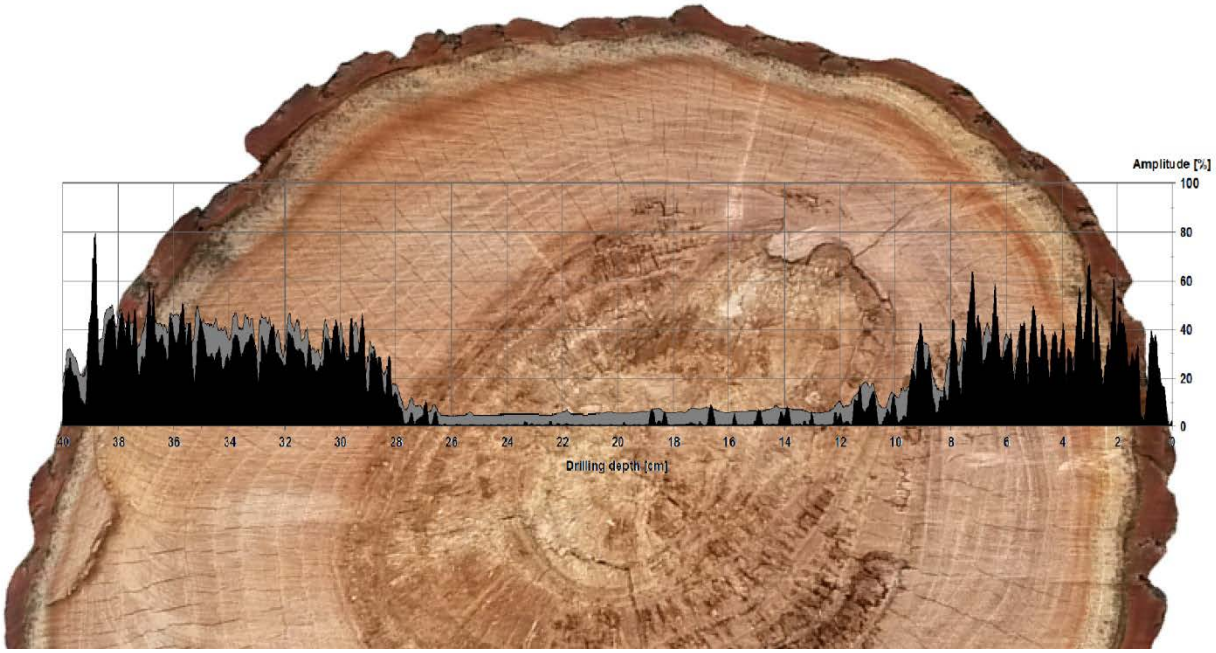

Figure 5 -- Drilling resistance profile of a Tipuana stem disc with central decay.
Drilling curve = grey; feed curve = black

Drilling resistance curve and feed curve drops down in the central decayed area (Figure 5). The dropdown is not abrupt indicating an ongoing decay activity towards the outside of the tree.

Drilling resistance profile of Arueira (*Lithraea molleoides*)

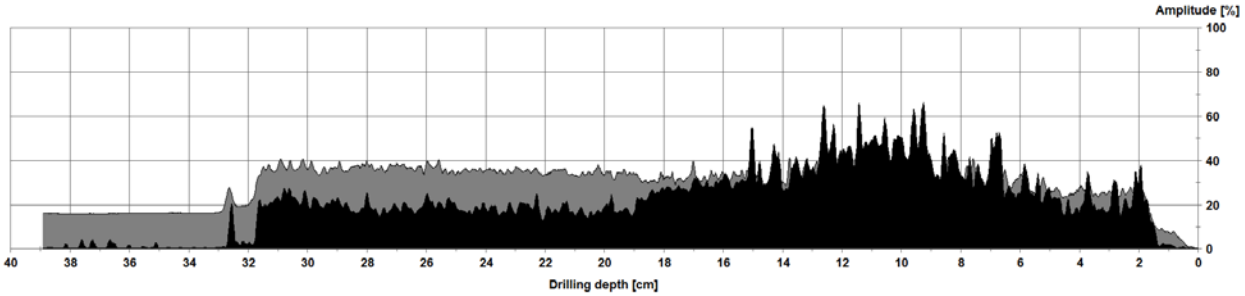

Figure 6 -- Drilling resistance profile of Arueira.
Drilling curve = grey; feed curve = black

Drilling resistance curve and feed curve show no sign of defect (Figure 6). The tree showed significant reaction wood formation with higher wood density due to a leaning stem. After 33 cm of drilling depth needle exits the tree and both curves drop down. The drilling curve increases from 20% to 40% amplitude due to shaft friction.

Drilling resistance profile of Imbuia (*Ocotea porosa*)

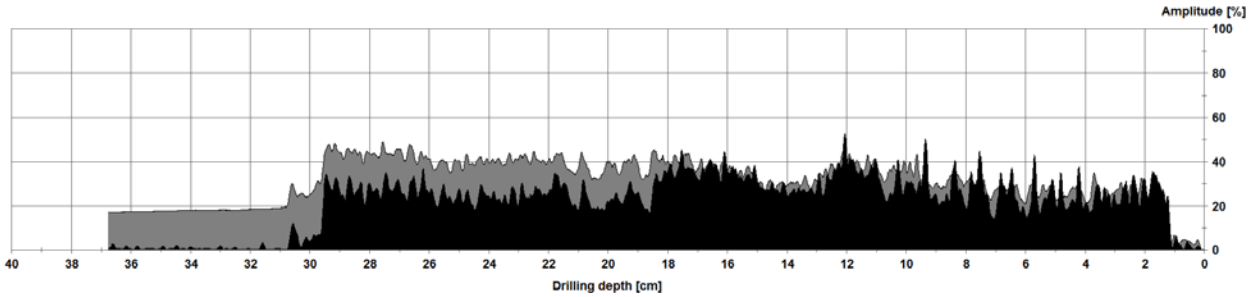

Figure 7 -- Drilling resistance profile of a Imbuia.
Drilling curve = grey; feed curve = black

Drilling resistance curve and feed curve show no sign of defect (Figure 7). After 31 cm of drilling depth needle exits the tree and both curves drop down. The drilling curve increases from 25 to 45% amplitude due to shaft friction.

Drilling resistance profile of a Imbuia crosscut (*Ocotea porosa*)

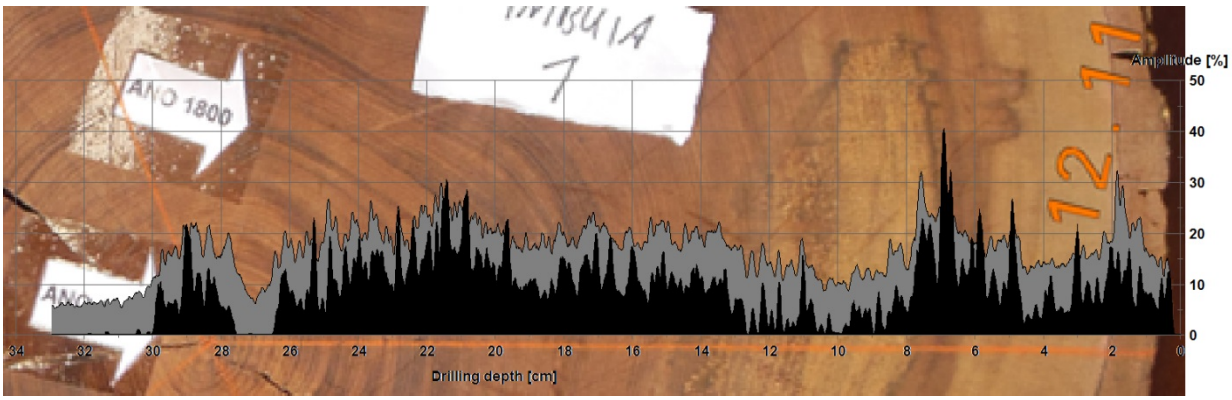

Figure 8 -- Drilling resistance profile of an Imbuia stem disc with decay area.
Drilling curve = grey; feed curve = black

Drilling resistance and feed curve drop down between 8 cm and 13 cm drilling depth indicating decay (Figure 8). At 30 cm drilling depth needle enters drying crack and resistances drop down.

Drilling resistance profile of Pitangueira *(Eugenia uniflora)*

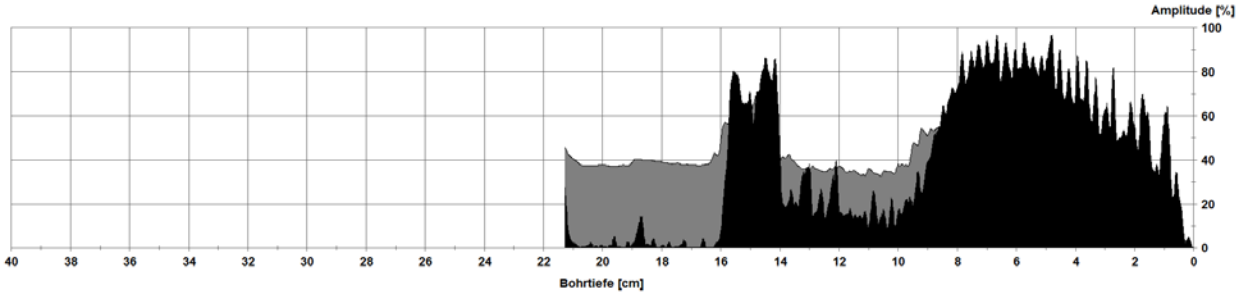

Figure 9 -- Drilling resistance profile of Pitangueira.
Drilling curve = grey; feed curve = black

Drilling resistance curve and feed curve rise steeply in the first 8 cm of drilling depth before dropping down in 9 cm to 14 cm visualizing a central decay. After 16 cm of drilling depth drilling needle exits the tree and drilling resistance amplitude remains at a 40% level due to shaft friction. The steep rise of the feed curve in the first 8 cm is due to high dense wound wood formation of the tree trying to compensate stability loss of the internal damage.

Drilling resistance profile of a Parana pine stem disc (*Araucaria angustifolia*)

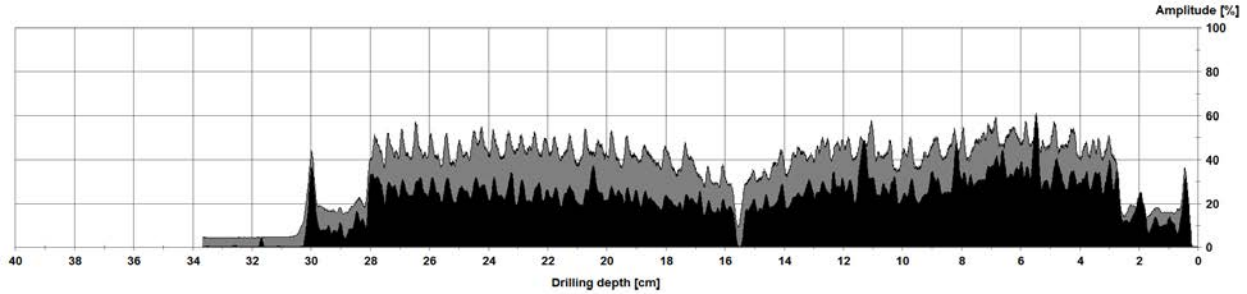

Figure 10 -- Drilling resistance profile of a Parana pine stem disc.
Drilling curve = grey; feed curve = black

Drilling resistance curve is less affected by shaft friction due to low wood density (Figure 10). At 15 cm drilling depth drilling hits the pith area and resistances drop down. Drilling and feed curve show high oscillation, indicating latewood and early wood variation inside the year ring.

Conclusions

The feed curve (feed force information) is only marginally affected by shaft friction and improves the identification and interpretation of defect (decayed) areas in wood especially when it is hard wood.
In Softwood with low wood density feed curve information is often not crucial for decay detection since shaft friction is of minor appearance. Nevertheless feed curve gives additional information for decision making if the tree has a defect or not.
The shaft friction and feed force information can be derived to other tree species of other countries that have similar hardness's. More research has to be done using drilling resistance with feed curve information on other tree species.
It has to be taken into account that site quality and growing space influence wood quality and wood density of the same tree species hence resistances amplitudes. It is recommendable to do more research

including cross cuts of the at measurement height, to complete the results of the drilling and feed curves with a visual identification of decayed areas in the tree.

References

Brashaw, B.; Dahlberg, J.; Hosteng, T.; Wacker, J. 2015. Development and Integration of Advanced Timber Bridge Inspection techniques for NBIS: Natural Resources Research Institute of University of Minnesota Duluth, Research Project Final Report 2015-0

Brashaw, B. K.; Vatalaro, R. J.; Wacker, J. P.; Ross, R. J. 2005. Condition Assessment of Timber Bridges: 1. Evaluation of a Micro-Drilling Resistance Tool. Gen. Tech. Rep. FPL-GTR-159. Madison, WI: U.S. Department of Agriculture, Forest Service, Forest Products Laboratory. 8 p.

Fruehwald, K.; Hasenstab, A.; Osterloh, K. 2011. Detection of Fungal Damage of Wood In Early Stages Using Drilling Cores and Drilling resistance Compared to Non-Destructive Testing Methods: SHATIS`11 International Conference on Structural Health Assessment of Timber Structures – Lisbon, Portugal – June 2011

Johnstone, D. M.; Ades, P. K.; Moore, G. M.; Smith, I. W. 2007. Predicting Wood Decay in Eucalypts Using an Expert System and the IML- Resistograph Drill. Arboriculture & Urban Forestry 2007. 33(2):76-82

Johnstone, D.; Moore, G.; Tausz, M.; Nicolas, M. 2010. The Measurement of Wood Decay in Landscape Trees: Arboriculture & Urban Forestry 2010. 36(3):121-127

Kubus, M. 2009. The Evaluation of Using Resistograph when Specifying the Health Condition of a Monumental Tree. Not.Bot.Hort.Agrobot.Cluj 37 (1) 2009, 157-164

Paula, J.E.; Alves, J.L.H. 1997. Madeiras Nativas – Anatomia, dendrologia, dendrometria, produção, uso. Fundação Mokiti Okada – MOA, Brasilia,Brasil.

Rinn, F. 2012. Basics of Typical Resistance-Drilling for Timber Inspection: Holztechnologie 53 (2012) 3 p. 24-29

Tannert, T.; Anthony, R.W.; Kasal, B.; Kloiber, M.; Piazza, M.; Riggio, M.; Rinn, F.; Widmann, R.; Yamaguchi, N. 2013: In situ assessment of structural timber using semi-destructive techniques. Materials and Structures DOI 10.1617/s11527-013-0094-5. July 2013

Wang, X.; Wiedenbeck, J.; Ross, R. J.; Forsman, J. W.; Erickson, J.R.; Pilon, C.; Brashaw, B. K. 2005. Nondestructive evaluation of incipient decay in hardwood logs. Gen. Tech. Rep. FPL-GTR-162. Madison, WI: U.S. Department of Agriculture, Forest Service, Forest Products Laboratory. 11p.

Wang, X.; Allison, R.B. 2008. Decay Detection in Red Oak Trees Using a Combination of Visual Inspection, Acoustic Testing, and Resistance Microdrilling. Arboriculture & Urban Forestry 2008. 34(1):1-4

Weber, K.; Mattheck, C. 2001. Manual of Wood Decay in Trees - Forschungszentrum Karlsruhe GmbH 2001

Session 4

Material Characterization—Other Techniques

Mechanical and physical properties of wood and bamboo in cell wall level: our recent progress

Siqun Wang
Center for renewable carbon, University of Tennessee, 2506 Jacob Dr., Knoxville, TN, US, swang@utk.edu
Guanben Du
Southwest Forestry University, Kunming, China,
gongben9@hotmail.com
Xinzhou Wang
College of Materials Science and Engineering, Nanjing Forestry University, Nanjing, China, xzwang_njfu@hotmail.com
Dong Xing
Material Science and Engineering College, Northeast Forestry University, Harbin, China, xing.dong@163.com
Yurong Wang
Research Institute of Wood Industry, Chinese Academy of forestry, Beijing, China, yur_wang@sohu.com
Chengjian Huang
College of Engineering, Zhejiang Agricultural and Forestry University, Hangzhou, China, hcj5236@yeah.net
Deliang Xu
College of Materials Science and Engineering, Nanjing Forestry University, Nanjing, China, xudl81@163.com
Yujie Meng
Center for renewable carbon, University of Tennessee, 2506 Jacob Dr., Knoxville, TN, US,
ymeng2@vols.utk.edu

Abstract

The nano-mechanics of wood and bamboo treated by several modification methods, an improved nanoindentation technique, and potential applications in wood science field were overviewed in this paper. With nanoindentation, the influence of thermal modification and genetic modification on nanomechanical properties of cell walls have been investigated. The quasi-static mechanics (modulus and hardness), dynamical mechanics (storage modulus and loss modulus), and creep behaviour of cell walls measured by nanoindentation provide a deeper knowledge of the cell wall properties and a theoretical support for developing a high-performance advanced design for wood and bamboo. Moreover, nanoindentation technique working at high temperature was attempted to evaluate the effects of temperature on the modulus and hardness of wood cell walls. This nondestructive testing method has proven to be an accessible and straightforward approach to analyze temperature-dependent materials.

Keywords: Nanoindentation; mechanical properties; wood; bamboo; cell wall

Introduction

As a biopolymer composite, both wood and bamboo have been extensively used for homes and other structures, and furniture due to their good machinability and good strength with its light weight. They, however, are prone to degrading, warping, and cracking under changing environmental conditions. Therefore, improving the environmental resistance of wood and bamboo, such as mechanical strength, dimensional stability, or resistance to biodegradation and to expand its application fields is of critical interest.

Both wood and bamboo consist of different cell types that are oriented in axial direction or in radial direction. The cell walls of fibers built up of layers of different thickness, spiral microfibril angles (MFA), and chemical components dominate the natural properties of wood and bamboo. To better understand the mechanism of weathering degradation and modification of wood and bamboo, investigating the mechanical and physical response in cell wall level is essential.

Nanoindentation with high-resolution testing equipment facilitates the measurement of properties at the micrometer or nanometer scales (Oliver and Pharr 1992). Accordingly, nanoindentation makes it possible to investigate the mechanical properties of small and heterogeneous biomaterials (Wimmer et al. 1997). During the past decade, a large number of useful engineering properties of biomaterials, such as wood (Xing et al. 2008; Wu et al. 2009; Meng et al. 2013), bamboo (Li et al. 2015), crop stalks (Wu et al. 2010; Wang et al. 2013; Li et al. 2013), cellulose fiber and others (Lee et al. 2007; Nair et al. 2010; Liu et al. 2014), have been investigated by means of nanoindentation in our previous study, including quasi-static properties (modulus, hardness, and fracture toughness), and viscoelastic properties (creep and stress relaxation). The primary purpose of this article is to provide an overview on how we implement the method to evaluate the effects of several modification methods on the mechanical and physical properties of wood and bamboo.

Quasi-static nanoindentation

Basic method

Nanoindentation experiments were performed at the Center for Renewable Carbon (University of Tennessee, USA); The instrument is a TriboIndenter system equipped with a diamond Berkovich tip (a three-sided pyramidal tip). The locations for NI experiments were chosen with precise positioning performed from scanning probe micrographs (SPM) taken with the indenter tip. Experiments were performed in load-controlled mode using a three-segment load ramp: loading, load holding, and unloading. When the indenter tip is driven into the material, both elastic and plastic deformations occur, generating an impression in the material that follows the geometric shape of the indenter and produces a contact depth. The test system will record some important quantities, such as peak load ($P_{\max}$), maximum depth ($h_{\max}$), and the slope of the upper portion of the unloading curve ($S = dP/dh$) , as shown in Figure 1. Young's modulus and the hardness can be obtained by analyzing the load-displacement curve according to the method of Oliver and Pharr (2012).

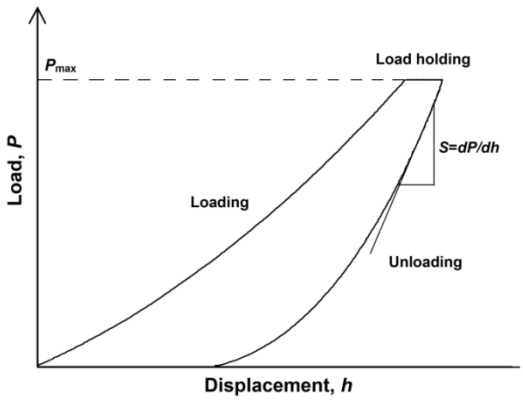

Figure 1 Schematic sample plot of load vs. displacement for Nanoindentation

Experimental applications

Wood genetic modification

Poplar trees including their hybrids have been considered as alternative wood source due to their characteristics of fast growth. However, there are few literatures regarding the mechanical and physical properties of hybrid poplar in cell wall level. In this experiment, two-year-old Populus deltoides, hybrid P.deltoides × P.maximowiczii, and hybrid P.deltoides × P.trichocarpa were selected. Microstructure, microfiber angle (MFA), and mechanical properties of cell wall in juvenile wood were investigated using Sliding section, X-ray diffraction, and Nanoidentation (NI), as shown in Figure 2. The relationship among the growth trait, the anatomical parameters and micromechanics of wood cell walls of the three kinds of poplar was discussed. The results indicated that P.Eltoides × P.maximowiczii grew fastest, whereas P.deltoides × P.trichocarpa grew slowest; the hybrid poplar with low growing rate has a smaller MFA and the hybrid poplar with high growing rate has a bigger MFA. The average reduced elastic modulus of P. deltoides, P.deltoides × P.maximowiczii and P.deltoides × P.trichocarpa is 7.59 GPa, 9.03 GPa and 12.58 GPa, respectively. The value of reduced elastic modulus of three kinds of poplar wood has the positive correlation relationship with value of their hardness. The bigger reduced elastic modulus and hardness have been found in hybrid poplars. It can be concluded that the poplars with a slower growth rate, thicker cell wall and smaller MFA, which present a higher mechanical properties in cell wall.

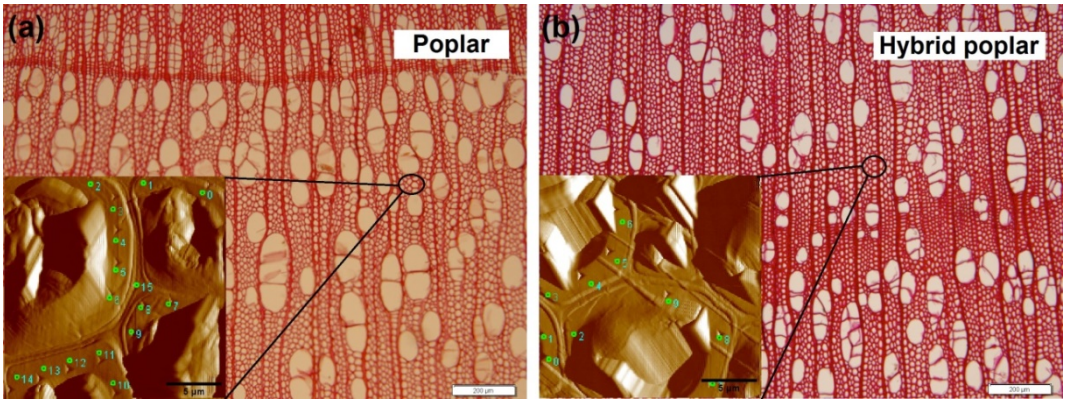

Figure 2 Microscope images showing the position of indents: (a) Poplar; (b) Hybrid poplar.

Bamboo thermal modification

Thermal treatment has been widely adopted in woody materials production and application to deepen the material's color for aesthetic purposes, and to improve the dimensional stability. An investigation of the mechanical properties of bamboo in cell wall level is of great importance to understand the thermal treatment mechanism.

Bamboo was thermally treated at 130°C, 150°C, 170°C, and 190°C for 2, 4, 6 h, respectively. The micromechanical properties of its cell walls were investigated by means of quasi-static nanoindentation (NI). The locations for NI experiments were chosen with scanning probe micrographs (SPM), as shown in Figure 3. With increasing treatment temperatures, the average dry density and mass of the bamboo decreased, whereas the already reduced elastic modulus increased. This finding agreed with Wang et al. (2014) that the increment of relative lignin content and crystallinity due to hemicellulose degradation and melting at elevated temperature has a positive effect on the mechanical properties of cell wall.

Furthermore, bamboo products always show significant viscoelastic effects under oscillation stress or strain condition (Jiang et al. 2009). The creep behaviour of thermal treated bamboo in cell wall level was also measured using nanoindentation. Figure 3d shows the influence of thermal treatment on the strain rate of bamboo with different treatment times at 190 °C. A slight decrease in strain rate occured after treatment. In other words, thermal modification is beneficial to improve creep resistance of bamboo. In addition, the treatment time has no significant effect on the creep behaviour of cell wall.

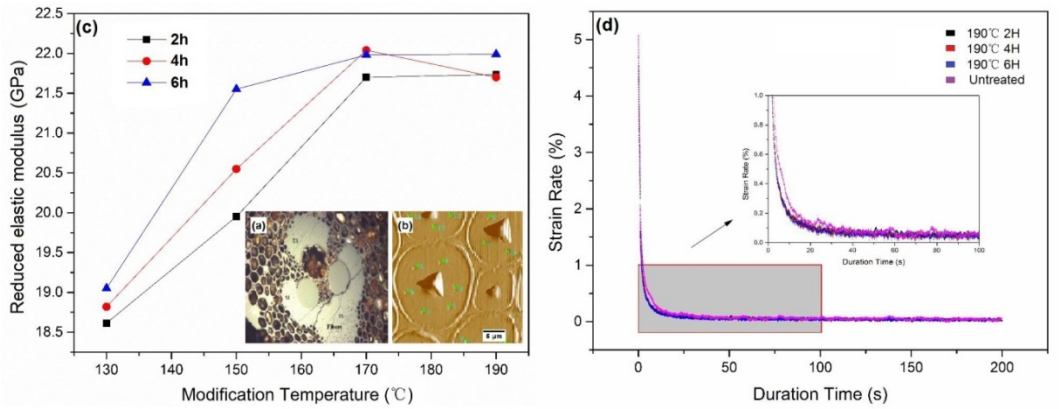

Figure 3 Nanoindentation of termal treated bamboo cell Wall: (a) Test area; (b) Positioning of indents; (c) Reduced elastic modulus; (d) Strain rate.

Dynamic nanoindentation

Basic method

Dynamic nanoindentation can reveal the viscoelastic properties of materials at the small scale (Herbert et al. 2008) and the viscoelastic properties of wood cell walls (Zhang et al. 2012). For this purpose, various instrumental setups can be used, and corresponding data can be analyzed to obtain the frequency domain measurements at ambient temperatures.

The nanoDMA tests were taken by the same Berkovich tip and Triboindenter equipped with a nanoDMA model transducer. The test was operated in a ramping dynamic frequency mode. The quasistatic load was 100 μN and the dynamic load was 10 μN. The harmonic frequencies were varied from 10 to 200 Hz with 100 cycles at each frequency. Data were recorded at 20 points for each indentation. At least 30 indentations were taken in five or six adjacent cells for each point. The analysis is based on the dynamic model introduced by Pethica and Oliver (1987) and developed by Asif et al. (1999).

Experimental applications

Combining dynamic and quasi-static indentation methods can provide more information about the elastic and viscoelastic properties of bamboo cell walls. Bamboo was thermally treated at 130 °C, 150 °C, 170 °C, and 190 °C for 2, 4, 6 h, respectively. The results of the dynamic indentation of bamboo cell walls for harmonic frequencies are presented in Figures 4. Figure 4a shows the storage modulus (E_r') and loss modulus (E_r") as a function of frequency at different temperatures. The E_r' and E_r"of heat-treated bamboo were higher than those of untreated bamboo cell walls and increased with increasing temperature. This was due to the increase in degree of crystallinity of cell walls. Moreover, the E_r' of heat-treated bamboo increased steadily with increasing frequency, whereas the E_r" decreased significantly. At lower frequency, the smaller E_r' was assigned to the relatively flexible molecular chains; at higher frequency, the main chain movements were probably frozen and small scale movements were dominant, resulting in a stiffer material (Zhang et al. 2013). The gradual decrease of E_r" with increasing harmonic frequency was attributed to the stiffening of the material due to the short time available for molecular chain rearrangement (Chakravartula and Komvopoulos 2006). Figure 4b gives the influence of E_r' and E_r" on the frequency of bamboo with different treatment times at 190 °C. It can be observed that the treatment time did not significantly affect the dynamic mechanical properties anymore.

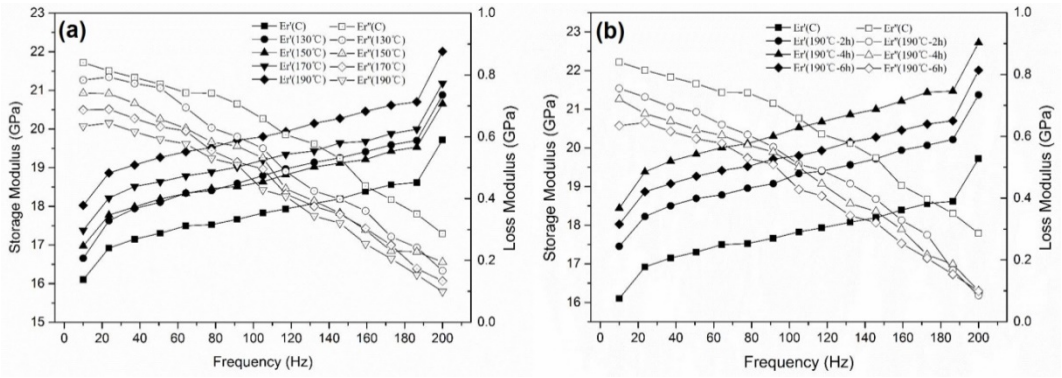

Figure 4 Dynamic indentation results of bamboo cell walls: (a) at different temperatures and (b) with different treatment times.

High-temperature nanoindentation

Basic method

Nanoindentation (NI) experiments were performed using a Hysitron TriboIndenter system with some proprietary modifications to enable its operation in a certain temperature environment. The

general arrangement of instrument components is shown schematically in Figure 5a. The sample stage was equipped with a temperature control stage allowing temperature control from room temperature to 200 ^{o}C by means of electric heater elements.

Experimental applications

The most nanoindentation tests are conducted at room temperature, in spite of the fact that wood materials are sensitive to temperature when they were put into service. There are rare study of the properties of treated wood under high temperature level, which is important to understand thermal behaviour of heat treated wood used in radiant heated floor.

Wood samples were treated at 180°C, 210°C, and 240°C, respectively. This improved technique was used to track changes in the micromechanical properties in the longitudinal direction and to obtain measurements for both the temperature-dependent reduced elastic modulus and hardness. The average reduced modulus of the cell wall slightly increased, while hardness tended to increase after heat treatment under room temperature conditions. The nanoindentation tests showed that both the reduced modulus and hardness of the wood cell walls tended to decrease as the load-temperature increased from 100°C to 180°C. Moreover, it was shown that heat treatment resulted in better heat resistance compared to that of untreated wood, especially in the samples indented at 180°C.

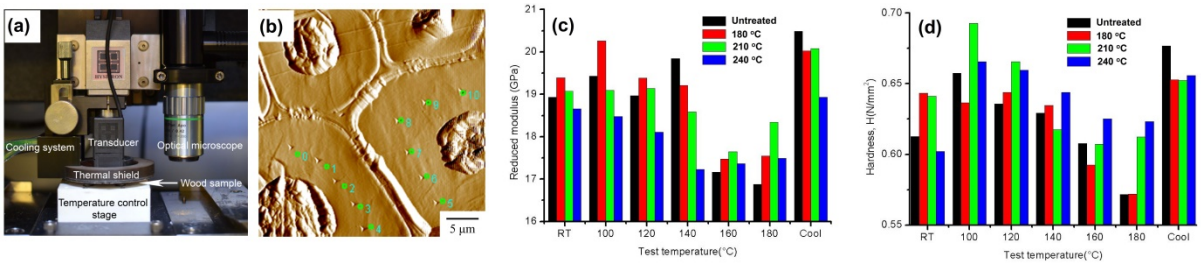

Figure 5 (a) Schematic of high temperature nanoindentation instrument; (b) Positions of indents; (c) Reduced elastic modulus; (d) Hardness

Conclusions

In this paper, the use of depth-sensing indentation to measure the mechanical properties of modified wood and bamboo cell walls was reviewed, including discussions of the applications of quasi-static indentation, dynamic indentation, and high-temperature indentation measurements. Quasi-static and dynamic indentation methods can provide detailed information about the elastic and viscoelastic properties of cell walls, improving the understanding of modification mechanism of wood and bamboo. The hybrid poplars with slower growth rate, thicker cell wall and smaller MFA, which present a higher mechanical properties in cell wall. Thermal modification showed a positive effect on the reduced elastic modulus, hardness, and creep resistance of bamboo fiber cell wall. High-temperature nanoindentation overcame the intrinsic limitations of ambient temperature to obtain the exact mechanical responses of wood at high temperatures has opened up significant new possibilities for investigating the weathering mechanism of wood products.

Acknowledgment

The Authors gratefully acknowledge financial support by the USDA Special Wood Utilization Grants R11-0515-041 and R11-2219-510, Zhejiang Key Level 1 Discipline of Forestry Engineering, the University of Tennessee Center for Renewable Carbon, and the Agricultural Experiment Station McIntire-Stennis Grant TENOOMS-101.

References

Asif, S.S.; Wahl, K.J.; Colton, R.J. 1999. Nanoindentation and contact stiffness measurement using force modulation with a capacitive load-displacement transducer. Review of scientific instruments, 70(5): 2408-2413.

Chakravartula, A.; Komvopoulos, K. 2006. Viscoelastic properties of polymer surfaces investigated by nanoscale dynamic mechanical analysis. Applied physics letters, 88(13): 1901.

Herbert, E.G.; Oliver, W.C.; Pharr, G.M. 2008. Nanoindentation and the dynamic characterization of viscoelastic solids. Journal of Physics D: Applied Physics, 41(7): 074021.

Jiang, J.; Lu, J.; Huang, R. [and others]. 2009. Effects of time and temperature on the viscoelastic properties of Chinese fir wood. Drying Technology, 27(11): 1229-1234.

Lee, S.H.; Wang, S.; Pharr, G.M. [and others]. 2007. Evaluation of interphase properties in a cellulose fiber-reinforced polypropylene composite by nanoindentation and finite element analysis. Composites Part A: Applied Science and Manufacturing, 38(6): 1517-1524.

Li, X.; Wang, S.; Du, G. [and others]. 2013. Variation in physical and mechanical properties of hemp stalk fibers along height of stem. Industrial Crops and Products, 42: 344-348.

Li, Y.; Yin, L.; Huang, C. [and others]. 2015. Quasi-static and dynamic nanoindentation to determine the influence of thermal treatment on the mechanical properties of bamboo cell walls. Holzforschung doi:10.1515/hf-2014-0112.

Liu, C.; Zhang, Y.; Wang, S. [and others]. 2014. Micromechanical properties of the interphase in cellulose nanofiber-reinforced phenol formaldehyde bondlines. BioResources, 9(3): 5529-5541.

Meng, Y.; Wang, S.; Cai, Z. [and others]. 2013. A novel sample preparation method to avoid influence of embedding medium during nano-indentation. Applied Physics A, 110(2): 361-369.

Nair, S.S.; Wang, S.; Hurley, D.C. 2010. Nanoscale characterization of natural fibers and their composites using contact-resonance force microscopy. Composites Part A: Applied Science and Manufacturing, 41(5): 624-631.

Oliver, W.C.; Pharr, G. 1992. An improved technique for determining hardness and elastic modulus using load and displacement sensing indentation experiments. J Mater Res; 7(6): 1564-1583.

Pethica, J.B.; Oliver, W.C. 1987. Tip surface interactions in STM and AFM. Physica Scripta, 1987(T19A), 61.

Wang, X.; Deng, Y.; Wang, S. [and others]. 2013. Nanoscale characterization of reed stalk fiber cell walls. BioResources, 8(2): 1986-1996.

Wang, X.; Deng, Y.; Wang, S. [and others]. 2014. Evaluation of the effects of compression combined with heat treatment by nanoindentation (NI) of poplar cell walls. Holzforschung, 68(2): 167-173.

Wimmer, R.; Lucas, B.N.; Oliver, W.C. [and others]. 1997. Longitudinal hardness and Young's modulus of spruce tracheid secondary walls using nanoindentation technique. Wood Science and Technology, 31(2): 131-141.

Wu, Y.; Wang, S.; Zhou D. [and others]. 2009. Use of nanoindentation and SilviScan to determine the mechanical properties of 10 hardwood species. Wood and Fiber Science, 41(1): 64-73.

Wu, Y.; Wang, S.; Zhou, D. [and others]. 2010. Evaluation of elastic modulus and hardness of crop stalks cell walls by nano-indentation. Bioresource technology, 101(8): 2867-2871.

Xing, C.; Wang, S.; Pharr, G.M. [and others]. 2008. Effect of thermo-mechanical refining pressure on the properties of wood fibers as measured by nanoindentation and atomic force microscopy. Holzforschung, 62(2): 230-236.

Zhang, T.; Bai, S.L.; Zhang, Y.F. 2012. Viscoelastic properties of wood materials characterized by nanoindentation experiments. Wood science and technology, 46(5): 1003-1016.

Pethica, J.B.; Oliver, W.C. 1987. Tip surface interactions in STM and AFM. Physica Scripta, 1987(T19A), 61.

Zhang, Y.M.; Yu, Y.L.; Yu, W.J. 2013. Effect of thermal treatment on the physical and mechanical properties of Phyllostachys pubescen bamboo. European Journal of Wood and Wood Products, 71(1): 61-67.

Use of the attenuation gamma radiation technique for qualification of heartwood and sapwood in *Eucalyptus*

Sabrina Galetti Cherelli
College of Agricultural Sciences, São Paulo State University. Rural Engineering Department - Lageado Farm - José Barbosa de Barros street, 1780, Botucatu-SP.
sabrina_galetti@hotmail.com

Adriano Wagner Ballarin
College of Agricultural Sciences, São Paulo State University. Rural Engineering Department - Lageado Farm - José Barbosa de Barros street, 1780, Botucatu-SP.
awballarin@fca.unesp.br

Marcos Antonio de Rezende
Bioscience Institute, São Paulo State University. Physics and Biophysics Department- Rubião Júnior district, S/N, Botucatu-SP.
rezende@ibb.unesp.br

Abstract

The presence of heartwood influences the use of wood in different ways (Hillis, 1987). The conceptual bases that allowed the precise definition and general physiological aspects involved in heartwood and sapwood formation were consolidated for some time, but some current techniques such as X-ray scans, infrared and gamma rays can be used for more detailed quantification and characterization of heartwood inside the main stem (Gominho, 2003). In this study we used the non-destructive method of gamma radiation attenuation to determine the basic and apparent density at 12% moisture content of wood portions (heartwood and sapwood) of mature trees of four forest species (*Eucalyptus grandis* Hill ex. Maiden - 18 years old, *Eucalyptus saligna* - 60 years old, *Eucalyptus tereticornis* - 35 years old and *Corymbia citriodora* - 28 years old). Six discs were sampled at breast height (DHB) of each species and the heartwood and sapwood were delimited by macroscopic analysis of the vessels (heartwood characterized by the presence of tyloses in the vessels, and sapwood, by the absence thereof) in each sample. The apparent density values ranged from 672 to 933 kg/m³ in the heartwood wood and 749 to 899 kg/m³ in the sapwood wood. The averages of apparent density did not differ significantly between the wood fractions. Despite the different ages of the plantations, the highest values of apparent density of wood, both in the heartwood and in the sapwood fraction were observed in *Corymbia citriodora* species.

keywords: density, gamma radiation, *Eucalyptus*, heartwood

Introduction

The genus *Eucalyptus* has potential as an alternative to native species for timber production due to its production capacity, adaptability to different environments and great diversity of species. Currently, is consensus in the brazilian forest sector that the wood of *Eucalyptus* is the main raw material to meet the various industries in the production of multiple wood products, not only to coal and cellulose (Caixeta et al. 2003).

The replacement of native wood by eucalyptus is mainly related to price and difficulty of obtaining other types of wood. Therefore, the *Eucalyptus* wood should be further studied and disseminated, in order to produce information that can generalize its use (Serpa et al., 2003).

Wood is a heterogeneous material formed by a set of cells with specific properties to perform the main functions of water conduction, storage of biochemicals and mechanical support of the plant body. The search for an interpretation increasingly detailed and in-depth of this complex and multifunctional system is an permanent scientific challenge. Today, with the availability and ease of access to equipment and greater potential techniques, themes once studied partial or limited way, gain new perspectives of analysis.

One of the most important characteristics that differentiates portions of wood of a tree is the formation of heartwood and sapwood. The presence of the heartwood influences the use of wood in different forms and affects uniformity (Hillis, 1987). The heartwood by its color and desirable properties, has, for some applications, a higher value and has been the target of interest of the timber users (Smith, 1996).

Due to the importance of the heartwood in the use of wood in certain applications and the possibility of using greater potential techniques, this study aimed the qualification of the wood of the heartwood and sapwood of four species of Eucalyptus with the use of attenuation gamma radiation technique.

Material and methods

Sampling procedures

Were selected and harvested six trees of *Eucalyptus grandis* Hill ex. Maiden (18 years old) provided by the College of Agricultural Sciences of Botucatu. The trees were obtained from a seminal plantation established in August 1996 at the Lageado Experimental Farm. Adult trees of *Corymbia citriodora* (28 years old), *Eucalyptus tereticornis* (35 years old) and *Eucalyptus saligna* (60 years old) were provided by PREMA Technology and Trade S.A. located in Rio Claro - SP. Were selected and harvested six trees of each species.

From each tree it was obtained a disk at breast height (DBH) approximately 30mm thick for the determination of basic and apparent density with the use of attenuation of gamma radiation technique.

Delimitation of the heartwood and sapwood

The disks had their cross section polished manually with a series of sandpapers - dry sandpaper (100, 150), and sandpaper water (320, 400, 600 and 1200). The polishing associated with the use of a stereo-microscope of 10x increase - Anatomy Wood Laboratory, College of Agricultural Sciences of Botucatu- made possible the observation of the cross section of the vessels and the exact delimitation between the regions of heartwood and sapwood. The heartwood was characterized by the presence of tyloses in the vessels, and the sapwood, the absence of them (Figure 1).

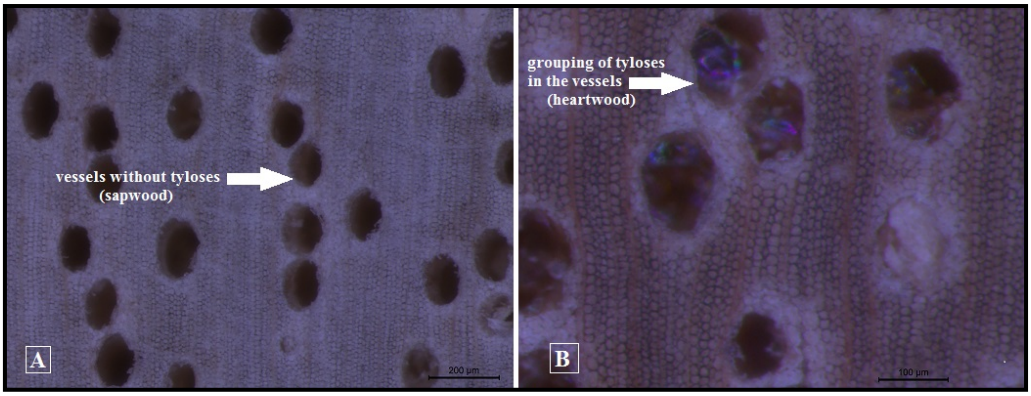

Figure 1— Vessels observed on the polished cross section of wood. A) vessels without tyloses, disc area characterized as sapwood; B) vessels filled with tyloses, disc area characterized as heartwood.

Apparent density (12% moisture content)

The apparent density of the wood (mass and volume at 12% MC) of the disks was determined by the attenuation gamma radiation technique - Figure 2- along the average radius of the discs, avoiding knots or cracks. The attenuation of gamma radiation analysis was performed in the Physics and Biophysics Department of the Biosciences Institute - Botucatu / SP, using an equipment developed and assembled in the same laboratory. This equipment is basically composed of:

- a radiation source sealed and shielded range with the radioisotope ^{241}Am with a half life of 458 years, 200 mCi of activity and photopeak 59.6 keV with emission intensity of 35.9% (Rezende et al., 1999; Palermo et al, 2004);
- a solid scintillation detector system with a crystal of sodium iodide with traces of thallium NaI (T1) inserted into a photomultiplier valve coupled to a source of high voltage GDM marks and connected to a signal amplifier GDM mark;
- a signal conversion board A / D (Analog / Digital) installed in a microcomputer for supplying the values of I and I_0 through a specific program of the GDM mark detection system running on Windows® platform ;
- an electromechanical apparatus for the automatic movement of the sample - wood discs.

According to Parrish (1961) and Ferraz and Mansel (1979), the density was determined by differential absorption of radiation, i.e., the higher the density, the greater the absorption and the lower the amount of radiation that pass through the absorber medium.

Equation 1 was used to calculate the point density expressing an adaptation to the Beer-Lambert law, with corrections provided by equation 2 and 3 due to the dead time of the electronic system.

$$\rho_U = \frac{\ln(I_{0C} - BG) - \ln(I_C - BG)}{\mu_m \cdot \chi_m} \quad (1)$$

$$I_{0C} = \frac{I_0}{1 - \tau I_0} \quad (2)$$

$$I_c = \frac{I}{1 - \tau I} \quad (3)$$

where ρ_U is the wood density at a given moisture content (U); μ_m is the mass attenuation coefficient of wood, in $cm^2.g^{-1}$; χ_m is the thickness of the wood specimen in cm; BG is the background radiation counts per minute; I_0 is a counting rate (counts per minute) obtained experimentally without absorbing material; I is a counting rate (counts per minute) obtained experimentally after passage through the absorber material (wood); I_{0c} is a I_0 value corrected due to the dead time of the electronic system by Equation 1; Ic: I value corrected due to the dead time of the electronic system by Equation 2 and τ is the is a dead time electronics system (1.0×10^{-7} minutes).

The disks were peeled, planed and sanded to acquire uniform thickness around 3.0 ± 0.5 cm which was measured using a digital caliper with a resolution of 0.01mm and accuracy of ± 0,005mm. Subsequently, the disks were stored in a room to reach moisture content of approximately 12%; then the masses of the disks were obtained using an electronic scale of precision , with a resolution of 0.01g and accuracy of ± 0.1 g.

After reaching the equilibrium moisture content (12%), the average radius of the disks was calculated from the disk perimeter, measured with a flexible tape. One radial orientation containing the average radius in the specimen was located and marked.

The disks were positioned in the equipment (Figure 2B) and slowly displaced to cross the radiation source at a speed adjusted to give an average of 2 points per millimeter along the average radius of the sample.

From data of gamma radiation were obtained the apparent densities point to point along the radius were obtained for each disk respectively.

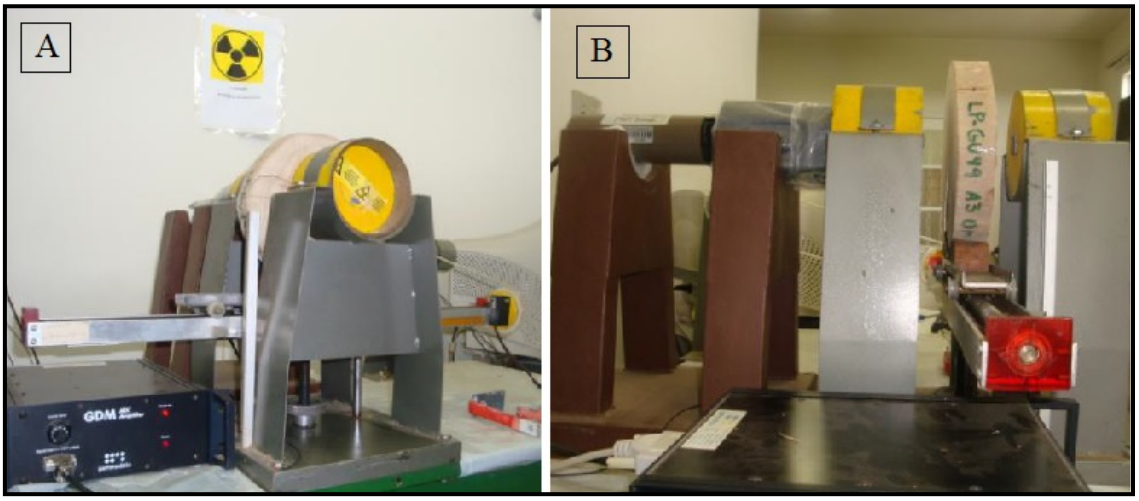

Figure 2— Attenuation gamma radiation technique. A) Overview of the system. B) Side detail side of the specimen movement between the source of radiation emission and the detection system.

Source: Jammal Filho (2011)

The weighted average density was calculated separately for each region of interest - heartwood and sapwood- using the assumption that the disk is formed by several thin and concentric rings with constant thickness: at the central region of the disk, the heartwood and in the peripheral ring, the sapwood. The juxtaposition of rings, one within another, reconstitutes each one of the regions (heartwood and sapwood) and, ultimately, the entire disc. Knowing the density at one point of each ring (Figure 3), it is assumed that this density is the average density of the ring. The weighted average density of the disc is obtained by weighting the point densities in the rings, wherein the weighting factor is the volume of the ring, i.e. the density of the ring with highest volume is more representative in the weighted average value of density.

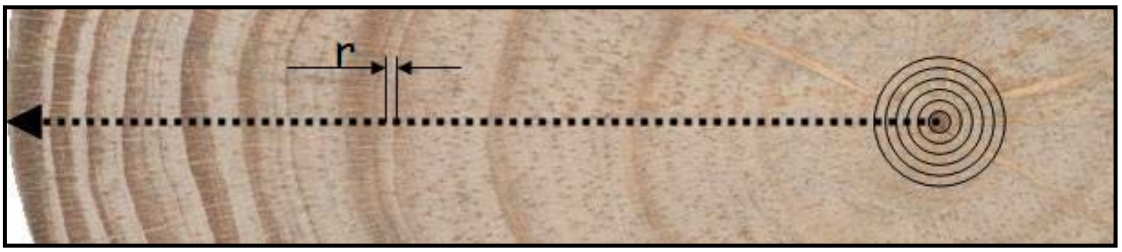

Figure 3— Idealization of composition of a wood disc: thin and concentric rings, of which the density (the center point of the ring) and volume are known ("r" is the distance between each measurement made by the technique).

Source: Costa (2006)

The weighted average density was calculated in the moisture of the sample (U) and then transformed into basic density (ρ_b) and density at 12% MC (ρ_{12}) by the equations 4, 5 and 6 proposed by Rezende (1997) and Rezende et al. (1998) and applied to *Pinus* and *Eucalyptus*.

$$\rho_0 = \frac{\rho_U}{(1+0{,}01\,U\%)\,[(1-0{,}0013U\%)-0{,}0050\,U\%\,\rho_0]} \quad (4)$$

$$\rho_b = \frac{0{,}98\,\rho_0}{1+0{,}24\rho_0} \quad (5)$$

$$\rho_{12} = 1{,}104\rho_0 - 0{,}067\rho_0{}^2 \quad (6)$$

where ρ_U is the apparent density at U% humidity, ρ_0 is the apparent density at 0% humidity, ρ_b is the basic density and ρ_{12} is the apparent density at 12% moisture content.

Results and discussion

Variation in density (12% moisture content) between species

Figures 4 and 5 show respectively one of the sampled (*Eucalyptus saligna*- tree nº 5) discs with the delimitation of heartwood and sapwood regions and its densitometric profile.

Figure 4— Demarcation of regions of heartwood and sapwood *Eucalyptus saligna*- tree nº 5.

Table 1 shows weighted basic and apparent densities results for heartwood and sapwood regions of the discs.

The basic density values ranged from 538 to 721 kg.m^{-3} in the heartwood and from 593 to 698 kg.m^{-3} in the sapwood. The values of apparent density of 12% moisture ranged from 672 to 933 kg.m^{-3} and at the heartwood and from 749 to 899 kg.m^{-3} in the sapwood.

There were no statistical differences between the mean values of both basic and apparent density for the two regions of the wood (heartwood and sapwood). This behavior may have been conditioned due to maturity of trees studied (trees older than 18 years).

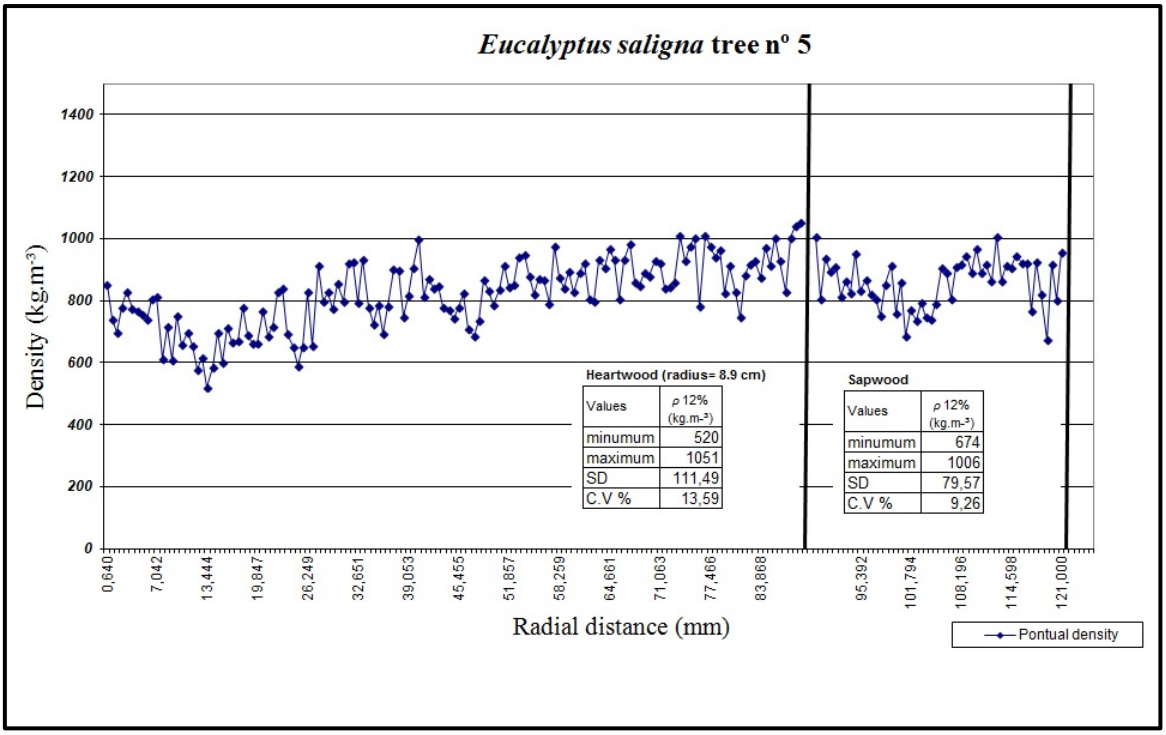

Figure 5— Densitometry profile of *Eucalyptus saligna*- tree nº 5.

Table 1— Weighted basic and apparent density data of the heartwood and sapwood regions.

Species	$\rho_{básica}$ (kg.m^{-3})		$\rho_{12\ \%}$ (kg.m^{-3})	
	Heartwood	Sapwood	Heartwood	Sapwood
Corymbia citriodora	721 (34.5) a A	698 (50.9) a A	933 (18.4) a A	899 (27.0) a A
Eucalyptus tereticornis	703 (59.6) a A	647 (86.9) ab A	910 (38.2) a A	826 (54.9) ab A
Eucalyptus saligna	680 (42.8) a A	667 (62.5) ab A	873 (58.3) a A	855 (86.0) ab A
Eucalyptus grandis	538 (43.5) b A	593 (60.1) b A	672 (62.1) b A	749 (87.5) b A

* In the same column, average followed by at least one lowercase same letter do not differ by Tukey test ($p < 0.05$).

** In the same row, for the same property, means followed by at least one capital letter like not differ by Student's t test ($p < 0.05$).

Comparing densities between the species, trees of *Corymbia citriodora* showed the highest values (both basic and apparent density) in the two regions of the wood, but these values did not differ statistically from the results obtained for *Eucalyptus tereticornis* and *Eucalyptus saligna* trees. *Eucalyptus grandi*s was the species that showed lower density values in both wood fractions, with statistical difference compared to the other three species studied for heartwood fraction; for the sapwood fraction, it differed statistically only from *Corymbia citriodora* trees.

Basic density of *Eucalyptus grandis* was studied by many authors, including Sturion et al. (1987) that found value of 525 kg.m^{-3} for trees with 10,5 years; Ciniglio (1998), studying the wood of the same species with 17 years old, obtained a basic density of 570 kg.m^{-3}; Ashley and Ozarska (2000), which studied the same species with 28 years old, reported a basic density of 690 kg.m^{-3} for juvenile wood and 750 kg.m^{-3} for adult wood; Gonçalez et al. (2006), who found for *E. grandis* wood - 17 years old - basic density of 590 kg.m^{-3} and Lopes et al. (2011) found for *E. grandis* wood - 18 years old - basic density of 580 kg.m^{-3}.

The values obtained in this study are similar to those found by Sturion et al. (1987), Ciniglio (1998), Gonçalez et al. (2006) and Lopes et al. (2011) and lower than those found by Ashley and Ozarska (2000). This inferiority in values when compared to the results obtained by these latter authors probably occurs due to the age of the trees used in the study of the authors (older trees than those used in this study).

Sturion et al. (1987) also evaluated the basic density of *Corymbia citriodora*, *Eucalyptus tereticornis* and *Eucalyptus saligna*. The values found by the authors were, respectively, 715 $kg.m^{-3}$, 592 $kg.m^{-3}$ and 562 $kg.m^{-3}$. The basic density of *Corymbia citriodora* found by the author is close to the values found in this study but for the other two species, the values found by the author are lower than those obtained here. Here again, the inferiority may be associated with younger trees (10,5 years).

Oliveira et al. (2005) studied the wood of seven species of *Eucalyptus* about 16 years old, including *Corymbia citriodora*, *Eucalyptus tereticornis* and *Eucalyptus grandis*, species that were studied in this work. The authors found basic density values of 730 $kg.m^{-3}$ for the *Corymbia citriodora*, 660 $kg.m^{-3}$ for *Eucalyptus tereticornis* and 490 $kg.m^{-3}$ for *Eucalyptus grandis*.

Oliveira et al. (2012), studying the wood of *Eucalyptus grandis* trees with 23 years and *Corymbia citriodora* with 17 years, found values of apparent density at 12% moisture content of 580 $kg.m^{-3}$ and 840 $kg.m^{-3}$, respectively. The values found by the authors are lower than those found in this study. Benjamin and Ballarin (2009) found apparent density values of 970-1200 $kg.m^{-3}$ for wood of *Corymbia citriodora* 29 years old.

Conclusions

The attenuation of gamma radiation is a low-energy technique that permits continuous and accurate nondestructive evaluation of wood density in regions of particular interest of disks.

For the trees and species studied from a physical point of view it can be stated that heartwood and sapwood fractions have the same quality because no significant differences were obtained in their basic and apparent densities

Acknowledgments

To São Paulo Research Foundation (FAPESP - 2012/18704-1), for their financial support.

References

ASHLEY, P.N.; OZARSKA, B. Furniture from young plantation eucalypts. In: The future of *Eucalyptus* for wood products, 2000, Launceston, Tasmania. Proceedings.... Launceston : IUFRO, 2000. p. 176-184. 2000.

BENJAMIM, C. S.; BALLARIN, A. W. Variação radial da densidade aparente da madeira de *Corymbia* (*Eucalyptus*) *citriodora* com 29 anos de idade. Energia na Agricultura, Botucatu, v. 24, n. 2, p. 29-46, 2009. (in portuguese)

CAIXETA, R. P. et al. Propriedades e classificação da madeira aplicadas à seleção de genótipos de *Eucalyptus*. Revista Árvore, Viçosa, MG, v. 27, n. 1, p. 43-51, 2003. (in portuguese)

CINIGLIO, G. Avaliação da madeira serrada de *Eucalyptus grandis* e *Eucalyptus urophylla*. Piracicaba, 1998. 73f. Dissertação (Mestrado) – Escola Superior de Agricultura Luiz Queiroz, Universidade de São Paulo, Piracicaba, 1998. (in portuguese)

COSTA, V. E. Caracterização físico-energética da madeira e produtividade de reflorestamentos de clones de híbridos de *Eucalyptus grandis* x *E.urophylla*. 2006. 99 f. Tese (Doutor em Energia na Agricultura) – Faculdade de Ciências Agronômicas, Universidade Estadual Paulista, Botucatu, 2006. (in portuguese)

FERRAZ, E. S. B.; MANSEL, R. S. Determining water content and bulk density of soil gamma Ray attenuations method. IFAS Technical Bulletin, Florida, n. 807, p. 51, 1979.

GOMINHO, J. Variação do cerne no eucalipto e a sua influência na qualidade da madeira para produção de pastas para papel. 2003. 264 f. Tese (Doutorado em Engenharia Florestal) – Universidade Técnica de Lisboa, Lisboa, 2003. (in portuguese)

GONÇALEZ, J.C. et al. Características tecnológicas da madeira de *Eucalyptus grandis* W.Hill ex Maiden e *Eucalyptus cloeziana* F.Muell visando ao seu aproveitamento na indústria moveleira. Ciência Florestal, Santa Maria, v. 16, n. 3, p. 329-341, dez. 2006. (in portuguese)

HILLIS, W. E. Heartwood and tree exudates. Berlin: Springer-Verlag, 1987. 268 p.

JAMMAL FILHO, F.A. Determinação da densidade da madeira de clones de *Eucalyptus* spp. a idades passadas com uso da técnica de atenuação de radiação gama. 2011. 81 f. Dissertação (Mestrado em Energia na Agricultura)-Faculdade de Ciências Agronômicas, Universidade Estadual Paulista, Botucatu, 2011. (in portuguese)

LOPES, C. S. D. et al. Estudo da massa específica básica e da variação dimensional da madeira de três espécies de eucalipto para a indústria moveleira. Ciência Florestal, Santa Maria, v. 21, n. 2, p. 315 - 322, 2011. (in portuguese)

OLIVEIRA, B. R. U. de. et al. Microdensitometria de raios X aplicada na determinação da variação da densidade do lenho de árvores de *Eucalyptus grandis* W. Hill. Scientia Forestalis, Piracicaba, v. 40, n. 93, p. 103-112, mar. 2012. (in portuguese)

OLIVEIRA, J. T. S.; TOMAZELLO FILHO, M; SILVA, J. C. Resistência natural da madeira de sete espécies de eucalipto ao apodrecimento. Revista Árvore, Viçosa, MG, v. 29, n. 6, p. 993-998, 2005. (in portuguese)

PALERMO, G. P. M. et al. Determinação da densidade da madeira de *Pinus elliottii* Engelm, através de atenuação de radiação gama comparada a métodos tradicionais. Floresta e Ambiente, Rio de Janeiro, v. 11, n. 1, p. 1-6, ago./dez. 2004. (in portuguese)

PARRISH, W. B. Detecting defects in wood by the attenuation of gamma rays. Forestry Science, Washington, DC, v. 2, p. 136-143, 1961.

REZENDE, M. A. Uma abordagem convencional sobre as principais características físicas da madeira, com ênfase para retratibilidade, massa específica e técnica de atenuação de radiação gama. 1987. 138 f. Tese (Livre Docência)- Faculdade de Ciências Agronômicas, Universidade Estadual Paulista, Botucatu, 1997. (in portuguese)

REZENDE, M. A.; SAGLIETTI, J. R. C.; CHAVES, R. Specific gravity variation of *Eucalyptus grandis* wood at 8 years old in function of a different productivity indexes. Scientia Forestalis, Piracicaba, n. 53, p. 71-78, 1998.

SERPA, P. N. et al. Avaliação de algumas propriedades da Madeira de *Eucalyptus grandis*, *Eucalyptus saligna* e *Pinus elliottii*. Revista Árvore, Viçosa-MG, v. 27, n. 5, p. 723-73, 2003. (in portuguese)

SMITH, H. G., WALTERS, J., WELLWOOD, R. W. Variation in sapwood thickness of Douglas-fir in relation to tree and section characteristics. Forest Science, Bethesda, v. 12, n. 1, p. 87-103, 1996.

STURION, J.A.; PEREIRA, J.C.D.; ALBINO, J.C. Avaliação da produtividade energética da madeira e do carvão de doze espécies de *Eucalyptus* em Uberaba-MG. Colombo: EMBRAPA-CNPF, 1987. (in portuguese)

Nondestructive testing of string musical instruments manufactured in wood

Voichita Bucur –CSIRO Commonwealth Scientific and Industrial Research Organisation, Ian Wark Laboratories, Bayview Avenue Clayton South- Victoria 3169, AUSTRALIA voichita.bucur@csiro.au

Abstract

This report describes three groups of nondestructive methods for testing string musical instruments for classical music, namely the instruments from violin family and guitar. The methods are the followings: *mechanical methods* - modal analysis, *optical methods*- holographic interferometry, laser Doppler vibrometry, near field acoustic holography, *X ray methods*- X-ray computed tomography and synchrotron radiation phase-contrast microtomography.

1.Background

In a very simplified way we can define a musical instrument like a device constructed to make musical sounds. A string instrument consists of a structure with a cavity which holds strings under tension. The structure radiates sounds if the strings vibrate. French and Bissinger (2001) noted "testing musical instruments is not conceptually different than testing other structures. Interpretation of the results is, however, somewhat non-traditional in that the enclosed air cavity is an integral part of the system and cannot be ignored. Instruments – particularly violins- are typically very light and flexible and very sensitive to boundary conditions. Special care needs to be taken so that the instrumentation, excitation methods, and support fixtures do not add mass or stiffness to the instrument".

2. Modal analysis

Modal analysis of musical instruments is the study of their dynamic properties under vibrational excitation. In other words ones can say that the modal analysis describes the dynamic properties of an instrument view as an elastic structure in terms of its normal modes of vibration. Theoretical aspects of modal analysis and experimental modal testing have been discussed in details by Fletcher and Rossing (2010) with application to a big diversity of musical instruments. The complex vibration of a musical instrument can be described in terms of normal modes of vibration. The frequency response of a musical instrument can be found by summing the modal responses of its sub structures in accordance with their degree of participation in the structural motion. Each mode of vibration is characterised by three main parameters: the mode shape, the natural frequency and the damping factor. Any deformation pattern of a musical instrument can be expressed by a combination of the mode shapes. Each mode shape shows how energy point on the violin (or other instrument) moves when it is excited at any point, and gives a list of displacements at various point of the instrument, in various directions. The damping factor of each mode is coupled with its natural frequency and is inversely proportional with the mass distribution (Rossing 2007). Modal testing may use continuous (sinusoidal), impulsive or random excitation and may measure the response mechanically, optically, or indirectly by observing the radiated sound field. Experimentally, the excitation force can be measured with a force transducer (load cell or piezoelectric transducer), the acceleration can be measured with an accelerometer and the velocity response of the structure with a laser velocimeter or by holographic interferometry. Data are converted in digitize analogue instrumentation signals and stored on a host computer. The analysis of experimental signals relies on Fourier analysis. The

resulting transfer function – frequency response function - will show characteristic peak resonances for different frequencies. The animated display of the mode shape is very useful for understanding vibration phenomena in musical instruments. Marshall (1985) was among the first authors to characterized violin vibrational modes with experimental modal analysis (Alonso Moral and Janson 1982). Graphical representation of experimental modal testing and finite element reconstruction of the vibration of the body of the violin is shown in Fig. 1, in which, for a resonant mode are represented the asymmetric vertical displacement and the flexural vibration of the violin.

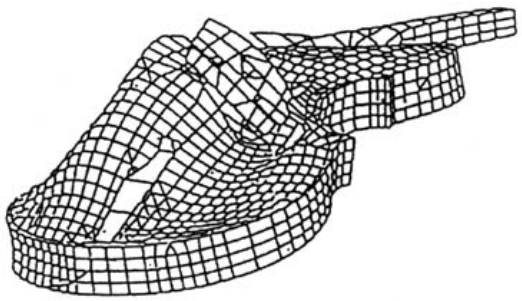

Figure 1 Asymmetric vertical displacement and flexural vibration of the violin are represented at an exaggerated scale, for a resonant mode (Knott 1987).

3. Optical methods

Optical methods are particularly appropriated for musical instruments vibrations studies. Being non-contact they do not involve any attaching devise to the surface of the instruments. Therefore the surface of the musical instrument can vibrate frailly, in its natural state. Typical applications of optical methods are related to modal analysis and reconstruction of sound fields radiated from the violins and other instruments (Molin 2002 , Molin and Zipser 2004). Holographic methods generally depend on the interference of coherent light to identify nodes and modes. Scanning laser vibrometry scans a laser beam across the surface of musical instrument and allows recording the return beam's frequency shift. This frequency is proportional to the velocity of the surface. Laser Doppler vibrometry compared to holography is more sensitive and operates well with multifrequency repeatable motions of the object, rather the holography works well with harmonic object motions.

Time average holographic interferometry was used for the study of body resonances by recording the nodal lines and producing a map of displacement amplitudes in antinodal zones (Reinecke and Cremer 1970, Jansson et al. 1970, Janson 1972). In these experiments a single frequency excitation was used, for a system demanding high stability. Technological advancements allowed the development of a TV- monitor for analysis of modal shapes in real time, on which monitor the vibrations over instrument surface are displayed as iso-amplitude lines (minimum amplitude 0.12μm) (Ek and Jansson 1986, Jansson et al. 1994). Real time observation of the vibration field allows search for resonant modes, amplitude and position of the exciters, settings of frequency, etc. Time-average technique requires recording of the vibration patterns on interferograms that permits a more detailed analysis of the vibration field. Currently for studies of vibrating objects as violins, a combination of the real time and time average holographic interferometry is used. Experimentally, iso-amplitude fringes that cover the surface of the violin are mapped and the corresponding intensity recorded. Practical resolution of vibration modes by visual observation in real time is about $\lambda/10$, which is about 100nm (Molin 2007). Figure 2 gives two images of a violin plate vibration, produced with Chladni pattern and with an interferogram of a free violin plate. This interferogram was obtained with a laser generating about 1 W of light at 514.5 nm. The system incorporated a speckle interferometer for real time visualisation of vibrations. This comparative presentation chosen by Richardson (2010) suggests the enormous progress realised in the last five decades in understanding violin acoustics.

a) Chladni pattern	b) holographic interfetrometry
	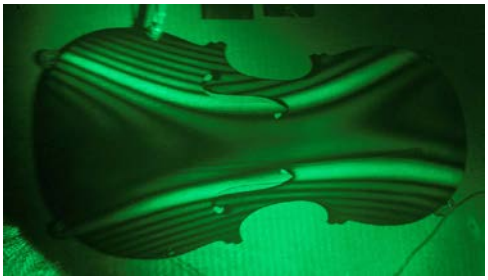

Figure 2 Vibration of a free violin plate observed with Chladni pattern (a) and with holographic interfetrometry (b) (Richardson 2010, fig 1, page 129)

The interferograms shows the resonance frequencies and bandwidth up to about 5 KHz, rather the Chladni pattern method works for the lowest two or three resonances observed inside the plate. With the interferograms, the fringes indicate the contours of constant vibration amplitude, as observed on the outside of the plate. As noted by Richardson (2010) "holographic interferometry has been superseded by scanning laser Doppler velocimetry, but holography does have the advantage of being able to measure static as well as dynamic displacements, it has better sensitivity at low frequencies and it also has applications in real time capture and distributed motion".

Laser Doppler vibrometry (LDVi) is an interferometric technique, very appropriate for measurements on vibrating surfaces (Drain 1980, Castellini et al. 1998) . The principle of LDVi is based on the conversion of the instantaneous velocity v into a Doppler frequency f_D, using a heterodyne interferometer. The investigation capabilities of experimental testing were enormously improved with respect to classic accelerometers, being non intrusive, giving high spatial resolution, with reduced testing time and superior performances expressed for example by the resolution in displacement in nm range and in velocity of about 0.5μm/s and bandwidth up to 200 kHz. This technique is less disturbed by the motion of the violin rigid body than holographic interferometry. By scanning the laser beam across the violin, the resonance frequencies and the corresponding modes are visualised and easy measured. Optical interference is observed when two coherent beams of light coincide. The resulting intensity varies with the phase difference between the two beams, which is a function of the different path lengths of the two beams. If one of the two beams is reflected back from a moving target, then the path difference can be observed as a function of time. From the interference fringe pattern which moves, the displacement of the target can be calculated by counting the passing fringe pattern. Scanning laser Doppler vibrometrs allows rapid and precisely moving the measurement point on the violin under test, analysing the entire surface, with high spatial resolution in a short testing time. The advantages of scanning laser Doppler vibrometry are the followings: capability of determining the velocity of vibration quantitatively; capability to measure vibration mode shapes with high speed sampling; capability to measure the vibration of objects of complex shape; frequency range up to 5000 Hz; measurement uncertainty below 3%. Figure 3 shows the superimposition of vibration modes of a violin plates obtained with scanning laser vibrometry and modal analysis. Simultaneous displacements of musical instruments in three directions can be obtained with devices allowing 3D scanning laser Doppler velocimetry.

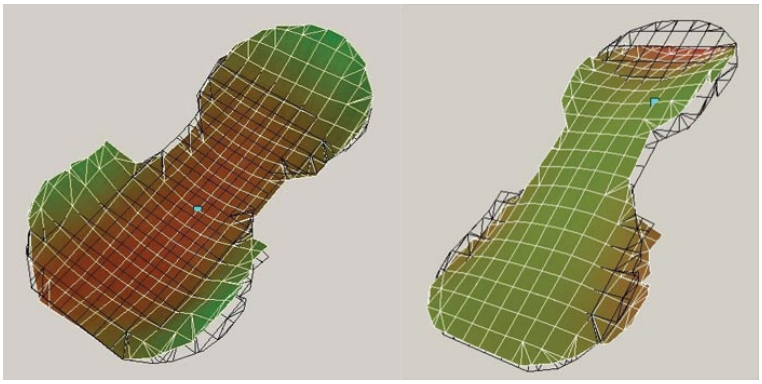

Figure 3 Superimposition of vibration modes of a violin plates obtained with scanning laser vibrometry and modal analysis (Photo courtesy of School of Engineering and Information Technology, University New South Wales , Canberra, Australia http://seit.unsw.adfa.edu.au/research/details2.php?page_id=746 access 20 August 2013)

A 3-Dimensional scanning laser system is comprised of three individual lasers measuring surface velocity from three different directions which allows extraction of motion components along three perpendicular directions. To measure all three components of the violin's velocity, a 3-D vibrometer should measure the violin vibrations with three independent beams, which strike the target from three different directions. This allows determination of the complete set of in-plane and out-of-plane velocities of the violin. Extensional in plane and flexural out of plane violin corpus mobilities can be visualised in top, back and ribs as developed and discussed by Bissinger and Oliver (2007) and can be presented with animations (http://www.strad3d.org/cms/).

Sound radiated from the violins can be visualised (mapped) and measured with regard to every measured frequency with near field acoustic holography. Theoretical foundation of this technique is explained by Maynard et al. (1985) and Kim (2007) and is based on the fact that the source can be completely reconstructed with measurements of exponentially decaying waves which propagate from the source. The sound field can be seen in frequency domain. Simulation of real bowing of a violin can be obtained with a mechanical device, bowing at constant frequency with a belt or, at variable frequency with a rotating mechanical bow. The sound radiated by real violins in these cases can be measured with near field acoustic holography. If the violin is excited by a rotating bow, several frequencies can also be excited and of course the eigenmodes can be determined (Gren et al. 2006). Figure 4 shows images of violin vibrations at 2265 Hz with a large number of antinodes.

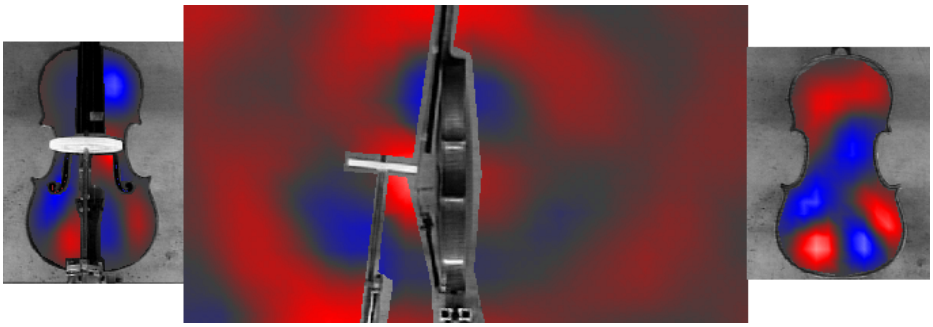

Top plate ± 0.5µm	Sound field at the eighth harmonic 2265 Hz Displacement ± 0.16 µm	Back plate ±0.12µm

Figure 4 Images of violin vibrations (Gren et al. 2006) Legend: The colour code blue red is set automatically. The displacement range is between 18µm and 40nm. Red areas vibrate in

anti-phase to the blue areas. Vibration at the 4th harmonic, at 2265 Hz (Gren et al. 2006, fig 12, page 642)

4. X ray methods

X-ray computed tomography has medical and industrial applications. X ray - computed tomography scanner produces three dimensional images of external and internal structure of the objects submitted to inspection. Applications of X ray computed tomography to wood imaging with a resolution of about 1μm for each side of the typical voxel, are described by Bucur (2003). (Note that a voxel or a volumetric pixel or volumetric picture element is a volume element, representing a value on a rectangular grid in 3D space). Density of inspected object depends on the atomic composition of the material and on the X-ray energy used in this process. Clinical scanners have been used to inspect the internal structure of Old Italian violins since 1997 (Sirr and Waddle 1997, Gattoni et al. 1999). The images obtained with this technique allowed univocal confirmation of the authenticity of these precious authentic historic instruments and identification of repairs, restoration works, damages by insects, etc. The accessibility of medical scanner for violin investigations produced hundred of images (Borman and Stoel 2009, Borman et al. 2005). The images were referred in three reference planes: the sagittal plane (from the side), the axial plane and the coronal plane (from the top). The violin is introduced into the scanner which produces images reconstructed from hundreds of thousands of measurement of X-ray absorption properties of the sample (Fig.5). Technical limitation of clinical equipment is due to the limited spatial resolution of the scanner which is of 0.4 x 0.4 x 0.6 mm^3. Every defect smaller than about 0.1 mm^3 cannot be detected with this kind of instrument. Image resolution depends on sample size and selected imaging technique. X-ray technique allows scanning of big objects of about 0.5 to 1.0 m with a resolution ranging from o.1 mm to less than 1mm; neutrons technique was used for scanning objects of about 5mm to 50 mm with a resolution of 0.02 mm to 0.1mm; synchrotron light imaging device can inspect objects of about 1 to 5 mm with a resolution of 0.001 to 0.005 mm. (Lehmann and Mannes 2012)

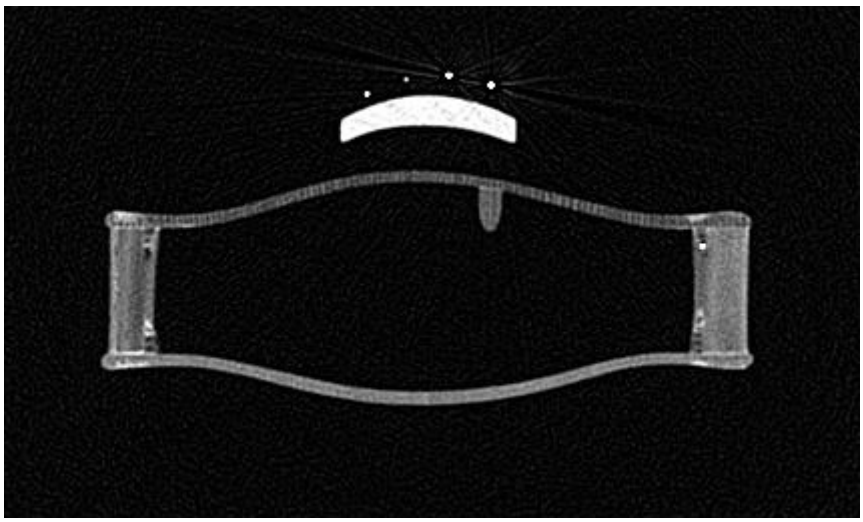

Figure 5 Transverse CT profile of a 1735 Guarneri ‘del Gesù’ violin at the widest section of the lower bout (photo courtesy http://www.bormanviolins.com/Images/1735.upper.c.web.jpg). Legend: end of bass-bar (within body) and part of tailpiece (above body) in ebony in white, of higher density and the section of the four strings. On the belly the transverse section of spruce is well visible with the alternating early wood (low density) and latewood (high density) in annual rings.

Recent development of synchrotron technology superseded the X-ray CT tomography and produced images of better resolution, but with very high cost equipment. Synchrotron radiation phase-contrast microtomography is considered an ideal technique for the non-destructive 3D analysis of samples of objects of cultural heritage in which low absorbing elements such as larvae and eggs can be detected in wood structural elements (Bentivoglio-Ravadio et al. 2011).

5. Conclusion

Testing musical instruments is not conceptually different than testing other structures. Interpretation of the results is, however, more complex because of the enclosed air cavity of musical instruments, which is an integral part of the system. Theoretical parameters of the vibration of musical instruments are given by modal analysis. Modal testing allows experimental identification of modal parameters of vibrating musical instruments (natural frequencies, modal damping and the mode shapes). Optical non-contact techniques - holographic and scanning laser - Doppler vibrometry - have been developed for experimental studies of violins. The advantages of scanning laser Doppler vibrometry are the followings: capability of determining the velocity of vibration quantitatively; capability to measure vibration mode shapes with high speed sampling; capability to measure the vibration of objects of complex shape; frequency range up to 5000 Hz; measurement uncertainty below 3%. X-ray (CT) computed tomography with clinical scanners is used to obtain data on wood density of different structural components and different maps such as map of thickness, map of density variation, map of arching. Technical limitation of clinical equipment is due to the limited spatial resolution of the scanner which is of 0.4 x 0.4 x 0.6 mm^3.Synchrotron radiation phase-contrast microtomography is considered an ideal technique for the non-destructive 3D analysis of samples of musical instruments and other objects of cultural heritage. These methods are discussed by Bucur (2003 and 2015) .

Acknowledgments

CSIRO Australia is acknowledged for supporting this reseach related to the materials for string musical instruments.

References

Alonso Moral J, Jansson E (1982) Eigenmodes, input admittance, and the function of the violin. *Acustica* 50: 329-337

Bentivoglio-Ravadio B, Dreossi D, Marconi E et al. (2011) Synchrotron radiation microtomography of musical instruments: a non-destructive monitoring technique for insecte infestation. *J. Ent. Acarol Res.* Ser. II 43, 2:149-155

Bissinger G, Oliver D (2007a) 3D laser vibrometry on legendary Old Italian violins. Sound and Vibrations July:10-14. http://wwwSandV.com (Access 30 July 2013)

Borman T, Stoel B (2009) Review of the uses of computed tomography for analysing instruments of the violin family with a focus on the future. *J. Violin Soc. Am. VSA Papers* XXII, 1: 1-12

Borman T, King AT, Loen JS (2005) Path Through the Woods .The Use of Medical Imaging in Examining Historical Instruments. *The Strad Magazine*, September: 68 - 75

Bucur V (2003) *Nondestructive characterisation and imaging of wood*. Springer Verlag, Berlin

Bucur V (2015) *Handbook of materials for string instruments* (in press) Springer Verlag.

Castellini P, Revel GM, Tomasini EP (1998) Laser Dopler vibrometry: a review of advances and applications. *Shock and Vibr. Digest* 30, 6: 443 - 456

Drain, L E (1980) *The Laser Doppler Technique*, John Wiley & Sons, New York

Ek L, Jansson EV (1986) Modal properties of wooden plates determined by TV –holography and electro-acoustical methods. *J. Sound Vibr.* 111, 1:115-124

Fletcher NH, Rossing T D (2010) *The physics of musical instruments*. Springer Verlag, Chapter 10.5.1 Experimental methods for modal analysis: 289- 291

French M, Bissinger G (2001) Testing of acoustic stringed musical instruments- an introduction. *Experimental Techniques.* January/February: 40-43. Part 2. Mechanics of stringed instruments. *Experimental Techniques* March/April : 34 – 37

Gattoni F, Melgara C, Sicola C, Uslenghi CM (1999) Unusual application of computerized tomography: the study of musical instruments. *Radiol. Med.* 97:170- 173

Gren P, Tatar K, Granström J, Molin NE (2006) Laser vibrometry measurements of vibration and sound fields of a bowed violin. *Measurement Sci. Techn.* 17: 635 – 644

Jansson EV (1972) An investigation of a violin by laser speckle interferometry and acoustical measurements. *Quarterly Progress and Status Report* 13, 1 : 025-033 http://www.speech.kth.se/qpsr

Jansson EV, Molin NE, Saldner HO (1994) On eigenmodes of the violin- Electronic holography and admittance measurements. *J. Acoust. Soc. Am.* 95: 1100 - 1105

Jansson EV, Molin NE, Sundin H (1970) Resonances of a violin body studied by hologram interferometry and acoustical methods. *Physica Scripta* 2: 243-256

Kim YH (2007) Acoustic holography. In "*Springer handbook of acoustics*" ed TD Rossing, Springer Verlag, Berlin: 1077-1100

Lehmann E, Mannes D (2012) Wood investigations by means of radiation transmission techniques *Journal of Cultural Heritage* 13, 3: S35-S43

Marshall KD (1985) Modal analysis of a violin. *J. Acoust. Soc. America* 77: 695-709

Maynard JD, Williams EG, Lee Y (1985) "Nearfield acoustic holography: I. Theory of generalized holography and the development of NAH". *J. Acoust. Soc. Am.* 78, 4: 1395–1413

Molin NE (2007) Optical methods for acoustics and vibration measurements. In "*Springer handbook of acoustics*" ed TD Rossing, Springer Verlag, Berlin: 1101-1126

Molin NE (2002) Vizualiastion instrument vibrations and sound fields – the state of the art. *Catgut Acoust. Soc. J.* Series II, 4, 5:21-29

Molin N E, Zipser L (2004) Optical methods of today for visualizing sound fields in musical acoustics. *Acta Acustica united with Acustica*, 90, 4: 618-628

Reinecke W, Cremer L (1970) Application of holographic interferometry to vibrations of the bodies of string instruments. *J. Acoust. Soc. Am.* 48: 988

Richardson BE (2010a) Mode studies of plucked stringed instruments: application of holographic interferometry. *Proc. Second Vienna Talk*, Sept. 19−21, 2010, University of Music and Performing Arts Vienna, Austria: 129-132

Rossing TD (2007) Modal analysis. In "*Springer handbook of acoustics*" ed TD Rossing, Springer Verlag, Berlin: 1127-1138

Sirr SA, Waddle JR (1997) CT analysis of bowed stringed instruments. *Radiology* 203: 801-805

Stoel BC, Borman TM, de Jongh R (2012) Wood densitometry in 17th and 18th century Dutch, German, Austrian and French Violins, compared to classical Cremoneses and modern violins. *PLoSOne*, October 7, 10: e46629

The effect of moisture content on nondestructive probing measurements

Daniel F. Llana
Department of Forest and Environmental Engineering and Management.Universidad Politécnica de Madrid, Madrid, Spain, danielfllana@gmail.com

Eva Hermoso
Forest Products Department.INIA-CIFOR,Madrid, Spain, hermoso@inia.es

Sara T. Izquierdo
Department of Forest and Environmental Engineering and Management. Universidad Politécnica de Madrid, Madrid, Spain, sarat.izquierdo.garcia@gmail.com

Ignacio Bobadilla
Department of Forest and Environmental Engineering and Management.Universidad Politécnica de Madrid, Madrid, Spain, i.bobadilla@upm.es

Guillermo Íñiguez-González
Department of Forest and Environmental Engineering and Management.Universidad Politécnica de Madrid, Madrid, Spain, guillermo.iniguez@upm.es

Abstract

When assessing existing timber structures it is not possible to obtain density as the ratio mass/volume, so nondestructive probing methods are used to predict density. As in other nondestructive techniques, moisture content influences measurements. The goal of this paper is to study the influence of timber moisture content on two nondestructive probing techniques (penetration resistance and pullout resistance). 25 large cross section specimens of laricio pine from Spain were measured. The moisture content ranged from 65.1% to 8.3%.

Penetration depth decreases and screw withdrawal strength increases when moisture content decreases below the fiber saturation point. There are lineal tendencies in both techniques. No moisture content influence was found in measures above fiber saturation point.

Keywords: moisture content, nondestructive techniques, penetration resistance, probing, pullout resistance

Introduction

Nondestructive probing methods are mainly used to evaluate existing timber structures. These techniques are used to estimate density (Bobadilla et al. 2007). Several factors affect nondestructive techniques, and one of the most important is moisture content (MC).

Some research works were found on the influence of MC over penetration depth tests. In 1978 several Pilodyn prototypes (with different diameter needles and 6, 9, 12 and 18 J energy release) were used on

Norway spruce (*Picea abies* (L.) Karst.), Scots pine (*Pinus sylvestris* L.) and European beech (*Fagus sylvatica* L.). An increase of from 1% to 2% in penetration depth for each 1% increase in MC was found in the 8% to 24% range of MC. However, above 30% of MC the increase is really low (Hoffmeyer 1978).

In another work using the Pilodyn 6J and Pilodyn 18J on 106 specimens 50 x 50 mm cross-section Douglas fir (*Pseudotsuga menziesii* (Mirb.) Franco), 2 different areas of influence were found. In MC range from 6% to 30% an increase of 0.19 mm in penetration depth using the Pilodyn 6J and an increase of 0.26 mm using the Pilodyn 18J was found for each 1% MC increase. However, above 30% no significant statistical influence of MC was found (Smith and Morrell 1986).

Research work using the Pilodyn 6J Forest device (Proceq, Switzerland) on Scots pine (*Pinus sylvestris* L.), radiata pine (*Pinus radiata* D. Don) and laricio pine (*Pinus* nigra Arn.) no variation in the MC range from 8% to 14% was found. This may be due to the variability of measurements (Calderón 2012). The same work also studied the effect of MC on the Screw Withdrawal Resistance Meter (SWRM) device (Fakopp, Hungary). The increase in screw withdrawal force when MC decrease was different for each species. A second order correction equation was proposed for each species.

Other authors mention the high sensitivity of screw withdrawal techniques to MC changes (McLain 1997). Screw withdrawal force at 7% MC is approximately 50% higher than above the fiber saturation point (FSP), and there are differences between species. For sugar maple (*Acer saccharum* Marsh.) it is 71% higher, while for white pine (*Pinus strobus* L.) it is 23% higher (Cockrell 1933).

Previous studies show the MC tendency in probing measurements, and they also indicate species and source influence on MC adjustments. Therefore, specific research is required, considering these factors in one of the most widely used Spanish structural timber species: laricio pine (*Pinus* nigra Arn. Ssp. *Salzmannii*).

Material and methods

In this study 25 planed large cross-section specimens of laricio pine (*Pinus nigra* Arn. Ssp. *Salzmannii*) of Spanish provenance with nominal dimensions of 100 x 150 mm cross-section and 500 mm length were used. Green specimens were selected in the sawmill and their ends were sealed to promote uniform drying. MC was determined by the oven drying method according to standard EN 13183-1:2002.

Needle impact penetration depth using the commercial device Pilodyn 6 J Forest (Proceq, Switzerland) and screw withdrawal force using the commercial device Screw Withdrawal Resistance Meter (Fakopp, Hungary) were measured at 14 different MC. Measurements were made avoiding areas close to the pith, following the same grain and with at least a 30 mm gap between them. The first one was performed at 65.1% average MC and the final one at 8.3% average MC. 181 days were necessary from the first measurement to the last one using the natural drying process.

Results and discussion

Figure 1 shows the evolution of MC in the natural drying process. At the beginning of tests, MC values were very disperse and variable. Table 1 summarizes measurements from both techniques (penetration resistance and pullout resistance).

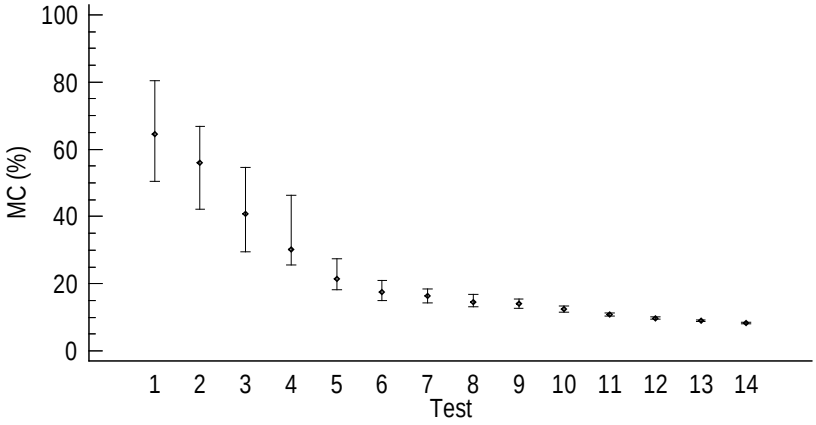

Figure 1— Average and range of MC values during the natural drying process.

Table 1— Pilodyn and SWRM mean results.

Nº Test	Day	Mean MC (%)	Mean Penetration Depth(mm)	COV (%)	Mean Screw Withdrawal Force (kN)	COV (%)
1	0	65.1	18	16.82	0.77	26.49
2	6	57.4	17	17.53	0.68	23.84
3	14	45.0	17	19.65	0.76	25.19
4	20	37.8	17	20.55	0.81	32.39
5	34	26.0	16	18.21	1.32	23.38
6	49	19.7	15	20.85	1.42	24.02
7	56	17.7	15	21.98	1.52	20.67
8	62	15.7	14	18.87	1.70	19.89
9	72	14.5	14	19.27	1.86	19.84
10	87	13.3	14	18.24	1.93	18.71
11	105	10.9	13	17.04	2.04	20.19
12	126	9.7	13	17.47	2.15	19.75
13	142	9.0	13	15.54	2.20	19.31
14	181	8.3	12	15.87	2.35	19.00

Figures 2 and 3 present the evolution of penetration depth and screw withdrawal force with MC changes. In both devices no statistical significant differences in MC range above FSP were found. The same results were found by other authors (Hoffmeyer 1978; Smith and Morrell 1986).

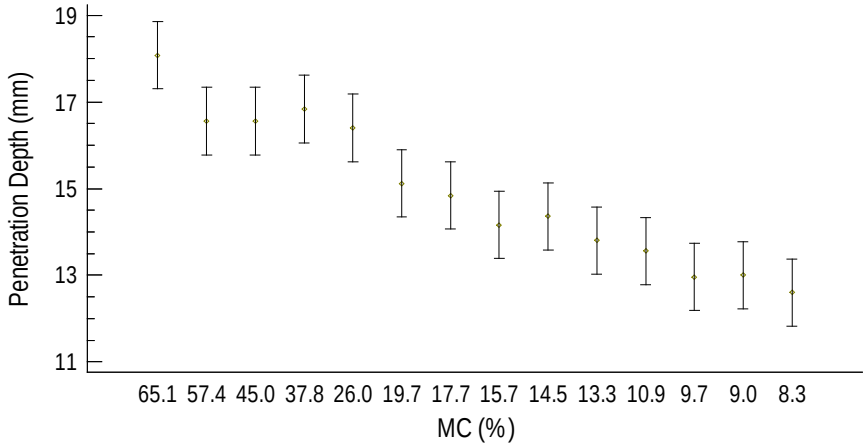

Figure 2— Means plot of one-way analysis of variance:Penetration depth vs. MC.

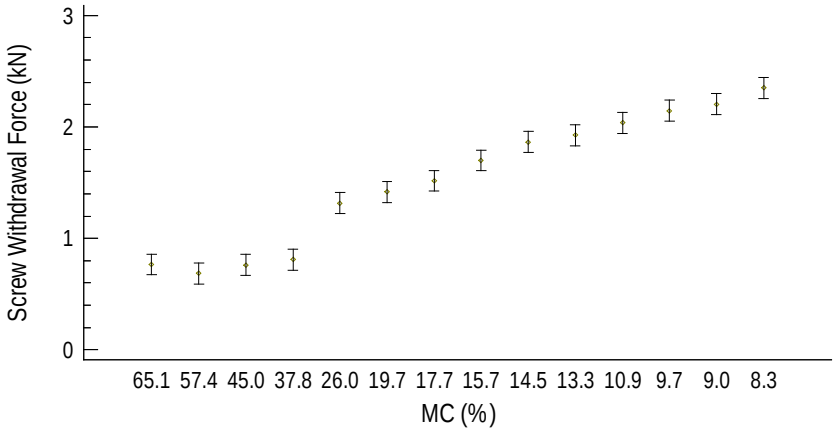

Figure 3— Means plot of one-way analysis of variance:Screw withdrawal force vs. MC.

To study tendencies below 30% of MC, figures 4 and 5 show linear regressions between penetration depth vs. MC and screw withdrawal force vs. MC, in the range from 8.3% to 30.0%. Equations and coefficients of determination are:

Pilodyn:	Depth=11.4121+ 0.194262*MC	R^2=15.39
SWRM:	Force=2.80006-0.0701658*MC	R^2=51.18

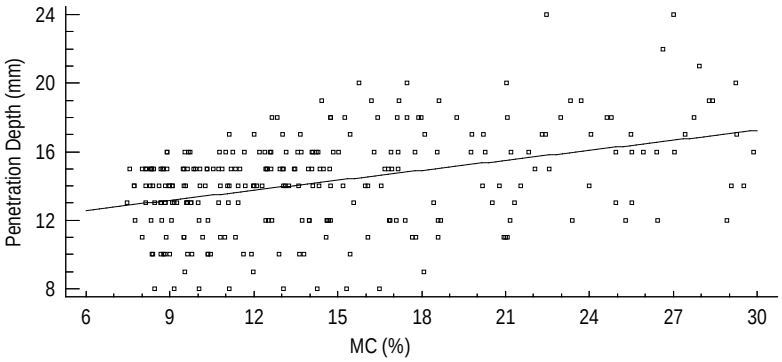

Figure 4— Linear regression: Penetration depth vs. MC.

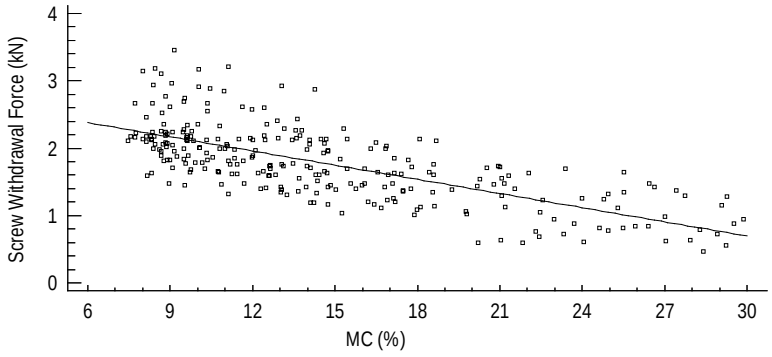

Figure 5— Linear regression: Screw withdrawal force vs. MC.

In the case of the Pilodyn 6J Forest device an increase of 0.19 mm (1.7%) was found in penetration depth for each 1% on MC increase. This is same value as was proposed by other authors (Smith and Morrell 1986) and the 1.7% increase is in the range from 1% to 2% proposed by Hoffmeyer (Hoffmeyer 1978).

In the SWRM device a decrease of 0.07 kN (2.5%) was found for each 1% MC increase. This value is inside the range 0.05 kN to 0.15 kN obtained by Calderon in laricio pine, and is within the range of 12% to 18% MC (Calderón 2012).

Conclusions

Pilodyn penetration depth and SWRM screw withdrawal force in laricio pine (*Pinus* nigra Arn. Ssp. *Salzmannii*) from Spain have a linear relationship with moisture content below 30%, although there is no statistically significant affect due to moisture content above 30%.

Penetration depth increases 0.19 mm and screw withdrawal force decreases 0.07 kN with each percentage increase in moisture content up to fiber saturation point.

These results correspond to a small number of specimens and only one species. Forthcoming studies will extend this research to cover other Spanish conifer species.

Acknowledgments

Ministerio de Economía y Competitividad. Plan NacionalI+D+i 2008-2011. Proy.: BIA 2010-18858. We would like to thank Ramón García Lombardero for his helpful work in the INIA lab, Spain.

References

Bobadilla, I.; Iñiguez, G.; Esteban, M.; Arriaga, F.; Casas, L. (2007). Density estimation by screw withdrawal resistance and probing in structural sawn coniferous timber.Proceedings of the 15th international symposium on nondestructive testing of wood.September 10-12, 2007. Duluth, MN, USA.

Calderón, L. (2012). Estudio sobre la influencia del contenido de humedad de la madera en ensayos no destructivos para *Pinus nigra* Arn., *Pinus radiata* D. Don y *Pinus sylvestris* L. [Study of wood moisture content influence on nondestructive measurements on*Pinus nigra*Arn., *Pinus radiata* D. Don and*Pinus sylvestris* L.]. PFC E.U.I.T. Forestal.UPM. Madrid. http://oa.upm.es/14396/

Cockrell, R. A. (1933). A study of the screw-holding properties of wood. Tech. Pub. 44. Bulletin of the New York State College of Forestry of Syracuse, N.Y. 27 pp.

EN 13183-1:2002. Moisture content of a piece of sawn timber. Part 1: Determination by oven dry method.

Hoffmeyer, P. (1978). The Pilodyn as a non-destructive tester of the shock resistance of wood.4th Nondestructive testing of wood symposium.Vancouver, Washington state. USA. Pp. 47-66.

McLain, T. E. (1997). Design axial withdrawal strength from wood: I. Wood screws and lag screws. Forest Products Journal. 47(5) pp. 77-84.

Smith, S.M.; Morrell, J.J. (1986).Correcting Pilodyn measurements of Douglas-Fir for different moisture levels.Forest Products Journal. Vol. 36, Nº 1.

Wood density measurement by microwave

Agnes Kinga Buza
Jozsef Bodig Non-destructive Testing Laboratory, University of West Hungary, Sopron, Hungary, agnes.kinga.buza@gmail.com

Ferenc Divos
Department of Physics and Electrotechnique, University of West Hungary, Sopron, Hungary, ferenc.divos@skk.nyme.hu

Abstract

Microwave radar is under development for evaluation of wood density. Tests were performed on air dry wood samples with the same size, thickness and moisture content (12%).
The samples were poplar (Populus, 295 kg/m^3), spruce (Picea, 371 kg/m^3), linden (Tilia, 477 kg/m^3), black walnut (Juglans nigra, 561 kg/m^3), black pine (Pinus nigra, 637 kg/m^3), ash (Fraxinus, 706 kg/m^3), and acacia (Robinia, 756 kg/m^3). All conditions were the same for them.
Each sample was placed between the microwave transmitter and receiver. The microwave signal penetrated into the samples, the amplitude and phase signal have changed due to the properties. The measured amplitude and phase data are density predictors. Linear relation could be established between the phase and density.
This is a preliminary study for a more complex density evaluation. The results are encouraging for further measures for developing a fast, nondestructive, and noncontact density measurement.

Keywords: wood density, microwave radar, phase signal

Introduction

The possibility of developing a fast, nondestructive and noncontact density measurement is important for wood industry. The long-term aim is to be able to predict the wood qualities from the trees' parameters. The measurement and results presented in this paper are the first steps of a development.
However, other researchers are also using radar/microwave techniques for their investigations of wood properties. For example there are researches with adapting GPR (ground penetration radar) technique for wood for determination of moisture (Rodriguez-Abad et al 2010) or dielectric anisotropy (Martinez-Sala et al 2013). Finding resin (Hislop et al 2009) or knots (Kaestner and Baath 2005) may also be possible by using microwave radars. Tomography is also under development (Salvade et al 2007). While the work of Schanjen and Orhan (2006), who used microwaves to measure wood grain angle, moisture content and density on hemlock and Douglas fir samples, also has to be mentioned,.
Theoretical background of the interaction of microwave signals and wood were summarized by Torgovnikov (1993). According to his work there is an exponential function between the decrease of the amplitude square of the signal and the wood density. However there also should be a change in the phase of the signal.
Both amplitude and phase were recorded during the signal traveled through the samples. The samples were made of different woods but all had the same thickness and all the other properties were the same except their density.

Methods and materials

Microwaves penetrate into wood and part of the signal is absorbed due to the interaction with material. This phenomenon was described by Torgovnikov (1993). The following equations show how the signal energy changes when microwave penetrate through material.

$$\frac{W}{W_0} = e^{-2\alpha\rho d} \quad (1)$$

where:
W_0 – initial energy reaching the surface,
W – energy of the signal after penetration,
d – sample thickness,
ρ – density,
α – attenuation coefficient.

The higher the frequency is, the higher the attenuation. The attenuation coefficient depends on material. The moisture content has influence attenuation coefficient. This relation makes possible the density determination by measuring the signal energy. The signal energy is proportional with the signal amplitude square.

$$A^2 \sim W \quad (2)$$

where
A – amplitude of the signal

The microwave velocity in material is less than the velocity in air. The higher the density of the material, the lower the signal velocity. It results phase change in signal penetrated through the material. For this reason phase change is another density predictor, independent from signal amplitude.
A Novelda impulse radar development kit was used for our measurements. The applied frequency was 4.4GHz. The sampling rate was 30 MHz while each data was the average of 25 measurements. As the impulse signal was detected a sine wave was fitted to the selected part of the curve. The amplitudes of the original and penetrated signals were calculated from the fitted function.
As the sine signal is:

$$A = A_0 \sin(\omega t + \beta) + C \quad (3)$$

where:
ω – the circular frequency
β – the phase angle
C – constant,
t – time.

From the fitted function both amplitude and phase angle were calculated, saved and investigated.
The measuring arrangement is shown in Figure 1. The emitting and receiving antennas were faced to each other, the distance between them was 7 cm. The original signal was digitalized by a high-speed AD converter. A screen shoot from the measuring program is seen in Figure 2. This figure shows the signal change while the sample was moving and crossing the antenna gap 3 times.

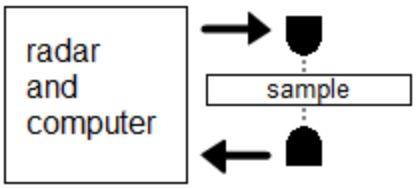

Figure 1 – The measurement setup. The microwave antennas (emitter and receiver) are faced to each other. The distance between antennas is 7 cm. The sample thickness is 2 cm.

The phase change can be greater than 360 degree - especially in case of thick samples. Handling this case, instead of phase angle we applied time delay (τ), calculated by the following expression $\tau=\beta/(f*360)$ where f is the wave frequency, β is the phase angle in degree.

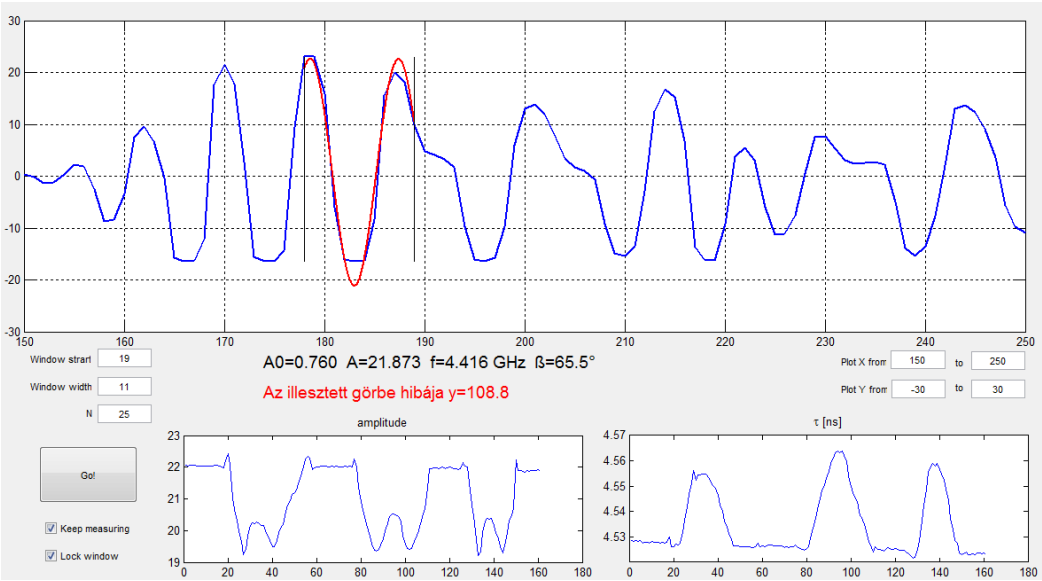

Figure 2 – A measurement as it is seen in the computer's screen. Up – the received signal and the fitted sine function. Down left – the amplitude of the fitted curve in time. Down right – the time delay (ns) in time.

Samples were poplar (Populus alba, 295 kg/m^3), spruce (Picea abies, 371 kg/m^3), linden (Tilia, 477 kg/m^3), black walnut (Juglans nigra, 561 kg/m^3), black pine (Pinus nigra, 637 kg/m^3), ash (Fraxinus, 706 kg/m^3), and acacia (Robinia, 756 kg/m^3). Both size (150 x 300 mm) and thickness (20 mm), moisture content (12%) were the same for all the samples. The samples were selected to cover wide density range.

Results and discussion

The measured signal amplitude was changing by time a bit, because the long term stability of the radar system was not perfect. For this reason we applied relative measurement. It is supported by the equation 1. The amplitude square ratio were calculated ($A_{penetrated}^2$ / $A_{original}^2$) where $A_{penetrated}$ is the measured amplitude after the signal penetrated through the sample and $A_{original}$ is the signal amplitude is the measured amplitude without sample. The expression ($A_{penetrated}^2$ / $A_{original}^2$) is identical with the signal's energy ratio (W/W_0) because equation 2. The measured amplitude ratio square is plotted versus sample density in Figure 3. We found moderate correlation.

The change in the time delay were calculated more simple ($\tau_{penetrated} - \tau_{original}$). The result is shown in Figure 4. We found high correlation between time delay and material density, indicating, that time delay is a reliable and good indicator of material density. The relative standard deviation was less than 1% for amplitude ratios and less than 5% for time delay.
In this work the material thickness and sample moisture content were constant. In case of practical application, further study of the influence of these parameters is necessary.

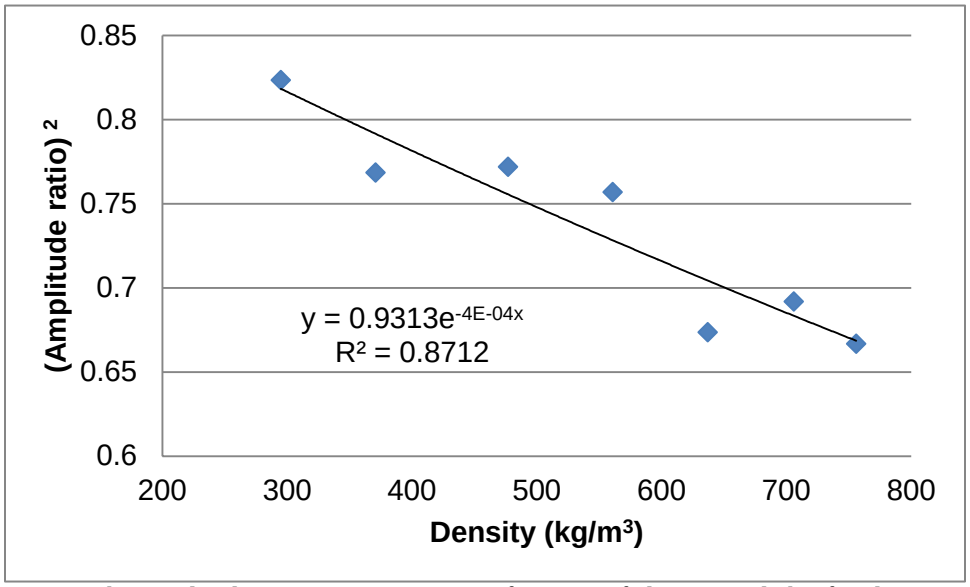

Figure 3 – The amplitude's squares ratios as a function of density and the fitted exponential function.

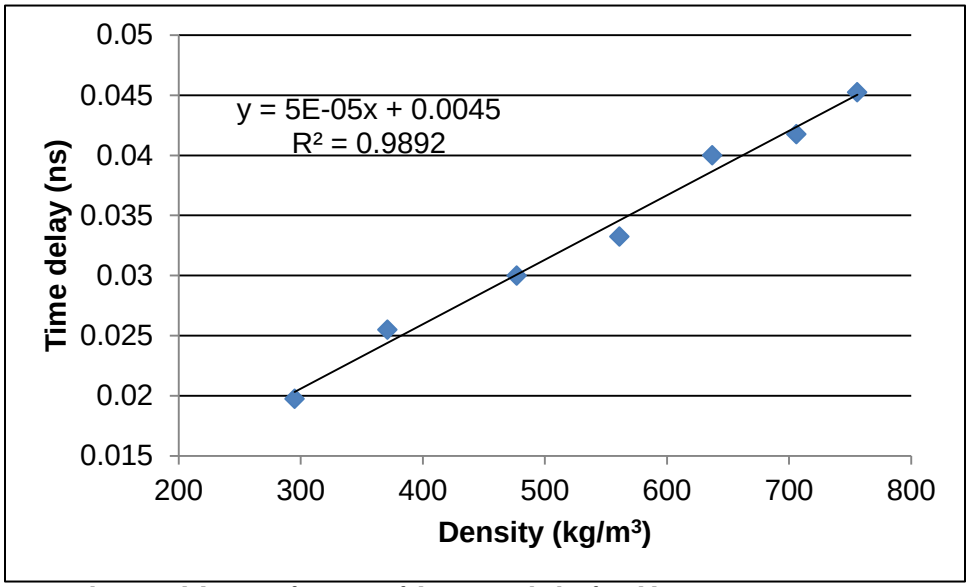

Figure 4 – The time delay as a function of density with the fitted line.

Summary and conclusion

Microwave signal interactions with air dry wood sample were tested. The sample's density covered wide range, from 295 kg/m^{3}to 756 kg/m^3. The microwave signal penetrated into the samples and traversed

through. The changes in the signal included the change in the amplitude and in the time delay caused by phase change. While all the conditions – like moisture content and sample thickness – were the same, the measured changes are related to the material density variation. Relation for the amplitude's change (R^2 = 0.871) and for the time delay change (R^2 = 0.989) are encouraging. It seems that the microwave has an opportunity to characterize wood material density. The obtained results are in good coincidence with previous measurements, Divos (2011).

Acknowledgement

This research - as a part of the Talentum Project for Science and Student Talent Fostering at WHU, TÁMOP-4. 2. 2. B - 15/1/KONV-2015-0005 - was sponsored by the EU/European Social Foundation. The financial support is gratefully acknowledged.

References

Divos F., Ther I. 2011. Wood density determination by microwave radar. Proceedings of the 17th International Nondestructive Testing and Evaluation of Wood Symposium, Sopron, Hungary, September 14-16, 2011

Hislop, G.; Hellicar, A.D.; Li, L.; Greene, K; Lewis, C.; Meder, R. 2009. Microwave radar for detection of resin defects in Pinus elliottii Engelm var elliottii. HOLZFORSCHUNG. 63(5): 571-574.

Kaestner, A.P.; Baath, L.B. 2005. Microwave polarimetry tomography of wood. Sensors Journal, IEEE. 5(2): 209-215.

Martinez-Salaa, R.; Rodríguez-Abada, I.; Diez Barrab, R.; Capuz-Lladróa R. 2013. Assessment of the dielectric anisotropy in timber using the nondestructive GPR technique. Construction and Building Materials. 38: 903-911.

Rodriguez-Abad, I.; Martinez-Sala, R.; Garcia-Garcia, F.; Capuz-Lladro, R. 2010. Non-destructive methodologies for the evaluation of moisture content in sawn timber structures: ground-penetrating radar and ultrasound techniques. Near surface geophysics. 8(6): 475-482.

Salvadè, A.; Pastorino, M.; Monleone, R.; Randazzo, A.; Bartesaghi, T.; Bozza, G. 2007. A numerical evaluation of an optimal setup for a microwave axial tomograph aimed at the inspection of wood. In Proceedings of IEEE International Workshop on Imaging Systems and Techniques, 2007. IST '07. 1-6.

Schajer, G.S.; Orhan, F.B. 2006. Measurement of wood grain angle, moisture content and density using microwaves. Holz als Roh- und Werkstoff. 64(6): 483-490.

Torgovnikov G. I.: Dielectric Properties of Wood and Wood-Based Materials (Springer Series in Wood Science); 196 S. ISBN 3-540-55394-0. Springer Verlag Berlin, Heidelberg, New York, 1993

Session 5

Evaluation of Solid Sawn Products

Characterization of the physical-mechanics properties of the Peruvian species, pino (*pinus patula*) and tornillo (*cedrelinga cateniformis*) by using non-destructives techniques.

Luis Yoza
Environmental, Physics and Meteorology Engineering Department, Universidad Nacional Agraria La Molina, Lima Peru, lyoza@lamolina.edu.pe.
Erik Baradit
Physics Department, Universidad del Bio Bio, Concepción Chile, ebaradit@ubiobio.cl
Moises Acevedo
Forestry Industry Department, Universidad Nacional Agraria La Molina, Lima Peru,macevedo@lamolina.edu.pe

Abstract

The objective of this survey was the determination of the physical-mechanical properties of two species of structural woods from the Peruvian forest: Pino (*Pinus patula*) and Tornillo (*Cedrelinga cateniformis*) by using non-destructive ultrasound methods.
For design structures, the information on the basic properties as the transverse elasticity module, module compression and shearing module are commonly used. In recent years, thanks to the progress achieved with ultrasound, acoustic non-destructive methods, the modulus of elasticity in other directions such as, E (RR); (E) (TT), G (RL), G (TR) has been able to be easily determined, allowing to improve the design of the structures.
By using the Parametric PR 5800 Ultrasound 1 MHz frequency equipment, the two above mentioned species were characterized. For that, the speeds of propagation of longitudinal and cross sectional waves were measured and then the respective elastic modules were calculated, obtaining values comparable with those obtained by traditional mechanical tests.

Keywords: Peruvian Woods, ultrasound, elastic modulus

Introduction

Knowing the physical-mechanical properties of timber plays an important role at the time of determining its use in both the construction and furniture industry. In this sense, it is increasingly necessary to improve the knowledge of the physical-mechanical properties of our forest species; on one hand to optimize the use of the resource and for the other hand, to make the national timber industry more competitive. For that, we will use non-destructive acoustic techniques and traditional mechanical tests to characterize the species Pino, *Pinus patula* and Tornillo, *Cedrelinga cateniformis*. In this sense, Pino is a species that is being introduced in the market thus; there is a growing interest for its exploitation. The other timber is Tornillo, this species is widely used in the design of structures, which serve as comparative reference in this study to evaluate the use of Pino as structural timber.

Pinus patula, Pino

This species grows in areas like forest humid or forest very humid montano low. In its native range, it is part of the cloud forests related to the following species: *Pinus ayacahuite, Michoacan Pinus*

lumholtzii and Pinus leiophylla. In Colombia and other countries where the species have been introduced, an excellent development have been presented, becoming a useful timber and reforestation programs in highlands species. In Peru, they are located in the Department of Cajamarca. It is a tree of 10 to 25m height, scaly and red bark, especially in the upper trunk of the tree. The stem is generally straight, commercial logs are between 10 and 20 m length and diameter from 25 to 50cm. The characteristics of the wood are: In dry-air conditions, the sapwood is yellowish white and the heartwood is yellowish brown to dark brown. It has undifferentiated growth rings, straight grain, fine texture and veining in overlapping arcs and parallel stripes.

At macro and microscopic level, the parenchyma is absent and the linear tracheid is visible under a 10x magnifier. They are long and wide cells with presence of aerolar pits inside. No marked difference between spring and summer tracheid. The length varies from 1150 to 4500µm and from 30 to 60µm wide. The pits in the crossing field are pinus type. The radius is uni-seriated and spindle, the latter with presence of resiniferous channel whose height is one to fourteen cells and of 141 to 471µm. There is presence of two types of resiniferous channel, longitudinal spread between the longitudinal and radial tracheid, included within the spindle radios. Figure 1 illustrates the cross-section and tangential sections.

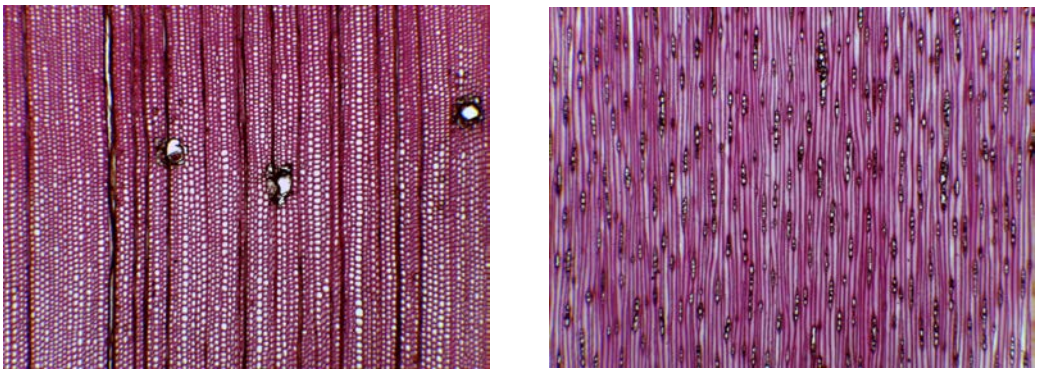

Figure 1-Microscopic views (40X) in cross section and longitudinal section of *Pinus patula*(Laboratory of Wood Anatomy UNALM)

***Cedrelinga cateniformis,* Tornillo**

This species is distributed in the Amazon region of Bolivia, Brazil, Colombia, Ecuador and Peru, at altitudes up 700 mosl. In Peru, they can be found in Cuzco, Huanuco, Loreto, Madre de Dios, San Martin and Ucayali.
It is a 20 to 40m total height tree, with a commercial height from 15 to 30m, cylindrical shaft and a diameter of 0.15 to 1.2 m. Its scientific name is *Cedrelinga cateniformis*, and its characteristics are:
In a dry open-air condition, the sapwood is light pink and dark pink heartwood, undifferentiated growth rings, straight to interlocked grain, coarse texture and absence of grain patterns.
At macro and microscopic level, the pores are visible at a plain eye, and they are solitary oval. They have diffuse porosity, mostly solitary with an oval shape and few radial 2-4 pore manifold. The average tangential diameter is 280 to 320µm; with 1 to 5 pores / mm2. The average length of the vascular elements ranges from 405 to 445µm, with simple perforation plate and alternate intervascular round-shape pits including opening. The parenchyma is visible under a 10x magnifier, vasicentric paratracheal; with presence of diffuse parenchymal apotracheal in longitudinal unstratified section. There is presence of gummy inclusions. The radius is visible under a 10x magnifier; it is fine and with few contrasted radial section. In tangential section, they are uniseriated, with a height between 240 and 345µm. In homocellular, radial section consists of procumbent cells. They have a 5-10 radios / mm; unstratified. They have radio vascular pits which are similar to intervascular pits. The fibers are libriform with simple unstratified pits; with a length between 1300 and 1450µm, total diameter of 15µm and cell wall thickness of 1,4µm. In Fig. 2 the cross, sectional and tangential cuts are illustrated.

This wood is used in spreaders , props , formwork, trusses , girders, beams , doors, windows , partitions, tongued , furniture in general , pallets and car body .

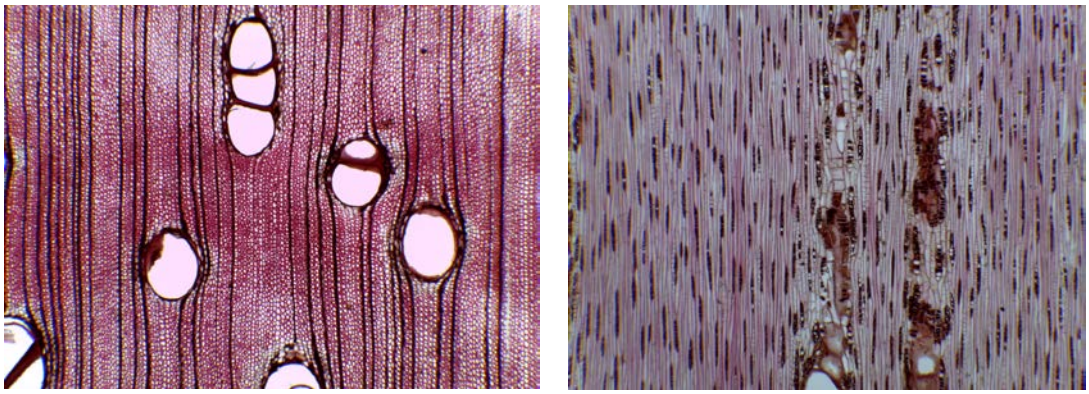

Figure 2-Microscopic views (40X) in cross and longitudinal section of Cedrelinga *cateniformis.* *(La*boratory of Wood Anatomy UNALM)

Non-destructive evaluation.

Typically, the information on the physical-mechanical properties comes out as a result of the implementation of several traditional measurements, where a testing machine plays the leading role. However, in recent years different non-destructive techniques have been implemented for materials evaluation and classification processes. Among these techniques, one of the most used is based on the propagation of mechanical waves of different frequency, mainly in the ultrasonic band. Whose advantage is to use them for example, to determine the elastic constants of different materials such as (Baradit 2012, Kranitz 2012) and in concrete and mortar (Rodriguez 2003, Lawson et al. 2011).
In particular the Young's modulus of elasticity (E) are obtained for the three main directions of the shaft by means of the following equation

$$E_{ii} = \rho v^2 \tag{1}$$

Where i = 1, 2, 3 indicates each of the major axes and V is the speed of propagation of longitudinal ultrasonic pulse (Bucur 2006). G shear modules are obtained through a similar expression

$$G_{ij} = \rho v^2 \tag{2}$$

Where $i \neq j$, V is the pulse velocity propagation with transverse polarization.

Materials and Methods

Samples.

Samples were selected from five species of Pino and Tornillo trees. Specimens for mechanical testing were prepared according to ASTM D143 (2008). The standard static bending tests were performed with a secondary method for dimensions of 25x25x410mm, with a total of 6 samples for Pino and 8 for Tornillo. For Parallel compression test, 50X50X200mm- dimensions samples were made with a total of 6 samples of Pino and 8 for Tornillo. In addition, finally shearing test was performed with 9 samples and 16 samples respectively.

Samples for ultrasound tests were taken in conjunction with the mechanical testing , preparing cubes of 30x30x30 mm, oriented in the LRT direction of the 5 trees selected per species, obtaining 19 samples for Pino and 18 for Tornillo respectively .

Equipment

The experimental setup is shown in the block diagram of Figure 3 and consists of an ultrasound generator PR Panametric 5800 brand and brand Tektronix oscilloscope. The used transducers were of 1 MHz frequency generation for both longitudinal and transverse waves polarization.

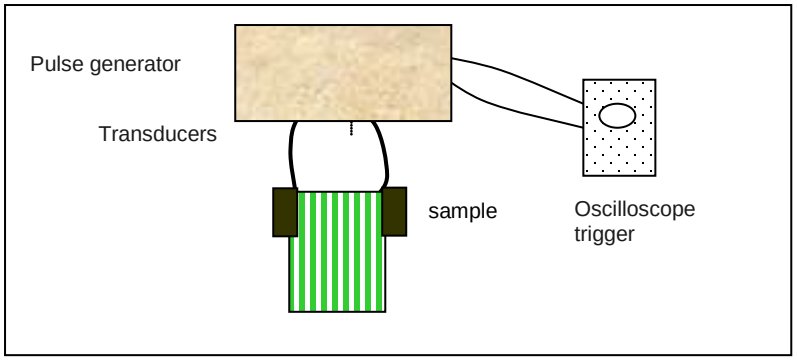

Figure 3-Layout of measuring equipment

Results and Discussion

The results of the speeds in the different directions are shown in Tables 1 and 2. The behavior is very similar rates in both species fulfilling the typical relationship V (LL) > V (RR) > V (TT). Other typical relations are linked to the symmetry of the shear speed V (LR) = V (RL) , V (LT) = V (TL) and V (RT) = V (TR) . These equalities as a result of experimental measurements are obviously approximate (Table 1 and 2).
We can point to the case of the Tornillo that the coefficients of variation for VTT, VTL and VLT speeds are significantly higher compared with Pino, possibly, because they were extracted from natural forest.

Table 1: Longitudinal and shear wave velocities for P*inus patula.*

Velocity(m/s)	$\mathbf{V_{LL}}$	$\mathbf{V_{RR}}$	$\mathbf{V_{TT}}$	$\mathbf{V_{RL}}$	$\mathbf{V_{TL}}$	$\mathbf{V_{TR}}$	$\mathbf{V_{LR}}$	$\mathbf{V_{LT}}$	$\mathbf{V_{RT}}$
Mean	4578	2022	1257	1523	1335	541	1603	1341	537
DS.	231	120	27	82	113	47	125	86	35
CV.%	5.0	5.9	2.2	5.4	8.4	8.7	7.8	6.4	6.5

Table 2: Longitudinal and shear sound velocities for Cedrelinga *cateniformis*

Velocity (m/s)	V_{LL}	V_{RR}	V_{TT}	V_{RL}	V_{TL}	V_{TR}	V_{LR}	V_{LT}	V_{RT}
Mean	4495	1860	1231	1411	1204	676	1330	1205	696
DS.	247	58	156	75	160	53,0	71	137	40
CV. %	5.5	3.1	12.7	5.3	13.2	7.8	5.4	11.3	5.7

The results of longitudinal speeds polarization exhibit elastic anisotropy in relation to the three major axes is similarly for both species. For Pino 1: 2.3: 3.6 whereas for the Tornillo 1 : 2.4 : 3.6 . Such anisotropy values are slightly higher than for Chilean softwoods (Softwoods) but lower than for hardwoods, (Baradit 2012).
In Tables 3 and 4, the values of the elastic modulus both Pino and Tornillo are shown. The Young's modulus are very similar for both species and in the radial direction only a small difference is observed, meanwhile, the shear modules for the difference between two species is most significant.

Table 3: Modulus of elasticity and shear modulus for *Pinus patula*

	Density (kg/m^3)	E_{LL} **(MPa)**	E_{RR} **(MPa)**	E_{TT} **(MPa)**	G_{LR} **(MPa)**	G_{TL} **(MPa)**	G_{TR} **(MPa)**
mean	508	10780	2077	805	1240	908	153
DS.	55.4	2087	98.8	10.5	140	85.0	34.6
CV. %	10.9	19.4	4.8	1.3	11.3	9.4	22.6

Table 4: Modulus of elasticity and shear modulus for *Cedrelinga cateniformis.*

	Density (Kg/m^3)	E_{LL} **(MPa)**	E_{RR} **(MPa)**	E_{TT} **(MPa)**	G_{LR} **(MPa)**	G_{LT} **(MPa)**	G_{RT} (MPa)
mean	528	10702	1831	814	997	777	251
DS.	28.9	1321	188	217	118	150	39.2
CV. %	5.3	12.3	10.3	26.6	11.9	19.3	15.6

Values of mechanical properties for both species are shown in Tables 5 and 6. pointing out the test results in static bending were: PL is the proportional limit stress ; MOR is the modulus of rupture; MOE is the modulus of elasticity and PL_L the proportional limit longitudinal stress; MORL is the longitudinal modulus of rupture; MOE_L is the modulus of longitudinal elasticity and finally the shear strength longitudinal modulus is the $SHEAR_L$.

Table 5: Mechanical Properties of the Pinus *patula.*

	Static Bending, *M (12%)* **(MPa)**			**Compression,** *M (16%)* **(MPa)**			**Shear,** *M (14%)* **(MPa)**
	Pl	**MOR**	**MOE**	**PL_L**	**MOR_L**	**MOE_L**	**$SHEAR_L$**
mean	72	110	8012	19	25	8453	10
SD.	25.5	33.7	1999	2.7	3.2	1859	2.3
CV. %	35.6	30.8	24.9	14.2	12.7	22.0	22.8

Table 6: Mechanical Properties of *Cedrelinga cateniformis*

	Static Bending, *M (12%)* **(MPa)**			**Compression,** *M (17%)* **(MPa)**			**Shear, *M*** *(12%)* **(MPa)**
	PL	**MOR**	**MOE**	**PL_L**	**MOR_L**	**MOE_L**	**$SHEAR_L$**
mean	35	58	8268	22	30	10404	10
SD.	6.2	9.45	1198	1.9	2.5	1455	1.2
CV. %	17.5	16.2	14.5	8.7	8.2	14.0	11.0

It is observed that for bending tests the modules of elasticity are similar for both species , being for the Tornillo highest in only about 256 MPa , while its modulus of rupture is almost half that for Pino. In parallel compression modulus of elasticity for the Tornillo was about 1951 MPa higher than for Pino, while breaking modules are similar in both species.

Conclusions.

The behavior of the velocities is very similar in both species fulfilling the typical ratio V (LL)> V (RR)> V (TT) and fulfilling relationships symmetry of the cutting speed V (LR) = V (RL) V (LT) = V (TL) and V (RT) = V (TR). We note that Tornillo coefficients of variation for VTT, VTL and VLT speeds are significantly higher compared with Pino, possibly because they were extracted from natural forest. Showing speeds polarized longitudinally elastic anisotropy of 1: 2.3: 3.6 and 1: 2.4: 3.6. for Pino and Tornillo respectively. The Young's modulus of elasticity are very similar for both species, meanwhile, shear modules for the difference is more significant.

Mechanical bending tests in the moduli of elasticity are similar in both species, being greater for the Tornillo in 256 MPa, while the modulus of rupture for the Tornillo is almost half that for Pino. In parallel compression, modulus of elasticity for the Tornillo was greater 1951 MPa, while shear modules are similar in both species.
In future studies measuring the Poisson coefficients evaluation for both species and samples of Tornillo belonging to plantations are recommended.

References

American Standard Test Methods, 2008. Standard Test Methods D 1432008 for small clear specimens of timber.

Baradit, E. and Niemz P. 2012 Some Elastic Constants of the Chilean Wood Species: tepa, olivillo, laurel, lenga, alerce and manio using ultrasound techniques. Wood Research 57(3):497-504.

Baradit, E.; et al 2012 Stifness Moduli of various extraneous species determined with ultrasound. Wood Research 57(1):173-178.

Bucur, V. 2006 Acoustic of Wood, Springer. Berlin.

Kranitz.K et al. 2012. Untersuchungen zu Eingenschaften von Mooreiche. Holztechnologie 53(1):11-17.

Lawson I. et al. 2011. Non-Destructive evaluation of concrete using ultrasound pulse velocity. Research Journal of Applied Sciences, Engineering and Technology 3(6):499-504.

Rodríguez G.and Pazini E. 2003. Módulo de elasticidad estático del hormigón determinado por medio de pruebas de ultrasonido. Materiales de Construcción, 53 (271-272): 47-55.

Rosell J. and Cantalapiedra I. 2011. Método simple para determinar el módulo de Young dinámico a partir de una excitación por impacto aplicado a morteros de cal y cemento. Materiales de Construcción, 61 (301): 39-48.

Laser based optical nondestructive method for evaluation of the pine timber strength

László Szalai
Insitute of Informatics and Economics, The Simonyi Karoly Faculty of Engineering, Wood Sciences and Applied Arts, University of West Hungary, Sopron, Hungary, szalai@inf.nyme.hu

Zoltán Pödör PhD
Insitute of Informatics and Economics, The Simonyi Karoly Faculty of Engineering, Wood Sciences and Applied Arts, University of West Hungary, Sopron, Hungary, podor@inf.nyme.hu

Abstract

Nowadays the fast and reliable strength classification of the timber becomes more important. The traditional visual methods can not provide sufficient accuracy and these are dependent on human factors, the destructive processes are slow and can not be used on every sample. We developed a complete technology, which is capable of determining the bending strength of spruce timber by nondestructive way. The He-Ne laser-based tool is able to scan the surface of the timber using a camera while feeding and transmit the data to the computer. Laser spots are projected to the timber surface. The computer software determines the knot locations, decays and grain anomalies based on the change of the laser spots. The final strength of the timber is calculated by analyzing the sets of the numerical vectors by various statistical method. The whole method is real time.
The big advantage of this method is that the results do not depend on color changes on the surface. The color change deceives the color-based optical systems in most cases. The analysis on the upper and bottom surface results more accurate 3D representation of the knot size and position inside the timber.

Introduction

Several standards exist in Europe to qualify timber strength. These standards (EN 408, EN 338) are coming to the focus of production companies, because without the use of these standards it is difficult to break into the European market. In many cases the strength classification of lumber is still through the conventional human visual method, which means that a worker visually determines the size of the defects contained in the timber. This latter method has disadvantages of slowness and the human factor. A not too old approach is the nondestructive testing of wood. Its biggest advantage is that during the process the timber is not broken. In fact, the wood fiber orientation and grain orientation anomalies heavily affect the strength (Tsoumins, 1991). A visual nondestructive test has been used in our previous research (Szalai, 2013). This earlier research focused on the timber surface profile based on the colors and classified it according to its estimated strength. In case of plain cut surface it also produced good result but when there were discontinuities or discoloration on the surface, it gave bad results. To eliminate this, the timber surface was projected by laser points/spots to determine the correct grain orientation. After analyzing the scattered laser spots the new profile was created. This result was more accurate than the previous method. Several research had already been with the laser inspection method (Simonaho et al., 2004) (Autologous, 2015) (Nieminen et al., 2012) and had been used in laser line technology (Åstrand, 2014). However, our method is able to estimate the main parameters necessary for the strength classification in real time and with fast speed.

Materials and methods

During our research spruce (Picea abies) timber (10 cm x 5 cm x 200 cm) was used as raw material, which was cut by traditional circular saw technology and then planed both sides. The moisture content was 18%. The timber was relatively straight at first sight, its twist and bow were less than 5 percent, so it was suitable for feeding with a winch. Our laboratory made system simulated the feeding machine of sawmill. The system's basic setup is shown in Figure 1.

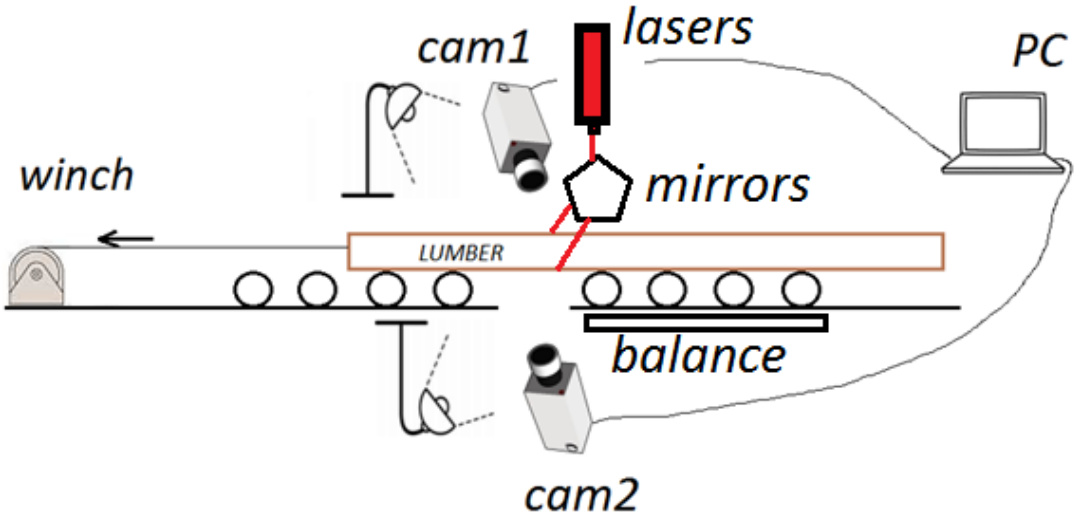

Figure 1 – The setup of the laser based lumber surface analyzer

The timber moves on a feeding roller table in longitudinal direction with the help of a winch. It pulls with a constant speed. It is a built-in balance which measures the weight of the timber and the software is able to calculate the density with the help of its dimensions. The surface of the timber is illuminated from above and below with a homogeneous light and also projected by red color He-Ne laser light. The laser light is divided by a semipermeable mirror system. The production and the assembly of the mirrors and the measurement of the scattering intensity were our task. It can reduce the system cost of raw materials. Similar method were used for the inspection of the timber (Jolma and Makynen, 2008). The wavelength of the laser was 633 nm, the strength was 2 mW. It had very high spectral purity. The laser dots were projected in two rows on the surface close to each other. The He-Ne laser plots normally a circle with the diameter 6 mm. The light scattering pattern image was a quasi-ellipse caused by the tracheid effect (Hu Cs., et al., 2004) (Faria de Oliveira et al., 2008). It can be seen in Figure 2.

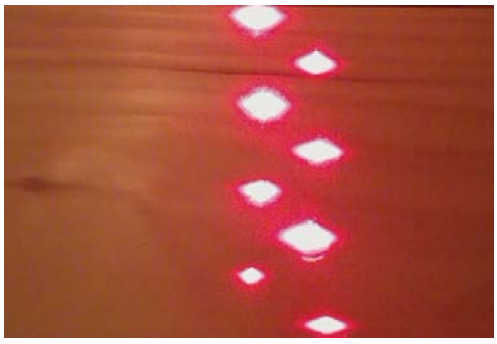

Figure 2 – Scattered laser dots on the surface

Two cameras scan the sawn surfaces above and below. The images are transmitted from the cameras to the computer that analyzes it. The cameras are good quality webcams that can be easily purchased in commercial trade. Their specifications include HD resolution and 30 frame per second capturing speed. The exact resolution was 960x720 pixel with 2700 Kbps bitrate. The capturing was made by a four-core computer. Of course, this is a laboratory hardware configuration. In industrial environment it is more reasonable to use professional tools for the analysis.

Strength classification and rating

According to the EN408, we used destructive testing to determine the maximum breaking force (f_{max}), the longitudinal modulus of elasticity (E_{mg}), the bending strength (f_m) and the density (ρ). The last three parameters classified the timber according to the EN338 standard. The lowest value gave the final strength class of the timber. We found that the density graded 67% of the cases, however 23% of the timber can be overclassified and 10% can be underclassified due to the modulus of elasticity. The bending strength classified only 0.2% of cases. The data showed that 33% of the cases was necessary to estimate both strength parameters because larger amount of timber represented significant financial value.

Processing in real time

Only pine wood material was tested by the system. Its grain orientation met the requirements most closely. 70% of the tested timber was cut radially, and 30% was cut tangentially. All pieces of timber had conspicuous grain orientation. Important defect included mainly the knot, since it obviously affected the grain orientation. In case of the intact timber we could see nearly parallel lines on the radial surface. In the case of the knotted material the grain orientation was no longer parallel. As we mentioned, two cameras scanned the both sides of the timber being fed, sent the video stream that the computer subsequently analyzed.

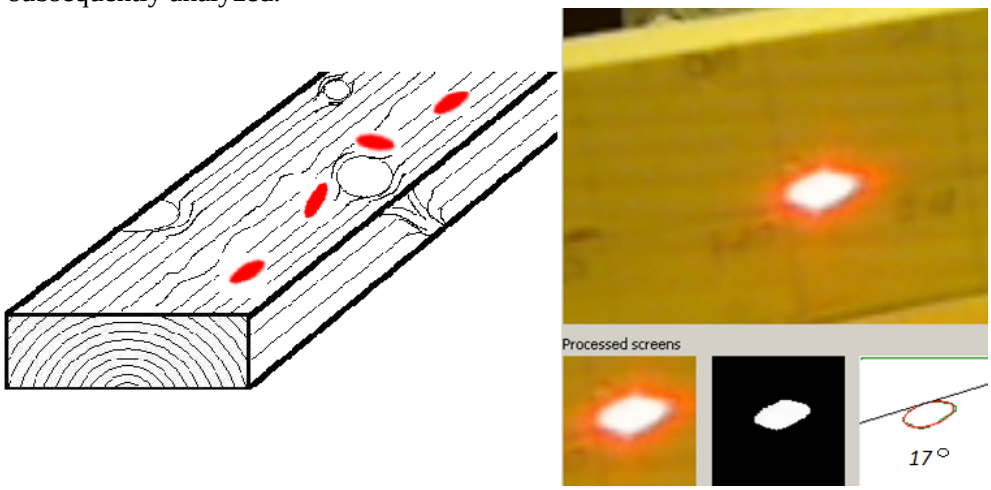

Figure 3 – The scattered laser dot and the „angle of ellipse”

Figure 3. shows that the collection of data is based on the change of the projected ellipse. The angle of the scattered ellipse’s major axis refers to the local grain orientation of the timber compared to the longitudinal fiber direction. Moreover we consider the ratio (r) of the ellipse major axis (Eb) and minor axis (Es) as well.

$$r = \frac{Eb}{Es} * 10 \quad (1)$$

If we determine this for all laser dots shown on Figure 2. we get a comprehensive database from the whole timber with good resolution. The processing software filters the colors of the scattered image to specify the shape of the ellipse then fits an ellipse and gives the angle and the length of the major axis.

Due to the 15 fps sampling speed, large number of measurement points have been collected on both sides, 16 lines. The processing and the analysis of this database are the key of the determination of the timber rating parameters.

Data processing and the estimation of parameters

As mentioned above, the strength classification depends on three parameters according to the EN338 standard. The estimation of these three characteristic values rates the timber to a strength class. The destiny is determined by a balance developed by us. The software based processing of the database estimates the other two parameters.

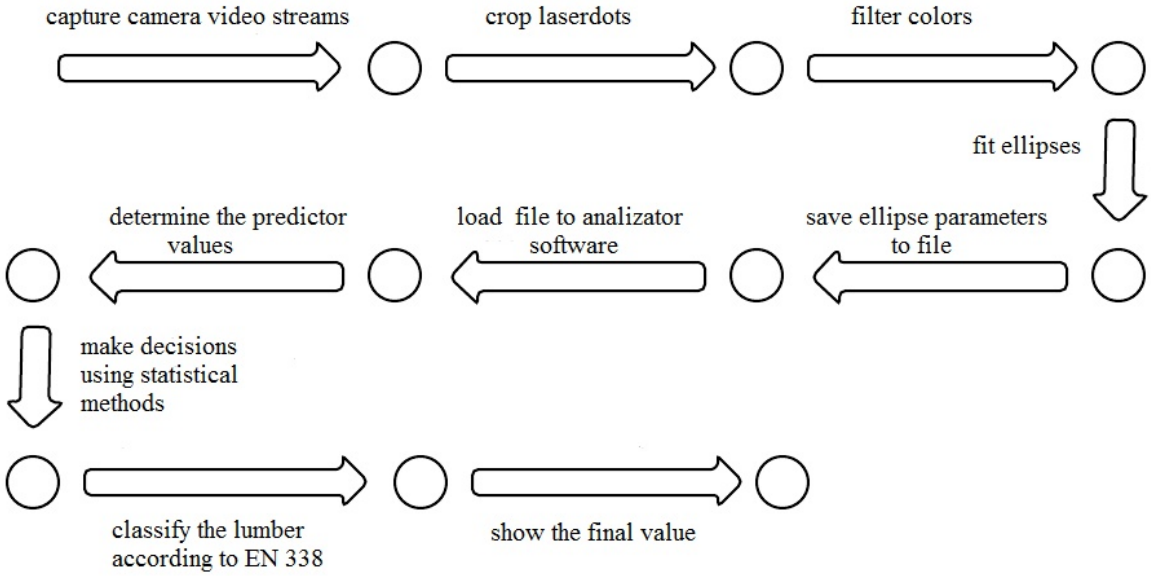

Figure 4 - Strength classification process

The Figure 4. shows the actual classification process. Two softwares perform the real data processing. The first software performs the data serialization of the scattered image then the second one processes and analyses the collected data. We developed a software that can handle the illegal data occurred by measurement errors.

The first step of processing the data sets has been prepared to the analysis. On the one hand the obviously wrong values (values no. 99999) have been converted to missing values (NA), on the other hand smoothing method has been used on raw data. Due to the data structure the smoothing method has been implemented by n-moving average, where n=5.

The mentioned ratio (r) value indicates the probability of the wrong data gathered by the measurement. We often found for ratio values 10 and 11 that the further values are not real, because we defined a ratio threshold to eliminate the data rows, which have lower ratio values than this threshold in the process.

A preliminary analysis was made in which we investigated the four parameters (ellipse width, height, ratio and angle) as dependent variables can be connect to the independent parameters (E_{mg}, f_m and ρ). We produced the average value of each timber that was typical for the given sample. Thus each timber had 16 average parameters. These 16 parameters as independent variables were compared with the four mentioned parameters as dependent parameters. To do this, stepwise linear regression was used (Montgomery et al., 2012). Though the models showed statistically significant relationships,

nevertheless it is hard to physically explain them. Noticeable that the parameter numbers were taken into the models were too many compared to database elements.
We assumed that due to the anomalies of the timbers better parameters can be defined regarding the modeling of the examined attributes.
From four parameters the ellipse's angle was chosen detecting the timber anomalies. Figure 5. shows the profile which was prepared for each sample. On this profile we can see the "grain vectors" calculated from the measured angles (the angle values were smoothing by 5-moving average method). Considering the data density of measurement method the data was displayed by three average values.

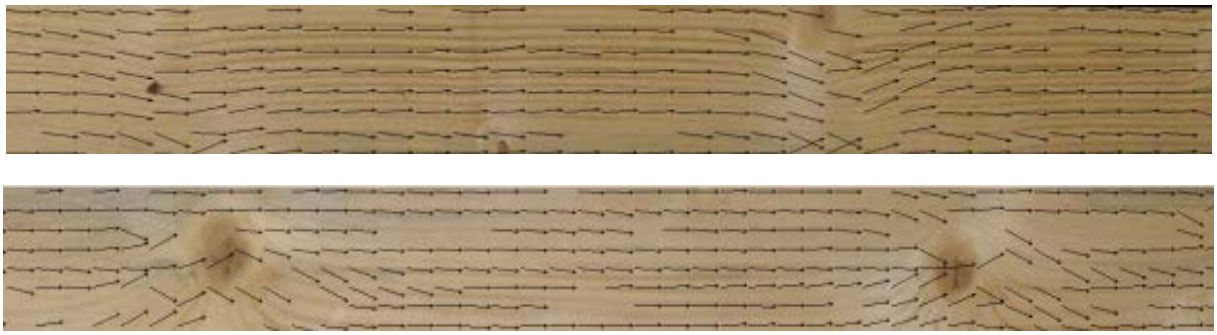

Figure 5 – Calculated „grain vectors" on the timber's surface

Visually reviewing the profiles we found that angle values showed the original grain orientation and the anomalies quite well.
Where the angle value differed from the mean value, and the difference was larger than the threshold, in this case there was an anomaly. The threshold value was interpreted by the method based on outlier data (Ramachandran and Tsokos, 2009). We calculated the mean and the standard deviation for each timber's each dataset of angle values. After this, we determined the threshold value. It was defined by the sum of mean value and the adequate constant-time of standard deviation. Where the ratio value was at least, and the angle value exceeded the above threshold in absolute value, we determined them like anomaly. With the help of these relevant angle values we were able to detect the anomalies and determined their specific attributes, like horizontal and vertical position, length, width and 3D position (knot goes through the timber or not).

Table 1 - Lumber # 1 detected anomalies

Lumber 1 / a					
	1	2	3	4	5
horizontal position	56	114	178	231	280
horizontal position (%)	17%	36%	55%	72%	89%
vertical position	middle	side	side	middle	side
length	18	14	6	5	12
height	7	5	2	3	4
3D	yes	yes	yes	no	no

It is necessary to take account, that one relevant unique angle value does not refer to anomaly, but measurement error or wrong anomaly detection can be based on the parametrization of the process. To handle this, the minimal angle distance can be defined by the user which refers to anomaly.
The free R software was used for the detection and analysis processes.

Results

The detected anomalies were displayed as rectangles. The size and location of every rectangle was based on the calculated anomaly parameters (Figure 6). Checking visually the results of the detection software was done and we determined that the accuracy of the anomaly detection was sufficient.

Figure 6 – Statistically calculated knots

The detection process produced parameters. These parameters were involved in the final process. The goal of this process was to estimate the longitudinal modulus of elasticity and the bending strength as dependent parameters. To do this, a Naive-Bayes classifier was used (Han and Camber, 2006) which is often used in data mining. Based on the analysis we finished, it is shown, this method is able to estimate the dependent parameters over than 80% accuracy. Important to mention, the analyzer process – which uses the parameters generated by the detection software – has been under development yet.

Conclusion

The complex procedure and system we have evaluated to measure the grain orientation and anomalies in wood appeared to provide objective information at a low cost. The reliability of methods and the classification can be improved, but it seems it is very promising solution. Handling the timber in 3D – real time analysis from above and below – unambiguously improves the estimation of the longitudinal modulus of elasticity, which is very relevant to classification.

References

Tsoumis G. 1991 Science and technology of wood: structure, properties, utilization. New York: Chapman & Hall.

Szalai. L. 2013 Camera based real time wood evaluation software in application. 18th International Nondestructive Testing and Evaluation of Wood Symposium, Madison, USA.

Simonaho, S.; Palviainen, J., Tolonen, Y.; Silvennoine, R., 2004 Determination of wood grain direction from laser light scattering pattern, Optics and Lasers in Engineering (41) : 95–103

Åstrand, E. 2014 Building a High Performance Camera for Wood Inspection Using the VITA1300 Image Sensor and the XEM5010 FPGA Integration Module, Vanserum, Sweden, https://www.opalkelly.com/customers/vanserum/ , [date: 2015.06.17]

Autolog Sawmill Automation, 2015, New tracheid sensor double laser technology, http://www.autolog.com/, [date: 2015.06.17]

Nieminen, S.; Heikkinen, J.; Lassila, E.; Alahautala, T, 2012 Application note – Industrial monitoring solutions - Process industry - Transillumination of wood, Cavitar Ltd. Finland

Jolma, I. P.; Makynen, A. J., 2008 The detection of knots in wood materials using the tracheid effect, Proceedings of SPIE – Vol 7022

Hu, Cs.; Tanaka, C.; Ohtani, T., 2004 On-line determination of the grain angle using ellipse analysis of the laser light scattering pattern image, J Wood Sci (50) 321–326

Oliveira Faria, R.; Alves Braga Jr.a,_R.; Elizeu da Rocha Neto, A.; Trindade, N.; Akira Mori, F.; Horgan, G.W., 2008 Reliability of wood grain orientation measurements using laser illumination, Biosystems engineering (100) 479 –

Ramachandran, K. M., Tsokos, C. P. (2009): Mathematical Statistics with Applications. Elsevier Academic Press, pp. 803.

Montgomery, D. C., Peck, A. E., Vining, G. G. (2012): Introduction to linear regression analysis (fifth edition). Published by John Wiley & Sons, pp. 672.

Han, J., Camber, M. (2006): Data Mining, Concepts and Techniques - second edition. Morgan Kaufmann Publishers, 2006, pp. 772.

EN 338, 2009. Structural timber. Stgrength classes.

EN 408, 2003. Timber structures. Structural and glued laminated timber. Determination of some physical and mechanical properties.

Assessing Southern Pine 2 x 4 Lumber Quality Using a Portable Device

Frederico J. N. França
fn90@msstate.edu

R. Daniel Seale
rds9@msstate.edu

Tâmara S. F. Amorim França
tsf97@msstate.edu

Rubin Shmulsky
rs26@msstate.edu

Department of Sustainable Bioproducts - Mississippi State University, Starkville, MS, USA

Abstract

The objective of this research was to demonstrate the use of smartphone technology in transverse vibration non-destructive testing techniques. A portable device with an adequate oscilloscope App was used to collect data from 30 eight-foot long samples of southern pine No. 2 2x4 lumber. The samples were subjected to transverse vibration and the frequencies were collected by a portable device, transverse vibration equipment, and a longitudinal stress wave velocity tool. A strong linear correlation was obtained between the transverse vibration frequencies collected with the smartphone accelerometer and a transverse vibration equipment (r^2=0.996; $p<0.0001$). The correlation between dynamic modulus of elasticity (MOE) calculated based on smartphone transverse vibration frequency and based on longitudinal stress wave timer was also high (r^2=0.935; $p<0.0001$). The results indicate a potential use of portable devices to determine the MOE of structural pieces of lumber and to expand the access of non-destructive techniques.

Keywords: non-destructive tests, modulus of elasticity, wood classification

Introduction

Wood is one of the main materials used in construction by presenting advantages when compared to materials, such as steel and concrete. It shows considerable mechanical strength being a light weight material that is easy to fasten, cut, and shape with relatively low cost tool compared to other materials. In addition, it is a sustainable, renewable and biodegradable bio-product; however, it needs to be classified for better use.

Ross et al. (1998) defines non-destructive assessment as the way to evaluate physical and mechanical properties of a piece of material without changing its characteristics. Non-destructive techniques, such as ultrasound, transverse vibration, longitudinal vibration, x-ray, and stress waves have been investigated, and have been adopted by industry because of their fast responses and high correlations (Brashaw et al., 2009).

According to Amishev and Murphy (2008), the modulus of elasticity (MOE) is one of the most important mechanical properties of wood since it is the indicator of load resistance most frequently used. The dynamic methods to characterize wood and other materials calculate the elastic modulus through the natural frequency of the specimen vibration and its geometric parameters. These methods have the advantage of being fast, using small samples, and being repeatable (Cossolino and Pereira, 2010).

As a building material, wood has many features which directly influence the quality of the chosen wood; therefore, a full knowledge of its structural potential is a necessity for its correct use in construction. Like other materials used in construction, the physical and mechanical properties of wood should be tested and then classified for structural use (Segundinho et al., 2012).

Since the 1960s, researchers from the forest products community have been developing non-destructive testing (NDT) tools for evaluating the quality of lumber products, especially with regard to mechanical grading (Divós and Tanaka, 2005). In the 1990's, Ross et al. (1991) developed personal computer software for making transverse vibration NDT tools available to a broader range of wood products manufacturers and users.

Predicting the MOE of lumber with longitudinal stress wave has received considerable research efforts in recent years in terms of lumber grading or pre-sorting (Wang, 2013). The assessment of the quality of raw wood materials has become a crucial issue in the operational value chain as forestry and the wood processing industry are increasingly under economic pressure to maximize its extracted value (Brashaw et al., 2009). New sensor technologies are improving the ability to determine with greater precision (Murphy, 2009).

Technological advancements in the communications industry in recent years transformed large low tech cell phones in small, lightweight and dynamic devices. These changes, added up to the advent of smartphones (cell phones that access to the Internet, download and run applications) involved in a new relationship between user and devices. Furthermore, these devices also offer an accelerometer, which is an electromechanical device that measures acceleration forces.

There are different types of accelerometers developed for wood evaluation, with the majority based on piezoelectric crystals. The sensors used in this equipment contain microscopic crystal structures that get stressed by accelerative forces, which cause a voltage to be generated (piezoelectric effect) (Ross et al., 2012). Micro electromechanical systems (MEMs) accelerometers can be smaller and could increase applicability in the wood/wood products evaluation field.

The aim of this study is to evaluate the reliability of portable devices and MEMs accelerometers in lumber quality evaluation as a quick way to determine the modulus of elasticity by comparing-longitudinal and transverse vibration techniques.

Materials and Methods

The specimens used in this study were kiln dried Southern pine No. 2 2x4 lumber. 30 eight-foot long boards (0.15 m x 0.35 m x 2.438 m) were conditioned to 12% moisture content before start the experimental procedure.

First, the lumber was vibrated using a transverse vibration technique. Boards were simply supported flatwise as a beam spanning the entire length of the board supported on one end by a knife-edge support and at the opposite end by a point support.

Each 2x4 was nondestructively examined using transverse vibration equipment. It can determine the MOE based on resonant vibration frequency and density using a Metriguard Model 340 Transverse Vibration E-Computer. The specimen was then set into vibration by gently tapping it near the center of the span. A load cell measured the frequency of vibration and board weight, and the E-Computer reached the transverse vibration frequency for each piece and calculated the dynamic MOE.

Using the same setup, vibration data was also collected using a portable device. The accelerometer (smartphone) was located in the middle of the lumber on the upside surface. Transversal vibration was initiated by impacting the middle part of the lumber. The signal collected by the smartphone app was a series of pulses with gradually decreasing (decaying) amplitude (Figure 1).

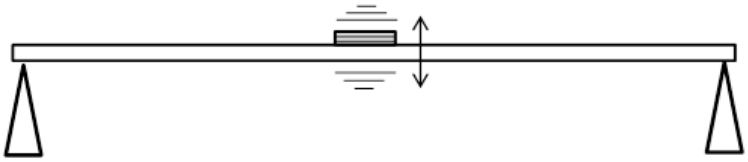

Figure 1 – Setup for frequency measurement using the portable device.

The application used worked as a vibration spectrum analyzer. It was written to emulate an oscilloscope based spectrum analyzer by recording the vibration of the material using the smartphone internal accelerometer. The app analyzed the vibratory motion. The parameter measured was resonant frequency (Fundamental frequency). It acquired the time series data, and performed and Fast Fourier Transformation (FFT) to produce frequency spectra, which allows the frequency analysis of the data.

The equation used to calculate the dynamic modulus of elasticity (MOE) was:

$$E_{tv} = \frac{f^2 W S^3}{K_d I g} \quad (1)$$

where E_{tv} is transverse vibration modulus of elasticity (Mpa), f is the frequency of oscillation (Hz), W is the weight of specimen (N), S is the span (m), K_d is the constant of free vibration of a simply supported beam, 2.47, I is specimen moment of inertia, $bd^3/12$ (m^4), b is width (m), d is depth (m), g is acceleration due to gravity (9,807 $m.s^{-2}$).

For both procedures, the specimens were positioned such that an equal portion of the length overhung each support. The overhang adopted was 0.98 (span (l) to length (lt) ratio), as recommended by ASTM D 6874 (2012).

Longitudinal vibration measurement was conducted on each board to obtain the stress wave velocity using a Hitman (Director HM-200^{TM}). A stress wave was initiated by a hammer impact on one end of the specimen. Stress wave propagation in the wood specimen was sensed by a piezoelectric transducer mounted on the same end of the sample. Stress wave velocity can be determined by Equation 2:

$$C = \frac{2.L}{\Delta t} \quad (2)$$

where C is stress wave velocity ($m.s^{-1}$), L is length of specimen (m), and Δt is time of flight (s).

The relation between acoustic velocity, density and wood stiffness is described by the fundamental wave equation (Bucur, 2003). The dynamic MOE of the specimens obtained by stress wave timer were determined using one-dimensional propagation waves, based on Equation 3.

$$E_{SW} = \rho . C^2 \quad (3)$$

where E_{sw} is dynamic modulus of elasticity, ρ is the density at 12% moisture content ($kg.m^{-3}$), and C is stress wave velocity ($m.s^{-1}$).

Results and Discussion

The average transverse frequency collected with the portable device was 14.12 Hz. The minimum was 11.08 Hz and the maximum was 16.05 Hz. According to ASTM D6874 (2012) best results are obtained when the frequency of oscillation is less than 30Hz.

The correlation between the smartphone and the Metriguard E-computer transverse vibration frequencies are shown in Figure 2.

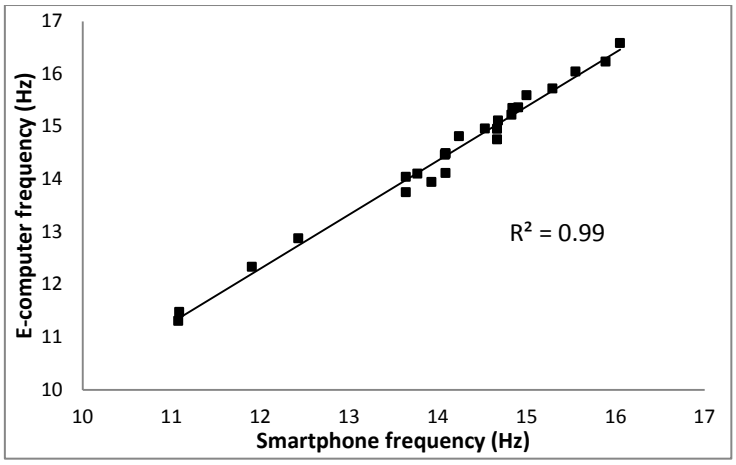

Figure 2 – Correlation between smartphone and E-computer vibration frequencies.

Transverse vibration frequency detected by MEM accelerometer was strongly correlated with the frequency detected by the E-computer. Strong linear correlations were obtained between the data collected with the smartphone and the dynamic modulus of elasticity (MOE) obtained with the E-Computer (r^2=0.996; p<0.0001).

The correlation between the smartphone and the Hitman dynamic MOEs are shown in Figure 3.

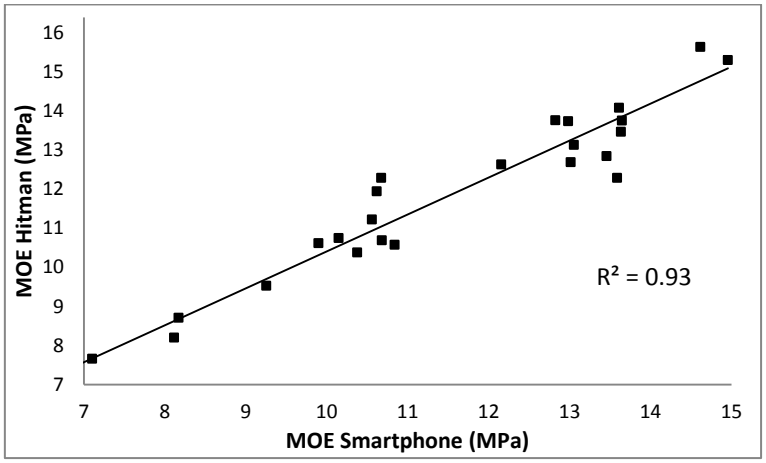

Figure 3 – Correlation between smartphone and Hitman dynamic MOEs.

Dynamic modulus of elasticity calculated based on MEM accelerometer frequency was strongly correlated with dynamic modulus of elasticity calculated based on longitudinal vibration (r^2=0.935; $p<0.0001$).

The micro electromechanical system (MEM) accelerometer inside smartphones includes a 3-channel accelerometer with sensitivity of approximately 0.02g and a range of +/-2g. Currently, MEM accelerometers built in smartphones are limited in 100 Hz. This provides access to sample data up to 50 Hz. This sampling vibration limitation is called Nyquist frequency.

According to the Nyquist sampling theorem, if the highest frequency contained in the signal of a transducer is equal to f, then the entire signal information can be captured if sampling is performed at a rate of at least 2f (Olshausen, 2000; McConnell, 1995).

The size of MEMs is getting smaller, whereas frequency response and sense range is getting wider. MEMs are more reliable and their sensitivity is becoming better. The price of MEMs accelerometers and other MEMs aren't expensive, but they still must decrease more if they want to expand massive consumption (Andrejašič, 2008). The results of this study indicate a potential use of portable devices to determine the MOE of structural pieces of lumber and to expand the access of non-destructive techniques.

Conclusions

- The MEMs accelerometer is able to capture wood transverse vibration;
- Smartphones are devices able to collect data from lumber, being useful in classifying wood;
- Increasing access to NDT tools can help reduce the cost of wood classification;
- By making wood evaluation easier, the quality control of wood products will improve;
- 50 Hz frequency limitation permits its use for real size lumber.

References

Amishev, D.; Murphy, G. E. 2008. In-forest assessment of veneer grade Douglas-fir logs based on acoustic measurement of wood stiffness. *Forest Products Journal*, 58(11):42-47.

Andrejašic M. 2008. MEMs Accelerometers. Seminar at Department of physics Faculty for mathematics and physics. University of Ljubljana.

ASTM D 6874-09, 2009. Standard Test Methods for Nondestructive Evaluation of Wood-Based Flexural Members Using Transversal Vibration.

Brashaw, B.K.; Bucur, V.; Divós, F.; Gonçalves, R.; Lu, J. X.; Meder, R.; Pellerin, R.F.; Potter, S.; Ross, R.J.; Wang, X.; Yin, Y.F. 2009. Nondestructive testing and evaluation of wood: A worldwide research update. *Forest Product Journal* 59:7-14.

Bucur, V. 2003. Nondestructive characterization and imaging of wood. Springer Verlag, Heidelberg.

Cossolino, L.C.; Pereira, A. H. A. 2010. Informativo Técnico-Científico/ATCP Engenharia Física. Módulos elásticos: visão geral e métodos de caracterização. 2010. Available at: <http://www.investagro.com.br>. Access in: 14 mar. 2013.

Divós, F.; Tanaka, T. 2005.Relation between Static and Dynamic Modulus of Elasticity of Wood, *Acta Silvatica et Lignatia Hungarica*, 1:105-110.

McConnell, E. 1995. Choosing data-acquisition method. *Electronic Design*, 43(6):147.

Murphy G. 2009. New Sensor Technologies for Forest Data Collection, Oregon State University, Corvallis, OR 97330, USA. IUFRO Division 4.01 Conference – Mount Gambier, South Australia 17–20 August 2009.

Olshausen, B.A. 2000. PSC 129 - Sensory Processes, Aliasing.

Ross, R. J.; Geske E. A.; Larson G. H.; Murphy J. F. 1991. Transverse Vibration Nondestructive Testing Using a Personal Computer. USDA Forest Service, Forest Products Laboratory RP-502. Madison, WI. 17 p.

Ross, R. J, Brashaw, B. K.; Pellerin, R. F. 1998. Nondestructively evaluation of wood. *Forest Products Journal*, 48(1):14-19.

Ross, R. J.; Kan, J.; Wang, X.; Blankenburg, J.; Stockhausen, J. I.; Pellerin, R.F. 2012. Wood and wood-based materials as sensors—a review of the piezoelectric effect in wood. 2012 USDA Forest Service, Forest Products Laboratory GTR-212. Madison, WI. 9 p.

Segundinho, P.G.A. 2012. Aplicação do método de ensaio das frequências naturais de vibração para obtenção do módulo de elasticidade de peças estruturais de madeira. *Revista Árvore*, 36(6):1155-1161.

Wang, X. 2013. Stress Wave E-Rating of Structural Timber—Size and Moisture Content Effects. In: Proceedings: 18th International NondestructiveTesting and Evaluation of Wood Symposium, Ross, R.J., Wang, X. (eds.) General Technical Report FPL-GTR-226, pp: 38-46, Madison, WI: U.S, Department of Agriculture, Forest Service, Forest Products Laboratory, USA.

Evaluation of European beech (*Fagus sylvatica* L.) roundwood for improved production of strength-graded lamellas

Lorenz Breinig
Department of Forest Utilisation, Forest Research Institute of Baden-Württemberg, 79100 Freiburg, Germany, lorenz.breinig@forst.bwl.de

Franka Brüchert
Department of Forest Utilisation, Forest Research Institute of Baden-Württemberg, 79100 Freiburg, Germany, franka.bruechert@forst.bwl.de

Anna Haas
Department of Forest Utilisation, Forest Research Institute of Baden-Württemberg, 79100 Freiburg, Germany, anna.haas@forst.bwl.de

Udo H. Sauter
Department of Forest Utilisation, Forest Research Institute of Baden-Württemberg, 79100 Freiburg, Germany, udo.sauter@forst.bwl.de

Abstract

Declining stocks of softwoods in European forests and, simultaneously, increased use of wood in the building sector which is both desired and anticipated will presumably lead to a future gap in wood supply for the production of glued structural timber. At the same time, increasing stocks of hardwoods such as European beech (*Fagus sylvatica* L.) with its favourable mechanical wood properties make utilisation of this resource for glued structural timber products a possible alternative. In the first part of a study on the suitability of lower-quality beech logs for the production of strength-graded lamellas for glued structural timber, a sample of 29 logs was evaluated for roundwood properties, including visual roundwood grading, measurement of dynamic modulus of elasticity (MOE) and X-ray computed tomography (CT) scanning. The results did not indicate any significant relationships between the measured roundwood properties. In a subsequent investigation, boards with common dimensions for glulam lamellas produced from the sample logs will be analysed including MOE measurements and visual strength grading. The data from the CT scans are planned to be used in sawing simulations for estimating the potential to optimise log breakdown for glulam lamellas.

Keywords: CT scanning, MOE measurement, hardwood, structural timber, glulam

Introduction

In central European forests there is a trend towards increasing standing stocks of hardwood species while the stocks of softwoods, especially spruce of medium dimensions, has started to decrease substantially. At the same time, an increased utilisation of wood in the building sector is sought and glued structural timber products such as glued laminated timber (glulam) and cross-laminated timber (CLT) are considered efficient construction materials, especially suited for multi-storey buildings. Currently, these products are

almost entirely made from softwoods and thus a gap in raw material supply can be expected for the future. A European research project aims to promote the establishment of hardwood glulam and CLT in the building sector by providing the information required for optimised lamella strength grading and glueing as well as harmonised product standards. Within the scope of this project, the possibilities of improving the production of strength-graded hardwood lamellas through roundwood pre-sorting as well as sawing optimisation by means of X-ray computed tomography (CT) log scanning are investigated.
European beech (Fagus sylvatica L.) is the most abundant hardwood species in central Europe with standing stocks of 635 M m³ in Germany (Schmitz et al. 2014) and 263 M m³ in France (Anonymous 2013). To date, about two thirds of the annual beech wood harvest is used for pulp and paper or as fuel wood with only roundwood of higher grades being allocated to sawn timber production. In this context, production of lamellas for glulam and CLT might be an interesting usage option for beech roundwood of average and lower quality with a higher value creation and the benefit of a more long-term carbon sequestration in buildings.
According to Aicher and Ohnesorge (2011), suitability of beech timber for glulam beams has been investigated since the 1960s and increasingly since the 2000s with different aspects covered such as lamella grading, finger jointing, bonding and the influence of red-heart discoloration. The overall conclusion is that, except for its low natural durability and high swelling/shrinkage factors, beech timber has favourable properties for usage in glued timber products. As Bernasconi (2004), who also reported high mechanical performance for beech glulam, pointed out, the limited availability of strength-graded beech lamellas for glulam production can still be seen as an impeding factor for its implementation.
Thus, efficient allocation of beech roundwood to the production of glued structural timber is required. This in turn warrants characterisation of roundwood representative for the available resource and evaluation of the sawn timber, i.e. glulam lamellas, that this roundwood can be converted into to allow for an estimation of the relationship between roundwood properties and lamella strength. Pre-sorting of beech roundwood could then be carried out so that only logs yielding sufficient volume of sawn timber which fulfils the strength requirements for glulam lamellas would be directed to this usage.
Beyond pre-sorting of roundwood, great potential for efficient sawn timber production can be expected from sawing optimisation by means of CT log scanning. It has been shown in sawing simulations that choosing the sawing position for a log according to wood features detected in CT scans can theoretically yield considerable improvement of value recovery. Berglund et al. (2014) observed that the value recovery for the production of strength-graded softwood boards could be increased by 11% through optimisation of log rotation. Also for European beech, promising results for a possible improvement of value recovery by choosing log rotation for sawing based on CT data, in this case for the production of appearance-graded lumber, have been reported (Stängle et al. 2014). It would thus be interesting to test the concept of CT-based sawing optimisation with the production of strength-graded boards from beech logs.
In the first part of the study, reported in this paper, a European beech log sample was evaluated for roundwood properties and the logs were CT-scanned. This evaluation shall be pursued by an analysis of sawn timber (glulam lamellas) produced from the logs, including visual strength grading. Analyses of the potential of sawing optimisation shall be tested as well.

Materials and methods

Roundwood sample

The European beech roundwood sample used in this study comprised 29 logs that had been cut from seven trees. The trees were sampled during the thinning of three beech stands in growth trial plots located in the north-eastern part of the Swabian Jura in southern Germany (48°33'37"N, 9°56'57"E). Six trees came from two 106-year old stands and one tree came from a 114-year old stand. The logs had lengths between 4.0 and 5.1 metres and their mid diameters under bark ranged from 16 to 42 cm with a mean

diameter of 28 cm. For six trees, four logs had been cut and numbered in sequence from the butt end, and from one tree, five logs were obtained.

Knot measurement and roundwood grading

The logs were visually examined for roundwood grading according to the rules in the German roundwood-trade framework agreement RVR (Anon. 2014) and according to the European standard EN 1316-1 (Anon. 2012). For each log, the diameter was measured at five positions: at the top and butt ends, 50 cm inward from top and butt end, respectively, and in the middle of the log. At each measurement position, two perpendicular measurements were taken and the arithmetic mean was rounded down to full centimetres according to forestry practice. For later analysis, the arithmetic mean of the five diameter values, rounded to full centimetres, was taken as mean diameter of a log.

Table 1—Excerpt of the RVR grading rules for European beech (Anon. 2014) – specifications on knots, spiral grain and crook

Roundwood feature	Grade			
	A	B	C	D
Occluded knot	Allowed if branch scar quotient ≤1:4	Allowed if branch scar quotient ≤1:2 and branch scar height ≤10 cm	Allowed	Allowed
Sound knot	Not allowed	2 per 4 m ≤10% of mid diameter	Normal amount of knots allowed	Allowed
Decayed knot	Not allowed	1 per 4 m ≤10% of mid diameter	2 per 4 m ≤20% of mid diameter, 12 cm maximum	Allowed
Spiral grain [cm/m]	≤2	≤6 for mid diameters ≤49 cm ≤7 for mid diameters ≥50 cm	No limitation	No limitation
Crook [cm/m]	≤2	≤3	≤4 for mid diameters ≤49 cm ≤6 for mid diameters ≥50 cm	No limitation

Knots visible on the log surface were recorded with their condition, size and longitudinal position along the log. Different size measurements were made depending on the condition of a knot which was classified as sound, decayed or occluded. For sound and rotten knots, the smallest diameter was taken, whereas for occluded knots, i.e. branch scars, the height and width of the branch scar were measured, in both cases with a precision of 0.5 cm. Only branch scars with a height of at least 1 cm were measured; smaller ones were counted only. In some cases, branch scars were recognizable on the log surface but could not be accurately measured, e.g. due to bark partly removed during skidding and handling of the logs. Such branch scars were counted as well.

Other wood features relevant for the applied grading rules such as spiral grain, crook, checks and bark damages were also recorded and measured if required by the grading rules. An excerpt of the RVR grading rules for European beech is presented in Table 1. In these rules, as in the case of the EN 1316-1 standard, four grades are distinguished. Grade “A” denotes roundwood of superior quality without any

defects restricting its usage and “B” corresponds to roundwood of regular quality with few or minor defects. Grade “C” is defined as roundwood quality slightly below average and roundwood graded as “D” may exhibit any number and size of defects as long as it can still be sawn into usable lumber.

Measurement of dynamic modulus of elasticity

For all logs, the dynamic modulus of elasticity (MOE) was determined using the interferometry or stress-wave technique. This method is based on measurement of the natural frequency of a wooden piece (board or log) when longitudinal oscillation is induced by impact. Natural frequency of the logs was measured with a MiCROTEC ViScan® laser interferometer. MOE (in N/mm²) was then calculated for each log according to

$$MOE = 4 \times \rho \times \nu^2 \times l^2 \quad (1)$$

where ρ is the green density of the log in kg/mm³, ν its natural frequency in Hz and l is its length in mm (cf. Pellerin and Ross 2002, Frese and Riedler 2010).

CT scans

After roundwood grading and laser interferometry measurement, the logs were CT scanned with a MiCROTEC CT.LOG® roundwood scanner (see Figure 1). Voltage and current of the X-ray tube were set at 180 kV and 14 mA, and the scans in spiral CT mode were run with 1000 projections per revolution at 8 rpm and a gantry forwarding speed of 1.3 mm/s.

a 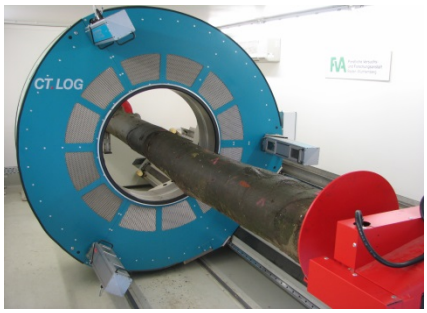

b 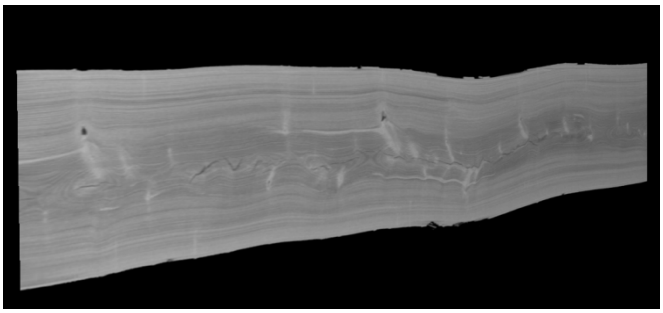

Figure 1—MiCROTEC CT.LOG scanner (a). During a scan the gantry with the rotating X-ray tube and detector assembly moves along the log resting on two end supports. CT image (axial section) of a beech log (b).

CT images with an image size of 768 by 768 pixels, a resolution of 1.1 mm/pixel in the cross-section plane and a slice thickness of 5 mm were reconstructed from the scans and stored as 16-bit TIFF files (cf. Figure 1). The mean green density of each log was calculated from the CT images which was feasible since the CT images of the CT.LOG were calibrated on water samples.

Results

The distribution of log grades when applying the grading rules for European beech in RVR and EN 1316-1 is presented in Table 2. When all roundwood properties were considered, none of the logs was better than grade “C” according to RVR or better than “D” according to EN 1316-1. Three logs were off-grade according to RVR and EN 1316-1, respectively, due to multiple and very strong crook (over 8 cm/m). One additional log was off-grade according to EN 1316-1 due to its small dimension, i.e. a mid diameter below 20 cm. When only knots were considered for grading, the number of “C” grade logs according to

RVR increased from 18 to 21 and two logs were graded as “B”, but still no log was better than “D” grade when EN 1316-1 was applied due to the more strict rules on knots in this standard.

Table 2—Frequency distribution of log grades according to RVR and EN 1316-1.

Grading rule	Properties considered	Grade				
		A	B	C	D	Off-grade
RVR	All	0	0	18	8	3
	Knots only	0	2	21	6	0
EN 1316-1	All	0	0	0	25	4
	Knots only	0	0	0	29	0

Green density of the logs varied between 901 and 1,037 kg/m³, mean green density (standard deviation) was 963 kg/m³ (34 kg/m³). Figure 2a shows the distribution of green density of the logs grouped by tree number, and in Figure 2b, green density is plotted against mean log diameter. As the scatterplot suggests, there was no significant correlation (Pearson’s r = 0.45) between these two properties.

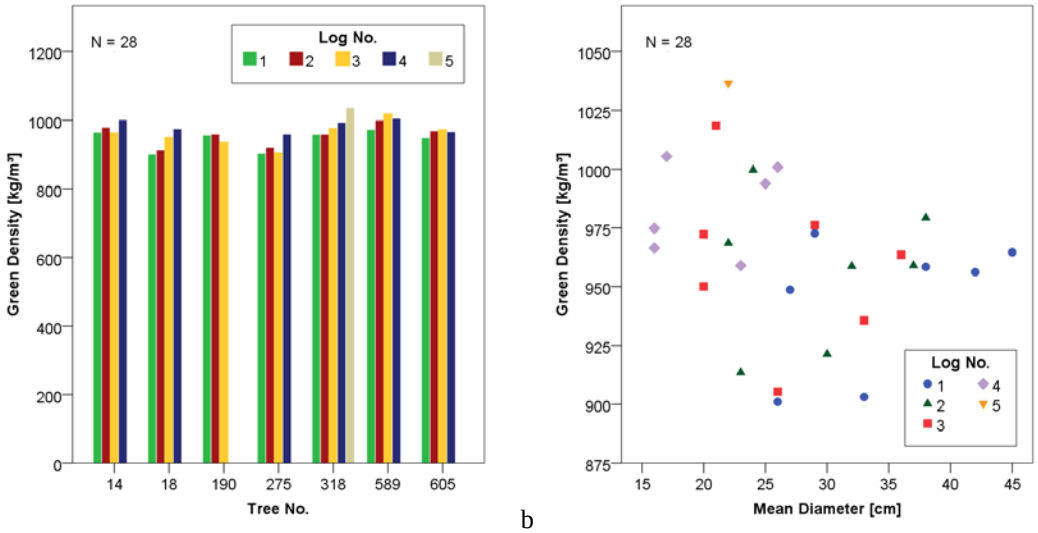

a b

Figure 2—Distribution of green density of the logs by tree number (a) and green density plotted against mean log diameter (b).

MOE measurements varied between 5,446 and 13,515 N/mm² with a mean of 11,258 N/mm² and a standard deviation of 1,996 N/mm² for the 28 logs that were analysed for MOE. One log had to be excluded since it was severely checked due to a large branch that had broken off, and ViScan measurement was not stable.

In Figure 3a, MOE is plotted against mean log diameter. It can be noted that the first and second logs from each tree had a rather close spread in MOE with means of 12,371 and 12,676 N/mm² and standard deviations of 504 and 455 N/mm², respectively, while the upper logs showed a larger variation with standard deviations of 2,827 N/mm² for the third and 1,466 N/mm² for the fourth lengths. Means were 10,093 and 10,034 N/mm² for these logs. No significant correlation (r = −0.34) was found for the relationship between MOE and green density of the logs (Figure 3b).

A slight dependency between MOE and log grade according to RVR (considering all roundwood properties) was suggested by the log sample (see Figure 3c). The logs graded as “C” had a mean MOE of 12,239 N/mm² with a rather small standard deviation of 714 N/mm², whereas the “D” grade logs had a mean of 10,258 N/mm² with a substantially larger standard deviation of 2,071 N/mm².

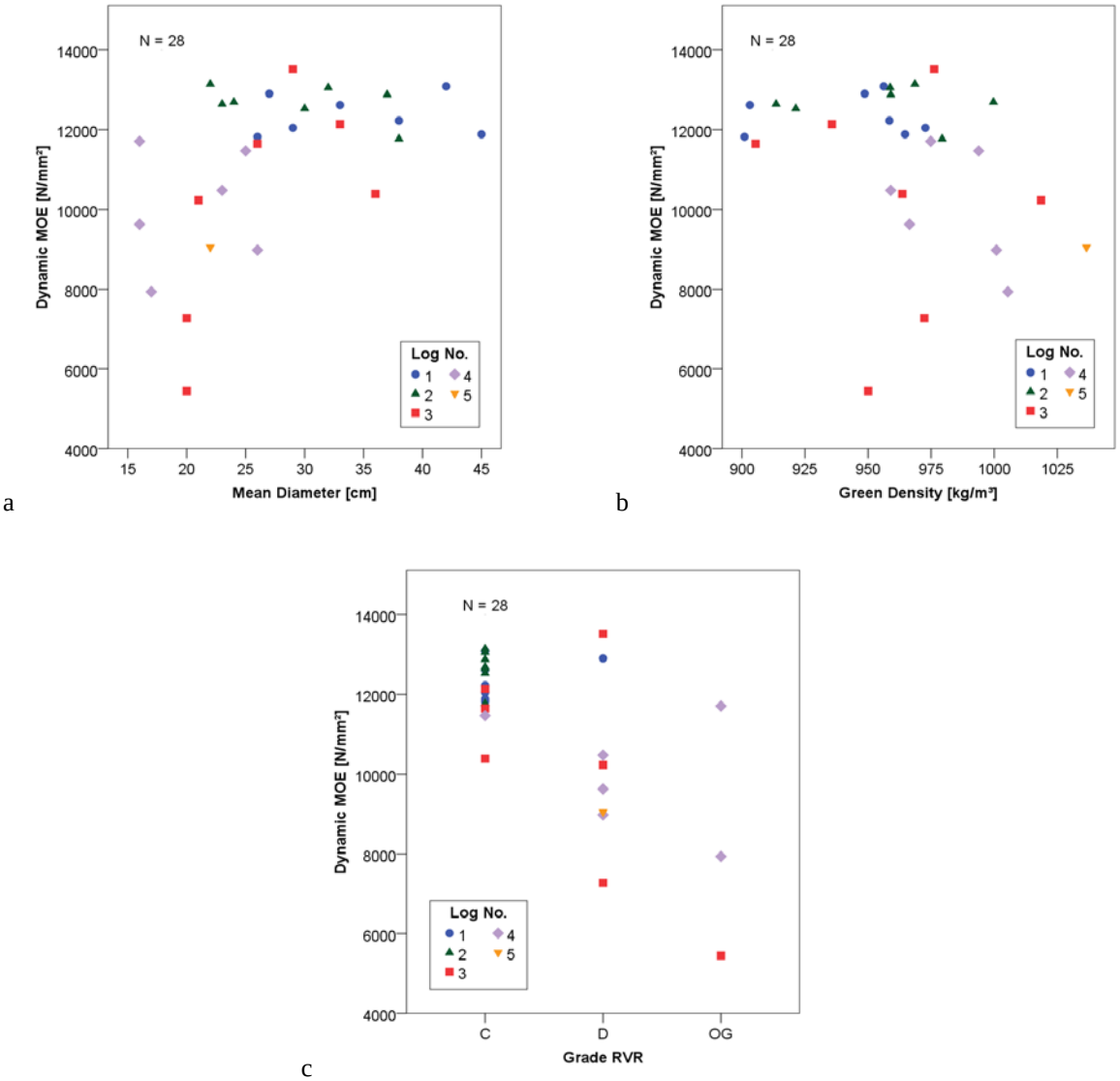

Figure 3—MOE plotted against mean diameter (a), green density (b) and grade according to the RVR rules (c).

Discussion and future work

The results of the roundwood grading indicated that the roundwood sample comprised logs of rather low quality but the fact that no log was better than grade "D" according to the EN 1316-1 rules also raises the question whether this grading standard might lead to grade distributions not fully reflecting the usage potential of a large part of the European beech resource, making analysis of the properties of sawn timber produced from the sample logs a relevant follow-up investigation.

Green density of the logs showed variations within the log groups and within trees on approximately the same level. On the basis of the small log sample, no differences in green density between different trees or between groups of logs from different heights within the stem were assumed but rather it was assumed that the variations in green density were to a large extent due to variations in moisture content. Density measurements on boards produced from the sample logs could further to explore the relationship between log green density and board density after drying.

The lack of significant correlation between log MOE and green density could be an indication of the presumably large influence of moisture content on green density. The apparent slight dependency between MOE and log grade according to RVR was probably mainly due to the fact that the first and second logs in the roundwood sample showed a somewhat higher and less variable MOE than the other logs – first and second logs made up the major part of the "C" grade logs. In this context, it might be interesting to investigate whether this would also be observable with other trees.
The observed MOE values of the logs were lower than the characteristic values for European beech reported in the literature, which range from 14,000 N/mm² (Anonymous 2003a) to 16,000 N/mm² (Anonymous 2003b). However, characteristic values are determined on small clear specimens dried to a moisture content of usually 12% whereas the sample logs in this investigation contained knots and were in green state.
In the next step after the measurements on the roundwood, the logs will be sawn into boards with typical dimensions for glulam lamellas, 30 mm by 150 mm and 30 mm by 200 mm. These boards will then be visually strength-graded applying the German standard for strength-grading of hardwood sawn timber, DIN 4074-5 (Anonymous 2008), and MOE measurement will be repeated for the individual boards. The relationships between roundwood properties such as MOE and the properties of the boards relevant for use in structural timber such as glulam can then be investigated with the objective to characterise the roundwood suitable for the production of glulam lamellas. This could help to identify the raw material needed for beech glulam production at an early stage in the conversion chain. The lack of clearly defined raw material is assumed to still be an obstacle for the establishment of an industrial production as stated by Frese and Riedler (2010). In contrast to the approach of allocating available appearance-graded lumber to glulam lamella production described in this study, allocation decisions at the roundwood stage might lead to a more efficient value chain.
This approach also motivates analysing the potential of sawing optimisation. Therefore, sawing simulations based on models of outer shape and internal knottiness of the sample logs that are extracted from the CT data are planned to obtain an estimation of the potential to produce boards meeting the requirements of the highest possible grades according to DIN 4074-5 from roundwood qualities as they are represented by the roundwood sample in this study.

Acknowledgements

This work was conducted within the framework of the *WoodWisdom-Net* project "European hardwoods for the building sector (EU Hardwoods)" funded in Germany by the *Fachagentur für Nachwachsende Rohstoffe e.V. (FNR)* under grant agreement 22004114 and was first presented at the 5th International Scientific Conference on Hardwood Processing (ISCHP 2015), September 15–17, 2015, Québec City, Canada. Parts of this work are also included in the bachelor thesis by Anna Haas supervised by Prof. Dirk Jaeger, Chair of Forest Operations at the University of Freiburg.

References

Aicher, S.; Ohnesorge, D. 2011. Shear strength of glued laminated timber made from European beech timber. European Journal of Wood and Wood Products 69: 143–154. DOI: 10.1007/s00107-009-0399-9

Anonymous. 2003a. Properties of wood species – Density, modulus of elasticity and strength. DIN 68364:2003-05. DIN Deutsches Institut für Normung e.V., Berlin, Germany.

Anonymous. 2003b. Wood species – Characteristic values to terms and symbols of OENORM EN 13556. OENORM B 3012:2003-12-01. ASI Austrian Standards Institute, Vienna, Austria.

Anonymous. 2008. Strength grading of wood – Part 5: Sawn hard wood. DIN 4074-5:2008-12. DIN Deutsches Institut für Normung e.V., Berlin, Germany.

Anonymous. 2012. Hardwood round timber – Qualitative classification – Part 1: Oak and beech. EN 1316-1:2012. CEN European Committee For Standardization, Brussels, Belgium.

Anonymous. 2013. Résultats d'inventaire forestier – Résultats standards (campagnes 2009 à 2013) – Tome national version régions administratives. Institut national de l'information géographique et forestière (IGN), Saint-Mandé, France. (In French)

Anonymous. 2014. Rahmenvereinbarung für den Rohholzhandel in Deutschland (RVR). Deutscher Forstwirtschaftsrat e.V., Deutscher Holzwirtschaftsrat e.V., Berlin, Germany.

Berglund, A.; Johansson, E.; Skog, J. 2014. Value optimized log rotation for strength graded boards using computed tomography. European Journal of Wood and Wood Products 72: 635 –642. DOI: 10.1007/s00107-014-0822-8

Bernasconi, A. 2004. Verleimung von Laubholz für den tragenden Einsatz. Schweizerische Zeitschrift für Forstwesen. 155:533–539. (In German)

Frese, M.; Riedler, T. 2010. Untersuchung von Buchenschnittholz (Fagus sylvatica L.) hinsichtlich der Eignung für Brettschichtholz. European Journal of Wood and Wood Products 68:445–453. DOI: 10.1007/s00107-009-0385-2 (In German)

Pellerin, R.; Ross,R. 2002. Nondestructive Evaluation of Wood. Publication No. 7250. Forest Products Society, Madison, Wisconsin, USA.

Stängle, S.; Brüchert, F.; Heikkila, A.; Usenius, T.; Usenius, A.; Sauter, U.H. 2014. Potentially increased sawmill yield from hardwoods using X-ray computed tomography for knot detection. Annals of Forest Science. DOI: 10.1007/s13595-014-0385-1

Schmitz, F.; Polley, H.; Hennig, P.; Kroiher, F.; Marks, A.; Riedel, T.; Schmidt, U.; Schwitzgebel, F.; Stauber, T. 2014. Der Wald in Deutschland – Ausgewählte Ergebnisse der dritten Bundeswaldinventur. Bundesministerium für Ernährung und Landwirtschaft (BMEL), Berlin, Germany. (In German)

Prediction of bending properties for Anatolian black pine (*Pinus nigra* T.) lumber using stress wave

Ergün Güntekin
Suleyman Demirel University, Faculty of Forestry, Department of Forest Products Engineering, 32260 Isparta Turkey, ergunguntekin@sdu.edu.tr

Zübeyde Bülbül
Istanbul University, Vocational School of Forestry, Bahçeköy, 34473 İstanbul, Turkey, zubeyde.bulbul@istanbul.edu.tr

İsmail Dutkuner
Suleyman Demirel University, Faculty of Forestry, Department of Forest Engineering, 32260 Isparta, Turkey, ismaildutkuner@sdu.edu.tr

Abstract

In this study; bending properties of black pine (*Pinus nigra* A.) lumber were predicted using stress – wave method and compared with static bending tests. First, total of 116 lumbers which were different in length, grade and cross section were weighed and dimensions were measured. Then, moisture contents were obtained via moisture meter. By using the density, moisture, and dimensions of the samples in MTG Timber Grader device, dynamic modulus of elasticity values were determined. Finally, samples were subjected to 3 point bending test. Modulus of elasticity and bending strengths were calculated using load – deformation curves. Regression models were developed to interpret relationships between dynamic modulus elasticity and bending properties. Results showed that there is a moderate regression coefficient (0.73) between dynamic modulus of elasticity and static modulus of elasticity. Regression coefficient between dynamic modulus of elasticity and static bending strength was measured as 0.55 while regression coefficient between static modulus of elasticity and static bending strength was measured as 0.54. More samples should be evaluated in order to predict bending properties of black pine lumber.

Keywords: bending properties, black pine, stress-wave

Introduction

Nondestructive evaluation (NDE) can be described as the assessment of a material's properties without damaging its end use (Ross et al. 1998). The oldest nondestructive evaluation of wood was visual inspection, mostly used for classification of load-carrying members (Bucur 2006). Later, a machine stress rating system, which is one of the most used methods in lumber grading, was introduced and has been commercially used since the 1960's (Galligan and McDonald 2000). Developments in instrumentation have made it possible to use scientific nondestructive tools for the last two decades. Transverse vibration and ultrasonic wave velocity are particularly important in obtaining the modulus of elasticity. Ultrasonic wave velocity has more advantages over other techniques in practical terms (Esteban et al. 2009).

Stress-wave-based NDE methods have been investigated extensively during the past few decades and have proven useful for predicting the mechanical properties of wood materials. The ultrasonic wave propagation method has been applied on standing trees for detecting defects (Najafi et al. 2009). Several studies have investigated the relationship between the stress-wave-based modulus of elasticity

of logs and the static MOE of lumber cut from log and have shown a correlation of 0.44 to 0.89 (Ross et al. 1997). A study by Wang et al. (2000) revealed that there can be a good correlation (R2 = 0.63 to 0.91) between stress wave speed and dynamic modulus of elasticity of standing trees and clear wood specimens. Stress wave base methods have been also used and good correlations have been achieved in the case of wood-derived products such as laminated veneer lumber, glued-laminated wood, and particleboard. Investigations also have been carried out to diagnose components of timber structures (Esteban et al. 2009).

Ross and Pellerin (1994) have summarized the results of different research reports related to the relationship between the modulus of elasticity in static and dynamic tests and stress wave methods. The correlation coefficient was scattered between 0.87 and 0.99. It was concluded that the stress wave method could be a nondestructive method for wood. Divos and Tanaka (2005) also confirmed that the correlation between dynamic and static modulus of elasticity is high.

Anatolian black pine covers the second largest area among the conifers grown in Turkey. The Turkish wood processing industry does not use any nondestructive based grading methods to assess the lumber quality. It is believed that these methods are expensive. However, in Turkey the increase in lumber prices could make these methods suitable for the lumber industry. Additionally, consumers could benefit by using classified material, which would have higher quality and reliability than unclassified one. The purpose of this study was to predict bending properties of Anatolian black pine lumber using stress wave method.

Materials and Methods

Black Pine lumber pieces were sawn from logs that came from the southwestern region of Turkey. The ages of tress were approximately 80 years. Logs were approximately 50 cm in diameter. The logs were transferred to a private mill and sawn to approximately 40 x 90 x 3000 mm lumber. After the lumber had been delivered to the laboratory, the boards were visually graded according to the Turkish standard TS 1611. In the Turkish standard the lumber is graded into three classes I, II, and III. These grades consider defects such as knots, checks, bows occurring in the lumber. Then, they were stored in a room for air drying. During the drying process, experimental procedures were performed. The moisture content (MC) of the lumbers was measured with a pinned moisture meter. Apparent density of the lumbers was calculated using their weighs and dimensions.

After the measurements, nondestructive testing was applied to the lumber. The stress wave timer used in this study is called Timber Grader MTG, which is a handheld grading device for sawn wood developed by Brookhuis Micro-Electronics and TNO. Timber grader MTG works on the principle of sound waves emission. It measures natural frequency and dynamic modulus of elasticity (MOE) of the lumbers when density, MC and dimensions are entered. Following stress wave measurement, all lumber samples were tested in flatwise bending to obtain static MOE. The static bending tests were conducted on each specimen using center-point loading (ASTM 2003)

Analysis of variance (ANOVA) general linear model procedure was run with SAS statistical analysis software to interpret the effects of measured physical properties on the dynamic MOE of the lumbers. Linear models for prediction of MOE and MOR based on dynamic MOE were developed.

Results and Discussions

Average static and dynamic MOE and some physical parameters of the lumbers are presented in Table 1. The moisture content of the lumbers ranged from 9 % to 25 % with an average of 14 % and coefficient of variation of 18%. Density of the lumber specimens varied 0.29 to 0.71 g/cm^3 with an average of 0.52 g/cm^3 and coefficient of variation of 15%.

Table 1. Some physical and mechanical properties of the lumbers used in the study.

Property	N	Mean	Max	Minimum	Coefficient of variation (%)
R (%)	116	14.43	25.8	9.3	18.09
D (g / cm^3)	116	0.52	0.71	0.29	15.70
E_{dyn} (N/mm^2)	116	10076	15221	4978	21.47
E_{stat} (N/mm^2)	116	7156	12879	3288	27.66
E_D (N/mm^2)	116	67	107	35	29.25

Linear regression analysis procedure was performed to establish relationships between dynamic MOE and bending properties. The relationship between static and dynamic MOE is shown in Figure 1. Generally, the values obtained through stress wave method were higher than static values. Several studies have reported that values of dynamic modulus of elasticity are often higher than those obtained using static bending tests (Teles et al. 2011; Passialis and Adamopoulos 2002; Barrett et al. 2008). The lower static MOE values were expected because static measurement includes shear deflection, whereas MTG results are essentially shear free MOE values (Barrett et al. 2008).

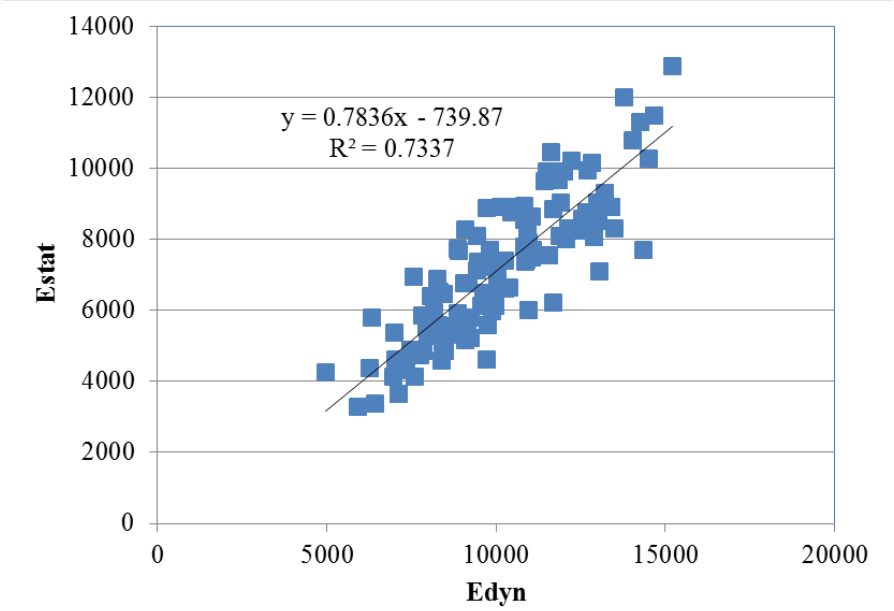

Figure 1. The relationship between static and dynamic MOE.

The coefficient of determination between dynamic MOE and bending strength is presented in Figure 2. The coefficient of determination between static MOE and bending strength is much lower than the coefficient between dynamic MOE and bending strength as shown in Figure 3. This means dynamic MOE is better predictor of bending strength than static MOE.

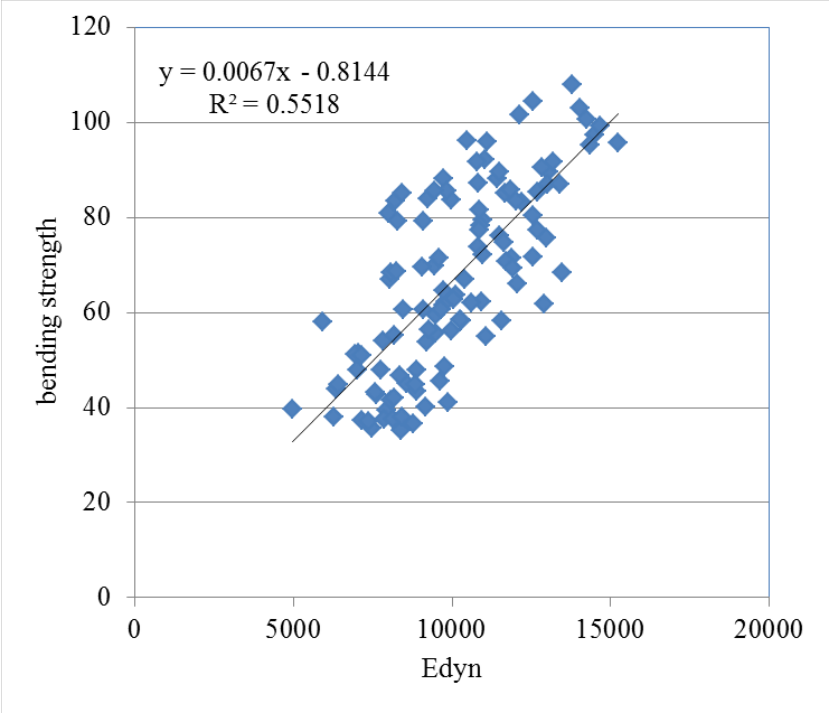

Figure 2. The relationship between dynamic MOE and bending strength.

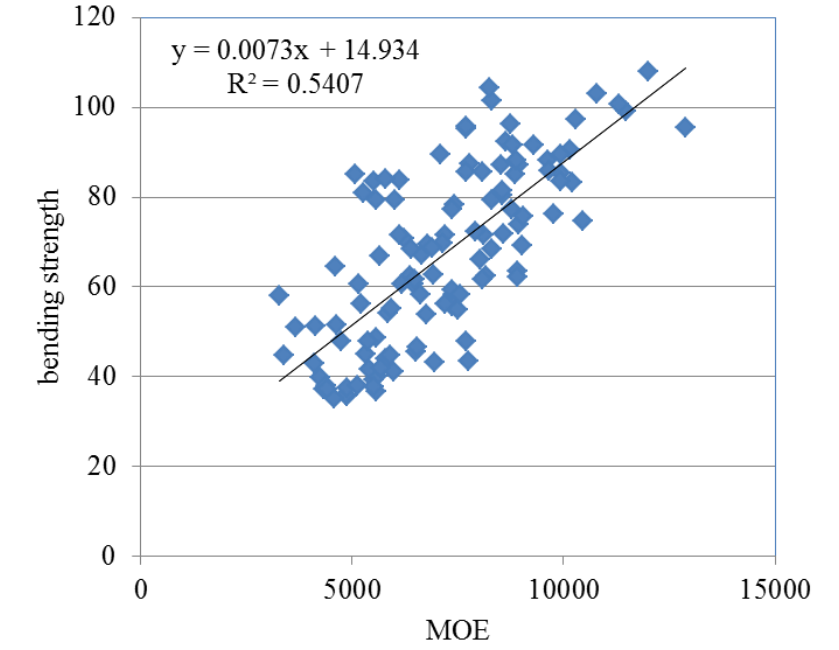

Figure 3. The relationship between static MOE and bending strength.

The coefficient of determination values for predicting bending properties were moderate, indicating that stress wave can be used in prediction of black pine lumber's bending properties. In non-destructive evaluation of wood, R^2 values are usually dependent on the methods, species used, moisture content, type of samples tested, etc. Results of nondestructive testing on wood were summarized by Ross and Pellerin (1994). They have stated that the R^2 value can be as high as 0.98 and 0.88 for clear wood species and dimension lumber, respectively. Divos and Tanaka (2005) reported that R^2 values between static and dynamic MOE values can be between 0.9 and 0.96, and dynamic MOE values are usually 10% higher than the static MOE values. Biechele et al. (2010) have reached

the coefficient of determination values of 0.80 and 0.97 for spruce timber using stress wave and transverse vibration methods, respectively while Teles et al. (2011) have reported the coefficient of determination values of 0.84 and 0.94 for tropical hardwood species using same methods. Ravenshorst and Kuilen (2006) evaluated bending properties of thirty different hardwood species using both destructive and non-destructive testing. They have reached a coefficient of determination of 0.62 and 0.85 for bending strength and bending elasticity, respectively. Krzosek et al. (2008) tested Polish grown structural pine lumber employing several nondestructive methods including MTG. They have reported a coefficient of determination of 0.84 for bending stiffness.

Conclusions

A total of 116 pieces of lumber were evaluated using stress wave method in order to determine bending properties. Linear statistical modeling was utilized to interpret relationship between the dynamic MOE and bending properties of the lumbers. The coefficient of determination between dynamic modulus and three-point bending modulus was 0.73. The coefficient of determination between dynamic MOE and bending strength of black pine sawn lumber was 0.55. Dynamic MOE seemed a better predictor for bending strength than static MOE which yielded a coefficient of determination of 0.54 for bending strength. It can be concluded that the stress wave method can be used for predicting bending properties of black pine lumber, more tests should be conducted. Timber Grader MTG provides fast elasticity measurements.

References

ASTM D 198. 2003. Standard test methods of static tests of lumber in structural sizes. Annual Book of ASTM Standards," West Conshohocken, PA, USA.

Barrett J.D.; Lam, F.; Chen, Y. 2008. Comparison of machine grading methods for Canadian hemlock, In: Proceedings of 10th WCTE Miyazaki, Japan.

Biechele, T.; Chui, Y.H.; Gong, M. 2010. Assessing stiffness on finger-jointed timber with different non-destructive testing techniques, In: The Future of Quality Control for Wood & Wood Products, 4-7th May 2010, The Final Conference of COST Action E53, Edinburgh.

Bucur, V. 2006. Acoustics of Wood, Springer-Verlag, Berlin.

Dıvós, F.; Tanaka, T. 2005. Relation between static and dynamic modulus of elasticity of wood, Acta Silv. Lign. Hung. 1, 105-110.

Esteban, L. G.; Fernandez, F. G.; de Palacios, P. 2009. MOE prediction in *Abies pinsapo Boiss*. timber: Application of an artificial neural network using non-destructive testing, Computers and Structures 87, 1360-1365.

Galligan, W. L.; McDonald, K. A. 2000. Machine grading of lumber. Practical concerns for lumber producers, General Technical Report FPL-GTR-7, USDA Forest Service.

Krzosek, S.; Grzeskiewicz, M.; Bacher, M. 2008. Mechanical properties of Polish – grown Pinus sylvestris L. Structural sawn timber, Conference COST E53, 29 – 30 October 2008, Delft, The Netherlands, pp. 253-260.

Najafi, S. K.; Shalbafan, A.; Ebrahimi, G. 2009. Internal decay assessment in standing beech trees using ultrasonic velocity measurement, Eur. J. Forest Res. 128, 345-350.

Passialis, C.; Adamopoulos, S. 2002. A comparison of three NDT methods for determining the modulus of elasticity in flexure of fir and black locust small clear wood specimens, Holz als Roh- und Werkstoff 60, 323-324.

Ravenshorst, G. J. P.; van de Kuilen, J. W. G. 2006. An innovative species independent strength grading model, In: 9th World Conference in Timber Engineering. August 6-10, 2006.

Ross R J, Bradshaw B K and Pellerin R F. 1998. Nondestructive evaluation of wood, Forest Products Journal. 48, 14-19.

Ross, R. J.;İ McDonald, K. A.;, Green, D. W.; Schad, K. C. 1997. Relationship between log and lumber modulus of elasticity, Forest Products Journal 47(2), 89-92.

Ross, R.J.; Pellerin, R. F. 1994. Nondestructive testing for assessing wood members in structures: A review, Gen. Tech. Rep. FPL- GTR-70 (Rev.), Madison, WI: U.S. Department of Agriculture, Forest Service, Forest Products Laboratory.

Teles, R. F., Del Menezzi, C. S., de Souza, F.; de Souza, M. R. 2011. Nondestructive evaluation of a tropical hardwood: Interrelationship between methods and physical-acoustical variables, Ciência da Madeira, Pelotas 2(1), 01-14.

TS EN 1611-1. 2002. Biçilmiş yapacak odun (kereste)- İğne yapraklı (yumuşak) odunların görünüşlerine göre sınıflandırılması, Bölüm 1: Avrupa ladinleri, göknarları, çamları ve duglas göknarları.

Wang, X.; Ross, R.J.; McClellan, M.; Barbour, R. J.; Erickson, J. R.; Forsman, J. W.; McGinnis, G. D. 2000. Strength and stiffness assessment of standing trees using a nondestructive stress wave technique. Research Paper FPL-RP-585. USDA Forest Service.

Strength grading based on high resolution laser scanning – performance of a procedure newly approved for the European market

Anders Olsson
Dept of Building Technology – Linnaeus University – SE-351 95, Växjö, Sweden , anders.olsson@lnu.se

Jan Oscarsson
Dept of Building Technology – Linnaeus University – SE-351 95, Växjö, Sweden , jan.oscarsson@lnu.se

Abstract

Strength grading of timber is necessary to ensure sufficient structural performance of the material, and machines based on different types of non-destructive measurements are available on the market. The purpose of this paper is to present results on an investigation of a new method and procedure for machine strength grading that is based on laser scanning and utilization of the tracheid effect, in combination with dynamic excitation and weighing. The investigated sample comprised more than 900 pieces of timber of Norway spruce (*Picea abies*) from Sweden, Norway and Finland. The coefficient of determination between the indicating property (IP) to bending strength and the measured bending strength was as high as $R^2 = 0.69$, while the coefficient of determination between dynamic MOE and measured bending strength was $R^2 = 0.53$. A comparison of the performance with what have been presented for machines that are based on X-ray in combination with dynamic excitation indicates that the new method/procedure will surpass such machines.

Keywords: grading, laser scanning, Norway spruce, strength class, structural timber, tracheid effect, yield

Introduction

Effective utilization of structural timber requires grading using indicating properties (IPs) that are able to predict strength with high accuracy, and machines that are able to measure the underlying board properties in a speed that corresponds to the production speed of saw mills. Many of the methods and machines used on the market today utilize longitudinal dynamic modulus of elasticity (MOE) for prediction of bending strength. The vibration signal from dynamic excitation, the weight and the dimensions of the board can be measured fast and accurately with machines that are comparatively inexpensive and the dynamic MOE is calculated using a simple equation. The relationship between longitudinal dynamic MOE and bending strength is, however, rather weak. For Norway spruce (*Picea abies*) the coefficient of determination, R^2, between longitudinal dynamic MOE and bending strength is about 0.5 which result in poor yield in high strength classes.

There are grading machines on the market that combine X-ray techniques with dynamic MOE (Microtec 2015) and these represent the most accurate strength grading that is utilized on the market today. The information added by the X-ray technique is high resolution information of the variation of density within a board which means that knot measures can be derived and used in definitions of IPs. In a large study performed by Hanhijärvi and Ranta-Maunus (2008), comprising more than 1000 pieces of spruce (*Picea abies*) and 1000 pieces of pine (*Pinus sylvestris*), mostly from Finland but also from North-Western Russia, assessments of various strength grading machines and IPs to tension and bending strength were

performed. The machine/IP that showed the best performance in the study was “GoldenEye+Viscan” of the company Microtec (Microtec 2015). On the basis of dynamic excitation, X-ray and knowledge of dimensions it gives information that are used for the establishment of an IP to bending strength. For the spruce timber that was evaluated with respect to bending strength the machine/IP gave a coefficient of determination to bending strength of $R^2 = 0.64$. When dynamic MOE (also assessed by equipment from Microtec) including information about density of individual boards was used for prediction of the bending strength a coefficient of determination between IP and bending strength of $R^2 = 0.57$ was achieved. When dynamic MOE based on a constant density for all boards, i.e. when the density of individual boards was not utilized, the coefficient of determination to bending strength was $R^2 = 0.48$. Other studies that give examples of the performance of the equipment of Microtec are presented by Bacher (2008) and Nocetti *et al.* (2010).

Olsson *et al.* (2013) suggested a strength grading method based on dot laser scanning, which gives high resolution information of the fibre orientation on board surfaces, to be used in combination with knowledge of dynamic MOE. Based on the fibre orientation, basic material wood properties, and cross-sectional integration schemes, a new IP defined as the lowest local edgewise bending MOE found along a board was established. A comparison of coefficients of determination of the new, suggested IP and dynamic MOE, respectively, to bending strength was performed and the result was very beneficial for the new IP. However, the investigation only comprised a small sample of 105 boards of one dimension, 45 × 145 × 3600 mm, and the examination of the boards was not performed under production conditions or at production speed. Between 2013 and 2015 the method was therefore examined again in an extensive study involving cooperation with both manufacturers of equipment for grading and saw milling companies. The timber sample examined was composed such that the results could be used as the basis for a formal approval of the method for the European market. The study was supervised by SP Technical Research Institute of Sweden and considered all parts that would be needed for an approval and successful market introduction, such as assessment of repetitiveness, significance of grading speed, evaluation of settings and yield in different strength classes, etcetera. A selection of results from this investigation is presented below.

Materials and methods

Sampling of material for evaluation

To derive machine settings that are valid for a new machine type, a minimum total number of 900 timber pieces originating from at least four different sub-samples shall, according to the European Standard EN 14081-2, clause 6.2.2, be sampled. Each sub-sample shall consist of at least 100 pieces and can include several board dimensions. The quality of the pieces shall be sawfalling, *i.e.* they must not be pre-graded. The sub-samples shall be distributed over a chosen geographic area with the purpose of reflecting the variation of growth conditions.

The present sample was divided in five subsamples representing timber from (1) northern Sweden, (2) mid Sweden, (3) southern Sweden, (4) Norway, and (5) Finland and included dimensions ranging from 30 – 70 mm in the thickness direction and from 70 – 245 mm in the depth direction. The sizes and numbers of boards from each region included in the investigated sample are presented in Table 1.

Table 1 Number of specimens and dimensions from each of the five subsamples/origins.

Sub-sample	Origin	Dimensions [mm][1] / No. specimens										
		30 × 95 × 3700	30 × 120 × 4400	40 × 70 × 3000	40 × 120 × 3600	45 × 95 × 3600	45 × 145 × 3600	45 × 170 × 5100	58 × 170 × 5800	70 × 220 × 5800	70 × 245 x 5800	Total
1	Sweden North					48	56					104
2	Sweden Mid					75	138	60				273
3	Sweden South			57	14		32		36	69	30	238
4	Norway	21				51	123	22				217
5	Finland		44				60					104
	Total	**21**	**44**	**57**	**14**	**174**	**409**	**82**	**36**	**69**	**30**	**936**

[1] The length given is the minimum length in any of the sub-samples.

Measurements and equipment for IP determining data

The IPs utilized in the grading method are based on local fibre orientation on the four longitudinal faces of the board and on the board longitudinal resonance frequency and mass assessed as described below. Also, knowledge of the moisture content of the batch to which the board belongs was required.

Resonance frequency and mass

The equipment employed for measurements of longitudinal resonance frequency and mass of each board was a Precigrader strength grading machine (Dynalyse 2015). When a board passes the machine the one end of it is excited with a blow of a piston. The response of it in terms of the sound that results from the blow of the piston is captured by means of two microphones, and by fast Fourier transform of the sound the lowest resonance frequency corresponding to the first longitudinal mode of vibration is extracted. The board weight is determined by means of a load cell placed in the production line.

Fibre orientation on wood surfaces

A WoodEye 5 scanner (Innovativ Vision 2015) equipped with four sets of dot lasers and multi-sensor cameras, one set for each longitudinal side of the board that is fed through it, is used for collecting high resolution data regarding fibre orientation. The fibre orientation in the plane of each of the four surfaces is obtained by means of the so-called tracheid effect where the major of the principal axes of the light intensity distribution around a laser dot is oriented in the direction of the wood fibres. This provides a practical method for measuring variations in grain angle on a wood surface. The resolution obtained in transverse direction of the board surfaces is 4.4 mm. The resolution obtained in the longitudinal direction, *i.e.* along the board, depends on the speed of the boards fed through the scanner. In a speed of 450 m/minute a resolution of 4.4 mm can be obtained also in this direction. Furthermore the scanner determines length, width and depth of the board.

Determination and requirements of grade determining properties

The grade determining properties, *i.e.* the properties that are decisive for the strength class to which a board should belong, are MOE, bending strength and density, with values of MOE and density adjusted to 12 % moisture content (MC), and strength adjusted according to the depth of the member, as defined in

EN 384. The grade determining properties are calculated on the basis of physical and mechanical properties that are determined according to the prescriptions in EN 408.

A four point bending test (EN 408) was used for assessment of both local and global MOE, which are here, after adjustment to 12 % MC, denoted $E_{\mathrm{local,corr}}$ and $E_{\mathrm{global,corr}}$, respectively. The stiffness property to be considered when grading timber into strength classes is defined as (EN 384)

$$\overline{E} = \left[\Sigma E_i / n\right] \cdot 1{,}3 - 2690 \qquad (1)$$

where E_{i} is the i$^{\mathrm{th}}$ value of $E_{global,corr}$ and n is the number of boards in the sample. For each of the strength classes defined in EN 338 there is a required value of average MOE which means that $\overline{E}$ of the boards, 1 to n, assigned to a strength class must exceed this required value.

The four point bending test is also used for assessment of the bending strength which, after adjustment to the depth of the member (EN 384), is here denoted $f_{\mathrm{m,corr}}$.

Density is determined for a piece of clear wood cut out from the board close to the position of failure in the four point bending test (the same piece is used for assessment of MC) and after adjustment to 12 % MC it is here denoted ρ_{corr}. The basic requirement on $f_{\mathrm{m,corr}}$ and ρ_{corr} in grading is that 95 % of the boards assigned to a strength class shall have values that exceed the characteristic strength and the characteristic density, respectively, of the class as defined in EN 338.

Calculation model and definitions of indicating properties

The principles of the grading method being assessed are given in brief in the section *Determination of local MOE valid for bending*. A complete account of the method is given by Olsson *et al.* (2013). The IPs employed for grading are formally defined in the section *Definitions of indicating properties*.

Determination of local MOE valid for bending

Wood is an orthotropic material having very high stiffness and strength in the fibre direction but low stiffness and strength in other directions. The local stiffness in the longitudinal direction of the board is thus strongly dependent on the local fibre orientation. Knowledge about the spatial distribution of the material orientation and the stiffness properties of the material everywhere within the board makes it possible to calculate the local stiffness in the longitudinal direction of the board and, by integration, to calculate the stiffness properties on the cross-sectional level. However, since the fibre direction is scanned on the surface, the information regarding the material orientation within the boards is limited. Thus, certain assumptions have to be made before the cross-sectional stiffness properties can actually be calculated and used in the definitions of IPs. In the presented grading method, it is therefore assumed that

- the density and the MOE in the fibre direction (E_{l}) are constant within a board,
- an initial, nominal value of the MOE in the fibre direction ($E_{\mathrm{l,0}}$), as well as nominal values for other stiffness parameters, are assumed (Olsson *et al.* 2013),
- when a value of E_{l} that should be valid for an examined board is determined it is assumed that the relationships between other board stiffness parameters (E_{r}, E_{t}, G_{lr}, G_{lt} and G_{rt}) and their corresponding nominal values ($E_{\mathrm{r,0}}$, $E_{\mathrm{t,0}}$, $G_{\mathrm{lr,0}}$, $G_{\mathrm{lt,0}}$ and $G_{\mathrm{rt,0}}$) are the same as the relationship between E_{l} and $E_{\mathrm{l,0}}$.
- fibre directions measured on the wood surface (Figure 1a) are located in the longitudinal−tangential plane of the wood material,
- the fibre direction coincides with the wood surface, *i.e.* the out of plane angle is set to zero, and

- the fibre direction measured on a surface is valid to a certain depth, which means that the fibre angle φ highlighted in Figure 1a, and the corresponding local MOE, *i.e.* $E_x(x,y,z)$, is assumed to be valid within the volume defined by the area dA (Figure 1b) times the length dx (Figures 1a and 1d).

On the basis of the described assumptions, the edgewise bending MOE of the segment shown in Figure 1d can be calculated by stiffness integration over the segment's cross-section. Information that originates from the dynamic excitation and weighing is used to get a value of E_l that is assumed to be representative for the board investigated.

Definitions of indicating properties

Three different IPs are defined and may be utilized for grading. The first one is suitable for prediction of the grade determining property ρ_{corr} and it is defined as

$$IP_{density} = \frac{m}{L \cdot h \cdot b}\left(1 - \frac{u_s - 12}{200}\right) \qquad (2)$$

where m is the mass [kg] of the board registered by the Precigrader, L, h and b [m] are the length, depth and thickness of the board registered by the WoodEye and u_s is the moisture content [%] measured by a device in the line of production or manually supplied by an operator. A value of u_s representative for the batch being graded is sufficient.

The second IP may be used for prediction of MOE and it is defined as

$$IP_{MOE} = 4\frac{m}{L \cdot h \cdot b} \cdot f^2 \cdot L^2\left(1 + \frac{u_s - 12}{100}\right) \qquad (3)$$

where f is the resonance frequency [Hz] corresponding to the first mode of axial vibration of the board determined by Precigrader and the other parameters are defined in the same way as for $IP_{density}$.

The third IP is used for prediction of bending strength, $f_{m,corr}$, and it can also be used for prediction of MOE. It is defined as

$$IP_{fb} = E_{b,90}\left(1 + \frac{u_s - 12}{100}\right) \qquad (4)$$

where $E_{b,90}$ is the lowest bending MOE over a 90 mm long section of the board determined on basis of information from WoodEye and Precigrader as described above and illustrated in Figure 1e.

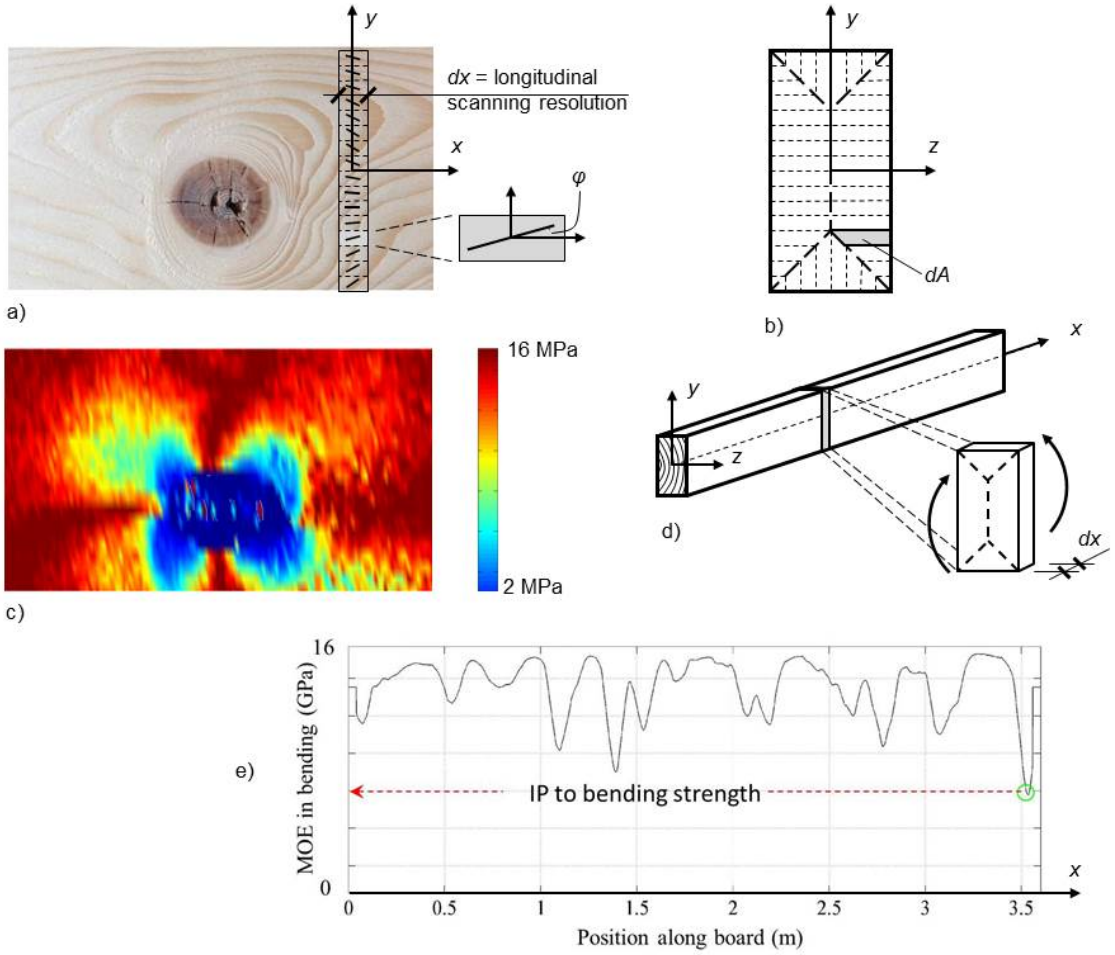

Figure 1 a) local fibre directions scanned on a member's surface by means of a row of laser dots, b) cross-section divided into sub-areas implying that the exhibited angle φ and corresponding MOE in the longitudinal direction, $E_x(x,y,z)$, is valid within the volume dA×dx, c) distribution of $E_x(x,y,z)$, d) segment of length dx for which the edgewise bending and axial MOE respectively is calculated by stiffness integration over the segment's cross-section, and e) a bending MOE profile, each value along the graph representing the average edgewise bending MOE of the surrounding 90 mm, and the lowest value along the profile defining the IP to bending strength. Figures 1a–d from Oscarsson *et al.* (2014). Figure 1e from Olsson *et al.* (2013).

Results

The relationships and coefficients of determination between IP_{fb} and $f_{m,corr}$, and between dynamic MOE, denoted as IP_{MOE}, and $f_{m,corr}$ are presented in Figure 2. For the relationship between IP_{fb} and $f_{m,corr}$ a linear regression coefficient of determination of 0.69 was achieved. For a slightly curved, exponential function for the relationship $R^2 = 0.70$ was reached. The linear regression coefficient of determination between IP_{MOE} and $f_{m,corr}$ was $R^2 = 0.53$. Table 2 shows the coefficient of determination between each of the grade determining properties and the indicating properties involved and Table 3 shows examples of yield in different strength classes when using different IPs or sets of IPs for assessment.

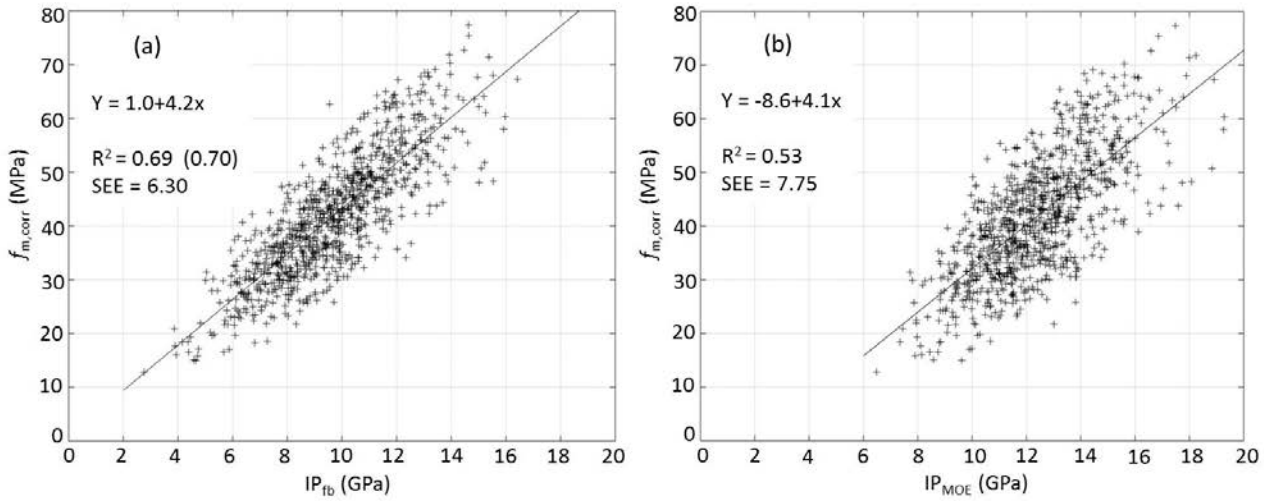

Figure 2 Scatter plots, lines of regression, coefficients of determination and standard error of estimates for the cases where (a) IP_{fb} and (b) IP_{MOE} are used as indication properties to bending strength, $f_{m,corr}$.

Table 2 Coefficient of determination, R^2, between grade determining properties and indicating properties.

R^2	$f_{m,corr}$	$E_{lokal,corr}$	$E_{global,corr}$	ρ_{corr}	IP_{fb}	IP_{MOE}	$IP_{density}$
$f_{m,corr}$	1	0.596	0.635	0.203	0.689	0.528	0.160
$E_{lokal,corr}$	0.596	1	0.833	0.316	0.730	0.681	0.273
$E_{global,corr}$	0.635	0.833	1	0.419	0.822	0.836	0.368
ρ_{corr}	0.203	0.316	0.419	1	0.333	0.526	0.838
IP_{fb}	0.689	0.730	0.822	0.333	1	0.836	0.300
IP_{MOE}	0.528	0.681	0.836	0.526	0.836	1	0.530
$IP_{density}$	0.160	0.273	0.368	0.838	0.300	0.530	1

Table 3 Examples of yield in strength classes using different IPs or sets of IPs.

Class or class combination	IPs used for prediction of grade determining properties / Yield (%)			
	IP_{MOE} [1)]	IP_{fb} [2)]	IP_{fb} & $IP_{density}$ [3)]	Ideal machine [4)]
C24	99,5	99,5	99,5	99,5
C30	95,4	96,4	96,8	97,1
C35	24,3	45,8	45,8	67,7
C40	14,5	27,9	30,3	45,4
C35	24,3	45,8	45,8	67,7
C18	75,2	53,6	53,6	31,7

1) IP_{MOE}, *i.e.* axial dynamic MOE, is used to predict all three grade determining properties

2) IP_{fb} is used to predict all three grade determining properties

3) IP_{fb} is used to predict $f_{m,corr}$ and $E_{global,corr}$, while $IP_{density}$ is used to predict ρ_{corr}

4) An imaginary machine able to predict all grade determining properties perfectly

Discussion and conclusions

The new strength grading method fulfils all the requirements laid down in EN 14081-2 and it has recently been approved for the European market. In the process for approval a timber sample of Norway spruce from Sweden, Norway and Finland was evaluated and the R^2 achieved between the IP to bending strength and the measured bending strength was as high as $R^2 = 0.69/0.70$, while the R^2 between dynamic MOE and measured bending strength was $R^2 = 0.53$. Although conclusions should always be draw with precaution when comparing coefficients of determination between IPs and grade determining properties of different timber samples, the results of this investigation indicates that the performance of the new method/procedure will surpass what is achieved by market leading techniques of today.

Regarding yield in strength classes the new method gives almost twice as high yield in high strength classes (C35 and above) than what grading methods based on dynamic MOE alone does.

References

Bacher, M. 2008. Comparison of different machine strength grading principles. COST E53, 29–30 October 2008, Delft, The Netherlands: 183–193.

Dynalyse AB (2015) Precigrader. http://dynalyse.se/precigrader/ (17 June 2015).

EN 338 (2009) Structural timber – Strength classes. European Committee for Standardization.

EN 384 (2010) Structural timber – Determination of characteristic values of mechanical properties and density. European Committee for Standardization.

EN 408 (2010) + A1 (2012) Timber structures – Structural timber and glued laminated timber – Determination of some physical and mechanical properties. European Committee for Standardization.

EN 14081-2 (2010) Timber structures – Strength graded structural timber with rectangular cross section – Part 2: Machine grading; additional requirements for initial type testing. European Committee for Standardization.

Hanhijärvi A.; Ranta-Maunus A. 2008. Development of strength grading of timber using combined measurement techniques. Report of the Combigrade-project – phase 2. VTT Publication 686.

Innovativ Vision AB (2015) http://woodeye.se/en/ (17 June 2015).

Microtec (2015) http://microtec.eu/ (17 June 2015).

Nocetti, M.; Bacher, M.; Brunetti, M.; Crivellaro, A.; van de Kuilen, J.-W. 2010. Machine grading of Italian structural timber: preliminary results on different wood species. Proceedings of the 11th World Conference on Timber Engineering, Trentino, Italy 2010:

Olsson, A.; Oscarsson, J.; Serrano, E.; Källsner, B.; Johansson, M.; Enquist, B. 2013. Prediction of timber bending strength and in-member cross-sectional stiffness variation on the basis of local wood fibre orientation. European Journal of Wood and Wood Products, 71(3): 319–333.

Oscarsson, J.; Olsson, A.; Enquist, B. 2014. Localized modulus of elasticity in timber and its significance for the accuracy of machine strength grading. Wood and Fiber Science, 46(4): 489–501.

Acoustic Velocity as Predictor of Strength Properties in Softwoods and Hardwoods Grown in Estonia

Taavi Korsar
Institute of Forestry and Rural Engineering, Estonian University of Life Sciences,
Kreutzwaldi 5, Tartu 51014, Estonia, taavi.korsar@gmail.com

Mirko Hani
Institute of Forestry and Rural Engineering, Estonian University of Life Sciences,
Kreutzwaldi 5, Tartu 51014, Estonia, mirko@streng.ee

Marko Teder
Institute of Forestry and Rural Engineering, Estonian University of Life Sciences,
Kreutzwaldi 5, Tartu 51014, Estonia, marko.teder@emu.ee

Abstract

The purpose of this study was to evaluate strength properties of timber using acoustical nondestructive methods. In this research ultrasound and stress wave methods were used to investigate the properties of timber, like bending strength and stiffness to find out which device is more reliable. The timber – Picea abies, Pinus sylvestris, Alnus glutinosa and Populus tremula – used in these experiments was cut from the forests of Estonia. All together 196 pieces with dimensions of 50x50x970…1100 mm were sawn from the collected material. The physical-mechanical properties of wood were determined in laboratory conditions according to standard practices. Acoustical measurements were performed in the longitudinal material directions. TICO Ultrasound Instrument fitted with 50 mm 54 kHz compressional wave transducers and Fakopp Microsecond Timer was used to conduct measurements.

Longitudinal measurements with alder characterized bending strength with r=0.59…0.60 and modulus of elasticity with r=0.81…0.82 and with aspen r=0.27…0.33 and r=0.48…0.59, respectively. In softwood, generally stronger correlations were found; longitudinal measurements with spruce characterized the bending strength with r=0.22…0.52 and the modulus of elasticity with r=0.55…0.86 and with pine r=0.73…0.74 and r=0.80…0.81, respectively.

Additionally, dynamic and static values of the modulus of elasticity were analyzed. The dynamic modulus of elasticity characterized static among hardwood samples R^2=0.28…0.65 and among softwoods R^2=0.44…0.79.

Keywords: stress wave timing, ultrasound, bending strength, modulus of elasticity

Introduction

When repairing buildings it is important to evaluate the physical state and strength of timber structures. Often there are situations where the timber elements need to be assessed on site and cannot be removed or sampled destructively and where visual assessment cannot be performed thoroughly. Thus we have got non-destructive acoustical methods as alternative to determine the strength properties of timber.

Sound and ultrasound are used rather widely, especially in sawmills, where the longitudinal measuring method is used to sort lumber into strength classes. Generally, sound consists of an elastic wave that propagates through material, its behaviour being different in various materials and or in different conditions within the same type of material. Consequently a correlation between the speed of sound wave and certain properties of a material as stiffness can be made (Lempriere 2002; Kettunen 2006). Ultrasound wave propagation is directly related to the elastic properties of the material through which it propagates. If wood is damaged, its stiffness is likely to decrease. Sound wave speed is a function of the square root of material stiffness. Lower speed or longer propagation times are generally indicative of poorer conditions in a sample (Drdácký, Kloiber 2006).

Generally, softwoods like spruce and pine are most widely used as structural timber in Estonia. However, hardwoods like alder (Alnus glutinosa) and aspen (Populus tremula) are also used in building structures, but not so widely and more in previous times. Still, there can be found timber buildings partly made of those mentioned species. Alder is widely known due to its good durability properties in wet conditions like in foundation piles, harbour docks and vessels (Klaassen 2008). Aspen was more used in walls and ventilated roof structures. Nowadays it is mostly used in buildings under renovation and restoration or in shingle roofs (Allikas and Kulbach 1962, Ussisoo and Veski 1943).

This study was aimed to test how well the mechanical properties correspond to acoustical ones. The relationship between ultrasound and stress wave timing velocities, the modulus of elasticity and the bending strength were investigated.

Materials and methods

All timber - Picea abies, Pinus sylvestris, Alnus glutinosa and Populus tremula - was cut from the same growth area located in the Southern part of Estonia. 96 (48+48) hardwood and 100 (50+50) softwood specimen with the dimensions of 50x50x970…1100 mm^3 were sawn from the collected material. The chosen dimensions were based on the standard EN 408:2010 (2010), which specifies that the length of the piece for the bending test should be at least 19 times of the height of the cross-section. The material was dried to the moisture content below 20% in a climate chamber. The experimental measurements were carried out in a laboratory at 21…23 °C and 20…40% relative humidity.

Two different devices - TICO Ultrasound Instrument (TUI) and Fakopp Microsecond Timer (FMT) - were used for acoustical measurements (Figure 1). TUI was fitted with 50 mm 54 kHz compressional wave transducers and the signal was induced to wood by equal hand-pressure. For better contact between the wood surface and the probes glycerine (propane-1,2,3-triol) was applied thinly onto the probes. This ensured effective transfer of the ultrasound wave between the surface of the sample and the probes. Before every test the measured length of the sample piece was entered into the device and the corresponding velocity reading in m/s was recorded. FMT is a portable microsecond stress-wave timer with two piezoelectric-type transducers equipped with 60 mm long nails. At the same time the nail performs as a wave guide and also fixes the transducer into the wood. The stress wave is induced by a simple hammer impact and the output is time of flight in microseconds between the transducers. Each sample was tested three times with both devices between the end surfaces in the longitudinal material direction (Figure 2).

Figure 1 - TICO Ultrasound Instrument with 50 mm 54 kHz compressional wave transducers (left) and Fakopp Microsecond Timer (right).

The bending strength of the test pieces was determined using an Instron 3369 device (Figure 2), based on standard EN 408:2010 (2010). According to this standard the sample was laid across two supports set 1000 mm apart and thereafter it was loaded with a static force at the center until failure. Here it should be noted that the force was applied in the tangential direction. Within this test the modulus of elasticity as well as the bending strength were measured.

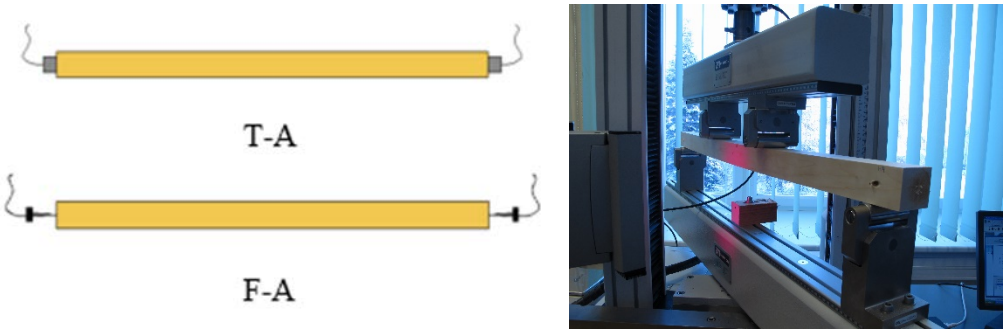

Figure 2 – Diagrams showing measuring methods applied with TICO Ultrasound Instrument (T-A) and Fakopp Microsecond Timer (F-A) (left) and 4-point bending test using Instron 3369 (right).

In order to define the moisture content of the samples, test pieces with dimensions of 50×50×50 mm^3 were sawn out from them. These pieces were weighed on an electronic scale with a readability of ±0.01 g and afterwards placed into a drying oven at a temperature of 103 ±2 °C. The pieces were dried until their differences of weighing at two-hourly intervals were less than 0.1% (EN 13183-1:2002). For determining the density, same test pieces were used. These were weighed on the same electronic scale and thickness, width and length were measured with a digital caliper (readability of ±0.01 m). The measurements were multiplied (EN 408:2010), and the density of wood was calculated according to ISO 3131: 1975 (1975).

After the experiments and based on the measured results the dynamic modulus of elasticity was calculated using the equation:

$$MoE_{dyn} = v^2 \cdot \rho \tag{1}$$

where MoE_{dyn} is longitudinal dynamical modulus of elasticity, v is longitudinal wave velocity, and ρ is bulk density of material.

All data processing was conducted by MS Excel and STATISTICA 10 software.

Results and discussions

The variability of density, bending strength and modulus of elasticity were regular and spread out, the variation was not mainly in one or the other end of extreme and was not closely clustered. Consequently, the experimental data were adequate to carry out the regression analysis (Table 1 and 2).

Table 1 - Characteristics of the statistical indicators of softwood specimen

Main indicators / Characteristics	Spruce (n=50)				Pine (n=50)			
	f_m (MPa)	MoE_{stat} (MPa)	MC (%)	ρ (kg/m^3)	f_m (MPa)	MoE_{stat} (MPa)	MC (%)	ρ (kg/m^3)
Mean	37.33	7821	14.17	426.9	52.36	10526	14.09	516.5
Median	36.64	7920	14.15	423.8	47.56	10569	14.01	506
Stan. deviation	14.85	1598	0.455	33	23.15	2489	0.533	76.28
Minimum	7.02	4291	13.22	379.4	8.22	6538	12.21	395.3
Maximum	66.27	11338	14.94	519.4	86.92	14667	15.39	711.1

Table 2 - Characteristics of the statistical indicators of hardwood specimen

Main indicators / Characteristics	Alder (n=48)				Aspen (n=48)			
	f_m (MPa)	MoE_{stat} (MPa)	MC (%)	ρ (kg/m^3)	f_m (MPa)	MoE_{stat} (MPa)	MC (%)	ρ (kg/m^3)
Mean	51.98	9516	13.60	517.8	61.43	11723	15.42	531.2
Median	56.45	9298	13.52	514.4	64.14	11923	15.05	530.7
Stan. deviation	13.72	1274	0.82	19.6	9.00	1023	1.42	20.8
Minimum	20.64	6667	11.92	487.2	40.30	9092	12.66	475.0
Maximum	72.10	11813	18.59	587.2	82.85	13985	20.72	581.4

While comparing the results of velocities acquired by different devices the variability among softwood specimen (Figure 3) is lower than among hardwood ones (Figure 4). The average speeds within softwood is between 5000 to 5500 m/s. Instead in hardwoods the average velocity is between 4500 to 5700 m/s. There is quite clear difference between the velocities in softwood samples.

Tables 3 to 6 show the correlation matrix between individual measured variables. Longitudinal measurements with alder characterized the bending strength with r=0.59…0.60 and the modulus of elasticity with r=0.81…0.82 and with aspen r=0.27…0.33 and r=0.48…0.59, respectively. In softwood, generally stronger correlations were found; longitudinal measurements with spruce characterized the bending strength with r=0.22…0.52 and the modulus of elasticity with r=0.55…0.86 and with pine r=0.73…0.74 and r=0.80…0.81, respectively. Other results with moisture content and density among all specimen tend to be rather floating and are not giving a clear tendency.

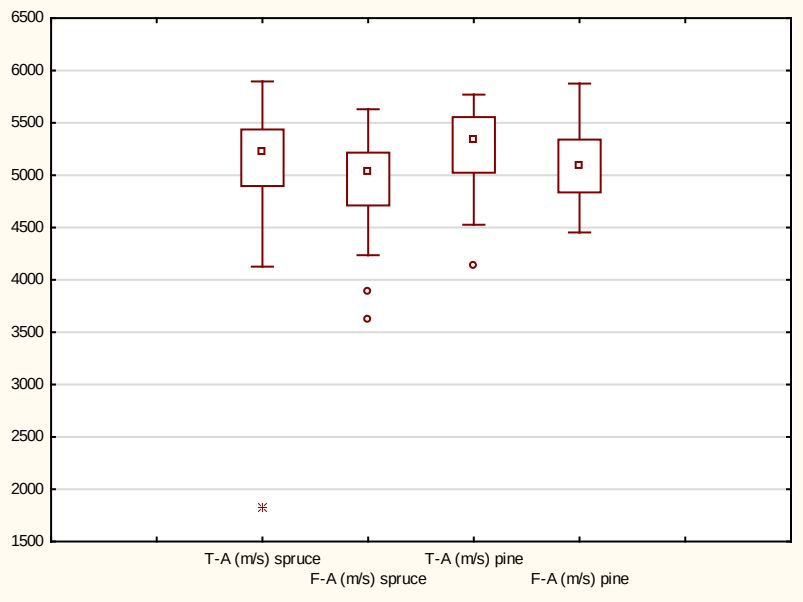

Figure 3 - Box plot charts of velocities for spruce and pine speciemen. T-A: measurements with TICO Ultrasound Instrument fitted with 50 mm 54 kHz compressional wave transducers; F-A: measurements with Fakopp Microsecond Timer.

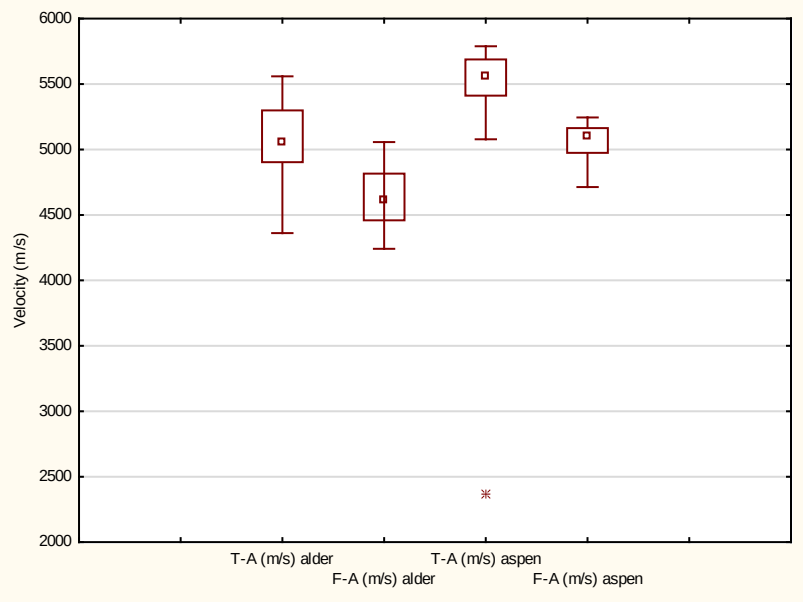

Figure 4 – Box plot charts of velocities for alder and aspen speciemen. T-A: measurements with TICO Ultrasound Instrument fitted with 50 mm 54 kHz compressional wave transducers; F-A: measurements with Fakopp Microsecond Timer.

Table 3 - The correlation matrix of characteristics of spruce samples (Correlation coefficient r)

Characteristic	T-A, m/s	F-A, m/s	f_m (MPa)	MoE_{stat} (MPa)
T-A, m/s	1			
F-A, m/s	0.57	1		
f_m (MPa)	0.22	0.52	1	
MoE_{stat} (Mpa)	0.55	0.86	0.76	1

Notes: figures marked light grey indicate a moderate relationship ($0.3 \leq |r| \leq 0.7$); figures marked dark grey indicate a strong relationship ($|r| \geq 0.7$).

Table 4 - The correlation matrix of characteristics of pine samples (Correlation coefficient r)

Characteristic	T-A, m/s	F-A, m/s	f_m (MPa)	MoE_{stat} (MPa)
T-A, m/s	1			
F-A, m/s	0.88	1		
f_m (MPa)	0.74	0.73	1	
MoE_{stat} (Mpa)	0.81	0.80	0.93	1

Notes: figures marked light grey indicate a moderate relationship ($0.3 \leq |r| \leq 0.7$); figures marked dark grey indicate a strong relationship ($|r| \geq 0.7$).

Table 5 - The correlation matrix of characteristics of alder samples (Correlation coefficient r)

Characteristic	T-A, m/s	F-A, m/s	f_m (MPa)	MoE_{stat} (MPa)
T-A, m/s	1			
F-A, m/s	0.83	1		
f_m (MPa)	0.60	0.59	1	
MoE_{stat} (Mpa)	0.82	0.81	0.76	1

Notes: figures marked light grey indicate a moderate relationship ($0.3 \leq |r| \leq 0.7$); figures marked dark grey indicate a strong relationship ($|r| \geq 0.7$).

Table 6 - The correlation matrix of characteristics of aspen samples (Correlation coefficient r)

Characteristic	T-A, m/s	F-A, m/s	f_m (MPa)	MoE_{stat} (MPa)
T-A, m/s	1			
F-A, m/s	0.63	1		
f_m (MPa)	0.27	0.33	1	
MoE_{stat} (Mpa)	0.48	0.59	0.80	1

Notes: figures marked light grey indicate a moderate relationship ($0.3 \leq |r| \leq 0.7$); figures marked dark grey indicate a strong relationship ($|r| \geq 0.7$).

The dynamic stiffness of wood prediction equations based on specific variables were examined. The variables (x) comprised acoustical velocities together with density according to the equation (1) (Tables 7 and 8). It can be concluded that the best prognosis of the static modulus of elasticity is given among softwoods, describing the variety of latter with ca 78…79% (except measurement T-A among spruce specimen). Lower results are with hardwood specimen, among alder the static modulus of elasticity is described with 63…65% and among aspen with 28…35%.

Table 7 – Predicting static modulus of elasticity (y) with different variables (x) individually among softwood samples

Species	Variable (x)	Regression equation	R^2
Spruce	MoE_{dyn} (T-A), MPa	y = 1,0021*x + 3243,7	0.44
	MoE_{dyn} (F-A), MPa	y = 0,9456*x + 3011,7	0.78
Pine	MoE_{dyn} (T-A), MPa	y = 1,2576*x + 1252,8	0.79
	MoE_{dyn} (F-A), MPa	y = 1,0898*x + 2038,1	0.79

Table 8 – Predicting static modulus of elasticity (y) with different variables (x) individually among hardwood samples

Species	Variable (x)	Regression equation	R^2
Alder	MoE_{dyn} (T-A), MPa	y = 1222,5 + 0,617*x	0.63
	MoE_{dyn} (F-A), MPa	y = 41,24 + 0,849*x	0.65
Aspen	MoE_{dyn} (T-A), MPa	y = 7767,3 + 0,247*x	0.28
	MoE_{dyn} (F-A), MPa	y = 1161,9 + 0,774*x	0.35

Conclusions

The main aim was to investigate the possibilities of applying acoustical measurements in assessment of the physical-mechanical properties of wood as bearing structure. For achieving this purpose two different devices - TICO Ultrasound Instrument fitted with 50 mm 54 kHz compressional wave transducers and Fakopp Microsecond Timer - were used. 96 hardwood and 100 softwood specimen were done for this study.

The analyses of the results using different measurement devices showed that Fakopp Microsecond Timer tend to be better as the correlation between the mechanical properties of wood and wave velocity were stronger, especially among softwood species. Further investigations with bigger cross-sectional dimensions are needed for the implementation of assessment of timber structures.

References

Allikas, L., Kulbach, V.1962. Puitkonstruktsioonid. Tallinn: Eesti riiklik kirjastus. 78 p.

Drdacky, M. F.; Kloiber, M. 2006. Non-destructive survey of historic timber. NSF/MŠMT supported US-Czech project and RILEM Workshop. Czech Republic.

EN 13183-1:2002. 2002. Moisture content of a piece of sawn timber - Part 1: Determination by oven dry method.

EN 408:2010. 2010. Timber structures - Structural timber and glued laminated timber - Determination of some physical and mechanical properties.

ISO 3131:1975. 1975. Wood – Determination of density for physical and mechanical tests. International Organization for Standardization. Switzerland.

Kettunen, O. P. 2006. Wood structure and properties. Switzerland: Trans Tech Publications Ltd. 401 p.

Klaassen, R. K.W.M.. 2008. Water flow through wooden foundation piles: A preliminary study, International Biodeterioration & Biodegradation, Volume 61, Issue 1: 61-68.

Lempriere, B. M. 2002. Ultrasound and elastic waves. USA: Academic Press. 241 p.

Ussisoo, T., Veski, A. 1943. Puit tarbematerjalina. Tartu: Trükikoda J. Mällo & Pojad. 172 p.

Influence of the moon phase on stress wave velocity and structural timber properties

Guillermo Íñiguez-González
Deparment of Forest and Environmental Engineering and Management, Escuela Técnica Superior de Ingeniería de Montes, Forestal y del Medio Natural, Universidad Politécnica de Madrid, Ciudad Universitaria s/n, 28040, Madrid, Spain. guillermo.iniguez@upm.es

María José Barriola
TKNIKA, Zamalbide Auzoa s/n, 20100, Errenteria, Gipuzkoa, Spain. mbarriola@tknika.net

Ernst Zürcher
Research Division Wood Engineering, Bern University of Applied Sciences BFH, Architecture, Wood and Civil Engineering AHB, Solothurnstrasse 102, CH-2500, Biel, Switzerland. ernst.zuercher@bfh.ch

Abstract

Traditional knowledge and some research works indicate that the date of tree felling (moon phase in addition to the season of the year) has an important influence on wood properties. Therefore, it is reasonable to think that variables obtained by nondestructive testing and related physical and mechanical properties could also be affected by this issue.

The objective of this research was to analyze this potential effect on stress wave velocity, density and mechanical properties (modulus of elasticity and modulus of rupture), by testing specimens felled at different moon phases.

The material studied involved 360 structural timber pieces obtained from 225 trees of Japanese larch (*Larix kaempferi* (Lamb.) Carr.) from Basque Country provenance. Trees were felled on moon`s waxing and waning phase (in two consecutive synodic lunar cycles), and processed in four sizes (from 70x150 mm to 200x250 mm). Additionally to the analysis of a possible influence of the moon phase on timber properties, linear regression models for estimation of mechanical properties by means of stress wave velocity are presented for this species.

Keywords: stress wave, structural timber, mechanical properties, moon phase

Introduction

The evaluation of material properties by means of nondestructive techniques is not a new concept. The fundamental hypothesis for the NDT of wood materials was initiated at 50`s. Since the first research works (Bell et al. 1950; Galiginaitis et al. 1954; James 1962; McKean and Hoyle 1962; Senft et al. 1962; Pellerin 1965) good methodologies results have been achieved.

Although it is relatively easy to conduct a NDT test, it is important to note that several factors affect NDT parameters. These factors can be divided into two categories: factors resulting directly from wood structure and properties, such as knot size, slope of grain, moisture content, etc. and, on the other hand, factors related to the test procedures and devices used, like transducer coupling, path length and the size and shape of specimens.

Thus, in order to gain uniform and reliable data and to develop procedures for the standardization of the NDT as predictors of structural timber properties, these factors have to be taken into account.

The influence of the moon on different wood properties is an ancient theme, as reflected by Theophrastus of Eresos (372-287 BC) in History of Plants (Vol 1, 3). He states that there is an appropriate season for cutting trees and (within the season) if cutting at the beginning of the waning moon, the wood is harder and less likely to rot. This popular knowledge has passed down to our times and to the local practices of felling trees during different moon positions depending on the specific forms of wood utilization (Zürcher 2000). There are even sawn wood producers that offer “moon wood” amongst their timber products.

Analyzing the influence of moon phase on the physical properties, researches have focused on the water loss during drying, on the calculated moisture content, the specific weight and the hygroscopic behavior (shrinkage) of wood. The importance of water as a decisive factor has been described in a diverging way in several studies (Seeling 1998, 2000, Bariska and Rösch 2000, Zürcher 2003, Ikeda 2006, Bues and Kretschmar 2008, Zürcher et al. 2010).

In the case of Norway spruce (*Picea abies* (L.) Karst.), Zürcher (Zürcher 2003, Zürcher et al. 2010) indicated significant relationships between the time of felling and the proportion of water lost during the drying process, while Seeling (2000) determined a significant difference of 6% in the dry density after the drying process, the denser samples being obtained from tree feelings in the waning moon phase..

The possible effect on density was also studied by Zürcher (Zürcher 2003, Zürcher et al. 2010, Zürcher et al. 2012) who detected a systematic change of this variable depending on the different moon phases. The results published in 2010 were based on samples from near 600 trees from four sites; the ones published in 2012 analyzed more in depth the properties on 144 of them, harvested in one of the four sites. However, other studies have found no relationship between all lunar phases with physical properties such as density or shrinkage (Villasante et al. 2010). It must be stressed out that in this last study four different dates in only one single lunar month were compared.

The influence of moon phase has been studied over Scots pine (*Pinus sylvestris* L.), sugi (*Cryptomeria japonica* (L. f.) D. Don) and Norway spruce (*Picea abies* (L.) Karst.), and very rarely in other species, as sweet chestnut (*Castanea sativa* Mill.) or oak (*Quercus humilis* Mill.). On the other hand, there is no evidence of any previous research on the influence of moon on values from nondestructive testing of structural timber sizes.

The objective of this research was to analyze this potential effect on stress wave velocity and linked mechanical properties, by testing structural specimens of Japanese larch (*Larix kaempferi* (Lamb.) Carr.) felled at different moon phases.

Material tested

The sample studied consisted of a total of 360 structural pieces obtained from 225 Japanese larch (*Larix kaempferi* (Lamb.) Carr.) trees from Basque Country provenance. Table 1 shows the number of specimens according to size (specimens were grouped into batches by cross section size).

Table 1— Number of specimens according to size.

Species	Batch	N pieces	Height (mm)	Width (mm)	Length (mm)
Larix kaempferi (Lamb.) Carr.	A	90	150	70	3000
	B	90	150	100	3000
	C	90	180	140	4000
	D	90	250	200	5000

Specimens were obtained from trees cut in two moon phases (waxing and waning moon) and two consecutive synodic lunar cycles (January and February, 2012), resulting 45 pieces by batch and moon phase. Additionally, up to four sawlogs were cut by tree so, specimens can also be grouped by different position in the trunk.

The test material presents random specimens of the population. The timber represents the timber source, sizes and quality that will be graded in production.

Methodology

Moisture content

The moisture content of specimens was evaluated using electrical resistance equipment, following the procedure defined in European standard EN 13183-2 (2002). Test pieces were conditioned at the standard environment of (20±2) ºC and (65±5)% relative humidity. The average moisture content measured is 17% (CoV: 17,4%).

Stress wave velocity

Stress wave velocity measurements were carried out in parallel (termed: longitudinal) to the grain on each piece. Measurements were carried out from end to end, taking one single reading in a central line of the specimen.

Equipment used to measure the stress wave velocity was the Microsecond Timer (MST), manufactured by Fakopp, in Hungary. In this equipment, the mechanical stress wave is induced by tapping one of the sensors by means of a hammer, and it then travels in a straight line to the opposite sensor. Equipment registers the time it takes the wave to pass between the two transducers. Pre-drilled contact holes are not necessary because this equipment has its transducers mounted directly on metal spikes, which provide direct contact points when the hammer is used to hit the transducers into the specimen.

As it is pointed out in the bibliography (Llana 2014), the moisture content of timber influences the propagation velocity of the wave. Therefore, this manufacturer recommends that when this equipment is used, velocity values should be corrected using the following ratio: for each 1% increase in moisture content there is a fall in velocity of approximately 1%. The values obtained and analyzed were corrected as explained.

The average stress wave velocity measured is 4.935 m/s (CoV: 5,9%). A multifactor analysis of variance (ANOVA Multifactor) was carried out in order to look for statistically significant differences by moon phase, cross section size and trunk position.

Density

As each piece of timber was weighed (a balance situated in one of the supports records the half mass), its global density was determined by dividing the total mass of each specimen by its volume. The result was then corrected to 12% of moisture content, according to EN 384 (2010), a 0,5% decrease in the density for each 1% increase in moisture content.

The mean density value for all species is 581 kg/m^3 (CV: 8,8%). Statistically significant differences were also analyzed.

Static modulus of elasticity and modulus of rupture

Finally, using destructive laboratory tests, the global elasticity modulus and bending strength of each specimen were obtained according to standard EN 408 (2010+A1:2012).

The static modulus of elasticity and modulus of rupture were measured using the European standard arrangement: the test piece was simply supported and symmetrically loaded in bending at the third points of a span of 18 times its depth, Figure 1.

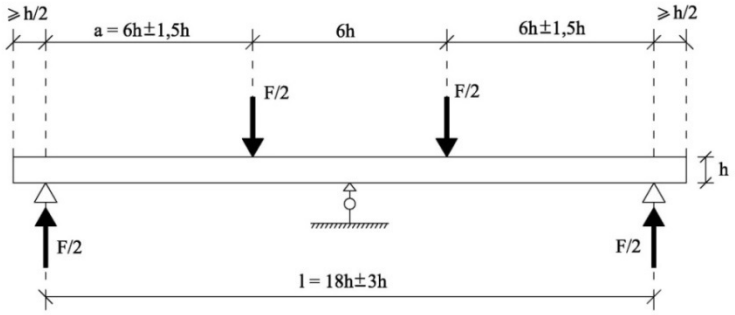

Figure 1— Arrangement for bending test according to European Standard EN 408 (2010+A1:2012).

Elasticity modulus values were adjusted to 12 % moisture content by the correction of standard EN 384 (2010), a 1% decrease in the elasticity modulus for each 1% increase in moisture content.

The mean values of the static modulus of elasticity and modulus of rupture are 11.564 N/mm^2 (CV: 16,3%), and 46,12 N/mm^2 (CV: 21,5%), respectively.

Results and discussion

Stress wave velocity vs. Moon phase

Multifactor analysis of variance (ANOVA Multifactor), carried out in order to look for statistically significant differences by moon phase, cross section size and trunk position in stress wave velocity, have been shown that clearly exists significant differences (p-value: 0,000) by trunk position, but do not exist for cross section size (p-value: 0,274).

Analyzing the hypothetic influence of moon phase, statistically significant differences were not found for stress wave within the complete sample, but a tendency according to the bibliography was found isolating the effect by cross section size and trunk position.

Physical and mechanical properties vs. Moon phase

On the other hand, when the influence of moon phase on density, MOE and MOR was evaluated, analyses of variance confirmed differences for density (p-value: 0,004). Statistically significant differences by moon phase were not found for MOE or MOR, but were found for cross section size and trunk position.

The tendency is for density to decrease in waxing moon. Means plot of one-way ANOVA analysis is shown in Figure 2.

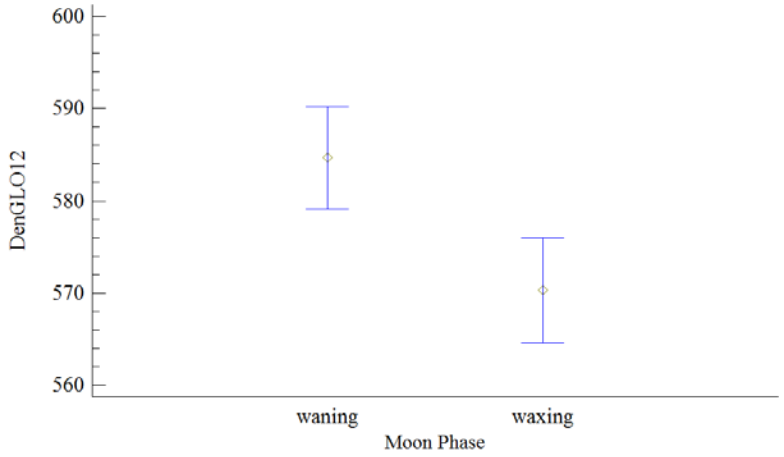

Figure 2— Means plot of global density by moon phase for the study sample.

Under the condition that the samples have been collected over two synodic lunar cycles, the statistical analysis indicates a significant difference of 2,52% in densities (being the samples obtained from the waning moon the denser ones). This observation is coherent with the published results in Seeling (2000), Zürcher (2003) and Zürcher et al. (2010 and 2012).

Static modulus of elasticity and modulus of rupture vs. longitudinal wave velocity

Using longitudinal wave velocity as a predictor of mechanical properties, the linear regression models which fitted are shown below, and the determination coefficients, R^2, obtained are 0,38 and 0,14, respectively.

$$MOE = - 8.148,07 + 3,9918 \cdot Vel_{EEmst12}$$

$$MOR = - 16,58 + 0,0127 \cdot Vel_{EEmst12}$$

Where:

MOE is the static modulus of elasticity adjusted to 12% moisture content, in N/mm^2.

$Vel_{EEmst12}$ is the longitudinal wave velocity adjusted to 12% moisture content and measured by the MST, in m/s.

MOR is the modulus of rupture, in N/mm^2.

Physical and mechanical properties of Japanese larch (*Larix kaempferi* (Lamb.) Carr.)

As part of the study carried out, physical and mechanical properties of Japanese larch were obtained. Not previous results of properties in structural sizes were available for this species till current research. Table 2 shows the physical and mechanical properties.

Table 2— Physical and mechanical properties of Japanese larch

Batch	N pieces	d_{mean} (kg/m^3)	E_{mean} (N/mn^2)	f_k (N/mn^2)
A	90	561	10.447	30,71
B	90	561	11.164	28,81
C	90	611	12.289	31,67
D	90	586	12.247	29,92

Where:

d_{mean} is the mean value of global density adjusted to 12% moisture content, in kg/m^3.

E_{mean} is the mean modulus of elasticity adjusted to 12% moisture content, in N/mm^2.

f_k is the characteristic value of modulus of rupture, in N/mm^2.

These results are coming for the mechanical characterization carried out in accordance with the methodologies and requirements of the European standards: EN 408 (2010+A1:2012), EN 384 (2010) and EN 338 (2009).

Conclusions

Comparative analyses of the variables measured were carried out to determine whether there are statistically significant differences between the moon phase, cross section size and trunk position. As result of these analyses, at times, significant differences were found for the variables studied.

For instance, when the influence of moon phase on density within groups was evaluated, analyses of variance showed a clear tendency and a significant difference of 2,52% in densities was found. Nevertheless, exits a big effect of cross section size and trunk position. Effects could not be isolated.

The ability of the stress wave velocity to act as a predictor of mechanical properties is well known and was confirmed in this research. Nevertheless, R^2 obtained were relatively low in comparison with other species and section sizes.

Results of physical and mechanical properties of Japanese larch presented adequate the use of Japanese larch as structural timber product.

The material tested in this study is insufficient to disaggregate the effects resulting of moon phase, cross section size and trunk position, but the authors believe that it would be necessary to carry out a more complete test program in order to verify the effect of moon phase in structural timber sizes.

Acknowledgments

D. Bixente Dorronsoro. Diputación Foral de Gipuzkoa. Donostia-San Sebastián.
Ministerio de Ciencia e Innovación: Proy.: BIA 2010-18858. Plan Nacional I+D+i 2008-2011.

SECOMA (Servicios Comerciales de la Madera de Guipuzkoa).
Maderas Larrañaga, Azpeitia.

References

Bariska, M.; Rösch, P. 2000. Felling date and shrinkage behavior of Norway spruce. Schweiz. Z. Forstwes. 151(11): 439-443.

Bell, E.R.; Peck, E.C.; Krueger, N.T. 1950. Young's modulus of wood determined by a dynamic method. Report 1775. Madison, WI: U.S. Department of Agriculture, Forest Service, Forest Products Laboratory.

Bues, C.T.; Kretschmar, K. 2008. Moisture content and insect infestation at timber of Norway spruce (*Picea abies* [L.] Karst.), which was harvested at specific moon phases. Forst. Holz. 63(9): 32-36.

European Standard EN 338: 2009. Structural timber. Strength classes.

European Standard EN 384:2010. Structural timber. Determination of characteristic values of mechanical properties and density.

European Standard EN 408:2010+A1:2012. Timber structures. Structural timber and glued laminated timber. Determination of some physical and mechanical properties.

European Standard EN 13183-2:2002. Moisture content of a piece of sawn timber. Part 2: estimation by electrical resistance method. European Committee for Standardization, Brussels, Belgium.

Galiginaitis, S.V.; Bell, E.R.; Fine, A.M. 1954. Nondestructive testing of wood laminates. Final Report. Louisville, KY: Office of Naval Research, Institute of Industrial Research, University of Louisville.

Ikeda, K. 2006. Green moisture content of sugi (*Cryptomeria japonica*) felled at the new of the moon and the full of the moon in every month. Bull. Shizuoka Prefecture Forestry Forest Prod. Res. 34: 25-30.

James, W.L. 1962. Dynamic strength and elastic properties of wood. Forest Products Journal. 12 (6): 253-260.

Llana, D.F.; Íñiguez-González, G.; Arriaga, F.; Niemz, P. 2014. Influence of temperature and moisture content on non-destructive measurements in Scots pine wood. Wood Research. 59 (5): 769 - 780.

McKean, H.B.; Hoyle, R.J. 1962. Stress grading method for dimension lumber. Special Tech. Pub. 353. Philadelphia, PA: American Society for Testing Materials.

Seeling, U. 1998. Doesn't non-wood shrink and burn?. AFZ/Der Wald, Allg. Forst Z. Waldwirtschaft Umweltvorsorge. 53(26): 1599-1601.

Seeling, U. 2000. Selected wood properties of Norway spruce *Picea abies* (L.) Karst and its dependence on the date of felling. Schweiz. Z. Forstwes. 151(11): 451-458.

Senft, J.F.; Suddarth, S.K.; Angleton, H.D. 1962. A new approach to stress grading of lumber. Forest Products Journal. 12(4): 183-186.

Pellerin, R.F. 1965. A vibrational approach to nondestructive testing of structural lumber. Forest Products Journal. 15(3): 93-101.

Villasante, A.; Vignote, S.; Ferrer, D. 2010. Influence of the Lunar Phase of Tree Felling on Humidity, Weight Densities, and Shrinkage in Hardwoods (*Quercus humilis*). Forest Products Journal. 60(5): 415-419.

Zürcher, E. 2000. Moon-related traditions in forestry and corresponding phenomena in tree biology. Schweiz. Z. Forstwes. 151(11): 417-424.

Zürcher, E. 2003. Drying and weathering behavior of Norway spruce *Picea abies* Karst wood felled according to moon phases. Schweiz. Z. Forstwes. 154(9): 351-359.

Zürcher, E.; Schlaepfer, R.; Conedera, M.; Giudici, F. 2010. Looking for differences in wood properties as a function of the felling date: lunar phase-correlated variations in the drying behavior of Norway Spruce (*Picea abies* Karst.) and Sweet Chestnut (*Castanea sativa* Mill.). Trees-Structure and Function. 24(1): 31-41.

Zürcher, E.; Rogenmoser, C.; Soleimany Kartalaei, A.; Rambert, D. 2012. Reversible Variations in Some Wood Properties of Norway Spruce (*Picea abies* Karst.), Depending on the Tree Felling Date. In: Spruce: Ecology, Management and Conservation. Eds. Nowak, K.I. and Strybel, H.F. Nova Science Publishers, Hauppauge, New York 2012; 75-94.

Grading of Parica Wood for Structural Purposes

Rodrigo Figueiredo Terezo
Forestry Department, Santa Catarina State University, Lages, Santa Catrina, Brazil, rodrigo.terezo@udesc.br

Carlos Augusto de Paiva Sampaio
Agronomy Department, Santa Catarina State University, Lages, Santa Catrina, Brazil, carlos.sampaio@udesc.br

Carlos Alberto Szücs
Civil Engineering Department, Federal University of Santa Catarina, Florianópolis, Santa Catarina, Brazil, carlos@szucs.com.br

Cleide Beatriz Bourscheid
Forestry Department, Santa Catarina State University, Lages, Santa Catrina, Brazil, cleidib@gmail.com

Talitha Rosa
Forestry Department, Santa Catarina State University, Lages, Santa Catrina, Brazil, rosa.talitha@gmail.com

Abstract

The planting of native species has been presented as an excellent alternative production for wood in the Amazon region. Among the various species planted, the parica (*Schizolobium amazonicum* Huber ex. Ducke) is among the first species exploited for such purposes. The aim of this study is to determine the modulus of elasticity (MOE) with different ages (6, 10, 19 and 28 years) by destructive and non-destructive testing, in order to identify its use in structures. In nondestructive testing, ultrasound equipment was used, according to NBR 15.521/2007 and destructive test was performed according to NBR 7.190/1997. The parica wood was graded as structural uses as much by the both methods. It was observe that according the NBR 7190/1997, the wood was grade as specie belonging to class strength C-20, since in the NBR 15.521/2007 the average was graded as C-30. It must be emphasized the possibility of using ultrasound as a classification tool, as well as the use of parica as structural timber.

Keywords: *Schizolobium amazonicum*, planted forest timber, non-destructive characterization.

Introduction

The Amazon rainforest is one of the largest suppliers of tropical native wood in the world market. However, due to a new commercial and environmental scenario that has been outlined for the planet, as well as by global pressures in order to preserve the Amazon rainforest, the planted forest with native species of rapid growth in the northern region of Brazil has shown as an economically viable alternative (TEREZO, et al.2010).

Although native species plantations have no tradition in Amazon region, planted forests are becoming more popular, showing potential as an alternative solution to the economic recovery of degraded areas is the use of fast growing species. This activity has been presented as an excellent alternative to production and marketing wood in the last twenty years in the Amazon region. Among the

various planted species, the paricá (*Schizolobium amazonicum* Huber ex. Ducke) is one of the pioneers (TEREZO, 2010).

The parica is considered a tall tree (20-30 mts of height). It occurs throughout Brazil, except in the Southern Region (CARVALHO and VIÉGAS, 2004). QUISEN et al. (1999) describe that the parica has vigorous inicial growth, reaching the age of 15 with 55 cm diameter at breast height (DBH), and approximately 150-340 m³ / hectare, depending on the planting density.

According to CORADIN et al. (1993), analyzing wood of native trees, the parica belongs to the *Leguminosae* family and *Caesalpinioideae* subfamily, with heartwood and sapwood slightly distinct, wood white color and indistinct growth rings. It is indicated for making essel, containers, pallets, toys, sporting goods and matchsticks. Its basic density is 490 kg / m³.

The use of wood in construction should be promoted considering its physical, mechanical and durability characteristics, defined in view of its final use, which involves technical classification standards that provide the product warranty.

The current technical standard in Brazil is the NBR 7190/97, Structural Design in Wood. This standard shows the test methods and dimensions of the test samples, which will determine the physical and mechanical wood properties. For the non-destructive testing of dicotyledons the standard is the NBR 15521/2007, Non-Destructive Testing - Ultrasound applied to the wood of dicotyledons. This standard specifies the requirements for use of ultrasound equipment in the wood and sets criteria for the evaluation of the resulting parameters of this application, aimed mechanical classification of sawn wood of dicotyledons, and can be used in laboratory conditions, sawmills and industry.

The mechanical classification may be performed by various equipment. This classification is to determine the longitudinal modulus of elasticity (MOE) of the blades through a non-destructive method. Among the methods used by companies and research laboratories the following are highlighted: (1) bending; (2) Machine Stress Rating - MSR; (3) Low frequency waves; and (4) ultrasound.

BUCUR (1995) defines that the ultrasound are mechanical waves inaudible by humans, being able to propagate through gases, liquid or solids. The frequency of oscillation of the particles is greater than 20,000 cycles per second (0.02 MHz) and lower than 100 million cycles per second (100 MHz). This frequency band is classified as ultrasound. According to MACHADO (2000), the frequencies most commonly used in wooden tests range from 20 kHz to 1 MHz.

The equipment basically consists of an issuing (generator transducer), where ultrasonic pulses are generated and transmitted; a receiver (receiving transducer), where the pulses are received; and a device to indicate the wave propagation time from the issuing transducer to the receiver transducer. SHAJI et al. (2000), explains that the ultrasonic pulse is generated by applying a rapid change of potential of a transducer plate for a piezoelectric transformer element that causes a known vibration frequency. The transducer is placed in contact with the material and this starts to receive vibrations. The vibrations pass through the material and are picked up by the receiver. The wave velocity is calculated using the pulse propagation time and distance between the transducers.

The aim of this study is to determine the elastic modulus (MOE) of parica wood of different ages through destructive and non-destructive testing, in order to use this in wood structures as well as their classification by ultrasound.

Materials and methods

The material of this research was parica wood, from planted forests from Pará State. The wood of trees aged 6 to 10 years were donated by plantations belonging to the company Tramontina S/A, in the city of Aurora do Pará. Trees of 19 and 28 years old were also donated from private plantations, belonging to Mr. João de Deus Francisco Neto, municipality of Tomé-açu.

The sampling of Aurora do Pará plantation was carried in two different reforestation areas. Eight trees were selected in each of five randomly-distributed samples within each area, thus totaling 80 trees in a population of 800 trees in the two different areas.

A random sampling of the research material was also conducted on the Tomé-Açu plantation. Due to the rapid growth of paricá, this plantation was created in order to protect cacao trees against the sunlight. Due to the large size of the trees of 19 and 28 years, five trees of each age were selected.

In the Aurora do Pará plantation, the logs were divided into small logs (short logs) of 2.5 m in length in order to be easily transported.

During the unfolding process, the bark is removed from the short logs and processed later into boards with thicknesses between 5 and 16 cm, with maximum optimization of the logs. For storage, the boards were stacked so that there was air circulation between them. In the drying process was expended 20 days to dry to 10% moisture. After this stage, it was noted that the woods without defects did not suffer warping and/or cracking. In order to facilitate removal of samples for laboratory tests the wood dried in kiln was sawn again. It were selected 13 trees of each age for the preparation of samples. The chosen boards had a thickness greater than or equal to 60 mm.

For the planting of Tomé-Açu, the logs transported to the mill of the company ARCA Lumber, were cut into short logs of 2.5 m and also sawn on the same day. Due to the highly favorable environment to fungi and drills, all the boards, after pick up the bark and offcuts, were immunized in tanks. The drying time was 15 days and it was held together with denser woods such as tauari (Couratari spp). The paricá boards were positioned in the central part of the dryer, which had a capacity of 100 m^3. Just a few defects were observed after drying. The wooden parts, after being sawn in band saw and subsequently dried, showed a wide variation in final dimensions. These imperfections did not allow the boards to be immediately flattened. In these cases, all wood boards were sawn again in a surfacer's machine.

Physical and mechanical characterization

The tests of physical and mechanical characterization of wood bundles followed the sampling criteria and test methods according to NBR-7190/97. Tests included: basic density; moisture content; and compression parallel to the fibers.

All samples were made from pieces of 250 cm in length, free from defects. The removal of the top 30 cm of each piece was done in order to avoid the influence of defects of fissure and cracks on the samples. Only the remaining central part of the pieces, with 190 cm long were used.

For parallel compression testing of fibers, it was used a universal testing machine Mohr & Federhaff®. It is a servo-hydraulic equipment in which are coupled, in addition to metallic devices for testing, electronic displacement transducers and load cell.

After storing all data in digital files, graphics tension-deformation were created and the maximum strain values were determined. The elasticity modulus values for the compression testings parallel to the fibers were also determined.

Non-destructive testing characterization

The propagation velocity of ultrasonic waves was measure in all the wood boards. The equipment used was the Sylvatest®. Has longitudinal wave transducer with conical shape and frequency of 30 kHz.

In this test, at first, the transducers were positioned on top, against each other to check the calibration of the equipment. Subsequently the transducers were placed on surface and on top of the boards. Four measures were performed on the surface of the board with distance of 1.50 mts between transducers. This measure was adopted so that possible defects on the top of the boards would not hinder the reading and to standardize the distance measured between samples.

The wave propagation is always given in the longitudinal direction of the board. Figure 1 illustrates the measurement points on the surface and the direction of wave propagation.

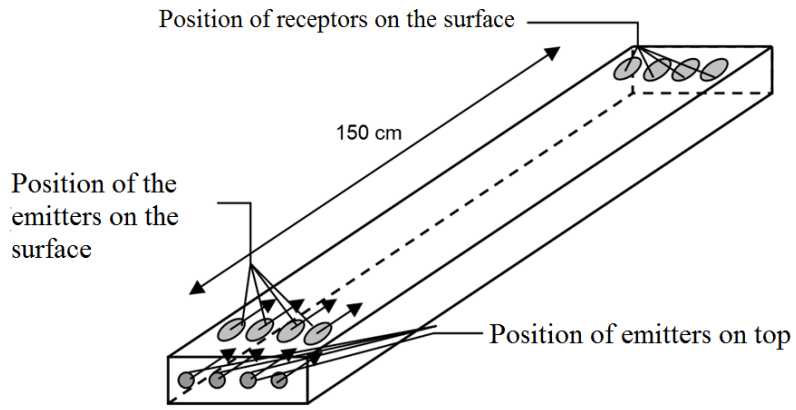

Figure 1 – Position scheme of the ultrasound transducers on the boards.

The classification of parts took place according to the recommendations of the current Brazilian standard, NBR-15521/2007 - Non-destructive testing - Ultrasound applied to wood of dicotyledons.

Also were performed measurements to determine the moisture content of each board of wood. This measurement was made through the application of a resistive hygrometer.

According to NBR 15521/2007, the wood moisture content significantly affects the results of the wave propagation speed in the longitudinal direction (V_{LL}), the speed intervals corresponding to the classes were developed based on saturated condition, so it is essential to determine moisture content of each board and perform V_{LL} correction whenever the wood moisture present less than 30% and more than 12%. The moisture contents found in the boards under consideration, using a resistive hygrometer, were averaged 15%, so the correction of the found values was performed. To according the NBR - 15521/2007 it must apply Eq. (1).

$$V_{LL_{SATURADA}} = -1745 + V_{LL} + 16xU + \rho_{ap} \qquad (1)$$

Where $V_{LL\ Saturada}$ = longitudinal speed in saturated board with humidity above 30% (m/s); V_{LL} = longitudinal velocity in board with humidity between 12% and 30% (m/s); U = wood moisture content (%) ρ_{ap} = apparent wood density (kg/m³).

Ranges of classification

With the average values of the velocities of wave propagation in the longitudinal direction, determined by Eq. (1) for the boards of wood in the saturated condition, it was used the classification table (Table 1) contained in NBR - 15521/2007.

Table 1 - Ranges of classification based on the saturated Speed Class chassis. Adapted from NBR - 15521/2007.

Class	V_{LLsat} (m/s)	E_M 12% (MPa)	$f_{c0,k}$ 12% (MPa)	$E_{c0,m}$ 12% (MPa)
UD - 20	V_{LLsat} < 3040	> 6750	20	8000
UD - 25	3040 - 3690	6750 – 10420	25	12000
UD - 30	3690 - 3950	10420 – 13020	30	14000
UD - 35	3950 - 4140	13020 – 14920	35	15000
UD - 40	4140 - 4300	14920 – 16520	40	16500

UD - 45	4300 - 4390	16520 – 17420	45	18500
UD - 50	4390 - 4490	17420 – 18420	50	19500
UD - 55	4490 - 4600	18420 – 19120	55	20500
UD - 60	V_{LLsat} > 4600	E_M > 19120	60	21200

$V_{LL\ Sat}$ = longitudinal speed in saturated piece with humidity above 30% (m/s); E_m = modulus of bending strain; $f_{c0,k}$ = characteristic compressive strain parallel to the fibers; $E_{c0,m}$ = modulus of compression parallel to the fibers

Processing data

Simple random

It refers to the sampling process used in the research, which is the choice and the number of trees to be felled and it is traditionally been used in forest inventories. The method adopted was the fully randomized.

A fully randomized is a congruent process, recommended for small forest areas with homogeneous characteristics with respect to the variables of interest, with easy accessibility framework.

Weibull statistical treatment

This treatment was used for the analysis of classification test plots by means of ultrasound. The frequencies found in each class have shown that tended to cluster data asymmetrically. In this case, it was used the Weibull method for the determination of mean values and standard deviations. To obtain the average in the distribution of Weibull should employ Eq. (2):

$$\overline{U} = \eta\Gamma\left[1+(1/\beta)\right] \qquad (2)$$

Where Γ = gamma function, determined by the value of β inverse factorial.

The value of the variance for the Weibull distribution is given by Eq. (3):

$$s^2 = \eta^2\left\{\Gamma\left[1+(2/\beta)-\Gamma^2\left[1+(1/\beta)\right]\right]\right\} \qquad (3)$$

Determinated the mean values and variances, were made the classification of each batch of wood. Later, the equality test between means were applied. For this study it was necessary to verify that the lots had their standard deviations equivalent. For this also was employed the Cochran test. Subsequently, there was checked significant existence between batches through variability of observations between groups. At the end were analyzed the variability of means and the significant difference of means between lots, through Duncan Test. The significance level used for all analyzes of this phase of the research was 5%.

Results and discussion

Sampling

The sampling carried out in planting 400 trees of 6 years and another 400 trees of 10 years, that was significant with an estimated error below 20%. This estimate only was possible to be calculated because in this planting were made annual measurements on the development of the same.

For sampling of the trees of 19 and 28 years old it was not possible to perform the determination of sampling errors and coefficients of variation, since there was no control over the development of trees as well as the total amount of the trees planting. It was used 8 trees by wich age.

Physical and mechanical characterization

Using the recommendations of the NBR-7190/97 to determine the physical and mechanical properties of wood lots, the results for the parica specie in four ages were obtained, as shown in Table 2.

Table 2 - Values of physical and mechanical properties of parica at different ages.

Properties		6 years old	-	10 years old	-	19 years old	-	28 years old	-
		Value		Value		Value		Value	
Density	Average	327,99 kg/m³		347,47 kg/m³		272,87 kg/m³		296,26 kg/m³	
	S.D.	45,75		39,94		32,21		48,24	
	C.V	13,95		11,49		11,81		16,28	
Properties		**6 years old**		**10 years old**		**19 years old**		**28 years old**	
		Resistance	**Modulus E**	**Resistance**	**Modulus E**	**Resistance**	**Modulus E**	**Resistance**	**Modulus E**
Parallel Compression	Charact	22,90 MPa		20,05 MPa		21,40 MPa		22,08 MPa	
	Average	30,84 MPa	11.418,09 MPa	30,03 MPa	10.479,19 MPa	26,96 MPa	11.751,65 MPa	29,46 MPa	10.582,63 MPa
	S.D.	4,66	2.309,00	5,53	1.869,49	4,72	2.100,83	5,02	2.222,20
	C.V	15,11 %	19,64 %	18,42 %	17,29 %	17,51 %	17,56 %	17,04 %	20,60 %

Charact - Characteristic values to 12% humidity; Average - Mean values at 12% humidity; S.D. - standard deviation; C.V. - Coefficient of Variation; N - samples number. * Adapted specimen of NF B 5-32.

The results of the Table 2 show that the wood of parica, regardless of age, can be termed as dicotyledon C-20 class, because it meets the requirements specified in item 10.6 of NBR-7190/97, where is deemed the characteristic value of strain to compression parallel to the fibers and the respective average elastic modulus, both at 12% moisture content. Thus, it becomes possible to use as a structural element.

Non-destructive testing characterization

Table 3 shows the average values of the speed of propagation of the ultrasonic wave on the saturated condition in each batch of wood and their respective strain class according to NBR 15521/07.

Table 3 - Mean values of the propagation speed of the ultrasonic wave and strain classes of lots of paricá according to NBR-15.521/07.

Reading	Age	Average Weibull (m/s)	Resistance Class	f_{c0} (MPa)	$E_{c0,m}$ 12% (MPa)
Surface	06 anos	4073	UD-35	35	15000
	10 anos	3881	UD-30	30	14000
	19 anos	4051	UD-35	35	15000
	28 anos	3626	UD-25	25	12000
Top	19 anos	4137	UD-35	35	15000
	28 anos	4073	UD-35	35	15000

f_{c0} = compressive strain parallel to the fibers; $E_{c0,m}$ = modulus of compression parallel to the fibers

It is observed that strains determined for compression parallel to the fibers are upper than medium and characteristic values found in destructive characterization tests (Table 2). Based on these results, only the batch of wood of 28 years, with reading measured on the surface, would be framed in the class C-20 NBR-7190/97, all the other, regardless of ultrasound scanning position, are classed in Class C -30 NBR 7190/97. However, these results are lower than the characteristic strain values to bending (Table 2), except for the value of top to top in woods with 28 years.

It is suggested, for parica wood, the use of a new constant in the equation of saturated longitudinal velocity in the NBR-15521/07 (Eq. (1)), so that it will have values near the destructive characterization tests.

Table 4 shows the values of constants for each lot and for each reading position of the wave propagation speed. These values were obtained based on the average values determined in non-destructive testing and in the determination of the physical properties of the lots. It is also suggests applying a constant with a value of 2,690 (Eq. (4)) for measurement performed on the surface, and 2,900 for readings made at the top of the pieces of parica (Eq. (5)).

$$V_{LL_{SATURADA}} = -2.690 + V_{LL} + 16U + \rho_{bas} \quad (4)$$

$$V_{LL_{SATURADA}} = -2.900 + V_{LL} + 16U + \rho_{bas} \quad (5)$$

Where V_{LL} Saturada = longitudinal speed in saturated piece with humidity above 30% (m/s); V_{LL} = longitudinal velocity in piece with humidity between 12% and 30% (m/s); U = wood moisture content (%) ρ_{ap} = apparent wood density (kg/m³).

Table 4 - Values of the constant used in determining V_{LL} sat for wood parica.

Reading	Age	V_{LL} ave (m/s)	ρ_{bas} kg/m³	humid %	Constant
Surface	06 anos	5314	328	15,49	2849,84
	10 anos	5102	347	14,93	2647,88
	19 anos	5347	273	16,93	2850,88
	28 anos	4898	296	16,58	2419,28
					2691,97
Top	19 anos	5433	273	16,93	2936,88
	28 anos	5345	296	16,58	2866,28
					2901,58

V_{LL} ave = average speed of wave propagation in the longitudinal direction; ρ_{bas} = basic density.

Although some batches were classified into distinct classes, as the differences were analyzed between the average values of saturated longitudinal velocity, there is an equality between batches with 95% confiability, for both kinds of reading. This reveals uniformity in the readings of the propagation speed regardless of the age of the trees.

For BUCUR (1995), the velocities of the waves with frequencies near 100 kHz may suffer dispersion and an increase in frequency, which also produces a significant increase in velocity in the longitudinal direction.

It is noteworthy that the database of ultrasound tests of NBR 15,521 / 2007 was carried out with use of pure longitudinal waves, ie, by propagation of waves obtained top to top.

It is noted that for the mechanical classification of parica by means of ultrasound was estimated in a smaller strain class (from 25 MPa to 35 MPa). In this sense, it is recommended to change the constant of Eq. (1) NBR 15521/07 when it use ultrasound and resistive hygrometer for this species, as well as the frequency of 33 kHz. Thus, one can get values closer to the strength class determined by means of tests of NBR 7190/97, which are employed in the design criteria of structural elements of wood.

Conclusions

In nondestructive classification model, which had reference in the NBR 15,521 / 2007, it used the acoustic emission equipment Sylvatest®, with frequency 33 kHz, and resistive hygrometer for

determining the moisture content. All parts of the lots were evaluated. Of the result set, it has the following conclusions:

- Based on these results, only the batch of wood with 28 years, with reading measured on the surface, would be framed in the class C-20 NBR-7190/97, and the others, regardless of ultrasound scanning position, in Class C-30 NBR 7190/97.
- It is suggested, for parica wood, the use of a new constant in the equation of saturated longitudinal speed on the NBR 15,521 / 2007, with a value of -2690 for readings taken at the surface, and -2900, for readings taken in top of the parica wood pieces, in order to have values near the destructive characterization tests.
- Was observed an equality between batches with 95% confiability, for both readings, on the surface and on the top. This reveals uniformity in the readings of the propagation speed regardless of the age of the trees.

It is noted the possibility of use of ultrasound as a classification tool, requiring an adjustment in the equation for determining velocity for the parica wood.

Finally, it can be concluded that the use of parica wood is possible, from planted forests in the Amazon region, in structural elements for construction.

References

Associação Brasileira de Normas Técnicas, ABNT, NBR 7190 - Projeto de Estruturas de Madeira. Rio de Janeiro, 1997. 107 P.

Associação Brasileira de Normas Técnicas, ABNT, NBR 15.521 - Ensaios Não Destrutivos - Ultrassom Aplicado à Madeira de Dicotiledônea. Rio de Janeiro, 2007.

Bucur, Voichita. Acoustics of Wood. Florida: CRC Press, 1995. 271 P. ISBN: 0-8493-4801-3.
Carvalho, J. G. De; Viégas, I. De J. M. Caracterização de Sintomas de Deficiências de Nutrientes em Paricá (Schizolobium Amazonicum Huber Ex. Ducke). Embrapa. Circular Técnica, N. 37, Belém, 2004. 6 P.

Coradin, V.T.R.; Camargos, J.A.A.; Marques, M. H.; Caracterização Tecnológica de Madeiras Denominadas Fava e/ou Faveira. Ibama. Brasília, 1993. 90p. ISSN 0104.1975.

Machado, José Maria S. R. S. Avaliação da Variação das Propriedades Mecânicas de Pinho Bravo (Pinus Pinaster Ait.) por Meio de Ultra-Sons. 2000. 199 F. Tese (Doutorado em Engenharia Florestal) – Instituto Superior de Agronomia, Universidade Técnica de Lisboa, Lisboa, 2002.

Quisen, R. C.; Rossi, L. M. B.; Vieira, A. H.; Teixeira, C. A. D. Bandarra: Essência Florestal de Rápido Crescimento. (Embrapa – Boletim Técnico). Brasília, 1999.

Shaji, T.; Somayaji, S.; Mathews, M. S. Ultrasonic Pulse Velocity Technique for Inspection and Evaluation of Timber. Journal of Materials in Civil Engineering, V. 12, N. 2, Maio 2000.

Terezo, R. F. Avaliação Tecnológica do Paricá e seu Uso em Estruturas de Madeira Laminada Colada. Tese (Doutorado em Engenharia de Estruturas) – Universidade Federal de Santa Catarina, Florianópolis, 2010.

Terezo, R. F.; Pigozzo, R. J. B.; Szücs, C. A. Estudo das Dimensões das Fibras do Lenho de Paricá com Idades de 6, 10, 19 E 28 anos. In: Xii Encontro Brasileiro em Madeira e em Estrutura de Madeira, 2010, Lavras, MG. Anais... Lavras: UFLA, 2010. 1 CD-Rom.

Strength grading of Turkish black pine (*Pinus nigra var. pallasiana arnold.*) structural timber by visual evaluation and nondestructive testing

Türker Dündar
Forest Industry Engineering – Faculty of Forestry - University of Istanbul, Bahcekoy, 34473, Sariyer, Istanbul, Turkey, dundar@istanbul.edu.tr

H. Volkan Görgün
Forest Industry Engineering – Faculty of Forestry - University of Istanbul, Bahcekoy, 34473, Sariyer, Istanbul, Turkey, volkan.gorgun@istanbul.edu.tr

Abstract

The objective of this study is to determine the compatibility between the visual strength grading and the mechanical strength properties performed by using nondestructive and destructive test methods in Turkish black pine (Pinus nigra var pallasiana Arnold.) structural timbers. Fifty three structural timbers were graded with three different visual strength grading standards; TS 1265, DIN 4074, and BS 4978. Dynamic modulus of elasticity (MOEd) was determined by using of longitudinal vibration non-destructive test method. Then, the static modulus of elasticity (MOEs) and the modulus of rupture (MOR) were determined on the timbers in structural size in accordance with EN 408.

The results indicated that the visual strength classes determined by using BS 4978 standard showed the best compliance with the MOEd determined by longitudinal vibration and the MOEs and MOR determined by destructive test. In general, the MOEd, MOEs, and MOR values of lumber were increased with increasing visual grading class for all standards used in this research. The differences in MOEd and MOEs values among the grading classes were found significant ($p<0.05$) for only BS 4788. However the differences in MOR values of lumber among the grading classes were found significant for all standards used. There were strong correlations between MOEd and MOEs ($R^2=0.86$) and MOR ($R^2=0.62$). The results showed that MOEd determined by longitudinal vibration nondetructive test can be used for strength grading of structural lumber instead of MOEs obtained from conventional bending test.

Keywords: nondestructive testing, visual grading, longitudinal vibration, dynamic modulus of elasticity, structural lumber.

Introduction

Regardless of species and size, lumber even if sawn from the same log, may show great variations in physical and mechanical properties due to its fibrous structure and the presence of irregularities. This is especially important for structural applications where the engineers are often frustrated with the performance variability found in structural members. Therefore, lumber used for structural applications must be graded and clearly marked to show it complies with the correct standards and strength requirements laid down by building codes and regulations.

Strength grading of structural lumber is a process by which lumber is sorted either by visual inspection or machine strength grading into strength classes- or strength grades- with ideally, similar structural properties in each group. In visual stress-grading, the lumber is sorted into groups based on the occurrences of strength-reducing features such as knots, slope of grain and splits. Machine strength grading is based on the relationship between the stiffness and strength properties of a lumber specimen. Machine-stress-rated (MSR), machine-evaluated-lumber (MEL), and E-rated lumber are three types of machine-graded lumber (Kretschmann and Green 1999). Machine-graded lumber allows for better sorting

of material for specific applications in engineered structures.

Vibration methods to predict static properties have been investigated since 1950s (Kitazawa 1950; Bell et al. 1950; Fukada 1950; Jayne 1959; Matsumoto 1962). As a potential lumber grading method, the transverse vibration testing technique measures natural frequencies of the vibration in a very short time, which in turn provides the MOE of the test material since the natural frequencies of a member are governed by its MOE and other easily measured parameters of test specimens (Ross and Pellerin 1994). The use of vibration techniques in lumber grading has evolved considerably, especially in the past several years. Jayne (1959) designed and conducted one of the first studies that utilized transverse vibration techniques for evaluating the strength of wood. The relationship between dynamic E and static E was further validated and improved (Jayne 1959; James 1964; Pellerin 1965). Static and dynamic MOE relationship was investigated by number of papers which good correlations have been reported between the two MOE values (Ross and Pellerin 1994; Divós and Tanaka 2005). The compliance between the visual strength grading and the mechanical properties has been also investigated by numerous researcher (Baltrušaitis and Pranckevičienė 2003, Piazza and Riggio 2008, Srpcic et al. 2010, Casado et. al. 2010, Vega et al. 2011).

The objective of this study is to determine the compatibility between the visual strength grading and the mechanical properties determined by using nondestructive and destructive test methods in Turkish black pine (*Pinus nigra* var *pallasiana* Arnold.) structural timbers. The specific objectives are (1) to examine the relationships between visual strength grading and dynamic modulus of elasticity (MOEd) determined by longitudinal vibration test (2) to examine the relationships between visual strength grading and static modulus of elasticity (MOEs) and modulus of rupture (MOR), (3) to compare the different visual strength grading standards in terms of their strength grading success and (4) to determine the relationships between MOEd and MOEs and MOR.

MATERIAL AND METHODS

In this study, 53 structural lumber of Black Pine (Pinus nigra spp.) in air-dry condition with the dimension of 6×8-10 cm (width×depth) and 2-m-length were used. The moisture content of the lumbers was measured using electrical resistance equipment by following the procedure defined in the EN 13183-2 standard. The average moisture content of the lumbers was determined as 15.4%.

The lumbers were first graded by visual inspection in accordance with three different visual strength grading standards; TS 1265 (Turkish), DIN 4074 (German), and BS 4978 (English). Table 1 shows the grading classes of these standards.

Table 1—Visual Grading Classes of the standards

Standards	**Classes (Best to worst)**			
TS 1265	I.	II.	III.	Out of grade
DIN 4074	S13	S10	S17	Out of grade
BS 4978	SS	GS	-	Out of grade

Following the visual examination, dynamic modulus of elasticity (MOEd) was determined by using of longitudinal vibration non-destructive test method. This method is based on measuring the resonance frequency of longitudinal vibration produced by the impact at one end of the piece, which crosses in its entirely. The test setup is represented in Figure 1.

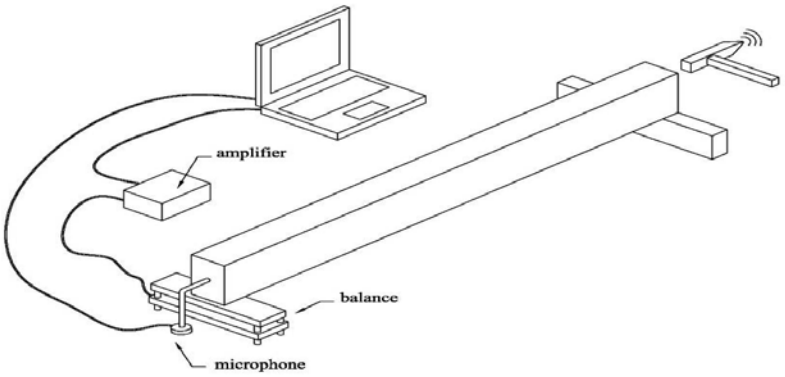

Figure 1— Longitudinal vibration test method with Portable Lumber Grader (PLG) of Fakopp.

Portable Lumber Grader (PLG) developed by Fakopp Enterprise was employed in order to determine MOEd of the timbers nondestructively. In the test procedure the specimens are placed on two supports with soft polyurethane pillows to ensure test pieces are free of vibration. One of these is simultaneously supported and balanced, recording the half mass of each piece. The end of a specimen is hit by a hammer and the impact induces a stress wave of longitudinal vibration caught as sound by a microphone set close to the other end of the test piece.

Using the specimen's mass (m, in kg), width (w, in m), length (l, in m), height (h in m), and the longitudinal vibration× frequency (f, in Hz), MOEd (in N/mm^2) is calculated with the following equation:

$$MOEd = \frac{m}{lwh}(2fl)^2 \tag{1}$$

After the vibration test, the static modulus of elasticity (MOEs) and the modulus of rupture (MOR) were determined on the timbers in structural size in accordance with EN 408 (Figure 2).

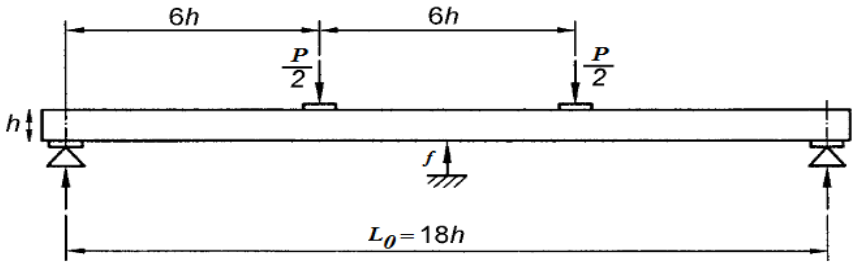

Figure 2— Static Four Point Bending Test Arrangement According to EN 408

Tests were carried out with the universal testing machine which was equipped with load cell of 100 kN. Global static modulus of elasticity (MOEs) was calculated as follows:

$$MOEs = \frac{L_0{}^3.(P_2 - P_1)}{b.h^3.(f_2 - f_1)}.\left[\left(\frac{3a}{4L_0}\right) - \left(\frac{a}{L_0}\right)^3\right] \tag{2}$$

where: *MOEs*: Destructive - static modulus of elasticity (N/mm^2)
L_0: Effective span distance (mm)

P_1-P_2: %10 and %40 of maximum load (N)
f_1-f_2: Deflection at %10 and %40 of Maximum Load (mm)
b: Width (mm)
h: Height (mm)
a: Distance between loading point and nearest support point (mm)

Modulus of rupture (MOR) was calculated as follows:

$$MOR = \frac{a.P_{\max}}{(b.h^3/12)} \quad (2)$$

where: MOR: Destructive and static bending strength (N/mm^2)
a: Distance between loading point and nearest support point (mm)
P_{max}: Maximum load (N)
b: Width (mm)
h: Height (mm)

In order to analyze the obtained data, first the percentages of the lumber sorted into each strength class according to different visual grading standards were compared each other. Than the relationships between the following parameters were examined; (1) visual strength classes vs. MOEd, (2) visual strength classes vs. MOEs and MOR, (3) MOEd vs. MOEs and MOR. The strength grading success of different visual grading standards were evaluated in consideration of the grading class-strength and stiffness relationships.

RESULTS AND DISCUSSION

The results of the visual strength grading of the lumbers according to three standards from different country are shown in Table 2. The lumbers graded according to TS 1265 took place mostly in high strength class while the lumber graded according to DIN 4074 and BS 4978 took place in a high proportion of medium strength class. The highest frequency of below-grade-lumber was found in grading according to BS 4978 while the lowest frequency was found for TS 1265. DIN 4074 showed the lowest frequency of high strength class lumber.

Table 2— Results of the Visual Strength Grading of the Lumbers According to Different Standards

Standard	Class	Frequency	Percentage
TS 1265	I	20	37.8
	II	15	28.3
	III	14	26.4
	Below grade	4	7.5
	Total	53	100.0
DIN 4074	S13	4	7.5
	S10	23	43.4
	S7	16	30.2
	Below grade	10	18.9
	Total	53	100.0
BS 4978	SS	15	28.3
	GS	24	45.3
	Below grade	14	26.4
	Total	53	100.0

Table 3 summarizes the average values of MOEd determined by longitudinal vibration nondestructive test and MOEs and MOR obtained from static bending test for grading classes of the standards. ANOVA was applied for investigating the compatibility between the mechanical properties and the grading classes of the

standards. The same letter on the numbers showed homogeneity groups for each standard. It was noted that the ANOVA was applied separately for each standard.

Table 3—Non-destructive and Destructive Tests Results

Standard	Class	MOEd (GPa)	MOEs (GPa)	MOR (MPa)
TS 1265	I	14,065 (3,23)[a]	13,259 (3,02)[e]	76,62 (14,17)[i]
	II	12,479 (2,67)[a]	12,031 (2,76)[e]	64,76 (18,92)[i]
	III	12,593 (1,70)[a]	12,706 (2,00)[e]	55,63 (17,27)[j]
	Below grade	12,527 (3,71)[a]	10,961 (2,79)[e]	57,31 (20,29)[i,j]
DIN 4074	S13	15,571 (3,48)[b]	14,579 (3,19)[f]	87,00 (6,99)[k]
	S10	12,973 (2,63)[b]	12,569 (2,75)[f]	68,65 (14,09)[l]
	S7	13,376 (2,56)[b]	12,968 (2,25)[f]	62,45 (21,39)[l]
	Below grade	12,022 (3,05)[b]	11,244 (2,80)[f]	58,56 (21,00)[l]
BS 4978	SS	15,420 (2,37)[c]	14,667 (2,12)[g]	82,91 (10,34)[m]
	GS	12,731 (1,97)[d]	12,217 (2,17)[h]	65,90 (13,12)[n]
	Below grade	11,289 (2,89)[d]	11,010 (2,85)[h]	49,03 (18,08)[o]

As seen on Table 3, the classes of BS 4978 showed the best compliance with the MOE and MOR values of lumbers. The average MOEd and MOEs values of the three grades of lumber decreased with decreasing visual class. However, only the MOEd and MOEs of lumber sorted in SS (select structural) class, which is the best class of BS4978, were significantly (at the $p<0.05$ level) higher than that of other classes. No significant differences were found between the grading classes of TS 1265 and DIN 4074 in terms of MOEd and MOEs values.

For MOR values, significant differences ($p<0.05$) were observed between the lumber graded visually according to all standards used. In general, the lower the visual grading class resulted in the lower average of MOR values. Only the exception of this was observed between class III and below grade of TS1265, whereas the below grade gave slightly higher MOR value than class III. The differences between the all grading classes were significant ($p<0.05$) for BS 4978. For TS 1265, class I and II showed significantly higher MOR values than that of class III and below grade. For DIN 4074, only the best class (S13) showed significantly higher MOR value than that of other classes, whereas there was no significant difference among the other classes.

The relationship between the MOEd and MOEs and MOR was also investigated. Figure 3 showed the linear regression analysis performed between MOEd and MOEs for all lumber. A strong correlation with an R square of 0.86 was found between the MOEd determined by longitudinal vibration and the MOEs determined by bending test. It was found also a strong correlation with an R square of 0.62 between the MOEd and MOR values of all lumber but this correlation were not as strong as MOEd-MOEs correlation as expected (Figure 4). It is well known that there is also a relatively weak correlation between static MOE and MOR values of wood.

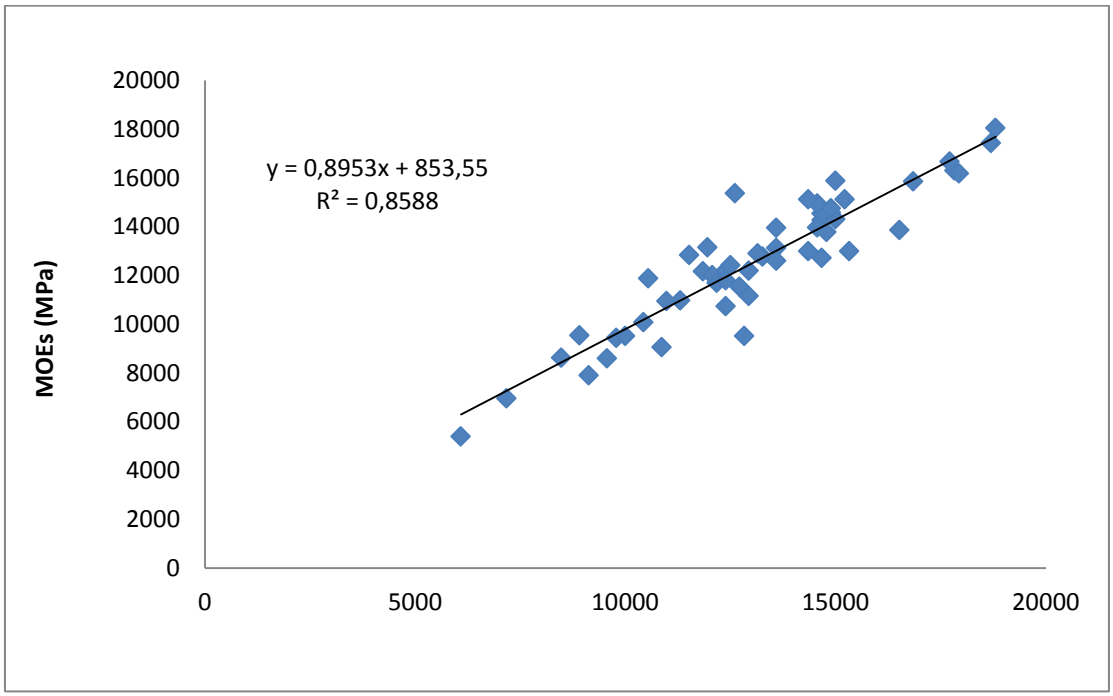

Figure 3-The relationship between the MOEd and MOEs values of lumber.

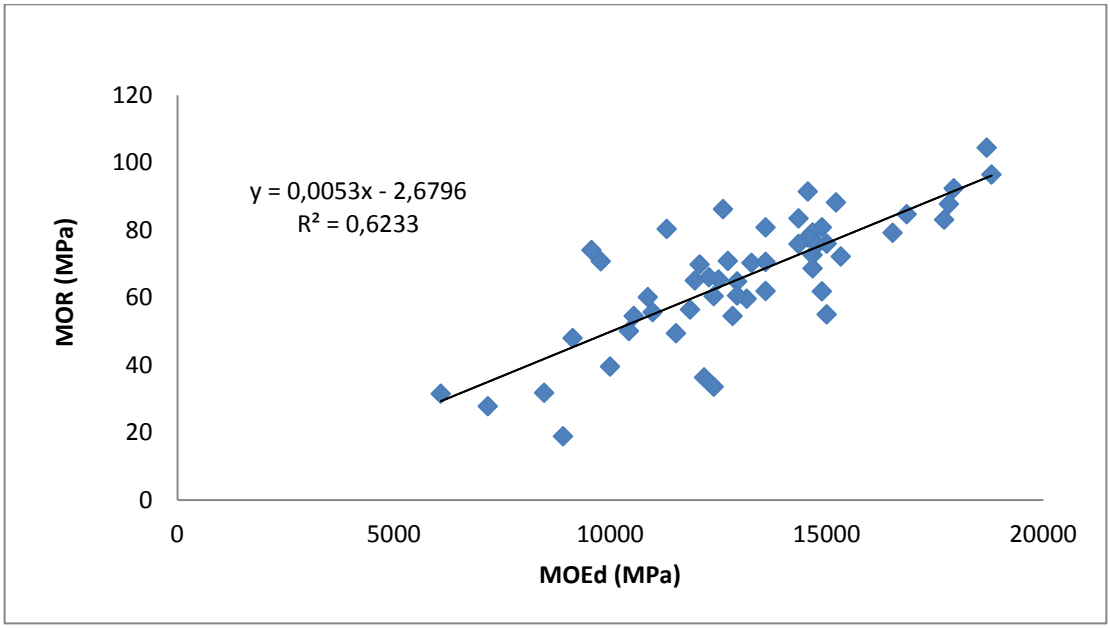

Figure 4-The relationship between the MOEd and MOR values of lumber.

CONCLUSIONS

The results indicate that the visual strength classes determined by using BS 4978 standard showed the best compliance with the MOEd determined by longitudinal vibration and the MOEs and MOR determined by destructive test. It was concluded that, in general, the MOEd, MOEs, and MOR values of lumber were increased with increasing visual grading class for all standards used in this research. This was more obvious for MOR values. The differences in MOEd and MOEs values among the grading classes were found significant ($p<0.05$) for only BS 4788. However the differences in MOR values of lumber among the grading classes were found significant for all standards used. There were strong correlations between MOEd and MOEs ($R^2=0.86$) and MOR ($R^2=0.62$). It can be concluded that MOEd determined by longitudinal vibration nondetructive test can be used for strength grading of structural lumber instead of

MOEs obtained from conventional bending test. It can be also concluded that the best results can be achieved with combining the visual grading and the strength grading.

Reference list

Baltrušaitis,A., Pranckevičienė V., 2003, Strength Grading of the Structural Timber, Materials Science (Medžıagotyra). Vol. 9, No. 3., ISSN 1392–1320.

Bell, E. R., Peck E. C., and Krueger.N. T., 1950, Young's modulus of wood determined by a dynamic method. U.S. Forest Products Laboratory Report 1775. WI: U.S. Department of Agriculture, Forest Service, Forest Products Laboratory.

Casado, M., Acuna, L., Vecılla, D., Relea, E., Basterra, A., Ramon, G., Lopez, G., 2010, The influence of size in predicting the elastic modulus of Populus x euramericana timber using vibration techniques, Structures and Architecture – Cruz (Ed.) , Taylor & Francis Group, London, ISBN 978-0-415-49249-2.

Divós, F., Tanaka, T., 2005, Relation between static and dynamic modulus of elasticity of wood. Acta Silv Lign Hung 1:105-110.

Fukada, E., 1950, The vibrational properties of wood. Jour. Phys. Soc. Japan. 5:321-327

James, W. L., 1964, Vibration, static strength and elastic properties of clear Douglas-fir at various levels of moisture content. Forest Prod. J. 14(9):409-413.

Jayne, B. A., 1959, Vibrational properties of wood as indices of quality. Forest Prod. J. 9(11): 413-416.

Kretschmann, D.E. and Green, D.W., 1999, Lumber Stress Grades and Design Properties, Wood handbook—Wood as an engineering material. Gen. Tech. Rep. FPL–GTR–113. Madison, WI: U.S. Department of Agriculture, Forest Service, Forest Products Laboratory. 463 p.

Kitazawa, G., 1950, Nondestructive testing for forest products. Proceedings: Forest Products Research Society 4:191-197

Matsumoto, I., 1962, Studies on the dynamic modulus E and logarithmic decrement of wood by transverse vibrations. Bull. of the Kyushu University Forests. 36. Fukuoka, Japan.

Pellerin, R. F., 1965, A vibrational approach to nondestructive testing of structural lumber. Forest Prod. J. 15(3):93-101.

Piazza, M., Riggio, M., 2008, Visual strength-grading and NDT of timber in traditional structures, Journal of Building Appraisal, 3, 267 – 296. doi: 10.1057/jba.2008.4.

Ross, R.J., Pellerin, R.F., 1994, Nondestructive testing for assessing wood members in structures: A review. U.S. Department of Agriculture. Forest Products Laboratory. Technical Report: 70, Madison. 42 p.

Srpcic, J., Plos, M., Pazlar, T. and Turk, G., 2010, Strength grading of Slovenian structural sawn timber, In Proceedings ‘The Future of Quality Control for Wood & Wood Products’, 4-7th May 2010, Edinburgh The Final Conference of COST Action E53.

Vega, A., Guaıta, M., Dıeste, A., Majada, J., Fernandez, I., Bano, V., 2011, Evaluation of the influence of visual parameters on wave transmission velocity in sawn chestnut timber, In. Proceedings 17th International Nondestructive Testing And Evaluation Of Wood Symposium, September 14-16, Hungary.

Use of visual and mechanical variables for structural grading of pine from Uruguayan plantations.

Andrea Cardoso
R&D Management Forestry Projects, Laboratorio Tecnológico del Uruguay, Montevideo, Uruguay, acardoso@latu.org.uy

Matías Cagno
R&D Management Forestry Projects, Laboratorio Tecnológico del Uruguay, Montevideo, Uruguay, mcagno@latu.org.uy

Hugo O´Neill
R&D Management Forestry Projects, Laboratorio Tecnológico del Uruguay, Montevideo, Uruguay, honeill@latu.org.uy

Abstract

The aim of this study is to determine the significant variables that predict the bending modulus of elasticity of the Uruguayan pine lumber, compare the results by including non-destructive testing as a predicting variable and analyze which structural grade of the European standard is achieved with the tested beams. It were used a hundred beams from two national plantations: *Pinus taeda* 14 years old and *P. elliottii* 27 years old. According to Chilean and European standards, were measured a series of visual variables, estimated the dynamic modulus of elasticity and determined the flexural strength and stiffness to build a model of classification. The limiting property to classify national pine in structural grades was the stiffness. The number of growth rings was the most relevant variable to classify the lumber in structural grades; besides using non-destructive testing improves the model of classification in structural grades and only a 40% of the 27 years old beams classified as C16.

Keywords: classification, pine, bending, regression trees

Introduction

In Uruguay, ninety eight percent of pine forest is planted with *Pinus elliottii* and *P. taeda,* principally located in the center-north of the country (MGAP 2012). The destination of this wood is not publicly indicated but because of the location and the proximity to industry areas, is estimated that is mechanically transformed. A study carried out by Dieste (2012) indicated that the average annual offer of pine lumber, between 2010 and 2030, will be about 3 millions of m^3. Uruguayan forestry plantations of pine are characterized by rapid growth, because of the climatic and soil conditions at the north of the country. These conditions generate a high percentages of juvenile wood and low values of bending elasticity modulus. The lowest value of the bending elasticity modulus is a problem for Uruguayan pine lumber classification in structural classes according to the European standards (Moya et al. 2015).

Currently, there is no structural classification of national pine lumber that indicates physical and mechanical features of the material. In consequence, there is a need to define a mechanical-visual classification to predict the structural properties of the national pine wood.

The presence and the position of the pith over the piece of lumber (Dahlen et al. 2014), the width or the number of the growth rings (Fenández-Golfín et al. 1994; INN 1999; Mascia and Cramer 2009), the knot diameter or the knot area (Guillaumet et al. 2007; Vega 2013; Moya et al. 2015) have influence in the mechanical properties: flexural stiffness and strength. The dynamic modulus of elasticity estimated by non-destructive testing is well correlated with the bending modulus of elasticity, strength and density (Acuña et al. 2001; O'Neill 2006; Iñiguez 2007). Many authors indicated that the prediction of mechanical properties is more precise by using non-destructive testing, than using only knot features and density of the pieces (Hermoso and Kessel cited by Iñiguez 2007). If the techniques of nondestructive testing and visual classification are combined, the correlation improves (Cecocotti cited by Iñiguez 2007).

Objectives

The aim of this paper is to determine the variables that predict the bending modulus of elasticity of the Uruguayan pine lumber under investigation , compare the results by including non-destructive testing as a predicting variable and analyze to which structural grade of the European standard achieved the beams.

Methods

The wood used was provided from two plantation located in the north of Uruguay. One of them situated in the province of Tacuarembó of *P. taeda,* 14 years old with pruning, and the other one from Rivera of *P. elliottii,* 27 years old without pruning and thinning. For this study it was used 99 commercial pine beams selected at sawmill, where were sawn, dried and planed. The final dimensions of the beams were of 2800 mm long, with an average section of 50 per 150 mm.

Based on Chilean (NCh1207:2005) and European (EN 56544:2011) standards, a series of visual variables were measured over the beams (Table 1). For the analysis of this study it were taken into consideration variables related to diameter, area[1] and positions of knots, growth rate estimated by the number of the growth rings per centimeter, presence and position of the pith. It was also considered a variable related to the sawing orientation.

Table 1 – Visual predicting variables used, type (N=numerical, C= categorical) and values.

Variable	Type	Value
Percentage of major diameter knot on face (DCARA)	N	1 to 100 (percentage)
Percentage of major diameter knot on edge (DCANTO)	N	1 to 100 (percentage)
Position of the major knot on face (PDCARA)	C	1 = center of beam, 2= extremes
Position of the major knot on edge (PDCANTO)	C	1 = center of beam, 2= extremes
Elongated knot area by section area (RANNA)	N	1 to 100 (percentage)
Individual knot area by section area (RANNI)	N	1 to 100 (percentage)
Knot area by section area (RANT)	N	1 to 100 (percentage)
Percentage of border area (AB)	N	1 to 100 (percentage)
Number of growth rings per centimeter (NAPCP2.8)	N	0 – 3
Pith (MEDULA)	C	0= absence, 1= centered, 2= off-centered pith
Sawing orientation (TC)	C	T= tangential, R= radial, S= combination

It was determined the dynamic modulus of elasticity (E_d) of the beams using a non-destructive ultrasonic test equipment (Fakopp Microsecond Timer). The beams were then tested in universal testing machine, determining the bending modulus of elasticity (El) and flexural strength (f) based on the European standard (AENOR 2011). According with this standard there were also determined the density (d) and moisture content of each piece.

[1] The variables related to area of knots were measured based on Chilean standard (INN 2005).

Based on tolerances of some singularities as warps, slits and cracks, wanes and resin pockets indicated in the European standard, 14 pieces were rejected because of wane presence and one because of resin pocket. Consequently, for this study it was taken into account 84 beams, from the 99 evaluated, as the data base.

The proceeding consisted of obtaining a measure of the visual and mechanical variables from each beam, founding the values of this singularities that allow to distinguish some beams as structural lumber. The data base was analyzed using the technique of automatic learning: regression trees with CART packages in R (Breiman et al. 1984). The principal idea of this technique is a value partition of the independent variables (called predicting variables), so that the values of the dependent variable (predicted variable) at terminal nodes have the least sum of squares (Wilkinson 2012). This technique take into account all the predicting variables in each partition. The trees were pruned with the criterions of "1-SE" recommended by Breiman et al. (1984), and the best tree was then plotted. Each plot is associated to a pseudo r^2, which indicates the adjustment of the model to the observations, and to a predicted error of the model. This error was estimated by cross-validation: it was obtained a regression tree using a sample of the data base (learn sample) and with the rest of the data (test data) it was calculated a predicting error of the tree. This exercise was randomly repeated 50 times, then was calculated an average model error and a standard deviation.

Results and discussion

In first place, the whole data base was analyzed without discrimination of age, species or silviculture management because it represents the lumber as it is commercially available in Uruguay. Secondly, it was meaningful to analyze the results per sampling, because in this way the variables previously mentioned take part of the entry features of the model of classification.

The tables 2 and 3 are a summary of the principal statistical indicators. In all cases, the mean and the characteristic value of El is lower than the minimum values indicated in the European standard EN 338 (2009) for the structural grades (mean=7000 MPa and 5^{th} percentile =4700 MPa). Consequently, for this study, it was analyzed the relation between the predicting variables and the values of El, as it was considered the limiting variable. It was observed that some beams showed high values of the principal properties, so they were analyzed in order to delimit a group with structural features.

Table 2—Descriptive indicators for bending strength, stiffness and density. Includes number of observations (n), the mean, the confidence interval for the mean at 95% (CI (95%)), the standard deviation (SD), minimum, maximum and the 5^{th} percentile (P(05)).

	f	El	d
	(MPa)	(MPa)	(g/cm^3)
n	84	84	84
Mean	27,33	6054,54	0,361
CI (95%)	±2,06	±351,83	±0,01
SD.	9,49	1621,22	0,04
Min	9,65	3483	0,296
Max	57,22	11914	0,465
P(05)	14,31	3948	0,306

Table 3—Descriptive indicators per sample for bending strength, stiffness and density

Sample	Tacuarembó, 14 years, with pruning	Rivera, 27 years, without pruning and thinning

	f	El	d	f	El	d
	(MPa)	(MPa)	(g/cm^3)	(MPa)	(MPa)	(g/cm^3)
n	46	46	46	38	38	38
Mean	26,56	5489	0,338	28,27	6739	0,389
CI (95%)	±1,99	±265	±0,007	±3,97	±661	±0,013
SD.	6,70	893	0,023	12,08	2012	0,038
Min	16,08	3483	0,296	9,65	3722	0,320
Max	39,51	7135	0,397	57,22	11914	0,465
P(05)	16,39	3948	0,302	10,91	3869	0,321

A preliminary evaluation of the relation between each predicting variable and the El was calculated by the Spearman correlation for the continuous variables. In table 4 is observed that Ed and the number of growth rings per centimeter are positively correlated with El. The variables related with the knot diameter have low correlation, but were better correlated than the variables related with the areas.

Table 4 - Correlation between El and continuous predicting variables.

Variable	Correlation
Ed	0,90
DCARA	-0,25
DCANTO	-0,22
NAPCP2.8	0,46
RANNI	-0,001
RANNA	0,002
RANT	-0,08
AB	0,08

It is necessary to evaluate all predicting variables together to understand which one is more relevant to predict the El and to describe the values of the variables that define groups of beams with structural characteristics.

Observing the graphics on figure 1, results that Ed is the most relevant variable to define a group with structural characteristics (a), and NAPCP2.8 is the significant variable detected if is not taken into account the non-destructive testing (b). On the first graphic it is defined a group on the right of eighteen beams that classify[2] as C16; the rests of the groups do not have structural grades by European standard. The other graphic determined a group of only seven beams, associated with the structural grade C18.

a) $r^2 = 0,74$; predicted error= 954±154 MPa (16% average model error)

[2] This classification is approximated, was made based in the EN 338:2009 standard, taken into account the mean and the characteristics values of the bending modulus of elasticity, stiffness and density.

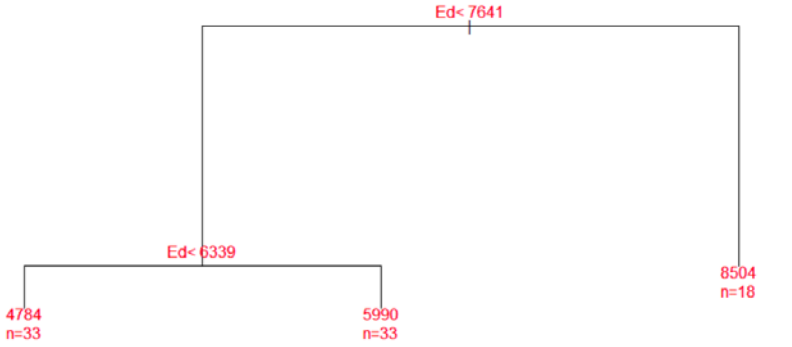

b) r^2 = 0,36 ; predicted error = 1494±268 MPa (25% average model error)

Figure 1— Regression trees for the bending modulus of elasticity (84 beams), comparing the result of using the non-destructive testing (a) or not (b).

This result is meaningful, because it demonstrates that the pine lumber in study has structural characteristics for being used in wood-framing. Through the graphics on figure 1, was observed the model taken into account non-destructive testing represent much better the data base than the model which no included it, looking forward the pseudo r^2 coefficient. In consequence using the predicting variable Ed is relevant to improve the classification. The model error using non-destructive testing is 16 % in average, whereas using only the visual variable NAPCP2.8, the error of the model was 25% in average. This value indicates the error made when a new beam is classified in one group or another.

An analysis per sample showed that the relevant predicting variable was Ed in cases where was used non-destructive testing (graphics c and d on figure 2), and NAPCP2.8 (graphic e) when only visual variables were used. In the latter model, it is observed that DCARA is an important predicting variable because was plotted on the model but it does not discriminate a group of beams with structural characteristics. It is also observed that no group of beams with 14 years old (c) has structural properties. On the other hand, a group of beams from plantation of 27 years old classify into C16 structural grade (d and e). This difference could be explained because of the age (Moya et al. 2015).

c) r^2 = 0,73 ; predicted error = 726 ± 108 MPa (13% average model error)

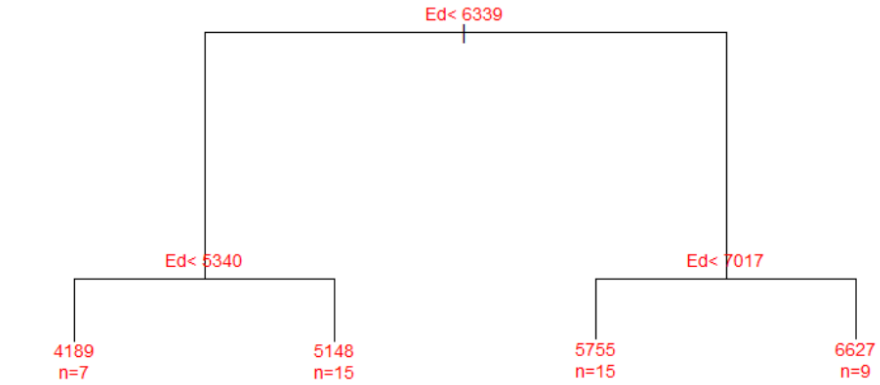

d) r^2 = 0,61 ; predicted error = 1196 ± 239 MPa (17% average model error)

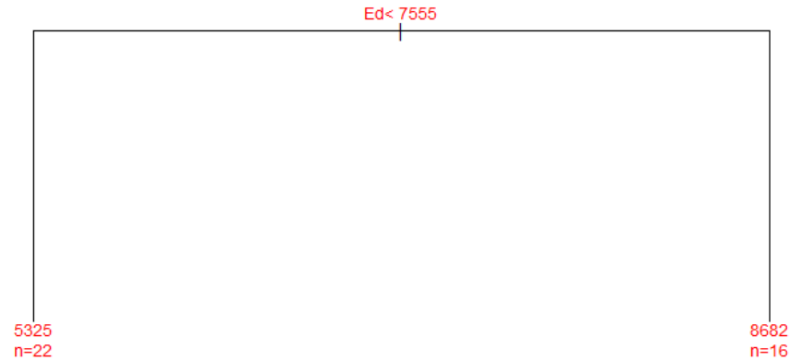

e) r^2 = 0,48 ; predicted error = 1849 ± 371 MPa (27% average model error)

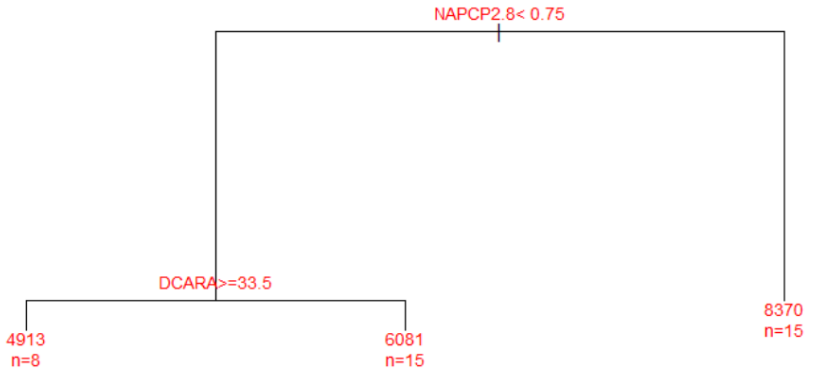

Figure 2— Regression trees for the bending modulus of elasticity per sampling. Graphic c) is the result for Tacuarembó´s beams using non-destructive testing, graphics d) and e) are the results for use Rivera´s beams using the non-destructive testing or not respectively.

The model error in this final analyzes were also minor when it is used non-destructive testing (13 and 17%) than when it is not used (27%).

Conclusions

The models obtained in this study, suggested that using a non-destructive testing to predict the bending modulus of elasticity is more effective than not using it, as it was observed in the analyzes of the models error taking into account all beams and per sampling. Ed and NAPCP2.8, were the most relevant variables to predict the bending modulus of elasticity.

One group that represents almost 40 % of the pine lumber from Rivera could be classified into C16 structural grade but no group of beams from Tacuarembó achieved this classification.

Acknowledgments

This study was developed in the framework of a timber visual-grading project on *Pinus sp*. conducted as a cooperative effort between the Forestry Projects Department of the Laboratorio Tecnológico del Uruguay (LATU) and the Dirección Nacional de Industria (DNI) of the Ministry of Industry, Energy and Mining (MIEM). Also thanks are due to Carolina Crisci for the statistical support.

References

Acuña, L. Llorente, A. Casado, M. Herrera, C. 2001. Clasificación de la madera de *Pinus sylvestris* L. mediante ensayos no destructivos. Spanish Forestal Congress (3, 2001, Granada)

AENOR (Asociación Española de Normalización y certificación). 2012. Estructuras de madera. Madera aserrada y madera laminada encolada para uso estructural. Determinación de algunas propiedades físicas y mecánicas UNE-EN 408. España, AENOR. 37 p.

AENOR (Asociación Española de Normalización y certificación). 2011. Clasificación visual de la madera aserrada para uso estructural. Madera de coníferas UNE 56544. España, AENOR. 25 p.

Breiman, L.; Friedman, J. H.; Olshen, R. A.; Stone, C. J. 1984. Classification and Regression Trees. Wadsworth.

Dahlen, J.; Jones, P D.; Seale, R D.; Shmulsky, R. 2014. Sorting Lumber by pith and tis effect on stiffness and strength in southern pine No. 2, 2x4 lumber. Wood and Fiber Science, 46(2) 186-194 pp.

Dieste A. 2012. Programa de promoción de exportaciones de productos de madera. http://gp.gub.uy/sites/default/files/documentos/programa_de_promocion_de_exportaciones_de_productos_de_madera_-_informe_preliminar_andres_dieste_-_2012.pdf [10November 2014].

Fernández-Golfín, J.I.; Díez, M.R.; Gutiérrez, A. 1997. Caracterización mecánica de la madera aserrada de pino silvestre de los sistemas Central e Ibérico mediante probetas de tamaño estructural. Revista de Investigación Agraria 6 (1 y 2): 183-215 pp.

Guillaumet, A A.; Manavella, R D.; Filippetti, M C.; Diab, J.; Armas, A. 2007. Clasificación visual resistente de la *Araucaria angustifolia* procedente de El Dorado, Misiones Argentina. En: Congreso Iberoamericano de productos forestales y no forestales (3, 2007, Buenos Aires) ISSN 1851-0973. 31 p.

INN (Instituto Nacional de Normalización). 2005. Pino radiata – Clasificación visual para uso estructural-Especificaciones de los grados de calidad NCh 1207.Of2005. Chile, INN. 20 p.

Iñiguez, G. 2007. Clasificación mediante técnicas no destructivas y evaluación de las propiedades mecánicas de la madera aserrada de coníferas de gran escuadría para uso estructural. Madrid, Universidad Politécnica de Madrid. Doctoral thesis.

Mascia, N T. Cramer, S M. 2009. On the effect of the number of annual growth rings, specific gravity and temperature on redwood elastic modulus. Maderas, Ciencia y Tecnología 11(1) 47-60 pp.

MGAP (Ministerio de Ganadería Agricultura y Pesca) 2012. Actualización de la cartografía forestal del Uruguay. http://www.mgap.gub.uy/portal/page.aspx?2,dgf,dgf-recurso-forestal,O,es,0,/superficietotaldebosques(cartografia2012) [10 of November].

Moya, L.; Cardoso, A.; Cagno, M.; O´Neill, H. 2015. Caracterización estructural de madera aserrada de pinos cultivados en Uruguay. Madera ciencia y tecnología 17. 25 p.

O'Neill, H. 2006. Estimación de la calidad de la madera producida en el Uruguay para uso estructural y su evaluación en servicio por métodos no destructivos. Nota Técnica N 4. LATU, Montevideo. 9 pp.

Vega, A. 2013. Caracterización mecánica de la madera estructural de *Castanea sativa* Mill. Clasificación visual y evaluación mediante métodos no destructivos. Lugo. Universidad de Santiago de Compostela. Doctoral thesis.

Wilkinson, L. 2012. Classification and regression Trees. http://cda.psych.uiuc.edu/multivariate_fall_2012/systat_cart_manual.pdf [10 of June of 2015]

Pearson Correlation between the Nondestructive Method of Radial Longitudinal Distension (DRL) and the Lumber Quality in Three Species of *Eucalyptus*

[1*]**Rui** André Maggi dos **Anjos**, [2]**Márcio** Pereira da **Rocha**, [3]**Gisele** Gimenes **Brochini**

[1,2,3]Forestry and Technology Engineering Department – Federal University of Curitiba – CEP 80210-170, Curitiba, Brazil.

*Adress: Avenida Prefeito Lothario Meissner, 632, Curitiba, Brasil. Phone: (41) 33604294. E-mail: rui@ufpr.br

ABSTRACT: This work aimed to study the correlation between Radial Longitudinal Distension (DRL) and the quality of lumber in clones of three species of *Eucalyptus*. The DRL method stands out for its ease of use and its speed. It also stands out because it is a methodology that can be applied to still-standing trees, without the cut its embodiments, avoid the need for applying destructive testing. The study found the DRL values of 75 clones of three species of Eucalyptus: *Eucalyptus grandis*, Eucalyptus *saligna* and *Eucalyptus dunnii*. The trees were properly processed and were observed the correlation of results obtained using the DRL with defects found in lumber. The results verified the difference of DRL between the three species. Positive relation were found between DRL, average diameter (DBH) and height (H) in Eucalyptus dunnii. The same was not observed in *Eucalyptus grandis* and *Eucalyptus saligna*. There was a significant correlation between DRL and the cracking rate in lumber for the three species analyzed. The results show the use of DRL as a promising methodology for observation of irregularities in quality lumber.

1 INTRODUCTION

The Pearson linear correlation is an important method of investigation of early characteristics of a forest planting. Suitable for non-destructive methods through this kind of relationship can be established between assumptions features observed in trees and peculiarities of the wood during processing.

One of the most common problems encountered in the mechanical processing of Eucalyptus wood is to determine which individual will be able to produce sawn products of superior quality, and the producer have to know in advance what will be the performance of the logs during processing, and what will be the quality of sawn products.

Non-destructive testing readily meet these aspirations since they can be applied in standing trees and early, without the overthrow of the same information of what will be the results of the mechanical wood processing . A quick and minimally invasive test is the Cirat -Foret method or determination of longitudinal residual strain (DRL). This test is to measure the strain of the external

tissues of the wood with the still living tree, and through this measure, relate that value the defects of lumber using Pearson's correlations.

The study of these correlations reduces the time required for evaluation of the mill able materials and creates conditions to predict the behavior of the log during the sawing process.

The main objective of this research was to establish Pearson correlations between DRL and features of the living tree and quality lumber from three species of Eucalyptus.

2 MATERIAL AND METHODS

2.1 Material Source

The wood used in this study originated in clonal trials Klabin SA of Paraná, in the municipality of Telemaco Borba. The species used are Eucalyptus grandis, E. saligna and E., derived from clonal plantations propagated by cuttings. The trees was planted in low slope sites, in homogeneous soils in plots protected by double surrounds, spaced 2.5 mx 3.0 m.

Table 1 shows the distribution of plants in the designs in the first half of 2007 when they began the study.

Table 1 number of species in trees

Área	Trees
E. grandis	468
E. dunnii	388
E. saligna	295

Fifty-five of each local trees were measured all diameters and heights of 1151 trees belonging to the study and the data were selected to the experiment. The choice sought greater diversity among the trees looking for possible lines plants without defects , diameters between 20-45 cm dbh (diameter at breast height of the average 1.30 m above the ground) . To ensure this completeness of each species, eight plants was chosen, with diameters from 20 to 26 cm, with eight DAPs between 27 and 33 cm and nine plants with more than 34 cm this division was employed after observing the frequency of diameters of the areas studied.

2.2 Analyzed parameters in Search

The parameters analyzed was in tree characteristics, logs and sawn products:

Characteristics measured DAP (cm) ; Overall height (m) ; Sawn wood yield (%), losses during processing due to warp and top cracks (loss of income) , the peripheral tissues of the trunk, arching and curving Index (mm /cm) cracking index (cm /m) and DRL (mm).

2.3 Parameter determination method

2.3.1 Determination of DRL

The longitudinal residual strain was measured in accordance with the recommendations made by CARDOSO JUNIOR (2002), PADUA (2002) and TRUGILHO (2002). All 75 trees have the DRL measured at four points, which correspond to the four cardinal points, and the measurement of the DRL for each tree was formed from an average of four measurements, north, south, east and west.

The measurement procedure was initiated by opening a window in the shell pentagonal shape, approximately 20 cm high and 10 cm wide. For this opening could be identified the orientation of the grain. The extensometer pins were set inside the window, parallel to the fibers. With the pins 45 mm apart and firmly attached to the timber, the apparatus was set to the realization of 2 cm in diameter and 25 mm deep hole. When starting drilling, the extensometer measured the spacing of the fibers, obtaining a reading of DRL.

After measuring the DRL, the trees were felled with the aid of chainsaws and subsequently transported. There was carried out no treatment for the relief of tensions, since the removal occurred simulating normal company operation in situations for logging in selective thinning. The cut was carefully avoiding, where possible injuries to the remaining plants.

The first log of each tree was transported from planting to unfold unit, and processed between 10-12 hours after the overthrow. The wood cut, measuring volumes and transport were performed during the day and overnight unfolding, to prevent loss of moisture that interferes with the expression of defects in the wood.

2.4 Withdrawal procedure and unfold

The main unfolding, the first and second cut was made, the log is rotated and 90^{o} were conducted at the third, fourth and fifth cutting. Secondary operations were made in horizontal band saw; the remaining portion, split into multiple circular saw that is shown in Figure 1.

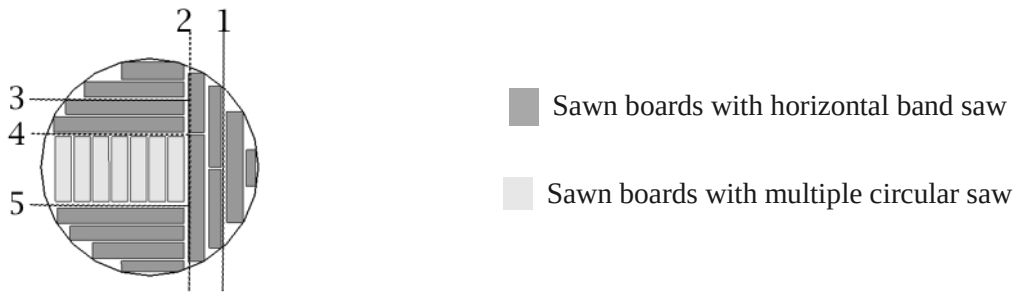

FIGURE 1 - chart unfold, adaptation of Mckimm et al chart. (1988), showing the sawn parts removed with the horizontal saw tape measure and the lumber with multiple circular saw. Note: the figures represent the cuts made by the main saw tape

2.5 Measuring boards

The arching index measurements were taken (mm/m) curving index (mm/m), the dimensions of length, width and thickness, in addition to the crack ratio (cm/m).

The boards were measured in accordance with relevant standards / NBR 14806 of February 2002 “Lumber Eucalyptus” and ABNT / NBR 7203 February 1982 " Timber and processed “.

The yields of the species in lumber were obtained by dividing the volume of the first log and the total volume measured by the boards unfold this log, described by equation:

$$Yie\square d = \left(\frac{Log\ volume\ m^3}{Log\ boards\ volume\ m^3}\right) x100$$

Losses in yield were calculated based on the volume of lumber that had to be cut due to the presence of cracks. As the equation:

$$Yield\ losses = \left(\frac{Log\ volume\ m^3}{Cut\log boards\ volume\ \ m^3}\right) x100$$

2.6 Statistical treatment

We used the Pearson correlation coefficients , significance levels in 1% and 5 % , to evaluate the association with DRL : DAP ; Total height; yield; Losses in yield; Curving index ; arching index; cracks index.

3 RESULTS

Table 1 shows the existence of correlation between DRL and the variables studied.

		DAP	Height	Yield	Yield losses	Incurve index	Arch index	Crack index
Eucalyptus dunnii	DRL	+*	+*	ns	+**	ns	ns	+*
Eucalyptus grandis	DRL	ns	ns	-*	-**	ns	ns	+*
Eucalyptus saligna	DRL	ns	ns	ns	-**	-*	ns	+*

NS not significant correlation; + * Positive correlation level of 5 %; ** + Positive correlation at a significance level of 1% - * negative correlation 5% - ** negative correlation to the 1% level of significance.

Note that the DRL was related to the loss of yield in the three species, it can be inferred that the distention of the logs of wood tissues is linked to the use of wood at the sawmill. However, the behavior of the species does not follow a pattern. The results show that the species are disparate in the interim, since the DRL increases for *E. dunnii* if related positively with the top cracks and losses and the opposite behavior was observed in *E. saligna* , higher values DRL were accompanied by smaller end splits and losses in the income values. Therefore, it can be said that early observation of DRL in live trees allowed relating these values to top cracks in the sawn material and losses in income. However, the behavior of the DRL may vary between species, as evidenced by the results of Table 1.

ANJOS (2013) to study the DRL between *Eucalyptus* clones found differences between genetic materials indicating that this characteristic is linked to the phenotype of the material. The author comments that the differences were more evident for *E. grandis* and *E. dunnii*.

Evaluation of the Pearson correlations and sawn timber yield losses in yield and cracking index can be seen in Table 2.

Table 2 Statement of Correlation Values between Measurements

		Yield	Yield losses	Crack index
E. dunnii		NS	0,276	NS
E. grandis	DRL	-0,408	-0,290	-0,181
E. saligna		NS	-0,402	-0,144

The correlations are low values , which does not mean they are nonexistent. What can explain these values are the differences between the studied materials and the actual mechanical processing of wood that interferes with the way the tensions present in the timber manifest.

E. dunnii stands out for presenting a different corpotamento the other two species. For this kind, the DRL increases were accompanied by greater losses in yield. As for the other species tested was noted perform differently.

What can be observed in Table 2 is that the DRL increases were accompanied by decreases, even subtle, the cracking rates. The theory advocated by TRUGILHO and CARDOSO JR (2004) is

that the DRL is an indirect measure of the tensions present in the tree. The results support the theory since the trees indicate that *E. grandis* and *E. saligna* DRL had higher with higher voltages, and logs derived from these plants generated lumber with low crack rates, or trees higher voltages showed slight smaller crack rates with lower losses in income. If theory is correct and the results indicate that the stress increases in *E. grandis* and *E. saligna* reduce the tendency to cracking , as in *E. dunnii* behavior is the inverse increased tensions trees is critical for causing sawing increased yield losses.

REFERENCES

ANJOS, R. A. M. *Estudo Sobre a Qualidade de Madeira Serrada de Três Espécies de Eucalipto*. Tese (Tese de Doutorado). Departamento de Engenharia e Tecnologia Florestal, Universidade Federal do Paraná, Curitiba. 2013. 153p.

ASSOCIAÇÃO BRASILEIRA DE NORMAS TÉCNICAS – ABNT - **NBR 7203:** Madeira Serrada e Beneficiada. Rio de Janeiro, 1982.

CARDOSO Jr. A. A. *Tensões de crescimento em Eucalipto e suas relações com espaçamento, idade e material genético*. (Dissertação de Mestrado), Universidade Federal de Lavras, Lavras, 2004, 85p.

MCKIMM J. R.; WAUGH G.; NORTHWAY R.L. *Utilization potential of plantation-grow Eucalyptus nites,* Australian Forestry, v52 n.1, 1988.

PÁDUA, F. A. de *Estimativas de Parâmetros Genéticos das Tensões de Crescimento em Clones de Eucalyptus*. (Dissertação de Mestrado), Universidade Federal de Lavras, Lavras, 2004, 65p.

TRUGILHO, P. F. et al. *Avaliação da Tensão de Crescimento em Clones de Eucalyptus*. Floresta e Ambiente, Rio de Janeiro, V9, n1, 2002, 38-44p.

Session 6

Evaluation of Engineered Wood Products

Nondestructive Evaluation of Laminated Veneer Lumber Bonded with High-density Polyethylene

Emanuela Lustosa
Department of Forest Engineering, University of Brasília, Brasília, DF, Brazil, emanuelacblustosa@gmail.com

Cláudio Del Menezzi
Department of Forest Engineering, University of Brasília, Brasília, DF, Brazil, cmenezzi@unb.br

Rafael Melo
Agrarian and Enviromental Sciences Institute, Federal University of Mato Grosso, Sinop, MT, Brazil, rrmelo2@yahoo.com.br

Abstract

The objective of this paper was evaluate the feasibility of using stress wave nondestructive technique to determine properties of a new wood veneer composite bonded with high-density polyethylene (LVL-HDPE). Twelve LVL-HDPE composite boards were produced and samples were cut and nondestructively tested using stress wave method and stress wave velocity (swv) and dynamic modulus of elasticity were calculated (E_d). Afterwards, the samples were tested up to rupture to assess bending properties (E_M, f_m), compression ($f_{c,0}$), hardness (f_H) and shear strength ($f_{v,0}$) properties. The sw and E_d data were utilized to predict the mechanical properties. The models obtained by treatment were non-significant. However, when all treatments were evaluated as a single group, only regressions between swv and E_M and between E_d and E_M were significant at 1% level. It was identified that the swv explained 34.35% of the E_M, while E_d explained 44.73%.

Keywords: stress wave, *Trattinnickia burseraefolia*, wood-plastic composite

Introduction

The wood-plastic composite (WPC) term refers to any composite that contains wood (of any form) and thermosetting or thermoplastic (Clemons 2002). Composites may be defined as materials made from two or more components with different compositions, structures and properties which are separated by an interface (Milagres 2004). The composites are distinguished by enabling the different materials combination, which may present higher in some properties regarding to individual components. They are products resulting from the mixture of two or more constituents, which have different shape and chemical composition (Correa 2004).

According to Milagres et al. (2006), most of the plastic residues are disposed in landfills and, due to its non-biodegradable nature, will remain at these places for many years, thus the plastic residues incorporation in the wood-plastic composite manufacture may contribute to reduce environmental pollution. Products made from recycled materials provide strength, durability and profitability equivalent to products made from raw materials, the ecological panel made from wood and recycled material has proven one of the most effective responses to the growing demand for materials (Pauleski at al. 2007).

Laminated veneer lumber (LVL) is a kind of engineered wood products that has been extensively used in construction sector. Nowadays, most of the wood I-beams used have LVL as flange, although it can be used alone as a single beam. LVL is only manufactured using thermosetting adhesives such as phenol-formaldehyde (PF) which presents durability and permanence required for structural purposes. The cost of these adhesives is relatively high, thus one possibility would be replace them by binding agent from recyclable sources, such as thermoplastics. Nevertheless, the utilization of thermoplastics in manufacturing LVL have not been tried so far, thus this paper present the first results about it. The proposed LVL composite board was made using post-consuming plastic bags as a binding agent. These bags are made from high-density polyethylene (HDPE) which belongs to PE thermoplastic class, the most used thermoplastic in the World (Lisperguer et al. 2010).

The utilization of nondestructive (NDT) methods to predict properties of veneer wood-based material (plywood or LVL) has been extensively studied. The common approach is use NDT methods to grade veneers before manufacturing the composite, as made by Del Menezzi et al. (2013), Bortoletto (2010) and Wang et al. (2004). Nevertheless, the evaluation of the properties of the consolidated veneer-based composites have be done (Melo and Del Menezzi 2014; Souza et al. 2011; Ferraz et al. 2009) and the results can be considered suitable. In this context, the present paper aimed at reporting the first results about nondestructive evaluation of this new kind of composite LVL.

Materials and methods

Composite manufacturing and testing

Wood veneers from amescla wood (*Trattinnickia burseraefolia*) were used to manufacture the composite boards. The veneers' size was 50 cm x 50 cm, and 3 to 4 mm thickness, and was subsequently sectioned into three 16.5 cm x 50 cm veneers. Four veneers interspersed with high-density polyethylene (HDPE) supermarket plastic bags were utilized for production of each board. The LVL-HDPE composite boards measuring 16.5 cm x 50 cm x 1.2-1.6 cm (width x length x thickness) were flat compressed using a hydraulic press. Each set was taken to press until the melting point of the HDPE (+/-140°C) for 20 minutes with adequate pressure to the set (≅1 N/mm²). Three treatments were studied varying the amount of HDPE to be used: 150g/m^2, 250g/m^2 and 350g/m^2. Four boards were manufactured for each treatment, totaling 12 LVL-HDPE composite boards.

Eight samples for each treatment were cut longitudinally after boards' production, totalizing 24 samples per test. These samples were put in air-conditioning room (20ºC/65%) up to achieve constant mass. All 24 samples were nondestructively evaluated lengthwise by stress wave (Metriguard Stress Wave Timer model 239A). The equipment has an impact pendulum that generates a stress wave which propagates through the sample. Two accelerometers are connected to the beam to measure the stress wave transit time (t, μs), which is the time required for the wave to travel between them. This value is used to determine the stress wave velocity (swv, m/s) and then the stress wave dynamic modulus of elasticity (E_d, MPa), according to equations 1 and 2, respectively.

$$swv\ (m/s) = \frac{L}{t \times 10^{-6}} \tag{1}$$

$$E_d\ (MPa) = \frac{swv^2 \times \rho}{g \times 10^{-5}} \tag{2}$$

Afterwards, the following mechanical properties were assessed according to ASTM D1037 (1998) and European Standard (2004): three-point static bending to obtain the modulus of rupture (f_m) and modulus

of elasticity (E_M), screw withdrawal resistance, Janka hardness (f_H), parallel compression strength ($f_{c,0}$); and parallel shear strength ($f_{v,0}$).

Statistical analysis

Initially Pearson correlations between all determined variables were calculated. Afterwards, the swv and E_d data were utilized to generate a simple linear regression model (y=a+bx), where these properties entering as independent variables (x) and mechanical properties (f_m, E_M, f_H, $f_{c,0}$, $f_{v,0}$) entering as dependent variables (y). In order to evaluate the effect of increasing amount of HDPE on swv and E_d, an analysis of variance (ANOVA) followed by Tukey test at α=0.05 was run.

Results and discussion

Table 1 presents the results of Pearson correlations (r) between nondestructive properties and LVL-HDPE materials properties. It can be seen that NDT properties had high r values with HDPE amount, density and modulus of elasticity. Janka hardness presented good correlation only with dynamic modulus of elasticity (E_d). It is clear that the higher the stress wave velocity the higher the bending stiffness of the LVL-HDPE composite board. It was found that increasing amount of HDPE improved significantly the density of the composite: 643 kg/m^3 (150 g/m^2 of HDPE), 664 kg/m^3 (250 and 350 kg/m^2). Both above mentioned results led obviously to a significant improvement of the E_d. Figure 1 shows the quadratic polynomial model fitted to describe this relationship.

Table 1—Pearson correlation between swv/E_d and LVL-HDPE material properties.

NDT Property	Material properties							
	HDPE	ρ	f_m	E_M	Screw	f_H	$f_{c,0}$	$f_{v,0}$
swv	0.657**	0.574**	0.279^{NS}	0.586**	0.108^{NS}	0.324^{NS}	0.049^{NS}	0.297^{NS}
E_d	0.714**	0.735**	0.347^{NS}	0.669**	0.156^{NS}	0.507*	0.119^{NS}	0.389^{NS}

Note: **,* statistically significant at α=0.01 and α=0.05, respectively; NS: non-significant

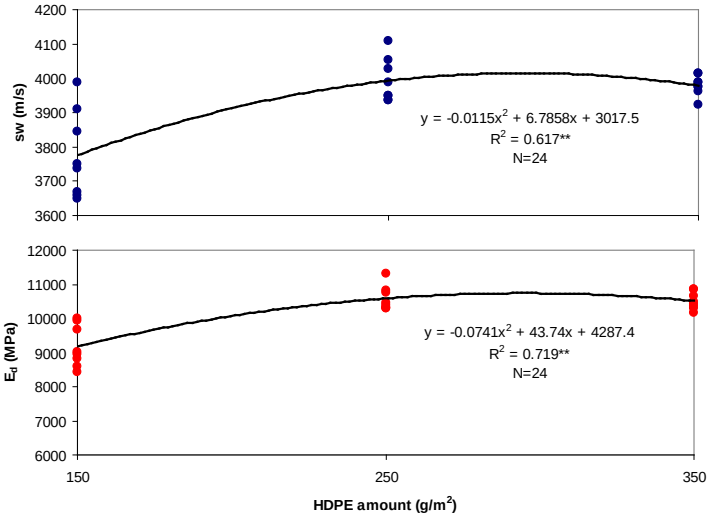

Figure 1—Effect of HDPE amount on stress wave velocity (sw) and dynamic modulus of elasticity (E_d) of the laminated veneer lumber (LVL). (Note: statistically significant at α=0.01)

The effect of increasing amount of HDPE might improve swv and Ed only at certain level, in this case 250 g/m^2. After this rate a trend of reduction in these NDT properties can be observed. It is well-know

that plastics show lower stiffness when compared with wood, and it is one the main reason wood flour is used for reinforcing WPC. In this context, the addition of higher amount of HDPE tends to reduce the ability of the composite to resist to the stress imposed when it is hit, and the strain is higher.

Figure 2 shows the linear models fitted to predict modulus of elasticity and Janka hardness. Although 10 possible linear models were run (swv/E_d x f_m/E_M/f_H/$f_{c,0}$/$f_{v,0}$) only three presented equations coefficient statistically significant. It was identified that the swv explained 34.35%, while that E_d explained 44.73% of the modulus of elasticity (E_M) data variation. Janka hardness (f_H) data variation could be poorly explained (25.75%) only by E_d.

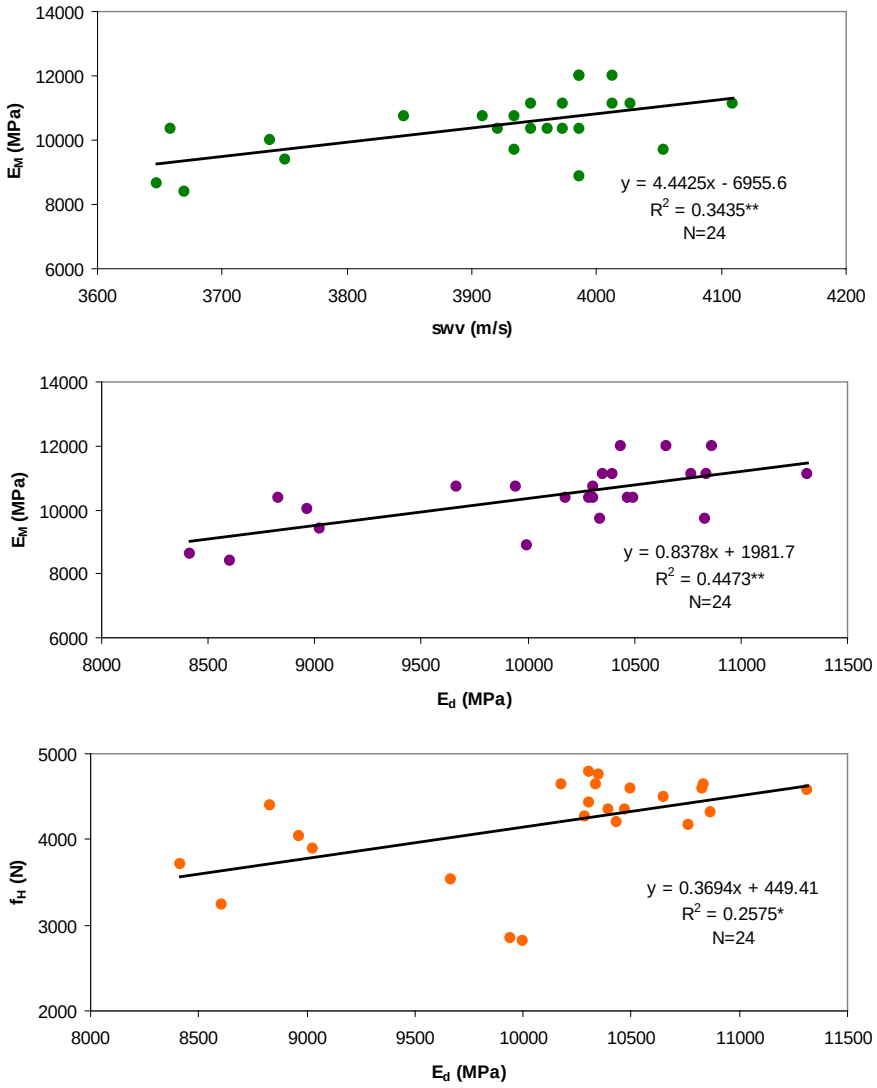

Figure 2—Linear regression models to predict modulus of elasticity (E_M) and Janka hardness (f_H) of the LVL-HDPE composite board using stress wave velocity (swv) and dynamic modulus of elasticity (E_d). (Note: **,*statistically significant at α=0.01 and α=0.05 respectively)

Souza (2009) evaluating LVL made from two pinus species and bonded with phenol-formaldehyde found that E_d could explain 58.6% of the E_M data variation while swv 47.6%. Recently, Melo and Del Menezzi (2014) employed the same method to predict bending stiffness of LVL made from *Schizolobium*

amazonicum. They found the relationship between E_d and E_M about R^2=0.58. Del Menezzi et al. (2013) graded veneer prior manufacturing LVL from *S. parahyba*. The R^2 values were higher and ranged from 0.622 to 0.769. In this context the models found here presented lower predictability than those found by others authors. One possible explanation is probably because they used thermosetting resins that present higher stiffness than thermoplastic.

Table 1 showed that HDPE amount had the highest values of Pearson correlation between evaluated properties. This way, in order to improve the predictability this was included in the model as a second factor affecting the properties of the composite LVL. The results are shown in Table 2. It can be observed that all models were highly significant and had theirs R^2 improved more than 20%. However, the prediction of f_H benefited much more and R^2 was doubled. The inclusion of this variable is advisable to improve the quality of the models without extra labor for measurement, since it is a manufacturing variable and must be known before production.

Table 2—Linear models .

Property	Model	R^2	F
E_M	680.5 + 5.41 HDPE + 2.147 swv	0.465	9.11**
E_M	4092.1 + 4.06 HDPE + 0.528 E_d	0.506	10.76**
f_H	3105.2 + 5.11 HDPE + 0.021 E_d	0.533	12.01**

Note: ** statistically significant at α=0.01.

Conclusions

A new kind of laminated veneer lumber (LVL) was produced using high-density polyethylene (HDPE) and it was nondestructively evaluated. It was found that the amount of HDPE affected significantly stress wave velocity (swv) and dynamic modulus of elasticity (E_d). Ten linear models were fitted to explain material properties using swv and E_d, but only three models were statistically significant to predict modulus of elasticity and Janka hardness.

Acknowledgments

The authors thank the Conselho Nacional de Desenvolvimento Científico e Tecnológico (CNPq) for granting the Scholarship to the first author and the Fundação de Aperfeiçoamento de Pessoal de Nível Superior (CAPES) for the travel grant conferred to the second author to attend this conference.

References

Bortoletto Jr. G. 2010. Effects of ply grading and assembly on the properties of plywood panels from *Pinus merkusii*. Cerne. 16(1): 145-153.

Clemons, C. 2002. Wood-plastic composites in the United States: the interfacing of two industries. Forest Products Journal. 52(6): 10-18.

Corrêa, G. R. 2004. Desenvolvimento, produção e caracterização de compósitos de madeira-plásticos para aplicação na indústria moveleira. Ouro Preto: MG: Universidade Federal de Ouro Preto. 107 p. M.S. thesis.

Del Menezzi, C. ; Mendes, L.; Souza, M. R.; Bortoletto Jr., G. 2013. Effect of nondestructive evaluation of veneers on the properties of laminated veneer lumber (LVL) from a tropical species. Forests. 4(2): 270-278.

Ferraz, J. M.; Del Menezzi, C. H. S.; Teixeira, D. E.; Okino, E. Y. A.; Souza, F.; Bravim, A. G. 2009. Propriedades de painéis de partículas laminadas paralelas utilizados com alternativa à madeira maciça. Cerne. 15(1): 67-74.

Lisperguer, J.; Bustos, X.; Saravia, Y. 2011. Thermal and mechanical properties of wood flour-polystyrene blends from postconsumer plastic waste. Journal of Applied Polymer Science. 119(1): 443-451.

Melo, R. R.; Del Menezzi, C. H. S. 2014. Estimativas das propriedades de compostos LVL produzidos com paricá (*Schizolobium amazonicum* Huber ex Ducke) por meio de stress wave. Revista Árvore. 38(6): 1155-1163.

Milagres, E. G. 2004. Compósitos de partículas de madeira de Eucalyptus grandis, polipropileno e polietileno de alta e baixa densidades. Viçosa, MG: Universidade Federal de Viçosa. 73 p. M.S. thesis.

Milagres, E. G.; Vital, B. R.; Lúcia, R. M. D.; Pimenta, A. S. 2006. Compósitos de partículas de madeira de *Eucalyptus grandis*, polipropileno e polietileno de alta e baixa densidades. Revista Árvore. 30(3): 463-470.

Pauliski, D. T.; Haselein, C. R.; Santini, E. J.; Rizzatti, E. 2007. Características de compósitos laminados manufaturados com polietileno de alta densidade (PEAD) e diferentes proporções de casca de arroz e partículas de madeira. Ciência Florestal. 17(2): 157-170.

Souza, F.; Del Menezzi, C. H. S; Bortoletto Jr. G. 2011. Material properties and nondestructive evaluation of laminated veneer lumber (LVL) made from *Pinus oocarpa* and *P. kesiya*. European Journal of Wood and Wood Products. 69(1): 183-192.

Wang, X; Ross, R. J.; Brashaw, B. K.; Verhey, S. A.; Forsman, J. W.; Erickson, J. R. 204. Flexural properties of laminated veneer lumber manufactured from ultrasonically rated red maple veneer. USDA/FS/FPL Research Note FPL-RN-0288. 5p

Determining Modulus of Elasticity of Full-Size Wood Composite Panels Using a Vibration Method

Cheng Guan
School of Technology, Beijing Forestry University, Beijing, China, 648911029@qq.com

Houjiang Zhang
School of Technology, Beijing Forestry University, Beijing, China, hjzhang6@bjfu.edu.cn

Lujing Zhou
School of Technology, Beijing Forestry University, Beijing, China, 229134038@qq.com

Wenhua Yu
School of Technology, Beijing Forestry University, Beijing, China, yuwenhua56@sina.com

Xiping Wang
USDA Forest Service, Forest Products Laboratory, Madison, Wisconsin, USA, xwang@fs.fed.us

Abstract

Traditionally, modulus of elasticity (MOE) of full-size wood composite panels is determined by mechanically testing multiple small specimens cut from the panels. The evaluation process is time consuming and destructive in nature. In manufacturing facilities, it is often desired to rapidly and non-destructively assess MOE of full size composite panels as a quality control procedure. The goal of this study was to develop a vibration-based measurement system that can be used to evaluate MOE of full-size panels in production settings. We first built a laboratory testing apparatus for measuring the fundamental frequency of 2440mm by 1220mm composite panels. A free vibration was initiated through a gentle push at the end of the panel away from the load cell and followed by a quick release. Vibration signal was collected through the laser sensor located in the middle of the panel, and the weight of the panel was measured by the load cell located at the 22.4% or the 77.6% in its length direction. Three hundred and three pieces of full-size composite panels were then tested using this vibration apparatus, including one hundred and one pieces of medium density fibreboard (MDF), one hundred pieces of particleboard and one hundred and two pieces of plywood. Following free vibration testing, six small specimens were cut from each panel and standard static bending test was then performed on each specimen to obtain static MOE. The results indicated the average dynamic MOE of full-size panels by vibration method was slightly higher (6.2%) than their average bending MOE. A good linear relationship (r=0.923) was found between dynamic MOE and average bending MOE of full-size panels. This study demonstrated that MOE of full-size wood composite panels can be potentially measured in production settings as a quality control procedure.

Key Words: full-size wood composite panel, modulus of elasticity (MOE), free vibration, dynamic testing.

Introduction

As an engineered wood product, wood composite panels are widely used in furniture manufacturing, building construction, packaging, transportation and other industrial sectors (Zhou 2010). Full-size wood composite panels refer to the panels with a standard size (length × width) of 2440 × 1220 mm that are most common in production sales. Modulus of elasticity (MOE) is a key index for evaluating the mechanical performance of wood composite panels. Studies have shown that MOE of a panel has a

statistical linear relationship with other mechanical performance indices.

Currently, the standard mechanical specimen testing method is used to determine MOE of full-size wood composite panels. According to this testing method, several small specimens have to be cut from different parts of a large-size panel, with (20h+50) × 50 × h (unit: mm) of the length × width × thickness (h). The small specimens are then destructively tested in a testing machine to obtain MOE and strength properties. With the measurement results of several standard specimens, the overall stiffness and strength of the full-size panel can be derived. This evaluation procedure is time-consuming and destructive in nature.

In recent years, many studies have been done on nondestructive evaluation of small wood composite specimens (Moslemi 1967; Shyamasunder et al.1994; Turk et al.2008; Yoshihara 2011; Wang et al. 2012; Yan et al. 2012; Hunt et al.2013). However, very limited information is available for nondestructive evaluation of full-size wood composite panels. A technique that has been investigated is a torsional-bending vibration method (Lau and Tardif 1996; Zhou et al.2007). During testing, a full-size wood composite panel is clamped at one end like a cantilever beam. Then an initial displacement is applied at one corner of the free end so that the panel is set into bending and torsional free vibrations. Through analysis of the vibration signals, MOE and shear modulus of the panel can be predicted.

This study presented a dynamic testing method that is based on the vibration theory of a “free-free” supporting condition. More specifically, the first order natural vibration frequency of the full-size wood composite panel supported at its two nodal lines was measured and used to predict MOE of the panel. Three hundred and three pieces of full-size wood composite panels were tested using a laboratory testing apparatus. The panels tested include a variety of thickness specifications of medium density fiberboard (MDF), particleboard and plywood. The results of vibration testing on full-size panels were then compared with those of static bending tests on small specimens. The relationships between the results of these two testing methods were examined.

Theoretical basis

“Free-free” support refers to the panel supported at its two nodal lines which are at 22.4% and 77.6% of the length on its length direction. And the panel’s free vibration in this supporting condition is called “free-free” supporting free vibration. Figure 1 shows the first vibration mode of the full-size wood composite panel supported in “free-free” condition. The first vibration mode of the full-size wood composite panel in this supporting condition is the same to the vibration mode of the beam supported in the same position (Zhou et al.2014). So, the calculation method for MOE of the beam in this supporting condition can be used to calculate MOE of the full-size wood composite panel. And, this MOE is correspond to the modulus of elasticity in the length direction of the panel. In this paper, this MOE is called the dynamic MOE of the full-size wood composite panel. Then, according to the Euler-Bernoulli vibration theory, the dynamic MOE of the full-size wood composite panel is calculated using Eq. (1):

$$E_d = \frac{4\pi^2 ML^3}{4.73^4 I} f^2 \qquad (1)$$

where E_d is the dynamic MOE of the panel (Pa), f is the first natural vibration frequency of the panel (Hz), M is the weight of the panel (Kg), L is the length of the panel (m), I is the inertia moment of the cross section (m^4). And $I = \frac{bh^3}{12}$, b is the width of the panel (m), h is the thickness of the panel (m). When panel geometry size (L, b, h) is given, MOE of the panel can be calculated in the condition of detecting the first natural vibration frequency f and the weight M. This is theoretical basis for dynamic determination of MOE of the full-size wood composite panel.

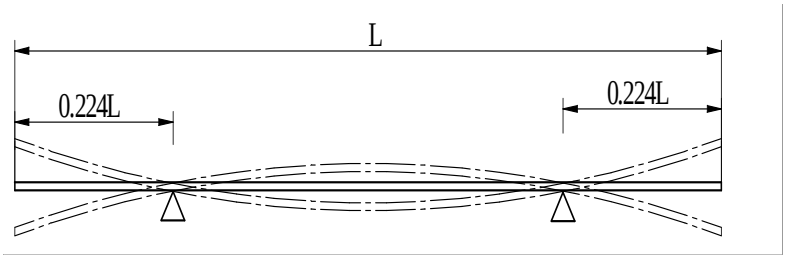

Figure 1-First vibration mode of the full-size wood composite panel supported in “free-free” condition

Materials and methods

Materials

Three hundred and three pieces of full-size wood composite panels were used in this study, including 101 pieces of medium density fiberboard (MDF) with 6 different thicknesses, 100 pieces of particleboard with 6 thicknesses, and 102 pieces of plywood with 8 thicknesses. The MDF panels were provided by Krono Beijing wood industry co., LTD., and the particleboard and plywood were purchased from local market. Table 1 shows the specifications of the panels. In order to facilitate recording test results, the panels were numbered. MDF represented medium density fiberboard, PW represented plywood and PB represented particleboard. The figure behind the letters represented the thickness of the panel. And the mantissa represented serial number of the panel. The nominal length and width of the panels were 2440 mm × 1220 mm, so they weren’t marked. For example, MDF8-1 meant the panel was medium density fiberboard, and in the “8-1” behind the letters, “8” represented the thickness was approximately 8 mm, while the “1” was the No. All the panels were stored in a chamber of a temperature of 21±2ºC and relative humidity of 60±2% before and during the test.

After conducting the dynamic detection test described below, measured panels were cut into standard small specimens according to the Chinese standards request (GB/T 2003; GB/T 2009). Six pieces of small specimens was cut from each full-size wood composite panel along the length of the panel. The cut-off small specimens were used for the center-loading bending test. Detailed dimension parameters are given in Table 2.

Testing apparatus and dynamic detection test

The Laboratory testing apparatus was developed by our research group for measuring mechanical performance of full-size wood composite panels, as shown in Figure 2. This apparatus was mainly composed of two load cells, one laser sensor and the supporting mechanism. Among of them, two load cells were used to measure the weight of the full-size wood composite panel, and the supporting rod on the two load cells made the panel achieve the right nodal line support; the laser sensor was used to sense vibration displacement signal at the middle of the full-size wood composite panel; the supporting mechanism, as the structural foundation of the apparatus, was used for standarding the panel’s placed location and fixing two load cells, and the supporting rod on the left side made the panel achieve the left nodal line support. The apparatus’s software was written by LabVIEW, to achieve the collecting and processing of the force signal and the laser vibration signal, MOE calculation and result storage.

In the dynamic detection test, the panel was first placed in the correct position on the apparatus, to make sure the panel supported by lines at the 22.4% and the 77.6% on its length direction; the testing software was run in the computer to collect the load cell signal and calculate the weight of the measured panel. Then pressing the panel at the end away from the load cell with both hands, the panel started free vibration. At this time, the panel’s vibration signal detected by the laser sensor was transmitted to the computer with a data acquisition card, and was processed through the testing software to get the first natural vibration frequency of the panel. According to Eq. (1), the calculation

module was compiled in the testing software and was finally used to calculate the dynamic MOE E_d of the panel.

Table 1-Specifications of full-size wood composite panels

Panel serial number	Material	Quantity (piece)	Panel average sizes (thickness × length × width, mm)	Average density (g/cm^3)	Average moisture content （%）
MDF5	MDF	10	5.92×1221.2×2442.7	0.76	9.0
MDF8	MDF	9	8.11×1220.8×2442.2	0.82	4.0
MDF12	MDF	25	11.94×1220.4×2439.7	0.79	6.8
MDF16	MDF	41	15.98×1220.0×2442.4	0.75	4.9
MDF18	MDF	7	18.04×1220.6×2439.4	0.79	4.7
MDF20	MDF	9	19.88×1220.3×2441.4	0.70	9.0
PB5	particleboard	8	4.64×1221.8×2444.9	0.73	9.0
PB9	particleboard	15	9.00×1222.9×2442.2	0.66	4.5
PB12	particleboard	17	12.20×1223.1×2442.2	0.71	4.1
PB16	particleboard	25	16.04×1223.1×2441.0	0.70	4.3
PB18	particleboard	25	18.03×1220.2×2437.0	0.66	5.7
PB25	particleboard	10	25.05×1220.9×2440.7	0.68	6.8
PW5	plywood	7	4.98×1218.6×2439.4	0.51	9.0
PW7	plywood	8	6.52×1218.9×2437.9	0.53	9.5
PW9	plywood	19	9.42×1219.1×2438.1	0.51	9.4
PW12	plywood	7	11.34×1224.9×2438.9	0.53	9.0
PW15	plywood	19	14.45×1220.8×2439.3	0.51	10.5
PW18	plywood	18	17.04×1221.1×2438.4	0.52	8.6
PW20	plywood	8	19.46×1218.0×2439.4	0.51	9.0
PW25	plywood	16	24.36×1219.2×2439.5	0.53	9.8

Table 2-Small specimens' sizes and quantities

Thickness *h* (mm)	Length *l* (mm)	Width *b* (mm)	Quantity(piece)
5	150	50	150
7	190	50	48
8	210	50	54
9	230	50	204
12	290	50	294
15	350	50	114
16	370	50	396
18	410	50	300
20	450	50	102
25	550	50	156

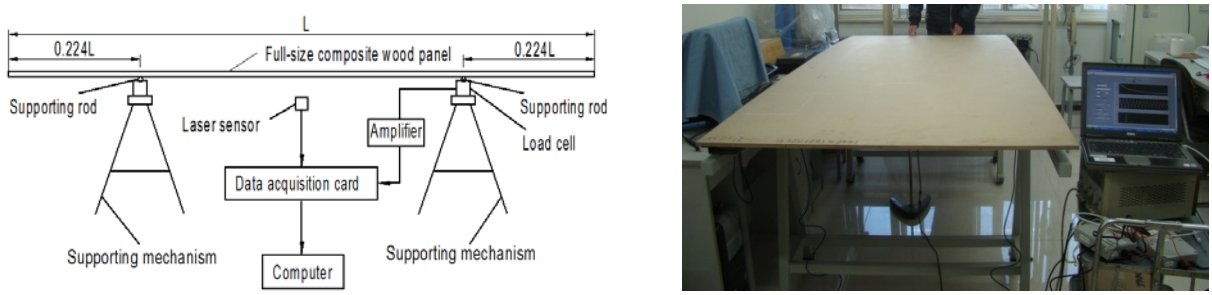

a-Schematic diagram b-Photo

Figure 2-Laboratory testing apparatus for measuring mechanical performance of full-size wood composite panels

Static bending test

In order to examine the feasibility and validity of dynamic testing method, according to the testing standard of GB/T 17657-2013 (GB/T 2014), the center-loading static bending test was carried out on the small specimens, as shown in Figure 3. The small specimens were loaded at the mid-span on the universal mechanical testing machine (RGW-3010, Shenzhen Reger instrument co., LTD., China) till failure to obtain MOE and flexural strength. The average value of MOE of the six small specimens represents the MOE of a full-size wood composite panel.

Figure 3-Static bending test on small specimens

Results and discussion

Comparison between the average measured results

The overall measurement results of 303 pieces of full-size wood composite panels in the dynamic detection method and center-loading bending method are given in Table 3, Table 4 and Table 5, including 6 kinds of thicknesses of MDF, 6 kinds of thicknesses of particleboard and 8 kinds of thicknesses of plywood. It can be seen from these tables, that the average MOE measured in the two methods are very close and their ratio are in the range of 0.94~1.18; in most cases, the dynamic MOE E_d is slightly higher than the bending MOE E_b; all the full-size wood composite panels as the research object, the average dynamic MOE E_d is 6.2% higher than the average bending MOE E_b.

Table 3- The results of MOE of MDF tested in the two methods

Panel serial number	MOE symbol	MOE（MPa）			SD	The ratio of the average MOE（E_d/E_b）
		Average	Min	Max		
MDF5	E_d	4183.87	3686.59	4498.42	285.45	1.04
	E_b	4010.97	3540.59	4235.60	247.14	
MDF8	E_d	3693.49	2803.25	4342.82	423.78	1.06
	E_b	3486.67	2582.42	4259.98	482.06	
MDF12	E_d	3933.18	3295.65	4378.28	336.06	1.02
	E_b	3841.25	3029.43	4344.10	359.60	
MDF16	E_d	3431.64	2561.00	4144.59	246.57	1.12
	E_b	3066.03	2010.00	4051.98	299.95	
MDF18	E_d	3660.69	2978.18	4042.61	355.05	1.09
	E_b	3354.88	2593.98	3541.57	341.51	
MDF20	E_d	3126.93	2709.59	3976.00	357.27	1.11
	E_b	2818.77	2446.91	3674.89	397.65	

Table 4- The results of MOE of particleboard tested in the two methods

Panel serial number	MOE symbol	MOE（MPa）			SD	The ratio of the average MOE（E_d/E_b）
		Average	Min	Max		
PB5	E_d	3855.73	3616.00	4204.55	179.58	1.01
	E_b	3831.28	3601.08	4118.91	148.60	
PB9	E_d	2946.55	2640.91	3531.00	241.87	1.08
	E_b	2732.01	2461.28	2975.18	139.46	
PB12	E_d	3704.77	2862.00	4379.50	424.11	1.02
	E_b	3632.47	2824.15	4193.67	485.57	
PB16	E_d	3677.43	3399.87	3949.61	143.24	1.07
	E_b	3421.19	3230.89	3750.44	122.20	
PB18	E_d	2368.07	1966.20	2725.30	166.29	1.14
	E_b	2083.80	1842.31	2520.79	187.93	
PB25	E_d	3060.73	2464.27	3595.15	427.96	1.13
	E_b	2697.27	2168.93	3236.42	433.03	

Table 5- The results of MOE of plywood tested in the two methods

Panel serial number	MOE symbol	MOE（MPa）			SD	The ratio of the average MOE（E_d/E_b）
		Average	Min	Max		
PW5	E_d	3760.75	3166.00	4121.00	339.72	1.12
	E_b	3355.19	3021.26	3821.71	273.47	
PW7	E_d	3419.63	2804.06	4308.03	473.24	1.18
	E_b	2907.57	2529.00	3406.03	316.38	
PW9	E_d	3728.86	2865.76	4250.21	322.92	1.07
	E_b	3480.46	2449.88	4320.78	459.50	
PW12	E_d	4739.48	4131.00	5142.68	329.43	0.94
	E_b	5034.74	4558.33	5384.30	283.65	
PW15	E_d	3288.14	2902.69	3747.11	226.07	1.04
	E_b	3159.08	2355.29	3664.01	338.82	
PW18	E_d	4683.79	4084.69	5331.54	336.72	1.09
	E_b	4301.59	3552.95	5346.43	522.49	
PW20	E_d	4611.26	4150.61	4888.84	242.00	0.96
	E_b	4810.87	4343.18	5176.44	317.65	
PW25	E_d	4781.30	4173.00	5372.02	297.64	1.12
	E_b	4260.87	3347.44	5011.19	452.91	

Table 3 shows the MOE measurement results of MDF in the two methods and their comparison. It can be seen that the average dynamic MOE E_d of six kinds of thicknesses of MDF is slightly higher than their average bending MOE E_b and their ratio are in the range of 1.02~1.12. Table 4 shows the MOE measurement results of particleboard in the two methods and their comparison. It can be seen that the average dynamic MOE E_d of six kinds of thicknesses of particleboard is slightly higher than their average bending MOE E_b and their ratio are in the range of 1.01~1.13. Table 5 shows the MOE measurement results of plywood in the two methods and their comparison. It can be seen that, in addition to the plywood with the thickness of 12 mm and 20 mm, the average dynamic MOE E_d of other six thicknesses of plywood is slightly higher than their average bending MOE E_b and their ratio are in the range of 0.94~1.18.

Correlation relationship between dynamic MOE E_d and bending MOE E_b of full-size wood composite panels

Through the laboratory testing apparatus for measuring mechanical performance of full-size wood composite panels and the universal mechanical testing machine for measuring MOE of the small specimens, the dynamic MOE E_d of three types of full-size wood composite panels and their bending MOE E_b are obtained, and the overall relationship between them are shown in Figure 4. Figure 5, Figure 6 and Figure 7 show that the relationships between MDF, particleboard, plywood's E_d and E_b respectively. It can be seen from the figures, whether three kinds of panels' measured results are put

together, or are analyzed separately, a statistical linear relationship is found between dynamic MOE E_d and bending MOE E_b of full-size wood composite panels.

Based on the R language modeling, these test data are analyzed using regression analysis in one variant linear regression analysis method, analysis of variance and t test (Wang et al.2014). The linear regression equations and the related parameters are given in Table 6. It can be seen from Table 6, regardless of three kinds of panels' overall data or each kind panel's data, that a positive linear relationship is found between E_d and E_b, and their relationships are all highly significant at the 0.001 level. In addition, the correlation coefficient of full-size wood composite panels' overall data between E_d and E_b is 0.923; the correlation coefficients of MDF and particleboard between E_d and E_b are 0.956 and 0.953 respectively, exceeding 0.95; the correlation coefficient of plywood between E_d and E_b is 0.838, but is more than 0.8. According to the experience of statistics theory, based on significant linear relationship between two groups of data, as long as the correlation coefficient is greater than or equal to 0.8, two groups of data' correlation are considered to be highly relevant. It can be concluded that the correlation of full-size wood composite panels' overall data and each full-size wood composite panel' data between E_d and E_b are highly relevant. Compared with other two kinds of panels, the correlation coefficient of plywood between E_d and E_b is smaller. The reason may be that plywood's material is most uneven and small specimen's material uniformity and density are rather changeable compared with other two kinds of panels. As a result the average MOE of small specimens of plywood fails to fully characterize MOE of their full-size wood composite panels.

In summary, a significant and highly correlated linear relationship is found between MOE of full-size wood composite panels obtained according to two kinds of detection methods, which proves that dynamic determination of MOE of full-size wood composite panels based on"free-free" supporting free vibration theory is feasible.

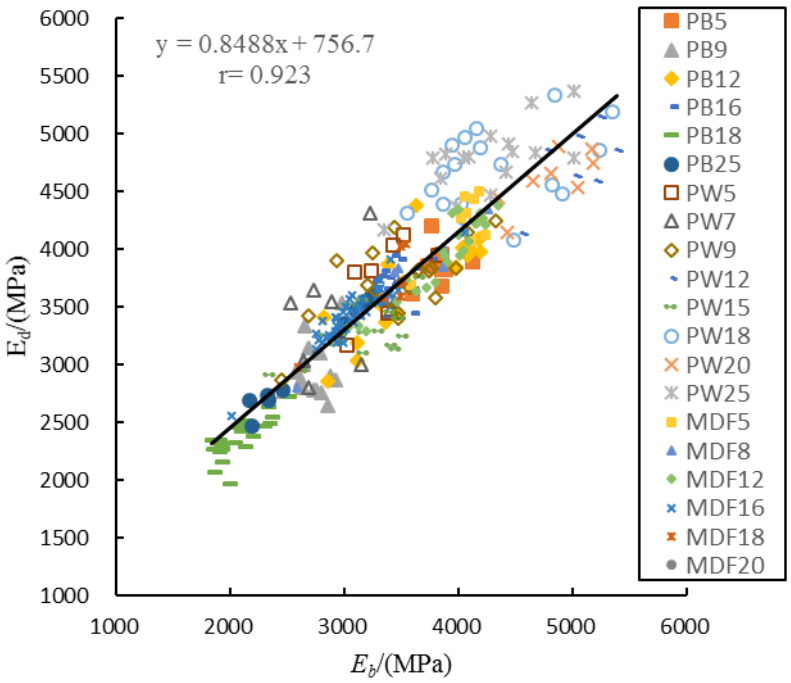

Figure 4-Relationship between full-size wood composite panels' dynamic MOE E_d and small specimens' bending MOE E_b

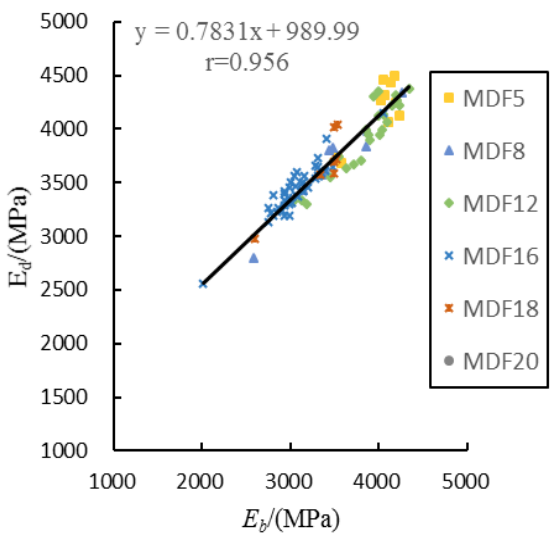

Figure 5-Relationship between the results of MOE tested of particleboard in the two methods

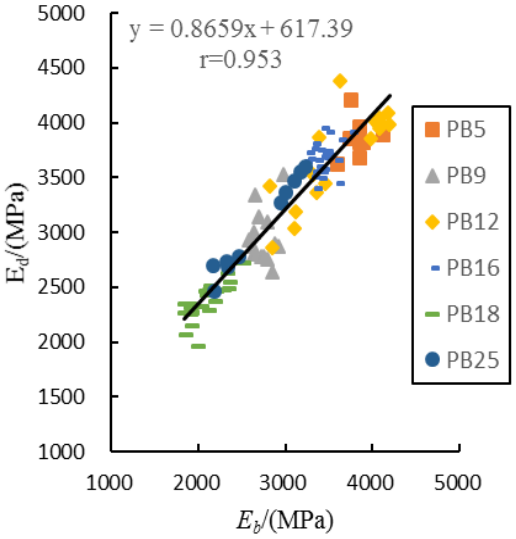

Figure 6-Relationship between the results of MOE tested of MDF in the two methods

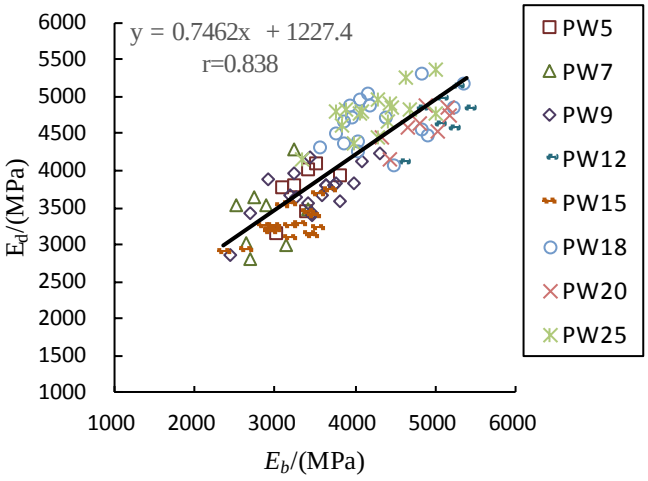

Figure 7-Relationship between the results of MOE of plywood tested in the two methods

Table 6- Linear regression equations and related parameters between dynamic MOE E_d and bending MOE E_b of full-size wood composite panels

Panel serial number	Quantity (piece)	y=ax+b		Correlation coefficient r	F	Significance*
		a	b			
MDF	101	0.7831	989.99	0.956	1039	significant（***）
PB	100	0.8659	617.39	0.953	963.8	significant（***）
PW	102	0.7462	1227.4	0.838	236.3	significant（***）
MDF、PB and PW	303	0.8488	756.7	0.923	1740	significant（***）

Note:*:‘***’0.001, ‘**’0.01, ‘*’0.05.

Conclusions

In this study, we proposed a dynamic testing method based on free vibration theory in a "free-free" supporting condition to predict MOE of full-size wood composite panels. Following the vibration testing of full-size panels, static bending tests were conducted to obtain static MOE of the panels. The feasibility and validity of dynamic testing method was examined by comparing the testing results with center-loading bending test. Based on the results and analysis, we concluded the following:

- Average MOE values of a specific thickness of MDF, particleboard and plywood obtained from two methods were very close and their ratio was in the range of 0.94 to 1.18. In most cases, the dynamic MOE of a specific thickness of the full-size wood composite panels was slightly higher than its static MOE.
- The average dynamic MOE of all full-size wood composite panels tested were 6.2% higher than their average static MOE.
- A significant linear relationship was found between E_d and E_b for three types of full-size wood composite panels (MDF, particleboard and plywood) tested.
- Compared with the static bending of small specimens, the vibration testing method proposed in this study has an advantage in achieving a rapid and nondestructive evaluation, which makes the on-line quality control possible in production settings.

Acknowledgements

This project was funded by the State Forest Administration of China through the Special Research Funds for Public Welfare. (Grant No. 201304512).

References

GB/T 4897.1-2003.2003. Particleboard-Part 1: General requirements for all board types. GB/T. Beijing: Standards Press of China.

GB/T 11718-2009.2009. Medium density fiberboard. GB/T. Beijing: Standards Press of China.

GB/T 17657-2013.2014. Test methods of evaluating the properties of wood-based panels and surfaces decorated wood-based panels. GB/T. Beijing: Standards Press of China.

Hunt J.F.; Zhang H.J.; Guo Z.R. [and others].2013. Cantilever beam static and dynamic response comparison with mid-point bending for thin MDF composite panels. BioResources. 8(1):115-129.

Lau P.W.; Tardif Y. 1996.Evaluation of moduli of elasticity and rigidity of panel products by torsional-bending vibration. Canadian Forest Service.

Moslemi A.A.1967. Dynamic viscoelasticity in hardboard. Forest Products Journal. 17(1):25-33.
Shyamasunder K.; Aswathanarayana B.S.; Naidu M.V.1994. Nondestructive evaluation of modulus of elasticity and modulus of rigidity of plywood by sonic methods. Ninth International Symposium on Nondestructive Testing of Wood. 113-116.

Turk C.; Hunt J.F.; Marr D.J.2008. Cantilever-beam dynamic modulus for wood composite products: part 1 apparatus. Research note FPL-RN-0308.Madison, WI: US Department of Agriculture, Forest Service, Forest Products Laboratory.

Wang B.H.2014. Multivariate statistical analysis and modeling for R language. 3th ed. Guangzhou: Jinan University Press.

Wang Z.; Li L.; Gong M.2012. Measurement of dynamic modulus of elasticity and damping ratio of wood-based composites using the cantilever beam vibration technique. Construction and Building Materials. 28(1): 831-834.

Yoshihara H. 2011.Measurement of the Young's modulus and shear modulus of in-plane quasi-isotropic medium-density fiberboard by flexural vibration. BioResources. 6(4): 4871-4885.

Yan H.C.; Zhang H.J.; Zhu L. [and others]. 2012. Dynamic and static modulus measurements for thin particleboard. Journal of Zhejiang A&F University. 29(1): 83-87.

Zhou H.B.; Ren H.Q.; Fei B.H. [and others].2007. Dynamical test on flexural and shear modulus of composite wood panels. Journal of Building Materials .10(5):561-565.

Zhou L.J.; Zhang H.J.; Guan C. [and others].2014. Analysis of vibration modal testing for the full-size artificial board. Journal of Multimedia .9(6): 816-821.

Zhou, X.Z. 2010.Study on development strategy of wood-based panel industry in China .Beijing: Beijing Forestry University.

Wood-based composite X-ray densitometry – attenuation effects on measurements

Konrad Solbrig
Laboratory for Timber Engineering, Products and Production, University of Applied Sciences Ostwestfalen-Lippe, Lemgo, Germany, konrad.solbrig@hs-owl.de

Katja Frühwald
Laboratory for Timber Engineering, Products and Production, University of Applied Sciences Ostwestfalen-Lippe, Lemgo, Germany, katja.fruehwald@hs-owl.de

Jörg B. Ressel
Center of Wood Sciences, University of Hamburg, Hamburg, Germany, joerg.ressel@uni-hamburg.de

Matthias Fuchs
Electronic Wood Systems GmbH, Hameln, Germany, info@electronic-wood-systems.de

Abstract

Wood densitometry serves as well-established nondestructive evaluation method since decades. In wood-based composite industry, reliable knowledge about density distributions is inevitable. Particular X-ray measuring devices are wide-spread, whereas their accuracy and capability seems questionable so far. Distinct density gradients themselves are observed to cause measuring insufficiencies. Hence, not exclusively elemental composition but structural conditions of wood-based composites, particularly porosity and respective raw density, affect actual radiation attenuation. At this, interdependent radiation-physical effects as beam hardening, multiple scattering, and radiation build-up occur. Considering X-ray spectra and setup influences additionally, subsequent detection of attenuated radiation was found not to follow conventional Beer's law anymore. Consequently introduced double-exponential attenuation law includes exponent κ beyond. This coefficient comprises the impact of present measuring conditions including material and serves as respective benchmark. The findings clarify X-ray interactions with wood-based composites and enable to derive approaches for enhancement of device setup, calibration, and data evaluation, thus, X-ray measuring systems for wood-based composite densitometry in general.

Keywords: porous media, beam hardening, multiple scattering, radiation build-up, energy spectrum, interdependencies, double-exponential attenuation

Introduction

Nondestructive methods for density profile determination by means of ionising radiation such as X- and γ-rays are well-known in several fields of wood evaluation. Manifold densitometry experiments on wood and wood-based composites were carried out hitherto both focussing on a particular application or material (e. g. wood species) as well as considering the ongoing technical progress. Furthermore, fundamental theoretical considerations complete current scientific knowledge of nondestructive density measurement and its influences, whereas also questionable applications and respective implications exist (e. g. Kim et al. (2014)).

Regarding wood, radiodensitometrical investigations of drilling cores for dendrochronological and dendroclimatological as well as mechanical purposes are common practice since decades. However, already Lenz et al. (1976) claimed methodological problems regarding calibration and feasible accuracy – just to name one study. Comprehensive theoretical wood densitometry considerations were presented by Liu and Olson (1988) and Olson et al. (1988) where they constructed parametric models for radiation attenuation and energy choice on theoretical basis under "good architecture" conditions. Beside plane techniques highlighted here, three-dimensional methods based on computed tomography (CT) are common for structural and also densitometrical investigations, where data acquisition starts out with two-dimensional projections of the object. Thus, same radiation-physical effects can be observed. Relevance and object scale of applied CT methods reaches from fundamental research over more or less worthy findings to industrial applications. Nowadays, preferably 3D applications with volumetric reconstructions from CT data gain attention due to their rising technical progress and availability. Nevertheless, this contribution concentrates on 2D projection data, where cumulation along the beam path in penetration direction arises. Finally, several findings can be transferred to CT methods. However, comprising literature review on wood densitometry is not aim of this contribution and can be found elsewhere.

Regarding wood-based composites (WBCs), radiometric methods receive growing interest both as a valuable tool in fields of material development, characterisation, and optimisation as well as regarding technical evaluation and improvement of the methods themselves. The latter case comprises measuring techniques which are industrially utilised for decades where laboratory and inline devices need to be distinguished. Their application for measurement of vertical raw density profile (RDP, lab and inline) and in-plane area density distribution (ρ_A, inline only) on WBC panels is state of the art by means of X- and γ-rays within this industrial sector. Such measuring systems and their results reveal a varying deep integration into individual process control and quality assurance depending on WBC type and plant performance. Notwithstanding the above, WBC producers need reliable nondestructive measuring devices due to both economical and ecological reasons to obtain high efficiency in raw material (wood and resin) and energy consumption, thus to save production costs and to go easy on resources.

First scientific investigations on in-plane area density distribution measurement were done by Walter and Wiechmann (1961) and Polge and Lutz (1969). The latter determined also vertical RDP utilising X-ray films likewise Nearn and Bassett (1968) as well as Henkel (1969) beside employing an ionisation chamber as detector. May et al. (1976) developed a viable detector-based measuring principle by means of radioisotope ^{241}Am and a scintillator, which still features today's lab devices but with X-ray tube instead. Various investigations followed meanwhile. However, a rethinking of X-ray systems utilised on WBCs is required by now. Contributions of Solbrig et al. (2014a) and Solbrig et al. (2015) give a technical overview, quantify measuring accuracy and validity, and point out demand and benefit of reliable measuring devices for WBCs. Fundamental considerations likewise Liu and Olson (1988) or Olson et al. (1988) are still pending on WBCs with practical regards. This contribution clarifies processes during irradiation of WBCs by X-rays considering the total beam path from source to detector and explains particular implications on measurement.

Empirical considerations

Motivation

Hitherto own work (partly unpublished) including numerous empiric experiments demonstrated potential failure sources and their impact on densitometric measuring results. Round robin test results and conclusions of Solbrig et al. (2014a) illustrate metrological consequences of radiation-physical effects considered hereafter. To outline all observations on insufficient X-ray devices, deviations from the real raw density occur in case of distinctly shaped gradients, i. e. with high ratios between maximum and

minimum raw density. Thus, sample heterogeneity itself biases its radiometric determination likewise Moschler Jr and Winistorfer (1990) and Rautkari et al. (2011) point out. As a consequence, ratio of extremes and shape of raw density gradient are flattened in general. This particularly becomes clear with more distinctive RDPs within WBCs (e. g. MDF 30 mm, ρ_{mean} = 770 kg/m³, ρ_{min} = 650 kg/m³, ρ_{max} = 1130 kg/m³, $ratio_{max/min}$ = 1.74). Not only in case of typical vertical RDPs or special sandwich composites, also regarding in-plane area density distribution, where the measuring device has to manage a wide product, i. e. area density, range and densification ratio differs significantly from furnish mat to final panel, similarly biased results are conceivable. Despite WBC applications, analogous conditions apply to tree-ring analyses with respective early and late-wood density ranges (e. g. pine 340…900 kg/m³, $ratio_{max/min}$ = 2.65) or densitometry on other lignocellulosic material with distinct raw density gradients (e. g. coconut palm 300…1050 kg/m³, $ratio_{max/min}$ = 3.50). To summarise, insufficiencies arose among others from replacement of (monoenergetic) radioisotopes by (polychromatic) X-ray sources without any adaption of calibration and data evaluation procedures to radiation-physical requirements in the past. Hence, energy-dependent attenuation mechanisms and subsequent beam hardening have to be considered additionally to scattering impact.

Interaction mechanisms

Within the suitable energy range for WBC applications E_{max} < 100 kVp, attenuation is caused by photoeffect (photo) and coherent (coh, Rayleigh) as well as incoherent (incoh, Compton) scattering as is known. Their respective prevalence depending on the actual energy (Figure 1) is considerable regarding the origin of detected radiation, which will be discussed in the section hereafter. Where interaction between radiation and matter happens, will be covered below whilst clarifying metrological consequences.

While penetrating radiation, i. e. photons of particular energy, travels through WBCs, its interaction with matter and the related information content of measurement have to be considered on distinct scales. The irradiated specimen appears on macroscopic scale as solid body featuring a certain raw density ρ [kg/m³] with, in turn, a potentially three-dimensional distribution. At this, cumulated radiation transmission is governed by the amount of matter along the beam path, i. e. area density ρ_A [kg/m²]. This corresponds to the measuring scale whose resulting information content equals a line integral from radiation source to detector surface averaging the information weighted along the travelled path. Wood is well-known not to be homogeneous material. Thus, radiation interaction distinguishes on microscopic scale representing the cell structure. Independ from wood species, cell wall substance shows approximately equal dry true density ρ_{true} ≈ 1500 kg/m³ (only minor differences between main components). Wood as hygroscopic material contains water as vapour within air-filled lumina or adsorbed within surrounding cell wall in equilibrium with ambient conditions. WBCs additionally contain adhesive resin and possibly further additives (e. g. paraffin or fire retardants) which partly penetrate into wood particle pores. Hereafter, resin considerations are limited to the economic and technical most important and chemical rather less complex resin type urea-formaldehyde (UF). Between macroscopic and microscopic level, WBCs require a mesoscopic scale for structural considerations to be characterised by a consolidated wood particle-resin matrix including voids filled with moist air. Wood particles of variously predefined shapes are both covered totally and incompletely by resin. Subsequently, wood particles touch each other either directly or with intermediate resin layer. Consolidation ratio causes final porosity and resulting raw density (bulk density). During penetration of WBCs, radiation does not travel constantly through condensed matter but the beam path shows permanent alternations of cell wall substance, water, resin, facultative additives, and moist air. Depending on void size, the latter allows infinitesimal free radiation propagation within air in between consolidated matter on account of comparatively low interaction probability which in turn facilitates divergence of scattered radiation. Furthermore, mineral components from wood itself, bark or impurities with varying amount due to WBC type have to be taken into account for attenuation. Thus, both structure and components are relevant for radiation attenuation on mesoscopic and microscopic scale whereas the actual photon interaction mechanisms with respective matter happen on sub-microscopic, i. e. atomic, scale.

To conclude in short, radiometric density measuring results (ρ [kg/m³] or ρ_A [kg/m²]) represent the macroscopic conditions of irradiated WBCs, whereas on the one hand their mesoscopic and microscopic structures affect total radiation transmission and on the other hand actual radiation-matter interaction happens on sub-microscopic (atomic) scale. Independent from consolidation ratio of wood furnish, the latter refers to respectively equal true densities of relevant components present, i. e. wood substance, resin, additives, and water. Consequently, transmitted radiation primarily contains information about irradiated mass of matter, i. e. area density ρ_A, expecting a homogeneous non-porous absorber. Hence, subsequent raw density evaluation requires mass attenuation coefficients μ/ρ [m²/kg] determined with a priori knowledge of structural conditions. Otherwise, tabulated μ/ρ, which refer to atomic cross sections, exclusively yield ρ_A and are not applicable for direct densitometry on porous media. Likewise, Liu and Olson (1988) confirm ρ_A as "[…] significant parameter that determines the degree of attenuation." Furthermore, they comprehensively consider "good architecture" conditions as

- linear source-absorber-detector alignment with vertical radiation incidence,
- convergent, narrow collimated (prior and behind absorber) beam,
- absorber of uniform thickness, and
- monochromatic radiation with optimal energy (according to Olson et al. (1988))

where radiation attenuation is described by exponential intensity diminution following well-known Beer's[1] law

$$I = I_0 \cdot e^{-\frac{\mu}{\rho}\cdot\rho\cdot t} \tag{1}$$

with transmitted I [-] and initial intensity I_0 [-], mass attenuation coefficient μ/ρ [m²/kg], raw density ρ [kg/m²], and penetration length t [m]. In practical WBC densitometry, these conditions cannot be reasonably met in any case due to following considerations.

Beam hardening, scattering and radiation build-up

Employing divergent beams of polychromatic X-rays for densitometry, structural conditions of WBCs and raw density distributions themselves, e. g. high void ratio of furnish mats or distinct vertical RDP of panels, lead to radiation-physical interdependencies of metrological relevance regarding desired measuring accuracy. On account of monotonically increasing $\mu/\rho(E)$ with decreasing energy and respectively prevalent photoeffect (Figure 1), low-energy radiation portions of polychromatic X-ray spectra gain accordingly stronger attenuation – particularly real absorption – during transmission through matter. The consequent rise of mean energy level, namely beam hardening, along the penetration length leads to correspondingly decreasing $\mu/\rho(E)$. Moreover, scattering as attenuation process does not absorb radiation but changes only its direction and (in case of incoherent Compton scattering) energy once or several times. In the latter case, scattered radiation passes secondary attenuation processes again, i. e. multiple scattering. As a result, scattering interaction subtracts the respective radiation portion only indirectly from the primary beam. Thus, scattered radiation is any longer present around the primary beam axis. Scatter-to-primary ratio differs from zero (SPR > 0) if scattered radiation superimposes transmitted primary radiation on detector. In case of pixel-wise X-ray imaging, scattering background leads to image blurring and poor contrast. Due to common signal integration across detector area in case of metrological applications, detector collects scattered radiation originating from sample ROI vertically above detector region or even beyond. Thus, detected scattering intensity I_S in addition to intensity of attenuated primary beam I_P appears as less diminished total transmitted intensity I. Hence, Eq. (1) is invalid for data evaluation because it supposes extraction of attenuated radiation from transmitted beam, i. e. absorbance, (cf. Kasperl (2005)). However, radiation build-up factor $B(E)$ enables quantitative

[1] Note, the shortest designation of this historically evolved physical law (cf. Perrin (1948)) was chosen.
Perrin, F. H. – Whose Absorption Law? Journal of the Optical Society of America 38 (1948) 1. p. 72-74.

consideration of scattered beside transmitted primary radiation on detector, whereas its experimental determination is non-trivial (cf. Halmshaw (1995)). Radiation build-up considerations were hitherto especially of dosimetric interest regarding radiation protection (e. g. build-up behind shieldings) and biological materials (e. g. differences between muscle, tissue, and bone) but emerge also in terms of metrology (cf. Halmshaw (1995) or Shirakawa (2000)). Within WBC-relevant energy range in general, build-up factor increases with increasing energy, decreasing atomic numbers, and increasing penetration length such as Sidhu et al. (2000) show theoretically for various biologic materials.

To conclude theory, both beam hardening and scattered radiation bias the linear slope of $\ln(I_0/I)$ along increasing material thickness (with constant homogeneous density) likewise Kasperl (2005) points out regarding his artefact reduction approaches for CT. I. e., non-linear context between ρ_A and $\ln(I_0/I)$ arises due to energy-dependent decreasing $\mu/\rho(E)$ with ongoing beam hardening as well as constant scattering intensity I_S in addition to decreasing primary intensity I_P (thus, increasing SPR I_S/I_P). Share of scattering in total attenuation is energy-dependent and increases with increasing energy (Figure 1, from 15 keV $\mu_{incoh}/\rho(E) \approx$ const. whereas $\mu_{photo}/\rho(E) \downarrow$). Beam hardening increases mean energy which in turn increases share of scattered radiation. As can easily be seen from these radiation-physical interdependencies, scattered radiation intensity appears higher in case of higher raw density at constant penetration thickness because SPR increases (e. g. RDP measurement). However, true density remains constant and increasing area density, i. e. increasing virtual thickness of homogeneous non-porous matter, implies beam hardening. Hitherto common calibration for furnish mat area density measurement was carried out on ready-pressed panels (cf. Fuchs (2010) and Solbrig et al. (2014b)). According to Fuchs (2010) and own observations employing the same cone beam setup on furnish mat and final panel, mass attenuation coefficients differ, i. e. $\mu/\rho_{mat} > \mu/\rho_{panel}$. Because of geometrical conditions, less scattered radiation reaches detector in case of irradiated furnish mat due to higher penetration length and interaction volume, whereas true density (i. e. matter responsible for interaction mechanisms) and area density ρ_A (i. e. virtual thickness of homogeneous non-porous matter) remain constant. Thus, likelihood of secondary attenuation (even absorption due to lower energy of incoherent scattered radiation) increases with increasing length of the beam path. Furthermore, interaction probability of scattered radiation is assumed to be higher around primary beam path through furnish mat in comparison to panel due to larger irradiated volume. Beyond that, irradiated mass per detector area (i. e. amount of irradiated matter) is higher in case of furnish mat compared to panel on account of divergent (fan or cone) beam. Irradiated panel cross section is smaller than detector area. To summarise, not beam hardening (whose influence nevertheless cannot be excluded) but detected scattered radiation and irradiation geometry cause this phenomenon to be considered for area density determination primarily. At this, likelihood of divergence of scattered radiation from primary beam axis increases with increasing material porosity (i. e. decreasing raw density at constant area density), which in turn decreases the portion of scattered radiation in detector signal on account of multiple scattering. Nevertheless, measuring signal as integrated intensity over detector area, exposure time, and energy spectrum furthermore differs from actually transmitted spectrum due to weighting by spectral detector sensitivity and characteristic output behaviour. Thus, detector response function $D(E)$, whether known or not, affects accuracy of X-ray densitometry additionally. Finally, consideration of interdependent radiation-physical effects and technical conditions results in

$$I = I_0 \cdot \int_E S(E) \cdot D(E) \cdot B(E) \cdot e^{-\frac{\mu}{\rho}(E) \cdot \rho_A} dE \tag{2}$$

according to Eq. (1) extended by initial energy spectrum $S(E)$, detector response function $D(E)$, and radiation build-up factor $B(E)$ as well as energy-dependent mass attenuation coefficient $\mu/\rho(E)$ and area density $\rho_A = \rho \cdot t$ with integration over the continuous energy range E.

X-ray energy choice and spectra modelling

Eq. (2) enables explicit quantitative consideration of emitted X-ray spectrum but requires knowledge about $S(E)$ and does not replace sophisticated energy predefinition. Estimation-driven setting of rather too high X-ray energy is state of the art and rarely brought into question so far. Nevertheless, reliable densitometry requires mean energies on an individually optimal level and spectra meeting certain conditions to increase measuring accuracy and sensitivity. Therefor, Rózsa (1987) and Walter and Wiechmann (1961) likewise suggest to adapt radiation properties to actually measured ρ_A to fulfil

$$\frac{\mu}{\rho}(E) = \left(1...1.5 \cdot \rho_A\right)^{-1} \tag{3}$$

which corresponds to radiation attenuation of 1/e. Olson et al. (1988) deliver a similar approach aiming at maximum radiation resolution in relation to maximum density range. Accordingly, ideal $\mu/\rho(E)$ has to be found following

$$\frac{\mu}{\rho}(E) = \frac{\ln\left(\rho_{\max}/\rho_{\min}\right)}{\left(\rho_{\max} - \rho_{\min}\right) \cdot t} \tag{4}.$$

Beyond that, intensity peak energy of spectral distribution $E_{I\text{peak}}$ is suggested to be set slightly below optimal energy due to expected beam hardening and already existing high-energy share of emitted spectrum. On account of lean total system design affordable by industrial customers, energy setting is preferably done via power adjustment of one installed X-ray tube with respective target (commonly W). Thus, continuous spectrum has to be modelled. The monoenergetic optimum is only obtainable by means of radioisotopes or a monochromator behind X-ray tube. Both are less convenient and deliver lower radiation flux (i. e. intensity) depending on isotope activity and tube power respectively. However, two practice-oriented solutions exist. Quasi-monoenergetic spectra are feasible by target material choice leading to characteristic high intensity K_α-energy (optimisable by filter application for pre-hardening and K_β-filtering, respectively). This is common practise for analytical X-ray applications (e. g. XRD, XRF, cf. Tsuji et al. (2004)) but less flexible and limited to one (rather too low for high ρ_A) energy each because of restricted choice of anode materials. A continuous bremsstrahlung spectrum (preferably from common W target, $E_{\max} < 57$ kVp) with well-defined filter application for spectrum pre-hardening allows to obtain narrow-band energy distributions. In both cases, certain amount of (density dependent) beam hardening and related interdependent effects on measurement still have to be expected. Despite cost aspects, to equip the X-ray source with a multi-metal target (cf. Hoffman and de Beer (2012)) is considered as highly sophisticated solution, which enables to utilise a specific spectrum on demand – not only via filter-supported shaping the bremsstrahlung spectrum but choosing predefined high intensity characteristic energies. The same applies for energy-selective detection. However, dual-energy applications to distinguish between constituents of WBC (such as water and wood matter) appear theoretically not advisable due to absence of absorption edges of present elements within the reasonable energy range.

Variable setups employing X-ray tubes with both tungsten (W) and silver (Ag) targets completed by radiation pre-filters on demand as well as collimators were available for X-ray transmission experiments. Emitted tube spectra including application- and energy-related pre-filtering were measured by X-ray spectrometer digiBASE 905-3 with MAESTRO-32 MCA software, ORTEC, Oak Ridge, USA. Figure 1 (right vertical axis) shows exemplary spectra of different setups and tube energy levels $E_{\max}$ [kVp] corresponding to particular ρ_A ranges. Theoretical mass attenuation coefficients $\mu/\rho(E)$ of laboratory-made MDF ($\omega_{UF,\,dry} = 10$ %), its components, and single attenuation processes (computation based on measured elemental compositions and data from MuPlot (2006) following mixture rule according to Jackson and Hawkes (1981)) are plotted over energy range additionally in Figure 1 (left vertical axis).

Accordingly, attenuation processes with prevailing contribution have to be taken into account. As an indication, scattering starts to dominate where the incoherent intersects the photoeffect line (Figure 1, from 25 keV for labMDF). For $E_{I\text{peak}}$ of the plotted spectra, following attenuation relations can be deduced from data behind Figure 1 (interpolated values from MuPlot (2006)) for labMDF at 9.5 % MC:

- $E_{I\text{peak}}$ = 13 keV | 86 % photo | 7 % coh | 7 % incoh,
- $E_{I\text{peak}}$ = 16 keV | 75 % photo | 10 % coh | 15 % incoh,
- $E_{I\text{peak}}$ = 22 keV | 56 % photo | 13 % coh | 31 % incoh,
- $E_{I\text{peak}}$ = 28 keV | 40 % photo | 13 % coh | 47 % incoh.

Hence, 16 kVp setup features almost solely photoelectric absorption. Despite its narrow-band spectrum, beam hardening appears during density measurement due to the steep slope of $\mu/\rho(E)$. The same applies more markedly for 20 kVp setup with increasing scattering influence in addition. In case of 35 kVp setup, scattering dominates attenuation conditions. Notwithstanding its pre-hardened spectrum, further shift of mean energy has to be expected during irradiation of matter. In between, 55 kVp setup shows distinctly pre-filtered low-energy share and the characteristic AgK_{α}-line around 22 keV (it appears less sharp than in reality due to spectrum measurement method). However, measured maximum energy of emitted spectra exceed tube energy level (peak tube voltage) $E_{\max}$ [kVp] due to common inaccuracy of respective high-voltage generators. Furthermore, Figure 1 (inset) illustrates similar $\mu/\rho(E)$ of WBC components each and mathematically resulting negligible moisture influence.

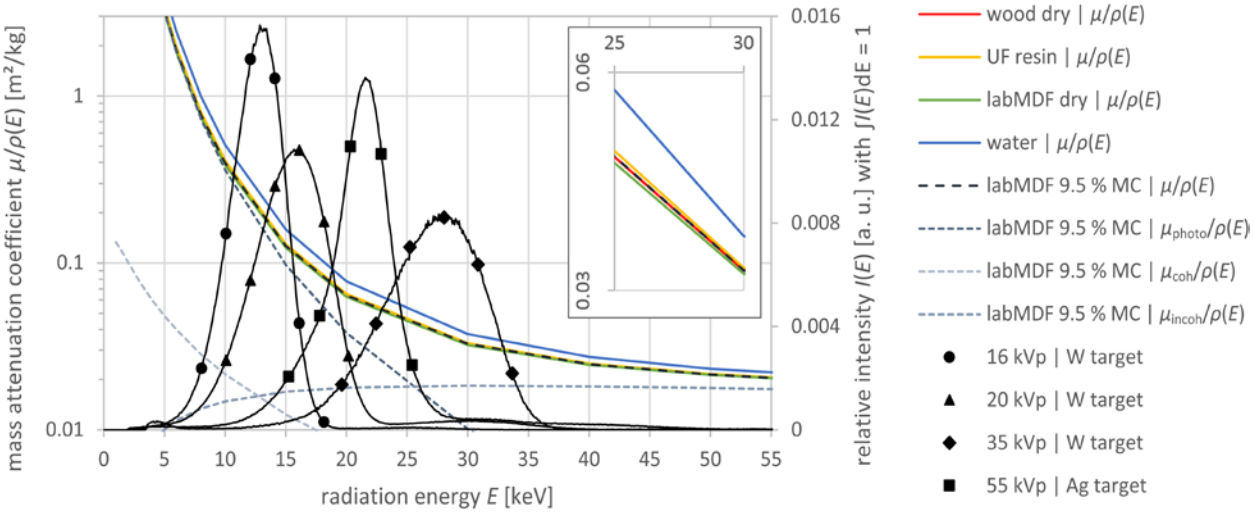

Figure 1—Plot of theoretical energy-dependent mass attenuation coefficients $\mu/\rho(E)$ of laboratory-made MDF, its components and single attenuation processes (left vertical axis, computation based on measured elemental compositions and data from MuPlot (2006) following mixture rule acc. to Jackson and Hawkes (1981)) with magnified $\mu/\rho(E)$ plot between 25…30 keV (inset) and exemplary spectra of different setups and tube energy levels $E_{\max}$ [kVp] for particular ρ_A ranges.

A reasonably high photoeffect share appears feasible on low energy levels for appropriate ρ_A ranges. Nevertheless, this does not apply for measuring conditions which require high penetration power. Beyond that, slope of $\mu/\rho(E)$ within related energy range of the applied spectrum has to be preferably flat. Finally, energy choice requires coordination between all those conditions and above discussed interdependent radiation-physical effects regarding WBCs. Additionally, radiation flux contributes to measuring accuracy and contrasts to intended reasonably low total power for efficiency and radiation protection reasons as well as preferably reduced beam dimensions according to scattering considerations. Notwithstanding that, practical WBC densitometry needs sufficiently implied agreements. A detector-specific minimum photon flux vertical to detector area is required to obtain good statistics in measuring results. Referring to this, Solbrig et al. (2015) quantify and discuss subsequent measuring performance and appropriate resolution in terms of distinguishability between ρ_A values. However, rigorous detector collimation or a scattering

grid on the one hand to reduce the scattering signal portion would be at the expense of detection statistics and signal-to-noise ratio (SNR). On the other hand, source collimation (or better focussing) is necessary to avoid irradiation of volumes beyond sensitive detector area whereas a pencil beam is out of proportion. Too narrow source collimation reduces available photon flux and complicates setup alignment. Beyond that, particularly ρ_A measurement requires signal integration across a distinct detector area not to map only structural inhomogeneities on mesoscopic scale of the particle mat. Hence, practical WBC densitometry requires well-defined lateral beam path dimensions.

Double-exponential attenuation law

On account of time-consuming and error-prone metrological scattering determination as well as the difficulty to define and implement $S(E)$, $D(E)$, and $B(E)$ comprehensively, a rather practice-oriented approach was explored as follows. From Eq. (1), the linear context between measuring signal $\ln(I_0/I)$ and area density ρ_A

$$\ln\left(I_0/I\right) = \frac{\mu}{\rho}(E) \cdot \rho_A \tag{5}$$

with appropriate energy-dependent mass attenuation coefficient $\mu/\rho(E)$ as constant of proportionality becomes obvious, which intersects point of origin (0; 0) under "good architecture" conditions. All deviations from this linear relationship are assumed to be caused by both technical conditions (e. g. non-linear detector response) and radiation-physical effects. From hitherto own WBC irradiation experiments (to be published elsewhere) it was found, that corresponding measuring result plots do not comply with Eq. (5) under holistic considerations. Particularly, an approximately linear slope exists only within a distinct range without zero-intersection but the curve is strictly monotonically increasing. Consequently, the relationship needs to be described by power function

$$\ln\left(I_0/I\right) = \left(\frac{\mu}{\rho}(E) \cdot \rho_A\right)^{\kappa} \quad \left\{\kappa \in \mathrm{R} \mid 0 < \kappa\right\} \tag{6}$$

in which the exponent κ [-] (lowercase Greek letter kappa) is introduced to conduce as dimensionless measure for deviation from the close linear context caused by previously discussed radiation-physical and technical effects subject to irradiation of inhomogeneous porous low-Z material by divergent polychromatic X-rays. Conversion of Eq. (6) into the pattern of exponential attenuation law yields

$$I = I_0 \cdot e^{-\left(\frac{\mu}{\rho}(E) \cdot \rho_A\right)^{\kappa}} \tag{7}$$

henceforth introduced as double-exponential attenuation law with κ raised to the power of the well-established Beer's law and corresponding to structural attenuation characteristics of divergent X-rays. Despite meeting the observed conditions, Eq. (7) totally differs from the approach regarding Eq. (2). However, additional terms in Eq. (2) just multiply exponentially attenuated primary intensity with a static factor resulting from integration over energy range. On the contrary, the double-exponent $-(\mu/\rho(E) \cdot \rho_A)^{\kappa}$ yields $\mu/\rho(E)$- and ρ_A-related fitting of the slope of exponential decrease with its $\lim_{\rho A \to 0} = 1$ suiting to reality. Via irradiation experiments individually determined, the numeric value of κ [-] serves as benchmark for the adaptable characteristics of one measuring situation to compare resulting impact of setup, beam hardening, multiple scattering, radiation build-up, and further metrological relevant influences quantitatively.

Conclusions and prospects

Attenuation of divergent X-rays in WBCs is considered to provide ρ_A information on macroscopic scale whereas interdependent radiation-physical effects are caused by interactions on subjacent structural levels. Finally, total measuring situation including material, setup, and technical conditions affect actually detected transmitted radiation. Comprehensive mathematical consideration of individual effect parameters is neither feasible nor viable. Densitometry requires calibration to establish the relation between measuring signal and target value (ρ [kg/m³] or ρ_A [kg/m²]), which consequently cannot be performed on exclusively theoretical data basis. Hence, application-oriented calibration data determination is inevitable for the respective X-ray measuring systems employed in WBC densitometry. Step wedges from homogeneous materials serve as a common tool for radiometric density calibration so far. As a matter of fact, their application is invalid in case of porous media because the single steps of predefined increasing penetration length only feature area density gradients not the dedicated structural conditions, i. e. raw density and porosity. Thus, each individual calibration procedure has to mimic actual measuring situation including material. Proper application presumed, calibration comprises all conditions by itself which are partially difficult to take into account separately. Subsequently derived data evaluation algorithm implies radiation-physical effects and results in reliable measuring results. Finally, realisation of the present attenuation considerations results in capable X-ray densitometry systems for WBCs. Where X-ray measuring device manufactures have to expend certain effort on appropriate equipment development, their customers are enabled to benefit from optimised measuring devices. Therefore, Solbrig et al. (2015) report achievable measuring accuracies in the range of ±0.2 % (repeatability on 99.73 % confidence level) exemplarily for area density measurement.

Subsequently introduced double-exponential attenuation law explicitly considers radiation-physical and technical effects during irradiation of WBCs by divergent X-rays. At this, exponent κ alters the exponential slope accordingly. Thus, this comprising coefficient quantifies the impact of present measuring conditions. Despite the approach for double-exponential attenuation law is based on hitherto own X-ray transmission experiments, its holistic validity for wood and WBC densitometry has to be proven. Presumably, proposed context and coefficient κ apply for porous media density measurement in general.

Acknowledgments

This work is based upon experiments within the scope of the research project ”Erforschung und Adaptierung von radiometrischen Verfahren zur Messung von Materialdichte und -feuchte an Holzwerkstoffen unter Berücksichtigung des strukturellen Aufbaus“ funded by German Federal Ministry of Economics and Technology on the basis of a decision by German Bundestag by the lead partner AiF Projekt GmbH. Additionally, free provision of X-ray spectrometer along with simulation software by BAM Federal Institute for Materials Research and Testing Division 8.3: Non-destructive Testing/ Radiological Methods is highly appreciated. Beyond that, first author gratefully acknowledges travel grant from Stiftung Holzwirtschaft, Hamburg, Germany, as valuable contribution to enable this conference visit.

References

Friedman, W. D. 2000 The criteria for measuring average density by X-ray attenuation: The role of spatial resolution. AIP Conference Proceedings. 509(1): 1939-1946.

Fuchs, M. 2010. Neues Kalibrierverfahren an MDF-Matten vor dem Pressvorgang. Holztechnologie. 51(1): 42-45.

Halmshaw, R. 1995. Industrial radiology - Theory and practice. 2nd edition. Chapman & Hall, London.

Henkel, M. 1969. Ermittlung von Dichteprofilen an Span- und Faserplatten mit Röntgenstrahlen. Holztechnologie. 10(2): 93-96.

Hoffman, J. W.; de Beer, F. C. 2012. Characteristics of the Micro-Focus X-ray Tomography Facility (MIXRAD) at Necsa in South Africa. In: Proceedings, 18th World Conference on Nondestructive Testing. Durban, South Africa: South African Institute for Non-Destructive Testing (SAINT): 1-12.

Jackson, D. F.; Hawkes, D. J. 1981 X-ray attenuation coefficients of elements and mixtures. Physics Reports. 70(3): 169-233.

Kasperl, S. 2005. Qualitätsverbesserungen durch referenzfreie Artefaktreduzierung und Oberflächennormierung in der industriellen 3D-Computertomographie. University of Erlangen-Nürnberg. 172 p. PhD thesis.

Kim, C.-K.; Oh, J.-K.; Hong, J.-P.; Lee, J.-J. 2014. Density calculation of wood by portable X-ray tube with consideration of penetrating depth. Journal of Wood Science. 60(2): 105-110.

Lenz, O.; Schär, E.; Schweingruber, F. H. 1976. Methodische Probleme bei der radiographisch-densitometrischen Bestimmung der Dichte und der Jahrringbreiten von Holz. Holzforschung. 30(4): 114-123.

Liu, C. J.; Olson, J. R. 1988. Theoretical wood densitometry. I: Mass attenuation equations and wood density models. Wood and fiber science. 20(1): 22-34.

May, H. A.; Schätzler, H. P.; Kühn, W. 1976. Measurement of the density profile of chipboard by means of gamma rays. Kerntechnik. 18(11): 491-494.

Moschler Jr, W. W.; Winistorfer, P. M. 1990. Direct scanning densitometry: an effect of sample heterogeneity and aperture area. Wood and fiber science. 22(1): 31-38.

MuPlot 2006. MuPlot v. 1.03 - A software tool for the computation of x-ray attenuation coefficients. http://shape.ing.unibo.it/html/muplot.htm. [06.2015].

Nearn, W. T.; Bassett, K. 1968. X-Ray Determination and Use Of Surface-to-Surface Density Profile in Fiberboard. Forest Products Journal. 18(1): 73-74.

Olson, J. R.; Liu, C. J.; Tian, Y.; Shen, Q. 1988. Theoretical wood densitometry. II. Optimal x-ray energy for wood density measurement. Wood and fiber science. 20(2): 187-196.

Polge, H.; Lutz, P. 1969. Über die Möglichkeit der Dichtemessung von Spanplatten senkrecht zur Plattenebene mit Hilfe von Röntgenstrahlen. Holztechnologie. 10(2): 75-79.

Rautkari, L.; Kamke, F.; Hughes, M. 2011. Potential error in density profile measurements for wood composites. European Journal of Wood and Wood Products. 69(1): 167-169.

Rózsa, S. 1987. Radiometrische Messungen in der Industrie - Grundlagen und Meßmethoden. Franzis, München.

Shirakawa, Y. 2000. A build-up treatment for thickness gauging of steel plates based on gamma-ray transmission. Applied Radiation and Isotopes. 53(4-5): 581-586.

Sidhu, G. S.; Singh, P. S.; Mudahar, G. S. 2000. A study of energy and effective atomic number dependence of the exposure build-up factors in biological samples. Journal of Radiological Protection. 20(1): 53-68.

Solbrig, K.; Fuchs, M.; Frühwald, K.; Ressel, J. B. 2014a. Accuracy of the radiometric determination of raw density gradients on wood-based composites. Holztechnologie. 55(6): 27-34.

Solbrig, K.; Fuchs, M.; Frühwald, K.; Ressel, J. B. 2014b. X-ray based process and quality control in wood-based composites production - needs and benefits. In: Villmer, F.-J.; Padoano, E., eds. Proceedings 4th International Conference Production Engineering and Management. University of Applied Sciences Ostwestfalen-Lippe, Lemgo, Germany: 179-192.

Solbrig, K.; Fuchs, M.; Frühwald, K.; Ressel, J. B. 2015. Zuverlässiger Einsatz quantitativer Röntgenmesstechnik zur Prozess- und Qualitätskontrolle in der Holzwerkstoffindustrie. In: Proceedings, DACH-Jahrestagung. Salzburg, Austria: 1-13.

Tsuji, K.; Injuk, J.; Grieken, R. V., eds. 2004. X-Ray Spectrometry: Recent Technological Advances. John Wiley & Sons Ltd: The Atrium, Southern Gate, Chichester, West Sussex.

Walter, F.; Wiechmann, H. 1961. Dichteuntersuchungen an Faser- und Spanplatten. Holztechnologie. 2(2): 172-178.

Non-Destructive Analysis Reveals Effect of Installation Details on Plywood Siding Performance

Christopher G. Hunt[1]*, Gregory T. Schueneman[1], Steven Lacher[1], Xiping Wang[2], R. Sam Williams[1,3]

[1] Forest Biopolymer Science and Engineering, USDA Forest Products Laboratory, 1 Gifford Pinchot Dr, Madison WI, 53726 USA
[2] Engineering Properties of Wood, Wood based Materials and Structures, USDA Forest Products Laboratory, 1 Gifford Pinchot Dr, Madison WI, 53726 USA
[3] Retired
* Corresponding author Tel. 608-231-9521 cghunt@fs.fed.us

Abstract

This study evaluated the influence of a variety of construction techniques on the performance of plywood siding and the applied paint, using both ultrasound and conventional visual inspection techniques. The impact of bottom edge contact, flashing vs. caulking board ends, priming the bottom edge, location (Wisconsin vs. Mississippi) and a gap behind the siding to facilitate drainage were tested. Test fences were constructed to provide outdoor exposure of 2 replicates of each permutation using full factorial design. Yellow poplar (*Liriodendron tulipifera*), a decay prone wood species was used for the plywood to accelerate the results. After four years of outdoor exposure, mushrooms were observed on the surface of some boards and all were removed for lab evaluation. Extensive water staining was seen on the backs of the boards caused by water travelling upward from the bottom edge. Sound velocities were measured to determine the degree of decay. Herein we will present an analysis of the relative merits of ultrasound vs. visual inspection. We also analyze factors impacting performance, including the poor performance obtained when the bottom of a piece of wood is in contact with another surface, and the unusually poor performance of the gap behind siding. The study will conclude with recommendations for construction practices.

Introduction

Paint and wood substrate performance testing has traditionally been evaluated with visual inspection methods. Physical testing of the wood properties has potential advantages because of the inherent problems of bias, training, repeatability, human error, rating standards, etc. associated with visual inspection methods. Automated methods also have the potential for continuous or more frequent monitoring, labor savings, and more. This study, then, evaluated the ability of NDT via ultrasonic wave propagation through the thickness of the wood specimen to detect changes in plywood properties over time, and compared the sensitivity and degree of property change to visual evaluations.

The construction methods used to install wood siding can have a large influence on the decay rate and overall performance of the siding. In this study several installation

methods known to be detrimental to performance, but still widely practiced, were tested to see just how important they are in siding performance, and also to test the NDT methodology.

Experimental

13mm thick, 5 layer rough sawn, T1-11 plywood panels of yellow poplar were manufactured for this study because this species is extremely prone to decay and would accelerate results. Strips 14cm tall x122cm wide, representing the bottom edge of a standard siding panel were coated with Sherwin Williams (Cleveland, OH) A-100 latex primer and A-100 latex paint facing South 90 degrees in outdoor exposure for 48 months (Mississippi) or 62 months (Wisconsin). A full factorial design with 2 replicates was used, with conditions and evaluated variables shown in Table 1.

Mississippi (MS) is subtropical hot and humid, Wisconsin (WI) is temperate ranging from -30 to +30C. The ends of boards were primed and then sealed with a caulk joint to the trim, as shown in Figure 1(common), or flashed (not commonly done), which basically leaves the left and right end of the siding unfinished except for the paint on the board ends. We also tested whether a gap at the bottom of each board was helpful, as it is expected to prevent water from wicking into the wood from the flat surface below. Whether the bottom edge had a coat of primer or not was another variable, with the intention that the primer would slow moisture entry. A gap behind the siding is normally recommended to allow drying of the siding through the back face, so we tested with and without a gap. The top edge of boards was unprimed but flashed to prevent water entry, and backs were unpainted.

A Sylvatest Duo (CBS-CBT, Les Ecorces, France) unit operating at 22 kHz was used to measure ultrasound transmission time and peak energy of compression waves through the thickness of the tested wood and some unexposed controls at the end of the study. The transmitter probe and the receiver probe were positioned at the selected test point, one on each side. A constant pressure of 207 kPa was applied to the probes during each measurement cycle through compressed air control. This probe–wood contact pressure was determined based on a series of repeatability tests with different pressures and proved to enable good coupling between the samples and the probes. Samples were equilibrated to the ambient laboratory environment before testing.

The ultrasound instrument outputs the mean of five consecutive measures. An average ultrasound transmission time (UTT) and peak energy of the ultrasound signals were recorded three different times in each of three regions of a panel: top, bottom, and end near caulking or flashing. Ultrasonic velocity was calculated by the thickness of the sample measured at the time of ultrasonic measurement divided by UTT. The peak energy represents the attenuation or propagation efficiency of the ultrasound waves through the sample.

Visual evaluations of the substrate integrity and paint cracking were done annually, where a rating of 10 represents pristine condition, 5 means repainting is needed, and 1 is complete failure (ASTM 1993).

Statistical analysis was conducted with JMP Pro 11 software (SAS Institute, Chicago, IL, USA). In table 1, "P" = probability that the treatment had no impact using student's t test. "Effect" is the difference between the means of the two possible values. "Sonic measurement location" data is expressed as the difference between each location and the mean of all locations.

Observations and Discussion

Visual vs NDT Evaluation

Figure 1 shows how ultrasonic measurements were obtained. Table 1 shows the results of statistical analysis. Yellow boxes indicate a probability under 0.5% of randomly obtaining the observed difference, and orange boxes under 5%. The most sensitive analysis technique is the ultrasound speed, based on the largest observed effects and most factors found to be statistically significant. Speed of sound is linearly correlated with stiffness, and stiffness is lost when wood rots. Therefore we interpret our measurements to indicate rot. Because the only thing typically preventing untreated wood from decaying is a lack of available water, we expect low sonic velocity to correlate with high typical moisture content of the wood in service and high decay rate. Peak energy was a very poor analysis technique, by comparison.

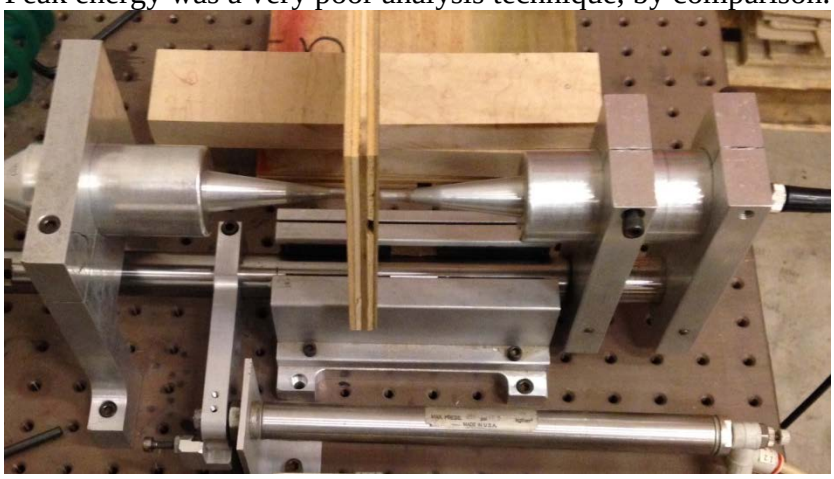

Figure 1: Apparatus for ultrasonic measurement with plywood sample in place.

Visual evaluation for paint cracking and ultrasonic velocity measurements both identified the same 3 variables as statistically significant (first three rows in Table1). The visual evaluations are faster, though they are prone to human bias, variability, and difficulties in clearly defining the various levels of the rating system.

The NDT measurements appeared to have more statistical power than visual measurements and also identified a fourth significant variable. Part of the power of the NDT evaluation is that more data points could be obtained from a given specimen than with visual evaluation (9 vs. 1 in our case). The NDT data could have been further improved because ~4.5% of the observed speeds were suspiciously fast, between 3500 and 4800m/s, even on the bottom edge of exposed boards showing signs of decay. We were not able to identify the source of these clearly erroneous measurements, and they were retained within the statistical analysis. Clearly the power and effect of the ultrasonic measurement would be dramatically improved if the sources of these outliers

were eliminated. We believe that measuring speed of ultrasound through the thickness of the panel, 12mm, reduced the reliability of the measurements. This is because the resolution of the timing electronics was only 8x faster than the average time and because this short sound wave travel distance resulted in very small volumes of wood being tested. Forcing the sound wave to travel a longer distance, as well as using shear waves of lower frequency, would probably improve the data. Shear waves travelling a longer distance could be sent and detected on the same side of the panel, and so allow monitoring of the samples on site over time. Finally, the compression force on the transducers may have closed delamination gaps in the plywood, affecting the results.

Table 1: Impact of exposure conditions on various properties. Positive effects indicate better performance under the first condition (ex. 9mm Bottom Gap is better than 0mm gap because effects are positive)

Effect of construction details on performance

		Sound Speed		Sound Energy		Substrate		Paint Crack	
		P	Effect	P	Effect	P	Effect	P	Effect
Mississippi vs Wisconsin		0.01	9%	0.34	-3%	0.00	-24%	0.00	-10%
Flashed vs. Caulked Ends		0.00	19%	0.08	5%	0.02	5%	0.01	-7%
Bottom Gap (9mm vs 0)		0.00	30%	0.00	13%	0.01	6%	0.04	5%
Primed Bottom (Yes vs No)		0.01	-8%	0.52	-2%	0.34	2%	0.40	-2%
Gap Behind (0 or 5cm)		0.12	5%	0.10	4%	0.08	-4%	0.40	-2%
Sonic Measurement Location	Bottom	0.00	-11%	0.23	-2%				
	End	0.00	-14%	0.00	6%				
	Top	0.00	25%	0.02	-4%				

Leaving a gap between the bottom of a board and the surface below it was the most important factor in good construction. The gap resulted in much lower decay rate (higher speed of sound, higher peak energy), as well as better visual substrate ratings and paint crack ratings. Leaving the gap allows boards to dry out faster after rain stops and potentially reduces the amount of water absorbed by the siding. This observation is consistent with many previous studies (Williams and Winandy, 2008).

Caulking the ends of boards is extremely widespread, though most installations apply caulk between board ends and trim as a fillet joint with caulk pressed into the corner between siding and trim, though manufacturer literature specifically discourage this practice (Dow Corning, 2011) because they are highly prone to sealant failure. After failure the caulk serves to trap moisture inside the structure rather than keep it out. In this study, we applied caulk and flashing properly (Figure 2). Still, the data shows that leaving a gap between the ends of the boards and vertical trim strip, with flashing, results in less decay and better substrate performance. Paint cracking is more severe, likely because moisture is able to enter the end grain of the wood and quickly swell the wood during rain events, putting stress on the paint film. Better sealing of the end grain of wood would likely improve cracking performance.

A **B** **C** **D**

Figure 2: End and bottom finishing details. A, schematic view from top of flashing between panel and trim. B, photo of flashing at end of panel. C, schematic of caulk joint. D, photo of caulked joint on end of test panel. D also shows a gap below the board (upper) and no gap (lower).

Exposure in warm and moist MS (30ºN Lat) resulted in a 9% faster average speed of ultrasound through the wood (less decay) than exposure in WI (43ºN Lat), which we attribute primarily to the shorter exposure time. By contrast, visual evaluations found Mississippi harder on the substrate and paint, in line with our previous experience.

Putting a coat of primer on the bottom edge has been shown in many previous studies to be beneficial to siding performance (Hunt 2009, Carll 2009), but not in this study. Usually primer is useful in preventing liquid water from entering the wood but allows vapor to escape wood. We do not know why in this study the primer was detrimental to performance, although it is known that some early alkyd emulsions (oil based paint dispersed in water) had problems with water barrier properties because of the specific surfactants used (Ekstedt 2003). Because these problems have been identified, we expect modern alkyd emulsions to perform much better, though using simply an oil based primer, rather than an emulsion, seems a safer bet for water repellency.

A secondary drainage plane or gap is made by adding furring strips between the vapor barrier and siding. This is typically referred to as a “rain screen”, or if vented at the top, “ventilated siding”, and is generally recommended. In this study, the bottom of the siding was open and no foundation was present, allowing the wind to pass under the wall. There was no significant effect of the gap but Figure 3 shows that siding on the

side with a gap (right) had more water stain, further up the backside of the board, than the side with no gap (left). This is clearly not the intent nor the typical performance of a rain screen. We believe the open space below the siding created a Venturi effect and a low pressure zone behind the siding, which would drive water up behind the siding. This highlights the need for careful attention to installation details. We refer the reader to Rousseau for a description of proper rain screen construction (Rousseau 1990).

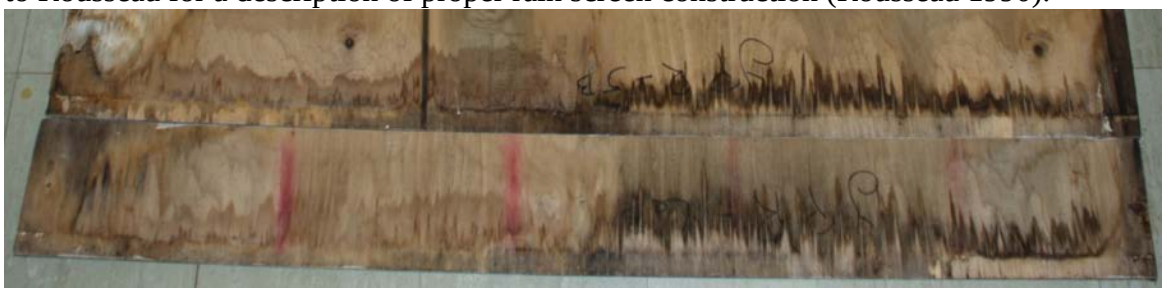

Fig 3: Back side of 2 panels after exposure, with caulked edges and no bottom gap showing water staining, more severe with the Venturi effect and gap behind boards (right) while end decay is more pronounced without gap behind boards (left).

Conclusions

In this experiment, ultrasonic velocity measurements were as good as, or better than visual evaluations at detecting performance differences. Several suggestions are made to improve ultrasonic NDT measurements which should improve the data quality significantly, suggesting that NDT evaluations for wood siding performance have the potential to be much more sensitive and reliable than visual evaluations.

When using wood siding, contact between the bottom of the board and the flashing below is significantly detrimental for every property we observed. Using caulk between ends of boards and vertical trim resulted in slower ultrasonic propagation and lower substrate ratings than flashing the ends, even though the caulking was applied properly. If the ends are to be flashed, however, special attention needs to be given to preventing water intrusion into the siding where it meets the vertical trim. Proper attention to several design details result in significant differences in siding decay rate and paint performance.

Literature

ASTM 1993 Standard D 661-93 (2000) Standard Test Method for Evaluating Degree of Cracking of Exterior Paints. ASTM International, West Conshohocken, NJ, USA

Carll, Charles G., Boardman, Charles R., Verrill, Steve P. (2009) Durability of Hardboard Lap Siding Performance in Laboratory Testing and in Long-Term Exterior Exposure; Forest Products Laboratory Research Paper FPL–RP–674

Dow Corning Americas Technical Manual 2011, p56 accessed June 10, 2015 http://www.dowcorning.com/content/publishedlit/62-1112a-01.pdf

Ekstedt, Jan. (2003) Influence of coating system composition on moisture dynamic performance of coated wood; Journal of Coatings Technology 75(938), pp 27-37

Hunt, C.G. Williams, R.S. Knaebe, M., Sotos, P., Lacher, S. (2009) Factors effecting paint performance on wood siding. accessed June 10, 2015 http://www.fpl.fs.fed.us/documnts/pdf2009/fpl_2009_hunt003.pdf

Rousseau, Madeleine Z, (1990) Facts and Fictions of Rain Screen Walls, Construction Canada 90 03 Vol. 32, No. 2 March/April pp. 40-47, NRCC 32332.

Williams, R. Sam and Winandy, Jerrold E. (2008) Effect of Flakeboard Manufacturing Variables on Composite Properties: Part 1. Effect of Resin Content, Wax Content, Pressing Conditions, and Edge Treatments on Paint Performance; Proceedings, One Hundred Fourth Annual Meeting of the American Wood Protection Association 2008. http://www.fpl.fs.fed.us/documnts/pdf2008/fpl_2008_williams001.pdf accessed June/10/2015

Influence of boundary condidtions on measurement of elastic constants of engineered wood-based panels using modal testing

Jianhui Zhou
Faculty of Forestry and Environmental Management, University of New Brunswick, Fredericton, New Brunswick, Canada, jh.zhou@unb.ca

Ying Hei Chui
Faculty of Forestry and Environmental Management, University of New Brunswick, Fredericton, New Brunswick, Canada, yhc@unb.ca

Abstract

Engineered wood-based panels (e.g. oriented strand board, plywood, cross laminated timber) are being used in wood construction. Elastic constants are the fundamental mechanical properties for structural design of these products. Modal testing based on the theory of transverse vibration of orthotropic plates has been proven to be an effective method to measure elastic constants of these panel products. Boundary condition (BC) and corresponding calculation method are key in affecting its practical application in terms of setup implementation, frequency identification, accuracy and calculation efforts. In order to find a suitable BC for non-destructive testing of engineered wood-based panels, three BCs with corresponding calculation methods were adopted for measuring elastic constants, namely in-plane elastic moduli (E_x, E_y) and shear modulus (G_{xy}), of wood-based panel products. As demonstration of the concept, the products used in this study were oriented strand board (OSB) and medium density fiberboard (MDF). The BCs with corresponding methods were, a) all sides completely free (FFFF) with one-term Rayleigh frequency equation, b) one side simply supported and the other three free (SFFF) with one-term Rayleigh frequency equation, c) a pair of opposite sides simply supported and the other pair free (SFSF) with improved three-term Rayleigh frequency equation. The results from different modal testing methods were compared with standard static testing method. It was found that the difference between modal and static results for different BCs were different to different extends.

Keywords: Wood-based panels, elastic constants, modal testing

Introduction

Engineered wood products have been gaining popularity in wood constructions for a long time. Engineered wood-based panels such as oriented strand board (OSB) are even more widely used in modern wood constructions, especially in light frame wood construction. Elastic constants are fundamental mechanical properties for structural design, which are also the key quality control parameters. The study of evaluating the elastic properties of wood-based panels by using modal testing for quality control purpose could be traced back to the 1980s. Different BCs with corresponding calculation methods have been applied for measuring the elastic constants of solid wood plates, particleboard, OSB, etc.

Completely free (FFFF) was the BC mostly used among the studies done for modal testing of panel-shaped wood products. As there is no analytical solution for FFFF boundary condition, the one-term

Rayleigh frequency solution was chosen for the calculation of elastic constants (Nakao and Okano 1987; Coppens 1988; Sobue and Kitazumi 1991; Schulte et al. 1996; Carfagni and Mannucci 1996; Bos and Casagrande 2003). The natural frequency of torsional mode was used for measuring the modulus of rigidity (G) by Nakao and Okano (1987). The method appeared to be much simpler than static plate-twist shear tests and LW-improved method (Okuma 1966). Coppens (1988) tested particleboard specimens to measure their elastic constants in the laboratory of the individual companies so that the quality of commercially-produced boards can be controlled non-destructively. The determination of orthotropic elastic constants of wood plate (western red cedar, hemlock, buna and keyaki) with FFFF BC using a vibration technique was studied and verified with static test results of beam specimen by Sobue and Kitazumi (1991). A simplified dynamic method based on experimental modal analysis for estimating the in-plane elastic properties of solid wood panels was proposed by Carfagni and Mannucci (1996), which is based on assessing whether the response and excitation were in or out of phase. The number of impact points was reduced from 24 to six for rectangular wood panels with FFFF BC. An on-line non-destructive evaluation system called VibraPann for quality control of wood-based panels was presented by Bos and Casagrande (2003). The in-plane moduli of elasticity in the two orthogonal directions of selected eight OSB panels, 260 plywood panels, one MDF panels were tested from the measurement of two vibration modes of bending, $f_{(2,0)}$ and $f_{(0,2)}$, using the system.

Besides Rayleigh frequency solution, finite element (FE) modelling was also used for the determination of elastic constants combined with modal analysis (Larsson, 1996; 1997; Martínez et al., 2011). The elastic constants were estimated by minimizing the difference between the experimental frequencies and FE modeled values using an iterative process. Full-size MDF and OSB, modeled as thin orthotropic plates under FFFF BC, were tested by Larsson (1996, 1997) using modal testing. An average of about 10% difference with corresponding static values was reported. A similar method was adopted to study the effects of moisture content on the in-plane elastic constants of wooden boards used in musical instruments (Martínez et al. 2011). Recently, experimental modal analysis was used to determine natural frequencies and mode shapes of rectangular cross laminated timber (CLT) specimens (Gsell et al. 2007). An analytical model based on Reddy's higher order plate theory (Reddy 1984) was applied to calculate natural frequencies and mode shapes numerically. All three shear moduli and the two in-plane modulus of elasticity were identified by minimizing the difference between measured and estimated natural frequencies based on the least-squares method. Gülzow further studied the modal testing method proposed by Gsell et al. (2007) to evaluate the elastic properties of CLT panels for quality control purposes (Gülzow 2008).

The other boundary conditions such as one edge simply supported and three edges free (SFFF) and one edge clamped and three edges free (CFFF) were also used for the determination of elastic constants of full-scale structural panels for the purpose of quality control in production. A simultaneous determination of orthotropic elastic constants of standard full-size plywood by vibration method was conducted with SFFF boundary condition (Sobue and Katoh 1992). The results, two moduli of elasticity and a shear modulus, were compared with static bending and torsional tests, which showed a fairly good agreement. Particleboard and MDF panels of full-scale dimensions were tested using a vibration technique in a vertical cantilever (CFFF) arrangement (Schulte et al. 1996).

So far none of the above reported methods with corresponding boundary conditions have been implemented for on-line evaluation of full-size composite panels. In this study a comparison of results obtained from three approaches with different BC (FFFF, SFFF and SFSF) and calculation procedure was conducted to produce recommendations for choosing BCs most suited for measurement of elastic constants by modal testing methods.

Theoretical background

The governing differential equation for the transverse vibration of a rectangular orthotropic plate neglecting the effects of shear deformation and rotatory inertia is expressed as follows (Leissa, 1969),

$$D_x \frac{\partial^4 w}{\partial x^4} + D_y \frac{\partial^4 w}{\partial y^4} + 2(D_1 + 2D_{xy}) \frac{\partial^4 w}{\partial x^2 y^2} + \rho h \frac{\partial^4 w}{\partial t^2} = 0 \quad (1)$$

where D's are the flexural and torsional rigidities: $D_x = \frac{E_x h^3}{12(1-\nu_{xy}\nu_{yx})}$, $D_y = \frac{E_y h^3}{12(1-\nu_{xy}\nu_{yx})}$, $D_1 = D_x \nu_{xy} = D_y \nu_{yx}$, $D_{xy} = \frac{G_{xy} h^3}{12}$. E_x, E_y and G_{xy} are the in-plane elastic moduli and shear modulus, ν_{xy} and ν_{yx} are the Poisson's ratios, and a, b, h are the length, width and thickness of the plate, respectively, and ρ is the mass density of the plate.

With the input of four elastic constants, dimensional information and density, all the natural frequencies of corresponding modes can be calculated under different boundary conditions, which is defined as the forward problem. However, due to the complexity of boundary condition, the analytical solution of forward problem cannot be simply generated from the governing differential equation. Therefore, numerical methods such as Rayleigh-Ritz and finite element were applied for solving the forward problem. With a proper forward solution and any four measured frequencies, the four elastic constants can be calculated through an inverse process theoretically, known as the inverse problem. However, the frequency of each mode is sensitive to different elastic constant. Only the sensitive frequencies result in approximate elastic constant values. Sensitivity analysis is always recommended before identifying the frequencies for calculation of elastic constants.

In this study, the forward problem solutions for FFFF and SFFF are both generated by Rayleigh method with one-term defromation expression (Sobue and Kitazumi 1991; Bos and Casagrande 2003). The frequency equation can be expressed as,

$$f_{(m,n)} = \frac{1}{2\pi} \sqrt{\frac{1}{\rho h}} \sqrt{D_x \frac{\alpha_{1(m,n)}}{a^4} + D_y \frac{\alpha_{2(m,n)}}{b^4} + 2D_1 \frac{\alpha_{3(m,n)}}{a^2 b^2} + 4D_{xy} \frac{\alpha_{4(m,n)}}{a^2 b^2}} \quad (2)$$

where $f_{(m, n)}$ is the natural frequency of mode (m, n), m and n are the number of node lines including the simply supported sides in y and x direction, respectively. $\alpha_{1(m, n)}$, $\alpha_{2(m, n)}$, $\alpha_{3(m, n)}$ and $\alpha_{4(m, n)}$ are the coefficients for each mode, which are usually presented in tables for different boundary conditions (Sobue and Kitazumi 1991; Bos and Casagrande 2003).

The frequency equation for each mode is scattered and the frequencies of some modes are linear to just one or two elastic constants, which makes it difficult to perform sensitivity analysis using analytical frequency equation. Thus, finite element modeling was employed for sensitivity analysis by changing 10% of each elastic constants. It was found that for FFFF boundary condition, the sensitive modes to E_x, E_y and G_{xy} are mode (2, 0), (0, 2) and (1, 1), respectively. With SFFF boundary condition, the sensitive modes to E_x, E_y and G_{xy} are mode (m (m≥2), 1), (0, 2) and (1, 1), respectively. The sensitivities of mode (m (m≥2), 1) to E_x increase with the increase of m. A desirable sensitivity can be found with m equals to 3 or 4 depending on the dimensions and mechanical properties of the panel. Natural frequency of mode (3, 1) is used in this study. The sensitivities of each mode to ν_{xy} is not significant for both boundary conditions considered here. Therefore, for FFFF BC, the elastic constants can be calculated using the following formulas (Nakao and Okano 1987; Bos and Casagrande 2003),

$$E_x = \frac{48\pi^2 \rho a^4 f_{(2,0)}^2 (1 - v_{xy} v_{yx})}{500.6 h^2} \quad (3)$$

$$E_y = \frac{48\pi^2 \rho b^4 f_{(0,2)}^2 (1 - v_{xy} v_{yx})}{500.6 h^2} \quad (4)$$

$$G_{xy} = 0.9\rho \left(\frac{ab}{h} f_{(1,1)}\right)^2 \quad (5)$$

and for SFFF BC, the elastic constants can be calculated using the following formulas (Sobue and Katoh, 1992),

$$E_x = \frac{12\pi^2 \rho a^4 (1 - v_{xy} v_{yx})(4 f_{(3,1)}^2 - 36.27 f_{(1,1)}^2)}{3805.04 h^2} \quad (6)$$

$$E_y = \frac{48\pi^2 \rho b^4 f_{(0,2)}^2 (1 - v_{xy} v_{yx})}{237.86 h^2} \quad (7)$$

$$G_{xy} = \frac{\pi^2 \rho a^2 b^2 f_{(1,1)}^2}{3h^2} \quad (8)$$

where $(1 - v_{xy} v_{yx})$ is about 0.99 for most wood materials.

A closed-form approximate frequency expression based on Rayleigh method with three-term defromation expression was adopted from Kim and Dickinson (1985) for SFSF BC. A calculation method with an analytical sensitivity analysis was developed using the improved frequency equation based on an iteration process. The initial value of E_x is first calculated using the fundamental frequency, $f_{(2, 0)}$. The other initial values are set as the ratios with E_x. The iteration stops when the total difference between measured and calculated frequencies is less than 1-5 %. The sensitive frequency modes to E_x, E_y and G_{xy} are mode (2, 0), (2, 1) and (2, n (n≥2)), respectively. The sensitivity of mode (2, n (n≥2)),) to E_x increases with the increase of n. In most cases, the frequency of mode (2, 2) or (2, 3) is sensitive enough for calculating E_y. Details about the calculation method can be found in Zhou and Chui (2014). Also, all the modes are not sensitive to v_{xy} for the panel dimensions evaluated in this study.

Material and Methods

Materials

Five full-size 11.1 mm thick APA rated sheathing OSB panels of dimension 2.44 m × 1.22 m and five full-size commercial industrial grade 15.7 mm thick MDF panels of dimension 2.46 m × 1.24 m were purchased from for this study. The average moisture contents and densities of OSB and MDF panels were about 4 % and 5%, 614 kg/m^3 and 697 kg/m^3, respectively. Each full-size panel was cut into four panels of dimension 1.21 m × 0.6 m equally. A total of twenty panels were obtained from each type of panel for modal testing. Then two panels with the closest masses were selected from four panels of the same full-size panel to glue a double-thick panel using a two-component structural polyurethane adhesive. A total of five panels were prepared from each type of panel for investigating the effect of thickness on the accuracy of modal tests. The average thicknesses of double-thick OSB (DOSB) and MDF (DMDF) panels were 22.1 mm and 31.2 mm, respectively. The remaining ten panels of each type were cut into square panels of dimension 0.6 m × 0.6 m for in-plane shear tests. Then three strips were cut from each strength direction from a square panel for bending tests. For the double-thick panels, they were cut into square panels for in-plane shear tests and panel bending tests as well. The cutting scheme is shown in Figure 1.

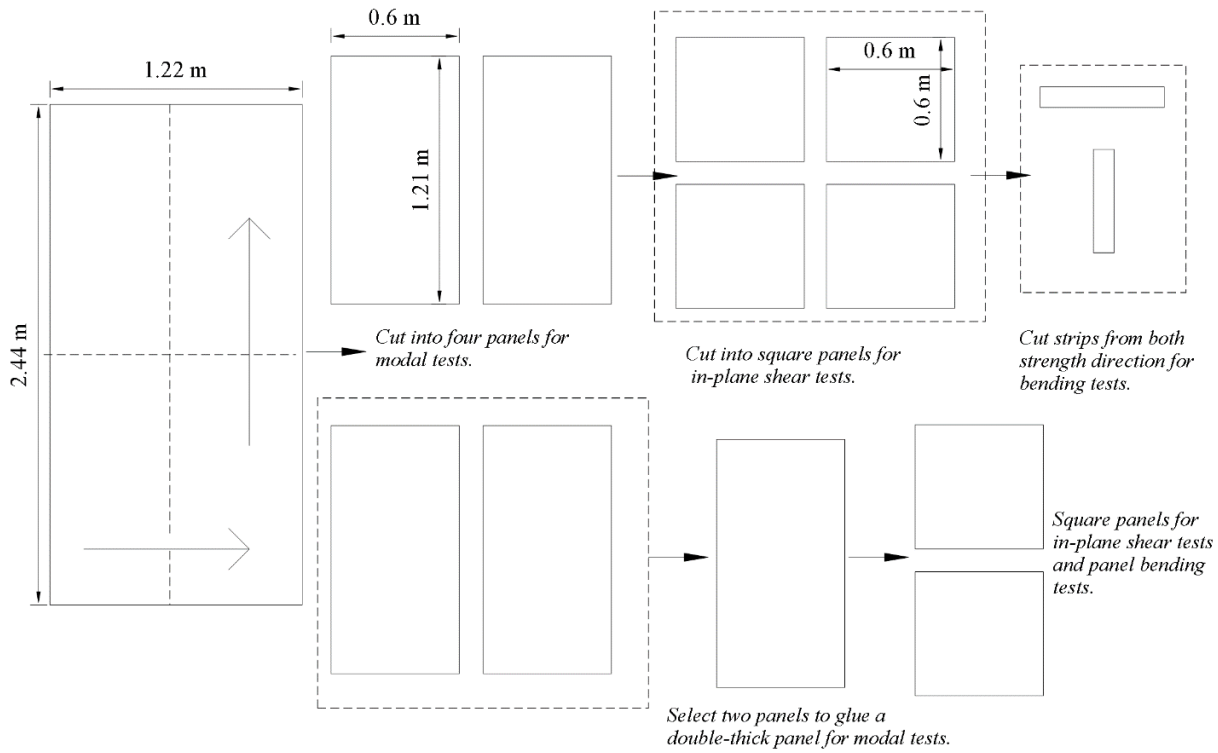

Figure 1 — Cutting Scheme for different tests

Dynamic test

The impact vibration tests were conducted on the specimen with three different BCs for both OSB and MDF panels. The BCs were realized using ropes and steel pipes in the lab. The panel was suspended with a pair of ropes on the steel frame as shown in Figure 2.a to simulate FFFF BC. A pair of steel pipes were used to clamp one side of the panel to simulate simply supported BC. As shown in Fig 2.b and c, the panels were clamped with proper pressure at one side parallel to major strength direction or a pair of two opposite sides parallel to minor strength direction to achieve SFFF or SFSF BC, respectively.

For FFFF and SFFF BCs, the accelerometer was attached at the left right corner of the panel, while for SFFF it was attached at 7/12 length of one free edge. The locations selected are not on the nodal lines of first several modes up to the first 15 modes including the sensitive natural frequencies. The impact and acceleration time signals were recorded by a data acquisition device (LDS Dactron, Brüel & Kjær) and the frequency response function (FRF) was calculated from the time signals using a data analysis software (RT Pro 6.33, Brüel & Kjær). The frequency spectrum was post-processed by MATLAB software for frequency identification and calculation of the elastic constants.

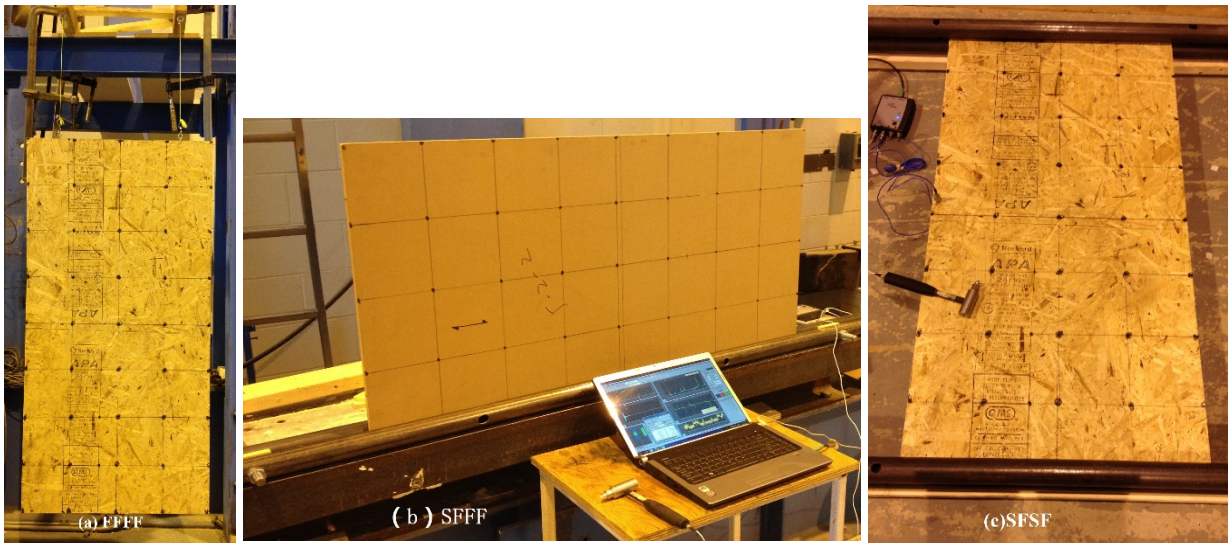

Figure 2 — Test setups for modal tests under different boundary conditions

Static tests

Static tests were conducted to verify the results obtained by modal tests. The E_x, E_y and G_{xy} of OSB and MDF panels were obtained from static centre-point flexure tests according to ASTM D3043 (ASTM, 2011a) and shear tests according to ASTM D3044 (ASTM, 2011b), respectively. A total of twelve strips along each strength direction cut from each full-size panel were tested for E values. A total of four square panels cut from each panel were tested for G_{xy} values. For the double-thick panels, the square panels are used for both in-plane shear tests and panel bending tests. The dimensions for static tests are listed in Table 1.

Table 1 — Dimensions of specimens for different static tests

Material	Strip bending tests				Inplane shear tests and panel bending tests (mm)
	Major (mm^2)	Span (mm)	Minor (mm^2)	Span (mm)	
OSB	600×50	540	450×50	270	600×600
MDF	600×50	570	450×50	380	600×600

Data analysis

The mean values of the elastic constants of four panels from the same full-size panel by dynamic tests were compared with the mean values of each elastic constants of the same full-size panel by static tests. The difference in percentage (Diff.) between static and dynamic method is calculated as follows

$$\text{Diff.} = \frac{p_{static} - p_{dynamic}}{p_{static}} \times 100\% \tag{9}$$

where Diff. is the difference of elastic constants between static and dynamic methods in percent, p is the elastic constant to be evaluated.

Besides comparison of mean values with static methods, paired-samples t-tests were also performed between static and dynamic results for evaluation of different approaches with corresponding boundary condition.

Results and discussion

The elastic constants of OSB and MDF panels measured by dynamic methods with different BCs and static methods are listed in Table 2. The dynamic values of four panels from the same full-size panel were averaged as the representatives of each full-size panel. It can be seen that, for all three BCs, dynamic E values of OSB panels were larger than their static E values, while dynamic G_{xy} values were smaller than static G_{xy} value. The differences between dynamic and static E_x values of OSB panels were -2.85%, -19.47% and -9.89% for SFFF, FFFF and SFSF BCs, respectively. The differences between dynamic and static E_y values of OSB panels were -30.40%, -42.98% and -23.83% for SFFF, FFFF and SFSF BCs, respectively. The differences between dynamic and static G_{xy} values of OSB panels were 22.15%, 30.50% and 16.27% for SFFF, FFFF and SFSF BCs, respectively. Among the three BCs, the three elastic constants of OSB panels obtained from FFFF BC exhibited the largest difference from the corresponding static values. The three elastic constants from SFSF BC were closer to static values than the other two BCs. If taking standard static test values as the reference values, dynamic values from SFSF boundary condition were the most acceptable for OSB panels.

For MDF panels, the differences between dynamic and static values were much smaller than those for OSB panels. The differences between dynamic and static E_x values of MDF panels were -4.42%, -10.57% and -6.38% for SFFF, FFFF and SFSF BCs, respectively. The differences between dynamic and static E_y values of MDF panels were 3.75%, -7.95% and 8.86% for SFFF, FFFF and SFSF BCs, respectively. The differences between dynamic and static G_{xy} values of MDF panels were 6.56%, 15.53% and 9.45% for SFFF, FFFF and SFSF BCs, respectively. Similarly, dynamic E_x values from all three BCs were larger than static value, and dynamic G_{xy} values from all three BCs were smaller than static value, but the differences were smaller than those for OSB panels. Dynamic E_y values from SFFF and SFSF BCs were a slightly smaller than static value, while dynamic E_y values from FFFF BC was larger than static values. Among the comparisons between dynamic and static values of MDF panels, the differences were with the same range less or around 10% except G_{xy} value from FFFF boundary condition, which was 15.53%.

Table 2 — Elastic constants of OSB and MDF measured by dynamic methods with different BCs and static methods

Panel #	Elastic constants measured by dynamic methods (MPa)									Elastic constants measured by static methods (MPa)		
	SFFF			FFFF			SFSF					
	E_x	E_y	G_{xy}	E_x	E_y	G_{xy}	E_x	E_y	G_{xy}	E_x	E_y	G_{xy}
OSB1	6533	3168	2092	7916	3607	1716	7496	3177	2045	6424	2654	2504
OSB2	6818	3060	1929	7871	3590	1732	7334	3071	2162	6732	2520	2589
OSB3	6994	3434	2119	8319	3008	1822	7542	3319	2243	6376	2627	2450
OSB4	6820	3225	1897	7852	3562	1704	6921	3049	1959	6808	2574	2488
OSB5	7223	3789	1763	7938	3774	1793	7386	3222	2155	6694	2555	2637
Mean	6878	3335	1960	7979	3508	1753	7336	3167	2113	6607	2586	2534
COV	6.52%	9.70%	9.95%	6.34%	6.01%	6.71%	6.34%	8.07%	8.76%	8.82%	9.22%	7.53%
Diff.	-2.85%	-30.40%	22.15%	-19.47%	-42.98%	30.50%	-9.89%	-23.83%	16.27%	/	/	/
MDF1	3273	2818	1324	3390	3483	1265	3297	3216	1341	3073	3162	1626
MDF2	3233	2938	1319	3358	3386	1253	3210	2906	1411	2929	3078	1450
MDF3	3276	3072	1406	3532	3633	1327	3473	3185	1492	3371	3453	1568
MDF4	3050	2848	1359	3286	3407	1223	3055	3017	1280	3041	3231	1492
MDF5	3280	3031	1434	3510	3510	1313	3403	3200	1526	3078	3251	1477
Mean	3222	2942	1368	3415	3484	1276	3288	3105	1410	3098	3235	1522
COV	5.34%	4.50%	4.91%	3.96%	3.45%	3.84%	5.44%	7.33%	7.63%	6.45%	5.78%	8.11%
Diff.	-4.42%	3.75%	6.56%	-10.57%	-7.95%	15.53%	-6.38%	8.86%	9.45%	/	/	/

Note: COV was the coefficient of variation.

In order to better compare the dynamic methods with static methods, the dynamic values from each BC were compared with static values through paired-sample t-tests. As shown in Table 3, most of the paired groups had a p value less than 0.05 at the 95% confidence level except paired group 'Static - SFFF' of E_x and paired group 'Static - SFSF' of E_y. Generally, the elastic values by dynamic methods have a significant difference with the elastic values by static methods at the 95% confidence level. The differences between each dynamic and static elastic constant value are illustrated in Figure 3 and 4. It can be seen that the trends generally agree with the trends of mean value comparisons. In Figure 3, the difference between dynamic and static E_x of each individual OSB panel ranges from -14 to 11% with most of them around -3% for SFFF boundary condition, from -40 to -3% with most of them around -20% for FFFF BC, from -30 to 6% with most of them around -10% for SFSF BC, respectively. The difference between dynamic and static E_y and G_{xy} values of each individual OSB panel is within -60% (except for one panel) and 40%, respectively. Most of the differences are distributed around their averaged differences for each BC. The exceptions happen when the static values are either too large or too small. However, corresponding dynamic values from three BCs shows quite good consistency, which appears to be more reliable. Unlike OSB panel, MDF panel results show much better uniformity in differences distribution for three elastic constants within an absolute difference of 20%.

Table 3 — Paired-Samples t-test results of each elastic constant between static and dynamic test values

Material	Elastic constants	Paired group	Paired Differences					t	df	Sig. (2-tailed)
			Mean	SD	SE Mean	95% Confidence Interval of the Difference				
						lower	upper			
OSB	E_x	Static - FFFF	-1372	652	146	-1677	-1067	-9.42	19	.000
		Static - SFFF	-271	675	151	-587	45	-1.80	19	.088
		Static - SFSF	-729	701	157	-1057	-401	-4.65	19	.000
	E_y	Static - FFFF	-922	788	176	-1291	-553	-5.23	19	.000
		Static - SFFF	-749	464	104	-966	-532	-7.22	19	.000
		Static - SFSF	-581	414	93	-775	-388	-6.28	19	.000
	G_{xy}	Static - FFFF	780	202	45	685	875	17.24	19	.000
		Static - SFFF	573	293	66	436	711	8.74	19	.000
		Static - SFSF	421	240	54	308	533	7.83	19	.000
MDF	E_x	Static - FFFF	-317	203	45	-412	-222	-6.98	19	.000
		Static - SFFF	-124	263	59	-247	-1	-2.11	19	.049
		Static - SFSF	-189	202	45	-284	-95	-4.20	19	.000
	E_y	Static - FFFF	-249	164	37	-326	-172	-6.78	19	.000
		Static - SFFF	293	181	40	208	378	7.25	19	.000
		Static - SFSF	130	282	63	-2	262	2.07	19	.053
	G_{xy}	Static - FFFF	246	138	31	181	310	7.97	19	.000
		Static - SFFF	154	147	33	85	223	4.68	19	.000
		Static - SFSF	113	187	42	25	200	2.70	19	.014

Note: Sig. refers to the significance of paired-samples t test of each group. The tests were performed using software SPSS 19.0. SD, SE and df are short for standard deviation, standard error and degree of freedom, respectively.

The differences between dynamic and static values can be mainly explained by the material structure of the panels and the nature of the test methods. As reported in most literature, usually a 10% or more difference can be observed between dynamic and static *E* values. Dynamic values by modal tests of panels are also said to be the general elastic constants as the representatives of the whole panel, while the static values are the local elastic constants. Sample size and sampling location have a great influence on the variance of test results. For each small panel in this study, due to the dimensions of the panel and the size equipment of bending specimen, only three strips were cut for bending test in each strength direction. Nakao and Okano (1987) reported differences between dynamic and static G_{xy} values for particleboard

and fiberboard such as hardboard and MDF panels of -35 to 18%, while the difference for plywood was -8 to 14%. However, the differences between each BC were primarily caused by the influence of BCs in practice, sensitivity level of selected frequency modes and the accuracy of chosen forward problem solutions.

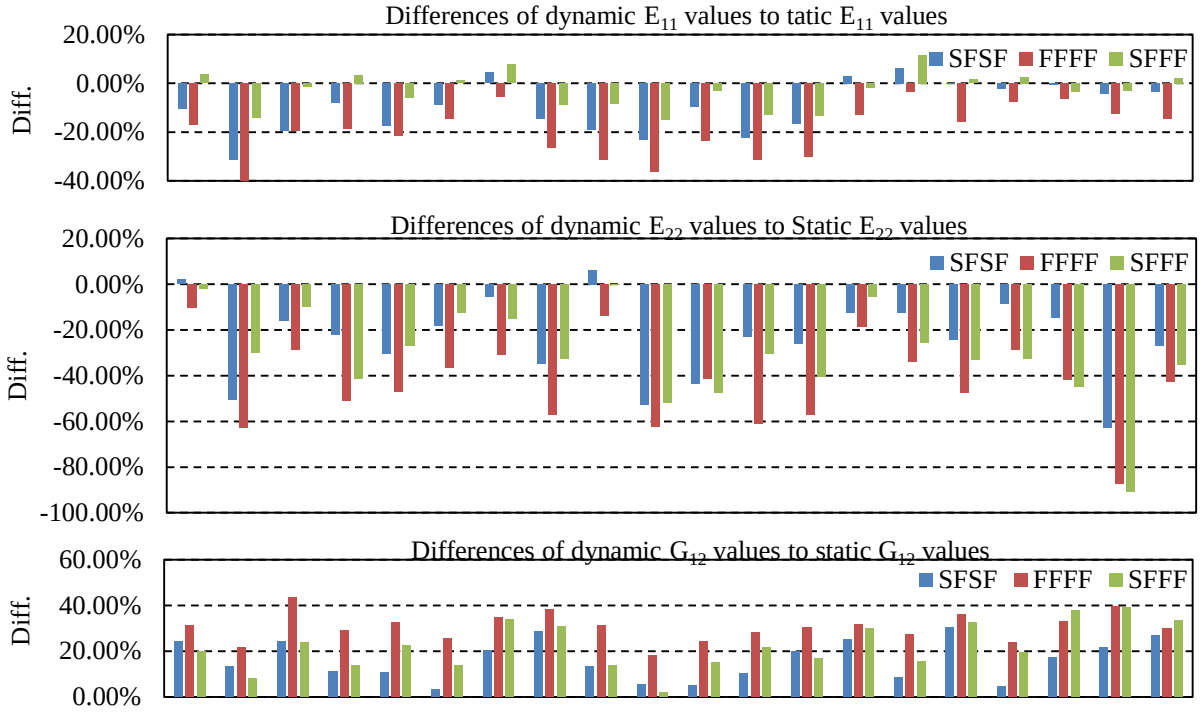

Figure 3 — Differences of dynamic elastic constants from different BCs to corresponding static values of OSB.

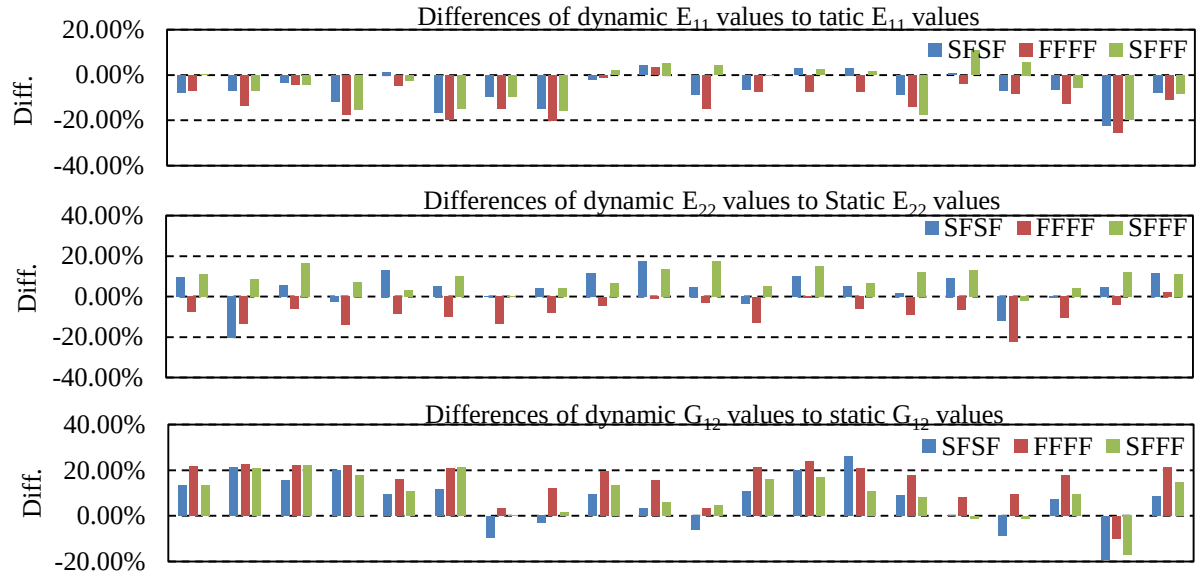

Figure 4 — Differences of dynamic elastic constants from different BCs to corresponding static values of MDF.

As SFFF BC is realized in a vertical position, it cannot be achieved as easy as FFFF and SFSF BCs in practice. Therefore, only modal tests with FFFF and SFSF boundary conditions were conducted for double-thick OSB and MDF panels. As shown in Table 4, the differences between dynamic and static values are much smaller than those for the thinner panels. Dynamic values with SFSF boundary condition are closer to static values than dynamic values with FFFF boundary conditions. The decrease in length to thickness ratio also has a negative effect on E_x and G_{xy} values due to increasing transverse shear deflection. It was found that in-plane shear modulus of western hemlock solid wood plates by static square-plate twist method increase from 0.5 to 1 GPa with the increase of length or width to thickness ratio from 14 to 60 (Yoshihara and Sawamura, 2006).

Table 4 — Elastic constants of double-thick OSB and MDF measured by modal methods with different BCs and static methods

Panel #	Elastic constants measured by dynamic methods (MPa)						Elastic constants measured by static methods (MPa)		
	FFFF			SFSF					
	E_x	E_y	G_{xy}	E_x	E_y	G_{xy}	E_x	E_y	G_{xy}
DOSB1	6567	4285	1639	6194	3909	1638	6141	4099	1716
DOSB2	6767	4833	1742	6325	4066	1557	6151	4430	1804
DOSB3	6886	4707	1733	6291	3734	1522	5908	3960	1672
DOSB4	6395	4242	1631	5514	4147	1782	5618	3877	1530
DOSB5	6550	4400	1637	6520	3715	1779	6231	4008	1814
Mean	6633	4493	1676	6169	3914	1656	6010	4075	1707
Diff.	-10.37%	-10.27%	1.79%	-2.65%	3.94%	3.01%	/	/	/
DMDF1	3198	3247	1129	2750	2812	1148	2772	2670	1128
DMDF2	2850	2786	1007	2611	2321	1046	2434	2440	1062
DMDF3	2770	2822	999	2252	2305	1040	2392	2468	1050
DMDF4	2689	2616	939	2420	2662	970	2208	2430	1107
DMDF5	2861	2790	994	2456	2663	969	2394	2405	1069
Mean	2874	2852	1014	2498	2553	1035	2440	2483	1083
Diff.	-17.77%	-14.90%	6.39%	-2.37%	-2.82%	4.45%	/	/	/

Conclusions

Through this study it is shown that different accuracy levels are achieved with the three modal evaluation approaches, which incorporate different boundary conditions and calculation procedures. However, it is difficult to conclude which one is best and gives the most accurate results. Modal test methods can be an option for measuring elastic constants of engineered wood-based panels due to its non-destructive nature and fast testing time. For two-way plate-like specimens, modal testing is recommended as it can account for the influence of coupling between elastic constants and is less tedious to conduct compared with one-way static testing approaches. All three BCs with corresponding calculation methods can be applied in the laboratory. FFFF is the easiest BC to be replicated in a testing environment and can be applied for panels of small to moderate dimensions, but further improvement of calculation method, such as iterative process using FE or other advanced forward problem solution is needed. SFFF is not strongly suggested as it requires some efforts in implementing the vertical simply supported BC. SFSF BC with the proposed calculation method shows great potential for laboratory and on-line application, especially for massive panels. Further studies should focus on support details such as clamping pressure, effect of panel dimensions and material types.

Acknowledgments

The authors greatly acknowledge the financial support provided by Natural Sciences and Engineering Research Council (NSERC) of Canada under the Strategic Research Network on Innovative Wood Products and Building Systems (NEWBuildS), New Brunswick Innovation Foundation and NSERC Vanier Canada Graduate Scholarship (Vanier CGS) program.

References

ASTM. 2011a. Standard Test Methods for Structural Panels in Flexure Designation D3043-00. American Society for Testing and Materials, West Conshohocken, PA.

ASTM. 2011b. Standard Test Method for Shear Modulus of Wood-Based Structural Panels. Designation D3044-94. American Society for Testing and Materials, West Conshohocken, PA.

Bos, F.; Casagrande, S. B. 2003. On-line non-destructive evaluation and control of wood-based panels by vibration analysis. J. Sound Vib. 268(2): 403-412.

Coppens, H. 1988. Quality control of particleboards by means of their oscillation behavior. Proceedings, FESYP Technical Conference, Munich: 143-165.

Carfagni, M.; Mannucci, M. 1996. A simplified dynamic method based on experimental modal analysis for estimating the in-plane elastic properties of solid wood panels. In: Sandoz, J.L., eds. 10th International Symposium on Nondestructive Testing of Wood. Lausanne, Switzerland, OR: Swiss Federal Institute of Technology Chair of Timber Construction: 247-258.

Gsell, D.; Feltrin, G.; Schubert, S. [and others]. 2007. Cross-laminated timber plates: Evaluation and verification of homogenized elastic properties. J. Struct. Eng. 133(1): 132-138.

Gülzow A. 2008. Zerstörungsfreie Bestimmung der Biegesteifigkeiten, von Brettsperrholzplatten. Nr 17944. Switzerland: ETH Zürich. 203 p. PhD thesis.

Kim, C. S.; Dickinson, S. M. 1985. Improved approximate expressions for the natural frequencies of isotropic and orthotropic rectangular plates. J. Sound Vib. 103(1): 142-149.

Leissa, A. W. 1969. *Vibration of plates*. Ohio State University, Columbus.

Larsson, D. 1996. Stiffness characterization of wood based panels by modal testing. In: Sandoz, J.L., eds. 10th International Symposium on Nondestructive Testing of Wood. Lausanne, Switzerland, OR: Swiss Federal Institute of Technology Chair of Timber Construction: 237-246.

Larsson, D. 1997. Using modal analysis for estimation of anisotropic material constants. J. Eng. Mech. 123(3): 222-229.

Martínez, M. P.; Poletti, P.; Espert, L. G. 2011. Vibration Testing for the Evaluation of the Effects of Moisture Content on the In-Plane Elastic Constants of Wood Used in Musical Instruments. In: Vasquens, C.M.A., Rodrigues, J.D., ed. Vibration and Structural Acoustics Analysis. Netherlands: Springer: 21-57. Chapter 2.

Nakao, T.; Okano, T. 1987. Evaluation of modulus of rigidity by dynamic plate shear testing. Wood and Fiber Science. 19(4): 332-338.

Okuma, M. 1966. Studies on the mechanical proeprties of plywood. Mokuzai Gakkaishi. 12(3): 123-128.

Reddy, J. N. 1984. A simple higher-order theory for laminated composite plates. Trans. ASME, J. Appl. Mech. 51 (4): 745–752.

Sobue, N.; Kitazumi, M. 1991. Identification of power spectrum peaks of vibrating completely-free wood plates and moduli of elasticity measurements. Mokuzai Gakkaishi. 37(1): 9-15.

Sobue, N.; Katoh, A. 1992. Simultaneous determination of orthotropic elastic constants of standard full-size plywoods by vibration method. Mokuzai Gakkaishi. 38(10): 895-902.

Schulte, M.; Frühwald, A.; Broker, F. W. (1996). Non-destructive testing of panel products by vibration technique. In: Sandoz, J.L., eds. 10th International Symposium on Nondestructive Testing of Wood. Lausanne, Switzerland, OR: Swiss Federal Institute of Technology Chair of Timber Construction: 259-268.

Yoshihara, H.; Sawamura, Y. 2006. Measurement of the shear modulus of wood by the square-plate twist method. Holzforschung. 60(5): 543-548.

Zhou, J.; Chui, Y. H. 2014. Efficient measurement of elastic constants of cross laminated timber using modal testing. In: Salenikovich, A., eds. World Conference on Timber Engineering. Quebec City, Canada, OR: FPInnovations, Université Laval and cecobois: Track 1, SESSION 1.2: 1-7.

Impact of grading on the mechanical behavior of CLT panels made from low quality timber.

Juliana Bello Mussi Alencar
Master Architecture and Urbanism – UEL – State University of Londrina – Centro de Tecnologia e Urbanismo. Rodovia Celso Garcia Cid (Pr445), Km 380 - Campus Universitário CEP: 86.051-990 - Londrina - Paraná - Brazil Fone 55 43 3020-3491 Email: juliana_mussi@hotmail.com

Dr. Jorge Daniel de Melo Moura
Associate Professor Department of Architecture, - UEL- State University of Londrina, Centro de Tecnologia e Urbanismo Rodovia Celso Garcia Cid (Pr445), Km 380 - Campus Universitário CEP: 86.051-990 - Londrina - Paraná - Brazil Fone 55 43 3371-4641 Email: jorda@uel.br

Abstract

The Cross Laminated Timber Construction System or CLT, first developed in Austria and Germany, has recently emerged as an excellent alternative for the construction industry. The region of Telemaco Borba-PR Brazil has a sawmill industry that produces a large amount of low-value wood pieces, including pieces of small length *Pinus* and boards from *Eucalyptus* pith, both materials used in this research. The objective of this work is to analyse the quality and structural performance of CLT panels, using plantation wood boards, *Pinus spp* and *Eucalyptus grandis*, previously visually and mechanically graded by ultrasound NDT method. After grading, all the boards were grouped into three levels according to the modulus of elasticity (MOE). These pieces were organized into 4 groups of panels, one exclusively of pine and one exclusively eucalyptus. The other types were developed combining these two species, a type of eucalyptus in the central layer and the pine in longitudinal layers and other with pine positioned in the central layer and eucalyptus in the outer layers of the panel. A fourth type of panel was produced using ungraded pine and eucalyptus, for the sake of comparison with the classified ones. The adhesive was Urea Formaldehyde Melanin (MUF). The panels were mechanically tested in bending according to ASTM D 198 (2009). Individual stiffness (MOE) of the panels was compared to the lumber MOE, showing the importance of non-destructive grading in the manufacture of the panels. The MOE panel values were also compared to the results found in literature and international standard that regulates the CLT (ANSI-APA / PGR 320 (2012)) showing the possibility of using both species successfully in the production CLT.
Keywords: CLT, ultrasound technique, eucalyptus, pine, visual grading.

Introduction

The pinewood and eucalyptus reforestation as raw material for construction is normally underused in Brazil, destined mainly to temporary concrete forms for structures such as beams, slabs and anchors. When it comes to eucalyptus pith and pine pieces resulting from cuts, with lengths less than 120 cm, the use for construction is virtually nonexistent. This fact is mainly due to the low density, mechanical properties and high shrinkage characteristic of the eucalyptus pith, central part of the logs, making this product, as well as the pine clippings, raw material destined to turn into charcoal and firewood. Therefore, the possibility of the use of this material - eucalyptus pith and pine clippings in construction is a way to lower production costs and add value to this raw material.

The construction system , Cross Laminated Timber (CLT) consists of layered boards glued transversely, forming a massive panel with structural features. Initially developed in Austria and Germany, in the 1990s, these panels have been used in various types of buildings, commercial and residential, with studies showing use even in tall buildings. CLT can be used exclusively in constructions for structure and sealing as well as in combination with other construction methods such as steel and concrete, particularly in buildings of more than two floors.

According to (Rivera 2012), traditionally, solid wood systems have used wood fibers oriented in one direction, both in vertical and horizontal applications. The main characteristic of CLT panel structural performance is that it can be used in all directions and may be considered as an isotropic structural element, because it is constructed from superimposed layers of wood pieces in transverse directions in order to increase the rigidity and stability. The panel thickness can be 3 to 10 layers, as illustrated in Figure 1.

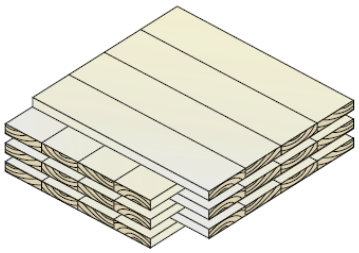

Figure 1- Configuration of the layers of CLT panels. Source: *FPInnovation* (2011) CLT *Handbook*

The panels can be formed with different types of wood species, which can alter their resistance, increasing or decreasing depending on the characteristics of the species. According to (ANSI / PRG APA 320 2012) which regulates the CLT in the United States, to avoid differences in the physical and mechanical properties of lumber, each species of wood must occupy a different layer when combined.

The (ANSI / APA PRG 320 2012), provides a grading of species available in the US through the physical and mechanical resistance, such as tension, bending, compression and shear. Based on these values, this standard requires minimal effort for the structural capacity of CLT panels, modulus of elasticity and rupture, which must be obtained through mechanical tests on specimens. They are tested for rigidity and resistance to bending, shear compression and traction. The flexural resistance tests are carried out in two directions, parallel and perpendicular to the direction of greater strength.

The coniferous wood for structural use should be classified according to NBR 7190/97. According to (Carreira 2005) this grading must evaluate each piece limiting its use according to the type, location and size of defects that can alter the structural strength of timber. As well as conifers, hardwoods are sorted for structural use according to the (NBR 9487 1986), however the (NBR 7190 1997) standard allows structural use without grading and instead applies the k_{mod} correction coefficient ranging from 1 for pieces without defects to 0.3 for less dense woods and with defects.

Among nondestructive grading techniques that can assist in structural timber evaluation process, stands the ultrasound technique. This technique consists of measuring the stiffness of the timber by the ratio of the propagation velocity of a high frequency sound wave. This speed can be changed by the presence of defects such as knots and insect attack, as well as the inclination of the fibers. The value of the modulus of elasticity (MOE) can be determined using the propagation velocity and the density of the material shown in equation (1):

$$MOE = V^2 \cdot \rho \qquad (1)$$

Where: V = the wave propagation velocity (m / s), and ρ = density of the wood (kg / m³).

Another factor that changes the resistance is the type of adhesive used in the manufacture of the panels, which according to (FPInnovations 2011), is the second most important component of the building system CLT. The adhesives used with success in the phenol type CLT are: phenol-resorcinol-formaldehyde, emulsion polymer isocyanate (EPI) and polyurethanes (PUR), but these adhesives exhibit a high cost. Structural adhesives melamine-urea-formaldehyde (MUF) and urea-formaldehyde (UF) become viable options for the manufacture of CLT panels because they have lower commercial value.

This study aimed to evaluate of the structural behavior in bending of CLT panels, made from pine and eucalyptus, by bending tests, with the minimum values specified in international standards and results obtained by other authors.

Materials and methods

The materials used in the study were wooden planks of the species *Pinus spp*, from the sawn dried boards and stored in the laboratory of structures of the Londrina State University and *Eucalyptus grandis* pith, coming from a planted forest in the Telemaco Borba-Pr region, oven dried and provided by Tecnomade, a sawmill company.

Non Destructive Rating

Visual Ranking

According to the (NBR 9487 1986), which ranks sawn hardwood, pith is a defect inadmissible in any of the four classes, so as all boards are composed mostly of pith, it is not suitable for structural use. However, aiming to add value to the material, these boards were included in the study.

The visual grading of the 147 eucalyptus pith pieces followed the selection criteria of the (NBR 9487 1986) for other defects, such as cracks and knots. A pre-selection was carried out on a group of 416 eucalyptus pith boards, from wich 35% were used for the preparation of panels. The other parts were discarded because they had more than 60% of visual defects in their length.

Concerning pine pieces, the visual grading was performed according to the standards of (NBR 11700 1990) and (ATSM D245 1998) as well as the grading manual produced by (Moura et al. 2012). Eigthy boards were visually graded 300 cm x 12,5 cm x 2,4 cm. The defects considered in the visual grading, both as eucalyptus pinus were: the number of nodes, the cracks and the cracks presented in pieces. Parts with defects such as wane, cupping, twisting and arching, were excluded in the pre-selection because such defects hinder the necessary contact between adjacent layers of the panel CLT.

Ultrasound test.

The ultrasonic test was carried out on pieces of pine and eucalyptus in order to obtain the dynamic modulus of elasticity of the wood. The equipment used was the Agricef brand and the model was USLab. It has an output of 700 V and metallic encapsulation transducers, which operate with a frequency of approximately 45 kHz to directly measure the propagation time of the waves in microseconds (μs).

The transducers were placed on the center at each end of the boards, with an application of a layer of approximately 1 mm alcohol gel in order to obtain the velocity of propagation of the waves in the middle, through the relationship between propagation time and the distance covered. The average length considered of the boards of both eucalyptus and pine was 3 m. Only one measurement was carried out on each board.

Development of CLT panels

Four types of CLT panels were prepared, two composed exclusively of pine (PPP) and eucalyptus (EEE). Two groups combining the two species with eucalyptus and pine: one with eucalyptus in the central layer and pine in the outer layers (PEP) and the other with pine in the central layer and eucalyptus in the outer layers (EPE).
Within these 4 types of panels, three categories were obtained from the observed values of dynamic elasticity module of the ultrasound method, as shown in table 1.

Table 1- Formation of CLT panels according to groups of dynamic MOE results (MPA). Source: Authors

	3 panels EEE	**3 panels EPE**	**3 panels PPP**	**3 panels PEP**
group 1	17.374 a 29.396	15.132 a 29.396	15.132 a 28.265	15.132 a 29.396
group 2	14.036 a 17.367	10.818 a 17.367	10.818 a 14.991	10.818 a 17.367
group 3	10.797 a 14.000	3.097 a 14.000	3.097 a 10.344	3.097 a 14.000

A category was created with unsorted parts, in order to compare panels made with classified wood.

Figure 2- Separation of the parts for dynamic modulus of elasticity groups (MPA). Source: Authors.

The panels were manufactured using melamine urea formaldehyde adhesive, 100 parts resin and 20 parts of catalyst. To obtain the weight of 400g / m² a precision scale was used. The assembly of CLT panels was carried out on a metal surface and to ensure that there was no bond between the boards and the surface, a plastic blanket was used.

The first layer was composed of 6 boards with a width of 10 cm, placed one beside the other and by applying the adhesive on the joint with the aid of a silicone spatula. After this process the layer of cross pieces was added, positioning the parts one next to the other, as figure 3 demonstrates.

Figure 3- Preparation of the CLT panels. Source: Authors

Immediately following placement of the transverse layers, the adhesive was applied again in the same amount as used in the previous layer. Above this second transverse layer, the longitudinal parts have been positioned, completing the panel assembly. According to the specifications of the manufacturer MUF adhesive, the time in which surfaces become bonded after contact is 50 minutes at 30° C and 150 minutes at 15 ° C. The ambient temperature at the time of preparation of the panels was 28 ° C and the assembly time occurred on an average 30 minutes. There was no gluing or pressing of the edges. After being mounted the panels were positioned in the press trays. The cold pressing time was 6 hours and the pressure set at 0.8 MPa.

Testing of CLT panels

The equipment used for the tests of the CLT panels, was the testing machine EMIC DL-30.000 model with 30.000 kgf load capacity (300KN) at the construction material lab at State University of Londrina (UEL). The values obtained in the tests were determined according to the prescribed test methodology in Annex B to (NBR 7190 1997). The standard load diagram has been transformed into a script by the TESC program that provided all the data during the test, such as: displacement, applied force to the panel, the time and the breaking load. The bending test panels followed the (NBR 7190 1997)standards Annex B and (ASTM D 198 2009). The load was applied by a "cleaver", perpendicular to the face of the panel according to the four bending method, as shown in Figure 4.

Figure 4 - The test panels CLT. Source: Authors

Results and Discussion

The results obtained for the non-destructive ultrasound rating on pieces of pine and eucalyptus showed that there was little variation in average values between the two species, as shown in Table 2. However, the coefficient variation of values were higher for the pinus because all the classified pieces were included in the study, which did not occur in the eucalyptus, as a pre-selection of the pieces were made and only the one with better assessment in the visual grading were used.

Table 2- Modules of Elasticity Dynamic, pine and eucalyptus (MPA). Source: Authors

Species		Density ρ_{apa} 12% (kg/m³)	V (m/s)	MOE_{din}
eucalipto	maximum	0,74	6.298	19.114
	minimum	0,37	2.164	5.028
	mean	0,51	4.908	12.410
	CV (%)	16	14	26
Pinus	maximum	0,72	5.899	24.009
	minimum	0,36	2.285	2.793
	mean	0,53	4.565	11.385
	CV (%)	14	17	37

The results reported in the literature correlate with the results found in the present study. (Targa et al. 2005) conducted a study to determine the elastic modulus on specimens prepared from three species of eucalyptus through the ultrasound method. Mean values were obtained for $MOE_{dinamic}$ 24.000 MPa for the *Eucalyptus citriadora* (density = 1.00 g / cm³), 17.000MPa for *Eucalyptus grandis* (density = 0.62 g / cm³) and 19.000PMa to *Eucalyptus saligna* (density = 0.87 g / cm³).

(Ballarin et al. 2005) conducted a study comparing the average values of dynamic modulus of elasticity of juvenile wood to mature wood of *Pinus taeda*, with average densities of 0.50 g / cm³ and 0.60 g / cm³, respectively. The results observed for $MOE_{dinâmic}$ were 11.816 MPa for juvenile wood and 17.914 MPa for mature wood.

Results of the panels tests.

The results of were analyzed and compared both with the values obtained between groups and combinations, as with values reported in the literature and in the specific technical standard for CLT (ANSI / APA 320 2012).

Table 2- Modulus of Elasticity result (MOE) MPA. Source: Authors

Panels	EEE	EPE	PPP	PEP
group 1	17.333	16.895	14.131	15.566
group 2	16.069	18.362	13.499	13.073
group 3	15.318	16.730	11.974	12.883
aleatory	15.815	16.910	14.884	10.693
mean	16.134	17.224	13.622	13.054
Standard Deviation	743,21	660,67	1.070,37	1.725,84
CV (%)	4,6	3,8	7,9	13,2

It can be seen in Table 3 that there were significant differences between the moduli of elasticity of the combination of the groups panels eucalyptus / pine / eucalyptus (EPE) and eucalyptus / eucalyptus / eucalyptus (EEA) compared with the combination of pine / eucalyptus / pine (PEP). In the elastic modulus of the EPE group, a value of 18.362MPa can be observed, 70% higher than the lowest results found in PEP group (10.693MPa).

These results show that panels produced entirely with eucalyptus and eucalyptus and pine in the central layer were stiffer. In this group of PEP composition, the panel consists of items unclassified or randomly presented the lowest result of all groups of elastic modulus (10,693 MPa). In combinations of EEE panels, PPP and PEP, the elastic modulus observed in the groups were decreasing in group 1 to group 3, maintaining an average for the random group, which was somehow expected because group 1 is formed with better grading of parts.

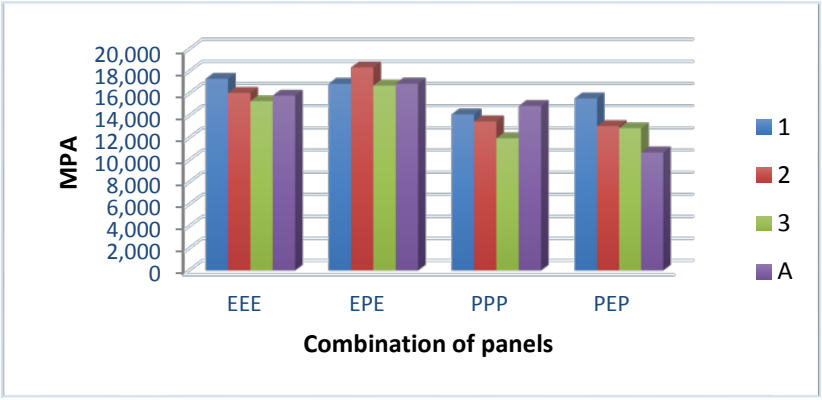

Figure 5- Modulus of Elasticity (MOE) MPA. Source: Authors

As seen in Figure 5, the group that showed the best MOE results was formed by eucalyptus / pine / eucalyptus unlike the group of panels prepared entirely with pine that had a lower elastic modulus value of all groups. Comparing the results of the pine and eucalyptus boards groups classified by ultrasound with the MOE values of the panels, these are lower than those of boards, is less flexible and more rigid.

The results obtained for bending tests performed on CLT panels compared to that found in the literature, show that the values achieved in this study were similar. (Wang et al. 2014) gave values for tensile modulus of 5.900 MPa to 8.700 MPa in flexural tests on panels CLT combining different species. (Flaig et al. 2014) in bending and rupture tests performed on CLT beams obtained average values for tensile modulus over density wood (0.45g / cm^3) and without finger joint 12.800 MPa. In this study, with less dense timber (0.40g / cm^3), the results obtained were 10.000 MPa for tensile modulus.

According to the minimum values for structural projects for CLT panels issued by (ANSI / APA 320 2012), the results for modulus of elasticity should not be less than 8.300 MPa. These values are relative to bending tests in the longitudinal direction, according to (ASTM D198 2009), the same methodology used in the tests performed in this study.

In most combinations, the results of unclassified groups were lower than those of the graded ones. However in some, values of panels with ungraded wood were higher because they could contain in board with high levels of $MOE_{dinamic}$. This fact confirm the importance of the grading process, both visual and non-destructive mechanical, in order to improve the structural behavior of these components, as well as the strutuctural safety levels CLT panels.

Conclusion

The results achieved in bending tests on 16 CLT panels showed values above those referenced in literature and the standard that regulates the CLT. The panels made with pine had the lowest values of MOE, i.e. panels with pine were less rigid than those with eucalyptus.

The combination between species, the panels containing pine in longitudinal layers and transverse eucalyptus layers (PEP) had the lowest average MOE values (13034 MPa). The panels with eucalyptus in longitudinal layers and pine in transverse layers (EPE) presented values of 17.224 MPa MOE. These results pointed to a greater stiffness and lower resistance for the panels with eucalyptus (EEA and EPE) while the ones containing pine (PPP and PEP) showed greater flexibility and resitence.

The structural behavior of the panels as the modulus of elasticity was compatible with the results of grading obtained by means of the ultrasonic non-destructive method. The panels made with boards without grading showed unpredictable structural behavior. Most of the time it was observed that MOE values were greater in groups with graded timber than the ungraded ones. However there were some results in the groups formed by ungraded boards which obtained MOE values above or similar to panels made with groups with classified lumber. So non-destructive grading proved to be an efficient method for determining the behavior of CLT structural panels.

Therefore the values achieved in this study, even the lower ones reached average values to those found in the literature, as well as above the minimum values published by (ANSI / APA 320 2012). Thus it was observed that eucalyptus pith, raw material considered inappropriate for structural use by the (NBR 9487 1986) standard, imparted acceptable stiffness and resistance levels to the composition of CLT panels, proving that material is suitable to structural use.

References.

American society for testing materials. 2009. ASTM D 198 - Standard Test Methods for Strength Properties of Adhesive Bonds in Shear by Compression Loading, Philadelphia.

American society for testing materials. 2002. ASTM D 245 - Standard Test Methods for Mechanical Properties of Lumber and Wood-Base Structural Material, Philadelphia.

Associação brasileira de normas técnicas, ABNT. 1997. NBR 7190 – Projeto de Estruturas de Madeira, Rio de Janeiro. 107 p.

Associação brasileira de normas técnicas, ABNT. 1986. NBR 9487 – Classificação de Madeira Serrada de Folhosas. Rio de Janeiro. 32 p.

Associação brasileira de normas técnicas, ABNT. 1990. NBR 11700 – Madeira serrada de coníferas proveniente de reflorestamento para uso geral. Rio de Janeiro. 6 p.

APA. The Engineered Wood Association. Standard for performance. 2012 Rated Cross-Laminated Timber, ANSI/APA PRG 320. Tacoma, Washington, USA.

Ballarin, A. W.; Nogueira, M. 2005. Determinação do Módulo de Elasticidade da Madeira Juvenil e Adulta de Pinus taeda por Ultrassom. Eng. Agric. Jaboticabal, v. 25, n,1, p. 19-28.

Carreira, M. R.; Dias, A. A. 2005. Classificação visual de coniferas: análise da aplicação do método norte-americano às espécies de Pinus sp plantadas no Brasil. Scientia Forestalis n. 67, p. 78-87.

Concu, G.; De Nicolo, B.; Valdés, M.; Fragiocomo, M.; Menis, A.; Trulli, N. 2013. Experimental Granding of Locally Grown Timber to be used as Structural Material. Revista Advances in Civil Engineering and Building Material, London.

Flaig, M.; Blad, H. J. 2014. Bending Strength of Cross Laminated Timber Beams Loaded in Plane. World Conference on Timber Engineer, Quebec-City, Canada.

FPINNOVATIONS. CLT Handbook : Cross laminated timber. FPInnovations Canadá. 2011.
Rivera, C. S. 2012. Expanding Opportunities for Mid-Rise Buildings in Chile Through the application of Timber Panel Sistems. 2012, (Master of Advanced Studies in Architecture) University of Bristish Columbia. Vancouver.
Moura, J. D. M.; Pletz, E.; Strass, M. C. 2012. Qualidade e Processo Produtivo da Madeira para Utilização em Mobiliario. State University of Londrina, Edition 1.

Targa, L. A.; Ballarin, A. W.; Biaggioni, M. A. M. 2005. Avaliação do Módulo de Elasticidade da Madeira com uso de Método Não-Destrutivo de Vibração Transversal. En. Agric., v. 25, n2, p. 291-299, Jaboticabal-SP.

Wang, Z.; FU, H.; Chui, Y.; Gong, M. 2014. Feasilibity of Using Poplar as Cross Layer to Fabricate Cross-Laminated Timber. World Conference on Timber Engineer, Quebec-City, Canada.

Effect of wood properties and production process on stiffness of charcoal studied by ultrasonic technique

Maíra Reis de Assis[1,2*], Loïc Brancheriau[2], Alfredo Napoli[1,2], Daniel Guibal[2], Nabila Boutahar[2], Paulo Fernando Trugilho[1]

[1] Federal University of Lavras/UFLA - Department of Forestry Sciences, Post Office Code 3037, 37200-000, Lavras, Minas Gerais, Brazil
[2] CIRAD - Research Unit BioWooEB, TA B114/16, 73 Rue J.F. Breton, 34398 Montpellier, France

[*] Corresponding author. Tel.: +33 (0) 782850062. E-mail: maira.reis_de_assis@cirad.fr

Abstract

Charcoal can replace coke in blast furnaces avoiding the use of reducing agents derived from fossil fuels. However, the main limitation of charcoal is its lower strength, which is essential for supporting the iron ore load inside the blast furnaces. In order to improve and control the charcoal quality, the objectives were then to study (i) the influence of radial position of the raw material and carbonization temperature on charcoal density and rigidity, and (ii) the link between properties of wood and charcoal taking into account the previous factors. It was found that: (a) The charcoal MOE increased with the final temperature of pyrolysis, but the temperature effect was less significant for the density. (b) The charcoal properties were higher for samples cut near the bark, but an elevated carbonization temperature seemed to reduce this phenomenon. (c) The best predictors to estimate the charcoal quality were the wood density and the carbonization temperature.

Keywords: charcoal quality, carbonization temperature, juvenile wood, ultrasounds

Introduction

World steel production is dependent on coking coal. Steel is an alloy based primarily on iron, and the iron ore must be converted, or 'reduced', using carbon during the making process. The primary source of this carbon is coking coal. During the iron-making process, the heated air (1200°C) is blown into the blast furnace, and causes the coke to burn, producing carbon monoxide which reacts with the iron ore, as well as heat to melt the iron. Charcoal has often been compared to coke and can replace it in blast furnaces avoiding the use of reducing agents derived from fossil fuels. However, the main limitation of charcoal as replacement coke is its low compression strength, which is essential for supporting the iron ore load inside the blast furnaces. The effect of wood properties as well as parameters of carbonization process on the strength of charcoal has been studied. Wood density was found to be positively correlated to the apparent density of charcoal (Antal and Grønli 2003). Charcoals produced with dense woods were characterized by a higher mechanical resistance. Blankenhorn et al. (1978) showed, when carbonizing Black Cherry wood, that charcoal density decreased until 600 °C, then increased with the increase of temperature until 900 °C. Vieira (2009) observed that the acoustic modulus of elasticity of charcoal from *Eucalyptus* sp. increased with the increase of the carbonization temperature from 350 to 900 °C. Considering the radial position, the mechanical resistance increased from the pith to the bark. Trugilho et al. (1996) showed that juvenile wood produced a less resistant charcoal than mature wood. Moore et al. (1974) tested carbonized wood from Birch trees in a temperature range of 200-700°C. The compression strength of charcoal decreased up to approximately 500 °C then increased. These tendencies were also observed by Oliveira et al. (1982) for *Eucalyptus* sp. Ultrasonic velocity was measured for yucca, before and after carbonization (Krzesińska and Zachariasz 2007). It was found that the velocity of charcoal decreased

up to 300°C, then increased between 300-750°C and was quasi-constant for higher temperatures. From previous results obtained by the cited authors, it is known that charcoal density and compression strength are linked to wood density and rigidity. Furthermore, this link is function of the radial position and the pyrolysis temperature. In order to improve and control the charcoal strength, our questions were thus: How to predict the charcoal properties from the wood properties? And what will be the accuracy of such estimates? The mechanical strength of the charcoal beds in the Brazilian context of iron and steel furnaces is very important and contribute for reduce the specific consumption of the industrial units. The purpose of this work was to study (i) the influence of radial position and carbonization temperature on charcoal density and rigidity and (ii) the link between properties of wood and charcoal taking into account the previous factors. Density and longitudinal modulus of elasticity were measured on wood samples before and after pyrolysis according to three radial positions and two final temperatures.

Material and Methods

Sample preparation

A total of 35 trees of one hybrid of *Eucalyptus urophylla* ST Blake (6 years old) were harvested. The trees came from a plantation belonging to GERDAU S.A., and were located in the same plot at Santo Antônio do Amparo, Minas Gerais - Brazil (20°56'48" S e 44°55'09" O). The plot was characterized by a flat soil with moderate winds. Cubic samples (30 mm in L, R and T directions; N = 57) were cut at 1.30 m height and at three radial positions from pith to bark. For diameters less than 18 cm, only one cubic sample was cut (identified as 'middle', N = 13). In the other case, two cubic samples were prepared (identified as 'internal', N = 22, and 'external', N = 22). After cutting, the samples were conditioned in a climatic room at 20°C and 65% of relative air humidity.

Experimental protocol

The density of the wood samples was first determined (volume computed by measuring the dimensions with a digital caliper). The modulus of elasticity was then assessed by ultrasonic measurements in the longitudinal direction. In a second step, the cubic samples were pyrolized. The bulk density of the charcoal samples was measured according to the ASTM D2395-07 (volume by water immersion). The samples were waterproofed with a very thin layer of grease before obtaining charcoal volume (grease used as couplant for the ultrasonic tests). The modulus of elasticity of the charcoal samples was finally determined by ultrasounds.

Pyrolysis process

The cubic samples were pyrolized at two final temperatures: 500°C and 900°C. The samples population was previously divided into two batches: the samples were sorted according to the wood density, and the even ranks were associated to a pyrolysis temperature of 500°C (odd ranks with a temperature of 900°C). Pyrolysis was performed in a specific electric reactor developed by Cirad (Macro-ATG), using a heating rate of 1.5 °C/min. After carbonization, the samples were conditioned in a climatic room at 20°C and 65% of relative air humidity.

Ultrasonic testing

Two contact transducers were used in transmission mode. Each sample was placed between the piezoelectric transducers with silicon grease used as coupling medium. The emission frequency was set to 1 MHz, and the received signal was digitized with a 12-bit resolution and a sampling period of 0.1 µs (the average propagation time is 6.4 µs for wood). A computer algorithm calculated the propagation time by determining a threshold based on an analysis of the statistical properties of the signal noise. This determination method was appropriate in this case given that the signal-to-noise ratio was greater than 30 dB. The ultrasonic modulus of elasticity (MOE) was determined by the

conventional Equation (1), where ρ is the density, L is the sample length, and τ is the propagation time. The mean of three measurements was used to determine the MOE value of each sample.

$$MOE = \rho\left(\frac{L}{\tau}\right)^2 \quad (1)$$

Statistical analysis

The comparison between averages was carried out by a nonparametric Wilcoxon test because of the low number of samples. The kernel density estimation method (KDE) was chosen to build the probability density function graphs. Analysis of covariance evaluated the influence of variables related to wood, carbonization process and their interaction on the charcoal mechanical property. The descriptive statistics, comparisons between means and the analysis of covariance were performed using the R statistical software (version 3.1.1, 2014).

Results

Influence of radial position on wood properties

Table 1 - Descriptive statistics of wood density and MOE according to radial position. SD: standard deviation.

Radial position	Number of samples	Density ($kg.m^{-3}$)				MOE (MPa)			
		Min.	Max.	Average	SD	Min.	Max.	Average	SD
Internal	22	473	610	518	40	8939	12546	10397	964
Middle	13	491	616	556	40	10347	17912	14315	2272
External	22	484	697	588	54	9765	17202	14116	1924

The descriptive statistics of wood density and MOE according to radial position were summarized in Table 1. Figure 1 showed the associated probability density functions. The wood properties were found to be lower near the pith. The density values varied from 473 kg/m^3 near the pith to 697 kg/m^3 near the bark, and from 8939 MPa to 17912 MPa for MOE. The variation patterns of density were similar to those of MOE (Figure 1). The 'middle' and 'external' curves were superimposed (average density of 556 kg/m^3 and 588 kg/m^3, average MOE of 14315 MPa and 14116 MPa), and these curves were different from the 'internal' probability density function (average density of 518 kg/m^3, average MOE of 10397 MPa). From this last observation it was deduced that the samples population should be divided into two groups and not into three groups prior further analysis.

Table 2 - Wilcoxon unpaired tests for wood density and MOE according to radial position. Significance levels: 0.0001 '***'; 0.001 '**'; 0.01 '*'; 0.05 '.'; Non-significant 'ns'.

Wood Properties	Wilcoxon *p* (bilateral)		
	Internal vs. Middle	Middle vs. External	Internal vs. External
Density ($kg.m^{-3}$)	0.01*	0.12^{ns}	<0.001**
MOE (MPa)	<0.001**	0.84^{ns}	<0.001**

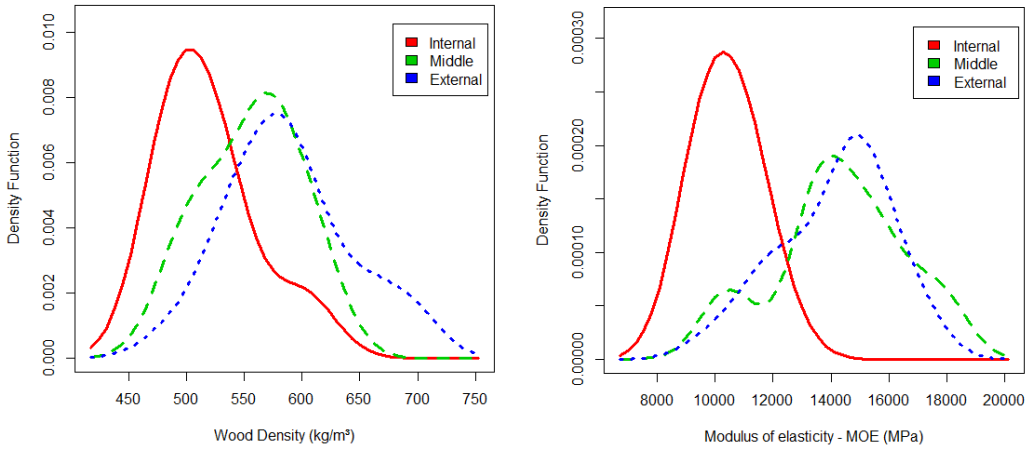

Figure 1 – Probability density function of wood density and MOE according to radial position.

The probability distributions were tested using the Kolmogorov–Smirnov test, and the Wilcoxon test was used to compare means. These tests led to the same conclusion, and confirmed the existence of two groups according to the radial positions. The Wilcoxon test results were presented in Table 2. In the following of the article, the samples population was thus divided into two groups identified as 'Internal' (N = 22) and 'Mid-Ext' (N = 35).

Influence of radial position and carbonization temperature on charcoal properties

Table 3 - Descriptive statistics of charcoal density and MOE according to radial position and carbonization temperature. SD: standard deviation.

Charcoal density ($kg.m^{-3}$)										
Radial position	500°C					900°C				
	N	Min.	Max.	Average	SD	N	Min.	Max.	Average	SD
Internal	11	224	328	250	27.8	11	251	334	291	23.2
Mid-Ext	17	246	369	309	35.4	18	259	484	341	58.2
Charcoal MOE (MPa)										
Radial position	500°C					900°C				
	N	Min.	Max.	Average	SD	N	Min.	Max.	Average	SD
Internal	11	985	1346	1052	100.5	11	2962	4237	3379	387.1
Mid-Ext	17	1089	1592	1372	137.3	18	2880	6153	4047	850.5

The descriptive statistics of charcoal density and MOE according to radial position and carbonization temperature were presented in Table 3. Wilcoxon tests were used to study the influence of the two factors (Table 4). The radial position and the carbonization temperature had significant effects on the density and the elastic modulus. The MOE increased with the final temperature of pyrolysis, from 1052 MPa to 3379 MPa for the internal position, and from 1372 MPa to 4047 MPa for the Mid-Ext position (the charcoal was 3 times more rigid at 900°C than at 500°C). This effect was less pronounced for the density, from 250 kg/m^3 to 291 kg/m^3 for the internal position, and from 309 kg/m^3 to 341 kg/m^3 for the Mid-Ext position (the density was 1.13 times greater at 900°C than at 500°C). The difference between 309 kg/m^3 and 341 kg/m^3 was non-significant (p=0.106) with the Wilcoxon test. The charcoal MOE and density were found to be higher for the Mid-Ext position than for the internal position. The relative difference between the radial positions was reduced for 900°C. The density ratio (Mid-Ext/Internal) was 1.24 at 500°C and 1.17 at 900°C; the MOE ratio was 1.30 at 500°C and 1.20 at 900°C (this observation was shown at Figure 2, the curves were overlapped at 900°C). Thus, a high carbonization temperature seemed to soften the effect of radial position.

Table 4 - Wilcoxon unpaired tests for charcoal density and MOE according to radial position and carbonization temperature. Significance levels: 0.0001 '***'; 0.001 '**'; 0.01 '*'; 0.05 '.'; Non-significant 'ns'.

Charcoal properties	Combination of factors	Wilcoxon *p* (bilateral)
Density (kg.m^{-3})	Internal and 500°C / 900°C	0.002*
	Mid-Ext and 500°C / 900°C	0.106^{ns}
	500°C and Internal / Mid-Ext	<0.001**
	900°C and Internal / Mid-Ext	0.016*
MOE (MPa)	Internal and 500°C / 900°C	<0.001**
	Mid-Ext and 500°C / 900°C	<0.001**
	500°C and Internal / Mid-Ext	<0.001**
	900°C and Internal / Mid-Ext	0.016*

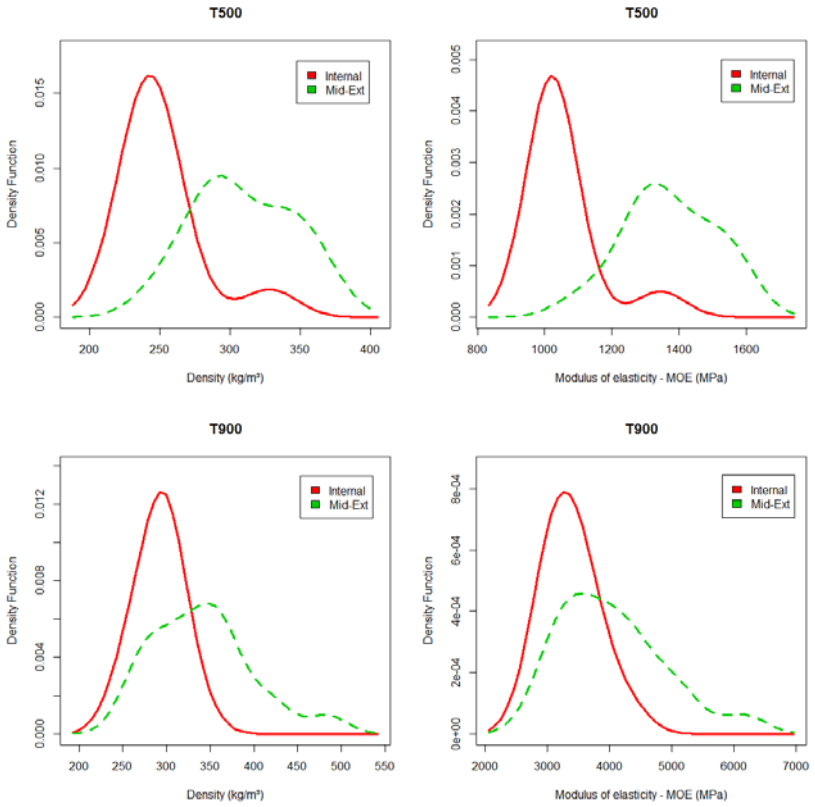

Figure 2 – Probability density function of charcoal density and MOE according to radial position (Internal, Mid-Ext) and carbonization temperature (T500, T900).

Link between properties of wood and charcoal according to radial position and carbonization temperature

The relationships between charcoal and wood properties according to the coupled effects of temperature and radial position were carried out with the analysis of covariance. The full influence of factors with interactions was initially taken into account for the modeling (wood density or MOE, final temperatures 500°C and 900°C, radial positions Internal and Mid-Ext). The models were then refined using the AIC criterion in a stepwise algorithm. At the end of the procedure, only the significant variables were kept in optimal models. The results were presented in Table 5. The effect of radial position was not present in the optimal models. The temperature effect was not included as an additive constant, but in the slope of the regression models (see the difference of slope in Figure 3).

Table 5 – Regression coefficients and model characteristics between charcoal and wood properties. T900: value of 1 for a temperature of 900°C and zero for 500°C. N = 57. RSE: Residual standard error.

Charcoal density (kg/m^3)				
Intercept	Wood density	Wood density * T900	RSE	Adjusted R^2
-151.1	0.792	0.060	17.3	0.89
Intercept	Wood MOE	Wood MOE * T900		
106.9	0.014	0.003	28.8	0.69
Charcoal MOE (MPa)				
Intercept	Wood density	Wood density * T900	RSE	Adjusted R^2
-1761	5.429	4.587	308	0.95
Intercept	Wood MOE	Wood MOE * T900		
543	0.055	0.203	335	0.94

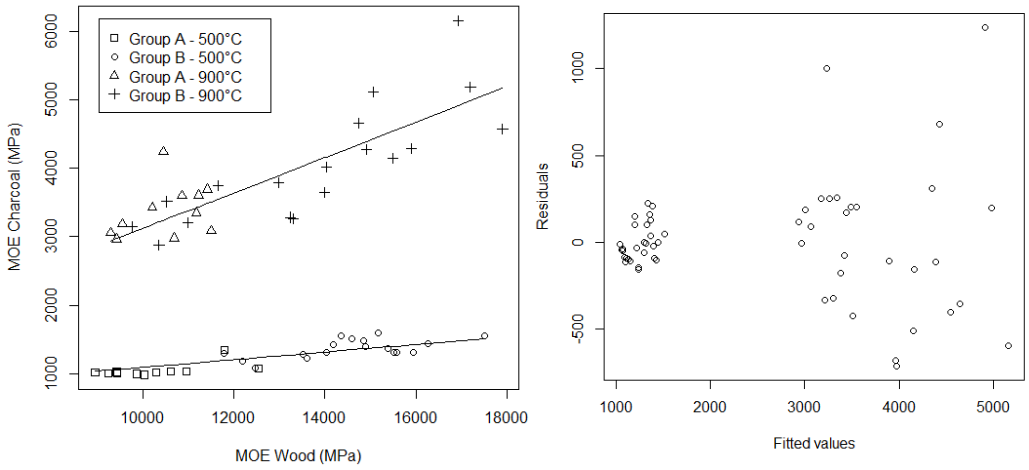

(a) (b)

Figure 3 - Relationship between charcoal and wood MOE (a) according to carbonization temperature and radial position (Group A for internal position and Group B for Mid-Ext position). (b) Dispersion of residues. N = 57.

The best predictor to estimate the charcoal density was the wood density (Adjusted R^2 of 0.89 with wood density, and 0.69 with wood MOE). The standard error of the charcoal density estimation by the wood density was 17.3 kg/m^3 associated with an average charcoal density of 287 kg/m^3 at 500°C and of 322 kg/m^3 at 900°C. However, the models with wood density or wood MOE were quasi-equivalent to predict the charcoal MOE (Adjusted R^2 of 0.95 with wood density, and 0.94 with wood MOE). The standard error of the charcoal MOE estimation by the wood density was 308 MPa associated with an average charcoal MOE of 1251 MPa at 500°C and of 3794 MPa at 900°C. The difference of adjusted determination coefficient between charcoal density (0.89; 0.69) and charcoal MOE (0.95; 0.94) was due to the difference of dispersion (coefficient of variation of 17% for charcoal density, and of 56% for charcoal MOE, considering the 57 samples). The model between charcoal and wood MOE was presented as example at Figure 3a. The model equation was: Charcoal MOE = 543 + 0.055 Wood MOE + 0.203 Wood MOE*T900. This equation was equal to: Charcoal MOE = 543 + 0.055 Wood MOE for 500°C and Charcoal MOE = 543 + 0.258 Wood MOE for 900°C. The scatterplot of the residuals was presented at Figure 3b. It was observed that the standard error of the residuals was different between 500°C (RSE=110 MPa) and 900°C (RSE=474 MPa); the RSE model being equal to 335 MPa (Table 5). The residues at 900 °C were more scattered than those at 500 °C.

Discussion

The samples population was divided into two groups in order to study the effect of radial position. For small diameters, only one cubic sample was cut in the middle of the radius; otherwise, two samples were taken. The pertinence of the sampling location was a question during the study; this was solved by a statistical analysis allowing to group locations with similar properties. The radial variation observed for the wood properties (density and MOE) was explained by the transition juvenile to mature wood. The wood properties were lower near the pith. From references cited in introduction, the charcoal density and the mechanical properties of charcoal are linked to wood properties. This link is function of the radial position and the pyrolysis temperature. Our observations were in agreement with the references cited. In the same way, the charcoal properties were found to be higher for the external position than for the internal position: this observation was in agreement with the cited references (denser wood produced denser charcoal). It was observed that the charcoal MOE increased with the carbonization temperature, but this phenomenon was less pronounced for the charcoal density. The density is linked to porosity. The porosity of charcoal is closely associated to the wood porosity, the temperature of carbonization, and the speed of carbonization (Blankenhorn et al. 1978, Oliveira et al. 1982). Blankenhorn et al. (1978) indicated that for *Prunus serotina* Ehrh., the porosity increased with the increase of temperature up to 600 °C and then decreased with temperatures up to 900 °C. Thus, the density decreased until 600 °C, and increased with the increase of temperature until 900 °C due to the occurrence of lower weight loss in relation to shrinkage. The rigidity is linked to the density (amount of matter per unit of area) and to the rigidity of matter. At temperatures above 375°C, lignin is the key component of the charcoal formation. The majority of the carbohydrate polymers have degraded between 300-375°C and mainly products from lignin conversion remain. Lignin has the highest heat of combustion, the highest charcoal yield and also the lowest percent of volatiles. Lignin starts to decompose at about 200°C, but is much more stable to thermal decomposition as compared to carbohydrate polymers. The increase of resistance from 500 °C is due to the structural rearrangement of the charcoal components, especially carbon (Beall et al. 1974, Moore et al. 1974, Oliveira et al. 1982). According to Oliveira et al. (1982) this structural rearrangement is accompanied by the increase of apparent density of charcoal. The carbonized wood presents graphite-type crystalline forms despite being considered as non-graphitic material (Emmerich 1987). It was suggested that the bonding between carbon atoms is modified between 600 °C and 800 °C, which is the starting point to formation of macromolecules (from amorphous structure to crystalline structure) (Manabe et al. 2007). The increase of temperature, between 500°C to 900°C, induced an increase of charcoal density coupled with a structure more and more crystalline and rigid. The effect of radial position on the charcoal properties was found to be reduced by a high carbonization temperature. The juvenile wood is characterized by a high cellulose microfibril angle in the S2 cell wall layer and a low density (short fibers with thin walls and low percentage of latewood in the annual rings). In hardwoods the chemical composition shows little change from pith to bark, while softwoods have wood cores with lower cellulose and higher lignin. Above 500°C, the cellulose was largely converted and the chemical composition was quasi-constant from pith to bark; only the wood density variation should induced a variation in the charcoal properties. However, between 500°C and 900°C, the charcoal density increased due to shrinkage of cell walls. The hypothesis to explain the link between the radial position effect and the carbonization temperature was that the wood density variation was counterbalanced by the shrinkage variation along the radial axis. The effect of radial position was not present in the regression models linking the properties of wood and charcoal. The radial position should be seen as a hidden variable because the cutting position in the radius allowed maximizing the variation of the wood properties. It was also found that the temperature effect was included in the slope value of the regression models. It was expected that the constant was nil (or non-significant) because when the wood MOE tends to zero, the charcoal MOE should tend to zero. The fact that the best predictor to estimate the charcoal properties was the wood density was explain by the known correlation between wood density and wood MOE coupled with low measurement error on wood density compared to wood MOE. Figure 3b showed that the residues at 900 °C were more scattered than those at 500 °C. The measurement error of charcoal MOE was higher at 900°C. The sides of the samples were not flat but irregular due to the occurrence of shrinkage between 500-900°C.

Conclusions

The radial position and the carbonization temperature had significant effects on charcoal density and rigidity. The charcoal MOE increased with the final temperature of pyrolysis; this effect was however less pronounced for the charcoal density. Furthermore, the charcoal MOE and density were found to be higher near the bark, but a high carbonization temperature seemed to soften this effect of radial position. The relationships between charcoal properties and wood properties were modeled taking into account the full influence of factors with interactions. The effect of radial position was not present in the final models. The temperature effect was present in the slope of the regression models. The best predictor to estimate the charcoal density was the wood density. The models with wood density or wood MOE were quasi-equivalent to predict the charcoal MOE. The wood density was then the adequate variable to estimate both charcoal density and MOE. Careful controls of raw material and pyrolysis conditions are required to produce charcoal with sufficient properties to substitute coke in blast furnaces. Taking into account the final pyrolysis temperature, the wood density is an important property which allows controlling the charcoal density, rigidity and strength.

References

Antal, M. J.; Grønli, M. 2003. The art, science and technology of charcoal production. Indian Engeneering Chemistry Research. 42: 1619-1640.

Beall, F. C.; Blankenhorn, P. R.; Moore G. R. 1974. Carbonized wood-physical properties and use as an SEM preparation. Wood Science and Technology. 6(3): 212-219.

Blankenhorn, P. R.; Barnes, D. P.; Kline, D. E.; Murphey, W. K. 1978. Porosity and pore size distribution of Black Cherry carbonized in an inert atmosphere. Wood Science and technology. 11(1):23–29.

Emmerich, F. G. 1987. Granular model, percolation-resistivity, ESR and elastic modulus of the carbon materials: application to the babassu endocarp carbon heat treated up to 2200ºC. PhD Thesis. Universidade Estadual de Campinas. Brazil.

Manabe, T.; Ohata, M.; Yoshizawa, S.; Nakajima, D.; Goto, S.; Uchida, K.; Yajima, H. 2007. Effect of carbonization temperature on the physicochemical structure of wood charcoal. Materials Research Society of Japan 32.4 1035.

Moore, G. R.; Blankenhorn, P. R.; Beall, F. C. Kline, D. E. 1974. Some physical properties of birch carbonized in a nitrogen atmosphere. Wood and Fiber Science. 6(3): 193-199.

Oliveira, J. B.; Gomes, P. A.; Almeida, M. R. 1982. Preliminary studies standardization of quality control tests of charcoal. Belo Horizonte, Fundação Centro Tecnológico de Minas Gerais. Brazil.

Trugilho, P. F.; Lima, J. T.; Mendes, L.M. 1996. Influência da idade nas características físico-químicas e anatômicas da madeira de Eucalyptus saligna. Cerne. 2(1): 94-116.

Vieira, R. S. 2009. Mechanical properties of Eucalyptus clones wood and charcoal produced between 350 ° C and 900 ° C. PhD Thesis. Universidade Federal de Lavras. Brazil.

Krzesińska, M.; Zachariasz, J. 2007. Correlation between the carbonization temperature and the physical parameters of porous carbons derived from Yucca flaccida. Journal Physics: Conference Series 79: Paper No. 012011.

Predicting Plywood Properties with Wood-Based Composite Models

Adam Senalik, USDA Forest Service, Forest Products Laboratory, Madison, WI, USA, christopherasenalik@fs.fed.us

Robert Ross, USDA Forest Service, Forest Products Laboratory, Madison, WI, USA, rross@fs.fed.us

Abstract

Previous research revealed that stress wave nondestructive testing techniques could be used to evaluate the tensile and flexural properties of wood-based composite materials. Regression models were developed that related stress wave transmission characteristics (velocity and attenuation) to modulus of elasticity and strength. The developed regression models accounted for over 94% of these materials' observed elastic properties and for over 90% of their observed strength. The original models were developed using wood-based particle composite specimens. The study presented in this paper investigated use of the developed statistical model to predict the modulus of elasticity and strength of veneer laminated materials, specifically plywood.

Introduction

In a previous study on the subject of nondestructive testing of wood-based composites conducted by Ross and Pellerin (1988), strong correlations ($r^2 > 0.90$) were drawn between dynamic modulus of elasticity (MOE), static flexural MOE, and modulus of rupture (MOR). At the time of the study, the use of ultrasonic stress wave propagation time as a non-destructive inspection tool for wood composites was not widespread. Since that study, ultrasonic inspection has become an accepted mean of assessing and evaluating wood and wood composites. The wood-based composites used in the original study did not include plywood.

Fundamental Hypothesis and First Studies

Jayne (1959) theorized that the mechanisms that controlled the dynamic properties of wood, such as stress wave speed and attenuation, also govern important static mechanical properties. The theory implied that identifiable relationships exist between stress wave behavior and mechanical properties of wood and wood-based composites; therefore, useful analytical models could be developed and used to nondestructively estimate the mechanical properties of these materials.

This concept has served as the working hypothesis for many studies, and resulting applications, that have focused on the use of dynamic properties as nondestructive indicators of the performance of wood-based materials and composites.

The first reported study that investigated use of stress wave speed to estimate the properties of wood-based particle composites was conducted by Pellerin and Morschauser (1974). They used stress wave speed to predict the flexural properties of underlayment particleboard. Szabo (1978)

published a reference that covered many aspects of the use of ultrasonic inspection on wood-based composites including anisotropy, coupling issues, wave types, attenuation, basic ultrasonic testing setups, transducer descriptions, and the advantages and disadvantages of higher frequency usage.

Koch and Woodson (1968) first reported on the use of stress wave technique to evaluate the properties of veneer to be used in laminated veneer lumber (LVL) based on results of a study conducted in cooperation with Washington State University. Kunesh (1978) reported on the industrial use of these concepts to grade veneer. Based on the results of an extensive field, laboratory and equipment development effort, he demonstrated that ultrasonic inspection was capable of grading wood veneer at rates usable on a production line. Sharp (1985) reported similar results and conclusions, and described the process of relating ultrasonic stress wave velocity to LVL strength and grade.

Development of Predictive Models for Elasticity and Strength

Subsequent to these early studies, there has been extensive research conducted on the use of ultrasonic test methods to inspect or grade wood-based composites. A literature review on the subject can be found in Senalik and others (2014). A critical analysis of that review revealed the following:

1. Most studies were aimed at investigating the possibility of adapting existing technologies that were developed for other materials to specific problems associated with wood-based composite materials,
2. A lack of investigations linking fundamental physical phenomena with composite product performance.

In an effort to develop a strong, fundamental model relating nondestructive parameters to mechanical properties, Ross and Pellerin (1988) developed an analytical model that was a marriage between theoretical and empirical approaches and was applicable to a broad spectrum of wood composites. Using a wide range of wood-based particle composites (Table 1) including particleboard, oriented strand board, and a high strength structural composite, they developed a model that predicted static properties at levels of accuracy thought at the time to be unattainable. It is important to note the following concerning their model:

1. The model is based on the assumption of a linear positive relationship between wave speed and static properties and an inverse relationship between wave attenuation and static properties;
2. No wood veneer products (plywood or laminated veneer lumber) were used in its development;

The fundamental form of the model they developed is expressed as Equation (1).

$$P = KN_0^x N_1^y N_2^z \quad (1)$$

Where
P is property being estimated,

K, x, y, and z are empirical constants, and
N_0, N_1, and N_2 are nondestructive parameters

The nondestructive parameters examined were specific gravity, wave attenuation, and wave speed. Given the wide range of values for the properties being estimated, natural log scale was used to express the relationship. Taking the natural logarithm of Equation (1) separated the nondestructive parameters, as shown in Equation (2), and allowed for further linear regression to be performed to determine which parameter had the highest correlation to flexural MOE and MOR.

$$\ln P = \ln K + x \ln N_0 + y \ln N_1 + z \ln N_2 \quad (2)$$

The dynamic MOE was found to have the combination of highest correlation and lowest standard error of the estimate. Dynamic MOE is the product of the wood density and the square of the wave speed, and is shown in Equation (3). Wood density is proportional to the specific gravity; therefore, dynamic MOE combined two nondestructive parameters into a single parameter.

$$E_d = \rho c^2 = \rho_{H_2 0} SG_w c^2 \quad (3)$$

Where
E_d is the dynamic modulus of elasticity (MOE),
ρ is the density of the wood specimen,
c is the wave speed through the wood specimen,
$\rho_{H_2 0}$ is the density of water (practically constant), and
SG_w is the specific gravity of the wood specimen.

The model shown in Equation (1) was implemented using the dynamic MOE as the sole nondestructive parameter. The model with reduced number of parameters is shown in Equation (4).

$$\ln P = \ln K + x \ln E_d \quad (4)$$

A linear regression analysis determined the values for the unknown empirical constants, K and x, for flexural MOE and MOR. The values for the constants and the related coefficients of determination, r^2, are given in Table 1. The research reported herein was conducted to examine use of this fundamental model to assess the properties of plywood products.

Table 1—Values predicted using dynamic modulus of elasticity as the nondestructive parameter

Parameter (P)	ln(K)	x	r^2 (Ross 1988)	r^2 (Reconstructed)[a]
Flexural Modulus	-0.109	0.934	0.92	0.93
Modulus of Rupture	8.321	1.211	0.85	0.89

[a] Reconstructed data had slightly higher coefficients of correlation than that of Ross and Pellerin (1988).

Materials and Methods

Specimens of untreated plywood were cut from six separate panels. The panels were previously unused and undegraded. The cut specimens had widths of 76 mm (3 in.) and lengths of 508 mm (20 in.). The panels had a variety of thickness between 11 mm (0.42 in.) to 18 mm (0.71 in.). The specimens were conditioned for 15 days at 24°C (75°F) and 65% relative humidity. At the end of the conditioning period, the specimens were assumed to contain 12% moisture content. Prior to destructive testing, the dimensions, mass, and dynamic wave speed were measured. The dynamic wave speeds were measured using a Metrigaurd 239A across a span of 457 mm (18 in.).

The specimens were then subjected to four point static bending tests in accordance with ASTM D3043. Load and deflection were recorded during testing. From the data, flexural MOE and MOR were extracted. The extracted values were compared against the values predicted using the dynamic MOE and the relationships given in Table 1.

Original data were no longer available from the Ross and Pellerin (1988) study. The diagrams from the paper were imported into AutoCAD. The diagrams were scaled within the 2D space and an estimate of location of each data point was made. The estimated data points were used to construct the diagrams in this report. While close to the original data, the reconstructed data did have some differences. The r^2 values of the reconstructed data were slightly higher than those of the original study, but did not exceed the original values by more than 5%. The r^2 values from the original study and the reconstructed data are given in Table 1.

Results

The relationship between the predicted flexural MOE and the flexural MOE from the specimen testing is shown in Figure 1. The data shown in Figure 1 was reconstructed from the original study. The r^2 value of the reconstructed data, 0.9271, was slightly higher than the original value of 0.92. In Figure 2, the flexural MOE results from the plywood tests were added to the reconstructed data shown in Figure 1. The additional data raises the r^2 value from 0.9271 to 0.9345. It can be concluded that the model accurately predicted the values of the flexural MOE from the dynamic MOE. Further, the additional plywood data strengthened the cumulative relationship between the predicted and tested values.

The relationship between the predicted MOR and the MOR from the specimen testing is shown in Figure 3. The data shown in Figure 3 was reconstructed from the original study. The r^2 value of the reconstructed data, 0.8865, was slightly higher than the original value of 0.85. In Figure 4, the results from the MOR results from the plywood tests were added to the reconstructed data shown in Figure 3. The additional data raises the r^2 value from 0.8865 to 0.9023. It can be concluded that the model accurately predicted the values of the MOR from the dynamic MOE.

Further, the additional plywood data strengthened the relationship between the predicted and tested values.

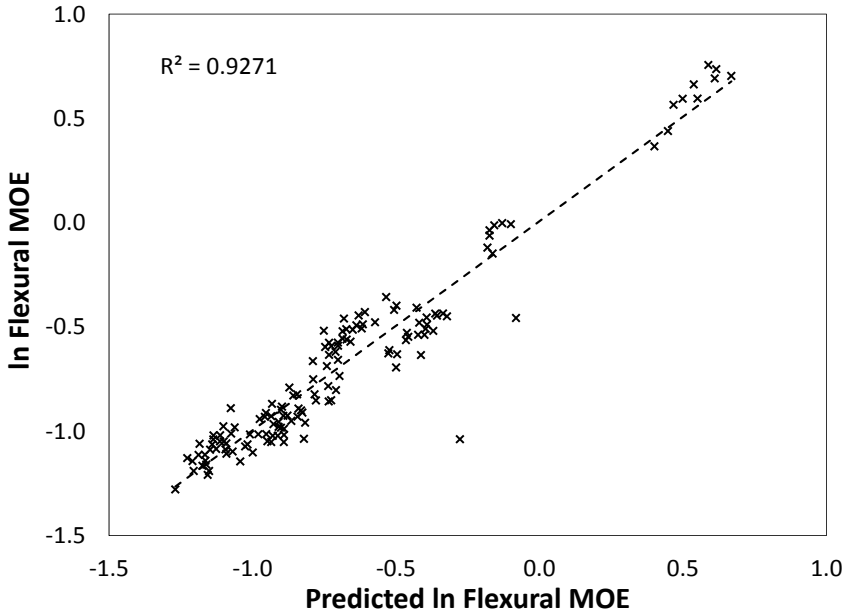

Figure 1—Natural logarithm of the predicted flexural modulus of elasticity (MOE) versus tested flexural MOE. Original data reconstructed from Ross and Pellerin (1988).

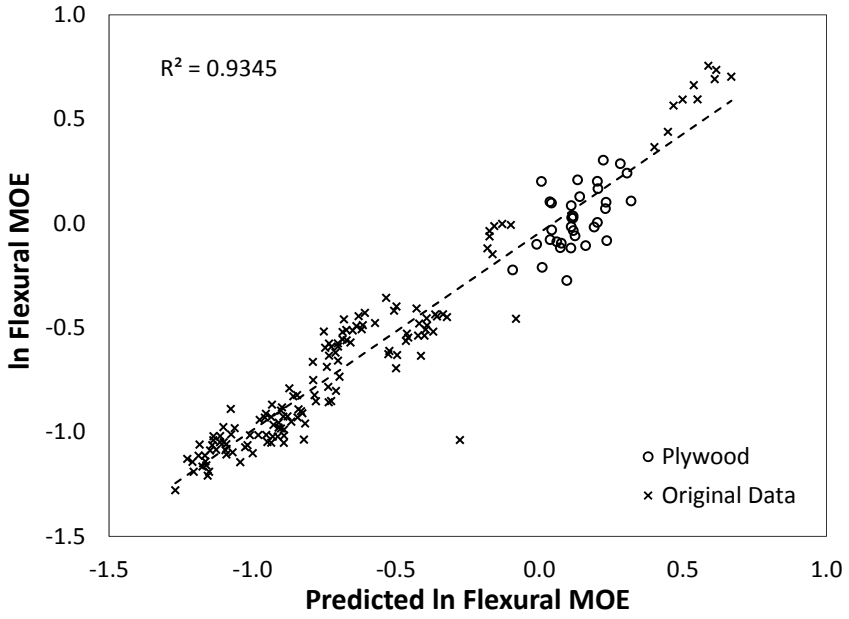

Figure 2—Natural logarithm of the predicted flexural modulus of elasticity (MOE) versus tested flexural MOE for the plywood. specimens. Plywood results are marked with “o”. Original data, marked with “x”, reconstructed from Ross and Pellerin (1988).

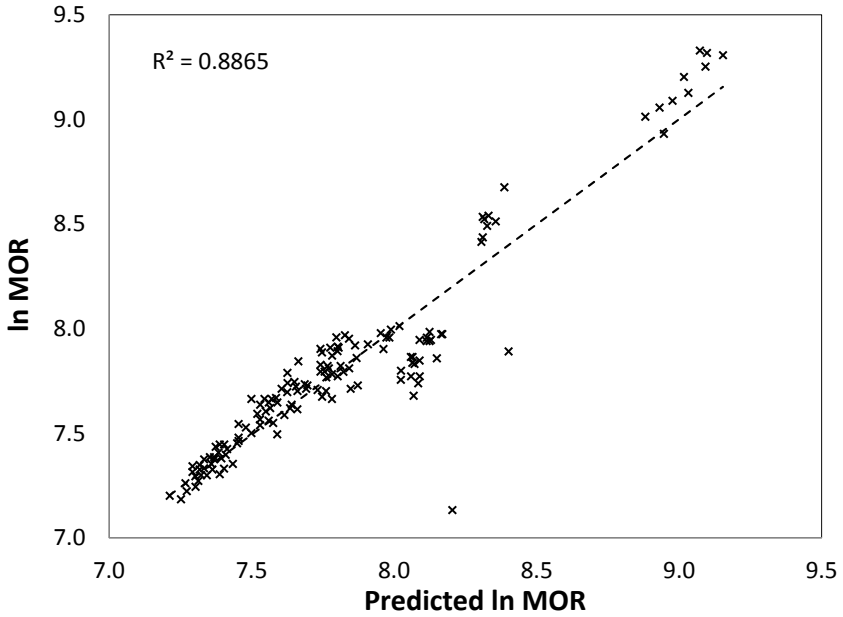

Figure 3—Natural logarithm of the predicted modulus of rupture (MOR) versus tested MOR. Original data reconstructed from Ross and Pellerin (1988).

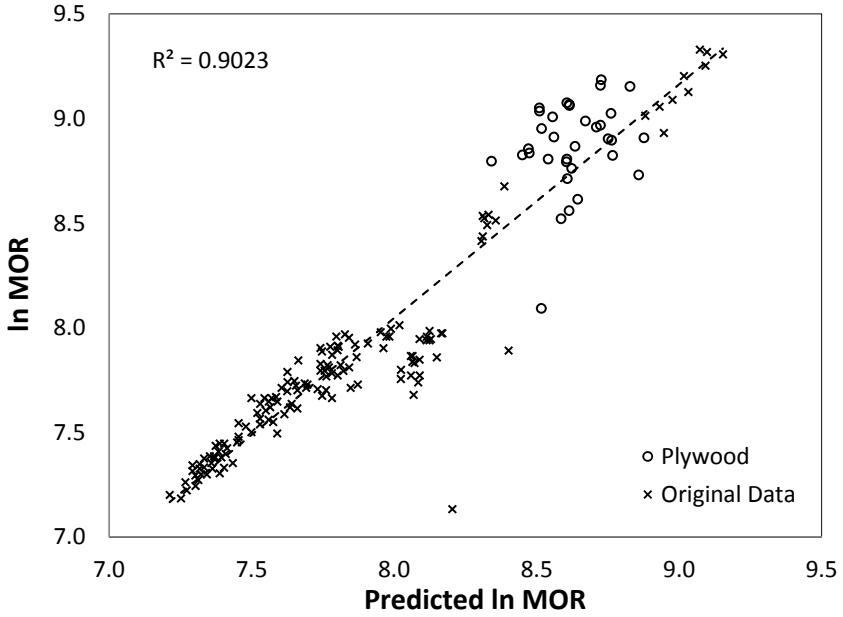

Figure 4—Natural logarithm of the predicted modulus of rupture (MOR) versus tested MOR for the plywood specimens. Plywood results are marked with "o". Original data, marked with "x", reconstructed from Ross and Pellerin (1988).

Conclusions

In this study, a model relating nondestructive parameters to mechanical properties for wood composites was applied to plywood specimens. Plywood was not among the wood composites originally used to develop the model. The nondestructive parameter used as the basis for predicting material properties was the dynamic modulus of elasticity (MOE). From the dynamic

MOE, flexural MOE and modulus of rupture (MOR) were predicted. The data used to create the original model was reconstructed using diagrams from the original report. The coefficients of determination, r^2, of the reconstructed data were slightly higher than those of the original data, but did not exceed the original values by more than 5%. In the predictions of both the flexural MOE and also the MOR, the inclusion of the plywood data caused the r^2 values to increase. The increase indicated that not only did the model accurately predict the mechanical properties of the plywood, but also the inclusion of the plywood to the body of data strengthened the correlation between the predicted values and the mechanical properties.

References

Jayne, B.A. 1959. Vibrational properties of wood as indices of quality. Forest Products Journal. 9(11): 413–416.

Kunesh, R.H. 1978. Using ultrasonic energy to grade veneer. In: Proceedings, 4th Symposium Nondestructive Testing of Wood. Vancouver, WA. pp. 275–278.

Koch, P. and G.E. Woodson. 1968. Laminating butt-jointed, log-run southern pine veneers into long beams of uniform high strength. Forest Products Journal. 18(10):45–51.

Pellerin, R.F.; Morschauser, C.R. 1974. Nondestructive testing of particleboard. In: Proceedings of the Seventh Particleboard Symposium. Washington State University, Pullman, WA. pp. 251–260.

Ross, R.J.; Pellerin, R.F. 1988. NDE of wood-based composites with longitudinal stress waves. Forest Products Journal. 35(5): 39–45.

Senalik, C.A.; Schueneman, G.; Ross, R.J. 2014. Ultrasonic-based nondestructive evaluation methods for wood: a primer and historical review. USDA Forest Service, Forest Products Laboratory, General Technical Report, FPL–GTR–235. 36 p.

Sharp, D.J. 1985. Nondestructive testing techniques for manufacturing LVL and predicting performance. In: Proceedings, 5th Symposium Nondestructive Testing of Wood. Pullman, WA. 99–108.

Szabo, T. 1978. Use of ultrasonics to evaluate or characterize wood composites. In: Proceedings, 4th Symposium Nondestructive Testing of Wood. Vancouver, WA. pp. 239–260.

The impact of grading on the structural performance of tensioned end-joints of nailed laminated timber - NLT

Emanuelle Graça Recco
Master in Architecture and Urbanism – UEL – State University of Londrina, Center for Technology and Urbanism - Rodovia Celso Garcia Cid (Pr445), Km 380 - Campus CEP: 86051-990 - Londrina - Paraná - Brazil Phone 55 43 3326-8551, email: emanuellegracarecco@yahoo.com.br

Jorge Daniel de Melo Moura
Associate Professor Department of Architecture, - UEL – State University of Londrina, Center for Technology and Urbanism - Rodovia Celso Garcia Cid (Pr445), Km 380 - Campus CEP: 86051-990 - Londrina - Paraná – Brazil Fone 55 43 3371-4641, email: jordan@ uel.br

Everaldo Pletz
Associate Professor Departmentof Civil Engineering – UEL – State University of Londrina, Center for Technology and Urbanism - Rodovia Celso Garcia Cid (Pr445), Km 380 - Campus CEP: 86051-990 - Londrina - Paraná - Brazil Fone 55 43 3371-4582, email: pletz@uel.br

Abstract

The most common use of wooden structure in Brazil is the structural frame for roofing. The wood from planted forests, especially southern pine – *Pinus spp*, is as a good alternative, given that it is a sustainable raw material and with great availability in the market. The trussed rafters system using soft lumber and metal plate connectors is widely used on roofs in other countries. This work proposes the development of the trussed rafters system in nailed laminated timber (NLT), using southern pine to enable the utilization of shorter pieces and smaller cross section compared to the traditional system. Before testing the trussed rafters, tensile tests on end joints were made in NLT specimens with dimension timber. The end joints were spaced 20 cm, each joint had 9 nails distributed in 3 rows and 3 columns spaced 5cm. Seven specimens and 03 metal nail types were tested: smooth nail, smooth with folded tip nail and spiraled ardox type nail, totaling 21 specimens. The lumber to the specimens were visual and ultrasound graded. The results were extremely encouraging, and a positive impact of grading in the mechanical performance of the end joint was observed.

Keywords: *Pinus spp*, trussed rafter in NLT (Nailed Laminated Timber), end-joints, grading.

Introduction

Most Brazilian homes have wooden roof from native forests and traditional construction process. There is need for development of new building systems using plantation lumber, in order to spread out their use in structures while adding value to the softwood, which has now great availability in the market.

Studying the sawmill industrial park in Telemaco Borba-PR county, Moura et al. (2012) found that the generation of by-products is associated with three aspects: grading, the presence of blue staining due to fungus and the log shape. Companies grade the boards removing knots, discarding often good-quality small length pieces for use in lower value-added activities such as fire wood for example. Also according to

Moura et al. (2012), from those by-products it is possible to design new components that might require specific cuts and reorient the sawing according to this new product.

The laminated timber consists of timber pieces, obtained from boards connected to one another, with the fibers parallel to the longitudinal axis of the element. This system allows obtaining structural elements with significant variety of shapes and sizes, which most often are limited only by transportation issues (Bono, 1996).

The connections between the wood pieces can be obtained in different ways: nails, screws, adhesives, among others. According to GAVA (2005), regardless of connection type, the laminated wood pieces show high resistance to mechanical stresses. The study of the behavior of these connections is important as it allows to identify their problems and point out solutions to improve load capacity, rigidity and ductility. As a result of these studies, there has been a change and even the creation of new arrangements of joint elements (Duarte, 2004).

In Brazil, the soil and climatic conditions (light and humidity) are highly favorable for the plantation of forests, such as *Pinus spp*, which features high productivity. However, due to this accelerated growth, wood from these forests grow with low density and many knots, making it necessary to carry out grading before being used as a structural component (CARREIRA and DIAS, 2005).

According to VALLE (2011), the architectural design and structure with clear criteria in compliance to standard specifications, the low density *Pinus spp* can be considered a great alternative to the more dense woods.

The visual grading is a process of separating wood pieces in groups of different quality, by analyzing the number and types of defects in the pieces. With the help of grading rules, the growth characteristics (growth rings) are an indication to place the wood into strength classes (CARREIRA, 2003).

The destructive evaluations are in general, the principal methods used to know the physical and mechanical properties of wood. Obtaining the results from this methodology is sometimes costly and time consuming. On the other hand, the non-destructive evaluations allow obtaining more accurate and more comprehensive information by measuring a greater number of samples (STANGERLIN et al., 2008).

According to Gonçalez et al. (2001), the acoustic wave frequency exceeding 20 kHz, is classified as ultrasound waves. The ultra-sound method is based on the analysis of the wave propagation and its relationship between the response to ultrasound and the elastic constants of the wood.

This work aims to study the impact of non-destructive (visual and ultrasound) grading, in the tension performance of nailed end-joints used in NLT to compose trussed rafters to be developed in a second phase of this research

Materials and methods

NLT end-joint arrangement

In order to determine the arrangement of nails between the end joints of the NLT, this work proposed a 20cm minimum distance between joints, about a "carpenter's hand". To minimize the weakness in the tensioned joints and increase security in the trussed rafter, the bars in NLT are composed by a continuous

centerpiece and discontinuous outer layers with staggered joints.

To connect the laminations, nine 18x36 (3,4 mm x 82,8 mm) nails on a grid of 3 x 3 were distributed. They spaced 2 cm from the edge and 5 cm from each other. This arrangement complies with the recommendations of minimum spacing of connections with metal pins specified in NBR 7190 / 97, as shown in Figure 1.

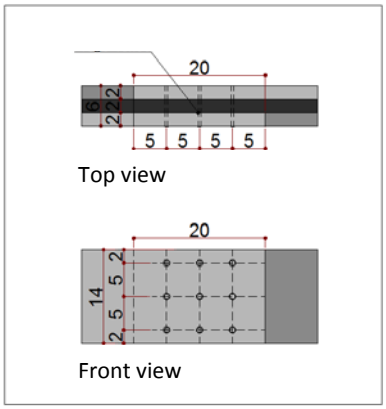

Figure 1 - Arrangement of the NLT end joints.

Once the connection arrangement of the NLT joints was defined, one proceeded to determine the types of nails to be tested. Three variations of nails were tested: smooth nail, smooth folded tip nail and spiral ardox type nail.

Mechanical testing

The test was performed according to the procedures of the NBR 7190-97Annex C in which, for determining the rigidity, the specimen resistance should be estimated ($ft_{0,\,est}$) by a destructive testing of a twin specimen. Once Known the estimated resistance of the sample ($ft_{0,\,est}$), the load was applied in two loading and unloading cycles (10% and 50% of $ft_{0,\,est}$). Linear Variable Differential Transformers (LVDTs) were installed at the time of the test in each side of the specimen for measuring the displacement of the connection.

For the tensile test specimens,an apparatus has been developed whose main objective was to ensure failure in the specimen middle section. The set up of the full-scale specimen was determined taking into account the length required to keep the ends of the link between the end-joints and the place of the apparatus claw, more resistant than the central section between the joints. In addition to the 9 nails between the staggered joints, 12 additional nails were distributed on each side, totaling 33 nails per specimen (Figure 2).

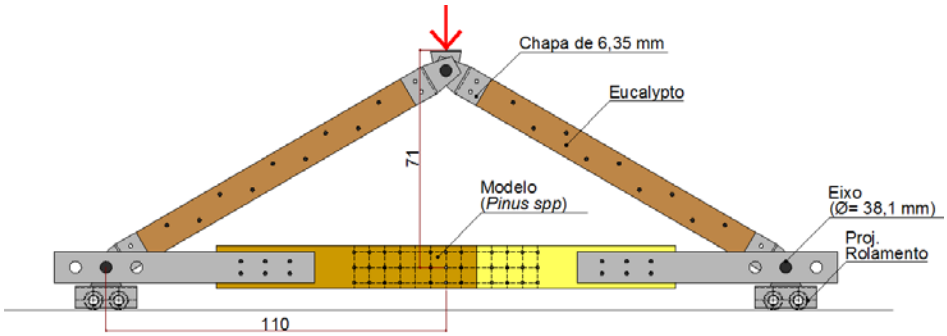

Figure 2 – Test apparatus and specimen for the tension test.

Lumber

The lumber used in this study was dry planks (average humidity equal to 12%) of southern pine-*Pinus spp*, whose average dimensions wer 3000 mm long, 280 mm wide and 40 mm thick.

Grading

On each plank non-destructive testing by ultrasound was carried out in order to obtain the dynamic modulus of elasticity of the lumber. The equipment used was the Agricef USLab with metallic encapsulated transducers operating at frequency of approximately 45 kHz to directly measure the propagation time of the waves in microseconds (μs).

All planks were placed on rectangular Styrofoam bases to avoid direct contact with the concrete countertop. The transducers were applied on the center of each longitudinal edge of the planks in order to obtain the velocity of the wave propagation, through the relationship between the travel time and the distance traveled by the wave. Only one measurement was carried out on each board. The modulus of elasticity (MPa) was obtained by the following equation:

$$E = v^2 * \rho \quad (1)$$

Where: v = wave velocity (m / s) and ρ = wood density (kg / m³).

After the measurements by ultrasound, the planks were split into four boards measuring 3000 mm long, 140 mm wide and 20 mm thick.

The visual grading was according to a visual grading manual (Moura et al., 2012), performed in accordance with the Brazilian standard NBR 11700-90 and the rules of American visual grading of SPIB (Southern Pine Inspection Bureau) and ASTM D245-93.

The pieces were graded by sections along the length of the piece according to the amount, type and location of the defects noted in a spreadsheet, as shown in Table 1. First of all, defects like knots, pitch pockets, galleries, and cracks were observed and then the references were made. When the defect was not limiting for the final performance of the board, it was allowed in the usable section. In some cases, the entire boards had to be discarded due either to excessive natural defects or size and location of these.

Table 1 – Spread sheet used for the visual grading

PIECE 10	**10A**		**10B**		**10C**		**10D**			
Length (mm)	3038		3040		3036		3035			
Thickness (mm)	139,8	140,3	139,9	140,6	140,5	140,0	141,3	140,6	140,6	140,0	139,8	141,0
Width (mm)	20,5	20,0	19,6	21,4	20,5	22,2	19,8	19,5	19,2	21,5	21,7	20,8
Humidity (%)	15		16		16		17			
Number of knots	1		2		3		5			
Growth Rings	6		11		9		7			
Cracks					X		X			
Pitch pockets							X			
Blue stain	<25%		<25%		<50%		<50%			
Vight Knots	X		X		X		X			
CLASSES	**2**		**2**		**3**		**3**			

The dimensions, length (in mm) thickness and width of three sections (in mm), equally spaced along the length of the piece were taken. The growth rings were counted and the natural defects were recorded. The maximum percentage of blue stain was also referenced as well as the number and type of knots. According to the defects, the board was ranked in classes 1 to 3.

Grouping of pieces

The Methodology of the grouping of pieces, was initiated by visual grading, discarding the main defect according to the grading manual. Then the grouping was performed according to classes of modulus of elasticity (MOE) of the pieces determined by means of ultrasound. Itcan be seen in Table 2, that the MOE values are similar for each specimen and there is the same mean variation for the 3 groups of nail types (PA, PB and PC).

Table 2 - MOE values of the pieces in each specimen

GROUPS		MOE piece 650mm (MPa)	MOE piece 650mm (MPa)	MOE piece 850mm (MPa)	MOE piece 850mm (MPa)	MOE piece 1500mm (MPa)	Average MOE (MPa)
PA (smooth nail)	PA 1	7.566,99	7.840,97	7.360,91	7.360,91	7.840,97	7594,147
	PA 2	7.404,63	7.566,99	7.543,33	7.534,31	7.590,16	7527,884
	PA 3	7.022,51	7.004,68	7.018,71	7.022,51	7.014,18	7016,519
	PA 4	8.074,82	8.151,88	7.884,28	7.930,36	8.203,47	8048,962
	PA 5	8.982,73	8.670,86	8.399,01	8.398,57	8.296,13	8549,46
	PA 6	9.285,96	9.143,91	8.732,96	8.450,61	8.660,27	8854,742
PB (smooth folded tip nail)	PB 1	7.796,25	7.886,29	7.543,33	7.456,73	8.931,40	7922,8
	PB 2	7.534,31	7.534,31	7.678,49	7.590,16	7.722,56	7611,963
	PB 3	7.004,68	7.018,71	7.004,68	7.088,83	7.139,48	7051,273
	PB 4	8.104,51	8.151,88	8.074,82	8.134,95	8.104,51	8114,134
	PB 5	8.399,01	8.398,57	8.167,72	7.590,16	8.263,14	8163,72
	PB 6	8.814,20	8.847,27	8.526,78	8.526,78	8.637,53	8670,512
PC (spiral ardox nail)	PC 1	7.884,28	7.884,28	7.758,27	7.886,29	8.053,98	7893,418
	PC 2	7.678,49	7.691,74	7.622,56	7.610,31	7.691,74	7658,968
	PC 3	7.248,04	7.266,77	7.167,85	7.167,85	7.260,61	7222,225
	PC 4	7.930,36	7.905,47	7.905,47	7.941,22	8.016,85	7939,874
	PC 5	8.203,47	8.263,14	8.104,51	8.134,95	8.388,09	8218,833
	PC 6	8.814,20	9.016,59	8.580,33	8.448,86	8.661,40	8704,274

The boards to compose each specimen after screening were organized into groups and cut to the required lengths being: two 650 mm long pieces, two 850 mm long pieces and one continuous central 150 0mm long piece (Figure 3).

Figure 3 - Cut pieces and grouped according to the MOE.

The nailing was performed with pre-drilling according to NBR 7190/97, which specifies for softwood a minimum diameter of 0.85 d_{ef}, (d_{ef} being the effective diameter of the nail to be used in millimeters). To this procedure, a template was developed in order to ease up the process (Figure 4).

Figure 4. - Template, pre-drilling and specimen nailing.

Results and discussion

For each test, load-deformation diagrams were drawn and the strength and stiffness of the end joint were recorded according to the NBR 7190/97 specifications. Once found the joint overall resistance, the resistance per nail for each cutting section was calculated as shown in Table 3. As expected, the smooth nail joints presentedthe smaller load capacity. The joints with folded tip nails presented a better record which can be attributed to the fact that the folded tip presented an additional anchoring against withdrawal. The best results were observed to the joints with spiral ardox type nail that were supposed to have greater adherence to the involving wood matrix.

As for the stiffness of the joints in the elastic range, it was also observed that the smooth nails produced more deformable joints than the other two types of nails. Nevertheless, they all showed ductility, a very important feature for connections to become more predictable and safe. The folded-tip nails behave as a bi-pinned beam at their ends, and as relative displacements increase, a extensional stiffness (rope effect according to Eurocode 5) appears, that increases the flexural rigidity. This made these folded-tip nail joints out performed ardox nail joints with regard to stiffness.

Also noteworthy was the variability of the failure results. The strength results showed greater variability than the stiffness ones during the elastic range. As shown above, the boards to the composition of the specimenswere grouped according to the dynamic MOE, which takes into account global aspects of the lumber.When submitted to tensile stress, the defects (local aspects of wood), influence more the strength than the stiffness.

In a comparative analysis of the three groupsin the early stages, smooth nails results demonstrated greater variability than the other two types of nails. In the initial phase, the nails presented low deformability, and therefore, the rigidity of the joints was less dependent on the heterogeneity of the timber. In the final stages as the load becomes critical, the rupture occurs in the sections containing knots.

Table 3 - stiffness and resistance per nail.

SAMPLES		Stiffness of the joints 200 mm (kN/cm)	Resist. per nail for each cutting section (kN)		Stiffness of the joints 200 mm (kN/cm)	Resist. per nail for each cutting section (kN)		Stiffness of the joints 200 mm (kN/cm)	Resist. per nail for each cutting section (kN)
1		167	1,94		235	2,04		153	1,94
2		169	1,89		190	2,80		175	2,15
3	**PA**	(*)	(*)	**PB**	210	1,55	**PC**	190	1,94
4		118	0,97		195	1,29		163	1,51
5		105	0,75		175	1,68		157	1,29
6		101	0,97		249	1,03		193	2,47
Average		132	1,30		209	1,73		172	1,88
Standard Deviation		33	0,57		28	0,62		17	0,43
Coefficient of variation		25%	43%		13%	36%		10%	23%

(*) The values for the PA 3 model were not considered due to problems that occurred at the time of the test.

Thanks to the grading and grouping of pieces according to the mechanical properties, a great similarity regarding the failure mode of the joints was observed. Initially, a large relative displacement was recorded, and as the nails bent and plasticized, the central lamination eventually failed. In the rupture, the displacement of the joints corresponded to deformations, ranging between 4% and 5%, extremely high values when compared to the deformation corresponding to the calculated resistance.

The rupture occurred in the joint, except in one of the specimens. The failure of central lamination was always accompanied by the presence of excessive deformation and rotation of the nails. There was one case of rupture caused by longitudinal shear in the wood, the joint line, and particularly the sinking of the nail heads in the wood, especially in the case of the folded-tip nails, (Figure 5).

Figure 5 – Failed specimens

Final considerations

The results show that in NLT it is necessary to ensure a minimum spacing between consecutive end joints of two-bladed components, determined from the level of the applied stresses. The experimental tests showed that the 3 types of nailed connections are different and therefore require specific mathematical models unlike the only approach specified in the NBR 7190/97.

Joints with smooth nail showed the worst performance of both resistance and rigidity. Joints with folded-tip nails showed the best results of rigidity, while joints with ardox nail reached the best results with respect to resistance. These last two end joint types presented performances close to each other.

The end joints studied had the necessary ductility and showed that the ardox type nail was the best one, with respect to both stiffness and failure. This nail is the one chose in the making of the trussed rafters to be tested in the next phase of this research.

The grading has enabled the lumber selection and grouping of pieces with similar MOE ensuring a safer comparative analysis among the types of nails to be appliedin end-joints of NLT. The methodology which takes into account global aspects of wood, proved to be efficient to predict stiffness with low variability of results. Concerning failure, the variability of the results was higher because local defects are more important than the overall stiffness of the piece.

The study highlights the importance of woodgrading to different purposes. In this case, it allowed the comparison of different types of nailed end-joints. The visual grading enabled the selective disposal of defects that would impair the performance of the joint, and NDT grading allowed the determination of the MOE for later assembly and production of the specimens. Being the ultrasound a very easy-to-apply and low cost method, it turns out to be a powerful tool to help building wooden structures safer and quicker. In this case, helped to enable to add value to small-length discarded lumber pieces to be used in NLT.

References

BONO, C, T. **Madeira laminada colada na arquitetura: sistematização de obras executadas no Brasil.** Departamento de arquitetura-EESC/USP, 1996. 365p. (Dissertação de mestrado).

CARREIRA, M. R.; DIAS, A. A. **Classificação visual de coníferas: análise da aplicação do método norte-americano às espécies de *Pinus spp.*** plantadas no Brasil. **ScientiaForestalis**, n.67, p.78-87, 2005.

DUARTE, R. S.: **Avaliação do Comportamento de Ligações com Parafusos Auto-Atarraxantes em Vigas de MLC** C. Dissertação de mestrado. Universidade Federal de Minas Gerais, Belo Horizonte, 248p, 2004. Orientador Prof. Dr. Edgar Vladimiro Mantilla Carrasco

GAVA, M. (2005). **"Viabilidade técnica e econômica da prodeção de componentes para habitação social utilizando madeira serrada de pinus de terceira classe de qualidade".** Dissertação (Mestrado em Arquitetura e Urbanismo), Programa de Pós-graduação em Arquitetura e Urbanismo da Escola de Engenharia de São Carlos, Universidade de São Paulo. São Carlos, SP.

GONÇALEZ, J.C.; VALLE, A.T.; COSTA, A.F. Estimativas das constantes elásticas da madeira por meio de ondas ultra-sonoras (ultra-som). Cerne, Lavras, v.7, n.2, p.81-92, 2001

MOURA, J. D. M.; PLETZ, E; RECCO, E. G. **Qualidade e processo produtivo da madeira para utilização em mobiliário**. Londrina, 2012.

MOURA, J.D.M.; PLETZ, E.; STRASS, M. C. **Panorama Geral e Perspectivas Preliminares de Continuidade dos Trabalhos em Relação às Visitas Técnicas Realizadas a Indústria do Setor Madeireiro do Parque Industrial de Telêmaco Borba a Convite da Secretaria Municipal do Trabalho e Industria Convencional.** 2012, Universidade Estadual de Londrina, Relatório Interno.

STANGERLIN, D. M.; CALEGARI, L.; SANTINI, E. J.; DOMINGUES, J. M. X.; GATTO, D. A.; MELO, R. R. Determinação do módulo de elasticidade em madeiras por meio de métodos destrutivo e não destrutivo. RevistaBrasileira de CiênciasAgrárias, v.3, n.2 p. 145-150, 2008.

Session 7

Standing Timber Assessment

Acoustic Evaluation of Thinning and Biosolid Fertilization Effects on Wood Quality of a Douglas-fir Stand

Xiping Wang*
USDA Forest Service, Forest Products Laboratory, Madison, WI 53726-2398, USA

Robert J Ross
USDA Forest Service, Forest Products Laboratory, Madison, WI 53726-2398, USA

Steve Verrill
USDA Forest Service, Forest Products Laboratory, Madison, WI 53726-2398, USA

Eini Lowell
USDA Forest Service Pacific Northwest Research Station, Portland, OR 97204, USA

Jamie Barbour
USDA Forest Service Pacific Northwest Research Station, Portland, OR 97204, USA

* Corresponding author. (1) 608-231-9461, xwang@fs.fed.us

Abstract

In this study, we examined the potential of using a time-of-flight (TOF) acoustic wave method to evaluate thinning and biosolid fertilization effects on acoustic velocity of trees and modulus of elasticity (MOE) of structural lumber in a 76-year-old Douglas-fir (*Pseudotsuga menziesii*, (Mirb., Franco)) experimental stand. The stand consisted of four treatments: control, thinned, biosolid fertilized, and a combined thinned and fertilized treatment, each with three replicates on 0.08 hectare plots. Four trees were selected in each plot using a stratified random sample based on the plot quadratic mean diameter, resulting in a total sample of 48 trees ranging from 14.2- to 53.3-cm diameter at breast height (DBH). The sample trees were first nondestructively tested using a TOF-based acoustic measurement system to obtain acoustic velocity in trees. The sampled trees were then harvested, bucked into merchantable-length stems and then mill-length logs that were sawn into lumber. Acoustic velocities of stems and logs and MOE of lumber were subsequently obtained. Our results indicated that biosolid fertilization had a statistically significant effect on acoustic velocities of trees, stems, and butt logs; thinning did not have a statistically significant effect on acoustic velocities; combining thinning with biosolids did not produce a change in acoustic velocity different from applying biosolids alone. These findings are consistent with the treatment effects that were reported on interannual ring specific gravity. At tree level, treatment had no significant effect on lumber stiffness.

Keywords: Acoustic velocity, biosolids, lumber, logs, trees, modulus of elasticity, thinning

Introduction

In-forest assessment of wood quality in individual trees and forest stands is important to both forest management decision-makers and forest operations. As world wood markets are becoming increasingly

competitive and complex, forest companies are under economic pressure to control cost, sort and allocate forest materials to the most appropriate markets, and maximize the value of the forest at the time of harvest (Wang et al. 2007a, Amishev and Murphy 2008). Although forestry has many widely accepted field tools, sampling procedures, and models for gathering and summarizing data and making projections of growth, yield, and tree size, counterparts for wood quality assessment have lagged far behind (Briggs et al. 2008). One of the reasons for this lag has been a lack of simple field tools permitting rapid collection of wood quality data from trees in a stand or sample plot.

Historically, trees and stands have been selected for harvest based on visual assessment of tree quality (diameter, height, straightness, taper, frequency and size of tree branches, observable defects, etc.) and stand characteristics (age, species composition, habitat type, presence of insects and diseases, and silvicultural objectives). These procedures do not incorporate estimates of any intrinsic wood properties and thus do not adequately assess the potential quality of the end products that might be manufactured from the trees. With the development and rapid growth of new engineered wood products such as laminated veneer lumber (LVL), I-joists, and cross laminated timber (CLT), there has been a parallel growth in non-destructive assessment of the stiffness of raw wood materials that go into these products. In addition, concerns with design values of structural lumber graded with visual methods are creating demand for stiffness verification of visually graded structural lumber. These trends have renewed the interest of forest companies in field non-destructive testing tools that can be used for in-forest assessment of wood quality in terms of stiffness. Mills seeking to capture a price premium by producing high-valued engineered products find that it is very expensive to process logs or purchase timber stands that have low yields of products with the stiffness and strength levels desired by their customers.

In recent years, research has been conducted to examine the concept of using acoustic wave propagation methods to evaluate standing trees and forest stands for general wood quality and intrinsic wood properties (Wang 1999, Harris and Andrews 1999, Huang 2000, Addis et al. 2000, Lindstrom et al. 2002, Wang et al. 2001, 2007b). The research has led to the development and commercialization of a series of acoustic tools that allow rapid assessment of wood resource quality at early stages of the forest operational value chain (Harris et al. 2002, Carter et al. 2005, Huang 2005, Wang et al. 2006, 2008, Divos 2010, Carter 2011). One particular technique, which uses the time-of-flight (TOF) method to measure longitudinal acoustic velocity near the base of standing trees, provides a means for silviculturists, forest managers, and planners to be able to predict the stiffness potential of stands prior to harvest and to assist in valuation, stumpage purchase, and harvest scheduling decisions (Briggs et al. 2008).

Although many studies have investigated the relationships between tree and log acoustic velocity and between tree/log velocity and wood stiffness of small clear wood and lumber or veneer for a variety of species (Wang et al. 2001, 2007b, Grabianowski et al. 2006, Chauhan and Walker 2006, Amishev and Murphy 2008, Mora et al. 2009, Achim et al. 2011), less is known about how silvicultural practices affect acoustic velocity of trees in a stand, information that is important to managers wishing to make informed decisions to enhance stiffness and value of plantations (Briggs et al. 2008, Raymond et al. 2008, Lowell et al. 2014). In 1998, a Douglas-fir (*Pseudotsuga menziesii* (Mirb.) Franco) stand, experimentally thinned and treated with bio-solids fertilization at age 55 in 1977, was scheduled for harvesting and provided an opportunity to evaluate the effects of these treatments on tree acoustic velocity and lumber quality. This study was initiated in conjunction with the mill recovery study conducted by the USDA Forest Service Pacific Northwest Research Station.

The specific objective of this study was to test the following hypothesis concerning the effects of thinning and biosolids treatments in the Douglas-fir stand: treatments caused no differences in 1) tree acoustic velocity; 2) log acoustic velocity, and 3) modulus of elasticity (MOE) of the dimensional lumber produced from the stand. The goal of our data analysis was to determine if acoustic velocity measured on trees and logs can be used to assess treatment effects.

Experimental Procedures

The study site was located on the University of Washington's Charles Lathrop Pack Experimental Forest near Eatonville, WA (Figure 1). The Douglas-fir stand naturally regenerated following a severe fire in 1922. When the study was established in 1977, the stand was estimated to be 55 years old and was heavily stocked with approximately 1977 trees/ha with about 75% under 18 cm in diameter at breast height (DBH) (Edmonds and Cole 1980, Sonne et al. 2004). During 1977, half of the stand was commercially thinned, which reduced density to about 250 trees per acre. Six 0.2-ac plots were randomly located in each of the thinned and unthinned portions of the stand. In the winter of 1977–1978, three plots in the thinned and unthinned areas were randomly selected and treated with 104.3 tons/ha of dewatered sewage (18% solids) depositing a 2.54 cm depth of biosolids (hereafter, fertilization with dewatered sewage application is referred to as biosolids treatment). Retreatment with 51.9 tons/ha occurred in 1980 and 1989, and the thinned area received a second commercial thinning in 1995. The site was scheduled for final harvest in 1998, providing the opportunity to evaluate the effects of the sequence of treatments on wood quality from various aspects, including 1) log and lumber visual grade and value (Sonne et al. 2004); 2) interannual ring specific gravity (Kantavichai et al. 2010); and 3) tree acoustic velocity and lumber stiffness (this study). Table 1 summarizes initial and final stand characteristics.

Table 1—Initial and final stand conditions

Treatment	Quad. mean DBH (cm)		Total height (m)		Trees/ac	
	1977	1998	1977	1998	1977	1978
Control	16.7	23.4	26.2	33.8	842	551
Biosolids	16.9	27.0	24.4	33.5	702	388
Thin	21.4	31.0	24.4	31.4	262	158
Thin/biosolids	22.0	35.4	24.1	32.9	250	120

Figure 1—Douglas-fir experimental stand located in Eatonville, Washington.

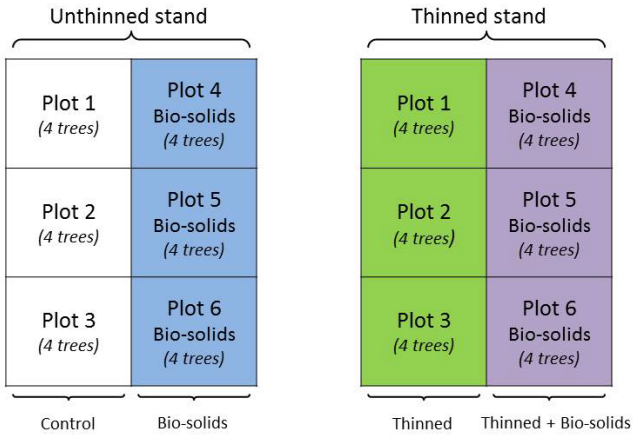

Figure 2—Experimental plots selected for the study.

In 1998, four trees in each plot (48 trees in total) were selected for field acoustic measurements. The tree samples were selected using a stratified random sample based on the plot quadratic mean diameter. Figure 2 shows the schematic of the experimental plots and tree samples selected for this study. We conducted acoustic measurements near the base of 48 sample trees using a prototype TOF measurement system. The setup consisted of two accelerometers, two spikes, a hand-held hammer, and a portable Fluke 97 50 MHz Scopemeter (Fluke UL Ltd, Norfolk, UK). Two spikes were inserted into the tree trunk at about a 45 degree angle to the trunk surface, one spike at each end of the section to be assessed. Accelerometers were mounted on the spikes using two specially designed clamps (Wang et al. 2001). An acoustic wave was introduced into the tree in longitudinal direction by impacting the lower spike with the hand-held hammer. The resulting signals were received by start and stop accelerometers and recorded on the Scopemeter. The TOF was determined by locating the two leading edges of the waveforms displayed. Acoustic velocity was then calculated by dividing the test span by the measured TOF (average of three readings). A span of 1.22 m was found to produce consistent readings and rapid measurements. Therefore, this span was used for all tree testing.

Following field acoustic measurements, the 48 sample trees were harvested, cut into merchantable length stems with a small end diameter of 15.2 cm, and then bucked into 171 mill-length logs (4.88 m). All stems and mill-length logs were acoustically tested using a resonance acoustic method to obtain acoustic velocity values for the stems and logs.

The logs were subsequently sawn into lumber with a portable WoodMizer™ sawmill. Sawing was limited to producing a 20.3-cm maximum width board and the majority of the lumber was 5.1 cm thick. Less than 10% of the volume was 2.5-cm thick jacket boards. Each piece of lumber was given a number that could be traced to the original log, tree, and treatment. The lumber was kiln dried, planed on four sides, and then E-rated using the E-computer (Metriguard Inc., Pullman, Washington), a transverse vibration testing equipment. The modulus of elasticity (MOE) of each piece of lumber was determined by the following equation:

$$MOE = \frac{f_r^2 W L^3}{2.46 I g}$$

Where
f_r —resonant frequency (Hz);
W—lumber weight (kg);
L—lumber span (m);
I—moment of inertia (m^4);
g—acceleration due to gravity (9.8 m/s^2).

Data Analysis

This study produced an interrelated acoustic data set from a stratified Douglas-fir tree sample across differing silvicultural treatments: 1) Acoustic velocity of 48 sample trees (12 trees per treatment × 4 treatments); 2) Acoustic velocity of 48 merchantable stems; 3) Acoustic velocity of 48 butt logs; and 4) Acoustic velocity of 171 mill-length logs obtained from 48 sample trees. All lumber pieces that could be sawn from the parent trees were assessed for stiffness. The lumber MOE data was then collated at the tree level to calculate volume-weighted mean lumber MOE.

Simple linear regression analyses were first conducted to examine the relationships between the tree velocity and stem/butt log velocities and between tree velocity and tree DBH. Statistical comparison analyses were used to examine the effect of treatment variables on wood quality in terms of acoustic

velocity and lumber MOE. A linear mixed effects model was fit to the data. Experimental plots were treated as random effects. Thinning, biosolids, and the thinning/biosolids interaction were treated as fixed effects. Plot statistics (for example, median, minimum, maximum) are presented graphically in box plots to show the effects of treatments on the acoustic velocities measured in trees, merchantable stems and butt logs, and the lumber MOE.

Results and Discussion

Acoustic velocities measured in trees, stems, and butt logs

Table 2 tabulates the statistics of acoustic velocities measured in trees, full-length stems, and butt logs. Distributions of acoustic velocities are shown in Figure 3. The velocity ranged from 3225 to 4763 m/s for standing trees, 3275 to 4416 m/s for stems, and 3805 to 4565 m/s for butt logs. Tree velocity had higher values than the stem and butt log velocities. This is consistent with what has been found in other studies (Wang 2013).

Figure 4 presents the plot of individual tree velocity versus tree DBH. One data point that had the lowest tree velocity (3225 m/s) was identified as a possible outlier. This tree had the largest DBH (53.3 cm) and thickest bark (4–5 cm) among all sample trees and was the first tree tested in the field. Based on the large velocity discrepancy observed for this tree and the recollection of the testing situation, we suspect that when this tree was tested, the sensor probes were likely not inserted into the trunk deeply enough to fully penetrate the bark and thus affected the TOF measurements (prolonged acoustic wave travel time and thus resulted in a low tree velocity). This technical issue was not recognized at the time of field testing and thus was left uncorrected. We decided not to include this data point in our analyses.

Overall, there is a general trend of decreasing tree velocity with tree DBH at tree level. The lower tree velocity with increased DBH seems associated with the higher growth rate in trees, which adversely affects specific gravity and stiffness of wood. It is also evident that there was a large variation in tree velocity for trees within the same diameter class. This may well reflect the natural variation among individual trees as well as the effects of prescribed treatments.

The accuracy and reliability of TOF measurements on standing trees are typically evaluated through a direct comparison with the corresponding log resonance measurements. Figure 5 shows the linear relationships between measured tree velocity and the corresponding stem/butt log velocities. The coefficient of determination (R^2) was 0.33 and 0.48 when the tree velocity was regressed against the butt log velocity and stem velocity, respectively. The strength of this relationship is moderate, but weaker than those obtained from Sitka spruce (*Picea sitchensis* (Bong.) Carr.) and western hemlock (*Tsuga heterophylla* (Raf.) Sarg.) (R^2 = 0.85-0.93, Wang et al. 2008), Douglas-fir (R^2 = 0.65, Briggs et al. 2008), radiata pine (*Pinus radiata* D. Don) (R^2=0.89, Chauhan and Walker 2006), and Loblolly pine (*Pinus taeda* L.) (R^2 = 0.81, Mora et al. 2009). Two possible causes could contribute to this lower correlation: 1) this was the first time that our TOF prototype measurement system with a manually operated Fluke ScopeMeter was used in field application (1998). Determination of TOF was based on the cursor measurement of the time arrivals of both impact and receiving signals. One of the goals of this field trial was to test the TOF measurement system and determine the applicability of the TOF approach in standing trees. The user had not yet developed operating experience with the system so the TOF data might be more variable. 2) The Douglas-fir sample trees tested in this study were in a 76-year-old mature stand, much older than the trees tested in the studies referenced above. Mature Douglas-fir trees have relatively thicker bark, which might have caused some measurement errors when the sensor probes were not inserted into the trunk deeply enough.

Treatment effects on acoustic velocity of trees, stems, and butt logs

Figure 6 provides boxplots of acoustic velocity of standing trees, stems, and butt logs versus treatment variables. The dark horizontal lines are the median values. Biosolid treatment was found to have a statistically significant effect on acoustic velocities measured in standing trees (p-value = 0.0243), stems (p-value = 0.0041), and butt logs (p-value = 0.0024). The effect on mean velocity for the plots that received biosolid treatment was –138 m/s from a base of 4400 m/s in standing trees, –192 m/s from a base of 4014 m/s in stems, and –156 m/s from a base of 4360 m/s in the butt logs. This finding is in agreement with the SG responses following the treatment (Kantavichai et al. 2010). In a parallel study of the same experimental plots, Kantavichai et al. (2010) examined the effect of thinning and biosolid fertilization on interannual ring specific gravity of the sample trees and found that biosolids significantly decreased SG, which is consistent with other studies involving application of fertilizer (Cahill and Briggs 1992) or biosolids (Briggs et al. 1986). Specific gravity averaged 0.517 over 1978–1989 without biosolids treatment and was reduced to 0.466 by biosolids. The significant decrease in SG explains the decreased acoustic velocity associated with biosolids treatment.

Table 2—Acoustic velocity measured in sample trees, merchantable stems, and butt logs

Treatment	DBH (cm)		Tree velocity (m/s)		Stem velocity (m/s)		Butt log velocity (m/s)	
	Mean	Stdev.	Mean	Stdev.	Mean	Stdev.	Mean	Stdev.
Control	29.0	11.49	4401	174.4	4061	216.0	4300	148.1
Biosolids	30.9	10.03	4232	215.9	3788	297.4	4162	149.0
Thin	32.9	6.43	4399	231.0	3977	141.7	4323	117.9
Thin/biosolids	37.5	8.65	4158	354.7	3780	180.4	4121	180.4

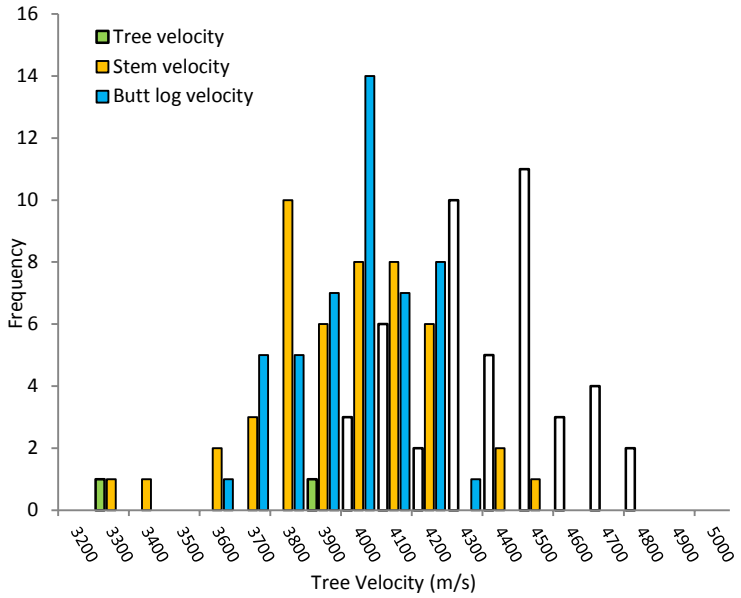

Figure 3—Histograms of acoustic velocities measured on Douglas-fir sample trees and the merchantable stems and butt logs obtained from the sample trees.

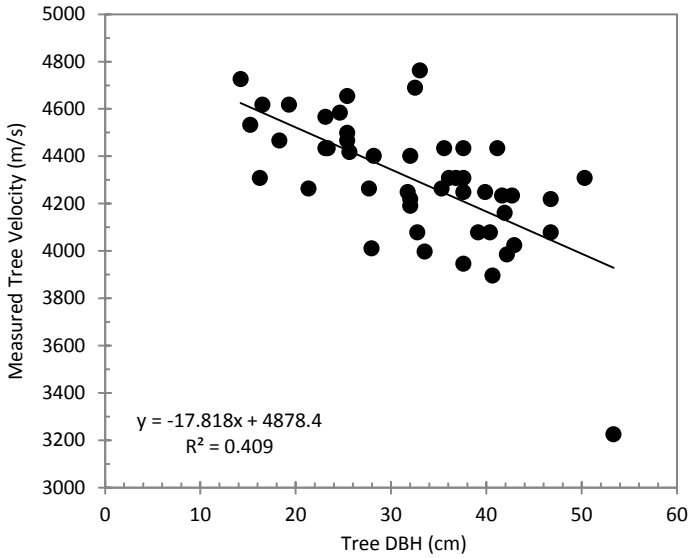

Figure 4—Relationship between tree velocity and tree DBH for the Douglas-fir sample trees.

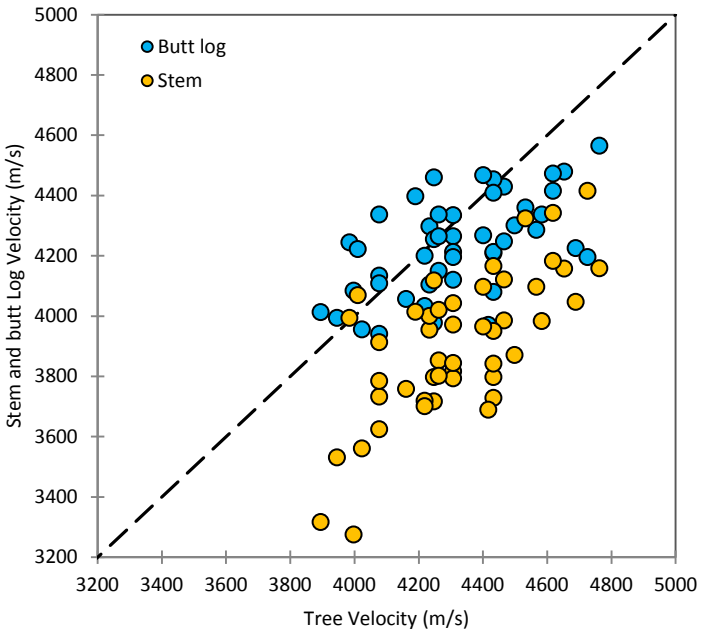

Figure 5—Relationships between tree velocity and stem/butt log velocity for the Douglas-fir sample trees.

Thinning treatment, on the other hand, did not have a statistically significant effect on acoustic velocities measured in standing trees (*p*-value = 0.7271), stems (*p*-value = 0.6065), and butt logs (*p*-value = 0.7280). The mean acoustic velocity only dropped 46 m/s in standing trees, 36 m/s in stems, and 69 m/s in butt logs from the base velocities of the control plots. This finding is different from those reported in some previous research. Wang et al. (2001) observed a decrease in tree velocity in young-growth Sitka spruce and western hemlock stands that had received medium and heavy thinning treatments. Briggs et al. (2008) reported lower acoustic velocity with increased DBH associated with the thinning in the 45- and 51-year-

old Douglas-fir installations. In contrast, Carter et al. (2005) found that thinning increased acoustic velocity in a stand with a late season moisture deficit. Briggs et al. (2008) reported that two young Douglas-fir installations (32- and 36-years old) exhibited increasing acoustic velocity with decreasing stand density and with increasing DBH. Differences in species, site conditions, and types of thinning produced seemingly contradictory thinning effects.

With respect to the immediate effect of thinning, we would expect that a thinning that removes smaller DBH trees from plots is removing the trees with higher SGs and thus higher acoustic velocities so that the mean acoustic velocity of the residual plots will likely be immediately lowered. However, for the plots under consideration in the current study, Kantavichai et al. (2010) found that thinning increased latewood width but did not change latewood percentage, earlywood SG or latewood SG, and the overall effect on SG was found not statistically significant. This could help explain why there was no significant change in acoustic velocity associated with thinning in this study. The temperature and precipitation data over the 1978–1989 response analysis period suggest that the Douglas-fir experiment stand at the Charles Lathrop Pack Forest may experience soil moisture deficit (SMD) in the summer (Kantavichai et al. 2010). Some studies report that water stress reduces growth and promotes latewood formation, which increases SG (Brix 1972, Cregg et al. 1988). However, extreme summer water stress can stop growth and production of latewood, reduce latewood percentage, and reduce SG (Bowyer et al. 2007). This effect was considered to be the situation on the drought-prone site of this study (Kantavichai et al. 2010).

Same as the SG response reported by Kantavichai et al. (2010), combining thinning with biosolids did not produce a change in acoustic velocity different from the change caused by applying biosolids alone. In contrast, others (Briggs et al. 1986, Cahill and Briggs 1992) report that combining thinning with fertilization or biosolids lowered SG more than either treatment alone. Larson et al. (2001) noted that the response of SG to treatments is likely to be site-specific, depending on the local soil, temperature, and precipitation conditions. We would also expect this dependence to apply to the acoustic velocity of trees.

Treatment effect on mean lumber MOE

Figure 7 shows a boxplot of volume-weighted mean lumber MOE versus treatment variables. The dark horizontal lines are the median values. We did not find a statistically significant effect of treatment on mean lumber MOE (p-value = 0.6614). The volume weighted mean lumber MOEs were 15.5, 15.3, 16.1, and 14.9 GPa for the control, biosolids, thinning, and thinning and biosolid treatments respectively. This indicates that there was no significant reduction in stiffness due to the prescribed treatments.

The mean lumber MOE at tree level was derived from MOE measurements of all possible pieces of lumber that could be produced from each tree, and then aggregated at the tree level. There was considerable quantities of wood that went to chips during the lumber conversion process. The lumber recovery rate is affected by log diameter, log taper, and the sawing techniques used. In addition, all lumber was processed and dried. Lumber MOE was measured at kiln-dried condition (moisture content less than 19%); In contrast, the acoustic velocity measured on a standing tree, stem, and butt log reflects the global stiffness of the tree/stem/butt log in green condition. A significant discrepancy between these two different measures is expected. This is evidenced by the low correlation between mean lumber MOE and acoustic velocities of the sample trees (r = 0.074, p-value = 0.6210), stems (r = 0.159, p-value = 0.2868), and butt logs (r = 0.387, p-value = 0.0072).

By treatment, the plots that received both the thinning and biosolids treatment had the lowest mean lumber MOE (14.9 GPa). This agrees with what we observed in acoustic variables (tree velocity, stem velocity, and butt log velocity) in Figure 6. The plots that received only the thinning treatment exhibited higher lumber MOE than the plots that received the biosolid or combined treatments, which is also

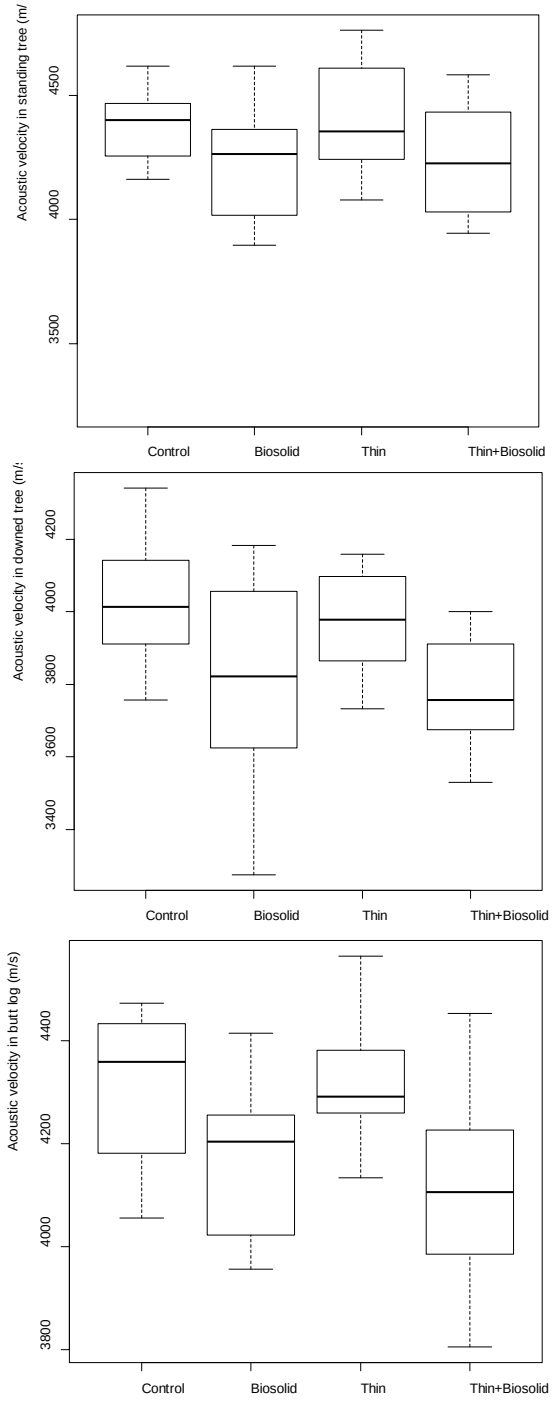

Figure 6—Effect of treatments on tree, stem, and butt log velocities.

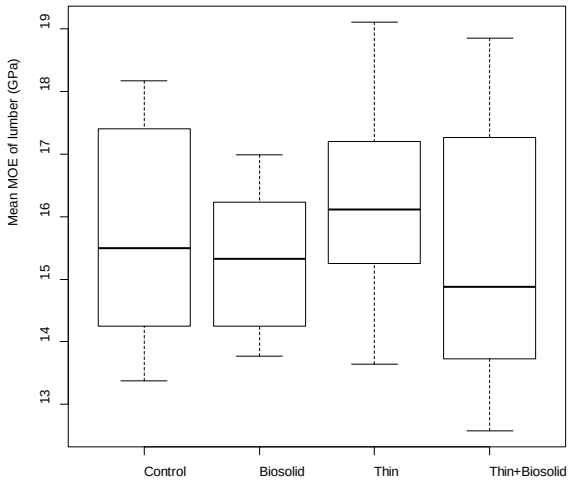

Figure 7—Effect of treatments on lumber MOE.

Table 3—Ranking of treatment based on mean acoustic velocity and mean lumber MOE

Property	High → Low			
Tree velocity	Control	Thin	Biosolid*	Thin + Biosolid*
Stem velocity	Control	Thin	Biosolid*	Thin + Biosolid*
Butt log velocity	Control	Thin	Biosolid*	Thin + Biosolid*
Lumber MOE	Thin	Control	Biosolid	Thin + Biosolid

* Significant at 5% level.

consistent with what we observed in acoustic variables. When the plots are ranked by mean acoustic velocity and mean lumber MOE, we noticed that the rank orders by mean acoustic velocities are consistent for the tree velocity, stem velocity, and butt log velocity; and the rank order by mean lumber MOE is generally consistent with that by acoustic velocity, except for the control and thinning plots (Table 3).

Conclusions

The effects of thinning and biosolid fertilization treatments on wood quality in a 76-year-old Douglas-fir stand were evaluated using a time-of-flight acoustic wave method. Field acoustic testing produced an interrelated acoustic data set from a stratified tree sample across control, thinned, biosolid fertilized, and combined treatments. Lumber stiffness data was collated to derive weighted mean lumber MOE at tree level. Analysis of the results indicated the following:

1. There was a general trend of decreasing tree velocity with increasing tree DBH across all experiment plots. There was a large variation in tree velocity for trees within the same diameter class, underlining the property variation among individual trees.
2. Biosolid fertilization treatment had a statistically significant effect on acoustic velocities measured in standing trees, stems, and butt logs; thinning did not have a statistically significant effect on acoustic velocities; the combined thinning with biosolids treatment could not be statistically distinguished from the biosolids treatment. These findings are consistent with the treatment effects on interannual ring specific gravity reported for the same sample of trees.
3. The thinning, biosolids, and combined treatments had no statistically significant effects on the mean lumber stiffness of a tree.

Acknowledgements

This project was initiated in conjunction with the mill recovery study conducted by the USDA Forest Service Pacific Northwest Research Station. The Stand Management Cooperative set up and maintained the experiment at the University of Washington College of Forest Resources Charles Lathrop Pack Forest, Eatonville, Washington, which provided the standing timber at harvest.

References

Addis T, Buchanan AH, Walker JCF. 2000. Selecting trees for structural timber. Holz Roh-Werkst 58:162–167.

Amishev D, Murphy GE. 2018. In-forest assessment of veneer grade Douglas-fir logs based on acoustic measurement of wood stiffness. Forest Products Journal 58(11): 42–47.

Achim A, Paradis N, Carter P, Hernandez RE. 2011. Using acoustic sensors to improve the efficiency of the forest value chain in Canada: A case study with laminated veneer lumber. Sensors 11:5716–5728.

Bowyer JL, Schmulsky R, Haygreen JG. 2007. Forest product and wood science. 5th ed. Blackwell Publishing, Oxford, UK.

Briggs DG, Smith WR. 1986. Effects of silvicultural practices on wood properties—a review. In, Douglas-fir: stand management for the future. College of Forest Resources, University of Washington, Seattle, Washington, USA. Contrib. no. 55. pp 246-257.

Briggs DG, Merifi F, Smith WR. 1986. Effect of sludge on wood properties – a conceptual review with results from a 60-year old Douglas-fir stand. In: The Forest Alternative: For Treatment and Utilization of Municipal and Industrial Wastes. Chp. 22, Edited by DE Cole, CL Henry and WL Nutter. University of Washington Press, Seattle, Wash. pp. 246–257.

Briggs DG, Thienel G, Turnblom EC, Lowell E, Dykstra D, Ross RJ, Wang X, Carter P. 2008. Influence of thinning on acoustic velocity of Douglas-fir trees in western Washington and western Oregon. In: Proceedings of the 15th International Symposium on Nondestructive Testing of Wood. September 10-12, 2007, Duluth, MN, USA. Forest Products Society: Madison, WI, USA. pp. 113–123.

Brix H. 1972. Nitrogen fertilization and water effects on photosynthesis and earlywood-latewood production in Douglas-fir. Canadian Journal of Forest Research 2(4): 467–478.

Cahill JM, Briggs DG. 1992. Effects of fertilization on wood quality and tree value. In: Proceedings of Forest Fertilization: Sustaining and Improving Nutrition and Growth of Western Forests. February 12–14, 1991, Seattle, WA, University of Washington, College of Forest Resources. pp. 145–161.

Carter P, Briggs D, Ross RJ, Wang X. 2005. Acoustic testing to enhance western forest values and meet customer wood quality needs. PNW-GTR-642, In: Harrington, CA, Schoenholtz SH, eds. Productivity of Western Forests: A Forest Products Focus. USDA Forest Service, Pacific Northwest Research Station, Portland, Oregon. pp. 121–129.

Carter P. 2011. Real-time measures of wood quality—transition from research to application. In: Proceedings, 17th International Nondestructive Testing and Evaluation of Wood Symposium, September 14-16, 2011, University of West Hungary, Sopron, Hungary. pp. 34–39.

Chauhan SS, Walker JCF. 2006. Variation in acoustic velocity and density with age, and their interrelationships in radiata pine. Forest Ecololgy Management 229: 388–394.

Cregg BM, Dougherty PM, Hennessey TC. 1988. Growth and wood quality in young loblolly pine trees in relation to stand density and climate factors. Canadian Journal of Forest Research 18(7): 851–858.

Divos F. 2010. Acoustic tools for seedling, tree and log selection. In: Proceedings, The Future and Quality Control for Wood & Wood Products, May 4-7, 2010, Edinburgh Napier University: Edinburgh, UK. p. 5.

Edmonds RL, Cole DW. 1980. Use of dewatered sludge as an amendment for forest growth: Vol III—Management and biological implications. Center for Ecosystem Studies, College of Forest Resources, University of Washington, Seattle, WA. 120 pp.

Grabianowski M, Manley B, Walker JCF. 2006. Acoustic measurements on standing trees, logs and green lumber. Wood Science Technology 40: 205–216.

Harris PD, Andrews MK. 1999. Tools and acoustic techniques for measuring wood stiffness. Emerging Technologies for Evaluating Wood Quality for Processing, 3rd Wood Quality Symposium Rotorua and Melbourne. Forest Industry Engineering Association, New Zealand.

Harris P, Petherick R, Andrews M. 2002. Acoustic resonance tools. In: Proceedings, 13th International Symposium on Nondestructive Testing of Wood, August 19-21, 2002, Berkeley, CA, pp. 195–201.

Huang CL. 2000. Predicting lumber stiffness of standing trees. In: Proceedings, the 12th International Symposium on Nondestructive Testing of Wood, University of Western Hungary, Sopron, September 13-15, 2000. pp. 173–179.

Huang CL. 2005. System and method for measuring stiffness in standing trees, US patent no. 6,872545.

Kantavichai R, Briggs DG, Turnblom EC. 2010. Effect of thinning, fertilization with biosolids, and weather on interannual ring specific gravity and carbob accumulation of a 55-year-old Douglas-fir stand in western Washington. Canadian Journal of Forest Research 40: 75–82.

Larson PR, Kretschmann DD, Clark A III, Isebrands JG. 2001. Formation and properties of juvenile wood in southern pines: a synopsis. USDA Forest Service. FPL-GTR-129. Madison, Wis.

Lindstrom H, Harris P, Nakada R. 2002. Methods for measuring stiffness of young trees. Holz Roh-Werkst 60:165–174.

Lowell EC, Todoroki CL, Dykstra DP, Briggs DG. 2014. Linking acoustic velocity of standing Douglas-fir trees to veneer stiffness: a tree-log-product study across thinning treatments. New Zealand Journal of Forestry Science 44(1): 1–16.

Mora CR, Schimleck LR, Isik F, Mahon JM, Clark A III, Daniels RF. 2009. Relationship between acoustic varaibles and different measures of stiffness in standing *Pinus taeda* trees. Canadian Journal of Forest Research 39:1421–1429.

Raymond CA, Joe B, Anderson DW, Watt DJ. 2008. Effect of thinning on relationships between three measures of wood stiffness in *Pinus radiata*: standing trees vs. logs vs. short clear specimens. Canadian Journal of Forest Research 38: 2870–2879.

Sonne E, Turnblom E, Briggs D, Becker G. 2004. Log and lumber grades and value from a Douglas-fir stand years after thinning and biosolids fertilization. WJAF 19(1): 34–41.

Wang X. 1999. Stress wave-based non-destructive evaluation (NDE) methods for wood quality of standing trees. Dissertation, Michigan Technological University, Houghton, Michigan. 187 p.

Wang X, Ross RJ, McClellan M, Barbour RJ, Erickson JR, Forsman JW, McGinnis GD. 2001. Nondestructive evaluation of standing trees with stress wave method. Wood and Fiber Science 33(4):522–533.

Wang X, Ross RJ, and others. 2006. System for and method of performing evaluation techniques on a log or round timber. US patent no. 7,043,990; New Zealand patent no. 527,569.

Wang X, Carter P, Ross RJ, Brashaw BK. 2007a. Acoustic assessment of wood quality of raw forest materials—a path to increased profitability. Forest Products Journal 57(5):6–14.

Wang X, Ross RJ, Carter P. 2007b. Acoustic evaluation of wood quality in standing trees. Part I. Acoustic wave behaviour. Wood and Fiber Science 39(1):28–38.

Wang X, Sharplin N, Carter P, Ross RJ. 2008. Method and apparatus for evaluation of standing timber. U.S patent no. 7,418,866 B2.

Wang X. 2013. Acoustic measurements on trees and logs: a review and analysis. Wood Science Technology 47:965–975.

Comparing usefulness of acoustic measurements on standing trees for segregation by timber stiffness

David Gil-Moreno
Centre for Wood Science & Technology, Edinburgh Napier University, Edinburgh, UK,
d.gil-moreno@napier.ac.uk

Dan Ridley-Ellis
Centre for Wood Science & Technology, Edinburgh Napier University, Edinburgh, UK,
d.ridleyellis@napier.ac.uk

Abstract

The paper presents a comparison of standard procedures to measure acoustic stiffness of standing trees and logs. The aim is to see how useful they are for predicting the properties of dry, sawn, timber for the purposes of resource segregation in industrial practice. Stress wave time-of-flight (TOF) measurements were made on 36 trees of four species. The TOF data were analyzed and compared with resonant frequency measurements made on cut logs and sawn dry timber, and, as the ultimate measurement, static stiffness measured by four point bending tests. A simplified model of segregation is used to examine the relative performance of the methods to sort the better grade timber; in this case defined by mean static bending stiffness. The research reveals that lengthening the TOF distance from 1 to 2 meters improves the performance for segregation in this case, particularly when segregating the higher stiffness proportion of the timber.

Keywords: resonance, time-of-flight, sawn dry timber, stiffness, grading, segregation, indicating property.

Introduction

Portable acoustic devices can be used for early segregation of timber, prior to making decisions about forest management, harvesting and processing into wood products. When segregating trees, it is less important that the acoustic measurement be a good predictor of the quality of the timber that can be made from that specific tree, than it is that the acoustic measurement can discern, specifically, the lower quality material that is unsuitable for timber. Therefore the common statistical comparisons of NDT methods, based on linear regression, are not so useful in comparing the actual practical performance of different NDT methods in industrial practice.

Acoustic tools currently used in forestry measure the speed of propagation of a sound wave in the wood, either by direct “time-of-flight” (TOF) measurement between two points (a technique which can be applied on standing trees, logs or sawn timber), or by impact excitation resonant frequency (which can be applied to logs and sawn timber, but not standing trees). The use of these techniques is particularly important in the UK, where stiffness is typically the limiting property when it comes to grading structural timber (Moore et al. 2011) and the ability to divert the lower stiffness timber to other markets at an early stage could reduce the cost of grading rejects after processing and drying.

It is already known that estimation of sawn timber quality can be achieved more successfully using the resonance of a log (Wang, 2013), but this can only be done after felling and cutting the log to length for a certain intended wood product. This study, aims to make better use of standing tree acoustic measurements in making decisions about the most appropriate end products. The method commonly used in research and industrial practice, measures the TOF of a stress wave between

transducers, which for practical reasons are usually about 1m apart on the same side of the tree at about breast height. However, the correlation between the TOF measurements made on individual trees and the stiffness of the timber cut from those trees is often weak. It has previously been suggested that this is because the short measurement distance of only 1m is not representative of the wood stiffness throughout the log and that a ratio of tree diameter to measurement length should be 0.1 or below (Zhang et al. 2011). The implication here is that if the measurement is over too short a distance, or the distance is not standardized, the measurements are confounded by other factors such as tree age, diameter and sapwood depth.

This study, conducted as part of a PhD, compares the performance of different standing tree TOF measurements for segregation on the basis of wood stiffness, comparing also to log and timber measurements and the ideal standard of a "perfect" machine simulated by use of the measured static stiffness (the best possible performance). The research is ongoing, but there is already sufficient data to make some preliminary recommendations for best practice standing tree measurement in the future.

Material and methods

This study uses material from four tree species, noble fir (*Abies procera*), western hemlock (*Tsuga heterophylla*), Norway spruce (*Picea abies*) and western red cedar (*Thuja plicata*), grown in even-aged plantations in Scotland, UK. For the exercise in this paper, the species are treated together, even though this would not normally happen in industrial practice because the species have different properties. This was done in order to provide more data over a wider range of wood stiffness.

Three trees were selected from three replicate plots for every species covering the range of diameter classes in each plot. Multiple TOF measurements using a Fakopp Tree Sonic device were collected on each of the 36 trees (nine per species), with a fixed origin over a measurement distance of 1, 2 and 3m on the north facing side (0 to 1, 0 to 2, and 0 to 3 in Figure 1). Further arrival times are compared on the south facing side of the tree with vertical distance between the transducers of 1m (A to B in Figure 1).

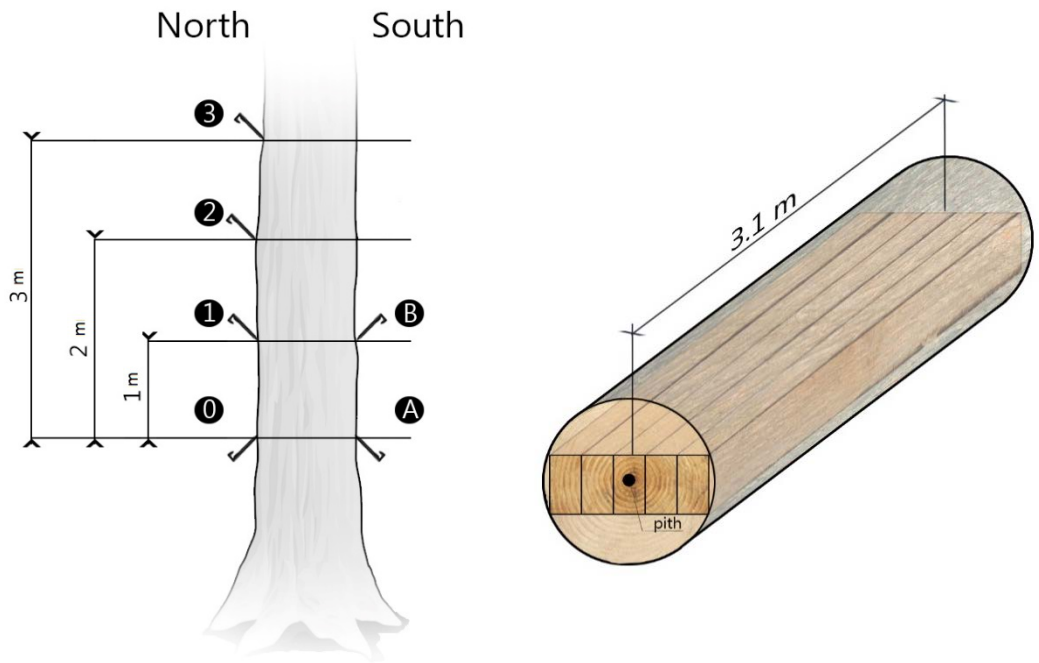

Figure 1—Left: Representation of TOF measurements collected per tree: 0-1; 0-2; 0-3; and A-B. Right: Cutting pattern of structural timber.

The trees were shortly after felled, and longitudinal resonance velocity of the logs (one per tree) measured with a HM-200 “Hitman” (Fibre-gen, Auckland, New Zealand). For the log resonance measurement the log length was 5 m for all species except the western red cedar, which was 3.1 m.

Dynamic modulus of elasticity (MOE_{dyn}) was calculated from measurements of wave speed using equation (1):

$$MOE_d = \rho V^2 \quad (1)$$

where ρ is the density and V is the speed of sound. In the case of TOF, V is calculated from straight line distance divided by time delay, and in the case of longitudinal resonance it is calculated from the frequency of the fundamental mode multiplied by the wavelength (twice the log or batten length). Wood density for standing trees and freshly felled logs was assumed to be 1000 kg/m^3 for all the trees.

Logs were next cross cut to 3.1 m length (retaining the lower part) and then processed into structural sized timbers, following a bark to bark pattern, with nominal cross sectional dimensions of 100x50 mm (Figure 1 right).These samples were aligned so as to match the orientation of the TOF measurements. The purpose of cutting bark to bark was to examine the radial trend in properties within the wider research project. This is not a normal industrial cutting pattern, but it is expected this will nevertheless provide good mean values per log. A total of 226 battens were obtained by this process: 47 noble fir, 51 Norway spruce, 61 western hemlock and 67 western red cedar.

The noble fir, Norway spruce and western hemlock material was kiln dried to 12%, whereas western red cedar was kiln dried to 20% due to the concerns over the risk of drying collapse for this species. The timber was then conditioned towards 12% and longitudinal resonance acoustic velocity was measured with a timber grading machine MTG960 (Brookhuis Microelectronics BV, Holland) with a connected balance to obtain whole batten density (in combination with manually measured dimensions). Finally, the specimens were subjected to destructive four point bending tests in accordance with EN408:2010, using a Zwick Z050 universal testing machine (Zwick Roell, Germany). The bending stiffness measurements used in this paper are the, as measured, “global” measurement adjusted to the reference conditions (12% moisture content), but not pure bending stiffness as in EN384:2010. Moisture content was measured by the oven dry method on the density samples cut from each batten immediately after testing. The measurements made with the MTG were not adjusted for moisture content (representative of a typical production scenario for this machine, grading a batch of timber within a moisture content range). Bending strength and density were also measured, but these data are not used for this paper.

For this paper, segregation means a process undertaken to sort trees and logs into categories based on wood properties. It can be used to improve grading of structural timber in the sawmill by diverting the lower quality material to other products so as to reduce grading rejects.

Like grading, segregation does not operate at the level of predicting the properties of individual trees or battens. Instead, segregation operates on the basis of predicting the characteristics of the portion of the population that passes a certain threshold “indicating property” (IP) measurement, which could be based on NDT, visual criteria, or category description.

Strength grading of structural timber is concerned with strength, stiffness and density, but this example is concerned only with stiffness. The reasons for this are simplicity, and because consideration of all three properties requires more data to work correctly, and may not work across a mix of species. Stiffness is the property that is most closely related to the acoustic measurements made, and it is also usually the critical (most limiting) property for production of graded timber in the UK. The relevant characteristic value for stiffness for this analysis is the mean of the static modulus of elasticity (after adjustment to 12% moisture content) of the timber passing the IP threshold.

The four species differed in average stiffness, so the most basic kind of segregation can operate on removal of species in ascending order of average static stiffness (Table 1). Any non-destructive measurement that performs less well than simple species segregation is not particularly useful.

In order that the NDT approaches can be compared to the simple species segregation, three grade targets have been defined to correspond with the result of the simple species segregation on this dataset with its particular ratio of species. The "low" grade has a target mean stiffness of 7947 N/mm^2, which corresponds to the result of removing the western red cedar. The "medium" grade has a target mean stiffness of 8358 N/mm^2, which corresponds to the result of also removing the noble fir. The "high" grade has a target mean stiffness of 8803 N/mm^2, which corresponds to the result of also removing the Norway spruce so that only the western hemlock remains. The low, medium and high grades are alternative levels of segregation (it is not segregation into three categories). NDT has the potential to outperform the species segregation because there is some overlap of wood stiffness within the species (even western red cedar contains some higher stiffness timber).

The best possible segregation that could be done is with an NDT machine that has perfect knowledge of the dry wood stiffness ("perfect segregation" being the equivalent of a "perfect grading machine", operating on trees rather than on battens as grading does), which can be simulated here because this has been measured. Real segregation approaches can be compared to the yield of perfect segregation to assess their performance.

Table 1—Summary of static bending stiffness for the four species

Species (in ascending order)	Mean static MoE [st dev] Adjusted to 12% mc (N/mm^2)	Mean moisture content at time of bending test (%)
Western red cedar (THPL)	6521 [1604]	12.0
Noble fir (ABPR)	6967 [1360]	9.3
Norway spruce (PCAB)	7826 [1426]	9.0
Western hemlock (TSHT)	8803 [2019]	15.7

Results

The correlation between the standing tree measurement and stiffness of the sawn dry timber is relatively weak. Figure 2 shows the apparent dynamic MOE calculated from the 1 and 3 m TOF measurements compared to the static MOE of the immediately adjacent (north side) batten (Figure 2, left) and the mean static MOE of all battens from that tree. The relationship is better for the 3 m measurement, and even more so for the mean static MOE of battens for that 3 m measurement. This is consistent with the wave propagating both up and outward, and not only through the sapwood in the outer part as Searles (2012) explains: "*when the excitation is initiated, the stress wave starts propagating both up toward the top probe and outward across the tree's cross section. It is not yet a plane wave but possibly, by the time it arrives at the top probe 1.0 – 1.5 m away, a measure of more of the tree's wood properties than simply the area directly between the probes*". The question to be answered is: are these correlations useful for segregation, and does the 3 m measurement afford any additional practical usefulness over the 1m measurement that would justify the additional effort required to make the measurement in practice.

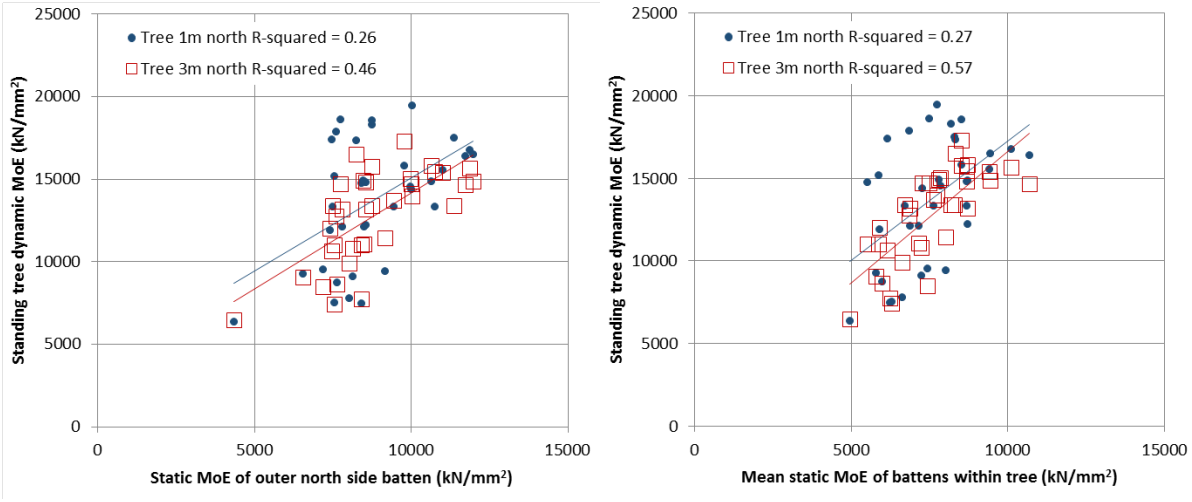

Figure 2—Comparison of 1m and 3m north side TOF measurements with the static MOE of the north side outer batten (left) and mean static MOE of all battens from the tree (right).

Correlation coefficients for each of the IP (indicating property) types against static MOE of individual battens are listed in Table 2. Ten segregation/grading approaches are assessed. This includes a perfect grading machine sorting individual battens (IP is static MOE) and perfect segregation sorting battens grouped by tree (IP is mean static MOE of battens within the tree), which are used as a reference to evaluate the effectiveness of the real world approaches.

Table 2—Effectiveness of different acoustic measurements to segregate timber.

Indicating property	R^2 vs Static MoE (note 1)	Segregation to "Grade" (note 2) Yield as a % of the perfect method yield [absolute yield %] Low	Medium	High
On standing tree / log				
Sorting by species	-	88% [70%]	79% [50%]	67% [27%]
1m TOF north side	16% (27%)	88% [70%]	51% [32%]	0% [0%]
1m TOF north & south	18% (31%)	92% [73%]	48% [30%]	0% [0%]
2m TOF north side	27% (50%)	88% [70%]	86% [54%]	80% [32%]
3m TOF north side	31% (57%)	92% [73%]	88% [55%]	47%* [19%]
Hitman velocity of log	35% (63%)	94% [76%]	79% [50%]	95% [38%]
Perfect tree segregation (mean)	*53% (100%)*	*100% [80%]*	*100% [63%]*	*100% [40%]*
On sawn dry timber				
MTG frequency only	63%	97% [84%]	96% [69%]	88% [49%]
MTG frequency & density	91%	99% [86%]	99% [71%]	94% [52%]
Perfect grading machine	*100%*	*100% [87%]*	*100% [72%]*	*100% [56%]*

Note 1: The R^2 value relate to correlations on a batten by batten basis. Values based on the mean of batten MOE per tree given in brackets
Note 2:Standing tree / log IP yields are compared to perfect tree segregation, batten IP (i.e. MTG) yields are compared to the perfect grading machine
* nearly achieves 89% [36%] (being just 0.4% short of the required mean stiffness at this yield)

Figure 3 shows the outcome of the thresholds of the different IPs being progressively increased to segregate the higher stiffness timber, described by the mean static stiffness of the timber passed (y-axis) and the simple proportion of the battens passing (x-axis). The figure also shows the MTG operating in frequency only mode on the battens, and in frequency plus density mode, the latter of which is close the performance of the perfect grading machine – indicating a high performance of this approach to grade timber (as expected when the only grading criteria is stiffness, as in this example) and also confirming that the relationship between dynamic and static stiffness is suitably similar for all species for the purposes of this analysis. Segregating trees cannot perform as well the (real or perfect) grading machine because the trees contain substantial variation of wood stiffness within them, but it can be seen that the perfect tree segregation works better than simple segregation by species - a near trivial kind of segregation in practice. Segregation by Hitman (log resonance) works better than by species, but not as well as perfect tree segregation.

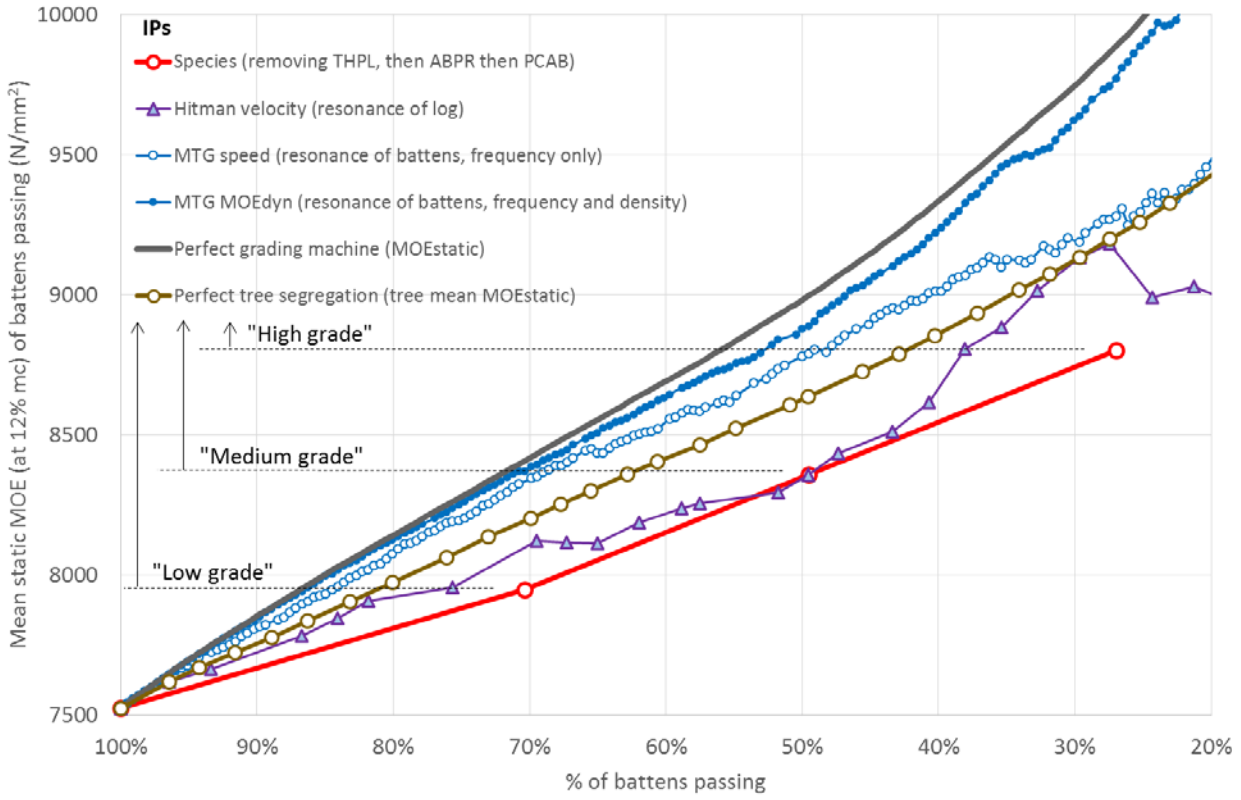

Figure 3—Segregation performance (for static stiffness) of the perfect grading machine, perfect tree segregation, MTG, Hitman, and simple species approach.

The performance of the standing tree measurements is shown in Figure 4, which indicates that the 2 and 3 m TOF measurement outperform the 1 m TOF measurement, except when segregation passes (approximately) more than three quarters of timber. When segregating the stiffest half of the timber, the 1 m TOF measurement performs less well than simple species segregation. This is consistent with the speed of stress wave propagation in trees being more similar to log resonance when TOF is made over more than a meter. This suggest a larger influence of the properties of the entire cross section as the distance increases rather than solely the outer part of the tree. In line with previous research, it is consistent with a change in the wave behavior from a dilatational or quasi-dilatational wave with short spans, to a one dimensional plane waves with longer spans (Wang et al. 2007; Andrews, 2003).

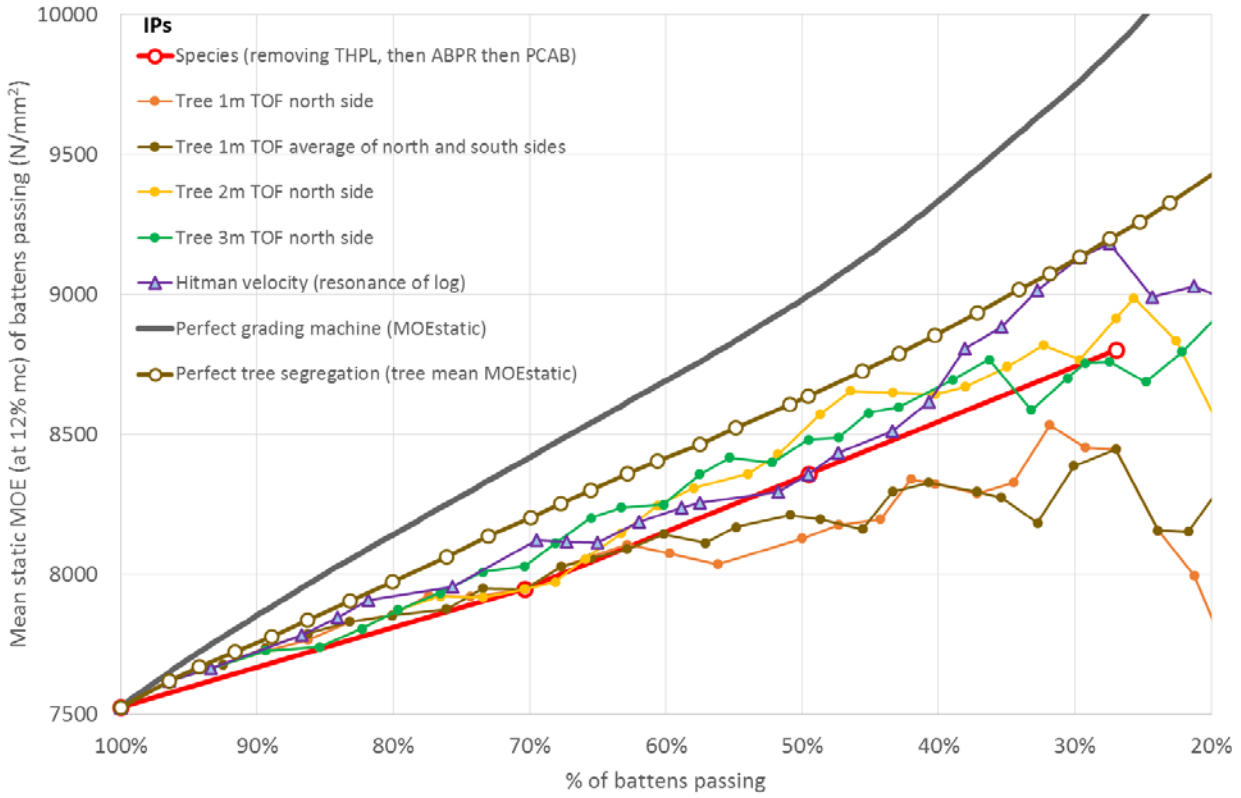

Figure 4—Segregation performance (for static stiffness) of the standing tree TOF measurements, compared to the simple species approach and perfect segregation.

To better illustrate the relative performance, three ‘grades’ were created that are equivalent to what is obtained by a simple species sort. The ‘low’ grade has a mean stiffness requirement equal to that of the timber when western red cedar is removed, ‘medium’ when noble fir is additionally removed, and ‘high’ when only western hemlock remains (see materials and methods above). Table 2 lists yields for these grades (when segregation to one grade only) expressed as a percentage of the yield obtained by the perfect segregation (in the case of the tree and log IP) and the yield of the perfect grading machine (in the case of the MTG, which operates on sawn dry timber rather than logs). The 2 and 3 m TOF measurements on the trees are seen to be similarly good, superior to simple segregation by species, and almost as good as resonance measurements on the logs. The case of the 3 m TOF yield for the high grade is special in that it very narrowly misses the required stiffness with a much higher yield (see table footnote), which is likely a random statistical effect of the low number of specimens for the high grade and an under representation of the performance.

Conclusions

As expected, the tree measurements are not as good as the log measurements, especially when the measurement distance is the usual 1 m. Increasing the measurement distance to 2 m is sufficient to add useful segregation potential, although, in this example, even a 1 m measurement performs as well as other standing tree measurements when it is desired to sort only the lower quarter of the timber.

Despite the variability of wood properties within a tree, the use of portable acoustic tools can help to segregate timber from standing trees and logs, and the correlations need not be strong if the requirement is only to segregate out the very worst timber. By establishing relationship between an indicating property and characteristic grade-determining property (which will depend on growth area and species) it is possible to set thresholds that would improve grading machine yields later down the line, and divert the less good timber to non-structural products.

This study also provides confirmation that stress wave do not travel only in the outer part of the tree, between the two probes, but likely up and across the tree's cross section with increasing measurement length.

Future work will take this approach further, adding more data to bring in consideration of cutting pattern, the performance within a single species, consideration of strength and density, and the more direct avoidance of machine grader rejects.

Acknowledgments

The financial support of the Scottish Forestry Trust, Forestry Commission Scotland and Cyfoeth Naturiol Cymru (Natural Resources Wales) is gratefully acknowledged. Andrew Price (Forest Research) is thanked for help finding suitable sample sites and organizing the necessary forest operations. The authors also thank Stefan Lehneke and Steven Adams (Edinburgh Napier University) for helping with the destructive tests.

References

Andrews, M. 2003. Which acoustic speed? Pages 159–165 in Proc. 13th International Symposium on Nondestructive Testing of Wood, August 19–21, 2002, Berkeley, CA.

CEN 2010. Structural timber—determination of characteristic values of mechanical properties and density. EN 384:2010. Brussels, European Committee for Standardization.

CEN 2012. Timber structures—structural timber and glued laminated timber—Determination of some physical and mechanical properties EN408:2010+A1:2012. European Committee for Standardization, Brussels.

Moore, J.R., Lyon, A.J., Searles, G.J., Lehneke, S.A., & Ridley-Ellis, D.J. Within- and between-stand variation in selected properties of Sitka spruce sawn timber in the UK: implications for segregation and grade recovery. Annals of Forest Science, 2013, 70(4): 403-414.

Searles, Gregory J (2012) Acoustic segregation and structural timber production. PhD thesis, Edinburgh Napier University.

Wang, X. Ross, R.J., Carter, P. 2007. Acoustic evaluation of wood quality in standing trees. Part 1. Acoustic wave behavior. Wood and Fiber Science, 39: 28-38.

Wang, X. (2013). Acoustic measurements on trees and logs: a review and analysis. Wood science and technology, 47(5), 965-975.

Zhang, H., Wang, X., Su, J. 2011. Experimental investigation of stress wave propagation in standing tree. Holzforschung. 65: 743-748.

10 years of experience using NIR in Arauco: from model development to operational use in *Eucalyptus* sp. commercial plantations assessment.

Mauricio Ramírez Vidal
División Propiedades de la Madera, Bioforest S.A. Concepción, Chile, mauricio.ramirez@arauco.cl

Miguel Peredo Lopez
División Propiedades de la Madera, Bioforest S.A. Concepción, Chile, miguel.peredo@arauco.cl

Abstract

Arauco's forest company has a *Eucalyptus* sp. plantation program focused to support the annual demand of 2.900.000 m^3 of solid wood required for producing kraft pulp at Nueva Aldea, Arauco and Valdivia pulp mills.

Considering the importance of raw material characteristics on the end pulp productivity, during 2005 Arauco choose the NIR method as a non-destructive technology as an evaluation tool. Since 2007, the NIR methodology has been used to predict basic density (BD), kraft pulp yield (KPY) and specific wood consumption (SWC), of commercial plantations included in the annual harvesting program. The samples of shaves were dried, milled and conditioned inside of the company laboratory. Then, two spectra per sample were generated using the spectrophotometer Foss NirSystems 6500. The NIR models were adjusted, calibrated and validated to obtain prediction values.

The calibrated models included samples of *E. globulus* and *E. nitens* between 4 and 20 years old. The standard errors of predictions were 23.1 kg/m^3, 1.29% and 0.22m^3/Adt, for BD, KPY and SWC, respectively. The main results of the operational use of NIR are the pulpability assessment of 35,657 ha of *E. globulus* and 12,500 ha of *E. nitens*.

After 10 years of NIR research at Arauco, it is expected that the main impact in the future will be the use of more homogenous raw material and a reduction of the SWC of the *Eucalypts* sp. raw material used for kraft pulp production.

Keywords: *Eucalyptus,* NIR, Arauco, basic density, pulp yield.

Introduction

Arauco's forest company has been developing a *Eucalyptus* sp. plantation program focused to support the annual demand of 2.900.000 m^3 of solid wood that is required to produce kraft pulp at Nueva Aldea, Arauco and Valdivia pulp mills. Actually, Arauco has in Chile 48,000 and 91,550 hectares of *E. nitens* and *E. globulus*, respectively.

Considering the high quality standard of the Arauco's pulp products, the raw material supply is based on the stability and the wood quality of the pulp logs coming into each yards. It also indicates that a productive and uniform wood raw material is sought in the long-term. All these goals are strongly related to raw material issues. In this sense, a full assessment of Arauco's forest resource pulpability

is desirable for planning purposes and for developing strategies for handling raw material variation. The information generated from a full assessment can easily complement other sources of information, such as forest inventories, helping to improve harvesting plans and wood supply plans to the mill.

However, a complete wood properties assessment by wet laboratory analysis is economically unfeasible. Near infrared (NIR) spectroscopy is increasingly being used to replace traditional methods of wood property assessment. This technology is particularly well-suited where large numbers of samples must be analyzed, but it can be utilized in any forestry application where the rapid provision of wood property data is required (Schimleck 2008). The earliest studies of NIR spectroscopy in forestry and wood quality concentrated on wood properties directly related to wood chemistry and were based on milled chips obtained from composite whole-tree samples. The range of applications rapidly expanded and NIR was used to estimate the moisture content (MC) and BD of intact chips, the physical and mechanical properties of solid wood, the characteristics of chemical pulps, and the density, microfibril angle and stiffness of radial strips cut from increment cores. Recent studies have shown that NIR spectra can also be collected directly from the ends of merchantable logs (Mora et al. 2011) and from few grams of wood material obtained at DBH from standing trees. The latter is the approach that is currently being used by Arauco for large scale eucalyptus plantation assessments (Meder et al. 2010). For more information, a comprehensive review of NIR applications in forestry and forest products industry is given in Schimleck and Workman (2004) and Tsuchikawa (2007).

The main goals were, to develop NIR calibration models for the prediction of whole-tree BD, KPY and SWC, in standing trees using non-destructive samples and to assess BD, KPY and SWC of commercial plantations included in the annual harvesting program, using the models developed.

Material and Methods

Tree sampling and spectra collection

The process of fitting NIR calibration models for large scale resource assessments considered the following steps: forest resource stratification (species and age) and selection of forest stands for each of the strata of interest. In total 1,126 samples of *E. globulus* and 4,265 samples of *E. nitens* were distributed on stands. From each tree, shavings were obtained at Breast Height (BH). All shaves were dried at 50°C for 24 hours and milled using a Willey and Cyclotec mill. Then two spectra from each sample were collected at 2 nm intervals over the wavelength range of 400 - 2500 nm in a Foss NIRSystems 6500 spectrophotometer, using a small sample cup on a spinning ring module. The instrument reference was a ceramic.

Selection of unique samples

The process to select the unique spectra was performed using the option included in WINISI III software (version 1.5) software package (Infrasoft International). The duplicate spectra were averaged and a standard normal variate plus detrend math pretreatment was used. The spectra (wavelengths 1100–2500 nm) were then converted to the second derivative using a gap width of 4 nm. The sample selection was based on the identification of spectral unique samples using the neighborhood distance. A total of 227 and 206 samples of *E. globulus* and *E. nitens* were selected, respectively. The selected trees were destructive sampled for wet chemical analyses

Wet laboratory analyses

Selected trees were felled, delimbed, and measured for total height and merchantable length (to 6 cm over-bark top diameter). Then five 1 m long logs were obtained for pulping analyses. These logs were extracted from the center of the resulting sections after splitting the merchantable length into fifths. All logs from each tree were properly identified and chipped. A sub sample of classified chips was analyzed at Arauco pulp mill laboratory. The chip classification prior cooking followed the standard SCAN CM 40 (2001) and to measure basic density, TAPPI T 258 (2011) standard method was used. Cookings of the raw material for yield at small scale were made using a MK digesters. To reach the targeted kappa number (15) the H-factor was adjusted. After cooking the pulp was washed, screened (slot 0.25 mm) and dried. Then, pulp was homogenized by hand and the yield, amount of reject and kappa number were measured.

NIR models, calibration and validation

From selected samples, calibration and validation set were split using the unique spectra option in WINISI II. Then, multivariate analyses were performed in The Unscrambler® X software (www.camo.com).

Calibration models were developed by using the partial least-squares algorithm considering the spectral range 1,100–2,500 nm and as math treatment Zavitzky-Golay second derivative with 4 nm gap. The root mean square error of full cross-validation (RMSECV), root mean square error of prediction (RMSEP), and the coefficient of determination (R^2) were used to assess calibration performance.

As part of the development, individual species models and multispecies models for *E. globulus* and *E.nitens* (Downes et al. 2010, Kothiyal et al. 2015) were explored.

Results

Models calibration and validation

Mora and Schimleck (2009) and Isik et al. (2011), have pointed out, that basic information regarding wood properties is becoming increasingly important with forest products companies aiming to optimize utilization of raw materials and tree breeders seeking to improve wood properties. It is essential that such information is provided rapidly, at low cost and preferably non-destructively, however methods typically employed to measure important wood properties are time consuming, expensive and often destructive, i.e. trees have to be cut down.

In general it is recommended that the development of NIR models must be specific for a particular species covering a range of plantation ages and growing areas. However in this project, the best option was to develop a multispecies models. The calibrated models included samples of *E. globulus* and *E. nitens* between 4 and 20 years old. The calibration and validation performance are showed in Table 1.

Table 1. Calibration and validation performance of NIR models

Model	Calibration				Validation		
	n samples	Factors	RMSCV	R^2	n samples	RMSEP	R^2
Basic Density (kg/m^3)	365	8	24.4	0.80	64	23.10	0.79
Pulp Yield (%)	365	8	1.18	0.80	64	1.29	0.77
Specific Wood Consumption (m^3/Adt)	362	7	0.25	0.81	64	0.22	0.84

A primary consideration is the accuracy and precision of NIR estimates of the property of interest. The accuracy of BD and PY measurements by wet laboratory analysis influences the performance of NIR calibrations. Careful consideration must also be given to the type of sample and what it represents: the use of few grams of material obtained at DBH from standing trees to estimate the whole-tree pulp ability is not free of error. While this issue is not specific to the utilization of NIR (e.g. Pilodyn penetrometers) the nature of sampling must always be considered when drawing conclusions from studies involving whole trees, particularly standing trees (Meder et al. 2010).

Eucalyptus sp. commercial plantations assessment

Since 2007samples from the stands included in the annual harvesting program were obtained. To secure representativeness by stand, 30 trees were selected (10 trees in 3 transects) for sampling. From each tree, bark to bark shavings were obtained at BH. All shaves were processed at Bioforest NIR laboratory and from their spectra, predictions of BD, PY and SWC were made.

The main results of the operational use of NIR are the pulpability assessment of 35,657 ha of *E. globulus* and 12,500 ha of *E. nitens* plantations (Figure 1).

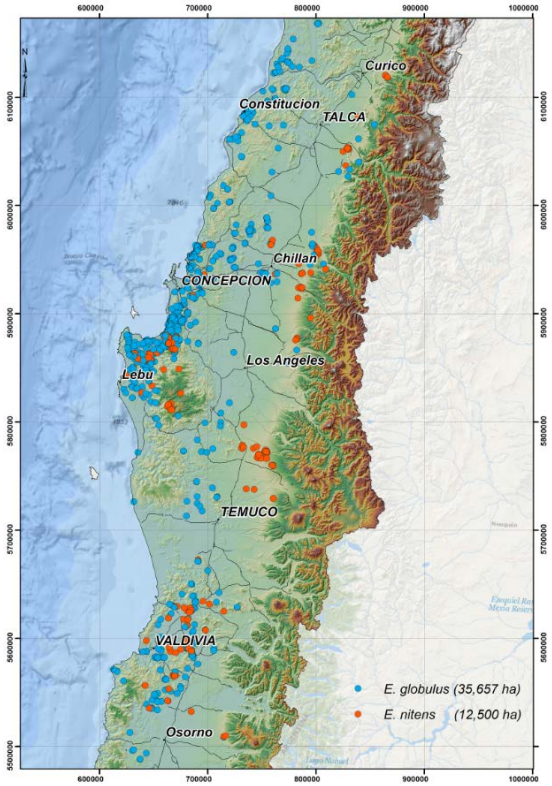

Figure 1. Distribution of stands with pulpability information.

In this context, after 10 years of NIR research at Arauco, it is expected that the main impact in the future will be the use of more homogeneous raw material to feed industrial plants and the reduction of the SWC of the *Eucalypts* sp. raw material used for kraft pulp production.

Conclusions

Near infrared models fitted to assess the raw material using non-destructive sampling on standing trees, allow to predict BD, PY and SWC with enough precision and accuracy.

The use of NIR as a non-destructive method to assess the pulpability of *Eucalyptus* sp., has been successfully implemented at operational level in Arauco.

Acknowledgments

The authors acknowledge the assistance of Yenny Lineros, Paola Pilgrín, Jessica Bustamante, Jhony Hidalgo and Jesus Castro for their help in data collection at the Bioforest NIR Laboratory, and also, the authors thanks Bioforest S.A. for support this work.

References

Downes, G.; Meder R.; Harwood J. 2010. A multi-site, multi-species near infrared calibration for prediction of cellulose content in eucalypt woodmeal. Journal of Near Infrared Spectroscopy. 18:381-387.

Isik, F.; Mora, C.R.; Schimleck, L.R. 2011. Genetic variation in *Pinus taeda* wood properties predicted using non-destructive techniques. Annals of Forest Science. 68 (2):283-293.

Kothiyal, V.; Jaideep; Bhandari, S.; Ginwal, H. S.; Gupta, S. 2015. Multi-species NIR calibration for estimating holocellulose in plantation timber. Wood Science and Technology, 49(4):769-793.

Meder, R.; Trung, T.; Schimleck, L. 2010. Seeing the wood in the trees: unleashing the secrets of wood via near infrared spectroscopy. Guest editorial. Journal of Near Infrared Spectroscopy. 18: v-vii.

Mora, C. R.; Schimleck, L.R. 2009. Determination of specific gravity of green *Pinus taeda* samples by near infrared spectroscopy: comparison of pre-processing methods using multivariate figures of merit. Wood Science and Technology. 43 (5-6):441-456

Mora, C.R.; Schimleck, L.R.; Clark III, A.; Daniels, R.F. 2011. Determination of basic density and moisture content of merchantable loblolly pine logs by near infrared spectroscopy. Journal of Near Infrared Spectroscopy. 19: 391-399.

SCAN CM 40. 2001. Wood chips for pulp production. Scandinavian Pulp, Paper and Board Testing Committee, Stockholm.

Schimleck, L.R. 2008. Near-infrared spectroscopy: A rapid non-destructive method for measuring wood properties, and its application to tree breeding. New Zealand Journal of Forestry Science. 38: 14-35.

Schimleck, L.R.; Workman, J. 2004. Applications in analysis of timber and paper. In: Near-Infrared Spectroscopy in Agriculture, Agronomy Monograph no. 44, American Society of Agronomy, Crop Science Society of America, Soil Science Society of America.

TAPPI T 258 om-11. 2011. Basic Density and Moisture Content of Pulpwood. TAPPI Press, Atlanta, GA.

Tsuchikawa, S. 2007. A review of recent near infrared research for wood and paper. Applied Spectroscopy Reviews. 42: 43-71.

Prediction of the velocity in logs and beams from the velocity in standing trees

Cinthya Bertoldo
Assistant Professor, Laboratory of Nondestructive Testing - LabEND, College of Agricultural Engineering - FEAGRI - University of Campinas - UNICAMP, Brazil
email: cinthya.bertoldo@feagri.unicamp.br

Raquel Gonçalves
Professor, Coordinator of the Laboratory of Nondestructive Testing – LabEND/FEAGRI/UNICAMP, Brazil, e-mail: raquel@feagri.unicamp.br

Bruno Piva Pellis
Master Student, Laboratory of Nondestructive Testing -LabEND/FEAGRI/UNICAMP, Brazil, e-mail: bruno.pellis@feagri.unicamp.br

Abstract

Velocities in trees, logs and beams are different each other. The objective of this work was to adjust, by models, the velocity obtained directly on trees to velocity obtained in logs and beams. We used six eucalyptus trees of three different species. From trees, we obtained the velocity of ultrasonic wave propagation (indirect measurement) and the diameter at breast height (DBH). From the freshly felled logs and beams in green condition we obtained the ultrasonic wave propagation in longitudinal direction (direct measurement). From specimens obtained from the beams we determined the Poisson's ratio by ultrasound. The regression models involving the velocity in the tree, the diameter at breast height and the Poisson's ratio showed coefficient of determination of 99% in predicting the velocity both in logs and beams.

Keywords: diameter at breast height; Poisson's ratio; adjusted velocity.

Introduction

The ultrasound velocity obtained in logs or the beams can predict, more accurately, the wood properties than the velocity obtained directly in standing trees. However, anticipate knowledge of the strength and stiffness properties of the wood from the living tree is important for making decisions in the forestry sector.

Acoustic measurements in standing trees occur differently from those in logs and beams. In standing trees is no access to the ends of the stem, as in the case of logs and beams. So, acoustic waves are introduced from the side surface, generating non uniaxial results of stress state in the stem. Thus, the unidimensional wave equation is not directly valid for trees (Wang, 2013). If the three-dimensional wave is considered for acoustic measurements in the trees, is required the Poisson's ratio (υ) of wood to describe the relationship between the wave velocity and the modulus of elasticity. The tri-dimensional velocity is bigger than the unidimensional wave velocity (Meyers 1994, Wang *et al.*, 2007a). As Poisson's ratio (υ) increase, the difference between tri-dimensional wave and unidimensional wave increase. For example, the relationship between tri-dimensional wave and unidimensional wave is 1.16 for $\upsilon = 0.30$. This relationship goes to 1.46 when the Poisson's ratio increase to 0.40 (Wang, 2013).

Furthermore, the tree is under loading while the beam is free of load, and the distance between transducers normally is smaller during the tests in trees than in beams, which can also cause disturbances in the wave propagation. In standing trees the transducers cannot be positioned at the ends, so, initially, there are surface waves (Rayleigh wave) and shear waves and after longitudinal waves. These conditions make the propagation and the wave dispersion different in trees from logs and beams.

Therefore, the velocity obtained in standing trees is affected by several parameters and in different ways, making its value not numerically equal to that obtained in freshly felled logs or saturated beams.

Thus, the objective of this work was to adjust, using regression models, the value of the velocity obtained directly in trees to values of velocity obtained in logs and beams.

Materials and methods

Material

The sample was composed of 6 trees of three different eucalyptus species (*Eucalyptus grandis*, *Corymbia citriodora* e *Eucalyptus pellita*), 18 logs obtained from these trees, 92 beams obtained from the logs and 12 polyhedrons with 26 faces removed from the beams.

Ultrasound tests in the trees, logs and beams

The ultrasonic tests in trees were performed using ultrasound equipment (AGRICEF, USLab, Brazil) with a 45-kHz dry contact transducer positioned on the same side of the tree (indirect measurement) – Figure 1. The vertical distance between the transducers was 0.70 m, including the breast height (~1.3 m above the ground). To ensure adequate contact between the transducers and the trunk, small holes (~0,003 m) were drilled at the measurements positions in order to remove the bark. The transducers were inserted at the holes an angle (~45º), favoring wave propagation in longitudinal direction (Fig. 1).

The diameter at breast height (DBH) was obtained for all tested trees. Three logs, with 3.5 m long, were obtained from each tree tested. The first log was cut from the base, the second from 7 m above the first one and the third from 14 m above the second one.

Figure 1 – Ultrasound test in the tree.

The ultrasound tests in logs were done in the longitudinal direction (compression wave), with the transducer positioned at the ends. In order to have an overall assessment of the log, the measurements were taken in three different parts of the log cross section, one of them positioned near to the bark, other near to the pith and the last point in the middle of the two ones.

The logs were sawed into beams with a 0.05 by 0.10-m nominal transversal section and 2.5 m long. The beams were tested by ultrasound in the longitudinal direction (compression wave) in green condition. The transducers were positioned at the ends of the beam in three points of the cross section, according to NBR 15521/2007.

The bulk green densities were calculated using freshly sawn wood taken from the logs, which were weighed and measured in this condition. The values used in the evaluations were the average densities of the beams taken from the logs.

Determination of Poisson's ratio

The polyhedrons used for Poisson's ratio determination were tested in the equilibrium moisture content (~12%).

Measurements were performed using ultrasound equipment (EPOCH 4, Panametrics, USA) and longitudinal and shear wave transducers, both with flat faces and 1000 kHz frequency (Figure 2) for determined the stiffness matrix.

The polyhedrons were obtained from 0.07 m edges cubes, oriented according to the longitudinal (L), radial (R) and transversal (T) axis (Figure 2). The dimension of the cub were adopted based on the transducer diameter, which should be confined to each face of the polyhedron.

The wave path length and the time of longitudinal wave propagations in L, R and T directions were used to calculate the compression wave velocities (V_{LL}, V_{RR} e V_{TT}). Considering the same directions, but with shear transducer, the transversals velocities (V_{LR}, V_{LT}, V_{RL}, V_{RT}, V_{TR} e V_{TL}) were calculated. The velocities corresponding to the out off principal symmetry axes was obtained on the faces of the polyhedral specimen cut at 45°.

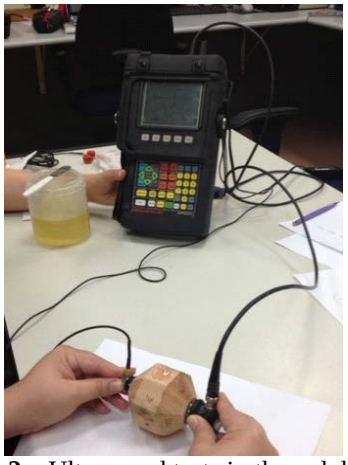

Figure 2 – Ultrasound tests in the polyhedron.

With the velocities we determined the coefficients of stiffness matrix [C] using the Christoffel equations. This inversion of the matrix [C] allowed to determine the compliance matrix [S] which contains all elastic parameters of the orthotropic material.

Determination of Regression Model

We used multiple regression to determining and to test models to adjust the values of the velocity obtained in trees to values of velocities obtained in logs and beams.

Results and discussions

We try to obtain the best regression model (maximum R^2 and minimum error) to infer the velocity in logs and beams by the velocity obtained in living trees The regression model that used the tree velocity (Vt), the Poisson's ratio (υ) and the DBH can explain 99% of the variability of the log velocity (Vl) and the error decrease in 87% when compared with the log velocity regression model considering only the tree velocity (Table 1). Additionally, all parameters considered in the models were statistically significant (Pvalue < 0.05 in Table 1). The smaller prediction error for log velocity prediction (Vl) was obtained by regression model including the velocity in living tree (Vt), the Poisson's ratio, the wood density in green condition (ρ) and the DBH, although υ, ρ and DAP were not statistically significant on the model at 95% significant level (Table 1).

Bertoldo and Gonçalves (2015) concluded that the velocities obtained at base logs are better correlated with the velocities measured in trees than those using the means velocities obtained from the logs of the whole tree. However, including the DBH in regression models the prediction accuracy was the same that those using only the base logs (Bertoldo and Gonçalves, 2015).

To infer velocity in beams (Vb) from velocity in trees (Vt), the insertion of Poisson's ratio, density in the green condition (ρ) and DBH, decrease the prediction error (Table 2). The highest coefficients of determination (R^2) and smallest errors were obtained including Poisson's ratio (υ) in the regression models (Table 2). The variability of the velocity in beams was 99% explained by the regression model that included the tree velocity (Vt), the Poisson's ratio (υ) and the DBH. The error decreased by 98%, compared to the prediction model using only the velocity in trees (Table 2). The inclusion of the density in green condition (ρ) decrease the error, although this parameter was not statistically significant for the model with 95% significance level (Table 2).

Table 1 – Models to predict the velocity in the log (Vl) using the independents variables tree velocity (Vt), Poisson's ratio (υ), bulk green density (ρ) of wood, and diameter at breast height (DBH), and corresponding regression analysis parameters.

Independent variables	Model	P value					R^2 (%)	Error ($m.s^{-1}$)
		Vt ($m.s^{-1}$)	υ	ρ ($kg.m^{-3}$)	DBH (m)	Model		
Vt	Vl = 2073 + 0.32*Vt	-	-	-	-	0.14	46	202
Vt and ρ	Vl = 2648 + 0.34*Vt – 0.70*ρ	0.11	-	0.21	-	0.16	70	172
Vt and DAP	Vl = 2520 + 0.27*Vt – 5.94*DBH	0.31	-	-	0.68	0.36	49	225
Vt and υ	Vl = 2960 + 0.34*Vt – 1308*υ	0.03	0.04	-	-	0.03	90	102
Vt, υ and ρ	Vl = 2977 + 0.33*Vt – 2145*υ + 0.67*ρ	0.06	0.10	0.34	-	0.09	94	93
Vt, υ and DBH	Vl = 2342 + 0.46*Vt – 1837*υ + 12.98*DBH	0.00	0.00	-	0.02	0.01	99	26
Vt, ρ and DBH	Vl = 1526 + 0.58*Vt – 1,68*ρ + 25.51*DBH	0.08	-	0.11	0.21	0.16	89	128
Vt, υ, ρ and DBH	Vl = 2206 + 0.48*Vt – 1617*υ - 0.27*ρ + 15.70*DBH	0.04	0.08	0.44	0.11	0.06	99	24

Table 2 – Models to predict the velocity in the beam (Vb) using the independents variables tree velocity (Vt), Poisson's ratio (υ), bulk green density (ρ) of wood, and diameter at breast height (DBH), and corresponding regression analysis parameters.

Independent variables	Model	P value					R^2 (%)	Error ($m.s^{-1}$)
		Vt ($m.s^{-1}$)	υ	ρ ($kg.m^{-3}$)	DBH (m)	Model		
Vt	Vb = 2720 + 0.37*Vt	-	-	-	-	0.19	39	263
Vt and ρ	Vb = 3752 + 0.40*Vt – 1.26*ρ	0.03	-	0.02	-	0.03	91	116
Vt and DBH	Vb = 4341 + 0.18*Vt – 21.54*DAP	0.45	-	-	0.18	0.16	70	213
Vt and υ	Vb = 4002 + 0.39*Vt – 1891*υ	0.00	0.00	-	-	0.00	99	28
Vt, υ and ρ	Vb = 3996 + 0.39*Vt – 1594*υ – 0.24*ρ	0.00	0.01	0.14	-	0.00	99	17
Vt, υ and DBH	Vb = 4172 + 0.36*Vt – 1745*υ – 3.57*DBH	0.00	0.00	-	0.01	0.00	99	5
Vt, ρ and DBH	Vb = 3428 + 0.47*Vt – 1,54*ρ + 7.36*DBH	0.12	-	0.14	0.66	0.12	92	133
Vt, υ, ρ and DBH	Vb = 4139 + 0.36*Vt – 1691*υ – 0.06*ρ – 2.90*DBH	0.00	0.01	0.14	0.04	0.00	99	2

The expected velocity in logs using the regression model including all statistically significant parameters (Vt, υ and DBH – Table 1) was named adjusted log velocity (Vl, adjust). The differences between the velocity in trees and logs and the adjusted log velocity and log velocity decreases for all species studied in this research (Figure 3). The mean relation between velocities (k), considering all trees of all species, were from 1.37 to 1.00 using the adjusted velocity instead of the tree velocity (Figure 3).

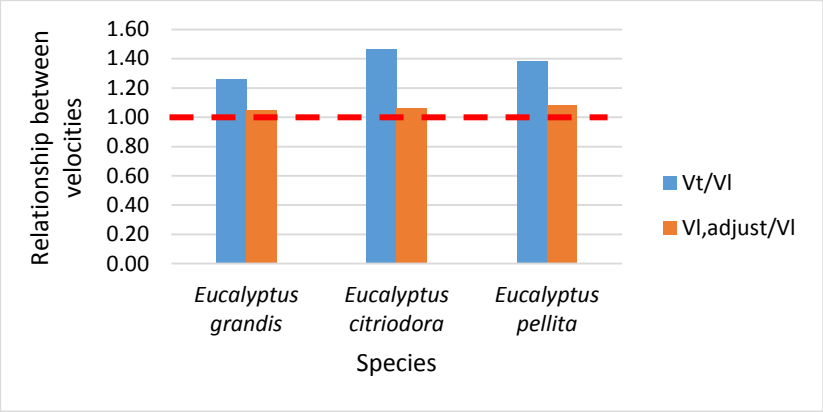

Figure 3 – Relationship between tree velocity (Vt) and log velocity (Vl) and between adjusted velocity in the log (Vl, adjust) and log velocity (Vl).

Wang et al. (2007b) present a linear regression model to correlate the velocity in trees and logs with a coefficient of correlation (R) ranging between 0.84 and 0.97. The coefficient of correlation (R) obtained by Bertoldo (2011) for the regression model to correlate tree and log velocities was 0.91. Gonçalves et al. (2011) obtained coefficients of correlation R = 0.93 for linear regression models to correlate the ultrasound velocity in the tree and the ultrasound velocity in the log. Bertoldo e Gonçalves (2015) obtained coefficients of correlation R = 0.89 to regression models to correlate velocity in the tree and average velocity obtained for all removed logs from the tree and, obtained R = 0.92 when regression model was between the velocity in the tree and the velocity only in the log base.

The mean relation (k) between velocities, considering all species was from 1.11 (Vt/Vb) to 1.00 (Vb, adjust/Vb) using the adjusted beam velocity instead the tree velocity (Figure 4).

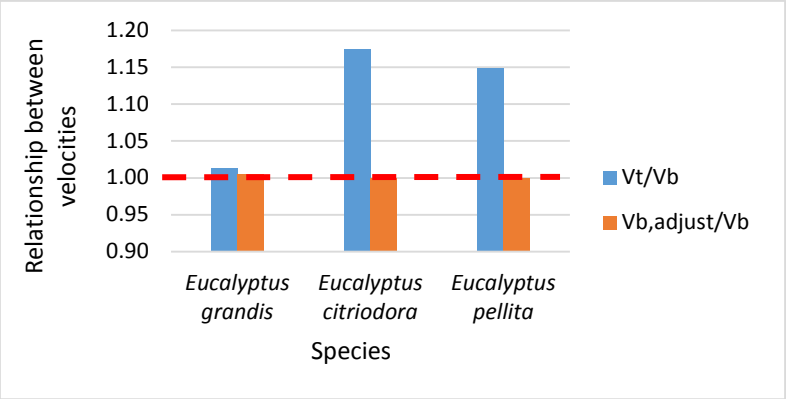

Figure 4 – Relationship between tree velocity (Vt) and beam velocity (Vb) and between adjusted velocity in the beam (Vb, adjust) and beam velocity (Vb).

Conclusion

Velocities obtained indirectly in standing trees, adjusted by regression models including the Poisson's ratio (υ) and the DBH, allow to infer the direct velocity in logs and in beams with coefficient of determination R^2 = 99%. The prediction errors are minimized if it is included the bulk green density (ρ) on the regression model.

Acknowledgement

The authors thank the São Paulo Research Foundation (FAPESP) for the PhD scholarship (Process: 2011/00904-1), the National Council for Scientific and Technological Development (CNPq) for Research Scholarship (306751/2011-9) and Dr. Mario Tomazello (Esalq/USP–Piracicaba, SP, Brazil) for the trees donation.

References

Bertoldo, C. 2011. Estimativa de propriedades de rigidez da madeira a partir de avaliação acústica na árvore e em toras recém abatidas. 2011. 85 f. Dissertação (Mestrado) - Faculdade de Engenharia Agrícola - Feagri, Universidade Estadual de Campinas - Unicamp, Campinas.

Bertoldo, C; Gonçalves, R. 2015. Influence of measurement Position, tree diameter, and bulk wood density on models that predict wave propagation velocity in logs according to the velocity in trees. Forest Products Journal, v. 65, nº3, p. 1-7.

Chauhan, S. S.; Walker, J. C. F. 2006. Variations in acoustic velocity and density with age, and their interrelationship in radiate pine. Foret Ecology and Management, v. 229, p. 388-394.

Gonçalves, R.; Bertoldo Pedroso, C.; Massak, M. V.; Batista, F.; Secco, C. B. 2011. Technical note: Velocity of ultrasonic waves in live trees and in freshly-felled logs. Wood and Fiber Science, v. 43, n. 2, p. 232-235.

Meyers, M. A. 1994. Dynamic behavior of materials. New York: John Wiley & Sons.

Wang, X.; Carter, P.; Ross, R. J.; Brashaw, B. K. 2007a. Acoustics assessment of wood quality of raw forest materials. Forest Products Journal, v. 57, p. 6-14.

Wang, X.; Ross, R. J.; Carter, P. 2007b. Acoustic Evaluation of Wood Quality in Standing Trees. Part 1. Acoustic Wave Behavior. Wood Science and Technology, p. 28-38.

Wang, X., S. Verrill, E. Lowell, R. J. Ross, and V. L. Heriant. 2013. Acoustic sorting models for improved log segregation. Wood Fiber Sci. 45:343–352.

Prediction of strength and stiffness of wood in bending using adjusted ultrasound velocities in standing trees

Cinthya Bertoldo
Assistant Professor, Laboratory of Nondestructive Testing - LabEND, College of Agricultural Engineering - FEAGRI - University of Campinas - UNICAMP, Brazil
email: cinthya.bertoldo@feagri.unicamp.br

Raquel Gonçalves
Professor, Coordinator of the Laboratory of Nondestructive Testing – LabEND/FEAGRI/UNICAMP, Brazil, e-mail: raquel@feagri.unicamp.br

Esther Merlo Sanchez
Empresa Madeira Plus, Galícia, Spain, e-mail: esther.merlo.sanchez@gmail.com

Oscar Santaclara
Empresa Madeira Plus, Galícia, Spain, e-mail: oscar.santaclara@gmail.com

Paulo G. Krejci Nunes
Agricultural Engineer, Technician of the Laboratory of Materials and Structures – LME/ FEAGRI/UNICAMP, Brazil, e-mail: paulo.nunes@feagri.unicamp.br

Abstract

Anticipating knowledge of the strength and stiffness properties of the wood from the living tree is important for decision-making in the forestry sector. The objective of this study was to validate the power of models, obtained in previous researches, which adjust the velocity obtained in the tree to predict the strength and stiffness of wood in bending. These models are based on the velocity obtained on live trees, the diameter at breast height (DBH) and the Poison's ratio. We tested the model using 20 Eucalyptus and Pinus trees. The correlation between the adjusted velocity and the modulus of rupture (f_m) and modulus of elasticity (E_M) was statistically significant with coefficient of determination R^2 = 87% and R^2 = 88%, respectively.

Keywords: velocity in log; velocity in beam; wood properties.

Introduction

The forest sector is looking forward to anticipate the knowledge of wood properties. If with measurements taken in living trees were possible to predict the qualities of the wood, the forest sector could give best destination to all material. Besides, the tree that the material do not meet the minimum quality required for a particular application could continue in the forest, avoiding, in this case, the tree cut.

The wave propagation methods are being widely used and accepted to predict the quality of wood from tests performed in the tree and/or in the log (Huang et al., 2003; Andrews, 2000; Dyck, 2002; Tsehaye et al., 2000a e b; Yin et al., 2010; Gonçalves et al., 2011; Wang et al., 2007a e b, Ross et al., 1997; Amishev e Murphy, 2008; Carter et al., 2005; Wang, 2013).

From tests in living trees, Wang et al. (2007 b) concluded that the precision obtained with wave propagation technology is sufficient to predict the wood quality and properties and correlate it with the structural performance of the final products. However, researches in this area (Tsehaye et al., 2000 a e b; Wang et al., 2007b; Wang et al., 2004; Wang et al., 2000; Gonçalves et al., 2011) showed that there were differences between the velocity wave propagation obtained in trees and in freshly felled logs of the same trees. The velocity in tree is, generally, higher than velocity in logs. Furthermore, the ultrasound velocity obtained in logs or in beams predicts, with greater precision, the wood properties than that obtained directly from living trees. According to the authors, these velocities variations can be justified by the mechanisms of the wave's propagation. The waves propagation would be influenced by the type of measurement (indirect in trees and direct in logs), the diameter and the age of the trees (higher proportion of juvenile and adult wood) and, also, by the static layout of the tree (cantilever).

The objective of this study was to validate the power of models obtained in previous researches, which use adjusted velocity from velocity and other parameters obtained in trees, to predict the strength and stiffness of wood in bending.

Materials and methods

Material

For the research we used 360 beams from 5 *Eucalyptus grandis* trees, from forest located in Lençóis Paulista/Brazil, 3 *Pinus pinaster* trees from forest located in La Coruña (Galícia/Spain), and 12 *Pinus elliottii* trees, with age from 8 to 23 years old, from forest located in Caçador/Brazil, (Table 1).

Table 1 - Species, number of trees (NT), ages, mean diameter at breast height (mean DBH), number of logs (NL) and number of beams (NB).

Species	NT	Age (years)	Mean DBH (m)	NL	NB
Eucalyptus grandis	5	34	0.54	15	255
Pinus pinaster	3	40	0.42	6	15
*Pinus elliottii**	12	8 to 23	0.26	28	90
Total	20	-	-	49	360

Ultrasound tests in standing trees

The ultrasonic tests in standing trees were performed using ultrasound equipment (AGRICEF, USLab, Brazil) with 45-kHz dry contact transducer positioned on the same side of the trunk (indirect measurement). The distance between the transducers was near 0.70 m, including the position of the breast height (~1.3 m above the ground). To ensure adequate contact between the transducers and the trunk, small holes (~0,003 m) were drilled at the measurements positions, in order to remove the bark. The transducers were inserted at the holes at an angle (~45º) favoring longitudinal wave propagation (Fig. 1).

The diameter at breast height (DBH) was obtained for all tested trees. Three logs, with 3.5 m long, were obtained from each tree tested. The first log was cut from the base, the second log 7 m above the first one and the third log 14 m above the second one. For each log was removed the largest number of beams with a 0.05 by 0.10 m nominal transversal section and lengths of 2.5 m.

Figure 1 – Tree measurement with ultrasound.

Bending tests

The beams were dried in chamber with control of relative humidity and temperature, until they reached ~12% of moisture content. Beams were tested in bending to determine the modulus of elasticity (E_M) and of rupture (f_m). The bending tests were performed according to ASTM D198-08 (2008).

The beams were tested in hydraulic framework (capacity 500 kN) with loads and displacements of the beam's center point obtained using a data acquisition system (Quantun, HBM, Germany) with 8 channels. The load cell and the electronic linear position transducer (0.001 mm resolution) were coupled in this system, allowing automated reading during the test.

The f_m and E_M were calculated according to ASTM D198-08 (2008). In this standard the f_m is calculated using the maximum load (P_{max}) absorbed by the beam (Equation 1).

$$f_m = \frac{3P_{\max}L}{2bh^2} \quad (1)$$

L is the span ; b is the width of the beam and h is the height of the beam.

The E_M was determined using the linear portion of the graph load x vertical displacement (Equation 2).

$$E_M = \frac{(P_{40\%} - P_{20\%})L^3}{4bh^3(\Delta_{40\%} - \Delta_{20\%})} \quad (2)$$

$P_{20\%}$ and $P_{40\%}$ are the corresponding loads at 20% and 40% from the maximum load P_{max}; $\Delta_{20\%}$ e $\Delta_{40\%}$ are the corresponding displacements to the loads $P_{20\%}$ e $P_{40\%}$; L is the span of the beam.

Regression models to obtain the Adjusted Velocity

The regression models to obtain the adjusted velocities, proposed by Bertoldo & Gonçalves (2015) – Equation 3 – and by Bertoldo (2014) – Equations 4 and 5, were tested to verify if its use can improve the correlation between the velocity obtained in standard tress and the strength and stiffness of wood.

$$V_{adjust1} = 671 + 0.46*V_t + 27.6*DBH \quad (3)$$

$$V_{adjust2} = 2342 + 0.46*V_t - 1837*\upsilon + 12.98*DBH \quad (4)$$

$$V_{adjust3} = 4172 + 0.36*V_t - 1745*\upsilon - 3.57*DBH \quad (5)$$

Where: V_t = velocity obtained in standard trees; υ = Poisson's ratio and DBH = diameter at breast height.

The models V_{ajust1} and V_{ajust2} were determined using the correlation between the velocity in standing trees and the velocity obtained in logs while the model V_{ajust3} were determined by the correlation between the velocity obtained in standing trees and the velocity obtained in beams.

As we did not have the Poisson's ratio (υ) of the wood from the tested trees, we use the correlation model ($\upsilon = 0.0006*\rho+0.14$) between the Poisson's ratio and the density (ρ), proposed by Bertoldo (2014). This model is statistically significant (P-value = 0.0165) with coefficient of correlation R = 0.89 and 6% of relative error.

Analysis of Results

The correlation between velocity of ultrasound wave propagation, obtained in living trees, and modulus of rupture (f_m) and of elasticity (E_M) obtained from bending tests in beams, were compared to the correlations of the adjusted velocities and the same parameters (f_m e E_M), in order to check if the adjustment has improved the prediction power of the ultrasound tests in living tree.

Results and discussions

The velocity obtained in standing trees (V_t) explain 79 percent of the variation of the modulus of elasticity obtained in beams (f_m) while the adjusted velocities using Equations 3 and 4 explain 87% e 82%, respectively (Table 2). Only the Model 1 (Equation 3) lowers the error of the regression. The Model 3 (Equation 5) reduced the correlation coefficients and increased the error compared with the use only the velocity obtained in standing trees (Vt).

For the modulus of elasticity (E_M), the velocity obtained in standing trees (V_t) explain 84% of its variation while the adjusted velocities (Equations 3 and 4) explain 86% e 88% %, respectively (Table 3). Also in this case, the Model 3 (Equation 5) reduced the coefficient of correlation and increased the regression error compared with the use only the velocity obtained in standing trees (Vt).

Table 2 – Regression models to predict the modulus of rupture in bending (f_m) using as independent variables the velocity in standing trees (V_t) and using adjusted velocities 1, 2 and 3 ($V_{adjust1}$, $V_{adjust2}$ e $V_{adjust3}$, respectively).

Models for predict f_m	R	R^2 (%)	P-value	Error (MPa)
$f_m = 26.4 + 0.0084*V_t$	0.89	79	0.000	7
$f_m = 13.1 + 0.0128*V_{adjust1}$	0.93	87	0.000	6
$f_m = 11.9 + 0.0135*V_{adjust2}$	0.90	82	0.000	7
$f_m = -27.3 + 0{,}0199*V_{adjust3}$	0.85	72	0.000	8

Table 3 – Regression models to predict the modulus of elasticity in bending (E_M) using as independent variables velocity obtained in standing trees (V_t) and using adjusted velocities 1, 2 and 3 ($V_{adjust1}$, $V_{adjust2}$ e $V_{adjust3}$, respectively).

Models for predict E_M	R	R^2 (%)	P-value	Error (MPa)
$E_M = 1144.5 + 2.76*V_t$	0.91	84	0.000	2015
$E_M = -2096.8 + 3.72*V_{adjust1}$	0.93	86	0.000	1700
$E_M = -2907.5 + 4.07*V_{adjust2}$	0.94	88	0.000	1614
$E_M = -17145.1 + 6.68*V_{adjust3}$	0.90	82	0.000	2132

Regarding the improvement of the coefficient of determination (R^2) obtained from use $V_{adjust1}$ and $V_{adjust2}$ (Tables 2 and 3) and considering the difficulty to obtain the Poisson's ratio, the DBH inclusion (Model 1, Equation 3) appears to be enough to improve the prediction power of the f_m and the E_M from tests in standing trees. The adjusted velocity by Model 3 (Equation 5) was not appropriate in no case.

The literature shows that many authors have studied the correlations between the velocity obtained directly in standing trees and the strength and stiffness properties of wood, indicating that this is an important question. Bertoldo (2014) using 26 trees of different species of eucalyptus and pine and 452 beams obtained from these trees, show that the velocity obtained in standing trees explained 62% of the strength and 67% of the stiffness. Auty and Achim (2008), using 11 trees and 40 specimens for the bending tests, presented values of R=0.77 for correlation between velocity in standing trees and strength properties and R=0.73 between velocity in standing trees and stiffness properties. Bending tests in pieces obtained from 56 trees of *Tsuga heterophylla* and *Picea sitchensis*, made by Wang et al. (2001) resulted in coefficient of correlation R = 0.66 and R = 0.64 between velocity in standing tree and stiffness and strength, respectively. These results shown that wave propagation tests in standing trees has potential to predict the strength and stiffness properties of the wood. As discussed in this paper, the prediction of the properties of wood, using the velocity in standing trees can become even better with adjustments, by inserting other parameters associated to the tree in regression models.

Conclusions

The adjusted velocity, obtained by inclusion, further the velocity in standing trees, the DBH and the Poisson's ratio, allowed to predict the strength and stiffness properties of the wood with more accuracy than that obtained using only the velocity in standing trees.

Acknowledgments

The authors thank the São Paulo Research Foundation (FAPESP) for the PhD scholarship (Process: 2011/00904-1) and the National Council for Scientific and Technological Development (CNPq) for Research Scholarship (306751/2011-9), Rotta Madeiras (Caçador, Santa Catarina, Brazil) and Duraflora (Lencóis Paulista, SP, Brazil) for trees donation, and Dr. Mario Tomazello (Esalq/USP–Piracicaba, SP, Brazil) and Esther Merlo (Madeira Plus Calidad Forestal, Galicia, Spain) for their collaboration.

References

American Society for Testing and Materials. 2008. ASTM D198-08: Static tests of Timbers in Structural Sizes. Philadelphia, Pa, USA.

Amishev, D.; Murphy, G. E. 2008. In-forest assessment of veneer grade Douglas-fir logs based on acoustic measurement of wood stiffness. Forest Products Journal, Inist-cnrs, Cote Inist, v. 58, n. 11, p. 42-47.

Andrews, M. 2000. Where are we with sonics? In: Proceedings, Capturing the benefits of forestry research: Putting ideas to work, Workshop 2000. Wood Technology Research Center, University of Canterbury. p. 57-61.

Auty, D.; Achim, A. 2008. The relationship between standing tree acoustic and timber quality in Scots pine and practical implications for assessing timber quality from naturally regenerated stands. Forestry, p. 475-487.

Bertoldo, C. 2014. Propriedades de resistência e de rigidez da madeira obtidas a partir de avaliação acústica na árvore. 122 f. Tese (Doutorado) - Faculdade de Engenharia Agrícola - Feagri, Universidade Estadual de Campias - Unicamp, Campinas.

Bertoldo, C; Gonçalves, R. 2015. Influence of measurement Position, tree diameter, and bulk wood density on models that predict wave propagation velocity in logs according to the velocity in trees. Forest Products Journal, v. 65, nº3, p. 1-7.

Carter, P.; Briggs, D.; Ross, R. J.; Wang, X. 2005. Acoustic testing to enhance western forest values and meet customer wood quality needs. PNW-GTR-642, Productivity of Western Forests: A Forest Products Focus. USDA Forest Service, Pacific Northwest Research Station, Portland, Oregon, p. 121-129.

Dyck, B. 2002. Precision forestry – the path to increased profitability! In: Proceedings, The 2nd International Precision Forestry Symposium. Seattle, Washington, USA. University of Washington, Seattle, Washington, p. 3-8.

Gonçalves, R.; Bertoldo Pedroso, C.; Massak, M. V.; Batista, F.; Secco, C. B. 2011. Technical note: Velocity of ultrasonic waves in live trees and in freshly-felled logs. Wood and Fiber Science, v. 43, n. 2, p. 232-235.

Huang, C.; Lindström, H.; Nakada, R.; Ralston, J. 2003. Cell wall structure and wood properties determined. *Holz Als Roh- Und Werkstoff*, p. 321-335.

Ross, R. J.; Mcdonald, K. A.; Green, D. W.; Schad, K. C. 1997. Relationship between log and lumber modulus of elasticity. Forest Products Journal, p. 89-92.

Tsehaye, A.; Buchanan, A. H.; Walker, J. C. F. 2000a. Selecting trees for structural timber. Holz Als Roh- Und Werkstoff, Springer Berlin, p. 162-167.

Tsehaye, A.; Buchanan, A. H.; Walker, J. C. F. 2000b. Sorting of logs using acoustics. Wood Science and Technology, Springer Berlin, p. 337-344.

Wang, X. 2013. Acoustic Measurements on Trees and Logs: a Review and Analysis. Wood Sci Technol. 47: 965-975.

Wang, X.; Carter, P.; Ross, R. J.; Brashaw, B. K. 2007a. Acoustics assessment of wood quality of raw forest materials. Forest Products Journal, v. 57, p. 6-14.

Wang, X.; Ross, R. J.; Carter, P. 2007b. Acoustic Evaluation of Wood Quality in Standing Trees. Part 1. Acoustic Wave Behavior. Wood Science and Technology, p. 28-38.

Wang, X.; Ross, R. J.; Brashaw, B. K.; Punches, J.; Erickson, J. R.; Forsman, J. W.; Pellerin, R. F. 2004. Diameter effect on stress-wave evaluation of modulus of elasticity of small-diameter logs. Wood Fiber Sci. 36(3):368–377.

Wang, X.; Ross, R. J.; Mcclellan, M.; Barbour, R. J.; Erickson, J. R.; Forsman, J. W.; Mcginnis, G. D. 2001. Nondestructive Evaluation of Standing Trees with a Stress Wave Method. Wood and Fiber Science, p. 522-533.

Wang, X.; Ross, R. J.; Mcclellan, M.; Barbour, R. J.; Erickson, J. R.; Forsman, J. W.; Mcginnis, G. D. 2000. Strength and Stiffness Assessment of Standing Trees Using a Nondestructive Stress Wave Technique. Research Paper FPL−RP−585. p. 1-9.

Yin, Y.; Nagao, H.; Liu, X.; Nakai, T. 2010. Mechanical properties assessment of *Cunninghamia lanceolata* plantation. J Wood Sci, p. 33-40.

Measures of crystallinity as a non-destructive indicator of wood hardness: Study on young fast grown plantation teak planted in dry and wet sites

Ratih Damayanti[1,2]
[1]Dept. of Forest and Ecosystem Sciences, The University of Melbourne, Burnley Campus, Richmond, Victoria, Australia; [2]The Center for Research and Development on Forestry Engineering and Forest Product Processing, FORDA, Ministry of Forestry, Bogor, Indonesia, rdamayanti@student.unimelb.edu.au/ratih_turmuzi@yahoo.com

Graham Brodie
Faculty of Veterinary and Agricultural Sciences, The University of Melbourne, Dookie Campus, Dookie, Victoria, Australia, grahamb@unimelb.edu.au

Jugo Ilic
Dept. of Forest and Ecosystem Sciences, The University of Melbourne, Burnley Campus, Richmond, Victoria, Australia, knowyourwood1@gmail.com

Barbara Ozarska
Dept. of Forest and Ecosystem Sciences, The University of Melbourne, Burnley Campus, Richmond, Victoria, Australia, bo@unimelb.edu.au

Gustan Pari
The Center for Research and Development on Forestry Engineering and Forest Product Processing, FORDA, Ministry of Forestry, Bogor, Indonesia, gustanp@yahoo.com

Peter Vinden
Dept. of Forest and Ecosystem Sciences, The University of Melbourne, Burnley Campus, Richmond, Victoria, Australia, pvinden@unimelb.edu.au

Abstract

Models for predicting wood hardness based on ultra-structural characteristics have been developed using crystallinity and other quantifiers of the cellulosic nature of wood including: degree of crystallinity (DC), crystallite dimension (width and length) and Micro Fibril Angle (MFA). Five factors, including sites (2 levels), ages (2 levels), tree diameter classes (3 levels), axial positions within tree (7 levels), and radial positions (3 levels) were analyzed using four response (dependent) variables: radial hardness, tangential hardness, side hardness and end-grain hardness. A study was conducted on five and six year old fast grown plantation teak. Variable selection and model development was carried out using Stepwise Multiple Regression and quadratic curve fitting with Matlab®. The results revealed that wood hardness along different structural directions was influenced by different ultramicroscopic characters of wood crystallinity. It was found that the DC was positively related only to end-grain hardness, while crystallite dimensions, mainly crystallite width and MFA, were negatively correlated to hardness along all structural directions. The proposed models offer intermediate power of prediction with adjusted R^2 values in the range of 0.53 and 0.63 when air dry density is included among the prediction variables.

Keywords: wood ultrastructure, crystallinity, NDT, young teak, Matlab

Introduction

Cellulose is the main component of wood, and occurs primarily in the S2 layer as a skeletal polysaccharide in the cell wall (Williams, 2005, Pereira et al., 2003). The cellulose molecules are combined into bundles termed microfibrils. The regular nearly parallel arrangement of the cellulose molecules forms crystalline cellulose/crystallites (Panshin et al., 1964). Cellulose microfibrils are not totally crystalline, but there are regions with a less ordered arrangement of the cellulose molecules, called amorphous region, occur along the chain length as well as across the chain. In wood, it is estimated that about 70% of the cellulose is crystalline (Pereira et al., 2003, Williams, 2005).

Wood crystallinity is defined as the weight fraction of crystalline material in wood (Jiang et al., 2007). It is an important property of woody materials that is affected by tree growth, anatomical structure, chemical properties, and is related to Young's modulus, dimensional stability, density, and hardness (Jiang et al. (2007) and Qu and Wang (2011)). Reportedly these properties increase with increasing crystallinity (Stuart and Evans, 1994, Jiang et al., 2007, Lee, 1961), while moisture regain, dye sorption, chemical reactivity, swelling, and flexibility decrease with decreasing crystallinity (Jiang et al., 2007, Lee, 1961).

Study of crystallinity by X Ray Diffracton (XRD) for genetic tree improvement programs includes two significant benefits: speed and accuracy (Hein and Brancheriau, 2011). Thus, the approach can be applied to develop non-destructive testing procedures for predicting wood properties which are usually carried out by routine destructive methods.

A study to relate Micro Fibril Angle (MFA) to wood hardness was conducted by Tze et al. (2007). By plotting ten longitudinal hardness of loblolly pine (*Pinus taeda* L.) wood as a function of Micro Fibril Angle (MFA), a high negative correlation was observed. However, they concluded that the relationship between wood hardness and MFA was orientation dependent; the preliminary indication was that - it could be caused by different amounts of cell wall extractives between the heartwood and sapwood regions. Thus, several of the data points which originated from the heartwood region as outliers were excluded.

Predicting of wood hardness using crystallinity and its quantifiers, that is, degree of crystallinity, crystallite dimension, and MFA using XRD has been developed by Damayanti et al. (2015). The study was conducted on 5-year old fast grown teak planted in Bogor, West Java, Indonesia. The study confirmed that hardness increases with increasing crystallinity in line with the findings from Jiang et al. (2007) and Lee (1961) which only referred to degree of crystallinity not the other crystallinity quantifiers. This current paper aims to explore crystallinity and other quantifiers of the cellulosic nature of wood fibres measured using XRD as a non-destructive indicator of wood hardness, and to study the relationships between crystallinity and wood hardness of fast grown plantation teak to investigate its growth characteristics across sites and different ages.

Materials and methods

Specimen preparation

Twenty tree stems ranging from small, medium and large diameter of 5- and 6-year old fast grown teak plantations in Indonesia (Table 1) were chosen and felled for wood hardness measurement using the Janka method (Mack, 1979). Bogor, West Java (Site 1) and Magetan, East Java (Site 2), were selected for representing wet and dry site plantations respectively. The average temperature and humidity of Site 1 and Site 2 are 26°C/ 83% and 27°C/77%, respectively. The average annual rainfall is 3,667 mm for Site 1, and 2,330 for Site 2. The number of rain months are 12 months and 9 months for Site 1 and Site 2, respectively, and the average number of rain days are 23 days per month for Site 1, and 16 days per month for Site 2.

One of the aims of the study was to develop non-destructive testing technique requirements for optimal sampling height. Raymond and Muneri (2001) who developed methods for whole tree sampling of wood properties for pulping indicated that samples should be easy to reach from the ground, be at a fixed convenient height above ground, and provide a high correlation with whole tree properties if they exhibit a large degree of variation that could have practical implications for the use of the wood. The test and sampling procedure are described in detail in Damayanti et al. (2015). From that study the optimal height representing the whole tree hardness was determined to be 130 cm above ground (BH-Breast Height). A total of 140 discs were cut and used for hardness and crystallinity assessments.

Table 1—Selected tree samples for hardness and crystallinity measurement

No	Tree code	Diameter [cm]	Height* [m]	Tree code	Diameter [cm]	Height* [m]
	Site 1: Wet (Bogor, West Java)			Site 2: Dry (Magetan, East Java)		
Class Diameter 1: large (>26 cm)						
1	SA22	30.25	16.00	K198	29.3	10.5
2	AC18	31.4	18.20	S12	29.3	12
3	AC23	32.2	13.60	S101`	28.7	9.2
Class Diameter 2: medium (17-25 cm)						
1	S 50	20.7	11.50	S108	21.5	8.5
2	S 74	21.3	9.10	S153	24.2	6.5
3	S 105	22.9	11.40	S78	24.5	8.65
Class Diameter 3: small (10-16 cm)						
1	S 89	14.3	9.65	S27	14.3	6.4
2	S 53	11.9	8.90	S2	16.6	6.7
3	S 120	14.6	10.10	S10	16.2	5.8
6-year old trees						
1				M73	27.7	10
2				Y56	27.4	12

*Economic height: height measured in the stem at top with diameter minimum 7 cm

Testing

Up to twenty samples (depend on the tree stem diameter), measuring 50x50x150 mm for Site 1 and 30x30x90 mm for Site 2, were prepared from each disc. These samples were identified as heartwood (HW), transition (TZ) and sapwood (SW) on the basis of wood color, and measured for hardness testing using the standard Janka test (employing an Instron® universal strength testing machine) according to the Australian Standards for mechanically testing small clear specimens of timber (Mack, 1979). Wood hardness was tested in the radial (R hardness), tangential (T hardness) and longitudinal (E hardness) grain directions. The reason for testing all faces was to ensure a more representative value of each specimen (Green et al., 2006), and to enable radial and tangential hardness to be tabulated as side hardness.

Three end matched specimens from each disc used for hardness measurements were used for crystallinity measurements. The samples were 50 mm (tangential direction) x 15 mm (longitudinal direction) and 30-40 µm (radial direction). Crystallinity and its quantifiers were measured using X-Ray Diffraction (XRD) (Shimadzu®). The X-ray beam was powered with a 40kV, 30mA source and scans made in the range from 0-40 degrees at a scan speed of 2 degrees per minute. The degree of crystallinity (DC) was calculated as the ratio between the crystalline and total-crystalline and

amorphous regions as shown in Figure 1. The dimension of crystallites (CW-width and CL-length) was determined using the Scherrer formula (Peura et al., 2008) at diffraction intensities (200) and (004) in the angular range from 20 to 24 degrees and from 32 to 37 degrees, respectively (Abe and Yamamoto, 2005). MFA was determined from the 200 reflection plane, and calculated by using equations in Stuart and Evans (1994) developed by Meylan (1967): MFA = 0.6 T, the T parameter was calculated according to Stuart and Evans (1994). Both hardness and crystallinity tests were conducted at Forest Product Testing Laboratory, The Center for Research and Development on Forestry Engineering and Forest Product Processing (FORDA), and Faculty of Forestry, Bogor Agricultural University, Bogor, Indonesia.

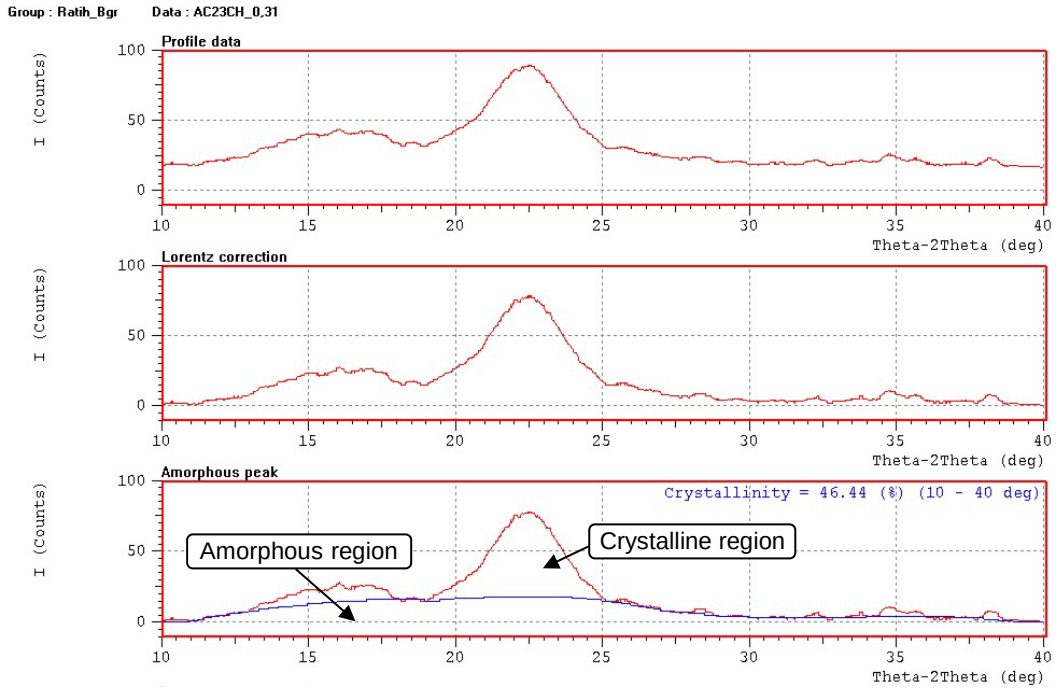

Figure 1—Data profile for Degree of Crystallinity (DC) measurement (Damayanti et al., 2015)

Data analysis

Models for predicting wood hardness were required to accommodate variations between sites, between ages, between tree diameter classes, and variations at different axial and radial positions. Shapiro Wilk-W Test (Statistica®), was used to test for normality of the data. Analysis of variance (ANOVA) was applied to test the variation between sites, ages, tree diameter classes, and different axial and radial positions using Statistica®.

Five independent variables and their transformations were applied to develop models for predicting wood hardness using Stepwise Multiple Regression, and a quadratic curve fitting was undertaken with MATLAB R2014a®. The five independent variables were: air dry density, Degree of Crystallinity (DC), crystallite width (CW), crystallite length (CL) and Micro Fibril Angle (MFA).

Results and Discussion

Wood hardness variation between sites, diameter classes, axial and radial positions

According to normality tests using the Shapiro Wilk-W Test (Statistica®), the data for radial and end-grain hardness were normally distributed (p=0.78 and p=0.81, respectively), while tangential and side hardness were not normally distributed (p= <0.001 and p=0.02, respectively).

Information on the variation between different plantation sites, age, tree diameter, axial and radial positions is very important for developing non-destructive tests (NDT) for predicting wood hardness and should accommodate these variations.

The wet site plantation produced significantly lower wood hardness than the dry site (Figure 2). Even though there was only one year difference between the plantations, the 6-year old fast grown teak plantation already produced significantly harder end-grain wood, but the increases for radial, tangential and side hardness (Figure 3) were not significant. Moreover and in general, small diameter trees of the same age produced statistically significant side hardness increases, but not end-grain hardness (Figure 4).

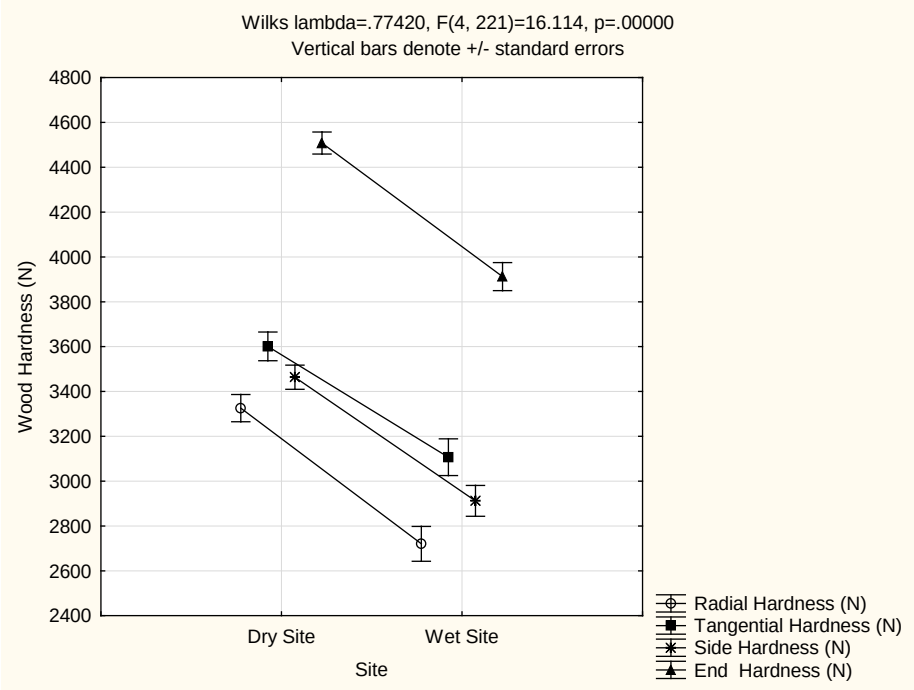

Figure 2—Whole tree wood hardness variation between dry and wet sites

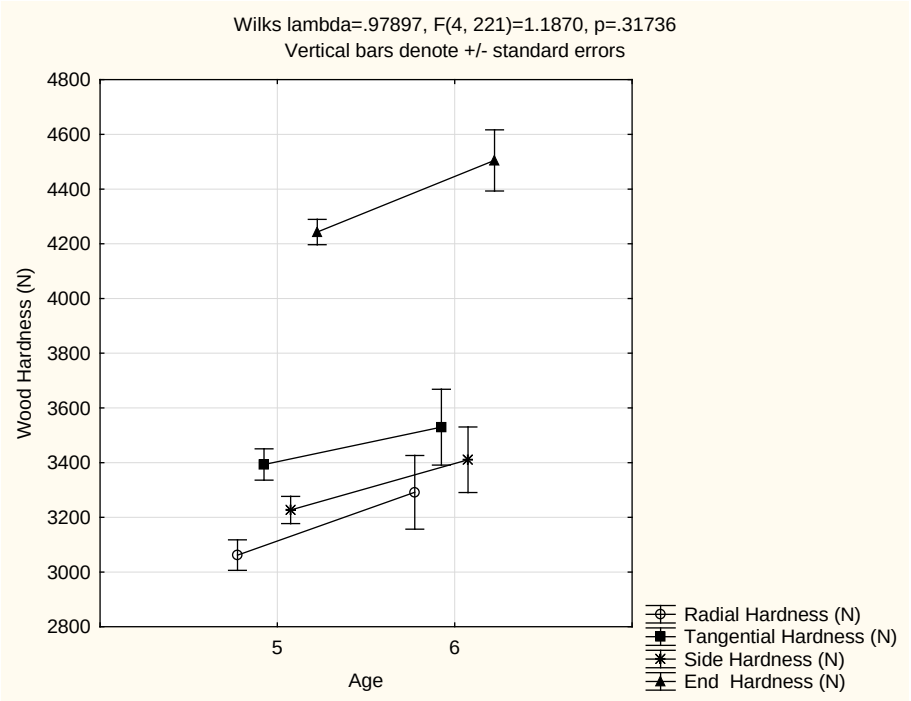

Figure 3—Whole tree wood hardness variation between 5- and 6-year old fast grown teak trees

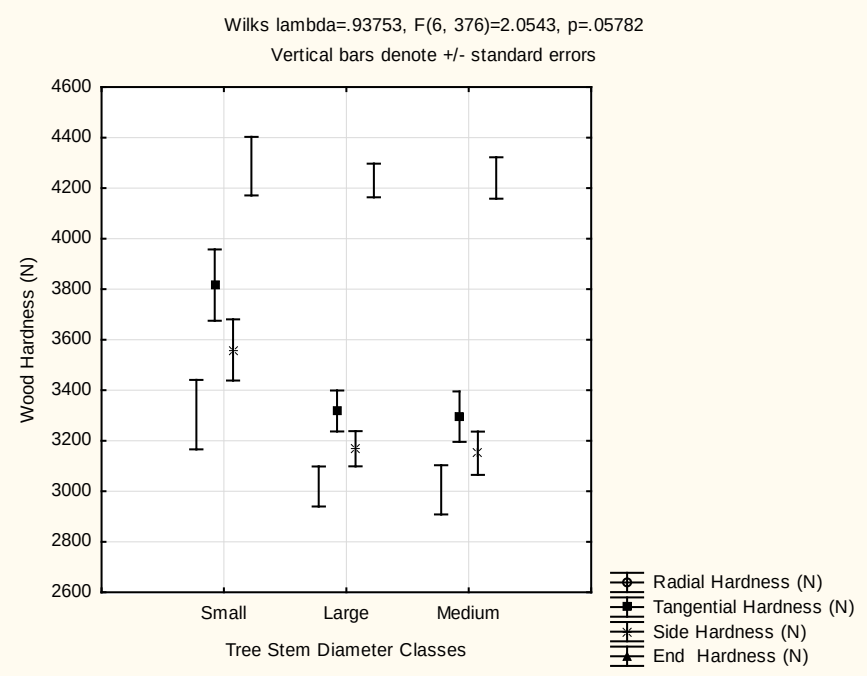

Figure 4—Whole tree wood hardness variation between different tree stem diameter classes

Furthermore, it was possible to fit parabolic relationships to the hardness data at different axial positions (Figure 5); the wood hardness was higher at the bottom, decreased with height to 120-130 cm above ground, then increased in the middle and top part of the tree. However, overall the axial wood hardness variations were not statistically significant.

On the other hand, radial variation showed that the transition zone had significantly higher wood hardness than the sapwood and heartwood zones. Even though the trees are still of a young age, they produced heartwood but the corresponding hardness was not consistently higher than that from the sapwood (Figure 6). The heartwood development of this very fast grown teak will be reported elsewhere.

The result was in line with Merela and Čufar (2013) who reported that hardness of mature white oak (*Qercus robur* or *Q. petrea*) and red oak (*Quercus cerris*) was not different between the heartwood and sapwood zones. The variation of wood hardness in the radial position can be explained by the variation of the air dry density (Figure 7). Density is positively correlated with wood hardness (Bustos et al., 2009, Thomas et al., 2009). In this study, density was significantly higher in the transition zone than that from the heartwood and sapwood regions.

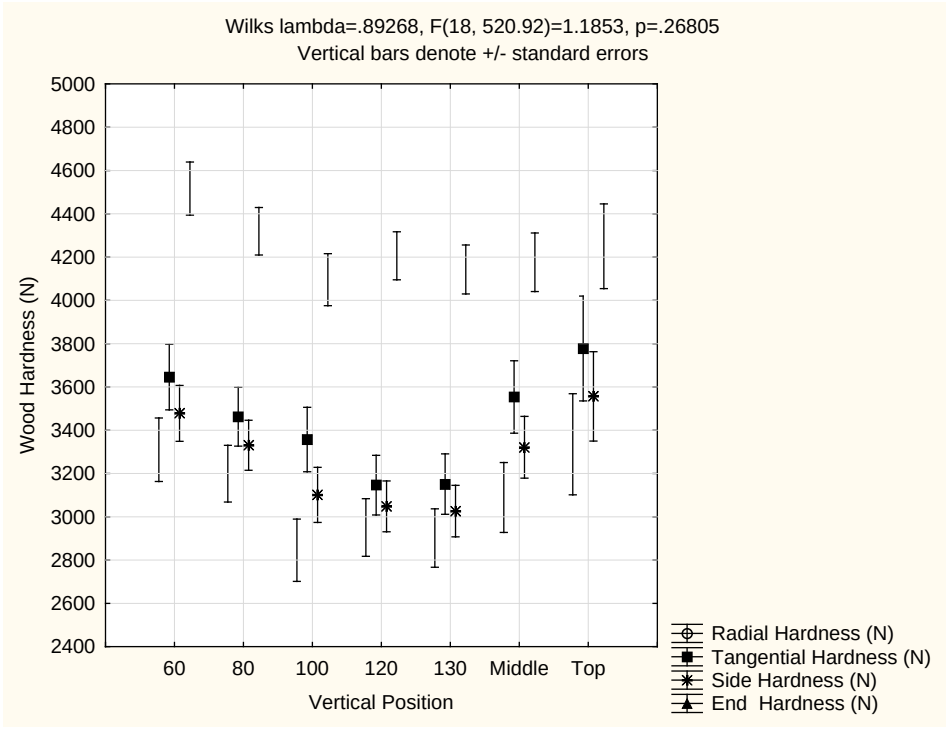

Figure 5—Whole tree wood hardness variation between different axial positions within trees

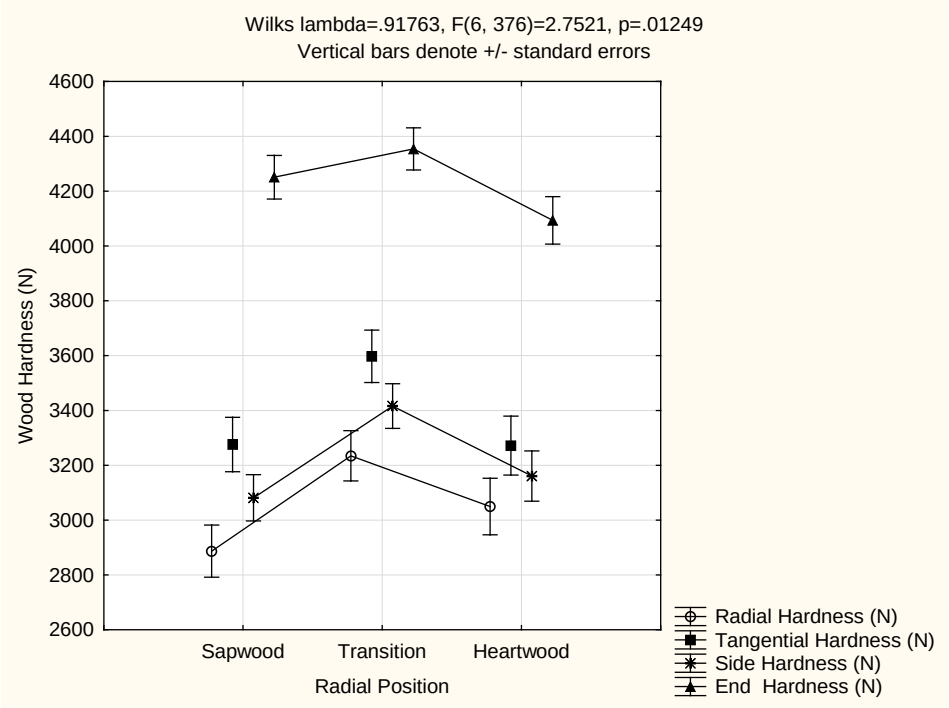

Figure 6—Whole tree wood hardness variation between different radial positions within trees

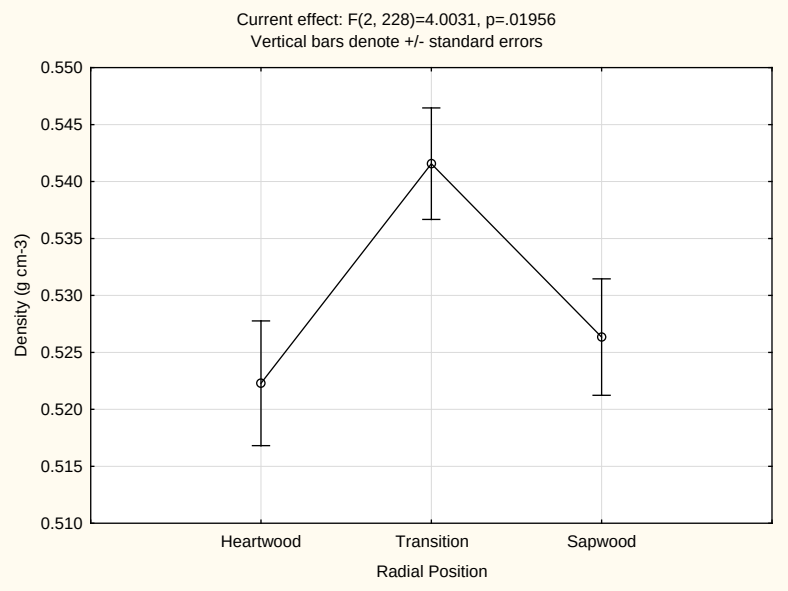

Figure 7—Variation of air dry wood density at radial position within tree

Models for Predicting Wood Hardness

Table 2 presents a simple correlation matrix between wood hardness and crystallinity quantifiers. Significant but low positive correlations were found between wood hardness (except tangential hardness) and the degree of crystallinity (DC), and between wood hardness values in all the structural directions with the square of DC. It was shown that there was a polynomial relationship between wood hardness and degree of crystallinity. Furthermore, the strongest positive correlations were observed between density and wood hardness.

Table 2—Simple correlation matrix between wood hardness, crystallinity characteristics and density

Wood Hardness (N)	MFA (°)	MFA^2	DC (%)	DC^2	CW (nm)	CW^2	CL (nm)	CL^2	Density (g cm^{-3})
Radial	0.08	0.08	0.15*	0.16*	-0.09	-0.07	0.12	0.06	0.65*
Tangential	-0.01	0.01	0.15	0.16*	-0.06	-0.05	0.13	0.08	0.74*
Side	0.04	0.05	0.17*	0.19*	-0.08	-0.07	0.15	0.08	0.79*
End	0.06	0.04	0.19*	0.20*	-0.14	-0.13	0.08	0.00	0.58*

*Marked correlations are significant at $p < .05$; N=201 (Casewise deletion of missing data)
MFA: Micro Fibril Angle (°); Dc: Degree of Crystallinity (%); SW: Crystallite Width (nm);
CL: Crystallite Length (nm)

Stepwise regression produced a greater variety of independent variables for inclusion in the models. It also accommodates for the interaction between variables and their squares. Selected independent variables and factors influencing wood hardness are summarized in Table 3.

Table 3— Selected independent variables (p value < 0.05) for each wood directions

Wood Hardness (N)	Variables included in the models	Influencing Factors
Radial	• CL (-) • Density (+) • CW (interaction with age) (-) • CW − MFA (in interaction) (-)	- Age - Site - Radial position - Axial position (as single variable and interaction radial position, CL, and CW)
Tangential	• CW (as single variable and interaction with diameter class) (-) • DC (-) • Density (interaction with site) (+) • DC − Density (in interaction) (+)	- Site (as single variable and interaction with diameter and density) - Diameter (as single variable and interaction with site, axial position and CW) - Axial positions (as single variable and interaction with diameter, DC and density)
Side	• CL(-) • DC(-) • CW (in interaction with diameter classes)(-) • CW^2(+) • CL − MFA (in interaction)(-) • CW − MFA (in interaction)(+) • DC − Density (in interaction)(+)	- Diameter classes (as single variable and interaction with CW) - Radial position - Axial position (interaction with radial position and CL)
End	• DC (+) • Density (+) • MFA (-) • CW (-) • Density − MFA (+) • $Density^2$ (-)	- Age(as single variable and interaction with axial position) - Site - Radial position(as single variable and interaction with diameter classes) - Axial position (interaction with CW, DC, and Density)

MFA: Micro Fibril Angle (°); DC: Degree of Crystallinity (%); CL: Crystallite Length (nm), CW: Crystallite Width (nm)

The models determined for predicting wood hardness for sampling position at 130 cm above ground (Breast Height) are as follows:

Radial Hardness *(R^2 0.57; Adj R^2 0.53)*

$$= -5113 + \frac{5225\ (5\ \text{yo})}{6270\ (6\ \text{yo})} - \frac{621\ (\text{Magetan})}{1242\ (\text{Bogor})} - \frac{77\ (\text{HW})}{\frac{154\ (\text{TW})}{231\ (\text{SW})}} - 38\ \text{CL} + 9031\ \text{Density} - \frac{1509\ (5\ \text{yo})}{1790\ (6\ \text{yo})}\ \text{CW} - 19.8\ (\text{CW.MFA}) \quad (1)$$

Tangential Hardness *(R^2 0.63; Adj R^2 0.60)*

$$= 7444 - \frac{4287\ (\text{Magetan})}{8574\ (\text{Bogor})} - \frac{989\ (\text{Small diameter})}{\frac{1796\ (\text{Medium diameter})}{2421\ (\text{Large diameter})}} + \frac{467\ (\text{Small diameter})}{\frac{934\ (\text{Medium diameter})}{1401\ (\text{Large diameter})}}\ (\text{Magetan}) + \frac{934\ (\text{Small diameter})}{\frac{1868\ (\text{Medium diameter})}{2802\ (\text{Large diameter})}}\ (\text{Bogor}) - 460\text{CW} - 124\ \text{DC} + \frac{7501\ (\text{Magetan})}{13676\ (\text{Bogor})}\ \text{Density} - \frac{166\ (\text{Small diameter})}{\frac{332\ (\text{Medium diameter})}{498\ (\text{Large diameter})}}\ \text{CW} + 240\ (\text{DC.Density}) \quad (2)$$

Side Hardness *(R^2 0.67; Adj R^2 0.63)*

$$= 4695 + \frac{691\ (\text{Small diameter})}{\frac{1382\ (\text{Medium diameter})}{2073\ (\text{Large diameter})}} - \frac{104\ (\text{HW})}{\frac{312\ (\text{TW})}{312\ (\text{SW})}} - 9.7\ \text{CL} - 136\ \text{DC} - \frac{152\ (\text{Small diameter})}{\frac{304\ (\text{Medium diameter})}{456\ (\text{Large diameter})}}\ \text{CW} + 0.3\ (\text{CL.MFA}) - 8.2\ (\text{CW.MFA}) + 261\ (\text{DC.Density}) + 54.4\ \text{CW}^2 \quad (3)$$

End Hardness *(R^2 0.62; Adj R^2 0.58)*

$$= -4670 - \frac{710\ (5\ \text{yo})}{930\ (6\ \text{yo})} - \frac{310\ (\text{Magetan})}{620\ (\text{Bogor})} - \frac{288\ (\text{HW})}{\frac{576\ (\text{TW})}{864\ (\text{SW})}} + \frac{147\ (\text{HW})}{\frac{294\ (\text{TW})}{441\ (\text{SW})}}(\text{Small Diameter}) + \frac{294\ (\text{HW})}{\frac{588\ (\text{TW})}{882\ (\text{SW})}}(\text{Medium Diameter}) + \frac{441\ (\text{HW})}{\frac{882\ (\text{TW})}{1323\ (\text{SW})}}(\text{Large Diameter}) + 22\ \text{DC} + 33796\ \text{Density} - 137\ \text{MFA} - 65\ \text{CW} + 279\ (\text{Density.MFA}) - 30110\ \text{Density}^2 \quad (4)$$

All proposed independent variables were included in the models using stepwise regression as single variables or as interactions with other variables, for the corresponding wood hardness directions. Goodness of fit for the proposed models based on adjusted R^2 values in the range of 0.53 to 0.63 was intermediate. This study showed that approximately 50-60% of the variation in wood hardness can be explained by wood density including the crystallinity quantifiers of cellulose.

Air dry wood density, as a single variable and as in interaction with other independent variables was consistently the best predictor of wood hardness. In all cases it showed a positive correlation. Bustos et al. (2009) and Holmberg (2000) also showed that wood density was positively related to hardness. In another study, the result was confirmed by Vincent et al. (2014) who showed that the main part of variation explaining the penetration of the Brinell ball is average ring density.

Radial hardness was negatively related to crystallite length and crystallite width (different ages resulting in different crystallite widths where older timber produced wider crystallites). An interaction between crystallite width and MFA was observed where MFA was positively related to crystallite width.

In the tangential direction, crystallite width and degree of crystallinity (DC) were better related to the wood hardness where wider crystallite and higher DC produced lower hardness. However, when the interaction is considered with wood density, DC was positively contributed to wood hardness. In this case, the higher the DC, the heavier the timber, showed by the greater wood density.

Crystallinity quantifiers appear to be more directly related to the end-grain hardness as single variables. DC was positively related to the end hardness, but CW and MFA were negatively correlated. As noted above, Tze et al. (2007) found that higher MFA contributed to the lower side hardness. However, Gindl et al. (2004) who studied the mechanical properties of spruce wood found that hardness determined by nano-indentation was independent of MFA, and suggested that indentation hardness was governed by yield processes in the matrix of the middle lamella. Furthermore, Ates et al. (2009) reported that tangential, radial and cross section Brinell hardness of *Pinus brutia* Ten. had high Pearson's correlation with holocellulose and lignin content ($r > 0.8$). While MFA is related to the wood elastic modulus, it is not likely to be useful for predicting wood hardness as confirmed by Konnerth et al. (2009).

It was shown in this study that wood hardness and crystallinity of the same timber from only one plantation site from Bogor (wet site) showed that MFA was negatively related with all the hardness directions. Crystallite width was only related to side hardness negatively, while DC was only positively related to the end-grain hardness (Damayanti et al., 2015).

Continuing the study by Damayanti et al. (2015), by including different sites and ages, produced more consistent results between crystallinity and wood hardness. It was shown that increased age influenced the radial and end-grain hardness where trees that are one year older produced higher hardness values. Furthermore, site had a significant influence on all individual hardness directions except side hardness. On the other hand, tree diameter classes were related to tangential and side hardness, while axial and radial positions were poorly related to wood hardness in the structural directions studied. Considering that wood of this age is most likely to be back-sawn for flooring products, prediction modeling for hardness in the tangential direction will be sufficient.

Concluding remarks

The proposed models provide intermediate power of prediction, as shown by the adjusted R^2 values between 0.53 and 0.63 when they included air dry density among the prediction variables. Crystallinity and its quantifiers obtained by XRD might also be useful as a non-destructive indicator of wood hardness as they were consistently related to wood hardness from plantation trees.

Acknowledgment

The first author would like to express her sincere gratitude and appreciation for the financial support provided by the Australian Centre for International Agricultural Research (ACIAR) during the PhD study at the University of Melbourne, Australia. Thanks is also directed to Didik Ahmad Sudika (FORDA) for helping in XRD testing and crystallinity measurement.

References

Abe, K.; Yamamoto, H. 2005. Mechanical interaction between cellulose microfibril and matrix substance in wood cell wall determined by X-ray diffraction. J Wood Sci. 51(4): 334-338.

Ates, S.; Akyildiz, M. H.; Ozdemir, H. 2009. Effects of heat treatment on Calabrian Pine (*Pinus brutia* Ten.) wood. BioResources. 4(3): 1032-1043.

Bustos, C.; Herna´ndez, R. E.; Fortin, Y. 2009. Effect of kiln-drying on the hardness and machining properties of tamarack wood for flooring. Forest Prod. J. 59(1/2): 71-76.

Damayanti, R.; Ilic, J.; Ozarska, B.; Pari, G.; Vinden, P. 2015. Crystallinity as a non-destructive indicator of wood hardness at standing trees. Applied Mechanics and Materials. 771: 232-241. DOI: 10.4028/www.scientific.net/AMM.771.232

Gindl, W.; Gupta, H. S.; Schöberl, T.; Lichtenegger, H. C.; Fratzl, P. 2004. Mechanical properties of spruce wood cell walls by nanoindentation. Applied Physics A: Materials Science & Processing. 79(8): 2069-2073. DOI: 10.1007/s00339-004-2864-y

Green, D. W.; Begel, M.; Nelson, W. 2006. Janka hardness using non standard specimens. Wisconsin: Forest Product Laboratory. 13p.

Hein, P. R. G.; Brancheriau, L. 2011. Radial variation of microfibril angle and wood density and their relationship in 14-year-old *Eucalyptus urophylla* S.T. Blake wood. BioResource. 6(3): 3352-3362.

Holmberg, H. 2000. Influence of grain angle on Brinell hardness of Scots pine (*Pinus sylvestris* L.). Holz als Roh-und Werkstoff. 58 (1-2): 91-95.

Jiang, Z.-H.; Yang, Z.; So, C.-L.; Hse, C.-Y. 2007. Rapid prediction of wood crystallinity in *Pinus elliotii* plantation wood by near-infrared spectroscopy. J Wood Sci. 53: 449-453.

Konnerth, J.; Gierlinger, N.; Keckes, J.; Gindl, W. 2009. Actual versus apparent within cell wall variability of nanoindentation results from wood cell walls related to cellulose microfibril angle. Journal of Materials Science. 44 (16): 4399-4406. DOI: 10.1007/s10853-009-3665-7

Lee, C. 1961. Crystallinity of wood cellulose fibers studies by X-ray methods. Forest Prod. J. 11: 108-112

Mack, J. 1979. Australian methods for mechanically testing small clear specimens of timber. Australia: Commonwealth Scientific and Industrial Research Organization (CSIRO). 19p.

Merela, M., & Čufar, K. (2013). Mechanical properties of sapwood versus heartwood in three. Drvna Industrija. 64(4): 323-334.DOI: 10.5552/drind.2013.1325

Panshin, A.J.; de Zeeuw, C.; Brown, H. 1964. *Textbook of Wood Technology. Volume I: Structure, identification, uses, and properties of the commercial woods of the United States*. New York: McGraw-Hill Book Company. 642 p.

Pereira, H.; Graca, J.; Rodrigues, J. C. 2003. Wood chemistry in relation to quality. In: J. R. Barnett & G. Jeronimidis, Eds. Wood quality and its biological basis. Oxford UK: Blackwell Publishing Ltd. 226 p.

Peura, M.; Muller, M.; Vainio, U.; Saren, M. P.; Saranpaa, P.; Serimaa, R. 2008. X-ray microdiffraction reveals the orientation of cellulose microfibrils and the size of cellulose crystallites in single Norway spruce tracheids. Trees. 22: 49-61.

Qu, Z.; Wang, L. 2011. Prediction of the crystallinity of White Pine using Near Infrared Spectroscopy. Advanced Materials Research. 183-185: 1215-1218.

Raymond, C.; Muneri, A. 2001. Nondestructive sampling of *Eucalyptus globulus* and *E. nitens* for wood properties. I. Basic density. Wood Science and Technology. 35: 27-39.

Stuart, S.; Evans, R. 1994. X-ray diffraction estimation of the microfibril angle variation in eucalypt increment cores. Australia: The CRC for Hardwood Fibre & Paper Science.

Thomas, D.; Henson, M..; Joe, B.; Boyton, S.; Dickson, R. 2009. Review of growth and wood quality of plantation-grown *Eucalyptus dunnii* Maiden. Australian Forestry. 72(1): 3-11.

Tze, W. T. Y.; Wang, S.; Rials, T. G.; Pharr, G. M.; Kelley, S. S. 2007. Nanoindentation of wood cell walls: Continuous stiffness and hardness measurements. Composites. 38(Part A): 945-953.

Vincent, M.; Tong, Q.; Terziev, N.; Daniel, G.; Bustos, C.; Escobar, W. G.; Duchesne, I. 2014. A comparison of nanoindentation cell wall hardness and Brinell wood hardness in jack pine (*Pinus banksiana* Lamb.). Wood Sci Technol. 46: 7-22.

Williams, R. S. 2005. Weathering of wood. In: Rowell, R.M., ed. Handbook of Wood Chemistry and Wood Composites. Florida: CRC Press: 139-185. Part II Chapter 7.

Stress Wave Propagation in Larch Plantation Trees—Numerical Simulation

Fenglu Liu
School of Technology, Beijing Forestry University, Beijing, China, liufenglu39@126.com

Fang Jiang
School of Technology, Beijing Forestry University, Beijing, China, jf0602@bjfu.edu.cn

Xiping Wang
USDA Forest Service Forest Products Laboratory, Madison, Wisconsin, USA, xwang@fs.fed.us

Houjiang Zhang
School of Technology, Beijing Forestry University, Beijing, China, hjzhang6@bjfu.edu.cn

Wenhua Yu
School of Technology, Beijing Forestry University, Beijing, China, yuwenhua56@sina.com

Abstract

In this paper, we attempted to simulate stress wave propagation in virtual tree trunks and construct two dimensional (2D) wave-front maps in the longitudinal-radial section of the trunk. A tree trunk was modeled as an orthotropic cylinder in which wood properties along the fiber and in each of the two perpendicular directions were different. We used the COMSOL Multiphysics® software to conduct numerical simulations. Field stress wave timing measurements were then conducted on three freshly cut larch (*Larix principis-rupprechtii* Mayr) logs to validate the simulation results. The 2D wave fronts observed through numerical simulations were in good agreement with those obtained through stress wave timing measurements. When a stress wave was introduced into the tree trunk through a point impact, it initially propagated in the impact direction with a spherical wave front; then the flow of stress wave energy gradually changed toward the longitudinal direction and its wave front became flattened perpendicular to the longitudinal axis. Our preliminary results indicate that the Structural Mechanics module of the COMSOL Multiphysics® software is capable of simulating the longitudinal wave propagation in standing trees.

Keywords: longitudinal stress wave, logs, standing trees, numerical simulation, time-of-flight, wave front.

Introduction

The use of stress wave technology for standing tree quality assessment has received a lot of attention in recent years (Carter et al. 2005, Chauhan and Walker 2006, Grabianowski et al. 2006, Wang et al. 2007a, Raymond et al. 2008, Mora et al. 2009, Mahon et al. 2009). By far, most research has been limited to direct measurement of stress wave velocity in trees. Subsequent wood property prediction was solely based on the measured velocity values (Addis et al. 2000, Huang 2000, Wang et al. 2001, Lindstrom et al. 2002, Wang et al. 2007b). A typical approach for measuring stress wave velocity in trees involves inserting two sensor probes (transmit probe and receiver probe) into the sapwood and introducing a stress wave impulse into the tree trunk from a mechanical impact (Wang et al. 2007a, b). The standing tree device essentially measures the time for the stress wave to travel from the transmit probe to the receiver probe. The stress wave velocity is subsequently calculated from the span between two sensor probes and the time of flight (TOF) data.

Although acoustic velocity has been proven to be an effective measure for predicting wood and fiber properties in standing trees, there is still a lack of understanding of how stress waves propagate in standing trees and how tree diameter, species, tree age, and environmental conditions affect wave propagation in a tree. Zhang et al. (2011) conducted stress wave timing measurements on red pine (*Pinus resinosa* Ait.) logs to obtain stress wave data needed for simulating stress wave propagation in standing trees. With the TOF data collected from a series of cross sections along the logs, they were able to construct two dimensional (2D) and three dimensional (3D) stress wave contour maps using a commercial software. Those stress wave contour maps represent the wave fronts in a time sequence, illustrating the flow of stress wave energy within a tree trunk. Although this experimental approach provides a way to study stress wave behavior in standing trees, the procedure requires cutting down trees and the TOF measurements are time consuming.

In this paper, we attempted to simulate stress wave propagation in virtual tree trunks and construct two dimensional wave front maps in the longitudinal-radial section of the trunk. We used a COMSOL Multiphysics® (Burlington, MA) software to conduct the numerical simulations. COMSOL Multiphysics® is a finite element analysis, solver, and simulation software package that is suited for various physics and engineering applications. It has been widely used in the areas of acoustics, biological science, structural mechanics and wave propagation (Zhou et al. 2015). Our goal was to prove the validity of using the COMSOL Multiphysics® software to simulate stress wave propagation in standing timber and pave the way for further investigation of stress wave behavior in plantation trees.

Fundamentals of Wave Propagation in Wood

When stress is applied suddenly to the surface of wood, the disturbance that is generated travels through the wood as stress waves. In general, three types of waves are initiated by such an impact: (1) longitudinal wave (compressive or P-wave), (2) shear wave (S-wave), and (3) surface wave (Rayleigh wave). A longitudinal wave corresponds to the oscillation of particles along the direction of wave propagation such that particle velocity is parallel to wave velocity. In a shear wave, the motion of the particles conveying the wave is perpendicular to the direction of the propagation of the wave itself. A Rayleigh (surface) wave is usually restricted to the region adjacent to the surface; particles move both up and down and back and forth, tracing elliptical paths. Although most energy resulting from an impact is carried by shear and surface waves, the longitudinal wave travels the fastest and is the easiest to detect in field applications (Meyers 1994). Consequently, the longitudinal wave is by far the most commonly used wave for material property characterization. A basic understanding of the relationship between wood properties and longitudinal wave velocity (hereafter referred to as wave velocity) can be acquired from fundamental wave theory.

One-dimensional stress wave theory

In a long, slender, isotropic material, strain and inertia in the transverse direction can be neglected and longitudinal waves propagate in a plane waveform (wave front). The free longitudinal motion for one-dimensional wave is governed by the following partial differential equation:

$$\frac{\partial^2 u}{\partial t^2} = \frac{E}{\rho}\frac{\partial^2 u}{\partial x^2} \tag{1}$$

Where u is the longitudinal displacement, E is longitudinal modulus of elasticity, and ρ is mass density of material. In this case, the wave velocity (C_0) is independent of Poisson's ratio and is given by the following equation:

$$C_0 = \sqrt{\frac{E}{\rho}} \tag{2}$$

Three-dimensional stress wave theory

In an infinite or unbounded isotropic elastic medium, a triaxial state of stress is present. The wave front of the longitudinal wave propagating through such a medium is no longer a plane. The partial differential equation that governs the three dimensional wave is as follows (Meyers 1994):

$$\frac{\partial^2 \Delta}{\partial t^2} = \frac{\lambda + 2\mu}{\rho} \nabla^2 \Delta \tag{3}$$

where λ , μ are the Lamé constants,

$$\Delta = \varepsilon_{ii} = \varepsilon_{11} + \varepsilon_{22} + \varepsilon_{33} \tag{4}$$

$$\nabla^2 = \frac{\partial^2}{\partial x_1^2} + \frac{\partial^2}{\partial x_2^2} + \frac{\partial^2}{\partial x_3^2} \tag{5}$$

From elastic theory, $\mu = \frac{E}{2(1+\nu)}$ and $\lambda = \frac{\nu E}{(1+\nu)(1-2\nu)}$, then the longitudinal velocity in unbounded medium can be determined as

$$C = \sqrt{\frac{1-\nu}{(1+\nu)(1-2\nu)} \frac{E}{\rho}} \tag{6}$$

Where ν is Poisson's ratio of the material. From Equation (6), it is clear that the wave velocity is dependent on density and two elastic parameters, modulus of elasticity (E) and Poisson's ratio (ν).

Numerical Simulation of Stress Wave Propagation in Standing Trees

Both Foundation Module and Structural Mechanics Module of the COMSOL Multiphysics® software were used for the task. Foundation module has main function of pre-processing, post-processing, and solving. Structural Mechanics Module is specifically for mechanical structural analysis under static or dynamic loads, including steady state, transient, quasi-static, frequency response, and pre-stressed. The Structural Mechanics module we selected is based on three-dimensional wave equations for elastic materials. Simulation of the wave propagation was achieved by solving the partial differential equations using finite element method under defined initial and boundary conditions.

Model geometry

To facilitate the comparison of simulation results and the field experimental results, we specifically set the longitudinal–radial sections of the logs cut from the trees as the geometry models for numerical simulation. The sizes of those three log samples are shown in Table 1. The geometry model is basically in a tapered solid cylindrical form.

Material properties

A tree trunk was considered as an orthotropic cylinder, with the axial, radial, tangential directions as three principal axes. Twelve elastic constants of green larch were determined through laboratory experiments in a previous study (Liu et al. 2015). The wood specimens used for determining the elastic constants were cut from the same logs that were used for validation experiment. The average values of the elastic constants are shown in Table 2. The measured average density (ρ) of green larch was 838 kg/m^3.

Impulse load

Stress waves used in tree measurements are typically produced through a mechanical impact on the start transducer and this impact-induced stress wave has a very short duration. We used the following half-sine pulse function to express this impact force:

$$F(\mathrm{t}) = \begin{cases} \mathrm{A}\sin(2\pi f\mathrm{t}), & t < (1/2f) \\ 0, & t \geq (1/2f) \end{cases} \tag{7}$$

Where A is the amplitude of pulse and f is the frequency.

According to the actual pulse signals collected from a hammer impact in a laboratory testing, the amplitudes of the pulse signals were about 200 N. Because the start sensor probe is typically inserted into a tree trunk in a 45-degree angle with respect to the longitudinal axis, the impact force acting on the start sensor is also in a 45-degree angle to the longitudinal axis of the trunk. Based on the principle of vector decomposition, *F(t)* can be decomposed into two orthogonal components: $F_y(t)$ and $F_z(t)$, and each component is 141.4N. According to the tested pulse force signal, the frequency of pulse was $f = 1\times10^8$ (Hz). The function graph of a single pulse force component is shown in Figure 1.

Table 1—Dimension of the larch logs

	Length (cm)	Large-end diameter (cm)	Small-end diameter (cm)
Log A	360	38	31
Log B	360	32	27
Log C	360	28	24

Table 2—Twelve elastic constants of larch wood obtained through laboratory experiments

Modulus of elasticity (MPa)		Modulus of rigidity (MPa)		Poisson's ratio μ	
E_L	4350.33	G_{RT}	523.18	μ_{LT}	0.41
E_T	1099.60	G_{LR}	460.32	μ_{LR}	0.23
E_R	1054.97	G_{LT}	412.42	μ_{TL}	0.10
				μ_{TR}	0.67
				μ_{RL}	0.08
				μ_{RT}	0.62

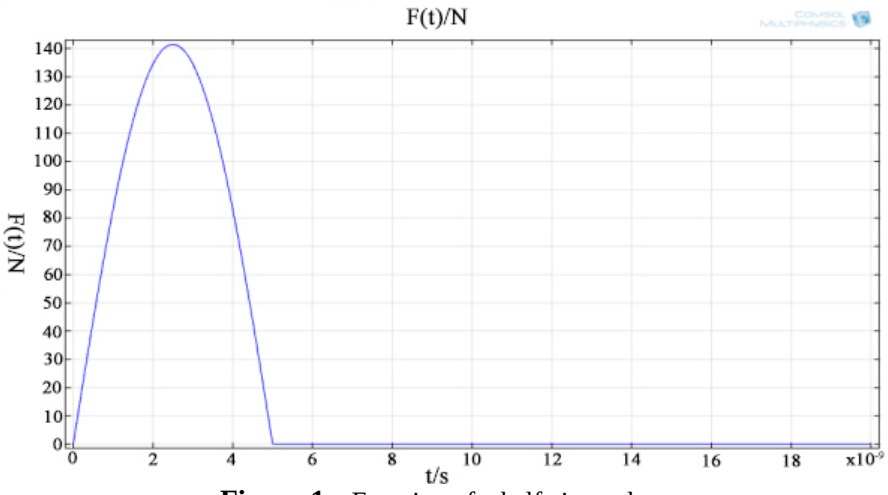

Figure 1—Function of a half-sine pulse.

Initial and boundary conditions

The initial displacement and initial velocity of each particle in wood were set as zero. *u* is used to represent the particle displacement, the mathematical expressions of these two initial conditions are shown below:

$$\textit{Initial displacement: } u_i = 0 \ (i = x, y, z) \tag{8}$$

$$\textit{Initial velocity: } \frac{\partial u_i}{\partial t} = 0 \ (i = x, y, z) \tag{9}$$

The virtual trunk model was set to have a free boundary condition, which means that the compression waves and reflected waves coexist with the wave attenuation when the stress wave propagates to the boundaries.

Meshing

The mesh was generated automatically with the triangular elements. Free meshing provided in COMSOL was used for the generation of mesh. The largest and smallest elements were 1.73 cm and 0.004 cm, respectively. Figure 2 shows the divided grid of longitudinal-radial section in a virtual tree trunk, which corresponds to log sample A. The mesh has been refined at the region below the excitation source. A free time step for transient solver was selected as initial step, 1e-9s; biggest step, 1e-4s. Output step of the result was 5.0e-7s. After all the settings were completed, the COMSOL program was run to obtain simulation results.

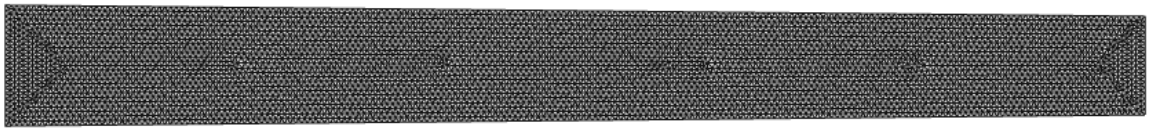

Figure 2—The geometry model of a virtual tree trunk with meshing grids.

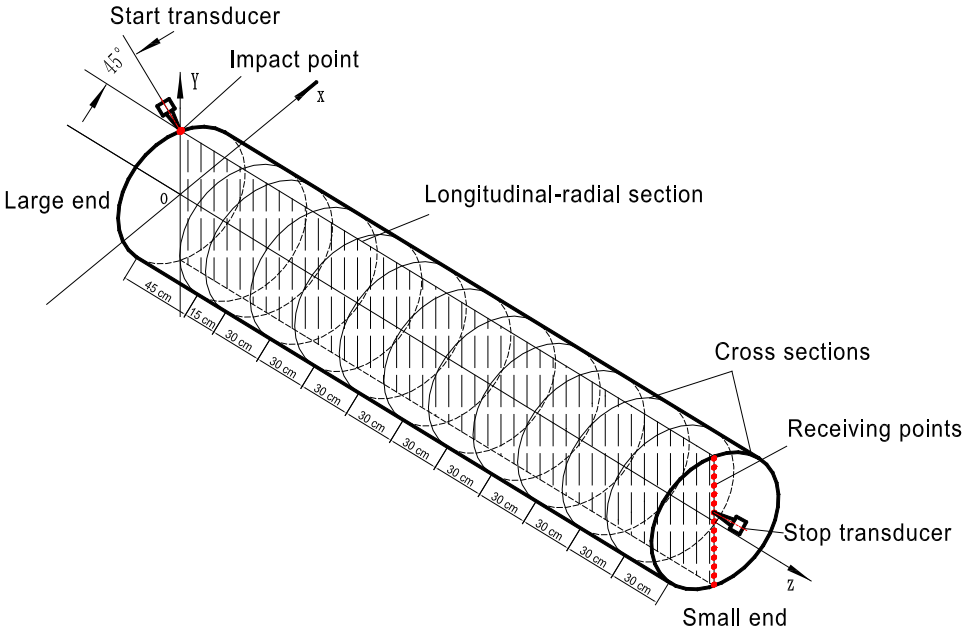

Figure 3—Schematic diagram of stress wave timing measurements on a log sample.

Experimental Validation

To validate the simulation results of stress wave propagation in standing trees, we conducted field stress wave measurements on freshly cut logs in a larch plantation stand. Three larch trees with different diameters at breast height were felled down and cut into 3.6-m long logs starting from the butt end. The first log from each tree was used to obtain stress wave data needed for developing wave front maps. Stress wave propagation time in the logs was measured using a battery-operated stress wave timer (FAKOPP Microsecond Meter, Fakopp Interprise, Hungary). Figure 3 shows the schematic diagram for conducting the field stress wave measurements.

Stress wave timing measurements were conducted when the log samples were laid flat on the ground. The start transducer was mounted on the log by inserting the spike 1-cm deep at the highest point of the large end, with an angle of 45 degrees with respect to the upper surface; while the stop transducer was mounted at the cross section of the small end by inserting the spike 1-cm deep through the end grain. The start transducer remained in the same position during the measurement process, while the position of stop transducer was continuously changed along the vertical middle lines. A constant impact on the start transducer was generated by a special pendulum device mounted onto the log. The stop transducer received stress wave signals and the time of flight (TOF) was displayed and recorded. A series of stress wave measurements were conducted by moving the stop transducer to different locations at the middle vertical lines of the end cross section. Once the stress wave measurements were completed at one end cross section, a 30-cm long section was cut off from the small end, and the same procedure was repeated on the new cross section. A total of 10 cross sections were tested for each log sample.

Results and Discussion

Contour maps of total displacement on the longitudinal-radial section were obtained through numerical simulations. The contour of displacement refers to the line in which each point has the same TOF as the stress wave propagated from the source point. As an example, Figure 4 shows the

simulated results at the times of T = 5e-5s, 1e-4s, 1.4e-4s, 1.9e-4s, 2.7e-4s, 3.5e-4s, 5e-4s, 7e-4s, 9e-4s, 1e-3s. The forefront line in the contour map for each time point represents the wave front, which is the boundary of stress wave disturbance zone and undisturbed areas during the propagation.

To visually display the propagation patterns of the impact-induced stress waves in the virtual tree trunks, we extracted the forefront contour lines from the displacement contour maps at various time points to form the wave front diagram. Figure 5 shows the 2D mapping of the simulated stress wave fronts for larch virtual trunks with three different diameters, which corresponds to the three logs used in the validation experiments. The numbers next to the wave front lines are the TOF in microsecond; the red dot on the upper left of the graph is the import source; horizontal and vertical axes are the length and diameter of the tree trunk, respectively. In all three simulation cases, the wave front initially propagated in the impact direction with a spherical wave front. As the wave continuously propagated, the flow of stress wave energy gradually changed toward the longitudinal direction and its wave front gradually became flattened and close to perpendicular to the longitudinal axis.

In order to verify the accuracy and reliability of numerical simulation results, the results of simulation and the results of the field experiments are compared and analyzed. Figure 6 is a summary of the experimental results of stress wave timing measurements showing the changing patterns of the wave fronts in the longitudinal-radial section of the larch logs. Note that the stress wave timing measurements in the larch logs began at the location 45 cm from the log end, therefore the display of contour maps after post-processing is 45 cm off the log end.

When compared Figure 5 with Figure 6, it is found that stress wave propagation patterns of the numerical simulation in virtual tree trunks are basically in agreement with the results from stress wave timing measurements. We also noticed that the shape of the stress wave fronts from the field experiments was not as smooth as those from numerical simulations. Some irregular TOF contour lines occurred in the latter part of the stress wave propagation path. This might be caused by the local defects such as knots in that part of the log. Knots typical exhibit distorted grain orientations and have very different physical and mechanical properties compared with normal wood. Whereas in numerical simulations, our analysis was based on the assumption that a tree trunk is orthotropic material without any defects.

Conclusion

Stress wave propagation patterns obtained through numerical simulations were in a good agreement with the results from field stress wave measurements. When a stress wave was introduced into the tree trunk through a point impact with a 45 degree angle with respect to the trunk surface, it initially propagated in the impact direction with a spherical wave front. Then the flow of stress wave energy gradually changed towards the longitudinal direction and its wave front became flattened perpendicular to the longitudinal axis. The preliminary results of this study indicated that the orthotropic assumption for the tree trunk model for numerical simulation is reasonable. The COMSOL Multiphysics® software is capable of simulating the longitudinal wave propagation in standing trees. This opens the way to further investigate the mechanism of stress wave propagation in standing trees and examine the effects of various factors (species, tree age, tree diameter, temperature etc.) on stress wave assessment of wood quality in plantation forests.

Acknowledgment

This project was conducted under the cooperative research agreement between Beijing Forestry University, Beijing, China, and the USDA Forest Service, Forest Products Laboratory (FPL), Madison, WI. Financial support to the project was provided by the National Natural Science Foundation of China (Grant No. 31328005).

References

Addis T, Buchanan AH, Walker JCF. 2000. Selecting trees for structural timber. Holz Roh-Werkst 58:162-167.

Carter P, Briggs D, Ross RJ, Wang X. 2005. Acoustic testing to enhance western forest values and meet customer wood quality needs. PNW-GTR-642, In: Harrington, CA, Schoenholtz SH, eds. Productivity of Western Forests: A Forest Products Focus. USDA Forest Service, Pacific Northwest Research Station, Portland, Oregon. pp 121-129.

Chauhan SS, Walker JCF. 2006. Variation in acoustic velocity and density with age, and their interrelationships in radiata pine. Forest Ecol Manag 229: 388-394.

Grabianowski M, Manley B, Walker JCF. 2006. Acoustic measurements on standing trees, logs and green lumber. Wood Sci Technol 40: 205-216.

Huang CL. 2000. Predicting lumber stiffness of standing trees. In: Proceedings, the 12th International Symposium on Nondestructive Testing of Wood, University of Western Hungary, Sopron, September 13-15, 2000. Pp. 173-179.

Lindstrom H, Harris P, Nakada R. 2002. Methods for measuring stiffness of young trees. Holz Roh-Werkst 60:165-174.

Liu F; Jiang F; Zhang J ; Zhang H; Wang X; Yang Z. 2015. Study on twelve elastic constant values of larch forest. Journal of Beijing Forestry University. (in press)

Mahon JM Jr, Jordan L, Schmileck LR, Clark A III, Daniels RF. 2009. A comparison of sampling methods for a standing tree acoustic device. South J Appl For 33(2): 62-68.

Meyers MA (1994) Dynamic behavior of materials. John Wiley & Sons. Inc., New York.

Mora CR, Schimleck LR, Isik F, Mahon JM, Clark A III, Daniels RF. 2009. Relationship between acoustic varaibles and different measures of stiffness in standing *Pinus taeda* trees. Can J For Res 39:1421-1429.

Raymond CA, Joe B, Anderson DW, Watt DJ. 2008. Effect of thinning on relationships between three measures of wood stiffness in *Pinus radiata*: standing trees vs. logs vs. short clear specimens. Can. J. For. Res. 38: 2870-2879.

Wang X, Ross RJ, McClellan M, Barbour RJ, Erickson JR, Forsman JW, McGinnis GD. 2001. Nondestructive evaluation of standing trees with stress wave method. Wood Fiber Sci 33(4):522-533.

Wang X, Ross RJ, Carter P. 2007a. Acoustic evaluation of wood quality in standing trees. Part I. Acoustic wave behaviour. *Wood and Fibre Science* 39(1):28-38.

Wang X, Carter P, Ross RJ, Brashaw BK. 2007b. Acoustic assessment of wood quality of raw forest materials—a path to increased profitability. Forest Products Journal 57(5):6-14.

Zhang H, Wang X, Su J. 2011. Experimental investigation of stress wave propagation in standing trees. Holzforschung 65(5):743-748.

Zhou J, Wei C, Li W, and others. 2015. Analysis of solid elasto-plastic mechanics based on mathematical module of COMSOL Multiphysics. Engineering Journal of Wuhan University. 48(2): 195-201.

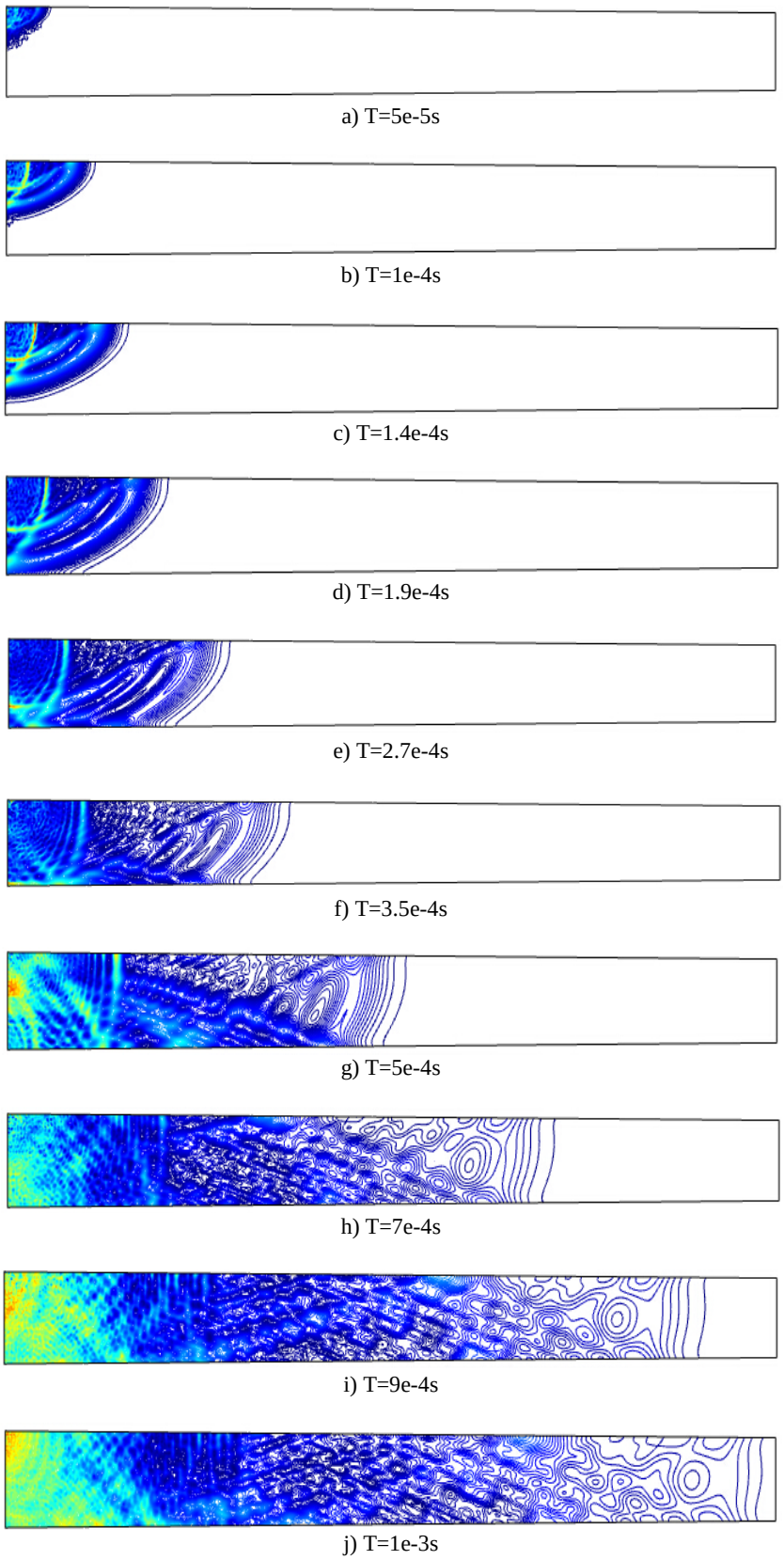

Figure 4—Contour maps of total displacement on longitudinal-radial section (log A).

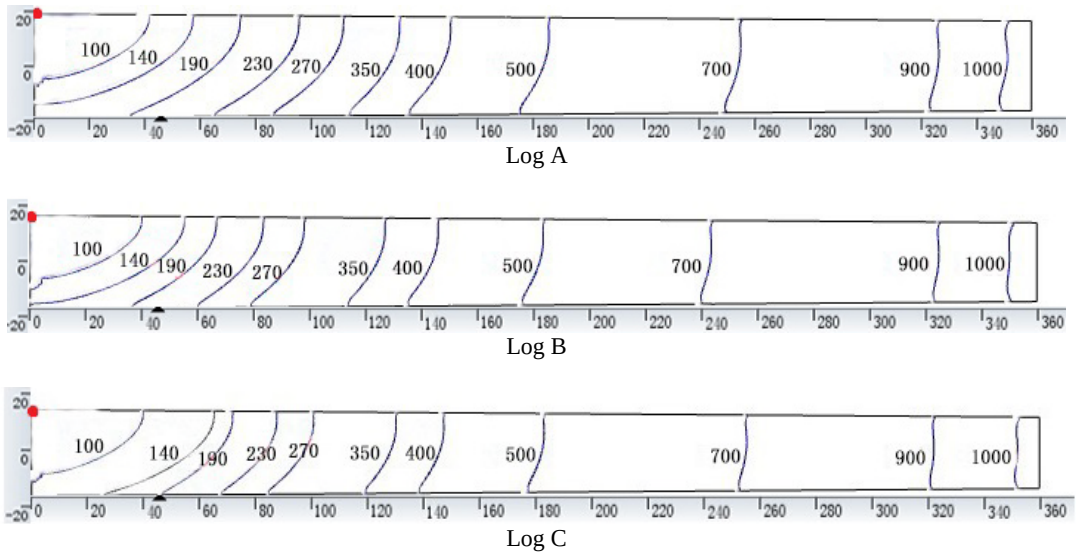

Figure 5—Wave fronts obtained through numerical simulation showing wave propagation patterns in the longitudinal-radial section of the virtual tree trunks.

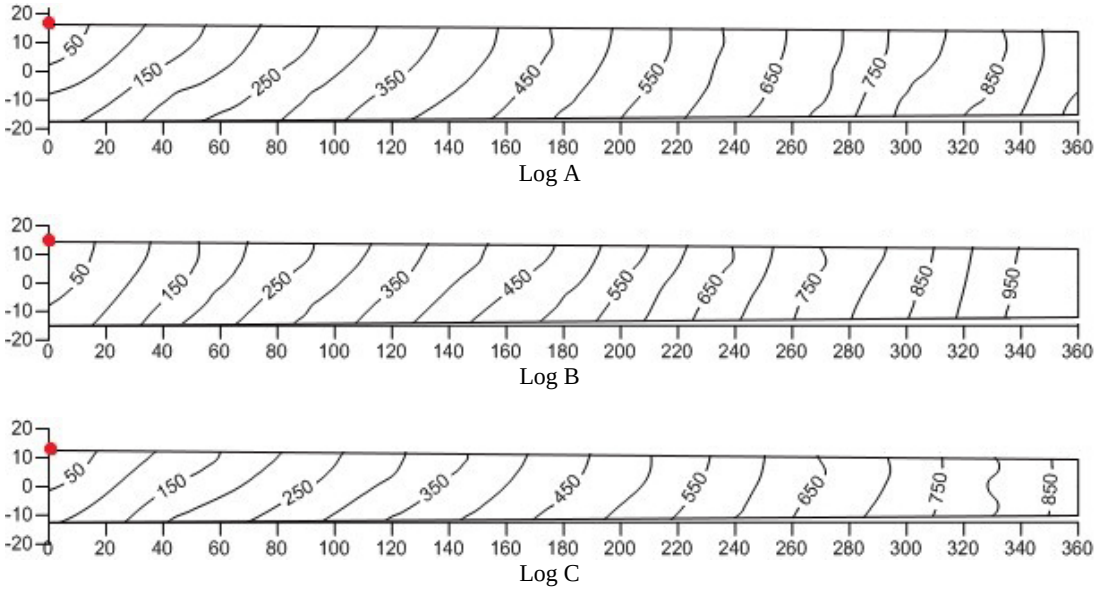

Figure 6—Experimental results of stress wave timing measurements showing the changing patterns of the wave fronts in the longitudinal-radial section of the larch logs.

Efficiency of Acoustic Segregation of *Castanea sativa* Standing Trees and Logs for Structural Timber Production

Oscar Santaclara Estévez
Madera Plus Calidad Forestal S.L., Ourense, Spain, maderaplus@maderaplus.es

Esther Merlo Sánchez
Madera Plus Calidad Forestal S.L., Ourense, Spain, maderaplus@maderaplus.es

Abstract

Sweet Chestnut (*Castanea sativa Mill.*) is one of the most important hardwood species traditionally used in construction in Spain. It has recently been included in the Spanish Standard for structural timber, UNE 56544, assigning the strength class according to European Standard EN 338. From the demonstrated effectiveness of acoustic techniques, this paper proposes classification models for trees and logs based on acoustic velocity to estimate the mechanical properties and improve the performance of structural timber processed. The acoustic velocity (ST300) was measured in a representative sample of 39 standing trees from Galicia region (northwest of Spain). 46 logs from these trees were obtained and resonance method (HM200) was used to measure the acoustic velocity and characterize the logs. The modulus of elasticity (MOE) was measured according to the European Standard EN 408 on 46 structural timber milled from the tested logs. The relationship between acoustic velocities and the average timber MOE was good for both models, R^2=0,75 for the log model and R^2=0,73 for tree model. An acoustic segregation of chestnut logs in three classes according to strength classes defined in EN 338 (D18 and D24) is proposed. The models will allow to select the best structural quality trees and logs and to increase the performance and profit of processing industry.

Keywords: sweet chestnut, trees, logs, acoustic evaluation, acoustic segregation, ST300, HM200.

Introduction

Sweet Chestnut is a species of great relevance in Spain and a much appreciated wood quality for numerous applications. It stands out by its natural durability and quite an acceptable strength for such a low dense timber. Roofs and frames building has been a traditional use of sweet chestnut timber, as well as the naval construction. In the last decades, its use has been reduced due to the competence with other materials (concrete, steel) and with the classified timber of conifers as for the lack of standards and sufficiently known strength properties to allow a realistic and trustworthy structural calculation. This situation has improved in 2013 thanks to the inclusion of the sweet chestnut timber in the Spanish visual grading Standard, UNE 56546:2013, being allocated to strength class D24, according to EN 338 (CEN 2010). Moreover its inclusion was approved in 2014 in the European System of strength classes from visual grading by species EN 1912 (CEN 2012). In a practical basis, this standardisation allows the CE mark implementation for structural sweet chestnut timber which is obligatory for its commercialisation. Therefore, in order to improve the performance and profit of the process, it is important to establish objective criteria of selection and segregation of standing trees and logs with adequated mechanical properties to produce structural timber according to current standards. The demonstrated good relationship of acoustic velocity and stiffness (Wang et al. 2000) allows to use the modulus of elasticity, MOE, as selection criteria and the acoustic technology as a tool capable of predicting the mechanical

properties of wood, due to the significant relationship between standing tree and log measurement and properties of timber processed from these trees and logs.
This paper estudies the relationship between the acoustic velocity measurements in trees and logs of Spanish sweet chestnut and the mechanical properties of timber processed from these trees and logs, and proposes an example of acoustic segregation of logs based on velocity ranges to obtain structural timber with the appropiatre strenght class and therefore, to improve the performance of industrial processes.

Material and Methods

39 Castanea sativa trees ranging from 37 to 50 cm diameter at breast height (DBH) were selected from three stands on Galicia region (northwest of Spain) according to criteria of morphological characteristics (diameter and straightness) in order to obtain large dimension timber. The acoustic characterization of standing trees was made using the Director ST300^{TM} (Fibre-Gen, New Zealand), which is based on the time-of-flight method to obtain the acoustic wave velocity (*Vtree*).
The trees were harvested and bucked into logs. The logs were tagged with a number that identified the tree and the position in the tree from which it came. A total number of 46 logs were obtained. Each log was acoustic characterized using an acoustic resonance technique with the Director HM200^{TM} (Fibre-Gen, New Zealand) to obtain an acoustic velocity of the log (*Vlog*).
The logs were processed into 46 large structural pieces, distributed in 7 pieces with cross-sectional dimensions of 200x200, 17 of 140x140, 57 of 100x100 and 26 of 65x30 mm. Each piece was identified by a number, indicating the log from which it came, and was acoustic characterized using the resonance technique in green condition (*Vgt*), above the fiber saturation point, and in dry condition after the kiln drying (*Vdt*), moisture content around 14%.
All the pieces were tested in accordance with EN 408:2010 (CEN 2010) to obtain the MOE in dry condition from the four-point bending test.
Summary statistics for measured variables are presented in Table 1.

Table 1—Summary statistics for measured variables

	Average	Min	Max	CV(%)
Vtree	3696	2755	4192	10,0
Vlog	2923	1932	3590	13,4
Vgt	3155	2520	3630	8,5
Vdt	4248	3445	5000	8,4
MOE	8898	4805	14716	16,6
MOElog	9315	5787	11651	15,9

Vtree: standing tree velocity (m/s); *Vlog*: log velocity (m/s); *Vgt*: timber velocity in green conditions (m/s); *Vdt*: timber velocity in dry conditions (m/s); MOE: MOE of structural pieces (N/mm^2); MOElog: average MOE of each log (N/mm^2).

Statistical Analysis

The statistics used for data analysis were the Pearson correlation coefficient to measure the degree of linear relationship between numerical variables, and the method of least squares adjustment for linear and nonlinear relationship between variables. The statistics used to analyze the goodness of fits are the Root Mean Squared Error (RMSE) and the coefficient of determination (R^2). Analysis of variance (ANOVA) was carried out to determine if there were significant differences in acoustic velocity of logs between strength classes. Multiple comparisons were made using Fisher's least significant difference (LSD) procedure, which identify any significant differences between groups.

Results and Discussion

Acoustic velocities in standing trees and logs

There was a good relationship observed between tree velocity (*Vtree*) and log velocity (*Vlog*) (Fig. 1), such that is possible to estimate *Vlog* from *Vtree*. The correlation between the two variables was 0,88 (P<0,001), taking into account that all of them are first and second logs and 3 outliers have been removed from data set. The wave velocities in trees before harvest were upper than for cut logs. The wave propagation and the velocity measurement between the time-of-flight and resonance methods are different (Wang 2013), as a result time-of-flight measures are typically 25 – 30% faster than resonance measures for harvest age trees or logs, but can more or less depending on a number of factors, primarily log diameter relative to time-of-flight probe spacing (Carter 2011).

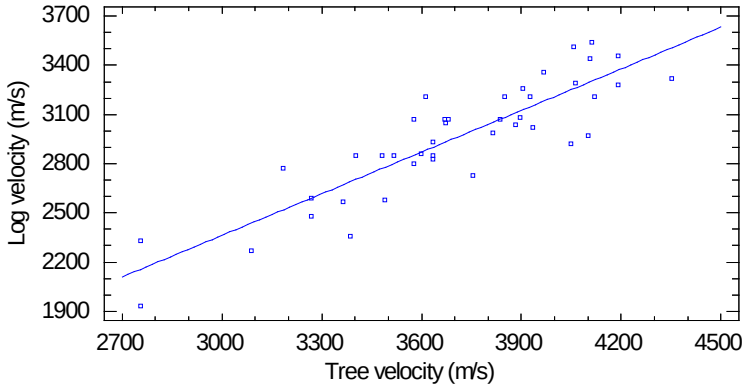

Figure 1—Relationship between tree velocity and log velocity (R^2=0,77).

Relationships between acoustic velocity and MOE

Table 1 shows the results of the relationships between the acoustic velocities and MOE and the fitted models. The tree and log level MOE was calculated as the arithmetic mean of the MOE measurements from all structural pieces obtained from each log.

Table 2—Fitted models for the relationships between velocities and MOE

	Fitted Model	R^2	RMSE
Tree Level	$MOE_{est} = f(Vtree)$	0,73	$103 \cdot 10^{-5}$
Log Level	$MOE_{est} = f(Vlog)$	0,75	$992 \cdot 10^{-6}$
Timber Level (green condition)	$MOE_{est} = f(Vgt)$	0,78	756,8
Timber Level (dry condition)	$MOE_{est} = f(Vdt)$	0,65	789,5

MOE_{est}: estimated MOE (N/mm^2); *Vtree*: standing tree velocity; *Vlog*: log velocity; *Vgt*: timber velocity in green conditions; *Vdt*: timber velocity in dry conditions.

Both standing tree as log level, a good relationship has been found to estimate the average MOE from the tree and log velocities, suggesting an opportunity to classify stands, trees and logs of sweet chestnut using acoustic technology.

Other studies found a negative and significant linear correlation between DBH and acoustic velocity and MOE (Moore et al. 2009, Santaclara et al. 2011). In this case, the relationship was not significant so the DBH has been removed from the model.

At timber level the acoustic velocity measured in green conditions has been a better estimator of MOE (R^2=0,78) than the velocity in dry conditions (R^2=0,65).

Acoustic segregation of logs

From this good relationship between acoustic velocity measured on logs and average MOE, to propose an acoustic segregation of logs would be interesting in order to improve the industrial performance in structural timber production. To stablish classes based on stiffness, each log has been characterized by a strength class (SClog) as a function of its average MOE and according to European Standard EN 338:2009. Thus, assigned classes ranging from R (rejected), D18, D24 and D30 or higher.
A Variance Analysis (ANOVA) with *Vlog* as a dependent variable and SClog as factor allows to know if there are differences in acoustic velocity between classes. To assess which classes were significantly different a multiple range test (LSD) was carried out. The results show three groups of acoustic velocity and stiffness significantly different (Table 2) and allow to establish three velocity ranges with the main objective to obtain timber with a strength class of D24 or higher according to strength class assigned to Spanish sweet chestnut in the European Standard EN1912 (Figure 2): R (rejected), D18 (D18 and D24) and D24 (D30 or higher).

Table 3—ANOVA table for *Vlog* by SClog

Source	*Sum of Squares*	*Df*	*Mean Square*	*F-Ratio*	*P-Value*
Between groups	3,10935E6	3	1,03645E6	14,30	0,0000
Within groups	2,82751E6	39	72500,3		
Total (Corr.)	5,93686E6	42			

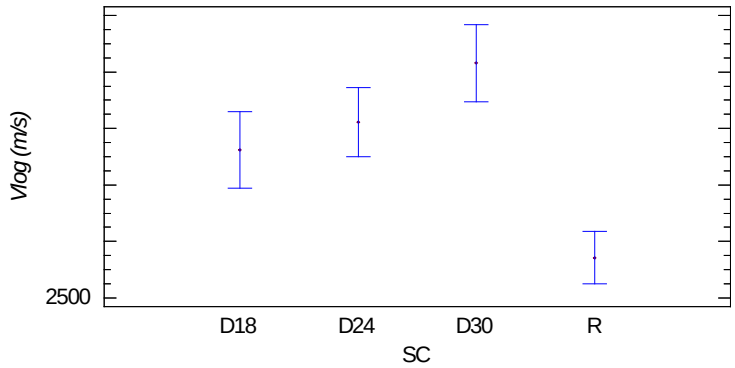

Figure 2—Means plot for *Vlog* by SClog

With the estimate standard error and using the inferior prediction limits of each group for safety reasons, the acoustic classification ranges were established: VCR, VCD18 and VCD24. The range velocity values are not exposed for confidentiality matters of the company that has financed the project. The distribution of SClog within each velocity range has been studied to evaluate the adequacy of the proposal (Figure 3).
Two important points are satisfied with these velocity ranges: no log average MOE has been overestimated, i.e. it has not been assigned to a higher class than its real SClog, and the rejections (non structural timber) are all in the VCR class, therefore safely set a minimum acoustic velocity for sorting logs is possible.
The VCD24 class would be the acoustic range to ensure chestnut timber with a strength class D24.
VCD18 is an intermediate range composed of logs of which are possible to obtain timber for structural purposes. The 57% is composed of logs with D24 and D30 of SClog which have been underestimated. In this case, a subsequent acoustic grading of sawn timber in green conditions could be proposed from the fitted model.

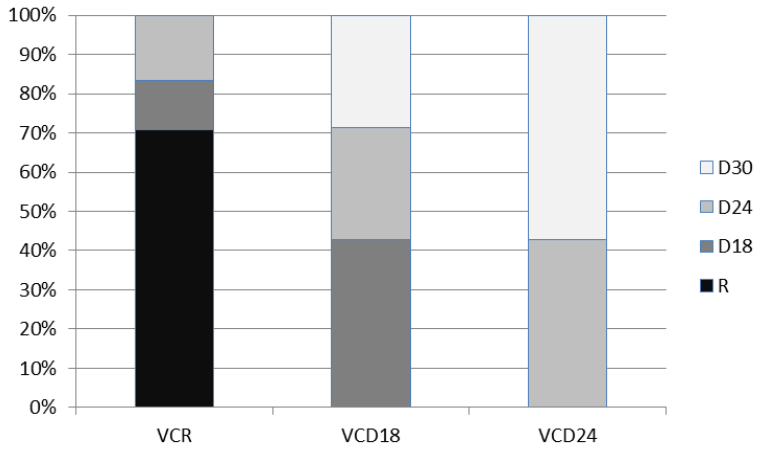

Figure 3—Bar plot: percentage of SClog within each Velocity Range

Conclusions

The acoustic technology has demonstrated a good efficiency for sweet chestnut trees and logs segregation and the possibility of establishing classification systems based on acoustic velocity.

The relationship at the three levels, tree, log and timber, between acoustic velocity and MOE has been good, and considering that in the fitted models the acoustic velocity was the only predictor variable. This fact would improve the practical application, avoiding measuring other variables. However, given the existing variability between stands and trees of Spanish *Castanea sativa* and in order to fit a more robust model to the changes, it would be necessary to try to include other parameters like the height or slenderness of the tree, diameter of the logs, etc., which have already proved to have a good relationship with the MOE for other species (Wang et al. 2009, Santaclara et al. 2011).

At tree level, from an industrial point of view, there is an opportunity to improve the mechanical properties of Spanish *Castanea sativa* and identify the best trees or stands for structural purposes. At log level, although the correlation is nowhere near perfect, it does not need to be, to segregate logs based on acoustic velocity should improve the quality of logs destined to structural timber production. Therefore, for industrial supplies, to carry out a previous classification based on acoustic velocity on standing trees or logs would increase the performance and resource optimization, achieving significant financial advantages in industry.

References

Carter, P. 2011. Real-time measures of wood quality – transition from research to application. In: 17th International Nondestructive Testing and Evaluation of Wood Symposium WoodNDT. Vol 1, pp.34-39, Sopron, Hungary.

CEN EN 1912:2012. Structural timber. Strength classes. Assignment of visual grades and species.

CEN EN 338:2010. Structural timber. Strength classes.

CEN EN 408:2010. Timber structures. Structural timber and glued laminated timber. Determination of some physical and mechanical properties.

Moore, J.R.; Lyon, A.J.; Searles, G.J.; Vihermaa, L.E. 2009. The effects of site and stand factors on the tree and wood quality of Sitka spruce growing in the United Kingdom. Silva Fenn, 43(3), 383-396.

Santaclara, O.; Álvarez, J.G.; Merlo, E. 2011. Modeling structural lumber quality for *Pinus pinaster* Ait. in northwestern Spain using standing trees acoustic assessment, tree characteristics and stand variables. In: 17th International Nondestructive Testing and Evaluation of Wood Symposium. Vol 1, pp.127-134, Sopron, Hungary.

UNE 56546:2013. Visual grading for structural sawn timber. Hardwood timber.

Wang, X; Verrill, S; Lowell, E; Ross, R; Herian, V. 2009. Acoustic sorting models for log segregation. In: Proceedings of the 16th International Symposium on Nondestructive Testing and Evaluation of Wood. p. 45-51. Beijing, China.

Wang, X. 2013. Acoustic measurements on trees and logs: a review and analysis. Wood Sci Technol. 47: 965-975.

Nondestructive Growth Study in *Araucaria angustifolia*

Ricardo A. Malinovski
Laboratório de Operações Florestais, UFPR- Rua Lothário Meissner, 632, Curitiba- PR, Brazil, ricardomalinovski@ufpr. br

Willian S. Wiese
Laboratório de Operações Florestais, UFPR- Rua Lothário Meissner, 632, Curitiba- PR, Brazil, willianswiese@gmail.com

Leif Nutto
Malinovski Florestal – Rua Itupava 1541, Alto da XV, Curitiba PR, Brazil, leif@malinovski.com.br

Tobias Biechele
IML System GmbH, Parkstraße 33, 69168 Wiesloch, Germany, tobias.biechele@iml.de

Silvia Martin
Laboratório de Operações Florestais, UFPR- Rua Lothário Meissner, 632, Curitiba- PR, Brazil, silviasmartin@gmail.com

Abstract

For developing management plans for protected tree species detailed data about tree growth are required, obtained applying a non-destructive method. *Araucaria angustifolia* is such an endangered species where even for research purpose no felling permit is given. The objective of the study was to test the precision of an IML-RESI PD® for non-destructive year ring analysis. The data of the PD were compared to a manual measurement of the year rings and the deviation between both methods was calculated. It turned out that the results of both methods do not differ significantly at a 5% level. The PD is an option for non-destructive growth data collection in *Araucaria angustifolia.*

Keywords: IML-RESI PD®, drilling resistance, year ring analysis, growth rings

Introduction

An extensive part of the southern Brazilian plateaus was covered by a forest formation called Mixed Ombrophilous Forest where the most characteristic species is the *Araucaria angustifolia* (Bortolini) Kuntze. According to Maack (1981), in the beginning of the 20th century, 83% of the Parana State was covered by this formation. However, in less than a hundred years, due to land changes and overexploitation, this area was reduced and the remaining forests areas in advanced successional stages correspond to less than 1% of the state (CASTELLA; BRITEZ, 2004). The *Araucaria angustifolia* is known for its good stem form, wood quality, aesthetics, and workability and, therefore, was one of the main commercialized species in the last century. In most cases there was no management plan for the exploitation. Facing this situation, environmental laws adopted a very protective attitude towards the species, making it difficult to obtain a license to explore it even with approved management plans. Nevertheless there exist perspectives for the rational use in the medium term under management plans. These plans will have to be developed using reliable data about growth and production in order to meet

sustainability goals and to be approved by the environmental authorities. One possibility for growth studies is the use of a non-destructive tool called Power Drill® from the company IML. The equipment provides a graphic representation of the energy consumed by the electric engine when penetrating a rotating needle into the wood sample, showing a resistance variation with change of internal wood quality. A series of variables can be determined relating the characteristics of the material (RINN ET AL. 1996). One variable that can be determined is wood density which is strongly correlated with wood resistance measured in terms of total energy consumed. Due to anatomic characteristics of the *Araucaria angustifolia*, early wood and late wood are visibly separated and the denser wood is formed during the fall and the winter, at the end of the vegetation period. The provided graphs show a succession of peaks, representing the higher or lower difficulty in the early or late wood as being components of an annual ring. The penetration of the needle in the radial direction shows the annual rings from bark to pith. This way all the annual rings are measured, enabling the determination of growth potential and the development of production tables. The study aimed to test the equipment and its methodology to verify their actual performance in measuring ring increment of the *Araucaria angustifolia* in a non-destructive way.

Material and Method

For this purpose, it was chosen to compare this methodology with the traditional methodology, where rings are counted and measured manually. Twelve samples of *Araucaria angustifolia* discs at approximately 0.2 m height were collected in a local sawmill in the city of União da Vitória, state of Paraná. After collection of the discs, the samples were sanded for manual measurement and afterwards perforated by the Power Drill®. For data interpretation the software PD-Tools was used, inclusive for the ring width measurement. The information generated this way was compared to the results of the manual measurement

Results

Assuming that the manual measurement was of a 100% precision, the T-Test at a 5% significance level was used to compare the average of the two measurements. The results showed that the manual and the PD measurements do not differ significantly. The Power Drill® can be used as a non-destructive tool for annual ring measurement of standing trees of *Araucaria angustifolia*. It may be used for non-destructive diameter growth analysis at standing trees, allowing the elaboration of management plans with an acceptable precision.

References

Castella, P. R.; Britez, R. M. de (Org.). A floresta com araucária no Paraná: conservação e diagnóstico dos remanescentes florestais. Projeto de Conservação e Utilização Sustentável da Diversidade Biológica Brasileira – PROBIO, Brasília, DF: Ministério do Meio Ambiente, 233 p, 2004.

MAACK, R. Geografia Física do Estado do Paraná. 2° Ed; J. Olympio; Curitiba; Secretaria da Cultura e do Esporte do Governo do Estado do Paraná. 1981.

Rinn, F., Schweingruber, F.H., and Schar, E. 1996. Resistograph and X- ray density charts of wood: comparative evaluation of drill resistance profiles and X- ray density charts of different wood species. Holzforschung 50: 303-311.

Session 8

In-Place Assessment of Structures

In-situ Synchrotron based micro-tomography and acoustic emission measurement of Norway spruce samples under tensile load

Peter Niemz
Wood Physics, Institute for Building Materials, ETH, Zurich, Switzerland, niemzp@retired.ethz.ch
Holz und Bau, Berner Fachhochschule Architektur, Biel, Switzerland, peter.niemz@bfh.ch

Franziska Baensch
Faculty of Wood Science and Technology, Eberswalde University for Sustainable Development, Eberswalde, Germany, franziska.baensch@hnee.de

Michaela Zauner
Wood Physics, Institute for Building Materials, ETH, Zurich, Switzerland, mzauner@ethz.ch

Andreas J. Brunner
Swiss Federal Laboratories for Materials Science, Empa, Dübendorf, Switzerland, Andreas.Brunner@empa.ch

Abstract

Damage mechanisms occurring in a material during increasing load lead to the emission of acoustic signals. Although a multitude of experiments have been done for acoustic emission measurements on wood, the assignment of signals to the initiating mechanisms was not yet possible. Therefore, in situ details of the structural changes generating the acoustic emission signals need to be known. To monitor these changes, additional imaging methods are necessary.

This contribution presents tensile tests on miniature samples of wood performed by means of a testing device that was implemented at the TOMCAT beam line (PSI, SLS, Villigen) to combine the in situ scanning of the structural changes with the monitoring of acoustic emission. Besides samples made of solid Norway spruce loaded in the longitudinal and in the radial direction, three different samples made of glued Norway spruce lamellae (either tangentially or longitudinally oriented) were investigated.

By means of this experimental setup it was possible to correlate the acoustic emission signals and the associated changes within the microstructure. Based on all results, comprising the individual failure mechanisms, their accumulation and their interactions, a detailed reconstruction of the failure evolution in the samples during loading could be realized.

Keywords: Synchrotron based micro-tomography, acoustic emission, in-situ, tension, Norway spruce, bonded wood

Introduction

General information

The observation of the complex hierarchical interdependency of damage phenomena within the wooden structure is a key challenge. Therefore, the acoustic emission (AE) measurement is a useful tool, because it enables a multi-scale analysis of the damage progress with respect to load history and over the whole specimen's volume (Grosse and Ohtsu 2008). An additional advantage of the AE method is the high time resolution with which the information of the defect generation is recorded. However, the key issue in AE analysis concerns the interpretation of the detected AE signals regarding their origin phenomena. To this aim, the present AE analysis focuses on the AE signals' frequency parameters due to the fact that similar damage mechanisms stimulate certain frequencies and, hence, introduce intrinsic similarities in the spectra. To identify classes of AE signals based on the similarities in their frequency spectra, a method of unsupervised pattern recognition (UPR) was employed (Sause et al. 2012, Baensch et al. 2015).

Furthermore, a substantial and detailed interpretation of these AE signal classes requires additional imaging information. To this purpose, the feasibility of real-time studies on sub-macroscopic damage mechanisms combining synchronous AE and tomographic monitoring was already proven for several materials (Chotard et al. 2003, Maire et al. 2007). To investigate anatomical features of the wooden microstructure, the suitability of computed micro-tomography (µCT) based on synchrotron radiation is proven satisfactory, since a spatial resolution down to $1\mu m^3$ is feasible (Steppe et al. 2004, Trtik et al. 2007, Van den Bulcke et al. 2009), and further, the micro-structure of wood under different moisture loads was investigated by µCT (Derome et al. 2011). For compression and bending tests on wood, the potential of the µCT method was already proven to evaluate deformations and details on structural changes at several loading steps (Forsberg et al. 2008, Zauner 2014).

In the light of these experiences, to investigate the damage evolution in wood at microscopic scale, tensile tests of miniature spruce wood specimens are presented, which are monitored by both AE and, simultaneously, µCT. The results received by the µCT provide complementary evidences for interpreting the AE signal clusters. Herein, the monitored results of tensile loading solid wood and glued wood are presented and discussed.

Material and Method

Solid and glued wood samples

The specimens were cut from clear spruce wood (Picea abies (L.) Karst.) grown in Switzerland. The mechanical properties of these wood samples are characterized by a low average raw density of approx. 340 kg/m^3. Two specimens differing in fiber-load-angle were investigated. The radial (R) specimen was loaded in the R direction and the longitudinal (L) specimen was loaded parallel to the grain, whereby a L specimen was selected that only contained earlywood within the test cross section (Fig. 1a). To ensure a defined crack initiation within the volume of interest (VOI), which can be monitored by both AE and µCT, the specimens were tapered. The L specimen was taper shaped at all four sides yielding a test cross section of 1 mm^2, whereas the R specimen had only a two-sided taper of approx. 4 mm^2 test cross section.

Moreover, the investigation was carried out on bonded wood specimens of miniature size made of clear spruce wood lamellae. Urea formaldehyde adhesive (UF) was used for gluing the wood lamellae. Three different specimen types were tested (Fig. 1c), whereby the geometry of these miniature specimens is similar to that of the miniature specimens made of solid spruce wood.

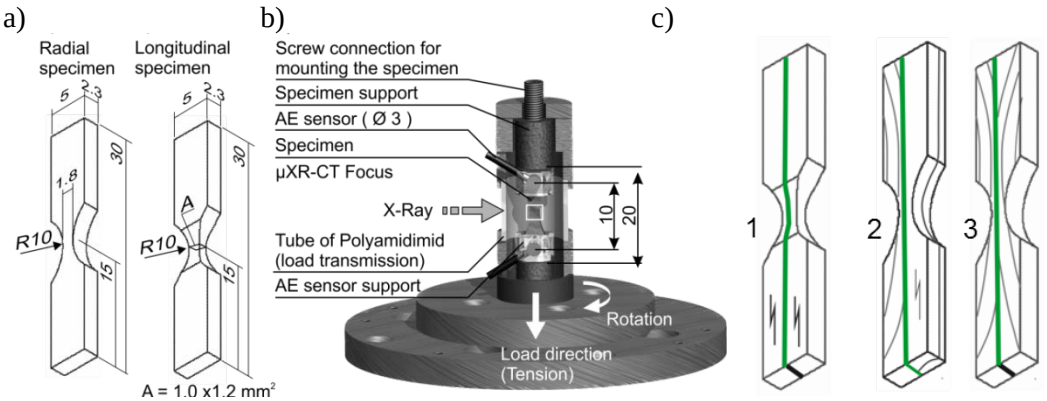

Figure 1—Specimens and testing device. a) Solid wood samples (R, L). b) Experimental setup. c) Glued samples (LL, TL, TT).

Test procedure and analysis

The tensile tests were performed with a loading device (load cell of 1kN) for miniature specimens designed for implementation at the synchrotron beam line TOMCAT at the Paul Scherrer Institute in Villingen, Switzerland (Fig. 1b) (Zauner et al. 2012). The tensile tests were performed stepwise by stopping the traverse at pre-determined positions, which were preliminarily defined with respect to the predicted AE occurrence. At each traverse stop, a µCT scan was performed. Before and after each load step, the quality of the AE sensor coupling was checked by auto-calibration (in the course of which each sensor served subsequently as emitter and sensor). AE and µCT data were synchronized by the load signal output of the testing device.

For AE analysis, the signals were windowed with a Hamming window function. For the unsupervised pattern recognition (UPR) method, nine features were chosen for input, namely, the peak frequency (PF), center of gravity frequency (CGF), weighted peak frequency (WPF) and six partial power levels. For more details on the UPR method, the reader is advised to Sause et al. 2012 and Baensch et al. 2015a.

Results and Discussion

Solid wood

For both specimen types, the signals of cluster A_R (radial tests) and A_L (longitudinal tests) contain WPFs below 500 kHz, while those of cluster B_R and B_L contain WPFs above 500 kHz (Fig. 2). The partial power level PP2 presents the ratio of the range of 200-400 kHz compared to the whole spectra (0-1000 kHz). The clusters can roughly be differentiated into signals with a relatively high share of low frequency (A clusters) and high frequency contents (B clusters), respectively.

Within the damage history, the brittle failure behavior of the R specimens is reflected, as the AE starts just shortly before the ultimate failure (above 70% of maximum load). Based on the reconstruction of the structure yielded by means of µCT, a first hypothesis was already outlined, which assigns the low-frequency signals of cluster A to cell separation mechanisms and the high-frequency cluster B to brittle trans-wall cracks (Baensch et al. 2015b).

Glued wood

Similarly to the AE cluster results from the tensile test on the solid spruce wood samples R and L, the UPR method yielded two signal classes for the three types of bonded spruce wood samples. Again, the signals of cluster A contain WPFs below 500 kHz, while those of cluster B contain WPFs above 500 kHz (Fig. 3). The clusters essentially differ with respect to higher shares of low and high frequency components. There is no indication of a separate, third signal cluster that can be attributed to the adhesive layer in the bonded wood in comparison with the solid wood samples.

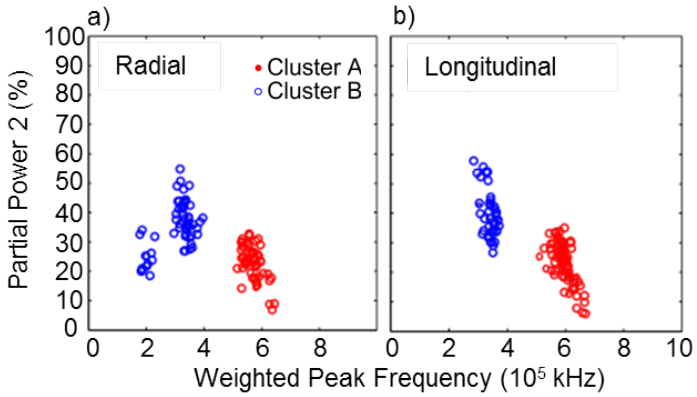

Figure 2—The clustering of the AE signals yields the two clusters A and B. Partial Power 2 (range of 200-400 kHz) vs. WPF are presented for AE signals detected during tensile testing of the spruce specimens in the radial (a) and longitudinal (b) direction.

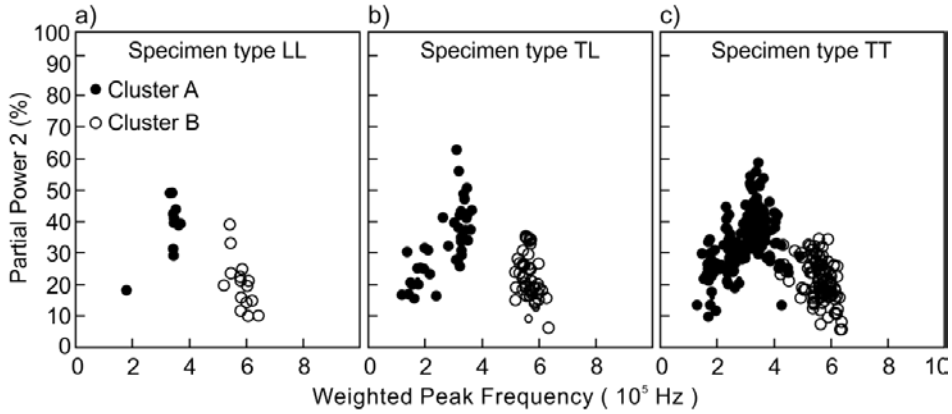

Figure 3—Clusters formed by pattern recognition of acoustic emission signal for bonded wood samples in different load directions. The partial power 2 (200-400kHz) is plotted against weighted peak frequency.

The different impact of the adhesive layer depending on grain orientation is demonstrated by the results from µCT scans recorded between the loading steps. Compared to the UF adhesive, the longitudinally loaded layers have stronger load bearing capabilities, whereas the tangentially loaded wood layers reveal greater weakness. The failure of the LL (Fig. 1c, 1) was mainly the result of the damage evolution within the wooden structure (Fig. 4). Especially the scan after ultimate failure (Fig. 4a-b) shows a crack path mainly running along the growth ring boundary (T direction) and along the grain (R direction), whereby passing the glue line seems to have no impact on crack path formation.

In contrast, for the TT sample, the adhesive acted as reinforcement of the structure and played a more important role. For the TT specimen, crack propagation within the adhesive layer was observed.

Furthermore, the cluster pattern of the low-frequency signals of cluster A (Fig. 4c) significantly differs compared to the cluster A patterns of all the other tested samples (Fig. 2, Fig 4a-b). Thus, it is assumed that AE signals generated by damage mechanisms of the adhesive layer might be covered by the A cluster (Baensch 2015).

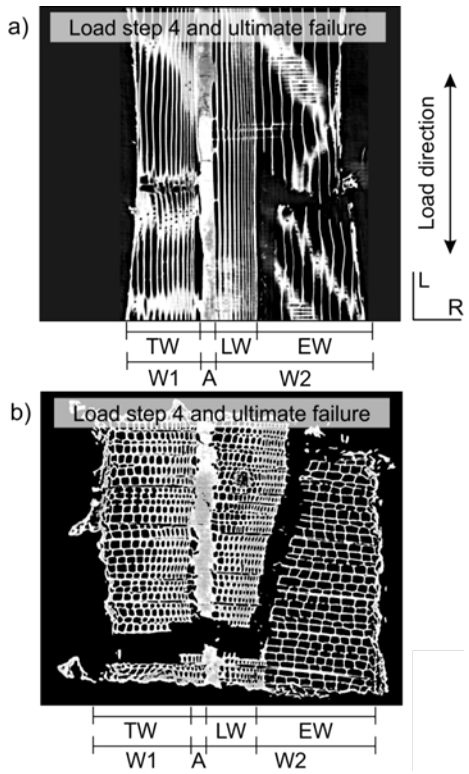

Figure 4—Fracture pattern of the bonded LL specimen with the view a) parallel and b) perpendicular to load after load step 4. Wood layers W1 and W2 bonded together with urea formaldehyde adhesive (A). Early wood (EW), transition wood (TW) and latewood (LW) tissue are distinguished.

Conclusions

The experiments allow the detection of the multi-scaled damage evolution in wood by combining the AE method with the in-situ μCT monitoring. By this, comprehensive datasets at different load states of the specimens were recorded. First tentative conclusions concerning the interpretation of the AE signal classes will have to be verified by further investigations (Baensch 2015).

An ongoing analysis of the reconstruction from the μCT monitoring will focus on describing structure and structural changes at microscopic scale. From these results, a dedicated segmentation and geometric parameterization of specific wood cells is currently being performed and, based on a 3D morphological approach, the volumetric strain fields at different load states are analyzed and discussed with regard to the final fracture path (Sanabria et al. 2015). Other tests with lap shear samples for glued wood are important for the next steps.

Anknowledgments

The authors acknowledge the financial support of the Swiss National Science Foundation under grant SNF-Project 127134.

References

Baensch, F.; Sause, M.G.R.; Brunner, A. J.; Niemz, P. 2015a. Damage Evolution in Wood - Pattern Recognition based on Acoustic Emission Frequency Spectra. Holzforschung. 69: 357-365.

Baensch, F.; Zauner, M.; Pinzer, B.; Sanabria, S.J.; Brunner, A.J.; Stampanoni, M.; Niemz, P. 2015b. Damage Evolution in Wood – X-ray micro-tomography and Complementary Evidence for Interpreting Acoustic Emission Behavior. Holzforschung, DOI: 10.1515/hf-2014-0152.

Baensch, F. 2015. Damage evolution in wood and layered wood composites monitored in situ by acoustic emission, digital image correlation and synchrotron based tomographic microscopy. PhD, ETH Zurich.

Chotard, T.J.; Smith, A.; Bonceur, M. P.; Fargeot, D.; Gault, C. 2003. Characterisation of early stage calcium aluminate cement hydration by combination of non-destructive techniques: acoustic emission and X-ray tomography. J. Eur. Ceram. Soc. 23(13):2211-2223.

Derome, D.; Griffa, M.; Koebel, M.; Carmeliet, J. 2011. Hysteretic swelling of wood at cellular scale probed by phase-contrast X-ray tomography. J. Struct. Biol. 173(1):180-190.

Forsberg, F.; Mooser, R.; Arnold, M.; Hack, E.; Wyss, P. 2008. 3D micro-scale deformations of wood in bending: synchrotron radiation muCT data analyzed with digital volume correlation. J. Struct. Biol. 164(3):255-262.

Grosse, C.; Ohtsu, M. (Eds.) 2008 Acoustic emission testing in engineering - Basics and applications. Springer publ., Heidelberg.

Maire, E.; Carmona, V.; Courbon, J.; Ludwig, W. 2007. Fast X-ray tomography and acoustic emission study of damage in metals during continuous tensile tests. Acta Mater. 55(20):6806-6815.

Sanabria, S.J.; Zauner, M.; Baensch, F.; Niemz, P. 2015. 3D morphological analysis of X-ray synchrotron tomograms of wood microstructure subjected to mechanical load for deformation measurements at the individual cell scale. In preparation.

Sause, M.G.R.; Gribov, A.; Unwin, A.R.; Horn, S. 2012. Pattern recognition approach to identify natural clusters of acoustic emission signals. Pattern Recognit. Lett. 33:17-23.

Steppe, K.; Cnudde, V.; Girard, C.; Lemeur, R.; Cnudde, J.-P.; Jacobs, P. 2004. Use of X-ray computed microtomography for non-invasive determination of wood anatomical characteristics. J. Struct. Biol. 148(1):11-21.

Trtik, P.; Dual, J.; Keunecke, D.; Mannes, D.; Niemz, P.; Stähli, P.; Kaestner, A.; Groso, A.; Stampanoni, M. 2007. 3D imaging of microstructure of spruce wood. J. Struct. Biol. 159(1):46-55.

Van den Bulcke, J.; Boone, M.; Van Acker, J.; Stevens, M.; Van Hoorebeke, L. 2009. X-ray tomography as a tool for detailed anatomical analysis. Ann. For. Sci. 66(5):508-520.

Zauner, M.; Keunecke, D.; Mokso, R.; Stampanoni, M.; Niemz, P. 2012. Synchrotron-based tomographic microscopy (SbTM) of wood: development of a testing device and observation of plastic deformation of uniaxially compressed Norway spruce specimens. Holzforschung 66(8):973-979.

Zauner, M. 2014. In -situ synchrotron based tomographic microscopy of uniaxially loaded wood: in –situ testing device, procedures and experimental investigations. PhD thesis, ETH Zürich

The influence of sensor placement on in-situ ultrasound wave velocity measurement

Francisco Arriaga
Department of Forest and Environmental Engineering and Management. Universidad Politécnica de Madrid, Madrid, Spain, francisco.arriaga@upm.es

Daniel F. Llana
Department of Forest and Environmental Engineering and Management. Universidad Politécnica de Madrid, Madrid, Spain, danielfllana@gmail.com

Roberto Martínez
Department of Agroforestry Engineering. Universidad Santiago de Compostela, Lugo, Spain, robertodmartinezlopez@gmail.com

Miguel Esteban
Department of Forest and Environmental Engineering and Management. Universidad Politécnica de Madrid, Madrid, Spain, miguel.esteban@upm.es

Guillermo Íñiguez-González
Department of Forest and Environmental Engineering and Management. Universidad Politécnica de Madrid, Madrid, Spain, guillermo.iniguez@upm.es

Abstract

Ultrasound wave velocity was measured in 30 pieces of Spanish Scots pine (*Pinus sylvestris* L.), 90 x 140 mm in cross-section and 4 m long. Five different sensor placement arrangements were used: end to end (V_0), face to opposite face, edge to opposite edge, face to same face and edge to same edge. The pieces were successively shortened to 3, 2 and 1 m, in order to obtain these velocities and their ratios to reference value V_0 for different lengths and angles with respect to the piece axis for the crossed measurements. The velocity obtained in crossed measurements is lower than V_0. A correction coefficient for crossed velocities is proposed, depending on the angle, to adjust them to the V_0 benchmark. The velocities measured on a surface, are also lower than V_0, and their ratio with respect to V_0 is close to 0.97 for distances equal to or greater than 18 times the depth of the beam.

Keywords: nondestructive techniques, sensors positioning, ultrasonic wave, wave velocity

Introduction

Non-destructive methods are used in the evaluation of existing timber structures, among other uses. For example, determination of wave transmission velocity makes it possible to estimate the mechanical properties of structural elements. Studies and laboratory research in this field are usually performed by measuring the Time-of-Flight (ToF) of the wave between the ends of the pieces.

This is the best way to measure ToF, in a direction parallel to the axis of the piece and approximately parallel to the grain. But in practice, during the in situ inspection of timber structures this is not possible,

and it is necessary to place sensors differently. It is usually impossible to access the ends of timber pieces in existing structures, and ToF has to be measured to determine wave velocity by placing one of the sensors on one face, and the other in the opposite face, in a segment with a length less than the total length of the piece. We term this arrangement 'crossed measurement'. There is therefore a small angle between the straight line joining both sensors and the grain. This angle is usually from 1.5 to 10º, and this deviation give rise to a slightly lower velocity compared with measurement parallel to the grain.

In cases such as timber floor joists where only the lower edges are visible, or in columns which are embedded in walls and covered with 1 or 2 cm of plaster, ToF measurements must be done by placing both sensors on the same face of the timber piece. We term this arrangement 'surface measurement'. The velocity obtained using this procedure usually gives slightly lower values than measurement parallel to the grain.

By these methods (crossed and surface measurements) ToF are measured in partial segments of the length of the piece, so the information collected by the wave is less representative of the overall quality of the piece. The correlation between mechanical properties and wave velocity varies depending on the segment length considered.

The objective of this research is to analyze the effect of these different sensor positions on ultrasound wave velocity measurement in existing timber structures (crossed and surface measurements) with respect to end-to-end measurement, together with the influence of the length of the tested central segment of the piece.

Material and methods

This study used 30 pieces of dry planed structural Spanish Scots pine (*Pinus sylvestris* L.) with nominal dimensions of 90 by 140 by 4000 mm. The moisture content (MC) of these timber specimens was measured using an electrical resistance moisture meter (Gann RTU600, Gann Mess-u, Regeltechnik Gmbh, Germany) according to the EN 13183-2 (2002) standard. The average MC of the pieces was 9.1%, with a coefficient of variation (COV) of 10.7%. The maximum and minimum values were 8 and 11.1%, respectively. No correction for MC was made for modulus of elasticity or for velocity, due to the low variation of MC in the timber pieces.

Time of flight measurements

Ultrasound wave Time-of-Flight (ToF) was measured using the Sylvatest Duo (CBS-CBT, France) with conical sensors at 22 kHz. This device determines an average ToF obtained from 5 consecutive readings for each measurement. Measurements were performed using five different sensor placement arrangements: longitudinal (parallel to the grain) by placing sensors at the ends of each specimen, one on each end (V_0); crossed, by placing one sensor on a face and the other on the opposite face (V_{cf}); crossed by placing one sensor on an edge and the other on the opposite edge (V_{ce}); and finally, surface measurement by placing both sensors on the same face (V_{sf}) or on the same edge (V_{se}), figure 1.

Wave velocity (V) was determined according to the following equation 1, where L is the distance between sensors (m) and T is the average time-of-flight measured.

$$V = L/T \quad (1)$$

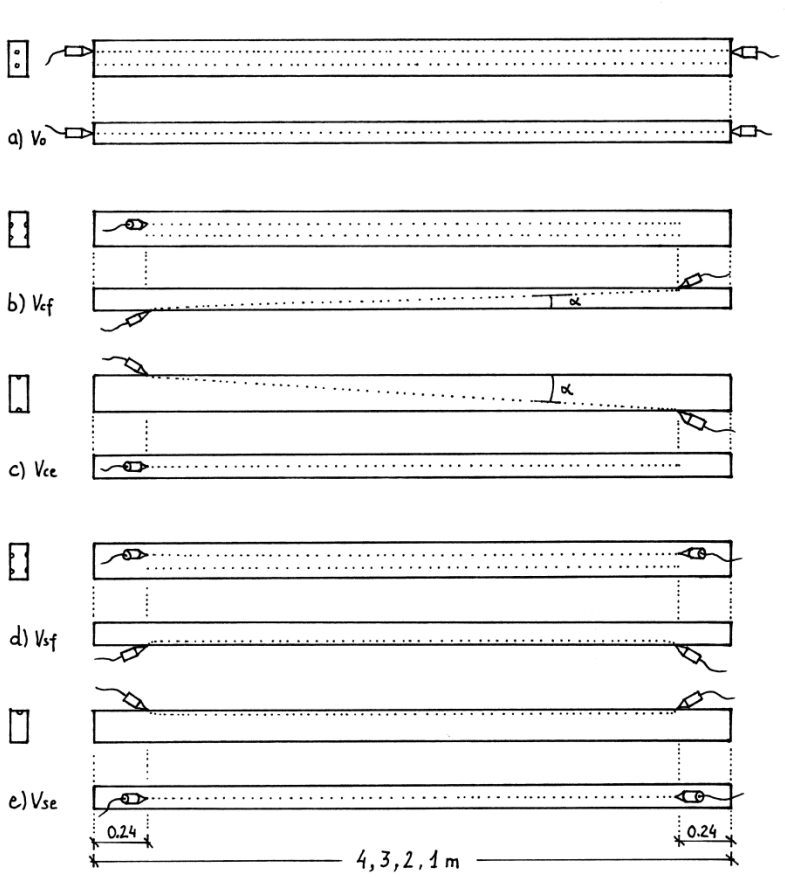

Figure 1— Sensor placement arrangements: a) Parallel to the grain; b) Crossed measurement between opposite faces; c) Crossed measurement between opposite edges; d) Surface measurement on the same face, and e) Surface measurement on the same edge.

Crossed and surface measurements were performed at a distance equal to 240 mm from the end of the piece in order to avoid any possible border effect. For each arrangement, two measurement points were considered, located at one and two thirds of the depth of the piece, except in edge measurement where due to its narrowness only one measurement was made, figure 2. Sensor orientation in crossed and surface measurements was at an angle equal to or slightly less than 45º with respect to the timber surface. The depth of the sensor point in the timber was 10 to 12 mm when parallel to the grain and inclined.

Following initial measurements on the 4-m-long wood specimens, each piece of wood was subsequently reduced to 3 m long by cutting a 0.5 m long section from each end. This procedure was repeated two more times to obtain wood specimens of 3, 2 and 1 m in length. Figure 3 shows the cutting procedures to obtain the target lengths. In this way, parallel to the grain ToF and velocity V_0 was obtained for pieces 4, 3, 2 and 1 m long, together with crossed measurements for 3.52, 2.52, 1.52 and 0.52 m lengths, corresponding to nominal distances between sensors and angles of 3.521 m/1.465º, 2.522 m/2.045º, 1.523 m/3.388º and 0.528 m/9.819º for V_{cf}, and 3.523 m/2.277º, 2.524 m/3.180º, 1.526 m/5.262º and 0.538 m/15.068º for V_{ce}. To summarize, velocities in crossed arrangements were obtained for 8 different angles from 1.627º to 15.068º and their ratios with respect to the benchmark value V_0 at the closest corresponding distance (4, 3, 2 and 1 m) were calculated.

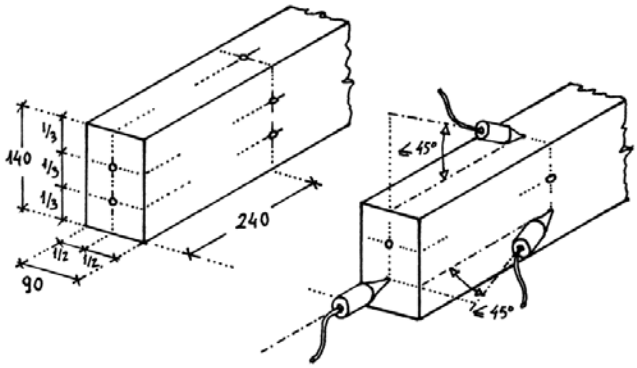

Figure 2— Sensor positioning.

In a similar way, ToF and velocity in surface measurement was obtained for each length (3.52, 2.52, 1.52 and 0.52 m) on the faces V_{sf} and the edges V_{se}, calculating the ratios with respect to the parallel velocity V_0.

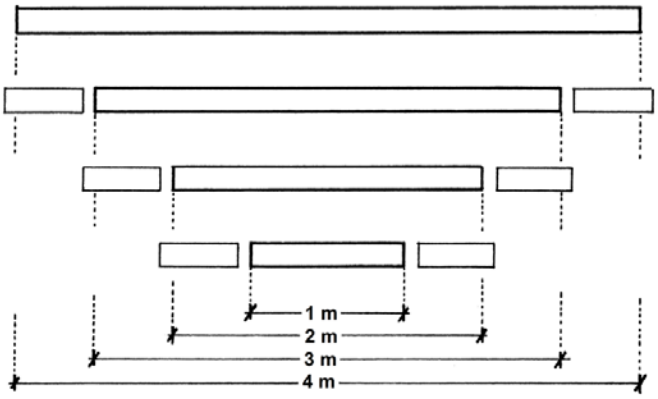

Figure 3— **Procedure** for reducing the length of the specimens.

Static modulus of elasticity

The static modulus of elasticity (*MOE*) of timber pieces were determined by static bending test according to European Standard EN 408 (2010+A1:2012). The test piece is simply supported and symmetrically loaded in bending at the thirds of a span equal to 18 times the depth of the piece, Figure 4. This test was performed when the timber pieces were 3 m long.

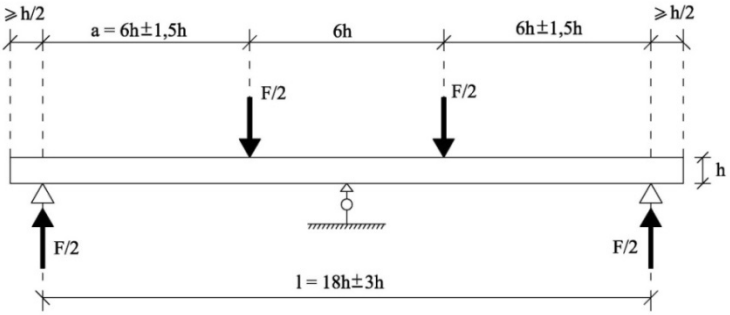

Figure 4— Arrangement for bending test according to European Standard EN 408 (2010+A1:2012).

One of the most relevant singularities of the timber grading process is knottiness, which can be characterized using a simplified parameter known as CKDR (Divos 2002). The knot diameter ratio (KDR) is knot diameter divided by the depth or width of the piece. The Concentrated KDR (CKDR) is the sum of the KDRs of the knots existing in any 15 cm length of a timber piece. The maximum CKDR which includes all 4 faces represents the quality of the piece, Figure 5. This value of CKDR is obtained for the worst cross section in the whole length of the piece, and it varies from 0 to 1. The CKDR was calculated for each length of the specimen (4, 3, 2 and 1 m) obtaining average values of 0.13, 0.13, 0.12 and 0.10, respectively. This means that knottiness is practically constant in all lengths.

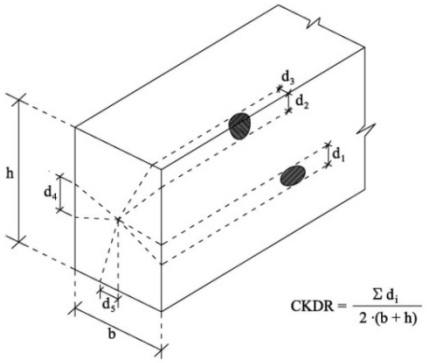

Figure 5— Knot Diameter Ratio (CKDR).

Results and discussion

Angle effect

Figure 6 shows the linear regression between the V_α/V_0 ratio and cos (α), where α is the angle formed by the line between sensors, in crossed measurements, and the direction of the axis of the piece. The coefficient of determination is $R^2 = 0.80$ and the equation is,

$$V_\alpha / V_0 = 5.2563 \cos\alpha - 4.28319 \quad (2)$$

If angle α=0 the ratio V_α/V_0= 0.973 which is approximately equal to the ratio between surface measurements and end to end measurements, as it will be shown later. This value, slightly different to 1, could be explained by an effect originated by the position of sensors in faces (or edges) and not in the ends of the piece.

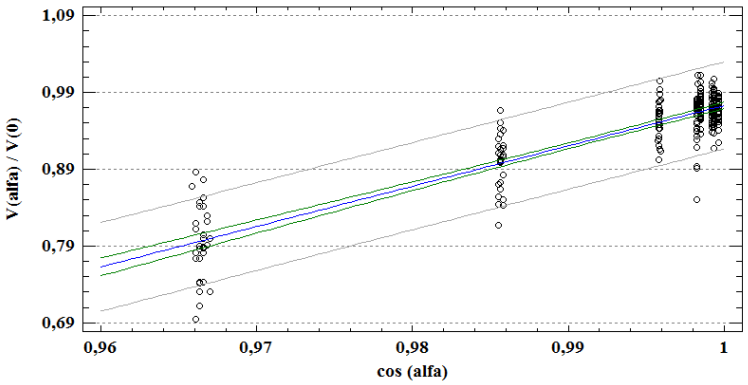

Figure 6— Linear regression: Vα/V_0 ratio vs. cos (α).

The influence of the angle of the grain can be estimated by means of the Hankinson formula (Hankinson 1921). If the property is known for the direction parallel and perpendicular to the grain (P_0 and P_{90}, respectively) the property for an inclined direction, P_α may be obtained according to the following equation,

$$P_\alpha = \frac{P_0}{\frac{P_0}{P_{90}} sin^2\,\alpha + cos^2\,\alpha} \tag{3}$$

and dividing both members of the equation by P_0 and denominating the P_0/P_{90} ratio k, equation 3 takes the following form,

$$\frac{P_\alpha}{P_0} = \frac{1}{k\,sin^2\,\alpha + cos^2\,\alpha} \tag{4}$$

According to some authors the ratio (k value) velocity at 0º over velocity at 90º to the grain is in the order of 2.7 (Gerhards 1982). A ratio of k=3 was obtained for ultrasound velocity in Scots pine in previous studies (Íñiguez et al. 2009). Better agreement with the experimental results obtained in this work for angles between 1.4 and 15º was deduced for k = 5.5. Figure 7a shows equation 4 for a k value of 5.5. Figure 7b compares the results obtained by equations 2 and 4 in the interval 1 to 15º. Although the curves are very close to each other, equation 2 presents a better fit with experimental results. The V_α/V_0 ratio will be termed the modification factor for angle k_α, and it will be used to correct the velocity obtained in crossed measurements.

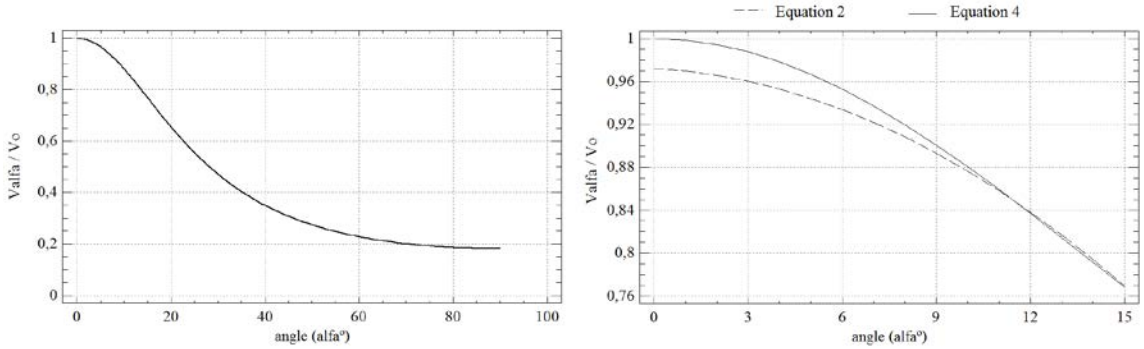

Figure 7— a) Hankinson – eq. 4; b) Equation 2.

Velocity decreases as grain angle increases, although there is no linear relationship. However, it is close to being a linear relationship at certain angles. Some authors estimate that there is 1% velocity loss per degree increase in grain angle up to about 30º (Gerhards 1982). In a previous work (Íñiguez 2007) the velocity parallel to the grain was measured end to end in 80 150x200 mm cross-section 4 m long pieces of radiata pine, obtaining a mean value of V_0 = 4859 m/s. The velocity from face to opposite face over a length equal to 18 times piece thickness was also measured with a mean value of V_{cf} = 4744 m/s. The angle between sensors and the axis of the piece was α = 2.38º. This fall in velocity is equivalent to a 1% fall in velocity for each 1º of angle to the grain.

Surface measurements

Table 1 shows the average ratios between the velocities obtained in surface measurements (sensors on the same face or the same edge) and the velocities measured parallel to the axis of the piece (sensors at the ends of the piece). Figure 8 includes the analysis of variance of these ratios and for each length interval. It can be seen that the "surface" velocity is slightly lower than the "parallel" velocity, except for interval distances of 1-0.52 m in edge measurements. Furthermore, the ratio seems to be close to 0.97 for distances equal to or bigger than 2.52 m. This ratio will be termed the correction factor for surface measurement (k_{sf} and k_{se} for face and edge measurements, respectively).

Table 1— Average values of ratios between velocity measured in the same face or edge (V_{sf} or V_{se}) and velocity measured from end to end (V_0) for each length.

Length (m)	4-3.52	3-2.52	2-1.52	1-0.52
$k_{sf} = V_{sf}/V_0$	0.964	0.967	0.945	0.978
$k_{se} = V_{se}/V_0$	0.971	0.983	0.985	1.041

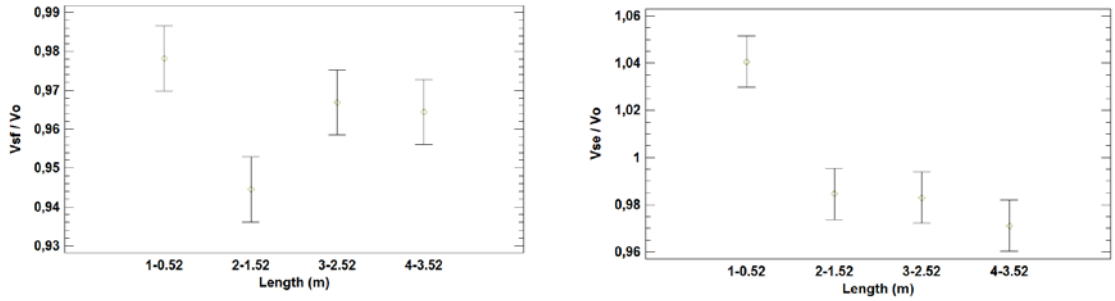

Figure 8— Means plot of one-way analysis of variance for each length. Left: the ratio between velocity measured in the same face (V_{sf}) and end to end velocity (V_0). Right: ratio between velocities measured in the same edge (V_{se}) and end to end velocity (V_0).

A similar value of the correction factor k_{sf} was obtained in previous studies (Íñiguez 2007, Arriaga et al. 2009). The velocity parallel to the grain (V_0) and the velocity from face to opposite face over a length equal to 18 times piece depth (V_{sf}), were measured in 80 150x200 mm cross-section 4 m long pieces of radiata pine. The ratio V_{sf}/V_0 obtained was 0.972, which is very close to the values of table 1.

MOE prediction

The mean MOE obtained was 11776 N/mm^2 with a coefficient of variation, CoV = 12% and the mean velocity from end to end of 3 m long timber pieces was V_0 = 5340 m/s with a CoV = 6%. Figure 9 shows the frequency histogram for both parameters.

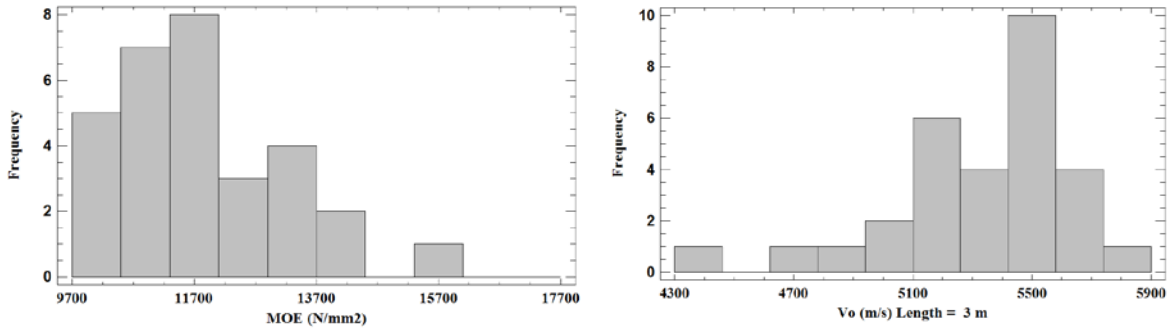

Figure 9— Frequency histogram. Left: MOE, and Right: velocity measured from end to end in 3 m long pieces.

The main purpose of determining wave transmission velocity is to correlate it with the MOE of timber pieces. In this work, the velocity was obtained for 4 different lengths (4, 3, 2 and 1 m) so that MOE can be predicted for each segment of length. Table 2 summarizes the linear regressions between MOE and velocity $V=V_0$ for each length segment, according to the equation,

$$MOE = A \cdot V + B \quad (5)$$

The coefficient of determination does not vary very much for different lengths (0.42 to 0.49), and the highest correlation corresponds to lengths 2 to 3 m long. This means that the best prediction of MOE would be obtained for a central segment of beams 2 to 3 m long (14 to 21 times the depth, h, of the beam).

In practice, in-situ ToF measurements have to be performed between opposite faces or edges, or even between two points of the same face or edge. In a similar way to the correlation established between MOE and V_0 in table 2, linear regressions can be established between MOE and "crossed" or "surface" velocities for 4 different lengths (3.52, 2.52, 1.52 and 0.52 m).

Table 2— Linear regression equation parameters for MOE vs. $V=V_0$ (equation 5).

L (m)	A	B	R^2
1	-4190	2.867	0.44
2	-6322	3.330	0.49
3	-4125	2.978	0.46
4	-3187	2.836	0.42

Table 3 summarizes the linear regressions between MOE and velocity $V=V_{cf}$ and $V=V_{ce}$ for each length segment, according to equation 5. Crossed velocity values have been corrected for angle using the k_α coefficient (equation 2). These results show that the correlation drops to unacceptable values for a measurement distance of 0.52 m (approximately 4 times the depth of the beam, h), while the best results are obtained for pieces 2.52 m long (18h). Using the mean value of both measurements does not give rise to a notable improvement in this prediction.

Table 3— Linear regression equation parameters for MOE vs. $V=V_{cf}$ and V_{ce} (equation 5).

	MOE vs V_{cf}/k_α			MOE vs V_{ce}/k_α			MOE vs $V_{c,mean}$		
L (m)	A	B	R^2	A	B	R^2	A	B	R^2
0.52	1458	1.848	0.18	5752	1.086	0.06	729	1.985	0.15
1.52	-1507	2.464	0.30	-6271	3.311	0.53	-5905	3.261	0.46
2.52	-2250	2.624	0.45	-4600	3.037	0.50	-3890	2.918	0.49
3.52	-2338	2.692	0.41	-735	2.376	0.35	-1746	2.573	0.38

$V_{c,mean}$ mean value of V_{cf}/k_α and V_{ce}/k_α

Table 4 summarizes the linear regressions between MOE and velocity $V=V_{sf}$ and $V=V_{se}$ for each length segment, according to equation 5. The values of surface velocities have been corrected using the k_{sf} or k_{se} coefficient (table 1). Although these results are similar to those of the crossed measurements, they show slightly lower coefficients of determination.

Table 4— Linear regression equation parameters for MOE vs. $V=V_{sf}$ and V_{se} (equation 5).

	MOE vs V_{sf}/k_{sf}			MOE vs V_{se}/k_{se}			MOE vs $V_{s,mean}$		
L (m)	A	B	R^2	A	B	R^2	A	B	R^2
0.52	1949	1.765	0.27	2538	1.661	0.22	-169	2.147	0.31
1.52	-788	2.313	0.33	3004	1.615	0.21	-506	2.261	0.31
2.52	-3353	2.833	0.46	-1791	2.542	0.39	-3570	2.875	0.45
3.52	-2721	2.747	0.43	-2016	2.614	0.42	-2696	2.743	0.43

$V_{s,mean}$ mean value of V_{sf}/k_{sf} and V_{se}/k_{se}

Conclusions

A correction coefficient of ultrasound wave velocity is proposed, to adjust ToF measurements in crossed faces or edges, depending on the cosine of the angle between the line connecting the sensors and the direction of the grain for angles of from 1.4 to 15º. The value is corrected to the reference velocity parallel to the grain. Hankinson's formula can be used for this correction, although it deviates from experimental mean values by around 2%, from 1.4 to 15 °.

A ratio equal to 0.97 was deduced between ultrasonic wave velocity obtained by means of surface measurement with respect to measurement the parallel to the grain, for distances equal to or greater than 2.52 m (18 times the depth of the beam, h). Under this distance surface measurement is not recommended.

The best prediction of MOE was obtained for a central segment of the beam of 2 to 3 m (14h to 21h) when velocity is determined by end to end measurement. The correlation between MOE and crossed and surface velocity is slightly lower than it is parallel to the grain. The best results obtained by crossed and surface velocity were for a central segment 2.52 m length (18h).

These results correspond to a small number of specimens, and therefore findings should be interpreted as preliminary. The authors will extend this research to cover more conifer species and other ToF measurement devices.

Acknowledgments

Ministerio de Economía y Competitividad. Plan Nacional I+D+i 2008-2011. Proy.: BIA 2010-18858. We would like to thank Ramón García Lombardero for his helpful work in the INIA lab, Spain.

References

Arriaga, F., Íñiguez-González, G., Esteban, M., Bobadilla, I. 2009. Proposal of a methodology for the assessment of existing timber structures in Spain. Proceedings of 16th International Symposium on Non-destructive Testing of Wood. Beijing, China.

Divos, F. (2002) Portable Lumber Grader. 13th International Symposium on Non-destructive Testing of Wood. Berkeley, California, USA.

EN 408:2010+A1:2012. Timber structures. Structural timber and glued laminated timber. Determination of some physical and mechanical properties.

EN 13183-2:2002. Moisture content of a piece of sawn timber. Part 1: Determination by electrical resistance method.

Gerhards, C.C. 1982. Longitudinal stress waves for lumber stress grading: factors affecting applications: state of the art. Forest Products Journal, Vol 32 (2), 21-25.

Hankinson, R.L. 1921. Investigation of crushing strength of spruce at varying angles of grain. Air Service Inform. Circular III, Nº 259. US Air Service, Washington DC, EEUU.

Íñiguez, G. 2007. Clasificación mediante técnicas no destructivas y evaluación de las propiedades mecánicas de la madera aserrada de coníferas de gran escuadría para uso estructural (Grading by non

destructive techniques and assessment of the mechanical properties of large cross section coniferous sawn timber for structural use). Doctoral Thesis. Universidad Politécnica de Madrid, ETS de Ingenieros de Montes. 223 p. PDF file: http://oa.upm.es/415

Íñiguez, G., Martínez, R., Bobadilla, I., Arriaga, F. and Esteban, M. 2009. Mechanical properties assessment of structural coniferous timber by means of parallel and perpendicular to the grain wave velocity. Proceedings of the 16th International Symposium on Nondestructive Testing of Wood. 2009, Beijing Forestry University. Pp. 79-84.

NBR 15521: Ensaios não destrutivos - Ultra-som - Classificação mecânica de madeira serrada de dicotiledôneas. (Non-destructive testing - Ultrasonic testing - Mechanical classification of dicotyledonous sawn wood). Abril 2007. Brasil.

NDT to identify biological damage in wood

Roberto Martínez
Department ofAgroforestalEngineering.Universidad Santiago de Compostela, Lugo, Spain, robertodmartinezlopez@gmail.com.

Francisco Arriaga
Department of Forest and Environmental Engineering and Management.ETS de Ingeniería de Montes, Forestal y del Medio Natural. Universidad Politécnica de Madrid, Madrid, Spain.
francisco.arriaga@upm.es

Daniel F. Llana
Department of Forest and Environmental Engineering and Management.ETS de Ingeniería de Montes, Forestal y del Medio Natural. Universidad Politécnica de Madrid, Madrid, Spain.
danielfllana@gmail.com

Javier Gallego
Department of Forest and Environmental Engineering and Management.ETS de Ingeniería de Montes, Forestal y del Medio Natural. Universidad Politécnica de Madrid, Madrid, Spain

Ignacio Bobadilla
Department of Forest and Environmental Engineering and Management.ETS de Ingeniería de Montes, Forestal y del Medio Natural. Universidad Politécnica de Madrid, Madrid, Spain
i.bobadilla@upm.es.

Abstract

Nondestructive techniques are widely used to assess existing timber structures. The models proposed for these methods are usually performed in the laboratory using small clear wood specimens. But in real situations many anomalies, defects and biological damage are found in wood. In these cases the existing models only indicate that the values are outside normality without providing any other information.
To solve this problem, a study of non-destructive probing methods for wood was performed, testing the behaviour of four different techniques (penetration resistance, pullout resistance, drill resistance and chip drill extraction) on wood samples with different biological damage, simulating an in-situ test. The wood samples were obtained from existing Spanish timber structures with biotic damage caused by borer insects, termites, brown rot and white rot.
The study concludes that all of the methods offer more or less detailed information about the degree of deterioration of wood, but that the first two methods (penetration and pullout resistance) cannot distinguish between pathologies. On the other hand, drill resistance and chip drill extraction make it possible to differentiate pathologies and even to identify species or damage location.
Finally, the techniques used were compared to characterize their advantages and disadvantages.

Key words: Nondestructive testing, probing, biological damage, identification.

Introduction

In the evaluation of existing structures, either in rehabilitation or consolidation works, non-destructive probing techniques can be of great help in decision-making. The application of these techniques to estimate physical and mechanical properties, especially density, requires knowledge of the characteristic values of each technique for each genus or species.

Many authors propose different models of density estimation for different tools, species and origins (Greaves, BL et al. 1996; Watt, MS et al. 1996; Walter, ITG et al. 2005 and Bobadilla et al. 2007, 2009).The models proposed for these methods are usually performed in the laboratory using small clear wood specimens. However, in real situations when these techniques are applied in-situ, many anomalies, defects and biological damage are found in wood. In these cases the existing models only indicate that the values are outside normality, without providing any other information.
But non-destructive methods are actually often used in addition to characterise wood, detecting and evaluating diseases or damage (Ross and Pellerin, 1994; Machado and Cruz, 1997; Casado et al. 2005; Lladró et al. 2006; Gallego and Bobadilla, 2011; Henriques et al. 2011). Analysis is complex due to the variability of results, since they depend on test location, timber anisotropy and density, the percentage of late wood, defects or decay, and the operator (Bonamini, 1995).

The main aim of this work is to organize and complete existing information on the use of non-destructive or semi-destructive probing methods in the detection and characterization of disease and damage in timber pieces, based on 10 years' professional experience and previous research works.

Materials, Equipment and Methods

Testing Material

Eighty six coniferous wood specimens with different types of biological damage were subjected to simulated in-situ testing. Wood samples were obtained from existing Spanish timber structures with biotic damage caused by borer insects, termites, brown rot and white rot, with different levels of damage.

Equipment and Methods

Firstly the pathology was identified, quantifying damage in the wooden pieces and determining the local density in the working area of the material tested.
Once the piece was tested the extent of attack and degradation depth was checked using an awl and gauge.
To quantify damage, visual inspection of the test zone was performed, distinguishing 4 depth damage groups: healthy wood (no degradation), surface degradation (1 to 10 mm depth), medium degradation (11 to 30 mm depth) and deep degradation (over 30 mm depth) (Bobadilla et al. 2009).
For local density calculation 8 cm^3 samples of the damaged tested areas as well as healthy wood of the same wood pieces were obtained. The density of the whole piece was measured by dividing its mass by its volume. The densities of the 4 damage classes (healthy wood, surface, medium and deep degradation) of the timber pieces tested were obtained in this way.

Penetration tester
The Penetrometer instrument (Pilodyn 6J Forest, Proceq, Switzerland) consists of a calibrated spring that drives a steel needle into timber. Depth of pin penetration can be used to evaluate the level of damage to the timber, depending on surface hardness and density (Hoffmeyer, 1978).

Screw Withdrawal Resistance Meter
Screw withdrawal resistance is measured using a test device designed specifically to record the maximum load required to extract a screw previously inserted into the timber. The assumption is that the greater the force needed to extract the screw, the higher the density of the timber (Iñiguezet al. 2010).
The screw withdrawal test was performed using the portable Screw Withdrawal Resistance Meter (SWRM), designed by Fakopp (Hungary). A 4 mm diameter 70 mm long Heco-Fix plus type screw with a penetration depth of 20 mm was selected for this study. Resistance can be used, as in the previous case, to evaluate the level of damage to the timber.

Resistograph
IML RESI F400S (IML, USA) drill equipment was used in this study. This equipment measures the torque or drill resistance applied to a 2.5 mm diameter drill bit in order to maintain constant penetration velocity into the wood piece. Density variations in the wood material will correspond to variations in the torque and result in a resistance drill profile down the depth of the wood element (Morales-Conde et al. 2014). This method involves obtaining and analyzing the drill resistance profile in the damaged wood area.

Wood extractor
The Wood Extractor is a device coupled to a commercial power drill to collect all the chips that are produced during drilling in a one-use paper bag filter (Bobadilla et al. 2013). This technique establishes a known volume of removed wood, at a constant setting of drill diameter (8 mm) and penetration (47 mm). After drilling, the collection of chips in the filter is studied for biological damage using a stereo microscope, and the percentage of small particles (<0.85 mm) is measured to discriminate between healthy and damaged wood.

Results and Discussion

Since the performance, behavior and information obtained with each tool is very different, analysis has been divided into three categories to clarify the results: Damage detection, quantification and identification.

Penetrometer

Damage detection: wood damage is detected when higher than normal penetration values for the analyzed species or family are obtained. If an existing density estimation model is applied, estimated density values are below the normal ones for healthy wood. It is only possible to detect damage of surface areas (up to 40 mm), as this is the measurement range of the equipment.

Quantification: with this tool, damage quantification is limited to the external area of the pieces. The degree of attack is well correlated with loss of density and increased needle penetration. The density of healthy and damaged areas of the same pieces was estimated using any of the existing models (Bobadilla et al. 2007, 2009), and the values obtained were compared. Thus surface degradation is difficult to detect due to measuring equipment variability, but in pieces with medium degradation, penetration values were duplicated for relatively low losses of density (17%), and in pieces with deep degradation, penetration is four times greater due to density loss of approximately 44%. Some of these results can be seen in Table 1. Another limitation of the penetrometer is that existing density estimation models do not work properly with deeply damaged timber, as they were designed for healthy wood.

Identification: Finally, with the information provided by this equipment it is not possible to identify the organism that caused the damage. Data provided by this tool is only about loss of wood density and hardness.

Table 1 - Results obtained with the Pilodyn in conifer wood pieces with different degrees of degradation. The density estimation model used is the one proposed by Bobadilla et al. 2007. (*) the density estimation models used do not work properly with deeply damaged timbers, as they were designed for healthy wood.

Sample	Mean penetration depth (mm)	CV (%)	Estimated density (kg/m^3)	CV (%)	Real density (kg/m^3)	CV (%)
Surface degradation	13	13.9	472	7.9	444	11.3
Medium degradation	16	26.0	414	20.5	436	12.8
Deep degradation	33	28.8	Out of range (*)	-	295	12.8
Healthy wood	8	20.6	570	6.2	528	8.5

Screw Withdrawal Resistance Meter

Damage detection: damage is detected when resistance values or estimated densities are below normal for the analyzed species or families. As in the previous case, the tool only detects damage in the outer part of pieces, because the range of use is 0 mm to 20 mm, although this could be increased if another type of screws is used and insertion depths are higher.

Damage quantification is achieved by the relationship between loss of withdrawal resistance and loss of density. Thus, the density of healthy and damaged areas of the same pieces has been estimated using one of the existing models (Bobadilla et al. 2007) and the values obtained have been compared. As happened with the penetrometer, this tool is not very precise about surface degradation due to the variability of the measuring equipment, but in pieces with medium degradation, resistance values decrease more than a half (53%) at relatively low losses of density (17%), while in pieces with deep degradation resistance drops by over 80% and density decreases by approximately half (44%). Some of these results are shown in Table 2. Similar results were obtained by other authors (Casado et al. 2005).

Table 2 - Results obtained with the Screw Withdrawal Resistance Meter in conifer wood pieces with different degrees of degradation. The density estimation model used is the one proposed by Bobadilla et al. 2007.

Sample	Mean withdrawal force (kN)	CV (%)	Estimated density (kg/m^3)	CV (%)	Real density (kg/m^3)	CV (%)
Surface degradation	1.20	28.3	421	8.8	444	11.3
Medium degradation	0.73	32.4	370	7.1	436	12.8
Deep degradation	0.25	92.9	317	8.0	295	12.8
Healthy wood	1.56	25.6	460	9.5	528	8.5

Identification: as in the previous case, with the information provided by this equipment it is not possible to identify the organism that caused the damage.

Resistograph

Damage detection: this is done by looking at abnormally low resistographic profiles. With this equipment it is also possible to compare densities through the values obtained using any of the regression models proposed by various authors (Machadoand Cruz, 1997; Lladró et al.2006; Gallego and Bobadilla, 2011). Some authors estimate that losses in density of from 3% to 12% can cause decreases in mechanical strength from 20% to 45% (Henriques et al. 2011).

Damage quantification is based on study of low resistographic profile surface locations affected by abnormalities in wooden pieces.

This tool now makes it possible to identify the pathogen affecting wood. This requires analysis of the shape and location of anomalies within the resistographic profile. Each destructive agent produces a characteristic attack, causing typical damage to timber and a different tool response.

Table 3 – Characteristic damage profiles and corresponding graphics produced by the most common pathogens in conifer timber.

Pathogens	Attack location	Shape	Pictures
Long horn beetle (Cerambicidae)	Sapwood	U	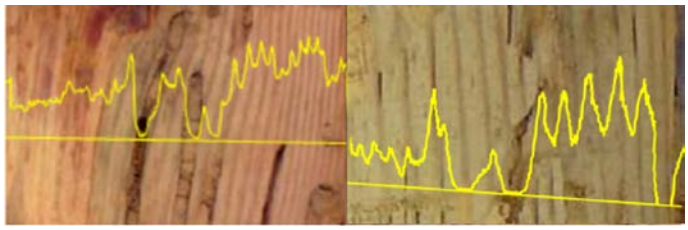
Furniture beetle (Anobiidae)	Sapwood	V	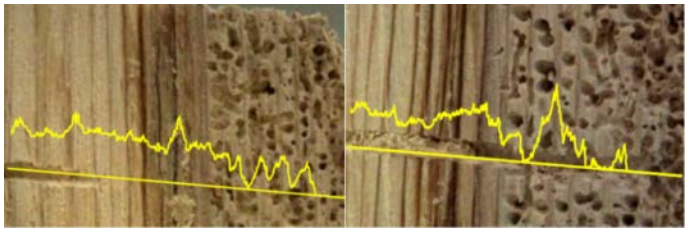
Termites (Reticulitermes spp)	Sapwood and Heartwood	⌊_/	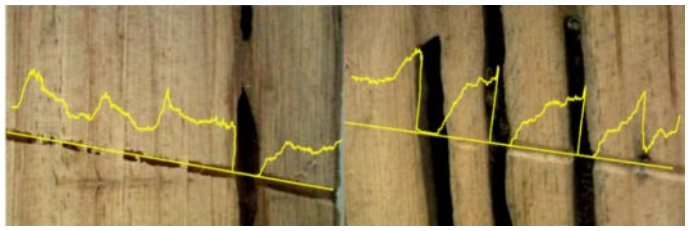
Brown and white rot	Sapwood and Heartwood	__/	

Given the characteristics of each of the pathogens taken from the study of such damaged wood samples, damage profiles were obtained for each of the different diseases. Table 3 shows the profile shape found and its most likely location in wood for each type of attack.

As a limitation of this method it should be noted that although profile analysis can provide some degree of information about pathogen type, it is still a complex and subjective method of identification. Furthermore, if different overlapping damage is found in the same piece, analysis and identification become more complex.

Wood Extractor

Damage detection begins with the feeling of loss of resistance to the drill. This loss of strength is transmitted to the hands of the technician continuously or discontinuously, depending on the type of damage to the wood. In a second phase, estimation of an abnormally low density based on the existing models or the appearance of the chips removed can also raise alarms (Bobadilla et al. 2013).

Degree of damage quantification estimates the above-mentioned density and greater or lesser amount of powder (minute debris<0.85 mm) in the extracted sample. The higher the small particle content and the lower the density, the greater is the damage. Table 4 presents the data obtained.

Table 4–Results obtained using the Wood Extractor on conifer wood pieces damaged by the most common timber pathogens.

Sample	Drill resistance feeling	Powder content	Distinctive feature on the extracted sample	Sample appearance	Pictures (X6)
Clear wood	Normal	15% Low	Wood scent	Splintery	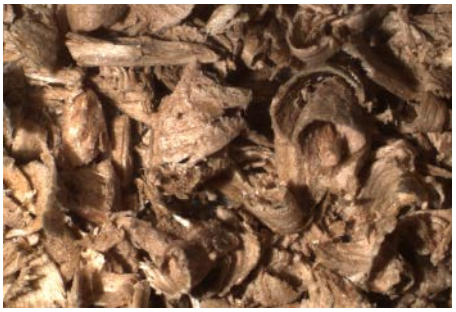
Borer insects (Cerambicidae, Anobiidae, Curculionidae… etc)	Low with gaps	40% High	Insects pellets	Powdery	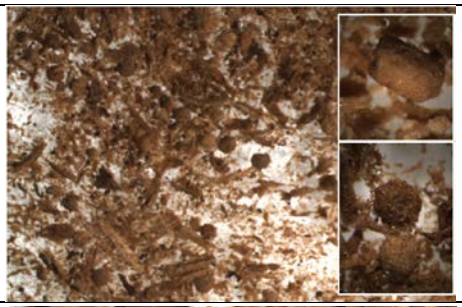
Termites (Reticulitermes spp)	Normal with gaps	30% High	Mud	Muddy powdery	

Brown rot	Low	40% High	Prism shaped bits	Powdery	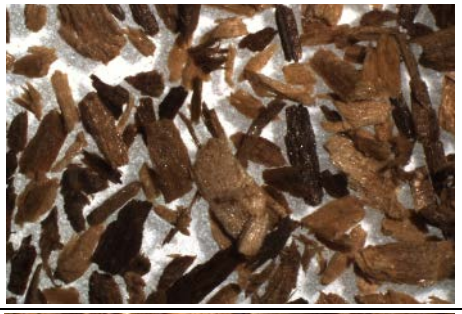
White rot	Low	30% High	Fiber shaped bits	Powdery fibrous	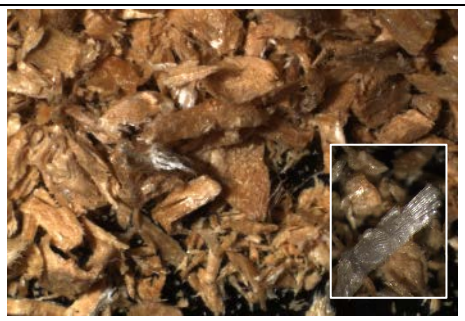

As with the resistograph, one of the advantages of this equipment is that it allows the identification of disease causing damage. To do this, quantification study of powder content (minute chips) and visual analysis of the presence of detritus (pellets), hyphae or characteristic remains of each pathogen in the extracted sample must be done (Bobadilla et al. 2008, 2013). Identification is therefore based on the detritus left by the degrading agent.

This technique is more effective and reliable than the resistograph in identifying different degrading agents, even if they overlap in the same piece of wood.

Finally, Table 5 shows a comparison of the techniques used.

Table 5 – Comparison of the different methods used in the study. Categories: Poor, Medium-Poor, Medium, Medium-Good and Good.

	Equipment cost	Handiness	Damage detection range	Damage quantification	Damage identification
Pylodin	Medium	Good	Surface 0 a 40 mm	Poor-Medium	-
Screw Withdrawal	Medium	Medium	Surface 0 a 20 mm (Depends on the screw)	Medium	-
Resistograph	Poor	Medium-Poor	All section (Depends on the tool)	Good	Medium-Good (Type, Family)
Wood extractor	Good	Medium-Good	Surface 0 a 50 mm (Depends on the drill bit)	Medium	Good (Family, sometimes Species)

Conclusions

The four probing and drilling tools and methods tested in this paper have proven their effectiveness for the detection and quantification of damage in construction timber. All the methods discussed objectively detect density losses caused by destructive agents, although detection is more reliable for medium or deep damage (affecting more than 1 cm below the surface).

Damage quantification reliability will depend on the method used, but they all allow estimation of abnormally low density, which is a clear indicator of the deterioration of wood.

The resistograph and wood extractor often also allow the identification of pathogens in wood. The resistograph does so by analyzing the shape of the graphic profile obtained, while the wood extractor does so by visual analysis of the sample taken with a magnifying glass.

The Screw Withdrawal Resistance Meter, Pilodyn and Wood extractor have an important limitation in terms of the test area, as this varies from 2 to 5 cm in depth in wooden pieces.

For better and more reliable analysis of damaged wood, and taking into account the fact that the characteristic values for each wood species and method used are not always known, the authors recommend testing areas of healthy and is free of defects wood in the same pieces tested in-situ and using the results obtained as a reference for comparison.

References

Bobadilla, I.; Iñiguez, G.; Esteban, M.; Arriaga, F.; Casas, L. (2007). Density estimation by screw withdrawal resistance and probing in structural sawn coniferous timber.Proceedings of the 15th International Symposium on Nondestructive Testing of Wood.Madison, Wisconsin.

Bobadilla, I.; Arriga, F.; Iñiguez, G.; Esteban, M.; Castro, N. (2008). Wood destroying insect identification in construction timber by means of the detritus morphologic analysis.Actas de las Segundas Jornadas de Investigación en Construcción. Madrid, Spain.

Bobadilla, I.; Iñiguez, G.; Arriaga, F. and Esteban, M. (2009). Técnicas no destructivas en la inspección de estructuras de madera 1: El Penetrómetro.(Non destructive technics on wooden building inspection 1: The penetrometer.)BIT de AiTiM nº 160. Pp 66-70.

Bobadilla, I. Martínez, R. Calvo, J. Arriaga, F. Iñiguez-González, G. (2013). First steps in wood density estimation using a conventional drill. Proceedings of the 18th International Symposium on Nondestructive Testing of Wood. Madison, Wisconsin.

Bonamini, G., (1995)Restoring timber structures – Inspection and evaluation in Timber Engineering STEP 2. Design – Details and structural systems, Edit. Centrum Hout, pp. D3/1-D3/9.

Casado, M.; Pinazo, O.; Basterra, A.; Acuña, L. (2005).Técnicas de ensayo no destructivas en madera estructural mediante el extractor de tornillos. Aplicación en viguetas de forjado de un edificio singular. Actas del IVº congreso nacional de protección de la madera. CIDEMCO (Ed.). Donostia-San Sebastian, Spain.

Gallego, J; Bobadilla, I. (2011). Identificación de patologías y singularidades de la madera mediante análisis resistográfico. PFC E.U.I.T. Forestal.UPM. Madrid.

Greaves, BL; Borralho, NMG; Raymond, CA; Farrington A. (1996).Use of a Pilodyn for the indirect selection of basic density in Eucalyptus nitens.Canadian Journal of Forest Research 26 (9), pp: 1643-1650.

Henriques, D., Nunes, L., Machado, J. S., & Brito, J. (2011). Timber in buildings: estimation of some properties using pilodyn and resistograph. In Proceedings of International conference on durability of building materials and components.Porto Portugal.

Hoffmeyer, P. (1978). The Pilodyn instrument as a non-destructive tester of the shock resistance of wood. In: Proc. Of the 4th Nondestructive Testing of Wood Symp., Washington State University, Pullman; WA. Pp. 47-66

Iñiguez, G.; Arriaga, F.; Esteban, M.; Bobadilla,I.; González, C.; Martínez, R.; (2010). In situ non-destructive density estimation for the assessment of existing timber structures.11th World Conference on Timber Engineering.

Lladró, R.C., Barra R.D., Botelho, J., Faria, J.A., (2006). Assessment of timber structures with in situ tests. PATORREB 2006, 20-21 March, Oporto, Portugal, pp. 139-148.

Machado, J.S.; Cruz H. (1997), Assessment of timber structures. Determination of density profile by non-destructive methods, Revista Por. de Engenharia de Estruturas, 42, pp. 15-18

Morales-Conde, M.J.; Rodríguez-Liñán, C.; Saporiti-Machado, J. (2014) Predicting the density of structural timber members in service.The combine use of wood cores and drill resistance data.Mater.Construcc.64 [315], e029 http://dx.doi.org/10.3989/mc.2014.03113.

Ross, R.J.; Pellerin, R.F. (1994).Non destructive testing for assessing wood members in structures.USDA.FPL-GTR-70.pp 1-40.

Walter, ITG; Norton, B; Lavery, DJ; Chapman, MJ.(2005). Screw ingress torque as a non-destructive determinant of timber compressive strength. Proceedings of the 14th International Symposium on Non-destructive Testing of Wood, pp: 144-145.

Watt, MS; Garnett, BT; Walker, JCF. (1996). The use of the Pilodyn for assessing outerwood density in New Zealand radiata pine. Forest Products Journal 46 (11-12), pp: 101-106.

Glue laminated timber structure evaluation by acoustic tomography

Balázs Major
József Bódig Wood NDT Laboratory, University of West Hungary, Simonyi Karoly Faculty of Engineering, Wood Sciences and Applied Arts, Sopron, Hungary, balazs.major@student.nyme.hu

Ferenc Divós
József Bódig Wood NDT Laboratory, University of West Hungary, Simonyi Karoly Faculty of Engineering, Wood Sciences and Applied Arts, Sopron, Hungary, ferenc.divos@skk.nyme.hu

Abstract

An approximately 40 year old, wooden lookout tower were examined in Budakeszi, Hungary. First we made the visual inspection of the structure and searched for damages for example due to decay or insects. The lookout tower was made of glue laminated timber, and because of their large cross-sections we have applied acoustic tomography. With this non-destructive testing method we got information about the internal conditions of the pillars, at the critical height. The purpose of the paper is to present the acoustic tomography, which can assist the work of structural engineers and wood preservation experts in case of large cross section glulam beams or pillars.

Keywords: acoustic tomography, lookout tower, glulam, fungi, wood preservation experts

Investigation supported by acoustic tomography

Hungarian wood preservation experts

The wood preservation experts had to pass an examination to get this qualification. This examination is at our university, about typical fungus, insects, wood preservation methods, wood properties, basic structures and law. These people are members of the Hungarian Chamber of Engineers. In the best case the applicants are MSc Wood Technology Engineers, after the exams they have to get 5 years of practice to get the rights from the Chamber of Engineers for starting their individual expertise.

Their tasks are examine new or old buildings, give advices to preserve wooden products, wooden structures. Since 2014, in the case of a building older than 80 years, their job is always necessary according to the Hungarian law. Their reports help the structural engineers and the architects in their mechanical calculations.

Techniques and methods used by wood preservation experts

Every evaluation of a structure, starts with a visual inspection, to search for damages caused by fungal and insect attack. The visual inspection means not just what they can see, it is a very difficult method, requires lot of practice. During the visual part of the evaluation, the expert have to use all of his/ her senses. For example several fungi have its own characteristic smell or fragrance, in other cases they can hear the sound of the drilling insects or they can see the wood meal cones made by insects.

At the beginning they mark the main wooden members of the structure with numbers or letters for their easier identification. This helps for the recording of the results of each examined structural element. There are lots of damages that can be recognised by visual inspection, but there are some cases when we don’t know exactly the extension of the damage due to the large cross-section or

because the structure is not accessible. Otherwise there are some insects and fungi which make their damage inside the structural elements. There are lots of types of non-destructive test equipment, which can make these presumptions surer.

The acoustic tomography equipment

In our laboratory there are several types of non-destructive testing equipments for wooden or timber structures. We chose the acoustic tomography for this investigation, because this is very good to determine the inside defects of glulam pillars with large cross section. The acoustic tomography was developed in Hungary, to determine by non-destructive techniques, areas attacked by fungi or hollows in the trunk of the standing trees. It is based on sound velocity measurement between several piezoelectric type sensors around the element. We could use with 10 or 12 sensors on the objective of the investigation (trunks or structure elements). The measurement principle is that sound velocity drops if there is a hollow or decayed area between two sensors. (Wang and Cai)

We have to hit the spike shaped sensors into the timber with a rubber hummer. We have to tap each transducer with a hammer, minimum 3 times to generate sound waves. The computer calculates and displays the internal sound-velocity distribution of the examined cross-section. The PC have to know the distances between each sensor. The software can assemble different measurements data from several heights into a 3D model (**Figure 1**).

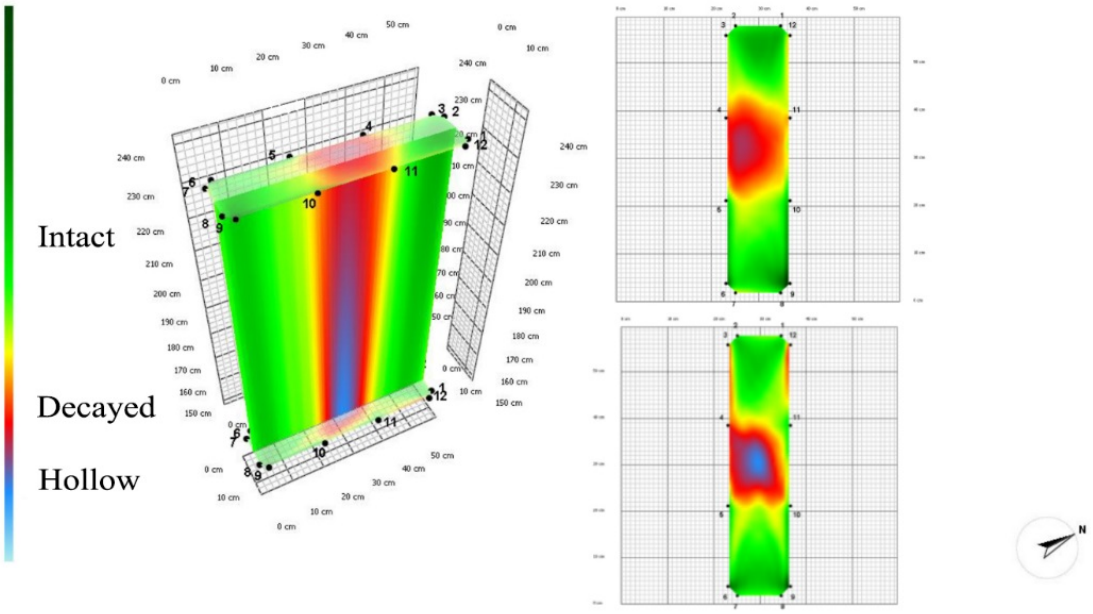

Figure 1—Acoustic tomography measured data, Budakeszi lookout tower pillar no. 4. On the right side you can see two layers from 1,5 m and 2,4 m height. On the left side of the picture there is a 3D model calculated by the PC from 2 layers

We have investigated a wooden lookout tower in Budakeszi. This structure is 14,5 m tall, and built with 6 large glue laminated timber pillars. The dimensions of the pillars: 17,5 x 60 cm. From the previous visual inspection it becomes apparent, that there are some pillars, which we had to measure by acoustic tomography. We made measurements at the critical points or heights of the pillars (**Figure 2**).

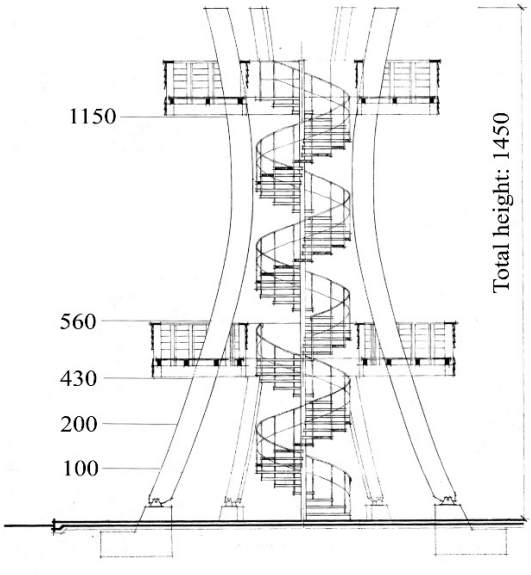

Figure 2—The acoustic tomography examination points on the pillars, measured from the ground [cm], lookout tower in Budakeszi

During the measurement we used 4 sensors on each 60 cm wide sides and 2 sensors on each 17,5 cm short sides. To make a roughly quadrilateral shaped layout we had to put two sensors close to each other at the edges.

Figure 3—The acoustic tomography setup on pillar no. 5., at about 2 m height

The internal fungi attack influence on the load capacity of glulam beams

The attack of *Gloeophyllum abietinum, Gloeophyllum sepiarium* or *Gloeophyllum trabeum* could cause very serious problems in large cross sections. They cause brown-rot, most of the time without any sign on the surfaces. These types of fungus attack through the cracks of the structure elements and start to impair from inside. In most cases remains a thinner layer of intact timber on the surface. We found *Gloeophyllum abietinum* in the pillars of the lookout tower.

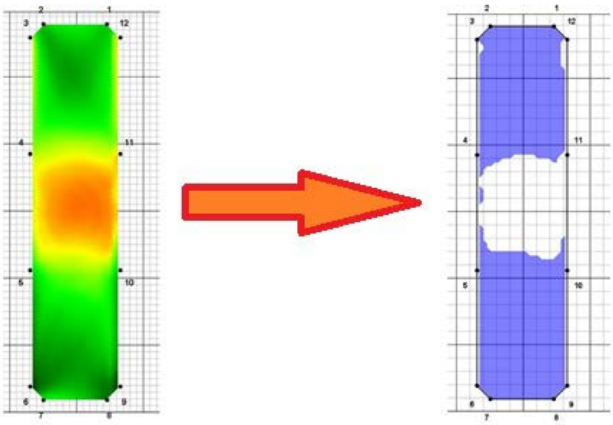

Figure 4—On the picture you can see the remained intact timber transformed from a measured data on a pillar.

After these kind of damage the load capacity of a beam or pillar can decrease critically. We can determine the damaged areas, so the structural engineers can calculate the load capacity of the elements according to Eurocode 5. In case of a pillar, the effective surface (A_{ef}) decreases, that increases the maximum compressive strength in the pillar, till the remained intact timber, may be unable to bear the increased load.

$$\sigma_{max} = \frac{F}{A_{ef}} \leq f_{d,0,c} \qquad (1)$$

where σ_{max} is maximal compressing strength in the element, F is compressive force, A_{ef} is the effective surface, $f_{(d,0,c)}$ is the maximal compressive strength according to the Eurocode 5 (Armuth and Bodnár 2011)

Conclusions

Finally we concluded that the pillar no. 4., 5. and no. 6. are in the worst condition according to the internal hollows and fungi attacks. The structure had also other damages from fungi and insects. The data, collected by the acoustic tomography helped the wood preservation expert to make a more precise and reliable evaluation.

Acknowledgements

We would like to thank Dr. László Németh for let us investigate the pillars of the wooden towerby with acoustic tomography equipment.

References

Armuth M., Bodnár M. 2011. Fa tartószerkezetek, Tervezés az Eurocode alapján, Artifex Kiadó Kft., Budapest, ISBN 978-963-7727-02-3, page 60.

Wang X., Cai Z. 2014. New Techniques and Technologies. In: White, Robert H.; Ross, Robert J. ed. 2014. Wood and timber condition assessment manual: second edition. Chapter 4.

Assessing the Performance in Service of an Cross Laminated Timber Structure Exposed to Extreme Conditions

Luís Jorge
Polytechnic Institute of Castelo Branco, Castelo Branco, Portugal, luisfc@ipcb.pt

Alfredo Dias
Department of Civil Engineering, University of Coimbra, Coimbra, Portugal, alfgdias@dec.uc.pt

Abstract

Cross-laminated timber panels (CLT panels) are one of the most enthusiastic construction systems for owners and designers nowadays, promising to overcome new challenges replacing concrete and steel for high demanding projects. However, its use in extreme environmental conditions is not well known and only few reports study the performance on high hygrometry environment. This paper report the assessment of the performance of a swimming-pool building, through moisture content and slip measurements. IF thermography is also showed and discussed for prospective work.

Keywords: CLT, monitoring, moisture content, IF thermography

Introduction

General information on CLT

Cross-laminated timber (English acronym: CLT) is produced from layers of spruce, pine or other wood species that are arranged crosswise on top of each other and glued to each other with a pressing power of at least 6 N/sqm to form large-sized solid wood elements. The crosswise arrangement of the longitudinal and transverse layers reduces the swelling and shrinkage of the wood in the plane of the panel to an insignificant minimum and considerably increases the static load-carrying capacity and dimensional stability. In order to rule out any damage caused by pests, fungi or insects, in compliance with the European Technical Approval, technically dried wood with a wood moisture of 12% (+/-2%) is used to produce CLT panels. To achieve high standard characteristics, all timber lamellae shall undergo rigorous sorting (usually, above the C18 strength class).

Cross laminated timber panels handle load transfer and stiffness trough bi-directional layers and massive cross section, which contributes to the main properties of the product, apart mechanical properties: good fire strength performance and low heat conductivity.

CLT panels are widely used across Europe and high rise buildings are being planned in recent years (Ceccoti, 2008) (Schickhofer, 2013) (Teibinger, 2008) but their use in extreme environmental conditions is not yet been established in a way owners and designers have enough confidence. Eurocode's Service Classe enable the design of timber structures taking in account, namely, environmental conditions. CLT panels are evaluated for structural applications in Service Classes 1 and 2 conditions (below the 20% of equilibrium on moisture content). The structural application in Service Class 3 (above the 20% of

equilibrium on moisture content) is not allowed, mainly because of (1) the high moisture content expected in timber and (2) some concerns related to the potential change in panels' size when significant moisture changes happen.

High moisture contents in CLT panels are not advisable, because it will lead to high level of stresses in glue lines. Several European Technical Approvals (ETA) state the insignificance of the dimensional variations of CLT panels due to moisture content variation; however, according to other technical documents, this kind of variation should be accounted for. After 3 year in service, this paper will report the assessment of the performance of one swimming-pool build with this technology, taken advantage of a monitoring program started when construction was completed. The monitoring program aims to evaluate the performance of CLT panels in places where high environmental humidity is expected. The major parameters monitored are (1) wood moisture content, to ensure that the CLT panels are in Service Classes 1 and 2 conditions and (2) the dimensional stability of the panels, to ensure that no unforeseen stresses will develop in the structure.

Building description

The building described here comprises a 25m long swimming-pool facility and 213sqm gym. The gym floor is composed by a flat slab made with 245 mm thick panels (Figure 1), supported on pairs of round steel columns arranged on a square mesh layout with 6 m side. At the top of each column is placed a steel plate to reduce stress compression perpendicular to grain. The panels are visible on both sides, and no thermal insulation was needed. A balcony surrounds the building and is made by a row of panels, in which each panel is half exposed to indoor conditioned environment and the other half is outdoor ceiling (in cantilever). The swimming-pool roof structure (Figure 1) is composed by steel trusses, supported by 128 mm thick CLT wall. Whenever there where are openings below, thicker panels were used in order to perform as a beam lintel. The ceiling of the roof is made by CLT panels suspended from the steel trusses. Due to the improved performance from the CLT panels used in the roof structure, it was possible to space the steel trusses by 6.35 m and additionally support higher loads.

Durability performance along all service life (50 years, according to Eurocodes) is the main challenge of the project, due to visible CLT walls and ceilings, high level of water vapor production inside the building and flat slab for gym floor with exterior visible surface. Load bearing walls of the swimming-pool, carrying the steel truss with high value of point loads also need special attention.

Figure 1—Gym floor.

Figure 2—Swimming-pool hall.

Figure 3—Bath room with visible wall and ceilings.

All places with hazard of direct water contact were coated with bituminous waterproof membrane (e.g. walls in shower rooms). Visible surfaces are protected with preservative biocide product, applied by painting, with certified performance for Use Class 3.1 (above the requirements for the building). In order to guarantee the desired penetration of the preservative product, pine species (*pinus sylvestris*) was used in alternative to most common spruce timber panels. After preservative painting, also varnish was applied as final coating to give protection to moisture income.

Moisture content assessment

According to the Eurocode 5 (CEN, 2006), the structural design of the timber structure is based on the rigorous assumption of the Service Class, ie. the evaluation of the moisture content of timber along the service life of the project. Due to mechanical ventilation systems, the relative humidity and temperature inside the building is, at most, conducting to Service Class 2, which is the equilibrium on moisture content below 20%. As reported previously on (Jorge and Dias, 2013) and (Jorge, Dias and Costa, 2015) moisture content fits with expected assumptions on design.

Figure 4, present the measurement and data logging system used, made with Scanntronik devices intended for this kind of use (Scanntronik, 2015). Special care was given to the distance between the devices and electric cables in order to avoid electromagnetic field distortion on measurements.

In order to obtain more robust data, measurements were also made on relative humidity and temperature, which can anticipate for the equilibrium on moisture content (FPL, 1999) (LNEC, 1997).

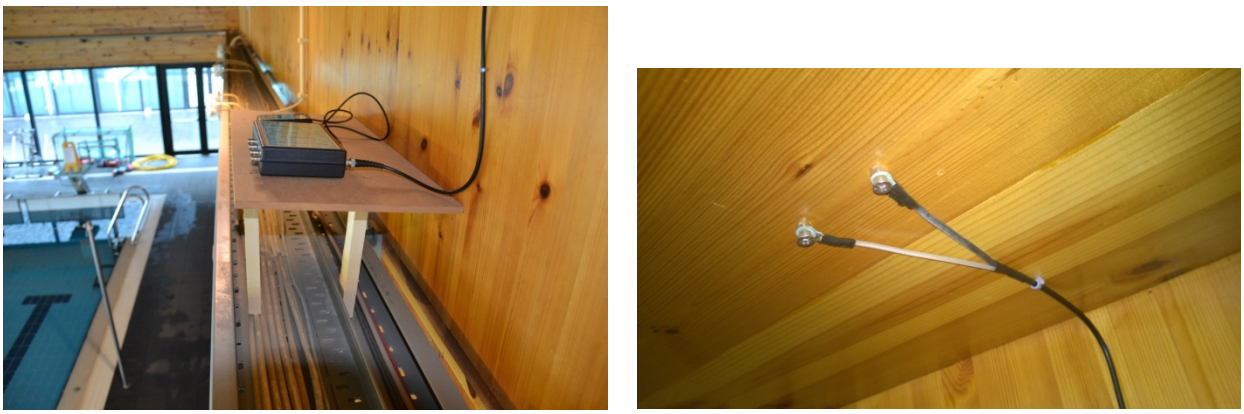

Figure 4—Moisture content measurement.

Crack measurement

Figure 5, present the crack measurement system, composed by the Rissfox Mini, which as a small shock-resistant and watertight housing combining a high resolution 12-bit crack analysis electronic, an air temperature sensor and air humidity sensor, a RISC microcontroller, memory for up to 64000 measuring values and a real-time clock into an enormously powerful analysis system. The fully calibrated crack sensor which can be connected to the system is characterized by especially easy handling, small dimensions, high reliability as well as high precision (Scanntronik, 2015).

The displacement measured between panels is below 1.0mm, along the last 12 months.

The pictures presented in Figure 5, show the vertical crack observed between two CLT wall panels with 13.0m long each. Those panels are made with 95mm thickness and 5 layer. Several French Avis Technique provides the value of 0.01mm/m for in-plane deformation (per percentage of timber moisture variation) and the TRADA Wood Information Sheet, WIS 2/3-62, refers to the maximum value of 0.02mm/m for the same conditions. The value of displacement can be related with a moisture variation between 3 and 7%.

Figure 5—Crack measurement.

IR Thermography

IR thermography was recently tried for the assessment of the timber structure in the building, however, few limitations were observed (which were already known from literature):

a) daily temperature change as thermal induction could be hard to use since heating inside the building keeps the temperature constant, however, the homogeneity of the heating along the assessed element can be an advantage;
b) only few millimeters depth can be assessed from surface;
c) varnish painting can behave like a mirror on thermal images;
d) air moisture content and air flow disrupts the thermal image;
e) for some observations (especially on the swimming-pool hall) the angle between the camera and the CLT panels is almost 60º, which is the reasonable limit for non-disrupts observations.

Figure 6 presents the thermography image of the technical room inside the building, where no ventilation is done and often high moisture values are observed. As it can be seen from the left side picture, disfiguring fungi appeared already. A few comments can be done on the right side picture: the angle to the grain (0º vs. 90º) is very well emphasized on the CLT roof panel; the temperature on the upper wall panel is bigger to the lower wall panel since the opposite side on the upper wall panel is exposed to exterior and the lower one is inside environment. Other temperature differences observed are difficult to relate with wood damage.

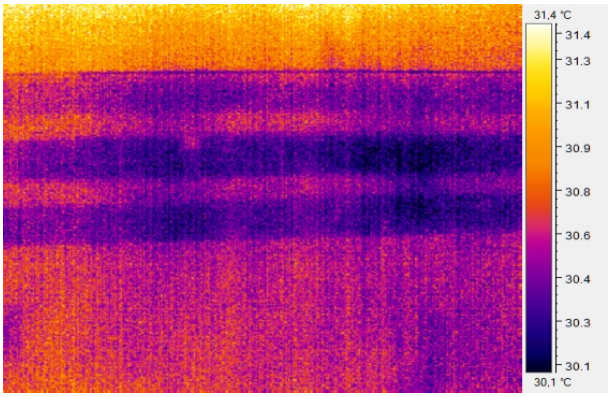

Figure 6—IR Thermography assessment.

For the strict purpose of monitoring the performance of the timber structure, qualitative thermography concept should be used. Therefore, emissivity determination is not the key-issue. However, better understanding on the influence of the disrupt factors mentioned here before should be carefully studied.

Thermography seems to have good potential for the assessment of the timber structures, and particularly, CLT elements on big areas, however, it observes temperature differences and reports just that…

Conclusions

Generally, the main issues on timber structures failures or malfunctions are: insufficient bracing of load bearing members and structures; consideration on performance of connections and how these are effected by variable moisture conditions; swelling and shrinking of timber members; cracks caused by shrinkage of moisture and orthotropic strength of wood. From these, we can conclude that moisture evaluation is the most relevant assessed parameter on such kind of structure.

Moisture induced damage occur, typically, on early ages due to differences on EMC between production and building site, and will lead to the following: increase deformation on members over time (higher k_{def}), decrease strength (lower k_{mod}), increase slip on connections (higher k_{def}) and origin induced stresses (mostly, perpendicular to the grain).

Two strategies can be assigned to this evaluation: (1) relative humidity and temperature measurements from which it is possible to estimate the equilibrium on moisture content or/and (2) direct measurement of moisture content.

Together with moisture evaluation and displacement measurements, visual inspections (with photographic report) are basic assessment works which can be done with very low budget for equipment (below 4000€). As far as all measurements are initiated a.s.a.p. from the completion of the construction works, gathering data should be done with more frequency at early stages (one time each 3 months in first year) in order to help define the best setup also for the mechanical ventilation system of the building.

IF thermography is believed to help in future assessments as long as the technique can overcame the points mentioned here before.

Acknowledgments

The authors acknowledge the Municipality of Almada for the financial support given in instrumentation of the monitoring works and to the company TISEM Lda for the IF thermography camera used.

References

Angst V, Malo KA. 2012. The effect of climate variations on glulam - an experimental study. Eur. J. Wood Wood Prod. 70(5):603-613DOI 10.1007/s00107-012-0594-y.

Brischke, C., Rapp, A., Bayerbach, R. 2008. Measuring system for long-term recording of wood moisture content with internal conductively glued electrodes. Building and Environment 43 (2008) 1566–1574

Ceccotti, A. (2008). New Technologies for Construction of Medium-Rise Buildings in Seismic Regions: The Xlam Case, Structural Engineering International, 2/2008, IABSE: 156-165.

CEN. 1994. EN 350-2 – Durability of wood and wood-based products. Natural durability of solid wood. Part 2: Guide to natural durability and treatability of selected wood species of importance in Europe.

CEN. 2006. EN 1995-1-1 – Eurocode 5: Design of Timber Structures. Part 1-1: General - Common rules and rules for buildings.

CEN. 2006. EN 335-1 – Durability of wood and wood-based products. Definition of use classes.

CEN. 2011. EN 14081-1 – Timber structures. Strength graded structural timber with rectangular cross section. Part 1: Requirements.

CEN. 2013. prEN 16351 Timber structures - Cross laminated timber – Requirements. CEN/TC 124 - Timber structures.

CSTB. 2011. Avis Technique 3/06-477, Panneaux bois à usage structural – Panneaux KLH.

CSTB. 2012. Document Technique d'Application (Avis Technique 3/11-704), Panneaux bois à usage structural – BBS.

CSTB. 2013. Document Technique d'Application (Avis Technique 3/12-724), Panneaux bois à usage structural – Panneaux LENO.

FPL. 1999. Wood Handbook – Wood as an Engineering Material. USDA Forest Service, 463p.

Fragiacomo M., Fortino S., Tononi D., Usardi I., Toratti T. 2011. Moisture-induced stresses perpendicular to grain in timber sections exposed to European climates. Engineering Structures, 2011, 33(11):3071-3078.

Gülzow A., Richter K., Steiger R. 2011. Influence of wood moisture content on bending and shear stiffness of cross laminated timber panels, J. Wood Prod. 69: 193–197.

Häglund M. 2008. Varying moisture content and eigen-stresses in timber elements. Wood Mater. Sci. Eng. 1-2:38-45.

Jönsson J. 2005. Internal stresses in the cross-grain direction in glulam induced by climate variations. Holzforschung. Volume 58, Issue 2, Pages 154–159, ISSN (Print) 0018-830, DOI: 10.1515/HF.2004.023.

Jorge, L., Dias, A. 2013. X-Lam panels in swimming-pool building - monitoring the environment and the performance. Advanced Materials Research. Volume 778, 2013, Pages 779-785

Jorge, L., Dias, A., Costa, R. 2015. Performance of X-Lam panels in a sports center with an indoor swimming-pool. Journal of Civil Structural Health Monitoring: Volume 5, Issue 2 (2015), Page 129-139. doi: 10.1007/s13349-014-0090-7

KLH, http://www.klh.at [accessed June 2015].

LNEC. 1997. Timber for Construction: Moisture in timber – Sheet M9 (in Portuguese).

OIB. 2011. European Technical Approval ETA 06/0138 – KLH solid wood slabs.

Onset, http://www.onsetcomp.com [accessed June 2015].

Scanntronik, http://www.scanntronik.de [accessed June 2015].

Schickhofer, G. 2011. CLT – European Experiences, Cross-Laminated Timber Symposium. Vancouver Convention Center. Canada.

Teibinger, M. 2008. Urban Timber Houses in Vienna, Structural Engineering International, 2/2008, IABSE: 114-117.

TRADA. 2009. Introduction to Specifiers, WIS 2/6-61. Wood Information Sheet.

New generation of non-destructive tool for in-field wood poles using combined parameters for improved reliability

Yann Benoit
Technology Dept., CBT SA, Saint-Sulpice, Switzerland, benoit@cbs-cbt.com

Jean-Daniel Gasser
Informatic Dept., CBT SA, Saint-Sulpice, Switzerland, benoit@cbs-cbt.com

Jean-Luc Sandoz
General Manager, CBS, Choisy le Roi, France, sandoz@cbs-cbt.com

Abstract

Non-destructive evaluation of in-field wood poles used in telecom and utilities overhead lines remains as a key issue for networks managers. If existing tools all have their own philosophies to give an estimation of the residual status of individual poles, the goals are usually the same:

- Security: Keep only safe poles in the networks
- Costs: Change as least poles as possible
- Productivity: Inspect as much poles as possible within a short period

For many years, CBT has been working on the topic to achieve those goals. If the tool – as called Polux – is considered as the reference on the market, the engineers have developed a newer generation taking into account new parameters to strengthen its performances.

This paper presents the very first results of this new generation of device born in 2015 using the existing Polux parameters plus new ones such as screw energy, local density graphics and density energy.

Keywords: in-field wood pole, non-destructive evaluation, security, maintenance, residual strength

Introduction

Telecom and utilities companies (TUC) have the responsibility to ensure the perfomances of their networks to guaranty:

1. The aim of their business (transport and distribution of telecom lines and/or energy)
2. The safety of any authorized crew for maintenance operations on their networks
3. The safety of anyone around their networks

Concerning overhead networks, the main risk consists in the failure of one pile or pole. In other words, TUC have the responsibility to ensure the adequate structural behavior of their poles.

To achieve this goal, TUC usually have inspection policies including a method and a strategy of maintenance with a short, medium or long term prospective.

If wood poles are excellent components for overhead lines, their inspections remain a challenge between the subjective traditional method (sound of the pole after a hammer shock) and a non-destructive tool to assess their residual performances.

Many devices are available on the market based on various non-destructive technologies and various results (Springer, 2008).

25 years ago, CBS and the Swiss Federal Institute of Technology developed the system Polux (Sandoz and Lorin, 1996) based on the measurements of local density and moisture content at the most critical zone for the wood pole, its ground line level, to evaluate its residual strength.

Over the years, the technology has built an impressive database to deliver optimized results for each case met in many countries over the world.

In 2015, CBS engineers launch the fifth generation of Polux device (Polux 5) to not only improve the ergonomic issue of the older versions, but to acquire new data thanks to additional sensors for an improved reliability.

This paper presents the development of this new device including the very first results collected in the field.

Development challenges

Polux technology

The fundamentals of Polux technology is the measurements of two parameters (Figure 1):

1. The local density of the pole: this measurement is made by introducing two small diameter (3mm) pins within the wood. A load sensor is connected to those pins and the force required to push the pins is recorded.
2. The moisture content of the wood: once the pins are within the wood (4cm inside) an electric current records the internal moisture content of the wood between the two pins.

Those two parameters give an estimation of the residual strength of the pole and propose a cycle for the next inspection. Measurements are performed at the pole's ground line level, the most critical area of the pole for both, mechanical and biodegradation issues.

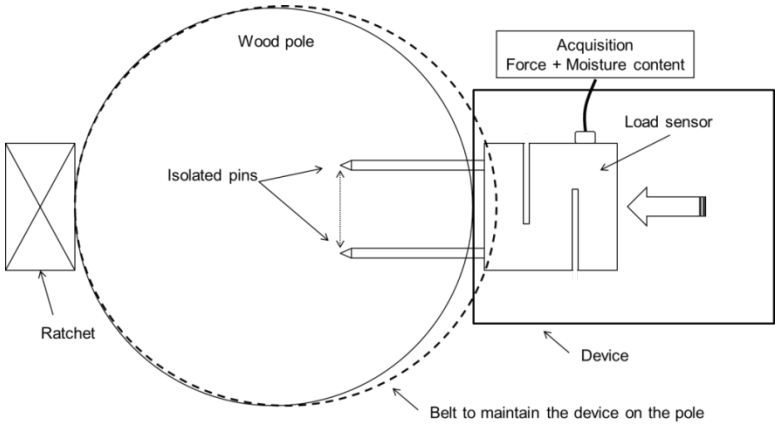

Figure 1- Fundamentals of Polux principle: The device is strapped on the pole thanks to a belt and a ratchet. Two isolated pins are set on a load sensor. The local density and the moisture content are registered.

Ergonomic issue

The main reason for the development of a newer device was to solve the ergonomic issue of the older devices generations what was considered as the most critical weakness of the technology.

Indeed, Polux results are accepted by main of the telecom and utilities operators, but the handling in the field was an identified obstacle, especially regarding both its weight (6.5kg for the 4th generation, 8kg for the older versions) and the system to strap the device on the pole combining a belt and a ratchet (weight of the ratchet: 1.5kg).

Knowing that an inspector can measure up to 120 poles per day (according to the field configuration), ergonomic issue is clearly a key one.

The following Figure 2 and Figure 3 illustrate the original idea, Polux 2 & Polux 4 respectively together with a field illustration with Polux 4 (Figure 4).

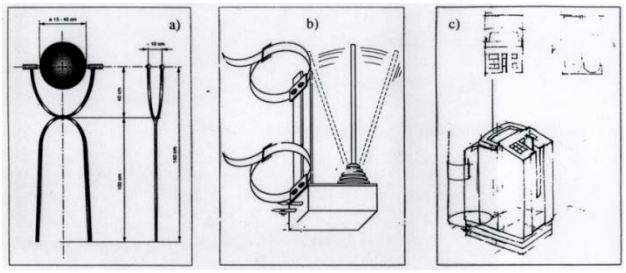

Figure 2- Illustrations of the original Polux concept

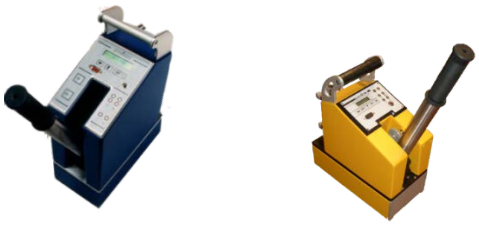

Figure 3- Polux generation 2 (left), 8kg and Polux 4 (right), 6.5kg

Figure 4- Polux 4 in the field, facing a pole in a slope situation.

In other terms, the main motivation in designing a newer Polux version was a consequent weight reduction and a way in simplifying the connection of the device to the pole without forgetting keeping the technology fundamentals of the original idea.

New technology design

Main objective

As explained in the previous chapter, the main objective is to imagine a solution to improve the setting of the device on the pole in order to avoid using a belt and a ratchet.

In the same direction, a consequent weight of reduction is expected in order to facilitate field operations.

Of course, Polux fundamentals principle must remain the same in order to use the previous patent and more important, the impressive database collected over the years.

The solution

In order to avoid using an embarrassing and heavy system to connect the device to the pole, the idea is to screw the device on the pole and, once fixed, launch Polux fundamentals process, meaning the pins within the wood to measure both the local density and the moisture content.

The protocol could be described as such:

1. Screw the device into the pole
2. Once the device is strongly set on the pole, launch the pins within the wood
3. Measure the penetration force of the pins to go within the pole (Polux fundamental number 1)
4. Once the pins are within the pole, the isolated pins measure the pole's moisture content (Polux fundamental number 2)
5. After the moisture content measurement, the unscrewing process frees the device

The Figure 5 illustrates the solution's principle.

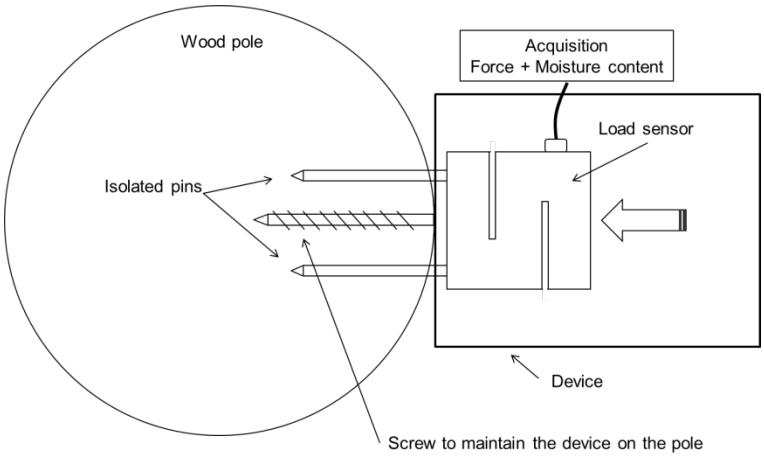

Figure 5- New device principles: instead of using an embarrassing and heavy belt and ratchet, a screw maintains the device on the pole on the same axis than the pins

The final solution looks like an electric screwdriver as presented by the Figure 6.

Figure 6- Polux 5. Fifth generation of Polux: Polux 5

The solution reaches the expected goals: a simplified setting of the device on the pole and a strong weight loss: 3.5kg.

The high performances of the solution

Although the major ergonomic gain, the new solution has many technology advantages in comparison to the older versions:

1. Possibility to measure with an angle below the ground line level as illustrated by the Figure 7.
2. Possibility to use a sensor on the screwing process in order to get additional data and improve the technology reliability
3. In situ utilization strongly improved especially for poles in a slope, double poles or poles with cables along them (ground cables for example).

Figure 7- Polux 5: Possibility to measure with an angle, below the ground line level

Parameters measured by the new device

In addition to the two main parameters of Polux technology, the local density and the moisture content, new values are registered by Polux 5:

Angle of the measurement

The angle of measurement is registered thanks to an integrated inclinometer.

This information is important in order to be able to compare the measurements the ones with the others.

Temperature

A thermometer measures the temperature of the environment.

This value is important because wood properties do vary with temperature. In order to be consistent and be able to compare measurements performed in winter or summer, temperature is registered to normalize the results.

Screwing energy

Thanks to the screw used to set up the device on the pole, another parameter can be easily used to improve the results.

The screwing coupling is then registered all along the screwing process. This measurement allows drawing a graphic of the screwing process. Any singularity met during this action can be visually observed and of course, managed with the adequate software.

Examples of field results

The first field results are presented in this section.

Each individual parameter can be displayed with graphs for each measurement.

Force analysis (local density)

The Figure 8 presents various results according to various poles qualities from a good plain pole, a weak plain pole and a pole with an internal cavity.

Moisture content analysis

The Figure 9 illustrates the moisture content measured in two different typical poles : a dry one and a wet one.

Screw power analysis (screwing energy)

The Figure 10 presents the diagrams of the screwing energy for both a strong and a weak pole.

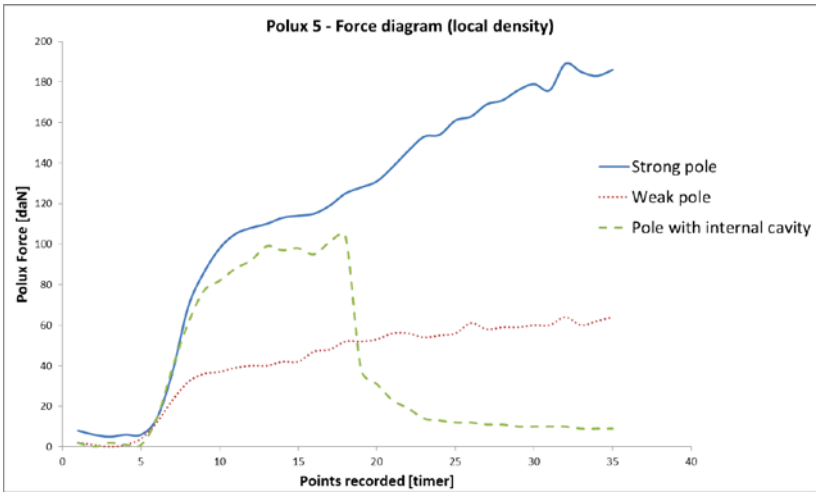

Figure 8- Polux 5: force diagram illustrating the local density. Comparison between a strong pole (solid line), weak pole (dots line) and a pole with an internal cavity (dash line). Measurements performed with the same angle (30°) and similar temperature (approx. 20°C) on a same wood species and impregnation (Spruce treated with CCB)

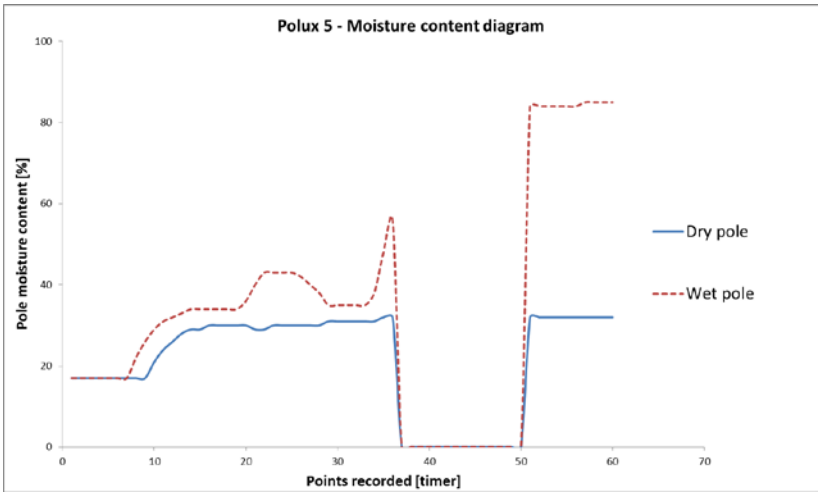

Figure 9- Polux 5: moisture content diagram. Comparison between a dry pole (solid line) and a wet pole (dash line). Measurements performed with the same angle (30°) and similar temperature (approx. 20°C) on a same wood species and impregnation (Spruce treated with CCB)

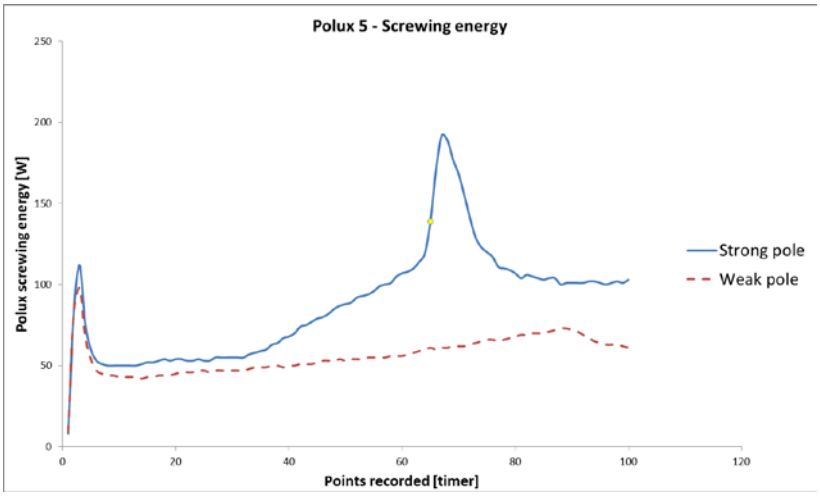

Figure 10- Polux 5: screwing energy diagram. Comparison between a strong pole (solid line) and a weak pole (dash line). Measurements performed with the same angle (30°) and similar temperature (approx. 20°C) on a same wood species and impregnation (Spruce treated with CCB)

Conclusions

The main development objective focusing on the ergonomic key issue is fully reached. A lighter and easier tool for in-situ NDT is born with the newest Polux generation, Polux 5.

The combination of the three recorded main parameters: the local density, the moisture content and the screwing energy – all normalized by the measurement's angle and temperature plus the species and treatments – ensures improved results especially for the weak poles.

Indeed, the comparison between a weak pole and a very weak pole can be better identified especially thanks to the diagrams displayed directly on the inspector's handheld computer. Costs of useless poles' replacements can be then saved. Of course, for a direct interpretation in the field, the curves are not mandatory: the software manages this directly for the inspector.

Nevertheless, the compatibility between the previous Polux generations and the newest one is guaranteed. Polux 5 can give the result according to Polux 4 algorithms and signals the difference obtained thanks to its new sensors. This represents a strong value for existing customers' databases.

Up to now only softwoods have been tested with Polux 5. The next step will be to check the feasibility to use this new device on stronger poles especially in the Southern hemisphere with stronger poles.

References

Springer, P. 2008. Wood Pole In-Service Assessment Methods. Neetrac, Research Center in the School of Electrical and Computer Engineering at the Georgia Institute of Technology. Atlanta, USA

Sandoz, J.-L., Lorin, P. 1996. Polux, a non-destructive technology for the security and the maintenance of in-field wood poles. Wood Laboratory, Swiss Federal Institute of Technology, Lausanne Switzerland.

Near infrared spectroscopy in wooden floor: application for wood discrimination and air-dry density estimation

Raphael Jaquier Bossler Pigozzo
Center for Forest Resource Technology – CTF, Institute for Technological Research – IPT, São Paulo, SP, Brazil, rpigozzo@ipt.br

Takashi Yojo
Center for Forest Resource Technology – CTF, Institute for Technological Research – IPT, São Paulo, SP, Brazil, yojos@ipt.br

Abstract

We evaluated the application of near-infrared spectroscopy as a non-destructive method for identification of wood floor parts and its potential to estimate the air-dry density. The classification model was developed to identify cumaru wood samples on an array of mix-wood floor parts from sucupira and garapa. The model was capable of discriminate all non-cumaru samples, a result that encourage the use of the NIR spectroscopy for wood floor inspections. For air-dry density estimation, the best model developed had satisfactory results just to initial screening and not for a quality control program.

Keywords: Near-infrared spectroscopy, wood identification, wooden floor.

Introduction

Wooden floor in Brazil have a high market price and their consumers have high standard demands for it. From time to time the Center for Forest Resource Technology at the Instituto de Pesquisas Tecnológicas de São Paulo (IPT) receives inquires from these consumers about the wood identification based on the colors patterns variation observed after the wooden floor has been applied. Although color is a useful character, for a reliable identification procedure it is required to access the cross section of the wood or to remove samples for microscopic observations of its anatomy.

Near-infrared spectroscopy has been tested for wood discrimination on a series of studies (Brunner et al. 1996; Tsuchikawa et al. 2003, Adedipe et al. 2008, Pastore et al. 2011) and proved to be a good non-destructive alternative method for wood anatomy. Therefore, the aim of this study was to develop a model to identify cumaru wood floor parts in a set of different timbers. Also, using the same acquired data, we created a model to estimate the air-dry wood density.

Materials and methods

Samples

A total of 180 samples from wood floor parts were assembled and grouped by their identification: 96 cumaru (*Dipteryx* sp.), 56 sucupira (*Diplotropis* sp.), 24 sucupira (*Bowdichia* sp.) and 4 garapa (*Apuleia leiocarpa*). The NIR spectrum of each sample at air dried condition was acquired by a diffuse reflectance spectrometer (Ocean Optics NIR 256-2.5) on the industrial finished surface. The range of the spectra varied from 900 to 2500 nm. Two mathematical pre-treatment were applied to the spectra collection: 1) Smoothing with a moving average of 5 points; 2) Scatter effect correction with the standard normal variation (SNV).

After collecting the spectrum, the moisture content and wood air-dry density from each sample were measured.

Wood discrimination

For the discrimination of cumaru from other timbers we used the Soft Independent Modeling of Class Analogies (SIMCA) method. The method consists in creating a model using principal component analysis (PCA) with the spectra of training group (Naes et al. 2004). The unknown samples are assigned to the group based on the Euclidian distance from the model and the distance from the projection on the model to the center of the group.

The training group was built from the 60 cumaru samples. After creating the model, we tested the other 36 samples of cumaru against it in order to confirm its validity. We also tested the spectra from the 84 mix-wood samples of sucupira and garapa against the model.

Wood air-dry density estimation

The models for wood estimation were developed with partial-least square regression (PLSR).
The first model was developed using the spectral collection of 60 Cumaru samples aforementioned and was applied for the prediction of the other 120 remain samples.

The second model was developed based on all the spectral collection. For the selection of the calibration group we used the Kernnard-Stone method (Kennard and Stone, 1969). First a PCA for all spectral collection was made. Then, 75% (108) of the samples were assigned as a calibration group and PLSR was performed. The model was test in a validation group from the other 72 samples.

Results and discussion

Samples properties

The mean moisture content of the 180 samples was 12% and the mean air-dried density was 901 kg/m^3. Table 1 summarizes the moist content within each timber group. Although water has a great influence over the NIR spectra, our results sample groups presents similar moisture content.

Table 1 – Samples moisture content and air-dried density

Timber	Moisture content	Air-dry density (kg/m^3)
Cumaru (*Dipteryx* sp.)	Mean = 12,3% Sd = 0,9%	Mean = 951 Sd = 66
Sucupira (*Diplotropis* sp.)	Mean = 11,5% Sd = 0,7%	Mean = 832 Sd = 80
Sucupira (*Bowdichia* sp.)	Mean = 12,2% Sd = 0,4%	Mean = 879 Sd = 104
Garapa (*Apuleia leiocarpa*)	Mean = 12,3% Sd =0,4%	Mean = 789 Sd =104
Total	Mean = 12,0% Sd =0,8%	Mean = 901 Sd =95

Wood discrimination

The model successfully discriminate all 84 non-cumaru samples using a 5% significance level. Among the cumaru samples, only two were not identified at this significance level. This corresponds to a Type 1 error, when a sample which belongs to the group is not assigned to it. Figure 1 shows the samples distance to the model and their distance from the model center. The samples not identified are very close to the limit area of the model. When we incur in the type 1 error, a re-acquisition of the spectrum can be used to confirm the identification.

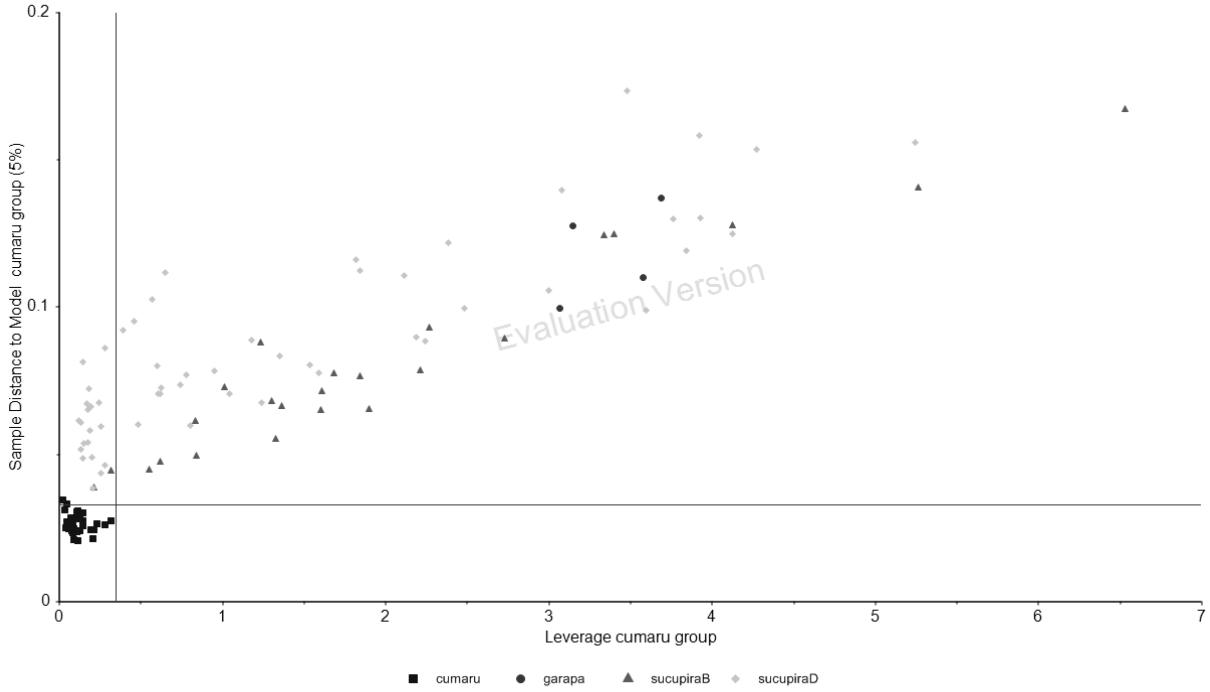

Figure 1 – Distance to model and samples leverage from the classification as cumaru timber. Samples inside the area on the bottom left corner defined by the two limit lines were identified as cumaru.

Wood air-dried density estimation

The resulting parameters from estimation of the two models are present in table 2.
The Standard error of Prediction (SEP) for the model build with the spectra of 60 cumaru samples was considered too high.

The model calibrated with 108 mix timber samples resulted in a lower prediction error. The ratio of the standard error of prediction to the standard deviation (SD) of the validation samples was 2.1, a value suitable for initial screening (Schimleck et al. 2003) but far from the one recommended for quality control (>5) (Williams, 2004).

Table 2 – Calibration models and prediction results for wood air-dry density estimation.

Model	Reference air-dry density (kg/m^3)	Factors	R^2 of prediction	SEP[a] (kg/m^3)
Cumaru based model				
Calibration: 60 cumaru samples	Mean = 953 SD = 80	-	-	-
Validation: 120 mix samples	Mean = 875 SD = 91	1	0,1	91
Kennard-Stone selection model				
Calibration: 108 mix samples	Mean = 885 SD = 93	-	-	-
Validation: 72 mix samples	Mean = 925 SD = 93	8	0,8	45

[a] Standard error of prediction of the air-dry density.

Conclusion

The results from these preliminary study show that NIR spectroscopy could be used as a tool on applied wooden floor evaluation, with focus on wood identification. The next steps is testing its application in site. For that we will have to consider other factors like finish variation and stained influence.

The better wood air-dry density estimation from the mix-timber samples model demonstrate that for calibration it is necessary to include wood samples from the role array of timbers to be tested. Application of one timber group calibration model for a mix-timber others results in poor prediction accuracy.

References

Adedipe, O.E.; Dawson-Andoh, B.; Slahor, J.; Osborn, L. 2008. Classification of red oak (*Quercus rubra*) and white oak (*Quercus alba*) wood using a near infrared spectrometer and soft independent modelling of class analogies. Journal of Near Infrared Spectroscopy. 16: 49-57.

Brunner, M.; Eugster, R.; Trenka, E.; Bergamin-Strotz, L. 1996. FT-NIR spectroscopy and wood identification. Holzforschung. 50(2): 130-134.
Kennard, R.W.; and Stone, L.A. 1969. Computer Aided Design of Experiments. Technometrics. 11(1): 137-148.

Naes, T.; Isaksson, T.; Fearn, T.; Davies, T. 2004. A user-friendly guide to Multivariate Calibration and Classification. Chichester, UK: NIR publications. 344 p.

Pastore, T.C.M.; Braga, J.W.B.; Coradin, V.T.R. [and others]. 2011. Near infrared spectroscopy (NIRS) as a potential tool for monitoring trade of similar woods: Discrimination of true mahogany, cedar, andiroba, and curupixá. Holzforschung. 65(1): 73-80.

Schimleck, L.R.; Evans, R.; Ilic, J. 2003. Application of near infrared spectroscopy to the extracted wood of a diverse range of species. IAWA Journal, 24 (4): 429 - 438.

Tsuchikawa, S.; Inoue, K.; Noma, J. 2003. Application of near-infrared spectroscopy to wood discrimination. Journal of Wood Science. 49: 29-35.

Williams, Phil; Norris, K., eds. 2004. Near-infrared techonology in the agricultural and food industries. 2nd ed., p.296. St. Paul, MN: American Association of Cereal Chemists, INC.

Design and experimental analysis of the trussed rafter system using nailed laminated softwood timber (NLT): Impact of grading on the structural performance

Emanuelle Graça Recco
Master in Architecture and Urbanism – UEL – State University of Londrina, Center for Technology and Urbanism - Rodovia Celso Garcia Cid (Pr445), Km 380 - Campus CEP: 86051-990 - Londrina - Paraná - Brazil Phone 55 43 3326-8551, email: emanuellegracarecco@yahoo.com.br

Jorge de Melo Daniel Moura
Associate Professor Department of Architecture, - UEL – State Universityof Londrina, Center for Technology and Urbanism - Rodovia Celso Garcia Cid (Pr445), Km 380 - Campus CEP: 86051-990 - Londrina - Paraná - BrazilFone 55 43 3371-4641, email: jordan@ uel.br

Everaldo Pletz
Associate Professor Departmentof Civil Engineering – UEL - StateUniversityof Londrina, Center for Technology and Urbanism - Rodovia Celso Garcia Cid (Pr445), Km 380 - Campus CEP: 86051-990 - Londrina - Paraná - BrazilFone 55 43 3371-4582, email: pletz@uel.br

Abstract

The roof system of social housing in Brazil generally consists of wood components from native forests of high market value. Taking into account the increasing number of planted forests, the need to develop new products and to add value to this wood, this work deals with the development and structural analysis of a roof system using plantation *Pinus spp*, a sustainable material even though presenting many defects. Therefore its use in structures implies grading. The NLT technology (Nailed Laminated Timber) was chosen mostly because it allows the use of shorter length and small cross section pieces, eliminating major defects. Seven samples of structural trussed rafter in NLT were tested; 06 with graded lumber and one ungraded in order to verify the impact of grading in the structural performance of the specimens. The results showed that the trussed rafter system in NLT meets the necessary structural performance requiring no sophisticated conditions of infrastructure for the manufacture process. The graded lumber specimens showed better results with respect to deflection than the one ungraded.

Keywords: *Pinus spp*, structural trussed rafter in NLT (Nailed Laminated Timber), grading.

Introduction

When considering the social circumstances of the Brazilian housing deficit and the precariousness of living conditions today, it appears that there is a vast field for research of manufacturing and use of prefabricated building systems with timber from plantations, especially those for social housing. Indeed, the civil construction sector has shown more and more the crucial need for development of products and processes that promote reduction of costs, improvement of quality of construction systems and housing.

The forest plantation timbers have great advantage of rapid growth and occupy a growing market space. *Pinus spp*, for example, is considered an easy handling and high workability, i.e., easy mechanical processing softwood. The growth of the reforestation area of *Eucalyptus spp*. and *Pinus spp* has increased

between 2005 and 2012, from over 300 000 hectares to 520 000 hectares (ABRAF, 2013) in the Paraná State alone.

The good quality wood is the one that presents fewer defects, whether related to the wood itself or those from the production chain. Although the wood of *Pinus spp* present good features that facilitate the transportation and use for various purposes, it also presents aspects that deserve further attention during the plantation process to obtain final product with better quality. In addition, the adoption of proper transportation procedures is necessary, sawing, drying and wood grading, which aim to make it a suitable raw material for the production of sawn wood, for the furniture industry, woodworking and civil construction.

In the production process of timber and wood products, there is a large amount of by products, often pieces of small length though with good quality that could be reused. According to Moura et al. (2012) it is impossible to eliminate the generation of waste in the production line, reason why this study proposes the use of short-length pieces in the composition of structural pieces to the construction industry.

The use of wood composite formed by connected pieces of commercial dimensions has gained importance in the wood structure sector in Brazil, mainly due to the gradual shortage of larger cross section pieces. The nailed timber composite (NLT - nailed laminated timber) allows wide range of application as structural material which main advantages are easeness of fabrication and low cost of production (GÓES & DIAS 2005).

The roof system in trussed rafter is not as spread out in Brazil as in other countries. The main feature of this system is the elimination of joists and traditional trusses and the adoption of trussed rafters. The roof structure is only formed by the trussed rafters and slats which are also a component of the bracing system. The rafters are generally spaced 100 cm from each other and allow spans ranging from 6 to 12 meters. The large spans are possible due to the large amount of trusses allowing better distribution of the loads acting among the structural components (VALLE, 2011).

All lumber presents uneven moisture levels that can cause damage to the structure when used in this condition. Thus, the lumber needs to be dried, operation that requires close attention to avoid stability defects (bending, twisting), collapse, hardening surface, cracks, stains and grain defects. All of these defects can be prevented by controlling the drying conditions (FAGUNDES, 2003).

According to NBR 7190/97, ungraded softwood is not allowed in structures. Two methods are used for structural grading of wood pieces, (CARREIRA 2003): a visual grading, in which, the classifier examines each piece and limits the type, location and size of the various defects that can affect the structural strength, and the mechanical grading, based on the use of an estimator to evaluate the resistance of the lumber.

Among other nondestructive grading techniques there are the ultrasound techniques, transverse vibration and stress wave technique, based on the tomographic image of wood.

In the ultrasound method the measure the stiffness of the timber is based on the propagation velocity of a high frequency sound wave, ≥20 kHz (Ross et al., 1999). The speed “C” at which the wave travels across the piece of wood as well as the mechanical properties depend on the inclination of the fibers and knots and thus can be determined by equation (1).

$$C = 2. L / D_t \quad (1)$$

Where: L = distance between the points of emission and reception of the wave (m), and D_t = time for the wave to travel across the piece(s).

The value of the MOE can be determined taking into account the propagation velocity and the density of the material shown in equation (2).

$$MOE = C^2 . \rho \quad (2)$$

Where: C = wave velocity (m/s), and ρ = density of the wood (kg/m³).

Materials and methods

NLT Trussed Rafters

The trussed rafter system in NLT consists of 03 layers of *Pinus spp* laminations, 1 central containing continuous pieces and two external layers containing discontinuous pieces (end jointed members), with approximately 6 m span and height of 1.2 m. All rafters were nailed with coiled nails ardox type 18x30 (3,4 mm x 69 mm) to overcome the total thickness of the NLT members (60 mm). The cross section of the NLT that composes the trussed rafter is 6x14 cm, corresponding to three boards of *Pinus spp*. The connections of the truss rafters were calculated according NBR 7190/97 and EUROCODE 5, and the connection between the end joints were determined in test performed on specimens in a previous article (RECCO et al., 2014). The minimum distance between the NLT end joints was 20 cm and and 9 nails were used as Figure 1.

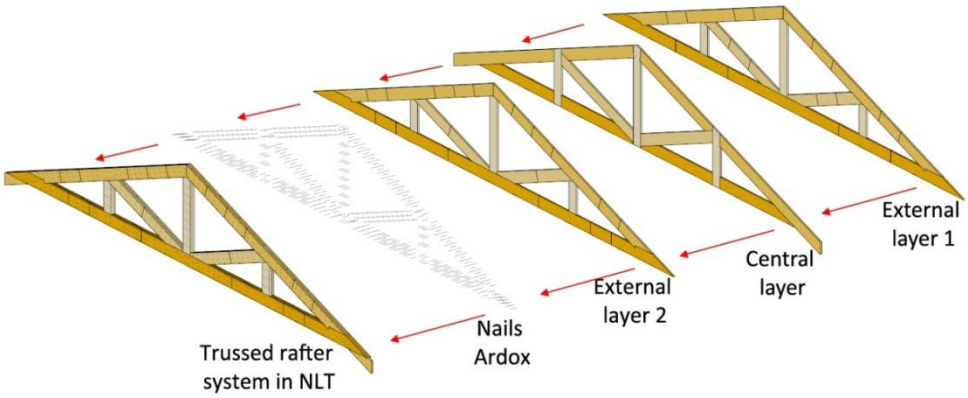

Figure 1 - Scheme of the trussed rafter in NLT.

The Brazilian standard NBR 7190/97 does not address dimension timber testing, only small specimens. Thus it was adopted as reference for this study the Annex B of the same standard for testing with small specimens establishing a minimum of 6 specimens. In addition to the 6 specimens with graded lumber, one specimen made out with ungraded lumber was also tested totaling 7 specimens.

Lumber

Altogether six specimens of rafters with gradade lumber were prepared. 40% of the whole batch of wood was discarded due to impermissible defects. As for the specimens with ungraded wood all pieces were included. Green wood was used in order to monitoring kiln drying.

It was observed that the boards had a large variation in density, observed through to the large difference in weight and growth ring (CARREIRA 2003).

Drying

Wood Drying was held in an experimental kiln built in the laboratory of structures at the State University of Londrina. The kiln drying process is a conventional one at low temperature and the microprocessor

system used to control the process was Digisystem Industry Electronic Systems Ltda., CRG model 08 KD/HT. The technique of air drying consists mainly of making a stack of sawn timber (with the layers of boards separated by stickers) as specified in the manufacturer's manual and accompanied drying cycles to ensure the quality of the wood. The final average moisture was 12%. The total time for drying of the wood was about 10 days.

Grading

The boards were removed from the kiln and placed in groups of 12 pieces for visual grading and measurement of dimensions (in 3 cross sections along the lenght): length, width and thickness in order to calculate density and MOE. Weighing was performed on a digital scale model C & F (maximum capacity. 30 kg), as illustrated in Figure 2.

Figure 2 - Visual grading and weighing.

The visual grading was performed following the instructions of the visual grading Manual of *Pinus spp* (Moura et al., 2012). Only allowable defects of classes EE and 01 were tolerated. The remainder wood was discarded. Another condition considered in the grading was the length; flawless pieces but smaller than 40 cm were discarded due to the minimum required lenght between end joints.

To help visual grading a template on acetate was prepared containing the allowable dimensions of defects in each class in accordance to the grading manual. The sections with defects to be discarded were marked with an X and when used were numbered and named. Finally, the pieces were all referenced and each one received a letter or number as a visual grading: E for structural class; and 1 for first class. For instance: AE 130, 130 B1, etc., as shown in Figure 3.

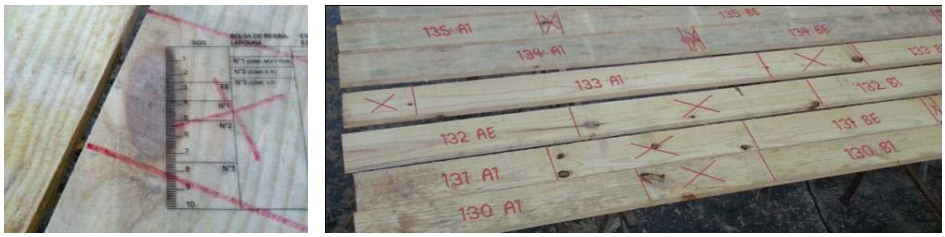

Figure 3 - Template and references on the pieces after visual grading.

The next step consisted in machining and cutting of the pieces according to the referencing made on the visual grading. Machining on the wider faces of the boards was necessary to avoid irregularities and allow full contact of the parts when assembling and nailing the NLT (Figure 4).

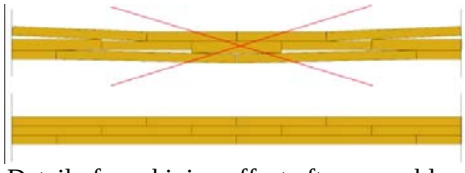

Figure 4 - Detail of machining effect after assembly of the NLT.

The pieces were grouped according to similar lengths to facilitate the organization for mechanical grading by ultrasound.

PUNDIT-6 ultrasound equipment (Portable Ultrasonic Non Destructive Digital Indicating Test) was used for mechanical grading. The time spent on the course was read on a digital display device. With the travel time and the distance traveled by the pulse (distance between the transducers), one could get the average velocity of the wave. For the transmission and reception of the pulse, the transducers should be fully in contact with the surface, because the existence of some air gap introduces error of the time reading, since the air transmits only a negligible portion of the pulse. To avoid this problem, a gel was applied.

The instrument calibration process was carried out frequently by plugging the appliance into a standard metal bar gage with known wave travel time (25.7 μs) as recommended by the manufacturer. In every measurement the pieces were placed on a polystyrene surface for insulation and transducers were placed on the surface of the two ends of the piece (figure 5).

Figure 5 - Photos of the grouped parts as lengths and measurement by ultrasound.

The wave velocity, the length and density values of the pieces were recorded in a spreadsheet to calculate the modulus of elasticity (MOE).

Choice Criteria of pieces

With lengths resulting from visual grading and MOE values obtained by ultrasound grading, a spreadsheet to distribution of pieces was drawn. It was necessary to make a distribution in such a way that all the rafters had similar characteristics: end joints of the outer layers at the same locations and similar MOE.

The pieces showed great variability of density and MOE, making it difficult even distribution throughout the specimens. The grouping and distribution were carried out in phases:

1) Pieces and end joints were distributed according to the lengths originated at the visual grading. Most pieces had small lengths ranging from 40cm to 70 cm, and therefore it was necessary to make a great number of end joints.

2) After setting up the lengths of the pieces and locating the end joints of the three layers, the boards to integrate the bottom chord, (where the greatest tension stresses appear), were separated. The goal was to group pieces with less MOE variation. The MOE of the bootom chord pieces showed a variation ranging from 8000 MPa to 14000 MPa and were distributed with the same average and the same variation of standard deviation between the six 6 specimens as Table 1.

3) The boards destined to the top chords and webs, showed high MOE variation, however, the pieces were distributed according to the required lengths, similar average MOE, standard deviation and coefficient of variation.

Table 1 - Model soreadsheet of the distribution of pieces according to the MOE.

BOOTOM CHORD						
PIECES (LENGTH.)	**MOE SAMPLES (MPa)**					
	1	**2**	**3**	**4**	**5**	**6**
PIECE (213,7 mm)	9001,7	13634,4	10756,5	13363,8	12784,9	13112,7
PIECE (173,7 mm)	12101,0	10121,4	13673,6	9605,4	12179,9	14162,0
PIECE (144,3 mm)	9408,6	9430,9	8408,6	8770,5	8408,6	8476,3
	14046,3	13916,0	13571,3	13295,3	12434,3	11281,7
PIECE (140 mm)	8093,6	8093,6	8604,2	8604,2	11069,3	10505,6
	12275,0	12275,0	11708,7	11708,7	11069,3	10505,6
PIECE (138,5 mm)	8374,8	9256,4	9256,4	8878,3	8374,8	9603,5
	9603,5	12151,0	12151,0	13671,7	14309,2	14309,2
PIECE (120 mm)	11905,4	10627,3	9176,1	8631,3	11767,8	8002,5
	14864,4	14790,1	13436,3	12422,2	12114,2	12047,9
PIECE (1m)	9193,4	9092,4	8377,2	8317,6	8094,4	8728,6
	11420,6	10071,0	10120,6	10928,0	8088,8	10960,3
	13782,8	13646,5	13202,9	13189,8	12813,5	11854,7
	14481,8	14601,7	14780,4	14796,1	14887,6	14937,8
Average	11663,0	11389,2	11232,6	11318,3	11941,0	11121,0
Standard deviation	2377,991	2284,625	2261,01	2309,713	2269,742	2224,703
Coefficient of variation	20,38916	20,05962	20,12903	20,4068	19,00798	20,00453

The underlying idea of this distribution piece was to fabricate specimens with mechanical properties as close as possible, therefore, with a similar structural behavior and thus, comparable.

Assembly steps of the Rafters

The assembly of the specimens was carried out in the laboratory of modelsof the university. The first specimen helped the set up of a template for assembling the remaining six copies. The set up of the first specimen demanded a great care in particular with the angular cuttings in order to allow maximum contact between pieces. The same was observed regarding the rectangular pieces.

Finished the assembling of the first specimen and all parts were cut and adjusted, one proceeded to cut the pieces to the remaing specimens. The pieces were cut and numbered from 1 to 6 according to the preset MOE. Thus, all parts were ready and screened for setting up and nailing. In order to assist in nailing the NLT, templates were made in MDF of the different arrangements of connections and pre-drilling was carried out according to NBR 7190/97 (minimum diameter of 0.85 d_{ef}, d_{ef} being the effective diameter in mm), as shown in Figure 6.

Figure 6 – Template for the execution of 6 samples, template utilization, assembly / pre-drilling of pieces.

Results and discussion

As previously mentioned, the test was performed according to Annex B of the NBR 7190/97. The estimated sample resistance f_{t0est}, was equal to 50 KN. The load was applied in two cycles of charge and discharge, 10 and 50% of the expected failure load. The last cycle was carried out to failure. The load was monotonically increasing with an approximate rate of 6MPaper minute, less than the established by the NBR 7190/97 (10 MPa per minute). Deflection measurements were made by means of three dial indicatorss installed below the bottom chord connections.

The results of tensile strength of the 7 specimens in NLT can be seen in Table 2 and it is possible to observe the high ultimate loads values averaging 60 KN and low variability of results (7, 5%).

Table 2 - Ultimate Load

Samples	1	2	3	4	5	6	Ungraded	Average	Standard deviation	Coefficient of variation
Tensiles trength (kN)	56,38	65,41	51,86	63,15	60,89	58,18	61,80	60,89	4,56	7,5%

In all samples the rupture occurred first in the connection between the end joints of the laminations of the bottom chord in the tensioned bar followed by the top chord failure. As expected the laminations approached the top of the end joints in the top chord due to the compressive stress. In the bottom chord the laminations moved away from the end joints due to the tensile stress, with greater loss of rigidity and overall strength of the tensioned bars.

The comparative graph of load versus displacement curves in the center of the span of the 7 samples to load application 47.35 KN at the time of the dial indicators withdrawal was prepared. All showed the same behavior, with a reduction of displacement after accommodation of the first cycle about 25 kN or 50% of the estimated load to failure. It is also noticeable that the specimen without ungraded lumber showed greater displacement during the first cycle of loading, demonstrating the positive impact of grading on the structure performance (Figure 7).

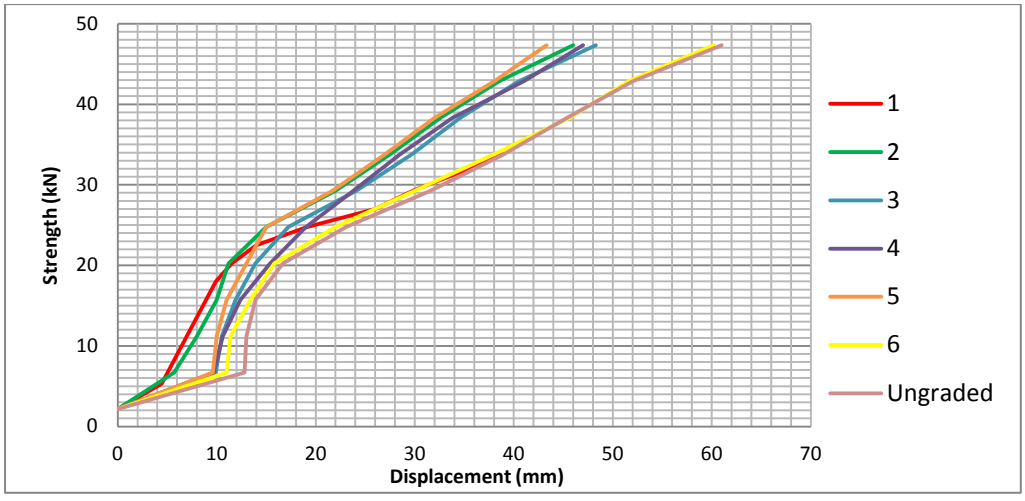

Figure 7 - Load Displacement Curve- measurements in the center of the span (up to 47.36 kN).

The results showed that the weakest point of the structure concerning failure, was the connection and not the timber since all the ultimate loads were very high and of low variability. However, concerning stiffness, the graded lumber specimens showed better performance. The ungraded timber specimen showed greater defletions, demonstrating the importance of grading in the development of new structural components.

Final considerations

The trussed rafters are widely used as roof structures in other countries and their effectiveness is proven. Through the results it was possible to show that the fabrication of these structures using NLT is a viable option considering the utilization of *Pinus* produced in Brazil.

The results could prove that through visual grading, disposal of major defects and determination of MOE of each piece through the use of ultrasound technique, it is possible to manufacture specimens with homogeneous mechanical properies. This methodology of structure composition allows the analysis of the results with safety and confirmation of the feasibility of the system.

The seven samples tested showed the same behavior throughout the test and the rupture occurred at the end joints of the tensioned bar. The results obtained concerning failure load are fairly high, with an average of 60 KN and low coefficient of variation. The vertical deflections were larger in the specimen with ungraded lumber, showing that grading performance benefits the structure, however in this case the absence of the grading did not disqualified the system as the load values, when the limit of deflection was reached, were higher than expected. In this case, the structure response of the system was found to be more dependent on joints in the NLT than properly the mechanical properties of timber.

References

ASSOCIAÇÃO BRASILEIRA DOS PRODUTORES DE FLORESTAS PLANTADAS - ABRAF. **Anuário estatístico ABRAF 2013: ano base 2012.** Brasília: ABRAF, 2013. p. 74

ASSOCIAÇÃO BRASILEIRA DE NORMAS TÉCNICAS, ABNT, **NBR 7190:** Projeto de estruturas de madeira. Rio de Janeiro, 1997. 107 p.

CARREIRA, M. R.; DIAS, A. A. **Classificação visual de coníferas: análise da aplicação do método norte-americano às espécies de *Pinus spp.*** plantadas no Brasil. **Scientia Forestalis**, n.67, p.78-87, 2005.

FAGUNDES, H. A. V. **Diagnóstico da produção de madeira serrada e geração de resíduos do processamento de madeira de florestas plantadas no Rio Grande do Sul.** Porto Alegre: Escola de Engenharia, UFRGS, 2003. 173 p. Dissertação (Mestrado).

GOÉS, J. L. N.; DIAS, A. A. **Análise de vigas de madeira pregadas com seção composta I.** São Carlos: Escola de Engenharia de São Carlos, USP, 2005. Cadernos de Engenharia de Estruturas, v. 7, n. 29, p. 57-77.

MOURA, J.D.M.; PLETZ, E.; STRASS, M. C. **Panorama Geral e Perspectivas Preliminares de Continuidade dos Trabalhos em Relação às Visitas Técnicas Realizadas a Indústria do Setor Madeireiro do Parque Industrial de Telêmaco Borba a Convite da Secretaria Municipal do Trabalho e Industria Convencional.** 2012, Universidade Estadual de Londrina, Relatório Interno.

RECCO, E. G. ; MOURA, J. D. M. ; PLETZ, E. . **Análise experimental de emendas tracionadas de barras de madeira laminada pregada de *Pinus spp***. In: XV Encontro Nacional do Ambiente Construído, 2014, Maceió. Anais do XV Encontro Nacional do Ambiente Construído. Maceió: ANTAC, 2014. v. 1. p. 3398-3407.

ROSS, R. J. ; PELLERIN, R. F. ; VOLNY, N. ; SALSIG, W. W. ; FALK, R. H. (1999**). "Inspection of Timber Bridges Using Stress Wave Timing Nondestructive Evaluation Tools".** Gen. Tech. Rep. FPL-GTR-114 USDA, Department of Agriculture, Forest Service, Madison, WI.17 p.

VALLE, I. M. R. **A pré-fabricação de dois sistemas de cobertura com madeira de florestas plantadas:** Estudos de casos: os assentamentos rurais Pirituba II e Sepé Tiaraju. São Carlos: Escola de Engenharia de São Carlos, USP, 2011. 352 p. Tese (Doutorado).

Inspection methodology and rehabilitation techniques of timber structural members of the suspension footbridge at Piracicaba River in Brazil

Leandro Dussarrat Brito
Department of Structural Engineering – SET, Laboratory of Wood and Timber Structures – LaMEM, University of São Paulo – USP, São Carlos School of Engineering – EESC, São Carlos, São Paulo. Avenida Trabalhador Sãocarlense, 400 - Caixa Postal 359 - Centro - Cep:13566-590 - São Carlos - SP – Brazil. dussarrat@sc.usp.br

Carlito Calil Junior
Department of Structural Engineering – SET, Laboratory of Wood and Timber Structures – LaMEM, University of São Paulo – USP, São Carlos School of Engineering – EESC, São Carlos, São Paulo. Avenida Trabalhador Sãocarlense, 400 - Caixa Postal 359 - Centro - Cep:13566-590 - São Carlos - SP – Brazil. calil@sc.usp.br

Abstract

This work was to propose rehabilitation techniques for decayed timber structural members on the case study for rehabilitation of the Suspension Footbridge of Piracicaba River, in Brazil. The structural system of the bridge is a suspension bridge system consists of two steel towers that support the cables leading steel suspension hangers and steel bars that fixed in the uprights of the lower trusses Lumber *Corymbia Citriodora* with 76.8 meters of free span. For the study a systematic literature survey of research was conducted followed by research "in situ" and experimental tests were conducted in the laboratory. On inspections were used to assessment the non-destructive techniques (NDT): superficial probing, pick test, sounding, visual inspection for evaluations of visual characteristics due to the presence of biodeterioration and defects, and the use of resources of topography on the deck for correction unevenness level of the deck. In the first stage the major pathological manifestations were investigated, indicating a proposed methodology for nondestructive inspection technique (NDT) by visual inspection technique to assessments for timber structural members, and assessment with use of the Resistograph® IML-RESI-F500-S. The methodology aimed at identifying and evaluating the main pathological manifestations found in each members. The second step consisted on the rehabilitation techniques with scabbing, whose experimental results of beams subjected to static bending tests were adequate, with better technical and economic feasibility.

Keywords: Structures, Timber, Pathologies, Assessment, Conservation, Rehabilitation

Introduction

The prefecture of Piracicaba, SP, Brazil, contacted the Laboratory of Wood and Timber Structures (LaMEM / EESC / USP), requesting an Inspection and rehabilitation at the suspension footbridge Pedestrian Pensil Bridge (Figure 1), which structural system is composed by timber trusses of *Corymbia Citriodora*, with 76.8 meters of free span over Rio Piracicaba (BRITO 2014). This Pedestrian Pensil

Bridge is situated on GPS coordinates 22º 43’06,50”S; 47º 39’ 14,75”O; 476 meters altitude (Figure 2).

Figure 1 - Overview of the Pedestrian Pensil Bridge above of the Piracicaba River. Photos: Authors

The Inspection aimed at identifying and evaluating possible existing pathologies and indicating the proper maintenance procedures to be performed (BRITO 2014). During the inspections, the following elements of the structure were investigated: suspension devices (cables, hangers and anchors), steel towers, metal guardrails, concrete bollards, stiffness trusses (wood parts, connections, support conditions); timber beams of the ramp (simply supported section); wood pieces of the board. However, the focus of this paper is only assessment of the wood structural elements of this pedestrian bridge, in inspection for evaluating decay.

a) Aerial view. b) Access ramp for Pedestrian Pensil Bridge.

Figure 2 - GPS coordinates 22º 43’06,50”S; 47º 39’ 14,75”O; 476 meters altitude. [Google Earth].

Description of the structure

The pedestrian bridge structural system is a suspension pensil system composed by two steel towers with approximately 15.0 meters height that support the main cables leading steel suspension hangers and steel bars fixed in the uprights of the lower timber trusses lumber of the wood *Corymbia Citriodora*, with 76.8 meters of free span and the deck with 4.0 meters wide. The Figure3 and Figure 4 shows the positioning of the schematic rigid lattice in elevation and in plan of the pedestrian suspension pensil bridge, for the purpose of description of parts (BRITO 2014).

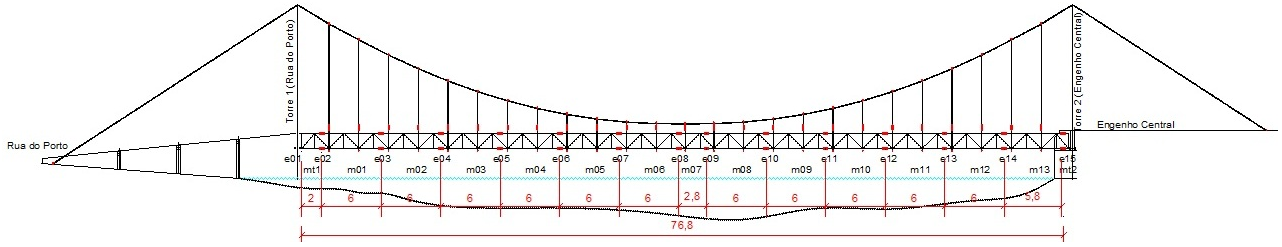

Figure 3 - Schematic elevation of the pedestrian suspension pensil bridge. (BRITO 2014)

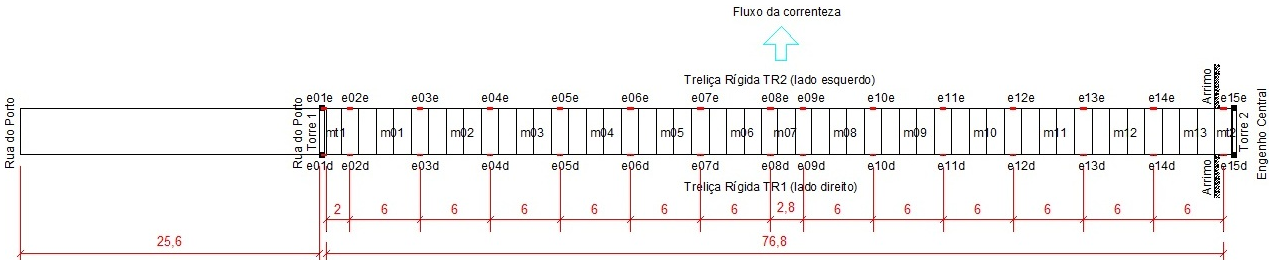

Figure 4 - Schematic plant of the of the pedestrian suspension pensil bridge. (BRITO 2014)

Inspection techniques to assess timber bridges

The wood is an amazing combination that exhibits both strength and durability as a structural material used for bridges. Nevertheless, from the time it is formed in the tree, wood is subject to deterioration by a variety of agents biotic and abiotic [1, 2, 3, 4, 5]. Damage ranges from relatively minor discolorations caused by fungi or chemicals to more serious decay and insect attack (RITTER; MORRELL 1990).
Timber inspection is a learned process that requires some knowledge of wood pathology, wood technology, and timber engineering [3]. This paper covers the fundamentals of timber structure pedestrian pensil bridge inspection for decay and deterioration; it identifies the agents of deterioration and outlines used inspection methods.
Timber structure bridge inspectors have the difficult task of accurately assessing the condition of an existing structure. They must understand the biotic and abiotic factors associated with wood deterioration as well as the relative rate at which these processes occur in a given environment (RITTER; MORRELL 1990).
For this there are the main methods that can be used for inspection and evaluation of timber bridges: types and areas for deterioration; inspection techniques; equipment and tools; NDE tool; performance monitoring.

Assessment by non-destructive techniques (NDT)

Nondestructive evaluation is the science of identifying the physical and mechanical properties of materials without altering its end-use capabilities and then using this information to make decisions regarding appropriate applications. Nondestructive evaluation (NDE) technologies have contributed significantly toward detect structural problems. Table 1 shows many tests and techniques evaluation categorized as nondestructive (PELLERIN; ROSS 2002).

Table 1 – Nondestructive techniques. Source: (PELLERIN; ROSS 2002)

Nondestructive evaluation of wood	
Evaluation of visual characteristics	Chemical tests

Color	Composition
Presence of defects	Presence of treatments
	- Preservatives
	- Fire retardants
Physical tests	Mechanical tests
Electrical resistance	Flexural stiffness
Dielectric properties	Proof loading
Vibrational properties	- Bending
Wave propagation	- Tension
Acoustic emissions	- Compression
X-Ray	Probes/coring

Simple methods are available for inspecting waterfront structures without sophisticated tools. These methods, which include visual characteristics, sounding, probing, pick test, moisture meter, microdrilling, and measuring moisture content, may be used singly or in combination:

a. Visual inspection technique

The visual inspection technique is used for evaluations of the visual characteristics due to the presence of defects, insects attacks and decay [1, 2, 3, 6, 7]. Camera can be used for picture a time to reflect existing damage, taking photos of the affected areas is quite important (ARRIAGA et al. 2002).

b. Sounding

Sounding, by rapping on the member with a hammer, may indicate the presence of interior deterioration. If the hammer does not rebound or produces a dull or hollow sound, a considerable amount of the internal wood is probably decayed. This method requires considerable experience and can be considered truly diagnostic only where decay is relatively severe, where large members are decayed, and where the decay extends to areas near the surface. If sounding suggests internal decay, the wood must usually be bored to verify the diagnosis [1, 2, 3, 7].

c. Pick test

The pick test is one of the simplest, yet most widely used, methods for detecting surface decay. A pointed pick, awl, or screwdriver is driven a short distance into the wood and used to pry out a sliver. The wood break is examined to determine if the break is brash (decayed) or splintered (sound). Sound wood has a fibrous structure and splinters when broken across the grain. Decayed wood breaks abruptly across the grain or crumbles into small pieces. Several studies indicate that the pick test is reasonably reliable for detecting surface decay. The only drawback to this method is having to remove a large sliver of wood for each test [1, 2, 3, 7].

d. Moisture meter

The moisture content of the wood and the walls is usually one of the most important factors for the development of some xylophage agents. These devices of moisture meters allow to determine the moisture content quickly [1, 2, 3, 7].

e. Microdrilling (Resistograph®)

Drilling and coring are the most common methods used to detect internal deterioration in wood members. Both techniques are used to detect the presence of voids and to determine the thickness of the residual shell when voids are present. Another drilling technique that has been commercially developed is the resistance drill system, like example the use of the Resistograph®. The resistance drill system measures

the resistance of wood members to a 1.5 mm drill bit with a 3.0 mm head that passes through them. The drill bit is fed at a fixed movement rate allowing the inspector to determine exact location and size of the damaged area. This system produces a chart showing the relative resistance over its travel path. This chart can be produced either as a direct printout or can be downloaded to a computer. Areas of sound wood have levels of resistance, with voids shoving no resistance. The user can determine areas of low, mild, and high levels of decay. Further, termite galleries can be identified by the characteristic of high resistance (solid wood) followed immediately by no resistance (gallery). Larger diameter holes can be drilled and inspected with a magnified inspection scope to verify live termites [1, 6, 7].

f. Probing test

Probing with a moderately pointed tool, such as an awl or knife, locates decay near the wood surface by revealing excessive softness or a lack of resistance to probe penetration. Although probing is a simple inspection method, experience is required to interpret results. It is good to take care to differentiate between decay and water-softened wood that may be sound but somewhat softer than dry wood. It is also sometimes difficult to assess damage in soft-textured woods [2, 3, 7].

Areas susceptible to deterioration

A good way to begin an inspection for decay is a visual inspection technique search for decay manifestations, emphasizing locations or conditions most conducive to prolonged wetting (Figure 5). Decay usually results in abnormal coloration of the wood. The first indication of decay is often brown streaks or blotches; purplish streaks are sometimes present. As wood approaches advanced stages of decay, it loses luster and may exhibit pronounced changes in color. Of course, judgments based on color necessitate familiarity with the appearance of sound wood. Sound, healthy softwood has a pleasant, fresh, resinous smell, whereas decayed wood usually has a mushroom-like, stale odor. However, a musty, moldy smell, though indicative of damage conditions favorable to decay, does not necessarily indicate the presence of decay (HIGHLEY; SCHEFFER T 1989).

The main pathological manifestations that can be observed by visual inspection technique are: signs of distress (collapsed, failed members, excessive deflections); missing members; fruiting bodies; sunken faces or localized surface depressions; staining or discoloration; insect activity; plant or moss growth in splits, cracks; grade stamps; checks.

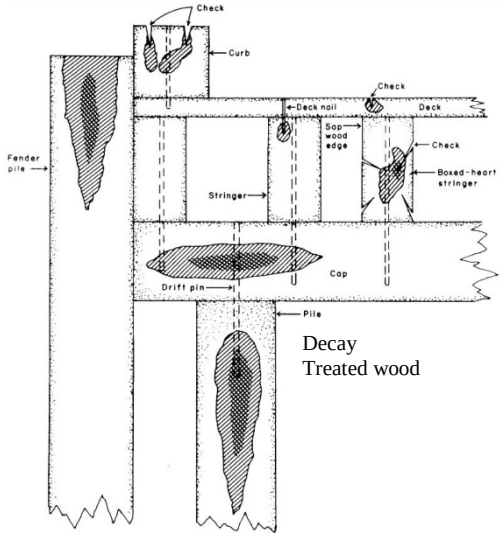

Source: (HIGHLEY; SCHEFFER 1989)

Figure 5 - Schematics of typical areas of decay in decking, stringers, pile covers (caps), curbing, and piling.

Assessment of timber structure members of the suspension footbridge at Piracicaba River

The nondestructive techniques (NDT) used in this work were evaluation of visual characteristics related to structural problems, that is, absence of bracing, buckland members, deterioration due wood humidity and deterioration due fungi and insects attacks. The pictures Figure 6 to Figure 11 shows this type of structural problems inspected by visual inspection technique. The fungi begin as minute spores that germinate and grow through the treated wood. Once enough energy has been obtained, the fungus produces a fruiting body and releases spores that spread and infect other wood (Figure 6 and Figure 7).

Figure 6 - Decay of woods by fungi at under board. Photos: (BRITO 2014)

The brown rot degrades the cellulose and hemi-celulose leaving the lignin as a framework which makes the wood dark brown and crumbly.

a) Characteristics brown rot fungi in an advanced stage. b) Note a lot of leaves, and the plants growing.

Figure 7 - Woods infected with characteristics brown rot fungi. The decayed wood has a darkened color with a cracked, brittle surface that resembles charred wood. Photos: (BRITO 2014)

During the inspection also were detected, frass and debris accumulations in the holes and tunnels of termites, at points located in wood beams and under wood board (Figure 8).

a) Holes and tunnels in beam. b) Tunnel in beam and board with termites.

Figure 8 - Termites and the wood damage they cause. In this case always note the frass and debris accumulations in the tunnels. Photos: (BRITO 2014)

During the inspection were also detected connections with splits (thru) checks (Figure 9). That is separation of the wood through the piece to the opposite surface or to an adjoining surface due to the tearing apart of wood cells.

Figure 9 - Splits (thru) checks at connections. Photos: (BRITO 2014)

In the inspection were detected connections with check (Figure 10). This is a separation of the wood normally occurring across or through the rings of annual growth and usually as a result of seasoning.

a) Diagonal: one check lateral. b) Other diagonal: check superior.

Figure 10 - Checks at diagonals. Photos: (BRITO 2014)

At certain points of the amendments trusses (Splice joint), were found loose bolts. As shown in pictures Figure 11.

Figure 11 – Splice joint with loose bolts. Photos: (BRITO 2014)

The pictures of the Figure 12 shows the case studies by BRITO 2014 for rehabilitation technique with juxtaposed scabbing on timber structural members of the Suspension Footbridge of Piracicaba-SP, Brazil.

(a) (b)

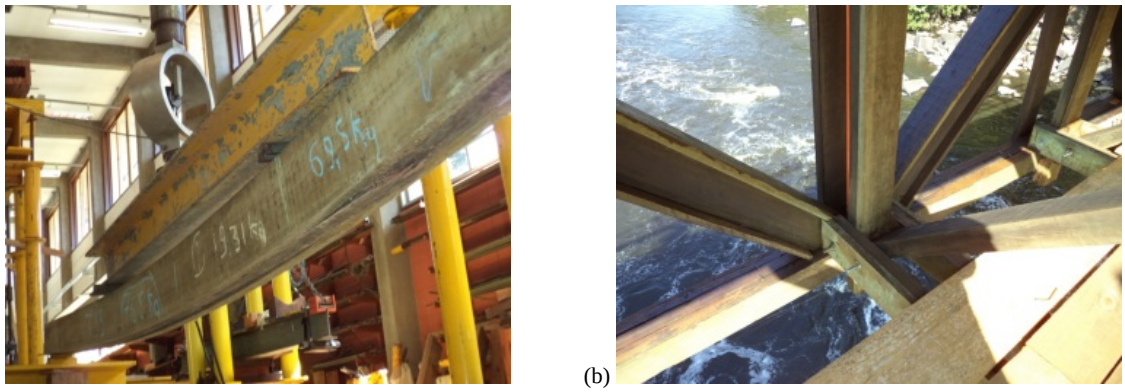

Figure 12 - Case study for rehabilitation of the Suspension Footbridge of Piracicaba-SP, Brazil: (a) making specimen; (b) experimental tests of beams subjected to static pure bending; (c) rehabilitation technique "in loco" with juxtaposed scabbing. Photos: (BRITO 2014)

Conclusions

Most of the types of deterioration has been analyzed using visual analysis and also mechanical equipment like resistograph technique. Detailed evaluation and technical report has been carried out with the support of the “Laboratory of Wood and Timber Structures” (LaMEM), São Carlos School of Engineering (EESC), University of São Paulo (USP), Brazil, in order to propose suggestions and recommendations for maintenance and rehabilitation of this timber structure bridge in Piracicaba in Sao Paulo state.

It is noteworthy that the pieces of wood were treated with CCA, however, even in the treatment process with a condom in autoclaves by impregnating the heartwood of hardwoods not guarantee effective treatment. For this reason, in case of use of sawn pieces of wood, especially bridge structures, it is always advisable, in addition to treatment by impregnation perform preventive maintenance with surface treatments such as painting with applications with varnish stain.

In this work, it was possible to detect pathologies in various structural elements of timber bridge, which could be avoided with regular inspections and preventive maintenance. There was a finding of lack of preventative maintenance and control of pedestrians and of timber bridges in Brazil. In this way the assessment, maintenance and rehabilitation of timber structures must be an important subject for the future of timber structures in Brazil.

The routine sequential for recommendation at the inspection process of timber bridges, can be used the

techniques as indicated below: the visual inspection technique, with records photos; the sounding technique with hammer; the probing test; the pick test with mortise chisel; the moisture meter; the microdrilling with Resistograph®; among others tests.

Acknowledgements

The authors thank CNPq for its financial backing of this work. And to LaMEM's researchers.

References

BRITO, L. D. 2014. Patologia em estruturas de madeira: metodologia de inspeção e técnicas de reabilitação. Tese (Doutorado) Departamento de Engenharia de Estruturas, Escola de Engenharia de São Carlos, Universidade de São Paulo. São Carlos, Brasil. [1]

HIGHLEY, T. L.; SCHEFFER, T 1989. Controlling decay in waterfront structures. Evaluation, Prevention, and Remedial Treatments. Department of Agriculture, Forest Service, Forest Products Laboratory. FPL-RP-494. Madison, WI, USA. [2]

RITTER, M. A.; MORRELL, J. J. 1990. Timber bridges. Depart. of Forest Products, Oregon State University. [3]

CALIL JR., C. et al 2006. *Manual de projeto e construção de pontes de madeira*. ISBN: 85-98156-19-1. Suprema, São Carlos, 2006. *Download (pdf):* <<*http://www.set.eesc.usp.br/portal/pt/livros/361-manual-de-projeto-e-construcao-de-pontes-de-madeira*>> [4]

CALIL JR., Carlito; BRITO, Leandro Dussarrat 2010. *Manual de Projeto e Construção de Estruturas com Peças Roliças de Madeira de Reflorestamento*. Departamento de Engenharia de Estruturas, Escola de Engenharia de São Carlos, Universidade de São Paulo. ISBN: 978-85-8023-000-0. Editora EESC. São Carlos. *Free Download (pdf):* <<*http://www.set.eesc.usp.br/portal/pt/livros/371-manual-de-projeto-e-construcao-de-estruturas-com-pecas-rolicas-de-madeira-de-reflorestamento*>> [5]

PELLERIN, Roy F.; ROSS, J. 2002. Nondestructive Evaluation of Wood. Forest Products Society, Madison, WI, USA. [6]

ARRIAGA, F.; PEZAZA, F.; ESTEBAN, M.; BOBADILLA, I.; GARCIA, F. 2002. Intervención en estructuras de madera. ISBN 84-87381-24-3. AITIM, Madrid. [7]

Historic “HAUFF” timber roofs in Poços de Caldas in Brazil

Leandro Dussarrat Brito
Department of Structural Engineering – SET, Laboratory of Wood and Timber Structures – LaMEM, University of São Paulo – USP, São Carlos School of Engineering – EESC, São Carlos, São Paulo. Avenida Trabalhador Sãocarlense, 400 - Caixa Postal 359 - Centro - Cep:13566-590 - São Carlos - SP – Brazil. dussarrat@sc.usp.br

Carlito Calil Junior
Department of Structural Engineering – SET, Laboratory of Wood and Timber Structures – LaMEM, University of São Paulo – USP, São Carlos School of Engineering – EESC, São Carlos, São Paulo. Avenida Trabalhador Sãocarlense, 400 - Caixa Postal 359 - Centro - Cep:13566-590 - São Carlos - SP – Brazil. calil@sc.usp.br

Abstract

This paper presents the assessment of historic structural systems timber roofs type “Hauff” of constructions existing in Poços de Caldas, Minas Gerais, Brazil. The large timber structures originated with the engineering company “Hauff”, whose production of timber structures contributed in great measure to the technological advance of the industry of construction engineering with wood in Brazil. Based on photographic by techniques of visual inspection (NDT) and descriptive documentation, this paper offers examples of timber roof structures that constitute most of type “Hauff” roof structural systems, such as, lamellar roof structure, sawn lumber nailed arch, plywood arch, shed truss roof, that were built between the years 40 and 60 in the city at Poços de Caldas in Minas Gerais. The timber structures with “Hauff” were built in various regions of Brazil at that time.

Keywords: timber structures, inspection, assessment, intervention, pathologies, sustainability

Introduction

According to a historical survey of the construction and engineering related to the history of type "Hauff" in timber structures, have recently been identified in several locations in the city Poços de Caldas, in Brazil, 12 timber roof structures, medium and large possession with various roof structural systems type "Hauff", still existing, built between the 1940s and 1960s. The major roof structural systems observed are the timber roof structures with lamellar roof structure, warehouses with roof structural system type sawn

lumber nailed arch, warehouses with roof structural system type plywood arches composed section, warehouse with shed truss roof, which were built at the time.

Restoring existing structures for reuse of the building is a major trend in the global issue of sustainability, (CÓIAS 2011). With this attitude you can reduce waste generation and material consumption that would result from the process of constructing a new building at the place of that existing old one.

Objective

Considering the lack of studies that provided evidence of the timber roof structures type "Hauff", built, and still existing in Poços de Caldas, it was observed the need to research a little more on this topic, aiming to identify structural systems adopted at that time.
The specific objective of this study sought to document the lifting of the main timber roof structures, which were built with roof structural systems type "Hauff," still existing in the city of Poços de Caldas in Minas Gerais, Brazil.

Methodology

The methodology used for the theoretical foundation of this study was performed a literature review on the roof structural systems type "Hauff". And for the lifting of existing structures in city Poços de Caldas, technical visits were made, where were photographed by techniques of visual inspection (NDT) outside areas, facades, and whenever possible, internal areas to identify details of roof structural systems, in order to catalog these buildings that still exist.

Theoretical foundation

Brief history of timber structures system type “Hauff” in Brasil

The Erwin Hauff, founder of the company “Hauff”, was born in Vienna, Austria and graduated in civil engineering from the Technical University of Munich in 1920. At the end of World War I, Mr. Hauff moved to Brazil, where he became fascinated in studies of Brazilian forest species upon observing the physical characteristics of their wood. He collected samples of a wide variety of species, observing their drying behavior, their defects such as cracking and warping, and their workability. All these observations were based on empirical trials (CÉSAR 1991). Hauff’s success in the 1920s, 30s and 40s was due, among other things, to the greater availability of skilled labor which was abundant in those days as a result of foreign immigration, which brought to Brazil a large contingent of individuals of medium level very experienced and highly qualified in carpentry trades, as well as in other general construction tasks. Also, at times, Hauff itself brought over several European technicians to train their workers, who were required to be qualified at a technical or specialized level in one area of carpentry, since the Brazilian labor market was going through a crisis, particularly in the late 40s and 50s. These foreign professionals were, in large part, responsible for training many excellent Brazilian carpenters, (CÉSAR 1991).
Of Hauff company’s three phases, the first stood out from the others for the technological innovation in wood structures which the company introduced into construction engineering, with timber truss system, known as “Hauff System”. These structures included road bridges, soffit scaffolding, framework scaffolding, antenna towers, falsework, roofing frameworks in general, and silos. Structures built according to the “Hauff System”, which was characterized by the presence of carved dowel connections and trusses, predominated in the first period of wood roofing projects and works. This initial period, in turn, was also divided into two phases. This division was marked by the type of tiles used in roofing, and the first phase, which occurred between 1925 and 1937, was characterized by the use of French-type fired clay tile roofing (CÉSAR 1991).

The second phase, which began in 1937, was characterized by the use of fiber cement corrugated roofing panels. The use French tiles required a roof framework composed of slats, rafters and purlins. Structural elements such as arches, rigid frames, trusses, etc. consisted of bars with more robust sections, since this type of roofing was heavier than fiber cement panels. Another important aspect of French tiles is the roof bracing system, which is simpler than the system used for frameworks for supporting fiber cement roofing panels, because clay tiles are not fixed to the roof web and therefore do not transfer the effect of wind suction to the structural elements. During this period, it was also common to use arch structures with two or three hinges and wood or steel ties. The combination of the shape of the arch and the mechanical characteristics of wood in resisting tensile and compressive loads parallel to the fibers resulted in a structural solution that could cope with large spans with the rational use of wood. This structural solution was widely used by Hauff for twenty to thirty meter spans, when the arches were braced and supported on, columns and reinforced concrete beams, or on timber columns (CÉSAR 1991).
During the second and third phase of "Hauff", according to the demand with the growth of construction in the country, have emerged in the market other manufacturers of timber structures for roofing, which was to highlight the criteria that they have achieved in the domestic market, but also the structural types offered by them (CÉSAR 1991).

Inspection techniques to assess timber structures

The wood is an amazing combination that exhibits both strength and durability as a structural material used for roof structures. Nevertheless, from the time it is formed in the tree, wood is subject to deterioration by a variety of agents biotic and abiotic [3, 4, 5, 11]. Damage ranges from relatively minor discolorations caused by fungi or chemicals to more serious decay and insect attack [4].
Timber inspection is a learned process that requires some knowledge of wood pathology, wood technology, and timber engineering [4]. This paper covers the fundamentals of timber roof structure inspection for decay and deterioration; it identifies the agents of deterioration and outlines used inspection methods.
For this, there are the main methods that can be used for inspection and evaluation of timber roofs: types and areas for deterioration; inspection techniques; equipment and tools; NDE tool; performance monitoring.
Nondestructive evaluation is the science of identifying the physical and mechanical properties of materials without altering its end-use capabilities and then using this information to make decisions regarding appropriate applications [6]. Nondestructive evaluation (NDE) technologies have contributed significantly toward detect structural problems.
The main methods that are available for inspecting timber structures, normally do not require sophisticated tools. These methods, which include visual characteristics by visual inspection technique; sounding with hammer; probing test; pick test with mortise chisel; measuring moisture content by moisture meter; and microdrilling by Resistograph, for example, may be used singly or in combination [3, 4, 6, 7, 11].
However, timber structure inspectors have the difficult task of accurately assessing the condition of an existing structure. They must understand the biotic and abiotic factors associated with wood deterioration as well as the relative rate at which these processes occur in a given environment [4].
The visual inspection technique is used for evaluations of the visual characteristics due to the presence of defects, insects attacks, decay and other deteriorations [3, 4, 6, 7, 11]. Camera can used for picture a time to reflect existing damage, taking photos of the affected areas is quite important [7, 8].
A good way to begin an inspection for decay is a visual inspection technique search for decay manifestations, emphasizing locations or conditions most conducive to prolonged wetting.
Decay usually results in abnormal coloration of the wood. The first indication of decay is often brown streaks or blotches; purplish streaks are sometimes present. As wood approaches advanced stages of decay, it loses luster and may exhibit pronounced changes in color. Of course, judgments based on color necessitate familiarity with the appearance of sound wood. Sound, healthy softwood has a pleasant, fresh,

resinous smell, whereas decayed wood usually has a mushroom-like, stale odor. However, a musty, moldy smell, though indicative of damage conditions favorable to decay, does not necessarily indicate the presence of decay [3].
The main pathological manifestations that can be observed by visual inspection technique are: signs of distress (collapsed, failed members, excessive deflections); missing members; fruiting bodies; sunken faces or localized surface depressions; staining or discoloration; insect activity; fungi, cracks; grade stamps; checks.

The City Poços de Caldas

Founded on November 6, 1872, Poços de Caldas is located at coordinates 21º47'10,77"S; 46º 33'47,16"O [Google Earth] and 1213 meters [IBGE] in the Serra da Mantiqueira, in the southern state of Minas Gerais, in Brazil. Mild climate and an average temperature of around 18ºC, with a population of approximately 140,000 inhabitants, the city has the highest life expectancy (78.2 years) in the state. It is a tourist town, known for his discovery of the hot springs, and 70 million square meters of green area spread over hundreds of parks, gardens, parks, day care they receive, and the Sierra de São Domingo, a nature reserve, tumbled the historical heritage of the state, [9].

Current Assessment of timber roof structures type "Hauff", in Poços de Caldas

Nowadays we still have in use important type "Hauff" timber roof structures and its assessment is recommended.
It is knowledge of the technical and scientific timber roof structural systems type "Hauff" played a role of great importance in the history of Brazilian construction industry, primarily with timber structures. In Poços de Caldas has been observed that various timber roof structural systems had such great acceptance between the 1940s and 1960s, and today was identified 12 buildings with these structures still exist. The covers were called here by RTH (Roof Type Hauff).
However, in assessment of some roofs structural systems identified, were observed by visual inspection technique, pathological manifestations of: moisture migration from tiles, staining or discoloration; signs of stain fungi; signs of distress with excessive deflections of purlins; missing members; irregular maintenance; among others.

Roof RTH-01: Hangar of the Aero club of Poços de Caldas

The first building of Poços de Caldas city, more known in the scientific-technical, for its beautiful timber roof structure lamellar type (Figure 1), with approximately 25 meters of free span, is the hangar Aero Club of Poços de Caldas. This building is located in the approximate coordinates of GPS 21º 50' 18,42"S; 46º 33' 46,56"O; altitude of 1261 meters [Google Earth]. With donations from members, beginning in 1943 the construction of the hangar in Aero Club of Poços de Caldas, [10].

a) Inside view of the hangar.

b) Details of lamellar roof: moisture migration from tiles.

Figure 1 - Details of the structural system of the lamellar timber roof structure [11]. Photos: Authors.

Roofs RTH-02 RTH-03 RTH-04 RTH-05

The second building identified in Poços de Caldas, also known in the scientific-technical, whose architectural design is subdivided into four independents areas of warehouses with timber roof structural systems medium to large spans: RTH-02 (Figure2a); RTH-03 (Figure2b); RTH-04 (Figure3a); RTH-05 (Figure3b). The main roof, these sheds, is situated on approximate coordinates of GPS 21º 50’ 18,42”S; 46º 33’ 46,56”O, and altitude of 1204 meters.

a) Roof RTH-02: Plywood arch ~30 m of span.

b) Roof RTH-03: Vertical sawn lumber nailed arch ~ 30 m.

Figure 2 – Timber roof structural systems: Roof RTH-02; RTH-03 [11]. Photos: Authors.

a) Roof RTH-04: Plywood arch ~ 45 m of span.

b) Roof RTH-05: Shed truss roof ~ 20 m.

Figure 3 – Timber roof structural systems: Roofs RTH-04; RTH-05 [11]. Photos: Authors.

Roofs RTH-06 RTH-07

The roof here identified by RTH-06 (Figure 4a) known in the scientific-technical, has structural system type plywood arch, with approximately 20 meters of span. This roof is situated on GPS coordinates 21º 47’ 29,10”S; 46º 33’ 48,19”O; and altitude of 1204 meters, [Google Earth].
The roof here identified by RTH-07 (Figure 4b) known in the scientific-technical, also has structural system type Plywood arch, with approximately 40 meters of span. This roof is situated on the GPS coordinates 21º 47’ 05,90”S; 46º 33’ 50,05”O; and altitude of 1204 meters, [Google Earth]. However it was not possible to photograph details of these roofs, because they were coated with PVC lining. Therefore, it was observed that the wood pieces were paintings with enamel in green, and the structural elements presented in excellent condition, including metal rods.

a) RTH-06: Plywood arch ~20m of span.

b) RTH-07: Plywood arch ~40m of span.

Figure 4 - Aerial view of rooftops: RTH-06; RTH7. Source: [Google Earth]

Roof RTH-08

The roof RTH-08 (Figure 5) has structural system type sawn lumber nailed arch, with approximately 15 meters of span. But it was also not possible to photograph details of this roof. This roof is situated on the GPS coordinates 21º 47’ 13,10”S; 46º 33’ 40,75”O; and altitude of 1216 meters. The leasing plan of this building is in L.

a) Aerial view of rooftops L.

b) Warehouse: RTH-08

Figure 5 – Warehouse with timber roof structural system: RTH-09. Source: [Google Earth]

Roof RTH-09

The roof RTH-09 (Figure 6) has structural system type plywood arch, with approximately 22 meters of span. That is situated on GPS coordinates 21º 47’ 33,20”S; 46º 33’ 48,85”O; and altitude of 1207 meters. The wooden parts of this structure were with enamel paintings in gray, and the structural elements and metal rods, had good repair. It is probable that the wood is Peróba Rosa, because pink staining of purlins.

Figure 6 – Roof RTH-09: Structural system type plywood arch ~ 22m of span. Photo: Autores

Roofs RTH-10 e RTH-11

The roof RTH-10 is located at GPS coordinates 21º 47’ 33,09”S; 46º 33’ 52,41”O; and altitude of 1210 meters. The roof RTH-11 is located in the GPS coordinates21º 47’ 32,58”S; 46º 33’ 52,31”O; and altitude of 1209 meters. The buildings of these roofs corresponds to 2 warehouses germinated (Figure 7a). The roof RTH-10 has structural system type plywood arch, with approximately 16 meters of span, and with skylight central projection of natural light (Figure 7b). The wooden parts of the roof RTH-10 were with enamel paintings in gray, and the structural elements and metal rods, presented in excellent condition.

a) Warehouses germinated: RTH-10 e RTH-11.

b) Plywood arch structural system ~16 m with skylight.

Figure 7 – Warehouses (RTH-10 e RTH-11) with timber roof structural systems. Photo: Autores

The roof RTH-11 is a dual-waters, with approximately 12 meters of span, also have skylight central to projection for natural lighting. However, it was not possible to photograph the internal area of the roof.

Roof RTH-12: Roof of the Gymnasium of the club "Associação Atlética Caldense"

The roof RTH-12 (Figure 8) of Gymnasium of the Club's "Caldense Athletic Association" has roof structural system type plywood arch, with approximately 30 meters span. This roof is situated on the GPS coordinates 21º 47' 06,30"S; 46º 33' 45,05"O; and altitude of 1208 meters. The wooden parts of the roof RTH-12 are structural system type plywood arch, with metal rods, and were in enamel paints green.

Figure 8 – Roof RTH-12: Structural system type plywood arch ~ 30m. Photo: Autores

Conclusions

Throughout its existence, "Hauff" played a highly relevant role in the history of civil engineering in Brazil, but particularly during the period of its greatest production, which corresponded to its wood structures phase. "Hauff" can be considered a company that introduced wood structure technologies in the country and which was in large part responsible for training artisans linked to the production of timber structures, master carpenters, draftsmen and designers, and for enriching the body of technical knowledge if many engineers who participated in this production. From the example of "Hauff", according to the demand with the growth of construction in the country, have emerged in the market other manufacturers of timber structures for roofing, which was to highlight the criteria that they have achieved in the domestic market, but also the structural types offered by them. During techniques visits, in assessment of some of these roofs identified, it was possible to detect, by visual inspection technique, pathological

manifestations in various structural elements of the timber roofs, which could be avoided with regular inspections and preventive maintenance. There is a lack of preventative maintenance and control of timber roof structures in Brazil. In this way the assessment, maintenance and rehabilitation of timber structures must be a important subject for the future of timber structures in Brazil. The routine sequential for recommendation at the inspection process of the timber roofs structures, can used: the visual inspection technique, with records photos; the sounding technique with hammer; the probing test; the pick test with mortise chisel; the moisture meter; the microdrilling with resistograph; among others tests.

Acknowledgements

The authors thank CNPq for its financial backing of this work.

References

CÓIAS, V. 2011. Qualificação dos profissionais e das empresas para a qualidade na reabilitação de estruturas de madeira. CIMAD 11 – 1º Congresso Ibero – Latino Americano da Madeira na Construção. Coimbra, Portugal. [1]

CÉSAR, S. F. 1991. As estruturas Hauff de Madeira no Brasil. (Master's Dissertation, Escola de Engenharia de São Carlos , USP. Orientador: Prof. Dr. Carlito Calil Junior. São Carlos. [2]

HIGHLEY, T. L.; SCHEFFER, T 1989. Controlling decay in waterfront structures. Evaluation, Prevention, and Remedial Treatments. Department of Agriculture, Forest Service, Forest Products Laboratory. FPL-RP-494. Madison, WI, USA. [3]

RITTER, M. A.; MORRELL, J. J. 1990. Timber bridges. *Depart. of Forest Products, Oregon State University*. [4]

CALIL JR., Carlito; BRITO, Leandro Dussarrat 2010. Manual de Projeto e Construção de Estruturas com Peças Roliças de Madeira de Reflorestamento. Departamento de Engenharia de Estruturas, Escola de Engenharia de São Carlos, Universidade de São Paulo. ISBN: 978-85-8023-000-0. Editora EESC. São Carlos. Free download: <<<*http://www.set.eesc.usp.br/portal/pt/livros/371-manual-de-projeto-e-construcao-de-estruturas-com-pecas-rolicas-de-madeira-de-reflorestamento*>>>. [5]

PELLERIN, Roy F.; ROSS, J. 2002. Nondestructive Evaluation of Wood. Forest Products Society, Madison, WI, USA. [6]

ARRIAGA, F.; PEZAZA, F.; ESTEBAN, M.; BOBADILLA, I.; GARCIA, F. 2002. Intervención en estructuras de madera. ISBN 84-87381-24-3. AITIM, Madrid. [7]

BRITO; L. D.; CALIL JR., C. 2012. Evaluation by visual inspection technique of "Hauff Type" timber roof structure at "São Carlos Clube" Gymnasium in Brazil. ICDS12 - International Conference Durable structures: from construction to rehabilitation. Lisbon, Portugal. [8]

PUC MINAS. História da cidade de Poços de Caldas. Disponível em: <<<*http://www.pucpcaldas.br/home.php?pagina=cidade_historia.php* >>> [Date accessed: 22 de jan. de 2013]. [9]

AEROCLUBE DE POÇOS DE CALDAS 1945. Homenagem do Aero Clube de Poços de Caldas ao pai de aviação Santos Dumont. Jornal Aero Clube de Poços de Caldas. Poços de Caldas. [10]

BRITO, L. D. 2014. Patologia em estruturas de madeira: metodologia de inspeção e técnicas de reabilitação. Tese (Doutorado) Departamento de Engenharia de Estruturas, Escola de Engenharia de São Carlos, Universidade de São Paulo. São Carlos, Brasil. [11]

Session 9

Urban Tree Assessment

Evaluation of the root system's stability based on actual wind intensity and inclination measurements

Ferenc Divos
Simonyi Karoly Faculty of Engineering, Wood Sciences and Applied Arts, University of West Hungary, Sopron, ferenc.divos@skk.nyme.hu

Laszlo Bejo
Simonyi Karoly Faculty of Engineering, Wood Sciences and Applied Arts, University of West Hungary, Sopron, laszlo.bejo@skk.nyme.hu

Lajos Puskas
Faculty of Forestry, University of West Hungary, Sopron, Hungary, puskas.lajos@emk.nyme.hu

Abstract

Tree root system stability assessment is the most difficult part of tree condition evaluation, because visual techniques are not applicable. The only reliable method adopted in today's practice is the pulling test, which simulates a wind storm, with wind speeds of 33 m/s, and an inclination of 0.2 degrees. This is an extreme wind load situation that typically occurs only once in every two years. Even in strong winds, actual wind speeds usually remain in the 10-15 m/s range, with wind loads approx. 5-10 times lower than those at 33 m/s. The pulling test is also a typical static test, while wind load is dynamic, because of the wind gusts.

Our investigation was aimed at measuring the wind load and inclination in real life situations. This requires high sensitivity inclination sensors with a resolution of .001 degree. The inclination of a sample tree was monitored over several weeks, using such sensors. Inclination data were collected 10 times per second in two directions, and compared to wind intensity measurements taken nearby. This allows the evaluation of the root system's stability under dynamic loading.

The comparison of inclination and wind intensity values shows a clear positive correlation between these two parameters. Anomalies typically occur after sudden gusts of wind, which cause excessive displacement, showing a loss of balance on behalf of the tree. Such imbalances may be responsible for most of the uprooting that occurs. A detailed analysis of the results is underway to create a suitable evaluation algorithm to predict the safety factor from the actual dynamic load and inclination measurements.

keywords: tree uprooting safety, root collar inclination, dynamic safety factor

Introduction

Urban tree safety has always been an important issue for cities. The visual evaluation of an urban tree is a quick and, in many cases, reliable tool for maintaining safety. In the meantime, detecting internal decay in a tree trunk, or detecting root failures, root decay is difficult, because these are not visible. For tree trunk evaluation, acoustic tomography is an accepted and rather quick method for safety evaluation, but the pulling test is the only available method for the determination of uprooting safety.

The pulling test has about 25 years of background in Germany (Wessoly, 1991) and a 5-year tradition in Hungary. The pulling test concept substitutes a stretched cable for wind load. The applied force is in the range of 10-40 kN, depending on the tree diameter and applied geometry conditions. The tree trunk inclination versus force is measured. By extrapolating the pulling curve, we get the uprooting force and the uprooting moment. Comparing the uprooting moment to the moment caused by wind, we are able to calculate the safety factor. The theoretical background of pulling tests is clear, but the following problems and limitations exist:

- The pulling test procedure is slow, usually takes 2 people and 1 hour of work.
- Handling 10-40 kN of load may be dangerous.
- Finding an anchor point (another tree nearby the examined tree) is not always possible. Sometimes, a heavy lorry may be used.
- The wind load is a dynamic load, while the pulling test uses a static process.

The goal of our investigation is developing a tree root evaluation technique, where tree inclination is measured under natural wind conditions. In this case, we do not need to use a pulling device, and the anchor point problem disappears. Using crown parameters, like crown area and crown central height, the drag coefficient is not necessary. On the other hand, the accurate detection of minor inclination – 0.001 degree – is necessary, because we want to utilize low (8 m/s) wind-gust speeds.

Fortunately storms occur only a few times per year, but the above mentioned wind condition happens about once a week. As of yet, the evaluation method is not fully developed. In this paper, we describe our proposal for a dynamic method for uprooting safety factor determination. The present state of tree biomechanics, the tree dynamic research is reviewed by James et al. (2014). Unfortunately, practically no research was found about tree root – soil dynamic interactions.

Materials and methods

A larch (*Larix decidua*) tree was selected for demonstrating the dynamic root evaluation technique. The tree is 23m tall, its breast height diameter (DBH) is 46 cm, and the crown surface area is 92 m^2. The tree is located in the Botanical Garden of the University of West Hungary – 20 m from Building "D", where the *Bódig József Wood NDT Laboratory* is located. The tree is surrounded by buildings and other trees as shown in Figure 1.

a. **b.**

Figure 1. The location of the examined tree and the anemometer (**a**), and the anemometer used in the study (**b**).

A high sensitivity biaxial inclinometer is fixed by a single screw at the ground level. The inclinometer is made by Measurement Specialties, powered by 9V DC. Its range is +/-2 degree, its resolution is 0.001 degree, and the sampling rate is 10 Hz (figure 2). The digital output is sent to the recording PC via a serial interface. The electronics is cased in waterproof housing.

Figure 2 The high sensitivity inclinometer board by Measurement Specialties (**a**), and the waterproof housing with the mounting device (b).

Data was captured over a longer period, using a PC located in the NDT laboratory. Data collection started in March 2015, and ended 2 months later. The wind data is provided by the Hungarian weather website www.idokep.hu. The location of the wind sensor is 500m North-East from the tree, identified as GGKI-Sopron. GGKI is an abbreviation of the Geodetic and Geophysical Institute, Hungarian Academy of Science. The measuring height of the wind sensor is 15m – located on top of a building, and the sampling rate is 1Hz, suitable for measuring wind gust speeds. A large amount of data was collected and analyzed.

Results and discussion

The tree trunk inclination (α) was calculated by the following formula, where α_x and α_y are the inclination in direction x and y.

$$\alpha = \sqrt{\alpha_x^2 + \alpha_y^2} \qquad (1)$$

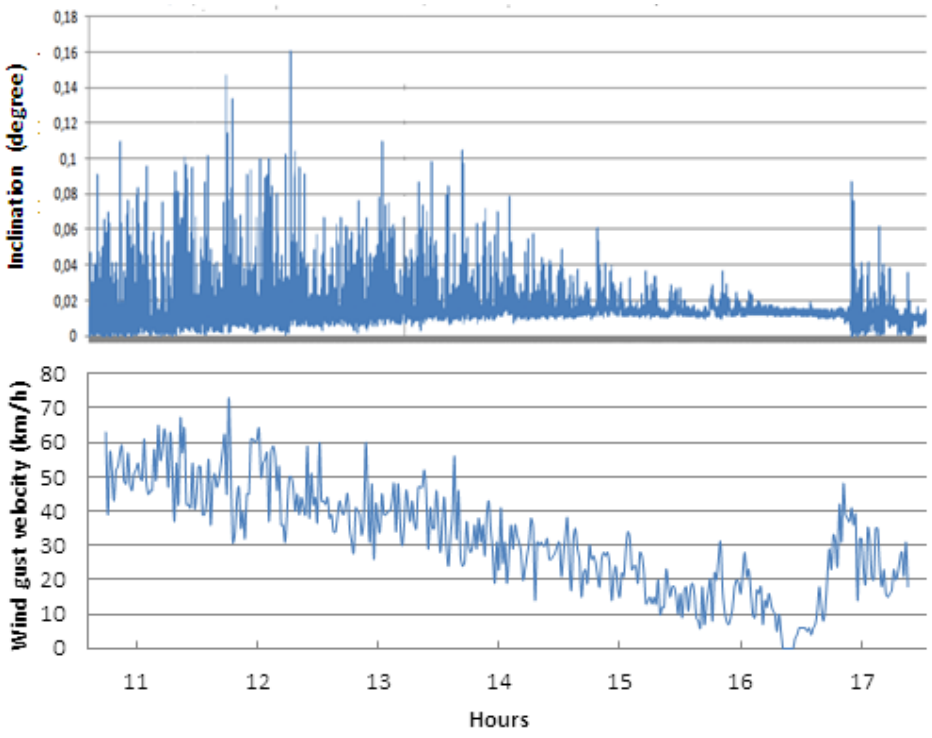

Figure 3 The calculated inclination and the measured wind gust velocity over a 7-hour period.

Figure 3 shows the calculated inclination and the measured wind gust velocity versus time. A 7-hour record is selected for demonstration. Characteristic peaks are recorded in the inclination plot. Sudden wind gusts cause excessive inclination, causing a loss of balance on behalf of the tree. Such imbalances may be responsible for most of the uprooting that occurs. Figure 4 shows the balance loss and the related inclination. To characterize the amplitude of the tree trunk inclination, the maximum inclination is calculated in the balance loss incident.

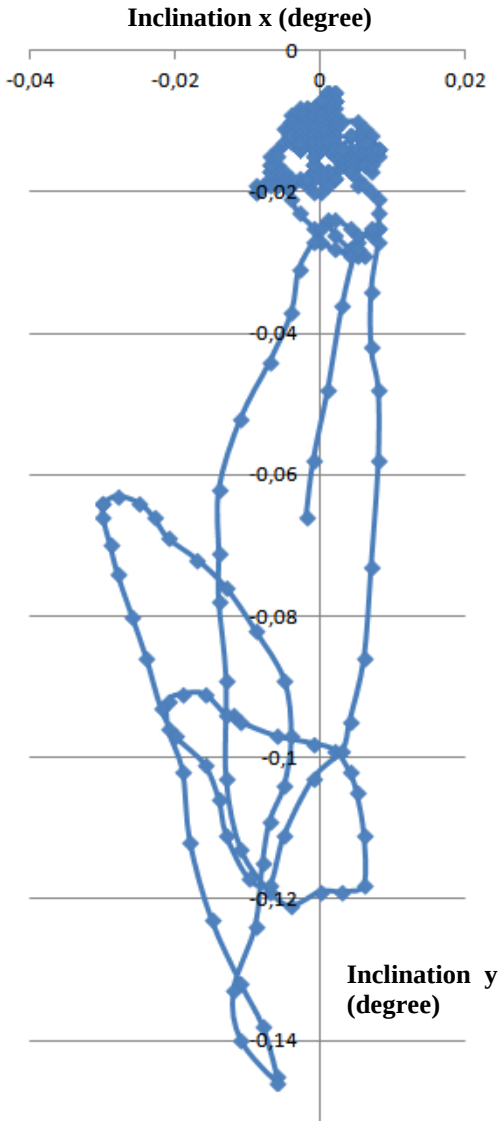

Figure 4 The movement of the root collar in a balance loss scenario.

Most of the time, the appropriate branch movements are able to dampen the effect of the wind gust. The relationship between tree trunk inclination and wind velocity is rather complex. In general, the larger the wind speed, the larger the inclination. Figure 3 indicates this relationship. The measured largest inclination around 12 o'clock does not correspondent to the largest wind speed. It is possible that the distance between the anemometer and the tree accounts for this phenomena.

Several inclination peaks were selected, at different wind velocities, and plotted against the wind pressure, see Figure 5. Wind pressure is calculated by the formula below:

$$p_{wind} = 0{,}5\rho V^2 \qquad (2)$$

where ρ is the air density, V is wind velocity. The relationship can be approximated using a modified tangent function:

$$\alpha = \frac{1}{3}\tan\left(1{,}354\frac{p}{p_{max}}\right) + \frac{1}{2}\left(\frac{p}{p_{max}}\right)^2 - \frac{1}{10}\left(\frac{p}{p_{max}}\right), \quad (3)$$

where α is the inclination of the tree, p is the wind pressure, as defined by equation (2), P_{max} is the critical wind pressure, where the uprooting may occur. The above equation is similar to the pulling function used in static pulling test. The only change is that, instead of force, wind pressure is used as the variable. The critical wind pressure (p_{max}) is determined by fitting equation 3 to the measured points, indicated in Figure 5. The best fit was found at p_{max} = 815. The tangent function looks like a straight line, because the measured wind pressure data are far from the critical wind pressure. The interpretation of safety factor (SF) is given by:

$$SF_{dynamic} = p_{max} / p_{local} \quad (4)$$

where p_{local} is the locally expected highest wind pressure, based on meteorological records at 10m height. In Hungary a maximum wind velocity of 120 km/h is used, which translates to 667 Pa, but in case of tree located on a hill top, this value is higher. The calculated dynamic safety factor is $SF_{dynamic}$ = 815/667= 1.22

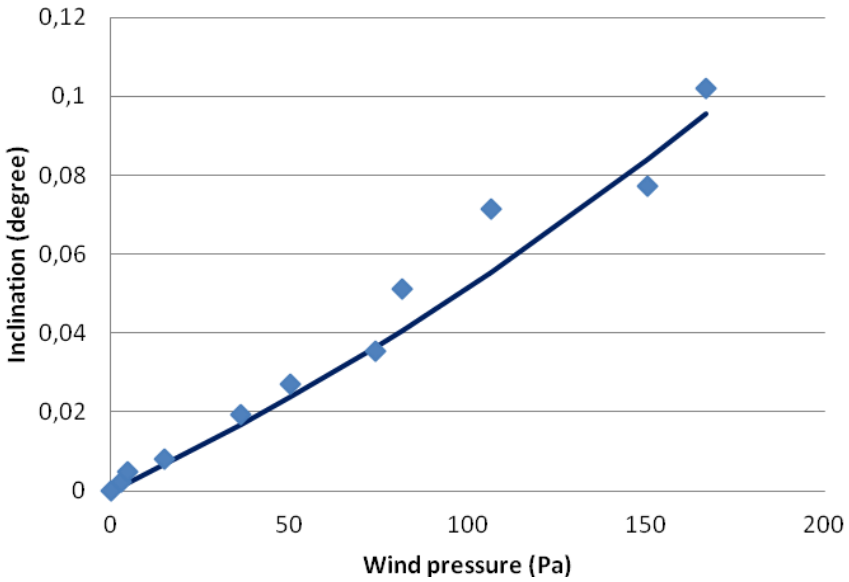

Figure 5. Inclination versus wind pressure. The critical pressure, p_{max} is 815 Pa.

According to data shown on figure 5 and other similar data set indicates: wind gust velocity 8 m/s or above is suitable for reliable extrapolation. Naturally, the calculation necessitates reliable wind velocity data.

The uprooting safety factor calculated from inclination and wind speed data is the dynamic safety factor ($SF_{dynamic}$). The static safety factor (SF_{staic}) was also measured on the same tree. Figure 6 shows the test results. The calculated static safety factor is SF_{static} = 1.52, compared to $SF_{dynamic}$ = 1.22. The dynamic value is markedly lower than the static value. The reason for this is unclear. The evaluation technique described above is based on the assumption that the static and dynamic uprooting curves are the same. This assumption may not be true. It may be necessary to collect data when the tree trunk inclination is high in strong winds, to verify the dynamic uprooting curve.

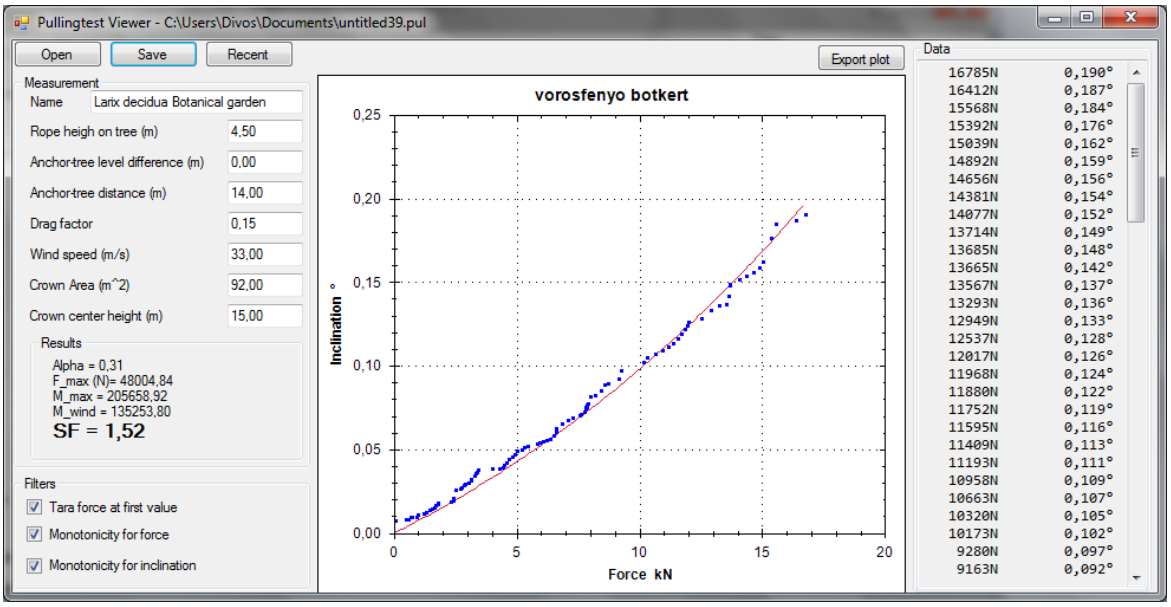

Figure 6 The results of the static pulling test. The pink line is the static uprooting curve. The safety factor is 1.52.

Conclusions

A method for dynamic uprooting safety factor determination is presented. The input data are the tree trunk inclination versus the wind velocity. Due to the high resolution (0.001 degree) of the inclinometer, reliable safety factor determination is possible using wind gust velocities of 8 m/s or higher. This makes the technique applicable for practical usage, because wind speeds in excess of 8 m/s are not rare. Compared to the static method, the determination of dynamic SF has the following advantages:

- aerodynamic drag coefficient is not necessary in the calculation,
- crown area is not necessary,
- crown center height is not necessary,
- no pulling device and anchor point is necessary.

disadvantages are:

- the dynamic uprooting curve is not known.
- the technique is applicable only if wind gust velocities reach 8m/s

Further verification of the method is necessary before arborists and tree experts can use this technique.

Acknowledgments

The work was supported by FAKOPP Bt and idokep.hu. They provided inclinometers and wind gust velocity data.

References

James, K.A., G.A. Dahle, J. Garbosky, B. Kane, A. Detter (2014): Tree Biomechanics Literature Review: Dynamics. Arboriculture & Urban Forestry 2014. 40(1): 1–15

Wessoly, L. (1991). Verfahren zur Bestimmung der Stand- und Bruchsicherheit von Bäumen. Holz als Roh- und Werkstoff 49:99-104.

Feasibility study on retrospective reconstruction method with X-ray radiographs to investigate inner state of wood

Chul-Ki Kim
Department of Forest Sciences, Seoul National University, Seoul, Korea, aries05@snu.ac.kr

Jung-Kwon Oh
Department of Forest Sciences/Research Institute of Agriculture and Life Sciences, Seoul National University, Seoul, Korea, jkoh75@hotmail.com

Hyeon-Jeong Lee
Department of Forest Sciences, Seoul National University, Seoul, Korea, dlguswjd0816@snu.ac.kr

Jun-Jae Lee†
Department of Forest Sciences/Research Institute of Agriculture and Life Sciences, Seoul National University, Seoul, Korea, junjae@snu.ac.kr

Abstract

In Korea, there are lots of historic traditional wooden structures with post and beam architecture style. Most of traditional wooden structures have wall between two columns. So, it is difficult to apply CT technique for investigating inner state of wood. Because of resolution and application, it is not proper way using stress wave or ultrasound testing, either. Therefore, this study conducted retrospective reconstruction with a couple of radiographs from limited rotating angle, from -20 to 20 degrees. For reconstructing a couple of radiographs, multiple projection algorithm and logarithmic subtraction method were used. To find feasibility of retrospective reconstruction, birch with heart rots and defect was prepared as specimen. Compared with single radiograph, retrospective reconstruction image can find defects and location of heart rots, easily. Using only 11 radiographs, heart rots could be investigated without any overlapped information. The 41 radiographs were needed to find small defect.

Keywords: X-ray, Retrospective reconstruction, multiple projection algorithm, Logarithmic subtraction

Introduction

Non-destructive testing and evaluation (NDT&E) is one of useful method to estimate mechanical properties or investigate inner state of wood. Especially, the East Asians (Korean, Chinese and Japanese) are interested in examining inner state of wooden member with NDT&E, because they have lots of historic traditional wooden structures, of which structural members were made by wood. In Korea, moreover, the importance of NDT&E have been emphasized as insert damages including termite damage in traditional wooden structure members is increasing by global warming (NRIC 2012).
The commonly used source for NDT&E of wood is stress wave, ultrasound, microwave, radiation, near infrared (NIR) and infrared ray. Among those sources, a stress wave or ultrasound testing, of which the equipment is simple or can be used for measuring mechanical properties of wood, has been adopted globally (Divos and Divos 2005; Nicolotti et al. 2003). However, they can make problems when those are

applied to investigate inner state of member at traditional wooden structure. First, a stress wave or ultrasound testing has low sensitivity to detect insect damage like termite damage. Second, a stress wave or ultrasound testing could scratch at the surface of wooden members, because they need probe to penetrate inside of wood or couplant gel to prevent inflow air between probe and wood. As mentioned above, most of Korean traditional wooden structures are suffering for insect damage, and they have special painting at their surface as shown Figure 1. Therefore, it is not proper way using a stress wave or ultrasound testing to investigate inner state of wood.

Figure 1—Throne Hall Compound in Gyeongbokgung palace (Korean national treasure no. 223)

Being used to investigate inner state of wood, nondestructive testing with X-rays has advantages of applying testing without contacts and making computed tomography (CT) with high resolution radiographs. Based on those advantages, it has been reported on lots of studies that X-rays and CT were used to measure air dried density, defect location and moisture content in wood (Olson et al 1988; Macedo et al. 2002; Lindgren et al. 1992; Oja and Temnerud 1999). There were also studies that soft X-rays, which has low penetrating energy compared with X-rays for industrial and medical purpose, was used to investigate inner state of wood (Nakada et al. 1999; Kim et al. 2014). With soft X-rays, X-rays testing could be applied in field where structures are located.

For conserving historic properties, CT, which can detect location of detect and investigate inner state of wood, can be better method than single radiograph. Because overlapped results must be contained in single radiograph. However, it is not easy to apply CT at Korean traditional wooden structure, because of their architectural style– post and beam. It might easy to apply CT at traditional wooden structure, where there are no walls between two columns, but most of traditional wooden structure has wall as shown in Figure 1. So, it is need to develop another method with containing high resolution results and having ability to find location of defect even though there is wall between columns.

With developing a radiation measurement technology, recently, it has been introduced the technique, which can make arbitrary cross section using several X-rays radiographs from single-acquisition sequence. This technique, a retrospective reconstruction method, is usually used to diagnose women breast cancer, and is reconstructing a low number of radiographs from a limited angle (Dobbins and Godfrey 2003). In view of the fact that a retrospective reconstruction methods show high image quality and have an information of interesting location with a low number of radiographs from a limited angle, this technique can be applied to investigate inner state of wood at traditional wooden structure. Therefore, it is necessary to assure feasibility for investigating inner state of wood using a retrospective reconstruction method. In this paper, wood having heart-rot and knot was prepared as specimen, and one of retrospective reconstruction methods was conducted to investigate inner state of wood.

Materials and Methods

Materials

A birch (*Betula platyphylla*) was prepared as a specimen to do retrospective reconstruction using being gained radiographs from limited angle, and contained knots and heart-rot the inside of that. The specimen was air-dried for a longtime, of which a moisture content and air-dried specific gravity was 18%, 0.64, respectively. The shape of specimen was round, and the longest diameter was 95 mm.

Methods

X-ray apparatus

In this study, X-ray tube, K-4 (Softex, Japan), was used. The maximum tube voltage and current are 60 kV, 5 mA, respectively. A digital detector, NX06 (RF system, Japan), was also prepared for gaining X-ray radiographs. NX06 is 2-dimensional detector consisted of a scintillator and 12 charge-coupled devices (CCD). The actual size and the maximum pixel of detector is 208 (w) × 214 (h) mm, 4040 (w) × 4040 (h) pixel, respectively. From the previous experiment for this specimen, 35 kV tube voltages and 5 mA tube currents were chosen to gain an X-ray radiograph. Radiographs were directly saved in laptop as DCM files after being exposed digital detector to radiation during 3 seconds for each X-ray radiograph. Those files were used for retrospective reconstruction method. The 41 radiographs were taken as X-ray tube and digital detector were rotated 1 degree from -20° to 20° as shown Figure 2a.

Retrospective reconstruction

Gained 41 radiographs were used to be reconstructed retrospectively by using multiple projection algorithm (MPA) method, which Kolitsi et. al (1992) introduced. Figure 2b shows MPA method, which is shifting the locations of pixels in each projected image so that they are aligned with an abstract image formation plane (Loukianos 2009).

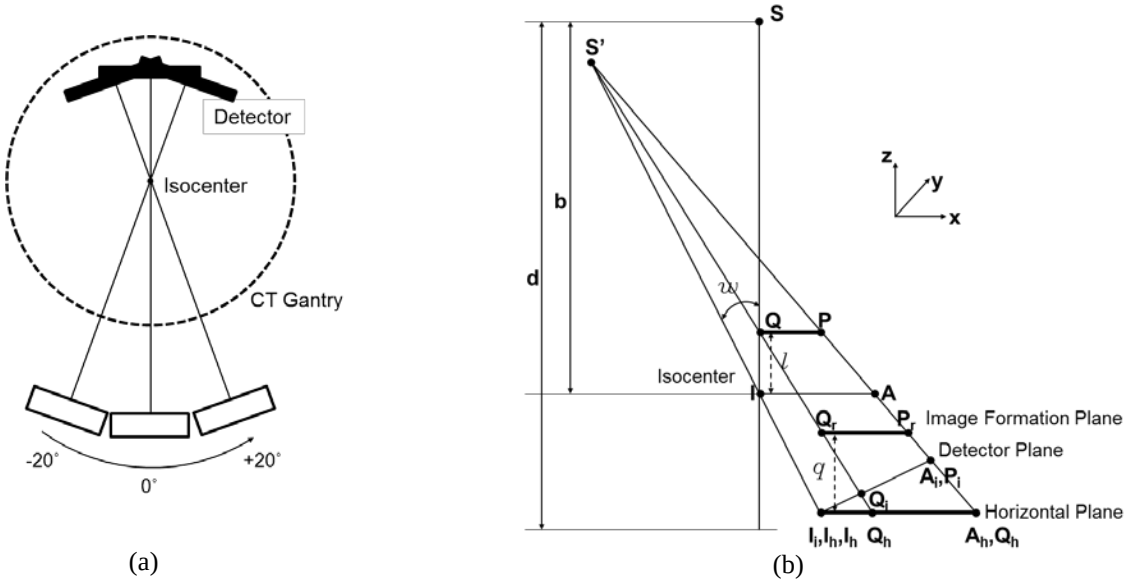

Figure 2—Schematic description of the acquisition data (a) and the principle of image formation (b) (revised Kolitsi et al. 1992)

A reconstruction image with MPA method shows a cross section image which is parallel to rotation axis of X-ray tube and digital detector, while CT reconstruction makes a cross section image which is perpendicular to rotation axis of those. So, MPA methods also called retrospective reconstruction. The reconstruction about standard horizontal plane could be expressed as Equation 1 and 2,

$$r = \left(h - \frac{ld \sin \omega}{b \cos \omega - l} \right) \left(1 - \frac{l}{b \cos \omega} \right) \tag{1}$$

$$h = id \big/ \left(d \cos \omega - i \sin \omega \right) \tag{2}$$

where, r is column shifting, h is the position of column in the image formation plane, s is position of tube at zero angle, s' is position of tube at ω angle, l is distance from isocenter to anatomic structure, d is distance from tube to detector, b is distance from tube to isocenter.

Logarithmic subtraction was also applied to reduce blur effect which was result of shift-adding algorithm. When X-rays penetrated compound, transmitted X-rays intensity can be expressed as Figure 3 according to Beer's law,

$$I = I_0 e^{-\mu \rho t} \tag{3}$$

where, I is transmitted X-rays intensity (mSv), I_0 is initial X-ray intensity (mSv), μ is mass attenuation coefficient (cm^2/g), ρ is air-dried density (g/cm^3), t is penetrating depth (cm).

Image intensity equation of reconstructed image can be changed to linear equation when it has been logarithmically processed. Therefore, logarithmic subtraction processing helps to remove blur in reconstructed image.

To compare the resolution of retrospective reconstruction image according to the number of radiographs, the image with 11 and 21 radiographs also reconstructed. The MPA algorithm and logarithmic subtraction were programmed using Matlab R2014 (Mathworks inc, USA).

Results and Discussion

Figure 3 and 4 shows the results of single radiograph when X-rays tube was located at zero angle and retrospective reconstruction with different number of radiographs, respectively. It was confirmed that a gray scale was different according to relative density; low density parts (close to white), high density parts (close to black). From the results, heart rot was detected in middle of specimen. However, the depth of heart rot and knots were hardly investigated with single radiograph.

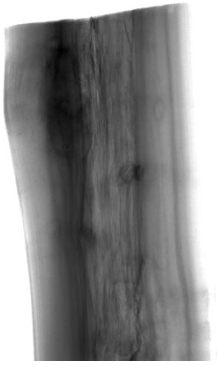

Figure 3—Single radiograph as X-rays tube was located at zero angle

Figure 4 shows the results of retrospective reconstruction with 11, 21 and 41 radiographs. It was determined that the quality of retrospective reconstruction was better as the number of radiographs for reconstructing images was large. It was also checked cross section images of which location was 1, 30 and 45 mm apart from the surface of specimen. In case of Heart rots which was located in the center of specimen, retrospective reconstruction with 11 radiographs could detect the location of Heart rots without knots. However, more radiographs were needed to detect the location of knots. In this study, retrospective reconstruction with 41 radiographs could detect knot and the location of that.

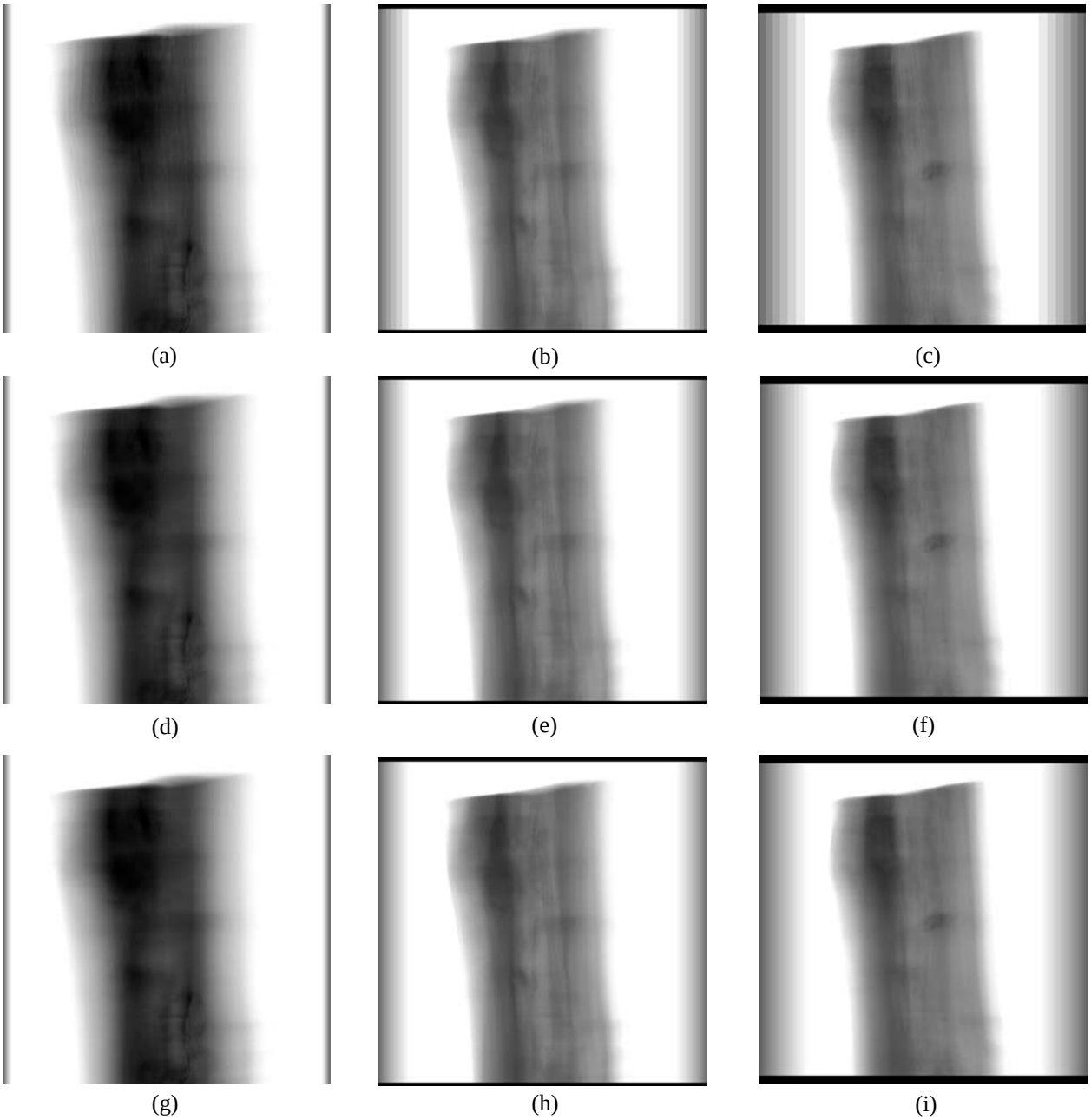

Figure 4—Retrospective reconstruction according to being used the number of radiographs. (a), (b) and (c): 11 radiographs, (d), (e), and (f): 21 radiographs, (g), (h) and (i): 41 radiographs

In this study, the feasibility of applying retrospective reconstruction for investigating inner state of wood was examined, and it was confirm that retrospective reconstruction can detect not only defect but location of that. That information couldn't be gain from single radiograph. Judging by retrospective reconstruction can be done with radiographs from limited angle of rotation, this technique can be applied at wooden structural even though they had wall between columns.
In further studies, relation between the number of radiographs for reconstructing and resolution of retrospective reconstruction according to a size of defect is going to be examined, and processing for quantification of reconstruction results will be developed.

References

Divos, F; Divos, P. 2005. Resolution of stress wave based acoustic tomography. In: 14th international symposium on nondestructive testing of wood, Shaker Verlag, Germany: 307-314

Dobbins, JT; Godfrey, DJ. Digital x-ray tomosynthesis: current state of the art and clinical potential. Phys Med Biol 48(19): R65-106

Kim, CK; Oh, JK; Hong, JP; LEE, JJ. 2014. Density calculation of wood by portable X-ray tube with consideration of penetrating depth. J Wood Sci 60(2): 105-110

Kolitsi, Z; Panayiotakis, G; Anastassopoulos, V; Scodras, A; Pallikarakis, N. A multiple projection method for digital tomosynthesis. Med Phys 19(4): 1045-50

Lindgren, O; Davis, J; Wells, P; Shadbolt, P. 1992. Non-destructive wood density distribution measurements using computed tomography. Holzforschung 50(7): 295-299

Loukianos, KF. 2009. Three dimensional breast imaging using digital tomosynthesis. Rio-Patras, Greece: University of Patras. M. Sc. Thesis

Macedo, A; Vaz, CMP; Pereira, JCD; Naime, JM; Cruvinel, PE; Crestana, S. 2002. Wood density determination by X- and gamma-ray tomography. Holzforschung 56(5): 535-540

Nakada, R; Fujisawa, Y; Hirakawa, Y. 1999. Soft X-ray observation of water distribution in the stem of Cryptomeria japonica D. Don Ⅱ: Types found in wet-area distribution patterns in transverse sections of the stem. J Wood Sci 45(3): 194-199

National research institute of cultural heritage. 2012. Conservation of wooden objects. Pointtech, Daejeon: 8

Nicolotti, G; Socco, LV; Martinis, R; Godio, A; Sambuelli L. 2003. Application and comparison of three tomographic techniques for detection of decay in tree. J of Arboric 29(2): 66-78

Oja, J; Temnerud, E. 1999. The appearance of resin pockets in CT-images of Norway spruce (*Picea abies (L.) Karst.*). Holzforschung 57(5): 400-406

Olson, JR; Liu, CJ; Tian, Y; Shen, Q. 1988. Theoretical wood densitometry: Ⅱ. Optimal X-ray energy for wood density measurement. Wood Fiber Sci 20(1): 187-196

Development of an Inexpensive Field and Research Tool for Acoustic Testing of Tree Decay

Richard Bruce Allison
Department of Forest and Wildlife Ecology, University of Wisconsin-Madison, Madison, Wisconsin, United States of America, rallison2@wisc.edu

Abstract

Advances in electronics and microprocessors plus significant reductions in costs, create opportunities for developing effective, low cost tools to measure the presence of decay and defect in standing timber. Single path acoustic testing tools in the hands of many field users combined with recording results in a large data base provide an opportunity for research and better understanding of interpreting measured results.

Introduction

Trees growing within an urban setting provide significant cooling, water management, wind control and other ecological contributions in addition to social and economic benefits. To capture these benefits, cities budget resources to maintain their trees. Healthy trees make the city more desirable and comfortable for the inhabitants. The urban forest like other biological communities exist on a condition continuum ranging from vigorous to decrepit. As large wooden structures subject to decay and environmental stresses, tree failure in close proximity to people and targets can cause harm. For the well-being and safety of their citizens, property, transportation and utility systems urban foresters and arborists need knowledge and tools to detect problem trees to avoid undesirable, unanticipated consequences from structural failure. (Allison, Wang 2015; Dunster, et al, 2013) Wood decay is closely associated with tree failure (Hayes, 2001).

Saprophytic fungal decay is a natural process affecting wood. When it enters living trees through wounds or root systems it can over time compromise the structural integrity of the standing tree leading to breaks or uprooting (Shigo, 1979, 1984; Weber and Mattheck 2003; Luley, 2005). Urban tree managers have various tools to detect decay or defect in trees including visual inspection (Mattheck, 1993), microdrills that measure resistance to a drill passing through the wood (Rinn 1988, 1989, 1990, 2012), and also acoustic tools measuring the movement of a sound wave through wood with time of flight varying by species and wood density properties (Nicolotti et al 2003; Wang, et al, 2004).

Single-Path Stress Wave Timing

Simple stress wave measuring devices are available for tree inspection to record the time it takes for an impact-induced stress wave to travel through the tree trunks. (Allison and Wang, 2015) This nondestructive testing procedure is often called single path stress wave timing measurement. A stress wave is generated with a strike to a nail or spike attached to the tree. An accelerometer mounted at the strike point senses the impact and sends a start signal to the measuring device that acts as a stop watch. A second accelerometer attached to the diametric opposite side of the tree senses the leading edge of the stress wave and sending a second signal to stop the timer. The

measured time between the start signal and stop signal is the time-of-flight (TOF) of the wave propagating across the tree trunk. The TOF data are measured in microseconds. Travel time per unit length, such as microseconds per meter and velocity, such as meters per second, are calculated using the known distance between the sensors and the TOF.

The first instruments using acoustics to determine forest product quality were developed by Metriguard, Inc., of Pullman, Washington, in the early 1960s to evaluate particleboards (Pellerin and Ross 2002). In the 1990s, foresters began using longitudinal stress wave testing on both cut logs and standing timber for log selection and grading based on material strength. The first report of the use of stress wave testing to determine internal degradation of living trees was by Claus Mattheck and Klaus Bethge in 1993 (Mattheck and Bethge 1993). Stress wave propagation in wood is related to the physical and mechanical properties of the wood. Stress waves travel faster in defect-free wood. Areas of cracks, cavities, or decay-induced low density will require longer times for the stress wave to arrive at the opposite timing sensor. By measuring TOF or wave transmission time through a tree stem in the radial direction, the internal condition of the tree can be determined. The presence of deterioration from decay can greatly affect TOF in wood. TOF for decayed wood are much greater than that for non-decayed wood. For example, TOF for nondegraded Douglas-fir is approximately 800 μs/m (244 μs/ft), whereas severely degraded members exhibit values as high as 3,200 μs/m (975 μs/ft) or greater (Wang et al. 2004). A study conducted by Pellerin and others (1985) demonstrated that a 30% increase in stress wave TOF implies a 50% loss in strength. A 50% increase indicates severely decayed wood. The speed of stress wave propagating perpendicular to grain is also affected by tree species. Mattheck and Bethge (1993) measured speed of sound in different species of healthy trees using a commercially available stress wave timing unit. The speed was determined by dividing the transit distance (tree diameter) by the TOF measured.

Generally, stress waves travel faster in hardwood trees than in softwood trees. To account for species difference, Divos and Szalai (2002) provided some baseline reference velocities for different species for field tree inspection . This reference velocity can be used to evaluate the actual measured wave velocity and assess the internal condition of the tree inspected. When measuring TOF across a tree trunk, an inspector should make sure that the start and stop sensor probes are aligned in a horizontal line across the diameter of the trunk. The nail or spike of a sensor probe should penetrate the bark and reach the sapwood so that the probe is securely attached to the trunk. A small hammer is typically used to tap the start sensor probe and obtain several consistent TOF readings.

Based on previous studies and tree inspection practice, (Allison, 2005; Allison et al, 2008; Wang and Allison (2008) have developed an effective tree decay inspection procedure that uses a combination of visual assessment, acoustic tools, and micro-drill. The steps of the procedure are the following: 1. Simple screening test using a combination of visual inspection and single-path acoustic testing. 2. Multi-sensor acoustic tomography to identify the location and approximate magnitude of defects. 3. Micro-drill resistance tool sampling to confirm defects or differentiate between decayed wood and internal cracks.

Though this combination of tools is effective, the cost of the tools creates an economic impediment to their wide use. To broaden the use of the well researched acoustic technology and to create opportunities for further research, an objective was established to develop a relatively inexpensive single-path stress wave timer that also had the capability of recording the wave form and transferring data to a computer for further analysis.

Development of the Tree Wave Timer

Allison working with wood engineers at the USDA Forest Products Laboratory, stated a project goal of developing a low cost electronic device to measure, display and store data on time of flight of an impacted induced acoustic wave traveling through wood. Engineers at the University of Wisconsin College of Engineering, Electrical and Computer Engineering Department were brought into the instruments development stage. We gathered information on the nature of the acoustic wave to enable us to select appropriate hardware. We considered the commercially available technology and identified opportunities to reduce costs while maintaining measurement quality and adding additional features. We explored various electric sensors and analog and digital signal processing components. Following is a detailed description of the parts chosen with a description of their capabilities and alternatives considered.

Sensor

The alternatives for measuring the acoustic wave were to use a displacement sensor, velocity sensor or an acceleration sensor (accelerometer). The first two were dismissed primarily on cost considerations. We considered instrument grade accelerometers but rejected due to their high costs. Inexpensive polymer piezo electric materials were considered but were rejected because of the extra costs required to build around the mechanics needed to guarantee a highly accurate and repeatable sensing device. We settled on a silicon based MEMS accelerometer. We chose a MEMS sensor that has a high frequency response and sensitivity specification appropriate for nondestructive testing of standing trees. (less than 5 G's). This tool differs substantially from other commercially available single path stress wave timers in that an analog processing circuit board has been placed at the sensor site . This guarantees the integrity of the acceleration signal when it arrives at the measurement and display until. This allowed us to use a very inexpensive, reliable and readily available telephone chord for transmission of the signal from the sensor.

Measurement and Display Unit

For the prototype measurement and display unit we chose a standard enclosure that fits comfortably within the hand plus houses the LCD display, SD memory chip, plug in cables, batteries and required electronics.

The measurement device receives two acceleration signals. The first is called the start signal from the sensor at the point of impact that initiates the wave that passed through the tree. The second is the stop signal which occurs when the wave arrives at the second accelerometer. To generate a digital number indicating time of flight, the analog start and stop signals are processed with comparators to determine at what times the acoustic wave amplitudes have achieved a predetermined threshold.

A unique characteristic of this unit is that it measures and records the entire acoustic wave arriving at the stop sensor. MEMS sensor signals usually need modification in the frequency domain due to a high frequency resonance inherent in the design. A special analog circuit was installed to compensate for this resonance. This compensated signal is converted to a digital form then displayed on the LCD screen and stored on the SD card. A further unique capability of this unit allows the user to listen to the compensated signal through a standard set of ear phones.

The time of flight information and stored compensated stop signal are achieved through the inclusion of the microprocessor within the Measurement and Display Unit. We chose a microprocessor based on the needed requirements:

1. ability to do an analog to digital conversion;
2. accurately measure a time difference between the start and stop signals;
3. display an image on an LCD;
4. store data on an SD card;
5. operate from standard battery power;
6. communicate wirelessly via Bluetooth;
7. reasonably priced, readily available and capable of increased functionality.

The system also has a test mode built in for each accelerometer to automatically verify functionality. Also the comparator circuitry is designed to allow very stable thresholds and independently adjustable thresholds.

Conclusion

Arborists and urban foresters need access to inexpensive, accurate tree decay detection tools. Researchers within the field of nondestructive wood evaluation have developed technology employing sound waves to differentiate normal from decayed wood. By carefully selecting electronic components for both functionality and cost, an accurate yet inexpensive measuring tool has been developed for both field application by practitioners and further study by researchers. Unlike other comparable tools currently on the market, this tool displays and records the acoustic wave form for further analysis. Production costs are under $100 US.

Literature Cited

Allison, R.B. 2005. Capitol park tree structural stability study. Report submitted to Wisconsin Department of Administration Division of Building & Police. Allison Tree Care, Inc. Fitchburg, WI. 308 p.

Allison, R.B.; Wang, X.; Ross, R.J. 2008. Visual and nondestructive evaluation of red pines supporting a ropes course in the USFS Nesbit Lake Camp, Sidnaw, Michigan. In: Proceedings of the 15th International Symposium on Nondestructive Testing of Wood. September 10–12, 2007, Duluth, MN. Madison, WI: Forest Products Society. p. 43–48.

Allison, R.B. , Wang, X. 2015. Nondestructive testing in the urban forest. P. 79 in Nondestructive Evaluation of Wood, Second Edition. R.J. Ross (ed) General Technical Report 238, USDA Forst Products Laboratory.

Divos, F.; Szalai, L. 2002. Tree evaluation by acoustic tomography. In: Proceedings of the 13th International Nondestructive Testing of Wood Symposium, August 19–21, 2002. Berkeley, CA. Madison, WI: Forest Products Society. p. 251–256.

Dunster, J.A.; Smiley, E.T.; Matheny, N.; Lilly, S. 2013. Tree risk assessment manual. Champaign, Illinois: International Society of Arboriculture.

Hayes, E. 2001. Evaluating tree defects: a field guide. Safetrees. ISBN-10: 0971412804. 30 p.

Luley, C.J. 2005. Wood decay fungi: common to urban living trees in the Northeast and Central United States. Naples, NY: Urban Forestry, LLC. 58 p.

Mattheck C. 1996. Body language of trees: a handbook for failure analysis. Research for Amenity Trees. London: Stationery Office Books (TSO). ISBN-10: 0117530670. 260 p.

Mattheck, C.G.; Bethge, K.A. 1993. Detection of decay in trees with the Metriguard Stress Wave Timer. Journal of Arboriculture. 19(6): 374–378.

Nicolotti, G.; Socco, L.V.; Martinis, R.; Godio, A.; Sambuelli, L. 2003. Application and comparison of three tomographic techniques for the detection of decay in trees. Journal of Arboriculture. 29: 66–78.

Pellerin, R.F.; Ross, R.J. eds. 2002. Nondestructive evaluation of wood. Madison, WI: Forest Products Society.

Rinn, F. 1988. A new method for measuring tree-ring density parameters. Physics diploma thesis, Institute for Environmental Physics, Heidelberg University. 85 p.

Rinn, F. 1989. A new drilling method for wood inspection. Holz Zentralblatt. 34: 529–530.

Rinn, F. 1990. Device for material testing, especially wood, by drill resistance measurements. German Patent 4122494.

Rinn, F. 2012. Basics of typical resistance-drilling profiles. Western Arborist. Winter: 30–36.

Shigo, A.L. 1979. Tree decay: An expanded concept. United States Department of Agriculture Forest Service Information Bulletin Number 419. Washington, DC.

Shigo, A.L. 1984. Compartmentalization: A conceptual framework for understanding how trees grow and defend themselves. Annual Review of Phytopathology. 22 (1): 189–214.

Wang, X.; Divos, F.; Pilon, C.; Brashaw, B.K.; Ross, R.J.; Pellerin, R.F. 2004. Assessment of decay in standing timber using stress wave timing nondestructive evaluation tools– A guide for use and interpretation. Gen. Tech. Rep. FPL–GTR–147. Madison, WI: U.S. Department of Agriculture, Forest Service, Forest Products Laboratory. 12 p.

Wang, X.; Allison, R.B. 2008. Decay detection in red oak trees using a combination of visual inspection, acoustic testing, and resistance microdrilling. Arboriculture & Urban Forestry. 34(1): 1–4.

Weber, K.; Mattheck C. 2003. Manual of wood decays in trees. Gloucestershire, UK: Arboricultural Association. 127 p.

Forestry Mobile Unit for hazard assessment of urban trees in Bogota

Yolima Cortés-Cortés[1*]

[1] Subdirección de Silvicultura, Flora y Fauna Silvestre – SSFFS – Secretaría Distrital de Ambiente – Av. Caracas No. 54 – 38, Bogotá, Colombia

[*] Telephone: +57 3166741967, Fax: +57 13778899, yolima.cortes@ambientebogota.gov.co; yocortesco@gmail.com

Abstract

The Forestry Mobile Unit operates in a hybrid vehicle equipped with measuring Rinntech® devices: acoustic tomographs and Resistograph® to establish the physical and internal health of the trees and recognize wood damage or defects.

The purpose of using these machines is to determine the most appropriate forestry treatments and thus reduce the number of accidents by falling branches or the tree itself; approximately 250 trees overturned or uprooted every year. This Unit has made 507 measurements of different trees and it has provided important information for decision- making through technical concepts.

It is necessary to differentiate the response of nondestructive tests for native and naturalized species in Bogota, which can be helpful for the management of health damages. The results are of significant value in the daily work being carried out within the process of evaluation, control and monitoring the implementation of urban forestry in the city.

Key words: nondestructives wood testing, hazardous trees, urban trees, Forestry Mobile Unit

Introduction

The risk assessment of trees that live in the cities is of great importance to avoid negative impacts such as failure caused by internal defects present in the trunks of the trees. Bogota has decided to use nondestructive technology on different fronts of work, in the search for tools that provide support to the evaluation, control and monitoring work of urban trees.

The project called Forestry Mobile Unit Is described, with an analysis of the experience of Bogota, by presenting, the implemented approach, the working procedure, the methodological needs in this operation and how technology used can support future research opportunities.

The intention of this paper is to share the experiences achieved with the functioning of the Unit in Bogota, Colombia, particularly the use of nondestructive testing devices in urban trees.

Bogota urban trees

In Colombia, the urban development of cities has not obeyed a prospective vision of land use planning to prevent the proliferation of informality; however the occupation of the territory has traditionally been the product of a mixture of many complexes political, economic and social order factors. Infrastructure development has largely contributed to the degradation of the main ecological structure that supports the processes of urban and regional development. Therefore, especially in Bogota (the capital city), urban forestry is a pending issue for the different factors that have to do with planning and urban development; explicitly, serious conflicts in the use of urban land devoted to building infrastructure within the urban forest (SDA, 2014).

Since 1998, the government of Bogota began to establish a set of standards that addressed forestry activities in the city and relevant entities in charge of this topic. The standards included emergency care related to woodland generating risk to life or citizens properties (Tovar Corzo, 2014). Bogota developed various tools for urban trees management, the Guide of urban forestry of Bogotá, the Information system for the management of urban trees (SIGAU), and the Local plans for urban reforestation (PLAU).

The District Secretariat of Environment (SDA, for its initials in Spanish) in the exercise of its duties as district environmental authority, is responsible for conducting the technical evaluation of urban trees, in order to grant permits and authorizations as well as to perform the control and monitoring of forestry administrative acts within its jurisdiction (SDA, 2014); this office examines the trees in the Capital District with the visual assessment method (Visual Tree Assessment - VTA), which allows for the determination of possible defects in stem, branches and foliage along with indications regarding the anchoring system, as far as possible with the available tools. The signs or symptoms suggesting major defects require further evaluation teams with the FMU, tomograph and Resistograph®.

According with JBB (2015) Bogota has a 100% inventory of trees in its urban area. JBB indicates there are 1,211,886 trees in public space and 762,000[1] in the private area for a total of approximately 2 million trees in the urban area of Bogota. Urban tree management in this city is particularly important because of effect of the urban renovation projects and the high risk due to the poor physical and sanitary conditions of many of these trees; as a result, there are frequent accidents by falling of branches or of the tree itself. (Tovar Corzo, 2014). On average, there have been 252 trees overturned or uprooted per year (between the years 2012 – 2014), as shown in Table 1.

Table 1 - Trees overturned in Bogota ((SDA, 2014))

Number of trees overturned	Year
188	2012
301	2013
269	2014

A statistical model indicates that more than 15,000 trees are likely to overturn (SDA, 2014). In 2011, the trees with symptoms of health impairment were: 44,502 in fair condition, 5,963 in poor condition and in critical condition 6,657 (JBB, 2015). This condition overview implies that the evaluation of urban trees is an important task in preventing damage to people and infrastructure.

Forestry Mobile Unit (FMU)

The FMU operates in a hybrid vehicle that works with electric propulsion system integrated into an advanced internal combustion engine. The unit is equipped with measuring devices such as

[1] Running inventory figure under review by the SDA

specialized brand Rinntech®: two acoustic tomographs and a Resistograph®, tools that establish the physical and internal health of the trees and help recognizing wood damage or cracks.

These devices are used with the purpose of determining of the most appropriate forestry treatments, thus reduce the number of felling of trees when this activity is not absolutely necessary and work for the conservation of forest resources in the city.

Acoustic tomography allows performing more accurate assessments of tree diagnostics and detecting the risk that defective trees may represent in an urban context. These kind of tests evaluate internal condition of trees, it functions by placing a certain number of transmitting and receiving sensors around the tree trunk perimeter and using a special software to calculate the measured values of the sound impulses received. The Resistograph®, on the other hand, is a micro drill that is introduced into a tree to measure the drill resistance of the wood.

The wood decay within a tree is often a cause of tree failure; because of that many field devices for measuring decay in trees are used (Johnstone et al. (2007). The principle of tomography technology is based on speed difference of sound waves through decaying wood and solid wood (Qi et al. (2013). In spite of this, a professional judgment is still necessary to make a technical decision. In Bogota the FMU as a diagnostic unit, schedules evaluations at the request of the forest engineer in charge of the procedure and who will issue the final technical concept to determine the treatment or forestry activity for each tree. When trees mean a risk because of their physical condition, but the internal state is unknown, then these trees are scheduled for a priority assessment.

The information obtained from the devices of FMU enables the acquisition and generation of knowledge about the urban trees and their behavior in accordance with the environmental and social conditions of the city. This information is useful for risk management and for the planning of new and ancient urban trees.

Measurement results

During the work period (2011 – 2014) of FMU, 507 measurements were carried out on different trees in Bogota. This unit has provided important information for decision-making through technical concepts issued by the SDA. The most frequently assessed species are those of a taller mature; most of them naturalized species, such as Blue Gum (*Eucalyptus globulus*), Australian Blackwood (*Acacia melanoxylon*) and Chinese Ash or Urapan (*Fraxinus chinensis*).

The tree assessment activity has verified the health of trees, according to height and carrying capacity of the tree, which results in community risk prevention. Tests have been conducted in trees that could cause damage or injury in case of fall, because they are located in areas of high vulnerability and its biomechanical conditions could be a risk; nondestructive testing has offered more knowledge of these species.

In this sense, Kolařik (2003) indicates that load analysis is crucial information to determinate tree safety, he points out that a defect (such as a cavity) correlates with height increasing structural failure; that is why in Bogota assessments have been focused on higher trees with basal cavities. However, especially in the urban landscape tree failures, Rinn (2013) shows that trunk diameter and thus age (and crown size), is also a safety factor, which needs to be analyzed from different approaches, because mature trees require less remaining shell wall thickness for acceptable stability, in comparison to younger trees.

Discussion

The operation of the FMU and its specialized equipment for the technical evaluation of urban trees, has offered multiple possibilities of analysis in this procedure, so as to detect the most appropriate and

timely forestry activity or those trees assessed. This unit constitutes a diagnostic tool and provides useful inputs into the decision making for the management and handling of trees in the city, for planning documents and for awareness campaigns to protect the trees in the city.

The visual assessment of the state of the base of the trunk is not enough to evaluate the physical and health condition of the roots; but the identification of areas without bark or areas with localized internal rot can provide clues that may be affecting the root system and can be detected by acoustic tomography, can provide clues what may be affecting the root system. Urban soil as a growing medium is an important issue of analysis but plantings are usually conducted with little appreciation to character and quality of the surface, this results in problems, such as soil compaction that arises and inhibits the growth of the plant, another consequence is supersaturated water, which can kill the roots around existing trees (Nilsson, Randrup, & Tvedt, 1997), this indicates the need for develop nondestructive methods to evaluate the roots health.

It is also necessary to find out decay resistance of species and to monitor the variation of pests and diseases identified in the city which frequently attack species like Sangregado (*Croton bogotensis*), Caucho Sabanero (*Ficus soatensis*), Falso Pimiento (*Schinus molle*) or Chicalá (*Tecoma stans*). These species are the object of endotherapy treatments. It is as well imperative to observe the effect of fertilization and nutrition programs in those species through nondestructive technics.

To prove accuracy of tomograms, for artificial defects, it was evident that the position of the defect regarding to the pith had an important effect in its detection (Espinoza et al. (2015). On the contrary, in the assessments of the natural defects, optimal velocity threshold detected the defect, but did not allow to locate and to quantify the precise area of the defect (Espinoza el al. (2015), Dolwin et al. (1999). It is necessary, to identify thresholds for determining specific sound velocity, accurate location segments and decay areas in tomograms for naturalized and native species, and specifically, to distinguish earlier and advanced decay stages detected in Bogota species.

An area of importance of nondestructive wood testing methods in the silvicultural management of trees in the city, is to determination of the effect of activities such as moving trees when there is interference with infrastructure, the results will be of significant value in the daily work carried out within the process of evaluation, control and monitoring of urban forestry activities in the Capital District and they also will help addressing the short- and medium-term prevention regarding the risk of falling trees in the city, according to current knowledge on development and behavior of trees in the urban context.

Conclusions

The FMU is a recent experience in Bogota, which has enabled more accurate technical evaluation of urban trees and it is the support for silvicultural treatments.

Although the use of the equipment requires care, time and dedication, the FMU has reduced these limitations and has allowed to get to places with difficult accessibility. The results of tests performed with the tomograph and complemented with Resistograph® provide easy understanding for ordinary people with no technical knowledge, especially when the assessment of trees generates dispute among the community. The FMU has helped supporting the decisions regarding the most appropriate management of trees in public areas where evaluation has been conducted.

Acknowledgments

I want to thank to the 19th International Nondestructive Testing and Evaluation of Wood Symposium to give me the opportunity to share the Bogota experience in the detection of hazardous trees by nondestructive testing.

References

Dolwina, J. A., Lonsdaleb, D., & Barnettc, J. (1999). Detection of decay in trees. *Arboricultural Journal: The International Journal of Urban Forestry, 23*(2), 139 - 149.

Espinosa, L. F., Arciniegas, A. F., Prieto, F. A., Cortes, Y., & Brancheriau, L. (2015). Standing tree decay detection by using acoustic tomography images. In O. A. Fabrice Meriaudeau (Ed.), *Twelfth International Conference on Quality Control by Artificial Vision. 9534*, pp. 77-82. Bellingham, WA: Proceedings of SPIE.

JBB. (2015, May 30). *Jardín Botánico José Celestino Mutis*. Retrieved from http://jbb.gov.co/jardin/sigau

Johnstone, D. M., Ades, P. K., Moore, G. M., & Smith, I. W. (2007). Predicting Wood Decay in Eucalypts Using an Expert System and the IML-Resistograph Drill. *Arboriculture & Urban Forestry, 33*(2), 76 - 82.

Kolařik, J. (2003, Jul 22). *The application of the static integrated approach for arboricultural.* Retrieved from http://www.treeworks.co.uk/downloads/2%20-%20JK_Static%20Integrated%20031203.pdf

Monk, B. (n.d.). *Evaluation of decay detection equipment in standing trees.* (U. S. Service, Ed.) Retrieved Jun 10, 2015, from http://www.fs.fed.us/t-d/programs/im/tree_decay/tree_decay_detect_equip.shtml

Nilsson, K., Randrup, T. B., & Tvedt, T. (1997). Aspectos tecnológicos del enverdecimiento urbano. In K. L., & J. R. Nascimento (Ed.), *Áreas Verdes Urbanas en Latinoamérica y el Caribe* (pp. 39 - 81). México: Banco Interamericano de Desarrollo.

Qi, Y., Foster, B., Ferchaud, V., & Collins, D. (2013). Detecting Internal Decay in Trees Using Sonic Tomography Technology. *Urban Forestry Natural Resources and Environment Station Bulletin*(605), 1 - 6.

Rinn, F. (2013). Shell-wall thickness and breaking safety of mature trees. *Western arborist*, 40 - 44.

SDA. (2014). *Documento Técnico de Soporte Subdirección de Silvicultura, Flora y Fauna Silvestre.* Bogotá: Secretaría Distrital de Ambiente.

Tovar Corzo, G. (2014, May 30). Management of urban woodlands. In FAO, & FAO (Ed.), *Trees connecting people in action together - Developing guidelines for decision and policy makers: trees and forest for healthy cities. Glasgow, United Kingdom, 30 - 31 May 2011* (Vol. Urban and Periurban Forestry working paper No. 9, pp. 12 - 13). Rome: FAO. Retrieved Jun 13, 2015, from Developing guidelines for decision and policy makers:: http://www.fao.org/3/a-i4206e.pdf

Biodeterioration and hazard assessment of tipuana trees in the sidewalks of São Paulo, SP

Sérgio Brazolin
Center for Forest Resource Technology, Institute for Technological Research - IPT, São Paulo, Brasil, brazolin@ipt.br

Mario Tomazello Filho
Department of Forest Science, São Paulo University - USP - Luiz de Queiroz College of Agriculture, Piracicaba, São Paulo, Brasil, mtomazel@usp.br

Takashi Yojo
Center for Forest Resource Technology, Institute for Technological Research - IPT, São Paulo, Brasil, yojos@ipt.br

Raquel D. A. M. Amaral
Center for Forest Resource Technology, Institute for Technological Research - IPT, São Paulo, Brasil, raquel@ipt.br

Abstract
In the sidewalks of São Paulo city, Brazil, 1109 tipuanas (*Tipuana tipu*) trees were evaluated for its biodeterioration process and hazard assessment, using biomechanical concepts. The trees were characterized taking into consideration the surroundings and target analysis, dendrometric variables and external and internal biodeterioration, using nondestructive equipment (resistograph) for the trunk prospection. The hazard assessment was estimated using a static structural model. The old aged trees did not show any sign of dieback, even though, the general aspect of their surroundings was critical by the inadequate places they were planted and inappropriate management and/or occurrence of injuries. The trees had their trunks deteriorated by xylophagous organisms, mainly decaying fungi and subterranean termites, which affected the heartwood. The decaying fungi observed were classified as white rot and soft rot, being the white rot more common in the heartwood of the trees. The infestation of the trees by the subterranean termite *Coptotermes gestroi* was at high levels, however, it was considered as a secondary plague-organism, because its attack was associated with the previously decayed heartwood by *Ganoderma* sp or *Pycnoporus sanguineus* fungi. The structural model categorized 177 (16%) tipuanas as hazardous trees and it was observed statistical significance with the external presence of fungi and termites, DBH and internal biodeterioration processes.

Keywords: decaying fungus, hazard assessment, resistograph, structural model, termite, tipuana, tree.

Introduction

Tipuana trees (*Tipuana Tipu*) were extensively used for about 60-70 years ago in arborization of São Paulo city due to its large size, flowering and fast growth, despite, it is an exotic species and the damage caused in the sidewalks and to the power grid (IPT, 2004; Silva et al., 2008). The wood of tipuana trees may be affected by wood-destroying organisms (fungi and termites), and this biodeterioration intensity is considered as a criterion for removal and cause of fall (Brazolin, Amaral, Tomazello-Filho, 2006;

Sampaio, 2006). Therefore, the present study, developed in the "Operação Árvore Saudável" project for São Paulo municipality (IPT, 2004), evaluates tipuana trees in the sidewalks, considering their surroundings and target analysis, dendrometric characteristics, trunk biodeterioration processes and fall risk, using a structural analysis model.

Method

In seven regions of São Paulo city (Cerqueira César; Pacaembu-Sumaré, Alto de Pinheiros, Alto da Lapa, Vila Nova Conceição, Paradise and Alto da Boa Vista) 1109 tipuana trees planted in public tours of seven regions in São Paulo were analyzed. In the analysis target and surrounding conditions was checked the type of traffic route (local, collector, arterial), sidewalk lifting and permeable area for its growth. The dendrometric characteristics as breast height diameter (BHD), first fork height, total height of the tree; canopy area and trunk inclination were obtained.The phytosanitary aspects or wood biodeterioration was evaluated by external analysis, considering the presence of decaying fungi (presence of mushroom and rot of the wood); subterranean termites by the presence of live insects in the wood, wood attack, tunnels in the bark and nest structure. These wood-destroying organisms were collected and identified in the Trees, Wood and Furniture Laboratory of IPT.

The internal analysis to determine the occurrence and intensity of biodeterioration (% deterioration of the wood) has been made at the trunk base, using a non-destructive equipment - resistograph (Figure 1).

Figure 1 - Resistograph used in the prospection of the trunk in tipuana trees

For the hazard assessment a static structural model developed by IPT (2004) was used. This model considers the following variables: i) the dendrometric measures; ii) the status of phytosanitary of the trunk (internal biodeterioration); iii) the physical and mechanical properties of wood; iv) wind velocity; v) the location of the trees in association with the wind statistical factors; vi) the root system (conceptual) and their interaction with the ground; and vii) the resistance of the root and trunk transition. This model assumes the rupture in the trunk and root-trunk area and categorized the trees minimum and maximum warning levels.

The association of wood-destroying organisms (external analysis), dendrometric characteristics and internal deterioration with the structural model response (minimum and maximum warning levels) were statistically analyzed by chi-square test, with signicance level of 5%.

Results and discussion

In the seven selected regions of São Paulo, the 1109 tree tipuana presented no sign of decline, with developed canopy, characteristic of the species and different levels of pruning, although 196 (17.6%) of the trees were observed with reduced canopy and epicormic branches.

Surroundings

Considering the traffic route, it was found 464 (43%) tipuanas in local route, 416 (37%) in collector routes and 229 (20%) in arterial. Therefore, 57% of the trees were in fast and heavy traffic roads (collector and arterial) representing, in case of fall, risk to the people and vehicle traffic in São Paulo city. Most trees (877, 79%) was planted in inadequate sidewalks (size) with insufficient permeable area (< 3 m²) for this species (São Paulo, 2005); 31% (269) of these trees were planted were fully cemented enveloping the stem base. There was also the presence of sidewalk lifting in 528 (48%) tipuana trees, indicating that physical barriers and/or soil compaction restricted the root system development (Lima, 1993) and can not be associated with the rot system and soil movimentation due to internal forces promoted by the wind. Inadequated condition diagnosed for most tipuana trees in São Paulo city can affect their growth and become more susceptible to attack by pests and diseases, increasing their risk of rupture (IPT, 2004).

Dendrometric characteristics

The dendrometric characteristics of tipuana trees of São Paulo (Table 1) indicated that 75% have BHD > 0.50 m and therefore classified as mature trees. The evaluation of the total height indicated that 50% have 10-14 m and 25% over 14 m. As most of these trees were planted in narrow sidewalks, your fall risk due to wind should be considered, since 831 (75%) of these trees have the more than 20 m² of canopy area. The inclination of 75% of tipuana trunk was less than 15º and only 15 trees (<1%) had trunk with inclination superior 30º. Albers, Pokorny and Johnson (2003), indicated that trees with trunk inclination greater than 40º must be removed or the target (equipment or property) removed. For 11(<1%) trees with first fork height lesse than 1,5 m and more than 10 m high are subject to breakage in this region.

Table 1 - Dendrometric characteristics tipuana trees in the urban area of São Paulo, SP

Dendrometric characteristics	Characteristics values of tipuana trees					
	Average	S. dev.	Min.	Max.	1ºQuartile	3ºQuartile
BHD (m)	0.60	0.16	0.16	1.06	0.50	0.70
Total height (m)	12.71	2.79	4.71	21.32	10.78	14.66
First fork height (m)	3.22	0.89	0.43	11.00	2.69	3.61
Trunk inclination (º)	11.0	6.8	0.1	48.7	5.8	14.7
Canopy area (m²)	32.44	18.85	0.92	133.21	21.64	40.50

Decaying fungi

The external evaluation of the phytosanitary condition of 1109 tipuana trees showed the presence of decaying fungi in 338 (30%), with characteristic symptoms of rotting in the root ant trunk injuries resulting from inadequated pruning. In 17 (1.5%) trees were detected mushrooms of *Picnoporus*

sanguineus and *Ganoderma* sp. on the exposed roots or bark, causing white rot in the wood (Brazolin, 2009). The presence of decaying fungi in the biodeterioration process of the tree is related to inadequated pruning, as mentioned by Amaral et al. (2003).

Termites

Subterranean termites were observed in 307 (29%) trees. Two species of Rhinotermitidae family were identified: *Coptotermes gestroi* in 119 trees and *Heterotermes* sp. just in one tree. The *C. gestroi* occurrence in high levels of infestation is due the great capacity for dispersion in urban centers and also causing damage to buildings (Zorzenon; Potenza, 1998; Amaral, 2002; Romgnano, 2004).The association between decaying fungi and *C. gestroi* and other species was reported by Brazolin et al. (2010), Sands (1969), Hickin (1971) and Grasse (1982).

Internal analysis

The results of internal deterioration showed 935 (84%) trees with different levels of damage and 142 (13%) evidenced in the open cavities as a reaction to injuries. The relative frequency of internal deterioration (%) indicated that 528 (48%) trees were healthy or less deteriorated (<11% internal deterioration); 412 trees (37%) between 11% to 44% and 169 (15%) more than 44%. Then, tipuana trees are suscetible to wood-destroying organisms, affecting the wood physical and mechanical properties, however, this species has good natural resistance, considering its longevity of 70 years and despite the inadequated planning and management of the São Paulo city.

Hazard Assessment

The structural model indicated a higher frequency of occurrence of trees classified into minimum warning level (932 trees; 84%) than maximum (177; 16%).

It was observed an association between external presence of wood-destroying organisms (decaying fungi and subterranean termites) and the fall risk for tipuana ($\chi 2 = 75.82$; $p < 0.05$) and a higher frequency of occurrence of fungi and termites was noted in maximum level.

For dendrometric chacracteristics, only the BHD variation showed a significant difference compared to fall risk ($\chi 2 = 75.82$; $p < 0.05$), indicating an association between these two parameters. The BHD values are higher for trees with maximum level and lower for minimum. The other characteristics of tipuana trees, represented by its total height, canopy area, first fork height and trunk inclination showed no statistical association ($p > 0.05$). It must be considered that the dendrometry of these trees has changed by management practices, mainly by pruning, modifying its architecture and, consequently, the interaction with the loading (wind and dead weight).

Regarding the internal deterioration of wood, the structural model showed a strong association with the internal deterioration, caused by wood-destroying organisms ($\chi 2 = 1107.32$, and $p < 0.05$). Trees classified as minimal level presented an average internal deterioration of 13 ± 14% and for maximum level 56 ± 14%, confirming the studies of Mattheck, Bethge and Tesari (2006), Wagener (1963), Smiley and Fraedrich (1992) and Mattheck and Breloer (1997) that related the rupture of trees to the mechanical resistance loss caused by internal cavities produced mainly by decaying fungi.

Conclusion

The old aged tipuana trees did not show any sign of dieback, even though, the general aspect of their surroundings was critical by the inadequate places they were planted and inappropriate management and/or occurrence of injuries. The trees had their trunks deteriorated by xylophagous organisms, mainly decaying fungi and subterranean termites, which affected the heartwood. In the hazard assessment, it was observed associations of external presence of decaying fungi and termites, the DBH and internal biodeterioration processes. The static structural model can be a useful tool for the municipality to prioritize the adequated management of trees.

References

Albers, J.S.; Pokorny, J.D.; Johnson, G.R. 2003. How to dectect and assess hazardous defects in trees. In: POKORNY, J. D. (Coord.). Urban tree risk management: a community guide to program design and implementation. St. Paul: USDA, Forest Service, Northeastern Area, Staty and Private Forestry, chap. 3, p. 41-116. (Technical Paper, NA-TP-03-03).

Amaral, R.D.A.M. 2002. Diagnóstico da ocorrência de cupins xilófagos em árvores urbanas do bairro de Higienópolis na cidade de São Paulo. 2002. 71 p. Dissertação (Mestrado em Recursos Florestais) - Escola Superior de Agricultura “Luiz de Queiroz”, Universidade de São Paulo, Piracicaba..

Brazolin, S. 2009. Biodeterioração, anatomia do lenho e análise de risco de queda de árvores de tipuana, Tipuana tipu (Benth.) O. Kuntze, nos passeios públicos da cidade de São Paulo, SP. 2009. 265 p. Tese (doutorado em Recursos Florestais - Escola Superior de Agricultura “Luiz de Queiroz”, Universidade de São Paulo, Piracicaba.

Brazolin, S.; Tomazello-Filho, M. Amaral, R. D. A. M. [and others] . 2010. Associação entre fungos apodrecedores e cupins-subterrâneos no processo de biodeterioração do lenho de árvores de Tipuana tipu (Benth.) O. Kuntze da cidade de São Paulo, SP. Scientia Forestalis, Piracicaba, v. 38, n. 86, p. 215-224, jun.

Brazolin, S.; Amaral, R.D.A.M.; Tomazello-Filho, M. 2006. Ocorrência de organismos xilófagos em árvores de *Tipuana tipu* (Benth.) Kuntze da cidade de São Paulo, SP. In: SIMPÓSIO DE PÓS-GRADUAÇÃO EM CIÊNCIAS FLORESTAIS, 4., 2006, Piracicaba. Anais.... Piracicaba: ESALQ. 1 CD-ROM.

Grassé, P.P. 1982. Termitologia. Paris: Masson, t. 1: Anatomie, physiologie, reproduction, 676 p.

Hickin, N.E. 1971. Termites: a world problem. London: Hutchinson. 232 p.

Instituto de Pesquisas Tecnológicas do Estado de São Paulo - IPT. 2004. Relatório técnico do diagnóstico e análise de risco de queda das árvores de vias públicas da cidade de São Paulo: Projeto Operação Árvore Saudável. São Paulo: IPT, Divisão de Produtos Florestais, v. 1, 45 p.

Lima, A.M.L.P. 1993. Piracicaba/SP: análise da arborização viária na área central e em seu entorno. 1993. 238 p. Tese (Doutorado em Solos e Nutrição de Plantas) – Escola Superior de Agricultura “Luiz de Queiroz”, Universidade de São Paulo, Piracicaba.

Mattheck, C.; Breloer, R.C. 1997.The body language of trees: a handbook for failure analysis. London: the Stationery Office. 239 p.

Mattheck, C.; Bethege, K.; Tesari, I. 2006. Shear effects on failure of hollow trees. Trees, New York, v. 20, p. 329-333.

Romagnano, L.F.T.D. 2004. Instrumentos de gestão ambiental integrada: diretrizes para o controle de cupins-subterrâneos em ambientes construídos. 2004. 126 p. Dissertação (Mestrado em Tecnologia Ambiental) – Instituto de Pesquisas Tecnológicas do Estado de São Paulo, São Paulo.

Sampaio, A.C.F. 2006. Análise da arborização de vias públicas das principais zonas do plano piloto de Maringa, PR. 2006. 117 p. Dissertação (Mestrado em Análise Regional e Ambiental) – Universidade Estadual de Maringá, Maringá.

Sands, A.W. 1969. The association of termites and fungi. In: KRISHNA, K; WESSNER, F.M. Biology of termites. New York: Academic Press. v. 2, p. 495-524.

São Paulo: Secretaria Municipal do Verde e do Meio Ambiente. 2005. Manual técnico de arborização urbana. 2. ed. São Paulo. 45 p.

Smiley, T.; Fraedrich, B.R. 1992. Determining strength loss from decay. Journal of Arboriculture, Champaign, v. 18, n. 4, p. 201-204, July/Dec.

Wagener, W.W. 1963. Judging hazard from native trees in California recreational areas: a guide for professional foresters. Berkeley: USDA, Agriculture Forest Service, Southwest Forest and Range Experiment Station, Research Paper: PSW-P1, 29p.

Zorzenon, F.J.; Potenza, M.R. 1995. Cupins: pragas em áreas urbanas. São Paulo: Instituto Biológico. 40 p. (IB. Boletim Técnico, 10).

Detecting defects in standing trees by an acoustic wave tomography with pseudorandom binary sequence code: simulation of defects using artificial cavity

Kana Yamashita
Department of Wood Properties, Forestry and Forest Products Research Institute, Tsukuba, Ibaraki, Japan, zaikana@ffpri.affrc.go.jp

Toshihiro Yamada
The University of Tokyo Chichibu Forest, The University of Tokyo, Chichibu, Saitama, Japan, yamari@uf.a.u-tokyo.ac.jp

Yuko Ota
Department of Forest Microbiology, Forestry and Forest Products Research Institute, Tsukuba, Ibaraki, Japan, yuota@affrc.go.jp

Hiroshi Yonezawa
JFE Civil Engineering and Construction Corporation, Taitou, Tokyo, Japan, yonezawa@jfe-civil.com

Izumi Tokue
Maghouse Inc., Shinagawa, Tokyo, Japan, to-5@mvc.biglobe.ne.jp

Abstract

This study aimed to evaluate the potential of Dr.Woods® acoustic tomography to detect internal defects in standing trees. Using the signals of pseudorandom binary sequence code, the sound velocities among sixteen test points around the trunk were measured at frequencies 10–40 kHz. In order to simulate different sizes and shapes of decay, different sizes and shapes of cavities were artificially chiseled in the trunk cross-sections. As cavity area increased, sound velocity of the path going around the cavity decreased.

Keywords: acoustic tomography, defect detection, trees

Introduction

Ultrasonic tomography with a high frequency acoustic wave has a possibility of high resolution imaging, whereas it requires a compromise between the resolution and the penetration power and suitable signal processing (Arciniegas 2014). Its resolution has been studied in previous papers (Bucur 2005, Divos and Divos 2005, Lin et al. 2008). Dr.Woods is a portable instrument for acoustic tomography to inspect internal state of a tree nondestructively. It injects a high frequency acoustic wave having accurately controlled amplitude and frequency into the tree (Yoshiyuki et al. 2006). We are testing the resolution with Dr.Woods using cross-sections having artificial cavities at different frequencies for several species. In this paper, the resolution of circular hole was examined at a frequency 20 kHz for *Zelkova serrata*. The effect of threshold to determine travel time at signal processing was also examined.

Materials and methods

Samples

Zelkova serrata is a popular species as street tree and for homestead woodland. It forms a thick trunk. Its wood is used as timber for building and furniture, and a drum etc. From a tree of *Zelkova serrata* grown in the Forestry and Forest Products Research Institute (Tsukuba, Ibaraki, Japan), two cross-sectional sound disks with diameters of 46 cm were cut. One disk with thickness of 5 cm was used for evaluating basic density (BD) and moisture content (MC), and the other disk with thickness of 15 cm was for acoustic tomography.

The thin disk was cut into 16 pieces in a circumference direction and 7 pieces in a radial direction (112 small pieces in total). BD was calculated from the volume in green condition and the weight in oven-dry condition. MC was calculated based on the weight in oven-dry condition.

Acoustic tomography with Dr.Woods (JFE Civil Eng. and Con. Co., Tokyo, Japan) was firstly performed on the sound disk without a cavity. Secondly, a small circular hole with diameter of 5 cm was chiseled around the pith, followed by acoustic wave tomography. The cavity diameter was successively enlarged from 10, 20 to 32 cm. Acoustic tomography was performed at every step. The ratio of cavity areas in the disk area increased from 0%, 1%, 5%, 20% to 50% at the five steps. During the acoustic tomography, the disk was kept in green condition.

Acoustic wave tomography

Sixteen sensors were set at the same level around the disk; this is how 240 sets of velocities between sensors were obtained. First, sixteen thin needles were inserted into the xylem and their positions were measured to get distances among sensors. Next, a sensor was connected to a needle, and then acoustic wave signal with pseudorandom binary sequence code was transmitted from every sensor (20 kHz, 50V), which was received by the other 15 sensors. The correlation coefficient was calculated between each pair of transmitted and received waves.

In signal processing, the first arrival point was recognized at the first wave top where exceeded the two threshold amplitudes: *thvn* and *thvc*. The *thvn* was calculated from the median and standard deviation of noise amplitude and noise level (*thnl*) input by a user. In this study *thnl* was set to 3, because the noise was comparatively small and didn't give a big effect on the first arrival point. The *thvc* was a division of the maximum amplitude in the anticipated velocity range, which was set to 0.1–1.5 km/s in this study, by the threshold noise criterion (*thnc*) input by a user. We input several *thnc* (2, 3, 5, 10, 15, 20, 25, and 30) and compared the results. After every first arrival point was confirmed, velocity was calculated from the flight time and the distance. A contour map was drawn by interpolation.

Results and discussion

Distribution of density and moisture content in a cross section

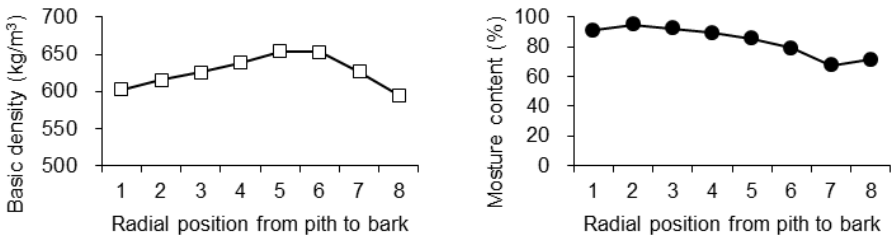

Figure 1—Radial trends from pith to bark for basic density and moisture content. Sixteen pieces from different positions in a circumference direction were averaged for each radial position.

Basic density (BD) was relatively smaller around the pith. In a radial direction, BD increased from pith outward, became a maximum at around 70% position of radius, and then decreased toward bark. Moisture content (MC) was relatively higher in the heartwood. In a radial direction, MC decreased gradually from pith outward. Average BD of all pieces was 626 kg/m^3, and moisture content was 84%.

Effect of threshold noise criteria at data processing

We investigated the effect of threshold noise criteria (*thnc*) on sound velocity and reconstructed image. For every tested disk, higher *thnc* dropped the threshold amplitude, enabled picking up first waves with smaller amplitude, and made sound velocity faster. Velocity histograms clearly showed the velocity shift by *thnc*. Figure 2 is the sound velocity of different paths analyzed with *thnc* of 30 and 5. The velocity was lower for *thnc* 5 than *thnc* 30. However, the trends of cavity diameter and path were similar between *thnc* 30 and *thnc* 5. When we compared the contour maps, there were not so markedly differences by *thnc*, either. These comparisons suggested that *thnc* would give apparent effect on velocity, but its effect on velocity distribution in the cross section might be less.

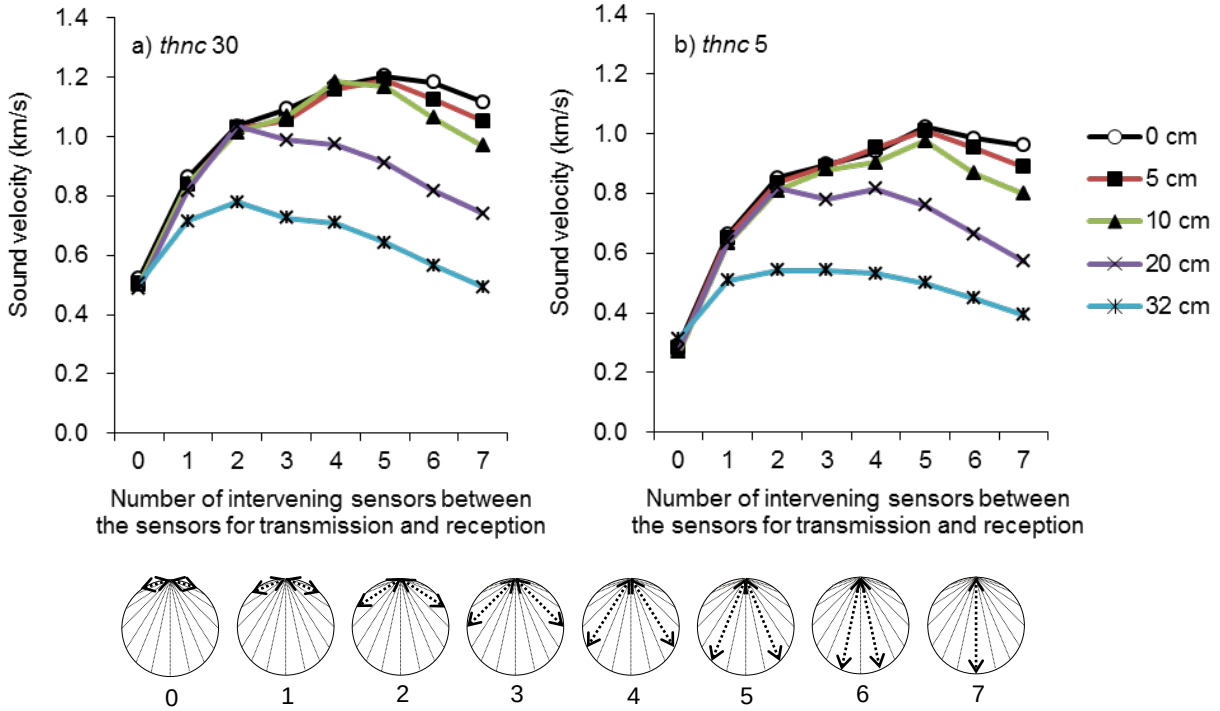

Figure 2—Sound velocities for a disk with five different diameters of circular cavities: 0, 5, 10, 20, and 30 cm by the number of intervening sensors between transmission and reception sensors. The number of sensors is 0 for adjacent sensors and 7 for sensors in the diagonal position. The threshold noise criteria (*thnc*) were set to 30 (a) and 5 (b).

Effect of cavity size on the sound velocity and reconstructed image

For the sound disk without a cavity, shown as circle marks with a black line in Figure 2, the sound velocity was the lowest for adjacent sensors, and increased as a path got close to a diagonal direction up to number of intervening sensors reaching five (Figure 2). It might be because of the wood anisotropy; sound velocity is faster in the radial direction than in tangential direction. The sound velocity slightly decreased for number of intervening sensors 6 and 7, which might be because of the lower density around the pith (Figure 1) and/or attenuation.

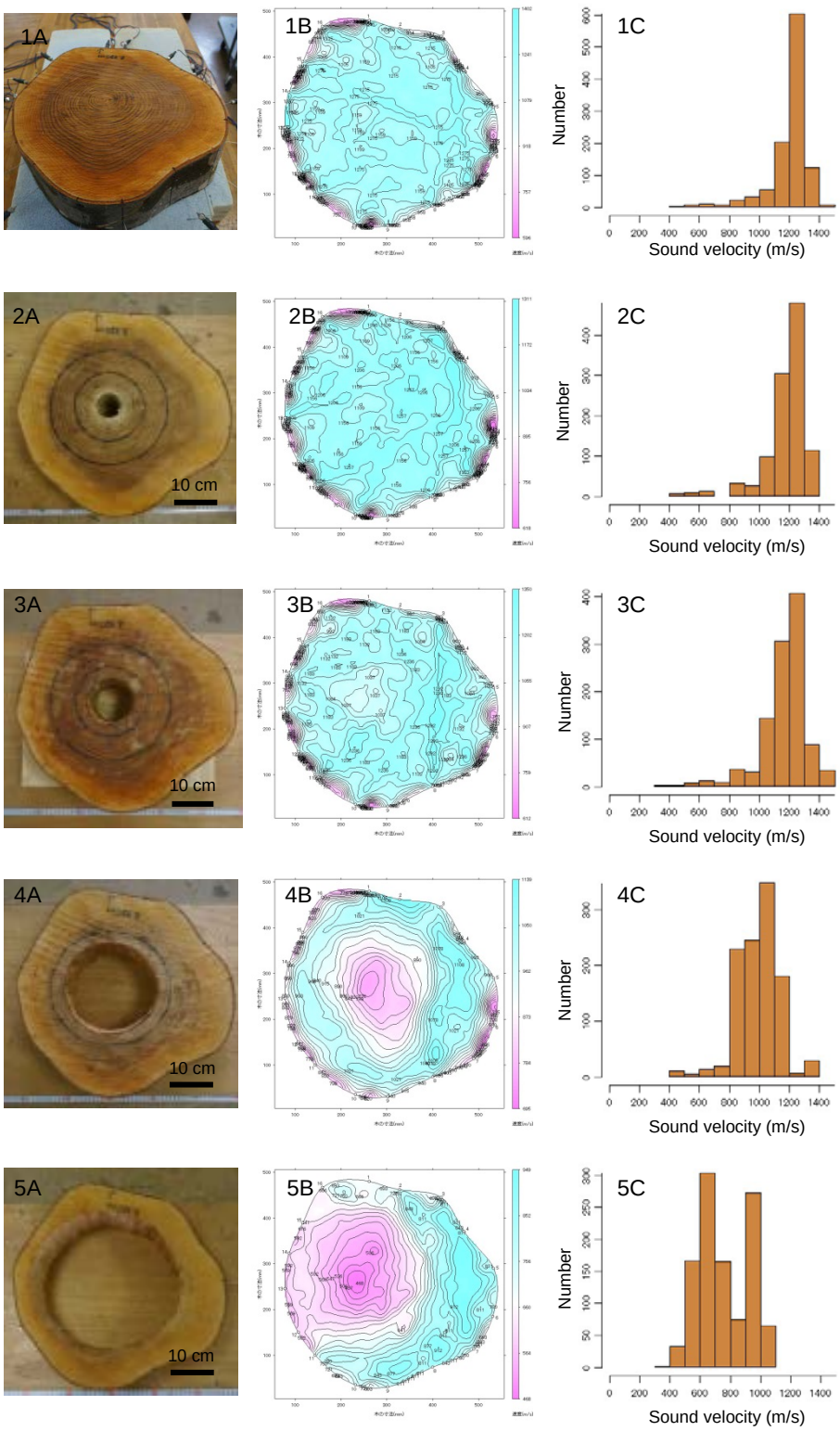

Figure 3—Sample image (A), reconstructed contour map by acoustic tomography (B), and sound velocity histogram by acoustic tomography (C) for a disk with five different diameters of circular cavities: 0, 5, 10, 20, and 32 cm. The threshold noise criteria (*thnc*) were set to 30. In contour map, the maximum and minimum velocities changes with cavity size. Blue and pink show high and low velocity. The histogram includes all sets of velocity in a cross-section.

As cavity diameter increased from 5 to 32 cm, the velocity between adjacent sensors didn't change, whereas the velocity in the diagonal direction decreased (Figure 2). It might be because that the waves in the diagonal direction passed around the cavity. As cavity diameter increased, more paths exhibited decrease in velocity. Those changes were clear for cavity diameters 20 and 32 cm.

Figure 3 shows contour maps and velocity histograms for five cavity diameters. Compared with the disk without a cavity, the frequency of lower velocity (1000–1200 m/s) increased for the disk with 5 cm cavity (Figure 3, 1C and 2C); however, low velocity contour was not observed on its contour map (Figure 3, 2B). For the disk with 10 cm cavity, low velocity contours were faintly visible (Figure 3, 3B). For the disk with 20 cm cavity, lower velocity contours were clear at the cavity area, which was shown in pink (Figure 3, 4B). For the disk with 32 cm cavity, the velocity was lower at the thinner part in the left side than the thicker part in the right side (Figure 3, 5B), which might be because the wave route went around the cavity at the narrow circumferential part.

Conclusions

Using a green disk of *Zelkova serrata* with different sizes of artificial circular cavities, ultrasonic sound velocity was measured with Dr.Woods. Compared with a sound disk, a disk with a cavity exhibited lower velocity where the wave went around the cavity. As cavity diameter increased, velocity decreased where the wave went around, and more portion exhibited lower velocity. On a contour map, small cavity with 5 cm diameter was not recognized, while larger cavities exhibited steep contours which suggested unsoundness.

Acknowledgments

This study was supported by the Japan Society for the Promotion of Science, Grant-in-Aid for Scientific Research No. 26292079.

References

Arciniegas, A.; Prieto, F; Brancheriau, L.; Lasaygues, P. 2014. Literature review of acoustic and ultrasonic tomography in standing trees. Trees. 28(6): 1559-1567.

Bucur, V. 2005. Ultrasonic techniques for nondestructive testing of standing trees. Ultrasonics. 43(4): 237-239.

Divos, F.; Divos P. 2005. Resolution of stress wave based acoustic tomography. Proceedings of the 14th International Symposium on Nondestructive Testing of Wood 309-314

Lin, C.J.; Kao, Y.; Lin, T. [and others]. 2008. Application of ultrasonic tomographic technique for detecting defects in standing trees. International Biodeterioration & Biodegradation 62: 434-441.

Yoshiyuki, M.; Sakakibara, J.; Yamamoto, T.; Tanaka, M. 2006. Nondestructive method and system of inspecting inside of tree by employing acoustic tomography. WO 2006/016520 A1. Patent.

Session 10

Logs and Round Wood Assessment

Analyzing the Accuracy of Internal Hardwood Log Defect Prediction Equations

R. Edward Thomas
Debbie Conner

U.S. Forest Service
Forest Products Laboratory
Madison, WI

Abstract

The type, size, and location of internal defects dictate the grade and value of lumber sawn from hardwood logs. Significant correlations have been documented among external log defect indicators and internal defect features. A series of prediction models for four hardwood species have been developed based on these correlations. The models are species and defect type specific and allow users to estimate internal defect size, shape, depth, and position. This paper examines the accuracy of the red oak and yellow-poplar prediction models by comparing defect attributes on actual sawn board faces with the predicted defect attributes on virtually sawn boards. In this validation test, 11 red oak and 9 yellow-poplar logs were sawn into a total of 209 boards. The outer face of the boards had a total of 218 observed surface defects of which the models predicted 68.3%. Overall, the yellow-poplar model performed slightly better than the red oak model. In addition, the models accurately predicted the sawing of 95 of 105 boards with no knot defects, an accuracy rate of 90.5%.

Keywords

Log defects; internal prediction; NDT; red oak; *Quercus rubra*; yellow-poplar; *Liriodendron tulipifera*

Introduction

The hardwood log grading rules are based on the relationship between defect occurrence and lumber recovery (Hanks et al. 1980). The ability to use internal defect information such as location, size, and shape during the sawing process has been shown to significantly improve the value of hardwood lumber sawn by as much as 10% to 21% (Steele et al. 1994; Wagner et al. 1990).

Because of the importance of internal defect information to the lumber sawing process, there have been several studies that seek to link external features to internal defect characteristics. Schultz (1961) studied German beech (*Fagus sylvatica* L.) and found that the ratio of the bark distortion width to length was the same ratio of the stem when the branch stub was encapsulated to the current stem diameter. However, for species with heavier, irregular bark, such as sugar maple (*Acer saccharum* L.), Schultz found that it was difficult to judge the clear area above the defect using this method. Similar results were found by Shigo and Larson (1969) where for many hardwoods the ratio of surface defect length to width indicated the depth of the defect with respect to the radius of the stem at the defect. Hyvärinen (1976) studied external bark distortion measurements and defect encapsulation depth for sugar maple and found strong correlations among encapsulation depth and distortion width, length, and rise using linear regression methods. More recently, Lemieux et al. (2001) examined knot defect correlations among external indicator and internal defect features for a sample of 21 black spruce (*Picea mariana* L.) trees collected in Northern Quebec. They found correlations ($r > 0.89$) among the width and length of internal defect areas on sawn board faces and external features such as branch stub diameter and length. Lemieux et al.'s 2001

study examined only branches that had not been dropped or pruned, thus preventing an examination of encapsulation depth.

An alternative approach to the x-ray/CT and MRI methods has been developed that uses high-resolution laser surface scanning coupled with internal defect prediction models. This approach uses intelligent software to locate and classify external log defects in the 3D laser data (Thomas et al. 2006). Once the external log defects are located, predictions of internal characteristics are made that estimate internal defect position, shape, and size based on measurements of the external indicator and log diameter (Thomas 2008; Thomas 2013b). These models are based on correlations among internal and external defect features. Different models were created for different species, defect types, and defect type groupings. The models were created by statistically analyzing 842 red oak (*Quercus rubra* L.) and 1,000 yellow-poplar (*Liriodendron tulipifera* L.) defect samples collected from three sites in the central Appalachian region (Fig. 1). These sites included the WVU experimental forest, a forest near Rupert, West Virginia, and the West Virginia State Forest at Camp Creek.

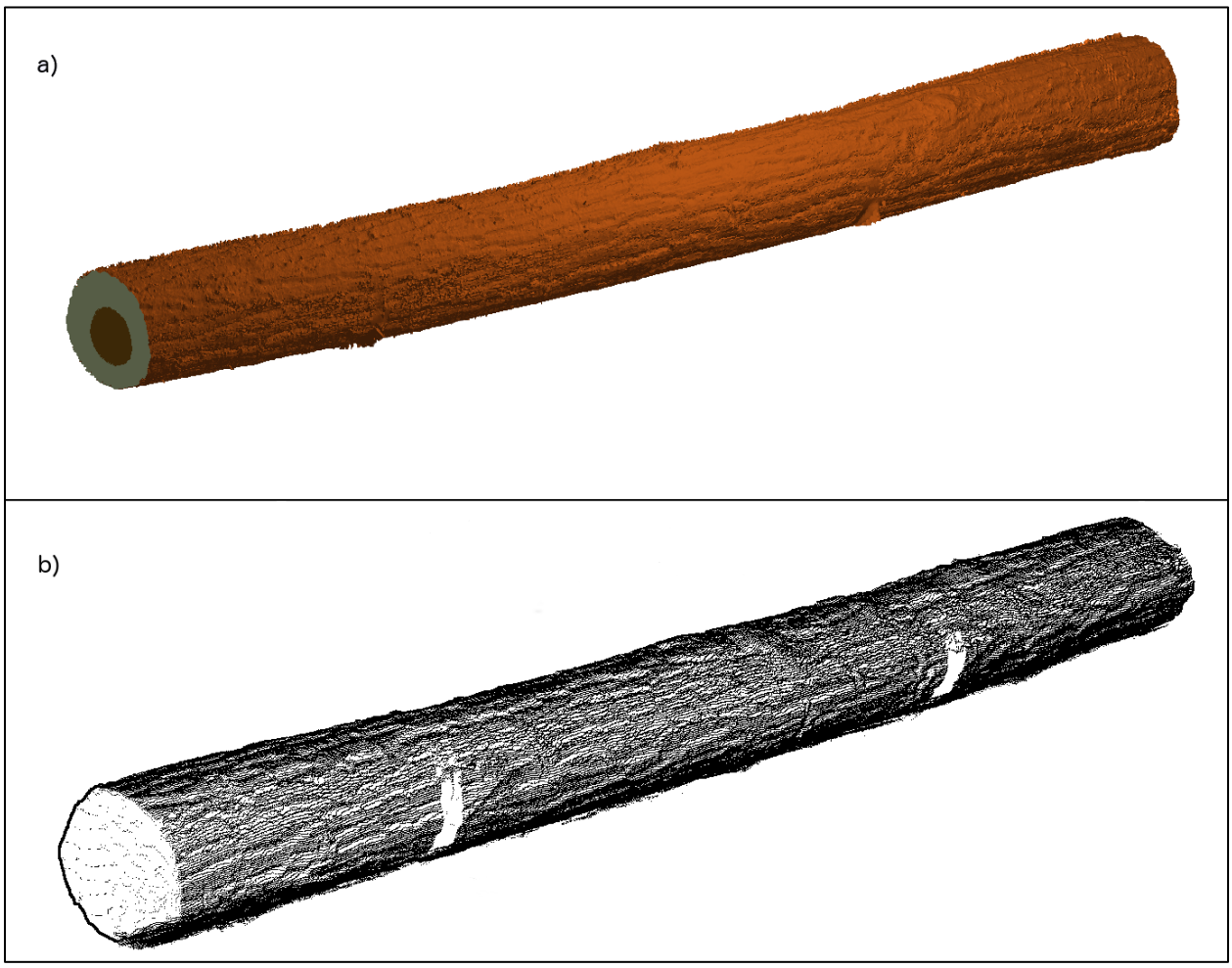

Figure 1—High-resolution scanned imagery of red oak log 21B: a) rendered surface, b) dot-cloud.

Methods

Three red oak (*Quercus rubra*) and three yellow-poplar (*Liriodendron tulipifera*) trees were harvested from the Fernow Experimental Forest located near Parsons, West Virginia. Eleven logs were bucked from the red oak trees and nine logs were bucked from the yellow-poplar trees. Table 1 lists the sizes and

grades of the logs. A high-resolution laser scanner (Thomas and Thomas 2011) was used to scan each log to obtain measurements, shape, and surface data. Figure 1 shows the scanned image of red oak log 21B whose measurement specifications are listed in Table 1.

Table 1—Summary of study log sizes, grades, and sawing results

Log	Species	U.S. Forest Service log grade	Length (in.)	Large end diameter (in.)	Small end diameter (in.)	Total boards sawn	Board volume(bd ft)	Cant volume(bd ft)	Cant size (in.)
17A	Y. poplar	Factory 1	146.7	20.6	17.2	19	159.8	13.3	4.3 × 3.1
17B	Y. poplar	Factory 2	143.5	16.9	15.8	16	114.4	12.6	5.4 × 2.6
17D	Y. poplar	Factory 2	144.2	14.8	13.9	10	67.6	21.1	6.3 × 3.4
21A	Red oak	Factory 2	142.3	18.1	13.3	12	78.8	12.9	4.3 × 3.3
21B	Red oak	Factory 2	143.2	13.0	12.2	8	43.8	16.8	4.9 × 3.8
21C	Red oak	Factory 2	145.3	12.4	12.3	8	37.3	25.7	4.6 × 5.6
21D	Red oak	Construction	120.2	11.9	10.6	6	23.4	15.8	5.6 × 3.4
29A	Y. poplar	Factory 1	152.3	17.6	16.9	17	129.8	15.0	5.0 × 3.0
29B	Y. poplar	Factory 2	146.8	15.3	13.6	10	65.8	24.8	5.5 × 4.5
29C	Y. poplar	Factory 3	131.6	13.8	13.4	11	56.0	18.6	6.3 × 3.6
31A	Y. poplar	Factory 2	143.0	16.3	16.0	8	45.4	16.2	4.9 × 3.6
31B	Y. poplar	Factory 2	144.9	11.4	10.7	5	26.4	15.8	5.5 × 2.9
31C	Y. poplar	Factory 3	111.4	10.1	10.0	5	24.0	11.6	5.9 × 2.6
33A	Red oak	Factory 2	145.7	15.5	12.0	11	57.3	11.0	4.0 × 2.8
33B	Red oak	Factory 2	145.6	11.8	11.1	8	36.8	17.3	5.8 × 3.0
33C	Red oak	Factory 3	143.8	10.6	11.9	5	24.5	16.0	5.0 × 3.5
36A	Red oak	Veneer	124.8	24.5	16.2	16	105.8	14.8	4.3 × 4.2
36B	Red oak	Factory 2	144.4	15.2	14.7	14	87.8	11.3	4.5 × 2.5
36C	Red oak	Factory 2	145.7	13.7	13.0	12	82.0	13.0	6.5 × 2.0
36D	Red oak	Factory 3	112.0	12.1	12.9	8	35.4	13.4	4.6 × 3.9
Average			138.9	14.8	13.4	10.5	65.1	15.8	5.2 × 3.4
Total						209	1301.8	316.9	

All surface defects were manually located, measured, and recorded. The defect, shape, and size information was used by the RAYSAW (Thomas 2013a) sawmill simulator to grade the logs to USDA Forest Service log grades (Rast et al. 1973). Overall, there was 1 veneer log, two Factory 1, 12 Factory 2, 4 Factory 3, and 1 Construction grade log. A total of 218 knot defects on the log surfaces were recorded, with red oak having 161 defects and yellow-poplar 57 defects (Table 2). Distortion-type defects were the most numerous comprising 63% of the total defect population. Overgrown knot defects were the next most common defect type with 16% of the defect population.

Table 2—Summary types and counts detected on log surfaces

Defect type	Total both species	Red oak	Yellow-poplar
Adventitious knot	12	11	1
Adventitious knot cluster	24	18	6
Bump	2	0	2
Heavy distortion	38	29	9
Light distortion	12	7	5
Medium distortion	88	65	23
Overgrown knot	31	23	8
Overgrown knot cluster	4	2	2
Sound knot	4	3	1
Sound knot cluster	1	1	0
Unsound knot	2	2	0
Total	218	161	57

The logs were sawn using a portable sawmill and the rotation and sawing pattern recorded. Table 1 lists the numbers of boards sawn from each log, the board volume, the cant volume, and the dimensions of the cant. The type and position of all knot defects on the outer face of every board were recorded. Where possible, all knot defects on the board faces were traced back to an originating surface defect. It is important to note that not all internal knots could be traced to such a surface indicator. Of the 280 total board knot defects, only 189 could be traced to a surface indicator (Table 3). The sawing process for each log was replicated using the RAYSAW sawmill simulator. The size and positions of internal defects were estimated using the models developed by Thomas (2008, 2013b). These methods use the size and type of the surface indicator to predict the size and location of the internal defect. When RAYSAW processes a log, it reports the overall shape of each board, as well as the positions and sizes of all predicted defects that fall on the board faces. Figure 2 shows a digital board alongside its real-world counterpart. RAYSAW represents defects such as knots as rectangles that describe the maximum width and length of the knot. Long defects such as wane are represented as a series of rectangles.

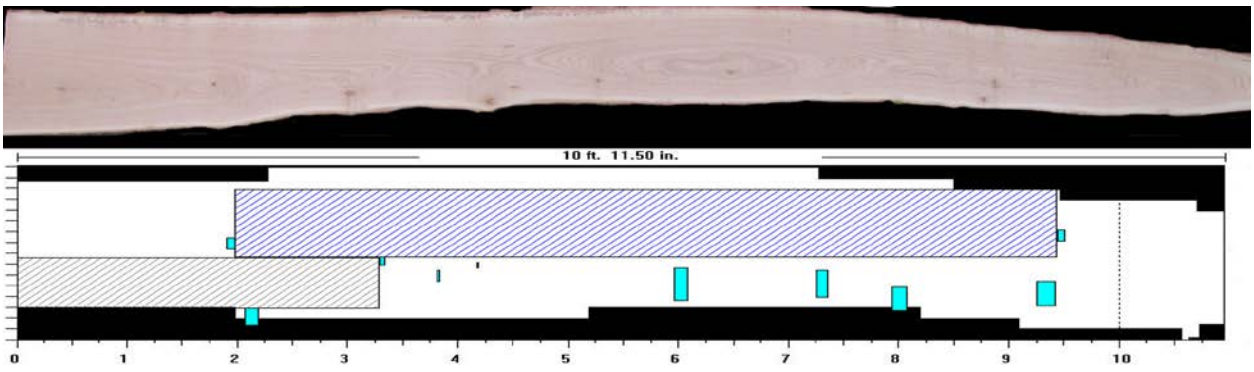

Figure 2—Sawing example showing RAYSAW simulated board with predicted defect areas alongside actual sawn board.

Discussion

In this study, a total of 209 boards, 108 red oak and 101 yellow-poplar, were sawn from the 20 sample logs. Of the actual boards, 105 were clear with no knot defects. The remaining 104 had a total of 280 observed knot defects, for an average of 2.7 defects per board. For the digitally sawn boards, the algorithms predicted a total of 95 clear boards and 114 with defects. Thus, the clear board face prediction had an accuracy rate of 90.5%. In addition, the algorithms predicted a total of 226 defects scattered among the 114 boards with defects, an average of 1.98 defects per board.

While the numbers of boards from the two species are approximately equal, the numbers of defects observed on board faces were not. A total of 191 defects were observed on the red oak board faces, while only 89 defects were observed on the yellow-poplar boards (Table 3). Table 3 lists the types and counts of defects observed on the board faces by species and overall. A number of the defects, 91, were attributed to defects not detected on the log surfaces during manual inspection. Deducting this number from the total defect population yields the maximum number of defects that the algorithms can reasonably predict. Thus, there were 132 defects in the red oak logs and 57 defects in the yellow-poplar logs for a total of 189 defects that the algorithm could predict (Table 3).

Table 3—Summary of defects on board faces attributed to detected surface defects

	Overall, both species				Red oak				Yellow-poplar			
Surface defect type	Defects (No.)	Matches (No.)	Match (%)	Misses (No.)	Defects (No.)	Matches (No.)	Match (%)	Misses (No.)	Defects (No.)	Matches (No.)	Match (%)	Misses (No.)
Not detected	91				59				32			
Adventi-tious knot	11	5	45.5	6	11	5	45.5	6	0	0		0
Light distortion	14	8	57.1	6	8	4	50.0	4	6	4	66.7	2
Medium distortion	18	10	55.6	8	15	7	46.7	8	3	3	100.0	0
Heavy distortion	13	11	84.6	2	8	7	87.5	1	5	4	80.0	1
Overgrown knot	66	58	87.9	8	48	40	83.3	8	18	18	100.0	0
Sound knot	17	11	64.7	6	14	9	64.3	5	3	2	66.7	1
Unsound knot	7	2	28.6	5	7	2	28.6	5	0	0		0
Bump	6	2	33.3	4	4	2	50.0	2	2	0	0.0	2
Adventi-tious knot cluster	24	12	50.0	12	10	7	70.0	3	14	5	35.7	9
Sound knot cluster	3	1	33.3	2	3	1	33.3	2	0	0		0
Overgrown knot cluster	10	9	90.0	1	4	3	75.0	1	6	6	100.0	0
Total from detected	189	129	68.3	60	132	87	65.9	45	57	42	73.7	15
Total observed	280				191				89			15

Overall, the models predicted the occurrence of 129 of 189 possible defects, at an overall accuracy rate of 68.3%. Model performance varied between the two species with the yellow-poplar model performing

slightly better. The yellow-poplar model had an accuracy rate of 73.7% and managed to predict all knots that originated from the medium distortion, overgrown knots, and overgrown knot cluster defect types (Table 3). The red oak model had an overall accuracy rate of 65.9%. The red oak model performed best with heavy distortions and overgrown knots for which it predicted the occurrence of 87.5% and 83.3%, respectively, of all resulting knot defects.

With respect to the knot defects that the models predict, there are two types of errors that can occur: positional and area. Positional error is the distance between the center of the actual defect and the center of the predicted defect. Area error is the difference between the actual defect surface area on the board and the predicted surface area. Table 4 summarizes the positional error for the models by species, overall, and by sawn board position. In Table 4 the "First 4 boards", "First 3 boards", and "First 2 boards" refer to subsamples combined of both species that consist of only the first specified number of boards sawn from the log from any face. There were a total of 137 boards sawn in the first 2 sawing passes, 173 in the first 3 passes, and 200 in the first 4 passes. Thus, the "First 2 boards" set is composed of the boards closest to log surface and are typically higher quality boards. It is important to note that boards were sawn from all four faces of the log. However, not all faces of all logs produced 2, 3, or 4 boards. In fact, some smaller logs were sawn only on two faces.

Table 4—Summary of positional differences between predicted and actual defects

Board and species grouping	Average (in.)	Minimum (in.)	Median (in.)	Maximum (in.)	Standard deviation (in.)
Red oak	1.28	0.06	1.03	5.00	0.98
Yellow-poplar	1.43	0.19	1.25	4.00	0.95
Both species	1.30	0.06	1.13	5.00	0.97
First 4 boards	1.33	0.06	1.13	5.00	0.97
First 3 boards	1.29	0.06	1.13	5.00	0.97
First 2 boards	1.33	0.13	1.00	4.00	0.88

The average positional error for all boards and defects was 1.30 in. with a median of 1.13 in. and an overall maximum of 5.00 in. The red oak positional errors were slightly less than those observed with yellow-poplar (Table 4). Red oak had an average positional error of 1.28 in. with a median of 1.03 compared to an average of 1.43 in. and a median of 1.25 in. for yellow-poplar. There was little difference among the boards from the different sawing passes, except that the median, maximum error size, and standard deviation were all lowest with the boards sawn in the first two passes. This tends to indicate that the models are slightly more accurate at predicting the position of the defect the closer it is to the surface of the log. This is logical when you consider it is in these sawing passes that the internal defects are closest to the surface indicator.

Table 5 summarizes the differences between the observed defect and predicted defect areas. The average area difference for both species combined was 10.50 $in.^2$, which corresponds to a 3.24-in. error in both the predicted width and length diameters of the board surface defect. The median error for both species was 5.96 $in.^2$ and indicates a width and length error of 2.40 $in.^2$ The maximum size error of 47.06 $in.^2$ occurred with the red oak model and a sound knot defect measuring 13.25 × 9.875 in. on the log surface. The actual defect dimensions on the board were 1.875 × 3.5 in. whereas the model predicted a knot of 5.5 ×

9.75 in. The standard deviation for all board and species groupings ranged from a low of 10.43 in. with red oak to a high of 11.73 in. with yellow-poplar.

Table 5—Summary of area differences between predicted and actual defects

Board and species grouping	Average ($in.^2$)	Minimum ($in.^2$)	Median ($in.^2$)	Maximum ($in.^2$)	Standard deviation ($in.^2$)
Red oak	9.46	0.13	5.06	47.06	10.43
Yellow-poplar	12.75	0.17	9.14	39.10	11.73
Both species	10.50	0.13	5.96	47.06	11.07
First 4 boards	10.63	0.13	6.02	47.06	10.94
First 3 boards	11.02	0.17	6.97	47.06	10.88
First 2 boards	12.04	0.17	8.88	47.06	11.24

The models predicted a total of 94 false positive defects, 70 on the red oak boards and 24 on the yellow-poplar boards. A false positive defect is one that the model predicts, which does not actually exist. The average yellow-poplar false positive was nearly 4 $in.^2$ larger than those predicted by the red oak model (Table 6). In addition, the median red oak false positive was 2.5 $in.^2$ while the yellow-poplar median was 6.19 $in.^2$ Examining the false positive errors from the different board sawing passes, we found that overall there was little to no difference among the results, with the exception the average size. Between the second and third passes and the third and fourth passes, the average size of the false positive decreased approximately 1 $in.^2$ in both cases. This is to be expected, as the prediction models anticipate the size of the defect decreasing as it nears the center of the log.

Table 6—Summary of false positive defect areas by species, overall, and board position.

Board and species grouping	Average ($in.^2$)	Minimum ($in.^2$)	Median ($in.^2$)	Maximum ($in.^2$)	Standard deviation ($in.^2$)	Defects (No.)
Red oak	6.10	0.13	2.50	70.69	11.84	70
Yellow-poplar	11.05	0.19	6.19	43.75	11.18	24
Both species	7.36	0.13	2.91	70.69	11.82	94
First 4 boards	7.36	0.13	2.91	70.69	11.82	94
First 3 boards	8.33	0.19	3.00	70.69	13.06	73
First 2 boards	9.29	0.19	3.00	70.69	13.95	61

Overall, there were 60 missed defect areas that were associated with a log surface indicator (Table 7). Of the 60, 15 were from yellow-poplar boards and on the whole were small in area. The average surface area was 1.64 $in.^2$ with a median of 1.25 $in.^2$. The red oak boards had a total of 45 missed defects with a much larger average size of 7.59 $in.^2$. The large average size was heavily influenced by nine knot defects that were greater than 10 $in.^2$. The majority of the knots were much smaller, 30 of 45 being less than 2 $in.^2$ in surface area. This observation is reflected in the low median surface area size of 1.13 $in.^2$. Examining the missed defect summaries by sawing pass, we saw no real difference between the defect size statistics for all defects versus those discovered on the first 4, 3, and 3 boards sawn from a face.

The other type of missed defects is those that we observed that did not have an associated log surface defect indicator. Table 8 summarizes the sizes and counts of these defects. There were a total of 91 of this type of defect on the board surfaces. In general, they were quite small with an overall average size of 0.63

in.^{2} with a median of 0.36 in.^{2}. Thirty-two of the defects were from the yellow-poplar boards and had an average size of 1.01 in.^{2} and a maximum of 6.56 in.^{2}. Most (58) of the defects were found on the boards sawn from the red oak logs. With an average size 0.41 in.^{2} and a maximum of 1.78 in.^{2}, the red oak defects were much smaller than the yellow-poplar knot defects.

Table 7—Summary of missed defect areas that had log surface indicators by species, overall, and board position.

Board and species grouping	Average (in.^{2})	Minimum (in.^{2})	Median (in.^{2})	Maximum (in.^{2})	Standard deviation	Defects (No.)
Red oak	7.59	0.02	1.13	50.75	14.26	45
Yellow-poplar	1.64	0.06	1.25	8.27	1.98	15
Both species	6.10	0.02	1.13	50.75	12.63	60
First 4 boards	6.34	0.02	1.29	50.75	12.55	59
First 3 boards	6.40	0.06	1.13	50.75	13.25	53
First 2 boards	6.45	0.06	1.13	50.75	13.31	41

Summary and Conclusion

There were a total of 218 defects recorded and measured on the surfaces of the 20 logs used in this validation study. Not all surface defects caused an internal defect to appear on a board face. Of the 218 surface defects, only 118 were linked to a board surface defect. One reason for this is that some of the surface defects such as the adventitious knots and clusters as well as bumps are often superficial and are completely removed from the log when the slabs are sawn from the log. The 118 log surface defects were linked to 189 defects observed on the outer face of the sawn lumber. The models predicted 129 of the 189 board surface defects, an overall accuracy rate of 68.3%. The yellow-poplar prediction model performed better than did the red oak model, 73.7% accuracy versus 65.9% accuracy (Table 3).

An additional 91 knot defects were found on the board faces that were not traceable to any detected surface defects. However, these defects were small with an average size of 0.63 in.^{2} and a median size of 0.36 in.^{2} (Table 8). A 0.36 in.^{2} defect would measure 0.6 in. on each edge. The defects found on the red oak boards were smaller than those encountered on the yellow-poplar boards with a median size of 0.20 in. versus 0.59 in.

Table 8—Summary of missed defects that had no surface indicator by species, overall, and board position.

Board and species grouping	Average (in.^{2})	Minimum (in.^{2})	Median (in.^{2})	Maximum (in.^{2})	Standard deviation (in.^{2})	Defects (No.)
Red oak	0.41	0.02	0.20	1.78	0.44	58
Yellow-poplar	1.01	0.06	0.59	6.56	1.41	32
Both species	0.63	0.02	0.36	6.56	0.96	90
First 4 boards	0.70	0.02	0.38	6.56	1.03	77
First 3 boards	0.77	0.02	0.41	6.56	1.18	50
First 2 boards	0.42	0.04	0.36	1.13	0.37	22

In the future we plan to expand prediction models to include additional species as well as look at ways of improving the accuracy of the existing models using different statistical and modeling methods. In addition, the combination of the log scanning and defect detection system and the internal defect prediction models need to be tested in a real sawmill environment. It is possible to develop a system that scans the board faces as sawing progresses. This would allow the system to determine its own accuracy, as well as give it the potential to add defect data to the system and allow it to learn from experience.

Literature Cited

Hanks, L. F., G. L. Gammon, R. L. Brisbin, and E.D. Rast. 1980. Hardwood log grades and lumber grade yields for factory lumber logs. Res. Pap. NE-468 Broomall, PA: U.S. Department of Agriculture, Forest Service, Northeastern Forest Experiment Station. 32 p.

Hyvarinen, M.J. 1976. Measuring quality in standing trees—Depth of knot-free wood and grain orientation under sugar maple bark distortions with underlying knots. PhD Dissertation. University of Michigan. 142 p.

Lemieux, H., M. Beaudoin, S.Y Zhang. 2001. Characterization and modeling of knots in black spruce (*Picea mariana*) logs. Wood and Fiber Science. 33(3): 465–475.

Rast, Everette D., D. L. Sonderman, and G. L. Gammon. 1973. A guide to hardwood log grading. Gen. Tech. Rep. NE-1. Upper Darby, PA: U.S. Department of Agriculture, Forest Service, Northeastern Forest Experiment Station. 32 p.

Schultz, H. 1961. Die Beurteilung der Qualitätsent wicklung junger Bäume. Forstarchiv XXXII (May 15 1961): 89–99.

Shigo, A.L.; Larson, E. vH. 1969. A photo guide to the patterns of discoloration and decay in living northern hardwood trees. Research Paper NE-127. Northeastern Forest Experiment Station, US Department of Agriculture, Forest Service. 100 p.

Steele, P.H.; T.E.G. Harless, F.G. Wagner, L. Kumar, and F.W. Taylor. 1994. Increased lumber value from optimum orientation of internal defects with respect to sawing pattern in hardwood logs. Forest Product Journal. 44(3): 69–72.

Stringer, K.W. Gottschalk, G.W. Miller, eds. In: Proceedings, 17th Central Hardwood Forest Conference; 2010 April 5-7; Lexington, KY. Gen. Tech. Rep. P-78. Newtown Square, PA: U.S. Department of Agriculture, Forest Service.

Thomas, L.; Mili, L,; Thomas, R.E.; Shaffer, C.A. 2006. Defect detection on hardwood logs using laser scanning. Wood and Fiber Science. 38(4): 682–695.

Thomas, L.; Thomas, R.E. 2011. A graphical automated detection system to locate external hardwood log surface defects using high resolution 3-D laser scan data. In: Fei, Songlin; Lhotka, John M.; Stringer, Jeffrey W.; Gottschalk, Kurt W.; Miller, Gary W., eds. Proceedings, 17th central hardwood forest conference; 2010 April 5-7; Lexington, KY; Gen. Tech. Rep. NRS-P-78. Newtown Square, PA: U.S. Department of Agriculture, Forest Service, Northern Research Station: 92-101.

Thomas, R. E. 2008. Predicting internal yellow-poplar log defect features using surface indicators. Wood and Fiber Science. 40(1): 14–22.

Thomas, R. E. 2013a. RAYSAW: a log sawing simulator for 3D laser-scanned hardwood logs. In: Miller, Gary W.; Schuler, Thomas M.; Gottschalk, Kurt W.; Brooks, John R.; Grushecky, Shawn T.; Spong, Ben D.; Rentch, James S., eds. Proceedings, 18th Central Hardwood Forest Conference; 2012 March 26-28; Morgantown, WV; Gen. Tech. Rep. NRS-P-117. Newtown Square, PA: U.S. Department of Agriculture, Forest Service, Northern Research Station: 325–334.

Thomas, R.E. 2013b. Predicting internal red oak (*Quercus rubra*) log defect features using surface defect measurements. In: G.W. Miller, T.M. Schuler, K.W. Gottschalk, J.R. Brooks, S.T. Grushecky, B.D. Spong, J.S. Rentch, eds. Proceedings, 18th Central Hardwood Forest Conference; 2012 March 26-28; Morgantown, WV; Gen. Tech. Rep. NRS-P-117. Newtown Square, PA: U.S. Department of Agriculture, Forest Service, Northern Research Station: 313–324. (Refereed)

Wagner, F.G.; Harless, T.E.G.; Steele, P.H.; Taylor, F.W.; Yadama, V.; McMillin, C.W. 1990. Potential benefits of internal log scanning. In Proceedings of Process Control/ Production Management of Wood Products: Technology for the 90’s. Athens, GA: 77–88.

Automated wood species identification by CT-technology

Udo H. Sauter
Forest Research Institute Baden-Württemberg (FVA), Department of Forest Utilisation, Wonnhaldestr. 4, 79100 Freiburg im Breisgau, Germany, udo.sauter@forst.bwl.de

Nicola Bertolini
Microtec GmbH Srl, Via Teano 1, 30174 Venezia, Italy, nicola.bertolini@microtec.eu

Norvin Laudon
Springer Microtec Inc., Suite#201 West Broadway, Vancouver, V6J1Y6, BC, Canada, norvin.laudon@springer-microtec.com

Rafael Baumgartner
Forest Research Institute Baden-Württemberg (FVA), Department of Forest Utilisation, Wonnhaldestr. 4, 79100 Freiburg im Breisgau, Germany, rafael.baumgartner@forst.bwl.de

Diana Hoyos-Montoya
Forest Research Institute Baden-Württemberg (FVA), Department of Forest Utilisation, Wonnhaldestr. 4, 79100 Freiburg im Breisgau, Germany, diana.hoyos@forst.bwl.de

Stefan M. Stängle
Forest Research Institute Baden-Württemberg (FVA), Department of Forest Utilisation, Wonnhaldestr. 4, 79100 Freiburg im Breisgau, Germany, stefan.staengle@forst.bwl.de

Franka Brüchert
Forest Research Institute Baden-Württemberg (FVA), Department of Forest Utilisation, Wonnhaldestr. 4, 79100 Freiburg im Breisgau, Germany, franka.bruechert@forst.bwl.de

Abstract

The introduction of X-ray computed tomography (CT) for automated detection of log internal features for value optimisation in real industry processes is in full progress. For the detection and identification of quality relevant log internal features, such as knots or cracks, species specific algorithms have been developed. The correct species identification in the mill is crucial to make use of the correct algorithms and attribute the logs to the right product line. In this study we developed an automated identification system using CT and Artificial Neural Networks (ANNs) for five different softwood species: Norway spruce (*Picea abie*s [L.] Karst), Silver fir (*Abies alba* [Mill.]), Scots Pine (*Pinus sylvestris* [L.]), Pinus nigra (*Pinus nigra* [Arn.]), and Douglas fir (*Pseudotsuga menziesii* [Mirb.] Franco). Based on the differentiation of biological characteristics, we developed a set of algorithms that allowed to extract the species information from the distribution of log internal features in CT-images. The developed system could distinguish between Norway spruce, Silver fir, Pine and Douglas fir with a true positive rate of over 0.97 for each of the species.

Keywords: X-ray computed tomography, artificial neural networks, log sorting, wood quality, optimisation

Introduction

The introduction of X-ray computed tomography (CT) for automated detection of log internal features for value optimisation in real industry processes is in full progress. First industrial CT scanners haven been successfully installed in saw mills. For the detection and identification of quality relevant log internal features, such as knots or cracks, species specific algorithms have been developed. Due to fully mechanised harvesting processes, arriving truck loads at mills often consist of logs of different tree species. The correct species identification in the mill is crucial to make use of the correct algorithms and attribute the logs to the right product line.
Different systems have been developed for automated species identification of wood. Mohan et al. (2014) developed a recognition system for the identification of wood species based on textural features using high digital cameras. This system was implemented for 10 Indian wood species and shows an accuracy of more than 95% (Mohan et. al. 2014) Another system was proposed for wood species classification based on a laser source and a spectrometer (Piuri and Scotti 2010). This system classifies the wood species by analysing the fluorescence spectra of the wood. In a next step, a processing system extracts wood features and uses them to train an inductive classification system. Another wood species identification system was developed using an industrial monochrome CCD camera and based on image processing, feature extraction and artificial neural networks (Khalid et al 2008). Wood species classification with CT was developed by Grundberg (1999).
The aim of this study was to develop an automated classification system based on CT-data using Artificial Neural Networks(ANNs) for five common softwood species in Europe: Norway spruce (*Picea abie*s [L.] Karst), Silver fir (*Abies alba* [Mill.]), Scots Pine (*Pinus sylvestris* [L.]), Pinus nigra (*Pinus nigra* [Arn.]), and Douglas fir (*Pseudotsuga menziesii* [Mirb.] Franco).

Material and Methods

Sample Logs

A total of 2700 logs of different length were selected and the tree species was manually determined by experts. Due to their similarity, the two species of the genus *Pinus* were grouped, making 1099 Norway spruce logs, 738 Silver fir logs, 333 Pine logs, and 530 Douglas fir logs. All logs were scanned with high speed CT scanner CT.Log (Microtec, Italy) at the sawmill SIAT Braun (France) at a feeding speed of 120 $m * min^{-1}$. The CT.Log scanner output is a 3D reconstruction of the logs, with a cross sectional resolution of 1x1mm and a longitudinal resolution of 11 mm.
CT images were analysed for species specific internal feature patterns to be able to distinguish one species from the others based on those features. Some of these features were known before the investigation. For example, it is well known that the absence of small branches between the knotty whorls can distinguish Pine from other species. Making use of this knowledge, we developed a set of algorithms, which allowed to identifying such features in our dataset. As follows, the examined features are listed.

Algorithm development

Algorithms were developed to extract the following feature information from each log:

- sapwood density
- heartwood density
- heartwood percentage
- mean radius of sapwood
- number of knots per meter
- inclinational angle of knots
- number of whorls

- whorl clustering
- knot distribution along the log
- spiral grain
- growth ring description
    - uniformity of growth rings
    - growth ring width

Feature Selection

To distinguish between species based on their feature distribution as a first step the feature distribution was compared for pairs of species.
For each of the listed features histograms of their occurrence were compared and sigmoid-based scoring functions were calculated for each pair of species. The scoring functions were fitted on 2/3 of random samples and evaluated with the remaining 1/3 of logs.

ANN Classifier

Making use of the information obtained by the feature selection we built our customized ANN binary classifier for each pair of species. It is composed of a single layer of neurons that are fed with the values from the features as input. The weighted sum of the scoring results gives the output, which can be interpreted as the species identification (Figure 1).

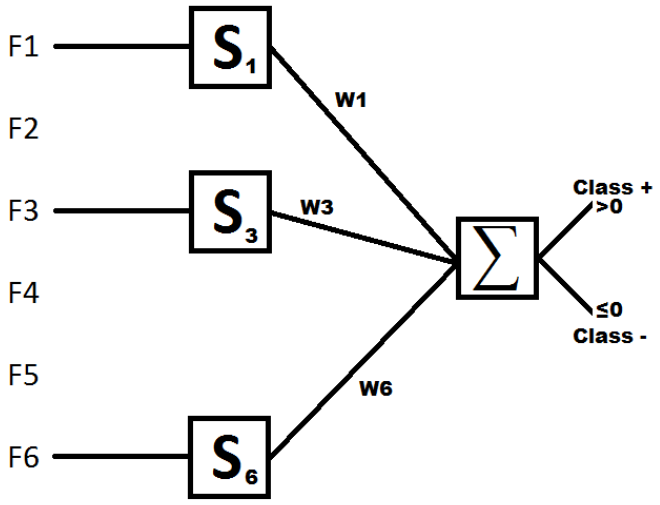

Figure 1—Structure of the artificial neural network binary species classifier. F1-F6 are values for log-internal features, S_1, S_2, S_3 are scoring functions, and W1-W3 the weights. $\sum$ is the sum.

The evaluation of the classifier was based on two metrics: the correctness of the scoring function and features usefulness. Once a good classifier for a given pair of species was built, we tried to eliminate features with the purpose to find the simplest classifier for a given pair of species.
The six developed binary classifiers were combined to an ANN Multiclass that was used to identify the tree species from all tested logs of the four species.

Results and Discussion

The developed classifier showed good performance with 2650 from 2700 correctly identified logs (Table 1). The true positive rates were above 0.97 for all tested species (Table 2).

Table 1—Confusion matrix of the results from the multiple ANN species identifier

		predicted			
		Norway spruce	Silver fir	*Pinus*	Douglas fir
actual	Norway spruce	1086	10	0	3
	Silver fir	8	719	0	11
	Pinus	0	2	331	0
	Douglas fir	10	6	0	514

Table 2— True positive rates for species identification with the multiple ANN

Species	True positive rate
Norway spruce	0.988
Silver fir	0.974
Pinus	0.994
Douglas fir	0.970
total	0.981

Conclusions

The developed species identification system based on data from high speed CT scanning proved to work well for the tested logs.
The classifier was trained on trees that were grown under similar climatic conditions. This classifier may not be valid in other areas with different climates. If new species are intended to be added, new classifiers need to be developed and the selection of new features has to be considered. We suggest using a training dataset of at least 300 logs per species to train the classifier in a new region or for a new species.
Further studies on additional features, especially for Norway spruce and Silver fir, are recommended.

References

Grundberg, S. 1999. An X-ray logscanner – a tool for the control of the sawmill process. Doctoral thesis. Division of Wood Technology, Luleå, University of Technology, Skelleftea, Sweden (ISSN 1402-1544). 210p.

Khalid, M., Lee, E. L. Y., Yusof, R. [and others]. 2008. Design of an intelligent wood species recognition system. International Journal of Simulation System, Science and Technology, 9(3): 9-19.

Mohan, S., Venkatachalapathy, K.,Sudhakar, P. 2014. An intelligent recognition system for identification of wood species. Journal of Computer Science, 10(7): 1231-1237.

Piuri, V., Scotti, F. 2010. Design of an automatic wood types classification system by using fluorescence spectra. Systems, Man, and Cybernetics, Part C: Applications and Reviews, IEEE Transactions on, 40(3): 358-366.

Influence of the diameter on the ultrasound waves velocity in Round timber

Monica Ruy
Laboratory of Nondestructive Testing - LabEND, College of Agricultural Engineering - FEAGRI - University of Campinas - UNICAMP, Campinas, São Paulo, Brazil – monica.ruy@hotmail.com.

Douglas Pereira Maraes
LabEND - Feagri,Unicamp, Campinas, São Paulo, Brazil, douglaspm1409@gmail.com

Cinthya Bertoldo
LabEND - Feagri,Unicamp, Campinas, São Paulo, Brazil, cinthyabertoldo@gmail.com

Raquel Gonçalves
LabEND - Feagri,Unicamp, Campinas, São Paulo, Brazil, raquel@feagri.unicamp.br

Abstract

The use of logs in its original shape, as round timber, has been considered economically competitive and sustainable, making the development of techniques that allow their classification important. The objective of this research was to evaluate the influence of the log diameter on velocity of ultrasound wave propagation. The ultrasound tests were performed in eucalyptus (*Eucalyptus grandis*, *Eucalyptus cloeziana*, *Eucalyptus resinifera*, *Eucalyptus maculata*) and *Pinus elliottii* round timber. For Eucalyptus there was found no statistical differences on velocity among the different diameter ranges. Using a specific sample (*Eucalyptus grandis*) the moisture conditions and the type of transducer didn´t interfere on the behavior of the analysis. For *Pinus elliottii* a statistical difference was detected, indicating different performances between the results for hardwoods and softwoods.

Keywords: ultrasound, round timber, diameter

Introduction

The use of logs in its original shape, as round timber, has been considered economically competitive and sustainable, making the development of techniques that allow their classification important.

Significant savings could be obtained if there were an evaluation of wood quality before the sawing process and drying the logs (Kretschmann & Hernandez, 2006). According to Sandoz (1994 *apud* Pelizan 2004) 80% to 90% quality measured by ultrasound in the logs will be kept in lumber. Thus, the round wood classification is also interesting to the lumber industry as it increases the reliability of the mechanical performance of the beams.

Tsehaye *et al* (2000) evaluated the profitability of the round wood rating, via nondestructive testing, by measuring the time of stress wave's propagation. Their data indicated that if there is the possibility of identifying low resistance logs before processing, unnecessary processing would be avoided and costs would be reduced.

The log resistance, low energy consumption for its processing, availability and easy handling make the round wood a highly competitive and sustainable material (Calil Jr. and Brito, 2010) and can be directly used as structure (poles , beams, columns etc.).

Wang *et al* (2002) analysed the influence of the logs' diameter on the wave propagation and they concluded that the larger the diameter of the log, the larger the difference between the static modulus of elasticity obtained in the bending tests, and dynamic elasticity modulus obtained in wave propagation tests. A study by Pelizan (2004) obtained similar results presenting significant effect of the log's diameter on wave propagation.

Research in progress on Feagri's Non-destructive Testing Laboratory aims to propose and evaluate Eucalyptus round timber grading through acoustic parameters. Therefore, it is important to know factors that may influence the classification in order to propose more efficient and accurate method. Thus, the present research aims to evaluate the influence of the diameter of round wood on ultrasound waves' propagation.

Material and Methods

Round timber of four species of Eucalyptus (*Eucalyptus grandis*, *Eucalyptus cloeziana*, *resinifera Eucalyptus*, *Eucalyptus maculate*) and *Pinus Elliottii* were used in this study. They were segregated in 10 different diameters ranges (Table 1).

Table 1— Predetermined diameter ranges.

Range	Diameter (m)
1	0,05 - 0,1
2	0,10 - 0,15
3	0,15 - 0,20
4	0,20 - 0,25
5	0,25 - 0,30
6	0,30 - 0,35
7	0,35 - 0,40
8	0,40 - 0,45
9	0,45 - 0,50
10	> 0,50

The ultrasound tests were performed with ultrasound equipment (USLab, Agricef, Brazil) and longitudinal transducer of 45 kHz. The measurements were made directly and parallel to the fibre (lengthwise) (Figure 1). Three repetitions were performed for each measurement point, in order to minimize any measurement error.

Figure 1— Direct testing with longitudinal ultrasound waves propagation on the log.

One of the species (*Eucalyptus grandis* 1) was chosen to verify whether the moisture condition (green or equilibrium) or the type of transducer (flat or dry point) would affect the result of the analysis factor that is the focus of this research - diameter. We know that moisture condition directly affects the ultrasound velocity. The purpose of this test is not to analyse this issue. The purpose of this test is to analyse if the relationship between the ultrasound velocity and the logs' diameter is different for green and equilibrium conditions. The same way, we know that if we use the same frequency transducer (45 kHz), the velocity should be very similar. Comparing these results is not the focus of this analysis, but the measurement methodology. The coupling of the dry point transducer is made through a small hole, whereas medicinal gel was used for the flat face transducer.

Thus, 18 logs were tested for one of the *Eucalyptus grandis* sample. These logs were segregated in three diameter ranges (6 logs in each range) and they were tested in two moisture conditions (green and equilibrium) and it was used two types of transducer (dry point and flat - Figure 2), both 45 kHz frequency. At first the logs were tested in green condition. Then they were placed in drying chamber until they reached the equilibrium moisture (around 12%) and tested again in this condition. The monitoring of moisture during drying was performed with contact moisture meter (pinless).

For the other species the number of logs in each diameter range depended on the sample (Figure 3). For statistical analysis was only considered the diameter ranges that contained at least 4 logs.

A B

Figure 2. Exponential (A) and flat (B) transducers

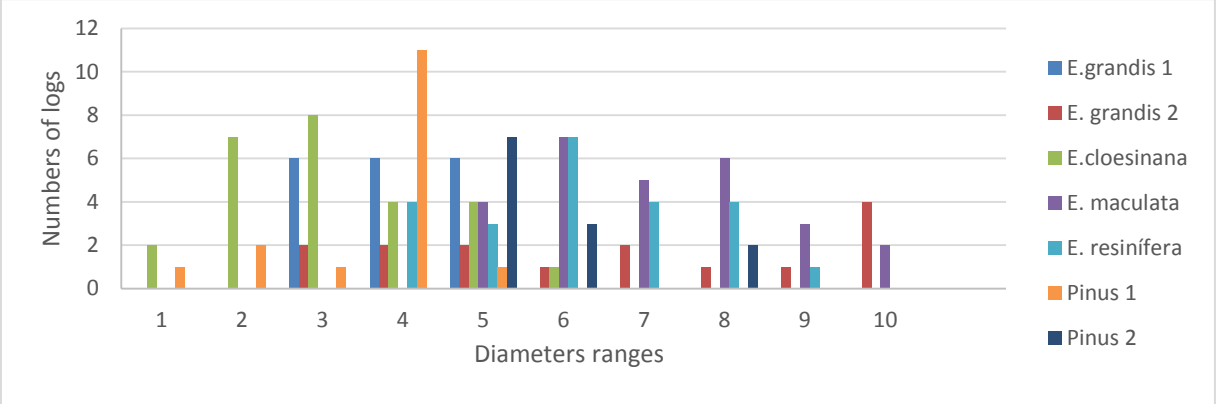

Figure 3. Number of logs by species in each diameter range.

Before starting the statistical evaluations of the main purpose of the research, the data's normality was checked. This evaluation was important to validate the statistical tests. For this analysis it was used parameters of skewing and kurtosis. The data is considered as normal distribution when these values are between -2 and +2.

The statistical significance of the difference in averages of velocities among the log diameter ranges was evaluated by P-value. When the P-value is less than or equal to 0.05 in the Anova Table, there is significant statistical difference in averages among the parameters evaluated, with 95% reliability.

Results and discussions

The values of skewing and kurtosis of the velocities obtained for each species were between -2 to +2, what indicated that the normality hypothesis can be accepted.

Statistical analysis of the *Eucalyptus grandis* 1 sample indicated that the type of transducer and moisture condition did not affect the outcome of the influence analysis of the diameter. In regards to the influence of diameter, the same result for green wood and dry wood was obtained, as well as for flat or dry point transducer, indicating that the result of diameter influence will not be affected by these parameters.

The multiple comparison analysis of velocities in the different samples indicated that for the *Eucalyptus* species, in general, velocity did not vary in different diameter ranges, except for the *Cloesiana Eucalyptus* (Table 2). For *Pinus*, only Sample 2 could be used, as in Sample 1 there were logs from just one diameter range, making impossible to perform statistical comparison (Table 2). The results obtained for *Pinus* corroborate previous conclusion of Wang *et al* (2002), that wave propagation velocity in round wood is influenced by its diameter. However, for hardwood the performance doesn't follow the same pattern.

Table 2 — Multiple comparision analysis parameters obtained for each sample on the different diameter ranges.

Sample	Coefficient of Variation (%)	P-Value	Analysis' Conclusion
E. cloeziana	9,67	0,00	There was statistical difference of the velocities in different diameter ranges
E. maculata	12,60	0,97	There was no statistical difference of the velocities in different diameter ranges
E. resinifera	6,51	0,55	There was no statistical difference of the velocities in different diameter ranges
E. grandis 1	5,16	0,19	There was no statistical difference of the velocities in different diameter ranges
E.grandis 2	9,67	0,39	There was no statistical difference of the velocities in different diameter ranges
Pinus 1	15,10	-	It was not possible to compare
Pinus 2	11,86	0,00	There was statistical difference of the velocities in different diameter ranges

Conclusions

For hardwoods, in general, it was not identified influence of diameters on the ultrasound waves' velocity, but a different result was obtained for the softwood.

Acknowledgments

We thank FAPESP for financially supporting research group (Proc. 2012 / 22599-9) and for the PhD scholarship (Proc. 2011 / 00904-1). We also thank CNPq for the Master's and undergraduate scholarships.

References

Calil Jr., C.; Brito, L.D. 2012. Manual de Projeto e Construção de Estruturas com Peças Roliças de Madeira de Reflorestamento. University of São Paulo, Escola de Engenharia de São Carlos. 332p.

Kretschmann, D.; hernandez, R. 2006. Grading timber and glued structural members. Primary wood processing: principles and practice. Dordrecht, Springer: 339-390.

Pelizan, T.R. 2004. Estudo de propriedades mecânicas de peças roliças de Eucalipto Citridora utilizando a técnica de ultra-som. São Carlos, SP: University of São Paulo. M.S. thesis.

Sandoz, J.L. 1994. Ultrasound applications to structural timber. In: Pacific Timber Engineering Conference – PTEC´94. Gold Coast, Australia. p. 740-744.

Tsehayve, A.; Buchanan, A.H.; walker, J.C.F. 2000. Sort of logs using acoustics. Wood Science and Technology, v. 34, p. 337-344.

WANG, X. [and others]. 2004. Diameter effect on stress-wave evaluation of Modulus of elasticity of logs. Wood and Fiber Science**.** 36(3): 368-377.

Two dimensional image construction of ultrasonic wave for detecting internal hole defect in log disc

Huadong Xu
College of Engineering& Technology, Northeast Forestry University, Harbin ,China,
huadongxu@yahoo.com

Lihai Wang
College of Engineering& Technology, Northeast Forestry University, Harbin ,China,
lihaiwang@yahoo.com

Shan Gao
College of Engineering& Technology, Northeast Forestry University, Harbin ,China,
gaoshan_2000@126.com

Shiquan Song
College of Engineering& Technology, Northeast Forestry University, Harbin ,China, 271204089
@qq.com

Abstract

The ultrasonic propagation parameters in Amur Linden (*Tilia amurensis Rupr.*) log specimen which was in intact and defective status respectively were measured and obtained. These parameters were then used as training set and test set to classify the hole size in log based on support vector machine (SVM). Furthermore, a kind of method to quantitatively determine the location of defect point on the cross section of log was proposed and improved. Based on this, the two dimensional simulation image of internal hole defect in log was constructed. The results show: (1) it is feasible to classify the hole size in log using SVM and the identification accuracy is 84.78%; (2) the two dimensional simulation image of hole defect in the cross section is in good agreement with the actual image of log specimen.

Keywords: ultrasonic wave, log, support vector machine, image construction

Introduction

Among several common techniques for nondestructive test of wood quality, the resolution of stress wave tomography is not high enough and the cost of computer tomography (X-rays) is not low (Ozyhar et al., 2013). Thus, it is essential to search new method to construct two-dimensional tomography. Recently, the image constructive method of two-dimensional tomography based on ultrasonic wave becomes a hot topic for detecting the internal decay of tree (Krause et al., 2013), but this technology is still no substantive breakthrough so far.

Support vector machine (SVM) was introduced to analyze the ultrasonic signal ontained from intact and defective log disc (Wang *et al*., 2008). Based on this, the location and size of hole defect were identified and then the identified results were displyed on two-dimensional plane.

Material and methods

In laboratory, a 5cm-thick *Tilia amurensis* disc, with a diameter of 34cm, was prepared to conduct the ultrasonic wave test at the environment temperature of 15 ℃.The moisture content (MC) of the disc

measured by oven drying method was 95%. Because the MC of wood affects the propagation parameters of ultrasonic wave（Sandoz,1993; Hasegawa et al.,2011）, the disc was tightly wrapped in a plastic bag and stored in a refrigerator at 0~5 ℃ temperature to prevent unintentional MC change before the test was taken.

During the test, thirty points were first drawn on the circumference of the disc (Figure1). Then the circumference was divided into three equal segments by point 1, point 11 and point 21, which were used as the exciting points of ultrasonic signal respectively. Several other points, the distance of which from each exciting point were larger than 33cm, were served as receiving points of ultrasonic signal in sequence. By attaching the exciting senor and the receiving senor, an ultrasonic instrument (RSM-SY5) was used to obtain the ultrasonic signal in the sample. After the intact disc was tested, four different size holes (d=4,6,8 and 10cm, respectively) were artificially drilled at the center of the cross section of the disc in sequence. The sample with different size hole defect was conducted the same above ultrasonic test. Then the ultrasonic signal for the intact and defective samples was obtained.

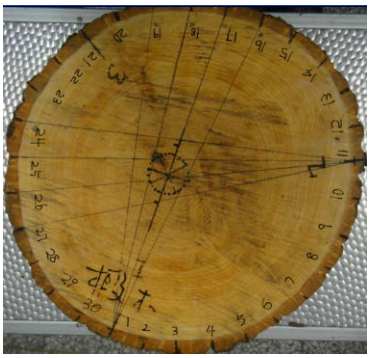

Figure 1— Illustration of ultrasonic wave testing point

Results and discussion

Identification of hole defect size by SVM

The eigenvalue data of the first wave of ultrasonic signal were acquired, which included its amplitude, starting time, period, half wave period, rise time, fall time and average propagation velocity. Thirty-two data sets for intact sample and ninety-one data sets for defective sample were used to analyze the effect of defect size on the ultrasonic wave propagation parameters. SVM was used to classify these data sets and then evaluate the hole defect size. The classification process included training set and test set selection, preliminary prediction of test set, optimization of the penalty parameter c and g, and SVM network training based on the optimal parameters. Finally, the actual classification and prediction results for the test set were shown in Figure 2 with Matlab software. Figure 2 shows that the wrong prediction number for the data set of different size hole defects (d=0cm, 4cm, 8cm and 10cm, respectively) is 1,1,0,2 and 3 respectively. In other words, the overall predictive accuracy rate is 84.78%, which indicates it is feasible to classify the size of internal hole defect in log based on SVM. Through above analysis, we know whether the ultrasonic signal travels through the defective area on the cross section of log when it is obtained by measurement.

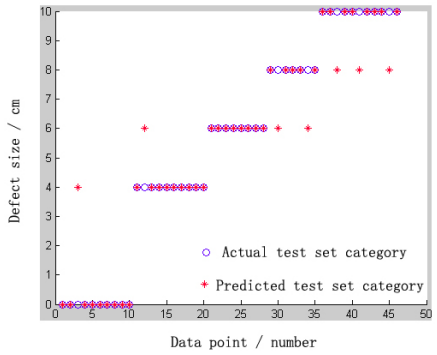

Figure 2— Distribution of real and predicting classification result of test data .Circle indicates the actual classification results, asterisk indicates the prediction results. If their position coincided with each other, which meaned the prediction result was right, otherwise it was wrong.

Localization of internal hole defect in log

After ultrasonic signals obtained from the disc sample were analyzed and classified, it need further to localize the defect position on the cross section of disc. Thus, we proposed an evaluation method: on the cross section of disc, if two lines intersected at point A(x,y) and these two lines were judged to travel through the defective area by SVM, the intersection point A(x,y) was considered as a defect point; otherwise it was not a defect point . Using this method, we can know all defect points.

After all defect points were determined, the location information (coordinate values) of each point should be well defined, which would be use to quantitatively show the position of hole defect on the cross section of log disc using Matlab software in the fallowing discussion. For this purpose, a two dimensional Cartesian coordinate system was artificially constructed. In this coordinate system, the coordinate plane coincided with the sample cross section, the signal exciting point 11 served as the origin, the direction of a connecting line from point 11 to point 26 served as Y axis, the vertical line of which served as X axis.Thus, the coordinate values of the intersection points of the connecting lines from exciting point1, 11 and 21 respectively to other points on the circumference of the log disc, could be determined. For example, when the hole defect sized=10 cm, the coordinate values of the intersection points of the connecting lines, which were from exciting point1and 11 and judged to travel through the defective area by SVM, were shown in Table 1.

Table 1— The coordinate values of intersection point of line through the hole with a diameter of 10 cm when point 1 and 11 are driving point respectively

Driving point-receiving point	11-24	11-25	11-26	11-27	11-28
1-15	(2.7,12.6)	(1.4,13.6)	(0,14.5)	(-1.6,15.9)	(-3.6,17.2)
1-16	(3.2,14.9)	(1.6,15.8)	(0,16.8)	(-1.9,17.9)	(-4.0,19.2)
1-17	(3.6,17.0)	(1.8,17.9)	(0,18.7)	(-2.1,19.7)	(-4.4,20.7)
1-18	(4.1,19.2)	(2.0,19.9)	(0,20.5)	(-2.3,21.1)	(-4.7,22.1)
1-19	(4.5,21.2)	(2.2,21.8)	(0,22.2)	(-2.4,22.8)	(-4.9,23.3)

Figure 3 shows the simulated two dimensional surface of the cross section of the log disc with a hole defect (d=10 cm) using Matlab. In Figure 3a, the big circle served as the edge of cross section , the small circles served as the edge of hole defect, and the symbol "+" served as the position of coordinate point shown in Table 1. The simulated graph showed that the predicting result with the evaluation method mentioned above did not completely cover the defect area. Some erroneous judgment points were found outside of the defect area, which indicated the proposed evaluation method was not perfect. When two lines were judged to travel through the defective area by SVM, the intersection point of them was considered as a defect point using this method, but in some cases it is inconsistent with the actual situation. For example, if two lines intersected at point A, when a line traveled through the defect area before point A and another line traveled through the defect area after point A, the results predicted by this method was obviously wrong. In order to accurately identify the location and shape of the hole defect and make up the deficiency of the method, the intersection points of each rays come from multiple exciting points were used to make the prediction.

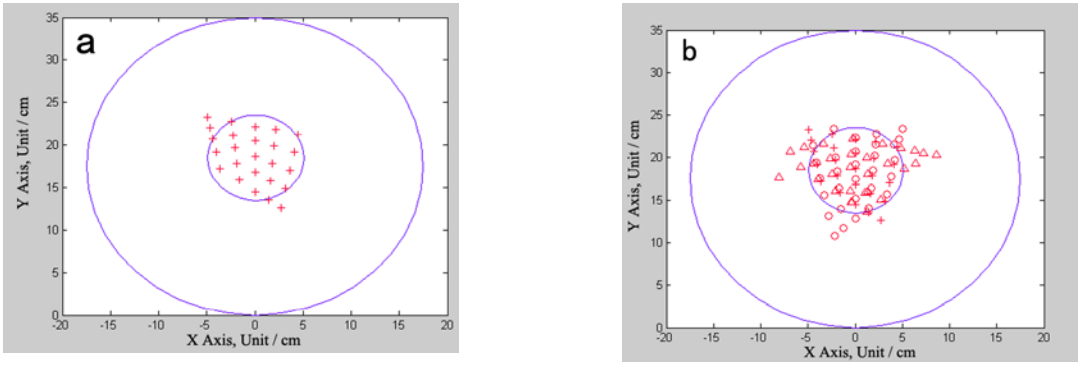

Figure 3— The plotted points simulation of a defective cross section (*d*=10 cm) diameter when point 1 and 11 are driving points (a) and when point 1, 11 and 21 are driving points (b).

Take for example again, the cross section of log disc with a 10cm diameter hole defect. If we used the three equal diversion points (point 1, point 11 and point 21) as exciting point respectively, the intersection points of each rays traveled through the hole defect were drawn in the simulated planar graph, as shown in Figure 3b. In Figure 3b, three different symbols were employed to mark the intersection points of each rays that come from various exciting points. The symbol "+" served as the intersection points of each rays from point 1 and point 11, the symbol "△" served as them from point 1 and point 21 and the symbol "○" served as them from point 11 and point 21. Compared with the actual defects, the comprehensively predicted defect area had a good fitness, although there were still some erroneous judgment points.

In order to make the simulated graph agree the actual hole defect better, it should find a way to remove those erroneous judgment points. Thus, we proposed a method to achieve this aim. If a point and the nearest point around it were marked by same symbol, this point would be removed. Figure 4 shows the plotted points simulation graph of a defective cross section (d=10 cm) when those erroneous judgment points were removed. The simulated plotted points graph predicted the hole defect accurately, which clearly demonstrated the size, location and shape of the actual defect.

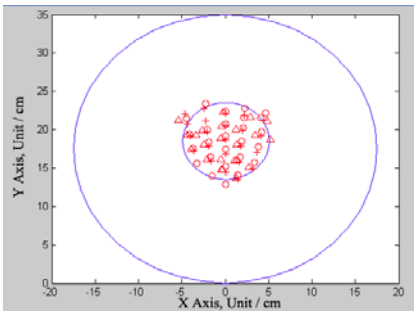

Figure 4—The plotted points simulation of a defective cross section (*d*=10 cm) when erroneous judgment points were removed.

Two dimensional visualization of internal defect in log based on SVM

To visually display the defect information such as size, location and shape on the cross section of log, two dimensional ultrasonic image was constructed. First, a two dimensional Cartesian coordinate system,which represented the cross section of log, was artificially constructed using Matlab. Second, each point on the two dimensional system was assigned a value with a number of 810. That's because the propagation velocity value of ultrasonic wave in intact wood is 810 $m \cdot s^{-1}$known by our previous experiment. Third, according to the above method, the location of all defective points were identified on the two dimensional plane. The value of each defective point was reassigned, the number of which was the larger number between the two propagation velocities of ultrasonic wave traveled through the point.
After assigning value for all points on the cross section, the simulated two dimensional plane was filled by different color based on the value assigned to each point, which would realize the visualization of image. In this process, interpolation processing was first done on the data composed of assigned value, then the plane was filled with bone color using matlab. Figure 5a and Figure 5b were the simulated 2D graph of log sample with a 10 cm hole which included some erroneous judgment points and didn't include the erroneous judgment points respectively. The color was dark in defect area but white in healthy area on the simulated graph (Figure 5). Compared with the actual photo of log sample, the coincidence degree of the simulated 2D graph that didn't include the erroneous judgment points was high, the simulation effect of which was well.

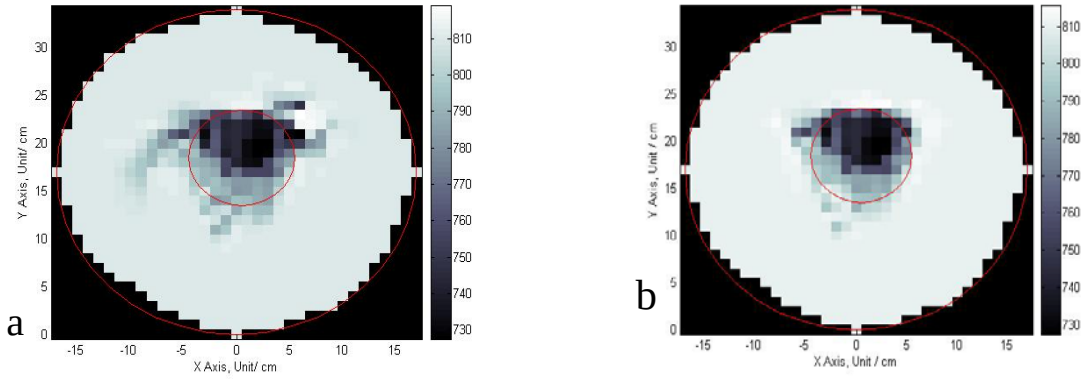

Figure 5— The simulated 2D graph of log sample with a 10 cm hole which includes some erroneous judgment points (a) and doesn't include the erroneous judgment points (b)

Figure 6— The actual photo of log sample

Conclusions

Support vector machine can be used to identify the size of defect on the cross section of log, the accuracy rate of which is 84.78%. We proposed an evaluation method: on the cross section of disc, if two lines intersected at point A(x,y) and these two lines were judged to travel through the defective area by SVM, the intersection point A(x,y) was considered as a defect point; otherwise it was not a defect point .The disadvantage of this method was analyzed and improved. Based on this, two dimensional ultrasonic image of internal defect in log was simulatively constructed based on SVM, which has a good the coincidence degree with actual photo of log sample.

Acknowledgments

This work was financially supported by “the national natural science foundation of China (31300474)”, “China Postdoctoral Science Foundation funded project (2014M551203)” and “the Fundamental Research Funds for the Central Universities of China (2572015CB03)”.

References

Hasegawa M, Takata M, Matsumura J, et al. 2011. Effect of wood properties on within-tree variation in ultrasonic wave velocity in softwood. Ultrasonics, 51(3): 296–302.

Krause M, Chinta P K, Mayer K, et al. 2013. NDT of structural timber members by means of 3D ultrasonic imaging techniques and modelling. Nondestructive Testing of Materials and Structures, 6, 6: 31-36.

Ozyhar T, Hering S, Sergio J. 2013. Determining moisture-dependent elastic characteristics of beech wood by means of ultrasonic waves. Wood Science and Technology, 47(2): 329-341.

Sandoz J L. 1993. Moisture content and temperature effect on ultrasonic timber grading. Wood Science and Technology, 27:373-380.

Wang L, Jia H, Li J. 2008. Training Robust Support Vector Machines with Smooth Ramp Loss in The Primal Space. Neurocomputing, 71（13/15）:3020-3025.

Session 11

Biomass and Pulpwood Assessment

Assessing Specific Gravity of Young *Eucalypt* Plantation Trees Using a Resistance Drilling Technique

José Tarcísio da Silva Oliveira
Forest and Wood Science Department, Federal University of Espírito Santo, Jerônimo Monteiro, ES, 29550-000, Brazil, jose.t.oliveira@ufes.br

Xiping Wang
USDA Forest Service, Forest Products Laboratory, Madison, WI 53726-2398, USA, xwang@fs.fed.us

Graziela BaptistaVidaurre
Forest and Wood Science Department, Federal University of Espírito Santo, Jerônimo Monteiro, ES, 29550-000, Brazil, grazividaurre@gmail.com

Abstract

The objective of this study was to evaluate the use of a resistance drilling technique for assessing wood specific gravity (SG) of young *Eucalyptus* plantation trees for pulpwood production. The genetic materials used in this study consisted of fifty 34-month-old and fifty 62-month-old trees from *Eucalyptus grandis* × *Eucalyptus urophylla* hybrid clonal plantations. A relative resistance profile was measured from each tree at the breast height (BH). Trees were then felled and a 3-cm-thick disc at BH level was removed for laboratory determination of specific gravity (SG) and moisture content (MC). For full drill penetration (drilling through the diameter), the relative resistance (average amplitude) showed a moderate linear relationship with SG (r, the correlation coefficient = 0.73) when two age groups were combined. For half-radius drill penetration, the relative resistance showed a relatively weak correlation (r = 0.49 for the first radius, r = 0.62 for the second radius) with SG. At increment drilling depths, the relative resistance showed a strong linear correlation (r = 0.87) with SG at 5 to 15 mm depths; however, the strength of the correlation decreased as the drilling depth increased.

Keywords: Specific gravity, resistance drilling, amplitude, plantation tress, *Eucalyptus*

Introduction

The genus *Eucalyptus* is an important source of wood supply for almost all wood uses. With many species available, *Eucalyptus* exhibits a wide range of wood properties and meets the requirements for almost all segments of wood industry as a raw material. In the Brazilian cellulose pulp industrial sector, *Eucalyptus* has become the main source of raw materials and the country has mastered wood processing technologies in this industrial sector for many years already. The large efforts toward research in tree breeding programs made by the private companies and research institutions have increased the production of genetic materials to more than 50 cubic meter per hectare a year in a commercial scale (Gomide et al. 2005).The high productivity levels were achieved mainly through cloning techniques. Clone selection begins with evaluation of silvicultural aspects, followed by a preliminary selection, and then wood property assessment of hundreds of clones. The clones are selected only after the silvicultural and wood quality studies have been completed and then the selected clones can be used for multiplication and formation of homogenous forests. After five to seven years of rotation, plantations attain high forest productivity and good quality for pulp production.

Basic density is one of the most important wood properties that affects the performance of the end products and it is also related to many other wood and fiber properties. Wood density is influenced by genetic, age, and edaphoclimatic factors. In addition to the variation among trees, there is a significant within-tree variation of density in both radial and longitudinal directions of a trunk (Oliveira 1998). The smaller the variation in radial direction, the more uniform and higher quality the wood becomes for different purposes. Fantuzzi Neto (2012) affirmed that basic density is a key property in pulp production and the easiness of determining it has stimulated its use as an measure index of wood quality. Considering that there are great inter-tree and intra-tree variations and differences among species and genera that affect wood density, Foelkel et al. (1990) pointed out that "the expression of the same basic density does not mean the same wood quality." They also stated that wood of different species with same density are not same in terms of its anatomical, physical, and mechanical properties.

Large areas of forest plantations characterize the cellulose industrial sector in Brazil and the evaluation of wood quality in these forests is a routine operation that requires accurate, rapid, and cost-effective assessment tools for field applications. Nondestructive techniques developed for evaluating the quality of standing trees may become essential tools to assess the forest resources and sort raw materials for industrial uses. Among the nondestructive evaluation tools developed for wood materials and timber resources, resistance drilling has a potential to be used for assessing the basic wood density of standing trees with a reasonable accuracy and a relatively low cost (Gao et al. 2012, Brashaw et al. 2013). It also has the capability to obtain basic density profiles through the tree diameter, which is otherwise difficult to achieve by using conventional methods.

A typical resistance drilling tool is a mechanical drilling system that measures the relative resistance (torque of the drill bit) when a small diameter drill is introduced into wood at a constant speed. Compared with other field methods, resistance drilling tool is easier to handle in both laboratory and field settings, providing fast and cost-effective data collection (Gao et al. 2012). Rinn et al. (1996) reported that the drill resistance measurement had a strong linear relationship with the gross density of dry wood with a correlation coefficient greater than 0.80. Rinn (2013) also noted that the performance of the resistance drilling machine and the needles used strongly influence the quality and reliability of the resulting profiles.

In addition, considering that resistance drilling is a relatively inexpensive and user-friendly method that allows the evaluation of a relatively large number of trees in a short time and causes minimal damage to the trees. Thus, it is possible that this technique can be applied in tree breeding programs for genetic improvement or used by forest companies to assess the quality of *Eucalyptus* trees as a material source for pulp production. The objectives of this study were to determine the relationships between radial resistance drilling results and the specific gravity (SG) of *Eucalyptus grandis* x *Eucalyptus urophylla* clones and evaluate the applicability of resistance micro-drilling technique as a field tool for assessing wood specific gravity of young *Eucalyptus* plantation trees for pulpwood production.

Material and Methods

The genetic materials used in this study consisted of 100 clonal hybrid *Eucalyptus grandis* x *Eucalyptus urophylla* trees in a forest plantation (owned by Fibria Cellulose Company) located in the north of Espírito Santo State, Brazil. Of the 100 trees selected, 50 trees were in a 34-month-old stand and 50 trees were in a 62-month-old stand. The sample trees were randomly selected at each stand and marked. The diameter at breast height (DBH) was measured for each sample tree using a diameter tape. For each sample tree, one resistance drilling measurement was made on the trunk at breast height (BH) (Figure 1), in the north-south direction, using an IML-RESI F300 Resistograph tool (IML System GmbH, Wiesloch, Germany).

Following data collection, the trees were felled and the total tree height was measured on each stem. Two disks of approximately 3.0-cm thickness, were removed from each tree at BH. The disks were labeled and immediately put in sealed plastic bags to prevent moisture loss.

A schematic for data collection and wood samples cutting is shown in Figure 2. The first disk (A) corresponded to the resistance drilling measurement and was used to determine the specific gravity and moisture content as well. The second disk (B), taken right below the first, was used for other laboratory evaluations.

Figure 1–Resistance drilling measurement on young *Eucalyptus* trees.

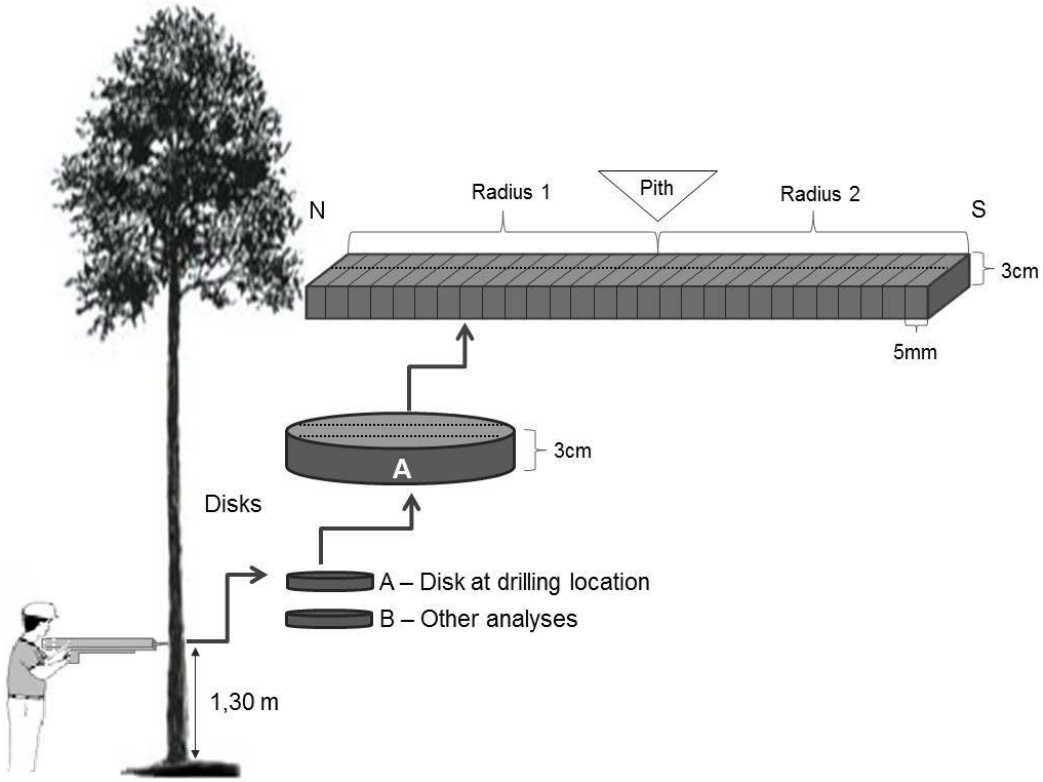

Figure 2–Field data collection and laboratory evaluation.

After the disks were brought to the laboratory, a 2.5-cm-wide center strip was cut from the first disk of each tree, then each strip was sliced into 5-mm-thick samples through the whole length. Both moisture content and specific gravity were determined for each individual sliced sample. The dimensions of the sliced samples were 5-mm × 25-mm × 30-mm (radial, tangential, and longitudinal directions, respectively). The hydrostatic balance method described in ASTM D2395-14 (ASTM 2014) was used to determine the volume of each wood sample in the green condition, replacing mercury with water. A precision scale (0.01 g) was used to determine the green and dry mass. The samples were then dried in a laboratory oven with forced ventilation and automatic temperature control, setting at 103 ± 2°C for 24 hours.

For the amplitude readings from the resistance drilling measurement on each tree, an average resistance value was first calculated for every 5-mm penetration, which corresponded to the 5-mm sample sliced from each the strip. Average amplitude was also calculated for each tree over a full penetration depth (through diameter) and half penetration depths (first radius and second radius). Data were first processed using Excel Software, and statistical analyses were performed using the S.A.E.G. program (S.A.E.G. 2012).

Results and Discussion

Resistance amplitude and wood specific gravity

Table 1 summarizes the statistics of tree DBH and average values of MC, SG, and resistance amplitude at each tree level in each stand. Variations in MC and SG among trees were small within each age class. The mean values of SG were 0.40 and 0.42 for 34-month-old and 62-month-old trees, respectively, with coefficients of variation (COV) of 3.4% and 3.3%, respectively. In contrast, the average resistance amplitude showed large variations among trees and especially between the two stands. The average amplitude values ranged from 3.1% to 11.2% for 34-month-old trees and from 8.7% to 18.5% for 64-month-old trees. The mean value of amplitude of 64-month-old trees was almost twice that of 34-month-old trees. This result is consistent with previous data with respect to tree ages. In two recent studies, the average amplitude of the resistance profile obtained at BH ranged from 10% to 17.4% for 7-year-old *Eucalyptus* clones (Lima et al. 2006) and from 12% to 33% for 16-year-old *Eucalyptus* clones (Lima et al. 2007). The increasing trend of average amplitude with age certainly contributed to the density increase as a tree matured, but it could also be related to the DBH increase. As drill penetration depth increases with diameter, the friction acting on the shaft of the drill bit could increase, which in turn results in high relative resistance readings.

Figures 3 and 4 show the variations of resistance amplitude (red diamonds) and SG (black triangles) in the radial direction for 34-month-old and 64-month-old trees, respectively. Each point of the data represents the average amplitude of 50 trees at a specific location over a 5-mm width, and the corresponding SG of the 5-mm sliced sample at that location. For the 34-month-old trees, the specific gravity was relatively constant across the diameter. This homogeneity is common in 2–3-year-old *Eucalyptus* plantations. In contrast, the resistance amplitude increased through the first radius, then remained high in the second radius and gradually decreased as the drill bit moved out of the tree at opposite side. This unique resistance drilling characteristics indicated that friction forces were built up during the drilling process, which could pose challenges for accurate SG prediction.

For the 64-month-old trees, the trend of SG showed a concavity across the diameter. SG was relatively constant in core wood, similar to the 34-month-old trees, but increased as the position moved toward the bark side. The resistance amplitude, on the other hand, showed a slight decrease within the first 40-mm penetration depth; then it gradually increased as the drill bit penetrated through the core wood. The rate of amplitude increase was much higher as the drill bit reached the opposite side of the tree trunk. This confirmed our speculation that as tree diameter increases, friction has a non-linear effect on SG prediction.

Relationships between resistance amplitude and wood specific gravity

Table 2 shows the correlation coefficients for linear regressions between average amplitude and specific gravity of *Eucalyptus* wood. The experimental data were analyzed on individual age class levels as well as on a combined age class level. The following scenarios were examined in the regression analysis:

1) at tree level (average, n = 50 or 100); 2) at sliced sample level, for entire strip (n = 2559); 3) at sliced sample level, for the first half of strip (from bark side to pith, n = 1303); 4) at sliced sample level, for the second half of strip (from pith to bark side, n = 1256); 5) at tree level, for drill penetration depths of 5, 10, 15, 20, 25, 30, and 35 mm.

Table 1 – Basic physical properties and resistance amplitude of clonal hybrid *Eucalyptus grandis* x *Eucalyptus urophylla* trees[a]

Stand age (month)	No. of trees		Height[1] (m)	DBH (cm)	Amplitude (%)	SG	MC (%)
		Average	16.58	12.24	6.3	0.40	179
		Min.	15.15	11.13	3.1	0.35	163
34	50	Max.	17.40	13.87	11.2	0.42	195
		Std. Dev.	1.24	0.87	1.5	0.01	7.0
		COV (%)	7.49	7.13	24.1	3.4	3.9
		Average	25.74	15.75	11.6	0.42	163
		Min.	23.70	13.98	8.7	0.39	143
62	50	Max.	27.00	17.43	18.5	0.46	179
		Std. Dev.	1.05	1.12	1.8	0.01	6.8
		COV (%)	4.07	7.10	15.5	3.3	4.2
		Average	21.16	14.00	8.9	0.41	171
		Min.	15.15	11.30	3.1	0.35	143
Combined	100	Max.	27	17.41	18.5	0.46	195
		Std. Dev.	4.83	2.03	3.1	0.02	10.6
		COV (%)	22.83	14.47	35.0	4.7	6.2

[a]Height: tree height based on data of 10 trees in each stand; DBH: Diameter at breast height; SG: specific gravity; MC: Moisture content; Std. Dev.: Standard deviation; COV: Coefficient of variation (%).

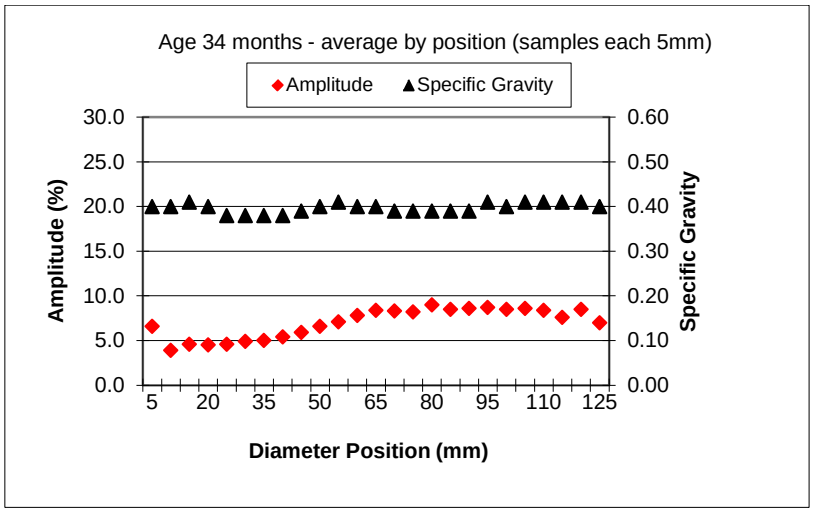

Figure 3–Average specific gravity and amplitude profiles across the diameter of 34-month-old *Eucalyptus* trees.

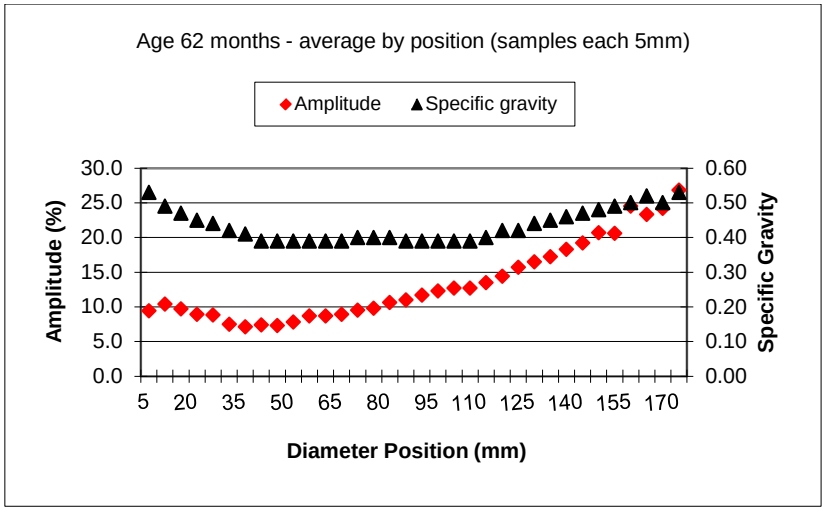

Figure 4 – Average specific gravity and amplitude profiles across the diameter of 62-month-old *Eucalyptus* trees.

Table 2–Pearson correlation coefficients between resistance drilling amplitude and specific gravity of *Eucalyptus grandis* x *Eucalyptus urophylla* trees

Stand age/Drill penetration depth	Correlation coefficient (r) ($p < 0.05$) Average amplitude vs. Specific gravity
34-month	
At sliced sample level, entire strip (n = 1089)	0.35
At sliced sample level, 1st half strip (n = 566)	0.10
At sliced sample level, 2nd half strip (n = 523)	0.45
At tree level, P = diameter (n = 50)	0.28
At tree level, P = 1st half(n = 50)	0.32
At tree level, P = 5mm (n = 50)	0.36
At tree level, P = 10mm (n = 50)	0.30
At tree level, P = 15mm (n = 50)	n.s[1]
At tree level, P = 20mm (n = 50)	n.s
At tree level, P = 25mm (n = 50)	n.s
At tree level, P = 30mm (n = 50)	n.s
At tree level, P = 35mm (n = 50)	n.s
At tree level, P = 40mm (n = 50)	n.s
At tree level, P = 45mm (n = 50)	n.s
At tree level, P = 50mm (n = 50)	0.30
At tree level, P = 55mm (n = 50)	0.34
At tree level, P = 60mm (n = 50)	0.33
At tree level, P = 65mm (n = 50)	n.s
62-month	
At sliced sample level, entire strip (n = 1470)	0.46
At sliced sample level, first half strip (n = 737)	0.48
At sliced sample level, 2nd half strip(n = 733)	0.65
At tree level, P = diameter (average, n = 50)	0.35
At tree level, P = 1st half (n = 50)	0.63
At tree level, P = 5mm (n = 50)	0.49
At tree level, P = 10mm (n = 50)	0.72
At tree level, P = 15mm (n = 50)	0.81
At tree level, P = 20mm (n = 50)	0.58
At tree level, P = 25mm (n = 50)	0.59
At tree level, P = 30mm (n = 50)	0.42
At tree level, P = 35mm (n = 50)	0.57

Continue Table 2 …

Stand age/Drill penetration depth	Correlation coefficient (r) ($p < 0.05$) Average amplitude vs. Specific gravity
At tree level, P = 40 mm (n = 50)	0.67
At tree level, P = 45 mm (n = 50)	0.56
At tree level, P = 50 mm (n = 50)	0.60
At tree level, P = 55 mm (n = 50)	0.67
At tree level, P = 60 mm (n = 50)	0.68
At tree level, P = 65 mm (n = 50)	0.64
At tree level, P = 70 mm (n = 50)	n.s
At tree level, P = 75 mm (n = 50)	0.34
At tree level, P = 80 mm (n = 50)	0.30
34- and 62-month combined	
At sliced sample level, entire strip (n = 2559)	0.49
At sliced sample level, 1st half strip (n = 1303)	0.49
At sliced sample level, 2nd half strip (n = 1256)	0.62
At tree level, P = diameter (average, n = 100)	0.71
At tree level, P = 1st half (n = 100)	0.77
At tree level, P = 5 mm (n = 100)	0.87
At tree level, P = 10 mm (n = 100)	0.86
At tree level, P = 15 mm (n = 100)	0.87
At tree level, P = 20 mm (n = 100)	0.74
At tree level, P = 25 mm (n = 100)	0.75
At tree level, P = 30 mm (n = 100)	0.53
At tree level, P = 35 mm (n = 100)	0.50
At tree level, P = 40 mm (n = 100)	0.38
At tree level, P = 45 mm (n = 100)	0.43
At tree level, P = 50 mm (n = 100)	0.40
At tree level, P = 55 mm (n = 100)	0.44
At tree level, P = 60 mm (n = 100)	0.39

[a]- not significant at 5% confidence level.

For 34-month-old *Eucalyptus*, the correlation coefficients were low for all scenarios considered, ranging from 0.10 to 0.45, and were not significant at 5% confidence level in some cases. Figure 5 shows the data plots for specific gravity and average amplitude at sliced wood sample level (A) and at tree level (B). Clearly, at both sliced wood sample level and tree level, resistance amplitude showed much larger variation (COV = 24.1%) than wood specific gravity (COV = 3.4%), and there seems no clear trend between amplitude and wood specific gravity. As discussed earlier, friction forces were built up during the drilling process, which could skew the relationship between amplitude and SG.

Figure 6 shows the data plots for specific gravity and average resistance amplitude at sliced wood sample level (A) and at tree level (B). Similar to what was observed in 34-month-old trees, resistance drilling amplitude showed much larger variation (COV = 15.5%) than wood specific gravity (COV = 3.3%). However the 62-month-old trees have a much clearer trend between amplitude and wood SG: drilling resistance increased as SG increased. At the sliced wood sample level, the correlation between resistance amplitude and specific gravity was improved compared to that for 34-month-old trees. At the individual tree level, the experimental data yielded moderate correlations, with a correlation coefficients ranging from 0.42 to 0.81 (Table 2).

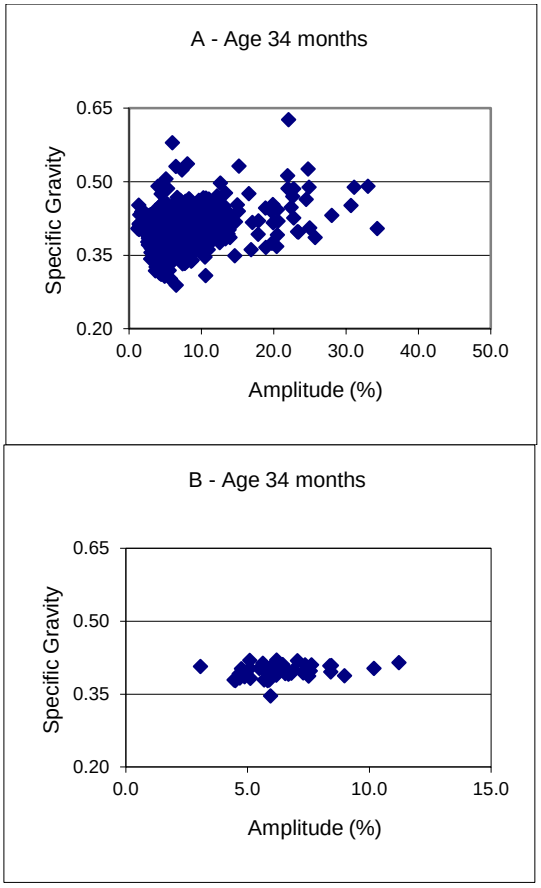

Figure 5–Plot of wood specific gravity and average resistance drilling amplitude for 34-month-old *Eucalyptus grandis* x *Eucalyptus urophylla* trees. A–at sliced sample level (entire strip); B–at tree level.

For 62-month-old *Eucalyptus* trees, the correlations were improved in all scenarios (0.42–0.81) compared to those for 34-month-old trees. It is not clear what caused this correlation improvement.

When the two age classes were combined, the relationships between average amplitude and wood specific gravity increased significantly at both the wood slice level (0.49 – 0.62) and the tree level (r = 0.73-0.87). Figure 7 shows the data plots for specific gravity and average amplitude for 34 and 62-month-old *Eucalyptus grandis* x *Eucalyptus urophylla* trees combined. Apparently, the greater variation in resistance readings and wood SG for the combined tree samples elevated the strength of the correlation between drilling resistance and wood specific gravity. This resistance-SG relationship is highly relevant to the physical and mechanical behavior of wood. For wood with higher specific gravity, the fibers tend to have thicker cell walls, which could increase the resistance as a drill needle penetrates into the wood, thus resulting in higher amplitude values.

The results obtained in this study are generally consistent with what was reported by Lima et al. (2006), who conducted resistance drilling measurements in two clones of *Eucalyptus* of seven years old provenance in Minas Gerais State, Brazil, and found correlation coefficients between amplitude and wood specific gravity at tree level varying from 0.71 to 0.81. Gouvea et al. (2011) also studied six *Eucalyptus* clones of three years old from different locations in Minas Gerais State, Brazil, and found a correlation coefficient of 0.60 for the linear relationship between amplitude and wood specific gravity. Theses authors concluded that the most significant correlation occurred between amplitude and average wood specific gravity of the whole tree. At the BH level, the correlations were not elevated to the clones.

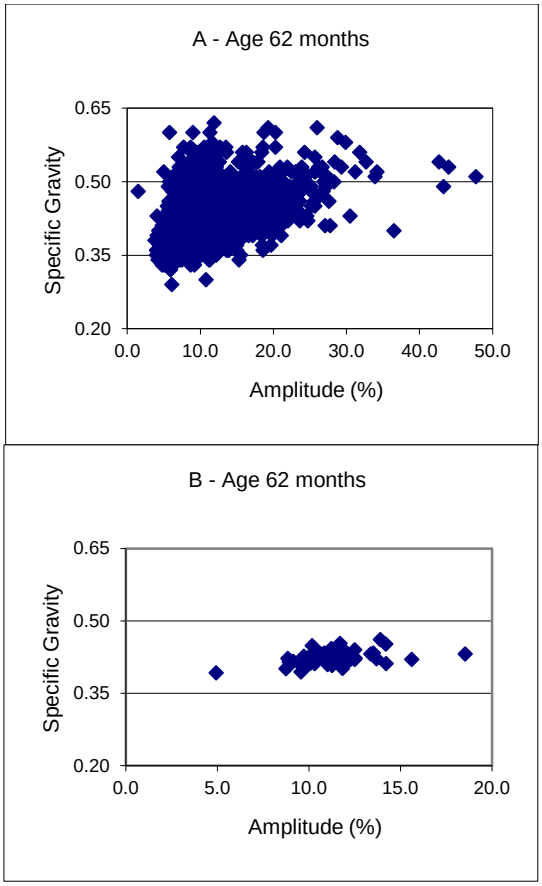

Figure 6–Plot of wood specific gravity and average resistance drilling amplitude for 62-month-old *Eucalyptus grandis* x *Eucalyptus urophylla* trees. A–at sliced sample level (entire strip); B–at tree level.

Effect of drill penetration depth

Another interesting finding in this study regards the effect of drill penetration depth. When age class was considered individually, there was no clear pattern on how drill penetration depth affected the correlations. But when two age classes were combined, a clear trend of weakening correlation as the drill penetration depth increased was observed. As Figure 5 shows, correlation coefficient remained relatively high at penetration depth of 5, 10, and 15 mm ($r \geq 0.86$), then it started decreasing as drill penetration depth further increased. The Pearson correlation coefficient dropped to 0.53 at 35-mm penetration depth. This was likely caused by the friction that was mounted onto the drill bit as the drill penetrated deeper into the tree.

Conclusions

The use of a resistance drilling technique for assessing wood specific gravity of young *Eucalyptus* plantation trees at two age classes was investigated. Based on the results from this study, the following conclusions were drawn:

- The average resistance amplitude was distinctly different between 34-month-old and 62-month-old *Eucalyptus* plantation trees. The average amplitude values ranged from 3.1% to 11.2% for 34-month-old trees and from 8.7% to 18.5% for 64-month-old trees.
- The average amplitude of a full penetration or a half penetration showed a relatively weak correlation with wood specific gravity for both 34-month-old and 62-month-old *Eucalyptus* plantation trees. When two age classes were combined, the strength of the relationship was

improved significantly, with correlation coefficients increased from 0.38 (34-month-old) and 0.42 (62-month-old) to 0.71 (34- and 64-month-old class combined).

- The drill penetration depth has a clear effect on the relationship between average amplitude and wood specific gravity. When two age classes were combined, there was a clear trend of weakening correlation as the drill penetration depth increased.

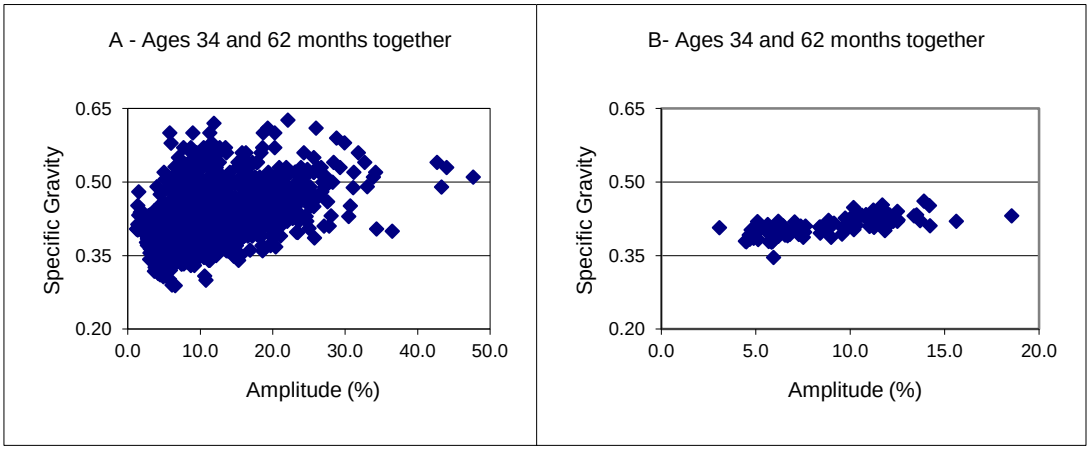

Figure 7–Plot of wood specific gravity and average resistance drilling amplitude for 34 and 62-month-old *Eucalyptus grandis* x *Eucalyptus urophylla* trees combined. A–at sliced sample level (entire strip); B–at tree level.

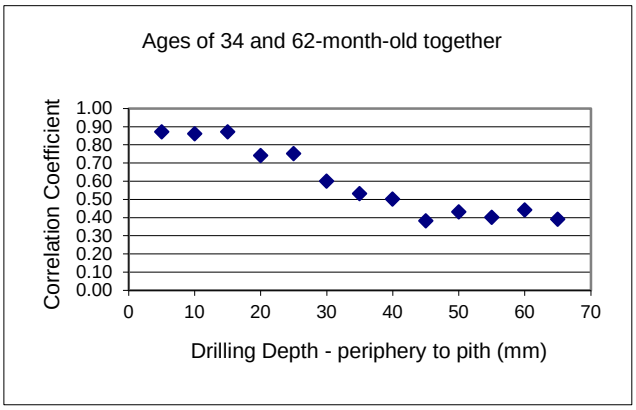

Figure 8–Values of Pearson correlation coefficients between resistance drilling amplitude and specific gravity of 34 and 62-month-old *Eucalyptus grandis* X *Eucalyptus urophylla* trees.

Acknowledgments

This project was conducted under cooperative research agreements among the Federal University of Espirito Santo and Fibria Cellulose Company in Brazil, and the USDA Forest Service, Forest Products Laboratory (FPL) in Madison, Wisconsin, USA. The financial support to Dr. Oliveira for his scientific exchange program at FPL was provided by CAPES-Brazil.

References

ASTM. 2014. D2395-14. Standard test methods for specific gravity of wood and wood based materials. American Society for Testing and Materials: West Conshohocken, PA.

Brashaw, B.K.; Wang, X.; Fellman, D.; Ross, R.J.; Xu, H. 2013. Acoustic assessment technologies for optimal wood products and biomass utilization. In: Proceedings of the 18th International Nondestructive Testing and Evaluation of Wood Symposium, Sept. 24–27, 2013, Madison, WI. p. 150–160.

Foelkel, C.E.B.; Mora, E.; Menochelli, S. 1990. Basic density: its true usefulness as a quality index of Eucalyptus pulpwood production. In: 6° CONGRESSO FLORESTAL BRASILEIRO, 22 a 27 de setembro, 1990, Campos do Jordão. Anais...Campos do Jordão. P. 719–728.

Gao, S.; Wang, X; Brashaw, B.K. [and others]. 2012. Rapid assessment of wood density of standing trees with nondestructive methods–A review. In: International Conference on Biobase Material Science and Engineering (BMSE), October 21-23, 2012, Changsha, China. p. 262–267.

Gomide, J.L.; Colodette, J.L.; Oliveira, R.C. [and others]. 2005.Technological characterization for pulpwood , the new generation of Eucalyptus clones of Brazil.. Revista Árvore. 29(1):129-137.

Gouvea, A.F.G.; Trugilho, P.F.; Colodete, J.L. [and others]. 2011. Relationship between characteristics of wood and pulp from Eucalyptus with non-destructive methods. Scientia Forestalis. 39(90): 205–220.

Lima, J.T.; Hein, P.R.G.; Trugilho, P.F. and others.2006.Resistograph performance in estimating the specific gravity of eucalyptus wood . In: ENCONTRO BRASILEIRO EM MADEIRAS E ESTRUTURAS DE MADEIRAS, 2006, São Pedro. Anais... São Pedro:... UNESP/CEVEMAD/IBRAMEM.(CD-ROM).

Lima, J.T.; Sartorio, R.S.; Trugilho, P.F. [and others]. 2007. Use of resistograph to estimate the basic density and resistance to drilling of Eucalyptus wood. Scientia Forestalis. 75:85–93.

Neto, F. 2012. Eucalypt wood quality to cellulose Kraft production.. Viçosa MG:Universidade Federal de Viçosa. 105 p. D.S. tese.

Oliveira, J.T.S. 1998. *Eucalyptus* wood characterization for civil construction. São Paulo SP:Universidade de São Paulo. 429 p. D.S. tese.

Rinn, F. 2013.Practical application of micro-resistance drilling for timber inspection. Holztechnologie 54(4): 32–38.

Rinn, F.; Schweingruber, F.H.; Schar, E. 1996. Resistograph and X-ray density charts of wood: comparative evaluation of drill resistance profiles and X-ray density charts of different wood species. Holzforschung 50:303–311.

S.A.G.E. 2012. Statistical analysis for genetic, Release 6.3: http://darwin.cwru.edu.

Prediction of basic density using parameters measured on trees

Rafael Gustavo Mansini Lorensani
PhD student, Laboratory of Nondestructive Testing – LabEND/FEAGRI/UNICAMP
e-mail: rafaelmansini@hotmail.com

Cilene da Silva Alves
Undergraduate Student, Laboratory of Nondestructive Testing –LabEND/FEAGRI/UNICAMP.
e-mail: cilenealves7@gmail.com

Raquel Gonçalves;
Professor, Coordinator of the Laboratory of Nondestructive Testing – LabEND, College of Agricultural Engineering – FEAGRI – University of Campinas – UNICAMP, Brazil
e- mail:raquel@feagri.unicamp.br.

Abstract

The measurement of the basic density of the wood in trees is laborious and time-consuming. The objective of this study was to analyze parameters that would allow predicting specific density in trees. We tested 180 trees in six different ages, with 30 trees per age. In all trees, we measured the total (TH) and canopy (CH) height, the diameter at breast height (DBH), the velocity of ultrasound wave propagation in the longitudinal (VL) and radial (VR) directions and the amplitude of drilling resistance (DA). We determine the basic density using cylindrical samples taken with increment borer (BDib) at DBH. No statistical correlations with BDib were found considering individual trees. For mean BDib by age the VL was the only parameter with statistical correlation with BDib (R^2 = 83%). The BDib do not shows growing with age, indicating that it was affected by the soil and climate. The same behavior was observed only on VL.

Key words: ultrasound, tree height, diameter at breast height, drilling resistance

Introduction

The proper use of wood depends directly on the knowledge of its physical and mechanical properties. Depending on the nature of use, the importance of some properties stand out, such as, for example, the paper and pulp mills, in which the density is an important property to be linked to the income.

For studies involving genetic improvement, monitoring the development of the wood density directly in the tree is important, because it allows more agile decision-making regarding the genetic material.

To determine the density of standing trees, nondestructive techniques have been indicated to prevent tree cutting, necessary to remove discs to be evaluated in the laboratory, therefore is more economical and agile. Downes et al. (1997) cited by Padua (2009) state that the determination of the density using discs from a single tree is 5 times longer, and 5 times more expensive than the density obtained using motorized borer sample; and 10 times longer and 9 times more expensive than the use of pylodin. However, for obtain the same accuracy in the

results, would be necessary, on average, six samples in the case of the trees discs, 7 in the case of the borer and 22 in the case of pylodin (Downes, 1997 cited by Padua, 2009). Carrasco & Azevedo (2003) and Couto et al. (2013) state that nondestructive techniques are essential for obtaining the density of the wood in the tree.

In addition to the use of the increment borer to determine the density of the wood directly on the tree, it is also reported studies (Sotomayor, 2013; Couto et al, 2013;. Padua, 2009; Isik and Li, 2003; Lima et al., 2007) using the resistance of penetration and drilling (pylodin and resistograph).

The objective of this research was to evaluate if the insertion of some parameters obtained in trees (total high, canopy high, diameter at breast high, drilling resistance, longitudinal ultrasound velocity and radial ultrasonic velocity) can improve the inference about basic density.

Material and Methods

In this study, 180 trees from a eucalyptus clone were used. The trees were 1, 2, 3, 4, 5 and 6 years old. From each age were chosen, randomly, 30 trees, respecting 30 meters from the edge of the plot to avoid interference of the growth caused by excessive exposure to wind (reaction wood).

For every tree we measured the total height (TH), canopy height (CH), the diameter at breast height (DBH), the time of flight of the ultrasound wave propagation in the longitudinal and radial direction and the drilling resistance. After taking these parameters, we removed a sample using the increment borer.

The total height and the height of the canopy were measured with hypsometer and the diameter at breast height with tape-measure.

For ultrasound test in the longitudinal direction (or fibers), the vertical distance between transducers was 0.70 m. This distance included the position of the DBH (0.35 m above and below this position). The test was performed indirectly, with transducers positioned on the same side and at an angle (approximately 45°) favoring the path of the wave in the longitudinal direction (Figure 1a). The ultrasound test in the radial direction (perpendicular to the fibers) - Figure 1b - was performed 0.35 m above and 0.35 below the DBH's position.

a b

Figure 1 – Ultrasound test in longitudinal (a) and radial (b) direction

The drilling resistance test (Figure 2a), performed with resistograph, and removal of the cylindrical sample with approximately 5 mm diameter (Figure 2b), performed with increment borer were accomplished in DBH position.

a b

Figure 2 – Drilling resistance test (a) and cylindrical sample obtained with the increment borer (b).

The cylindrical samples were packed in small plastic bags, sealed and stored on ice to maintenance of field moisture. At the laboratory the samples were measured to obtain the saturated weight. The samples were then placed in an oven with temperature of 103 ± 2°C until anhydrous condition, in which they were weighed to obtain the dry weight. The basic density was calculated by the relationship presented by ABNT: NBR 11941 (2003).

With these results, we used statistical software to evaluate the normality of the data and the simple and multiple regressions between the parameters and the basic density.

Results and discussions

The basic density, obtained from the sample taken with the borer, do not increased with age. The statistical analysis of mean comparison (Multiple-Sample comparison and Multiple Range Test) indicated, with 95% confidence level, 3 statistically different groups: the clone with 5 years (smaller value); Clones 1, 2, 3 and 6 years (intermediate values) and clone 4 years (higher value) - Figure 3. The basic densities presented coefficients of variation less than 8% in each age and 6.6% for all trees (Table 1).

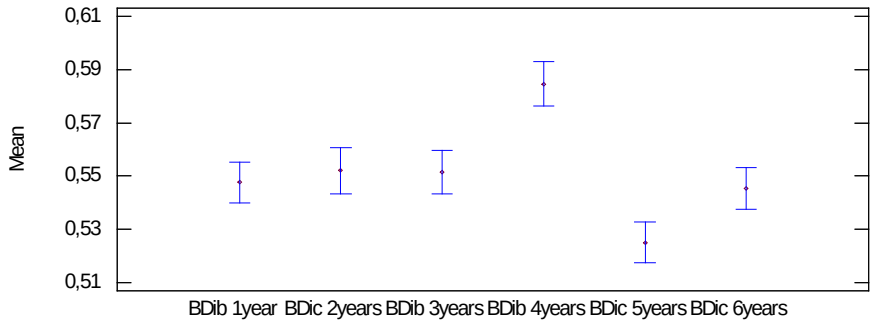

Figure 3 – Means plot of Basic Density (BDib) in g.cm^{-3} obtained using the increment borer from different ages trees

Table 1 – Statistical summary of the basic density at different ages

Age	Mean [g.cm^{-3}]	Variation coefficient [%]	Minimum [g.cm^{-3}]	Maximum [g.cm^{-3}]
1	0,55	5,0	0,50	0,60
2	0,55	5,4	0,50	0,61
3	0,55	7,5	0,47	0,65
4	0,58	3,2	0,56	0,63
5	0,53	6,5	0,47	0,59
6	0,55	4,4	0,50	0,60
All	**0,55**	**6,3**	**0,47**	**0,65**

Raymond (2002), cited by Padua (2009), comments that it is expected that the basic density increases with age, but this parameter varies widely within and between trees of up to 3 years old.

The sample used in this study (30 trees) was bigger than that proposed by Downes et al. (1997), cited by Padua (2009), that indicates 7 trees using increment borer to calculate the density. Nevertheless, our results did not follow the pattern of growth expected over the age of 3 years.

Despite all trees are of the same clone, they were located in plots belonging to different farms of the company and in different regions. Thus, the density may have been influenced by climate and soil factors, which reflected in increased density. Also, the basic density used in this part of the research was determined only by the cylinder removed by the increment borer. Several researchers have shown that the density obtained with the auger has a good correlation with the density obtained on discs, but the value is not the same. In addition, there is controversy regarding the underestimation (Padua, 2009) or overestimation (Sotomayor, 2013) of the value obtained by the cylinder sample in relation to the value obtained using discs.

Analyzing the behavior of the tree height and of the canopy height, parameters strongly associated with age, we observed growth (Figure 4). Statistically each means belongs to a different group, indicating that, in this case, the climate and soil factors did not interfere so remarkable as in the density.

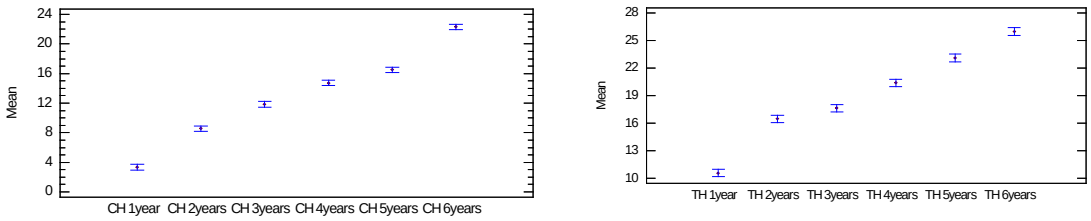

a b

Figure 4 – Means and 95% limit standard deviation intervals for Canopy high (CH) (a) and Total high (TH) (b) in meters.

The diameter at breast height (DBH) is also strongly linked to growth parameter and evolved with age much like the TH and CH (Figure 5). The Multiple Range Test indicated four distinct groups: 1 year; 2 years; 3 to 5 years and 6 years.

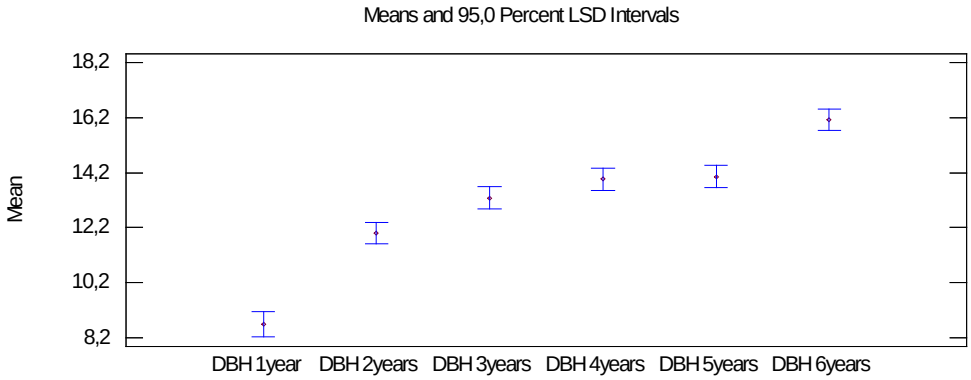

Figure 5 – Means and 95% limit standard deviation intervals for Diameter at Breast Hight (DBH) in centimeters.

In the case of Drilling Amplitude (DA) the Multiple Range Test showed similar behavior to that obtained for the DBH (Figure 6), but with only three statistically different groups (1 year, 2 to 5 years, 6 years old). This result is consistent and expected (increase with age) but also different from that obtained for the density.

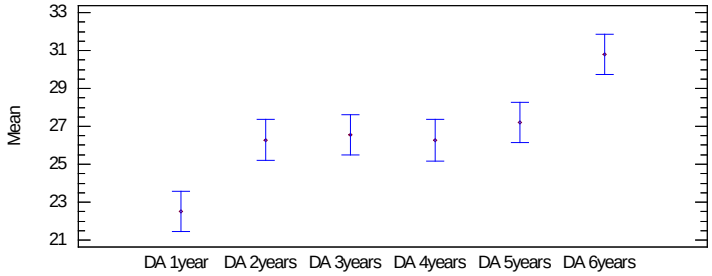

Figure 6 – Means and 95% limit standard deviation intervals for Drilling Amplitude (DA) in percentage.

The longitudinal velocity (VL) indicated 3 statistically differentiated groups (5 years; 1,2,3 and 6 years, 4 years) with same behavior of the basic density obtained from the sample of the increment borer. The radial velocity had no similar behavior, compared to VL or other parameters (BDib, TH, CH, DBH, DA) (Figure 7). Considering that, the longitudinal velocity correlates better with rigidity, this result it may reflect differences in soil and climate conditions that surpass the age issue. The radial velocity is more strongly influenced by irregularities (fiber deviation, resin pockets, etc.) and it may reflect silviculturais parameters, more than age.

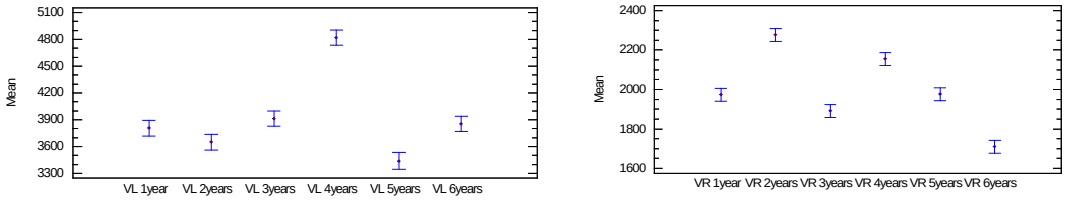

a b

Figure 7 – Means and 95% limit standard deviation intervals for Longitudinal Velocity (VL) and Radial Velocity (VR) in meters per second.

Using as a sample the values obtained in each tree (not the average), none of the nondestructive technologies allowed to explain adequately the variability of the density obtained from the increment borer sample. The longitudinal and radial velocities of ultrasound showed a statistically significant correlation with basic density (Pvalue <0.05) but the correlation coefficients were very low R = 0.29 and R = 0.16, respectively. The drilling amplitude had no statistically significant correlation with basic density (Pvalue = 0.2637). This result shows that, in our research, the ultrasound or the drilling resistance were not able to differentiate the basic density among trees.

Couto et al. (2013) managed to get significant correlations between drilling resistance and the average density (obtained through the mean of different disks removed from the tree) using data from 49 trees from two clones (24 clones of 42 months and 25 clones of 54 months). The models obtained by Couto et al. (2013) explained 54% to 67% of variability of the average density of the trees. Kahl et al. (2009), cited by Couto et al. (2013), obtained results very close, (R2 = 65%) for the correlation between basic density and drilling resistance. These results shows that these authors found significant models with good predictive ability to individually separate trees using the amplitude of the drilling resistance as a variable.

The statistically significant multiple regression (Pvalue = 0.001) that best fitted was the one that contained the longitudinal velocity (Pvalue = 0.0001), amplitude of drilling resistance (Pvalue = 0.0227) and tree height (Pvalue = 0.050), but this model explain only 14% of the variability of the density obtained from the borer sample. Once more, it appears that, with our results, it was not feasible to differentiate individually the trees, even with the inclusion of other parameters.

To evaluate whether there was a model that could differentiate the average basic density of the clone obtained in a plot, we used the average of the properties obtained in each of the blocks (ages). The amplitude obtained with the resistograph and the radial velocity showed no statistically significant correlation with the basic density obtained from the borer (Pvalue = 0.8258 and Pvalue = 0.3453, respectively), while the longitudinal velocity showed a statistically significant correlation with the basic density obtained from the borer (Pvalue = 0.0113) and the correlation coefficient was R = 0.91 (R^2 = 83%). The use of longitudinal velocity associated with other parameters (multiple regression) indicates no statistically significance (Pvalue > 0.05).

Conclusions

Considering the trees of the clone as a single block there was no statistically significant correlation between the basic density of trees obtained from the auger sample in DBH (BDib) and any of the variables evaluated in this study (simple regression) or between their composition (multiple regression).

Considering the average per block (age), the longitudinal velocity of ultrasonic waves propagation (VL) was the only variable that showed a statistically significant correlation with specific density obtained from the auger sample in DBH (BDib).

Acknowledgements

We thank National Council of Technological and Scientific Development (CNPq) and São Paulo Research Foundation (FAPESP) for scholarships (FAPESP Proc. 2013/03449-9). We also thank the International Paper and FAPESP (Proc. 2012/22599-9) for the research support.

References

ASSOCIAÇÃO BRASILIERA DE NORMAS TÉCNICAS. NBR 11941: Determinação da Densidade Básica. Rio de Janeiro, 2003. 6 p.

Carrasco EVM, Azevedo AP. 2003. Avaliação não destrutiva de propriedades mecânicas de madeira através de ultrassom: fundamentos físicos e resultados experimentais. Cerne, v.9, n.2, p. 178-191.

Couto AL, Trugilho RF, Neves TA, Protásio TP, Sá VA. 2013. Modeling of basic density of wood from Eucalyptus grandis and Eucalyptus urophylla using nondestructive methods. Cerne, v.19, n.1, p.27-34.

Isik F, Li B. 2003. Rapid assessment of wood density of live trees using the Resistograph for selection in tree improvement programs. Canadian Journal of Forestry Research.2003; 33:2426–2435.

Lima JT, Sartório RC, Trugilho PF, Cruz CR, Vieira RS. 2007. Uso do resistógrafo para estimar a densidade básica e a resistência a perfuração da madeira de Eucalyptus. Scientia Forestalis, v.75, p.107-116.

Pádua FA. 2009. Amostragem para avaliação da densidade básica da madeira de um híbrido de Eucalyptus grandis e Eucalyptus urophylla. Tese de Doutorado. Universidade Federal de Lavras, MG, Brasil. 79p.

Pádula RR. 2013. Estudo comparativo de métodos para determinação da densidade básica de cavacos e discos de madeira. Dissertação de Mestrado. Universidade Estadual Paulista/UNESP, Botucatu. 57p.

Stomayor JFM. 2013. Determinação de Biomassa aérea em florestas nativas num ambiente agrícola do Estado de São Paulo. Tese de Doutorado. Universidade de São Paulo/ESALq. 130p.

Session 12

Poster Session

Velocity variation in wood as a function of defects

Alex J. Trinca
PhD, Visiting Professor, Laboratory of Nondestructive Testing - LabEND, College of Agricultural Engineering - FEAGRI - University of Campinas - UNICAMP, Brazil – E-mail: alexjuliotrinca@gmail.com

Mariana R. Guerra
Master student, Laboratory of Nondestructive Testing – LabEND, College of Agricultural Engineering - FEAGRI - University of Campinas - UNICAMP, Brazil – E-mail:ma.nagle.reis@gmail.com

Raquel Gonçalves
Professor, Coordinator of the Laboratory of Nondestructive Testing – LabEND, College of Agricultural Engineering - FEAGRI - University of Campinas - UNICAMP, Brazil – E-mail: Raquel@agr.unicamp.br

Abstract

In wood the defects may be present in different ways; the most frequent are internal holes and degradation by the presence of fungi and termite attack. The objective of this study was to evaluate the variation of ultrasound velocity in different types of defects in wood, using equipment developed in Brazil and 45 kHz dry points transducers. To achieve this goal we used 14 *Pinus sp* discs. Five discs were inoculated with fungi *Lentinula*, six infested by termites *Coptotermes gestroi* and 3 drilled artificially. Using the ultrasonic results, we obtained the velocity variation caused by the action of fungi, termites and the drilled parts. The direct comparison is not possible, because the integrity of the wood varied in the three conditions. Nevertheless, for the three conditions the decay was detected by the variation of the velocity of wave propagation.

Keywords: Ultrasonic tomography, degradation by fungi, degradation by termites, holes in wood.

Introduction

The wave propagation is affected by presence of materials with different characteristics of acoustic impedance, for example, defects or irregularities (grain deviation, resin bags, etc.) and abnormalities caused by biological attacks or by insects (Bucur et al., 2006). As the propagation is affected there is variation in wave velocity and amplitude of the signal, which can be detected by the ultrasound equipment and studied for the development of a behavioral profile related to the defect or degradation.

It is expected that there are different profiles for different anomalies, defects or degradation in the wood. Understanding the behavior of these profiles is important for applications that aim the inspecting of the condition of the wood through wave propagation techniques.

Several authors have studied the behavior of the propagation of ultrasound waves on wood for different defects or anomalies. Among them we can mention Puccini et al. (2002), which valuated the influence of the knots, pith and fiber deviation in the velocity of ultrasound wave propagation. The velocity was highly significant on models involving as independent variable, the presence of knots, the pith or fiber deviation (Puccini et al., 2002).

Analyzing the wave propagation behavior in wood with fungal attack, Kim et al. (2007) concluded that the symptoms of fungi attack could not be detected by visual analysis, but images generated by ultrasound tomography allowed the identification of regions with a maximum deterioration.

The changes on behavior of wave propagation due to the presence of artificial holes with increasing dimensions were studied by Secco (2011) and Lin et al. (2008). These authors showed a relation between the increase of the size of the hole and the velocity variation. Considering the results in sound wood and in wood with the biggest hollow, Secco (2001) obtained velocities from 2000 ms- 1 to 600 ms- 1 while Lin et al. (2008) velocities from 1600 ms- 1 to 600 ms -1, so, very close variation.

This research aimed to evaluate the velocity change in disks with holes and degradation caused by termites and fungi.

Methodology

In all discs the measurements were performed with ultrasound equipment developed in the research group in partnership with spin-off company (USlab , AGRICEF , Brazil) and 45 kHz transducers with dry point.

The sample was composed of 14 Pinus sp disks taken from trees with 8 years old and, therefore, the entire disk consisted of juvenile wood. Of these discs, 6 were used for the study of termites, 5 for the study of fungi and 3 for the study with holes.

The Lentinula edodes (shitake), used in this research, is a fungus belongs to the class of Basidiomycetes, classified as white rot. Its action occurs by decay, with no distinction between polysaccharides and lignin. The attack of this fungus causes gradual erosion of the cell wall, but also the lignin (Rowell 2005). Although lignin resists the attack of most microorganisms, white rot fungi are also capable of efficiently degrade lignin (Wong 2009). After inoculation, the disks were placed in a climatic chamber with temperature and moisture control, keeping the saturation condition.

The termites used in this research were the *Coptotermes gestroi*. This species of subterranean termites is considered one of the most destructive, both for the urban arboriculture and agricultural areas (Passos et al., 2014). Despite it´s Asiatic origin, now it has been observed in many tropical and subtropical regions of the world. In Brazil, the state with most cases of infestation is the Southeast (Veiga, 1998).

For the velocity variation test as a function of the holes, we generated artificial holes on the disks (Table 1 and Figure 1). The cracks on the disk 12 (Figure 1c) was due to the drying, but it was not present when we performed the ultrasound measurements.

Table 1. Details of the disks on which were performed artificial holes

Disc	Diameter of the disc (mm)	Number of holes	Position of the hole	Diameter of the hole (mm)
7	370	2	Central e externo	50 mm cada
10	350	1	Central	50 mm
12	350	2	Central e externo	50 mm o central 60 mm o externo

a b c

Figure 1. Image disks 7 (a), 10 (b) and 12 (c), with artificial holes.

We measured all disks (Figure 2) using diffraction mesh, that is used by several researchers (Divos, 2002 and Secco, 2011). For these measurements the transmitter transducer is positioned at one point of the mesh while the receiver transducer is placed at the other points, so the wave propagate in different routes (Figure 2). Using the path length of the measurement routes and the propagation times in each route, the velocities were calculated.

Figure 1. Example of ultrasound measurement in the disc

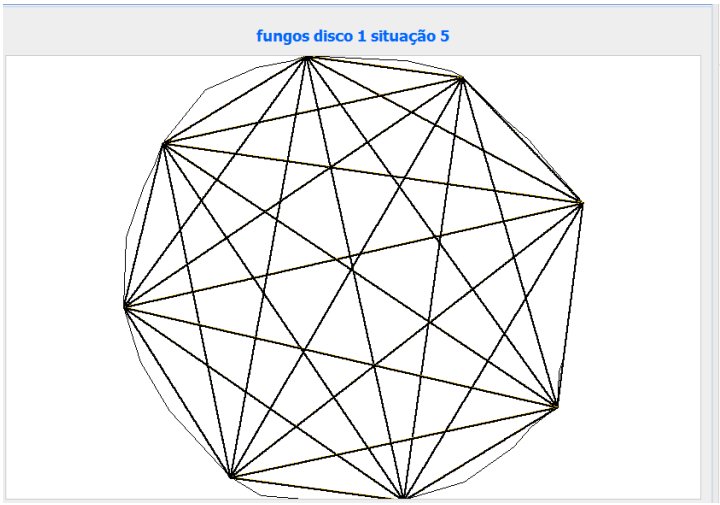

Figure 2. wave propagation routes in diffraction mesh

All discs were initially measured without any attack or hole - initial condition. New measurements were performed as the progress of decay by fungi and termites occurred and also after drilling the holes.

Results

During the fungal attack we verified that the velocities ranges have been modified, showing gradual and constant reduction values (Table 2). It is important to highlight that the disks were not degraded equally in the 11 months of observation, because it is a biological material. After 11 months of inoculation, the disks had visual deterioration.

Table 2. Ranges of velocity variation (minimum and maximum) (m.s-1) on the disks before and during the wood degradation process by fungi

Disc	T0	T1	T2	T3	T4	T5
1	218-1051	213-1014	207-912	182-806	104-753	82-668
2	250-1382	242-1367	220-1216	154-1192	121-991	61-966
3	261-1656	215-1752	177-1507	115-892	99-846	59-384
4	260-1536	259-1229	259-1042	258-1003	258-680	116-588
5	245-1711	228-1543	208-1331	180-1234	117-1155	99-696

T0 = before inoculation; T1 = 3 months after inoculation; T2 = 5 months after inoculation; T3 = 7 months after inoculation; T4 = 9 months after inoculation and T5 = 11 months after inoculation.

Using mean velocity in regressions it was possible to obtain linear models between the velocity and the elapsed time of inoculation, with correlation coefficients (R) ranging from 0.94 to 0.98; depending on the disc. The slope of the regression line also varied among discs (-72 to -25) indicating that the speed of degradation was not equal on all discs, even though they were initially very similar. The average slope (assuming all disks) was -49 with 18.5 % coefficient of variation between discs.

In discs inoculated by termites, visually there is still no degradation after 7 months of inoculation, but the external signals (waste) indicate that the degradation has already begun. The velocities ranges showed gradual and small reduction up to 7 months after inoculation (T3 in Table 3) and practically constant values in the last measurement (T4). The slower degradation caused by termites as compared with fungi has been depicted by the velocity variation.

Table 3. Ranges of velocity variation (minimum and maximum) ($m.s^{-1}$) on the disks before and during the degradation of wood by termites

Disc	T0	T1	T2	T3	T4
1	385 - 1507	363 -1507	334 -1507	331 - 1475	331 - 1475
2	940 - 1252	827 - 1267	891 - 1222	693 - 1033	533 -1033
3	947 - 1284	929 - 1226	793 - 1127	856 - 1160	837 - 1160
4	921 - 961	917 - 961	824 - 961	741 - 961	560 - 961
5	757 - 1172	877 - 1247	660 - 1076	595 - 1047	595 - 1047
6	530 - 1058	567 - 1134	515 - 1030	550 - 1100	550 -1100

T0= before inoculation; T1 = 3 months after inoculation; T2 = 5 months after inoculation; T3 = 7 months after inoculation; T4 = 9 months after inoculation

Using the mean velocity values, linear correlations also represented the velocity variation rate with elapsed time of inoculation ($0.76 < R < 0.97$), except for the disc 6, which showed no correlation between the velocity and time, indicating that degradation had not yet started or could not be captured by ultrasound. The average slope was -19 (disregarding the disc 6) with a coefficient of variation of 58 % between the disks. This result confirms that the degradation is still well below the discs attacked by fungi and the variation between the discs is much greater than that caused by fungi.

In the case of the disks with the simulation of hollow, we have only two points of observation (before and after the artificial hollow - Table 4), so, it is not appropriate to analyze the correlation coefficient of the regression. Linear regression was performed to compare the angular coefficient with the discs inoculated with fungi and termites. The average slope (assuming all disks) was -290 with a 29% coefficient of variation between discs. In the case of disks with holes the change in speed occurs sharply in minimum value and in the maximum there are little variation. This result is expected, once around the hole we have sound wood.

Table 4. Velocity ranges (minimum and maximum) (ms -1) and mean velocity before (T0) and after (T1) holes and variation between mean velocities at T1 and T0

Disc	T0	T1	Mean velocity In sound wood	Mean velocity after hole	Variation (%)
7	860-2387	340-2329	1623	1335	22
10	1009-1825	572-1850	1417	1211	17
12	1212-2255	553-2165	1734	1359	28

CONCLUSION

Direct comparison among velocities in discs degraded by fungi and termites and with hollow was not possible, because the wood integrity condition varied in all three cases. However, it was observed that, in all cases, it was possible capture the variation of the health condition of the wood by varying the wave propagation velocity. In the case of wood degraded by fungi discs it was found that the velocity variation occurs for the maximum and minimum value obtained in the disk, once the material degradation is broader than in the case of hollow or degradation by termites, where there are galleries surrounded by sound wood.

ACKNOWLEDGEMENTS

The authors thank the São Paulo Research Foundation (FAPESP - Proc n.2012/22599-9; Proc 2011/08286-5 and Proc 2015/05692-3) for the support; São Paulo State University "Julio de Mesquita Filho" (UNESP), Bioscience Institute Centre for Study of Social Insects, for the partnership; Sguario Forest Company S/A, for the wood material (logs of *Pinus elliottii*) and Fungi and Flora Company for the fungal strains.

REFERENCES

BUCUR, V. (2005). Ultrasonic techniques for nondestructive testing of standing trees. Ultrasonics, 43:237-239.

DIVOS, F.; SZALAI, L. 2002. Tree evaluation by acoustic tomography. In: Proceedings of the 13th International symposium on nondestructive testing of wood; 2002 August 19. 21; Berkeley, CA. Madison, WI: Forest Products Society: 251.256. 2002.

KIM, Kwang-Mo; PARK, Joo-Saeng; LEE, Sang-Joon; YEO, Hwanmyeong; LEE, Jun-Jae. Development of a portable ultrasonic computed tomography system for detecting decay in wood. In: International Symposium on Nondestructive Testing of Wood, 15., 2007, Duluth, Minnesota, USA. Anais Duluth: Forest Products Society, 2007, v.1, p. 191-195.

PASSOS, E.M.; ALBUQUERQUE, A.C.; MARQUES, E.J.; TEIXEIRA, V.W.; SILVA, C.C.M.; OLIVEIRA, M.A.P. (2014). Efeitos de isolados do fungo Isaria (Persoon) sobre o cupim subterrâneo *Coptotermes gestoi*. Arq. Inst. Biol. V.81(3), pp.232-237

PUCCINI, C. T.; **Avaliação de aspectos de qualidade da madeira utilizando o ultra-som,** 139p. Tese (Doutorado em Engenharia Agrícola) – Na área de concentração de Construções Rurais, Faculdade de Engenharia Agrícola, Universidade Estadual de Campinas, Campinas (SP), 2002.

ROEWLL, R. M.; Handbook of Wood Chemistry and Wood Composites, 1st ed., CRC Press: Madison, 2005.

SECCO, C.B. Detecção de ocos em toras utilizando métodos de propagação de ondas. ultrassonicas.112p. Tese (Mestrado em Engenharia Agrícola), Na área de concentração de Construções Rurais, Faculdade de Engenharia Agrícola, Universidade Estadual de Campinas, Campinas (SP), 2011.

WONG, D.W. (2009). Structure and action mechanism of ligninolytic enzymes. Applied Microbiology and Biotechnology, v.157 (2), pp.174-209

Condition Assessment of a Historic Trout Rearing Station In Upper Michigan

Frederico J. N. França
Department of Sustainable Bioproducts, Mississippi State University, Starkville, Mississippi, USA, fn90@msstate.edu

Tâmara S. F. Amorim França
Department of Sustainable Bioproducts, Mississippi State University, Starkville, Mississippi, USA, tsf97@msstate.edu

Lon A. Yeary
Director of Development & Outreach, Engineering Intern, Forest Products Laboratory, Madison, Wisconsin, USA, muskie.yeary15@gmail.com

Christopher Hohnholt
Assistant Research Scientist, School of Forest Resources and Environmental Science Michigan Technological University, Houghton, Michigan, USA, cahohnho@mtu.edu

John W. Forsman
School of Forest Resources and Environmental Science Michigan Technological University, Houghton, Michigan, USA, jwforsma@mtu.edu

Robert J. Ross
Supervisory Research General Engineer Forest Products Laboratory, Madison, Wisconsin, USA, rjross@fs.fed.us

Abstract

Michigan Technological University's (Michigan Tech) School of Forest Resources and Environmental Science maintains a log cabin on the north branch of the Otter River in southern Houghton County (Portage Township), Michi- gan. The cabin was built in 1934–1935 and measures 150 m2. The cabin's location is less than 10 m from the river, and when combined with the region's high snowfall (5+ m per year) and subsequent spring melting, is highly susceptible to occasional flooding and subsequent water damage and decay. The history and use of the cabin dates back to the mid- 1930s. The Michigan Conservation Department (predeces- sor of the Michigan Department of Natural Resources) and the Civilian Conservation Corps built the cabin in 1934–1935 to house workers who used the site as a trout hatchery. Since 1998 Michigan Tech, in cooperation with the USDA Forest Products Laboratory (FPL), has conducted periodic inspections of the cabin. This report summarizes results obtained from the inspection conducted in 2013. It includes a brief summary of the nondestructive testing techniques used, observations, and data from tests conducted on the cabin.

Keywords: Non-destructive assessment, decay, moisture content

Introduction

Michigan Technological University's (Michigan Tech) School of Forest Resources and Environmental Science maintains a log cabin on the north branch of the Otter River in southern Houghton County (Portage Township), Michigan, USA. The cabin was built in 1934–1935 and measures 150 m2. Untreated red pine (*Pinus resinosa*) logs were used as the primary construction material. The cabin's location is less

than 10 m from the river, and when combined with the region's high snowfall (5+ m/year) and subsequent spring melting, results in it being highly susceptible to occasional flooding and subsequent water damage and decay.

The history and use of the cabin dates back to the mid- 1930s. The Michigan Conservation Department (predeces- sor of the Michigan Department of Natural Resources) and the Civilian Conservation Corps built the cabin in 1934– 1935 to house workers who used the site as a trout hatchery. Grayling (*Thymallus arcticus*), rainbow (*Oncorhynchus mykiss*) and German brown (*Salmo trutta*) trout were propa- gated at the site. The cabin was transferred to Michigan Tech in 1955 with the reservation that public rights of hunt- ing, fishing, and trapping would be maintained. The cabin has been used regularly by students of Michigan Tech's School of Forest Resources and Environmental Science. Access to the cabin is also granted to a variety of user groups within the local community.

Ongoing maintenance of the cabin is required because of its proximity to the river and the region's heavy annual snow fall. Excessive water exposure as a consequence of flooding of the nearby river has resulted in the deterioration of several of the logs of the cabin during its service life. For example, in 1959, deteriorated logs were removed and re- placed with a ventilated crawl space using a red sandstone foundation. Several attempts to mitigate the effects of snow on the roof have been undertaken. Asphalt shingles replaced the original cedar shake roof in 1956, and in 1990 a metal roof was installed.
Since 1998, Michigan Tech has conducted periodic inspections of the cabin in cooperation with the USDA Forest Products Laboratory (FPL). This research note summarizes results obtained from the inspection conducted in 2013. It includes a brief summary of the techniques we used and observations and data from tests conducted on the cabin.

Methods

We inspected the cabin on July 30, 2013. Figure 1 is the cabin, and Figure 2 illustrates the location of the cabin relative to the Otter River.
Similar inspections of the cabin were completed in 1998 and 2008. In these inspections, we used accepted inspection techniques to assess the condition of the timbers that comprise the cabin. These techniques are discussed in detail in *Wood and Timber Condition Assessment Manual*, *Second Edition* (White and Ross 2014). A brief description of the techniques we used follows.

Figure 1 – Otter River cabin, 2013.

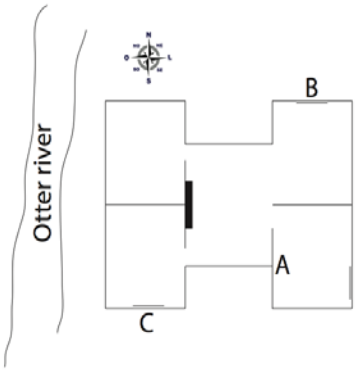

Figure 2 – Orientation of the cabin relative to the Otter River. Note the location of walls A, B, and C.

Visual Inspection

The simplest method for locating deterioration in wood members is visual inspection. An inspector observes the structure for signs of actual or potential deterioration, noting areas that require further investigation. Visual inspection is useful for detecting intermediate or advanced surface decay, water damage, mechanical damage, or failed members. Visual inspection cannot detect early stage decay or deterioration. Several key indicators are looked for in visual inspections: fruiting bodies (evidence of advanced decay), staining or discoloration of members (indicators of water damage), evidence of insect activity (holes, frass, and powder posting), plant or moss growth in a member, deep checks or splits, and failed or missing members.

In our inspection of the cabin, we specifically looked for the following: 1. Evidence of water intrusion and subsequent damage, especially near its foundation, and 2. Evidence of structural failure of the timbers and noting collapsed timbers near the foundation and at hips and valleys of the roof.

Sound Transmission

A significant volume of research has been devoted to the use of sound waves for locating areas of deterioration in timber structures, and a practical set of guidelines for their use has been prepared by FPL (Ross et al., 1999). In summary, the transmission of sound in wood is affected significantly by the presence of deterioration. Consequently, ultrasound and stress-wave based technologies have been developed and are widely used to inspect wood structures (Allison et al., 2008; Brashaw et al., 2005; Clausen et al., 2001; Emerson et al., 2002; Ross et al., 1999; Ross et al., 2006) and have been used for the assessment of culturally significant historic ships and artifacts (Ross et al., 1998; Wang et al., 2008; Dundar and Ross, 2012).

We used a simple, inexpensive stress-wave timer in our inspection (Fig. 3). Sensors were placed on opposite sides of a timber. The timber was then struck, generating a stress wave. The time it took for the wave to travel between the sensors was measured by the timer and recorded. Transmission times for wood from several species are known and were used as a baseline. Transmission times significantly longer than baseline values indicated the presence of deteriorated wood.

Figure 3 – Testing of wall timbers using a stress-wave timing device.

Micro-Drilling Resistance

Simple mechanical tests are frequently used for in-service inspection of wood members in structures. Drilling and coring are the most common, simple tests used to detect internal deterioration. Both are used to detect the presence of voids and to determine the thickness of the residual shell when voids are present. Micro-drilling resistance is a commercially developed technique originally developed for use by arborists and tree care professionals to evaluate the condition of urban trees and locate voids and decay. It is now being used to identify and quantify decay, voids, and termite galleries in wood beams, columns, poles and piles (Fig. 4) (Brashaw et al., 2005). The underlying premise for this technique is that de- graded wood is relatively soft and will have low resistance to drill penetration.

Figure 4 – Micro-drilling resistance of wall timber in Otter River cabin.

Our tests were conducted using a micro-drilling resistance device manufactured by IML, Inc. (Instrument Mechanic Labor, Inc., Kennesaw, Georgia). We conducted micro-drilling resistance tests in areas of the timbers that we believed contained deteriorated wood, based on results from our visual assessments and stress-wave testing.

Results

Visual Inspection

Figures 5 and 6 illustrate examples of the types of deterioration we found in our visual inspection. Note that the logs used in the construction of the cabin were not treated with a wood preservative; hence they are highly prone to deterioration from decay fungi. Many of the logs that are in direct contact with the sandstone foundation showed signs of significant deterioration. The log shown in Figure 3 is an excellent example of the type of deterioration we observed. It contained significant splits and cracks, and upon probing with a pocket knife was found to be soft, both indicators of advanced deterioration.
Many of the logs showed signs of severe deterioration, as shown in Figure 5, with the ends of several having been entirely destroyed. Several showed signs of mechanical failure.

Figure 5 – Visual evidence of deterioration of wall timbers.

Figure 6 – Visual evidence of severe deterioration of wall timbers.

Sound Transmission

Table 1 summarizes results from sound transmission tests for logs from several locations of the camp. Note that a baseline reading of approximately 200 micro-seconds or smaller indicates solid wood. Transmission times greater than 200 micro-seconds indicate deteriorated wood, and values greater than 250 indicate severe deterioration. Note that an electrical resistance moisture meter was used to determine their moisture content. Moisture content of the cabin's timbers ranged from 8.0% to 20.4%.

Table 1 – Results from stress wave tests of timbers in the Otter River cabin

Wall	Timber Position in the Wall	Stress Wave Transmission Time (μs)	Comments
A	1	250	Deteriored
	2	289	
	3	262	Deteriored
	4	289	Deteriored
	5	246	
	6	319	
	7	248	Deteriored
	8	526	Severe Deterioration
B	1	135	
	2	130	
	3	145	
	4	153	
	5	145	
	6	235	Deteriored
C	1	174	
	2	232	Deteriored
	3	187	
	4	207	
	5	250	Deteriored
	6	256	Deteriored

Micro-Drilling Testing

Tests results from logs that compromised Wall Section A confirmed that many were deteriorated. Most had an outer shell of solid material, whereas their core was severely deteriorated. Similarly, micro-drilling testing of several timbers in Wall Section C confirmed that they were significantly compromised (Fig. 7).

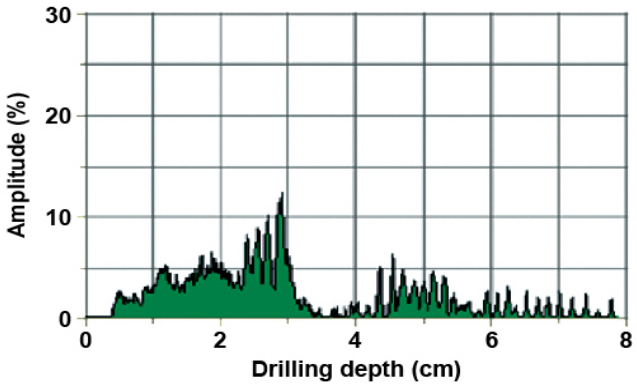

Figure 7 – Typical results obtained from a micro-drilling resistance test of a deteriorated timber from the Otter River cabin.

Conclusions

Because of its close proximity to the Otter River, the Camp's cabin has significant water damage. Several areas of the cabin have significantly deteriorated timbers. Wall A is directly underneath a valley in the cabin's roof. Prior inspections revealed significant water damage. The roof was repaired subsequent to the 1998 inspection. The logs that comprise this wall section have been water damaged because of flooding from the river and water entering through the roof. All of the logs in this section are deteriorated, some severely. The logs in Wall B of the cabin showed no signs of deterioration. Several of the logs in Wall C were deteriorated.

References

Allison, R.B.; Wang, X.; Ross, R.J. 2008. Visual and nonde- structive evaluation of red pines supporting a ropes course in the USFS Nesbit Lake Camp, Sidnaw, MI. Proceedings, 15th Nondestructive Testing of Wood Symposium, Sep- tember 10–12, 2007, Duluth, MN. Forest Products Society: 43–48.

Brashaw, B.K.; Vatalaro, R.J.; Wang, X.; Ross, R. J.; Wack- er, J.P. 2005. Condition assessment of timber bridges. 2. Evaluation of several stress wave tools. General Technical Report FPL–GTR–160. Madison, WI: U.S. Department of Agriculture, Forest Service, Forest Products Laboratory. 11 p.

Clausen, C.A.; Ross, R.J.; Forsman, J.W.; Balachowski, J.D. 2001. Condition assessment of roof trusses of Quincy mine blacksmith shop in Keweenaw National Historical Park. Re- search Note FPL–RN–0281. Madison, WI: U.S. Department of Agriculture, Forest Service, Forest Products Laboratory. 4 p.

Dundar, T.; Ross, R.J. 2012. Condition assessment of 2500 year old wood coffin. Research Note FPL–RN–0327. Madison, WI: U.S. Department of Agriculture, Forest Service, Forest Products Laboratory. 3 p.

Emerson, R.; Pollock, D.; McLean, D.; Fridley, K.; Pellerin, R.; Ross, R.J. 2002. Ultrasonic inspection of large timber bridge members. Forest Products Journal. 52(9): 88–95.
Ross; R.J.; Soltis, L.A.; Otton, P. 1998. Assessing wood members in the USS Constitution using nondestructive eval- uation methods. APT Bulletin. 29(2): 21–25.

Ross, R.J.; Volny, N.; Pellerin, R.F.; Salsig, W.W.; Falk, R.H. 1999. Inspection of timber bridges with stress wave nondestructive evaluation tools. A guide for use and interpretation. General Technical Report FPL–GTR–114. Madison, WI: U.S. Department of Agriculture, Forest Service, Forest Products Laboratory.

Ross, R.J.; Brashaw, B.K.; Wang, X. 2006. Structural condition assessment of in-service wood. Forest Products Journal. 56(6): 4–8.

Wang X.; Wacker, J.P.; Ross, R.J.; Brashaw, B.K. 2008. Condition assessment of the main structural members of historic steam schooner Wapama. Research Paper FPL–RP– 649. Madison, WI: U.S. Department of Agriculture, Forest Service, Forest Products Laboratory.

White, R.H.; Ross, R.J. 2014. Wood and timber condition assessment manual. Second Edition. General Technical Re- port FPL–GTR–324. Madison, WI: U.S. Department of Agriculture, Forest Service, Forest Products Laboratory. 102 p.

Assessment of biomass for energy industry in Arauco Forest Company

Simón Sandoval
Bioforest S.A., ARAUCO Chile. Camino Coronel Km 15 S/N, Coronel, Región del Bio-Bio, Chile. simon.sandoval@arauco.cl.

Juan José Quiroga
Bioforest S.A., ARAUCO Chile. Camino Coronel Km 15 S/N, Coronel, Región del Bio-Bio, Chile. juan.quiroga@arauco.cl.

Miguel Peredo
Bioforest S.A., ARAUCO Chile. Camino Coronel Km 15 S/N, Coronel, Región del Bio-Bio, Chile. miguel.peredo@arauco.cl.

ABSTRACT

The biomass from *Pinus radiata* stands with different productivity indexes, sites, seasons and industry sub-product biomass was assessed. The biomass extraction activities were classified by slope types. Stands with low and high productivity were selected for sampling, which were located in the northern and central areas of Arauco forestry land, during the summer and winter harvest seasons.

As a result, it was determined that there was an increase of the total biomass in high-productivity stands, with 250 dry tons/ha of total above-ground biomass and 177 dry tons/ha of total above-ground biomass in the central and northern areas, respectively. Also, in those different areas, the potential exploitable biomass (*PEB*) varied within a range of 22% to 31% compared to the total above-ground biomass (*TAB*) per hectare. The average PEB was composed of branches (40%), tree topping (20%), bark (20%) and needles (20%).

The moisture content of the biomass was determined using a portable measuring analyzer, MARRARI model M75D. Preliminary functions for determining moisture content were generated in different types of biomass for seven industrial plants. The calibration functions were generated following two phases: the first considered general functions, only differentiating between products, during the second phase local functions were calibrated, setting for both, product and industry type.

Keywords: Energy industries, ARAUCO Chile, Biomass assessment, MARRARI M75D.

INTRODUCTION

In Chile, Arauco has 12 energy industrial plants that use forest biomass as fuel, which is obtained from the by-products of industrial processes and forest harvesting operations. In 2015, the installed capacity of Arauco in Chile is 606 MW, allowing it provide over 80% of the energy requirements for the industrial processes, and has an energy surplus of 195 MW, which is injected into the Central Interconnected System (CIS).

Biomass consumption of the company is over 11 million m^3; mainly including sawdust, bark, wood chips, shavings and forest biomass. About 20% is supplied by the local external market, but the demand for biomass is steadily growing. Thus, bioenergy generation should primarily strive for more efficient management processes for biomass, in order to improve the purchasing strategy. In this context, knowledge of the quality of biomass is a tool to improve the procurement and supply processes.

Another important issue is to know and determine the amount of biomass extracted from forest harvesting sites. There are some studies that have determined these amounts (Howard 1972, Spichiger and Verdugo

2008, Moore 2010, Ximenes et al. 2012), but in Chile there still is not much literature associated to this research area. Overall, the research concludes that the residual biomass that remains after the tasks of harvesting and extraction is not related to site productivity (Moore 2010, Ximenes et al. 2012).

This study was focused on the characterization of biomass in three phases:

a) Determination of amount of above-ground biomass in the forest in different site indexes of the stands.
b) Quantifying and assessing the different types of biomass; total biomass and each of its components (stem, bark, branches, needles and cones), and of commercial biomass (*TCB*), potential exploitable biomass (*PEB*), total extracted biomass (*TEB*) and total residual biomass (*TRB*).
c) Assessing the industrial biomass and its quality parameters. The moisture content of the biomass was determined using a portable measuring analyzer, MARRARI model M75D. Preliminary functions for determining moisture content were generated in different types of biomass for seven industrial plants.

METHODOLOGY

The biomass from *Pinus radiata* stands with different productivity indexes, sites, seasons and industry sub-product biomass was assessed. The main objective was to quantify and evaluate the quality of the biomass. Slope types classified the biomass extraction activities. Stands with low and high productivity were selected for sampling, located in the northern and central areas of Arauco forestry land, during summer and winter harvest seasons **(Table 1)**.

Table 1. Sampling matrix for forest biomass assessment in both Northern and Central areas.

Season	Stands	
	Silviculture	Productivity
Summer	Managed	High
	Managed	Low
	Unmanaged	Low
Winter	Managed	High
	Managed	Low
	Unmanaged	Low

Biomass system production in tons was classified into five types: total above-ground biomass (*TAB*), total commercial biomass (*TCB*), potential exploitable biomass (*PEB*), total extracted biomass (*TEB*) and total residual biomass (*TRB*); which are subject to *TAB*=*TCB*+*PEB*, with *PEB*=*TEB*+*TRB*. Biomass models for total above-ground biomass for each tree component (*i.e.* stem, bark, branches, cones and needles) was generated by the use of simultaneous modeling and macro-nutrients data.

An industrial biomass assessment, mainly of sawdust, bark, wood chips and shavings was performed. This was done in seven industrial energy plants, using a portable moisture analyzer, MARRARI M75D, to measure moisture content. Sampling in seven industrial plants and 10 kinds of raw material was performed. Each function was performed with fresh material (under the arrival conditions of each industry) and was conditioned for outdoor summer months for about two weeks. This allowed for reducing its moisture content and for generating a set of validation functions for extreme moisture ranges. The required volume of each sample was ground ± 30 L. Each sample was processed with M75D equipment and 3 sub-samples were extracted. The moisture content sub-samples were later determined after drying them at 103°C ± 1 to constant weight. In total, 710 samples with MARRARI M75D and 2,130 laboratory samples to determine the moisture content were processed.

RESULTS

As a result, it was determined that there was an increase of the total biomass in high productivity stands with 250 dry tons/ha of total above-ground biomass and 177 dry tons/ha in the central and northern areas, respectively (see Figures 1 and 2). Also, in those different areas, the potential exploitable biomass (*PEB*) varied within a range of 22%-31% compared to total above-ground biomass (*TAB*) per hectare. The average PEB was composed of branches (40%), tree topping (20%), bark (20%) and needles (20%).

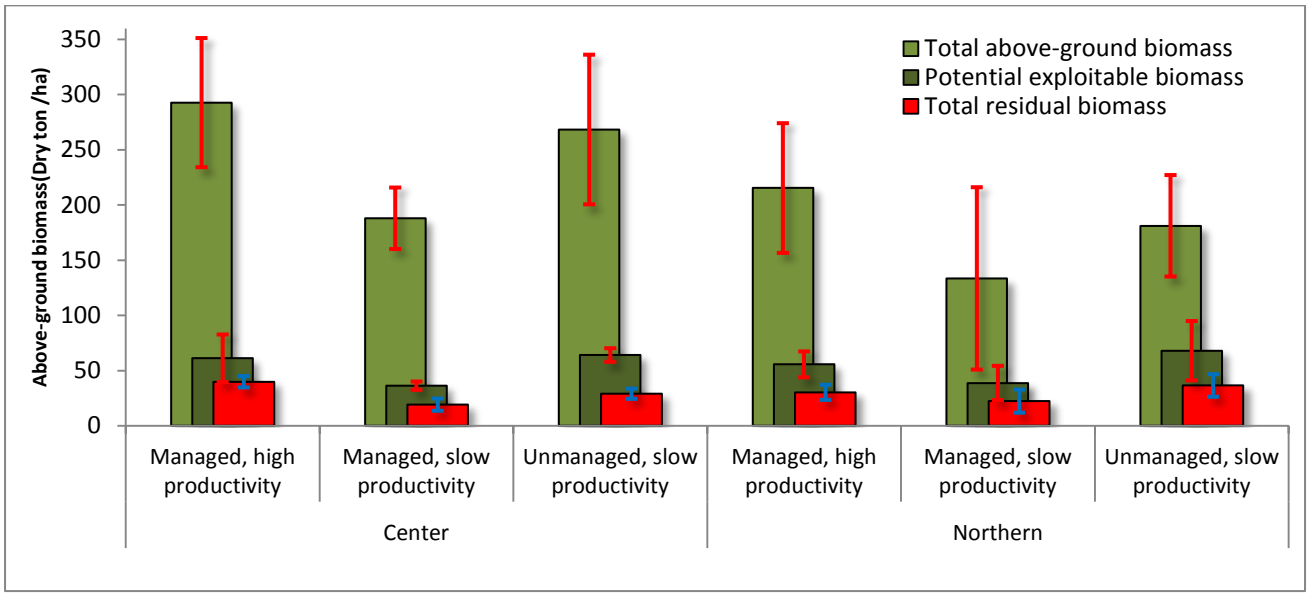

Figure 1. Biomass assessment by utilization.

Potential exploitable biomass in the Central and Northern areas was, on average, 54 dry tons/ha, corresponding to 22% and 31% with regard to the total above-ground biomass, respectively (see Figure 2). These differences were generated because of small trees in the Northern Area, where the extracted wood volume is less and it produces more potential exploitable biomass for use as energy.

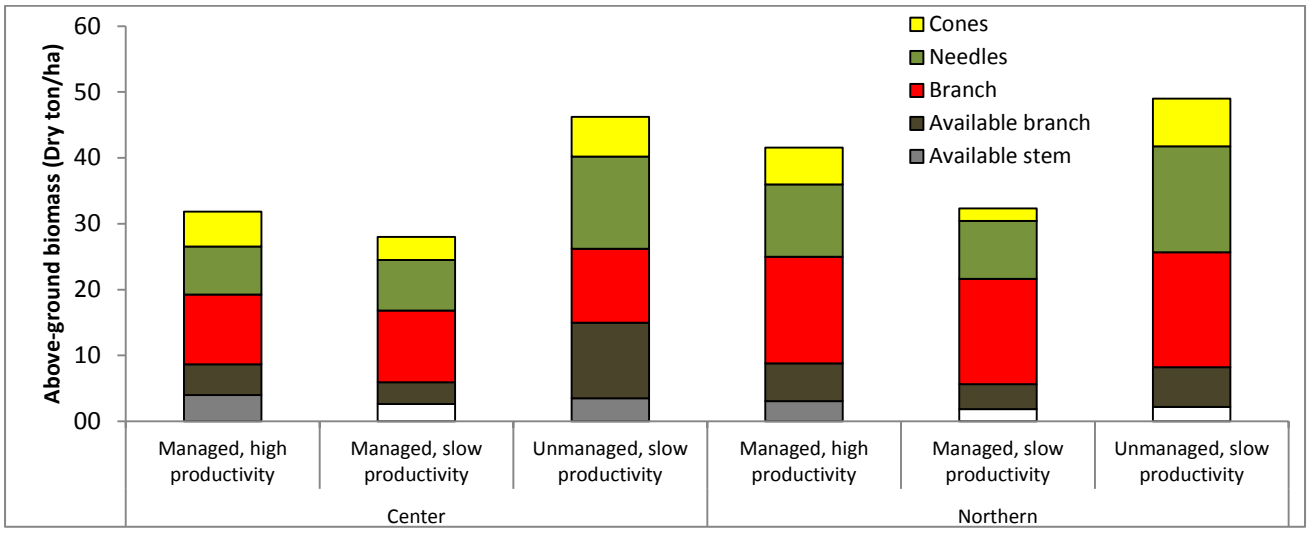

Figure 2. Potential exploitable biomass assessment by its components.

The quality of biomass was determined by removing the forest; bark and needles from the trees, which are the components with a highest calorific value with 5,300 and 5,000 cal/g, respectively, while the wood stems and branches had an average caloric value of 4,600 cal/g. Notwithstanding those variations in calorific value, the moisture content was the main determining factor of the quality of the biomass extraction activities. Moisture content had a negative proportional effect on the calorific value, which occurs in the biomass that is exported in winter and contains up to 20% inert material (i.e. mud, rocks, sand, etc.) (see Figure 3).

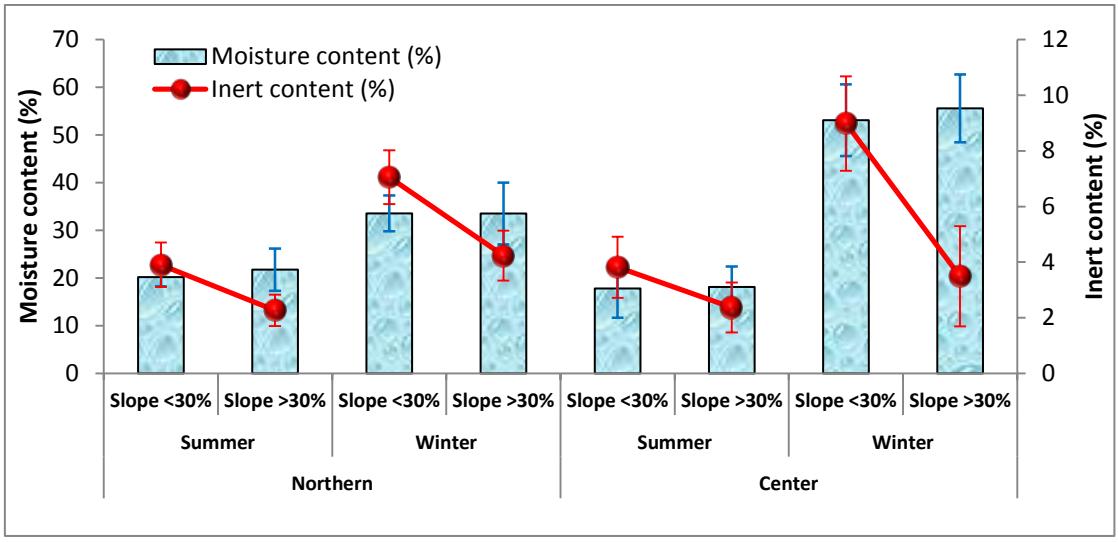

Figure 3. Moisture and inert content in the biomass by zone, season and utilization.

The calibration functions were generated by completing two phases: the first phase considered general functions, only differentiated between products, and the second phase calibrated local functions, which were set for both, product and industry type (see Figure 4).

Configured local functions improved the accuracy of moisture content determinations, demonstrating an average error of 3.1% to 14.7% when compared to moisture values determined in the laboratory (see Figure 4). Thus, the equipment demonstrated a high potential to be implemented in industries as a sampling and assessment tool for raw material. The analysis of means method demonstrated that all of the averages are statistically equal, demonstrating the robustness of the measurements made with the equipment and concluding that the functions are bias free in estimates of average moisture content. In general, the difference between the average moisture determination by using the M75D and the average moisture determination made in the laboratory did not exceed one percentage point. In only some cases, the bias in these estimates was higher; but it was not over 4 percentage points.

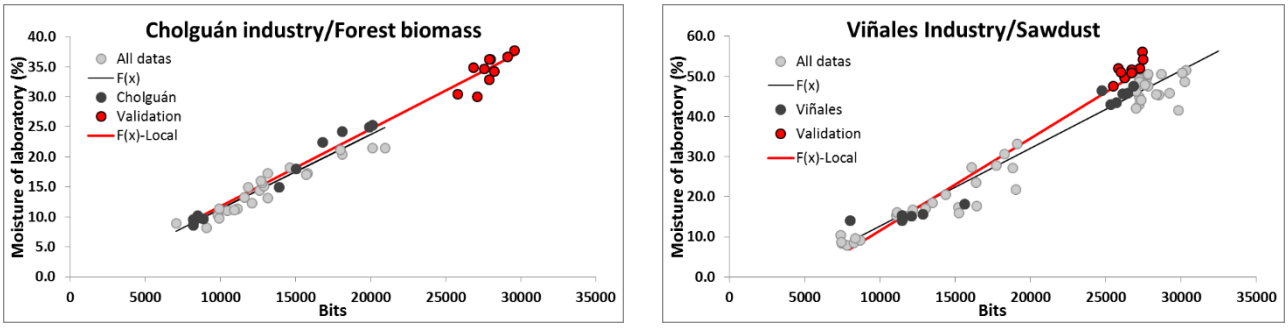

Figure 4. Functions calibration for estimating moisture using an MARRARI M75D. This is just an example considering that 70 functions (i.e., 10 biomass types and 7 industries) in total were calibrated.

CONCLUSIONS

The total above-ground biomass is higher in forests with high productivity. On average they scored 250 and 177 dry tons/ha of total biomass in the central and northern areas of the company, respectively.

The potential exploitable biomass is 22% to 31% with respect to the total above-ground biomass per hectare.

The residual biomass left on site mainly consisted of branches, stems and cones. The sum of these components was more than 90% of the total.

Residual biomass utilization in winter had higher moisture content and inert content in the form of clay and sand, which was generated. This figure was even higher when mechanical harvesting was performed using a tractor.

The portable equipment demonstrated great potential for being implemented at an industrial level as a characterization tool, for sampling and for a raw material census, mainly because of its ease of use and quick measuring time.

REFERENCES

Howard J. 1972. Measurement of logging residue: alternative applications of the line intersect method. Portland, Ore: Pacific Northwest Forest and Range Experiment Station, Forest Service, U.S. Dept. of Agriculture, 1972.

Moore J. 2010. Allometric equations to predict the total above-ground biomass of radiata pine trees. Ann. For. Sci. (67) 806. Pages 1-11.

Spichiger J., Verdugo E. 2008. Energy generation potential for forestry waste management in Chile. Non-Conventional Renewable Energy in Chile (CNE/GTZ), pages 56.

Ximenes F., Ramos J., Huiquan B., Cameron N., Pal Singh B., Blasi M. 2012. Determining Biomass in Residues Following Harvest in Pinus radiata Forests in New South Wales. Rural Industries Research and Development Corporation. Pages 78.

Early age evaluation by the stress wave speed for the breeding of high Young's modulus Japanese cedar

Kiyohiko Ikeda
Shizuoka Prefectural Research Institute of Agriculture and Forestry, Negata2542-8 Hamakita, Hamamatsu, Shizuoka Japan, kiyohiko1_ikeda@pref.shizuoka.lg.jp

Shigehiro Yamamoto
Shizuoka Prefectural Agriculture and Forestry College, Oro4034-5 Hamakita, Hamamatsu, Shizuoka Japan, shigehiro1_yamamoto@pref.shizuoka.lg.jp

Tetuji Hakamata
Shizuoka Prefectural Research Institute of Agriculture and Forestry, Negata2542-8 Hamakita, Hamamatsu, Shizuoka Japan, tetuji1_hakamata@pref.shizuoka.lg.jp

Shinya Yamada
Shizuoka Prefectural Research Institute of Agriculture and Forestry, Negata2542-8 Hamakita, Hamamatsu, Shizuoka Japan, shinya1_yamada@pref.shizuoka.lg.jp

Akira Kondo
Shizuoka Prefectural Research Institute of Agriculture and Forestry, Negata2542-8 Hamakita, Hamamatsu, Shizuoka Japan, akira1_kondo@pref.shizuoka.lg.jp

Abstract

The purpose of this study is to inspect the effectiveness of the wood quality evaluation technique of standing tree by stress wave speed in the early age (2- 7 years) for the creation of the high Young's modulus Japanese cedar (*Cryptomeria japonica*). About the Japanese cedar of selected clone tree among mating families of plus tree, we investigated the standing tree by a stress wave of velocity propagation (Vp) and growth traits from two years to seven years after planting and the log by dynamic Young's modulus (Efr) felled for the early period in two examinations forest. The individual tree difference of Vp was appeared between 1.5 to 2.5 km/sec, and the high correlation was recognized of the Vp for two years and three-six years. Furthermore, as a result of investigated of tree Vp in different test forest from four years to seven years, a similar tendency was confirmed. A high correlation was recognized between trees Vp of two or six years and Efr of log in felled six years. In addition, as for most of standing tree when Vp in four years showed more than 2.5 km/sec, it was esteemed that Efr in seven years showed higher than 6 kN/mm^2 that became the index of the high Young's modulus. A significant correlation was not recognized concerning the quantity of change of growth trait (diameter and height) and the quantity of change of Vp in during growth period.
Keywords: Japanese cedar, Stress wave propagation, early period evaluation, young’s modulus

Introduction

Japanese cedar is adapted to grow in climate and soil of Japan, it has been planted in each region as artificial silviculture softwood species. There are problem that the Young's modulus of Japanese cedar to using structural is lower than other conifers, improvement by breeding has been demanded. Therefore, it is need to improvement by breeding and it was selected a high Young's modulus individual from plus tree,

create new varieties by cuttings or mating, early evaluation of their material juvenile period is required. So far, for the purpose of early evaluation of high Young's modulus by breeding, we have been considering the possibility of standing trees Young's modulus evaluation by stress wave of velocity propagation method of cedar and cypress in the young age. In addition, inter-individual differences in the same stand it was clarified young period and the Young's modulus of the relevance of maturity, and the features of the stem within the variation of high Young's modulus cedar (Ikeda et al. 2009). Other, Miyashita et al evaluated the Young's modulus of the trunk in 10-year old cedar clone by stress wave velocity propagation (Miyashita et al. 2009). Others, in radiata pine, with 7 ~ 8 year old of trees or with 3 year old of logs, were evaluated the Young's modulus by the stress wave propagation velocity method (Matheson et al. 2008, Lindstorm et al. 2004).
In this study, in order to produce a high Young's modulus varieties, for cuttings seedlings were selected from plus tree mating family or the like as a mother tree candidates trees, trees of stress wave propagation speed over the time when to 7 year after planting 2 years (Young's modulus) and growth traits of annual variation, we examined the application as early material evaluation technique from the Young's modulus of the relevance of raw wood that was cut down to young period.

Materials and Methods

Test specimen of Japanese cedar tree is the cuttings seedlings, those were selected from Sugi plus tree and planted in Shizuoka forest and forestry product research center at 2 test plots. Test plot A was planted seedlings in 2008. Test plot B was planted seedlings in 2007. 175 trees of 50 cultivars selected from sugi plus trees has planted at test plot A, and 115 trees of 40 clones selected from sugi plus trees has planted at test plot B.
Stress wave propagation velocity (described as “Vp”) and diameter and the tree height were measured at the time of 2, 3, 4 and 6 years after planting by test stand A. When 5 years per 4 years and 7 years per 6 years had passed after planting by test B of woods, stress wave propagation speed, a diameter from the base of 80cm height and the tree height were measured. Stress wave propagation velocity (described as Vp) measured by sensor in the location of the ground clearance 20cm and 80cm using “FAKKOP”.
70 test trees were felled at the time of a distance for 6 years after planting by test plot A of woods. 50 test trees were felled at the time of a distance for 7 years after planting by test plot B of woods.
By cutting the logs of 0.2 ~ 1.2m from the roots part from tree, it were measured dynamic Young's modulus (described as Efr :$Efr = 4 \times fr2 \times L2 \times d$ lfr(Hz) is the fundamental resonance frequency, L (cm) is the length of the log and d is its green density (g/cm3) by a longitudinal vibration method.
It also cut from logs the circular disk specimen with a thickness of 40mm, it measured green density,oven-dried density and moisture content by oven-dried method.

Table1-Summary of test plots and Japanese cedar tree specimens

Test plot	Year	Measure tree age	Clone N	Specimens : N	
	Plant - Thinning			Tree	Log
A	2008 - 2014	2,3,4,6	50	175	70
B	2007 - 2014	4,5,6,7	40	115	50

Results and Discussion

Vp of the Standing tree at test plot A, the difference between individuals was observed 1.6 ~ 2.6 km/sec after two years of growth. In addition, the coefficient of variation of the Vp was the same 10% at the time of growth of 2 years to 6 years. Most of the trees had become faster Vp in accordance with the elapsed years increase in after planting. Increase of Vp according to the growth of one year, was about 0.125 ㎞ / sec after planting 2 years to 6 years. It was observed same results at test plot B from 7 years to 4 years after planting (Table 2).

Table2 -Velocity propagation、diameter and height of sugi standing tree at two test stands

	Velocity Propagation (Vp) (km/sec)				Diameter of 0.8m height (cm)				Height (m)			
Test plot A	2-year	3-year	4-year	6-year	2-year	3-year	4-year	6-year	2-year	3-year	4-year	6-year
Average	2.04	2.20	2.34	2.54	1.9	3.2	4.5	6.5	2.1	3.0	3.5	4.9
Max	2.63	2.74	2.91	3.25	4.0	5.5	8.6	10.8	3.5	4.2	5.3	7.6
Min	1.57	1.74	1.82	1.96	0.7	1.4	2.0	2.2	0.8	1.7	1.9	2.1
C.V(%)	10	10	10	10	37	26	26	31	24	16	17	22
Test plot B	4-year	5-year	6-year	7-year	4-year	5-year	6-year	7-year	4-year	5-year	6-year	7-year
Average	2.66	2.73	2.98	3.03	4.8	5.6	7.0	7.6	4.2	4.8	5.4	6.2
Max	3.29	3.37	3.58	3.63	9.5	11.6	14.2	15.7	6.8	7.3	7.8	9.3
Min	2.09	2.12	2.27	2.30	1.8	1.9	2.5	2.5	2.4	2.6	2.9	3.2
C.V(%)	10	10	9	9	35	36	36	37	23	23	21	23

C.V:Coefficient of variatio Vp:velocity propagation of stress wave

In Figure1, it shows the relationship between the Vp of 2 year-old and Vp of 3 -6 year-old or between the Vp of 4 year-old and Vp of 5 -7 year old. At the test plot A, high correlation between each measurement year was observed, the correlation coefficient was 0.7 or more. Correlation coefficient in the test plot B showed a higher correlation with 0.8 or more. From these results, Individual differences of Vp appeared at the time of early age the stem was lignified, It was suggested that estimate the Young's modulus.
Between the Vp and the diameter and height, significant correlation was not recognized at plot B. On the other hand, a weak positive correlation was seen in part of the measured year at plot A between them (Table 3). About the amount of variation in growth period from four years to one year, the correlation between the trees Vp and growth traits were not observed in both plot A and plot B. From these results, growth traits and the Young's modulus of the stem was suggested that an independent genetic trait to each other, and it was considered both can create both excellent varieties.
Efr of thinning the log is test plot A 3.5-8 kN / mm^2, is test plot B 4-8.5 kN mm^2, and the average value of plot B was about 1.5 kN /mm^2 faster than plot A (Figure 2). Also, comparing the Vp average value at 4 years, plot B was faster than plot A.From these results, individuals of high Young's modulus at test plot B appeared to be more as compared to plot A. In the test plot A, high correlation was observed between Efr of log and Vp of tree at 6 years old. Furthermore between Vp of trees measured at 2 years old, and Efr of log measured at 6 years old, a high correlation was observed.

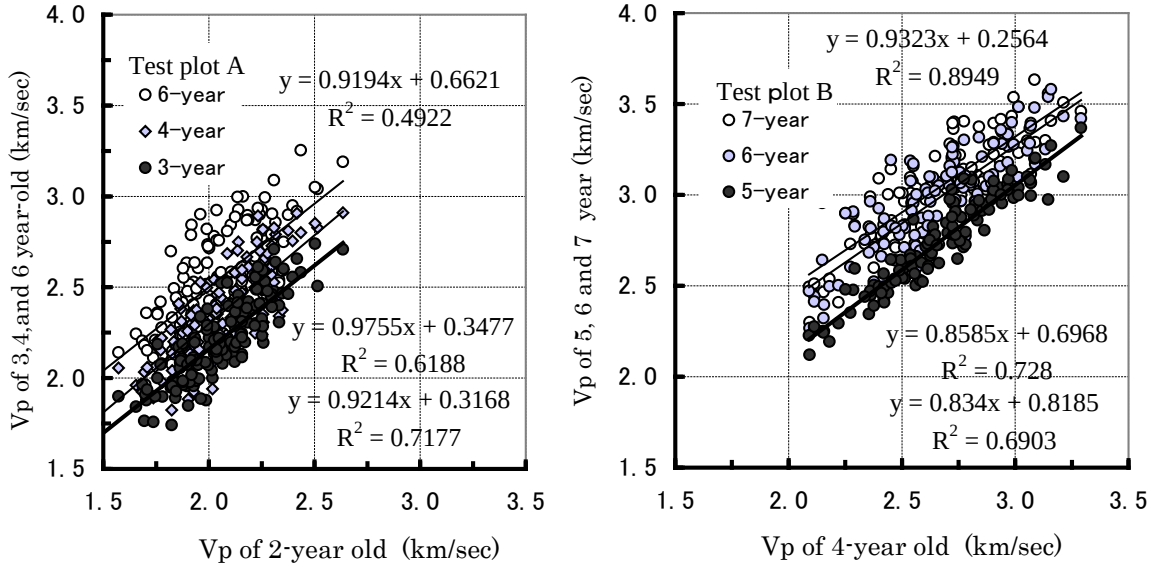

Figure1 - Comparison in the measurement-year of Vp of tree trunk in juvenile period after planting.

Table3-Correlation coefficient of Vp, diameter and height growth between each years

Test plot A N=175					Test plot B N=115				
	2-year	3-year	4-year	6-year		4-year	5-year	6-year	7-year
Vp	Vp				Vp	Vp			
2-year					4-year				
3-year	0.853				5-year	0.946			
4-year	0.786	0.890			6-year	0.853	0.896		
6-year	0.702	0.772	0.825		7-year	0.831	0.860	0.904	
Vp	Diameter 0.8m height				Vp	Diameter 0.8m height			
2-year	0.391				4-year	0.141			
3-year		0.051			5-year		0.057		
4-year			0.040		6-year			0.045	
6-year				0.250	7-year				0.173
Vp	Height				Vp	Height			
2-year	0.478				4-year	0.030			
3-year		0.348			5-year		0.159		
4-year			0.203		6-year			0.063	
6-year				0.375	7-year				0.084

Vp:velocity propagation of stress wave

In the test stand B was thinning at 7 years old, similarly high correlation was observed between Efr of l ogs and Vp of trees. It also has been suggested that 7 years old Efr of logs can be estimated from a four-year Vp of trees.

By dividing the cedar lumber examined the Young's modulus in our previously reported, if the Young's modulus of the tree wick to 5 annual rings is more than 5kN/mm^2, the Young's modulus of 20 annual rings since have been found to be it likely will be 8kN/mm^2 or higher (JAS Solid timber Mechanical Grade E90). In addition, we have inferred that if Vp of the tree at five years showed more than 2.5km/sec, the Young's modulus of the tree after 20 years will be 8kN/mm^2 or more (Ikeda et al 2009). Fujisaki was multiple regression analysis using cambial age and annual ring width as predictor variable for estimating MOE of sugi lumber (Fujisaki. 1983).

We tried to re-verification of these results. From cedar large square timber beams (Young's modulus 8kN /mm^2 or 10kN/mm^2 or more), it was sampling small test pieces of the site and subsequent annual ring sites from pith to 5 rings. Specimens was measured Young's modulus in the longitudinal vibration method. Also, it was measured visually the number of tree rings from the pith.

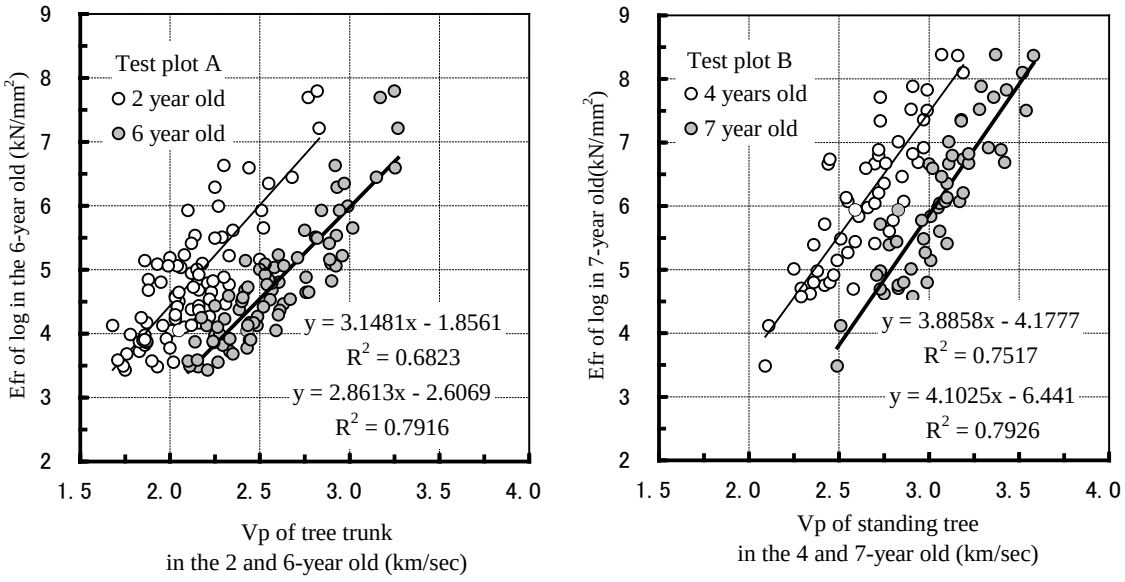

Figure2-Relationship between Vp of standing tree and Efr of log in the early age at two test plots

Table4 -Efr of log ,green or ovendrid density, moisture content and effective density

Test plot		Efr	G-Density	Od-density	MC	Effective Density 1	2	3
		(kN/mm^2)	(kg/m^3)		(%)	(kg/m^3)		
A	Average	4.8	1029	431	172	909	924	911
	C.V.(%)	20	4	10	14	4	4	4
B	Average	6.1	968	417	166	884	899	886
	C.V.(%)	19	6	9	12	6	6	6

Efr: Dynamc young modulus of sugi butt log, G-density:Green density,
Od-density: Oven-dried density, MC: moisture content
Effective density:1-3 :Calculated G and Od density, G-density and MC, Oddensity and MC, respectvely.

Relationship between Efr and annual ring number (assumed to cambial age) from pith was shown in Figure 3. The relationship between them was a high determining coefficient in the case of applying the logarithmic regression. According to a logarithmic regression equation, if the Young's modulus of lumber beams of more than $10kN/mm^2$ is, Efr from the pith to 5th annual ring was $6kN/mm^2$.
From their logarithmic regression equation, we induced the reference line for assessing when grown from 2 to 10 years, for tree stem expected to be a high Young's modulus in the maturation period.
In addition, the effective density calculated from the green density and oven-dried density and moisture content, the average value was approximately $900kg/m^3$ at 2 test plots both (Sobue.1993). Dynamic Young's modulus (Ev) of standing-trees at both plots in each year were calculated by following formula, using Vp of each year and effective density ($900 kg/m^3$: a constant value assumed).

$$Ev = Vp^2 \times 900$$

Ev of each years at plot A were exceeded an estimated line $8kN/mm^2$, and at plot B were exceeded an estimated line $10kN/mm^2$ (Figure 4). From these things, it was speculated that about more than half of both the plot of trees will be high Young's modulus at maturation period and later growth.
According to some previous reports, by examining MFA (S2 microfibril angle) of 2 -3 rd annual ring, it has been suggested to be a possible early evaluation of good individual, and to be able to select a high Young's modulus cedar (Nakada et al. 2003, Ishidoh et al.2009). To summarize the above results, it appeared to be able to evaluated of the Young's modulus of standing tree at the stage of 4 years from 2 years after planting of seedlings period without felling the trees.

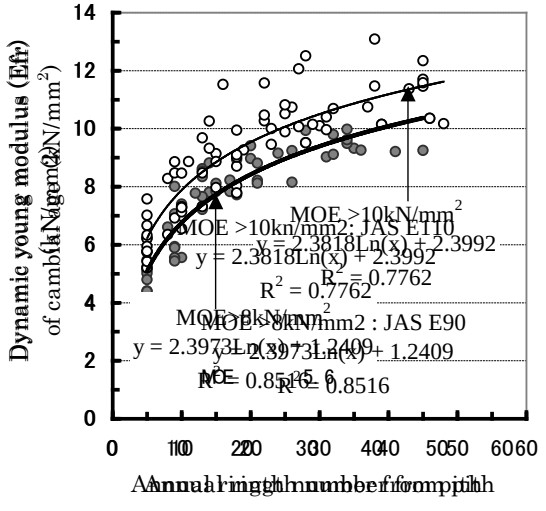

Figure3-Relationship between dynamic young modulus (Efr) of cambial age and annual ring number from pith

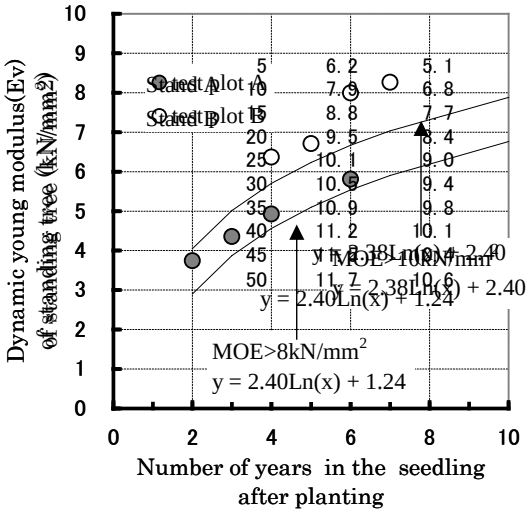

Figure4-The reference line for assessing the high Young's modulus cedar during 2-10 year growth、and the average value of

Conclusions

In the 2-4 year growth period stem was lignified after planting cedar sapling, we were examined whether it is possible to Young's modulus evaluation of the young period by the measurement of stress wave propagation. Vp of the difference between individuals was observed 1.6 ~ 2.6km/sec after two years of growth. In addition, the coefficient of variation of the Vp was the same 10% at the time of growth of 2 years to 6 years. Most of the trees had become faster Vp in accordance with the elapsed years increase in after planting. Vp of trees measured at 2 years old, and Efr of log measured at 6 years old, a high correlation was observed. Individual differences of Vp appeared at the time of early age the stem was lignified, It was suggested that estimate the Young's modulus.

.

References

Fujisaki K. 1983, Multiple regression analysis of the MOE of sugi wood using cambial age and ring width as predictor variable. Bulletin of the Ehime University Forest. 22. 1-6.

Ikeda, K.; Yamamoto, S; Kondo, A. 2009, Young modulus variations of Sugi and Hinoki in the early growth period and in the direction of the trunk radiation. Technical bulletin of the Shizuoka research institute report of agriculture and forestry, 2: 69-74.

Ishidoh, M.; Ishiguri, F.; Iizuka, K.; Yokota, S.; Ohno, H.;Yoshizawa, N. 2009, The evaluation of modulus of elasticity at an early stage of growth in Sugi wood using S2 microfibril angle of latewood tracheids as a wood quality indicator. Mokuzai Gakkaishi, 55(1):10-17.

Lindstorom, H.; Harris, P.; Sorensson, S.T. 2004, Stiffness and wood variation of 3-year old Pinus radiata clone. Wood Science technology. 38:579-597.

Matheson, A,C.; Gapare, W,J.; Ilic, J.;Wu, H,X. 2008, Inheritance and genetic gain in wood stiffness in radiata pine assessed acoustically in young standing trees. Silvae Genetica, 57(2): 56-64.

Miyashita, H.; Orita, H.; Handa, T. 2009, Evaluation of the wood quality of young *Cryptomeria japonica* clones. Mokuzai Gakkaishi, 55(3):136-145.

Nakada, R.; Fujisawa, Y.; Hirakawa, Y. 2003, Effects of Clonal Selection by Microfibril Angle on the Genetic Improvement of Stiffness in Cryptomeria japonica D. Don. Holzforschung, 57(5): 553-560.

Sobue, N. 1993, Simulation study on stress wave velocity in wood above fiber saturation point. Mokuzai Gakkaishi, 39(3): 271-276.

Nondestructive evaluation of coconut palm wood by means of ultrasonic and natural frequency methods

Matthias Wolters
Laboratory for Timber Engineering, Products and Production, University of Applied Sciences Ostwestfalen-Lippe, Lemgo, Germany, matthias.wolters@stud.hs-owl.de

Timm Hüls
Laboratory for Timber Engineering, Products and Production, University of Applied Sciences Ostwestfalen-Lippe, Lemgo, Germany, timm.huels@stud.hs-owl.de

Konrad Solbrig
Laboratory for Timber Engineering, Products and Production, University of Applied Sciences Ostwestfalen-Lippe, Lemgo, Germany, konrad.solbrig@hs-owl.de

Katja Frühwald
Laboratory for Timber Engineering, Products and Production, University of Applied Sciences Ostwestfalen-Lippe, Lemgo, Germany, katja.fruehwald@hs-owl.de

Abstract

The application of nondestructive methods such as measurements of ultrasonic velocity and natural frequency to determine elasto-mechanical properties is widely spread for dicotyledonous wood species. The aim of this research study was to examine the applicability of these methods on monocotyledonous coconut wood. Dynamically determined MOE values were found considerably higher compared to static MOE resulting from the anatomic structure of coconut wood combined with respective test conditions. Natural frequency measurement seems to be well-suited for small-sized specimens under laboratory conditions via flexural vibration and for larger specimens in industrial environment via longitudinal vibration. In case of ultrasonic measurements, coupling of the conical probes appears difficult to implement into an industrial process, whereas the results are promising for laboratory use.

Keywords: coconut wood, ultrasonic, natural frequency, dynamic MOE, static MOE

Introduction

Coconut trees (Cocos nucifera L.) are mainly cultivated in large plantations for food production and as an industrial raw material. Their productivity decreases markedly at an age around 50…60 years. It is common practice to replace the trees at this stage. Each year, large quantities of coconut palm trunks are obtained. Traditionally, these trunks have been waste. In recent years, potential commercial uses for coconut wood were explored. It can substitute tropical hardwoods for various purposes, e. g. as construction timber. For utilisation as load-bearing products, defined elasto-mechanical properties – and therefore strength grading of the lumber – are indispensable.

Anatomic wood structure of monocotyledonous palms differs from deciduous and coniferous trees. Palms have no secondary growth, due to absence of cambium layer. Palm wood consists of high density vascular bundles embedded in soft (lower density) parenchymatous ground tissue (without knots). Bulk density of

palm wood depends on size, number, and anatomical structure of vascular bundles. Thus, palm trunks show a significant bulk density gradient both over trunk height and cross section. The number of vascular bundles decreases logarithmically from cortex to the centre of the trunk (Killmann 1993). According to Fathi (2014), the amount of vascular bundles increases with increasing stem height. Because of varying anatomical structure of vascular bundles with increasing stem height, bulk density and mechanical properties decrease accordingly. Knots as probably the most important grading criteria for deciduous and coniferous lumber are not present in palm lumber. Hence, palm wood is more homogeneous compared to dicotyledonous wood. Elasto-mechanical properties of coconut wood, especially MOE and MOR, correlate with bulk density (Frühwald et al. 1992). Presumably, bulk density resp. size and number of vascular bundles per area are the most important visual grading criteria for coconut lumber. In an exploratory research study, the applicability of ultrasound and natural frequency measurements for grading purposes of coconut wood was evaluated by comparing dynamic MOE from ultrasound (MOE_{US}) and longitudinal ($MOE_{NF,\ long}$) as well as flexural vibration ($MOE_{NF,\ flex}$) with static MOE and bulk density.

Material and methods

Dry coconut lumber from Indonesia (region Manado, North Sulawesi) was sawn and planed aiming at test specimens with preferably even cross-sectional bulk density distribution. Two sizes of test specimens were prepared: medium-sized (1,100 × 58 × 22 mm³, $n = 23$) and small-sized (380 × 22 × 22 mm³, $n = 77$) specimens. Due to sample size and anatomic structure, medium-sized specimens show a more distinct bulk density gradient over the cross section in comparison to the small-sized specimens. Bulk density of small-sized test specimens ranges from 304 kg/m³ to 1,043 kg/m³ as shown in Figure 1. All samples were categorised in bulk density classes. Prior to all measurements, all samples were conditioned to constant weight at 20 °C and 65 % relative humidity (according to DIN 50014:1985).

Figure 1—Cross sections of exemplary small-sized test specimens with bulk density range 320…450…560…780…960 kg/m³ (from left to right).

Considering all test specimens, ultrasonic time-of-flight and natural frequency were measured with subsequent dynamic modulus of elasticity (MOE_{dyn}) computation. Three point bending tests (according to DIN 52186:1987 with a support span of 15 × thickness) were carried out for comparative purposes. For nondestructive reasons, load application was stopped within the elastic range (at 33 % F_{max}). Ultrasonic time-of-flight measurements in longitudinal wood direction were carried out by means of ultrasonic device STEINKAMP BP 5, Bremen, Germany, with conical probes for longitudinal waves (50 kHz). Coupling was performed directly without coupling agent. On medium-sized specimens, measurements were performed at three measuring points within the cross section, because of their substantially bulk density gradient. The samples were fixed free-floating between spring-loaded ultrasonic probes in order to keep testing conditions (especially contact pressure) constant. MOE computation was done by the equation according to Steiger (1991). For sound intensity and damping effect determination based on electrical signal measurement, a two-channel digital oscilloscope was used. The ratio of

received maximum voltage amplitudes to zero amplitudes is used for calculation of sound attenuation coefficient α [m^{-1}] (cf. Bucur 2006). Natural frequency of longitudinal and flexural vibrations was determined employing Grindo*Sonic* MK5, J.W. Lemmens N.V., Leuven, Belgium ($MOE_{NF,\ long}$ and $MOE_{NF,\ flex}$),
a portable device of VISCAN, Microtec, Brixen, Italy ($MOE_{NF,\ long}$), and a miniature (2.4 g weight) piezoelectric accelerometer KS94B.10/01, MMF, Radebeul Germany ($MOE_{NF,\ flex}$). Longitudinal vibrations were used for intentionally comparison to ultrasound results (MOE_{US}). Flexural vibrations were determined to illustrate the differences between respective vibration modes. The miniature piezoelectric accelerometer was used as a comparison method in addition to Grindo*Sonic* and VISCAN measurements to analyse the general suitability of involving a mass vibration sensor coupled by wax to the specimen as well as to ascertain the influence of sensor mass on natural frequency. During vibration measurement, test specimens were supported on rectangular foam stripes in the region of the nodal points. Impulse was initiated by a small impact hammer. Dynamic MOE for flexural and longitudinal vibrations were calculated using the equations according to Görlacher (1984).

Results

A compilation of all measurement results and evaluated material properties is presented in Table 1 with mean values representing respective bulk density classes.
Subject to the bulk density,

- static MOE ranges between 1,760…17,131 N/mm²,
- dynamic MOE from longitudinal vibration (Grindo*Sonic*) between 2,568…23,470 N/mm², and
- dynamic MOE from longitudinal waves (STEINKAMP) between 3,486… 25,723 N/mm².

According to Table 1, both dynamic MOEs (MOE_{US} and $MOE_{NF,\ long}$) show higher values compared to the static MOE (MOE_{stat}). Furthermore, MOE determined by ultrasonic measurement (MOE_{US}) is higher than MOE of longitudinal vibration measurement ($MOE_{NF,\ long}$). For medium-sized specimens, MOE_{US} is 20 % higher than $MOE_{NF,\ long}$ and 75 % above MOE_{stat}, where $MOE_{NF,\ long}$ is 44 % higher than the MOE_{stat}. For small-sized specimens, a tendency towards minor differences can be found: MOE_{US} is about 12 % higher than $MOE_{NF,\ long}$ and 59 % above MOE_{stat}, where $MOE_{NF,\ long}$ is 41 % higher than MOE_{stat}. All computed MOE values from longitudinal vibration ($MOE_{NF,\ long}$) are higher compared to those from flexural vibration ($MOE_{NF,\ flex}$), i. e. 12.4 % in case of small-sized and 5.7 % for medium-sized specimens (on average). Table 2 shows coefficients of determination R^2 between dynamic and static MOEs, between MOEs and bulk density, and within the dynamic methods. To summarise, small-sized specimens show a higher correlation than the medium-sized.

Mean sound attenuation coefficients α [m^{-1}] for individual bulk density classes are shown in Table 1. In general, sound attenuation coefficient decreases with increasing density. Further investigations considering different coupling points indicate significantly higher sound attenuation coefficients via coupling to parenchymal tissue (10.38 m^{-1}) than via coupling to a vascular bundle (7.18 m^{-1}). In addition to sound attenuation coefficient, mass attenuation coefficient (total attenuation coefficient) μ_m [m²/kg] is presented in Table 1 which shows an exponential decrease with increasing bulk density. Mass attenuation coefficient is preferred for comparison of various materials.

Divergence of absolute dynamic and static MOE values with increasing bulk density becomes obvious from Figure 2. In contrast, the percentage difference between MOE_{stat} and MOE_{NF} decreases with increasing bulk density. For statistic reasons, two medium-sized specimens with distinctly higher bulk density are henceforth not taken into consideration for computation of linear regressions. These outliers are left in the charts to clarify the trend of linear regression graphs. The close linear relation between respective dynamic and static MOEs becomes obvious from Figure 3. From exemplary experiments with one test specimen beyond that, an influence of support span on static MOE was found. At this, MOE_{stat}

equals 8,090 N/mm² for support span of 15 × thickness (corresponding to DIN 52186:1987), whereas it increases to 9,140 N/mm² for 21 × thickness and further to 9,740 N/mm² for 40 × thickness.
Sound velocity and natural frequency are the basis to calculate dynamic MOE. To evaluate sound velocity and natural frequency as an own grading criteria, their relation to bulk density is analysed in Figure 4. Both dynamic methods show a strong correlation with $R^2 = 0.6$ in case of small-sized specimens and a moderate correlation with $R^2 = 0.3$ resp. $R^2 = 0.5$ for medium-sized specimens.

Table 1—Results (mean values) according to specimen size and bulk density.

bulk density class [kg/m³]	MOE_{stat} [N/mm²]	MOE_{NF} [N/mm²]		MOE_{US} [N/mm²]	natural frequency [Hz]		sound velocity [m/s]	sound attenuation coefficient α [m^{-1}]	mass attenuation coefficient μ_m [m²/kg]
		long	flex		long	flex			
small-sized specimens (NF longitudinal vibration | flexural vibration both via Grindo*Sonic*)									
300-413	3,129	4,549	4,041	5,225	4,548	508	3,717	11.09	0.03
413-580	5,755	8,687	7,118	9,007	5,310	578	4,185	10.32	0.02
580-769	9,407	13,248	11,738	14,870	5,778	642	4,627	9.05	0.013
769-900	12,908	17,165	16,216	20,027	5,973	675	4,794	8.02	0.009
900-1043	14,763	19,399	17,416	21,803	5,940	667	4,781	7.68	0.008
medium-sized specimens (NF longitudinal vibration via VISCAN | flexural vibration via Grindo*Sonic*)									
400-490	4,278	6,002	5,712	7,792	1,652	67	4,139	5.38	0.012
490-580	5,951	8,802	8,163	10,690	1,823	73	4,430	5.32	0.01
580-769	7,916	11,279	10,787	13,178	1,911	77	4,542	4.63	0.007
>769	12,525	18,121	17,220	20,230	2,113	85	4,911	3.97	0.005

Table 2—Coefficients of determination R^2 between respective MOEs and bulk density for natural frequency (NF) and ultrasonic (US) measurements.

small-sized specimen *n* = 77 (NF with Grindo*Sonic*)			**medium-sized specimen *n* = 23**		
relation between		**R^2**	**relation between**		**R^2**
$MOE_{NF, long}$	density	0.91	$MOE_{NF, flex}$ (Grindo*Sonic*)	density	0.82
$MOE_{NF, flex}$	density	0.93	$MOE_{NF, long}$ (VISCAN)	density	0.82
$MOE_{NF, long}$	$MOE_{NF, flex}$	0.99	$MOE_{NF, long}$ (Grindo*Sonic*)	density	0.81
MOE_{US}	$MOE_{NF, long}$	0.98	$MOE_{NF, long}$ (VISCAN)	$MOE_{NF, long}$ (Grindo*Sonic)*	0.99
MOE_{US}	$MOE_{NF, flex}$	0.98	MOE_{US}	density	0.78
MOE_{US}	density	0.92	MOE_{US}	$MOE_{NF, long}$ (VISCAN)	0.91
MOE_{stat}	density	0.96	MOE_{stat}	density	0.83
MOE_{stat}	$MOE_{NF, long}$	0.97	MOE_{stat}	$MOE_{NF, long}$ (VISCAN)	0.94
MOE_{stat}	MOE_{US}	0.96	MOE_{stat}	MOE_{US}	0.8
natural frequency	density	0.60	natural frequency	density	0.49
sound velocity	density	0.63	sound velocity	density	0.31

Virtually contactless and mass connected measuring sensor methods (Grindo*Sonic* and miniature sensor MMF) were compared considering small- and medium-sized specimen. According to sensor manufactures, mass of miniature piezoelectric accelerometer should not exceed 10 % of object mass to be measured aiming at negligible effects on vibration frequency. For medium-sized specimen (sensor equals 0.2…0.4 % of specimen mass), sensor has no traceable impact on natural frequency. In case of small-

sized specimen (sensor equals 1.3…3.3 % of specimen mass) the error caused by sensor mass increases with decreasing bulk density from 1 % to 3 % in comparison to the values of Grindo*Sonic* device.

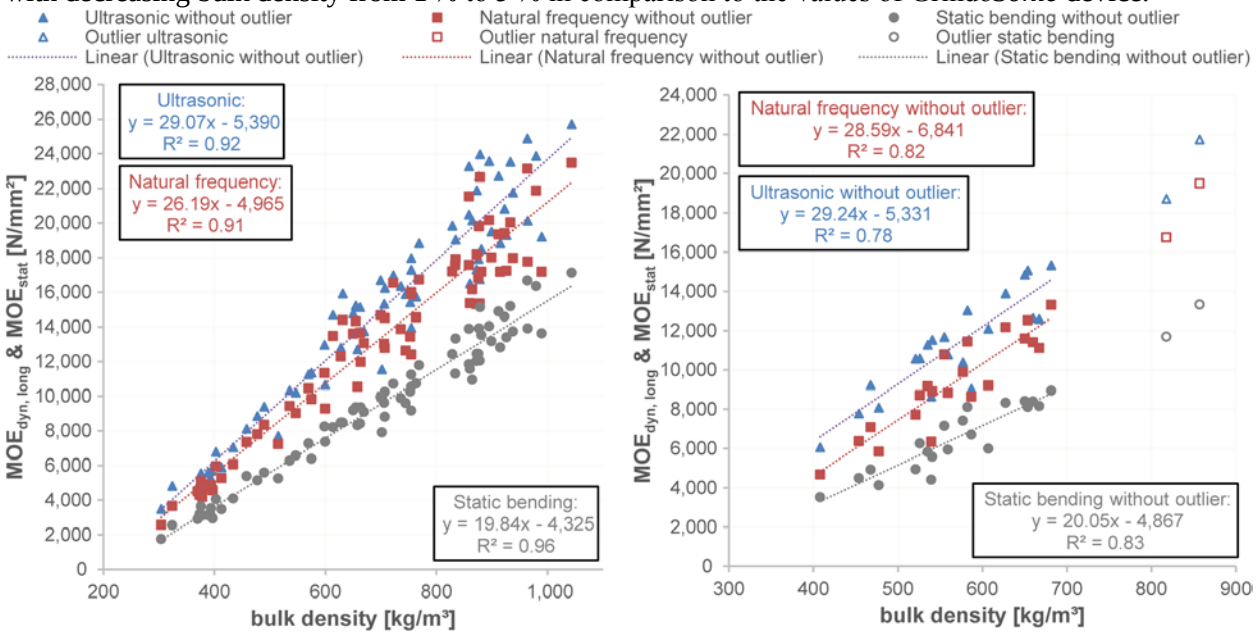

Figure 2—Relation between dynamic MOEs by ultrasonic resp. natural frequency with longitudinal vibration (small-sized Grindo*Sonic* and medium-sized VISCAN) or static MOE by bending test and bulk density for small-sized specimen (left) and medium-sized specimen (right).

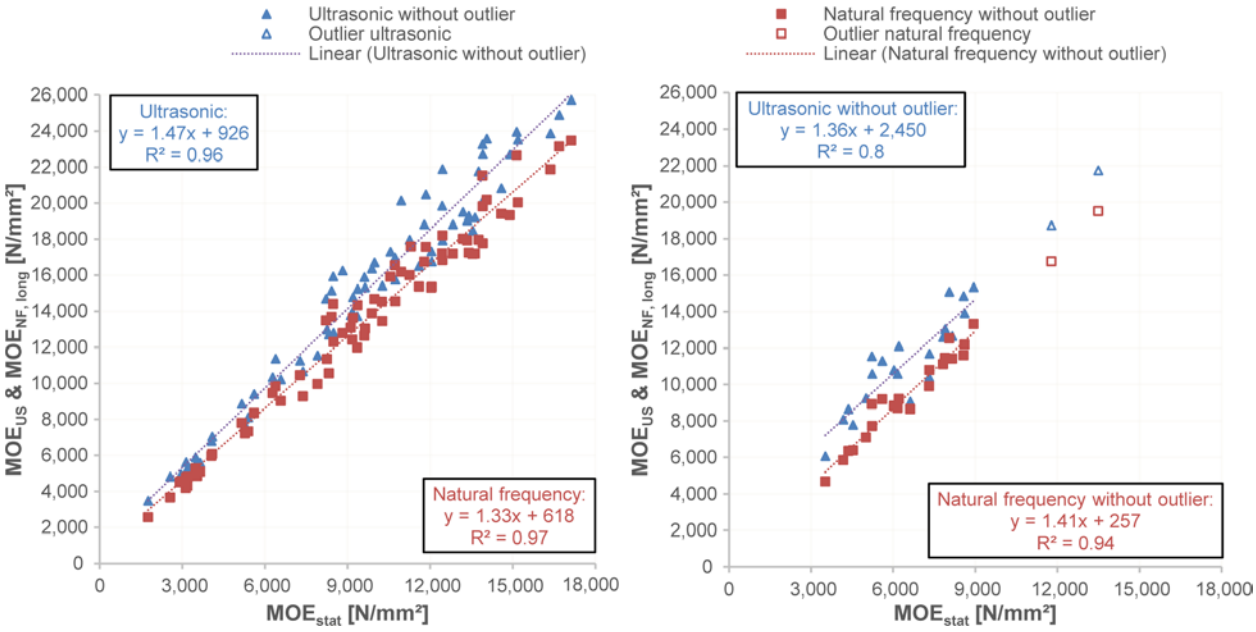

Figure 3—Relation between dynamic MOEs by ultrasonic resp. natural frequency with longitudinal vibration (small-sized Grindo*Sonic* and medium-sized VISCAN) and static MOE by bending test for small-sized specimen (left) and medium-sized specimen (right).

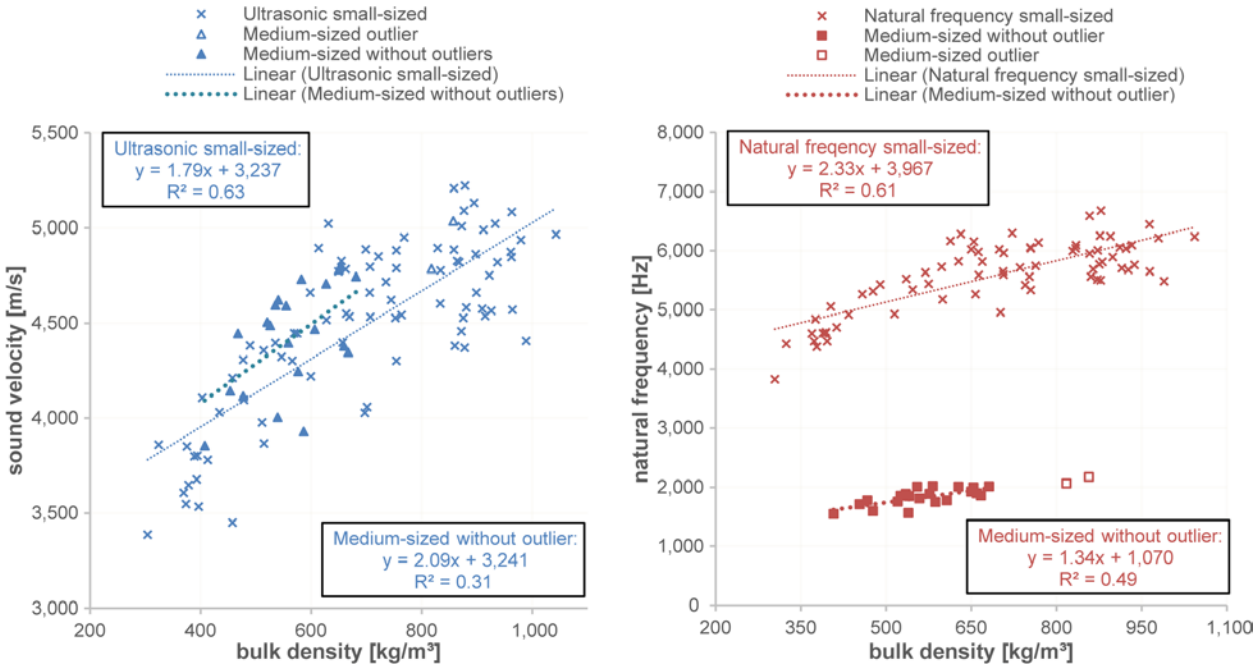

Figure 4—Relation between sound velocity and bulk density (left) and natural frequency from longitudinal vibration (small-sized Grindo*Sonic* and medium-sized VISCAN) and bulk density (right).

Discussion

Coconut wood features lower shear strength compared to dicotyledonous wood species with similar bulk densities. Shear strength of coconut wood with a bulk density of 610 kg/m³ equals 7.7 N/mm² (Fathi 2014), whereas Carolina pine with a bulk density of 600 kg/m³ shows a shear strength of 10.5 N/mm² and ash wood with 700 kg/m³ has 13 N/mm² (DIN 68364:2003). Consequently, rather considerable differences between MOE_{dyn} and MOE_{stat} appear for coconut wood in comparison to dicotyledonous wood species. With increasing bulk density (i. e. lower amount of parenchymatous ground tissue), influence of shear modulus on the bending test decreases caused by correspondingly higher shear strength. According to Fathi (2014), shear strength of coconut wood correlates directly with bulk density of parenchymatous ground tissue. This results in lower percentage differences between $MOE_{NF, long}$ and MOE_{stat} with increasing bulk density. Regarding support span of 15 × thickness according to the German standard, shear modulus has significant influence on MOE_{stat}. Comparatively low shear strength and the anatomic structure of coconut wood affects shear modulus more than in case of dicotyledonous wood species.

According to Burmester (1965) and Greubel and Plinke (1995), sound velocity is mainly influenced by the area with the highest permeability within test specimen, thus, the area with the highest density (fibre caps of the vascular bundles in case of coconut wood). Therefore, coupling point of the conical probes influences measurement results (here, 7.24 V signal amplitude for vascular bundles and 2.32 V for parenchyma). Hence, coupling at parenchymatous tissue results in dynamic MOE which is on average 448 N/mm² lower compared to coupling at vascular bundles. The difference in maximum amplitudes are supposed to correspond to the lower fibre lengths of parenchymatous ground tissue compared to vascular bundles leading to a higher number of fibre to fibre interfaces within the same specimen length.

Correlation of bulk density and sound velocity (Figure 4, left) is weaker in case of medium-sized specimens compared to small-sized (Table 2) because of bulk density gradient over the cross section of

the investigated medium-sized specimens. As mentioned above, sonic waves propagate within the region of highest permeability, i. e. region of highest density. Hence, sound velocity within the medium-sized specimen increases between the three measuring points with increasing bulk density (e. g. 4,368 m/s → 4,536 m/s → 4,593 m/s).

Minor sound attenuation coefficients indicate high permeability and vice versa. According to Table 1, low density coconut wood shows high sound attenuation coefficients and therefore a higher damping effect resp. a lower permeability. This is probably due to the small proportion of vascular bundles, their dimension, and number in low density material (Fathi 2014). Shorter fibres of parenchymatous ground tissue and associated higher number of interfaces within the specimen increase damping compared to longer fibres in the vascular bundles. On average, sound attenuation coefficient of small-sized specimens is twice as high as sound attenuation coefficient of medium-sized specimens at the same bulk density (Table 1). At this, damping appears lower in case of medium-sized specimen due to averaging of three measuring points and apparent bulk density gradient over the cross section. However, sonic waves propagate within the region of highest permeability as already mentioned.

Higher values of dynamic MOE determined via ultrasound compared to dynamic MOE via natural frequency measurements are caused by bulk density gradients within specimens, varying sound velocities in parenchymatous ground tissue and vascular bundles, and corresponding higher sound velocity in the area with the highest permeability. In contrast, natural frequencies are only marginally affected by the anatomical structure because the specimen vibrates through its entire dimensions. Thus, mean elasto-mechanical properties are analysed.

The employed natural frequency methods differ regarding their simplicity of application. In this investigation, medium-sized specimen under flexural vibration revealed problems related to specimen support on the utilised foam stripes. Considerably low frequencies with high amplitudes tended to lift up the specimen from their supports apparently. Longitudinal vibrations were detected without problems. In case of small-sized specimens under flexural vibrations, high repeating accuracy was obtained. However, longitudinal natural frequencies up to 6 kHz were detected on small-sized specimens. According to Holz (1967), damping effect depends on frequency and increases above 2 kHz explicitly. Consequently assumed high damping effect, particularly observed on specimen with low density, seems to explain accordingly lower repeating accuracy.

Conclusions

In general, both ultrasonic and natural frequency measurements in longitudinal and flexural vibration are suitable for a further development of strength grading of palm lumber. Flexural vibration measurements are appropriate especially for investigation of small test specimens under laboratory conditions. Longitudinal vibrations are well-suited to determine MOE of medium-sized specimens and indicate potential for specimens in component dimensions in an industrial production environment (but further investigations are necessary). The utilisation of miniature sensors fixed on the specimen implies minor measuring errors for small-sized specimen, but is an appropriate method for laboratory applications considering sensor mass less than 1 % of specimen. Because of the influence of coupling with conical ultrasonic probes on either ground tissue or vascular bundles, ultrasonic coupling can be difficult to integrate into an industrial process. Therefore, coupling modes especially in an industrial context have to be investigated further.

Considering MOE determination via static bending test, influence of shear modulus seems to be higher for coconut wood compared to dicotyledonous wood species because of its anatomic structure with (high

density) vascular bundles embedded in (low density) parenchymatous ground tissue. Further investigations of the influence of support span on test results for different dimensions of coconut timber have to be carried out.

Acknowledgement

The authors thankfully acknowledge financial support from the German Federal Ministry of Education and Research through the “KMU-innovativ” project "Technologies for Lumber Processing from Oil Palm Trunks (02PK2458)", project coordinator: Simon Möhringer Anlagenbau GmbH, Wiesentheid, Germany. Additionally, free provision of Grindo*Sonic* MK5, STEINKAMP BP 5, and coconut lumber by the Centre of Wood Sciences, University of Hamburg, Germany, a further STEINKAMP BP 5 by Department of Civil Engineering, University of Applied Sciences Ostwestfalen-Lippe, Germany, and VISCAN by Microtec, Brixen, Italy is gratefully appreciated.

References

Bucur, V. 2006. Acoustics of Wood. 2nd edition. Springer-Verlag, Berlin, Heidelberg.

Burmester, A. 1965. Zusammenhang zwischen Schallgeschwindigkeit und morphologischen, physikalischen und mechanischen Eigenschaften von Holz. Holz als Roh- und Werkstoff. 23(6): 227-236.

DIN 50014: 1985-07. Klimate und ihre technische Anwendung: Normalklimate. Deutsches Institut für Normung e.V. Beuth Verlag GmbH, Berlin.

DIN 52186:1978. Prüfung von Holz - Biegeversuch. Deutsches Institut für Normung e.V. Beuth Verlag GmbH, Berlin.

DIN 68364:2003. Kennwerte von Holzarten - Rohdichte, Elastizitätsmodul und Festigkeiten. Deutsches Institut für Normung e.V. Beuth Verlag GmbH, Berlin.

Fathi, L. 2014. Structural and mechanical properties of the wood from coconut palms, oil palms and date palms. University of Hamburg. 248 p. PhD thesis.

Frühwald, A.; Peek, R.-D.; Schulte, M. 1992. Nutzung von Kokospalmenholz am Beispiel von Nordsulawesi, Indonesien. Bundesforschungsanstalt für Forst- und Holzwirtschaft Hamburg. Kommissionsverlag Max Wiedebusch, Hamburg.

Greubel, D.; Plinke, B. 1995. Zerstörungsfreie Festigkeitsuntersuchungen an Spanplatten mit Ultraschallmeßtechniken. Holz als Roh-und Werkstoff. 53(3): 193-200.

Görlacher, R. 1984. Ein neues Meßverfahren zur Bestimmung des Elastizitätsmoduls von Holz. Holz als Roh- und Werkstoff. 42(6): 219-222.

Holz, D. 1967. Untersuchungen an Resonanzholz – 3. Mitteilung. Holztechnologie. 8(4): 221-224.

Killmann, W. 1993. Struktur, Eigenschaften und Nutzung von Stämmen wirtschaftlich wichtiger Palmen. University of Hamburg. 213 p. PhD thesis.

Steiger, R. 1991. Festigkeitssortierung von Kantholz mittels Ultraschall. Holzforschung und Holzverwertung. 43(2): 40-46.

Monitoring of wood Degradation caused by termites using ultrasonic tomography with Brazilian technology

Alex J. Trinca
PhD, Visiting Professor, Laboratory of Nondestructive Testing - LabEND, College of Agricultural Engineering - FEAGRI - University of Campinas - UNICAMP, Brazil – E-mail: alexjuliotrinca@gmail.com

João P.R. Nascimento
PhD student, Laboratory of Nondestructive Testing – LabEND, College of Agricultural Engineering - FEAGRI - University of Campinas - UNICAMP, Brazil – E-mail:jprn.rc_unesp@yahoo.com.br

Mariana R. Guerra
Master student, Laboratory of Nondestructive Testing – LabEND, College of Agricultural Engineering - FEAGRI - University of Campinas - UNICAMP, Brazil – E-mail: ma.nagle.reis@gmail.com

Stella S.S.A. Palma
Master student, Laboratory of Nondestructive Testing – LabEND, College of Agricultural Engineering - FEAGRI - University of Campinas - UNICAMP, Brazil – E-mail:ssapalma@gmail.com

Raquel Gonçalves
Professor, Coordinator of the Laboratory of Nondestructive Testing – LabEND, College of Agricultural Engineering - FEAGRI - University of Campinas - UNICAMP, Brazil – E-mail: Raquel@agr.unicamp.br

Abstract

Termites create galleries in the late wood, following the grain and causing cracks and irregularities. The objective of this research was to evaluate the performance of ultrasonic tomography, using Brazilian technology (equipment and software), to estimate the evolution of degradation on wood attacked by termites. To achieve this goal we used 6 *Pinus sp*. discs inoculated with subterranean termite *Coptotermes gestroi*, grown for 11 months. During the period, we visually followed the conditions on the discs and we performed ultrasound measurements with 45 kHz exponential transducers. In the generated images were used only two velocities ranges to evidence the zones with low ones. Considering that the attack is still incipient, we didn´t identify visual changes, however, the images showed early degradation on the disks. Although preliminary, the results indicate that the technology shows sensitivity in detecting changes in wood caused by the termite attack.

Keywords: Ultrasonic tomography, degradation by termites, degradation of wood.

Introduction

Ultrasonic tomography, to evaluate the internal condition of trees, is viable and can be accomplished using different wave propagation parameters like the time, amplitude or frequency response (Bucur 2005).

The equipment of Tomographic are already commercialized in the international market. However, the Nondestructive testing Laboratory from University of Campinas (LabEnd) has been working on researches aiming the improvement of equipment and software developed in Brazil. For achieve this purpose, the research group have deepened the theoretical knowledge involved and its application on Brazilian species, both forest and urban.

Within the broader scope of researches developing by the group there is the study of ultrasonic tomography applied in different situations, such as in samples with knots (Trinca & Gonçalves, 2014), with displaced pith (Trinca & Gonçalves, 2014),with hollows of different sizes (Secco, 2011 and Trinca & Gonçalves, 2014), with degradation by fungi (Trinca & Gonçalves, 2014) and with degradation by termites (Trinca & Gonçalves, 2014).

Subterranean termites prefer to attack juvenile wood, but it creates galleries through the late wood, following its grain, causing cracks and irregularities (Koehler, 1996) that can be detected by wave propagation methods. In living trees these termites begin the attack at the roots and, even if the heartwood is destroyed, the tree can not to give external signs of the attack (Spring, 1998), making it important to use technologies that allow this detection.

Great attenuation of the signal was observed in researches that used wood discs with holes filled with adhesive and sawdust to simulate the condition of an attack by fungi and termites (Lasaygues et al., 2007), showing that this detection may be more complex than in discs with hollows.

Subterranean termites as the specie *Coptotermes gestroi*, used in this study, are considered as the most destructive species, both in urban trees as in cultivated area (Passos et al., 2014). Despite its Asiatic origin, they have been observed in many tropical and subtropical regions of the world. In Brazil, the state with more significant presence of this species is the Southeast (Veiga, 1998).

Therefore, the objective of this research was to evaluate the performance of ultrasonic tomography, using Brazilian technology (equipment and software), to estimate the evolution of degradation on wood attacked by termites.

Methodology

To inoculate and follow the development of the degradation caused by termites, we used 6 *Pinus elliottii* discs with diameters between 290mm and 355 mm and 440 $kg.m^{-3}$ mean apparent density (at 12% moisture content). Three discs were taken from 6 years old trees (disks 1, 4 and 5) and three from 18 years old trees (disks 2, 3 and 6). The disks were free of contamination.

In general, studies with termites are performed on very small samples, but this search used discs, to obtain conditions to perform the usual test for ultrasonic tomography.

Each disc received three plastic pots, one central and two adjacent, connected with plastic tubes 100 mm in length and 5 mm in diameter (Figure 1). One of the adjacent containers served as house for the termite population (container nest). In this container we introduced 4 grams of termite workers (approximately 1200 individuals) and 60 termite soldiers. The central container (supply container) served as the arena for the wood attack of termites and the adjacent container (depot container) served as its waste barn.

Previously, the containers received sterile sand and moistened with distilled water, which served as substrate for the termites. The container nest received 200 grams of sand with 12.5 ml of water and the depot container 20 grams of sand with 1.5 mL of water. The food container received neither sand nor

water because it was in direct contact with the wood sample. The bioassays were held in the laboratory with controlled relative humidity and temperature, 60 ± 20 UR and 25 ± 2 ° C respectively.

We weigh and measure the discs with ultrasond before the insertion of the colony and new measurements (weight and ultrasound) were made throughout the follow-up period of the attack of termites to the wood.

For ultrasound measurements we used diffraction mesh with 8 points (Figure 2), 45 kHz frequency transducers with dry faces and ultrasound equipment (USLab, AGRICEF, Brazil) developed by the group in partnership with a spin-off company. For the creation of the images we used the software *ImageWood 2.0*, also developed by the research group in partnership with an IT area specialist. The ultrasound measurements were performed close to the face directly in contact with the bioassay and close to the other side.

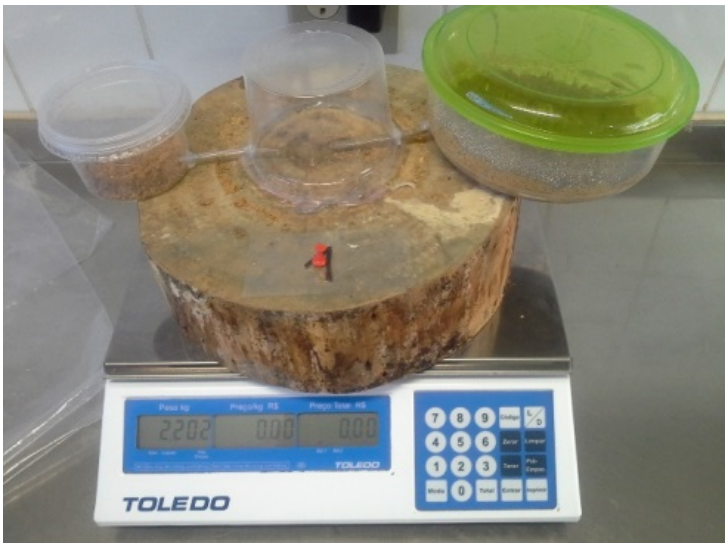

Figure 1. System for termite maintenance and inoculation of the discs.

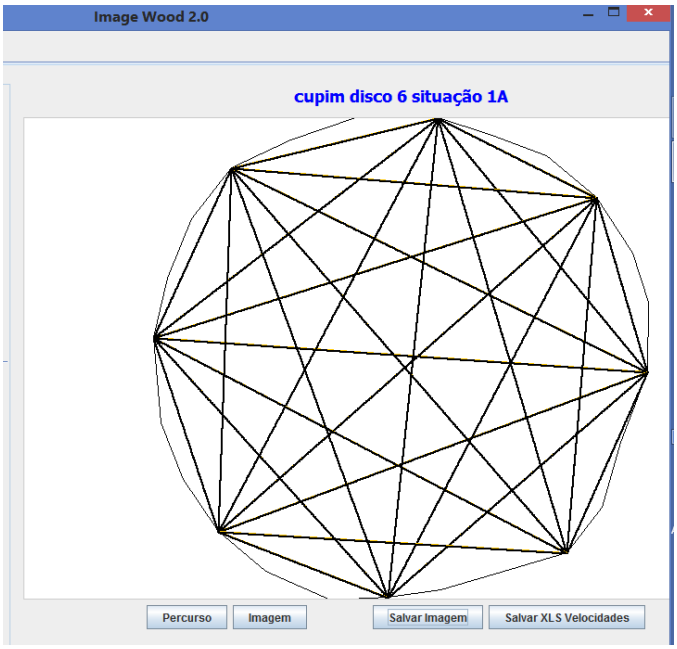

Figure 2. Measurement points of the diffraction mesh and routes of wave propagation.

Results

The weight of the disks during the termite activity period remained approximately constant up to 75 days of insertion of the colony, except for some oscillations caused by moisture content changes (Figure 3).

From 105 days we observed, for all disks, small and increasing loss until the last measurement, when new increase occurs (Figure 3). Except for the first weighing, the others were done with the whole set of plastic containers used, since we cannot move the bioassay without affecting the colony. However, as the weight of the containers was known, this value was subtracted from the final weight on each day of measurement. According to the expert researchers on termites, mass loss is more apparent when the part is already well under attack, since while the termites feed on wood, they also left material, such as saliva, excrements and remains of the wood itself. This issue may have affected the reduction in mass loss of the last measurement.

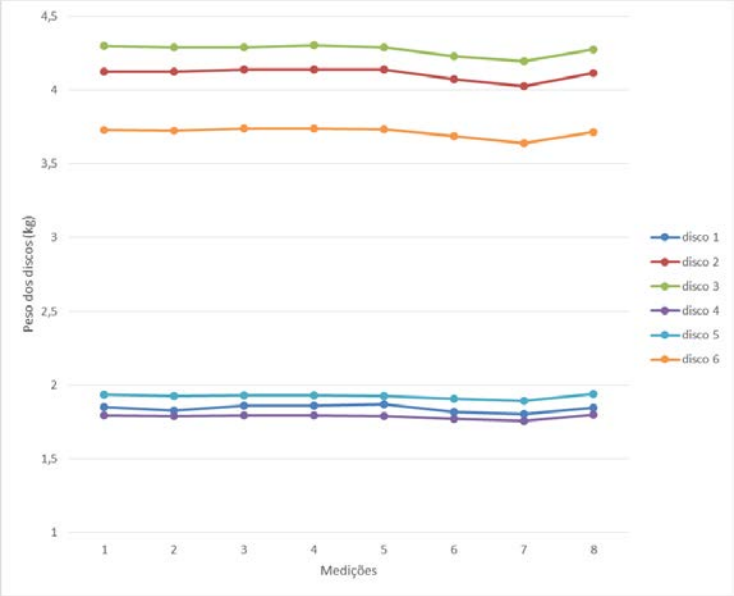

Figure 3. Behaviour of Mass loss in discs inoculated with termites.

Measurement 1: before inoculation; Measurement 2: 15 days; Measure 3: 30 days; Measurement 4: 45 days; Measurement 5: 75 days; Measuring 6 105 days; Measuring 7 135 days; measuring 8: 195 days

To verify if similar results would be obtained by images generated by ultrasonic tomography in the disks, we prepared the images for each measurement period (initial condition up to 195 days of incubation). The minimum velocity obtained in the initial condition was used as a reference to check if there was an increase of the lower velocities zones.

For this analyse, 96 images (6 discs x 8 conditions x 2 faces) were generated. The images were studied in detail to determine at what point the presence of damaged areas began to be noticed on the disks.

The tomographic images of the disks 1, 2, 4 and 6 indicated no signs of degradation until 195 days of inoculation (Figure 4). The disc 3 showed early signs of action of the termite in the region of the pith 195

days after inoculation (Figure 5). The disc 5 was the only one who presented change in image after 135 days, highlighting a narrow zone of low velocity values, as a gallery (Figure 6b). On this disc, after 195 days the most significant changes were observed leaving the narrow range (gallery) and forming larger pockets near to the edge (Figure 6c). It should be noted that the disc 5 consisted only of juvenile wood, while the disc 3 had juvenile wood in the centre and externally mature wood.

a b

Figure 4. Example of images generated from the discs 1,2,4 and 6 in the initial stage (a) and 195 days after inoculation with termites (b)

a b

Figure 5. Images generated from disk 3 in an initial phase (a) and 195 days after inoculation with termites (b)

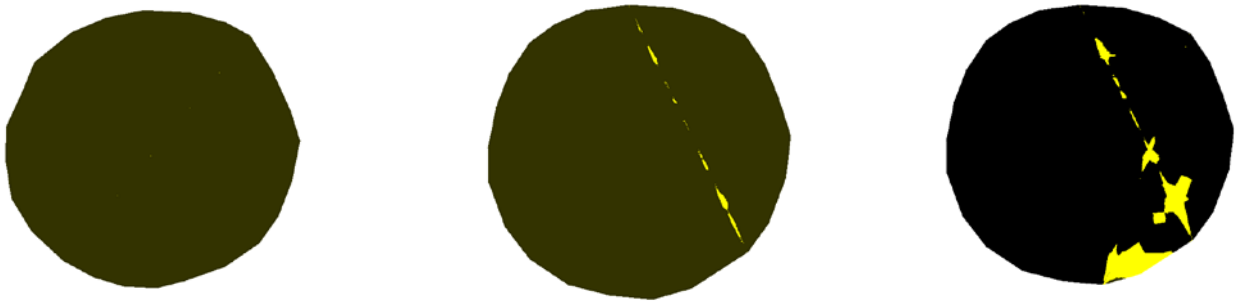

a b c

Figure 6. Images generated from the disc 5 in the initial stage (a) after 135 days (b) and 195 days after inoculation with termites (c)

Considering that the attack of termites is still incipient, the bioassay was not dismantled and the research group will continue the measurements until the disks present advanced degradation.

CONCLUSION

The degradation of the discs by termites is still incipient, and we should continue rehearsals for the final analyze of the image pattern and the evaluation of the velocity variation level. However, as in two disks it was possible to see a variation in velocity, it is verified that the methodology, equipment and software used have the sensitivity to detect changes in the internal structure of the wood.

ACKNOWLEDGEMENTS

The authors thank the São Paulo Research Foundation (FAPESP - Proc n.2012/22599-9; Proc 2011/08286-5 and Proc 2015/05692-3) for the support; São Paulo State University "Julio de Mesquita Filho" (UNESP), Bioscience Institute Centre for Study of Social Insects, for the partnership and the Sguario Forest Company S/A, for the wood material (logs of *Pinus elliottii*).

REFERENCES

BUCUR, V. (2005). Ultrasonic techniques for nondestructive testing of standing trees. Ultrasonics, 43:237-239.

DIVOS, F.; SZALAI, L. 2002. Tree evaluation by acoustic tomography. In: Proceedings of the 13th International symposium on nondestructive testing of wood; 2002 August 19. 21; Berkeley, CA. Madison, WI: Forest Products Society: 251.256. 2002.

ELEOTÉRIO, E.S.R. (2000). Levantamento e identificação de cupins em área urbana de Piracicaba, SP. Dissertação (Mestrado). Escola Superior de Agricultura Luiz de Queiróz, USP.
KOEHLER, P.G. (1996). Drywood and other non-subterranean termites. Umiversity of Florida. Gainesville, 4p. (www.hammock.ifas.ufl.edu).

LASAYGUES, Philippe; FRANCESCHINI, Emilie; DEBIEU, Eric; BRANCHERIAU, Loïc. Non-destructive diagnosis of the integrity of green wood using ultrasonic computed tomography. In: International Congress on Ultrasonics, 2007, Vienna, Austria, v.1, p.1-4.

LI, G.; WANG, X.; WIEDENBECK, J.; ROSS, R.J. (2013). Analysis of wave velocity patterns in Black Cherry trees and its effect on internal decay detection. In: 18th International symposium on nondestructive testing of wood; Madison, WI: Forest Products Society: 79-91.

MYLES, T.G. (1999). Termite prevention (www.utoronto.ca/forest/termite/tips).

PASSOS, E.M.; ALBUQUERQUE, A.C.; MARQUES, E.J.; TEIXEIRA, V.W.; SILVA, C.C.M.; OLIVEIRA, M.A.P. (2014). Efeitos de isolados do fungo Isaria (Persoon) sobre o cupim subterrâneo *Coptotermes gestoi*. Arq. Inst. Biol. V.81(3), pp.232-237.

TRINCA, Alex Julio; GONÇALVES, Raquel. 2014. Relatório de Pesquisa apresentado à Fundação de Amparo de Pesquisa do Estado de São Paulo (FAPESP), Proc. n. Proc. 2011/08286-5.

Measurement of stiffness of tree stems using acoustic velocity measurements made across the stem

Mathew Legg
Physics Department, University of Auckland, Auckland, New Zealand, m.legg@auckland.ac.nz

Stuart Bradley
Physics Department, University of Auckland, Auckland, New Zealand, s.bradley@auckland.ac.nz

Abstract

Standing tree stiffness measurements are commonly calculated using acoustic Time of Flight (TOF) velocity measurements. These are generally obtained by measuring the propagation time of an acoustic signal between two probes inserted into the “same face” of the tree. Studies have suggested that these TOF measurements are biased to measure the outerwood stiffness rather than that of the tree stem as a whole. However, the stiffness of tree stems increase from pith to bark. In this paper, a technique is investigated, which uses TOF measurements on the "opposite faces" of the tree stem to attempt to obtain an average stiffness through the tree stem. Unlike previous studies, this technique allows for the anisotropic nature of wave propagation in wood. The measured Modulus of Elasticity (MOE) values are compared to MOE values obtained using the "same face" TOF and acoustic resonance techniques.

Keywords: stiffness, time of flight, opposite face, anisotropic

Introduction

The stiffness of wood is related to the Modulus of Elasticity (MOE), or Young's E modulus, of the wood. Bending tests can be used to measure the static modulus of elasticity. However, these are generally destructive tests. Acoustic nondestructive testing (NDT) techniques have, therefore, been developed to measure the dynamic modulus of elasticity *E*. This is calculated using

$$E = \rho c^2 \tag{1}$$

where c is the acoustic wave velocity in the longitudinal direction, see Figure 1, and ρ is mass density of material (Ross and Pellerin, 1994). For logs, the velocity is usually measured using acoustic resonance. The end of the log is hit with a hammer and the signal is recorded and the spectrum obtained. The resonance acoustic velocity is then calculated for the n^{th} resonance frequency f_n using

$$c_{RES} = \frac{2Lf_n}{n}, \tag{2}$$

where L was the length of the log. Resonance techniques have been reported to give stiffness measurements that compare well with static MOE values obtained using bending tests (Harris, Petherick and Andrews, 2002). Different resonance harmonics may generate different results. According to Chauhan and Walker (2006), the second harmonic appears to be that used by the commercial resonance tool Hitman[1].

[1] http://www.fibre-gen.com

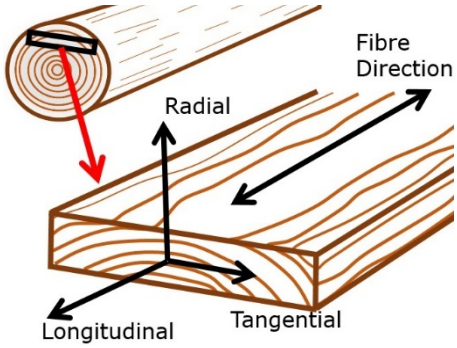

Figure 1: Diagram illustraiting the longitudinal, radial, and tangential orthotropic axis directions for wood.

Resonance cannot be used for standing trees. Instead the stiffness is measured using TOF techniques (Wang et al., 2001). These measurements are generally obtained by inserting two probes into a tree stem on the "same face" of the tree, separated vertically by a distance *z*, usually about a meter, see Figure 2(a). The acoustic velocity is calculated from the acoustic propagation time *T* between the two probes using

$$c_{TOF} = \frac{z}{T}, \tag{3}$$

The TOF is measured by detecting the start time of the signal. TOF techniques have been reported to provide stiffness measurements that are higher than those obtained using resonance or bending tests (Wang, Ross and Carter, 2007). This has been suggested to be due to the increase in stiffness and hence acoustic velocity in tree stems from pith to bark (Hsu, 2003; Wang et al., 2004; Chauhan and Walker, 2006; Lasserre, Mason and Watt, 2007). An alternative explanation is that the TOF method measures a "dilation speed", while the resonance measures the "rod speed" (Andrews, 2002; Wang, 2013).

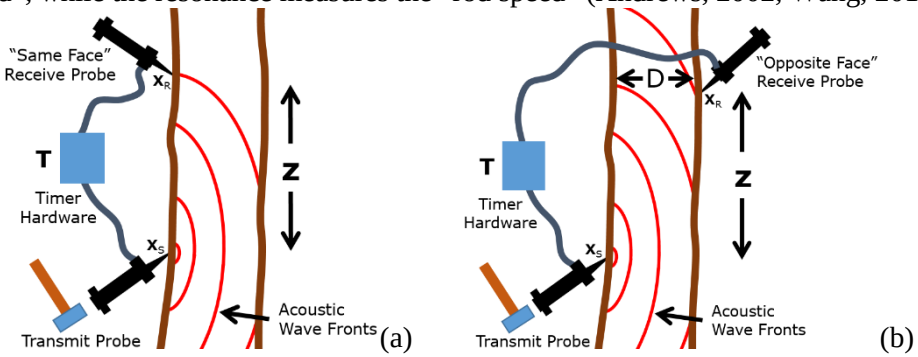

Figure 2: Diagrams illustrating time of flight velocity measurements made using (a) "same face" and (b) "opposite face" techniques.

There has been results which suggest that "same face" TOF stiffness measurements are more closely correlated to with outerwood stiffness (Grabianowski, Manley and Walker, 2006; Mora et al., 2009). To try to compensate for this, some studies have been made TOF measurements on "opposite faces" of the tree with the probes separated vertically by about a meter, see Figure 2(b) (Joe et al., 2004; Mahon et al., 2009; Matheson et al., 2002; Dickson, Raymond, Joe and Wilkinson, 2003; Dickson et al., 2004; Mahon, 2007). However, none of these studies have allowed for the anisotropic nature of wood, where the velocity in the radial direction is significantly less than that in the longitudinal direction. This resulted in stiffness measurements that were too low. Also, most have not included the true propagation path distance in the TOF velocity measurements, which has resulted in stiffness measurements that varied with the diameter of the tree stem. This means that the longitudinal velocity cannot be calculated using Equation (3).

In order for the “opposite face” method to be used for longitudinal velocity measurements, a model of the anisotropic wave propagation in tree stems needs to be obtained for the longitudinal-radial plane. Acoustic TOF measurements in logs have been presented in references (Zhang, Wang and Su, 2011; Zhang, Wang and Ross, 2009; Su, Zhang and Wang, 2009), though wave propagation models were not provided. Searles (2012) analyzed the data provided by Zhang, Wang and Su (2011) and suggested the wave fronts in the longitudinal-radial plane could be explained by elliptical velocities with the ellipse axes being the longitudinal and radial velocities. Anisotropic wave propagation models in the radial-tangential plane have been investigated in references (Dikrallah et al., 2006; Maurer et al., 2006; Li et al., 2014) for 2D tomography corrections. Maurer et al. (2006) provided a model which was a first order approximation of an ellipse. An 3D anisotropic model may be derived from Kelvin-Christoffel equation (Carcione, 2007a; Bucur, 2006). However, papers verifying this model experimentally for tree stems were not found in the literature.

In this paper, “same face” and “opposite face” techniques are investigated using multi-path TOF measurements. The “opposite face” data is analyzed and a propagation model is presented, which attempts fit the measurements for this log. This model includes the anisotropic nature of wave propagation in wood and the propagation distance. Longitudinal acoustic velocity values obtained using this techniques are compared the “same face” technique and acoustic resonance.

Radiata Pine Log

Acoustic velocity measurements were made in the Acoustics Lab of the Physics Department, the University of Auckland. Measurements were made on a 2.5 meter long radiate pine log, see Figure 3. The diameter of the log at the thin and thick ends of the log was respectively 290 and 340 mm. At the time of measurements, the log had been in the lab for several month and was relatively dry. The transducers were attached directly to surface of log, with the bark removed in the area where the transducers were attached.

Figure 3: Photo log used for measurements with a transducer attached to the surface of the log using a strap.

Resonance Measurements

Acoustic resonance measurements were made for the log. This involved hitting the end of the log with a hammer and recording the resulting signal using a low noise Gras microphone and a Data Translation DT9836 board. A fast Fourier transform of this signal was obtained and the frequencies at which the spectral peaks occurred were measured. Spectral peaks at 566 and 1067 kHz were obtained. Equation (2) was used to obtain the first and second harmonic resonance velocities of 2830 and 2670 m/s. The average of these two is 2750 m/s.

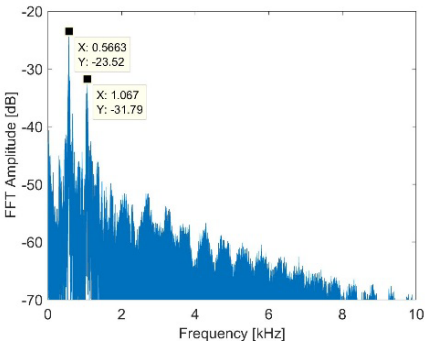

Figure 4: Spectrum for a hammer hit on the end of the log recorded using a microphone. Resonance peaks can be seen at frequencies f_n of 566 and 1067 Hz.

Time of Flight Measurements

Acoustic excitation and reception was made using custom built hardware/software. The excitation signal used was 20 cycles of a Maxim Length Sequence (MLS). This is a series of digital high and low values which has a wide, flat frequency response (0 to 112.5 kHz in this case). These signals were generated using MatLab and played using the analog output of a Data Translation DT9836 board using a sampling rate of 225 kHz. This was amplified to about 250 V_{pp} using a MOSFET/step-up transformer power amplifier (Svilainis and Motiejunas, 2006) and used to drive a shear wave transducer. The resulting signal was measured using one or more shear transducers. This signal was amplified using preamplifier circuits and sampled using an analog input channel of the DT9836 using a sampling rate of 225 kHz.

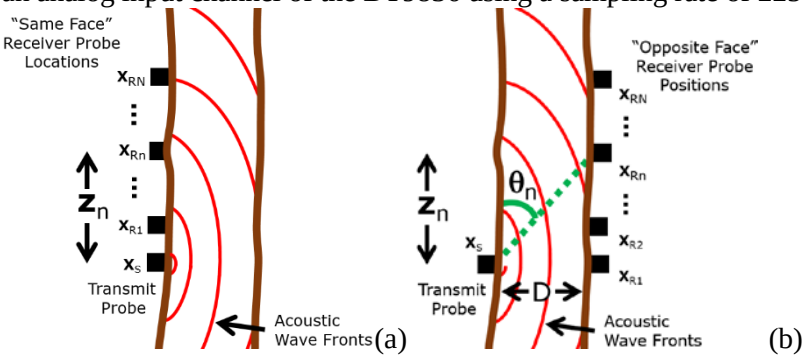

Figure 5: Diagrams showing (a) "same face" and (b) "opposite face" multi-path TOF measurement locations.

The transducers were oriented to excite vibration in the longitudinal direction. The transmit transducer was kept a one location while the receive transducer was move to multiple locations on the log, see Figure 5. The first arrival time T of acoustic signal were calculated using an AIC algorithm Picker (Zhang, Thurber and Rowe, 2003).

Same Face Measurements

"Same face" measurements were made at the thin end of the log. The transmit transducer was kept stationary while the receiver transducer was moved incrementally along the log in steps of 50 mm, see Figure 5(a). Example plots of the raw data and AIC picker algorithm output can be seen in Figure 6. With increase propagation distance, the signal was increasingly attenuated. It also appeared that higher frequency components of the signal were increasingly filtered out with propagation distance.

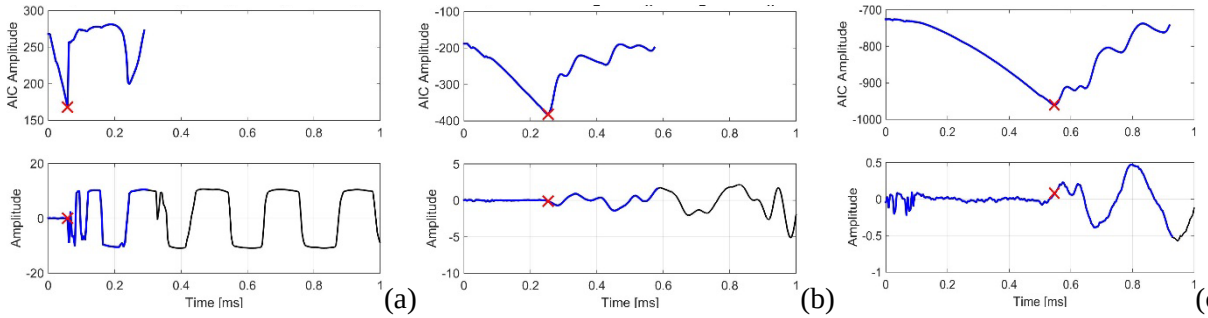

Figure 6: Example plots of raw data (lower) and AIC picker output (upper) for "same face" measurements made at distance z_n of (a) 300, (b) 550, and (c) 800 mm. The first arrival time obtained by the AIC picker is shown in red.

The calculated TOF values were plotted as a function of distance, see Figure 7. It can be seen that the data appears to lie on three straight lines. The sudden jumps may be due to the AIC picker algorithm triggering on different parts of the received signal due to attenuation. Therefore, velocities were calculated using the slope of a least squared fitted line through the data. Three velocities were 4490, 3120, and 3150 m/s were obtained. It appears that the signal initially propagates at a higher velocity (4490 m/s) but subsequently drops to a lower velocity (3120 or 3150 m/s). Potentially the two different velocities could be related a different frequencies components propagating at different velocities but experiencing different attenuation rates. As expected, both these velocities values are higher than that obtained using resonance. The lower of the two velocities is greater by 1.14.

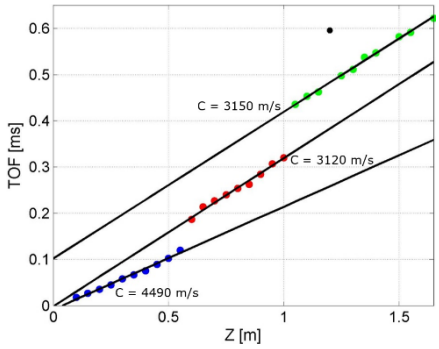

Figure 7: "Same face" AIC time of flight measurements at increamental positions along log. The velocity c is measured using the slope of a fitted line through data points. The two in TOF at about 1 meter appears to be caused by in the AIC picker triggering on a different parts of the received signal.

Opposite Face Measurements

"Opposite face" TOF measurements were also made on the thin end of the log. The transmit transducer was kept stationary, while the receive transducer was moved along the opposite side of the log in steps of 50 mm, see Figure 5(a). The TOF measurements were plotted as a function of distance z_n, see Figure 8(a). It was observed that the data points initially followed a curve but jumped to a higher level after 1050mm. This jump may be caused by the AIC picker algorithm triggering on different parts of the received signal due to attenuation. Velocities were calculated using the measured time of flights T_n and propagation distance R_n

$$c_n = \frac{R_n}{T_n} = \frac{\sqrt{D^2 + z_n^2}}{T_n}. \tag{5}$$

These velocities were analysed and plotted as a function of different parameters. It was observed that the measured velocity data points formed a relatively straight line when plotted as a function of the sin of the angle

$$\sin(\theta) = \frac{D}{\sqrt{D^2 + z_n}}, \tag{6}$$

see Figure 8(b). This indicates that the velocity could be described as

$$c = b - a\sin(\theta), \tag{7}$$

where parameters *a* and b can be obtained from a least squares fit. Taking the limits as the angle θ goes to 0 and 90 degrees, this model suggests that the longitudinal and radial velocities can be obtained from the least squares fitted parameters using

$$c_L = b, \quad c_R = b - a. \tag{8}$$

For the fitted data points, the longitudinal and radial velocities were calculated as 3908 and 1446 m/s respectively. This is higher than that obtained using resonance and the lower of the two velocities obtained using the "same face" technique. Other models, especially one using the Kelvin-Christoffel equation should be investigated.

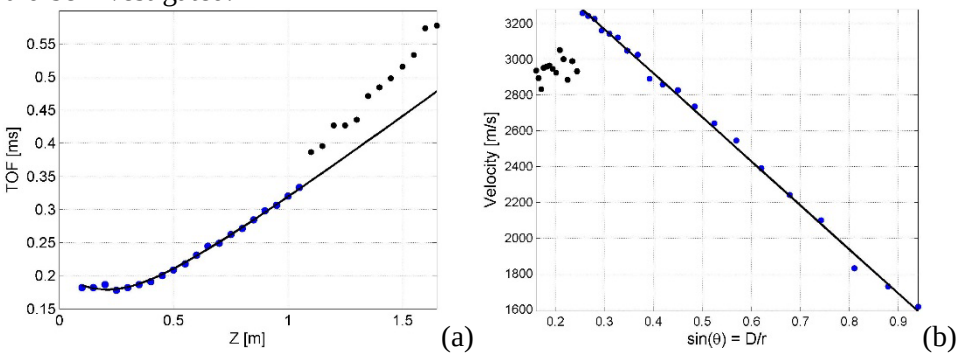

Figure 8: "Opposite face" measured (a) TOF and (b) velocity data points. Overlaid are linear least squared fitted lines. Beyond about a meter, the signal appears to have been attenuated too much for the AIC picker to pick the first arrival time of the signal.

The previous measurement had been made with an impulsive excitation signal using MLS signal and a MOSFET/set-up transformer power amplifier. "Opposite face" measurements were repeated using an arbitrary power amplifier and a transmit signal composed for five cycles of a sine wave (tone burst) and transmit frequencies ranging from 8 to 50 kHz in 0.5 kHz increments. These measurements were made with the transmit receiver both the thin and thick end of the log. The calculated velocities are plotted in Figure 9 as a function of the sin of the angle θ. Relatively similar results were obtained for the different transmit frequencies. However, different lines were obtained for the two ends of the log. This may be related to the thinner end having a lower moisture content than the thicker end and hence higher velocity.

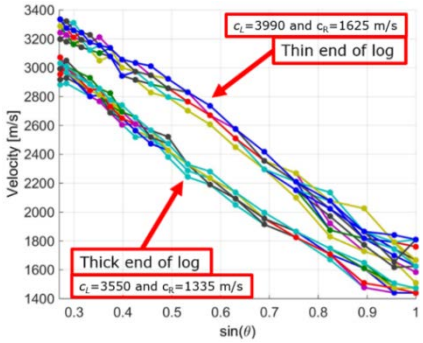

Figure 9: Measured "opposite face" velocities for frequency range of 8 to 50 kHz for two different locations in the log. Estimated values of longitudinal and radial velocities were estimated using Equation (8).

Table 1: Acoustic velocities obtained using different techniques.

Technique	Longitudinal Velocity
Resonance	2830 and 2670 m/s
TOF – "Same Face"	4490, 3120, and 3150 m/s
TOF – "Opposite Face" Model	3550 and 3908 m/s

Conclusions

There have been suggestion in some literature that time of flight measurements made on the same face of the tree tends to provide results that are biased to the outerwood stiffness. Measurements made with the receiver on the opposite face of the stem to the transmitter probe have been proposed as a potential way of obtaining stiffness measurements that are more of an average through the tree stem. However, this technique requires an anisotropic velocity model for the longitudinal-radial plane in order to extract the longitudinal velocity. This paper investigated both the "same face" and "opposite face" techniques using multiple propagation paths TOF measurements. A basic model was presented that explained the "opposite face" measured data for the log being investigated. This provided longitudinal velocities that were higher than those obtained using acoustic resonance and the lower of the two "same face" velocities. This was used with least squares fitting to estimate the longitudinal and radial velocity. Measurements were made using transducers on a log that was relatively dry. More experiments need to be made on standing trees or freshly cut logs to see if similar results are observed. Measurements could also be made using hammer impact on spikes. Also, other models should be investigated, such as that provided by the Kelvin-Christoffel equation.

Acknowledgments

This work was performed as part of the Growing Confidence in Forestry Future project (http://gcff.nz/). Funding was provided through Scion, the New Zealand Ministry of Business, Innovation and Employment and the New Zealand Forest Growers Levy Trust. Authors would like to acknowledge John Moore and Grant Emms of Scion for their help and guidance.

References

Andrews, M., 2002. Which acoustic speed. In: *Proceedings of the 13th International Symposium on Nondestructive Testing of Wood*. pp.159–165.

Bucur, V., 2006. *Acoustics of wood*. 2nd ed. New York: Springer.

Carcione, J.M., 2007a. Anisotropic elastic media. In: *Wave fields in real media: Wave propagation in anisotropic, anelastic, porous and electromagnetic media*. Oxford, Elsevier.

Chauhan, S. and Walker, J., 2006. Variations in acoustic velocity and density with age, and their interrelationships in radiata pine. *Forest Ecology and Management*, 229(1), pp.388–394.

Dickson, R., Matheson, A., Joe, B., Ilic, J. and Owen, J., 2004. Acoustic Segregation of *Pinus radiata* logs for sawmilling. *New Zealand Journal of Forestry Science*, 34(2), pp.175–189.

Dickson, R.L., Raymond, C.A., Joe, W. and Wilkinson, C.A., 2003. Segregation of *Eucalyptus dunnii* logs using acoustics. *Forest Ecology and Management*, 179(1), pp.243–251.

Dikrallah, A., Hakam, A., Kabouchi, B., Brancheriau, L., Baillères, H., Famiri, A. and Ziani, M., 2006. Experimental analysis of acoustic anisotropy of green wood by using guided waves. *Proceedings of the ESWM-COST Action E*, 35, pp.149–154.

Grabianowski, M., Manley, B. and Walker, J., 2006. Acoustic measurements on standing trees, logs and green lumber. *Wood Science and Technology*, 40(3), pp.205–216.

Harris, P., Petherick, R. and Andrews, M., 2002. Acoustic resonance tools. In: *Proceedings, 13th International Symposium on Nondestructive Testing of Wood.* pp.195–201.

Hsu, C.Y., 2003. Radiata pine wood anatomy structure and biophysical properties. PhD thesis, Forestry Department, University of Canterbury, New Zealand.

Joe, B., Dickson, R., Raymond, C., Ilic, J. and Matheson, A., 2004. Prediction of *Eucalyptus Dunnii* and *Pinus Radiata* Timber Stiffness Using Acoustics*: A Report for the RIRDC/Land and Water Australia/FWPRDC/MDBC Joint Venture Agroforestry*

Program. RIRDC.

Lasserre, J.-P., Mason, E.G. and Watt, M.S., 2007. Assessing corewood acoustic velocity and modulus of elasticity with two impact based instruments in 11-year-old trees from a clonal-spacing experiment of *Pinus radiata* D. Don. *Forest Ecology and Management*, 239(1), pp.217–221.

Li, G., Wang, X., Feng, H., Wiedenbeck, J. and Ross, R.J., 2014. Analysis of wave velocity patterns in black cherry trees and its effect on internal decay detection. *Computers and Electronics in Agriculture*, 104, pp.32–39.

Mahon, J.M., 2007. The use of acoustics for the wood quality assessment of standing *P. taeda* trees. PhD Thesis. University of Georgia.

Mahon, J.M., Jordan, L., Schimleck, L.R., Clark, A. and Daniels, R.F., 2009. A comparison of sampling methods for a standing tree acoustic device. *Southern Journal of Applied Forestry*, 33(2), pp.62–68.

Matheson, A.C., Dickson, R.L., Spencer, D.J., Joe, B. and Ilic, J., 2002. Acoustic segregation of *Pinus radiata* logs according to stiffness. *Annals of Forest Science*, 59(5-6), pp.471–477.

Maurer, H., Schubert, S.I., Bächle, F., Clauss, S., Gsell, D., Dual, J. and Niemz, P., 2006. A simple anisotropy correction procedure for acoustic wood tomography. *Holzforschung*, 60(5), pp.567–573.

Mora, C.R., Schimleck, L.R., Isik, F., Mahon, J.M., Clark, A. and Daniels, R.F., 2009. Relationships between acoustic variables and different measures of stiffness in standing *Pinus taeda* trees. *Canadian Journal of Forest Research*, 39(8), pp.1421–1429.

Ross, R.J. and Pellerin, R.F., 1994. Nondestructive testing for assessing wood members in structures. *General Technical Report FPL-GTR-70, Forest Products Laboratory, US Department of Agriculture*.

Searles, G., 2012. *Acoustic segregation and structural timber production.* PhD thesis. Edinburgh Napier University.

Su, J., Zhang, H. and Wang, X., 2009. Stress Wave Propagation on Standing Trees-Part 2. Formation of 3D Stress Wave Contour Maps. In: *Series: Conference Proceedings*.

Svilainis, L. and Motiejunas, G., 2006. Power amplifier for ultrasonic transducer excitation. *Ultragarsas*, 1(58), pp.30–36.

Wang, X., 2013. Acoustic measurements on trees and logs: a review and analysis. *Wood Science and Technology*, 47(5), pp.965–975.

Wang, X., Ross, R.J. and Carter, P., 2007. Acoustic evaluation of wood quality in standing trees. Part I. Acoustic wave behavior. *Wood and Fiber Science*, 39(1), pp.28–38.

Wang, X., Ross, R.J., McClellan, M., Barbour, R.J., Erickson, J.R., Forsman, J.W. and McGinnis, G.D., 2001. Nondestructive evaluation of standing trees with a stress wave method. *Wood and Fiber Science*, 33(4), pp.522–533.

Wang, X.R.R.J., Brashaw, B.K., Punches, J., Erickson, J.R., Forsman, J.W. and Pellerin, R.F., 2004. Diameter effect on stress-wave evaluation of modulus of elasticity of logs. *Wood and Fiber Science*, 36(3), pp.368–377.

Zhang, H., Thurber, C. and Rowe, C., 2003. Automatic P-wave arrival detection and picking with multiscale wavelet analysis for single-component recordings. *Bulletin of the Seismological Society of America*, 93(5), pp.1904–1912.

Zhang, H., Wang, X. and Ross, R.J., 2009. Stress wave propagation on standing trees: Part 1. Time-of-flight measurement and 2D stress wave contour maps. In: *16th International Symposium on NDT/NDE of Wood*. Beijing, China, pp.12–14.

Zhang, H., Wang, X. and Su, J., 2011. Experimental investigation of stress wave propagation in standing trees. *Holzforschung*, 65(5), pp.743–748.

Eucalyptus Wood Evaluation by Non-destructive Assessment

Frederico J. N. França
Department of Sustainable Bioproducts, Mississippi State University, Starkville, Mississippi, USA, fn90@msstate.edu

Tâmara S. F. Amorim França
Department of Sustainable Bioproducts, Mississippi State University, Starkville, Mississippi, USA, tsf97@msstate.edu

Franco S. Poletti
Departament of Forest and Wood Scienc, Federal University of, Jerônimo Monteira, Espírito Santo, Brazil, franco.s.poletti@gmail.com

Graziela B. Vidaurre Dambroz
Departamento de Ciências Florestais e da Madeira, Universidade Federal do Espírito Santo, Jerônimo Monteira, Espírito Santo, Brasil, grazividaurre@gmail.com

Abstract

The objective of this study aimed to evaluate the reliability of acoustic assessment in longitudinal and transverse directions as non-destructive test (NDT) way to predict the modulus of elasticity (MOE) and modulus of rupture (MOR) of 13-year-old Eucalyptus grandis x Eucalyptus urophylla hybrid clones wood. A total of 42 trees, 13-year-old *Eucalyptus grandis* x *Eucalyptus urophylla* hybrid clones were cut from a plantation in Alcobaça, Brazil. The logs were cut into boards and air dried to reach equilibrium moisture content (EMC). The specimens were removed from the diametrical board and cut into static bending test dimensions, 50 x 50 x 760 mm (ASTM D 143, 2006). All samples were conditioned to 12% moisture content before testing. Velocities were measured in longitudinal direction using stress wave timer equipment (Metriguard) and also using a microphone with specific computer software to read the longitudinal and transverse vibration frequencies. All three methods are reliable to predict MOE. High positive correlation were found between static MOE and dynamic MOE but both longitudinal direction techniques got higher correlation compared to the transverse direction method. Elastic waves such stress waves are not reliable to predict MOR but the transverse vibration exhibiting a slightly higher correlation between dynamic MOE and MOR, compared to the two longitudinal methods used.

Keywords: static bending, longitudinal vibration, transverse vibration

Introduction

Wood is one of the main materials used to construction to present advantages when compared with other materials like steel and concrete. It has considerable mechanical strength even being a light weight material. It is sustainable bio-product since it is renewable and biodegradable.

Like other materials used in construction, wood should be tested for physical and mechanical properties and then classified for structural use (Segundinho et al., 2012). The Brazilian standard NBR 7190 (ABNT, 1997) recommend the use of wood based on its strength characteristics required to meet the demands required.

Ross et al. (1998) defines non-destructive assessment as the way to evaluate physical and mechanical properties of a piece of material without changing its characteristics and uses.

Non-destructive techniques such as ultrasound, transverse vibration, longitudinal vibration, x-ray, and stress waves have been investigated and adopted by industry since they are able to offer fast response and high correlations with inexpensive equipment (Brashaw et al., 2009).

According to Amishev and Murphy (2008), the modulus of elasticity is one of the most important mechanical properties since it is the indicator of load resistance most frequently used in the case of wood.

The dynamic methods to characterize wood and other materials calculate the elastic modulus through the natural frequency of vibration of the specimen and its geometric parameters. These methods have the advantage of being fast, use small samples, and be repeatable (Cossolino and Pereira, 2010).

As a building material, wood offers many features that influences directly from the quality of the chosen wood and it is necessary the full knowledge of its structural potential for the correct use of wood in construction.

The objective of this study aimed to evaluate the reliability of stress wave, longitudinal vibration and transverse vibration as fast assessment ways to determine the modulus of elasticity and modulus of rupture of Eucalyptus grandis x Eucalyptus urophylla wood.

Materials and methods

Test specimens

A total of 42 trees, 13-year-old Eucalyptus grandis x Eucalyptus urophylla hybrid clones were cut from a plantation in Alcobaça, Brazil. The logs were cut into boards and air dried during 6 months to reach equilibrium moisture content (EMC). In this work, 56 specimens, eight samples from each clone, were removed from the diametrical board and cut into static bending test dimensions, 50 x 50 x 760 mm, according to ASTM D 143 (2006).

All samples and conditioned to 12% moisture content before testing. The specimens were evaluated using stress wave timer, longitudinal vibration and transverse vibration techniques, seeking to correlate with the static bending results.

Stress wave timer

Stress wave measurement was conducted on each wood specimen to obtain the stress wave velocity. A stress wave was initiated by a hammer impact on one end of the specimen. Stress wave propagation in the wood specimen was sensed by a piezoelectric transducer mounted on the other end of the sample. Stress wave velocity can be determined by Equation 1.

$$C = L/\Delta t \quad (1)$$

where C = stress wave velocity ($m.s^{-1}$), L = length of the specimen (m), Δt = time of flight (s).

Predicting the MOE of lumber with longitudinal stress wave has received considerable research effort in recent years in terms of lumber grading or pre-sorting (Wang, 2013). The relation acoustic velocity, density and wood stiffness is described by the fundamental wave equation (Bucur, 2003).

The dynamic MOE of the specimens were determined using one-dimensional propagation waves, based on Equation 2.

$$\boldsymbol{E_{sw} = \rho . C^2} \tag{2}$$

where Esw = dynamic modulus of elasticity obtained by stress wave timer, ρ = density at 12% moisture content ($kg.m^{-3}$), C = stress wave velocity ($m.s^{-1}$).

Longitudinal vibration

To achieve the longitudinal and transverse frequencies a microphone was used to capture the vibration. A computer with specific software, Fast Fourier Vibration Analyzer reads the natural frequency of each type of vibration.

An impact was applied on each test specimen in the longitudinal direction as according to ASTM E 1876 (2009). The direction of the wave motion occurs in the same direction as the longitudinal vibration mode. Dynamic modulus of elasticity due to the first longitudinal vibration resonance frequency is given by Equation 3.

$$\mathrm{E_L} = 4.\left(\frac{\mathrm{m.f_1^2}}{\mathrm{b}}\right).\left(\frac{\mathrm{l}}{\mathrm{h}}\right) \tag{3}$$

where EL = dynamic modulus of elasticity obtained by longitudinal vibration (MPa), m= mass (kg), f1 = first harmonic longitudinal vibration frequency (Hz), b = width (mm), h = height (mm), l = length (mm).

Transverse vibration

The transverse vibration test was performed similarly to longitudinal vibration but with a different direction of impact and sound capture. The impact was applied and the signal captured on the transverse direction of the wood according to ASTM E 1876 (2009). The calculation of the elastic modulus due to the first transverse vibration resonant frequency is given by Equation 4.

$$\mathrm{E_{VT}} = \left(\frac{2.\mathrm{f_1}}{\gamma_1.\pi}\right)^2.\left(\frac{\mathrm{m.l^3}}{\mathrm{I}}\right) \tag{4}$$

where E_{VT} = dynamic modulus of elasticity obtained by transverse vibration (MPa); F1 = first harmonic transverse vibration frequency (Hz); $\gamma 1 = (n+0.5)^2$ with n is the number of the fundamental wave; m = mass (kg); l = length (m); I = moment of inertia (m^4).

Static bending test

Following the non-destructive measurements, all specimens were mechanically tested in static bending with an Instron instrument in order to obtain the MOE and MOR. The static bending tests were conducted on each specimen using center-point loading, according to ASTM D 143 (2006). The load-deflection data was recorded by the machine and the flexural modulus of elasticity is calculated by Equation 5.

$$MOE = \frac{P.L^3}{48.\delta.I} \quad (5)$$

where MOE = Static bending modulus of elasticity (MPa), P = Force (N), L = distance between load points (m), d = midspan deflection (m), I = moment of inertia (m4).

Modulus of rupture (MOR) was calculated based on Equation 6:

$$MOR = \frac{P.L}{b.h^2} \quad (6)$$

where P = maximum transverse load on specimen (N), L = span of the specimen (m), b = thickness of the specimen (m), and h = depth of the specimen (m).

Density and moisture content

The dimension (cross section size and length) and weight of each specimen were measured. Density of each specimen was calculated based on the weight and volume. After static bending tests were completed, two moisture samples were cut from each specimen and its moisture content was determined using the oven dry method following ASTM D 4442 (ASTM, 2006).

Results and Discussion

Density and dynamic MOE of Eucalyptus wood measured with three techniques are show in Table 1. Density between clones ranged from 400 to 800 kg.m^{-3}. Dynamic MOEs obtained with the stress wave timer were higher if compared with the other two techniques.

Table 1 - Density and dynamic MOE of Eucalyptus clones wood measured with three techniques

CLONE	ρ_{AP}	E_{SW}	E_L	E_{VT}
No. 1	739	21.91	16.66	17.63
	(4.73)*	(6.32)	(12.12)	(8.40)
No. 2	675	21.53	15.14	16.59
	(2.30)	(4.84)	(6.01)	(7.06)
No. 3	712	18.83	14.15	16.49
	(7.69)	(12.38)	(11.34)	(9.79)
No. 4	701	18.00	13.08	16.11
	(3.18)	(5.71)	(6.18)	(6.18)
No. 5	723	15.63	11.74	15.43
	(4.81)	(6.15)	(11.46)	(2.78)
No. 6	572	17.01	10.19	13.98
	(3.90)	(7.15)	(10.18)	(9.56)
No. 7	629	18.39	11.91	14.78
	(10.03)	(10.00)	(18.70)	(10.98)

ρ_{AP} – Density at 12% MC (kg.m^{-3}); E_{sw} – Stress wave dynamic modulus of elasticity (MPa); E_L – Longitudinal vibration dynamic modulus of elasticity (MPa); E_{VT} – Transverse vibration dynamic modulus of elasticity (MPa); * Coeficient of variation (%).

Mechanical characteristics of the wood

Table 2 - MOE and MOR of the Eucalyptus clones wood samples

CLONE	MOE (GPa)			MOR (MPa)		
	Average	Min.	Max.	Average	Min.	Max.
No. 1	17.27 A (5.46)*	16.17	18.54	113.95 A (7.32)	100.52	123.07
No. 2	16.09 AB (4.11)	15.29	17.28	108.46 AB (6.44)	102.19	123.66
No. 3	14.68 BC (22.61)	9.35	16.34	96.17 B (20.31)	72.18	112.48
No. 4	13.88 CD (4.84)	12.70	14.42	99.17 B (5.54)	93.75	109.74
No. 5	12.69 D (5.71)	11.61	13.69	97.75 B (4.93)	90.42	104.24
No. 6	12.81 D (9.65)	10.96	14.39	82.54 C (11.87)	73.06	98.95
No. 7	13.71 CD (10.63)	11.37	15.73	95.30 BC (14.73)	78.16	110.91
AVERAGE	14.39			98.23		

MOE – Modulus of elasticity (GPa); MOR – Modulus of rupture (MPa); Min – Minimum value; Max. Maximum value; * Coeficient of variation (%).

The values of MOE found in this study ranged from 10.96 to 18.54 GPa. There are some variations between clones with Clone No. 1 exhibiting higher MOE and MOR if compared to the other clones.

Technique comparison

The relationship between static MOE and dynamic MOE obtained with the stress wave timer, longitudinal vibration, and transverse vibration are shown on Figure 1. All three methods got high positive correlation between static MOE and dynamic MOE.

Stress wave timer got the highest correlation (r^2=0.8682), followed by longitudinal vibration (r^2=0.8461) and then transverse vibration (r^2=0.6092). Both longitudinal direction techniques got higher correlation compared to the transverse direction method.

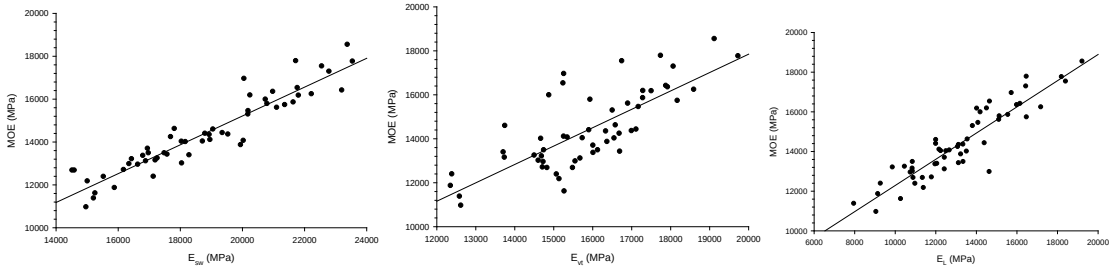

a b c

Figure 1 – Relationship between static MOE and dynamic MOE obtained with the stress wave timer (a), longitudinal vibration (b), and transverse vibration (c).

The relationship between MOR and dynamic MOE obtained with the stress wave timer, longitudinal vibration, and transverse vibration are shown on Figure 2. Linear relationship between dynamic MOE and MOR were not strong as already expected. All three methods exhibited moderate positive correlation between dynamic MOE and MOR.

Transverse vibration technique got the highest correlation ($r^2 = 0.6048$), followed by stress wave timer ($r^2 = 0.5195$) and then longitudinal vibration technique ($r^2 = 0.4255$). Transverse vibration technique had a slightly higher correlation compared to the two longitudinal methods used.

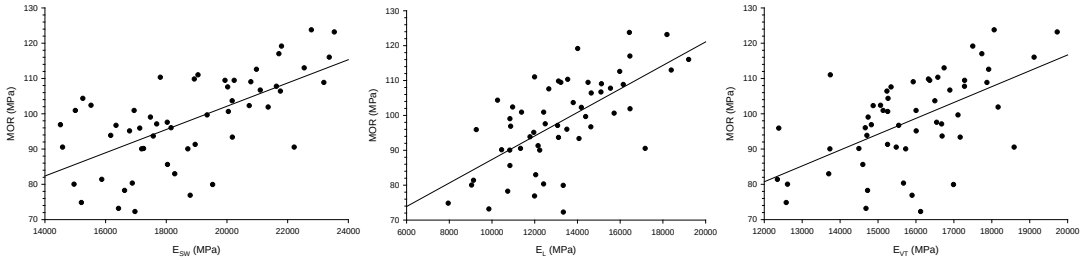

a b c

Figure 2 – Relationship between MOR and dynamic MOE obtained with the stress wave timer (a), longitudinal vibration (b), and transverse vibration (c).

McDonald et al. (1990) found a correlation between the static MOE and acoustic wave techniques. The author stated that it is more difficult to relate strength with the dynamic elastic constant, since the presence of defects and the inclination of the fibers have great effect in longitudinal speed of ultrasound wave.

Calil Junior and Miná (2003) found correlation between the static MOE and the dynamic MOE obtained through bending tests and transverse vibration in *Pinus* sp. wood. Carreira (2012) tested the transverse vibration method with Eucalyptus sp. logs in bending test and concluded that this technique was not efficient to provide reliable estimates of the logs MOR.

Conclusions

- Clones exhibit different values of MOE and MOR as expected;
- All three methods tested are able to predict MOE;
- Stress wave timer showed higher correlation between dynamic MOE and static MOE;
- Transverse vibration exhibited a slightly higher correlation between dynamic MOE and MOR;
- Elastic waves such stress waves are not reliable to predict MOR.

References

American Society For Testing And Materials. 2006. *ASTM D 143*: Standard methods of testing small clear specimens timber. Annual Book of ASTM Standards. v. 4.10, West Conshohocken.

American Society of Testing and Material. 2006. *ASTM D 4442*: Test Method for Direct Measurement of Wood and Wood-Base Materials. Annual Book of ASTM Standards. v. 4.10, West Conshohocken.

American Society of Testing and Material. 2009. *ASTM E 1876*: Standard Test Method for Dynamic Young's Modulus, Shear Modulus, and Poisson's Ratio by Impulse Excitation of Vibration. West Conshohocken, Pennsylvania, USA.

Amishev, D.; Murphy, G. E. 2008. In-forest assessment of veneer grade Douglas-fir logs based on acoustic measurement of wood stiffness. Forest Products Journal, Inistcnrs, Cote Inist, 58(11):42-47.

Associação Brasileira de Normas Técnicas. *NBR 7190: 1997*: Projeto de Estruturas de Madeira: 1997. Rio de Janeiro, 1997.

Brashaw, B.K.; Bucur, V.; Divós, F.; Gonçalves, R.; Lu, J. X.; Meder, R.; Pellerin, R.F.; Potter, S.; Ross, R.J.; Wang, X.; Yin, Y.F. 2009. Nondestructive testing and evaluation of wood: A worldwide research update. *Forest Product Journal*. 59:7-14.

Bucur, V. 2003. Nondestructive Characterization and Imaging of Wood, *Springer Series in Wood Science.*

Carlil Júnior, C.; Miná, A. J. S. 2003. Vibração transversal: Um método eficiente para classificação de peças estruturais de madeira. *Revista Brasileira de Engenharia Agrícola e Ambiental*, 7(2):335-338.

Carreira, M. R. 2012. Avaliação da Rigidez à Flexão de Toras de Madeira por meio de Vibração Transverse. 2012. Tese (Doutorado em Engenharia de Estruturas e Área de Concentração em Engenharia de Estruturas)–Escola de Engenharia de São Carlos, Universidade de São Paulo.

Cossolino, L. C.; Pereira, A. H. A. Informativo Técnico-Científico/ATCP Engenharia Física. Módulos elásticos: visão geral e métodos de caracterização. 2010. Disponível em: <http://www.investagro.com.br>. Acesso em: 14 mar. 2013.

McDonald, K. A.; Falk, R. H.; Mallory, M. P. 1990. Nondestructive testing of wood products and structures: state of the art and research needs. Madison, WI: U.S. Department of Agriculture, Forest Service, Forest Products Laboratory. p. 137-147.

Ross; R.J.; Soltis, L.A.; Otton, P. 1998. Assessing wood members in the USS Constitution using nondestructive eval- uation methods. *APT Bulletin*. 29(2): 21–25.

Segundinho, P. G. A. Aplicação do método de ensaio das frequências naturais de vibração para obtenção do módulo de elasticidade de peças estruturais de madeira. *Revista Árvore*, 36(6):1155-1161.

Wang, X. 2013. Stress Wave E-Rating of Structural Timber—Size and Moisture Content Effects. In: Proceedings: 18th International NondestructiveTesting and Evaluation of Wood Symposium, Ross, R.J., Wang, X. (eds.) General Technical Report FPL-GTR-226, pp: 38-46, Madison, WI: U.S, Department of Agriculture, Forest Service, Forest Products Laboratory, USA.

Influence of drying defects in the velocity of ultrasonic waves and in the compression strength of wood

Lucas Verissimo S. Castro
Undergraduate Student, Laboratory of Nondestructive Testing - LabEND, College of Agricultural Engineering – FEAGRI – University of Campinas – UNICAMP, Campinas, Brazil – e-mail:

Nádia Schiavon da Veiga
PhD Student, Laboratory of Nondestructive Testing - LabEND, College of Agricultural Engineering – FEAGRI – University of Campinas – UNICAMP, Campinas, Brazil – e-mail: nadiasveiga@gmail.com

Julio Soriano
Assistant Professor, Laboratory of Nondestructive Testing – LabEND, College of Agricultural Engineering – FEAGRI – University of Campinas – UNICAMP, Campinas, Brazil –
e-mail: julio.soriano@feagri.unicamp.br. Tel +55-19-35211040; fax +55-19-35211005

Abstract

Cracks and checks originated from drying the wood are more evident at the ends of structural lumber. Standards indicate that the characterization of wood must be done with the material extracted out of discard area. In this research, were evaluated implications of drying defects in the velocity of ultrasonic waves and on compression strength parallel to grain. We used structural lumber of tropical species (*Cedrela ssp, Apuleia leiocarpa, Goupia glabra* and *Dipteryx odorata)*. From discard area we extracted two specimens, one from each end of the longitudinal direction. To determine the wave propagation velocity of ultrasound we used a 45 kHz frequency longitudinal transducer. Afterwards we subjected the specimens to compression parallel to the grains. The results shown that is not possible to distinguish the specimens of both ends of discard. We conclude that drying defects do not affect significantly the behavior of wave propagation and parallel compression.

Keywords: characterization of wood, cracks, checks, timber discard area.

Introduction

Researches related to wood strength properties and their variations in consequence of humidity are extremely important for the qualification of the species and the adequacy of its various uses in the constructions. The knowledge of physical and mechanical properties of species is also required to specification of appropriate preservative treatment (IPT, 2009).

To obtain the properties of the wood, the ABNT NBR 7190 (1997) instructs that the specimens should be extracted out of the disposal areas, which are located at the ends of the structural piece. This procedure aims to obtain specimens free from defects, due physical damage or uncontrolled drying. The drying defects are characterized by changes that can do the wood unusable or make more difficult the workability and machining (Gonçalves, 2010). Among the defects caused by uncontrolled drying, there are the cracks, checks, warping and collapses (Wood Handbook, 2010; Jankowsky, 1995; IPT, 2009 and Jankowsky, 1979). In the case of eucalyptus, a susceptible species to drying defects, the lack of a more strict control while drying the pieces causes losses of the material that may reach 30% (Jankowsky, 1979 and Jankowsky, 1995).

Defects resulting from the drying of wood can cause variances in the results of non-destructive testing. Bucur and Bönhke (1994), researching the classification of structural pieces of wood by ultrasound, mentioned that variations in ultrasound tests may occur as a result of the wood defects and its moisture content. This approach is also presented by Bartholomeu (2001) and Calegari (2006).

This study aimed to evaluate the influence of drying defects in the results of ultrasonic velocity and compression strength parallel to grain in pieces of structural wood.

Material and Methods

The tests were performed with four hardwood species: Cupiúba (Goupia glabra), Cumaru (Dipteryx odorata), Cedar (Cedrela spp) and Garapa (Apuleia leiocarpa). For each species were selected 12 different boards with commercial sections measuring 80 mm x 200 mm.

In accordance with the procedures of ABNT NBR 7190 (1997), to characterize the physical and mechanical properties of wood, for the extraction of specimens should be excluded the ends of the pieces (Figure 1), called disposal areas. Thus, for the object of this study, each beam has taken a disposal area of the prism with a length of 40 cm from the tip of the beam. These prisms were used because of the greater concentration of drying defects (cracks and checks). During the cutting of these pieces, the wood was dry and the moisture in balance with the protected building.

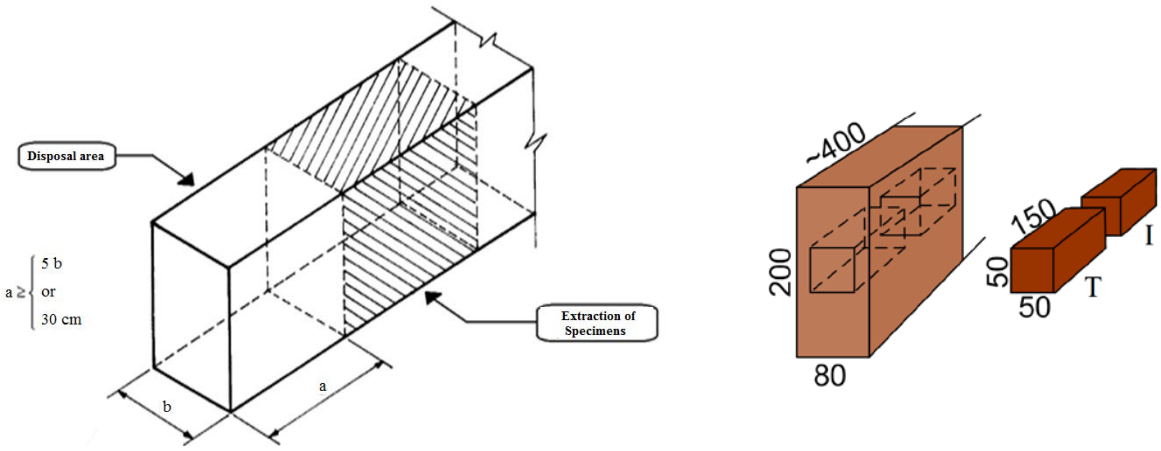

a) Disposal areas and areas to specimens extraction. Adapted from ABNT NBR 7190 (1997).

b) Positioning of specimens inside the disposal area (dimensions in mm).

Figure 1. Disposal region at the tip of a beam.

Of each disposal prism, two specimens (Figure 1) were extracted for tests of compression parallel to grain and ultrasound. The specimens were fabricated with cross-section measuring 50 mm x 50 mm and 150 mm long. The samples extracted from the tips of the beams were identified by T and the extracted specimens from the inner region were identified by the letter I. Some of the specimens had visibly drying defects (Figure 2). Also, for each prism was extracted a sample for determine the moisture content, with cross-section measuring 20 mm x 30 mm and 50 mm long, according to ABNT NBR 7190 (1997).

a) longitudinal view b) cross-sectional view

Figure 2. Specimens with visible defects.

All specimens made for parallel compression to grain test were at first submitted to ultrasound test, which was used for measuring the time of wave propagation in the longitudinal direction. In that direction were calculated spread velocities of ultrasonic waves. The ultrasound machine used was the USLab (USLab, AGRICEF, Brazil) and flat faces transducers, with frequency 45 kHz, attached to the faces of the wood with medicinal gel. Compression tests were performed on a universal machine (DL30.000, EMIC, Brazil).

To determine the moisture content according to ABNT NBR 7190 (1997), the specimens were weighed then they were kept in a kiln at temperature of 103ºC ± 2ºC until the difference between two consecutive readings of mass (every 6 hours) were less than 0.5%.

Results and Discussion

The moisture contents for each species are presented in Table 1. The results shows that all the species researched were next to the Brazilian standard moisture content, 12%. Note also that the highest coefficient of variation resulted equal 7.54%.

Table 1. Moisture content of the tested pieces for all species.

	Cumaru	**Cupiúba**	**Cedar**	**Garapa**
N	12	12	12	12
Mean (%)	11.31	12.30	12.87	11.34
StDev (%) [(1)]	0.85	0.88	0.58	0.51
C.V. (%) [(2)]	7.54	7.16	4.53	4.53

[(1)] Standard deviation [(2)] Coefficient of variation

Table 2 shows the groupings of wave propagation velocities for each species, referring to specimens taken from tips and inner regions of the prism. Note that there is no statistical difference between the values

obtained for tips and centers. The Table 3 shows the same grouping analysis in relation to the compression resistance parallel to grain.

Table 2. Ultrasound velocity and grouping for each species.

	Samples	Mean (m s^{-1})	StDev (m s^{-1}) [1]	CV (%)	Grouping [2]
Cumaru	Tip	4704.2	106.2	2.26	A
	Inner	4703.8	109.7	2.33	A
Garapa	Tip	4535.9	166.3	3.67	A
	Inner	4585.6	248.2	5.41	A
Cedar	Tip	4421.4	110.5	2.50	A
	Inner	4420.5	137.7	3.12	A
Cupiuba	Tip	4296.3	202.0	4.70	A
	Inner	4380.3	229.9	5.25	A

[1] Standard deviation; [2] Based on the LSD Tukey test with a 5.0% margin of error, there is no statistically significant difference between the values denoted by the same letter.

Table 3. Compression strength parallel to grain and grouping for each species.

	Samples	Mean (MPa)	StDev (MPa) [1]	CV (%)	Grouping [2]
Cumaru	Tip	74.7	6.7	8.91	A
	Inner	75.7	6.3	8.29	A
Garapa	Tip	75.6	5.0	6.61	A
	Inner	73.9	3.4	4.57	A
Cedar	Tip	44.6	5.9	13.27	A
	Inner	46.1	4.6	10.03	A
Cupiuba	Tip	60.8	9.8	16.08	A
	Inner	60.5	10.5	17.36	A

[1] Standard deviation; [2] Based on the LSD Tukey test with a 5.0% margin of error, there is no statistically significant difference between the values denoted by the same letter.

For each studied species, the distribution of the results obtained for both the specimen, tips and centers, was similar. If the drying defects interfere in the results of ultrasound parallel to the fibers (Table 2), the results for the tips should have smaller values than those obtained for the centers. Similarly, if the drying defects interfere in the compression strength parallel to grain (Table 3) for each species, the tip results would be lower than those of the inner pieces.

For the results of ultrasonography (Table 2), considering each species, the largest coefficients of variation were obtained for the specimen of central region, with the highest value of 5.41% corresponding to Garapa species. For compressive strength, the highest coefficient of variation (17.36%) was obtained for the specimens from the internal region of Cupiúba species. However, for the other three species the largest coefficients of variation were obtained for the samples taken from the tip region (Table 3). With respect to the coefficients of variation for the compression strength parallel to grain, were obtained all values below 18%. For design purposes, ABNT NBR 7190 (1997) admits the coefficient of variation up

to 18%, with which is possible to estimate the characteristic strength equal to 70% of the average strength.

Before conducting the tests, by visual inspection, the cracks were highlighted on the faces of the specimens. Figure 3 presents specimens after fracture by compression parallel to the fibers. Although the drying defects have not produced significant differences in the results of ultrasound and compression strength parallel to the fibers, it is evident that such defects have a direct influence on the material failure mode.

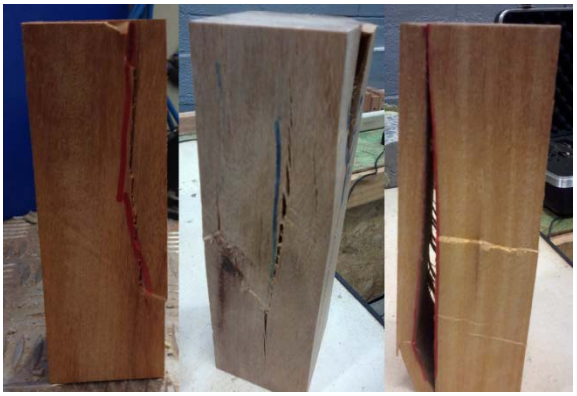

Figure 3. Specimens ruptured in the fissures previously highlighted.

Conclusions

Based on the results obtained by ultrasound testing and compression parallel to the fibers it was concluded that:

- Drying defects characterized by fissures and cracks, which are most evident at the tips of the timber, did not influence the results of these test methods. The grouping of results for each species studied showed no significant difference in the disposal area.
- Variations of the ultrasound results were lower than the variations in compressive strength parallel to the fibers, with maximum values of the coefficients of variation of 5.41% and 17.36% respectively.
- The presence of cracks, evident on the surfaces of the specimens, although it has not caused reduction of compressive strength parallel to the fibers, influenced the failure mode of the specimens.

Acknowledgments

The authors would like to thank the support of the National Council of Technological and Scientific Development (CNPq) for the undergraduate research scholarship, to the Brazilian Federal Agency of Coordination for the Improvement of Higher Education Personnel (CAPES) for the PhD research scholarship and the Fund to Support to Teaching, Research and Extension (FAEPEX) from the University of Campinas for the financial support.

References

ABNT. 1997. Design of timber structures. NBR 7190 - Brazilian Association of Technical Standards. Rio de Janeiro. (in Portuguese)

Bartholomeu, A. 2001. Grading of structural lumber using ultrasound. Campinas, SP: University of Campinas. Doctorate thesis. (in Portuguese)

Bucur, V.; Böhnke, I. 1994. Factors affecting ultrasonic measurements in solid wood. Ultrasonics. 32(5): 385-390.

Calegari, L. 2006. Use of the ultrasonic wave as a means of controlling the wood-drying process. Santa Maria, RS. University of Santa Maria. M.S. thesis. (in Portuguese)

Gonçalves, C. N. P. 2010. Contributions to a higher and better use of wood brave pine in Portugal. Porto. Universidade do Porto. M.S. thesis. (in Portuguese)

IPT - Institute for Technological Research of the State of Sao Paulo. 1989. Sheets characteristics of Brazilian woods. São Paulo: IPT. 418p. (in Portuguese)

Jankowsky, I. P. 1979. Wood Juvenile, training and industrial use. IPEF - Institute of Research and Forestry Studies. http://www.ipef.br/publicacoes/ctecnica/nr081.pdf. [accessed 2014]. (in Portuguese)

Jankowsky, I. P. 1995. Equipment and processes for wood drying. In: International seminar of use of eucalyptus wood for sawmill. Piracicaba: IPEF - Institute of Research and Forestry Studies: 109-118. (in Portuguese)

U. S. Department of Agriculture. Forest Products Laboratory. 2010. Wood Handbook-Wood as an engineering material. Madison, 508 p.

Effects of non-linearity and variability in the study of natural frequency of Eucalyptus grandis wood using a impulse excitation non-destructive technique

Carlos Alberto Oliveira de Matos
Experimental Campus of Itapeva – UNESP, São Paulo State University, Itapeva, São Paulo, Brazil, carlos@itapeva.unesp.br

Rafaele Almeida Munis
Experimental Campus of Itapeva – UNESP, São Paulo State University, Itapeva, São Paulo, Brazil, rafaele.munis@grad.itapeva.unesp.br

Elen Aparecida Martines Morales
Experimental Campus of Itapeva – UNESP, São Paulo State University, Itapeva, São Paulo, Brazil, elen@itapeva.unesp.br

Abstract

The influence of length of piece wood on natural frequency vibration was evaluated to determine the natural frequency range to calculate the longitudinal modulus of elasticity in bending of Eucalyptus grandis with ten years old. The results obtained from the average of the data of frequencies indicate which the longitudinal frequency depends linearly on the length of the piece (p-value=0.0001399). The high quality of the fitted model (adjusted R^2=0.92) with this approach underestimates important effects of the natural variability. Simulations (Monte Carlo) were performed with coefficients of variation between 5 and 25% and a non-linear model (logarithm of the frequency as a function of length). The low value R^2 median obtained (0.49) for the most coefficient of variation indicates the need to consider the role of variation more appropriately; R^2 median for the nonlinear model indicated no substantive gain of quality in relation to the linear model.

Keywords: variability, non-linearity, natural frequency range, length of piece wood

Introduction

In the impulse excitation method, the specimen is submitted to a short impact vibrations and reacts with its natural vibration frequency in accordance with the imposed boundary conditions. This method was developed in the 1960s and 1970s in conjunction with the Grindosonic equipment that spread the characterization of the dynamic elastic moduli and expanded the scope of this method for quality control and inspection. The Grindosonic is marketed with the same features (non-destructive, portable, simple, results available quickly, no need calibration or adjustment, widest range of materials, sample size from less than 100 mg to over a ton, modulus values from 0.05 to over 900 GPa, suitable for industrial and laboratory use, high accuracy and reproducibility) until now, but in the 1990s have been developed and are currently being improved, automated measurement systems for the characterization of elastic moduli of refractory materials as a function of time and temperature. These systems are computer-based and have several advantages over the traditional Grindosonic, particularly the discrimination of frequencies. The Sonelastic by example enumerates the existing harmonic frequencies and its damping besides the

fundamental frequency. Characterization procedures for nondestructive dynamic methods were standardized (ASTM 2000; ASTM 2007) as a result of its dissemination and increasing importance. Preparation of studies and guides to good characterization practices (Morrel 1996; Morrel 2006) and harmonization efforts between laboratories and techniques (Wolfenden et al. 1989) were also a result of this process.

Wood from species of Eucalyptus presents itself as an efficient alternative for use in structures, sector in which there is a lack of studies in Brazil. Among the methods used for the mechanical characterization of materials (longitudinal modulus of elasticity in bending, in case) the Impulse Excitation Technique (IET) has had recent use (Munis et al. 2013).

The influence of length of piece wood on natural frequency vibration was evaluated to determine the natural frequency range to calculate the longitudinal modulus of elasticity in bending of Eucalyptus grandis with ten years old. The results obtained from the average of the data of frequencies indicate which the longitudinal frequency depends linearly on the length of the piece (p-value=0.0001399). The high quality of the fitted model (adjusted R^2=0.92) with this approach underestimates important effects of the natural variability. Additionally the graphical analysis of the data indicated a probable non-linearity. Our objectives were assess the effects of non-linearity and variability in the study of natural frequency of Eucalyptus grandis wood.

Review and Methodology

The determination coefficient is a measure of the quality of obtained fit with regression models. However, the coefficient of determination value depends on the number of sample observations, tending to grow when n decreases. On limit for n = 2, we would always have the determination coefficient equal to one, as two points determine a straight, deviations are therefore nulls. In an attempt to overcome this drawback, it is defined the coefficient of determination adjusted for degrees of freedom. (Hoffmann and Vieira 1998)

$$R^2_{adj} = R^2 - \frac{1}{n-2}\left(1 - R^2\right) \tag{1}$$

When apply regression analysis to study the functional relationship between two variables, the problem of the specification is to determine the mathematical shape of the function to be adjusted. The mathematical form of the function it can be determined in two different ways and often complementary: using a priori knowledge we have about the phenomenon or using knowledge acquired by inspection the available numerical data. Often we adjusted more than one model and choose the model that best fits the data based on the statistical results (coefficient determination, residual mean squares, etc.). When the best models that fit are examples of non-linear models we can transforms them in linear models using anamorphosis ,that is, by replacing values of one or more variables by functions of these variables. The graphical analysis of the results indicated an exponential function to model the functional relationship between the longitudinal frequency and length (Munis et al. 2013). These models (non-linear and linear obtained with the anamorphic process) are presented in equations (2) e (3).

$$Y_i = \alpha\beta^{X_i}\varepsilon_i \tag{2}$$

$$\log Y_i = \log \alpha + \log X_i \log \beta + \log \varepsilon_i \tag{3}$$

We can estimate the Y value corresponding to the X value which does not exist in the sample (Y_h). $\hat{Y}_h$ is not-biased prediction of the Y_h value. The prediction interval assesses the precision of $\hat{Y}_h$ as prediction of the value the new observation. The concept of prediction interval is analogous to the confidence interval, with the difference that while confidence interval referred to a constant (mathematical expectation of Y_h in the case), the prediction interval refers to a random variable (Y_h in the case). Narrow confidence and prediction intervals are extremely desirable when the objective is disseminate the applicability of models specified for the prevision purposes. The width of the confidence and prediction intervals is inversely proportional to the quality of the model measured by the coefficient of determination.

The pseudo-random number generator used in the Monte Carlo simulations was the so-called Mersenne Twister algorithm that uses multiple recursive matrix method for generating pseudo-random numbers. It is a variation of generators type TGFSR (twisted generalized feedback shift register) which produces an astronomical period approximately equal to 2^{19937}-1 on the basis of selected parameters (Matsumoto and Nishimura 1998). This generator, according has undergone tests of randomness rather strict, including the DieHard battery of tests, without accusing any detection of deterministic patterns and is currently implemented in matrix languages such as matrix R (Cribari Neto and Zarkos 1999). Simulations (Monte Carlo) were performed with coefficients of variation between 5 and 25% and a non-linear model (logarithm of the frequency as a function of length). Each simulation condition comprises five levels of variance and two models was run 20,000 times.
R is a programming language and integrated development environment available for free for statistical computing and graphics. It is a GNU project which is similar to the S language and environment which was developed at Bell Laboratories (formerly AT&T, now Lucent Technologies) by John Chambers and colleagues. In this work we used the R x64 3.1.3 version. The functions used belong to package base (R Core Team 2015).

Results and Conclusion.

Table 1 shows the results of raising the coefficient of variation in the quality of the linear models. Even for the smallest coefficient of variation, quality (summarized by adjusted coefficient of determination median) was smaller than given in the original paper that supported our simulations. The low value R^2 median obtained (0.49) for the most coefficient of variation indicates the need to consider the role of variation more appropriately.

Table 1—Linear Model

Coefficient of variation	Adjusted R^2 Median
(%)	(%)
5	89.29
10	81.16
15	70.41
20	59.16
25	49.28

The hypothesis of a possible non-linear model that relates functionally the horizontal frequency with the length is refuted in Table 2. There are no significant differences between quality of fit exponential model linearized by anamorphosis with the linear model. R^2 median for the nonlinear model indicated no substantive gain of quality in relation to the linear model.

Table 2—Non Linear Model

Coefficient of variation	Adjusted R^2 Median
(%)	(%)
5	91.84
10	81.84
15	68.72
20	55.10
25	42.60

The results recommend caution in the use of the model originally specified. Figure 2 illustrates this recommendation. It has been drafted on coefficient of determination approximately equal to ($R^2 \approx 50\%$) obtained in the simulation with the highest coefficient of variation (25%).

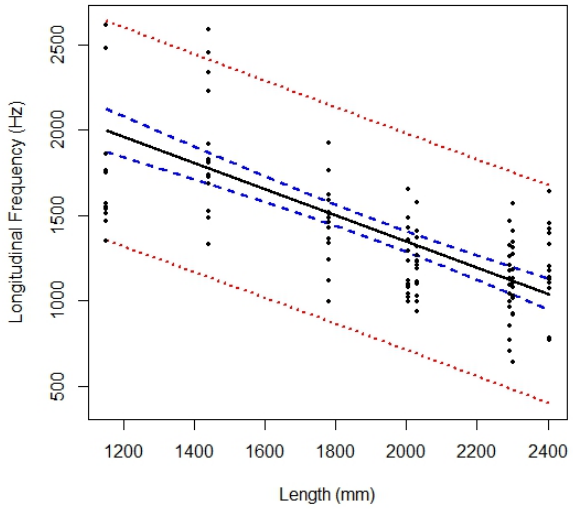

Figure 1—Linear model: Longitudinal Frequency = f (Length). Widths of confidence interval (blue) and prediction interval (red). Adjusted coefficient of determination $R^2 \approx 0.50$.

The big widths of confidence and prediction intervals demonstrates the limitations related to the use of the present model for predictive purposes in situations where there are moderate levels of natural variability.

Acknowledgments

We thank to all the challenging students and the relevant employees of Experimental Campus of Itapeva, UNESP - Universidade Estadual Paulista.

References

ASTM International. 2000. ASTM E1875 – 00: Standard Test Method for Dynamic Young's Modulus, Shear Modulus, and Poisson's Ratio by Sonic Resonance. 7 p.

ASTM International. 2007. ASTM E1876 – 07: Standard Test Method for Dynamic Young's Modulus, Shear Modulus, and Poisson's Ratio by Impulse Excitation of Vibration. 15 p.

Cribari Neto, F.; Zarkos, S. G. 1999. R: Yet Another Econometric Programming Environment. Journal of Applied Econometrics. 14: 319-329.

Hoffmann, R.; Vieira, S. 1998. Análise de Regressão. Uma Introdução à Econometria. São Paulo: HUCITEC. 379 p.

Matsumoto, M.; Nishimura, T. 1998. Mersenne Twister: A 623-Dimensionally Equidistributed Uniform Pseudo-Random Number Generator. ACM Transactions on Modeling and Computer Simulation. 8: 3-30.
Morrel, R. 1996. Measuring Elastic Properties of Advanced Technical Ceramics – A review. UK National Physical Laboratory Report - 42. 41p.

Morrel, R. 2006. NPL Measurement Good Practice Guide - Elastic Module Measurement. UK National Physical Laboratory Report - 98. 100 p.

Munis, R. A.; Morales, E. A. M.; Fé, A. D. [and others]. 2013. Estudo da frequência natural da madeira de dez anos de Eucalyptus grandis utilizando a técnica não destrutiva de excitação por impulso. http://prope.unesp.br/cic/admin/ver_resumo.php?area=100077&subarea=23284&congresso=35&CPF=41296251870

R Core Team. 2015. R: A language and environment for statistical computing. R Foundation for Statistical Computing. Vienna. http://www.R-project.org/. [Date accessed unknown].
Wolfenden, A.; Harmouche, M.R.; Blessing, G.V. 1989. Dynamic modulus measurements in metallic materials: results of an interlaboratory testing program. Journal of Testing and Evaluation. 17(1): 2-13.

Evaluation of growth stresses in living trees of *Corymbia citriodora* Hill & Johnson *(Eucalyptus citriodora* Hook*)* by determining the Longitudinal Residual Strain

Carolina N. Xavier
Department of Forest Products, Federal Rural University of Rio de Janeiro, Seropédica – RJ, Brazil.
ncarolx@gmail.com

Carlos Eduardo S. da Silva
Department of Forest Products, Federal Rural University of Rio de Janeiro, Seropédica – RJ, Brazil.
c.eduardo_silveira@yahoo.com.br

Marcondes G. Coelho Junior
Department of Forest Products, Federal Rural University of Rio de Janeiro, Seropédica – RJ, Brazil.
marcondescoelho22@gmail.com

Alexandre M. de Carvalho
Department of Forest Products, Federal Rural University of Rio de Janeiro, Seropédica – RJ, Brazil.
amcarvalho.ufrrj@gmail.com

Abstract

The equipment called extensometer, is the responsible for the measurement of longitudinal residual strain (LRS). This deformation is caused by growth stress which is a natural force whose objective is the support of the tree, being responsible for defects in the wood after tree felling. The objective of this study was to measure the longitudinal residual strain in *Corymbia citriodora Hill & Johnson*, checking in 4 different positions in the trunk and their correlation with diameter at breast height (DBH), height and thickness of the shell.

On the campus of the Rio de Janeiro Rural Federal University (UFRRJ), Seropédica/RJ eight trees of *Corymbia citriodora Hill & Johnson* were chosen randomly. In each tree the following measurements were taken: DBH, bark thickness, tree height and the LRS in four different positions around the trunk (north, south, east and west). The LRS were measured in DBH with the aid of the extensometer. For install the extensometer is necessary to remove the bark forming a square of 15cm x 15cm on the tree trunk. From this, for performing each measurement, inside this panel are fixed two metal pins at a distance of 45mm from each other and with the aid of a hand drill a hole was made between the pins, thus the growth stresses were released, thus enabling the measurement of the strain gauge through the LRS.

After statistical analysis there was a low correlation between LRS and the variables DBH, height and thickness of the shell. Concerning the measurement of the position of LRS in the trunk there is no significant difference. It can be concluded that there is a need for a more precise evaluation in a larger number of trees can be adopted lowest number of reviews on each tree to provide a better understanding of the correlates of longitudinal residual strain and other variables evaluated in the population.

Keywords: wood, extensometer, longitudinal residual strain (LRS), correlation, growth.

Introduction

The wood has historically been used for various purposes. He has served for our predecessors such as housing, as a building material and the passage of time pillars and beams were discovered in prehistory in various civilizations, before the fire. Each civilization, climate, terrain, cataclysms that determined a different approach in the use of wood (UFSC, 2014).

Thus, the man saw the wood a range of opportunities for your use. Wood floats, therefore boats were created. It is easy workability, new forms, furniture and objects emerged. Varying with locality and their types of trees, the wood was and is always present in human history and is used naturally or combined with some other element (UFSC, 2014).

According to Cunha (2012), Wood choice of woody species for a particular job can only be done with economy and safety, with knowledge of the values that define their behavior, both from the physical point of view of their resistance when subjected to mechanical stress. To obtain these values can be used for destructive sampling methods and non-destructive.

According to Padua (2009), methods or non-destructive tests are important tools for evaluating the properties of wood, as are techniques to qualify the material without compromising its future use. Thus, the methods provide a saving of time and costs in the preparation of the samples, unlike destructive sampling.

Currently forest research organizations are used for nondestructive evaluations (HANSEN, 2000). According Ross, Brashaw and Pellerin (1998 cited by Couto, 2011 and FLÓREZ, 2012), the non-destructive evaluation can be defined as the science of identifying the physical and mechanical properties of a part of a material without affecting the usability end.

In addition to cost savings, the non-destructive tests also have great utility for species where vegetative propagation is unreliable (Raymond, 2002 cited by Padua, 2009).

Silva (1992) cited by Palermo (2010), deals with that for anatomical analysis the selection of raw materials with minimal cellular variation is important for the quality control of wood products. However, the evaluation based on these characteristics is difficult because of the wide variation that occurs between and within species.

This variation second Hughes (1968), can be divided into three aspects. The first is the variation between species, gener and families. The second is the variation within the same species and the third is the variation found in relation to age. The size, proportion and arrangement of various forms of structural elements of wood make a species can be distinguished from other (Palermo, 2010).

This variation of the anatomical elements directly affect the performance of the species when they are subjected to physical tests, thus defining potential as the commercial use (Burger & Richter, 1991 cited by PALERMO, 2010).

According to Lima (2004), cited by Flórez (2012), among the methods considered non-destructive or semidestrutivos for measuring deformations associated to the growth stresses are developed by the CIRAD-Forêt (BAILLÈRES; DURAND, 2000), which consists of measuring, with the aid of a dial indicator, the deformation experienced in the central area between two pins fixed to 45 mm apart along the grain, the surface of the trunk without bark.

The strain measurements are carried out by releasing tension and drive pins process. For this, it made a hole with a drill of 20 mm in diameter (Lisbon, 1993 LIMA, 2004, cited by FLOREZ, 2012).

These stresses may vary in intensity and can be tensile or compressive depending on the location within the xylem and its direction of operation: longitudinal, tangential and radial (STERN, 2002 cited by TRUGILHO et al., 2006).

Measurements with extensometer provide digital data od longitudinal residual strain (LRS), which is directly related to longitudinal stress growth, this smaller shape is the value of the LRS, lower levels of internal stresses growth and wood most favorable to use as a solid product.

According to Lima (2004), cited by Flórez (2012), among the methods considered non-destructive or semidestrutivos for measuring deformations associated to the growth stresses are developed by the CIRAD-Forêt (BAILLÈRES; DURAND, 2000), which consists of measuring, with the aid of a dial indicator, the deformation experienced in the central area between two pins fixed to 45 mm apart along the grain, the surface of the trunk without bark.

The strain measurements are carried out by releasing tension and drive pins process. For this, it made a hole with a drill of 20 mm in diameter (Lisbon, 1993 LIMA, 2004, cited by FLOREZ, 2012).

The objective of this study was to measure the longitudinal residual strain in *Corymbia citriodora* Hill & Johnson, checking in 4 different positions in the trunk and their correlation with diameter at breast height (DBH), height and thickness of the shell.

MATERIAL AND METHODS

Eight trees of *Corymbia citriodora*, from the campus of the Rio de Janeiro Rural Federal University (UFRRJ), Seropédica/RJ were chosen randomly. In each tree the following measurements were taken: DBH, bark thickness (Figure 1), tree height and the LRS in four different positions around the trunk (north, south, east and west).

Figure 1. Measurement of the thickness of the bark of the trunk

The LRS were measured in DBH with the aid of the extensometer. For install the extensometer is necessary to remove the bark forming a square of 15cm x 15cm on the tree trunk (Figure 2).

Figure 2. Window made in the tree for equipment fixing

From this, for performing each measurement, inside this panel are fixed two metal pins at a distance of 45mm from each other and with the aid of a hand drill a hole was made between the pins, thus the growth stresses were released, thus enabling the measurement of the strain gauge through the LRS (Figure 3).

Figure 3. Measurement of longitudinal residual strain

RESULTS AND DISCUSSION

Residual Longitudinal Deformation (LRS) average was observed at 0,081mm (Table 1). In the analysis of variance (ANOVA) had a p value of 0,2007, so the average between 4 LRS (measured in directions north, south, east and west) are equivalent.

Table 1. Results of longitudinal residual strain (LRS), diameter at breast height (DBH), height and thickness of the bark.

Tree	DBH (cm)	Height (m)	Bark thickness (mm)	LRS 1 (mm)	LRS 2 (mm)	LRS 3 (mm)	LRS 4 (mm)	Average LRS
1	35,97	18	4	0,051	0,033	0,015	0,037	0,034
2	69,71	21	11	0,060	0,068	0,045	0,048	0,055
3	61,43	20	12	0,120	0,190	0,155	0,070	0,134
4	35,33	15	5,5	0,139	0,136	0,164	0,094	0,133
5	19,42	13	4	0,024	0,033	0,044	0,013	0,028
6	26,10	12	6	0,090	0,129	0,118	0,101	0,110
7	36,29	20	3	0,084	0,149	0,138	0,033	0,101
8	53,32	23	5	0,047	0,096	0,039	0,022	0,051
Average	42,20	17,75	6,31	0,077	0,104	0,090	0,052	0,081
Standard derivation	17,52	3,99	3,35	0,039	0,057	0,060	0,033	0,044
Minimum	19,42	12,00	3,00	0,024	0,033	0,015	0,013	0,028
Maximum	69,71	23,00	12,00	0,139	0,190	0,164	0,101	0,134
CV (%)	41,53	22,48	53,04	50,75	54,71	66,90	62,84	54,05

Gonçalves (2007) obtained in their research the average value of longitudinal residual strain (LRS) for *Eucalyptus citriodora* and *Eucalyptus urophylla*, respectively, 0.106 and 1.92 mm. Lima (2004), in *Eucalyptus* spp clones. LRS observed an average of 0.079 mm and Trugilho et al. (2006) of 0.093 mm in *Eucalyptus* clones.

Therefore, the results of this study are within the range of values reported in the literature.

Table 2. Pearson correlation between the longitudinal residual strain (LRS), diameter at breast height (DBH), height and bark thickness.

	DBH (cm)	Height (m)	Bark thickness (mm)	LRS 1 (mm)	LRS 2 (mm)	LRS 3 (mm)	LRS 4 (mm)
DBH (cm)	1	0,8086	0,7817	0,1527	0,2502	-0,0368	-0,0163
Height (m)		1	0,3007	-0,0899	0,1409	-0,1922	-0,4205
Bark thickness (mm)			1	0,3398	0,3570	0,1982	0,3425
LRS 1 (mm)				1	0,8282	0,9048	0,8193
LRS 2 (mm)					1	0,90142	0,5768
LRS 3 (mm)						1	0,6813
LRS 4 (mm)							1

It is observed in Table 2 that most of the LRS values there is a negative correlation with variables DBH and height as the variable thickness of the bark has a low positive correlation to DRL.

Gonçalves (2007) noted in his research a negative and significant correlation between LRS and height to *Eucalyptus urophylla*. According to Beltrame (2010), the longitudinal residual strains showed significant correlations with the bark thickness. According Muneri et al. (2000), there are significant positive correlations of LRS to the height and diameter of *Eucalyptus cloeziana* trees.

Thus, it is observed how distinct is the LRS interactions with the growth characteristics of one species to another.

Conclusions

- The longitudinal residual strain average observed was 0.081 mm;
- The longitudinal residual strain measured in the four directions (north, south, east and west) does not differ statistically;
- There is a negative correlation between height and LRS and a positive correlation between LRS and the bark thickness.

REFERENCES

Baillères, H.; Durand, P. Y. Non -destructive techniques for wood quality assessment of plantation grown teak. Bois et Forest dês Tropiques, Montpellier, v. 54, n. 263, p. 17-20, 2000.

Beltrame, R. Determination of longitudinal residual strains arising from the growth stresses in Eucalyptus spp. 2010. 81p. Dissertation. Santa Maria Federal University, Santa Maria, RS. 2010.

Couto, A. M. Modeling of basic density and chemical characterization of clones of *Eucalyptus urophylla* e *Eucalyptus grandis*. 2011. 71 p. Master in Science and Wood Technology. Lavras Federal University – UFLA) Lavras, Brazil.

Cunha, A.B. Analysis of Physical Properties, Mechanical and Energy Air Party and Trunk of Algaroba (*Prosopis Juliflora*). Monograph (Forest Engineer). 40p. 2012. Brazília University, Brazil.

Gonçalves, M. da P.M. Correlations of height and diameter growth stresses in *Eucalyptus citriodora* Hook and *Eucalyptus urophylla* s. t. Blake P. Monograph 24 2007 - Rural Federal University of Rio de Janeiro, RJ. Seropédica-2007.

Hansen, C. P. Application of the pilodyn in forest tree improvement. Humlebaek: Danida Forest Seed Centre, 2000. 15 p. (Series of Technical Notes, TN55).

Lima, J. T et al. Longitudinal residual strains due to growth stresses in eucalypts and their association with other properties. Árvore Paper, v.28, n.1, p.107-116, 2004.

Muneri, A. et al. Relationships between surface longitudinal growth strain and tree size, wood properties and timber distorcion of 4 years old plantation grown *Eucalyptus cloeziana*. In: IUFRO CONFERENCE – The Future of *Eucalyptus* for Wood Products, 2000, Lauceston, Australia, IUFRO. Proceedings… Launceston. 2000. p .292-300.

Pádua, F.A. Amostragem para Avaliação da Densidade Básica da Madeira de um Híbrido de *Eucalyptus grandis* W.Hill ex Maiden x *Eucalyptus urophylla* S. T. Blake. 99p., 2009. Tese (Doctor in Science and Wood Technology. Lavras Federal University – UFLA) Lavras, Brazil.

Palermo, G.P.M. Properties and Wood Technological Behavior of Eucalyptus grandis W. Hill ex-Maiden Aiming its Use in High Value Added Products. 2010. 249p. Doctor in Environmental and Forest Sciences, 2010. Federal Rural University of Rio de Janeiro, Seropédica – RJ, Brazil.

Trugilho, P. F. et al. Longitudinal residual strain (LRS) and tangential (TRS) in six clones of *Eucalyptus spp*. Cerne, Lavras, v. 12, no. 3, p. 279-286, July / SET button. 2006.

UFSC. Federal University of Santa Catarina, Brazil. Wood history. http://www.arq.ufsc.br/arq5661/Madeiras/historia.html. Date accessed: June 16, 2014.

MODULE EVALUATION OF DYNAMIC ELASTICITY, DETERMINED BY ULTRASOUND, IN THREE SPECIES OF TROPICAL WOOD

Joaquim Carlos Goncalez
Prof. University of Brasília - Department of Forest - Campus Darcy Ribeiro – Asa Norte -707919-900 Brasília DF, Brazil. goncalez@unb.br

Lucas Fonseca Goncalez
Student Production Engineering, University of Brasília - Campus Darcy Ribeiro – Asa Norte Brasília DF, Brazil. lucasgoncalez@gmail.com

Claudene Menezes Atayde Calderon
Profa. University Federal of Acre – Campus Floresta - Cruzeiro do Sul AC, Brazil. goncalez@unb.br

Newton Jordão Zerbini
Eng. Forest PhD., Superintendent of Environment, Eletronorte, Brasilia, DF, Brazil. newton.zerbini@bmte.com.br

ABSTRACT

The objective of this research was to determine the modulus of elasticity (MOE) and rupture module (MOR) of three Amazonian species: Axixá (*Sterculia pruriens*); Amarelinho or Peroba Mico (*Aspidosperma macrocarpom*) and Jatoba (*Hymenaea courbaril*) with the aid of ultrasound technique and testing in bending by checking their correlations. The samples of 2 x 2 x 30cm (width, height and length) at 12% moisture content were subjected to non-destructive testing (ultrasound equipment USLab, resolution 0.1 μs and frequency of 45 kHz) and destructive flexion static (equipment EMIC DL 30 kN), which was determined to MOEd dynamic, static MOE and MOR. The anatomical structure of the studied species influenced the displacement determined by ultrasound waves. The results for the static and dynamic tests do show close links between these two measures. The break modules showed good correlations with dynamic MOE for the three species.

Keywords: ultrasound, tropical wood, properties

INTRODUCTION

The mechanical characteristics are important technological basis for rational use of wood. Several methods can be used to evaluate the wood quality, among these are non-destructive techniques that has been gaining ground not only in scientific circles but also in industries.
The methods that use ultrasonoras waves are being employed primarily to determine the elastic constant illustrate the structural and biological modifications timber evaluate the quality of sawing. Methods employing the resonance frequency, ultrasonic velocity, acoustic emission, can assess the structural and functional integrity of various wood-based products. Through ultrasonoras waves it is possible to estimate the elastic constants of the wood.

The equations of Christoffel (Guitard, 1987) provide the relationship between the elastic constants and speeds of ultrasonoras waves.
Spycher et al. (2008) showed that the structure of wood and size of cells influence some property values calculated by means of evaluation by resonance.
OUIS (2002) analyzed the reasons for the frequency dependence of the static timber modulus of elasticity. It took into consideration several publications showing that the value of the MOE depends on how often will be evaluated. The main conclusion drawn theory, also supported by experiments, it is that the dynamic module is an increasing function of frequency, and the static value corresponds to the smallest possible value taken by the dynamic MOE.
Gonçalez et al. (2001) found in his research with Amazonian woods, values of dynamic modulus of elasticity (the ultrasound technique) higher than the static elasticity module (AFNOR and COPANT standards). Relations between dynamic and static modules are between 1.4 and 1.6. The author considered two hypotheses to help explain these differences: the highest value determined by ultrasound is attributed to the nature of the "request" because it is known that the static test because the body of evidence changes in their rheological properties, and the dynamic test does not cause changes in the specimen structure (KOLIAS, 1980; quoted by BUCUR, 1984); the static modulus of elasticity is driven by an isothermal phenomenon, whereas the dynamic modulus is primarily governed by an adiabatic law (HEARMON, BUCUR 1961 and 1984).
Research on the ultrasound technique is more common with planted forests woods. The application of this methodology with native species, especially the Amazon is rarer. Thus, this work aims to contribute with information about three Amazonian species characterized with the help of ultrasound technique in determining their elastic properties and modulus of rupture.
The objective of this research was to determine the modulus of elasticity (MOE) and rupture module (MOR) of three Amazonian species: Axixá (*Sterculia pruriens*); Amarelinho or Peroba Mico (*Aspidosperma macrocarpom*) and Jatoba (*Hymenaea courbaril*), with the aid of ultrasound technique and in bending test.

MATERIAL AND METHODS

We used 10 samples (2 x 2 x 30 cm) from three plates of each species: Axixá (*Sterculia pruriens*); Amarelinho/Peroba Mico (*Aspidosperma macrocarpom*) and Jatoba (*Hymenaea courbaril*), collected from sawmills in the Brazilian Amazon. These woods have been identified in the laboratory of anatomy to confirm the species. The study was conducted in Wood Technology Laboratory of the Department of Forestry at the University of Brasilia. The specimens were used for nondestructive evaluation (ultrasound) and destructive, static bending test to determine the static modulus of elasticity (MOE) and modulus of rupture (MOR), as COPANT (555) (1973). The samples were placed in a room (65% UR, 20°C), as required by COPANT norm, to obtain a final moisture content of 12%.
The non-destructive test using wave propagation, was carried out Agricef USLab equipment for timber, which can determine the elastic properties and thus to sort the quality of the material analyzed by the speed of wave propagation material. The device has output of 700V, resolution of 0.1μs and the longitudinal wave transducers and flat section operating at a frequency of 45kHz. For the determination of the dynamic elastic modulus (ultrasound) it was necessary to calculate the density of the test material. The density at 12% moisture was obtained by stereometric method.
To determine the dynamic modulus of elasticity (Moed) used the equation:

$$MOEd = D_{12\%} x Vel^2 \qquad \text{Eq (1)}$$

where: MOEd = Dynamic Elastic Modulus (MPa); $D_{12\%}$ = wood density at 12% moisture (kg/m3); Vel = velocity of ultrasonic wave (m/s).

The bending test was conducted on a universal testing machine EMIC DL model 30 kN. The following equations were used to determine their modulus of elasticity (MOE) and modulus of rupture (MOR):

$$MOE = \frac{PL^3}{48bdh^3} \quad \text{Eq (2)}$$

where: MOE = Modulus of elasticity in flexure (kg/cm2); P = load on the proportional limit (kg); d = Deformation corresponding to the load on the proportional limit (cm).

$$MOR = \frac{3PL}{2bh^2} \quad \text{Eq (3)}$$

where: MOR = static flexural modulus of rupture (kg/cm2, P = maximum load applied (kg), L = sample length (cm) b = the basis of the sample (cm) h = height of sample (cm .) Note: The results of the MOE and MOR were expressed in MPa.

Data were evaluated by descriptive statistics and Pearson correlation at 5% probability.

RESULTS AND DISCUSSION

Wood Axixá (*Sterculia pruriens*) is characterized anatomically by presenting large and rare pores, visible rays to the naked eye, straight grain and coarse texture (ZERBINI, 2008). The Amarelinho species (*Aspidosperma macrocarpom*) has small pores and large amounts barely visible rays, fine, grain straight to slightly crooked and fine texture (CALDERON, 2012). The wood Jatoba (*Hymenaea courbaril*) for visible pores with the naked eye, numerous and very visible rays, irregular grain, medium texture (D'AMBROS, 2011).
The density at 12% moisture content displayed by the woods of Axixá, Amarelinho and Jatoba was respectively 674 kg/m3, 683 kg/m3 and 860 kg/m3. The average speeds of ultrassonoras waves found for the woods were, respectively, 5296m/s, 4903m/s and 5196m/s.
Table 1 shows the average, minimum and maximum values of modules of static elasticity (MOE) and dynamic (MOEd) of the three species.

Table 1 - Values of modules of static elasticity (MOE) and dynamic (MOEd) of the three species.

	Wood					
	Axixá		**Amarelinho**		**Jatobá**	
	MOE static (MPa)	**MOEd dynamic (MPa)**	**MOE static (MPa)**	**MOEd dynamic (MPa)**	**MOE static (MPa)**	**MOEd dynamic (MPa)**
Average	14.138	20.163	8.914	16.438	14.079	24.645
Minimum	12.233	18.599	5.045	15.493	11.518	22.660
Maximum	15.314	21.248	12.109	18.684	16.171	28.086
Standard deviation	851	780	2260	905	212	1855

Wood Axixá showed a higher average velocity of the wave of ultrasound, while Amarelinho species had the lowest average speed. It seems that the anatomical structure of Axixá and Amarelinho showed influence on the displacement of the wave. The straight grain and the bit number of pores in wood Axixá favored the displacement wave form still more. Moreover, the large amount of pores and grain presence of winding on wooden Amarelinho ultrassonora hindered the continuity of the wave. The high density of the wood Jatoba, lots of fiber was favorable to the displacement wave in this species.

The dynamic elasticity module (MOEd) were greater for the three mixed studied in relation to the static elasticity module (MOE). In wood Axixá the average percentage was 43%, in Amarelinho 84% and 75% Jatoba. The superiority of Moed in relation to the MOE can be explained by the viscoelastic nature of wood. According Gonçalez (2001) the lower the excitation frequency of the material, the greater the proximity between the results from dynamic tests and their static counterparts. These results are according to those found by other researchers (BAAR et al., 2015, TELES, 2014; CALDERON, 2012; ZERBINI, 2008; BALLARIN et al 2005; GONÇALEZ et al., 2001).
It was determined also the break module (MOR) average in bending of the three species, 12% humidity. The wood Axixá, Amarelinho and Jatoba, presented, respectively, the MOR 120,85MPa, 80,91MPa and 154,87MPa. The timber Amarelinho had an average MOR value of below those found in the literature (LPF, 2015). Perhaps the small sample number, coupled with no control of local boards of where the samples were taken may have influenced the results.
Table 2 shows the correlation values between the MOEd (dynamic elasticity module), MOE (static elasticity module) and MOR (static rupture module) for the three studied woods.
Table 2 - Pearson correlation between MOEd, MOE and MOR for wood Axixá, Amarelinho and Jatoba.

Wood		**MOEd**	**MOE**	**MOR**
Axixá	**MOEd**	1		
	MOE	0,531*	1	
	MOR	0,593*	0,641*	1
Amarelinho	**MOEd**	1		
	MOE	0,293	1	
	MOR	0,523*	0,617*	1
Jatobá	**MOEd**	1		
	MOE	0,606*	1	
	MOR	0,681*	0,712*	1

* Significant correlation at 5% probability

It is observed in Table 2 that all the experimental correlations have good properties, significant at the 5% probability, except MOE x MOEd Amarelinho wood which was not significant. The wood Jatoba presented the best correlations, while the Amarelinho presented the lowest correlations. Gonçalez 2001, studying the wood mahogany tamarin (Amarelinho), found a correlation of 0.6800 between the MOE x MOEd variables. The literature presents other works (BAAR et al, 2015;. TELES, 2014; CALDERON 2012; ZERBINI, 2008; Gonçalez et al 2001) with tropical wood that follow the same trend of positive correlation between the properties studied, particularly among MOE x MOR and MOE x MOEd.
Interestingly, the MOEd x MOR showed a significant correlation for the three species. This correlation between these two variables is not always reported in the literature. According to Falk et al. (1990), high correlations have been observed between the elasticity modulus obtained from the ultrasound wave techniques and found in the static bending test; It is more difficult to bond to the modulus of rupture modulus obtained from the technique. As the defects present in the wood affect the slope of the fibers, the method is sensitive to this will have high potential for determining the resistance of the wood. Gonçalez 2001 states that the anatomical structure and the chemical constituents present in each species can influence differently the studied properties.

CONCLUSION

The anatomical structure of the studied species seems to have influenced the displacement determined by ultrasound waves. The high density of the wood Jatoba, presence of high amount of fiber, favored the displacement of the wave in this species, which showed the highest value of the dynamic elasticity modulus between the studied species.
The results for the static and dynamic tests do show close links between these two measures. Therefore, it can be deduced that the study of static and ultrasonic methods can be used to characterize the elastic timber.
Despite the absolute values of the elastic constants obtained in static and dynamic regime are different mainly due to the viscoelastic nature of wood, the ultrasound method is interesting due place quickly and simply the differences in the quality of the wood. The break modules showed good correlations with dynamic MOE for the three species. It is interesting to invest in more studies for these variables in an attempt to use them to estimate the MOR through the dynamic MOE.

REFERENCES

BAAR J; TIPPNER J.; RADEMACHER P. Prediction of mechanical properties - modulus of rupture and modulus of elasticity - of five tropical species by nondestructive methods. **Madera. Ciencia y Tecnologia**, 17(2): 239 - 252, 2015.

BALLARIN, A. W.; NOGUEIRA, M. Determinação do módulo de elasticidade da madeira juvenil e adulta de *Pinus taeda* por ultra-som. **Engenharia Agrícola**, v.25, n.1, p. 19-28, 2005.

BUCUR V. **Ondes ultrasonores dans le bois. Caractérisation mécanique et qualité de certaines essences de bois**. ISMCM, 1984.126p. (Thèse de docteur Ingenieur).

CALDERON, C.M.A. **O segmento moveleiro na região do Alto Juruá – AC: Perfil e uso de tecnologias alternativas para a caracterização das principais espécies madeireiras**. 2012. (Tese) Doutorado em Ciências Florestais, Universidade de Brasília, Brasília, DF, 158p. 2012.

GONÇALEZ, J.C.; VALLE, A.T.; COSTA, A.F. Estimativas das constantes elásticas da madeira por meio de ondas ultra-sonoras (ultra-som). **Cerne**, Lavras, v. 7, n. 2, p. 81-92, jul./dez. 2001.

GUITARD D. **Mécaniques du matériau bois et composites**. CEPADUES, 1987. 238 p.

HEARMON R. F. S. **An introduction to applied anisotropic elasticity**. Oxford University Press. 1961.

LPF, 2015 Laboratório de Produtos Florestais, Serviço Florestal Brasileiro. Ficha técnica de madeiras tropiciais. Consulta on line. www.florestal.gov.br

OUIS, D. On the frequency dependence of the modulus of elasticity of wood. **Wood Science and Technology**, v.36, n. 4, p. 335-346, aug. 2002

SPYCHER, M.; SCHWARZE, F.W.M.R.; STEIGER, R. Assessment of resonance wood quality by comparing its physical and histological properties. **Wood Science and Technology**, v.42, n. 4, p. 325-342, april. 2008.
ZERBINI, N.J. **Madeiras tropicais com potencial comercial na região do rio Xingu (Pará, Brasil):** propriedades tecnológicas e cadeia produtiva. (Tese) Doutorado em Engenharia Florestal, Brasília, Universidade de Brasília. 2008. 187p.

Methods for Nondestructive Investigation of Heritage Listed Timber Buildings to Support Restoration Projects and Preservation Initiatives

Janice Bernardo
Architecture and Urban Planning, Faculdades Ponta Grossa, Ponta Grossa, PR, Brasil, janicebs@gmail.com

Gabriel Ruiz
Architecture and Urban Planning College, University of São Paulo, São Paulo, SP, Brasil, ruiz_oliveira@yahoo.com.br

Jacqueline Collucci Stella
Departament of Civil Construction – DACOC, Federal Technological University of Paraná, Curitiba, PR, Brasil, jacque.coluccis@gmail.com

Abstract

This paper presents methods and instrumental standards for restoration and preservation studies of heritage listed timber buildings through nondestructive techniques. The analyzed constructions were built in the beginning of the twentieth century using Araucaria wood at the Murici Colony of polish immigrants in the county of São José dos Pinhais, south of Brazil, and are important examples of the building techniques development, the region's environment and the immigrant's cultural contribution. The nondestructive techniques were proven effective and worthwhile to ensure the maintenance and preservation of heritage listed buildings. Further studies concerning the evaluation of historical wood elements are also recommended, in order to set standards to support the structural analysis.

Keywords: Deterioration, historical architecture, Methodology Analysis (diagnostic);

Introduction

Since the settling of the Murici Colony, at the end of the XIX century in the county of São José dos Pinhais, south of Brazil, the *Araucaria angustifolia* wood has been utilized as the main source of power and profit, among other uses. It was colonized by polish immigrants whose first houses were built of corner jointed logs through a handmade process on which the trees were processed with manual saws. (Marochi 2006). The Polishes built their houses using timber and, along with the German and Italian immigrants, contributed to the development of woodworking knowledge and techniques at the south of Brazil (Kersten 2000).

One of the innovations brought by the immigrants was the construction of small water-powered sawmills. These shared-use mills took advantage of the local watercourses to improve the processing of grains and the wood (Bernardo 2013).

For more than a decade, the lumbering activity at the Paraná State was limited to these small water powered sawmills that only attended the local needs, but after 1885, with the State's railway network

increase, the lumbering industry developed significantly, so that in 1939, lumber represented Paraná's main export good (Simioni and Keinert Jr 1976; Imaguire Jr 1993).

There are still remaining *Araucaria angustifolia* architecture examples at the Murici Colony, like houses and storehouses, where it is possible to identify the use of wood joinery, demonstrating the assembling of the European traditional building technical knowledge with the use of local materials. At the Colony there are also many houses with vertical timber boards cladding and lambrequins decoration, which exemplify the logs processing mechanization and the standardizing of its dimensions (Figure 1).

Figure 1— (a) Storehouse built with Araucaria logs longitudinally jointed (b) House with vertical timber boards cladding and lambrequins decoration (Bernardo 2013)

Heritage conservation principles are opposed to the structural elements replacement, defending the preservation of the building's originality through the maintenance of its material and intangible values towards the future (Brandi 2004). La Rosa and Ventimiglia (2009) point out the building diagnosis importance, an indispensable interdisciplinary action for the restoration project's effectiveness.

This paper's objective is to present nondestructive methods to support heritage preservation studies, evaluating the effectiveness of the methods utilized for a survey at the Murici Colony historical buildings in order to promote the valorization of the region's cultural property.

The nondestructive methods utilized at this survey were: wood macroschopic analysis, conservation conditions evaluation, deteriorating insects identification and structural verification. This survey is part of the doctorate thesis "Murici Colony: diagnostic methods in historical heritage restoration and preservation projects" (Bernardo 2014).

Investigation methods

One of the primary stages on elaborating restoration projects is to identify the wood deterioration causes and agents. The diagnosis helps to comprehend the structures current safety state addressing the problems in order to guarantee the property's conservation and the safety of its users (Jurina 2009). Historical properties evaluation is recommended to be undertaken by a team of multidisciplinary specialist who will visually analyze and diagnose the building, preferably by using nondestructive techniques, according to information obtained by in situ inspections. (Tampone 1996; UNI EN 11119:2004; Augelli 2006; Valle et al 2006).

Melo Junior (2012) avers about the importance of identifying the utilized lumber species and presents positive results about the microscopic anatomy taxonomy identification system. "Restoration requires previous knowledge of the botanical species and the proprieties of the wood used on a specific site". The

macroscopic analyses is the most indicated one, as it does not require samples removal and can be easily done in situ without sophisticated equipments (UNI EN11118:2004). The Italian code UNI EN11118:2004 defines goals, procedures and criteria for the evaluation of the wood conservation conditions, its resistance and hardness, particularly for structural bearing timber used on cultural properties. The code requires that in situ analyses must be complemented by nondestructive tests to determine the elements resistance.

To identify the wood species, macroscopic analysis was used, visually inspecting the building structural elements. Based on the procedures defined at the code UNI 11118:20004, the roof structural elements were analyzed and photographed, with relevant aspects being noted down, just as color, texture, grain and growth rings. As Augeli (2006) recommends, the superficial pellicle was removed with the help of sandpaper or a chisel.

The wood deterioration agents classification, specially fungi and xylophagous insects, is considered an important requisite to evaluate the damages intensity, particularly on buildings subject to the Brazilian tropical weather. Biological deterioration caused by several orders of xylophagous insects is responsible significant losses to heritage, mainly those from the orders Coleoptera and Isoptera (Liotta 1998).

Badalini (et al 2009) consider the resistograph an efficacious equipment for depth survey of the materials consistence, specially to inspect internal areas that are difficult to be reached. Its minimum invasion approach enables it to be used on heritage structures experiments. The resistograph can be used to locate deteriorations and determine the residual bearing section of a damaged element, as long as identify variations on the wood density when compared to a standard reference (Boviar 2008).

The use of the resistograph to evaluate the timber conservation conditions and resistance was established according to the UNI 11119:2004 and follows the following procedures: wood moist check; elements geometry and morphology identification; indication, location and extension of the timber defects and deteriorations; definition of the critical sections. The xylophagous insects infestations were determined by indications on the timber elements, such as the presence of holes, galleries and residual material. The collected insects were classified at the Coleoptera Systematic and Bio Ecology Laboratory (LSBC), Zoology Department, Federal University of Paraná.

For the Murici Colony historical buildings structural verification it was important to determine the timber consistency and resistance variations, as long as defects and deteriorations on the structural elements may contribute to compromising situations. The structural bearing capacity was estimated determining the critical and effective section of the buildings timber elements as set at the UNI 11119:2004. Critical section corresponds to a representative transversal section where all the defects and damages influence the elements resistance. Effective section is the timber element transversal section obtained by the subtraction of the critical section area.

The structural elements transversal section dimensions were measured in situ, and the critical section of the deteriorated parts determined according to the information provided by the resistograph's diagrams.

Considering these definitions and the standards set by the Brazilian codes NBR 7190:1997 [timber structures calculations] and NBR 6123:1988 [wind loads] the structures were verified in two different geometrical situations, named "integral situation" and "modified situation" (Bernardo et al. 2012). Besides the wind loads, the verification also considered the dead loads of all the structural elements, including rafters, battens and wet roof tiles. These loadings were factored according to the Ultimate Limit State Design criteria defined at NBR 7190 for a medium duration loading combination.

At the "integral situation" it was considered the elements integral transversal section, while the modified situation" was calculated using the "effective section" dimensions. The "modified situation" bearing capacity

reduction is due to the lost of stiffness caused by the effective section's smaller dimensions, and is indicated by a reduction factor given by the acting axial stress on the integral section divided by the axial stress on the effective section. These two verifications obtained values were compared with the material's resistance to estimate the structural safety margin.

Results

The macroscopic analysis identified similar characteristics in the different buildings woods. On the timbers without paint, or on which the superficial pellicle was removed (Figure 2a) longitudinally parallel ground tissues were observed, with knots less than 1 meter frequent were visible in most of the structural elements (Figure 2b). The centennial houses' timber color has darkened, tending to a rosy tone. These macroscopic aspects support the buildings wood species to be classified as *Araucaria angustifolia.*

Figure 2— (a) Superficial pellicle removal, parallel wood grain; (b) knots at the roof battens

Figure 3 illustrates the location of some of the defects and deterioration agents that alter the material proprieties and affect the building conservation conditions. Physical deteriorations, mainly moist, are indicated in blue; Defects and mechanical deteriorations, like knots and fissures are indicated in red; Biological deterioration caused by fungi and insects are shown in green. The numbered arrows in the figure indicate the elements with critical sections selected for the resistograph's drills.

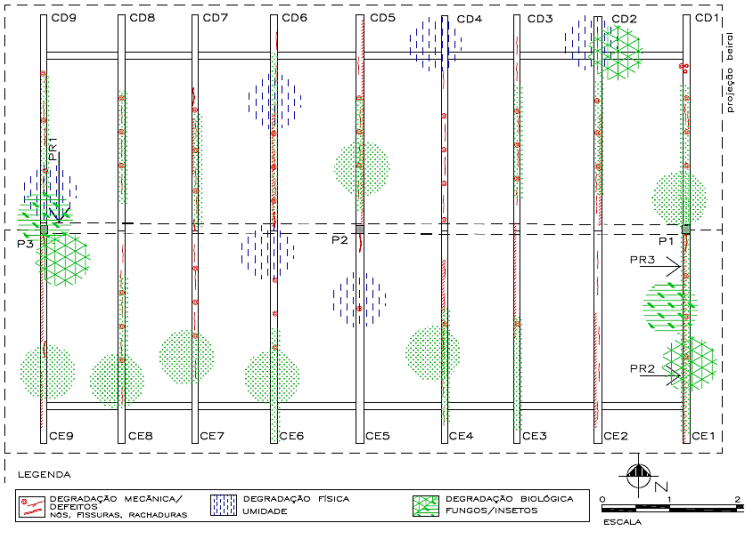

Figure 3— Defects and Deteriorations

Figure 4 examples of one of the resistograph's test results. The test no.PR2, drilled on the rafter CE1 basis demonstrates healthy timber conditions, except for the first and last centimeter. The graphic shows null resistance close to the element surface, in accordance with the insects deterioration identified during the visual inspection. The graphic also shows a relative resistance reduction from the centimeter 7 to 8.

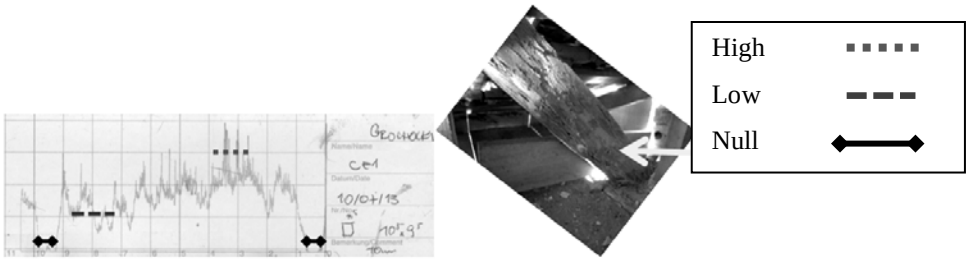

Figure 4— Resistograph test undertaken on a rafter basis indicating timber internal conditions

The visual analysis of the biological deterioration informed the presence of emerging holes with signs of active attack on the timber elements. The galleries and residuals characterize deterioration caused by infestations of insects from the orders Isoptera and Coleoptera, in some of which the material and section losses represent potential risks for the timber elements of the structures.

Figure 5— (a) Rafter deteriorated by Isoptera insects (b) Prop deteriorated by Coleoptera insects

Through data obtained with the resistograph's inspection it was possible to determine the critical areas of the elements, establishing the damaged area dimensions of the structural elements. In the case of the rafter CE1 (Figure 6), 1,5cm of wood on the left side and 1,0 cm on the right side were deteriorated and subtracted to define the effective section. Therefore, while the integral section had 10,5 x 9,5 cm dimensions, the effective section had only 8,5 x8,5cm.

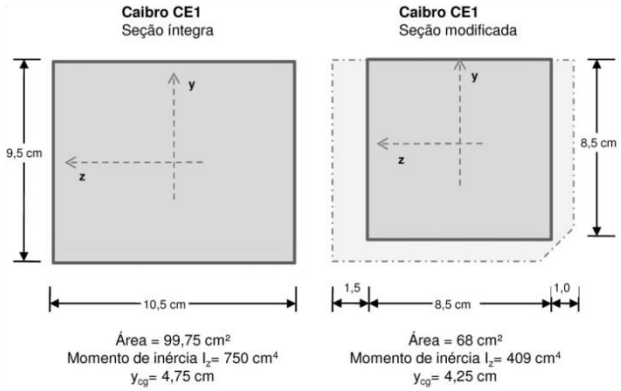

Figure 6— Rafter CE1 transversal sections: integral and effective, with the reduced area

Verifying the axial stress loads for the integral and modified situations with the timber bearing capacity it is possible to estimate the structural safety margin for each geometrical assumption. Most of the evaluated structural elements demonstrated a safety margin superior to 30%. For some elements, though, like the rafter CE1 (Table 1), the modified situation produced by the deterioration has reduced the safety margin to -6,9%, which is coherent with the visual analysis and the resistograph's instrumental evaluation.

Table 1 – Grochocki House – Comparisons between bearing capacity and axial stress.

Grochocki House	Araucaria wood Axial Bearing Capacity (MPa)	Axial Stress Load (MPa)		Comparison Bearing Capacity and Axial Load – Structural Safety Margin (%)	
		Integral	**Modified**	**Integral**	**Modified**
CE1	14	9,34	14,97	33,2	-6,9

By using this calculation method it was possible to determine the bearing capacity of the structural elements of the analyzed buildings, estimating their structural safety margin. Through these analysis the buildings structural stability was verified, and specific situations that required consolidation were identified and addressed, avoiding unnecessary replacements of the historical structure elements.

Conclusions

Through visual analyzes it was possible to identify the wood, its deterioration agents and to evaluate its conservation conditions. The macroscopic investigation proved to be a valid instrument to identify the *Araucaria angustifolia* on historical buildings, thought the woods must have reasonable conservation and visibility conditions.

The resistograph's instrumental analyzes effectively provided the qualitative register of internal modifications of the building elements in order to determine their critical sections. It is necessary to associate other analyses to obtain more accurate quantitative results about the damaged material loading capacity and to reduce the drilling quantity, guarantying minimal intrusive actions.

The calculations by comparing integral and modified situations has also been proved valid as it was possible to estimate structural safety margins and predict the structure's more risky areas, defining conservation priorities. It is recommended to probe the material's appraisal to define more precise resistance standards to support structural analyzes. Nondestructive investigation techniques have been proven efficient and effective for the diagnosis, maintenance and preservation of built heritage.

It is important to undertake correction treatments to eliminate and prevent the physical and biological deterioration favorable conditions, as long as a restoration project to consolidate the damaged building parts. Periodic inspections and frequent maintenance are recommended to conserve the heritage buildings.

Acknowledgments

To CNPq for the financial support. To the Departamento de Ciências Florestais (LCF) from the Escola Superior de Agricultura Luiz Queiroz (ESALQ-USP) for lending the Resistograph.

References

Associação brasileira de normas técnicas. 1997. NBR 7190: Projeto de Estruturas de Madeira, Rio de Janeiro.

Associação brasileira de normas técnicas.1988. NBR 6123: Forças devidas ao vento em edificações, Rio de Janeiro.

Augelli, F.2006.La diagnosi delle opere e delle strutture lignee. Le ispezioni.In: Xilema. Milano: Il prato. 165 p.

Badalini, J; Barbo, S; Del Curto, D. 2009. La prova resistografica per l'analisi e La diagnostica di strutture lignee in opera: letteratura, normativa, applicazioni sul costruito storico. In: SCIENZA E BENI CULTURALI,XXV.Bressanone – Itália. Atti...Venezia: Arcádia Ricerche S.r.l. p.400-413.

Bernardo, J.; Penner, E; Stella, J.C.; Augelli, A ; Rocha, M.P. 2012. Análise estrutural da cobertura de madeira de uma edificação histórica. In: XIII EBRAMEM, UFES/Vitória.

Bernardo, J. 2013. Madeira e técnica: as edificações históricas da colônia Murici. Curitiba: (Ed. Autora).168 p.

Bernardo, J. 2014. Colônia Murici: métodos para diagnóstico em projetos de restauração e preservação do patrimônio histórico. Curitiba: Universidade Federal do Paraná. 168 p. D. Thesis.

Boviar. 2008. Strumentazione per la diagnostica e Il monitoraggio. [CD-ROM]. Milão.

Brandi, C. 2004 Teoria da restauração. Cotia, SP: Ateliê Editorial. 261 p.

Imaguire Jr.,K.1993. A Casa de Araucária: Arquitetura Paranista.Curitiba: UFPR. 134 p.

Jurina, L. 2003. Strutture in legno: soluzioni leggere per il consolidamento. In: Recupero e conservazione, Milão-Itália, n°50, p. 65-68. http://www.jurina.it/pubblicazioni03c4.html?id_pg=1 [Date accessed 12/08/2009].

Kersten, M.S.A. 2000. Os rituais de tombamento e a escrita da história: bens tombados no Paraná entre 1938-1990. Curitiba: UFPR. 300 p.

La Rosa, N.; Ventimiglia, G. M. 2009. I soffitti lignei dipinti e le strutture di copertura nella architettura religiosa della Sicilia barocca: Conoscenza e diagnosi per il progetto di restauro. In: SCIENZA e BENI CULTURALI XXV. Bressanone – Itália. Atti...Venezia: Arcadia Ricerche S.r.l.p. 317-334.

Liotta, G. 1998. Gli insetti e i danni del legno: Problemi di restauro. 3. ed. Firenze: Nardini.150 p.

Marochi, M.A. 2006. Imigrantes 1870 – 1950: Os europeus em São José dos Pinhais. Curitiba, Travessa dos Editores.323p.

Melo Jr., J.C.F. 2012. Anatomia de madeiras históricas: um olhar biológico sobre o patrimônio cultural. Joinville: Univille.132 p.

Norma italiana. 2004. UNI 11119, Beni culturali Manufatti lignei Strutture portanti degli edifici – Ispezione in sito per la diagnosi degli elementi in opera.

Norma italiana. 2004.UNI EN 11118, Beni culturali – Manufatti lignei - Identificazione delle specie legnose.

Simioni, A.; Keinert JR.,S. 1976. Evolução da exploração Madeireira no Brasil. In: Revista Floresta, Curitiba, v. 7, n.2, p. 41-44.

Tampone, G.1996. Il restauro delle strutture di legno. Milano: HOEPLI. 401 p.

Valle, A; Brittes, R. D.; Lourenço, P.B. 2006. Uso da perfuração controlada na avaliação de deterioração da madeira em edificações antigas. In: X EBRAMEM, São Paulo.

Study on Termites Detection using Two-frequency CW Radar System

Dan Zhang[#1], Yunfei Liu[1], Ling Jiang[1], Qiong Zhang[1] and Takayuki Inaba[2]

[#1] College of Information Science and Technology, Nanjing Forestry University, Nanjing 210037, China
[2]Graduate school of Informatics and Engineering, The University of Electro-Communications
Chofu-Shi, 182-8585 Japan

[#1] Corresponding author: +86-25-85427693, zhangdan@njfu.edu.cn

***Abstract* — In this paper, we introduce two-frequency CW system principle using software radar device for the termite detection, and propose the detection method to detect the Doppler shift of the received signal from the activities of termites. We have verified detection experiment of termites in the cavity of the timber that mimics the damage caused by termites using this method.**

***Index Terms* — two-frequency CW radar, termite detection, Doppler frequency.**

I. INTRODUCTION

As we know, the termite damage of the wooden structure is a serious problem in modern society. That due to erosion in favor of the dark humid, it has become an extensive damage when it discovers visually often termites.

As a method for detecting termites, AE based on ultrasonic measurement (Acoustic Emission) method has been proposed [1]. However, AE method is necessary to make contact with the wood of the sensor. As a detection method for non-contact detection by X-ray can be considered, there is a problem apparatus and systems become expensive, it is necessary radiation management.

Recently, researchers consider termite detection method using electromagnetic wave [2]-[4]. The termite detection performed by detecting the Doppler shift of the received signal to an electromagnetic wave irradiated wood, resulting from the activity of termites within the timber. According to the detection method, it is believed that it can be performed efficiently in non-contact sensing termites. Furthermore, it is considered to be a possible at low cost and detection is performed easily without requiring special qualifications during operation.

The CW radar has the advantages of low power consumption and simple radio architecture. Moreover, CW radar can also cancel out clutter noise by proper adjustment of the radio front-end architecture. The two-frequency CW system transmits signals with two almost same frequencies using time division method, transmission and reception system may be made simply. In the two-frequency CW system, the occupied frequency bandwidth is narrow, it is good in interference. Other more, the two-frequency CW system has excellent suitability for detection close targets, according to the distance accuracy which is dependent on the S/N instead of frequency bandwidth.

In this paper, we propose the detection method to detect the Doppler shift of the received signal from the activities of termites and verify detection experiment of termites in the cavity of the timber that mimics the damage caused by termites using two-frequency CW system method. First, we will explain the termite detection principle by dual-frequency CW system. Then, we will go to termite detection experiments using a software radar device.

II. METHOD

As shown in Fig.1, the two-frequency method is a method that can detect the distance and speed of the target in a very narrow frequency band. The CW (Continuous Wave) which transmission frequency f_1 and f_2 separated slightly from f_1 is sent in interval of time T, respectively.

On the receiving system, in each time section, transmission frequency f_1 and f_2 is mixed with each local signal. After eliminating the sum signal with LPF (Low Pass Filter), the beat signals can be obtained as following.

$$B_{f1}(t) = \exp\left\{ j\left[2\pi f_d \cdot t - \frac{4\pi f_1}{c} R \right] \right\}$$

$$B_{f2}(t) = \exp\left\{ j\left[2\pi f_d \cdot t - \frac{4\pi f_2}{c} R \right] \right\}$$

Where, f_d is the Doppler frequency $f_d=2v/\lambda$, R is target distance, c is the speed of light, v is the target speed, and λ is the wavelength of the transmitted wave. Since the difference of transmission frequency f_1 and f_2 is little, the received signals from the same target are observed with the same Doppler frequency f_d in the each time interval.

Transmission frequency	24.15GHz
Frequency difference of f_1 and f_2	65MHz
Sampling frequency	20kHz
Frequency switching time	50μs
Measurement time	100sec
Transmission power	10mW

The each beat signal in time interval is transformed to frequency domain by Fourier transform. We easily know the Doppler frequency and target speed, then the target distance can be obtained by the phase of the Doppler frequency as fowling:

$$R = \frac{c \cdot \Delta\phi}{4\pi(f_2 - f_1)} \quad (1)$$

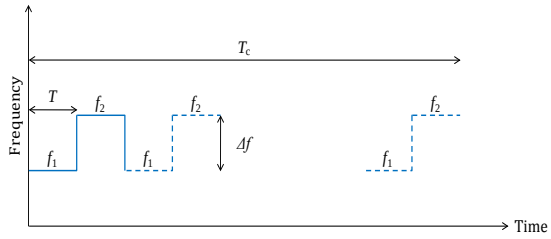

Fig.1. Transmission sequence diagram of a two-frequency CW system

III. EXPERIMENT

In order to simulate the environment that the wood's cavity is eaten by termites, the termites are sealed in the timber hole. Termites' length is about 6mm. We can detect the reflected wave which is Doppler shifted from termites. The transmission frequency is 24.15GHz, If the moving speed of termites is assumed to 1~10mm/sec, Doppler frequency is 0.16~0.8Hz and the power may increase in the frequency spectrum. We think the difference of the phase becomes substantially constant regardless of the frequency when the of the power increase. This is because the distance between the antennas and each termite in termites group can be seen as almost the same values. Therefore, the value of the phase difference dispersion may be the index for determining termites in the power increasing frequencies range. If the value of the dispersion is small, termites are present.

The radar parameters of the system used here is shown in Table 1. It is possible to detect the presence of termites by detecting the increase in the power. The distance is selected to 10cm, 20cm and 50 cm between the antenna and wood, respectively as shown in Fig.2. The spectral analysis time is selected to 100sec, so the frequency resolution is 0.01Hz.

Table 1 Two-frequency CW radar Parameters

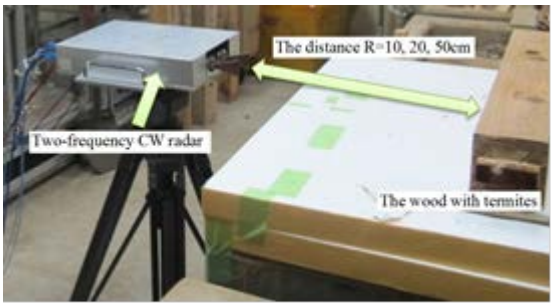

We show the power and the phase difference in the frequency spectrum for the environment noise and each case from Fig. 3 to Fig.6. Compared to the environment noise, the largest power increase is observed about 20dB and the phase difference variation is small for R=50cm at frequency band -0.5Hz ~0.5Hz. It is considered that this is due to the reflected wave from the termites which are active within the wood.

IV. CONCLUSION

The termites are detected in the experimental timber using a two-frequency CW system radar device that conformed to specified low power radio station standard at 24GHz in this paper. We have shown the sufficient signal strength to detect termites at the distance between the timber and the antenna even for 50cm. Further, it is also shown that the phase information can been seen as an important index for determining the presence of termites. We will investigate termite detection algorithms high accuracy using the phase information in the future.

REFERENCES

[1] Y. Fujii, "non-destructive detection of termite feeding damage by AE monitoring," material, Vol.51, No.5, pp.594-595, 2002.

[2] K. Shigeno, and T. Inaba, "The detection of termites using electromagnetic radiation," *IEICE Society Conference* 2011 B-2-18, Sep. 2011 (in Japanese).
[3] A. Z. Tirkel, J. C. S. Lai, T. A. Evans, and G. A. Rankin, "Effects of Millimeter Wave Exposure on Termite Behavior," *Progress In Electromagnetics Research Symposium Proceedings*, pp.1581-1585, Marrakesh,Mar.2011.
[4] Y. Fujii, Y. Fujiwara, Y. Yanase, S. Okumura, et al., "Nondestructive detection of termites using a millimeter-wave imaging tech- nique," *Forest Products Journal*, Vol. 57, No. 10, 75-79, 2007.

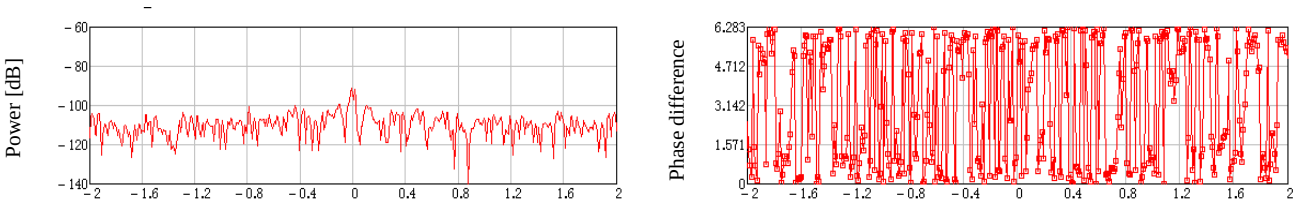

Fig.3. Measurement results of environment noise. (a) Power (b) Phase difference

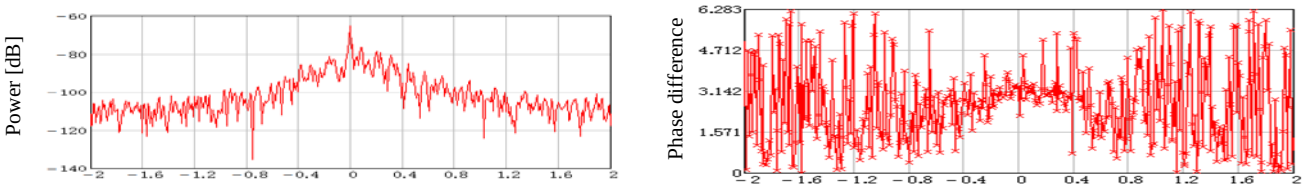

Fig.4. Measurement results of the distance R=10cm. (a) Power (b) Phase difference

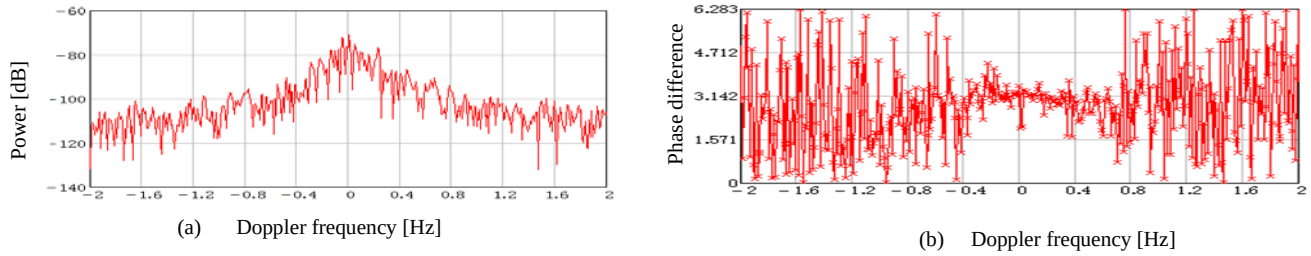

Fig.5. Measurement results of the distance R=20cm. (a) Power (b) Phase difference

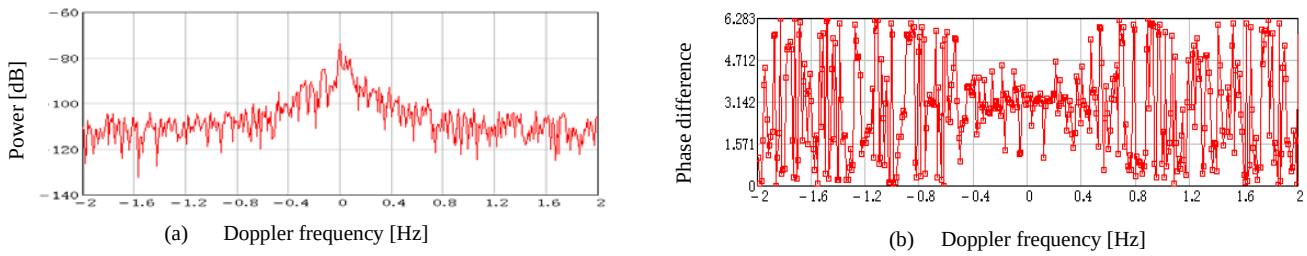

Fig.6. Measurement results of the distance R=50cm. (a) Power (b) Phase difference

Experimental measurement of acoustic guided wave propagation in logs

Mathew Legg
Physics Department, University of Auckland, Auckland, New Zealand, m.legg@auckland.ac.nz

Stuart Bradley
Physics Department, University of Auckland, Auckland, New Zealand, s.bradley@auckland.ac.nz

Abstract

The stiffness of wood can be estimated using acoustic velocity. For standing trees, velocity measurements are generally obtained by driving two pikes into the tree stem, hitting one with a hammer, and measuring the time for the signal to first reach the second transducer. This time of flight method only uses the start time of the signal. This paper investigates if additional information that can be obtained from the acoustic signal could be used to measure wood properties. Wave propagation was investigated using shear transducers. These transducers were initially attached to spikes. It was found that the angle and orientation of the spikes significantly affected the received signal. Measurements were also made with transducers attached directly to the logs. The alignment of the transducers allowed different guided wave modes, such as longitudinal and torsional wave modes, to be excited and measured.

Keywords: tree, stiffness, time of flight, wave modes, guided waves

Introduction

The stiffness of standing trees can be estimated using Time of Flight (TOF) techniques (Wang et al., 2001). Two probes are usually inserted into the tree stem, one probe is hit with a hammer and the first arrival T of the signal at the second probe is obtained. The acoustic velocity is calculated using

$$c_{TOF} = \frac{z}{T}, \tag{1}$$

where z is the separation of the probes, see Figure 1. The dynamic modulus of elasticity is calculated using

$$E = \rho c^2, \tag{2}$$

where ρ is the density. This technique only uses the first arrival time and the rest of the signal is ignored.

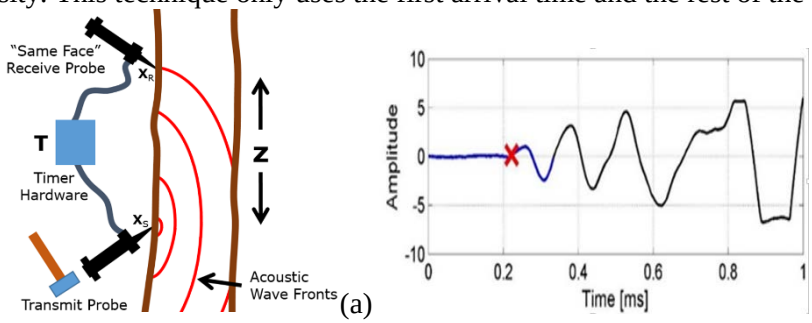

Figure 1: Diagram (a) showing the method generally used to measure the stiffness of standing trees. A stress wave is excited at one probe and the velocity is calculated using the first arrival time of a signal at the receiver second probe. Plot (b) shows an example of this first arrival time (red cross).

The acoustic velocity of logs is generally measured using an alternative technique referred to as acoustic resonance (Harris, Petherick and Andrews, 2002). The end of the log is hit with a hammer, the resulting

acoustic signal is measured, and the frequency f_n of n^{th} harmonic peaks in the spectrum is used to calculate the resonance velocity using

$$c_{RES} = \frac{2Lf_n}{n}, \tag{3}$$

where L is the length of the log. TOF techniques provide stiffness measurements that are higher than those obtained on felled logs using acoustic resonance (Harris, Petherick and Andrews, 2002) or bending tests. It has been suggested that the TOF technique measures a "dilation" or "bulk" wave speed due to the short propagation distance between probes. In contrast, the resonance technique may measure a "rod speed" given by Equation (2) due to the fact that the acoustic velocity has propagated many lengths of the log (Andrews, 2002; Wang, 2013). This suggests that the acoustic signal used for the resonance technique is a guided wave. There have also been references to the velocity of ultrasonic waves in timber being dependant on the dimension of the sample or the transmit frequency (Marra, Pellerin and Galligan, 1966; de Oliveira, Miller, Candian and Sales, 2006; Bartholomeu, Goncalves and Bucur, 2003; Dikrallah et al., 2010; Baltruvsaitis, Ukvalbergiene, Pranckevivciene and Kaunas, 2010; Bucur, 2006). This phenomina may also be explained by guided waves.

An acoustic signal initially propagates in a rod-like structure as bulk waves. However, with sufficient propagation distance, it eventually becomes guided waves. Three types of vibrations (wave modes) may be expected to be excited; longitudinal, torsional, and flexural, see Figure 2. These wave modes travel at different velocities and can be dispersive. This means that different frequency components in the signal propagate at different velocities resulting in the signals that spreading out spatially with propagation distance. The used of Ultrasonic Guided Waves (UGW) is well developed as a non-destructive testing technique for structures such as metal pipes, rods, or plates (Lowe, Alleyne and Cawley, 1998). However, only a few studies have investigated guided waves in timber (Dahmen, Ketata, Ben Ghozlen and Hosten, 2010) or logs (Martin and Berger, 2003; Yang, Wang and Li, 2011; Martin and Berger, 2001; Subhani, Li and Samali, 2013). It is possible that techniques developed for inspection of structures, such as pipes, may be able to be used to improve the measurement of the properties of wood.

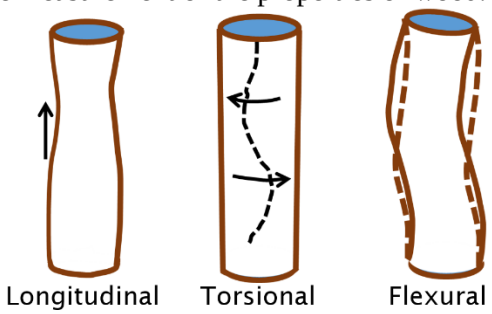

Figure 2: Diagram showing the different types of vibrations that could be expected to occur on a rod like structure.

This paper investigates if there is more information in acoustic TOF measurement signals that could potentially be used for improved measurement of the properties of wood. Experimental results are presented that look at different methods of exciting and measuring the acoustic signals in wood. Results indicate that some degree of control can be achieved with the signals that are excited and measured.

Procedure

TOF excitation and reception are generally made using spikes inserted into a tree stem. In contrast, UGW inspection techniques commonly use transducers attached directly to the surface of the structure, such as a pipe. This is done to control the wave modes that are excited and received. Measurements were, therefore, made with PZT shear transducers attached to spikes and then to the surface of the log. Shear transducers have their direction of vibration parallel to the surface of the transducer head, see Figure 3. Two

transducers were used, one for transmission and one for reception (pitch-catch configuration). The transducers were made by Plant Integrity[1].

The excitation signal used was five cycles of a sine wave, which was windowed using a Hann window. This is commonly done in UGW inspection to reduce the bandwidth and hence potential for dispersion of the signal. The signal was generated in Matlab and converted to an analogue signal using a Data Translation DT9836 with a sampling rate of 225 kHz and resolution of 16 bits. This was amplified using a custom built power amplifier, which was capable of outputting arbitrary waveforms with an output peak-to-peak voltage of up to 400 V. This signal was used to drive the transmit shear mode transducer. The received signal was measured on a second shear transducer. This signal was amplified using a custom built preamplifier. This was then sampled using an analogue input channel of the DT9836 board with a sampling rate of 225 Hz and a resolution of 16 bits. These signals were saved to file and processed using MatLab. It was found that an attenuated version of the transmit signal appeared on the received signals as channel cross talk, but this was removed by subtracting the signal with no transducer on it from the signal from the receiver transducer.

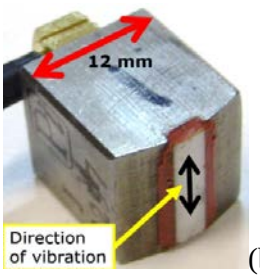

(b)
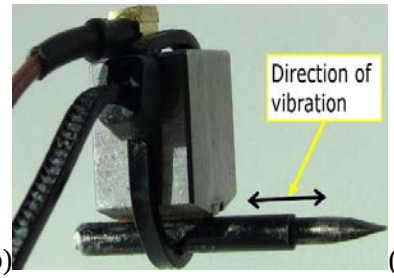

(b)

Figure 3: Photo (a) shows one of the shear PZT transducers used for transmission and receiption. These transducers were either attached directly to the surface of the log or attached to spikes which were driven into the log.

Measurements were made on two *Pinus radiata* logs referred to as “Log 1” and “Log 2”. The thin and thick end diameters of “Log 1” were 290 and 340 mm, while those of “Log 2” were 220 and 275 mm.

Results

Short (300 mm) Propagation Distance Experiments

Measurements were initially made on “Log 2” using a transducer spacing of 300 mm. These measurement were performed to see what wave shapes were observed with transducers attached to spikes and directly to the surface of the log. The transmit signal frequency for these measurements was 25 kHz.

Measurements were initially made with the transducers attached to spikes (small screw drivers) pushed into the log. It was observed that the received signal varied significantly depending on the angle of the spike and the orientation of the transducer on the spike. Figure 4 shows two examples of the received signal for two angles of the transmit spike.

[1] http://www.plantintegrity.com/

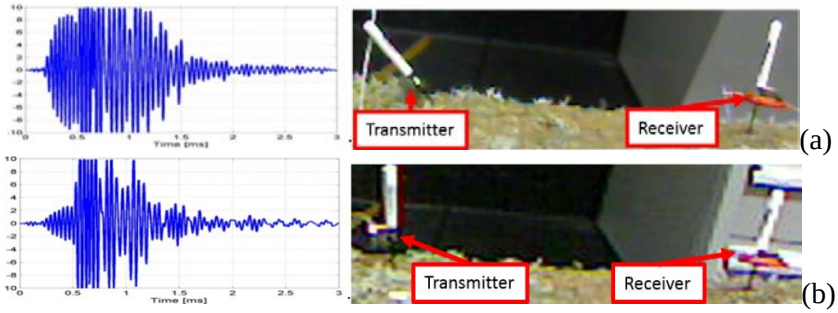

Figure 4: Example plots showing the variation in received signal when the angle transmit transducer spike was varied from (a) 42 to (b) 82 degrees relative to vertical, while the angle of the receiver transducer was held constant.

Measurements were then made with the transmitter transducer attached to the surface of the log (onto the bark) using a ratchet tie. This transducer was aligned to generate vibration in the longitudinal direction. The receiver was attached to a spike. Again, it was found that the angle and orientation of the receiver spike had a significant effect on the revived signal shape, see Figure 5.

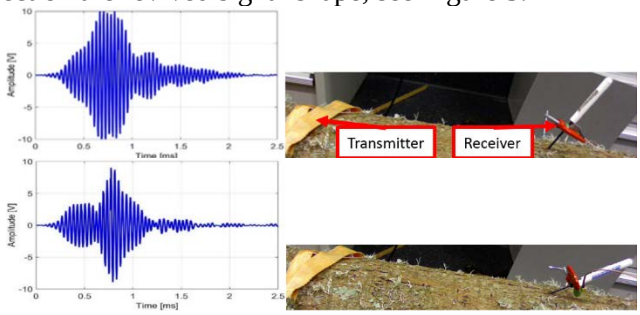

Figure 5: Example plots showing the variation in received signal when the angle the receiver transducer spike was varied from (a) 70° to (b) 38°, while the angle of the receiver transducer was held constant.

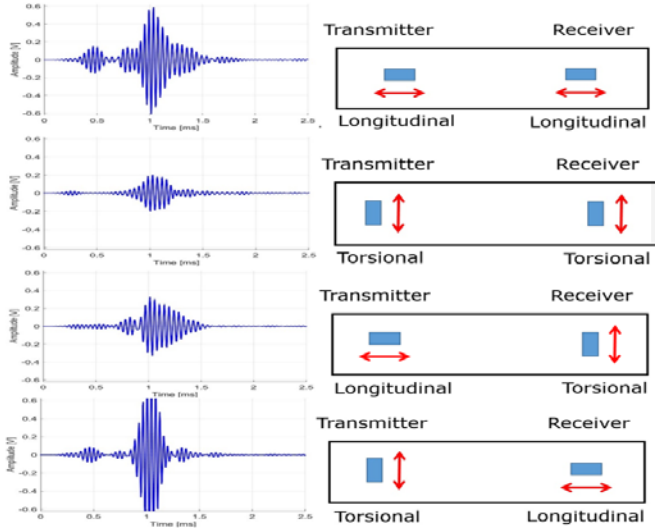

Figure 6: Plots of the received signals and the relative orientation of the transducers when pushed directly to the surface of the log (without the use of spikes). The diagrams to the right show the orientations of the transducers.

Experiments were then made with both transmit and receive transducers attached directly to the surface of the log. The alignment of both transducers was varied. Significant variation of the received signal was observed with each orientation of the transducers, see Figure 6. The separation of individual shapes wasmore pronounced with transducers attached directly to the surface of the log, when better control of the transmitted and received vibrations was able to be achieved.

Longer (2.5 m) Propagation Distance Experiments

Experiments were conducted on "Log 1" with transmit and receive transducers at opposite ends of the log. The bark was thicker for this log and was found to attenuate the received signal. Therefore, the bark was removed around the transducer locations, and transducers were placed directly on the bare log surface. Acoustic resonance measurements had been made for this log. Resonance peaks were observed at frequencies of 566 and 1067 Hz. This corresponded to first and second harmonic resonance velocities of 2830 and 2670 m/s, or an average speed of 2750 m/s. TOF measurements made on the same face of the log had obtained velocities of 3135 m/s for propagation distances of 0.6 to 1.6 meters and using a square wave power amplifier.

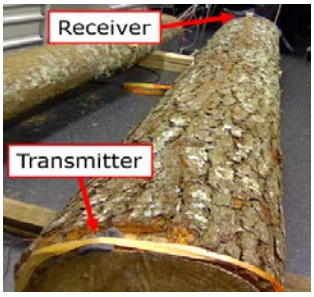

Figure 7: Photo of the larger of the two logs with transmit and recieve transducers attached at opposite ends of the log. The bark was removed around where the transducers were attached.

Transmit and Receive Transducers Attached to Log Surface

Measurements were made with the transducers attached directly to the surface of the log for a range of transmit frequencies. The longer propagation distance resulted in higher attenuation. It was found that frequencies above 16 kHz where highly attenuated. Figure 8 shows the received signal for two transmit frequencies. In these plots, the transmit signal channel cross talk has not been removed. Red crosses have been added where peaks in the transmit signal occurred. Black crosses have been plotted where these peaks would be expected to occur in the received signal, assuming that the acoustic velocity was the mean of the first and second harmonic velocity of 2750 m/s (assuming no dispersion). From these plots, it appears that the longitudinal wave velocity is close to that of the mean of the resonance velocities. This was not expected from previous TOF measurements with probes separated by about a meter and using a square wave power amplifier.

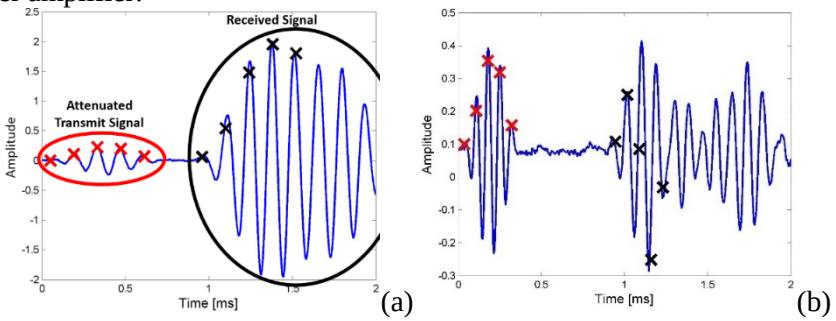

Figure 8: Example plots of the received signal for the transmit and receive transducers attached directly to the surface of the log aligned in the longitudinal direction. The separation of the transducers was 2.5 meters. The transmit signal frequencies were (a) 7 and (b) 14 kHz.

Measurements were them made with the transmit and receive transducers attached to the log in either the longitudinal or the torsional direction. The resulting signals for a transmit frequency of 7 kHz can be seen in Figure 9. It can be seen that the torsional alignment of the transducers resulted in significantly different

signals compared to longitudinal alignment. The arrival times for the torsional alignment was about three time later than for longitudinal alignment.

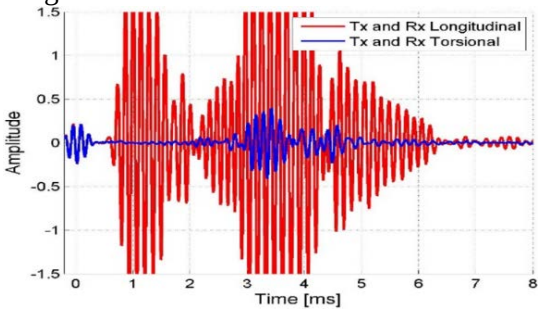

Figure 9: Example plot showing the received signal for the transmit and receive transducers pushed against the surface of the log and both aligned in either the (red) longitudinal or (blue) torsional directions. The transmit signal frequency was 7 kHz. The time axis for this plot has been shifted so that the centre of the transmit signal was at the origin.

Figure 10 shows a time-frequency plot for longitudinal and torsional alignment of the transducers. The plots show the absolute value of a matrix, where each row is the receive signal for a different transmit frequency. The transmit signal frequencies ranged from 3 to 16 kHz in 100 Hz increments The received signal in each matrix row has been shifted in the time axis so that the time corresponding to the centre of the transmit signal was at the origin in the time axis. This was to allow for the increased duration of the transmit signal with reduced frequency. Again it can be seen that significant differences in arrival times can be seen for the longitudinal and torsional alignment of the transducers.

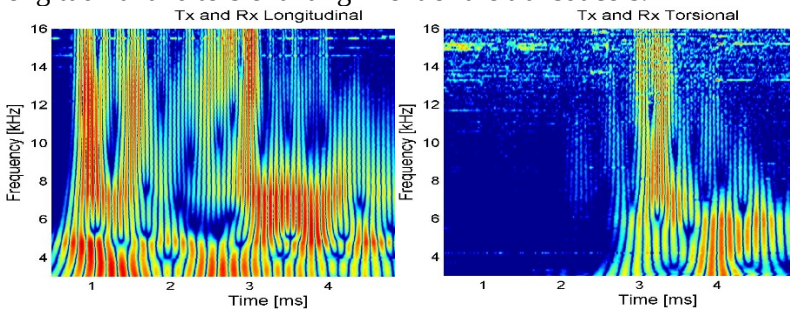

Figure 10: Time frequency plots for the transmit and receive transducers pushed against the log surface and aligned in either the (a) longitudinal or (b) torsional directions.

Transmit and Receive Transducers Attached to Spikes

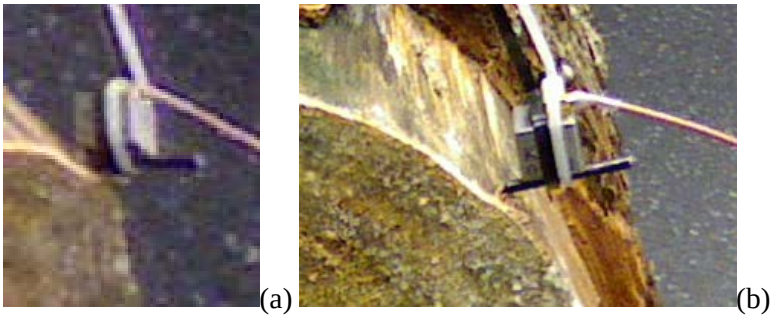

Figure 11: Photos showing transducers attached to spikes aligned to excite vibration in (a) the longitudinal or (b) the torsional directions.

The above process was repeated with transmit and receive transducers attached to spikes at each end of the log, see Figure 11. The received signals for 7 kHz can be seen in Figure 12. Similar results to those in Figure 9 can be seen, where the transducers were attached directly to the log. A time- frequency analysis

of the received signals can be seen in Figure 13. Again, somewhat similar results to Figure 10 can be seen.

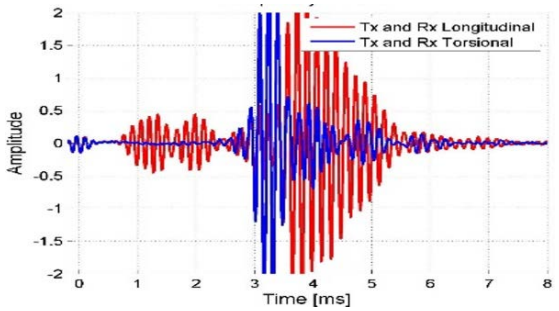

Figure 12: Example plot showing the received signal for the transmit and receive transducers atteched to spikes in the log and both aligned either in the (red) longitudinal or (blue) torsional directions. The transmit signal frequency was 7 kHz. The time axis has been shifted so that the centre of the transmit signal was at the origin.

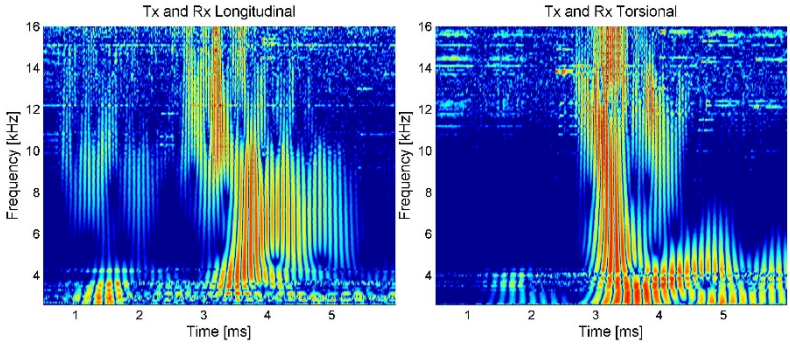

Figure 13: Time frequency plots for the transmit and receive transducers attached to spikes pushed into the log aligned in either the (a) longitudinal or (b) torsional directions.

Conclusions

This work has looked at different ways of exciting and receiving signals on logs using shear transducers. Considerable differences in the received signals were observed if the transducers were attached to spikes or directly to the log surface and depending on the alignment of the transducers. For shear transducers on the log aligned in the longitudinal direction and separated by 2.5 meters, the acoustic velocity appeared to be similar to the mean of the first and second harmonic resonance velocity. This was not expected, based on reports in the literature and also from TOF measurements made over a shorter propagation distance. More work is needed comparing these results with those obtained using an impact in a spike for different propagation distances. Torsional alignment of the transducers resulted in arrival times that were about three time later than that for longitudinal alignment. Additional work is needed to see if this torsional velocity can be used to for measuring wood properties of interest. More work on guided wave modes in tree stems may provide improved measurements of wood properties.

Acknowledgments

This work was performed as part of the Growing Confidence in Forestry Future project (http://gcff.nz/). Funding was provided through Scion, the New Zealand Ministry of Business, Innovation and Employment and the New Zealand Forest Growers Levy Trust. Authors would like to acknowledge John Moore and Grant Emms of Scion for their help and guidance.

References

Andrews, M., 2002. Which acoustic speed. In: *Proceedings of the 13th International Symposium on Nondestructive Testing of Wood*. pp.159–165.

Baltruvsaitis, A., Ukvalbergiene, K., Pranckevivciene, V. and Kaunas, L., 2010. Nondestructive evaluation of viscous-elastic changes in ammonia-modified wood using ultrasonic and vibrant techniques. *Wood Research*, 55(4), pp.39–50.

Bartholomeu, A., Goncalves, R. and Bucur, V., 2003. Dispersion of ultrasonic waves in eucalyptus lumber as a function of the geometry of boards. *Scientia Forestalis*, 1(63), pp.235–240.

Bucur, V., 2006. *Acoustics of wood*. 2$_nd$ ed. New York: Springer.

Dahmen, S., Ketata, H., Ben Ghozlen, M.H. and Hosten, B., 2010. Elastic constants measurement of anisotropic Olivier wood plates using air-coupled transducers generated Lamb wave and ultrasonic bulk wave. *Ultrasonics*, 50(4), pp.502–507.

Dikrallah, A., Kabouchi, B., Hakam, A., Brancheriau, L., Bailleres, H., Famiri, A. and Ziani, M., 2010. Study of acoustic wave propagation through the cross section of green wood. *Comptes Rendus Mécanique*, 338(2), pp.107–112.

Harris, P., Petherick, R. and Andrews, M., 2002. Acoustic resonance tools. In: *Proceedings, 13th international symposium on nondestructive testing of wood*. pp.195–201.

Lowe, M.J., Alleyne, D.N. and Cawley, P., 1998. Defect detection in pipes using guided waves. *Ultrasonics*, 36(1), pp.147–154.

Marra, G., Pellerin, R. and Galligan, W., 1966. Nondestructive determination of wood strength and elasticity by vibration. *Holz als Roh-und Werkstoff*, 24(10), pp.460–466.

Martin, P. and Berger, J., 2001. Waves in wood: free vibrations of a wooden pole. *Journal of the Mechanics and Physics of Solids*, 49(5), pp.1155–1178.

Martin, P. and Berger, J., 2003. Waves in wood: axisymmetric guided waves along boreholes. *Chinese J. Mech. A*, 19, pp.105–111.

De Oliveira, F.G.R. de, Miller, K.P., Candian, M. and Sales, A., 2006. Effect of the Size of the Specimen on Ultrasonic Velocity. *Revista Árvore*, 30(1), pp.141–145.

Subhani, M., Li, J. and Samali, B., 2013. A comparative study of guided wave propagation in timber poles with isotropic and transversely isotropic material models. *Journal of Civil Structural Health Monitoring*, 3(2), pp.65–79.

Wang, X., 2013. Acoustic measurements on trees and logs: a review and analysis. *Wood Science and Technology*, 47(5), pp.965–975.

Wang, X., Ross, R.J., McClellan, M., Barbour, R.J., Erickson, J.R., Forsman, J.W. and McGinnis, G.D., 2001. Nondestructive evaluation of standing trees with a stress wave method. *Wood and Fiber Science*, 33(4), pp.522–533.

Yang, H., Wang, L. and Li, L., 2011. Frequency equation of axisymmetric guided waves in logs. In: *Electronic and Mechanical Engineering and Information Technology (EMEIT), 2011 International Conference on*. pp.1964–1967.